Published in Journals: Axioms, Computation, Fractal and Fractional, Mathematics and Symmetry

Topic Reprint

Fractional Calculus

Theory and Applications, 2nd Edition

Edited by
António Lopes, Liping Chen, Sergio Adriani David and Alireza Alfi

mdpi.com/topics

MDPI

Fractional Calculus: Theory and Applications, 2nd Edition

Fractional Calculus: Theory and Applications, 2nd Edition

Topic Editors

António Lopes
Liping Chen
Sergio Adriani David
Alireza Alfi

MDPI

Basel • Beijing • Wuhan • Barcelona • Belgrade • Novi Sad • Cluj • Manchester

Topic Editors

António Lopes
Faculty of Engineering
University of Porto
Porto
Portugal

Liping Chen
School of Electrical
Engineering and Automation
Hefei University of Technology
Hefei
China

Sergio Adriani David
Department of Biosystems
Engineering
University of São Paulo
Pirassununga
Brazil

Alireza Alfi
Faculty of Electrical Engineering
Shahrood University of Technology
Shahrood
Iran

Editorial Office
MDPI AG
Grosspeteranlage 5
4052 Basel, Switzerland

This is a reprint of the Topic, published open access by the journals *Axioms* (ISSN 2075-1680), *Computation* (ISSN 2079-3197), *Fractal and Fractional* (ISSN 2504-3110), *Mathematics* (ISSN 2227-7390) and *Symmetry* (ISSN 2073-8994), freely accessible at: https://www.mdpi.com/topics/FractionalCalculus2.

For citation purposes, cite each article independently as indicated on the article page online and as indicated below:

Lastname, A.A.; Lastname, B.B. Article Title. *Journal Name* **Year**, *Volume Number*, Page Range.

ISBN 978-3-7258-9215-0 (Hbk)
ISBN 978-3-7258-9216-7 (PDF)
https://doi.org/10.3390/books978-3-7258-9216-7

© 2026 by the authors. Articles in this reprint are Open Access and distributed under the Creative Commons Attribution (CC BY) license. The reprint as a whole is distributed by MDPI under the terms and conditions of the Creative Commons Attribution-NonCommercial-NoDerivs (CC BY-NC-ND) license (https://creativecommons.org/licenses/by-nc-nd/4.0/).

Contents

Preface . . . . . **vii**

Asad Khan, Muhammad Awais Javeed, Saadia Rehman, Azmat Ullah Khan Niazi and Yubin Zhong
Advanced Observation-Based Bipartite Containment Control of Fractional-Order Multi-Agent Systems Considering Hostile Environments, Nonlinear Delayed Dynamics, and Disturbance Compensation
Reprinted from: *Fractal Fract.* **2024**, *8*, 473, https://doi.org/10.3390/fractalfract8080473 . . . . . **1**

Suleman Alfalqi, Hamid Khiar, Ahmed Bchatnia and Abderrahmane Beniani
Polynomial Decay of the Energy of Solutions of the Timoshenko System with Two Boundary Fractional Dissipations
Reprinted from: *Fractal Fract.* **2024**, *8*, 507, https://doi.org/10.3390/fractalfract8090507 . . . . . **28**

Abdelkader Amara, Mohammed El-Hadi Mezabia, Brahim Tellab, Khaled Zennir and Loay Alkhalifa
Study of a Coupled Ψ–Liouville–Riemann Fractional Differential System Characterized by Mixed Boundary Conditions
Reprinted from: *Fractal Fract.* **2024**, *8*, 510, https://doi.org/10.3390/fractalfract8090510 . . . . . **47**

Juan Luis González-Santander and Francesco Mainardi
Some Fractional Integral and Derivative Formulas Revisited
Reprinted from: *Mathematics* **2024**, *12*, 2786, https://doi.org/10.3390/math12172786 . . . . . **69**

Asra Hadadfard, Mohammad Bagher Ghaemi and António M. Lopes
Existence of Solutions for a Coupled Hadamard Fractional System of Integral Equations in Local Generalized Morrey Spaces
Reprinted from: *Axioms* **2024**, *13*, 688, https://doi.org/10.3390/axioms13100688 . . . . . **82**

Maryam Ahmad Alyami and Abdeljabbar Ghanmi
Multiple Solutions for a Critical Steklov Kirchhoff Equation
Reprinted from: *Fractal Fract.* **2024**, *8*, 598, https://doi.org/10.3390/fractalfract8100598 . . . . . **93**

Ramzi Alsaedi
A Note on a Min–Max Method for a Singular Kirchhoff Problem of Fractional Type
Reprinted from: *Mathematics* **2024**, *12*, 3269, https://doi.org/10.3390/math12203269 . . . . . **108**

Yutong Zhang, Bin Li and Mingfa Fei
Linearly Implicit Conservative Schemes for the Nonlocal Schrödinger Equation
Reprinted from: *Mathematics* **2024**, *12*, 3339, https://doi.org/10.3390/math12213339 . . . . . **119**

Muhammad Younis, Ahsan Mehmood, Muhammad Samraiz, Gauhar Rahman, Salma Haque, Ahmad Aloqaily and Nabil Mlaiki
Computational Representation of Fractional Inequalities Through 2D and 3D Graphs with Applications
Reprinted from: *Computation* **2025**, *13*, 46, https://doi.org/10.3390/computation13020046 . . . . **132**

Rongbo Zhang, Kun Qiu, Chuang Liu, Hongli Ma and Zhaobi Chu
Comparison Principle Based Synchronization Analysis of Fractional-Order Chaotic Neural Networks with Multi-Order and Its Circuit Implementation
Reprinted from: *Fractal Fract.* **2025**, *9*, 273, https://doi.org/10.3390/fractalfract9050273 . . . . . **165**

Arsalane Chouaib Guidoum, Fatimah A. Almulhim, Mohammed Bassoudi, Kamal Boukhetala and Mohammed B. Alamari
Fractional and Higher Integer-Order Moments for Fractional Stochastic Differential Equations
Reprinted from: *Symmetry* **2025**, *17*, 665, https://doi.org/10.3390/sym17050665 . . . . . **181**

Ahmed S. Rashed, Mahy M. Mahdy, Samah M. Mabrouk and Rasha Saleh
Fractional Order Mathematical Model for Predicting and Controlling Dengue Fever Spread Based on Awareness Dynamics
Reprinted from: *Computation* **2025**, *13*, 122, https://doi.org/10.3390/computation13050122 . . . **204**

Fang Wang, Lishan Liu, Haibo Gu, Lina Ma and Yonghong Wu
Existence and Uniqueness of Solutions for Singular Fractional Integro-Differential Equations with p-Laplacian and Two Kinds of Fractional Derivatives
Reprinted from: *Axioms* **2025**, *14*, 890, https://doi.org/10.3390/axioms14120890 . . . . . **220**

Dmitriy Tverdyi and Roman Parovik
A Study of the Efficiency of Parallel Computing for Constructing Bifurcation Diagrams of the Fractional Selkov Oscillator with Variable Coefficients and Memory
Reprinted from: *Computation* **2024**, *8*, 32, https://doi.org/10.3390/computation14020032 . . . . . **258**

Sheng-Hu Xu and Liang-Jia Dong
Global Dynamics of a Fractional-Order Anthrax Transmission Model with Distributed Delays and Beddington–DeAngelis Incidence
Reprinted from: *Fractal Fract.* **2026**, *10*, 175, https://doi.org/10.3390/fractalfract10030175 . . . . **278**

Zhichao Lu, Shiyou Lin and Tingting Hu
Partial Approximate Controllability of a Three-Parameter Damped Fractional Diffusion Control System with Nonlinear Perturbations
Reprinted from: *Symmetry* **2026**, *18*, 721, https://doi.org/10.3390/sym18050721 . . . . . **305**

Sixuan Chen, Xiaobo Wu, Tao Wang, Hongli Ma, Xiang Li and Lisheng Yin
Complex-Order Gold Rush Optimizer Algorithm
Reprinted from: *Computation* **2026**, *14*, 124, https://doi.org/10.3390/computation14060124 . . . **325**

Hanifah Al Affiani, Muhamad Deni Johansyah, Endang Rusyaman, Sukono, Nurfadhlina Binti Abdul Halim, Alim Jaizul Wahid, et al.
Hydrometeorological Disaster Insurance Modeling Based on Fractional Differential Equations for Climate Change Mitigation Within the Framework of SDG 13
Reprinted from: *Mathematics* **2024**, *14*, 2277, https://doi.org/10.3390/10.3390/math14132277 . . **352**

Zhi-Chao Lu, Ting-Ting Hu and Shi-You Lin
Optimal Control of Riemann–Liouville Fractional Stochastic Systems with Three-Parameter Damping
Reprinted from: *Fractal Fract.* **2026**, *10*, 490, https://doi.org/10.3390/fractalfract10070490 . . . . **394**

Zafer Bekiryazici
On the Solution Variability of Random-Order Fractional Differential Equations with Orders on Bounded Supports
Reprinted from: *Fractal Fract.* **2026**, *10*, 561, https://doi.org/10.3390/fractalfract10080561 . . . . **423**

Preface

This Reprint presents recent theoretical, computational, and applied advances in fractional calculus, a framework that extends differentiation and integration to noninteger orders and provides effective tools for describing memory, nonlocality, and complex dynamics. The presented studies develop analytical results for fractional differential and integral equations, including existence, uniqueness, stability, inequalities, and variational problems. They also introduce numerical and computational methods for simulation, bifurcation analysis, optimization, and the accurate treatment of nonlocal models. Applications span nonlinear and chaotic systems, neural networks, multiagent control, circuit implementation, biological and epidemiological modeling, stochastic processes, and climate-related risk assessment. Together, these contributions demonstrate how fractional-order models connect rigorous mathematical analysis with practical problems in science, engineering, and economics. The Reprint offers researchers a focused overview of current methods, emerging applications, and continuing challenges in the theory and use of fractional calculus.

António Lopes, Liping Chen, Sergio Adriani David, and Alireza Alfi
Topic Editors

fractal and fractional

MDPI

Article

Advanced Observation-Based Bipartite Containment Control of Fractional-Order Multi-Agent Systems Considering Hostile Environments, Nonlinear Delayed Dynamics, and Disturbance Compensation

Asad Khan [1,†], Muhammad Awais Javeed [2,†], Saadia Rehman [3], Azmat Ullah Khan Niazi [3] and Yubin Zhong [4,*]

[1] Metaverse Research Institute, School of Computer Science and Cyber Engineering, Guangzhou University, Guangzhou 510006, China; asad@gzhu.edu.cn
[2] School of Transportation, Southeast University, Nanjing 211189, China
[3] Department of Mathematics and Statistics, The University of Lahore, Sargodha 40100, Pakistan; azmatullah.khan@math.uol.edu.pk (A.U.K.N.)
[4] School of Mathematics and Information Science, Guangzhou University, Guangzhou 510006, China
* Correspondence: zhong_yb@gzhu.edu.cn
† These authors contributed equally to this work.

Abstract: This paper introduces an advanced observer-based control strategy designed for fractional multi-agent systems operating in hostile environments. We take into account the dynamic nature of the agents with nonlinear delayed dynamics and consider external disturbances affecting the system. The manuscript presents an improved observation-based control approach tailored for fractional-order multi-agent systems functioning in challenging conditions. We also establish various applicable conditions governing the creation of observers and disturbance compensation controllers using the fractional Razmikhin technique, signed graph theory, and matrix transformation. Furthermore, our investigation includes observation-based control on switching networks by employing a typical Lyapunov function approach. Finally, the effectiveness of the proposed strategy is demonstrated through the analysis of two simulation examples.

Keywords: observation error; fractional-order multi-agent system; bipartite containment control; observation error; Lyapunov function; signed directed network

1. Introduction

Multi-agent systems (MASs) are composed of multiple interacting autonomous subsystems that utilize shared information to tackle challenging or complex tasks. Consensus is a critical aspect of MASs' collective actions and ensures that through effective distributed control based solely on local knowledge, each agent's state converges to a desired common state. The existing literature has proposed several significant results addressing consensus problems under conditions of limited communication, dynamically changing topologies, uniform or non-uniform time delays, and external disturbances [1–5]. Additionally, the exploration of output containment control strategies has been a focal point of research efforts [6]. Various techniques, ranging from those leveraging the principles of Laplace transforms to sophisticated frequency domain analysis approaches, have been employed to address this intricate problem space [7]. In contrast to the cooperative frameworks typically studied in academia [8], real-world MASs frequently operate within environments characterized by a delicate interplay of cooperative and hostile connections among agents [9]. This detailed dynamic is enclosed within the framework of signed networks, where positive and negative edge weights encode the nature of the connection between agents [10]. These signed networks find widespread application across different domains, including social networks and multi-robot systems, where understanding and navigating

the complex inter-dependencies between agents is preeminent [11,12]. The appreciation of these antagonistic–cooperative dynamics underscores the need for adaptive and robust control strategies capable of accommodating the intricate interplay between the agents within such networks. Numerous significant investigations have focused on bipartite containment control. References [13–15] present fascinating works in this field. In reference [16], the authors convert bipartite containment control into a general form using matrix transformation techniques. An observer-based strategy to tackle bipartite containment control is introduced in [17]. Reference [18] explores the bipartite output containment issue by developing various control protocols. Moreover, other approaches have been employed, such as an output feedback method [19], a fuzzy observer method [20], and a delayed event-triggered mechanism [21]. It is important to note that the majority of existing research focuses on bipartite containment control for integer-order multi-agent systems (MASs). However, fractional calculus has demonstrated substantial benefits in modeling complex phenomena, including the transient response of elastomers and the motion of objects in viscoelastic materials [22,23]. In recent years, there has been significant research on control systems for connected vehicle platooning. Niazi et al. have made important contributions in this area [24]. The latest advancements in multi-agent system control have addressed various challenges, including communication delays and nonlinear couplings. Given the inherent uncertainties and nonlinearities in physical applications, substantial research has focused on the robust formation and consensus control problems in uncertain multi-agent systems (MASs). Studies such as those in [25,26] have introduced a fully distributed adaptive consensus protocol for higher-order systems with general linear and Lipschitz nonlinear dynamics. This protocol effectively reduces the consensus error to a small neighborhood around the origin and implements exponential convergence. In a similar way, adaptive techniques have been used to deal with the formation tracking problem in teams of uncertain systems with nonlinear terms satisfying Lipschitz conditions [27,28]. The motivation for studying fractional-order multi-agent systems (FMASs) with delays is grounded in both practical applications and theoretical advancements. Practically, FMASs can model complex systems in engineering, biology, and social networks and capture memory effects and long-term dependencies more accurately than traditional models. Communication delays are inherent in distributed systems and smart devices, necessitating robust control strategies. Theoretically, this research fills a gap in existing studies by providing new insights into the stability and control of FMASs with delays, leading to improved performance and resilience in real-world applications.

Inspired by these findings, this paper proposes advanced observer-based bipartite containment control of fractional multi-agent systems considering hostile environments, nonlinear delayed dynamics, and disturbance compensation. The specific contributions of this paper are given below.

- As compared to [29], we use a fractional-order multi-agent system instead of an integer-order derivative; our work contributes to the field by providing a more general and flexible framework for modeling and controlling dynamic behaviors in complex networks.
- By incorporating disturbances into the controller, our work enhances the robustness and practical applicability of the control strategy for fractional-order multi-agent systems, addressing real-world uncertainties.
- By incorporating a nonlinear delayed function in the dynamics, our work provides a more accurate and comprehensive framework for modeling and controlling fractional-order multi-agent systems, capturing complex temporal interactions and delays that have not been addressed in previous studies [29].

1. Section 1 is the introduction of the paper.
2. Section 2 presents the foundational knowledge that is useful for our main results.
3. Observation-based analyses of bipartite containment control for fixed and switching signed digraphs are discussed in Sections 3.2 and 4.
4. Numerical examples are presented in Section 5.
5. The paper is summarized in Section 6.

Figure 1 represents the framework of this paper.

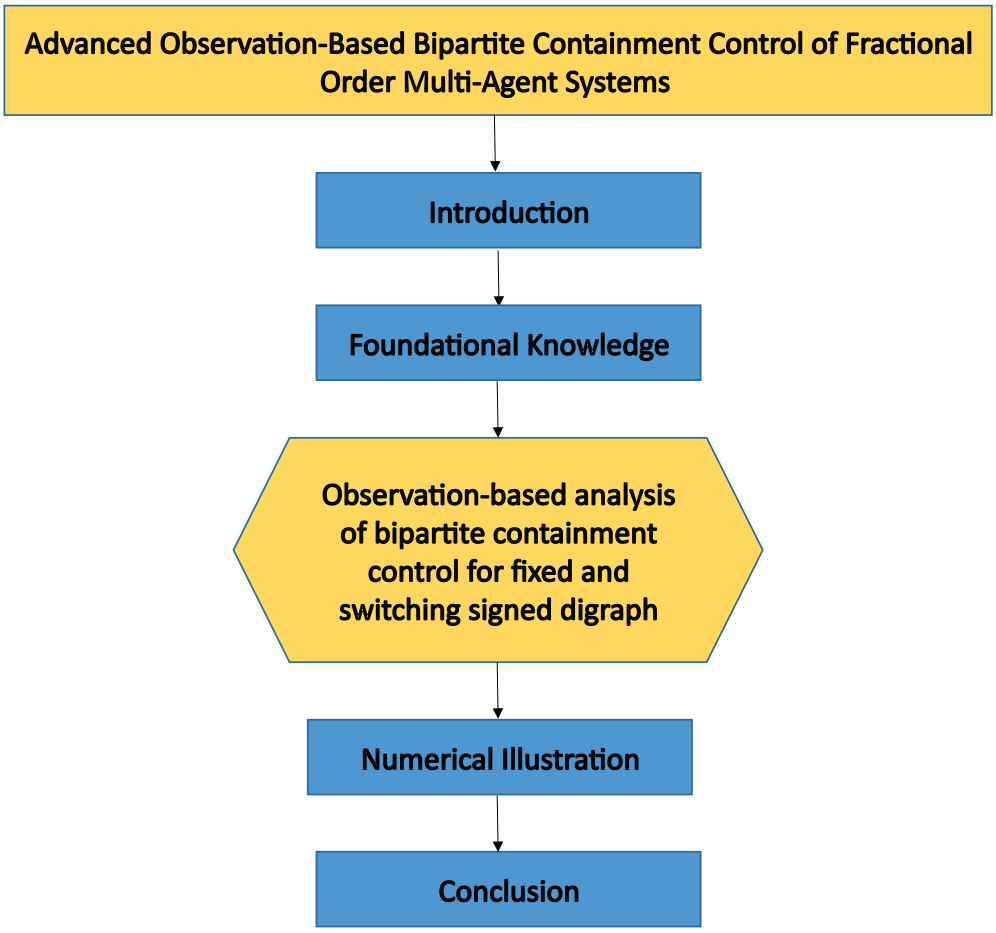

Figure 1. Framework of the paper.

2. Foundational Knowledge

2.1. Graph Theory

Consider a weighted signed digraph $\mathcal{G} = (\mathtt{N}, \mathtt{E})$, where $\mathtt{N} = \{n_1, \ldots, n_{\mathcal{N}}\}$ is the set of nodes and $\mathtt{E} \subseteq \mathtt{N} \times \mathtt{N}$ is the set of directed edges. The adjacency matrix $\mathtt{F} = [f_{ij}]_{\mathcal{N}\times\mathcal{N}}$ is defined such that $f_{ij} \neq 0$ if $(n_i, n_j) \in \mathtt{E}$ and $f_{ij} = 0$ otherwise. An edge (n_i, n_j) means that node n_i is capable of receiving information from node n_j; $f_{ij} > 0$ indicates a cooperative relationship, and $f_{ij} < 0$ indicates a hostile connection between nodes n_i and n_j. The Laplacian matrix $L = [\ell_{ij}]_{\mathcal{N}\times\mathcal{N}}$ for $\mathcal{G}$ is defined such that $\ell_{ij} = -f_{ij}$ for $i \neq j$ and $\ell_{ii} = \sum_{j=1, j\neq i}^{\mathcal{N}} |f_{ij}|$. Additionally, $\mathcal{G}$ is considered to be structurally balanced if the node set $\mathtt{N}$ of the signed graph $\mathcal{G}$ can be divided into two disjoint subsets $\mathtt{N}_1$ and $\mathtt{N}_2$ such that $f_{ij} > 0$ for any $n_i, n_j \in \mathtt{N}_1$ or $n_i, n_j \in \mathtt{N}_2$ and $f_{ij} < 0$ for any $n_i \in \mathtt{N}_1$ and $n_j \in \mathtt{N}_2$.

2.2. Basic Lemmas and Fractional Operators

In this subsection, various valuable definitions and lemmas are revisited.

Definition 1 ([30]). *The Caputo derivative of order γ for a function $\psi(s)$ that is c-differentiable is expressed as:*

$$D^{\gamma}\psi(s) = \frac{1}{\Gamma(c-\gamma)} \int_{s_0}^{s} \frac{\psi^{(c)}(t)}{(s-t)^{\mu-c+1}} dt, \;\; 0 \leq c-1 < \gamma \leq c, \;\; c \in \mathbb{Z}^{+}.$$

Lemma 1 ([31]). *If $\mathcal{Q}(s) \in \mathbb{R}^n$ is an absolutely continuous and differentiable function, then the following property holds:*

$$\frac{1}{2}D^{\gamma}(\mathcal{Q}^T(s)\mathcal{Q}(s)) \leq \mathcal{Q}^T(s)[D^{\gamma}\mathcal{Q}(s)] \leq 0, \quad \gamma \in (0,1).$$

Remark 1. *It is significant to observe that the Leibniz rule for the Caputo fractional derivative does not have a simple form. The fractional Leibniz rule, which is appropriate for the Caputo derivative, includes complex integral expressions that account for the non-local properties of the fractional derivative. For detailed discussions on the Leibniz rule for fractional derivatives, refer to foundational works on fractional calculus like [32].*

Lemma 2 ([31]). *Let $\beta_1, \beta_2 \in \mathbb{R}^n$ and $\rho > 0$; then the following inequality holds:*

$$2\beta_1^T\beta_2 \leq \rho\beta_1^T\beta_1 + \frac{1}{\rho}\beta_2^T\beta_2$$

Consider a delayed fractional-order system for $0 < \gamma < 1$ that can present both switching and non-switching behaviors:

$$\begin{aligned} D^{\gamma}z(s) &= k^{\sigma(s)}(s, z_s), \quad s \geq s_0 \\ z_{s_0}(\theta) &= \phi(\theta), \quad \theta \in [-e_2, 0] \end{aligned} \tag{1}$$

where $z_s(\theta) = z(s+\theta)$, $\theta \in [-e_2, 0]$, for any $s \geq s_0$ and time delay $e_2 > 0$, $\phi \in \mathcal{P}$. The function $k^{\sigma(s)}$ maps $\mathbb{R}\times$ (bounded sets of $\mathcal{P}$) into bounded sets of $\mathbb{R}^n$ and $k^{\sigma(s)}(s, 0) = 0$. Here, $\sigma(s)$ is a piecewise constant switching signal that can be constant in both cases (switching or non-switching).

Lemma 3. *The equilibrium point at zero of system (1), whether it presents switching or non-switching behavior, is asymptotically stable provided there exist positive numbers c_1, c_2, c_3 and a quadratic Lyapunov function $\mathcal{V} : \mathbb{R}^n \to \mathbb{R}$ such that*

$$c_1\|z(s)\|^2 \leq \mathcal{V}(z(s)) \leq c_2\|z(s)\|^2$$

and whenever

$$\begin{aligned} &\mathcal{V}(z(s+\theta)) \leq \kappa\mathcal{V}(z(s)), \quad \theta \in [-e_2, 0], \\ &D^{\gamma}\mathcal{V}(z(s)) \leq -c_3\|z(s)\|^2, \end{aligned}$$

where $\kappa > 1$; for more details see [33].

3. Observation-Based Bipartite Containment Control Analysis

In this section, we examine observation-based bipartite containment control of nonlinear FMASs with delays and disturbance in controllers for fixed signed directed networks as well as switching signed directed networks employing the common Lyapunov function approach. This is done by using the fractional Razmikhin technique, signed graph theory, and matrix transformation.

3.1. Model Building

In a fractional-order multi-agent system (FMAS) containing $\mathcal{F}$ followers and $\mathcal{N} - \mathcal{F}$ leaders, represented as $\mathbb{F} = \{1, 2, \ldots, \mathcal{F}\}$ and $\mathbb{B} = \{\mathcal{F}+1, \mathcal{F}+2, \ldots, \mathcal{N}\}$, respectively, the behavior of the followers is governed by:

$$\begin{aligned} D^{\gamma} y_i(s) &= Dy_i(s) + p(s, y_i(s)) + p_1(s, y_i(s - e_2)) + E\int_{-e_1}^{0} y_i(s+\phi)d\phi + Fv_i(s) + \Delta v_i(s) \\ z_i &= Gy_i(s) \quad i \in \mathbb{F} \end{aligned} \tag{2}$$

and the behavior of the leaders is described by

$$\begin{aligned} D^{\gamma} y_i(s) &= Dy_i(s) + p(s, y_i(s)) + p_1(s, y_i(s - e_2)) + E\int_{-e_1}^{0} y_i(s+\phi)d\phi \\ z_i &= Gy_i(s) \quad i \in \mathbb{B} \end{aligned} \tag{3}$$

Each agent i in the system is described by its state $y_i \in \mathbb{R}^n$, output $z_i \in \mathbb{R}^a$, and control input $v_i \in \mathbb{R}^b$; also, e_2 and e_1 are positive constants representing the communication and distributed delay, respectively. The function $p : \mathbb{R} \to \mathbb{R}^n$ is continuous and odd with respect to y_i and satisfyies $p(s, 0) = 0$ and $p(s, -y_i) = -p(s, y_i)$. The term p_1 is the nonlinear known function satisfying the Lipschitz condition. Matrices D, $E \in \mathbb{R}^{n\times n}$, $F \in \mathbb{R}^{n\times b}$, and $G \in \mathbb{R}^{a\times n}$ are constant. Furthermore, we assume that every agent can access relative output measurements of its neighboring agents and that the $i-th$ agent belongs to the set $\mathbb{B}$; the control input v_i is equal to zero.

Definition 2 ([1]). *The set $\delta \in \mathbb{R}^n$ is convex if, for any pair of points x_1, x_2 in δ and any λ, where $0 < \lambda < 1$, the point $\lambda x_1 + (1-\lambda)x_2$ is also in δ. The convex hull formed by a finite set of points $x_1, x_2, \ldots, x_n \in \mathbb{R}^n$ is the set of all possible convex combinations of these points and is defined as follows: it consists of all points of the form*

$$co\{x_1, x_2, ...x_n\} = \left\{ \sum_{i=1}^{n} \lambda_i x_i | \lambda_i \geq 0, \sum_{i=1}^{n} \lambda_i = 1 \right\} \tag{4}$$

Definition 3. *Observation-based bipartite containment control of the FMAS described in Equations (2) and (3) is achieved if certain followers converge to the convex hull of y_q for $q \in \mathbb{B}$, while others converge to $-co\{y_q, q \in \mathbb{B}\}$.*

Assumption 1. *If the functions p_i are Lipschitz continuous, then for each p_i, there exists a constant $k_i > 0$ such that for any vectors θ and α in $\mathbb{R}^n$, the condition below is satisfied:*

$$||p_i(s, \theta) - p_i(\theta, \alpha)|| \leq k_i ||\theta - \alpha||, \;\; i = 1, 2. \tag{5}$$

Assumption 2. *The nonlinear function p complies with the following inequality: for any $z, z_i \in \mathbb{R}^n$, where $\lambda_i \geq 0$ and $\sum_{i=1}^{\mathcal{N}-\mathcal{F}} \lambda_i = 1$, and for a given $r > 0$,*

$$\|p(s, z) - \sum_{i=1}^{\mathcal{N}-\mathcal{F}} \lambda_i p(s, z_i)\| \leq r\|z - \sum_{i=1}^{\mathcal{N}-\mathcal{F}} \lambda_i z_i\|.$$

Assumption 3. *The signed digraph $\mathcal{G}$ exhibits structural balance.*

Assumption 4. *Each follower within the signed digraph $\mathcal{G}$ is connected by a directed link to at least one leader.*

Remark 2. *If Assumption 2 holds, this implies that the Lipschitz condition is fulfilled; however, the converse is not true. The condition outlined in Assumption 2 guarantees both the existence and uniqueness of the solution for a nonlinear fractional-order system under delays [34]. Assumption 4 is crucial to ensure the absence of isolated vertices, ensuring that every agent can receive information from its neighboring agent. This configuration is commonly encountered in various containment control problems [35].*

Remark 3. *If Assumption 3 holds, then the followers may be split into two separate non-overlapping subsets: $\mathbb{F}_1$ and $\mathbb{F}_2$. Within each subset, agents connect cooperatively, while connections between agents from different subsets are hostile in behavior. By using Definition 3, observation-based bipartite containment control of the system defined by (2) and (3) is accomplished if the following conditions are satisfied:*

$$\lim_{s\to\infty} \|y_i - co\{y_q, q \in \mathbb{B}\}\| = 0, \ \forall\, i \in \mathbb{F}_1,$$
$$\lim_{s\to\infty} \|y_i + co\{y_q, q \in \mathbb{B}\}\| = 0, \ \forall\, i \in \mathbb{F}_2.$$

3.2. Observation-Based Analysis of Bipartite Multi-Agent System for Fixed Signed Digraph

Based on the idea from the containment control protocols presented by [9,29], we introduce an observation-based bipartite containment controller for every $i \in \mathbb{F}$. This study leverages the state, which is observed information, to enhance the system's performance:

$$\begin{aligned} D^{\gamma}\hat{y}_i(s) &= D\hat{y}_i(s) + p(s,\hat{y}_i(s)) + p_1(s,\hat{y}_i(s-e_2)) + E\int_{-e_1}^{0} \hat{y}_i(s+\phi)d\phi + Fv_i(s) + \Delta v_i(s) \\ &\quad + \mu A\left(\sum_{j=1}^{\mathcal{F}} |f_{ij}|(z_i - sgn(f_{ij})z_j) - \sum_{j=1}^{\mathcal{F}} |f_{ij}|(\hat{z}_i - sgn(f_{ij})\hat{z}_j) + \sum_{j=\mathcal{F}+1}^{\mathcal{N}} |f_{ij}|(z_i - \hat{z}_i))\right), \\ \hat{z}_i &= G\hat{y}_i(s) \quad i \in \mathbb{F} \end{aligned} \tag{6}$$

$$\begin{aligned} v_i = -\beta T\left(\sum_{j=1}^{\mathcal{N}} |f_{ij}|\big(\hat{y}_i(s-e_2) - \mathrm{sgn}(f_{ij})\hat{y}_j(s-e_2)\big) + \sum_{j=\mathcal{F}+1}^{\mathcal{N}} |f_{ij}|\big(\hat{y}_i(s-e_2) - \mathrm{sgn}(f_{ij})y_j(s-e_2)\big)\right) \\ + \Delta v_i(s) \end{aligned} \tag{7}$$

Here, $\hat{y}_i$ denotes the state estimate of y_i for each $i \in \mathbb{F}$, and $\hat{z}_i$ is the output of the observer. The parameters μ and $A \in \mathbb{R}^{n\times a}$ are the coupling strength and the gain matrix of the observer, respectively, both of which are designed; $e_2 > 0$ represents the input delay. Moreover, $T \in \mathbb{R}^{b\times n}$ and β represent the gain matrix and coupling constant for the controller, respectively. The term f_{ij} refers to entries of the adjacency matrix of digraph $\mathcal{G}$, and $\Delta v_i(s)$ is the disturbance in the controller. Since $v_i = 0$ for all $i \in \mathbb{B}$, the Laplacian matrix L of the signed digraph $\mathcal{G}$ is defined as:

$$L = \begin{pmatrix} L_{\mathcal{F}} & L_{\mathcal{B}} \\ 0_{(\mathcal{N}-\mathcal{F})\times\mathcal{F}} & 0_{(\mathcal{N}-\mathcal{F})\times(\mathcal{N}-\mathcal{F})} \end{pmatrix}$$

where $L_{\mathcal{F}} \in \mathbb{R}^{\mathcal{F}\times\mathcal{F}}$ and $L_{\mathcal{B}} \in \mathbb{R}^{\mathcal{F}\times(\mathcal{N}-\mathcal{F})}$. If Assumption 3 is met, a diagonal matrix exists such that $\psi = \mathrm{diag}(\psi_1, \psi_2, \ldots, \psi_{\mathcal{F}}, \psi_{\mathcal{F}+1}, \ldots, \psi_{\mathcal{N}})$; the matrix is defined by its elements as:

$$\begin{cases} \psi_i = 1 \ if \ i \in \mathbb{F}_1 \cup \mathbb{B} \\ \psi_i = -1 \ if \ i \in \mathbb{F}_2 \end{cases}$$

such that

$$L = \psi L \psi = \begin{pmatrix} \overline{L}_{\mathcal{F}} & \overline{L}_{\mathcal{B}} \\ 0_{(\mathcal{N}-\mathcal{F})\times\mathcal{F}} & 0_{(\mathcal{N}-\mathcal{F})\times(\mathcal{N}-\mathcal{F})} \end{pmatrix}$$

Here, $\overline{L}_{\mathcal{F}} = [\overline{\ell}_{ij}]_{\mathcal{F}\times\mathcal{F}}$ if $i \neq j$; then $[\overline{\ell}_{ij}]_{\mathcal{F}\times\mathcal{F}}$ is equal to $-|f_{ij}|$; otherwise, it is equal to $\sum_{j=1}^{\mathcal{N}} |f_{ij}|$. Also, $\overline{L}_{\mathcal{B}} = [\overline{\ell}_{ij}]_{\mathcal{F}\times(\mathcal{N}-\mathcal{F})}$ $\overline{\ell}_{ij} = -|f_{ij}| \leq 0$ for $i = 1, 2, 3, ...\mathcal{F}$, $j = \mathcal{F}+1, ..., \mathcal{N}$.

Lemma 4 ([1]). *If Assumption 4 holds, $\overline{L}_{\mathcal{F}}$ is a non-singular M-matrix, and each component of $-\overline{L}_{\mathcal{F}}^{-1}\overline{L}_{\mathcal{B}}$ is nonnegative, with each row summing to 1.*

Remark 4. *Dealing with fractional-order systems is significantly more complex than handling integer-order systems [15]. Fractional-order systems have memory effects and non-locality, meaning*

their future states depend on their entire past history rather than just the current state. This complexity requires more advanced mathematical tools, such as fractional derivatives and integrals, which often lack closed-form solutions and require numerical methods and approximations. Analyzing the stability of fractional-order systems is more intricate and requires extensions or adaptations of traditional methods like Lyapunov functions. Controller design is also more challenging due to the need to account for fractional dynamics, demanding more sophisticated techniques. Additionally, the application of fractional-order Laplace transforms and the formulation of linear matrix inequalities (LMIs) introduce further complexities. These factors collectively make the analysis and control of fractional-order systems significantly more challenging than that of integer-order systems [21].

Theorem 1. *Observer-based bipartite containment control of the FMAS defined by Equations (2) and (3), with the controller given in Equation (7) and under Assumptions 1, 2, 3, and 4, can be successfully realized if there exists a diagonal matrix $\Phi = diag(\phi_1, \ldots, \phi_{\mathcal{F}}) > 0$ such that $\Phi L_{\mathcal{F}} + L_{\mathcal{F}}^T \Phi > 0$ along with positive definite matrices S_1 and S_2 satisfying the following set of inequalities:*

$$\begin{pmatrix} (1-r)S_1 & S_1 E \\ E^T S_1 & -S_1 \end{pmatrix} < 0 \tag{8}$$

$$\begin{pmatrix} S_1 D + D^T S_1 + S_1^2 + (k^2+\ell^2) I_n + (1+re_1) S_1 - \rho G^T G & S_1 \\ S_1 & -I_n \end{pmatrix} < 0 \tag{9}$$

$$\begin{pmatrix} (1-b)S_2^{-1} & E S_2^{-1} \\ S_2^{-1} E^T & -S_2^{-1} \end{pmatrix} < 0 \tag{10}$$

$$\begin{pmatrix} D S_2^{-1} + S_2^{-1} D^T + (1+be_1) S_2^{-1} + (2+\frac{q}{\nu}) I_n + \omega F F^T (\ell^2 I_n + S_2^{-1})^{-1} S_2 F F^T & k S_2^{-1} \\ k S_2^{-1} & -I_n \end{pmatrix} < 0 \tag{11}$$

Given the parameters $\rho, \omega > 0$ and $r, b > 1$, the observer and controller are designed with the following specifications:

- $A = S_1^{-1} G^T$
- $\mu \geq \frac{\rho \phi_{\max}}{\lambda_1}$, *where:*
  - $\lambda_1 = \lambda_{\min}\{\Phi \overline{L}_{\mathcal{F}} + \overline{L}_{\mathcal{F}}\}$
  - $\phi_{\max} = \max_{1 \leq j \leq \mathcal{F}}\{\phi_j\}$
- $T = F^T S_2$
- $0 < \beta \leq \sqrt{\frac{\omega \phi_{\min}}{\lambda_2}}$, *where:*
  - $\lambda_2 = \lambda_{\max}\{\overline{L}_{\mathcal{F}}^T \Phi \overline{L}_{\mathcal{F}}\}$
  - $\phi_{\min} = \min_{1 \leq j \leq \mathcal{F}}\{\phi_j\}$

Proof. First, we define the observed state $\hat{y}_i$ and the state y_i for each $i \in \mathbb{F}$ using Equations (2), (6) and (7):

$$
\begin{aligned}
&D^{\gamma}y_i(s) = Dy_i(s) + p(s, y_i(s)) + p_1(s, y_i(s-e_2)) + E\int_{-e_1}^{0} y_i(s+\phi)d\phi \\
&- \beta FT\left(\sum_{j=1}^{\mathcal{N}}|f_{ij}|\big(\hat{y}_i(s-e_2) - \operatorname{sgn}(f_{ij})\hat{y}_j(s-e_2)\big) + \sum_{j=\mathcal{F}+1}^{\mathcal{N}}|f_{ij}|\big(\hat{y}_i(s-e_2) - \operatorname{sgn}(f_{ij})y_j(s-e_2)\big)\right) \\
&+ 2\Delta v_i(s) \\
&D^{\gamma}\hat{y}_i(s) = D\hat{y}_i(s) + p(s, \hat{y}_i(s)) + p_1(s, \hat{y}_i(s-e_2)) + E\int_{-e_1}^{0} \hat{y}_i(s+\phi)d\phi \\
&- \beta FT\left(\sum_{j=1}^{\mathcal{N}}|f_{ij}|\big(\hat{y}_i(s-e_2) - \operatorname{sgn}(f_{ij})\hat{y}_j(s-e_2)\big) + \sum_{j=\mathcal{F}+1}^{\mathcal{N}}|f_{ij}|\big(\hat{y}_i(s-e_2) - \operatorname{sgn}(f_{ij})y_j(s-e_2)\big)\right) \\
&+ 2\Delta v_i(s) + \mu A\left(\sum_{j=1}^{\mathcal{F}}|f_{ij}|(z_i - sgn(f_{ij})z_j) - \sum_{j=1}^{\mathcal{F}}|f_{ij}|(\hat{z}_i - sgn(f_{ij})\hat{z}_j) + \sum_{j=\mathcal{F}+1}^{\mathcal{F}}|f_{ij}|(z_i - \hat{z}_j)\right)
\end{aligned}
$$

Consider the coordinate transformation $x_i = \psi_i y_i$ and $\hat{x}_i = \psi_i \hat{y}_i$, where $\psi_i = 1$ for $i \in \mathbb{F}_1 \cup \mathbb{B}$, and $\psi_i = -1$ for $i \in \mathbb{B}_2$. Hence, we can obtain

$$
\begin{aligned}
&D^{\gamma}x_i(s) = Dx_i(s) + p(s, x_i(s)) + p_1(s, x_i(s-e_2)) + E\int_{-e_1}^{0} x_i(s+\phi)d\phi \\
&- \beta FT\psi_i(\sum_{j=1}^{\mathcal{N}}|f_{ij}|\big(\psi_i\hat{x}_i(s-e_2) - \operatorname{sgn}(f_{ij})\psi_j\hat{x}_j(s-e_2)\big) + \sum_{j=\mathcal{F}+1}^{\mathcal{N}}|f_{ij}|(\psi_i\hat{x}_i(s-e_2) \\
&- \operatorname{sgn}(f_{ij})\psi_j x_j(s-e_2))) + 2\Delta v_i(s), \quad i \in \mathbb{F} \qquad (12) \\
&D^{\gamma}\hat{x}_i(s) = D\hat{x}_i(s) + p(s, \hat{x}_i(s)) + p_1(s, \hat{x}_i(s-e_2)) + E\int_{-e_1}^{0} \hat{x}_i(s+\phi)d\phi \\
&- \beta FT\psi_i\left(\sum_{j=1}^{\mathcal{N}}|f_{ij}|\big(\psi_i\hat{x}_i(s-e_2) - \operatorname{sgn}(f_{ij})\psi_j\hat{x}_j(s-e_2)\big) + \sum_{j=\mathcal{F}+1}^{\mathcal{N}}|f_{ij}|\big(\psi_i\hat{x}_i(s-e_2) - \operatorname{sgn}(f_{ij})\psi_j x_j(s-e_2)\big)\right) \\
&+ \mu AG\psi_i\left(\sum_{j=1}^{\mathcal{F}}|f_{ij}|\psi_i(x_i - sgn(f_{ij})\psi_j x_j) - \sum_{j=1}^{\mathcal{F}}|f_{ij}|(\psi_i\hat{x}_i - sgn(f_{ij})\psi_j\hat{x}_j) + \sum_{j=\mathcal{F}+1}^{\mathcal{F}}|f_{ij}|(\psi_i x_i - \psi_j\hat{x}_j)\right) \\
&+ 2\Delta v_i(s), \quad i \in \mathbb{F} \qquad (13) \\
&D^{\gamma}x_i(s) = Dx_i(s) + p(s, x_i(s)) + p_1(s, x_i(s-e_2)) + E\int_{-e_1}^{0} x_i(s+\phi)d\phi \quad i \in \mathbb{B} \qquad (14)
\end{aligned}
$$

Let $X_{\mathcal{F}}(s) = (x_1^T(s), x_2^T(s), \ldots, x_{\mathcal{F}}^T(s))^T$; $X_{\mathcal{B}}(s) = (x_{\mathcal{F}+1}^T(s), x_{\mathcal{F}+2}^T(s), \ldots, x_{\mathcal{N}}^T(s))^T$;
$P(s, X_{\mathcal{F}}) = (p^T(s, x_1), p^T(s, x_2), \ldots, p^T(s, x_{\mathcal{F}}))^T$; $P(s, X_{\mathcal{B}}) = (p^T(s, x_{\mathcal{F}+1}), p^T(s, x_{\mathcal{F}+2}), \ldots, p^T(s, x_{\mathcal{N}}))^T$
$\hat{X}_{\mathcal{F}}(s) = (\hat{x}_1^T(s), \hat{x}_2^T(s), \ldots, \hat{x}_{\mathcal{F}}^T(s))^T$; $P(s, \hat{X}_{\mathcal{F}}) = (p^T(s, \hat{x}_1), p^T(s, \hat{x}_2), \ldots, p^T(s, \hat{x}_{\mathcal{F}}))^T$;
$P_1(s, X_{\mathcal{F}}(s-e_2) = (p_1^T(s, x_1(s-e_2)), p_1^T(s, x_2(s-e_2), \ldots, p^T(s, x_{\mathcal{F}}(s-e_2))^T$;
$P_1(s, X_{\mathcal{B}}(s-e_2) = (p_1^T(s, x_{\mathcal{F}+1}(s-e_2)), p_1^T(s, x_{\mathcal{F}+1}(s-e_2), \ldots, p^T(s, x_{\mathcal{N}}(s-e_2))^T$;
$P_1(s, \hat{X}_{\mathcal{F}}(s-e_2) = (p_1^T(s, \hat{x}_1(s-e_2)), p_1^T(s, \hat{x}_2(s-e_2), \ldots, p^T(s, \hat{x}_{\mathcal{F}}(s-e_2))^T$;

From Equations (12)–(14), we derive the following results:

$$D^{\gamma}X_{\mathcal{F}} = (I_{\mathcal{F}} \otimes D)X_{\mathcal{F}} + P(s, X_{\mathcal{F}}) + P_1(s, X_{\mathcal{F}}(s-e_2)) + \int_{-e_1}^{0} (I_{\mathcal{F}} \otimes E)X_{\mathcal{F}}(s+\phi)d\phi$$
$$- (\overline{L}_{\mathcal{F}} \otimes \beta FT)\hat{X}_{\mathcal{F}}(s-e_2) - (\overline{L}_{\mathcal{B}} \otimes \beta FT)X_{\mathcal{B}}(s-e_2) + 2\Delta v_i(s) \quad (15)$$
$$D^{\gamma}\hat{X}_{\mathcal{F}} = (I_{\mathcal{F}} \otimes D)\hat{X}_{\mathcal{F}} + P(s, \hat{X}_{\mathcal{F}}) + P_1(s, \hat{X}_{\mathcal{F}}(s-e_2)) + \int_{-e_1}^{0} (I_{\mathcal{F}} \otimes E)\hat{X}_{\mathcal{F}}(s+\phi)d\phi$$
$$- (\overline{L}_{\mathcal{F}} \otimes \beta FT)\hat{X}_{\mathcal{F}}(s-e_2) - (\overline{L}_{\mathcal{B}} \otimes \beta FT)X_{\mathcal{B}}(s-e_2) + (\overline{L}_{\mathcal{F}} \otimes \mu AG)X_{\mathcal{F}}$$
$$- (\overline{L}_{\mathcal{F}} \otimes \mu AG)\hat{X}_{\mathcal{F}} + 2\Delta v_i(s) \quad (16)$$
$$D^{\gamma}X_{\mathcal{B}} = (I_{\mathcal{N}-\mathcal{F}} \otimes D)X_{\mathcal{B}} + P(s, X_{\mathcal{B}}) + P_1(s, X_{\mathcal{B}}(s-e_2)) + \int_{-e_1}^{0} (I_{\mathcal{N}-\mathcal{F}} \otimes E)X_{\mathcal{B}}(s+\phi)d\phi \quad (17)$$

Let observation error $\alpha_1(.) = \hat{X}_{\mathcal{F}}(.) - X_{\mathcal{F}}(.)$ and bipartite containment control error $\alpha_2(.) = X_{\mathcal{F}}(.) - (-\overline{L}_{\mathcal{F}}^{-1}\overline{L}_{\mathcal{B}} \otimes I_n)X_{\mathcal{B}}(.)$; one has

$$D^{\gamma}\alpha_1 = (I_{\mathcal{F}} \otimes D)\alpha_1 + P(s, \hat{X}_{\mathcal{F}}) - P(s, X_{\mathcal{F}}) + P_1(s, \hat{X}_{\mathcal{F}}(s-e_2)) - P_1(s, X_{\mathcal{F}}(s-e_2))$$
$$\int_{-e_1}^{0} (I_{\mathcal{F}} \otimes E)\alpha_1(s+\phi)d\phi - (\overline{L}_{\mathcal{F}} \otimes \mu AG)\alpha_1. \quad (18)$$

$$D^{\gamma}\alpha_2 = (I_{\mathcal{F}} \otimes D)X_{\mathcal{F}} + (\overline{L}_{\mathcal{F}}^{-1}\overline{L}_{\mathcal{B}} \otimes D)X_{\mathcal{B}} + P(s, X_{\mathcal{F}}) + (\overline{L}_{\mathcal{F}}^{-1}\overline{L}_{\mathcal{B}} \otimes I_n)P(s, X_{\mathcal{B}}) + P_1(s, X_{\mathcal{F}}(s-e_2))$$
$$+ (\overline{L}_{\mathcal{F}}^{-1}\overline{L}_{\mathcal{B}} \otimes I_n)P_1(s, X_{\mathcal{B}}(s-e_2)) + \int_{-e_1}^{0} (I_{\mathcal{F}} \otimes E)X_{\mathcal{F}}(s+\phi)d\phi + \int_{-e_1}^{0} (\overline{L}_{\mathcal{F}}^{-1}\overline{L}_{\mathcal{B}} \otimes E)X_{\mathcal{B}}(s+\phi)d\phi$$
$$- (\overline{L}_{\mathcal{F}} \otimes \beta FT)\hat{X}_{\mathcal{F}}(s-e_2) + (\overline{L}_{\mathcal{F}} \otimes \beta FT)X_{\mathcal{F}}(s-e_2) - (\overline{L}_{\mathcal{F}} \otimes \beta FT)X_{\mathcal{F}}(s-e_2)$$
$$- (\overline{L}_{\mathcal{B}} \otimes \beta FT)X_{\mathcal{F}}(s-e_2) + 2\Delta v_i(s). \quad (19)$$

$$D^{\gamma}\alpha_2 = (I_{\mathcal{F}} \otimes D)\alpha_2 + +P(s, X_{\mathcal{F}}) + (\overline{L}_{\mathcal{F}}^{-1}\overline{L}_{\mathcal{B}} \otimes I_n)P(s, X_{\mathcal{B}}) + P_1(s, X_{\mathcal{F}}(s-e_2))$$
$$+ (\overline{L}_{\mathcal{F}}^{-1}\overline{L}_{\mathcal{B}} \otimes I_n)P_1(s, X_{\mathcal{B}}(s-e_2)) + \int_{-e_1}^{0} (I_{\mathcal{F}} \otimes E)\alpha_2(s+\phi)d\phi \quad (20)$$
$$- (\overline{L}_{\mathcal{F}} \otimes \beta FT)\alpha_1(s-e_2) - (\overline{L}_{\mathcal{F}} \otimes \beta FT)\alpha_2(s-e_2) + 2\Delta v_i(s)$$

Let $\alpha(.) = [\alpha_1^T(.), \alpha_2^T(.)]^T$ represent the error system and

$$D^{\gamma}\alpha = R_1\alpha + \overline{P}(s, \alpha) + \overline{P}_1(s, \alpha(s-e_2)) + R_2\alpha(s-e_2) + \int_{-e_1}^{0} R_3\alpha(s+\phi)d\phi + 2\Delta v_i(s), \quad (21)$$

where

$$R_1 = \begin{pmatrix} (I_F \otimes D) - (\overline{L}_{\mathcal{F}} \otimes \mu AG) & 0 \\ 0 & I_F \otimes D \end{pmatrix}; \quad R_2 = \begin{pmatrix} 0 & 0 \\ -\overline{L}_{\mathcal{F}} \otimes \beta FT & -\overline{L}_{\mathcal{F}} \otimes \beta FT \end{pmatrix};$$

$$R_3 = \begin{pmatrix} I_F \otimes E & 0 \\ 0 & I_F \otimes E \end{pmatrix};$$

$$\overline{P}(s, \alpha) = \left[P(s, \hat{X}_{\mathcal{F}}) - P(s, X_{\mathcal{F}})\right]\left[P(s, X_{\mathcal{F}}) + (\overline{L}_{\mathcal{F}}^{-1}\overline{L}_{\mathcal{B}} \otimes I_n)P(s, X_{\mathcal{B}})\right],$$

$$\overline{P}_1(s, \alpha(s-e_2) = \left[P_1(s, \hat{X}_{\mathcal{F}}(s-e_2) - P_1(s, X_{\mathcal{F}}(s-e_2)\right]\left[P_1(s, X_{\mathcal{F}}(s-e_2) + (\overline{L}_{\mathcal{F}}^{-1}\overline{L}_{\mathcal{B}} \otimes I_n)P_1(s, X_{\mathcal{B}}(s-e_2)\right].$$

Let us delve into the asymptotic stability analysis of the error system (21). Given that $\overline{L}_{\mathcal{F}}$ is a non-singular M-matrix according to Lemma 4, then there exists a positive definite

diagonal matrix $\mathbf{\Phi} = \text{diag}(\phi_1, \phi_2, \ldots, \phi_{\mathcal{F}})$ such that $\Phi\overline{L}_{\mathcal{F}} + \overline{L}_{\mathcal{F}}^T\Phi > 0$. With this in mind, let us formulate the following Lyapunov function:

$$\begin{aligned}\mathcal{V}(\alpha(s)) &= \mathcal{V}_1(\alpha_1(s)) + \mathcal{V}_2(\alpha_2(s)) \\ &= \alpha_1^T(\Phi \otimes S_1)\alpha_1 + \alpha_2^T(\eta\Phi \otimes S_2)\alpha_2\end{aligned} \tag{22}$$

where $\eta > 0$ is very small scalar.

Remark 5. *Our method extends traditional Lyapunov techniques, which typically rely on a single positive definite matrix P. Instead of using P, we introduce a matrix Φ with a structured diagonal form, offering greater versatility and adaptability to various system dynamics. Recent research on adaptive and robust control also supports the use of structured Lyapunov functions [29]. Our approach aligns with these recent advancements, as it provides a structured yet adaptable framework to guarantee stability even when dealing with changing system parameters.*

It follows from Lemma 1 that

$$\begin{aligned}&D^\gamma\mathcal{V}_1(\alpha_1(s)) = D^\gamma[\alpha_1^T(\Phi \otimes S_1)\alpha_1] \le 2\alpha_1^T(\Phi \otimes S_1)[D^\gamma\alpha_1] \\ &2\alpha_1^T(\Phi \otimes S_1)[(I_{\mathcal{F}} \otimes D - \overline{L}_{\mathcal{F}} \otimes \mu AG)\alpha_1 + P(s, \hat{X}_{\mathcal{F}}) - P(s, X_{\mathcal{F}}) + P_1(s, \hat{X}_{\mathcal{F}}(s - e_2)) \\ &- P_1(s, X_{\mathcal{F}}(s - e_2)) + \int_{-e_1}^{0}(I_{\mathcal{F}} \otimes E)\alpha_1(s + \phi)d\phi] \\ &= \alpha_1^T\Big[\Phi \otimes (S_1D + D^TS_1) - (\Phi\overline{L}_{\mathcal{F}} \otimes \mu S_1AG) - (\overline{L}_{\mathcal{F}}^T\Phi \otimes \mu G^TA^TS_1)\Big]\alpha_1 \\ &+ 2\alpha_1^T(\Phi \otimes S_1)\big[P(s, \hat{X}_{\mathcal{F}}) - P(s, X_{\mathcal{F}})\big] + 2\alpha_1^T(\Phi \otimes S_1)\big[P_1(s, \hat{X}_{\mathcal{F}}(s - e_2)) - P_1(s, X_{\mathcal{F}}(s - e_2))\big] \\ &+ \int_{-e_1}^{0} 2\alpha_1^T(\Phi \otimes S_1E)\alpha_1(s + \phi)d\phi\end{aligned} \tag{23}$$

Notice that

$$2\alpha_1^T(\Phi \otimes S_1)\big[P(s, \hat{X}_{\mathcal{F}}) - P(s, X_{\mathcal{F}})\big] = \sum_{i=1}^{\mathcal{F}} 2\phi_i\alpha_{1i}^TS_1[p(s, \hat{x}_i) - p(s, x_i)];$$

one has from Assumption 2 and Lemma 2

$$2\phi_i\alpha_{1i}^TS_1[p(s, \hat{x}_i) - p(s, x_i)] \le \phi_i\Big[\alpha_{1i}^TS_1^2\alpha_{1i} + (p(s, \hat{x}_i) - p(s, x_i))^Tp(s, \hat{x}_i) - p(s, x_i)\Big] \le \phi_i\Big[\alpha_{1i}^TS_1\alpha_{1i}^2 + k^2\alpha_{1i}^T\alpha_{1i}\Big]$$

Due to $\alpha_1^T\big[\Phi \otimes (S_1^2 + k^2I_n)\big]\alpha_1 = \sum_{i=1}^{\mathcal{F}}\phi_i\big[\alpha_{1i}^TS_1^2\alpha_{1i} + k^2\alpha_{1i}^T\alpha_{1i}\big]$, we can derive that

$$2\alpha_1^T(\Phi \otimes S_1)\big[P(s, \hat{X}_{\mathcal{F}}) - P(s, X_{\mathcal{F}})\big] \le \alpha_1^T\Big[\Phi \otimes (S_1^2 + k^2I_n\Big]\alpha_1 \tag{24}$$

$$2\alpha_1^T(\Phi \otimes S_1)\big[P_1(s, \hat{X}_{\mathcal{F}}(s - e_2) - P_1(s, X_{\mathcal{F}}(s - e_2)\big] = \sum_{i=1}^{\mathcal{F}} 2\phi_i\alpha_{1i}^TS_1[p_1(s, \hat{x}_i(s - e_2) - p_1(s, x_i(s - e_2)],$$

using Assumption 1 and Lemma 2, we have

$$\begin{aligned}&2\phi_i\alpha_{1i}^TS_1[p_1(s, \hat{x}_i(s - e_2) - p_1(s, x_i(s - e_2)] \le \phi_i[\alpha_{1i}^TS_1^2\alpha_{1i} \\ &+ (p_1(s, \hat{x}_i(s - e_2) - p_1(s, x_i(s - e_2))^Tp_1(s, \hat{x}_i(s - e_2) - p_1(s, x_i(s - e_2)] \\ &\le \phi_i\Big[\alpha_{1i}^TS_1\alpha_{1i}^2 + \ell^2\alpha_{1i}(s - e_2)^T\alpha_{1i}(s - e_2)\Big]\end{aligned}$$

Due to

$$\alpha_1^T(s)\Big[\Phi \otimes S_1^2\Big]\alpha_1(s) + \alpha_1^T(s - e_2)\Big[\Phi \otimes \ell^2I_n\Big]\alpha_1(s - e_2) = \sum_{i=1}^{\mathcal{F}}\phi_i\Big[\alpha_{1i}^TS_1^2\alpha_{1i} + \ell^2\alpha_{1i}^T(s - e_2)\alpha_{1i}(s - e_2)\Big],$$

we can derive that

$$2\alpha_1^T(\Phi\otimes S_1)\left[P_1(s,\hat{X}_{\mathcal{F}}(s-e_2)-P_1(s,X_{\mathcal{F}}(s-e_2)\right]\leq\alpha_1^T(s)\Big[\Phi\otimes S_1^2\Big]\alpha_1(s)+\alpha_1^T(s-e_2)\Big[\Phi\otimes\ell^2I_n\Big]\alpha_1(s-e_2) \tag{25}$$

By (23)–(25), we have

$$\begin{aligned}D^{\gamma}\mathcal{V}_1&\leq\alpha_1^T\Big[\Phi\otimes(S_1D+D^TS_1+2S_1^2+k^2I_n)-(\Phi\overline{L}_{\mathcal{F}}\otimes\mu S_1AG)-(\overline{L}_{\mathcal{F}}^T\Phi\otimes\mu G^TA^TS_1)\Big]\alpha_1\\&+\alpha_1^T(s-e_2)\Big[\Phi\otimes\ell^2I_n\Big]\alpha_1(s-e_2)+\int_{-e_1}^{0}2\alpha_1^T(\Phi\otimes S_1E)\alpha_1(s+\phi)d\phi\end{aligned}$$

Substituting the gain matrix $A=S_1^TG^T$ into the above equation yields

$$\begin{aligned}D^{\gamma}\mathcal{V}_1&\leq\alpha_1^T\Big[\Phi\otimes(S_1D+D^TS_1+2S_1^2+k^2I_n)-\mu(\Phi\overline{L}_{\mathcal{F}}+\overline{L}_{\mathcal{F}}^T\Phi)\otimes G^TG\Big]\alpha_1\\&+\alpha_1^T(s-e_2)\Big[\Phi\otimes\ell^2I_n\Big]\alpha_1(s-e_2)+\int_{-e_1}^{0}2\alpha_1^T(\Phi\otimes S_1E)\alpha_1(s+\phi)d\phi\end{aligned} \tag{26}$$

Now, we utilize the fractional Razumikhin technique on Equation (26). Notice that

$$\begin{aligned}&2\alpha_1^T(\Phi\otimes S_1E)\alpha_1(s+\phi)=2\alpha_1^T(I_{\mathcal{F}}\otimes S_1E)(\Phi^{\frac{1}{2}}\otimes S_1^{-\frac{1}{2}})(\Phi^{\frac{1}{2}}\otimes S_1^{\frac{1}{2}})\alpha_1(s+\phi)\\&\leq\alpha_1^T(I_{\mathcal{F}}\otimes S_1E)(\Phi^{\frac{1}{2}}\otimes S_1^{-\frac{1}{2}})(\Phi^{\frac{1}{2}}\otimes S_1^{-\frac{1}{2}})(I_{\mathcal{F}}\otimes E^TS_1)\alpha_1\\&\alpha_1^T(s+\phi)(\Phi^{\frac{1}{2}}\otimes S_1^{\frac{1}{2}})(\Phi^{\frac{1}{2}}\otimes S_1^{\frac{1}{2}})\alpha_1(s+\phi)\\&=\alpha_1^T\Big(\Phi\otimes S_1ES_1^{-1}E^TS_1\Big)\alpha_1+\alpha_1^T(s+\phi)(\Phi\otimes S_1)\alpha_1(s+\phi),\ \ \phi\in[-e_1,0]\end{aligned} \tag{27}$$

For some $\kappa>1$, whenever $\mathcal{V}_1(s+h)\leq\kappa\mathcal{V}_1(s),\quad h\in[-e_1,0]$. That is,

$$\alpha_1^T(s+h)(\Phi\otimes S_1)\alpha_1(s+h)\leq\kappa\alpha_1^T(\Phi\otimes S_1)\alpha_1;\quad h\in[-e_1,0]. \tag{28}$$

When we substitute (27) and (28) into Equation (26), then for a suitably small $\delta>0$, the value of κ equals $1+\delta$, and we have following result:

$$\begin{aligned}D^{\gamma}\mathcal{V}_1&\leq\alpha_1^T\Big[\Phi\otimes\Big(S_1D+D^TS_1+2S_1^2+k^2I_n)+\Big(S_1ES_1^{-1}E^TS_1+S_1\Big)e_1\Big)-\mu(\Phi\overline{L}_{\mathcal{F}}+\overline{L}_{\mathcal{F}}^T\Phi)\otimes G^TG\Big]\alpha_1\\&+\alpha_1^T(s-e_2)\Big[\Phi\otimes\ell^2I_n\Big]\alpha_1(s-e_2)\end{aligned}$$

Denote $\lambda_1=\lambda_{min}\{\Phi\overline{L}_{\mathcal{F}}+\overline{L}_{\mathcal{F}}^T\Phi\}$, $\phi_{max}=max_{1\leq\mathcal{F}}\{\phi_j\}$; the following inequality with $\mu\geq\frac{\rho\phi_{max}}{\lambda_1}$ and $\rho>0$ holds:

$$\begin{aligned}D^{\gamma}\mathcal{V}_1&\leq\alpha_1^T\Big[\Phi\otimes\Big(S_1D+D^TS_1+2S_1^2+k^2I_n)+\Big(S_1ES_1^{-1}E^TS_1+S_1\Big)e_1\Big)-\rho G^TG\Big]\alpha_1\\&+\alpha_1^T(s-e_2)\Big[\Phi\otimes\ell^2I_n\Big]\alpha_1(s-e_2)\\&=\alpha_1^T(\Phi\otimes\Lambda_1)\alpha_1+\alpha_1^T(s-e_2)\Big[\Phi\otimes\ell^2I_n\Big]\alpha_1(s-e_2)\end{aligned} \tag{29}$$

Now, again from Lemma 1,

$$\begin{aligned}&D^{\gamma}\mathcal{V}_2(s)=D^{\gamma}[\alpha_2^T(\eta\Phi\otimes S_2)\alpha_2]\leq2\alpha_2^T(\eta\Phi\otimes S_2)[D^{\gamma}\alpha_2]\\&=2\alpha_2^T(\eta\Phi\otimes S_2)[(I_{\mathcal{F}}\otimes D)\alpha_2+P(s,X_{\mathcal{F}})+(\overline{L}_{\mathcal{F}}^{-1}\overline{L}_{\mathcal{B}}\otimes I_n)P(s,X_{\mathcal{B}})+P_1(s,X_{\mathcal{F}}(s-e_2))\\&+(\overline{L}_{\mathcal{F}}^{-1}\overline{L}_{\mathcal{B}}\otimes I_n)P_1(s,X_{\mathcal{B}}(s-e_2))+\int_{-e_1}^{0}(I_{\mathcal{F}}\otimes E)\alpha_2(s+\phi)d\phi-(\overline{L}_{\mathcal{F}}\otimes\beta FT)\alpha_1(s-e_2)\\&-(\overline{L}_{\mathcal{F}}\otimes\beta FT)\alpha_2(s-e_2)+2\Delta v_i(s)]\end{aligned}$$

By simplifying the above equation, we have

$$
\begin{aligned}
D^{\gamma}\mathcal{V}_2(\alpha_2(s)) &= \alpha_2^T\Big[\eta\Phi\otimes(S_2D+D^TS_2)\Big]\alpha_2+2\alpha_2^T(\eta\Phi\otimes S_2)[P(s,X_{\mathcal{F}})+(\overline{L}_{\mathcal{F}}^{-1}\overline{L}_{\mathcal{B}}\otimes I_n)P(s,X_{\mathcal{B}})]\\
&+2\alpha_2^T(\eta\Phi\otimes S_2)[P_1(s,X_{\mathcal{F}}(s-e_2))+(\overline{L}_{\mathcal{F}}^{-1}\overline{L}_{\mathcal{B}}\otimes I_n)P_1(s,X_{\mathcal{B}}(s-e_2))]+\int_{-e_1}^{0}2\alpha_2^T(\eta\Phi\otimes S_2E)\alpha_2(s+\phi)d\phi \qquad (30)\\
&-2\alpha_2^T(\eta\Phi\otimes S_2)(\overline{L}_{\mathcal{F}}\otimes\beta FT)\alpha_1(s-e_2)-2\alpha_2^T(\eta\Phi\otimes S_2)(\overline{L}_{\mathcal{F}}\otimes\beta FT)\alpha_2(s-e_2)+4\alpha_2^T(\eta\Phi\otimes S_2)\Delta v_i(s)
\end{aligned}
$$

Let $-\overline{L}_{\mathcal{F}}^{-1}\overline{L}_{\mathcal{B}}=[\overline{\ell}_{ij}]_{\mathcal{F}\times(\mathcal{N}-\mathcal{F})}$; then

$$
2\alpha_2^T(\eta\Phi\otimes S_2)[P(s,X_{\mathcal{F}})+(\overline{L}_{\mathcal{F}}^{-1}\overline{L}_{\mathcal{B}}\otimes I_n)P(s,X_{\mathcal{B}})]=\sum_{i=1}^{\mathcal{F}}2\phi_i\alpha_{2i}^TS_2[p(s,x_i)-\sum_{j=1}^{\mathcal{N}-\mathcal{F}}\overline{\ell}_{ij}p(s,x_{\mathcal{F}+j})].
$$

From Assumption 2 and Lemma 2, we have

$$
\begin{aligned}
&2\eta\phi_i\alpha_{2i}^TS_2[p(s,x_i)-\sum_{j=1}^{\mathcal{N}-\mathcal{F}}\overline{\ell}_{ij}p(s,x_{\mathcal{F}+j})]\le\eta\phi_i[\alpha_{2i}^TS_2^2\alpha_{2i}+\left(p(s,x_i)-\sum_{j=1}^{\mathcal{N}-\mathcal{F}}\overline{\ell}_{ij}p(s,x_{\mathcal{F}+j})\right)^T\\
&\left(p(s,x_i)-\sum_{j=1}^{\mathcal{N}-\mathcal{F}}\overline{\ell}_{ij}p(s,x_{\mathcal{F}+j})\right)]\le\eta\phi_i[\alpha_{2i}^TS_2^2\alpha_{2i}+k^2\alpha_{2i}^T\alpha_{2i}]
\end{aligned}
$$

Due to

$$
\alpha_2^T[\eta\Phi\otimes(S_2^2+K^2I_n)]\alpha_2=\sum_{i=1}^{\mathcal{F}}\eta\phi_i[\alpha_{2i}^TS_2^2\alpha_{2i}+k^2\alpha_{2i}^T\alpha_{2i}]
$$

we can derive that

$$
2\alpha_2^T(\eta\Phi\otimes S_2)[P(s,X_{\mathcal{F}})+(\overline{L}_{\mathcal{F}}^{-1}\overline{L}_{\mathcal{B}}\otimes I_n)P(s,X_{\mathcal{B}})]\le\alpha_2^T[\eta\Phi\otimes(S^2+k^2I_n)]\alpha_2 \qquad (31)
$$

Also, we have

$$
2\alpha_2^T(\eta\Phi\otimes S_2)[P(s,X_{\mathcal{F}})+(\overline{L}_{\mathcal{F}}^{-1}\overline{L}_{\mathcal{B}}\otimes I_n)P(s,X_{\mathcal{B}})]=\sum_{i=1}^{\mathcal{F}}2\phi_i\alpha_{2i}^TS_2[p(s,x_i)-\sum_{j=1}^{\mathcal{N}-\mathcal{F}}\overline{\ell}_{ij}p(s,x_{\mathcal{F}+j})],
$$

Again, by using Assumption 1 and Lemma 2, we have

$$
\begin{aligned}
&2\eta\phi_i\alpha_{2i}^TS_2[p_1(s,x_i(s-e_2))-\sum_{j=1}^{\mathcal{N}-\mathcal{F}}\overline{\ell}_{ij}p_1(s,x_{\mathcal{F}+j}(s-e_2))]\\
&\le\eta\phi_i[\alpha_{2i}^TS_2^2\alpha_{2i}+\left(p_1(s,x_i(s-e_2))-\sum_{j=1}^{\mathcal{N}-\mathcal{F}}\overline{\ell}_{ij}p_1(s,x_{\mathcal{F}+j}(s-e_2))\right)^T\times \qquad (32)\\
&\left(p_1(s,x_i(s-e_2))-\sum_{j=1}^{\mathcal{N}-\mathcal{F}}\overline{\ell}_{ij}p_1(s,x_{\mathcal{F}+j}(s-e_2))\right)\\
&\le\eta\phi_i[\alpha_{2i}^TS_2^2\alpha_{2i}+\ell^2\alpha_{2i}(s-e_2)^T\alpha_{2i}(s-e_2)]
\end{aligned}
$$

Due to

$$
\alpha_2^T(\eta\Phi\otimes S_2^2)\alpha_2+\alpha_2^T(s-e_2)(\eta\Phi\otimes\ell^2I_n)\alpha_2(s-e_2)=\sum_{i=1}^{\mathcal{F}}\eta\phi_i[\alpha_{2i}^TS_2^2\alpha_{2i}+\ell^2\alpha_{2i}^T(s-e_2)\alpha_{2i}(s-e_2)]
$$

we can derive that

$$
2\alpha_2^T(\eta\Phi\otimes S_2)[P_1(s,X_{\mathcal{F}}(s-e_2))+(\overline{L}_{\mathcal{F}}^{-1}\overline{L}_{\mathcal{B}}\otimes I_n)P_1(s,X_{\mathcal{B}}(s-e_2))]\le\alpha_2^T(\eta\Phi\otimes S_2^2)\alpha_2+\alpha_2^T(s-e_2)(\eta\Phi\otimes\ell^2I_n)\alpha_2(s-e_2) \qquad (33)
$$

By (30), (31), and (33),

$$
\begin{aligned}
&D^{\gamma}\mathcal{V}_2(\alpha_2(s)) \leq \alpha_2^T\Big[\eta\Phi\otimes(S_2D+D^TS_2+2S_2^2+k^2I_n)\Big]\alpha_2+\int_{-e_1}^{0}2\alpha_2^T(\eta\Phi\otimes S_2E)\alpha_2(s+\phi)d\phi\\
&-2\alpha_2^T(\eta\Phi\otimes S_2)(\overline{L}_{\mathcal{F}}\otimes\beta FT)\alpha_1(s-e_2)-2\alpha_2^T(\eta\Phi\otimes S_2)(\overline{L}_{\mathcal{F}}\otimes\beta FT)\alpha_2(s-e_2)+\\
&\alpha_2^T(s-e_2)(\eta\Phi\otimes\ell^2I_n)\alpha_2(s-e_2)+4\alpha_2^T(\eta\Phi\otimes S_2)\Delta v_i(s)
\end{aligned}
\tag{34}
$$

To simplify (29) and (34), we define
$\mathcal{Q}_1(.)=(I_{\mathcal{F}}\otimes S_2)\alpha_1(.)$
$\mathcal{Q}_2(.)=(I_{\mathcal{F}}\otimes S_2)\alpha_2(.)$
$\mathcal{Q}(.)=(I_{2\mathcal{F}}\otimes S_2)\alpha(.)$

By applying the above condition on Equation (29), we have

$$
D^{\gamma}\mathcal{V}_1(\alpha_1(s)) \leq \mathcal{Q}_1\Big(\Phi\otimes S_2^{-1}\Lambda_1S_2^{-1}\Big)\mathcal{Q}_1+\mathcal{Q}_1^T(s-e_2)(\Phi\otimes S_2^{-1}\ell^2I_nS_2^{-1})\mathcal{Q}_1(s-e_2) \tag{35}
$$

and also, from (34), we have

$$
\begin{aligned}
&D^{\gamma}\mathcal{V}_2 \leq \mathcal{Q}_2^T\Big[\eta\Phi\otimes(DS_2^{-1}+S_2^{-1}D^T+2I_n+k^2S_2^{-2})\Big]\mathcal{Q}_2\\
&\int_{-e_1}^{0}\mathcal{Q}_2^T(\eta\Phi\otimes ES_2^{-1})\mathcal{Q}_2(s+\phi)d\phi-2\mathcal{Q}_2^T(\eta\Phi\overline{L}_{\mathcal{F}}\otimes\beta FTS_2^{-1})\mathcal{Q}_2(s-e_2)\\
&-2\mathcal{Q}_2^T(\eta\Phi\overline{L}_{\mathcal{F}}\otimes\beta FTS_2^{-1})\mathcal{Q}_1(s-e_2)+\mathcal{Q}_2^T(s-e_2)(\eta\Phi\otimes\ell^2S_2^{-2})\mathcal{Q}_2(s-e_2)+4\mathcal{Q}_2^T(\eta\Phi\otimes I_n)\Delta v_i(s)
\end{aligned}
\tag{36}
$$

Substituting the gain matrix $T=F^TS_2$ into (36), we have

$$
\begin{aligned}
&D^{\gamma}\mathcal{V}_2 \leq \mathcal{Q}_2^T\Big[\eta\Phi\otimes(DS_2^{-1}+S_2^{-1}D^T+2I_n+k^2S_2^{-2})\Big]\mathcal{Q}_2\\
&\int_{-e_1}^{0}\mathcal{Q}_2^T(\eta\Phi\otimes ES_2^{-1})\mathcal{Q}_2(s+\phi)d\phi-2\mathcal{Q}_2^T(\eta\Phi\overline{L}_{\mathcal{F}}\otimes\beta FF^TS_2^{-1})\mathcal{Q}_2(s-e_2)\\
&-2\mathcal{Q}_2^T(\eta\Phi\overline{L}_{\mathcal{F}}\otimes\beta FF^TS_2^{-1})\mathcal{Q}_1(s-e_2)+\mathcal{Q}_2^T(s-e_2)(\eta\Phi\otimes\ell^2S_2^{-2})\mathcal{Q}_2(s-e_2)+4\mathcal{Q}_2^T(\eta\Phi\otimes I_n)\Delta v_i(s)
\end{aligned}
\tag{37}
$$

Now, from (35) and (37), we have

$$
\begin{aligned}
&D^{\gamma}\mathcal{V}(\alpha(s))=D^{\gamma}\mathcal{V}_1(\alpha_1(s))+D^{\gamma}\mathcal{V}_2(\alpha_2(s))\\
&\leq\mathcal{Q}_1\Big(\Phi\otimes S_2^{-1}\Lambda_1S_2^{-1}\Big)\mathcal{Q}_1+\mathcal{Q}_1^T(s-e_2)(\Phi\otimes\ell^2S_2^{-2}\mathcal{Q}_1(s-e_2)\\
&+\mathcal{Q}_2^T\Big[\eta\Phi\otimes(DS_2^{-1}+S_2^{-1}D^T+2I_n+k^2S_2^{-2})\Big]\mathcal{Q}_2\\
&\int_{-e_1}^{0}\mathcal{Q}_2^T(\eta\Phi\otimes ES_2^{-1})\mathcal{Q}_2(s+\phi)d\phi-2\mathcal{Q}_2^T(\eta\Phi\overline{L}_{\mathcal{F}}\otimes\beta FF^T)\mathcal{Q}_2(s-e_2)\\
&-2\mathcal{Q}_2^T(\eta\Phi\overline{L}_{\mathcal{F}}\otimes\beta FF^T)\mathcal{Q}_1(s-e_2)+\mathcal{Q}_2^T(s-e_2)(\eta\Phi\otimes\ell^2S_2^{-2})\mathcal{Q}_2(s-e_2)+4\mathcal{Q}_2^T(\eta\Phi\otimes I_n)\Delta v_i(s)
\end{aligned}
\tag{38}
$$

For some $\kappa>0$, whenever

$$
\mathcal{V}_1(s+h)\leq\kappa\mathcal{V}_1(s),\mathcal{V}_2(s+h)\leq\kappa\mathcal{V}_2(s),\ h\in[-e_3,0], \tag{39}
$$

where $e_3=max\{e_1,e_2\}$, then we can derive

$$
\begin{aligned}
&D^{\gamma}\mathcal{V}(\alpha(s)) \leq \mathcal{Q}_1\Big(\Phi\otimes S_2^{-1}\Lambda_1 S_2^{-1}\Big)\mathcal{Q}_1 + \mathcal{Q}_1^T(s-e_2)(\Phi\otimes \ell^2 S_2^{-1}S_2^{-1})\mathcal{Q}_1(s-e_2)\\
&+\mathcal{Q}_2^T\Big[\eta\Phi\otimes(DS_2^{-1}+S_2^{-1}D^T+2I_n+k^2S_2^{-2})\Big]\mathcal{Q}_2\\
&\int_{-e_1}^{0}\Big[2\mathcal{Q}_2^T(\eta\Phi\otimes ES_2^{-1})\mathcal{Q}_2(s+\phi)+\kappa\mathcal{Q}_2^T(\eta\phi\otimes S_2^{-1})\mathcal{Q}_2-\mathcal{Q}_2^T(s+\phi)(\eta\Phi\otimes S_2^{-1})\mathcal{Q}_2(s+\phi)\Big]d\phi\\
&-2\mathcal{Q}_2^T(\eta\Phi\overline{L}_{\mathcal{F}}\otimes\beta FF^T)\mathcal{Q}_2(s-e_2)+\kappa\mathcal{Q}_1^T(\phi\otimes S_2^{-1}S_1S_2^{-1})\mathcal{Q}_1+\kappa\mathcal{Q}_2^T(\eta\Phi\otimes S_2^{-1})\mathcal{Q}_2\\
&-\mathcal{Q}_1^T(s-e_2)(\phi\otimes S_2^{-1}S_1S_2^{-1})\mathcal{Q}_1(s-e_2)-\mathcal{Q}_2^T(s-e_2)(\eta\Phi\otimes S_2^{-1})\mathcal{Q}_2(s-e_2)\\
&-2\mathcal{Q}_2^T(\eta\Phi\overline{L}_{\mathcal{F}}\otimes\beta FF^T)\mathcal{Q}_1(s-e_2)+\mathcal{Q}_2^T(s-e_2)(\eta\Phi\otimes\ell^2S_2^{-2})\mathcal{Q}_2(s-e_2)+4\mathcal{Q}_2^T(\eta\Phi\otimes I_n)\Delta v_i(s)
\end{aligned}
\tag{40}
$$

Let $\kappa\to 1^+$; one has for some $b>1$

$$
\begin{aligned}
&D^{\gamma}\mathcal{V}(\alpha(s)) \leq \mathcal{Q}_1\Big(\Phi\otimes S_2^{-1}(\Lambda_1+S_1)S_2^{-1}\Big)\mathcal{Q}_1 + \mathcal{Q}_1^T(s-e_2)(\Phi\otimes S_2^{-1}(\ell^2I_n+S_1)S_2^{-1})\mathcal{Q}_1(s-e_2)\\
&+\mathcal{Q}_2^T\Big[\eta\Phi\otimes(DS_2^{-1}+S_2^{-1}D^T+2I_n+k^2S_2^{-2}+(1+be_1)S_2^{-1}\Big]\mathcal{Q}_2\\
&\int_{-e_1}^{0}\Big[2\mathcal{Q}_2^T(\eta\Phi\otimes ES_2^{-1})\mathcal{Q}_2(s+\phi)+\mathcal{Q}_2^T(\eta\phi\otimes(1-b)S_2^{-1})\mathcal{Q}_2-\mathcal{Q}_2^T(s+\phi)(\eta\Phi\otimes S_2^{-1})\mathcal{Q}_2(s+\phi)\Big]d\phi\\
&-2\mathcal{Q}_2^T(\eta\Phi\overline{L}_{\mathcal{F}}\otimes\beta FF^T)\mathcal{Q}_2(s-e_2)-\mathcal{Q}_2^T(s-e_2)(\eta\Phi\otimes S_2^{-1}(\ell^2+S_2^{-1}))\mathcal{Q}_2(s-e_2)\\
&-2\mathcal{Q}_2^T(\eta\Phi\overline{L}_{\mathcal{F}}\otimes\beta FF^T)\mathcal{Q}_1(s-e_2)+\mathcal{Q}_2^T(s-e_2)(\eta\Phi\otimes\ell^2S_2^{-2})\mathcal{Q}_2(s-e_2)+4\mathcal{Q}_2^T(\eta\Phi\otimes I_n)\Delta v_i(s)
\end{aligned}
\tag{41}
$$

Inequality (10) implies

$$
\begin{pmatrix}\mathcal{Q}_2^T & \mathcal{Q}_2^T(s+\phi)\end{pmatrix}\begin{pmatrix}\eta\Phi\otimes(1-b)S_2^{-1} & \eta\Phi\otimes ES_2^{-1}\\ \eta\Phi\otimes S_2^{-1}E^T & -\eta\Phi\otimes S_2^{-1}\end{pmatrix}\begin{pmatrix}\mathcal{Q}_2\\ \mathcal{Q}_2(s+\phi)\end{pmatrix}<0
$$

Then

$$
\begin{aligned}
&\int_{-e_1}^{0}\Big[2\mathcal{Q}_2^T(\eta\Phi\otimes ES_2^{-1})\mathcal{Q}_2(s+\phi)+\mathcal{Q}_2^T(\eta\phi\otimes(1-b)S_2^{-1})\mathcal{Q}_2-\mathcal{Q}_2^T(s+\phi)(\eta\Phi\otimes S_2^{-1})\mathcal{Q}_2(s+\phi)\Big]d\phi\\
&<0
\end{aligned}
\tag{42}
$$

Substituting (42) into (41), we have

$$
\begin{aligned}
&D^{\gamma}\mathcal{V}(\alpha(s)) \leq \mathcal{Q}_1\Big(\Phi\otimes S_2^{-1}(\Lambda_1+S_1)S_2^{-1}\Big)\mathcal{Q}_1 + \mathcal{Q}_1^T(s-e_2)(\Phi\otimes S_2^{-1}(\ell^2I_n+S_1)S_2^{-1})\mathcal{Q}_1(s-e_2)\\
&+\mathcal{Q}_2^T\Big[\eta\Phi\otimes(DS_2^{-1}+S_2^{-1}D^T+2I_n+k^2S_2^{-2}+(1+be_1)S_2^{-1}\Big]\mathcal{Q}_2\\
&-\mathcal{Q}_2^T(\eta\Phi\overline{L}_{\mathcal{F}}\otimes\beta FF^T)\mathcal{Q}_2(s-e_2)-\mathcal{Q}_2^T(s-e_2)(\eta\Phi\overline{L}_{\mathcal{F}}\otimes\beta FF^T)\mathcal{Q}_2\\
&-\mathcal{Q}_2^T(s-e_2)(\eta\Phi\otimes S_2^{-1}(\ell^2I_n+S_2^{-1}))\mathcal{Q}_2(s-e_2)-\mathcal{Q}_2^T(\eta\Phi\overline{L}_{\mathcal{F}}\otimes\beta FF^T)\mathcal{Q}_1(s-e_2)\\
&-\mathcal{Q}_1(s-e_2)^T(\eta\Phi\overline{L}_{\mathcal{F}}\otimes\beta FF^T)\mathcal{Q}_2+4\mathcal{Q}_2^T(\eta\Phi\otimes I_n)\Delta v_i(s)
\end{aligned}
\tag{43}
$$

Now, let $\mathcal{J}=(\mathcal{Q}^T,\mathcal{Q}^T(s-e_2))$, where $\mathcal{Q}(.)=(I_{2\mathcal{F}}\otimes S_2)\alpha(.)$. Also let $\Lambda_2=DS_2^{-1}+S_2^{-1}D^T+2I_n+k^2S_2^{-2}+(1+be_1)S_2^{-1}$, $\nu=\mathcal{Q}_2$, and $q=4\Delta v_i(s)$. We can reduce the above equation in the following matrix:

$$
\begin{aligned}
&\mathcal{J}^T\begin{pmatrix}\Phi\otimes S_2^{-1}(\Lambda_1+S_1)S_2^{-1} & 0 & 0 & 0\\ 0 & \eta\Phi\otimes(\Lambda_2+\frac{q}{\nu}I_n) & -\eta\Phi\overline{L}_{\mathcal{F}}\otimes\beta FF^T & -\eta\Phi\overline{L}_{\mathcal{F}}\otimes\beta FF^T\\ 0 & -\eta\overline{L}_{\mathcal{F}}\Phi\otimes\beta FF^T & -\Phi\otimes S_2^{-1}(\ell^2I_n+S_1)S_2^{-1} & 0\\ 0 & -\eta\overline{L}_{\mathcal{F}}\Phi\otimes\beta FF^T & 0 & -\eta\Phi\otimes S_2^{-1}(\ell^2I_n+S_2^{-1})\end{pmatrix}\mathcal{J}\\
&\triangleq\mathcal{J}^T\lambda_3\mathcal{J}\\
&=\begin{pmatrix}\alpha^T(s) & \alpha^T(s-e_2)\end{pmatrix}(I_{4\mathcal{F}}\otimes S_2)\Lambda_3(I_{4\mathcal{F}}\otimes S_2)\begin{pmatrix}\alpha(s)\\ \alpha(s-e_2)\end{pmatrix}
\end{aligned}
$$

Let

$$\mathcal{U}_1 \triangleq \begin{pmatrix} \eta\Phi \otimes (\Lambda_2 + \frac{q}{\nu} I_n) & -\eta\Phi\overline{L}_{\mathcal{F}} \otimes \beta FF^T & -\eta\Phi\overline{L}_{\mathcal{F}} \otimes \beta FF^T \\ -\eta\overline{L}_{\mathcal{F}}\Phi \otimes \beta FF^T & -\Phi \otimes S_2^{-1}(\ell^2 I_n + S_1)S_2^{-1} & 0 \\ -\eta\overline{L}_{\mathcal{F}}\Phi \otimes \beta FF^T & 0 & -\eta\Phi \otimes S_2^{-1}(\ell^2 I_n + S_2^{-1}) \end{pmatrix} \tag{44}$$

Then there is an invertible matrix

$$\mathcal{W} = \begin{pmatrix} 0 & I_{\mathcal{F}} \otimes I_n & 0 \\ I_{\mathcal{F}} \otimes I_n & 0 & 0 \\ 0 & 0 & I_{\mathcal{F}} \otimes I_n \end{pmatrix}$$

that is used as

$$\mathcal{W}^{-1}\mathcal{U}_1\mathcal{W} = \begin{pmatrix} -\Phi \otimes S_2^{-1}(\ell^2 I_n + S_1)S_2^{-1} & -\eta\overline{L}_{\mathcal{F}}\Phi \otimes \beta FF^T & 0 \\ -\eta\Phi\overline{L}_{\mathcal{F}} \otimes \beta FF^T & \eta\Phi \otimes (\Lambda_2 + \frac{q}{\nu} I_n) & -\eta\Phi\overline{L}_{\mathcal{F}} \otimes \beta FF^T \\ 0 & -\eta\overline{L}_{\mathcal{F}}\Phi \otimes \beta FF^T & -\eta\Phi \otimes S_2^{-1}(\ell^2 I_n + S_2^{-1}) \end{pmatrix} \triangleq \mathcal{U}_2. \tag{45}$$

From Equations (44) and (45), one can easily say that matrices $\mathcal{U}_1$ and $\mathcal{U}_2$ are similar matrices and have the same eigenvalues. Now, we divide matrix $\mathcal{U}_2$ into matrix

$$\begin{pmatrix} -\Phi \otimes S_2^{-1}(\ell^2 I_n + S_1)S_2^{-1} & -\eta\mathcal{C}_1^T \\ -\eta\mathcal{C}_1 & -\eta\mathcal{C}_2 \end{pmatrix}$$

where matrices $\mathcal{C}_1$ and $\mathcal{C}_2$ are defined as

$$\mathcal{C}_1 = \begin{pmatrix} \Phi\overline{L}_{\mathcal{F}} \otimes \beta FF^T \\ 0 \end{pmatrix}, \mathcal{C}_2 \begin{pmatrix} -\Phi \otimes (\Lambda_2 + \frac{q}{\nu} I_n) & \Phi\overline{L}_{\mathcal{F}} \otimes \beta FF^T \\ \overline{L}_{\mathcal{F}}\Phi \otimes \beta FF^T & \Phi \otimes S_2^{-1}(\ell^2 I_n + S_2^{-1}) \end{pmatrix}$$

Next, we have to prove that $\mathcal{U}_2$ is less than zero. Since by Lemma 4, $\overline{L}_{\mathcal{F}}$ is invertible,

$$\begin{aligned} &\implies \text{for any non-zero vector x}(\overline{L}_{\mathcal{F}}x)^T\Phi\overline{L}_{\mathcal{F}}x = x^T(\overline{L}_{\mathcal{F}}^T\Phi\overline{L}_{\mathcal{F}})x > 0 \\ &\implies \overline{L}_{\mathcal{F}}^T\Phi\overline{L}_{\mathcal{F}} > 0 \end{aligned}$$

Suppose that $0 < \beta \leq \sqrt{\frac{\omega\phi_{min}}{\lambda_2}}$, where $\lambda_2 = \lambda_{max}\{\overline{L}_{\mathcal{F}}^T\Phi\overline{L}_{\mathcal{F}}^T\}, \phi_{min} = min_{1\leq j\leq\mathcal{F}}\{\phi_j\}$,

$$\begin{aligned} &-\Phi \otimes \Lambda_2 + \frac{q}{\nu} I_n - \overline{L}_{\mathcal{F}}^T\Phi\overline{L}_{\mathcal{F}} \otimes \beta^2 FF^T(\ell^2 I_n + S_2^{-1})^{-1}S_2FF^T \\ &\geq -\Phi \otimes \left(\Lambda_2 + \frac{q}{\nu} I_n + \frac{\lambda_2}{\phi_{min}}\beta^2 FF^T(\ell^2 I_n + S_2^{-1})^{-1}S_2FF^T\right) \\ &\geq -\Phi \otimes \left(\Lambda_2 + \frac{q}{\nu} I_n + \omega FF^T(\ell^2 I_n + S_2^{-1})^{-1}S_2FF^T\right) \end{aligned}$$

From (11) $\Lambda_2 + \frac{q}{\nu} I_n + \omega FF^T(\ell^2 I_n + S_2^{-1})^{-1}S_2FF^T < 0$; hence, $-\Phi \otimes \Lambda_2 + \frac{q}{\nu} I_n - \overline{L}_{\mathcal{F}}^T\Phi\overline{L}_{\mathcal{F}} \otimes \beta^2 FF^T(\ell^2 I_n + S_2^{-1})^{-1}S_2FF^T > 0$, which implies that $\mathcal{C}_2 > 0$.

Now, by choosing a small scalar $\eta > 0$ such that

$$-\Phi \otimes S_2^{-1}(\ell^2 I_n + S_1)S_2^{-1} + \eta\mathcal{C}_1\mathcal{C}_2^{-1}\mathcal{C}_1 < 0$$

$\implies \mathcal{U}_2 < 0$; hence, we proved that $\mathcal{U}_1 < 0$. As a result $\Lambda_1 + S_1 < 0$ and $\mathcal{U}_1 < 0$ from (8)–(11). Hence,

$$\Lambda_3 = \begin{pmatrix} \Phi \otimes S_2^{-1}(\Lambda_1 + S_1)S_2^{-1} & 0 \\ 0 & \mathcal{U}_1 \end{pmatrix} < 0$$

Then, from (43), $D^\gamma\mathcal{V}(\alpha(s)) < 0$. Hence, there exists a scalar $\kappa > 0$ such that

$$D^\gamma\mathcal{V}(\alpha(s)) \leq -\kappa||\alpha(s)||^2. \tag{46}$$

Based on Lemma 3, it can be concluded that $\lim_{s\to\infty} \alpha = 0$, indicating that the zero solutions of systems (18) and (21) are asymptotically stable. As a result, observer-based bipartite containment control of the FMAS described by Equations (2) and (3) with the delayed controller (7) is achieved. □

4. Observation-Based Analysis of Bipartite Containment Control for Switching Signed Digraph

Firstly, some important preliminaries on switching signed digraphs are introduced. Let $\sigma : [s_0, \infty) \to \mathcal{T} = \{1, 2, \ldots, \mathcal{M}\}$ be a piecewise switching signal, and let $\mathcal{G}^{\sigma(s)} = (N, E^{\sigma(s)})$ show a switching signed digraph. When $\sigma(s) = t \in \mathcal{T}$ for $s \in [s_g, s_{g+1})$, where s_g is a switching instant, the t-th topology is activated. Suppose that there is an arbitrarily small Ξ such that $s_{g+1} - s_g \geq \Xi$ for all s_g and $qg \in \mathbb{Z}^+ \cup \{0\}$ to avoid Zeno behavior. The matrices $\mathbb{F}^{\sigma(s)} = [f_{ij}^{\sigma(s)}]_{\mathcal{N}\times\mathcal{N}}$ and $L^{\sigma(s)} = [\ell_{ij}^{\sigma(s)}]_{\mathcal{N}\times\mathcal{N}}$ are called the adjacency matrices and Laplacian matrices of $\mathcal{G}^{\sigma(s)}$, respectively. For any $\sigma(s) = w \in \mathcal{T}$, it holds that $\mathcal{G}^w = \mathcal{G}$. Next, we propose the following state observer and observation-based switching controller for each $i \in \mathbb{F}$.

$$\begin{aligned} D^{\gamma}\hat{y}_i(s) &= D\hat{y}_i(s) + p(s, \hat{y}_i(s)) + p_1(s, \hat{y}_i(s - e_2)) + E\int_{-e_1}^{0} \hat{y}_i(s+\phi)d\phi + Fv_i(s) + \Delta v_i(s) \\ &\quad + \mu A\left(\sum_{j=1}^{\mathcal{F}} |f_{ij}^{\sigma(s)}|(z_i - sgn(f_{ij}^{\sigma(s)})z_j) - \sum_{j=1}^{\mathcal{F}} |f_{ij}^{\sigma(s)}|(\hat{z}_i - sgn(f_{ij}^{\sigma(s)})\hat{z}_j) + \sum_{j=\mathcal{F}+1}^{\mathcal{N}} |f_{ij}^{\sigma(s)}|(z_i - \hat{z}_i))\right), \\ \hat{z}_i &= G\hat{y}_i(s) \quad i \in \mathbb{F} \end{aligned} \tag{47}$$

$$\begin{aligned} v_i = -\beta T\left(\sum_{j=1}^{\mathcal{N}} |f_{ij}^{\sigma(s)}|\left(\hat{y}_i(s - e_2) - \mathrm{sgn}(f_{ij}^{\sigma(s)})\hat{y}_j(s - e_2)\right) + \sum_{j=\mathcal{F}+1}^{\mathcal{N}} |f_{ij}^{\sigma(s)}|\left(\hat{y}_i(s - e_2) - \mathrm{sgn}(f_{ij}^{\sigma(s)})y_j(s - e_2)\right)\right) \\ + \Delta v_i(s) \end{aligned} \tag{48}$$

Assumption 5. *The signed digraph $G^{\sigma(s)}$ exhibits structural balance for any $\sigma(s) \in \mathcal{T}$.*

Assumption 6. *Every follower in the signed digraph $\mathcal{G}^{\sigma(s)}$ has a directed link from at least one leader for any $\sigma(s) \in \mathcal{T}$.*

Remark 6. *Since $v_i = 0$ for all $i \in \mathbb{B}$, the Laplacian matrix L of the signed digraph $\mathcal{G}^{\sigma(s)}$ for some $\sigma(s) \in \mathcal{T}$ is defined as:*

$$L^{\sigma(s)} = \begin{pmatrix} L_{\mathcal{F}}^{\sigma(s)} & L_{\mathcal{B}}^{\sigma(s)} \\ 0_{(\mathcal{N}-\mathcal{F})\times\mathcal{F}} & 0_{(\mathcal{N}-\mathcal{F})\times(\mathcal{N}-\mathcal{F})} \end{pmatrix}$$

Here, $L_{\mathcal{F}}^{\sigma(s)} \in \mathbb{R}^{\mathcal{F}\times\mathcal{F}}$ and $L_{\mathcal{B}}^{\sigma(s)} \in \mathbb{R}^{\mathcal{F}\times(\mathcal{N}-\mathcal{F})}$. If Assumption 5 is met, a diagonal matrix exists such that $\psi = diag(\psi_1, \psi_2, \ldots, \psi_{\mathcal{F}}, \psi_{\mathcal{F}+1}, \ldots, \psi_{\mathcal{N}})$ for which the elements are defined as

$$\begin{cases} \psi_i = 1 \; if \; i \in \mathbb{F}_1 \cup \mathbb{B} \\ \psi_i = -1 \; if \; i \in \mathbb{F}_2 \end{cases}$$

such that

$$\overline{L}^{\sigma(s)} = \psi L^{\sigma(s)}\psi = \begin{pmatrix} \overline{L}_{\mathcal{F}}^{\sigma(s)} & \overline{L}_{\mathcal{B}}^{\sigma(s)} \\ 0_{(\mathcal{N}-\mathcal{F})\times\mathcal{F}} & 0_{(\mathcal{N}-\mathcal{F})\times(\mathcal{N}-\mathcal{F})} \end{pmatrix}$$

where $\overline{L}_{\mathcal{F}}^{\sigma(s)} = [\overline{\ell}_{ij}^{\sigma(s)}]_{\mathcal{F}\times\mathcal{F}}$ if $i \neq j$ then $[\overline{\ell}_{ij}^{\sigma(s)}]_{\mathcal{F}\times\mathcal{F}}$ is equal to $-|f_{ij}^{\sigma(s)}|$ otherwise it is equal to $\sum_{j=1}^{\mathcal{N}} |f_{ij}^{\sigma(s)}|$, also $\overline{L}_{\mathcal{B}}^{\sigma(s)} = [\overline{\ell}_{ij}^{\sigma(s)}]_{\mathcal{F}\times(\mathcal{N}-\mathcal{F})}$ $\overline{\ell}_{ij}^{\sigma(s)} = -|f_{ij}^{\sigma(s)}| \leq 0$ for $i = 1, 2, 3, \ldots\mathcal{F}$, $j = \mathcal{F}+1, \ldots, \mathcal{N}$

Lemma 5 ([1]). *If Assumption 6 holds, then for any $\sigma(s) \in \mathcal{T}\overline{L}_{\mathcal{F}}^{\sigma(s)}$, is a non-singular M-matrix, and every element of -$\left(\overline{L}_{\mathcal{F}}^{\sigma(s)}\right)^{-1}\overline{L}_{\mathcal{B}}^{\sigma(s)}$ is nonnegative, with each row summing to 1.*

Theorem 2. *Observer-based bipartite containment control of FMAS* (2) *and* (3) *with controller* (48) *under Assumptions* 1, 2, 5, *and* 6 *is successfully realized if there exists a diagonal matrix $\Phi = diag(\phi_1, \ldots, \phi_{\mathcal{F}}) > 0$ such that $\Phi L_{\mathcal{F}}^{\sigma(s)} + \left(L_{\mathcal{F}}^{\sigma(s)}\right)^T \Phi > 0$ along with positive definite matrices S_1 and S_2 that satisfy the following set of inequalities:*

$$\begin{pmatrix} (1-r)S_1^{-1} & ES_1^{-1} \\ S_1^{-1}E^T & -S_1^{-1} \end{pmatrix} < 0 \tag{49}$$

$$\begin{pmatrix} S_1D + D^TS_1 + S_1^2 + (k^2+\ell^2)I_n + (1+re_1)S_1 - \rho G^TG & S_1 \\ S_1 & -I_n \end{pmatrix} < 0 \tag{50}$$

$$\begin{pmatrix} (1-b)S_2^{-1} & ES_2^{-1} \\ S_2^{-1}E^T & -S_2^{-1} \end{pmatrix} < 0 \tag{51}$$

$$\begin{pmatrix} DS_2^{-1} + S_2^{-1}D^T + (1+be_1)S_2^{-1} + (2+\frac{q}{\nu})I_n + \omega FF^T(\ell^2 I_n + S_2^{-1})^{-1}S_2FF^T & kS_2^{-1} \\ kS_2^{-1} & -I_n \end{pmatrix} < 0 \tag{52}$$

Given the parameters $\rho, \omega > 0$ and $r, b > 1$, the observer and controller are designed with the following specifications:

- $A = S_1^{-1}G^T$
- $\mu \geq \frac{\rho\phi_{\max}}{\lambda_1}$, *where:*
  - $\lambda_3 = min_{\sigma(s)\in\mathcal{T}}\left\{\lambda_{\min}\left\{\Phi\overline{L}_{\mathcal{F}}^{\sigma(s)} + \left(\overline{L}_{\mathcal{F}}^{\sigma(s)}\right)^T\Phi\right\}\right\}$
  - $\phi_{\max} = \max_{1\leq j\leq\mathcal{F}}\{\phi_j\}$
- $T = F^TS_2$
- $0 < \beta \leq \sqrt{\frac{\omega\phi_{\min}}{\lambda_2}}$, *where:*
  - $\lambda_4 = max_{\sigma(s)\in\mathcal{T}}\left\{\lambda_{\max}\left\{\left(\overline{L}_{\mathcal{F}}^{\sigma(s)}\right)^T\Phi\overline{L}_{\mathcal{F}}^{\sigma(s)}\right\}\right\}$
  - $\phi_{\min} = \min_{1\leq j\leq\mathcal{F}}\{\phi_j\}$

Proof. Suppose that $\alpha_1(.) = \hat{X}_{\mathcal{F}}(.) - X_{\mathcal{F}}(.)$ denotes the observation error and

$\alpha_2(.) = X_{\mathcal{F}}(.) - \left(-\left(\overline{L}_{\mathcal{F}}^{\sigma(s)}\right)^{-1}\overline{L}_{\mathcal{B}}^{\sigma(s)} \otimes I_n\right)X_{\mathcal{B}}(.)$ is the bipartite containment control error; then under controller (48),

$$\begin{aligned} D^\gamma\alpha_1 &= (I_{\mathcal{F}} \otimes D)\alpha_1 + P(s, \hat{X}_{\mathcal{F}}) - P(s, X_{\mathcal{F}}) + P_1(s, \hat{X}_{\mathcal{F}}(s-e_2)) - P_1(s, X_{\mathcal{F}}(s-e_2)) \\ &\int_{-e_1}^{0}(I_{\mathcal{F}} \otimes E)\alpha_1(s+\phi)d\phi - (\overline{L}_{\mathcal{F}}^{\sigma(s)} \otimes \mu AG)\alpha_1. \end{aligned} \tag{53}$$

and

$$\begin{aligned} D^\gamma\alpha_2 &= (I_{\mathcal{F}} \otimes D)\alpha_2 + +P(s, X_{\mathcal{F}}) + \left(\left(\overline{L}_{\mathcal{F}}^{\sigma(s)}\right)^{-1}\overline{L}_{\mathcal{B}}^{\sigma(s)} \otimes I_n\right)P(s, X_{\mathcal{B}}) + P_1(s, X_{\mathcal{F}}(s-e_2)) \\ &+ \left(\left(\overline{L}_{\mathcal{F}}^{\sigma(s)}\right)^{-1}\overline{L}_{\mathcal{B}}^{\sigma(s)} \otimes I_n\right)P_1(s, X_{\mathcal{B}}(s-e_2)) + \int_{-e_1}^{0}(I_{\mathcal{F}} \otimes E)\alpha_2(s+\phi)d\phi \\ &- (\overline{L}_{\mathcal{F}}^{\sigma(s)} \otimes \beta FT)\alpha_1(s-e_2) - (\overline{L}_{\mathcal{F}}^{\sigma(s)} \otimes \beta FT)\alpha_2(s-e_2) + 2\Delta v_i(s) \end{aligned} \tag{54}$$

Let $\alpha(.) = [\alpha_1^T(.), \alpha_2^T(.)]^T$ represent the error system, and

$$D^{\gamma}\alpha = \overline{R}_1\alpha + \overline{P}(s,\alpha) + \overline{P}_1(s,\alpha(s-e_2)) + \overline{R}_2\alpha(s-e_2) + \int_{-e_1}^{0} \overline{R}_3\alpha(s+\phi)d\phi + 2\Delta v_i(s), \quad (55)$$

where

$$\overline{R}_1 = \begin{pmatrix} (I_F \otimes D) - (\overline{L}_{\mathcal{F}}^{\sigma(s)} \otimes \mu AG) & 0 \\ 0 & I_F \otimes D \end{pmatrix}; \quad \overline{R}_2 = \begin{pmatrix} 0 & 0 \\ -\overline{L}_{\mathcal{F}}^{\sigma(s)} \otimes \beta FT & -\overline{L}_{\mathcal{F}}^{\sigma(s)} \otimes \beta FT \end{pmatrix}; \overline{R}_3 = \begin{pmatrix} I_F \otimes E & 0 \\ 0 & I_F \otimes E \end{pmatrix};$$

$$\overline{P}(s,\alpha) = \left[P(s,\hat{X}_{\mathcal{F}}) - P(s,X_{\mathcal{F}})\right]\left[P(s,X_{\mathcal{F}}) + \left(\left(\overline{L}_{\mathcal{F}}^{\sigma)s)}\right)^{-1}\overline{L}_{\mathcal{B}}^{\sigma(s)} \otimes I_n\right)P(s,X_{\mathcal{B}})\right],$$

$$\overline{P}_1(s,\alpha(s-e_2) = \left[P_1(s,\hat{X}_{\mathcal{F}}(s-e_2) - P_1(s,X_{\mathcal{F}}(s-e_2)\right]\times$$
$$\left[P_1(s,X_{\mathcal{F}}(s-e_2) + \left(\left(\overline{L}_{\mathcal{F}}^{\sigma(s)}\right)^{-1}\overline{L}_{\mathcal{B}}^{\sigma(s)} \otimes I_n\right)P_1(s,X_{\mathcal{B}}(s-e_2)\right].$$

Let us delve into the asymptotic stability analysis of the error system in Equation (55). Given that $\overline{L}_{\mathcal{F}}^{\sigma(s)}$ for any $\sigma(s) \in \mathcal{T}$ is a non-singular M-matrix according to Lemma 4, then there exists a positive definite diagonal matrix $\mathbf{\Phi} = \text{diag}(\phi_1, \phi_2, \ldots, \phi_{\mathcal{F}})$ such that $\Phi\overline{L}_{\mathcal{F}}^{\sigma(s)} + \left(\overline{L}_{\mathcal{F}}^{\sigma(s)}\right)^T\Phi > 0$. In this context, the following Lyapunov function is proposed for the stability analysis:

$$\begin{aligned} \mathcal{V}(s) &= \mathcal{V}_1(s) + \mathcal{V}_2(s) \\ &= \alpha_1^T(\Phi \otimes S_1)\alpha_1 + \alpha_2^T(\eta\Phi \otimes S_2)\alpha_2 \end{aligned} \quad (56)$$

where $\eta > 0$ is very small scalar.

By using Theorem 1,

$$D^{\gamma}\mathcal{V}_1 \leq \alpha_1^T\left[\Phi \otimes \left(S_1D + D^TS_1 + 2S_2^{2_1} + k^2I_n) + \left(S_1ES_1^{-1}E^{TS_1} + S_1\right)e_1\right) - \mu(\Phi\overline{L}_{\mathcal{F}}^{\sigma(s)} + \left(\overline{L}_{\mathcal{F}}^{\sigma(s)}\right)^T\Phi) \otimes G^TG\right]\alpha_1$$
$$+ \alpha_1^{T(s-e_2)}\left[\Phi \otimes \ell^2I_n\right]\alpha_1(s-e_2)$$

Denote $\lambda_3 = \lambda_{min}\{\Phi\overline{L}_{\mathcal{F}}^{\sigma(s)} + \left(\overline{L}_{\mathcal{F}}^{\sigma(s)}\right)^T\Phi\}$, $\phi_{max} = max_{1\leq\mathcal{F}}\{\phi_j\}$. The following inequality with $\mu \geq \frac{\rho\phi_{max}}{\lambda_3}$ and $\rho > 0$ holds:

$$\begin{aligned} D^{\gamma}\mathcal{V}_1 &\leq \alpha_1^T\left[\Phi \otimes \left(S_1D + D^TS_1 + 2S_2^{2_1} + k^{2I_n}) + \left(S_1ES_1^{-1}E^{TS_1} + S_1\right)e_1\right) - \rho G^TG\right]\alpha_1 \\ &+ \alpha_1^T(s-e_2)\left[\Phi \otimes \ell^2I_n\right]\alpha_1(s-e_2) \\ &= \alpha_1^T(\Phi \otimes \Lambda_1)\alpha_1 + \alpha_1^T(s-e_2)\left[\Phi \otimes \ell^2I_n\right]\alpha_1(s-e_2) \end{aligned} \quad (57)$$

Now, by using Theorem 1 and Equation (48),

$$\begin{aligned} &D^{\gamma}\mathcal{V}(s) \leq \mathcal{Q}_1\left(\Phi \otimes S_2^{-1}(\Lambda_1 + S_1)S_2^{-1}\right)\mathcal{Q}_1 + \mathcal{Q}_1^T(s-e_2)(\Phi \otimes S_2^{-1}(\ell^2I_n + S_1)S_2^{-1})\mathcal{Q}_1(s-e_2) \\ &+ \mathcal{Q}_2^T\left[\eta\Phi \otimes (DS_2^{-1} + S_2^{-1}D^T + 2I_n + k^2S_2^{-2} + (1+be_1)S_2^{-1}\right]\mathcal{Q}_2 \\ &- \mathcal{Q}_2^T(\eta\Phi\overline{L}_{\mathcal{F}}^{\sigma(s)} \otimes \beta FF^T)\mathcal{Q}_2(s-e_2) - \mathcal{Q}_2^T(s-e_2)(\eta\Phi\overline{L}_{\mathcal{F}}^{\sigma(s)} \otimes \beta FF^T)\mathcal{Q}_2 \\ &- \mathcal{Q}_2^T(s-e_2)(\eta\Phi \otimes S_2^{-1}(\ell^2I_n + S_2^{-1}))\mathcal{Q}_2(s-e_2) - \mathcal{Q}_2^T(\eta\Phi\overline{L}_{\mathcal{F}}^{\sigma(s)} \otimes \beta FF^T)\mathcal{Q}_1(s-e_2) \\ &- \mathcal{Q}_1(s-e_2)^T(\eta\Phi\overline{L}_{\mathcal{F}}^{\sigma(s)} \otimes \beta FF^T)\mathcal{Q}_2 + 4\mathcal{Q}_2^T(\eta\Phi \otimes I_n)\Delta v_i(s) \\ &= \mathcal{J}^T\begin{pmatrix} \Phi \otimes S_2^{-1}(\Lambda_1 + S_1)S_2^{-1} & 0 \\ 0 & \mathcal{U}_3 \end{pmatrix}\mathcal{J} \end{aligned} \quad (58)$$

where

$$\mathcal{U}_3 \triangleq \begin{pmatrix} \eta\Phi \otimes (\Lambda_2 + \frac{q}{\nu} I_n) & -\eta\Phi\overline{L}_{\mathcal{F}}^{\sigma(s)} \otimes \beta FF^T & -\eta\Phi\overline{L}_{\mathcal{F}}^{\sigma(s)} \otimes \beta FF^T \\ -\eta\overline{L}_{\mathcal{F}}^{\sigma(s)}\Phi \otimes \beta FF^T & \Phi \otimes S_2^{-1}(\ell^2 I_n + S_1)S_2^{-1} & 0 \\ -\eta\overline{L}_{\mathcal{F}}^{\sigma(s)}\Phi \otimes \beta FF^T & 0 & \eta\Phi \otimes S_2^{-1}(\ell^2 I_n + S_2^{-1}) \end{pmatrix}$$

$$\Lambda_2 = DS_2^{-1} + S_2^{-1}D^T + 2I_n + k^2 S_2^{-2} + (1 + be_1)S_2^{-1} and q = 4\Delta v_i(s)$$

Then there is an invertible matrix

$$\mathcal{W} = \begin{pmatrix} 0 & I_{\mathcal{F}} \otimes I_n & 0 \\ I_{\mathcal{F}} \otimes I_n & 0 & 0 \\ 0 & 0 & I_{\mathcal{F}} \otimes I_n \end{pmatrix}$$

which is used as

$$\mathcal{W}^{-1}\mathcal{U}_3\mathcal{W} = \begin{pmatrix} \Phi \otimes S_2^{-1}(\ell^2 I_n + S_1)S_2^{-1} & -\eta\overline{L}_{\mathcal{F}}^{\sigma(s)}\Phi \otimes \beta FF^T & 0 \\ -\eta\Phi\overline{L}_{\mathcal{F}}^{\sigma(s)} \otimes \beta FF^T & \eta\Phi \otimes (\Lambda_2 + \frac{q}{\nu} I_n) & -\eta\Phi\overline{L}_{\mathcal{F}}^{\sigma(s)} \otimes \beta FF^T \\ 0 & -\eta\overline{L}_{\mathcal{F}}^{\sigma(s)}\Phi \otimes \beta FF^T & \eta\Phi \otimes S_2^{-1}(\ell^2 I_n + S_2^{-1}) \end{pmatrix} \triangleq \mathcal{U}_4. \tag{59}$$

One can easily say that matrices $\mathcal{U}_3$ and $\mathcal{U}_4$ are similar matrices and have the same eigenvalues. Now, we divide matrix $\mathcal{U}_4$ into matrix

$$\begin{pmatrix} \Phi \otimes S_2^{-1}(\ell^2 I_n + S_1)S_2^{-1} & -\eta\mathcal{C}_1^T \\ -\eta\mathcal{C}_3 & -\eta\mathcal{C}_4 \end{pmatrix}$$

where matrices $\mathcal{C}_3$ and $\mathcal{C}_4$ are defined as

$$\mathcal{C}_3 = \begin{pmatrix} \Phi\overline{L}_{\mathcal{F}}^{\sigma(s)} \otimes \beta FF^T \\ 0 \end{pmatrix}, \mathcal{C}_4 \begin{pmatrix} \Phi \otimes (\Lambda_2 + \frac{q}{\nu} I_n) & \Phi\overline{L}_{\mathcal{F}}^{\sigma(s)} \otimes \beta FF^T \\ \overline{L}_{\mathcal{F}}^{\sigma(s)}\Phi \otimes \beta FF^T & \Phi \otimes S_2^{-1}(\ell^2 I_n + S_2^{-1}) \end{pmatrix}$$

Next, we have to prove that $\mathcal{U}_4$ is less than zero. Since, by Lemma 5, $\overline{L}_{\mathcal{F}}^{\sigma(s)}$ is invertible,

$$\implies \text{for any non-zero vector } x \left(\overline{L}_{\mathcal{F}}^{\sigma(s)} x\right)^T \Phi \overline{L}_{\mathcal{F}}^{\sigma(s)} x = x^T \left(\left(\overline{L}_{\mathcal{F}}^{\sigma(s)}\right)^T \Phi \overline{L}_{\mathcal{F}}^{\sigma(s)} \right) x > 0$$

$$\implies \left(\overline{L}_{\mathcal{F}}^{\sigma(s)}\right)^T \Phi \overline{L}_{\mathcal{F}}^{\sigma(s)}$$

Suppose that $0 < \beta \leq \sqrt{\frac{\omega\phi_{min}}{\lambda_4}}$, where $\lambda_4 = \lambda_{max}\left\{ \left(\overline{L}_{\mathcal{F}}^{\sigma(s)}\right)^T \Phi \overline{L}_{\mathcal{F}}^{\sigma(s)} \right\}, \phi_{min} = min_{1 \leq j \leq \mathcal{F}}\{\phi_j\}$,

$$\begin{aligned} &-\Phi \otimes \Lambda_2 + \frac{q}{\nu} I_n - \left(\overline{L}_{\mathcal{F}}^{\sigma(s)}\right)^T \Phi \overline{L}_{\mathcal{F}}^{\sigma(s)} \otimes \beta^2 FF^T (\ell^2 I_n + S_2^{-1})^{-1} S_2 FF^T \\ &\geq -\Phi \otimes \left(\Lambda_4 + \frac{q}{\nu} I_n + \frac{\lambda_2}{\phi_{min}} \beta^2 FF^T (\ell^2 I_n + S_2^{-1})^{-1} S_2 FF^T \right) \\ &\geq -\Phi \otimes \left(\Lambda_4 + \frac{q}{\nu} I_n + \omega FF^T (\ell^2 I_n + S_2^{-1})^{-1} S_2 FF^T \right) \end{aligned}$$

From (52) $\Lambda_2 + \frac{q}{\nu} I_n + \omega FF^T (\ell^2 I_n + S_2^{-1})^{-1} S_2 FF^T < 0$; hence

$$-\Phi \otimes \Lambda_2 + \frac{q}{\nu} I_n - \left(\overline{L}_{\mathcal{F}}^{\sigma(s)}\right)^T \Phi \overline{L}_{\mathcal{F}}^{\sigma(s)} \otimes \beta^2 FF^T (\ell^2 I_n + S_2^{-1})^{-1} S_2 FF^T > 0$$

$\implies$ that $\mathcal{C}_4 > 0$. Now, by choosing a small scalar $\eta > 0$ such that

$$-\Phi \otimes S_2^{-1}(\ell^2 I_n + S_1)S_2^{-1} + \eta\mathcal{C}_3\mathcal{C}_4^{-1}\mathcal{C}_3 < 0$$

$\Longrightarrow \mathcal{U}_4 < 0$; hence, we proved that $\mathcal{U}_3 < 0$. As a result, $\Lambda_1 + S_1 < 0$, and $\mathcal{U}_3 < 0$ from (49)–(52). Hence,

$$= \begin{pmatrix} \Phi \otimes S_2^{-1}(\Lambda_1 + S_1)S_2^{-1} & 0 \\ 0 & \mathcal{U}_3 \end{pmatrix} < 0$$

Then from (58), $D^{\gamma}\mathcal{V}(s) < 0$. Hence, there exists a scalar $\kappa > 0$ such that

$$D^{\gamma}\mathcal{V}(\alpha(s)) \leq -\kappa||\alpha(s)||^2. \tag{60}$$

Based on Lemma 3, it can be concluded that $\lim_{s\to\infty} \alpha = 0$, indicating that the zero solution of the system (55) is asymptotically stable. As a result, observer-based bipartite containment control of the FMAS described by Equations (2) and (3) with the delayed controller (48) is achieved. □

5. Numerical Illustrations

Two examples will be offered to illustrate the practical significance of the conclusions drawn.

Example 1. *In the context of observation-based bipartite containment control having five followers and two leaders, the signed digraph illustrated in Figure 2 is noted for its structural balance and division into bi-partitioned subgroups $\mathbb{F}_1$ and $\mathbb{F}_2$, where $\mathbb{F}_1 = \{0, 1\}$ and $\mathbb{F}_2 = \{2, 3, 4\}$. First, we define the matrices that are used in FMAS Equations (2) and (3) as follows:*

$$D = \begin{pmatrix} 1.25 & 0.05 \\ 0.05 & 1.6 \end{pmatrix}, \quad G = \begin{pmatrix} 0.5 & 0.25 \\ 0.1 & 0.3 \end{pmatrix}$$

$$E = \begin{pmatrix} 0.2 & 0.1 \\ 0.05 & 0.07 \end{pmatrix}, \quad F = \begin{pmatrix} 1 \\ 0.5 \end{pmatrix}$$

and

$$p_1(s, y_i(s - e_2)) = y_i(s)\frac{4}{7}y_i(s)\sin(s - e_2),$$

$$p(s, y_i(s) = cos(y_i(s)$$

$\Longrightarrow$ *we can take the value of constant $k = 0.5$ and $\ell = 0.4$. We take $\Delta v_i(s) = 30cos(0.3)$ and $\nu = 0.3$. Now, by using Figure 2,*

$$F = \begin{pmatrix} 0 & 0.9 & 0 & 0 & 0 & 0.7 & 0 \\ 0 & 0 & 0 & 0 & -1 & 0 & 0.5 \\ -0.5 & 0 & 0 & 0.2 & 0 & -0.5 & 0 \\ 0 & 0 & 0 & 0 & 1 & 0 & 0 \\ 0 & 0 & 0.5 & 0 & 0 & 0 & -0.6 \\ 0 & 0 & 0 & 0 & 0 & 0 & 0 \\ 0 & 0 & 0 & 0 & 0 & 0 & 0 \end{pmatrix} \text{ then } L = \begin{pmatrix} 1.6 & -0.9 & 0 & 0 & 0 & -0.7 & 0 \\ 0 & 1.5 & 0 & 0 & 1 & 0 & -0.5 \\ 0.5 & 0 & 1.2 & -0.2 & 0 & 0.5 & 0 \\ 0 & 0 & 0 & 1 & -1 & 0 & 0 \\ 0 & 0 & -0.5 & 0 & 1.1 & 0 & 0.6 \\ 0 & 0 & 0 & 0 & 0 & 0 & 0 \\ 0 & 0 & 0 & 0 & 0 & 0 & 0 \end{pmatrix}$$

$$\psi = \begin{pmatrix} 1 & 0 & 0 & 0 & 0 & 0 & 0 \\ 0 & 1 & 0 & 0 & 0 & 0 & 0 \\ 0 & 0 & -1 & 0 & 0 & 0 & 0 \\ 0 & 0 & 0 & -1 & 0 & 0 & 0 \\ 0 & 0 & 0 & 0 & -1 & 0 & 0 \\ 0 & 0 & 0 & 0 & 0 & 1 & 0 \\ 0 & 0 & 0 & 0 & 0 & 0 & 1 \end{pmatrix}$$

Now, since $\overline{L} = \phi L \phi$,

$$\Longrightarrow \overline{L} = \begin{pmatrix} 1.6 & -0.9 & 0 & 0 & 0 & -0.7 & 0 \\ 0 & 1.5 & 0 & 0 & -1 & 0 & -0.5 \\ -0.5 & 0 & 1.2 & -0.2 & 0 & -0.5 & 0 \\ 0 & 0 & 0 & 1 & -1 & 0 & 0 \\ 0 & 0 & -0.5 & 0 & 1.1 & 0 & -0.6 \\ 0 & 0 & 0 & 0 & 0 & 0 & 0 \\ 0 & 0 & 0 & 0 & 0 & 0 & 0 \end{pmatrix}$$

from the above matrix, one can obtain

$\overline{L}_{\mathcal{F}} = \begin{pmatrix} 1.6 & -0.9 & 0 & 0 & 0 \\ 0 & 1.5 & 0 & 0 & -1 \\ -0.5 & 0 & 1.2 & -0.2 & 0 \\ 0 & 0 & 0 & 1 & -1 \\ 0 & 0 & -0.5 & 0 & 1.1 \end{pmatrix}$ *and* $\overline{L}_{\mathcal{B}} = \begin{pmatrix} -0.7 & 0 \\ 0 & -0.5 \\ -0.5 & 0 \\ 0 & 0 \\ 0 & -0.6 \end{pmatrix}$. *Suppose that* $e_1 = 0.4$*;*
then by solving inequalities (8)–(11), one can have $\rho = 0.0213$ *and* $r = 0.2148$.

$$S_1 = \begin{pmatrix} 0.3208 & 0.0021 \\ 0.0021 & 0.2145 \end{pmatrix}$$

$\omega = 0.0023, b = 0.2312$

$$S_2^{-1} = \begin{pmatrix} 0.4521 & 0.0123 \\ 0.0123 & 0.4325 \end{pmatrix} \Longrightarrow S_2 = \begin{pmatrix} 2.2136 & -0.0630 \\ -0.0630 & 2.3139 \end{pmatrix}$$

We can select $\Phi = I_5$ *for* $\Phi \overline{L}_{\mathcal{F}} + \overline{L}_{\mathcal{F}}^T \Phi > 0$*; thus,* $\phi_{min} = \phi_{max} = 1$.

$$\lambda_1 = 0.6414$$

and

$$\lambda_2 = 5.2776$$

$\mu \geq \frac{\rho \phi_{max}}{\lambda_1} = 0.0332$ *and* $0 < \beta \leq \sqrt{\frac{\omega \phi_{min}}{\lambda_2}} = 0.02085$

Now If we take $\beta = 0.02$ $\mu = 0.1$ *gain matrices* $A = \begin{pmatrix} 1.5511 & 0.3026 \\ 1.1503 & 1.3956 \end{pmatrix}$ *and* $T = \begin{pmatrix} 2.1821 & 1.0939 \end{pmatrix}$

Now, if $\gamma = 0.7$ *and* $e_2 = 0.7$*, then the state of the agents and the observation error of FMAS (2) and (3) are given in Figures 3 and 4, respectively. Figure 3 shows that*

$$\lim_{s \to \infty} \|\alpha_1\| = 0 \text{ and } \lim_{s \to \infty} \|\alpha_1\| = 0$$

where

$$\alpha_1 = \begin{cases} \hat{y}_i - y_i, \ i = 0, 1 \\ -\hat{y}_i + y_i, \ i = 2, 3, 4 \end{cases} \quad \alpha_2 = \begin{cases} y_i - co\{y_5, y_6\} \ i = 0, 1 \\ -(y_i + co\{y_5, y_6\}) \ i = 2, 3, 4. \end{cases}$$

Notice that

$$\lim_{s \to \infty} \|\hat{y}_i - y_i\| = 0, i = 0, 1, 2, 3, 4$$
$$\lim_{s \to \infty} \|y_i - co\{y_5, y_6\}\| = 0, i = 0, 1,$$
$$\lim_{s \to \infty} \|y_i + co\{y_5, y_6\}\| = 0, i = 2, 3, 4.$$

Drawing from the simulation results, it is determined that the observation-based bipartite containment control for FMAS (2) and (3) using controller (7) is successfully implemented. Furthermore, the results confirm that the asymptotic stability of the observation error is assured.

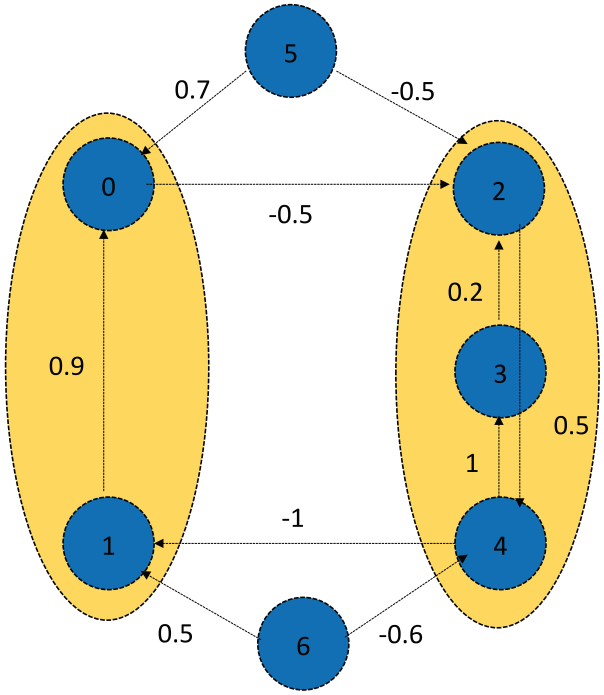

Figure 2. Signed digraph of $\mathcal{G}$.

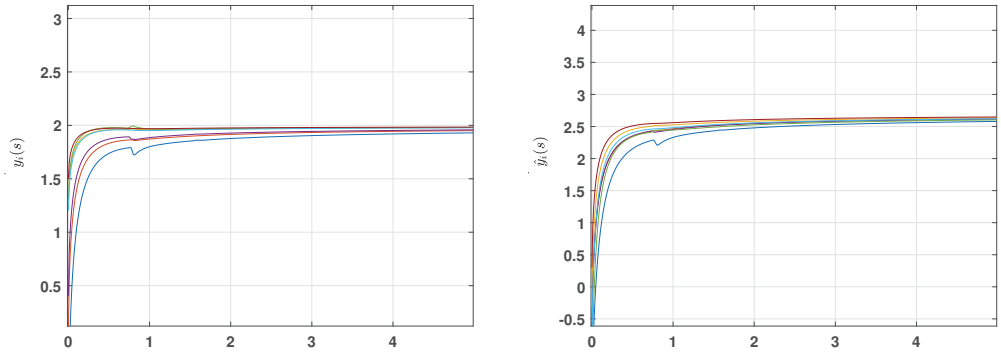

Figure 3. Agent state $y_i(s)$ and $\hat{y}_i(s)$, where $i = \{1, 2, ..., 7\}$, for fixed signed digraph.

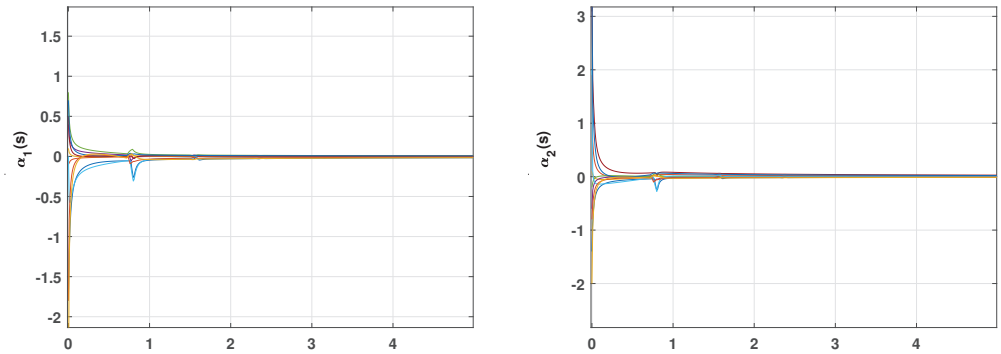

Figure 4. Observation error $\alpha_1(s)$ and bipartite containment error $\alpha_2(s)$ for fixed signed digraph.

Example 2. *Consider the bipartite containment control for a system having five followers and two leaders. The system's dynamics are governed by switching topology graphs $\mathcal{G}_1$, $\mathcal{G}_2$, and $\mathcal{G}_3$, which are*

illustrated in Figures 5 and 6. These graphs, $\mathcal{G}_1$, $\mathcal{G}_2$, and $\mathcal{G}_3$, are signed digraphs that are structurally balanced, meaning that they can be split into bipartition subgroups where each link connecting nodes of the same subgroup is positively signed, and each edge connecting nodes of different subgroups is negatively signed. Specifically, the bipartition subgroups are $F_1 = \{0,1\}$ and $F_2 = \{2,3,4\}$. The coefficient matrices used in the finite multi-agent system (FMAS) Equations (2) and (3) are the same as those presented in Example 1, ensuring consistency in the system's behavior and analysis.
From Figures 5 and 6.

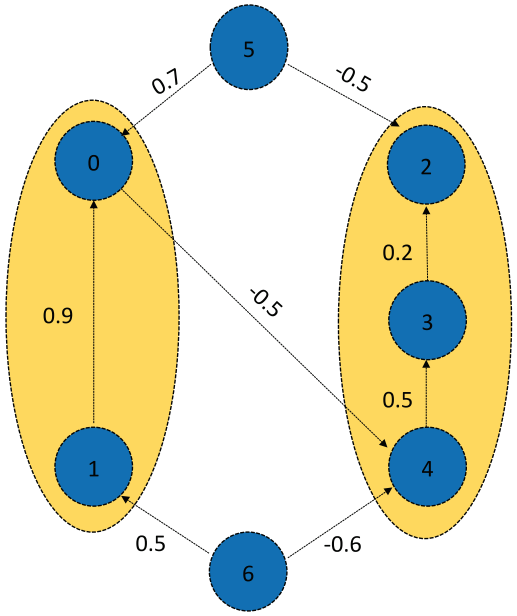

Figure 5. Signed digraph of $\mathcal{G}_1$.

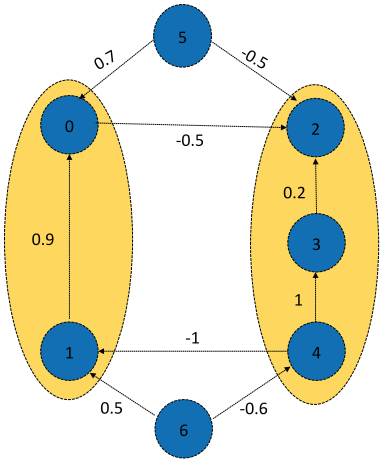

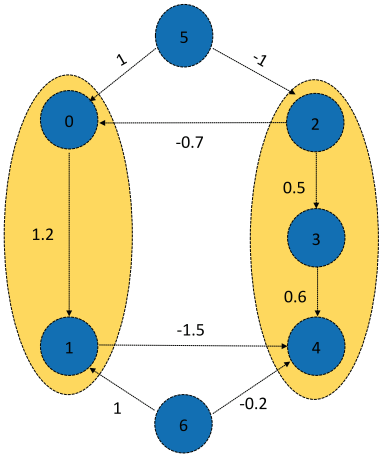

Figure 6. Signed digraphs of $\mathcal{G}_2$ and $\mathcal{G}_3$.

$$F^1 = \begin{pmatrix} 0 & 0.9 & 0 & 0 & 0 & 0.7 & 0 \\ 0 & 0 & 0 & 0 & 0 & 0 & 0.5 \\ 0 & 0 & 0 & 0.2 & 0 & -0.5 & 0 \\ 0 & 0 & 0 & 0 & 1 & 0 & 0 \\ -0.5 & 0 & 0 & 0 & 0 & 0 & -0.6 \\ 0 & 0 & 0 & 0 & 0 & 0 & 0 \\ 0 & 0 & 0 & 0 & 0 & 0 & 0 \end{pmatrix} \quad F^2 = \begin{pmatrix} 0 & 0.9 & 0 & 0 & 0 & 0.7 & 0 \\ 0 & 0 & 0 & 0 & -1 & 0 & 0.5 \\ -0.5 & 0 & 0 & 0.2 & 0 & -0.5 & 0 \\ 0 & 0 & 0 & 0 & 1 & 0 & 0 \\ 0 & 0 & 0 & 0 & 0 & 0 & -0.6 \\ 0 & 0 & 0 & 0 & 0 & 0 & 0 \\ 0 & 0 & 0 & 0 & 0 & 0 & 0 \end{pmatrix}$$

$$F^3 = \begin{pmatrix} 0 & 0 & -0.7 & 0 & 0 & 1 & 0 \\ 1.2 & 0 & 0 & 0 & 0 & 0 & 1 \\ 0 & 0 & 0 & 0 & 0 & -1 & 0 \\ 0 & 0 & 0.5 & 0 & 0 & 0 & 0 \\ 0 & -1.5 & 0 & 0.6 & 0 & 0 & -0.2 \\ 0 & 0 & 0 & 0 & 0 & 0 & 0 \\ 0 & 0 & 0 & 0 & 0 & 0 & 0 \end{pmatrix}$$

$$\psi = \begin{pmatrix} 1 & 0 & 0 & 0 & 0 & 0 & 0 \\ 0 & 1 & 0 & 0 & 0 & 0 & 0 \\ 0 & 0 & -1 & 0 & 0 & 0 & 0 \\ 0 & 0 & 0 & -1 & 0 & 0 & 0 \\ 0 & 0 & 0 & 0 & -1 & 0 & 0 \\ 0 & 0 & 0 & 0 & 0 & 1 & 0 \\ 0 & 0 & 0 & 0 & 0 & 0 & 1 \end{pmatrix}$$

Then

$$\overline{L}_{\mathcal{F}}^1 = \begin{pmatrix} 1.6 & -0.9 & 0 & 0 & 0 \\ 0 & 0.5 & 0 & 0 & 0 \\ 0 & 0 & 0.7 & -0.2 & 0 \\ 0 & 0 & 0 & 0.5 & -0.5 \\ -0.5 & 0 & 0 & 0 & 1.1 \end{pmatrix} \overline{L}_{\mathcal{B}}^1 = \begin{pmatrix} -0.7 & 0 \\ 0 & -0.5 \\ -0.5 & 0 \\ 0 & 0 \\ 0 & -0.6 \end{pmatrix}$$

$$\overline{L}_{\mathcal{F}}^2 = \begin{pmatrix} 1.6 & -0.9 & 0 & 0 & 0 \\ 0 & 1.5 & 0 & 0 & -1 \\ -0.5 & 0 & 1.2 & -0.2 & 0 \\ 0 & 0 & 0 & 1 & -1 \\ 0 & 0 & 0 & 0 & 0.6 \end{pmatrix} \overline{L}_{\mathcal{B}}^2 = \begin{pmatrix} -0.7 & 0 \\ 0 & -0.5 \\ -0.5 & 0 \\ 0 & 0 \\ 0 & -0.6 \end{pmatrix}$$

$$\overline{L}_{\mathcal{F}}^3 = \begin{pmatrix} 1.7 & 0 & -0.7 & 0 & 0 \\ -1.2 & 2.2 & 0 & 0 & 0 \\ 0 & 0 & 1 & 0 & 0 \\ 0 & 0 & -0.5 & 0.5 & 0 \\ 0 & -1.5 & 0 & -0.6 & 2.3 \end{pmatrix} \overline{L}_{\mathcal{B}}^3 = \begin{pmatrix} -1 & 0 \\ 0 & -1 \\ -1 & 0 \\ 0 & 0 \\ 0 & -0.2 \end{pmatrix}$$

In this scenario, the dynamical equations governing each agent remain unchanged; only the communication switching among the agents is different. Consequently, the feasible solutions to inequalities (49)–(52) are identical to those in Example 1. We can select $\Phi = I_5$ *for* $\Phi\overline{L}_{\mathcal{F}}^{\sigma(s)} + \left(\overline{L}_{\mathcal{F}}^{\sigma(s)}\right)^T \Phi > 0$ *thus* $\phi_{min} = \phi_{max} = 1$.

$$\lambda_{min}\left\{\Phi\overline{L}_{\mathcal{F}}^1 + \left(\overline{L}_{\mathcal{F}}^1\right)^T\Phi\right\} = 0.6372\lambda_{min}\left\{\Phi\overline{L}_{\mathcal{F}}^2 + \left(\overline{L}_{\mathcal{F}}^2\right)^T\Phi\right\} = 0.2234\lambda_{min}\left\{\Phi\overline{L}_{\mathcal{F}}^3 + \left(\overline{L}_{\mathcal{F}}^3\right)^T\Phi\right\} = 0.6467$$

Hence, $\lambda_3 = 0.2234$. *Also,*

$$\lambda_{max}\left\{\overline{L}_{\mathcal{F}}^1\Phi\left(\overline{L}_{\mathcal{F}}^1\right)^T\right\} = 3.7233\lambda_{max}\left\{\overline{L}_{\mathcal{F}}^2\Phi\left(\overline{L}_{\mathcal{F}}^2\right)^T\right\} = 4.9827\lambda_{max}\left\{\overline{L}_{\mathcal{F}}^3\Phi\left(\overline{L}_{\mathcal{F}}^3\right)^T\right\} = 10.7194$$

Hence, $\lambda_4 = 10.7194$, $\mu \geq \frac{\rho\phi_{min}}{\lambda_3} = 0.09534$, *and* $0 < \beta \leq \sqrt{\frac{\omega\phi_{max}}{\lambda_4}} = 0.0144$

Now, if we take $\beta = 0.1$ *and* $\mu = 0.01$,

and we choose $\gamma = 0.7$ and $e_2 = 0.9$, then the states of the agents and the observation error under switching topologies of FMAS (2) and (3) are given in Figures 7 and 8, respectively.

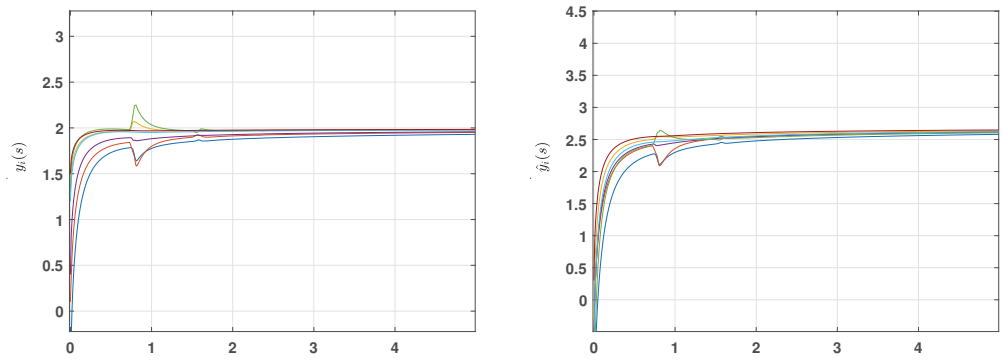

Figure 7. Agent state $y_i(s)$ and $\hat{y}_i(s)$, where $i = \{1, 2, ..., 7\}$, for switching signed digraph.

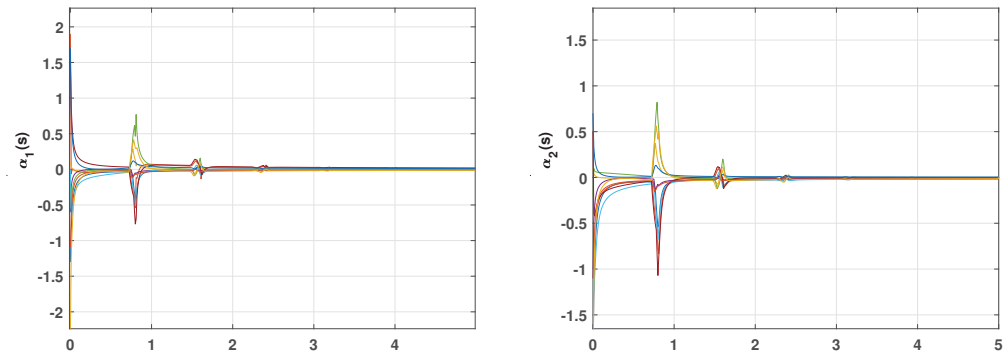

Figure 8. Observation error $\alpha_1(s)$ and bipartite containment error $\alpha_2(s)$ for switching signed digraph.

6. Conclusions

In networks that incorporate both fixed and switching attributes along with signed directed edges where both cooperative and hostile agent interactions occur, observation-based bipartite containment control of nonlinear FMASs has been investigated. Assuming the associated signed digraph is structurally balanced and at least one leader has a directed link to each follower, delayed and disturbance compensation control methods have been developed for both fixed and switching signed directed systems to address observation-based bipartite containment control networks. Using the Lyapunov function approach and the fractional Razumikhin technique, a reliable and practical solution has been proposed to tackle the issues resulting from switching topologies, fractional calculus, and delay. Basic matrix inequalities have been employed to guarantee multiple bipartite containment control. The validity and feasibility of the main findings are demonstrated through concrete numerical examples.

Author Contributions: Conceptualization, A.U.K.N.; Software, A.K. and M.A.J.; Validation, Y.Z.; Resources, A.K. and M.A.J.; Data curation, S.R.; Writing—original draft, S.R.; Writing—review and editing, A.U.K.N.; Supervision, A.U.K.N. and Y.Z.; Project administration, Y.Z., A.K. and M.A.J. All authors have read and agreed to the published version of the manuscript.

Funding: This research was sponsored by the Key Laboratory of Philosophy and Social Sciences in Guangdong Province of Maritime Silk Road of Guangzhou University (GD22TWCXGC15), the National Natural Science Foundation of China (grant No. 622260-101 and 12250410247), and also by the Ministry of Science and Technology of China (No. WGXZ2023054L).

Data Availability Statement: The code is considered intellectual property of the Guangzhou government project and is therefore not publicly available.

Acknowledgments: This work has been carried out at the University of Lahore, Sargodha Campus. The authors are also grateful for the support from Guangzhou University, China.

Conflicts of Interest: The authors declare that they have no conflicts of interest.

References

1. Dai, J.; Guo, G. Event-triggered leader-following consensus for multi-agent systems with semi-Markov switching topologies. *Inf. Sci.* **2018**, *459*, 290–301. [CrossRef]
2. Zhang, J.; Peng, S. Exponential Consensus of Multi-Agent Systems under Event-Triggered Impulsive Control with Actuation Delays. *Entropy* **2023**, *25*, 877. [CrossRef]
3. Zhang, Y.; Liu, Z.; Wang, F.; Chen, Z. Rotating Consensus for Leader-Follower Multi-Agent Systems with a Smart Leader. In Proceedings of the 2023 42nd Chinese Control Conference (CCC), Tianjin, China, 24–26 July 2023; pp. 5719–5724.
4. Ali, M.S.; Agalya, R.; Orman, Z.; Arik, S. Leader-following consensus of non-linear multi-agent systems with interval time-varying delay via impulsive control. *Neural Process. Lett.* **2021**, *53*, 69–83. [CrossRef]
5. Ali, M.S.; Agalya, R.; Shekher, V.; Joo, Y.H. Non–fragile sampled data control for stabilization of non-linear multi-agent system with additive time varying delays, Markovian jump and uncertain parameters. *Nonlinear Anal. Hybrid Syst.* **2020**, *36*, 100830. [CrossRef]
6. Zhao, L.; Chen, X.; Yu, J.; Shi, P. Output feedback-based neural adaptive finite-time containment control of non-strict feedback nonlinear multi-agent systems. *IEEE Trans. Circuits Syst. Regul. Pap.* **2021**, *69*, 847–858. [CrossRef]
7. Mohammed, K.S.; Pata, U.K. Linking the utilization of mineral resources and climate change: A novel approach with frequency domain analysis. *Geosci. Front.* **2024**, *15*, 101683. [CrossRef]
8. Jiang, Y.; Fan, J.; Gao, W.; Chai, T.; Lewis, F.L. Cooperative adaptive optimal output regulation of nonlinear discrete-time multi-agent systems. *Automatica* **2020**, *121*, 109149. [CrossRef]
9. Khan, A.; Niazi, A.U.K.; Rehman, S.; Ahmed, S. Hostile-based bipartite containment control of nonlinear fractional multi-agent systems with input delays: A signed graph approach under disturbance and switching networks. *AIMS Math.* **2024**, *9*, 12678–12699. [CrossRef]
10. Yang, R.; Liu, S.; Li, X.; Xiao, J. Bipartite containment control of fractional multi-agent systems with input delay on switching signed directed networks. *ISA Trans.* **2023**, *135*, 130–137. [CrossRef]
11. Yin, M.; Liu, L.; Cheng, L.; Li, Z.; Tu, Y. A novel group multi-criteria sorting approach integrating social network analysis for ability assessment of health rumor-refutation accounts. *Expert Syst. Appl.* **2024**, *238*, 121894. [CrossRef]
12. Madridano, Á.; Al-Kaff, A.; Martín, D.; De La Escalera, A. Trajectory planning for multi-robot systems: Methods and applications. *Expert Syst. Appl.* **2021**, *173*, 114660. [CrossRef]
13. Meng, X.; Gao, H. High-order bipartite containment control in multi-agent systems over time-varying cooperation-competition networks. *Neurocomputing* **2019**, *359*, 509–516. [CrossRef]
14. Liu, Z.; Zhan, X.; Han, T.; Yan, H. Distributed adaptive finite-time bipartite containment control of linear multi-agent systems. *IEEE Trans. Circuits Syst. II Express Briefs* **2022**, *69*, 4354–4358 [CrossRef]
15. Zhu, Z.H.; Hu, B.; Guan, Z.H.; Zhang, D.X.; Li, T. Observer-based bipartite containment control for singular multi-agent systems over signed digraphs. *IEEE Trans. Circuits Syst. I Regul. Pap.* **2020**, *68*, 444–457. [CrossRef]
16. Ahsan, M.; Ma, Q. Bipartite containment control of multi-agent systems. In Proceedings of the 2019 IEEE/ASME International Conference on Advanced Intelligent Mechatronics (AIM), Hong Kong, China, 8–12 July 2019; pp. 895–900.
17. Wang, L.; Han, T.; Zhan, X.S.; Wu, J.; Yan, H. Bipartite containment for linear multi-agent systems subject to unknown exogenous disturbances. *Asian J. Control* **2022**, *24*, 1836–1845. [CrossRef]
18. Zuo, S.; Song, Y.L.; Lewis, F.; Davoudi, A. Bipartite output containment of general linear heterogeneous multi-agent systems on signed digraphs. *IET Control Theory Appl.* **2018**, *12*, 1180–1188. [CrossRef]
19. Zhou, Y.; Zhang, H.; Yu, L.; Sun, S. Cooperative bipartite containment control for heterogeneous networks with structurally balanced graph. *IEEE Trans. Circuits Syst. II Express Briefs* **2021**, *68*, 2885–2889. [CrossRef]
20. Zhou, Q.; Wang, W.; Liang, H.; Basin, M.V.; Wang, B. Observer-based event-triggered fuzzy adaptive bipartite containment control of multiagent systems with input quantization. *IEEE Trans. Fuzzy Syst.* **2019**, *29*, 372–384. [CrossRef]
21. Cai, Y.; Zhang, H.; Zhang, J.; He, Q. Distributed bipartite leader-following consensus of linear multi-agent systems with input time delay based on event-triggered transmission mechanism. *ISA Trans.* **2020**, *100*, 221–234. [CrossRef]
22. Rahman, R.U.; Hammouch, Z.; Alsubaie, A.S.A.; Mahmoud, K.H.; Alshehri, A.; Az-Zo'bi, E.A.; Osman, M.S. Dynamical behavior of fractional nonlinear dispersive equation in Murnaghanan's rod materials. *Results Phys.* **2024**, *56*, 107207. [CrossRef]
23. Di Paola, M.; Alotta, G.; Burlon, A.; Failla, G. A novel approach to nonlinear variable-order fractional viscoelasticity. *Philos. Trans. R. Soc. A* **2020**, *378*, 20190296. [CrossRef] [PubMed]
24. Khan, A.; Hassan, W.U.; Manzor, A.; Ahmed, S.; Niazi, A.U.K. Strengthening stability with centralized event-triggered control system with the disturbances and artificial time delay in wireless connected vehicle platooning (CVSs). *Syst. Sci. Control Eng.* **2024**, *12*, 2342818. [CrossRef]

25. Wenlong, Y.; Ruiliang, D.; Weixian, Z.; Zongying, S.; Yisheng, Z. Fully Distributed Robust Adaptive Formation Control for Linear Multi-agent System with Uncertainties and Communication Delays. *IFAC-PapersOnLine* **2023**, *56*, 9227–9232. [CrossRef]
26. Luo, L.; Mi, W.; Zhong, S. Adaptive consensus control of fractional multi-agent systems by distributed event-triggered strategy. *Nonlinear Dyn.* **2020**, *100*, 1327–1341. [CrossRef]
27. Hua, Y.; Dong, X.; Li, Q.; Ren, Z. Distributed time-varying formation robust tracking for general linear multiagent systems with parameter uncertainties and external disturbances. *IEEE Trans. Cybern.* **2017**, *47*, 1959–1969. [CrossRef] [PubMed]
28. Yu, J.; Wu, M.; Yang, W.; Ji, J. A system decomposition method for region tracking control of a non-holonomic mobile robot with dynamic parameter uncertainties. *Asian J. Control* **2024**, *26*, 1459–1471. [CrossRef]
29. Yang, R.; Liu, S.; Li, X. Observer-based bipartite containment control of fractional multi-agent systems with mixed delays. *Inf. Sci.* **2023**, *626*, 204–222. [CrossRef]
30. Zhou, Y. *Basic Theory of Fractional Differential Equations*; World Scientific: Singapore, 2023.
31. Sevinik Adigüzel, R.; Aksoy, Ü.; Karapinar, E.; Erhan, İ.M. On the solution of a boundary value problem associated with a fractional differential equation. *Math. Methods Appl. Sci.* **2020**, *early view*. [CrossRef]
32. Huseynov, I.T.; Ahmadova, A.; Mahmudov, N.I. Fractional Leibniz integral rules for Riemann-Liouville and Caputo fractional derivatives and their applications. *arXiv* **2020**, arXiv:2012.11360.
33. Wen, Y.; Zhou, X.F.; Zhang, Z.; Liu, S. Lyapunov method for nonlinear fractional differential systems with delay. *Nonlinear Dyn.* **2015**, *82*, 1015–1025. [CrossRef]
34. Arık, I.A.; Araz, S.I. Delay differential equations with fractional differential operators: Existence, uniqueness and applications to chaos. *Commun. Anal. Mech.* **2024**, *16*, 169–192. [CrossRef]
35. Ye, Y.; Wei, H.; Lu, R.; Su, H.; Wu, Y. Containment control for networked fractional-order systems with sampled position data. *IEEE Trans. Circuits Syst. I Regul. Pap.* **2021**, *68*, 3881–3889. [CrossRef]

Disclaimer/Publisher's Note: The statements, opinions and data contained in all publications are solely those of the individual author(s) and contributor(s) and not of MDPI and/or the editor(s). MDPI and/or the editor(s) disclaim responsibility for any injury to people or property resulting from any ideas, methods, instructions or products referred to in the content.

fractal and fractional

MDPI

Article

Polynomial Decay of the Energy of Solutions of the Timoshenko System with Two Boundary Fractional Dissipations

Suleman Alfalqi [1,†], Hamid Khiar [2,†], Ahmed Bchatnia [3,*,†] and Abderrahmane Beniani [2,†]

[1] Department of Mathematics, Applied College in Mahayil, King Khalid University, Abha 61421, Saudi Arabia; salfalqi@kku.edu.sa
[2] Engineering and Sustainable Development Laboratory, Faculty of Science and Technology, University of Ain Temouchent, Ain Temouchent 46000, Algeria; hamid.khiar@univ-temouchent.edu.dz (H.K.); abderrahmane.beniani@univ-temouchent.edu.dz (A.B.)
[3] LR Analyse Non-Linéaire et Géométrie, LR21ES08, Department of Mathematics, Faculty of Sciences of Tunis, University of Tunis El Manar, Tunis 2092, Tunisia
* Correspondence: ahmed.bchatnia@fst.utm.tn
† These authors contributed equally to this work.

Abstract: In this study, we examine Timoshenko systems with boundary conditions featuring two types of fractional dissipations. By applying semigroup theory, we demonstrate the existence and uniqueness of solutions. Our analysis shows that while the system exhibits strong stability, it does not achieve uniform stability. Consequently, we derive a polynomial decay rate for the system.

Keywords: Timoshenko systems; fractional derivatives; $\mathcal{C}_0$ semi-group

MSC: 35L05; 34K35; 93D20

1. Introduction

In this study, we investigate the well-posedness and stabilization of a one-dimensional Timoshenko system of the following form:

$$\begin{cases} \rho_1 \varphi_{tt} - d_1(\varphi_x + \psi)_x = 0, & (x,t) \in (0,L) \times (0,+\infty), \\ \rho_2 \psi_{tt} - d_2 \psi_{xx} + d_1(\varphi_x + \psi) = 0, & (x,t) \in (0,L) \times (0,+\infty). \end{cases} \tag{1}$$

The initial conditions are

$$\begin{aligned} \varphi(x,0) = \varphi_0(x), \quad \varphi_t(x,0) = \varphi_1(x), \quad x \in (0,L), \\ \psi(x,0) = \psi_0(x), \quad \psi_t(x,0) = \psi_1(x), \quad x \in (0,L), \end{aligned} \tag{2}$$

and the following boundary conditions:

$$\begin{aligned} \varphi(0,t) = 0, \quad \psi(0,t) = 0, \quad \text{in } (0,+\infty), \\ (\varphi_x + \psi)(L) = -\gamma_1 \partial_t^{\alpha,\eta} \varphi(L), \quad (\psi_x + \psi)(L) = -\gamma_2 \partial_t^{\alpha,\eta} \psi(L), \quad \text{in } (0,+\infty), \end{aligned} \tag{3}$$

where ρ_1, ρ_2, d_1, d_2, γ_1, and γ_2 are positive constants, η is a non-negative constant, and α is in $(0,1)$.

The notation $\partial_t^{\alpha,\eta}$ represents the generalized Caputo fractional derivative of order α (where $0 < \alpha < 1$) with respect to time t. It is defined as

$$\partial_t^{\alpha,\eta} f(t) = \frac{1}{\Gamma(1-\alpha)} \int_0^t (t-s)^{-\alpha} e^{-\eta(t-s)} \frac{df}{ds}(s)\, ds, \quad \eta \geq 0.$$

The Timoshenko system, traditionally used to model the behavior of beams in mechanical structures, is extended in this study to incorporate fractional derivatives on the

boundary conditions. This extension is significant because fractional derivatives are known to provide more accurate models for systems with memory effects and complex dissipation properties, which are often encountered in practical applications, such as material microstructure analysis. The introduction of fractional derivatives into the boundary conditions is novel in the context of the Timoshenko system. This allows us to model more realistic dissipative effects that occur in various materials and structures. Our results provide new insights into the stability characteristics of systems with fractional boundary dissipation, contributing to both the theoretical understanding and practical applications in engineering and materials science.

Fractional calculus has developed into a well-established theory with a solid mathematical foundation, and its applications have gained significant interest in various research fields, including electrical circuits, chemical processes, signal processing, bioengineering, viscoelasticity, and control systems (see [1]). Fractional-order control is not only theoretically important but also has practical implications. It generalizes classical integer-order control theory, enabling more accurate modeling and enhanced control performance. Experimental observations reveal that many phenomena cannot be fully described using traditional Newtonian terms. For example, in viscoelastic materials, the material's microstructure leads to a combined response involving both elastic solid and viscous fluid characteristics.

The literature (see [2]) establishes that the fractional derivative ∂_t^α enforces dissipation in the system and ensures that the solution converges to an equilibrium state. Consequently, when applied at the boundaries, fractional derivatives can act as controllers to suppress or attenuate undesirable vibrations.

In [3], B. Mbodje explored the asymptotic behavior of solutions with the following system:

$$\begin{cases} \partial_t^2 u(x,t) - u_x^2(x,t) = 0, \quad (x,t) \in (0,1) \times (0,+\infty), \\ u(0,t) = 0, \\ \partial_x u(1,t) = -k\partial_t^{\alpha,\eta} u(1,t), \quad \alpha \in (0,1), \eta \geq 0, k > 0, \\ u(x,0) = u_0(x), \\ \partial_t u(x,0) = v_0(x). \end{cases}$$

He demonstrated strong asymptotic stability of the solutions when $\eta = 0$ and a polynomial decay rate of t^{-1} as time approaches infinity when $\eta \neq 0$. The polynomial decay rate was established using the energy method.

Kim and Renardy [4] investigated (1) with two boundary controls of the following form:

$$K(\varphi_x + \psi)(L) = -\gamma_1 \partial^\alpha t \varphi(L), \quad b\psi x(L) = -\gamma_2 \partial_t^\alpha \psi(L), \quad \text{for,,} t \in (0,+\infty),$$

and employed multiplier techniques to prove an exponential decay result for the natural energy of (1). Additionally, Yan [5] established a polynomial decay result when examining two boundary frictional damping terms with polynomial growth near the origin.

Benaissa and Benazzouz [6] investigated the stabilization of the following Timoshenko system with two dynamic boundary control conditions involving fractional derivatives:

$$\begin{cases} \rho_1 \phi_{tt} - K(\phi_x + \psi)x &= 0, \quad (x,t) \in (0,L) \times (0,+\infty), \\ \rho 2\psi_{tt} - b\psi_{xx} + K(\phi_x + \psi) &= 0, \quad (x,t) \in (0,L) \times (0,+\infty). \end{cases}$$

The system is subject to the following boundary conditions:

$$\begin{cases} m_1 \phi_{tt}(L,t) + K(\phi_x + \psi)(L,t) &= -\gamma_1 \partial_t^{\alpha,\eta} \phi(L,t) \text{ for } t \in (0,+\infty), \\ m_2 \psi_{tt}(L,t) + b\psi_x(L,t) &= -\gamma_2 \partial_t^{\alpha,\eta} \psi(L,t) \text{ for } t \in (0,+\infty), \\ \phi(0,t) = 0, \quad \psi(0,t) &= 0 \text{ for } t \in (0,+\infty), \end{cases}$$

where m_1 and m_2 are positive constants. They demonstrated that the system (1) is not uniformly stable using the spectrum method. Polynomial stability was established through semigroup theory and by applying a result from Borichev and Tomilov.

M. Akil et al. [7] studied the Timoshenko system with a single fractional derivative described by

$$\begin{cases} au_{tt} - (u_x + y)_x &= 0, \quad (x,t) \in (0,1) \times (0,+\infty), \\ by_{tt} - y_{xx} + c(u_x + y) &= 0, \quad (x,t) \in (0,1) \times (0,+\infty), \end{cases} \tag{4}$$

where a, b, and c are positive constants. The system is subject to the following boundary conditions:

$$\begin{cases} u_x(1,t) + y(1,t) + \gamma \partial_t^{\alpha,\eta} u(1,t) &= 0, \quad t \in \mathbb{R}^+, \\ u(0,t) = y_x(0,t) = y_x(1,t) &= 0. \end{cases} \tag{5}$$

They demonstrated that the energy of the system (4) and (5) decays polynomially over time. References such as [8–14] present a comprehensive collection of published works that support the mathematical formulation of problems related to fractional differential equations and the decay rate of the associated energy.

This paper is organized as follows: in Section 2, we demonstrate the well-posedness of system (1) with the boundary conditions (3) using semigroup theory. In Section 3, we prove that the Timoshenko system (1) with the boundary conditions (2) is not exponentially stable, whether the wave propagation speeds are equal ($\frac{\rho_1}{d_1} = \frac{\rho_2}{d_2}$) or not ($\frac{\rho_1}{d_1} \neq \frac{\rho_2}{d_2}$). In Section 5, we show that the solution decays polynomially to zero when $\eta > 0$, employing a frequency domain approach and a theorem by Borichev and Tomilov.

2. Augmented Model and Well-Posedness of the System

In this section, we focus on reformulating the model (1) into an augmented system. To proceed, we first require the following theorem:

Theorem 1 ([3]). *Let μ be the following function:*

$$\mu(\xi) = |\xi|^{(2\alpha - n)/2}, \quad \xi \in \mathbb{R}^n, \quad 0 < \alpha < 1.$$

Consider the system governed by the equation:

$$\partial_t \varphi(\xi,t) + \left(|\xi|^2 + \eta\right)\varphi(\xi,t) - U(t)\mu(\xi) = 0, \quad \xi \in \mathbb{R}^n, \eta \geq 0, t > 0,$$

with the initial condition

$$\varphi(\xi,0) = 0,$$

and the output defined as

$$O(t) = \frac{2\sin(\alpha\pi)\Gamma\left(\frac{n}{2}+1\right)}{n\pi^{\frac{n}{2}+1}} \int_{\mathbb{R}^n} \mu(\xi)\varphi(\xi,t)d\xi.$$

The relationship between the 'input' U and the 'output' O is then given by

$$O(t) = I^{1-\alpha,\eta}U(t) = D^{\alpha,\eta}U(t),$$

where

$$[I^{\alpha,\eta}f](t) = \frac{1}{\Gamma(\alpha)} \int_0^t (t-\tau)^{\alpha-1} e^{-\eta(t-\tau)} f(\tau)d\tau.$$

Lemma 1 ([15]). *If $\lambda \in D = \{\lambda \in \mathbb{C} \mid \Re(\lambda) + \eta > 0\} \cup \{\Im(\lambda) \neq 0\}$, then*

$$\tau(\alpha) \int_{\mathbb{R}^n} \frac{\mu^2(\xi)}{\lambda + \eta + \xi^2} d\xi = (\lambda + \eta)^{\alpha - 1},$$

where $\tau(\alpha) = \pi^{-1}\sin(\alpha\pi)$.

Using the previous theorem, the system (1) can be rewritten as the following augmented model:

$$\begin{cases} \rho_1\varphi_{tt} - d_1(\varphi_x+\psi)_x = 0, \quad (x,t)\in(0,L)\times(0,+\infty), \\ \rho_2\psi_{tt} - d_2\psi_{xx} + d_1(\varphi_x+\psi) = 0, \quad (x,t)\in(0,L)\times(0,+\infty), \\ \partial_t\phi_1(\xi,t) + (\xi^2+\eta)\phi_1(\xi,t) - \mu(\xi)\partial_t\varphi(L,t) = 0, \quad t\in(0,+\infty), \quad \xi\in\mathbb{R}, \\ \partial_t\phi_2(\xi,t) + (\xi^2+\eta)\phi_2(\xi,t) - \mu(\xi)\partial_t\psi(L,t) = 0, \quad t\in(0,+\infty), \quad \xi\in\mathbb{R}, \\ (\varphi_x+\psi)(L) = -\gamma_1\dfrac{\sin(\alpha\pi)}{\pi}\displaystyle\int_{\mathbb{R}}\mu(\xi)\phi_1(\xi,t)d\xi, \quad t\in(0,+\infty), \\ \psi_x(L) = -\gamma_2\dfrac{\sin(\alpha\pi)}{\pi}\displaystyle\int_{\mathbb{R}}\mu(\xi)\phi_2(\xi,t)d\xi, \quad t\in(0,+\infty), \end{cases} \tag{6}$$

with the following initial conditions:

$$\begin{aligned} &\varphi(x,0) = \varphi_0(x), \quad \varphi_t(x,0) = \varphi_1(x), \quad x\in(0,L), \\ &\psi(x,0) = \psi_0(x), \quad \psi_t(x,0) = \psi_1(x), \quad x\in(0,L). \end{aligned}$$

For a solution $U = (\varphi, \varphi_t, \psi, \psi_t, \phi_1, \phi_2)$ of (6), we define the energy by

$$E(t) = \frac{1}{2}\|U\|^2_{\mathcal{H}}, \tag{7}$$

where

$$\begin{aligned} \|U\|^2_{\mathcal{H}} &= \frac{1}{2}\int_0^L\Big(\rho_1|\varphi_t|^2 + \rho_2|\psi_t|^2 + d_1|\varphi_x+\psi|^2 + d_2|\psi_x|^2\Big)dx \\ &+ \frac{\xi_1}{2}\int_{\mathbb{R}}|\phi_1|^2d\xi + \frac{\xi_2}{2}\int_{\mathbb{R}}|\phi_2|^2d\xi, \end{aligned}$$

with constants $\xi_i = \frac{\gamma_i}{d_i}\frac{\sin(\alpha\pi)}{\pi}$.

Lemma 2. *Let $U = (\varphi, \varphi_t, \psi, \psi_t, \phi_1, \phi_2)$ be a regular solution of the problem* (6)*. Then, the energy functional defined in* (7) *satisfies the following relation:*

$$\frac{d}{dt}E(t) = -\xi_1\int_{\mathbb{R}}\Big(|\xi|^2+\eta\Big)|\phi_1(\xi,t)|^2\,d\xi - \xi_2\int_{\mathbb{R}}\Big(|\xi|^2+\eta\Big)|\phi_2(\xi,t)|^2\,d\xi.$$

Proof. Multiplying Equations $(6)_1$ and $(6)_3$ by φ_t and ψ_t, respectively, integrating by parts over $(0,L)$, and then summing the resulting equations, we obtain

$$\frac{1}{2}\frac{d}{dt}\left(\int_0^L\Big(\rho_1|\varphi_t|^2 + \rho_2|\psi_t|^2 + d_1|\varphi_x+\psi|^2 + d_2|\psi_x|^2\Big)dx\right) - (\varphi_x+\psi)(L)\varphi_t(L) = 0. \tag{8}$$

Multiplying Equations $(6)_2$ and $(6)_4$ by $\xi_1\phi_1$ and $\xi_2\phi_2$, respectively, integrating over $\mathbb{R}$, and adding the resulting equations gives us

$$\begin{aligned} &\frac{1}{2}\frac{d}{dt}\left(\xi_1\int_{\mathbb{R}}|\phi_1|^2d\xi + \xi_2\int_{\mathbb{R}}|\phi_2|^2d\xi\right) + \xi_1\int_{\mathbb{R}}(\xi^2+\eta)|\phi_1(\xi,t)|^2\,d\xi \\ &+ \xi_2\int_{\mathbb{R}}(\xi^2+\eta)|\phi_2(\xi,t)|^2\,d\xi - \xi_1\varphi_t(L)\int_{\mathbb{R}}\mu(\xi)\phi_1(\xi,t)\,d\xi \\ &- \xi_2\psi_t(L)\int_{\mathbb{R}}\mu(\xi)\phi_2(\xi,t)\,d\xi = 0. \end{aligned} \tag{9}$$

Combining Equations (8) and (9), we obtain

$$\frac{d}{dt}E(t) = -\xi_1\int_{\mathbb{R}}\Big(\xi^2+\eta\Big)|\phi_1(\xi,t)|^2\,d\xi - \xi_2\int_{\mathbb{R}}\Big(\xi^2+\eta\Big)|\phi_2(\xi,t)|^2\,d\xi.$$

This concludes the proof of the lemma. □

We now address the well-posedness of (6). To this end, we introduce the following Hilbert space, referred to as the energy space:

$$\mathcal{H} = \Big(H_L^1(0,L) \times L^2(0,L)\Big)^2 \times L^2(\mathbb{R}),$$

where $H_L^1(0,L)$ is defined as

$$H_L^1(0,L) = \{\varphi \in H^1(0,L) \mid \varphi(0) = 0\}.$$

For $U = (u_1, u_2, u_3, u_4, \phi_1, \phi_2)^T$ and $\tilde{U} = (\tilde{u}_1, \tilde{u}_2, \tilde{u}_3, \tilde{u}_4, \tilde{\phi}_1, \tilde{\phi}_2)^T$, we define the inner product in $\mathcal{H}$ as follows:

$$\begin{aligned}\langle U, \tilde{U}\rangle_{\mathcal{H}} &= \int_0^L \big(\rho_1 u_2 \overline{\tilde{u}_2} + \rho_2 u_4 \overline{\tilde{u}_4}\big)dx + \int_0^L d_1(u_{1x} + u_3)\overline{(\tilde{u}_{1x} + \tilde{u}_3)}dx \\ &+ \int_0^L d_2 u_{3x}\overline{\tilde{u}_{3x}}dx + d_1^2\xi_1 \int_{\mathbb{R}} \phi_1 \overline{\tilde{\phi}_1}\, d\xi + d_2^2\xi_2 \int_{\mathbb{R}} \phi_2 \overline{\tilde{\phi}_2}\, d\xi.\end{aligned}$$

We transform the system described by (6) into a semigroup framework. By defining the vector function $U = (u_1, u_2, u_3, u_4, \phi_1, \phi_2)^T$, we express the system (6) in the equivalent form

$$\begin{cases} U' = \mathcal{A}U, \quad t > 0, \\ U(0) = U_0, \end{cases}$$

where $U_0 = (\varphi_0, \varphi_1, \psi_0, \psi_1, \phi_1^0, \phi_2^0)^T$.

The operator $\mathcal{A}$ is linear and defined by

$$\mathcal{A}\begin{pmatrix} u_1 \\ u_2 \\ u_3 \\ u_4 \\ \phi_1 \\ \phi_2 \end{pmatrix} = \begin{pmatrix} u_2 \\ \frac{d_1}{\rho_1}(u_{1x} + u_3)_x \\ u_4 \\ \frac{d_2}{\rho_2}u_{3xx} - \frac{d_1}{\rho_2}(u_{1x} + u_3) \\ -(\xi^2 + \eta)\phi_1 + u_2(L)\mu(\xi) \\ -(\xi^2 + \eta)\phi_2 + u_4(L)\mu(\xi) \end{pmatrix}.$$

The domain of $\mathcal{A}$ is then

$$D(\mathcal{A}) = \left\{ \begin{array}{l} (u_1, u_2, u_3, u_4, \phi_1, \phi_2)^T \in \mathcal{H} : u_1, u_3 \in H^2 \cap H_L^1, \\ \xi\phi_1, \xi\phi_2 \in L^2(\mathbb{R}), -\big(|\xi|^2 + \eta\big)\phi_1 + u_2(L)\mu(\xi) \in L^2(\mathbb{R}^n), \\ (u_{1x} + u_3)(L) = -\gamma_1 \dfrac{\sin(\alpha\pi)}{\pi} \displaystyle\int_{\mathbb{R}} \mu(\xi)\phi_1(\xi, t)d\xi, \\ -\big(|\xi|^2 + \eta\big)\phi_2 + u_4(L)\mu(\xi) \in L^2(\mathbb{R}), \\ u_{3x}(L) = -\gamma_2 \dfrac{\sin(\alpha\pi)}{\pi} \displaystyle\int_{\mathbb{R}} \mu(\xi)\phi_2(\xi, t)d\xi. \end{array} \right\}. \tag{10}$$

We state the following theorem on existence and uniqueness:

Theorem 2.

1. *If $U_0 \in D(\mathcal{A})$, then the system* (6) *has a unique strong solution*

$$U \in \mathcal{C}^0(\mathbb{R}_+, D(\mathcal{A})) \cap \mathcal{C}^1(\mathbb{R}_+, \mathcal{H}).$$

2. *If $U_0 \in \mathcal{H}$, then the system* (6) *has a unique weak solution*

$$U \in \mathcal{C}^0(\mathbb{R}_+, \mathcal{H}).$$

Remark 1. *Note that, while strong solutions satisfy the differential equation pointwise and require higher regularity, weak solutions are defined in an integral sense with lower regularity requirements.*

Proof. First, we demonstrate that the operator $\mathcal{A}$ is dissipative.

For any $U = (u_1, u_2, u_3, u_4, \phi_1, \phi_2) \in D(\mathcal{A})$, we have

$$\begin{aligned} \mathcal{R}e\langle \mathcal{A}U, U\rangle_{\mathcal{H}} &= -d_1^2\xi_1 \int_{\mathbb{R}} \Big(\xi^2+\eta\Big)|\phi_1(\xi,t)|^2 d\xi - d_2^2\xi_2 \int_{\mathbb{R}} \Big(\xi^2+\eta\Big)|\phi_2(\xi,t)|^2 d\xi \\ &\leq 0. \end{aligned}$$

Hence, $\mathcal{A}$ is dissipative.

We will show that the operator $I - \mathcal{A}$ is surjective.

Given $F = (f_1, f_2, f_3, f_4, f_5, f_6) \in \mathcal{H}$, we prove that there exists $U = (u_1, u_2, u_3, u_4, \phi_1, \phi_2) \in D(\mathcal{A})$ satisfying

$$(I - \mathcal{A})U = F.$$

That is,

$$\begin{cases} u_1 - u_2 &= f_1, \\ u_2 - \frac{d_1}{\rho_1}(u_{1x} + u_3)_x &= f_2 \\ u_3 - u_4 &= f_3, \\ u_4 - \frac{d_2}{\rho_2}u_{3xx} + \frac{d_1}{\rho_2}(u_{1x} + u_3) &= f_4 \\ \phi_1(1 + \xi^2 + \eta) - \mu(\xi)u_2(L,t) &= f_5, \\ \phi_2(1 + \xi^2 + \eta) - \mu(\xi)u_4(L,t) &= f_6. \end{cases} \tag{11}$$

Then, $(11)_1$, $(11)_2$, $(11)_5$, and $(11)_6$ yield

$$\begin{cases} u_2 &= u_1 - f_1, \\ u_4 &= u_3 - f_3, \\ \phi_1 &= \frac{f_5}{1+\xi^2+\eta} + \frac{\mu(\xi)u_2(L,t)}{1+\xi^2+\eta}, \\ \phi_2 &= \frac{f_6}{1+\xi^2+\eta} + \frac{\mu(\xi)u_4(L,t)}{1+\xi^2+\eta}. \end{cases} \tag{12}$$

Inserting Equations $(11)_1$ in $(11)_2$ and $(11)_3$ in $(11)_4$, we obtain

$$\begin{cases} \rho_1 u_1 - d_1(u_{1x} + u_3)_x &= \rho_1(f_1 + f_2), \\ \rho_2 u_3 - d_2 u_{3xx} + d_1(u_{1x} + u_3) &= \rho_2(f_3 + f_4). \end{cases} \tag{13}$$

Solving system (13) is equivalent to finding $u_1, u_3 \in H^2(0,L) \cap H_L^1(0,L)$ such that

$$\begin{cases} \int_0^L [\rho_1 u_1 - d_1(u_{1x} + u_3)_x]\chi dx &= \int_0^L \rho_1[f_1 + f_2]\chi dx, \\ \int_0^L [\rho_2 u_3 - d_2 u_{3xx} + d_1(u_{1x} + u_3)]\zeta dx &= \int_0^L \rho_2(f_3 + f_4)\zeta dx, \end{cases} \tag{14}$$

for all $\chi, \zeta \in H_L^1(0,L)$.

Inserting Equations $(12)_3$ in $(14)_1$ and $(12)_4$ in $(14)_2$, we obtain

$$\begin{cases} \int_0^L [\rho_1 u_1 \chi + d_1(u_{1x} + u_3)\chi_x]dx + k_1 u_2(L)\chi(L) \\ = \int_0^L \rho_1[f_1 + f_2]\chi dx - d_1^2\xi_1\chi(L)\int_{\mathbb{R}} \frac{f_5\mu(\xi)}{1+\xi^2+\eta}d\xi, \\ \int_0^L [\rho_2 u_3\zeta + d_2 u_{3x}\zeta_x + d_1(u_{1x} + u_3)\zeta]dx + k_2 u_4(L)\zeta(L) \\ = \int_0^L \rho_2(f_3 + f_4)\zeta dx - d_2^2\xi_2\zeta(L)\int_{\mathbb{R}} \frac{f_6\mu(\xi)}{1+\xi^2+\eta}d\xi, \end{cases} \tag{15}$$

where $k_i = d_i^2 \xi_i \int_{\mathbb{R}} \frac{\mu^2(\xi)}{1+\xi^2+\eta} d\xi$ and with the following boundary conditions:

$$u_2(L) = u_1(L) - f_1(L), \quad u_4(L) = u_3(L) - f_3(L). \tag{16}$$

Inserting (16) into (15), we obtain

$$\begin{cases} \int_0^L [\rho_1 u_1 \chi + d_1(u_{1x} + u_3)\chi_x]dx + k_1 u_1(L)\chi(L) \\ = \int_0^L \rho_1 [f_1 + f_2]\chi dx - d_1^2 \xi_1 \chi(L) \int_{\mathbb{R}} \frac{f_5 \mu(\xi)}{1+\xi^2+\eta} d\xi + k_1 f_1(L)\chi(L), \\ \int_0^L [\rho_2 u_3 \zeta + d_2 u_{3x}\zeta_x + d_1(u_{1x} + u_3)\zeta]dx + k_2 u_3(L)\zeta(L) \\ = \int_0^L \rho_2 (f_3 + f_4)\zeta dx - d_2^2 \xi_2 \zeta(L) \int_{\mathbb{R}} \frac{f_6 \mu(\xi)}{1+\xi^2+\eta} d\xi + k_2 f_3(L)\zeta(L). \end{cases} \tag{17}$$

Thus, the problem (17) can be reformulated as the following problem:

$$a((u_1, u_3), (\chi, \zeta)) = \mathcal{L}(\chi, \zeta), \tag{18}$$

where

$$\begin{aligned} a((u,v),(\chi,\zeta)) &= \int_0^L [\rho_1 u\chi + d_1(u_x + v)(\chi_x + \zeta) + \rho_2 v\zeta + d_2 v_x \zeta_x]dx \\ &+ k_1 u(L)\chi(L) + + k_2 v(L)\zeta(L), \end{aligned}$$

and

$$\begin{aligned} \mathcal{L}(\chi,\zeta) &= \int_0^L \rho_1 [f_1 + f_2]\chi dx - d_1^2 \xi_1 \chi(L) \int_{\mathbb{R}} \frac{f_5 \mu(\xi)}{1+\xi^2+\eta} d\xi + k_1 f_1(L)\chi(L) \\ &+ \int_0^L \rho_2 (f_3 + f_4)\zeta dx - d_2^2 \xi_1 \zeta(L) \int_{\mathbb{R}} \frac{f_6 \mu(\xi)}{1+\xi^2+\eta} d\xi + k_2 f_3(L)\zeta(L). \end{aligned}$$

It is straightforward to verify that a is continuous and coercive and that $\mathcal{L}$ is continuous. By applying the Lax–Milgram Theorem A1, we conclude that, for all $(\chi, \zeta) \in H_L^1(0, L) \times H_L^1(0, L)$, the problem (18) has a unique solution $(u_1, u_3) \in H_L^1(0, L) \times H_L^1(0, L)$.

Using classical elliptic regularity results, it follows from (17) that $(u_1, u_3) \in H^2(0, L) \times H^2(0, L)$. Consequently, the operator $I - \mathcal{A}$ is surjective. Finally, Theorem 2 follows from the Lumer–Phillips Theorem A2. □

3. Asymptotic Stability

In this section, we analyze the asymptotic stability of the system described by (1)–(3), which requires

$$\lim_{t \to +\infty} E(t) = 0, \quad \forall U_0 \in \mathcal{H}.$$

We will examine the spectrum and investigate the strong stability of the C_0 semigroup associated with the system (1)–(3) using the criteria of Arendt–Batty [16].

The main results of this paper are summarized as follows:

Theorem 3. *The semigroup of contractions $(S(t))_{t \geq 0}$ is strongly stable on the energy space $\mathcal{H}$, meaning that*

$$\lim_{t \to \infty} \left\| e^{\mathcal{A}t} U_0 \right\|_{\mathcal{H}} = 0 \quad \forall U_0 \in \mathcal{H}.$$

First, we need to prove the following lemmas:

Lemma 3. *The point spectrum of the operator $\mathcal{A}$ does not intersect with the imaginary axis, i.e.,*

$$\sigma_p(\mathcal{A}) \cap i\mathbb{R} = \emptyset,$$

where

$$\sigma_p(\mathcal{A}) = \{\lambda \in \mathbb{C} \mid \ker(\lambda I - \mathcal{A}) \neq \{0\}\}.$$

Proof. For clarity, we divide the proof into two steps.

Step 1. By direct computation, the equation

$$\mathcal{A}U = 0$$

with $U \in D(\mathcal{A})$ admits only the trivial solution, i.e., $U = 0$. Hence, $0 \notin \sigma_p(\mathcal{A})$.

Step 2. Suppose that there exists $\beta \in \mathbb{R}^*$ such that

$$\ker(i\beta I - \mathcal{A}) \neq \{0\}.$$

Thus, $\lambda = i\beta$ is an eigenvalue of $\mathcal{A}$. Let U be an eigenvector in $D(\mathcal{A})$ associated with λ, satisfying

$$(i\beta I - \mathcal{A})U = 0.$$

Equivalently, we have

$$\left\{\begin{array}{lcl} u_2 & = & i\beta u_1, \\ \frac{d_1}{\rho_1}(u_{1x} + u_3)_x & = & i\beta u_2 \\ u_4 & = & i\beta u_3, \\ \frac{d_2}{\rho_2}u_{3xx} - \frac{d_1}{\rho_2}(u_{1x} + u_3) & = & i\beta u_4 \\ -\phi_1(\xi^2 + \eta) + \mu(\xi)u_2(L,t) & = & i\beta\phi_1, \\ -\phi_2(\xi^2 + \eta) + \mu(\xi)u_4(L,t) & = & i\beta\phi_1. \end{array}\right. \tag{19}$$

First, a straightforward computation shows that

$$\begin{array}{rcl} 0 & = & \Re < (i\beta I - \mathcal{A})U, U >_{\mathcal{H}} \\ & = & d_1^2\xi_1 \int_{\mathbb{R}} \Big(\xi^2 + \eta\Big)|\phi_1(\xi,t)|^2 d\xi + d_2^2\xi_2 \int_{\mathbb{R}} \Big(\xi^2 + \eta\Big)|\phi_2(\xi,t)|^2 d\xi. \end{array}$$

We deduce that $\phi_1 = \phi_2 = 0$ a.e. in $\mathbb{R}$.
On the other hand, by $(19)_5$ and $(19)_6$, we obtain,

$$\phi_j = \frac{\mu(\xi)u_{2j}(L,t)}{\xi^2 + \eta + i\beta}, \; j = 1, 2,$$

which yields $u_2(L,t) = u_4(L,t) = 0$. Hence, from $(19)_1$ and $(19)_3$, we obtain

$$u_1(L,t) = u_3(L,t) = 0, \quad \text{and from (10)}, \quad (u_{1x} + u_3)(L,t) = u_{3x}(L,t) = 0. \tag{20}$$

Otherwise, replacing $(19)_1$ into $(19)_2$ and $(19)_3$ into $(19)_4$ and setting $v = u_{1x} + u_3$, we obtain

$$\left\{\begin{array}{lcl} \beta^2 u_1 + \frac{d_1}{\rho_1}v_x & = & 0, \\ \beta^2 u_3 + \frac{d_2}{\rho_2}u_{3xx} - \frac{d_1}{\rho_2}v & = & 0. \end{array}\right. \tag{21}$$

We can rewrite (21) and (20) as

$$\left\{\begin{array}{l} \frac{d}{dx}X = \mathcal{B}X, \quad t > 0, \\ X(L) = 0, \end{array}\right.$$

where $X := (u_1, v, u_3, u_{3x})^T$. The operator $\mathcal{B}$ is linear and defined by

$$\mathcal{B}\begin{pmatrix} u_1 \\ v \\ u_3 \\ u_{3x} \end{pmatrix} = \begin{pmatrix} v - u_3 \\ -\frac{\rho_1\beta^2}{d_1}u_1 \\ u_{3x} \\ \frac{d_1}{d_2}v - \frac{\rho_2\beta^2}{d_2}u_3 \end{pmatrix}.$$

According to Picard's theorem for ordinary differential equations, the system (3) has a unique solution, which is $X = 0$. Thus, $u_1 = u_3 = 0$. It follows from (19) that $u_2 = u_4 = 0$. Consequently, we obtain $U = 0$ over the interval $(0, L)$, which contradicts the assumption that $U \neq 0$. □

Lemma 4. *The operator* $\Big(i\beta I - \mathcal{A}\Big)$ *is surjective.*

Proof. Let $F = (f_1, f_2, f_3, f_4, f_5, f_6) \in \mathcal{H}$ be looking for $U = (u_1, u_2, u_3, u_4, \phi_1, \phi_2) \in D(\mathcal{A})$ such that

$$i\beta U - \mathcal{A}U = F.$$

That is,

$$\begin{cases} i\beta u_1 - u_2 &= f_1, \\ i\beta u_2 - \frac{d_1}{\rho_1}(u_{1x} + u_3)_x &= f_2 \\ i\beta u_3 - u_4 &= f_3, \\ i\beta u_4 - \frac{d_2}{\rho_2}u_{3xx} + \frac{d_1}{\rho_2}(u_{1x} + u_3) &= f_4 \\ \phi_1(i\beta + \xi^2 + \eta) - \mu(\xi)u_2(L,t) &= f_5, \\ \phi_2(i\beta + \xi^2 + \eta) - \mu(\xi)u_4(L,t) &= f_6, \end{cases}$$

which is equivalent to

$$\begin{cases} u_2 &= i\beta u_1 - f_1, \\ -\beta^2 u_1 - \frac{d_1}{\rho_1}(u_{1x} + u_3)_x &= f_2 + i\beta f_1, \\ u_4 &= i\beta u_3 - f_3, \\ -\beta^2 u_3 - \frac{d_2}{\rho_2}u_{3xx} + \frac{d_1}{\rho_2}(u_{1x} + u_3) &= f_4 + i\beta f_3 \\ \phi_1 &= \frac{f_5 + \mu(\xi)u_2(L,t)}{i\beta + \xi^2 + \eta}, \\ \phi_2 &= \frac{f_6 + \mu(\xi)u_4(L,t)}{i\beta + \xi^2 + \eta}. \end{cases} \tag{22}$$

To solve the last system (22), it is enough to study the following:

$$\begin{cases} \beta^2\rho_1 u_1 + d_1(u_{1x} + u_3)_x &= -\rho_1\Big(f_2 + i\beta f_1\Big), \\ \beta^2\rho_2 u_3 + d_2 u_{3xx} - d_1(u_{1x} + u_3) &= -\rho_2\Big(f_4 + i\beta f_3\Big), \end{cases} \tag{23}$$

with the conditions

$$\begin{cases} u_1(0) &= 0, \\ u_3(0) &= 0, \\ (u_{1x} + u_3)(L) &= -d_1\xi_1\Big((f_5 + i\beta u_1(L))I_1(\beta,\eta) - f_1(L)I_2(\beta,\eta)\Big), \\ u_{3x}(L) &= -d_2\xi_2\Big((f_6 + i\beta u_3(L))I_1(\beta,\eta) - f_3(L)I_2(\beta,\eta)\Big), \end{cases}$$

where $I_1(\beta,\eta) = \displaystyle\int_{\mathbb{R}} \frac{\mu(\xi)}{i\beta + \xi^2 + \eta} d\xi$ and $I_2(\beta,\eta) = \displaystyle\int_{\mathbb{R}} \frac{\mu^2(\xi)}{i\beta + \xi^2 + \eta} d\xi$.

We now distinguish two cases.

Step 1. $\beta = 0$ and $\eta > 0$: System (23) is equivalent to finding $u_1, u_3 \in H^2(0,L) \cap H_L^1(0,L)$ such that

$$\left\{ \begin{array}{rcl} -\int_0^L d_1(u_{1x}+u_3)_x \chi dx & = & \int_0^L \rho_1 f_2 \chi dx, \\ \int_0^L [-d_2 u_{3xx} + d_1(u_{1x}+u_3)]\zeta dx & = & \int_0^L \rho_2 f_4 \zeta dx, \end{array} \right. \tag{24}$$

for all $\chi, \zeta \in H_L^1(0,L)$.

Using integration by parts in (24), we deduce that (22) is equivalent to

$$b((u_1,u_3),(\chi,\zeta)) = \mathcal{M}(\chi,\zeta), \tag{25}$$

where

$$b((u,v),(\chi,\zeta)) = \int_0^L [d_1(u_x+v)(\chi_x+\zeta) + d_2 v_x \zeta_x] dx,$$

and

$$\begin{array}{rcl} \mathcal{M}(\chi,\zeta) & = & \int_0^L \big(\rho_1 f_2 \chi + \rho_2 f_4 \zeta\big) dx - d_1^2 \xi_1 [f_5 - f_1(L) I_2(0,\eta)] \chi(L) \\ & - & d_2^2 \xi_2 [f_6 - f_3(L) I_2(0,\eta)] \zeta(L). \end{array}$$

It is straightforward to verify that the bilinear form b is continuous and coercive and that the operator $\mathcal{M}$ is continuous. By applying the Lax–Milgram theorem, we conclude that, for all $(\chi,\zeta) \in H_L^1(0,L) \times H_L^1(0,L)$, the problem (25) has a unique solution $(u_1,u_3) \in H_L^1(0,L) \times H_L^1(0,L)$. Utilizing classical elliptic regularity, it follows from (24) that $(u_1,u_3) \in H^2(0,L) \times H^2(0,L)$. Consequently, the operator $-\mathcal{A}$ is surjective.

Step 2. $\beta \neq 0$ and $\eta \geq 0$:

Now, we consider the following system:

$$\left\{ \begin{array}{rcl} -d_1(u_{1x}+u_3)_x & = & g_1, \\ -d_2 u_{3xx} + d_1(u_{1x}+u_3) & = & g_2, \end{array} \right. \tag{26}$$

with the conditions

$$\left\{ \begin{array}{rcl} u_1(0) & = & 0, \\ u_3(0) & = & 0, \\ (u_{1x}+u_3)(L) & = & -i\beta d_1 \xi_1 u_1(L) I_1(\beta,\eta), \\ u_{3x}(L) & = & -i\beta d_2 \xi_2 u_3(L) I_1(\beta,\eta), \end{array} \right.$$

where $(g_1,g_2) \in \Big(L^2(0,L)\Big)^2$.

Let us note that $\mathcal{L} : (u_1,u_2) \longrightarrow (-d_1(u_{1x}+u_3)_x, -d_2 u_{3xx} + d_1(u_{1x}+u_3))$ with domain $D(\mathcal{L}) = \{(u_1,u_3) \in \Big(H_L^1(0,L)\Big)^2,\ u_1(0)=0,\ u_3(0)=0,\ (u_{1x}+u_3)(L) = -i\beta d_1\xi_1 u_1(L) I_1(\beta,\eta),\ u_{3x}(L) = -i\beta d_2 \xi_2 u_3(L) I_1(\beta,\eta)\}$.

Multiplying $(26)_1$ by χ and $(26)_2$ by ζ, one obtains:

$$\begin{array}{rcl} & & \int_0^L [d_1(u_x+v)(\chi_x+\zeta) + d_2 v_x \zeta_x] dx + i\beta d_1^2 \xi_1 I_1(\beta,\eta) u_1(L) \chi(L) \\ & + & i\beta d_2^2 \xi_2 I_2(\beta,\eta) u_3(L) \zeta(L) = \int_0^L \big(g_1 \chi + g_2 \zeta\big) dx, \end{array} \tag{27}$$

for all $(\chi,\zeta) \in \Big(H_L^1(0,L)\Big)^2$.

By applying the Lax–Milgram theorem once more, we deduce that there exists a unique strong solution $(u_1,u_3) \in \big(H_L^1(0,L)\big)^2 \cap D(\mathcal{L})$ for the variational problem (27).

Consequently, it follows that $\mathcal{L}^{-1}$ is compact in $\Big(L^2(0,L)\Big)^2$ and therefore (23) is equivalent to

$$\Big(\beta^2\mathcal{L}^{-1} - I\Big)U = \Phi,$$

where $U = (u_1, u_3)$ and $\Phi = \Big(-\rho_1(f_2 + i\beta f_1), -\rho_2(f_4 + i\beta f_3)\Big)$ and, by Fredholm's alternative, it suffices to prove that $Ker\Big(\beta^2\mathcal{L}^{-1} - I\Big) = \{0\}$.

For this purpose, let $(y_1, y_2) \in Ker\Big(\beta^2\mathcal{L}^{-1} - I\Big)$; then, we have

$$\left\{\begin{array}{rcl} \beta^2\rho_1 y_1 + d_1(y_{1x} + y_3)_x &=& 0, \\ \beta^2\rho_2 y_3 + d_2 y_{3xx} - d_1(y_{1x} + y_3) &=& 0, \end{array}\right. \tag{28}$$

with the conditions

$$\left\{\begin{array}{rcl} y_1(0) &=& 0, \\ y_3(0) &=& 0, \\ (y_{1x} + y_3)(L) &=& -i\beta d_1\xi_1 y_1(L) I_1(\beta,\eta), \\ y_{3x}(L) &=& -i\beta d_2\xi_2 y_3(L) I_1(\beta,\eta). \end{array}\right.$$

Multiplying $(28)_1$ by $\overline{y_1}$ and $(28)_2$ by $\overline{y_3}$, integrating over $(0, L)$, one obtains

$$\begin{array}{rcl} & \displaystyle\int_0^L \Big(\beta^2\rho_1|y_1|^2 + \beta^2\rho_2|y_3|^2 - d_2|y_{3x}|^2 - d_1|y_{1x} + y_3|^2\Big)dx & \\ = & -i\beta I_1(\beta,\eta)\Big(d_1^2\xi_1|y_1(L)|^2 + d_2^2\xi_2|y_3(L)|^2\Big). & \end{array}$$

Taking the imaginary part, we deduce that

$$d_1^2\xi_1|y_1(L)|^2 + d_2^2\xi_2|y_3(L)|^2 = 0.$$

Hence, we deduce that (y_1, y_2) is the solution of

$$\left\{\begin{array}{rcl} \beta^2\rho_1 y_1 + d_1(y_{1x} + y_3)_x &=& 0, \\ \beta^2\rho_2 y_3 + d_2 y_{3xx} - d_1(y_{1x} + y_3) &=& 0, \\ y_1(0) = y_3(0) = (y_{1x} + y_3)(L) &=& y_{3x}(L). \end{array}\right.$$

Using the same argument used in Lemma 3, we infer that $(y_1, y_2) = (0, 0)$.
This completes the proof of Lemma 4. □

From Lemmas 3 and 4, we conclude the following result.

Proposition 1. $\sigma(\mathcal{A}) \cap i\mathbb{R} = \{0\}$.

Proof of Theorem 3. Due to Proposition 1, the operator $\mathcal{A}$ lacks pure imaginary eigenvalues, and the intersection $\sigma(\mathcal{A}) \cap i\mathbb{R}$ is countable. By applying the general criterion from Arendt and Batty in [17], the $\mathcal{C}^0$ semigroup $(S(t))_{t\geq 0}$ of contractions is strongly stable. □

4. Lack of Exponential Stability

The primary result of this section is encapsulated in the following theorem.

Theorem 4. *The semigroup generated by the operator $\mathcal{A}$ fails to exhibit exponential stability in the energy space $\mathcal{H}$.*

Proof. Our objective is to demonstrate that an infinite number of eigenvalues of the operator $\mathcal{A}$ approach the imaginary axis, thereby preventing the Timoshenko system (1)–(3)

from achieving exponential stability. To begin, we derive the characteristic equation that determines the eigenvalues of $\mathcal{A}$.

Given that $\mathcal{A}$ is dissipative, we choose a sufficiently small $\alpha_0 > 0$ and examine the asymptotic behavior of the eigenvalues λ of $\mathcal{A}$ within the set $S = \lambda \in \mathbb{C} : \alpha_0 \leq \mathrm{Re}(\lambda) \leq 0$.

We first establish the characteristic equation that the eigenvalues of $\mathcal{A}$ must satisfy. Let $\lambda \in \mathbb{C}^*$ be an eigenvalue of $\mathcal{A}$ and let $U = (u_1, \lambda u_1, u_3, \lambda u_3, \phi_1, \phi_2) \in D(\mathcal{A})$ be a corresponding eigenvector such that $|U| = 1$.

The resulting eigenvalue problem is then given by

$$\begin{cases} \lambda^2 u_1 - \frac{d_1}{\rho_1} u_{1xx} - \frac{d_1}{\rho_1} u_{3x} &= 0, \\ \lambda^2 u_3 - \frac{d_2}{\rho_2} u_{3xx} + \frac{d_1}{\rho_2} u_{1x} + \frac{d_1}{\rho_2} u_3 &= 0, \\ \phi_1 = \frac{\mu(\xi) u_1(L,t)}{\xi^2+\eta+\lambda}, \quad \phi_2 = \frac{\mu(\xi) u_3(L,t)}{\xi^2+\eta+\lambda}, & \\ u_1(0) = u_3(0) = 0, \ \ (u_{1x} + u_3)(L) &= -d_1 \xi_1 u_1(L) I_\alpha(\lambda, \eta) \\ u_{3x}(L) &= -d_2 \xi_2 u_3(L) I_\alpha(\lambda, \eta). \end{cases}$$

where $I_\alpha(\lambda, \eta) = \displaystyle\int_{\mathbb{R}} \frac{|\xi|^{2\alpha-1}}{\xi^2 + \eta + \lambda} d\xi$.

Equivalently, we have

$$\begin{cases} u_{1xxxx} - \lambda^2 \left(\frac{\rho_1}{d_1} + \frac{\rho_2}{d_2}\right) u_{1xx} + \lambda^2 \frac{\rho_1 \rho_2}{d_1 d_2} \left(\lambda^2 + \frac{d_1}{\rho_2}\right) u_1 &= 0, \\ u_1(0) = u_3(0) &= 0, \\ \left(\frac{\rho_1}{d_1} \lambda^2 - \gamma_1 \gamma_2 (\lambda + \eta)^{2\alpha-2}\right) u_1(L) - \gamma_2 (\lambda + \eta)^{\alpha-1} u_{1x}(L) - u_{1xx}(L) &= 0, \\ \frac{\rho_2 \gamma_1}{d_2} \left(\lambda^2 + \frac{d_1}{\rho_2}\right) u_1(L) (\lambda + \eta)^{\alpha-1} + \left(\frac{\rho_1}{d_1} + \frac{\rho_2}{d_2}\right) \lambda^2 u_{1x}(L) - u_{1xxx}(L) &= 0, \end{cases} \tag{29}$$

where we used $I_\alpha(\lambda, \eta) = \dfrac{\gamma_i}{d_i \xi_i} (\lambda + \eta)^{\alpha-1}$, $i = 1, 2$ (see Lemma 2.1 in [6] for the proof).

The characteristic polynomial associated with System (29) is given by

$$P(r) := r^4 - \lambda^2 \left(\frac{\rho_1}{d_1} + \frac{\rho_2}{d_2}\right) r^2 + \lambda^2 \frac{\rho_1 \rho_2}{d_1 d_2} \left(\lambda^2 + \frac{d_1}{\rho_2}\right) = 0.$$

Our goal is to analyze the asymptotic behavior of the large eigenvalues λ of $\mathcal{A}$ within the set S. A detailed examination reveals that the polynomial P has four distinct roots when $\left(\frac{\rho_1}{d_1} - \frac{\rho_2}{d_2}\right)^2 \lambda^2 \neq 4 \frac{\rho_1}{d_2}$.

Thus, the four distinct roots of P are given by $r_1(\lambda)$, $r_2(\lambda)$, $r_3(\lambda) = -r_1(\lambda)$, and $r_4(\lambda) = -r_2(\lambda)$, where

$$\begin{cases} r_1(\lambda) = \frac{\lambda}{\sqrt{2}} \sqrt{\left(\frac{\rho_1}{d_1} + \frac{\rho_2}{d_2}\right) + \sqrt{\left(\frac{\rho_1}{d_1} - \frac{\rho_2}{d_2}\right)^2 - 4 \frac{\rho_1}{d_2} \lambda^{-2}}}, \\ r_2(\lambda) = \frac{\lambda}{\sqrt{2}} \sqrt{\left(\frac{\rho_1}{d_1} + \frac{\rho_2}{d_2}\right) - \sqrt{\left(\frac{\rho_1}{d_1} - \frac{\rho_2}{d_2}\right)^2 - 4 \frac{\rho_1}{d_2} \lambda^{-2}}}. \end{cases}$$

The general solution to (29) can be expressed as

$$u_1(x) = c_1 \sinh(r_1(\lambda) x) + c_2 \sinh(r_2(\lambda) x) + c_3 \cosh(r_1(\lambda) x) + c_4 \cosh(r_2(\lambda) x).$$

Applying the boundary conditions in (29) at $x = 0$ yields $c_3 = c_4 = 0$. Additionally, the boundary conditions at $x = L$ in (29) can be expressed as

$$
\begin{array}{l}
M(\lambda)C = \\
\left(\begin{array}{ll} f_1(r_1)\sinh(r_1L) - f_2(r_1)\cosh(r_1L) & f_1(r_2)\sinh(r_2L) - f_2(r_2)\cosh(r_2L) \\ H_1\sinh(r_1L) + g(r_1)\cosh(r_1L) & H_1\sinh(r_2L) + g(r_2)\cosh(r_2L) \end{array} \right)
\left(\begin{array}{l} c_1 \\ c_2 \end{array} \right) \\
= \left(\begin{array}{l} 0 \\ 0 \end{array} \right)
\end{array}
$$

where

$$
\begin{array}{l}
f_1(r) = \frac{\rho_1}{d_1}\lambda^2 - \gamma_1\gamma_2(\lambda+\eta)^{2\alpha-2} - r^2, \quad f_2(r) = \gamma_2\lambda(\lambda+\eta)^{\alpha-1}r, \\
H_1 = \frac{\rho_2\gamma_1}{d_2}(\lambda^2 + \frac{d_1}{\rho_2})(\lambda+\eta)^{\alpha-1}, \quad g(r) = \left(\frac{\rho_1}{d_1} + \frac{\rho_2}{d_2}\right)\lambda^2 r - r^3 \text{ and } C = (c_1\, c_2)^T.
\end{array} \tag{30}
$$

Let $\det(M)$ represent the determinant of the matrix M. Then, it follows that

$$
\begin{array}{rcl}
detM(\lambda) & = & (f_1(r_1) - f_1(r_2))H_1\sinh(r_1L)\sinh(r_2L) \\
& - & (f_2(r_1)g(r_2) - f_2(r_2)g(r_1))\cosh(r_1L)\cosh(r_2L) \\
& + & (f_1(r_1)g(r_2) + f_2(r_2)H_1)\sinh(r_1L)\cosh(r_2L) \\
& - & (f_2(r_1)H_1 + f_1(r_2)g(r_1))\cosh(r_1L)\sinh(r_2L).
\end{array}
$$

The Equation (29) has a non-trivial solution if and only if $\det(M) = 0$.
Case 1. Assuming that $\frac{\rho_1}{d_1} = \frac{\rho_2}{d_2}$, and applying the asymptotic expansion, we obtain

$$
\begin{array}{l}
r_1 = \lambda\sqrt{\frac{\rho_1}{d_1}}\sqrt{1 + i\frac{d_1}{\sqrt{\rho_1 d_2}}\frac{1}{\lambda}} = \sqrt{\frac{\rho_1}{d_1}}\lambda + \frac{i}{2}\sqrt{\frac{d_1}{d_2}} + \frac{1}{8}\frac{d_1^{3/2}}{\sqrt{\rho_1}d_2}\frac{1}{\lambda} + o(\frac{1}{\lambda}), \\
r_2 = \lambda\sqrt{\frac{\rho_1}{d_1}}\sqrt{1 - i\frac{d_1}{\sqrt{\rho_1 d_2}}\frac{1}{\lambda}} = \sqrt{\frac{\rho_1}{d_1}}\lambda - \frac{i}{2}\sqrt{\frac{d_1}{d_2}} + \frac{1}{8}\frac{d_1^{3/2}}{\sqrt{\rho_1}d_2}\frac{1}{\lambda} + o(\frac{1}{\lambda}).
\end{array} \tag{31}
$$

Next, inserting (31) into (30), we obtain

$$
\left\{ \begin{array}{rcl}
(f_1(r_1) - f_1(r_2))H_1 & = & -2i\gamma_1\sqrt{\frac{\rho_1}{d_2}}\lambda^{2+\alpha} + O(\lambda^{1+\alpha}), \\
f_2(r_1)g(r_2) - f_2(r_2)g(r_1) & = & 2i\gamma_2\sqrt{\frac{\rho_1}{d_2}}\lambda^{3+\alpha} + O(\lambda^{2+\alpha}), \\
f_1(r_1)g(r_2) + f_2(r_2)H_1 & = & -i\sqrt{\frac{\rho_1}{d_2}}\lambda^3 + O(\lambda^2), \\
f_2(r_1)H_1 + f_1(r_2)g(r_1) & = & i\gamma_1\gamma_2\frac{\rho_1}{d_2}\sqrt{\frac{\rho_1}{d_2}}\lambda^{2+2\alpha} + O(\lambda^{1+2\alpha}).
\end{array} \right. \tag{32}
$$

where we used

$$
(\lambda+\eta)^{\alpha-1} = \lambda^{\alpha-1} + O\left(\lambda^{\alpha-2}\right).
$$

From (31), we obtain

$$
\left\{ \begin{array}{ll}
\sinh(r_1L) = \sinh\left(\sqrt{\frac{\rho_1}{d_1}}\lambda L\right) + O(\frac{1}{\lambda}) & \cosh(r_1L) = \cosh\left(\sqrt{\frac{\rho_1}{d_1}}\lambda L\right) + O(\frac{1}{\lambda}), \\
\sinh(r_2L) = \sinh\left(\sqrt{\frac{\rho_1}{d_1}}\lambda L\right) + O(\frac{1}{\lambda}) & \cosh(r_2L) = \cosh\left(\sqrt{\frac{\rho_1}{d_1}}\lambda L\right) + O(\frac{1}{\lambda}).
\end{array} \right. \tag{33}
$$

Therefore, from (32) and (33), we obtain

$$
\begin{array}{rcl}
\frac{\det M}{\lambda^{3+\alpha}} & = & 2i\gamma_2\sqrt{\frac{\rho_1}{d_2}}\cosh^2\left(\sqrt{\frac{\rho_1}{d_1}}\lambda L\right) - i\sqrt{\frac{\rho_1}{d_2}}\frac{1}{\lambda^\alpha}\frac{1}{2}\sinh\left(2\sqrt{\frac{\rho_1}{d_1}}\lambda L\right) \\
& - & i\gamma_1\gamma_2\frac{\rho_1}{d_2}\sqrt{\frac{\rho_1}{d_2}}\frac{1}{\lambda^{1-\alpha}}\frac{1}{2}\sinh\left(2\sqrt{\frac{\rho_2}{d_2}}\lambda L\right) + O\left(\lambda^{-1}\right).
\end{array} \tag{34}
$$

Let λ be a large eigenvalue of $\mathcal{A}$. Then, according to (34), λ is an approximate root of the following asymptotic equation:

$$\varphi(\lambda) = \varphi_0(\lambda) + \frac{\varphi_1(\lambda)}{\lambda^{\min(\alpha,1-\alpha)}} + O(\lambda^{-1}),$$

where $\varphi_0(\lambda) = 2i\gamma_2\sqrt{\frac{\rho_1}{d_2}}\cosh^2\left(\sqrt{\frac{\rho_1}{d_1}}\lambda L\right)$ and $\varphi_1(\lambda) = c\sinh\left(2\sqrt{\frac{\rho_1}{d_1}}\lambda L\right)$.

It is important to note that φ_0 and φ_1 remain bounded within the strip $\alpha_0 \leq \mathrm{Re}(\lambda) \leq 0$.

The roots of φ_0 are given by $i\frac{(2n+1)\pi}{2L}\sqrt{\frac{d_2}{\rho_1}}$, $k \in \mathbb{Z}$, and we conclude using Rouché's theorem.

Case 2. $\frac{\rho_1}{d_1} \neq \frac{\rho_2}{d_2}$ is treated in a similar way.

The proof of Theorem 4 is thus concluded. □

5. The Rate of Decay of the $\mathcal{C}_0$ Semigroup

This section focuses on analyzing the asymptotic behavior of the solution to the system (1)–(3). We demonstrate the polynomial stability of the system (1)–(3):

Theorem 5. *Let $(S(t))_{t\geq 0}$ be the bounded C_0 semigroup on the Hilbert space $\mathcal{H}$; with generator $\mathcal{A}$, we have*

$$\|S(t)\mathcal{A}(I-\mathcal{A})^{-1}\| = O(t^{-1}), \quad t \to \infty.$$

The following corollary follows from Theorem 5 and Remark 8.5 in [16].

Corollary 1. *Given $(u_0, u_1) \in D(\mathcal{A}) \cap R(\mathcal{A})$. There exist constants C, $t_0 > 0$ such that, for all $t \geq t_0$,*

$$\|S(t)(u_0, u_1)\| \leq \frac{C}{t}\|(u_0, u_1)\|_{D(\mathcal{A})\cap R(\mathcal{A})}.$$

To establish Theorem 5, we derive a specific resolvent estimate using a result from Batty, Chill, and Tomilov as presented in [16]. More precisely, we have the following lemmas:

Lemma 5. *The operator $\mathcal{A}$ defined by* (2) *and* (10) *satisfies*

$$\limsup_{\beta\in\mathbb{R},|\beta|\to+\infty} \|\left(i\beta I - \mathcal{A}\right)^{-1}\|_{\mathcal{L}(\mathcal{H})} < \infty.$$

Proof. By contradiction, suppose that

$$\limsup_{\beta\in\mathbb{R},|\beta|\to\infty} \|\left(i\beta I - \mathcal{A}\right)^{-1}\|_{\mathcal{L}(\mathcal{H})} = \infty.$$

There exists a sequence of real numbers $\beta_n > 0$ with $\beta_n \to \infty$ and a sequence of vectors $(U_n)_n \in D(\mathcal{A})$ such that

$$\|U_n\|_{\mathcal{H}} = 1,$$

and

$$(i\beta_n I - \mathcal{A})U_n =: F_n = o(1) \text{ in } \mathcal{H}. \tag{35}$$

Our objective is to show that U_n converges to zero, leading to a contradiction.

Note that (35) is equivalent to

$$\left\{\begin{array}{rcl} i\beta_n u_1^n - u_2^n &=& f_1^n \longrightarrow 0 \text{ in } H_L^1,\\ i\beta_n u_2^n - \frac{d_1}{\rho_1}\left(u_{1x}^n + u_3^n\right)_x &=& f_2^n \longrightarrow 0 \text{ in } L^2,\\ i\beta_n u_3^n - u_4^n &=& f_3^n \longrightarrow 0 \text{ in } H_L^1,\\ i\beta_n u_4^n - \frac{d_2}{\rho_2}u_{3xx}^n + \frac{d_1}{\rho_2}\left(u_{1x}^n + u_3^n\right) &=& f_4^n \longrightarrow 0 \text{ in } L^2,\\ \phi_1^n(i\beta_n + \xi^2 + \eta) - \mu(\xi)u_2^n(L,t) &=& f_5^n \longrightarrow 0 \text{ in } L^2,\\ \phi_2^n(i\beta_n + \xi^2 + \eta) - \mu(\xi)u_4^n(L,t) &=& f_6^n \longrightarrow 0 \text{ in } L^2,\\ (u_{1x}^n + u_3^n)(L) &=& -\gamma_1\dfrac{\sin(\alpha\pi)}{\pi}\displaystyle\int_{\mathbb{R}}\mu(\xi)\phi_1^n(\xi,t)d\xi,\\ u_{3x}^n(L) &=& -\gamma_2\dfrac{\sin(\alpha\pi)}{\pi}\displaystyle\int_{\mathbb{R}}\mu(\xi)\phi_2^n(\xi,t)d\xi. \end{array}\right. \tag{36}$$

First, taking the real part of the inner product of (35) with U_n in $\mathcal{H}$, we obtain

$$\begin{array}{rl} & \mathcal{R}e\langle i\beta_n I - \mathcal{A})U_n, U_n\rangle_{\mathcal{H}}\\ = & d_1^2\xi_1\displaystyle\int_{\mathbb{R}}\left(\xi^2+\eta\right)|\phi_1^n(\xi,t)|^2d\xi + d_2^2\xi_2\int_{\mathbb{R}}\left(\xi^2+\eta\right)|\phi_2^n(\xi,t)|^2d\xi. \end{array} \tag{37}$$

Then, from (35) and (37), we obtain

$$\|\phi_1^n\|_{L^2} = \|\phi_2^n\|_{L^2} = o(1),$$

and we deduce that

$$(u_{1x}^n + u_3^n)(L) = o(1) \text{ and } u_{3x}^n(L) = o(1).$$

Note also that we deduce from $(36)_1$ and $(36)_3$ that $\|u_1^n\|_{L^2} = o(1)$ and $\|u_3^n\|_{L^2} = o(1)$. Now, inserting $(36)_1$ into $(36)_2$ and $(36)_3$ into $(36)_4$, we obtain

$$\left\{\begin{array}{rcl} u_2^n &=& i\beta u_1^n - f_1^n,\\ -\beta^2 u_1^n - \frac{d_1}{\rho_1}(u_{1x}^n + u_3^n)_x &=& f_2^n + i\beta f_1^n,\\ u_4^n &=& i\beta u_3^n - f_3^n,\\ -\beta^2 u_3^n - \frac{d_2}{\rho_2}u_{3xx}^n + \frac{d_1}{\rho_2}(u_{1x}^n + u_3^n) &=& f_4^n + i\beta f_3^n\\ \phi_1^n &=& \frac{f_5^n + \mu(\xi)u_2^n(L,t)}{i\beta+\xi^2+\eta},\\ \phi_2^n &=& \frac{f_6^n + \mu(\xi)u_4^n(L,t)}{i\beta+\xi^2+\eta}. \end{array}\right. \tag{38}$$

We will break the proof into several steps, and, for simplicity, we will omit the index n.

Step 1. Multiplying $(38)_2$ by $x\overline{u_{1x}}$ and integrating over $(0,L)$, one obtains

$$\begin{array}{rl} & \beta^2\displaystyle\int_0^L\frac{|u_1|^2}{2}dx - \frac{\beta^2 L}{2}|u_1(L)|^2 + \frac{d_1 L}{\rho_1}\int_0^L\frac{|u_{1x}|^2}{2}dx - \frac{d_1}{\rho_1}|u_{1x}(L)|^2\\ - & \dfrac{d_1}{\rho_1}\displaystyle\int_0^L x\Re(u_{3x}\overline{u_{1x}})dx\\ = & \Re\big[\displaystyle\int_0^L xf_2\overline{u_{1x}}dx - i\beta\int_0^L(f_1 + xf_{1x})\overline{u_1}dx + i\beta L f_1(L)\overline{u_1(L)}\big]. \end{array}$$

Using the fact that $\displaystyle\int_0^L xf_2\overline{u_{1x}}dx = o(1)$, $\displaystyle\int_0^L(f_1 + xf_{1x})\overline{\beta u_1}dx = o(1)$ and $|f_1(L)| = |\displaystyle\int_0^L f_{1x}dx| \le \sqrt{L}\|f_1\|_{H_L^1(0,L)} = o(1)$.

Therefore,

$$\begin{aligned} & \beta^2 \int_0^L \frac{|u_1|^2}{2} dx - \frac{\beta^2 L}{2} |u_1(L)|^2 + \frac{d_1}{\rho_1} \int_0^L \frac{|u_{1x}|^2}{2} dx - \frac{d_1 L}{\rho_1} |u_{1x}(L)|^2 \\ - \quad & \frac{d_1}{\rho_1} \int_0^L x \Re(u_{3x} \overline{u_{1x}}) dx = o(1) \Big(1 + \Re(\beta \overline{u_1(L)} \Big). \end{aligned} \tag{39}$$

Analogously, by multiplying Equation $(38)_4$ by $x\overline{u_{3x}}$, we obtain

$$\begin{aligned} & (\beta^2 - \frac{d_1}{\rho_2}) \int_0^L \frac{|u_3|^2}{2} dx + L(\frac{d_1}{\rho_2} - \beta^2) \frac{|u_3(L)|^2}{2} + \frac{d_2}{\rho_2} \int_0^L \frac{|u_{3x}|^2}{2} dx - \frac{d_2 L |u_{3x}|^2}{2\rho_2} \\ + \quad & \frac{d_1}{\rho_2} \int_0^L x \Re(u_{1x} \overline{u_{3x}}) dx = o(1) \Big(1 + \Re(\beta \overline{u_3(L)} \Big). \end{aligned} \tag{40}$$

Consequently, estimates (39) and (40) give

$$\begin{aligned} & \beta^2 \rho_1 \int_0^L \frac{|u_1|^2}{2} dx - \frac{\beta^2 \rho_1 L}{2} |u_1(L)|^2 + d_1 \int_0^L \frac{|u_{1x}|^2}{2} dx - d_1 L |u_{1x}(L)|^2 \\ + \quad & (\beta^2 \rho_2 - d_1) \int_0^L \frac{|u_3|^2}{2} dx + L(d_1 - \beta^2 \rho_2) \frac{|u_3(L)|^2}{2} + d_2 \int_0^L \frac{|u_{3x}|^2}{2} dx \\ = \quad & o(1) \Big(1 + \Re(\beta \overline{u_1(L)} + \Re(\beta \overline{u_3(L)} \Big). \end{aligned} \tag{41}$$

Step 2. From $(38)_5$ and $(38)_6$, we have

$$\begin{cases} \phi_1^2 = \frac{f_5^2}{\beta^2 + (\xi^2 + \eta)^2} + \frac{\mu^2(\xi) u_2^2(L,t)}{\beta^2 + (\xi^2 + \eta)^2} + 2\mathcal{R}e \frac{f_5 \mu(\xi) u_2(L,t)}{\beta^2 + (\xi^2 + \eta)^2}, \\ \phi_2^2 = \frac{f_6^2}{\beta^2 + (\xi^2 + \eta)^2} + \frac{\mu^2(\xi) u_4^2(L,t)}{\beta^2 + (\xi^2 + \eta)^2} + 2\mathcal{R}e \frac{f_6 \mu(\xi) u_4(L,t)}{\beta^2 + (\xi^2 + \eta)^2}. \end{cases}$$

Given that $\|\phi_1\|_{L^2} = \|\phi_2\|_{L^2} = o(1)$ and $\int_{\mathbb{R}} \frac{\mu(\xi)}{\beta^2 + (\xi^2 + \eta)^2} \, d\xi > 0$, we can deduce that

$$u_2(L) \longrightarrow 0 \text{ and } u_4(L) \longrightarrow 0.$$

Consequently, using $(38)_1$ $(38)_3$, and the fact that $|f_i(L)| \leq \sqrt{L} \|f_i\|_{H_L^1} = O(1)$, $i = 1, 3$, we obtain

$$\beta u_1(L) \longrightarrow 0 \text{ and } \beta u_3(L) \longrightarrow 0,$$

and, next, $u_{1x}(L) = o(1)$.

Combining this with (41), $(38)_1$, and $(38)_3$, we obtain that $\|u_2\|_{L^2} = o(1)$ and $\|u_4\|_{L^2} = o(1)$ and, next, $\|U\|_{\mathcal{H}} = o(1)$, which contradicts the hypothesis that $\|U\|_{\mathcal{H}} = 1$.

Thus, the proof of the lemma is complete. □

Lemma 6. *The operator $\mathcal{A}$ defined by* (2) *and* (10) *satisfies*

$$\limsup_{\beta \in \mathbb{R},\, \beta \to 0} \|\beta (i\beta I - \mathcal{A})^{-1}\|_{\mathcal{L}(\mathcal{H})} < \infty.$$

Proof. By contradiction, suppose that

$$\limsup_{\beta \in \mathbb{R},\, \beta \to 0} \|\beta (i\beta I - \mathcal{A})^{-1}\|_{\mathcal{L}(\mathcal{H})} = \infty. \tag{42}$$

Put $\beta = \dfrac{1}{\gamma}$ so (42) is equivalent to

$$\limsup_{\gamma \in \mathbb{R},\, |\gamma| \to +\infty} \|\gamma^{-1} (i\gamma^{-1} I - \mathcal{A})^{-1}\|_{\mathcal{L}(\mathcal{H})} = \infty.$$

Then, there exists a sequence of real numbers $\gamma_n > 1$ with $\gamma_n \to \infty$ and a sequence of functions $(U_n)_n \in D(\mathcal{A})$ such that

$$\|U_n\|_{\mathcal{H}} = 1, \tag{43}$$

and

$$\gamma_n(i\gamma_n^{-1}I - \mathcal{A})U_n =: F_n = o(1), \quad \text{in } \mathcal{H}. \tag{44}$$

We will demonstrate that $\|U_n\|_{\mathcal{H}} = o(1)$, which contradicts the assumption regarding U_n. To simplify, we will drop the index n in the following and divide the remainder of the proof into two steps for clarity.

Step 1. In fact, (44) can be written as

$$\begin{cases} iu_1 - \gamma u_2 = f_1 & \longrightarrow 0 \quad in \quad H_L^1, \\ iu_2 - \frac{\gamma d_1}{\rho_1}(u_{1x} + u_3)_x = f_2 & \longrightarrow 0 \quad in \quad L^2, \\ iu_3 - \gamma u_4 = f_3 & \longrightarrow 0 \quad in \quad H_L^1, \\ iu_4 - \frac{\gamma d_2}{\rho_2}u_{3xx} + \frac{\gamma d_1}{\rho_2}(u_{1x} + u_3) = f_4 & \longrightarrow 0 \quad in \quad L^2, \\ \phi_1(i + \gamma\xi^2 + \gamma\eta) - \gamma\mu(\xi)u_2(L,t) = f_5 & \longrightarrow 0 \quad in \quad L^2, \\ \phi_2(i + \gamma\xi^2 + \gamma\eta) - \gamma\mu(\xi)u_4(L,t) = f_6 & \longrightarrow 0 \quad in \quad L^2. \end{cases} \tag{45}$$

Since U_n is bounded by 1 in $\mathcal{H}$ and F_n converges to 0 in $\mathcal{H}$, $(45)_1$ and $(45)_3$ imply that

$$\|u_2\|_{L^2} = \|u_4\|_{L^2} = o(1). \tag{46}$$

By taking the real part of the inner product of (44) with U in $\mathcal{H}$, we obtain

$$\begin{aligned} \mathcal{R}e\Big\langle \gamma(i\gamma^{-1}I - \mathcal{A})U, U\Big\rangle_{\mathcal{H}} &= \gamma d_1^2\varsigma_1 \int_{\mathbb{R}} \Big(\xi^2 + \eta\Big)|\phi_1^n(\xi,t)|^2 d\xi \\ &+ \gamma d_2^2\varsigma_2 \int_{\mathbb{R}} \Big(\xi^2 + \eta\Big)|\phi_2^n(\xi,t)|^2 d\xi. \end{aligned}$$

Then, from (43) and (44), we obtain

$$\|\phi_1\|_{L^2} = \|\phi_2\|_{L^2} = o(1). \tag{47}$$

Considering that $U \in D(\mathcal{A})$, we deduce that

$$(u_{1x} + u_3)(L) = o(1) \text{ and } u_{3x}(L) = o(1). \tag{48}$$

Next, we use the same steps used in the previous lemma to obtain

$$\gamma u_2(L) \longrightarrow 0 \text{ and } \gamma u_4(L) \longrightarrow 0,$$

and we infer that

$$u_1(L) \longrightarrow 0 \text{ and } u_3(L) \longrightarrow 0. \tag{49}$$

Step 2. Now, from $(45)_2$, $(45)_4$, and (46), we obtain

$$\begin{cases} \gamma(u_{1x} + u_3)_x &= -\frac{\rho_1}{d_1}(f_2 - iu_2) := g_1 \longrightarrow 0 \text{ in } L^2, \\ \gamma u_{3xx} - \frac{\gamma d_1}{d_2}(u_{1x} + u_3) &= -\frac{\rho_2}{d_2}(f_4 - iu_4) := g_2 \longrightarrow 0 \text{ in } L^2. \end{cases}$$

Consequently, $V := (u_1, u_{1x} + u_3, u_3, u_{3x})^T$ is the solution of

$$\begin{cases} \frac{d}{dx}V &= CV + G \\ V(L) &= (u_1(L), (u_{1x} + u_3)(L), u_3(L), u_{3x}(L))^T. \end{cases}$$

Here, C is defined as

$$C = \begin{pmatrix} 0 & 1 & -1 & 0 \\ 0 & 0 & 0 & 0 \\ 0 & 0 & 0 & 1 \\ 0 & \frac{d_1}{d_2} & 0 & 0 \end{pmatrix}$$

and $G := (0, \frac{1}{\gamma}g_1, 0, \frac{1}{\gamma}g_2)^T$.

On one hand, by Duhamel's formula, one obtains

$$V(x) = \exp\big(C(x-L)\big)V(L) + \int_L^x \exp\big(C(x-s)\big)G(s)ds.$$

Conversely, a straightforward calculation yields the characteristic polynomial of C:

$$P(\lambda) = \lambda^4.$$

Hence, we obtain

$$\exp(Cx) = \begin{pmatrix} 1 & x - \frac{d_1 x^3}{6d_2} & -x & -\frac{x^2}{2} \\ 0 & 1 & 0 & 0 \\ 0 & \frac{d_1 x^2}{2d_2} & 1 & x \\ 0 & \frac{d_1 x}{d_2} & 0 & 0 \end{pmatrix}, \ \forall x \in \mathbb{R}.$$

Therefore,

$$\begin{aligned} u_1 &= u_1(L) + \Big(x - L - \frac{d_1(x-L)^3}{6d_2}\Big)(u_{1x} + u_3)(L) - (x-L)u_3(L) \\ &- \frac{(x-L)^2}{2}u_{3x}(L) + \frac{1}{\gamma}\int_L^x \Big((x-s-\frac{d_1(x-s)^3}{6d_2})g_1 - \frac{(x-s)^2}{2}g_2\Big)ds, \end{aligned}$$

and, from (48) and (49), it is simple to show that u_1 converges to 0 in L^2. We also show that u_{1x}, u_3 and u_{3x} converge to 0 in L^2.

Finally, combining the last result with (46) and (47), we find that $\|U\|_{\mathcal{H}} = o(1)$, which contradicts the assumption that $\|U\|_{\mathcal{H}} = 1$. □

Proof of Theorem 5. It follows immediately from Lemma 5, Lemma 6, and Theorem 7.6 in [16] that

$$\|S(t)\mathcal{A}(I-\mathcal{A})^{-1}\| = O(t^{-1}), \quad t \to \infty.$$

□

Author Contributions: Conceptualization, S.A. and H.K.; Methodology, A.B. (Ahmed Bchatnia) and A.B. (Abderrahmane Beniani); Validation, A.B. (Ahmed Bchatnia); Investigation, S.A.; Resources, S.A., H.K. and A.B. (Ahmed Bchatnia); Writing—original draft, S.A., H.K., A.B. (Ahmed Bchatnia) and A.B. (Abderrahmane Beniani); Visualization, A.B. (Abderrahmane Beniani); Supervision, A.B. (Ahmed Bchatnia). All authors have read and agreed to the published version of the manuscript.

Funding: This research received no external funding.

Data Availability Statement: Data are contained within the article.

Acknowledgments: The authors extend their appreciation to the Deanship of Research and Graduate Studies at King Khaled University for funding this work through Large Research Project under grant number RGP2/37/45.

Conflicts of Interest: The authors declare no conflicts of interest.

Appendix A

In this appendix, we present several key theorems from the literature that have been utilized in various proofs throughout this article. We begin with the Lax–Milgram theorem, which serves as a type of representation theorem for bounded linear functionals on a Hilbert space $\mathcal{H}$:

Theorem A1. *Let B be a bounded, coercive bilinear form on a Hilbert space $\mathcal{H}$. Then, for every bounded linear functional ℓ on $\mathcal{H}$, there exists a unique element $x_\ell \in \mathcal{H}$ such that $\ell(x) = B(x, x_\ell)$ for all x in $\mathcal{H}$.*

We then proceed to the Lumer–Phillips theorem, which provides a necessary and sufficient condition for a linear operator in a Banach space to generate a contraction semigroup:

Theorem A2. *Let $\mathcal{A}$ be a densely defined operator on X. Then, $\mathcal{A}$ generates a $\mathcal{C}_0$-semigroup of contractions on X if and only if*

1. *$\mathcal{A}$ is dissipative;*
2. *$(I - \mathcal{A})D(\mathcal{A}) = X$, where $D(\mathcal{A})$ is the domain of the operator $\mathcal{A}$.*

References

1. Podlubny, I. Fractional Differential Equations. In *Mathematics in Science and Engineering*; Academic Press: London, UK, 1999; Volume 198.
2. Mbodje, B.; Montseny, G. Boundary fractional derivative control of the wave equation. *IEEE Trans. Automat. Contr.* **1995**, *40*, 368–382. [CrossRef]
3. Mbodje, B. Wave energy decay under fractional derivative controls. *SIAM J. Control Optim.* **2006**, *23*, 237–257. [CrossRef]
4. Kim, J.U.; Renardy, Y. Boundary control of the Timoshenko beam. *SIAM J. Control Optim.* **1987**, *25*, 1417–1429. [CrossRef]
5. Yan, Q.X. Boundary stabilization of Timoshenko beam. *Syst. Sci. Math. Sci.* **2000**, *13*, 376–384.
6. Benaissa, A.; Benazzouz, S. Well-posedness and asymptotic behavior of Timoshenko beam system with dynamic boundary dissipative feedback of fractional derivative type. *Z. Angew. Math. Phys.* **2017**, *68*, 94. [CrossRef]
7. Akil, M.; Chitour, Y.; Ghader, M.; Wehbe, A. Stability and exact controllability of a Timoshenko system with only one fractional damping on the boundary. *Asymptot. Anal.* **2020**, *119*, 221–280. [CrossRef]
8. Akil, M.; Wehbe, A. Stabilization of multidimensional wave equation with locally boundary fractional dissipation law under geometric conditions. *Math. Control Relat. Fields* **2019**, *9*, 97–116. [CrossRef]
9. Bchatnia, A.; Mufti, K.; Yahia, R. Stability of an infinite star-shaped network of strings by a Kelvin-Voigt damping. *Math. Methods Appl. Sci.* **2022**, *45*, 2024–2041. [CrossRef]
10. Beniani, A.; Bahri, N.; Alharbi, R.; Bouhali, K.; Zennir, K. Stability for Weakly Coupled Wave Equations with a General Internal Control of Diffusive Type. *Axioms* **2023**, *12*, 48. [CrossRef]
11. Bagley, R.L.; Torvik, P.J. A theoretical basis for the application of fractional calculus to viscoelasticity. *J. Rheol.* **1983**, *27*, 201–210. [CrossRef]
12. Batty, C.J.K.; Duyckaerts, T. Non-uniform stability for bounded semi-groups on Banach spaces. *J. Evol. Equ.* **2008**, *8*, 765–780. [CrossRef]
13. Lyubich, I.; Phng, V.Q. Asymptotic stability of linear differential equations in Banach spaces. *Stud. Math.* **1988**, *88*, 37–42. [CrossRef]
14. Soufyane, A. Stabilisation de la poutre de Timoshenko. *C. R. Acad. Sci. Paris Sér. I Math.* **1999**, *328*, 731–734. [CrossRef]
15. Achouri, Z.; Amroun, N.; Benaissa, A. The Euler Bernoulli beam equation with boundary dissipation of fractional derivative. *Math. Methods Appl. Sci.* **2017**, *40*, 3837–3854. [CrossRef]
16. Batty, C.J.K.; Chill, R.; Tomilov, Y. Fine scales of decay of operator semigroups. *J. Eur. Math. Soc.* **2016**, *18*, 853–929. [CrossRef]
17. Arendt, W.; Batty, C.J.K. Tauberian theorems and stability of one-parameter semigroups. *Trans. Am. Math. Soc.* **1988**, *306*, 837–852. [CrossRef]

Disclaimer/Publisher's Note: The statements, opinions and data contained in all publications are solely those of the individual author(s) and contributor(s) and not of MDPI and/or the editor(s). MDPI and/or the editor(s) disclaim responsibility for any injury to people or property resulting from any ideas, methods, instructions or products referred to in the content.

fractal and fractional

MDPI

Article

Study of a Coupled Ψ–Liouville–Riemann Fractional Differential System Characterized by Mixed Boundary Conditions

Brahim Tellab [1], Abdelkader Amara [1], Mohammed El-Hadi Mezabia [1], Khaled Zennir [2] and Loay Alkhalifa [2,*]

[1] Applied Mathematics Laboratory, Kasdi Merbah University, BP511, Ouargla 30000, Algeria; brahimtel@yahoo.fr (B.T.); amara.abdelkader@univ-ouargla.dz (A.A.); hadimzabi@gmail.com (M.E.-H.M.)
[2] Department of Mathematics, College of Science, Qassim University, Buraydah 51452, Saudi Arabia; k.zennir@qu.edu.sa
* Correspondence: loay.alkhalifa@qu.edu.sa

Abstract: This research is concerned with the existence and uniqueness of solutions for a coupled system of Ψ–Riemann–Liouville fractional differential equations. To achieve this objective, we establish a set of necessary conditions by formulating the problem as an integral equation and utilizing well-known fixed-point theorems. By employing these mathematical tools, we demonstrate the existence and uniqueness of solutions for the proposed system. Additionally, to illustrate the practical implications of our findings, we provide several examples that showcase the main results obtained in this study.

Keywords: fractional differential equation; iterative methods; Banach space; Ψ–Liouville–Riemann fractional operators

1. Introduction

Numerous authors have tackled boundary value problems (BVPs) encompassing various types of fractional derivative operators, including, but not limited to, Caputo–Liouville, Riemann–Liouville, Ψ–Riemann–Liouville [1], Hilfer [2], κ–Riemann–Liouville [3], and ψ–Hilfer [4]. Recent research papers [5–7] delve into multivalued BVPs that incorporate Hilfer and Caputo–Hadamard-type fractional derivative operators. To grasp the fundamental concepts of fractional calculus, consult references such as the book [8]. Notably, the Hilfer fractional derivative offers a unified definition for both Riemann–Liouville and Caputo fractional derivatives. For practical applications involving the Hilfer fractional derivative operator, readers are referred to [9–12]. Traditionally, derivatives are taken with respect to variables. However, fractional derivatives can also be taken with respect to other functions. This type of derivative is a generalization of the traditional derivative, and it is commonly used in fractional calculus to describe complex systems with non-integer-order dynamics. By taking the fractional derivative with respect to another function, researchers can better model the behavior of these systems and gain a deeper understanding of their underlying dynamics; for more details, see [13–20]. In recent years, fixed-point theory has emerged as a crucial tool in the analysis of differential equations, including fractional differential systems. The Banach Fixed-Point Theorem provides a foundational result, establishing conditions for the existence and uniqueness of fixed points for contraction mappings in complete metric spaces [21]. Further extending these ideas, Krasnoselskii's fixed-point theorem handles mappings composed of a compact continuous operator and a contraction, broadening the scope of applicable systems [22]. The Nonlinear Alternative of the Leray–Schauder type provides another powerful tool, offering alternatives for the existence of fixed points in Banach spaces under compactness assumptions [23]. These theoretical advancements have found significant applications in the study of fractional differential equations. For instance, recent works have successfully applied fixed-point theorems to establish existence results

for fractional pantograph equations and advection–diffusion equations under various initial and boundary conditions [24]. These contributions underscore the versatility of fixed-point theory in addressing complex problems in fractional calculus. The study of fractals and their applications in various fields has garnered significant attention in recent years. Fractals, which are complex structures characterized by self-similarity and fractional dimensions, have been found to be particularly useful in modeling and analyzing natural phenomena. For instance, recent research has demonstrated the effectiveness of fractal analysis in understanding complex systems and improving algorithmic approaches in mathematics and computer science (see [25,26]). In particular, advancements in mathematical methods have shown promise in enhancing our understanding of fractal dimensions and their applications in signal processing and image analysis [27]. These methods not only provide insights into the intrinsic properties of fractals but also open up new avenues for practical applications in various scientific and engineering disciplines. In recent studies [15–17], significant attention was directed towards establishing findings pertaining to a specific category of coupled system of fractional integral problems. These problems were associated with fractional differential equations (FDEs) and featured movable boundary conditions. In [28], the researchers focused their efforts on investigating and analyzing the following form of problem structure:

$$\begin{cases} {}^{c}D_{0^+}^{\ell_1} u(\varsigma) = \gamma_1(\varsigma, \omega(\varsigma)), \quad \varsigma \in [0,1], \\ {}^{c}D_{0^+}^{\ell_2} \omega(\varsigma) = \gamma_2(\varsigma, u(\varsigma)), \quad \varsigma \in [0,1], \\ u(0) = 0, \quad \omega(0) = 0, \\ u(1) = \int_0^a u(s)ds, \quad \omega(1) = \int_0^b \omega(s)ds, \end{cases} \tag{1}$$

with $\gamma_1, \gamma_2 \in C([0,1], \mathbb{R}_+)$, $1 < \ell_1, \ell_2 < 2$, and $0 < a, b < 1$. Recently, Rezapour [29] constructed a new analysis studying the problem

$$\begin{cases} {}^{C}D^{\xi_1}\left({}^{C}D^{\xi_2}\xi\right)(\varsigma) = K\left(\varsigma, \zeta(\varsigma), {}^{C}D^{\xi_2}\zeta(\varsigma)\right), \qquad \varsigma \in [0,1], \\ {}^{C}D^{\xi_1^*}\left({}^{C}D^{\xi_2^*}\zeta\right)(\varsigma) = M\left(\varsigma, \xi(\varsigma), {}^{C}D^{\xi_2^*}\xi(\varsigma)\right), \qquad \varsigma \in [0,1], \\ \gamma\xi(0) = \delta\xi(1) = \alpha\,{}^{C}D^{\xi_2}\xi(0) = \beta\,{}^{C}D^{\xi_2}\xi(1) = 0, \\ \gamma^*\zeta(0) = \delta^*\zeta(1) = \alpha^*\,{}^{C}D^{\xi_2^*}\zeta(0) = \beta^*\,{}^{C}D^{\xi_2^*}\zeta(1) = 0, \end{cases} \tag{2}$$

such that $\xi_1, \xi_1^* \in (1,2]$, $\xi_2, \xi_2^* \in (1,2]$ and $\gamma, \delta, \alpha, \beta, \gamma^*, \delta^*, \alpha^*, \beta^* \in \mathbb{R}_+$. In addition, the authors used the operator ${}^{C}D^{(\cdot)}$ to deal with fraction derivatives according to Caputo's definition. Furthermore, the continuous single-valued functions K and M, defined on $[0,1] \times \mathbb{R}^2$ are considered, taking values in $\mathbb{R}$. In [30], the authors proposed a new formulation, marking the first instance of a coupled system of three-point integral pantograph FDEs using the corresponding Caputo's operators in

$$\begin{cases} {}^{CC}D_{\varsigma_0}^{\mu,\xi_1}\varphi(\varsigma) = \omega_1(\varsigma, \Psi(\varsigma), \Psi(\lambda\varsigma)), \qquad \varsigma \in \mathbb{O} = [\varsigma_0, Z], \\ {}^{CC}D_{\varsigma_0}^{\mu,\xi_2}\Psi(\varsigma) = \omega_2(\varsigma, \varphi(\varsigma), \varphi(\lambda\varsigma), \\ \varphi(\varsigma_0) = 0, \quad a_1\varphi(Z) + a_2\,{}^{RC}I_{\varsigma_0}^{\mu,\theta}\varphi(c) = m_1, \qquad c \in \mathbb{O}, \\ \Psi(\varsigma_0) = 0, \quad b_1\Psi(Z) + b_2\,{}^{RC}I_{\varsigma_0}^{\mu,\theta}\Psi(d) = m_2, \qquad d \in \mathbb{O}, \end{cases} \tag{3}$$

where ${}^{CC}D_{\varsigma_0}^{\mu,\xi_i}$ stands for the corresponding Caputo's derivatives of order $\xi_i \in (1,2)$ with $\mu \in (0,1)$ for $i = 1,2$, and ${}^{RC}I_{\varsigma_0}^{\mu,\theta}$ denotes the RL-corresponding integral of order $\theta > 0$. Furthermore, $a_1, a_2, b_1, b_2, m_1, m_2 \in \mathbb{R}$, $\lambda \in (0,1)$, with

$$\omega_i : [\varsigma_0, Z] \times \mathbb{R}^2 \longrightarrow \mathbb{R},$$

are continuous for $i = 1,2$.

In this work, we aim to extend the results of the aforementioned articles within the context of Ψ–Riemann–Liouville fractional derivatives. Specifically, we focus on the existence and uniqueness of solutions by employing Banach's fixed-point theorem and Krasnoselskii's fixed-point theorem, similar to the previous studies. Additionally, we introduce the use of another fixed-point theorem, the nonlinear alternative of the Leray–Schauder type. Furthermore, we explore the Ulam–Hyers stability of the solutions. The importance of Ψ–Riemann–Liouville fractional-order derivatives lies in their ability to generalize and extend traditional derivatives. For example, if we make $\Psi(\varsigma) = \varsigma$, we obtain the classical Riemann–Liouville fractional operator, and if we make $\Psi(\varsigma) = \ln(\varsigma)$, we obtain the Hadamard fractional operator. Conversely, Ψ–Riemann–Liouville fractional-order derivatives enhance the ability to model and analyze systems with complex, non-local, or memory-dependent behaviors, making them a valuable tool in theoretical and applied contexts. In particular, we delve into the coupled fractional BVP formulation, which can be described as follows:

$$\begin{cases} D_{0^+}^{\varrho,\Psi}\vartheta(\varsigma) & = \hat{\ell}(\varsigma,\vartheta(\varsigma),\chi(\varsigma)), \quad \varsigma \in \mathcal{O} = [0,1] \\ D_{0^+}^{\omega,\Psi}\chi(\varsigma) & = \check{\ell}(\varsigma,\vartheta(\varsigma),\chi(\varsigma)), \quad \varsigma \in \mathcal{O} = [0,1], \end{cases} \tag{4}$$

subject to the following mixed boundary conditions:

$$\begin{cases} \vartheta(0) = 0, \quad \vartheta(1) = P_1 D_{0^+}^{\sigma_1,\Psi}\chi(\xi_1) + P_2 D_{0^+}^{\sigma_2,\Psi}\chi(\xi_2), \quad P_1, P_2 \in \mathbb{R} \\ \chi(0) = 0, \quad \chi(1) = Q_1 I_{0^+}^{\omega_1,\Psi}\vartheta(\eta_1) + Q_2 I_{0^+}^{\omega_2,\Psi}\vartheta(\eta_2), \quad Q_1, Q_2 \in \mathbb{R}, \end{cases} \tag{5}$$

where $D_{0^+}^{\theta,\Psi}$ denotes the Ψ–RL fractional derivative of order $\theta \in \{\varrho, \omega, \sigma_1, \sigma_2\}$, $1 < \varrho, \omega < 2$, $0 < \sigma_1, \sigma_2 < 1$, $\hat{\ell}, \check{\ell} \in C\big([0,1] \times \mathbb{R}^2, \mathbb{R}\big)$, $I_{0^+}^{\omega_1,\Psi}$, $I_{0^+}^{\omega_2,\Psi}$ are the Ψ–RL fractional integrals with order $\omega_1 > 0$, $\omega_2 > 0$, respectively, and $0 < \xi_1, \xi_2, \eta_1, \eta_2 < 1$.

The rest of the article is structured as follows: In Section 2, we recall the main tools, preliminaries, and basic definitions with useful auxiliary propositions to be used later. In Section 3, we state and prove the existence and uniqueness of the results for our main problem. To illustrate our results, a series of examples are presented and discussed in Section 4. Finally, a concluding section is given to summarize the main steps of our work.

2. Preliminary Findings and Essential Tools

We will commence this section by introducing the definitions associated with the coupled Ψ–Riemann–Liouville system (4) and (5).

Definition 1 ([1]). *For $\varphi : (0, +\infty) \longrightarrow \mathbb{R}$, the integral*

$$\big(I_{0^+}^{\varrho}\varphi\big)(\varsigma) = \frac{1}{\Gamma(\varrho)}\int_0^{\varsigma}(\varsigma - s)^{\varrho-1}\varphi(s)ds,$$

is referred to as the Riemann–Liouville fractional integral of order $\varrho > 0$, where $\Gamma(\varrho)$ is the gamma function

Definition 2 ([1]). *For a continuous function $\varphi : (0, +\infty) \longrightarrow \mathbb{R}$, the equation*

$$\mathcal{D}_{0^+}^{\varrho}\varphi(\varsigma) = \frac{1}{\Gamma(n-\varrho)}\left(\frac{d}{d\varsigma}\right)^n \int_0^{\varsigma}(\varsigma - s)^{n-\varrho-1}\varphi(s)ds = \left(\frac{d}{d\varsigma}\right)^n I_{0^+}^{n-\varrho}\varphi(\varsigma),$$

is called the Riemann–Liouville derivative of order $n - 1 < \varrho \leq n$.

Definition 3 ([31]). *Consider a function $\varphi : [a,b] \to \mathbb{R}$ that is integrable, and let $\Psi \in C^n[a,b]$ be an increasing mapping satisfying the condition $\Psi'(\varsigma) \neq 0$ for all $\varsigma \in [a,b]$. The Ψ–Riemann–Liouville integral of order $\varrho > 0$ for the function φ is defined as:*

$$I_{a^+}^{\varrho;\Psi}\varphi(\varsigma) = \frac{1}{\Gamma(\varrho)}\int_a^{\varsigma} \Psi'(s)\big(\Psi(\varsigma)-\Psi(s)\big)^{\varrho-1}\varphi(s)ds.$$

Similarly, the Ψ–Riemann–Liouville derivative of order $\varrho > 0$ for the same function is given by:

$$\begin{aligned} D_{a^+}^{\varrho;\Psi}\varphi(\varsigma) &= \left(\frac{1}{\Psi'(\varsigma)}\frac{d}{d\varsigma}\right)^n I_{a^+}^{n-\varrho;\Psi}\varphi(\varsigma) \\ &= \frac{1}{\Gamma(n-\varrho)}\left(\frac{1}{\Psi'(\varsigma)}\frac{d}{d\varsigma}\right)^n \int_a^{\varsigma} \Psi'(s)\big(\Psi(\varsigma)-\Psi(s)\big)^{n-\varrho-1}\varphi(s)ds, \end{aligned}$$

where $n-1 < \varrho \leq n$.

For any positive values of μ and a, the following semigroup specification holds true

$$I_{a^+}^{\mu;\Psi} I_{a^+}^{a;\Psi} u(\varsigma) = I_{a^+}^{\mu+a;\Psi} u(\varsigma).$$

In the case where $\Psi(\varsigma) = \varsigma$, the Ψ-operators given in Definition 3 coincide with the classical Riemann–Liouville integral and derivative, as presented in Definitions 1 and 2, respectively. This establishes a direct correspondence between the Ψ-operators and the well-known Riemann–Liouville fractional operators. Conversely, when $\Psi(\varsigma) = \ln(\varsigma)$, the Ψ-operators return to the Hadamard fractional integral and derivative, as previously defined in references [1,31,32]. This relationship highlights the versatility of Ψ-operators, allowing them to encompass both the classical and Hadamard fractional operators depending on the choice of the weight function $\Psi(\varsigma)$.

Lemma 1. *For $1 < \varrho < 2$, and $\vartheta : [a,b] \to \mathbb{R}$, the following relation holds*

$$I_{0^+}^{\varrho,\Psi} D_{0^+}^{\varrho,\Psi}\vartheta(\varsigma) = \vartheta(\varsigma) - a_1(\Psi(\varsigma)-\Psi(0))^{\varrho-1} - a_2(\Psi(\varsigma)-\Psi(0))^{\varrho-2}.$$

Definition 4 ([31]). *Let $\Psi \in C^m[a,b]$ with $\Psi'(\varsigma) \neq 0$ for all $\varsigma \in [a,b]$. Then, we present the spaces*

$$\mathcal{AC}[a,b] = \Big\{ f : [a,b] \to \mathbb{R}, \quad f(x) = f(a) + \int_a^x g(t)dt, \quad g \in L^1([a,b]) \Big\}.$$

$$\mathcal{AC}^{m;\Psi}[a,b] = \Big\{ g : [a,b] \to \mathbb{R}, \quad g^{[m-1]} = \left(\frac{1}{\Psi'(\varsigma)}\frac{d}{d\varsigma}\right)^{m-1} g \in \mathcal{AC}[a,b] \Big\}.$$

Theorem 1 (Banach's fixed-point theorem [21,31]). *Let $(Y, \|\cdot\|)$ be a non-empty Banach space, and let $F : Y \to Y$ be a contraction mapping. That is, there exists a constant $k \in (0,1)$ such that for all $x, y \in Y$,*

$$\|F(x) - F(y)\| \leq k\|x - y\|.$$

Then, F has a unique fixed point $x^* \in Y$ (i.e., $T(x^*) = x^*$).

Theorem 2 (The Nonlinear Alternative of the Leray–Schauder Type [31]). *Let X be a convex closed subset of a Banach space Y. Let B be an open subset of X with $0 \in B$, and let $G : \bar{B} \to X$ be a continuous and compact mapping.*

Then, either:

(1) The mapping G has a fixed point in $\bar{B}$, or
(2) There exists $x \in \partial B$ and $0 < \kappa < 1$ such that $x = \kappa G x$.

Theorem 3 ((Krasnoselskii's fixed-point theorem [22,31]). *Let $\mathcal{N}$ be a closed, bounded, convex, and nonempty subset of a Banach space Y. Moreover, let the operators G_1 and G_2 have the properties:*

(a) $G_1x + G_2y \in \mathcal{N}$ *for all* $x, y \in \mathcal{N}$,
(b) G_1 *is compact and continuous,*
(c) G_2 *is a contraction.*

Then, $\exists z \in \mathcal{N}$ *so that* $z = G_1z + G_2z$.

To transform our problem into an equivalent integral equation, we require the following Proposition

Proposition 1. *Let $\omega_i > \sigma_i$, for i = 1, 2. Then, (ϑ, χ) is a solution of the Problem*

$$\begin{cases} D_{0^+}^{\varrho,\Psi}\vartheta(\varsigma) & = \hat{h}(\varsigma), \quad \varsigma \in \mathcal{O} = [0,1], \\ D_{0^+}^{\omega,\Psi}\chi(\varsigma) & = \check{h}(\varsigma), \quad \varsigma \in \mathcal{O} = [0,1], \\ \vartheta(0) = 0, & \vartheta(1) = P_1 D_{0^+}^{\sigma_1,\Psi}\chi(\xi_1) + P_2 D_{0^+}^{\sigma_2,\Psi}\chi(\xi_2), \quad P_1, P_2 \in \mathbb{R}, \\ \chi(0) = 0, & \chi(1) = Q_1 I_{0^+}^{\omega_1,\Psi}\vartheta(\eta_1) + Q_2 I_{0^+}^{\omega_2,\Psi}\vartheta(\eta_2), \quad Q_1, Q_2 \in \mathbb{R}, \end{cases} \tag{6}$$

and it is equivalent to

$$\begin{aligned} \vartheta(\varsigma) = I_{0^+}^{\varrho,\Psi}\hat{h}(\varsigma) + \frac{(\Psi(\varsigma) - \Psi(0))^{\varrho-1}}{\Lambda} \\ \times \Bigg[k_1(\Delta_1\Delta_2 + \Lambda)\Big(P_1 I_{0^+}^{\omega-\sigma_1,\Psi}\check{h}(\xi_1) + P_2 I_{0^+}^{\omega-\sigma_2,\Psi}\check{h}(\xi_2) - I_{0^+}^{\varrho,\Psi}\hat{h}(1)\Big) \\ + \Delta_1 Q_1 I_{0^+}^{\varrho+\omega_1,\Psi}\hat{h}(\eta_1) + \Delta_1 Q_2 I_{0^+}^{\varrho+\omega_2,\Psi}\hat{h}(\eta_2) - \Delta_1 I_{0^+}^{\omega,\Psi}\check{h}(1)\Bigg], \end{aligned} \tag{7}$$

and

$$\begin{aligned} \chi(\varsigma) = I_{0^+}^{\omega,\Psi}\check{h}(\varsigma) + \frac{(\Psi(\varsigma) - \Psi(0))^{\omega-1}}{\Lambda}\Bigg[\frac{Q_1}{k_1} I_{0^+}^{\varrho+\omega_1,\Psi}\hat{h}(\eta_1) + \frac{Q_2}{k_1} I_{0^+}^{\varrho+\omega_2,\Psi}\hat{h}(\eta_2) - \frac{1}{k_1} I_{0^+}^{\omega,\Psi}\check{h}(1) \\ + \Delta_2 P_1 I_{0^+}^{\omega-\sigma_1,\Psi}\check{h}(\xi_1) + \Delta_2 P_2 I_{0^+}^{\omega-\sigma_2,\Psi}\check{h}(\xi_2) - \Delta_2 I_{0^+}^{\varrho,\Psi}\hat{h}(1)\Bigg], \end{aligned} \tag{8}$$

where

$$\Delta_1 = \frac{P_1\Gamma(\omega)}{\Gamma(\omega-\sigma_1)}(\Psi(\xi_1) - \Psi(0))^{\omega-\sigma_1-1} + \frac{P_2\Gamma(\omega)}{\Gamma(\omega-\sigma_2)}(\Psi(\xi_2) - \Psi(0))^{\omega-\sigma_2-1}, \tag{9}$$

$$\Delta_2 = \frac{Q_1\Gamma(\varrho)}{\Gamma(\varrho+\omega_1)}(\Psi(\eta_1) - \Psi(0))^{\varrho+\omega_1-1} + \frac{Q_2\Gamma(\varrho)}{\Gamma(\varrho+\omega_2)}(\Psi(\eta_2) - \Psi(0))^{\varrho+\omega_2-1}, \tag{10}$$

$$\Lambda = (\Psi(1) - \Psi(0))^{\varrho-1}(\Psi(1) - \Psi(0))^{\omega-1} - \Delta_2\Delta_1, \tag{11}$$

$$k_1 = (\Psi(1) - \Psi(0))^{1-\varrho}, \tag{12}$$

with $\Lambda \neq 0$ and $k_1 \neq 0$.

Proof. The first implication: (6) implies (7) and (8).

Suppose that (ϑ, χ) is the solution (6). Applying $I_{0^+}^{\varrho,\Psi}$ and $I_{0^+}^{\omega,\Psi}$ on the first and second $D_{0^+}^{\varrho,\Psi}$ FDEs in (6), respectively, and by Lemma 1, we find

$$\vartheta(\varsigma) = I_{0^+}^{\varrho,\Psi}\hat{h}(\varsigma) + a_1(\Psi(\varsigma) - \Psi(0))^{\varrho-1} + a_2(\Psi(\varsigma) - \Psi(0))^{\varrho-2}, \tag{13}$$

$$\chi(\varsigma) = I_{0^+}^{\omega,\Psi}\check{h}(\varsigma) + b_1(\Psi(\varsigma) - \Psi(0))^{\omega-1} + b_2(\Psi(\varsigma) - \Psi(0))^{\omega-2}, \tag{14}$$

with constants a_1, a_2, b_1, and b_2. By exploiting the boundary conditions $\vartheta(0) = 0$ and $\chi(0) = 0$ in (13) and (14), we obtain $a_2 = 0$ and $b_2 = 0$. By using the Ψ–RL fractional integral and derivative of order δ_1 and δ_2, respectively, with $\delta_1 \in \{\omega_1, \omega_2\}$, $\delta_2 \in \{\sigma_1, \sigma_2\}$, we obtain

$$I_{0^+}^{\delta_1,\Psi}\vartheta(\eta_1) = I_{0^+}^{\varrho+\delta_1,\Psi}\hat{h}(\eta_1) + a_1\frac{\Gamma(\varrho)}{\Gamma(\varrho+\delta_1)}(\Psi(\eta_1) - \Psi(0))^{\varrho+\delta_1-1},$$

and

$$D_{0^+}^{\delta_2,\Psi}\chi(\xi_1) = I_{0^+}^{\omega-\delta_2,\Psi}\check{h}(\xi_1) + b_1\frac{\Gamma(\omega)}{\Gamma(\omega-\delta_2)}(\Psi(\xi_1) - \Psi(0))^{\omega-\delta_2-1}.$$

$$\vartheta(1) = P_1 D_{0^+}^{\sigma_1,\Psi}\chi(\xi_1) + P_2 D_{0^+}^{\sigma_2,\Psi}\chi(\xi_2), \quad P_1, P_2 \in \mathbb{R}.$$

By replacing the values $\delta_1 = \omega_1$, $\delta_1 = \omega_2$, $\delta_2 = \sigma_1$, and $\delta_2 = \sigma_2$ and using the second condition of (6), we obtain

$$I_{0^+}^{\varrho,\Psi}\hat{h}(1) + a_1(\Psi(1) - \Psi(0))^{\varrho-1} = P_1 I_{0^+}^{\omega-\sigma_1,\Psi}\check{h}(\xi_1) + P_2 I_{0^+}^{\omega-\sigma_2,\Psi}\check{h}(\xi_2) + b_1\Delta_1, \tag{15}$$

and

$$I_{0^+}^{\omega,\Psi}\check{h}(1) + b_1(\Psi(1) - \Psi(0))^{\omega-1} = Q_1 I_{0^+}^{\varrho+\omega_1,\Psi}\hat{h}(\eta_1) + Q_2 I_{0^+}^{\varrho+\omega_2,\Psi}\hat{h}(\eta_2) + a_1\Delta_2, \tag{16}$$

where Δ_1 and Δ_2 are defined in (9) and (10), respectively, which leads to

$$\begin{aligned} a_1 =& (\Delta_1\Delta_2 + \Lambda)\frac{P_1 I_{0^+}^{\omega-\sigma_1,\Psi}\check{h}(\xi_1) + P_2 I_{0^+}^{\omega-\sigma_2,\Psi}\check{h}(\xi_2) - I_{0^+}^{\varrho,\Psi}\hat{h}(1)}{(\Psi(1) - \Psi(0))^{\varrho-1}\Lambda} \\ &+ \frac{\Delta_1 Q_2}{\Lambda} I_{0^+}^{\varrho+\omega_1,\Psi}\hat{h}(\eta_1) + \frac{\Delta_1 Q_2}{\Lambda} I_{0^+}^{\varrho+\omega_2,\Psi}\hat{h}(\eta_2) - \frac{\Delta_1 I_{0^+}^{\omega,\Psi}\check{h}(1)}{\Lambda}, \end{aligned}$$

and

$$\begin{aligned} b_1 =& \quad \frac{(\Psi(1)-\Psi(0))^{\varrho-1}Q_1}{\Lambda} I_{0^+}^{\varrho+\omega_1,\Psi}\hat{h}(\eta_1) + \frac{(\Psi(1)-\Psi(0))^{\varrho-1}Q_2}{\Lambda} I_{0^+}^{\varrho+\omega_2,\Psi}\hat{h}(\eta_2) \\ &- \frac{(\Psi(1)-\Psi(0))^{\varrho-1} I_{0^+}^{\omega,\Psi}\check{h}(1)}{\Lambda} + \frac{\Delta_2 P_1 I_{0^+}^{\omega-\sigma_1,\Psi}\check{h}(\xi_1) + \Delta_2 P_2 I_{0^+}^{\omega-\sigma_2,\Psi}\check{h}(\xi_2) - \Delta_2 I_{0^+}^{\varrho,\Psi}\hat{h}(1)}{\Lambda}. \end{aligned}$$

Upon substituting the prescribed values for the constants a_1 and b_1 into Equations (13) and (14), we derive Equations (7) and (8).

The reverse implication: (7) and (8) implies (6)

We have

$$\begin{aligned}\vartheta(\varsigma) &= I_{0^+}^{\varrho,\Psi}\hat{h}(\varsigma) + \frac{(\Psi(\varsigma)-\Psi(0))^{\varrho-1}}{\Lambda} \\ &\times \left[k_1(\Delta_1\Delta_2+\Lambda)\Big(P_1 I_{0^+}^{\omega-\sigma_1,\Psi}\check{h}(\xi_1) + P_2 I_{0^+}^{\omega-\sigma_2,\Psi}\check{h}(\xi_2) - I_{0^+}^{\varrho,\Psi}\hat{h}(1)\Big)\right. \\ &+ \left.\Delta_1 Q_1 I_{0^+}^{\varrho+\omega_1,\Psi}\hat{h}(\eta_1) + \Delta_1 Q_2 I_{0^+}^{\varrho+\omega_2,\Psi}\hat{h}(\eta_2) - \Delta_1 I_{0^+}^{\omega,\Psi}\check{h}(1)\right], \end{aligned} \tag{17}$$

and

$$\begin{aligned}\chi(\varsigma) &= I_{0^+}^{\omega,\Psi}\check{h}(\varsigma) + \frac{(\Psi(\varsigma)-\Psi(0))^{\omega-1}}{\Lambda}\left[\frac{Q_1}{k_1} I_{0^+}^{\varrho+\omega_1,\Psi}\hat{h}(\eta_1) + \frac{Q_2}{k_1} I_{0^+}^{\varrho+\omega_2,\Psi}\hat{h}(\eta_2)\right. \\ &- \left.\frac{1}{k_1} I_{0^+}^{\omega,\Psi}\check{h}(1) + \Delta_2 P_1 I_{0^+}^{\omega-\sigma_1,\Psi}\check{h}(\xi_1) + \Delta_2 P_2 I_{0^+}^{\omega-\sigma_2,\Psi}\check{h}(\xi_2) - \Delta_2 I_{0^+}^{\varrho,\Psi}\hat{h}(1)\right], \end{aligned} \tag{18}$$

By using the Ψ–RL fractional derivative of order ϱ and ω on Equations (17) and (18), respectively, we obtain

$$\begin{cases} D_{0^+}^{\varrho,\Psi}\vartheta(\varsigma) &= \hat{h}(\varsigma), \quad \varsigma \in \mathcal{O} = [0,1], \\ D_{0^+}^{\omega,\Psi}\chi(\varsigma) &= \check{h}(\varsigma), \quad \varsigma \in \mathcal{O} = [0,1]. \end{cases} \tag{19}$$

We now check that the integral equations satisfy all three conditions.

1. From (17), we obtain $\vartheta_1(0) = 0$.
2. For the second condition

$$\vartheta(1) = P_1 D_{0^+}^{\sigma_1,\Psi}\chi(\xi_1) + P_2 D_{0^+}^{\sigma_2,\Psi}\chi(\xi_2). \tag{20}$$

From Equation (17), we have

$$\begin{aligned}\vartheta(1) &= I_{0^+}^{\varrho,\Psi}\hat{h}(1) + \frac{(\Psi(1)-\Psi(0))^{\varrho-1}}{\Lambda} \\ &\times \left[k_1(\Delta_1\Delta_2+\Lambda)\Big(P_1 I_{0^+}^{\omega-\sigma_1,\Psi}\check{h}(\xi_1) + P_2 I_{0^+}^{\omega-\sigma_2,\Psi}\check{h}(\xi_2) - I_{0^+}^{\varrho,\Psi}\hat{h}(1)\Big)\right. \\ &+ \left.\Delta_1 Q_1 I_{0^+}^{\varrho+\omega_1,\Psi}\hat{h}(\eta_1) + \Delta_1 Q_2 I_{0^+}^{\varrho+\omega_2,\Psi}\hat{h}(\eta_2) - \Delta_1 I_{0^+}^{\omega,\Psi}\check{h}(1)\right]. \end{aligned} \tag{21}$$

Conversely, by using the Ψ–RL fractional derivative of order σ_1 and σ_2 on Equation (18), we obtain

$$\begin{aligned} D_{0^+}^{\sigma_1,\Psi}\chi(\xi_1) &= I_{0^+}^{\omega-\sigma_1,\Psi}\check{h}(\xi_1) + \frac{\Gamma(\omega)}{\Gamma(\omega-\sigma_1)}(\Psi(\xi_1)-\Psi(0))^{\omega-\sigma_1-1} \\ &\times \left[\frac{(\Psi(1)-\Psi(0))^{\varrho-1}Q_1}{\Lambda} I_{0^+}^{\varrho+\omega_1,\Psi}\hat{h}(\eta_1) + \frac{(\Psi(1)-\Psi(0))^{\varrho-1}Q_2}{\Lambda} I_{0^+}^{\varrho+\omega_2,\Psi}\hat{h}(\eta_2)\right. \\ &- \left.\frac{(\Psi(1)-\Psi(0))^{\varrho-1} I_{0^+}^{\omega,\Psi}\check{h}(1)}{\Lambda} + \frac{\Delta_2 P_1 I_{0^+}^{\omega-\sigma_1,\Psi}\check{h}(\xi_1) + \Delta_2 P_2 I_{0^+}^{\omega-\sigma_2,\Psi}\check{h}(\xi_2) - \Delta_2 I_{0^+}^{\varrho,\Psi}\hat{h}(1)}{\Lambda}\right], \end{aligned} \tag{22}$$

and

$$D_{0^+}^{\sigma_2,\Psi}\chi(\xi_2) = I_{0^+}^{\omega-\sigma_2,\Psi}\check{h}(\xi_2) + \frac{\Gamma(\omega)}{\Gamma(\omega-\sigma_2)}(\Psi(\xi_2)-\Psi(0))^{\omega-\sigma_1-1} \tag{23}$$
$$\times\left[\frac{(\Psi(1)-\Psi(0))^{\varrho-1}Q_1}{\Lambda}I_{0^+}^{\varrho+\omega_1,\Psi}\hat{h}(\eta_1) + \frac{(\Psi(1)-\Psi(0))^{\varrho-1}Q_2}{\Lambda}I_{0^+}^{\varrho+\omega_2,\Psi}\hat{h}(\eta_2)\right.$$
$$\left. - \frac{(\Psi(1)-\Psi(0))^{\varrho-1}I_{0^+}^{\omega,\Psi}\check{h}(1)}{\Lambda} + \frac{\Delta_2P_1I_{0^+}^{\omega-\sigma_1,\Psi}\check{h}(\xi_1)+\Delta_2P_2I_{0^+}^{\omega-\sigma_2,\Psi}\check{h}(\xi_2)-\Delta_2I_{0^+}^{\varrho,\Psi}\hat{h}(1)}{\Lambda}\right].$$

Substituting the value of $D_{0^+}^{\sigma_1,\Psi}\chi(\xi_1)$ and $D_{0^+}^{\sigma_2,\Psi}\chi(\xi_2)$ into the following equation

$$P_1D_{0^+}^{\sigma_1,\Psi}\chi(\xi_1) + P_2D_{0^+}^{\sigma_2,\Psi}\chi(\xi_2) = P_1I_{0^+}^{\omega-\sigma_1,\Psi}\check{h}(\xi_1) + \frac{P_1\Gamma(\omega)}{\Gamma(\omega-\sigma_1)}(\Psi(\xi_1)-\Psi(0))^{\omega-\sigma_1-1} \tag{24}$$
$$\times\left[\frac{(\Psi(1)-\Psi(0))^{\varrho-1}Q_1}{\Lambda}I_{0^+}^{\varrho+\omega_1,\Psi}\hat{h}(\eta_1) + \frac{(\Psi(1)-\Psi(0))^{\varrho-1}Q_2}{\Lambda}I_{0^+}^{\varrho+\omega_2,\Psi}\hat{h}(\eta_2)\right.$$
$$\left. - \frac{(\Psi(1)-\Psi(0))^{\varrho-1}I_{0^+}^{\omega,\Psi}\check{h}(1)}{\Lambda} + \frac{\Delta_2P_1I_{0^+}^{\omega-\sigma_1,\Psi}\check{h}(\xi_1)+\Delta_2P_2I_{0^+}^{\omega-\sigma_2,\Psi}\check{h}(\xi_2)-\Delta_2I_{0^+}^{\varrho,\Psi}\hat{h}(1)}{\Lambda}\right]$$
$$+ P_2I_{0^+}^{\omega-\sigma_2,\Psi}\check{h}(\xi_2) + \frac{P_2\Gamma(\omega)}{\Gamma(\omega-\sigma_2)}(\Psi(\xi_2)-\Psi(0))^{\omega-\sigma_1-1}$$
$$\times\left[\frac{(\Psi(1)-\Psi(0))^{\varrho-1}Q_1}{\Lambda}I_{0^+}^{\varrho+\omega_1,\Psi}\hat{h}(\eta_1) + \frac{(\Psi(1)-\Psi(0))^{\varrho-1}Q_2}{\Lambda}I_{0^+}^{\varrho+\omega_2,\Psi}\hat{h}(\eta_2)\right.$$
$$\left. - \frac{(\Psi(1)-\Psi(0))^{\varrho-1}I_{0^+}^{\omega,\Psi}\check{h}(1)}{\Lambda} + \frac{\Delta_2P_1I_{0^+}^{\omega-\sigma_1,\Psi}\check{h}(\xi_1)+\Delta_2P_2I_{0^+}^{\omega-\sigma_2,\Psi}\check{h}(\xi_2)-\Delta_2I_{0^+}^{\varrho,\Psi}\hat{h}(1)}{\Lambda}\right].$$

Simplifying Equation (24), we obtain

$$\begin{aligned}
&P_1D_{0^+}^{\sigma_1,\Psi}\chi(\xi_1)+P_2D_{0^+}^{\sigma_2,\Psi}\chi(\xi_2)\\
&\qquad= I_{0^+}^{\varrho,\Psi}\hat{h}(1) + \frac{(\Psi(1)-\Psi(0))^{\varrho-1}}{\Lambda}\\
&\qquad\times\left[k_1(\Delta_1\Delta_2+\Lambda)\Big(P_1I_{0^+}^{\omega-\sigma_1,\Psi}\check{h}(\xi_1)+P_2I_{0^+}^{\omega-\sigma_2,\Psi}\check{h}(\xi_2)-I_{0^+}^{\varrho,\Psi}\hat{h}(1)\Big)\right.\\
&\qquad\left.+\Delta_1Q_1I_{0^+}^{\varrho+\omega_1,\Psi}\hat{h}(\eta_1)+\Delta_1Q_2I_{0^+}^{\varrho+\omega_2,\Psi}\hat{h}(\eta_2)-\Delta_1I_{0^+}^{\omega,\Psi}\check{h}(1)\right]\\
&\qquad=\vartheta(1).
\end{aligned}$$

3. Similarly, we obtain

$$\chi(0)=0,\ \chi(1)=Q_1I_{0^+}^{\omega_1,\Psi}\vartheta(\eta_1)+Q_2I_{0^+}^{\omega_2,\Psi}\vartheta(\eta_2).$$

Hence, the proof is completed.

A series of computations demonstrate that the converse aspect of the argument is valid. Hence, the proof is finalized. □

Let us consider $\mathcal{E}$ as the space of continuous functions gifted with the norm $\|\vartheta\| = \max_{\varsigma\in[0,1]}|\vartheta(\varsigma)|$. This makes $\mathcal{E}$ a Banach space. Now, if we take the Cartesian product $\mathcal{E}\times\mathcal{E}$, and define the norm on this space as $\|(\vartheta,\chi)\| = \|\vartheta\|+\|\chi\|$, we obtain another Banach space.

Using Proposition 1, we define the operator $F:\mathcal{E}\times\mathcal{E}\to\mathcal{E}\times\mathcal{E}$ as

$$F(\vartheta,\chi)(\varsigma) = (F_1(\vartheta,\chi)(\varsigma), F_2(\vartheta,\chi)(\varsigma)),$$

where

$$
\begin{aligned}
F_1(\vartheta,\chi)(\varsigma) &= I_{0^+}^{\varrho,\Psi}\hat{\ell}(\varsigma,\vartheta(\varsigma),\chi(\varsigma)) + \frac{(\Psi(\varsigma)-\Psi(0))^{\varrho-1}}{\Lambda} \\
&\times \Big[k_1(\Delta_1\Delta_2+\Lambda)\Big(P_1 I_{0^+}^{\omega-\sigma_1,\Psi}\check{\ell}(\xi_1,\vartheta(\xi_1),\chi(\xi_1)) \\
&+ P_2 I_{0^+}^{\omega-\sigma_2,\Psi}\check{\ell}(\xi_2,\vartheta(\xi_2),\chi(\xi_2)) - I_{0^+}^{\varrho,\Psi}\hat{\ell}(1,\vartheta(1),\chi(1))\Big) \\
&+ \Delta_1 Q_1 I_{0^+}^{\varrho+\omega_1,\Psi}\hat{\ell}(\eta_1,\vartheta(\eta_1),\chi(\eta_1)) \\
&+ \Delta_1 Q_2 I_{0^+}^{\varrho+\omega_2,\Psi}\hat{\ell}(\eta_2,\vartheta(\eta_2),\chi(\eta_2)) - \Delta_1 I_{0^+}^{\omega,\Psi}\check{\ell}(1,\vartheta(1),\chi(1))\Big], \\
F_2(\vartheta,\chi)(\varsigma) &= I_{0^+}^{\omega,\Psi}\check{\ell}(\varsigma,\vartheta(\varsigma),\chi(\varsigma)) + \frac{(\Psi(\varsigma)-\Psi(0))^{\omega-1}}{\Lambda}\Big[\frac{Q_1}{k_1} I_{0^+}^{\varrho+\omega_1,\Psi}\hat{\ell}(\eta_1,\vartheta(\eta_1),\chi(\eta_1)) \\
&+ \frac{Q_2}{k_1} I_{0^+}^{\varrho+\omega_2,\Psi}\hat{\ell}(\eta_2,\vartheta(\eta_2),\chi(\eta_2)) - \frac{1}{k_1} I_{0^+}^{\omega,\Psi}\check{\ell}(1,\vartheta(1),\chi(1)) \\
&+ \Delta_2 P_1 I_{0^+}^{\omega-\sigma_1,\Psi}\check{\ell}(\xi_1,\vartheta(\xi_1),\chi(\xi_1)) \\
&+ \Delta_2 P_2 I_{0^+}^{\omega-\sigma_2,\Psi}\check{\ell}(\xi_2,\vartheta(\xi_2),\chi(\xi_2)) - \Delta_2 I_{0^+}^{\varrho,\Psi}\hat{\ell}(1,\vartheta(1),\chi(1))\Big].
\end{aligned}
$$

It is worth noting that the problem of finding a fixed point (ϑ,χ) satisfying $F(\vartheta,\chi)=(\vartheta,\chi)$ is equivalent to the nonlinear problem represented by Equations (4) and (5). To simplify the computational process, we introduce the following notation for the sake of convenience:

$$
\begin{aligned}
R_1 &= \frac{(\Psi(1)-\Psi(0))^{\varrho}}{\Gamma(\varrho+1)} + \frac{(\Psi(1)-\Psi(0))^{\varrho-1}}{|\Lambda|}\Big[k_1(|\Delta_1\Delta_2|+|\Lambda|)\frac{(\Psi(1)-\Psi(0))^{\varrho}}{\Gamma(\varrho+1)} \\
&+ |\Delta_1||Q_1|\frac{(\Psi(1)-\Psi(0))^{\varrho+\omega_1}}{\Gamma(\varrho+\omega_1+1)} + \Delta_1|Q_2|\frac{(\Psi(1)-\Psi(0))^{\varrho+\omega_2}}{\Gamma(\varrho+\omega_2+1)}\Big], \\
R_2 &= k_1(|\Delta_1\Delta_2|+|\Lambda|)\Big(|P_1|\frac{(\Psi(1)-\Psi(0))^{\omega-\sigma_1}}{\Gamma(\omega-\sigma_1+1)} + |P_2|\frac{(\Psi(1)-\Psi(0))^{\omega-\sigma_2}}{\Gamma(\omega-\sigma_2+1)}\Big) \\
&+ |\Delta_1|\frac{(\Psi(1)-\Psi(0))^{\omega}}{\Gamma(\omega+1)}, \\
R_3 &= \frac{(\Psi(1)-\Psi(0))^{\omega}}{\Gamma(\omega+1)} + \frac{(\Psi(1)-\Psi(0))^{\omega-1}}{|\Lambda|}\Big(\frac{1}{k_1}\frac{(\Psi(1)-\Psi(0))^{\omega}}{\Gamma(\omega+1)} \\
&+ |\Delta_2 P_1|\frac{(\Psi(1)-\Psi(0))^{\omega-\sigma_1}}{\Gamma(\omega-\sigma_1+1)} + |\Delta_2 P_2|\frac{(\Psi(1)-\Psi(0))^{\omega-\sigma_2}}{\Gamma(\omega-\sigma_2+1)}\Big), \\
R_4 &= \frac{(\Psi(1)-\Psi(0))^{\omega-1}}{|\Lambda|}\Big[\frac{|Q_1|}{k_1}\frac{(\Psi(1)-\Psi(0))^{\varrho+\omega_1}}{\Gamma(\varrho+\omega_1+1)} + \frac{|Q_2|}{k_1}\frac{(\Psi(1)-\Psi(0))^{\varrho+\omega_2}}{\Gamma(\varrho+\omega_2+1)} \\
&+ |\Delta_2|\frac{(\Psi(1)-\Psi(0))^{\varrho}}{\Gamma(\varrho+1)}\Big].
\end{aligned} \tag{25}
$$

3. Results of Existence and Uniqueness

Here, we utilize Banach and Krasnoselskii fixed-point theorems and the Leray–Schauder nonlinear alternative (referenced as [33]) to to establish our main results of the existence and uniqueness ($\mathbb{E}.\mathbb{U}$). Together, these two powerful fixed-point theorems provide a solid theoretical foundation for analyzing and characterizing the solutions of (4) and (5).

Theorem 4. *Let $\hat{\ell}, \check{\ell} : [0,1] \times \mathbb{R}^2 \to \mathbb{R}$ satisfy the Lipschitz condition, that is, for all $\varsigma \in [0,1]$ and $\wp_i, \wp_i^* \in \mathbb{R}$, $i = 1,2$,*

$$\begin{aligned} |\hat{\ell}(z, \wp_1, \wp_2) - \hat{\ell}(z, \wp_1^*, \wp_2^*)| &\leq m_1|\wp_1 - \wp_1^*| + m_2|\wp_2 - \wp_2^*|, \\ |\check{\ell}(z, \wp_1, \wp_2) - \check{\ell}(z, \wp_1^*, \wp_2^*)| &\leq n_1|\wp_1 - \wp_1^*| + n_2|\wp_2 - \wp_2^*|, \end{aligned} \tag{26}$$

with real constants $m_i, n_i, i = 1,2$. In addition, we assume that

$$1 > (R_2 + R_3)(n_1 + n_2) + (R_1 + R_4)(m_1 + m_2), \tag{27}$$

where $R_i, i \in \{1,2,3,4\}$, are expressed by (25). Thus, the fractional boundary value problem (FBVP) (4) and (5) admits only one solution on $[0,1]$.

Proof. We define the set $\mathcal{B}_r = \{(\vartheta, \chi) \in \mathcal{E} \times \mathcal{E} : \|(\vartheta, \chi)\|| < r\}$, such that

$$\frac{(R_1 + R_4)D_1 + (R_2 + R_3)D_2}{1 - (R_2 + R_3)(n_1 + n_2) - (R_1 + R_4)(m_1 + m_2)} \leq r,$$

$$\sup_{\varsigma \in [0,1]} |\hat{\ell}(\varsigma, 0, 0)| = D_1 < \infty \text{ and } \sup_{\varsigma \in [0,1]} |\check{\ell}(\varsigma, 0, 0)| = D_2 < \infty. \tag{28}$$

Then, under the assumptions (26) and (28), taking (ϑ, χ), we obtain

$$\begin{aligned} & |F_1(\vartheta, \chi)(\varsigma)| \\ \leq\ & I_{0^+}^{\varrho, \Psi}\left[|\hat{\ell}(\varsigma, \vartheta(\varsigma), \chi(\varsigma)) - \hat{\ell}(\varsigma, 0, 0)| + |\hat{\ell}(\varsigma, 0, 0)|\right] \\ +\ & \frac{(\Psi(\varsigma) - \Psi(0))^{\varrho - 1}}{|\Lambda|}\Bigg[k_1(|\Delta_1\Delta_2| + |\Lambda|)\Big(|P_1| I_{0^+}^{\omega - \sigma_1, \Psi}\left[|\check{\ell}(\xi_1, \vartheta(\xi_1), \chi(\xi_1))\right. \\ -\ & \left.(\xi_1, 0, 0)| + |(\xi_1, 0, 0)|\right] \\ +\ & |P_2| I_{0^+}^{\omega - \sigma_2, \Psi}\left[|\check{\ell}(\xi_2, \vartheta(\xi_2), \chi(\xi_2)) - (\xi_2, 0, 0)| + |(\xi_2, 0, 0)|\right] \\ +\ & I_{0^+}^{\varrho, \Psi}\left[\hat{\ell}(1, \vartheta(1), \chi(1)) - \hat{\ell}(1, 0, 0) + \hat{\ell}(1, 0, 0)\right]\Big) \\ +\ & |\Delta_1 Q_1| I_{0^+}^{\varrho + \omega_1, \Psi}\left[|\hat{\ell}(\eta_1, \vartheta(\eta_1), \chi(\eta_1)) - (\eta_1, 0, 0)| + |(\eta_1, 0, 0)|\right] \\ +\ & |\Delta_1 Q_2| I_{0^+}^{\varrho + \omega_2, \Psi}\left[|\hat{\ell}(\eta_2, \vartheta(\eta_2), \chi(\eta_2)) - (\eta_2, 0, 0)| + |(\eta_2, 0, 0)|\right] \\ +\ & |\Delta_1| I_{0^+}^{\omega, \Psi}\left[|\check{\ell}(1, \vartheta(1), \chi(1)) - \check{\ell}(1, 0, 0)| + |\check{\ell}(1, 0, 0)|\right]\Bigg] \\ \leq\ & \frac{(\Psi(1) - \Psi(0))^{\varrho}}{\Gamma(\varrho + 1)}(m_1\|\vartheta\| + m_2\|\chi\| + D_1) \\ +\ & \frac{(\Psi(1) - \Psi(0))^{\varrho - 1}}{|\Lambda|}\Bigg[k_1(|\Delta_1\Delta_2| + |\Lambda|)\Big(|P_1|\frac{(\Psi(1) - \Psi(0))^{\omega - \sigma_1}}{\Gamma(\omega - \sigma_1 + 1)}(n_1\|\vartheta\| + n_2\|\chi\| + D_2) \\ +\ & |P_2|\frac{(\Psi(1) - \Psi(0))^{\omega - \sigma_2}}{\Gamma(\omega - \sigma_2 + 1)}(n_1\|\vartheta\| + n_2\|\chi\| + D_2) + \frac{(\Psi(1) - \Psi(0))^{\varrho}}{\Gamma(\varrho + 1)} \\ \times\ & (m_1\|\vartheta\| + m_2\|\chi\| + D_1)\Big) + |\Delta_1 Q_1|\frac{(\Psi(1) - \Psi(0))^{\varrho + \omega_1}}{\Gamma(\varrho + \omega_1 + 1)}(m_1\|\vartheta\| + m_2\|\chi\| + D_1) \\ +\ & |\Delta_1 Q_2|\frac{(\Psi(1) - \Psi(0))^{\varrho + \omega_2}}{\Gamma(\varrho + \omega_2 + 1)}(m_1\|\vartheta\| + m_2\|\chi\| + D_1) \end{aligned}$$

$$
\begin{aligned}
&+ \quad |\Delta_1|\frac{(\Psi(1)-\Psi(0))^{\omega}}{\Gamma(\omega+1)}(n_1\|\vartheta\|+n_2\|\chi\|+D_2)\Big]\\
&= \quad \Big[\frac{(\Psi(1)-\Psi(0))^{\varrho}}{\Gamma(\varrho+1)}+\frac{(\Psi(1)-\Psi(0))^{\varrho-1}}{|\Lambda|}\Big[k_1(|\Delta_1\Delta_2|+|\Lambda|)\frac{(\Psi(1)-\Psi(0))^{\varrho}}{\Gamma(\varrho+1)}\\
&+ \quad |\Delta_1 Q_1|\frac{(\Psi(1)-\Psi(0))^{\varrho+\omega_1}}{\Gamma(\varrho+\omega_1+1)}+|\Delta_1 Q_2|\frac{(\Psi(1)-\Psi(0))^{\varrho+\omega_2}}{\Gamma(\varrho+\omega_2+1)}\Big]\Big](m_1\|\vartheta\|+m_2\|\chi\|+D_1)\\
&+ \quad \frac{(\Psi(1)-\Psi(0))^{\varrho-1}}{|\Lambda|}\Big[k_1(|\Delta_1\Delta_2|+|\Lambda|)\Big(|P_1|\frac{(\Psi(1)-\Psi(0))^{\omega-\sigma_1}}{\Gamma(\omega-\sigma_1+1)}\\
&+ \quad |P_2|\frac{(\Psi(1)-\Psi(0))^{\omega-\sigma_2}}{\Gamma(\omega-\sigma_2+1)}\Big)+|\Delta_1|\frac{(\Psi(1)-\Psi(0))^{\omega}}{\Gamma(\omega+1)}\Big](n_1\|\vartheta\|+n_2\|\chi\|+D_2)\\
&= \quad R_1(m_1\|\vartheta\|+m_2\|\chi\|+D_1)+R_2(n_1\|\vartheta\|+n_2\|\chi\|+D_2)\\
&\leq \quad (R_1m_1+R_2n_1+R_1m_2+R_2n_2)r+R_1D_1+R_2D_2.
\end{aligned}
$$

Analogously, we have

$$
\begin{aligned}
&\quad |F_2(\vartheta,\chi)(\varsigma)|\\
&\leq \quad \frac{(\Psi(1)-\Psi(0))^{\omega}}{\Gamma(\omega+1)}(n_1\|\vartheta\|+n_2\|\chi\|+D_2)+\frac{(\Psi(1)-\Psi(0))^{\omega-1}}{|\Lambda|}\\
&\quad \Big[\frac{|Q_1|}{k_1}\frac{(\Psi(1)-\Psi(0))^{\varrho+\omega_1}}{\Gamma(\varrho+\omega_1+1)}(m_1\|\vartheta\|+m_2\|\chi\|+D_1)\\
&+ \quad \frac{|Q_2|}{k_1}\frac{(\Psi(1)-\Psi(0))^{\varrho+\omega_2}}{\Gamma(\varrho+\omega_2+1)}(m_1\|\vartheta\|+m_2\|\chi\|+D_1)\\
&+ \quad \frac{1}{k_1}\frac{(\Psi(1)-\Psi(0))^{\omega}}{\Gamma(\omega+1)}(n_1\|\vartheta\|+n_2\|\chi\|+D_2)\\
&+ \quad |\Delta_2P_1|\frac{(\Psi(1)-\Psi(0))^{\omega-\sigma_1}}{\Gamma(\omega-\sigma_1+1)}(n_1\|\vartheta\|+n_2\|\chi\|+D_2)\\
&+ \quad |\Delta_2P_2|\frac{(\Psi(1)-\Psi(0))^{\omega-\sigma_2}}{\Gamma(\omega-\sigma_2+1)}(n_1\|\vartheta\|+n_2\|\chi\|+D_2)\\
&+ \quad |\Delta_2|\frac{(\Psi(1)-\Psi(0))^{\varrho}}{\Gamma(\varrho+1)}(m_1\|\vartheta\|+m_2\|\chi\|+D_1)\Big]\\
&= \quad \Big[\frac{(\Psi(1)-\Psi(0))^{\omega}}{\Gamma(\omega+1)}+\frac{(\Psi(1)-\Psi(0))^{\omega-1}}{|\Lambda|}\Big(\frac{1}{k_1}\frac{(\Psi(1)-\Psi(0))^{\omega}}{\Gamma(\omega+1)}\\
&+ \quad |\Delta_2P_1|\frac{(\Psi(1)-\Psi(0))^{\omega-\sigma_1}}{\Gamma(\omega-\sigma_1+1)}\\
&+ \quad |\Delta_2P_2|\frac{(\Psi(1)-\Psi(0))^{\omega-\sigma_2}}{\Gamma(\omega-\sigma_2+1)}\Big)\Big](n_1\|\vartheta\|+n_2\|\chi\|+D_2)\\
&+ \quad \frac{(\Psi(1)-\Psi(0))^{\omega-1}}{|\Lambda|}\Big[\frac{|Q_1|}{k_1}\frac{(\Psi(1)-\Psi(0))^{\varrho+\omega_1}}{\Gamma(\varrho+\omega_1+1)}\\
&+ \quad \frac{|Q_2|}{k_1}\frac{(\Psi(1)-\Psi(0))^{\varrho+\omega_2}}{\Gamma(\varrho+\omega_2+1)}+|\Delta_2|\frac{(\Psi(1)-\Psi(0))^{\varrho}}{\Gamma(\varrho+1)}\Big](m_1\|\vartheta\|+m_2\|\chi\|+D_1)\\
&= \quad R_3(n_1\|\vartheta\|+n_2\|\chi\|+D_2)+R_4(m_1\|\vartheta\|+m_2\|\chi\|+D_1)\\
&\leq \quad (R_3n_1+R_4m_1+R_3n_2+R_4m_2)r+R_3D_2+R_4D_1.
\end{aligned}
$$

We obtain

$$\begin{aligned}\|F(\vartheta,\chi)\| &= \|\Big(F_1(\vartheta,\chi),F_2(\vartheta,\chi)\Big)\| = \|F_1(\vartheta,\chi)\| + \|F_2(\vartheta,\chi)\| \\ &\leq \Big[(R_2+R_3)(n_1+n_2)+(R_1+R_4)(m_1+m_2)\Big]r \\ &\quad + (R_1+R_4)D_1 + (R_2+R_3)D_2 \leq r,\end{aligned}$$

which yields that $F(\mathcal{B}_r) \subseteq \mathcal{B}_r$, and since $(\vartheta,\chi) \in \mathcal{B}_r$ is an arbitrary element. Conversely, for (ϑ_1,χ_1), $(\vartheta_2,\chi_2) \in \mathcal{E}\times\mathcal{E}$ and $\varsigma \in [0,1]$, we obtain

$$\begin{aligned}&|F_1(\vartheta_2,\chi_2)(\varsigma) - F_1(\vartheta_1,\chi_1)(\varsigma)| \\ \leq\ & I_{0^+}^{\varrho,\Psi}(|\hat{\ell}(\varsigma,\vartheta_2(\varsigma),\chi_2(\varsigma)) - \hat{\ell}(\varsigma,\vartheta_1(\varsigma),\chi_1(\varsigma))|) \\ +\ & \frac{(\Psi(\varsigma)-\Psi(0))^{\varrho-1}}{|\Lambda|}\Big[k_1(|\Delta_1\Delta_2|+|\Lambda|)\Big(|P_1|I_{0^+}^{\omega-\sigma_1,\Psi}(|\check{\ell}(\xi_1,\vartheta_2(\xi_1),\chi_2(\xi_1)) \\ -\ & \check{\ell}(\xi_1,\vartheta_1(\xi_1),\chi_1(\xi_1))|) + |P_2|I_{0^+}^{\omega-\sigma_2,\Psi}(|\check{\ell}(\xi_2,\vartheta_2(\xi_1),\chi_2(\xi_2)) - \check{\ell}(\xi_2,\vartheta_1(\xi_1),\chi_1(\xi_2))|) \\ +\ & I_{0^+}^{\varrho,\Psi}(|\hat{\ell}(1,\vartheta_2(1),\chi_2(1)) - \hat{\ell}(1,\vartheta_1(1),\chi_1(1))|)\Big) \\ +\ & |\Delta_1 Q_1|I_{0^+}^{\varrho+\omega_1,\Psi}(|\hat{\ell}(\eta_1,\vartheta_2(\eta_1),\chi_2(\eta_1)) - \hat{\ell}(\eta_1,\vartheta_1(\eta_1),\chi_1(\eta_1))|) \\ +\ & |\Delta_1 Q_2|I_{0^+}^{\varrho+\omega_2,\Psi}(|\hat{\ell}(\eta_2,\vartheta_2(\eta_2),\chi_2(\eta_2)) - \hat{\ell}(\eta_2,\vartheta_1(\eta_2),\chi_1(\eta_2))|) \\ +\ & |\Delta_1|I_{0^+}^{\omega,\Psi}(|\check{\ell}(1,\vartheta_2(1),\chi_2(1)) - \check{\ell}(1,\vartheta_1(1),\chi_1(1))|)\Big] \\ \leq\ & (R_1m_1+R_2n_1)\|\vartheta_2-\vartheta_1\| + (R_1m_2+R_2n_2)\|\chi_2-\chi_1\|.\end{aligned}$$

Thus, we obtain

$$\begin{aligned}&\|F_1(\vartheta_2,\chi_2)(\varsigma) - F_1(\vartheta_1,\chi_1)(\varsigma)\| \\ &\qquad \leq (R_1m_1+R_2n_1+R_1m_2+R_2n_2)\big[\|\vartheta_2-\vartheta_1\| + \|\chi_2-\chi_1\|\big].\end{aligned} \tag{29}$$

Similarly, one can find that

$$\begin{aligned}&\|F_2(\vartheta_2,\chi_2)(\varsigma) - F_2(\vartheta_1,\chi_1)(\varsigma)\| \\ &\qquad \leq (R_3n_1+R_4m_1+R_3n_2+R_4m_2)\big[\|\vartheta_2-\vartheta_1\| + \|\chi_2-\chi_1\|\big].\end{aligned} \tag{30}$$

Thus, in view of (29) and (30) it follows that,

$$\begin{aligned}&\|F(\vartheta_2,\chi_2)(\varsigma) - F(\vartheta_1,\chi_1)(\varsigma)\| \\ &\qquad \leq \Big[(R_2+R_3)(n_1+n_2)+(R_1+R_4)(m_1+m_2)\Big]\big[\|\vartheta_2-\vartheta_1\| + \|\chi_2-\chi_1\|\big].\end{aligned}$$

Considering the condition (27), it can be observed that the mapping F satisfies the criteria for being a contraction. Consequently, from Banach's contraction, we conclude that F possesses a single, distinct fixed point. As a result, the problem (4) and (5) unequivocally possesses one solution within the interval $[0,1]$. □

Theorem 5. *Let $\hat{\ell},\check{\ell} \in C([0,1]\times\mathbb{R}^2,\mathbb{R})$ such that, for all $\varsigma \in [0,1]$ and $\vartheta_i,\chi_i \in \mathbb{R}$, $i \in \{1,2\}$,*

$$\begin{aligned}|\hat{\ell}(\varsigma,\vartheta_1,\chi_1)| &\leq \kappa_0 + \kappa_1|\vartheta_1| + \kappa_2|\chi_1| \\ |\check{\ell}(\varsigma,\vartheta_2,\chi_2)| &\leq \nu_0 + \nu_1|\vartheta_2| + \nu_2|\chi_2|\end{aligned} \tag{31}$$

with real constants $\kappa_i, \nu_i, i \in \{0,1,2\}$, *with* $\kappa_i, \nu_i > 0$. *Then, the System (4) and (5) has at least one solution on* $[0,1]$ *provided that*

$$(R_1+R_4)\kappa_1 + (R_2+R_3)\nu_1 < 1 \quad \textit{and} \quad (R_1+R_4)\kappa_2 + (R_2+R_3)\nu_2 < 1,$$

such that $R_i, i \in \{1,2,3,4\}$, *are given by (25).*

Proof. Note that, since $\hat{\ell}$ and $\check{\ell}$ are continuous, it follows that the mapping F is continuous as well. Moreover, we can demonstrate that F is also completely continuous.

Let us consider a bounded set S in $\mathcal{E} \times \mathcal{E}$. Thus, within this set, there exist positive constants L_1 and L_2 such that

$$|\hat{\ell}(\varsigma, \vartheta(\varsigma), \chi(\varsigma)| \leq L_1, \quad |\check{\ell}(\varsigma, \vartheta(\varsigma), \chi(\varsigma)| \leq L_2, \ \ (\vartheta, \chi) \in S.$$

Therefore, for all $(\vartheta, \chi) \in S$, we obtain

$$\begin{aligned}
|F_1(\vartheta,\chi)(\varsigma)| &\leq \Bigg[\frac{(\Psi(1)-\Psi(0))^{\varrho}}{\Gamma(\varrho+1)} + \frac{(\Psi(1)-\Psi(0))^{\varrho-1}}{|\Lambda|}\Big[k_1(|\Delta_1\Delta_2|+|\Lambda|)\frac{(\Psi(1)-\Psi(0))^{\varrho}}{\Gamma(\varrho+1)} \\
&+ |\Delta_1 Q_1|\frac{(\Psi(1)-\Psi(0))^{\varrho+\omega_1}}{\Gamma(\varrho+\omega_1+1)} + |\Delta_1 Q_2|\frac{(\Psi(1)-\Psi(0))^{\varrho+\omega_2}}{\Gamma(\varrho+\omega_2+1)}\Big]\Bigg] L_1 \\
&+ \frac{(\Psi(1)-\Psi(0))^{\varrho-1}}{|\Lambda|}\Bigg[k_1(|\Delta_1\Delta_2|+|\Lambda|)\Big(|P_1|\frac{(\Psi(1)-\Psi(0))^{\omega-\sigma_1}}{\Gamma(\omega-\sigma_1+1)} \\
&+ |P_2|\frac{(\Psi(1)-\Psi(0))^{\omega-\sigma_2}}{\Gamma(\omega-\sigma_2+1)}\Big) + |\Delta_1|\frac{(\Psi(1)-\Psi(0))^{\omega}}{\Gamma(\omega+1)}\Bigg] L_2 \\
&= R_1 L_1 + R_2 L_2,
\end{aligned}$$

which yields

$$\|F_1(\vartheta,\chi)(\varsigma)\| \leq R_1 L_1 + R_2 L_2.$$

Analogously, one can obtain

$$\|F_2(\vartheta,\chi)(\varsigma)\| \leq R_3 L_1 + R_4 L_2.$$

Hence,

$$\|F(\vartheta,\chi)(\varsigma)\| \leq (R_1+R_3) L_1 + (R_2+R_4) L_2.$$

As a result, the operator F exhibits uniform boundedness. To demonstrate the equicontinuity of F, consider ς_1 and ς_2 in the interval $[0,1]$ such that $\varsigma_1 < \varsigma_2$. Consequently, we obtain

$$\begin{aligned}
&|F_1(\vartheta,\chi)(\varsigma_2) - F_1(\vartheta,\chi)(\varsigma_1)| \\
\leq\ & \frac{1}{\Gamma(\varrho)}\Bigg|\int_0^{\varsigma_1}[\Psi(s)'(\Psi(\varsigma_2)-\Psi(s))^{\varrho-1} - \Psi(s)'(\Psi(\varsigma_1)-\Psi(s))^{\varrho-1}]\hat{\ell}(s,\vartheta(s),\chi(s))ds \\
+\ & \frac{1}{\Gamma(\varrho)}\int_{\varsigma_1}^{\varsigma_2}[\Psi(s)(\Psi(\varsigma_2)-\Psi(s))^{\varrho-1}]\hat{\ell}(s,\vartheta(s),\chi(s))ds\Bigg| \\
+\ & \frac{(\Psi(\varsigma_2)-\Psi(0))^{\varrho-1} - (\Psi(\varsigma_1)-\Psi(0))^{\varrho-1}}{|\Lambda|} \\
\times\ & \Bigg[|k_1(\Delta_1\Delta_2+\Lambda)|\Big(|P_1|I_{0^+}^{\omega-\sigma_1,\Psi}|\check{\ell}(\xi_1,\vartheta(\xi_1),\chi(\xi_1))|
\end{aligned}$$

$$
\begin{aligned}
&+ \quad |P_2| I_{0^+}^{\omega-\sigma_2,\Psi} |\check{\ell}(\xi_2, \vartheta(\xi_2), \chi(\xi_2))| + I_{0^+}^{\varrho,\Psi} |\hat{\ell}(1, \vartheta(1), \chi(1))| \Big) \\
&+ \quad |\Delta_1 Q_1| I_{0^+}^{\varrho+\omega_1,\Psi} |\hat{\ell}(\eta_1, \vartheta(\eta_1), \chi(\eta_1))| \\
&+ \quad |\Delta_1 Q_2| I_{0^+}^{\varrho+\omega_2,\Psi} |\hat{\ell}(\eta_2, \vartheta(\eta_2), \chi(\eta_2))| + |\Delta_1| I_{0^+}^{\omega,\Psi} |\check{\ell}(1, \vartheta(1), \chi(1))| \Bigg] \\
&\leq \quad \frac{L_1}{\Gamma(\varrho+1)} \Big| [2|(\Psi(\varsigma_2) - \Psi(\varsigma_1))^{\varrho-1}| + |(\Psi(\varsigma_2) - \Psi(0))^{\varrho-1} - (\Psi(\varsigma_1) - \Psi(0))^{\varrho-1}|] \\
&+ \quad \frac{(\Psi(\varsigma_2) - \Psi(0))^{\varrho-1} - (\Psi(\varsigma_1) - \Psi(0))^{\varrho-1}}{|\Lambda|} \Bigg[|k_1(\Delta_1\Delta_2 + \Lambda)| \Big(L_2|P_1| \frac{(\Psi(\xi_1) - \Psi(0))^{\omega-\sigma_1}}{\Gamma(\omega-\sigma_1+1)} \\
&+ \quad L_2|P_2| \frac{(\Psi(\xi_2) - \Psi(0))^{\omega-\sigma_2}}{\Gamma(\omega-\sigma_2+1)} + L_1 \frac{(\Psi(1) - \Psi(0))^{\varrho}}{\Gamma(\varrho+1)} \Big) + L_1|\Delta_1 Q_1| \frac{(\Psi(\xi_1) - \Psi(0))^{\varrho+\omega_1}}{\Gamma(\varrho+\omega_1+1)} \\
&+ \quad L_1|\Delta_1 Q_2| \frac{(\Psi(\xi_1) - \Psi(0))^{\varrho+\omega_2}}{\Gamma(\varrho+\omega_2+1)} + L_2|\Delta_1| \frac{(\Psi(1) - \Psi(0))^{\omega}}{\Gamma(\omega+1)} \Bigg] \to 0 \text{ as } \varsigma_2 - \varsigma_1 \to 0,
\end{aligned}
$$

independently of $(\vartheta, \chi) \in S$. Hence, $F_1(\vartheta, \chi)$ is equicontinuous. Similarly, we can establish the equicontinuity of $F_2(\vartheta, \chi)$. Hence, based on the preceding arguments, we can conclude that the operator $F(\vartheta, \chi)$ is completely continuous.

Finally, we will demonstrate that the set

$$\mathcal{D} = (\vartheta, \chi) \in \mathcal{E} \times \mathcal{E} : (\vartheta, \chi) = wF(\vartheta, \chi), 0 \leq w \leq 1,$$

is bounded. Let $(\vartheta, \chi) \in \mathcal{D}$, then $(\vartheta, \chi) = wF(\vartheta, \chi)$ for all $\varsigma \in [0, 1]$ and that

$$\vartheta(\varsigma) = wF_1(\vartheta, \chi)(\varsigma), \quad \chi(\varsigma) = wF_2(\vartheta, \chi)(\varsigma).$$

Thus, we have

$$
\begin{aligned}
|\hat{\ell}(\varsigma, \vartheta_1, \chi_1)| &\leq \kappa_0 + \kappa_1|\vartheta_1| + \kappa_2|\chi_1|, \\
|\check{\ell}(\varsigma, \vartheta_2, \chi_2)| &\leq \nu_0 + \nu_1|\vartheta_1| + \nu_2|\chi_2|,
\end{aligned}
$$

$$
\begin{aligned}
|\vartheta| \quad \leq \quad & \Bigg[\frac{(\Psi(1) - \Psi(0))^{\varrho}}{\Gamma(\varrho+1)} + \frac{(\Psi(1) - \Psi(0))^{\varrho-1}}{|\Lambda|} \Big[k_1(|\Delta_1\Delta_2| + |\Lambda|) \frac{(\Psi(1) - \Psi(0))^{\varrho}}{\Gamma(\varrho+1)} \\
&+ \quad |\Delta_1 Q_1| \frac{(\Psi(1) - \Psi(0))^{\varrho+\omega_1}}{\Gamma(\varrho+\omega_1+1)} + |\Delta_1 Q_2| \frac{(\Psi(1) - \Psi(0))^{\varrho+\omega_2}}{\Gamma(\varrho+\omega_2+1)} \Big] \Bigg] (\kappa_0 + \kappa_1|\vartheta_1| + \kappa_2|\chi|) \\
&+ \quad \frac{(\Psi(1) - \Psi(0))^{\varrho-1}}{|\Lambda|} \Bigg[k_1(|\Delta_1\Delta_2| + |\Lambda|) \Big(|P_1| \frac{(\Psi(1) - \Psi(0))^{\omega-\sigma_1}}{\Gamma(\omega-\sigma_1+1)} \\
&+ \quad |P_2| \frac{(\Psi(1) - \Psi(0))^{\omega-\sigma_2}}{\Gamma(\omega-\sigma_2+1)} \Big) + |\Delta_1| \frac{(\Psi(1) - \Psi(0))^{\omega}}{\Gamma(\omega+1)} \Bigg] (\nu_0 + \nu_1|\vartheta_1| + \nu_2|\chi|),
\end{aligned}
$$

$$
\begin{aligned}
|\chi| &\leq \Big[\frac{(\Psi(1)-\Psi(0))^{\omega}}{\Gamma(\omega+1)}+\frac{(\Psi(1)-\Psi(0))^{\omega-1}}{\Lambda}\Big(\frac{1}{k_1}\frac{(\Psi(1)-\Psi(0))^{\omega}}{\Gamma(\omega+1)}\\
&+ |\Delta_2 P_1|\frac{(\Psi(1)-\Psi(0))^{\omega-\sigma_1}}{\Gamma(\omega-\sigma_1+1)}\\
&+ |\Delta_2 P_2|\frac{(\Psi(1)-\Psi(0))^{\omega-\sigma_2}}{\Gamma(\omega-\sigma_2+1)}\Big)\Big](\nu_0+\nu_1|\vartheta_1|+\nu_2|\chi|)+\frac{(\Psi(1)-\Psi(0))^{\omega-1}}{|\Lambda|}
\end{aligned}
$$

$$
\times\Big[\frac{|Q_1|}{k_1}\frac{(\Psi(1)-\Psi(0))^{\varrho+\omega_1}}{\Gamma(\varrho+\omega_1+1)}+\frac{|Q_2|}{k_1}\frac{(\Psi(1)-\Psi(0))^{\varrho+\omega_2}}{\Gamma(\varrho+\omega_2+1)}+|\Delta_2|\frac{(\Psi(1)-\Psi(0))^{\varrho}}{\Gamma(\varrho+1)}\Big]
$$

$$
\times\Big(\kappa_0+\kappa_1|\vartheta_1|+\kappa_2|\chi|\Big).
$$

Consequently, we obtain

$$
\begin{aligned}
\|\vartheta\|+\|\chi\| &\leq (R_1+R_4)\kappa_0+(R_2+R_3)\nu_0+[(R_1+R_4)\kappa_1+(R_2+R_3)\nu_1]\|\vartheta\|\\
&+ [(R_1+R_4)\kappa_2+(R_2+R_3)\nu_2]\|\chi\|,
\end{aligned}
$$

which can be expressed as

$$
\|(\vartheta,\chi)\| \leq \tfrac{(R_1+R_4)\kappa_0+(R_2+R_3)\nu_0}{\mathbb{M}_0},
$$

where

$$
\mathbb{M}_0=\min\{1-(R_1+R_4)\kappa_1-(R_2+R_3)\nu_1, 1-(R_1+R_4)\kappa_2-(R_2+R_3)\nu_2\}.
$$

Consequently, the Leray–Schauder alternative (Theorem 2) can be invoked, leading to the conclusion that the operator F possesses at least one fixed point. As a result, System (4) and (5) exhibits at least one solution on the interval $[0,1]$. □

Theorem 6. *Consider the assumptions that $\hat{\ell}$ and $\check{\ell}$ are continuous functions defined on $[0,1]\times\mathbb{R}\times\mathbb{R}$, satisfying Condition (31) of Theorem 5. Additionally, we assume that:*
(Con_1) There exist P and $Q\in C([0,1],\mathbb{R}_+)$ such that

$$
|\hat{\ell}(\varsigma,\vartheta,\chi)|\leq P(\varsigma),\ \ \check{\ell}(\varsigma,\vartheta,\chi)\leq Q(\varsigma),\ \ \textit{for each}\ \ (\varsigma,\vartheta,\chi)\in[0,1]\times\mathbb{R}\times\mathbb{R}.
$$

Then, the problem (4) and (5) possesses at least one solution on $[0,1]$, provided that

$$
(R_2+R_3)(n_1+n_2)+(R_1+R_4)(m_1+m_2)<1. \tag{32}
$$

Proof. To start the decomposition process, we will express the operator F as a combination of four individual operators: $F_{1,1}$, $F_{1,2}$, $F_{2,1}$, and $F_{2,2}$, as

$$
\begin{aligned}
F_{1,1}(\vartheta,\chi)(\varsigma) &= I_{0^+}^{\varrho,\Psi}\hat{\ell}(\varsigma,\vartheta(\varsigma),\chi(\varsigma)),\ \ \varsigma\in[0,1],\\
F_{1,2}(\vartheta,\chi)(\varsigma) &= \frac{(\Psi(\varsigma)-\Psi(0))^{\varrho-1}}{\Lambda}\Bigg[k_1(\Delta_1\Delta_2+\Lambda)\Big(P_1 I_{0^+}^{\omega-\sigma_1,\Psi}\check{\ell}(\xi_1,\vartheta(\xi_1),\chi(\xi_1))\\
&+ P_2 I_{0^+}^{\omega-\sigma_2,\Psi}\check{\ell}(\xi_2,\vartheta(\xi_2),\chi(\xi_2)) - I_{0^+}^{\varrho,\Psi}\hat{\ell}(1,\vartheta(1),\chi(1))\Big)\\
&+ \Delta_1 Q_1 I_{0^+}^{\varrho+\omega_1,\Psi}\hat{\ell}(\eta_1,\vartheta(\eta_1),\chi(\eta_1))\\
&+ \Delta_1 Q_2 I_{0^+}^{\varrho+\omega_2,\Psi}\hat{\ell}(\eta_2,\vartheta(\eta_2),\chi(\eta_2)) - \Delta_1 I_{0^+}^{\omega,\Psi}\check{\ell}(1,\vartheta(1),\chi(1))\Bigg],\ \ \varsigma\in[0,1],\\
F_{2,1}(\vartheta,\chi)(\varsigma) &= I_{0^+}^{\omega,\Psi}\check{\ell}(\varsigma,\vartheta(\varsigma),\chi(\varsigma)),\ \ \varsigma\in[0,1],\\
F_{2,2}(\vartheta,\chi)(\varsigma) &= \frac{(\Psi(\varsigma)-\Psi(0))^{\omega-1}}{\Lambda}\Bigg[\frac{Q_1}{k_1} I_{0^+}^{\varrho+\omega_1,\Psi}\hat{\ell}(\eta_1,\vartheta(\eta_1),\chi(\eta_1))\\
&+ \frac{Q_2}{k_1} I_{0^+}^{\varrho+\omega_2,\Psi}\hat{\ell}(\eta_2,\vartheta(\eta_2),\chi(\eta_2)) - \frac{1}{k_1} I_{0^+}^{\omega,\Psi}\check{\ell}(1,\vartheta(1),\chi(1))\\
&+ \Delta_2 P_1 I_{0^+}^{\omega-\sigma_1,\Psi}\check{\ell}(\xi_1,\vartheta(\xi_1),\chi(\xi_1))\\
&+ \Delta_2 P_2 I_{0^+}^{\omega-\sigma_2,\Psi}\check{\ell}(\xi_2,\vartheta(\xi_2),\chi(\xi_2)) - \Delta_2 I_{0^+}^{\varrho,\Psi}\hat{\ell}(1,\vartheta(1),\chi(1))\Bigg],\ \ \varsigma\in[0,1].
\end{aligned}
$$

Observe that $F_1 = F_{1,1} + F_{1,2}$ and $F_2 = F_{2,1} + F_{2,2}$. Consider the set

$$B_\mu = \{(\vartheta,\chi)\in\mathcal{E}\times\mathcal{E} : \|(\vartheta,\chi)\|\le\mu\},$$

with $(R_1+R_4)\|P\| + (R_2+R_3)\|Q\| \le \mu$. Similarly to the proof of Theorem 5, one can derive:

$$|F_{1,1}(\vartheta,\chi)(\varsigma) + F_{1,2}(\vartheta,\chi)(\varsigma)| \le R_1\|P\| + R_2\|Q\|,$$

and

$$|F_{2,1}(\vartheta,\chi)(\varsigma) + F_{2,2}(\vartheta,\chi)(\varsigma)| \le R_4\|P\| + R_3\|Q\|.$$

Therefore, we obtain

$$\|F_1(\vartheta,\chi) + F_2(\vartheta,\chi)\| \le \|P\|(R_1+R_4) + \|Q\|(R_2+R_3) < \mu.$$

Consequently, $F_1(\vartheta,\chi) + F_2(\vartheta,\chi) \in B_\mu$. Next, it will be established that the operator $(F_{1,2}, F_{2,2})$ is a contraction. As demonstrated during the proof of Theorem 4, for (ϑ_1,χ_1), $(\vartheta_2,\chi_2)\in B_\mu$, one can find that

$$
\begin{aligned}
& |F_{1,2}(\vartheta_2,\chi_2)(\varsigma)-F_{1,2}(\vartheta_1,\chi_1)(\varsigma)| \\
\leq\ & \frac{(\Psi(\varsigma)-\Psi(0))^{\varrho-1}}{|\Lambda|}\Bigg[k_1(|\Delta_1\Delta_2|+|\Lambda|)\Big(|P_1|I_{0^+}^{\omega-\sigma_1,\Psi}(|\check{\ell}(\xi_1,\vartheta_2(\xi_1),\chi_2(\xi_1)) \\
-\ & \check{\ell}(\xi_1,\vartheta_1(\xi_1),\chi_1(\xi_1))|) \\
+\ & |P_2|I_{0^+}^{\omega-\sigma_2,\Psi}(|\check{\ell}(\xi_2,\vartheta_2(\xi_1),\chi_2(\xi_2))-\check{\ell}(\xi_2,\vartheta_1(\xi_1),\chi_1(\xi_2))|) \\
+\ & I_{0^+}^{\varrho,\Psi}(|\hat{\ell}(1,\vartheta_2(1),\chi_2(1))-\hat{\ell}(1,\vartheta_1(1),\chi_1(1)))|\Big) \\
+\ & |\Delta_1 Q_1|I_{0^+}^{\varrho+\omega_1,\Psi}(|\hat{\ell}(\eta_1,\vartheta_2(\eta_1),\chi_2(\eta_1))-\hat{\ell}(\eta_1,\vartheta_1(\eta_1),\chi_1(\eta_1))|) \\
+\ & |\Delta_1 Q_2|I_{0^+}^{\varrho+\omega_2,\Psi}(|\hat{\ell}(\eta_2,\vartheta_2(\eta_2),\chi_2(\eta_2))-\hat{\ell}(\eta_2,\vartheta_1(\eta_2),\chi_1(\eta_2))|) \\
+\ & |\Delta_1|I_{0^+}^{\omega,\Psi}(|\check{\ell}(1,\vartheta_2(1),\chi_2(1))-\check{\ell}(1,\vartheta_1(1),\chi_1(1))|)\Bigg] \\
\leq\ & (R_1m_1+R_2n_1)\|\vartheta_2-\vartheta_1\|+(R_1m_2+R_2n_2)\|\chi_2-\chi_1\|, \qquad (33)
\end{aligned}
$$

and

$$
\begin{aligned}
& |F_{2.2}(\vartheta_2,\chi_2)(\varsigma)-F_{2.2}(\vartheta_1,\chi_1)(\varsigma)| \qquad (34) \\
& \qquad \leq (R_3n_1+R_4m_1)\|\vartheta_2-\vartheta_1\|+(R_3n_2+R_4m_2)\|\chi_2-\chi_1\|
\end{aligned}
$$

From Equations (33) and (34), we obtain

$$
\begin{aligned}
& \|(F_{1.2},F_{2.2})(\vartheta_2,\chi_2)-(F_{1.2},F_{2.2})(\vartheta_1,\chi_1)(\varsigma)\| \\
& \qquad \leq \big((R_2+R_3)(n_1+n_2)+(R_1+R_4)(m_1+m_2)\big)(\|\vartheta_2-\vartheta_1\|+\|\chi_2-\chi_1\|).
\end{aligned}
$$

This indicates that the operator $(F_{1,2},F_{2,2})$ can be regarded as a contraction, thanks to the satisfaction of Condition (32). Moreover, considering the continuity properties of $\hat{\ell}$ and $\check{\ell}$, we can conclude that the operator $(F_{1,1},F_{2,1})$ is continuous. also, we have:

$$
\|(F_{1.1},F_{2.1})(\vartheta,\chi)\| \leq \frac{(\Psi(1)-\Psi(0))^{\varrho}}{\Gamma(\varrho+1)}\|P\|+\frac{(\Psi(1)-\Psi(0))^{\omega}}{\Gamma(\omega+1)}\|Q\|,
$$

as

$$
\|F_{1.1}(\vartheta,\chi)\| \leq \frac{(\Psi(1)-\Psi(0))^{\varrho}}{\Gamma(\varrho+1)}\|P\|,
$$

and

$$
\|F_{2.1}(\vartheta,\chi)\| \leq \frac{(\Psi(1)-\Psi(0))^{\omega}}{\Gamma(\omega+1)}\|Q\|.
$$

Thus, $(F_{1.1},F_{2.1})B_\mu$ is uniformly bounded.

In the next step, we establish that the set $(F_{1.1},F_{2.1})B_\mu$ is equicontinuous. For $\varsigma_1,\varsigma_2 \in [0,1]$, $\varsigma_1<\varsigma_2$ and for all $(\vartheta,\chi)\in B_\mu$, we have

$$
\begin{aligned}
&|F_{1,1}(\vartheta(\varsigma_2),\chi(\varsigma_2)) - F_{1,1}(\vartheta(\varsigma_1),\chi(\varsigma_1))| \\
&\quad \leq \frac{1}{\Gamma(\varrho)}\Bigg| \int_0^{\varsigma_1} [\Psi(s)(\Psi(\varsigma_2)-\Psi(s))^{\varrho-1} - \Psi(s)(\Psi(\varsigma_1)-\Psi(s))^{\varrho-1}]\hat{\ell}(s,\vartheta(s),\chi(s))ds \\
&\quad + \frac{1}{\Gamma(\varrho)}\int_{\varsigma_1}^{\varsigma_2} [\Psi(s)(\Psi(\varsigma_2)-\Psi(s))^{\varrho-1}]\hat{\ell}(s,\vartheta(s),\chi(s))ds\Bigg| \\
&\quad \leq \frac{\|P\|}{\Gamma(\varrho+1)}\Big|[2|(\Psi(\varsigma_2)-\Psi(\varsigma_1))^{\varrho-1}| + |(\Psi(\varsigma_2)-\Psi(0))^{\varrho-1} - (\Psi(\varsigma_1)-\Psi(0))^{\varrho-1}|] \to 0 \\
&\quad \text{as } \varsigma_2-\varsigma_1 \to 0,
\end{aligned}
$$

independently of $(\vartheta,\chi) \in B_\mu$. Analogously, one can obtain that

$$F_{2,1}(\vartheta(\varsigma_2),\chi(\varsigma_2)) - F_{2,1}(\vartheta(\varsigma_1),\chi(\varsigma_1)) \to 0, \text{ as } \varsigma_1 \to \varsigma_2.$$

Consequently, as ς_1 approaches ς_2, then $|(F_{1,1},F_{2,1})(\vartheta,\chi)(\varsigma_2) - (F_{1,1},F_{2,1})(\vartheta,\chi)(\varsigma_2)| \to 0$. This implies that $(F_{1,1},F_{2,1})$ exhibits equicontinuity. By applying the Arzel'a–Ascoli theorem, we can deduce that the operator $(F_{1,1},F_{2,1})$ is compact on B_μ. Consequently, the conditions required by the Krasnoselskii fixed-point theorem (Theorem 3) are satisfied. Thus, we can conclude that the System (4) and (5) possesses at least one solution on the interval $[0,1]$. □

4. Illustrative Examples

Example 1. *Consider the FBVP:*

$$
\begin{cases}
D_{0^+}^{1.84,1+\varsigma^3}\vartheta(\varsigma) &= \frac{1}{\varsigma+2023}\frac{|\vartheta+\chi|}{|\vartheta+\chi|+1} + \frac{1}{2024}\varsigma + 0.2025, \quad \varsigma \in [0,1], \\
D_{0^+}^{1.22,1+\varsigma^3}\chi(\varsigma) &= \frac{1}{5\varsigma^2+50}\sin(\frac{|\vartheta+\chi|}{|\vartheta+\chi|+1}) + \exp(\varsigma+2000) + 0.2222, \quad \varsigma \in [0,1],
\end{cases} \tag{35}
$$

supplemented with the mixed boundary conditions

$$
\begin{cases}
\vartheta(0) = 0, \quad \vartheta(1) = 5D_{0^+}^{0.18,1+\varsigma^3}\chi(0.3) + 20.5D_{0^+}^{0.27,1+\varsigma^3}\chi(0.4), \\
\chi(0) = 0, \quad \chi(1) = Q_1 I_{0^+}^{5.33,1+\varsigma^3}\vartheta(0.2) + Q_2 I_{0^+}^{10.22,1+\varsigma^3}\vartheta(0.2),
\end{cases} \tag{36}
$$

Here, $\rho = 1.84$, $\omega = 1.22$, $\omega_1 = 5.33$, $\omega_2 = 10.22$, $\sigma_1 = 0.18$, $\sigma_2 = 0.27$, $Q_1 = 20$, $Q_2 = 10$, $P_1 = 5$, $P_2 = 20.5$, $\eta_1 = 0.2$, $\eta_2 = 0.2$, $\xi_1 = 0.3$, $\xi_2 = 0.4$, $\Psi = 1+\varsigma^3$.

A simple computation gives:

$$\mathbb{K} = 1, R_1 \approx 1.1716, R_2 \approx 13.3695, R_3 \approx 1.7953, R_4 \approx 0.0028.$$

Consider the nonlinear Lipschitzian unbounded functions $\hat{\ell}$ and $\check{\ell}$ defined on $[0,1]\times\mathbb{R}\times\mathbb{R}$ as follows:

$$\hat{\ell}(\varsigma,\vartheta,\chi) = \frac{1}{\varsigma+2023}\frac{|\vartheta+\chi|}{|\vartheta+\chi|+1} + \frac{1}{2024}\varsigma + 0.2025, \tag{37}$$

$$\check{\ell}(\varsigma,\vartheta,\chi) = \frac{1}{5\varsigma^2+50}\sin(\frac{|\vartheta+\chi|}{|\vartheta+\chi|+1}) + \exp(\varsigma+2000) + 0.2222, \tag{38}$$

which satisfy the Lipschitz condition:

$$|\hat{\ell}(\varsigma,\vartheta_1,\chi_1) - \check{\ell}(\varsigma,\vartheta_2,\chi_2)| \leq \frac{1}{2023}|\vartheta_1-\vartheta_2| + \frac{1}{2023}|\chi_1-\chi_2|,$$

$$|\check{\ell}(\varsigma,\vartheta_1,\chi_1) - \check{\ell}(\varsigma,\vartheta_2,\chi_2)| \leq \frac{1}{50}|\vartheta_1-\vartheta_2| + \frac{1}{50}|\chi_1-\chi_2|,$$

with Lipschitz constants $m_1 = m_2 = 1/2023$, $n_1 = n_2 = 1/50$. *Furthermore,*

$$(R_2 + R_3)(n_1 + n_2) + (R_1 + R_4)(m_1 + m_2) \approx 0.6077 < 1.$$

Hence, the conditions of Theorem 4 are verified and its implies that Problem (35) and (36) possesses one solution on $[0, 1]$.

Example 2. *Let us consider the system:*

$$\begin{cases} D_{0^+}^{1.91,1+\varsigma^2}\vartheta(\varsigma) &= \frac{\pi}{\varsigma+2\pi^2} + \frac{1}{5\pi^2}\vartheta + \frac{3}{(1+\pi)^4}\sin(|\chi|), \quad \varsigma \in [0,1], \\ D_{0^+}^{1.44,1+\varsigma^2}\chi(\varsigma) &= \frac{1+\cos^2(\vartheta\chi)}{\varsigma+2\pi^2} + \frac{\vartheta^2\exp(-|\chi|)}{5(1+\vartheta)} + \frac{\chi(1+\cos^8(\vartheta))}{(\varsigma^5+20)}, \quad \varsigma \in [0,1], \end{cases} \tag{39}$$

subject with the mixed boundary conditions

$$\begin{cases} \vartheta(0) = 0, \quad \vartheta(1) = 0.77D_{0^+}^{0.28,1+\varsigma^2}\chi(0.39) + 0.88D_{0^+}^{0.37,1+\varsigma^2}\chi(0.47), \\ \chi(0) = 0, \quad \chi(1) = 0.44I_{0^+}^{51.33,1+\varsigma^2}\vartheta(0.19) + 0.99I_{0^+}^{15.22,1+\varsigma^2}\vartheta(0.29). \end{cases} \tag{40}$$

Here, $\rho = 1.91$, $\omega = 1.44$, $\omega_1 = 51.33$, $\omega_2 = 15.22$, $\sigma_1 = 0.28$, $\sigma_2 = 0.37$, $Q_1 = 0.44$, $Q_2 = 0.99$, $P_1 = 0.77$, $P_2 = 0.88$, $\eta_1 = 0.19$, $\eta_2 = 0.29$, $\xi_1 = 0.39$, $\xi_2 = 0.47$, $\Psi = 1 + \varsigma^2$.

A simple computation leads to:

$$\mathbb{K} = 1, R_1 \approx 1.0848, R_2 \approx 2.5626, R_3 \approx 1.5679, R_4 \approx 1.9175 \times 10^{-15}$$

Consider the functions $\hat{\ell}$ *and* $\check{\ell}$ *defined as nonlinear Lipschitzian unbounded functions on the domain* $[0, 1] \times \mathbb{R} \times \mathbb{R}$, *given by:*

$$\hat{\ell}(\varsigma, \vartheta, \chi) = \frac{\pi}{\varsigma + 2\pi^2} + \frac{1}{5\pi^2}\vartheta + \frac{3}{(1+\pi)^4}\sin(|\chi|), \tag{41}$$

$$\check{\ell}(\varsigma, \vartheta, \chi) = \frac{1 + \cos^2(\vartheta\chi)}{\varsigma + 2\pi^2} + \frac{\vartheta^2\exp(-|\chi|)}{5(1+\vartheta)} + \frac{\chi(1+\cos^8(\vartheta))}{(\varsigma^5+20)}. \tag{42}$$

Clearly, $|\hat{\ell}(\varsigma, \vartheta, \chi)| \leq \frac{1}{2\pi} + \frac{1}{5\pi^2}|\vartheta| + \frac{3}{(1+\pi)^4}|\chi|$ *and* $|\check{\ell}(\varsigma, \vartheta, \chi)| = \frac{1}{\pi} + \frac{1}{5}|\vartheta| + \frac{1}{10}|\chi|$ *with* $\kappa_0 = \frac{1}{2\pi}$, $\kappa_1 = \frac{1}{5\pi^2}$, $\kappa_2 = \frac{3}{(1+\pi)^4}$, $\nu_0 = \frac{1}{2\pi^2}$, $\nu_1 = \frac{1}{5}$, $\nu_2 = \frac{1}{10}$. *Moreover,*

$$(R_1 + R_4)\kappa_1 + (R_2 + R_3)\nu_1 \approx 0.8532 < 1 \quad \textit{and} \quad (R_1 + R_4)\kappa_2 + (R_2 + R_3)\nu_2 \approx 0.4267 < 1.$$

Consequently, based on the result obtained from Theorem 5, we can conclude that Problem (39) *and* (40) *possesses at least one solution on the interval* $[0, 1]$.

Example 3. *Consider the following FBVP:*

$$\begin{cases} D_{0^+}^{1.33,1+\varsigma^4}\vartheta(\varsigma) &= \frac{\exp(-\varsigma^2-1)\arctan(\vartheta)}{45} + \frac{1}{\pi^5}\sin(\chi) + \frac{1}{22}\varsigma + \frac{1}{\pi^5}, \quad \varsigma \in [0,1], \\ D_{0^+}^{1.04,1+\varsigma^4}\chi(\varsigma) &= \frac{|\vartheta|}{20(|\vartheta|+1)} + \frac{|\chi|}{50|\chi|+50} + \exp(\varsigma^2+2) + \frac{3}{100}, \quad \varsigma \in [0,1], \end{cases} \tag{43}$$

subject with the mixed boundary conditions

$$\begin{cases} \vartheta(0) = 0, \quad \vartheta(1) = 1.77D_{0^+}^{0.47,1+\varsigma^4}\chi(0.89) + 1.88D_{0^+}^{0.77,1+\varsigma^4}\chi(0.77), \\ \chi(0) = 0, \quad \chi(1) = 0.77I_{0^+}^{33.33,1+\varsigma^4}\vartheta(0.69) + 0.88I_{0^+}^{22.22,1+\varsigma^4}\vartheta(0.69). \end{cases} \tag{44}$$

Here, $\rho = 1.33$, $\omega = 1.04$, $\omega_1 = 33.33$, $\omega_2 = 22.22$, $\sigma_1 = 0.47$, $\sigma_2 = 0.87$, $Q_1 = 0.77$, $Q_2 = 0.88$, $P_1 = 1.77$, $P_2 = 1.88$, $\eta_1 = 0.69$, $\eta_2 = 0.79$, $\xi_1 = 0.89$, $\xi_2 = 0.77$, $\Psi = 1 + \varsigma^4$.

By a simple computation, we obtain

$$\mathbb{K} = 1, R_1 \approx 1.6832, R_2 \approx 6.1372, R_3 \approx 1.9654, R_4 \approx 5.9581 \times 10^{-24}.$$

Consider the functions $\hat{\ell}$ and $\check{\ell}$ defined as nonlinear Lipschitzian unbounded functions on the domain $[0,1] \times \mathbb{R} \times \mathbb{R}$, given by:

$$\hat{\ell}(\varsigma, \vartheta, \chi) = \frac{\exp(-\varsigma^2 - 1)\arctan(\vartheta)}{45} + \frac{1}{\pi^5}\sin(\chi) + \frac{1}{22}\varsigma + \frac{1}{\pi^5},$$
$$\check{\ell}(\varsigma, \vartheta, \chi) = \frac{|\vartheta|}{20(|\vartheta| + 1)} + \frac{|\chi|}{50|\chi| + 50} + \exp(\varsigma^2 + 2) + \frac{3}{100}.$$

Then, we have

$$|\hat{\ell}(\varsigma, \vartheta, \chi)| = \frac{\exp(-\varsigma^2 - 1)}{45} + \frac{2}{\pi^5} + \frac{1}{22}\varsigma,$$
$$|\check{\ell}(\varsigma, \vartheta, \chi)| = \frac{1}{10} + \exp(\varsigma^2 + 2),$$

and

$$|\hat{\ell}(\varsigma, \vartheta_1, \chi_1) - \check{\ell}(\varsigma, \vartheta_2, \chi_2)| \leq \frac{1}{45}|\vartheta_1 - \vartheta_2| + \frac{1}{\pi^5}|\chi_1 - \chi_2|,$$

$$|\check{\ell}(\varsigma, \vartheta_1, \chi_1) - \check{\ell}(\varsigma, \vartheta_2, \chi_2)| \leq \frac{1}{20}|\vartheta_1 - \vartheta_2| + \frac{1}{50}|\chi_1 - \chi_2|,$$

with Lipschitz constants $m_1 = 1/45, m_2 = 1/\pi^5, n_1 = 1/20, n_2 = 1/50$.

Furthermore, $(R_2 + R_3)(n_1 + n_2) + (R_1 + R_4)(m_1 + m_2) \approx 0.6218 < 1$. Consequently, according to the statement in Theorem 6, we can deduce that Problem (43) and (44) possesses at least one solution within the interval $[0,1]$.

5. Conclusions and Perspectives

In this research, we have proven the existence, uniqueness, and stability of solutions for a coupled fractional differential system characterized by mixed boundary conditions and incorporating fractional ψ–Riemann–Liouville operators. To solve this problem, we used a fixed-point approach by reformulating the original problem into an equivalent fixed-point problem, which allowed us to exploit specific fixed-point theorems due to Banach, Krasnoselskii, and Leray–Schauder, which are particularly appropriate for our analysis. It is important to note that the problem we investigated introduces a unique setup that extends the scope of traditional studies. The results of this work have broad applicability, offering insights that go beyond the limitations of previously investigated cases.

The techniques and results presented in this paper can be potentially generalized to other types of fractional differential equations and boundary conditions. Future research could explore these generalizations to broaden the applicability of the methods, while the paper focuses on analytical results, developing robust numerical methods to approximate solutions for the discussed fractional boundary values problems would be an important next step. This would help in validating the theoretical results and in solving real-world problems in which analytical solutions are difficult to obtain. The fractional differential equations studied in this paper have applications in various fields, including physics, engineering, and finance. Investigating specific applications in which these types of equations model real phenomena could lead to new insights and practical advancements.

Author Contributions: Writing—original draft preparation, A.A. and M.E.-H.M.; writing—review and editing, B.T. and L.A.; supervision, K.Z. All authors have read and agreed to the published version of the manuscript.

Funding: This research received no external funding.

Data Availability Statement: No new data were created or analyzed in this study. Data sharing is not applicable to this article.

Acknowledgments: The Researchers would like to thank the Deanship of Graduate Studies and Scientific Research at Qassim University for financial support (QU-APC-2024-9/1).

Conflicts of Interest: The authors declare no conflicts of interest.

References

1. Kilbas, A.A.; Srivastava, H.M.; Trujillo, J.J. *Theory and Applications of Fractional Differential Equations*; Elsevier: Amsterdam, The Netherlands, 2006.
2. Hilfer, R. *Applications of Fractional Calculus in Physics*; World Scientific: Singapore, 2000.
3. Dorrego, G.A. An alternative definition for the k-Riemann–Liouville fractional derivative. *Appl. Math. Sci.* **2015**, *9*, 481–491. [CrossRef]
4. da Sousa, J.V.C.; de Oliveira, E.C. On the ψ-Hilfer fractional derivative. *Commun. Nonl. Sci. Numer. Simul.* **2018**, *60*, 72–91. [CrossRef]
5. Nuchpong, C.; Ntouyas, S.K.; Tariboon, J. Boundary value problems of Hilfer-type fractional integro-differential equations and inclusions with nonlocal integro-multipoint boundary conditions. *Open Math.* **2020**, *18*, 1879–1894. [CrossRef]
6. Subramanian, M.; Gopal, T.N. Analysis of boundary value problem with multi-point conditions involving Caputo-Hadamard fractional derivative. *Proyecciones* **2020**, *39*, 155–1575. [CrossRef]
7. Belbali, H.; Benbachir, M.; Etemad, S.; Park, C.; Rezapour, S. Existence theory and generalized Mittag–Leffler stability for a nonlinear Caputo-Hadamard FIVP via the Lyapunov method. *AIMS Math.* **2022**, *7*, 14419–14433. [CrossRef]
8. Zhou, Y. *Basic Theory of Fractional Differential Equations*; World Scientific: Singapore, 2014.
9. Thabet, S.T.M.; Al-Sa'di, S.; Kedim, I.; Rafeeq, A.S.; Rezapour, S. Analysis study on multi-order ϱ-Hilfer fractional pantograph implicit differential equation on unbounded domains. *AIMS Math.* **2023**, *8*, 18455–18473. [CrossRef]
10. Thabet, S.T.M.; Kedim, I. Study of nonlocal multiorder implicit differential equation involving Hilfer fractional derivative on unbounded domains. *J. Math.* **2023**, *2023*, 8668325. [CrossRef]
11. Hilfer, R. Experimental evidence for fractional time evolution in glass forming materials. *Chem. Phys.* **2002**, *284*, 399–408. [CrossRef]
12. Garra, R.; Gorenflo, R.; Polito, F.; Tomovski, Z. Hilfer-Prabhakar derivatives and some applications. *Appl. Math. Comput.* **2014**, *242*, 576–589. [CrossRef]
13. Thabet, S.T.M.; Matar, M.M.; Salman, M.A.; Samei, M.E.; Vivas-Cortez, M.; Kedim, I. On coupled snap system with integral boundary conditions in the *G*-Caputo sense. *AIMS Math.* **2023**, *8*, 12576–12605. [CrossRef]
14. Sousa, J.V.d.C.; De Oliveira, E.C. On the Ulam-Hyers-Rassias stability for nonlinear fractional differential equations using the ψ-Hilfer operator. *J. Fixed Point Theory Appl.* **2018**, *20*, 96. [CrossRef]
15. Jiang, J.; Li, C.; Shen, J. Existence and uniqueness results for fractional differential equations with Riemann–Liouville fractional integral boundary conditions. *J. Math. Anal. Appl.* **2017**, *450*, 618–633.
16. Sivaprakasam, S.; Muthukumar, R. Analysis of a coupled system of fractional differential equations with Riemann–Liouville fractional derivatives. *J. Math. Anal. Appl.* **2018**, *465*, 1033–1046.
17. Wang, J.; Zhang, S. Coupled fractional differential systems involving Riemann–Liouville derivatives: Existence results and applications. *Nonlinear Anal. Real World Appl.* **2019**, *46*, 124–138.
18. Ahmed, I.; Kumam, P.; Shah, K.; Borisut, P.; Sitthithakerngkiet, K.; Demba, M.A. Stability results for implicit fractional pantograph differential equations via ϕ-Hilfer fractional derivative with a nonlocal Riemann–Liouville fractional integral condition. *Mathematics* **2020**, *8*, 94. [CrossRef]
19. Elsayed, E.; Harikrishnan, S.; Kanagarajan, K. Analysis of nonlinear neutral pantograph differential equations with ψ-Hilfer fractional derivative. *MathLAB* **2018**, *1*, 231–240.
20. Zhou, J.; Zhang, S.; He, Y. Existence and stability of solution for nonlinear differential equations with ψ-Hilfer fractional derivative. *Appl. Math. Lett.* **2021**, *121*, 107457. [CrossRef]
21. Banach, S. Sur les opérations dans les ensembles abstraits et leur application aux équations intégrales. *Fundam. Math.* **1922**, *3*, 133–181. [CrossRef]
22. Krasnoselskii, M.A. Two remarks on the method of successive approximations. *Uspekhi Mat. Nauk.* **1955**, *10*, 123–127.
23. Leray, J.; Schauder, J. Topologie et équations fonctionnelles. *Ann. Sci. L'école Norm. Supér.* **1934**, *51*, 45–78. [CrossRef]
24. Ali, I.; Malik, N. Hilfer fractional advection-diffusion equations with power-law initial condition; a numerical study using variational iteration method. *Comput. Math. Appl.* **2014**, *68*, 1161–1179. [CrossRef]
25. Thabet, S.T.M.; Vivas-Cortez, M.; Kedim, I.; Samei, M.E.; Ladh Ayari, M. Solvability of a ϱ-Hilfer Fractional Snap Dynamic System on Unbounded Domains. *Fractal Fract.* **2023**, *7*, 607. [CrossRef]
26. Thabet, S.T.M.; Vivas-Cortez, M.; Kedim, I. Analytical study of ABC-fractional pantograph implicit differential equation with respect to another function. *AIMS Math.* **2023**, *8*, 23635–23654. [CrossRef]
27. Boutiara, A.; Etemad, S.; Thabet, S.T.M.; Ntouyas, K.; Rezapour, S.; Tariboon, J. A mathematical theoretical study of a coupled fully hybrid (k, ϕ)-fractional order system of BVPs in generalized Banach spaces. *Symmetry* **2023**, *15*, 1041. [CrossRef]
28. Shah, K.; Wang, J.; Khalil, H.; Khan, R.A. Existence and numerical solutions of a coupled system of integral BVP for fractional differential equations. *Adv. Differ. Equ.* **2018**, *2018*, 149. [CrossRef]

29. Rezapour, S.; Tellab, B.; Deressa, C.T.; Etemad, S.; Nonlaopon, K. H-U-type stability and numerical solutions for a nonlinear model of the coupled systems of Navier BVPs via the generalized differential transform method. *Fractal Fract.* **2021**, *5*, 166. [CrossRef]
30. Thabet, S.T.M.; Etemad, S.; Rezapour, S. On a coupled Caputo conformable system of pantograph problems. *Turk. J. Math.* **2021**, *45*, 496–519. [CrossRef]
31. Miller, K.S.; Ross, B. *An Introduction to the Fractional Calculus and Fractional Differential Equations*; Wiley: New York, NY, USA, 1993.
32. Etemad, S.; Tellab, B.; Deressa, C.T.; Alzabut, J.; Li, Y.; Rezapour, S. On a generalized fractional boundary value problem based on the thermostat model and its numerical solutions via Bernstein polynomials. *Adv. Diff. Equ.* **2021**, *2021*, 458. [CrossRef]
33. Granas, A.; Dugundji, J. *Fixed Point Theory*; Springer: New York, NY, USA, 2003.

Disclaimer/Publisher's Note: The statements, opinions and data contained in all publications are solely those of the individual author(s) and contributor(s) and not of MDPI and/or the editor(s). MDPI and/or the editor(s) disclaim responsibility for any injury to people or property resulting from any ideas, methods, instructions or products referred to in the content.

mathematics

MDPI

Article

Some Fractional Integral and Derivative Formulas Revisited

Juan Luis González-Santander [1,*,†] and Francesco Mainardi [2,†]

[1] Department de Mathematics, University of Oviedo, C Leopoldo Calvo Sotelo 18, 33007 Oviedo, Spain
[2] Department of Physics and Astronomy, University of Bologna, and INFN, Via Irnerio 46, I-40126 Bologna, Italy; francesco.mainardi@bo.infn.it
* Correspondence: gonzalezmarjuan@uniovi.es
† These authors contributed equally to this work.

Abstract: In the most common literature about fractional calculus, we find that ${}_aD_t^\alpha f(t) = {}_aI_t^{-\alpha} f(t)$ is assumed implicitly in the tables of fractional integrals and derivatives. However, this is not straightforward from the definitions of ${}_aI_t^\alpha f(t)$ and ${}_aD_t^\alpha f(t)$. In this sense, we prove that ${}_0D_t^\alpha f(t) = {}_0I_t^{-\alpha} f(t)$ is true for $f(t) = t^{\nu-1}\log t$, and $f(t) = e^{\lambda t}$, despite the fact that these derivations are highly non-trivial. Moreover, the corresponding formulas for ${}_{-\infty}D_t^\alpha |t|^{-\delta}$ and ${}_{-\infty}I_t^\alpha |t|^{-\delta}$ found in the literature are incorrect; thus, we derive the correct ones, proving in turn that ${}_{-\infty}D_t^\alpha |t|^{-\delta} = {}_{-\infty}I_t^{-\alpha} |t|^{-\delta}$ holds true.

Keywords: Riemann–Liouville fractional integral; Riemann–Liouville fractional derivative; Weyl fractional integral; Weyl fractional derivative

MSC: 26A33

1. Introduction

From the very beginning of the invention of differential calculus, important inquiries regarding the significance of the non-integer operations of integrals and derivatives calculus were brought up. In this sense, it is well known that Leibniz initially introduced a symbolic approach and employed the notation $d^n y/dt^n = D^n y$ to represent the n-th derivative, with n being a non-negative integer. However, L'Hospital asked in a letter to Leibniz dated in 1695 [1]: "What if n is $1/2$?" Leibniz replied, "It will lead to a paradox." But he added, "From this apparent paradox, one day useful consequences will be drawn". From this initial "paradox", fractional calculus was developed through contributions from mathematicians such as Euler, Lagrange, Laplace, Fourier, and others during the 18th and early 19th centuries (a comprehensive summary of its historical progression can be found in [2] [Chap. I]). Despite the efforts of these great mathematicians, a satisfactory expression for the generalization of integration to fractional powers was not developed until the mid-19th century, through the work of Liouville [3]. However, it is worth noting that Abel set the notation that was used later by Liouville (and also used nowadays) for fractional-order integration when solving the generalization of the tautochrone problem (see [4] and the references therein). For a rigorous understanding of fractional calculus as a theory involving operators of integration and differentiation of arbitrary order, we recommend the book by Samko, Kilbas, and Marichev [5].

Definition 1 (Riemann–Liouville fractional integral)**.** *For $\alpha > 0$ [6] ([Chap. XIII])*

$$ {}_aI_t^\alpha f(t) = \frac{1}{\Gamma(\alpha)} \int_a^t (t-\tau)^{\alpha-1} f(\tau)\, d\tau. \tag{1}$$

Remark 1. *Usually, $a = 0$ in many textbooks and applications [7] [Eqn. 1.2]. However, when $a \to -\infty$ in (1), we obtain the Weyl fractional integral, i.e.,*

$$ {}_{-\infty}I_t^{\alpha} f(t) = \frac{1}{\Gamma(\alpha)} \int_{-\infty}^{t} (t-\tau)^{\alpha-1} f(\tau)\, d\tau. \tag{2} $$

It is worth noting that in [6] [Chap. XIII], we find other definition of the Weyl fractional integral, i.e.,

$$ \mathfrak{B}_{\alpha}\{f(\tau);t\} = \frac{1}{\Gamma(\alpha)} \int_{t}^{\infty} (\tau-t)^{\alpha-1} f(\tau) d\tau. $$

It is easy to prove that

$$ {}_{-\infty}I_t^{\alpha} f(t) = \mathfrak{B}_{\alpha}\{f(-\tau);-t\}. $$

As pointed out in [7] [Sect. 1.2], one is tempted to substitute α with $-\alpha$ in (1) in order to obtain a definition for the fractional derivative ${}_aD_t^{\alpha} f(t)$. Nevertheless, some care is required in the integration for this generalization, and the theory of generalized functions has to be invoked. In order to avoid the use of generalized functions, we find in [8] [Sect. 2.3.3] the following definition:

Definition 2 (Riemann–Liouville fractional derivative)**.** *For $m \in \mathbb{N}$, and $\alpha > 0$*

$$ {}_aD_t^{\alpha} f(t) = \begin{cases} \dfrac{1}{\Gamma(m-\alpha)} \dfrac{d^m}{dt^m} \displaystyle\int_a^t \frac{f(\tau)}{(t-\tau)^{\alpha+1-m}} d\tau, & m-1 < \alpha < m, \\ \dfrac{d^m}{dt^m} f(t), & \alpha = m. \end{cases} \tag{3} $$

Remark 2. *Usually, $a = 0$ in many textbooks and applications [7] [Eqn. 1.13b]. However, when $a \to -\infty$ in (3), we obtain the Weyl fractional derivative [7] [Eqn. 1.108], i.e., for $m \in \mathbb{N}$, and $\alpha > 0$*

$$ {}_{-\infty}D_t^{\alpha} f(t) = \begin{cases} \dfrac{1}{\Gamma(m-\alpha)} \dfrac{d^m}{dt^m} \displaystyle\int_{-\infty}^t \frac{f(\tau)}{(t-\tau)^{\alpha+1-m}} d\tau, & m-1 < \alpha < m, \\ \dfrac{d^m}{dt^m} f(t), & \alpha = m. \end{cases} \tag{4} $$

Nonetheless, in the existing literature, we find tables of Riemann–Liouville fractional derivatives, wherein they just substitute α with $-\alpha$ in the corresponding Riemann–Liouville fractional integral. For instance, if $E_{\mu,\nu}(z)$ denotes the Mittag–Leffler function, and $\psi(z)$ denotes the digamma function, we find in [6] [Eqn. 13.1.(24)] and [9] [Table IV.1], respectively,

$$ {}_0I_t^{\alpha}\left[t^{\nu-1}\log t\right] = \frac{t^{\alpha+\nu-1}\,\Gamma(\nu)}{\Gamma(\alpha+\nu)}[\log t + \psi(\nu) - \psi(\alpha+\nu)], \tag{5} $$

$$ {}_0I_t^{\alpha} e^{\lambda t} = t^{\alpha} E_{1,1+\alpha}(\lambda t), \tag{6} $$

Nevertheless, in [8] [Appendix], we find that α is changed by $-\alpha$ in (5) and (6) in order to obtain the corresponding fractional derivatives, i.e., ${}_0D_t^{\alpha}\left[t^{\nu-1}\log t\right]$ and ${}_0D_t^{\alpha} e^{\lambda t}$.

Also, we find in [7] [Eqn. 1.112]

$$ {}_{-\infty}D_t^{\alpha}|t|^{-\delta} = \frac{\Gamma(\delta+\alpha)}{\Gamma(\delta)}\,|t|^{-\alpha-\delta} = {}_{-\infty}I_t^{-\alpha}|t|^{-\delta}. \tag{7} $$

However, according to our numerical experiments, it seems that (7) does not hold true. Consequently, the aim of this paper is twofold. On the one hand, we want to justify that

$$ {}_0D_t^{\alpha}\left[t^{\nu-1}\log t\right] = {}_0I_t^{-\alpha}\left[t^{\nu-1}\log t\right], $$

$$ {}_0D_t^{\alpha} e^{\lambda t} = {}_0I_t^{-\alpha} e^{\lambda t}, $$

from the definitions given in (1) and (3). We will see that these proofs are highly non-trivial. On the other hand, we would like to calculate the Weyl fractional integral and derivative for the power function, i.e., ${}_{-\infty}I_t^\alpha |t|^{-\delta}$ and ${}_{-\infty}D_t^\alpha |t|^{-\delta}$, as well as to justify that

$${}_{-\infty}D_t^\alpha |t|^{-\delta} = {}_{-\infty}I_t^{-\alpha} |t|^{-\delta}.$$

This paper is organized as follows. Section 2 collects all the definitions of the special functions and polynomials that appear throughout the paper. Section 3 calculates the fractional integrals ${}_0I_t^\alpha \left[t^{\nu-1}\log t\right]$, ${}_0I_t^\alpha e^{\lambda t}$, and ${}_{-\infty}I_t^\alpha |t|^{-\delta}$. Despite the fact that ${}_0I_t^\alpha \left[t^{\nu-1}\log t\right]$, and ${}_0I_t^\alpha e^{\lambda t}$ are found in the existing literature, it is worth performing these calculations, as they will be useful in the following section. In Section 4, we calculate ${}_0D_t^\alpha \left[t^{\nu-1}\log t\right]$, ${}_0D_t^\alpha e^{\lambda t}$ and ${}_{-\infty}D_t^\alpha |t|^{-\delta}$. Finally, we collect our conclusions in Section 5.

2. Preliminaries

In this section, we collect all the definitions of the special functions and polynomials that appear throughout the paper.

Definition 3. *For* $\operatorname{Re}\alpha > 0$*, the gamma function is defined as [10] [Eqn. 1.1.1]*

$$\Gamma(z) = \int_0^\infty t^{z-1}e^{-t}dt. \tag{8}$$

Definition 4. *The digamma function is defined as [10] [Eqn. 1.3.1]*

$$\psi(z) = \frac{\Gamma'(z)}{\Gamma(z)}. \tag{9}$$

Definition 5. *The Pochhammer polynomial is defined as [11] [Eqn. 18:12:1]*

$$(x)_n = x\,(x+1)(x+2)\cdots(x+n-1) = \frac{\Gamma(x+n)}{\Gamma(x)}. \tag{10}$$

Definition 6. *For* $\operatorname{Re}a > 0$, $\operatorname{Re}b > 0$*, the beta function is defined as [10] [Eqns. 1.5.2&5]*

$$\mathrm{B}(a,b) = \int_0^1 t^{a-1}(1-t)^{b-1}dt = \frac{\Gamma(a)\,\Gamma(b)}{\Gamma(a+b)}. \tag{11}$$

Remark 3. *Note that if we are considering* $a, b \in \mathbb{R}$*, then the condition* $\operatorname{Re}a > 0$, $\operatorname{Re}b > 0$*, becomes* $a, b > 0$*.*

Definition 7. *The lower incomplete gamma function is defined as [11] [Eqn. 45:3:1]*

$$\gamma(\alpha, z) = \int_0^z t^{\alpha-1}e^{-t}dt. \tag{12}$$

Definition 8. *The two-parameter Mittag–Leffler function is defined as [12] [Eqn. 10.46.3],*

$$E_{\mu,\nu}(z) = \sum_{k=0}^{\infty} \frac{z^k}{\Gamma(\mu\,k+\nu)}. \tag{13}$$

Definition 9. *The generalized hypergeometric function is defined as [12] [Eqn. 16.2.1]*

$${}_pF_q\left(\begin{array}{c} a_1,\ldots,a_p \\ b_1,\ldots,b_q \end{array}\middle| z\right) = \sum_{k=0}^{\infty} \frac{(a_1)_k\cdots(a_p)_k}{(b_1)_k\cdots(b_q)_k}\frac{z^k}{k!}. \tag{14}$$

3. Fractional Integrals

3.1. Fractional Integral of the Power Function

Theorem 1. *For $\alpha > 0$, $\gamma > -1$, and $t > 0$, we have [6] [Eqn. 13.1.(7)]*

$$ {}_0I_t^{\alpha} t^{\gamma} = \frac{\Gamma(1+\gamma)}{\Gamma(1+\gamma+\alpha)} t^{\gamma+\alpha}. \tag{15} $$

Proof. Apply definition (1), and perform the change in variables $t - \tau = st$, with $t > 0$ to obtain

$$ \begin{aligned} {}_0I_t^{\alpha} t^{\gamma} &= \frac{1}{\Gamma(\alpha)} \int_0^t (t-\tau)^{\alpha-1} \tau^{\gamma} \, d\tau \\ &= \frac{t^{\alpha+\gamma}}{\Gamma(\alpha)} \underbrace{\int_0^1 s^{\alpha-1}(1-s)^{\gamma} \, d\tau}_{\mathrm{B}(\alpha,1+\gamma)}. \end{aligned} $$

Finally, apply (11) to obtain (15) as we wanted to prove. Note that we consider $\alpha, \gamma \in \mathbb{R}$; thus, according to Remark 3, we have $\alpha > 0$, $\gamma > -1$. □

As mentioned in the Introduction, the Weyl fractional integral for the power function given in (7) does not seem to hold true. Therefore, next, we are going to calculate ${}_{-\infty}I_t^{\alpha}|t|^{-\delta}$. For this purpose, let us first prove the following lemma.

Lemma 1. *For $\alpha < -\beta - 1 < 0$, and $t > 0$, the following integral formula holds true:*

$$ \begin{aligned} \mathcal{I}_{\alpha,\beta}(t) &= \int_{-\infty}^0 (t-\tau)^{\alpha} |\tau|^{\beta} d\tau \\ &= t^{\alpha+\beta+1} \frac{\Gamma(-1-\alpha-\beta)\,\Gamma(\beta+1)}{\Gamma(-\alpha)}. \end{aligned} \tag{16} $$

Proof. Perform the change in variables $u = -\tau$ to obtain

$$ \begin{aligned} \mathcal{I}_{\alpha,\beta}(t) &= \int_{-\infty}^0 (t-\tau)^{\alpha} (-\tau)^{\beta} d\tau \\ &= \int_0^{\infty} (t+u)^{\alpha} u^{\beta} du. \end{aligned} $$

Perform the change in variables $u = st/(1-s)$ with $t > 0$, and use the definition of the beta function (11) to obtain

$$ \begin{aligned} \mathcal{I}_{\alpha,\beta}(t) &= \int_0^1 \left(t + \frac{st}{1-s}\right)^{\alpha} \left(\frac{st}{1-s}\right)^{\beta} t \frac{ds}{(1-s)^2} \\ &= t^{\alpha+\beta+1} \underbrace{\int_0^1 (1-s)^{-\alpha-\beta-2} s^{\beta} ds}_{\mathrm{B}(-\alpha-\beta-1,\beta+1)}. \end{aligned} $$

Applying again (11), we finally arrive at (16), as we wanted to prove. According to Remark 3, we have $\alpha < -\beta - 1 < 0$. □

Theorem 2. *For $0 < \alpha < \delta < 1$, and $t > 0$*

$$ {}_{-\infty}I_t^{\alpha}|t|^{-\delta} = \frac{\Gamma(\delta-\alpha)}{\Gamma(\delta)} \frac{\cos\left(\frac{\pi\delta}{2} - \pi\alpha\right)}{\cos\left(\frac{\pi\delta}{2}\right)} t^{\alpha-\delta}. \tag{17} $$

Proof. Note that

$$ {}_{-\infty}I_t^{\alpha}|t|^{-\delta} = {}_{-\infty}I_0^{\alpha}|t|^{-\delta} + {}_0I_t^{\alpha}|t|^{-\delta}. $$

Also, from (1) and (15), for $\alpha > 0$, $\delta < 1$ and $t > 0$, we have

$$ {}_0I_t^{\alpha}|t|^{-\delta} = {}_0I_t^{\alpha}\, t^{-\delta} = \frac{\Gamma(1-\delta)}{\Gamma(1-\delta+\alpha)} t^{\alpha-\delta}. \tag{18} $$

Moreover, from definition (1) and lemma (16), we have for $\alpha < \delta < 1$, and $t > 0$

$$ {}_{-\infty}I_0^{\alpha}|t|^{-\delta} = \frac{1}{\Gamma(\alpha)} \underbrace{\int_{-\infty}^{0} (t-\tau)^{\alpha-1}|\tau|^{-\delta}}_{\mathcal{I}_{\alpha-1,-\delta}(t)} = t^{\alpha-\delta}\frac{\Gamma(\delta-\alpha)\,\Gamma(1-\delta)}{\Gamma(1-\alpha)}, \tag{19} $$

and thus, according to (18) and (19), we obtain

$$ \begin{aligned} & {}_{-\infty}I_t^{\alpha}|t|^{-\delta} \\ = \;& t^{\alpha-\delta}\,\Gamma(1-\delta)\left[\frac{\Gamma(\delta-\alpha)}{\Gamma(\alpha)\,\Gamma(1-\alpha)} + \frac{1}{\Gamma(1+\alpha-\delta)}\right] \\ = \;& t^{\alpha-\delta}\,\frac{\Gamma(\delta-\alpha)\,\Gamma(1-\delta)\,\Gamma(\delta)}{\Gamma(\delta)} \\ & \left[\frac{1}{\Gamma(\alpha)\,\Gamma(1-\alpha)} + \frac{1}{\Gamma(1+\alpha-\delta)\,\Gamma(\delta-\alpha)}\right]. \end{aligned} $$

Now, apply the property [10] [Eqn. 1.2.2]

$$ \Gamma(z)\,\Gamma(1-z) = \frac{\pi}{\sin(\pi z)} \tag{20} $$

to obtain

$$ {}_{-\infty}I_t^{\alpha}|t|^{-\delta} = t^{\alpha-\delta}\,\frac{\Gamma(\delta-\alpha)}{\Gamma(\delta)\sin(\pi\delta)}[\sin(\pi\alpha) + \sin(\pi(\delta-\alpha))]. $$

Finally, apply the property [13] [Eqn. 5.61]

$$ \sin A + \sin B = 2\sin\left(\frac{A+B}{2}\right)\cos\left(\frac{A-B}{2}\right), \tag{21} $$

to arrive at (17) as we wanted to prove. □

3.2. Fractional Integral of the Exponential Function

Lemma 2. *The following identity holds true:*

$$ \gamma(\alpha, z) = z^{\alpha}\,\Gamma(\alpha)\,e^{-z}\,E_{1,1+\alpha}(z). \tag{22} $$

Proof. Consider the expansion [11] [Eqn. 45:6:2]

$$ e^{z}\,\gamma(\alpha, z) = \frac{z^{\alpha}}{\alpha}\sum_{k=0}^{\infty}\frac{z^{k}}{(\alpha+1)_k}. $$

Taking into account the factorial property of the gamma function [10] [Eqn. 1.2.1], i.e.,

$$ \Gamma(z+1) = z\,\Gamma(z), \tag{23} $$

and the definition of the Pochhammer symbol (10), we have

$$ e^{z}\,\gamma(\alpha, z) = z^{\alpha}\,\Gamma(\alpha)\sum_{k=0}^{\infty}\frac{z^{k}}{\Gamma(\alpha+1+k)}. $$

Finally, apply the definition of the Mittag–Leffler function (13) to complete the proof. □

Theorem 3. *For $t > 0$, and $\alpha > 0$, the following fractional integral holds true [9] [Table IV.1]:*

$$ {}_0I_t^{\alpha} e^{\lambda t} = t^{\alpha} E_{1,1+\alpha}(\lambda t). \tag{24}$$

Proof. According to the definition of the Riemann–Liouville fractional integral (1), we have

$$\begin{aligned} {}_0I_t^{\alpha} e^{\lambda t} &= \frac{1}{\Gamma(\alpha)} \int_0^t (t-\tau)^{\alpha-1} e^{\lambda \tau} d\tau \\ &= \frac{\lambda^{-\alpha}}{\Gamma(\alpha)} \int_0^t (\lambda t - \lambda \tau)^{\alpha-1} e^{\lambda \tau} \lambda d\tau, \end{aligned}$$

thus performing the change in variables $u = \lambda(t-\tau)$, and taking into account the definition of the lower incomplete gamma function (12), we obtain

$$\begin{aligned} {}_0I_t^{\alpha} e^{\lambda t} &= \frac{\lambda^{-\alpha} e^{\lambda t}}{\Gamma(\alpha)} \int_0^{\lambda t} u^{\alpha-1} e^{-u} du \\ &= \frac{\lambda^{-\alpha} e^{\lambda t}}{\Gamma(\alpha)} \gamma(\alpha, \lambda t). \end{aligned}$$

Finally, apply (22) to complete the proof. □

3.3. Fractional Integral Formula of the Logarithmic Function

Lemma 3. *The following integral formula holds true:*

$$\int_0^1 t^{a-1}(1-t)^{b-1} \log t \, dt = \frac{\Gamma(a)\,\Gamma(b)}{\Gamma(a+b)} [\psi(a) - \psi(a+b)], \tag{25}$$
$$\operatorname{Re} a > 0, \operatorname{Re} b > 0.$$

Proof. Perform the derivative with respect to the first parameter in the beta function definition (11),

$$\begin{aligned} &\frac{\partial}{\partial a} \mathrm{B}(a,b) \\ &= \int_0^1 t^{a-1}(1-t)^{b-1} \log t \, dt = \Gamma(b) \, \frac{\Gamma'(a)\,\Gamma(a+b) - \Gamma(a)\,\Gamma'(a+b)}{\Gamma^2(a+b)}, \end{aligned} \tag{26}$$

and take into account the definition of the digamma function (9) to complete the proof. □

Theorem 4. *The following fractional integral holds true [6] [Eqn. 13.1.(24)]:*

$$ {}_0I_t^{\alpha} \left[t^{\nu-1} \log t \right] = \frac{t^{\alpha+\nu-1}\,\Gamma(\nu)}{\Gamma(\alpha+\nu)} [\log t + \psi(\nu) - \psi(\alpha+\nu)], \tag{27}$$
$$\operatorname{Re} \alpha > 0, \operatorname{Re} \nu > 0.$$

Proof. Apply the definition (1) and perform the change in variables $\tau = t\,u$ with $t > 0$ to obtain

$$\begin{aligned} &{}_0I_t^{\alpha} \left[t^{\nu-1} \log t \right] \\ &= \frac{1}{\Gamma(\alpha)} \int_0^t (t-\tau)^{\alpha-1} \tau^{\nu-1} \log \tau \, d\tau \\ &= \frac{t^{\alpha+\nu-1}}{\Gamma(\alpha)} \left\{ \log t \int_0^1 (1-u)^{\alpha-1} u^{\nu-1} du + \int_0^1 (1-u)^{\alpha-1} u^{\nu-1} \log u \, du \right\}. \end{aligned} \tag{28}$$

Use the definition of the beta function (11) to calculate the first integral in (28) as

$$\int_0^1 (1-u)^{\alpha-1} u^{\nu-1} du = \frac{\Gamma(\nu)\,\Gamma(\alpha)}{\Gamma(\alpha+\nu)}, \tag{29}$$
$$\operatorname{Re}\alpha > 0,\ \operatorname{Re}\nu > 0.$$

The second integral in (28) is given in lemma (25). Therefore, substituting (25) and (29) in (28), we arrive at (27) as we wanted to prove. □

4. Fractional Derivatives

4.1. Fractional Derivative of the Power Function

Lemma 4. *The following n-th derivative formula holds:*

$$\frac{d^n}{dt^n} t^a = \frac{\Gamma(a+1)}{\Gamma(a-n+1)} t^{a-n}. \tag{30}$$

Proof. According to the definition of the Pochhamer symbol (10), we have

$$\begin{aligned} \frac{d^n}{dt^n} t^a &= a(a-1)\cdots(a-n+1)t^{a-n} \\ &= (a-n+1)_n\, t^{a-n} \\ &= \frac{\Gamma(a+1)}{\Gamma(a-n+1)} t^{a-n}. \end{aligned}$$

□

Theorem 5. *For $\alpha > 0$, $\gamma > -1$, and $t > 0$ [9] [Table IV.1], [8] [Appendix], the following fractional derivative holds true:*

$${}_0D_t^\alpha t^\gamma = \frac{\Gamma(1+\gamma)}{\Gamma(1+\gamma-\alpha)} t^{\gamma-\alpha}. \tag{31}$$

Proof. According to definition (3), and the results given in (15) and (30),

$$\begin{aligned} {}_0D_t^\alpha t^\gamma &= \left(D_t^m \circ {}_0I_t^{m-\alpha}\right) t^\gamma \\ &= \frac{\Gamma(1+\gamma)}{\Gamma(1+\gamma+m-\alpha)} \frac{d^m}{dt^m} t^{\gamma+m-\alpha} \\ &= \frac{\Gamma(1+\gamma)}{\Gamma(1+\gamma+m-\alpha)} \frac{\Gamma(\gamma+m-\alpha+1)}{\Gamma(\gamma-\alpha+1)} t^{\gamma+m-\alpha-m}, \end{aligned}$$

as we wanted to prove. □

Now, we calculate the Weyl fractional derivative corresponding to the Weyl fractional integral calculated in (17).

Theorem 6. *For $0 < \delta < 1$, $\alpha > 0$, and $t > 0$,*

$${}_{-\infty}D_t^\alpha |t|^{-\delta} = \frac{\Gamma(\delta+\alpha)}{\Gamma(\delta)} \frac{\cos\left(\frac{\pi\delta}{2} + \pi\alpha\right)}{\cos\left(\frac{\pi\delta}{2}\right)} t^{-\alpha-\delta}. \tag{32}$$

Proof. According to the definition of the Weyl fractional integral (4), we have

$${}_{-\infty}D_t^\alpha |t|^{-\delta} = {}_{-\infty}D_0^\alpha |t|^{-\delta} + {}_0D_t^\alpha |t|^{-\delta}. \tag{33}$$

On the one hand, apply definition (3), taking into account that $\alpha \notin \mathbb{N}$ and $m - \alpha > 0$,

$$ {}_{-\infty}D_0^{\alpha}|t|^{-\delta} = \frac{1}{\Gamma(m-\alpha)}\frac{d^m}{dt^m}\underbrace{\int_{-\infty}^{0}\frac{|\tau|^{-\delta}}{(t-\tau)^{\alpha+1-m}}d\tau}_{\mathcal{I}_{m-1-\alpha,-\delta}(t)}. $$

Now, apply lemmas (16) and (30) to obtain for $m - \alpha < \delta < 1$

$$ \begin{aligned} {}_{-\infty}D_0^{\alpha}|t|^{-\delta} &= \frac{\Gamma(\alpha+\delta-m)\,\Gamma(1-\delta)}{\Gamma(m-\alpha)\,\Gamma(1+\alpha-m)}\frac{d^m}{dt^m}t^{m-\alpha-\delta} \\ &= \frac{\Gamma(\alpha+\delta-m)\,\Gamma(1-\delta)}{\Gamma(m-\alpha)\,\Gamma(1+\alpha-m)}\frac{\Gamma(m-\alpha-\delta+1)}{\Gamma(-\alpha-\delta+1)}t^{-\alpha-\delta}. \end{aligned} \tag{34} $$

On the other hand, taking into account that $t > 0$ and $\alpha \notin \mathbb{N}$, apply (31) to obtain for $\delta < 1$,

$$ {}_0D_t^{\alpha}|t|^{-\delta} = {}_0D_t^{\alpha}\,t^{-\delta} = \frac{\Gamma(1-\delta)}{\Gamma(1-\delta-\alpha)}t^{-\delta-\alpha}. \tag{35} $$

Substitute results (34) and (35) in (33) to arrive at

$$ {}_{-\infty}D_t^{\alpha}|t|^{-\delta} = \frac{t^{-\alpha-\delta}\,\Gamma(1-\delta)}{\Gamma(1-\alpha-\delta)}\left[\frac{\Gamma(\alpha+\delta-m)\,\Gamma(1-\alpha-\delta+m)}{\Gamma(m-\alpha)\,\Gamma(1+\alpha-m)}+1\right]. $$

Now, apply (20)

$$ \begin{aligned} & {}_{-\infty}D_t^{\alpha}|t|^{-\delta} \\ = \;& t^{-\alpha-\delta}\frac{\Gamma(\alpha+\delta)}{\Gamma(\delta)}\frac{\Gamma(1-\delta)\,\Gamma(\delta)}{\Gamma(1-\alpha-\delta)\,\Gamma(\alpha+\delta)}\left[\frac{\sin\pi(m-\alpha)}{\sin\pi(\alpha+\delta-m)}+1\right] \\ = \;& t^{-\alpha-\delta}\frac{\Gamma(\alpha+\delta)}{\Gamma(\delta)}\frac{\sin\pi(\alpha+\delta)}{\sin\pi\delta}\left[1-\frac{\sin\pi\alpha}{\sin\pi(\alpha+\delta)}\right] \\ = \;& t^{-\alpha-\delta}\frac{\Gamma(\alpha+\delta)}{\Gamma(\delta)}\left[\frac{\sin\pi(\alpha+\delta)-\sin\pi\alpha}{\sin\pi\delta}\right]. \end{aligned} $$

Finally, apply (21) and simplify to arrive at (32) as we wanted to prove. □

4.2. Fractional Derivative of the Exponential Function

Theorem 7. *For $\alpha > 0$, $\alpha \notin \mathbb{N}$, and $t > 0$*

$$ {}_0D_t^{\alpha}e^{\lambda t} = t^{-\alpha}E_{1,1-\alpha}(\lambda t). \tag{36} $$

Proof. Apply the definition (3) and expand the exponential fraction in its Maclaurin series to obtain

$$ \begin{aligned} {}_0D_t^{\alpha}e^{\lambda t} &= \frac{1}{\Gamma(m-\alpha)}\frac{d^m}{dt^m}\int_0^t(t-\tau)^{m-\alpha-1}e^{\lambda\tau}d\tau \\ &= \frac{1}{\Gamma(m-\alpha)}\frac{d^m}{dt^m}\int_0^t(t-\tau)^{m-\alpha-1}\sum_{k=0}^{\infty}\frac{(\lambda\tau)^k}{k!}d\tau \\ &= \frac{1}{\Gamma(m-\alpha)}\frac{d^m}{dt^m}\left(\sum_{k=0}^{\infty}\frac{\lambda^k}{k!}\int_0^t\frac{\tau^k}{(t-\tau)^{\alpha-m+1}}d\tau\right). \end{aligned} \tag{37} $$

Perform the change in variables $\tau = u\,t$ with $t > 0$ in (37), and apply the definition of the beta function (11). Thus, for $m - \alpha > 0$, we have

$$\begin{aligned} {}_0D_t^{\alpha} e^{\lambda t} &= \frac{1}{\Gamma(m-\alpha)} \frac{d^m}{dt^m} \left(t^{m-\alpha} \sum_{k=0}^{\infty} \frac{(\lambda t)^k}{k!} \int_0^1 u^k \,(1-u)^{m-\alpha-1} du \right) \\ &= \frac{1}{\Gamma(m-\alpha)} \frac{d^m}{dt^m} \left(t^{m-\alpha} \sum_{k=0}^{\infty} \frac{(\lambda t)^k}{k!} \,\mathrm{B}(k+1, m-\alpha) \right) \\ &= \frac{d^m}{dt^m} \sum_{k=0}^{\infty} \frac{\lambda^k \, t^{m-\alpha+k}}{\Gamma(m-\alpha+k+1)}. \end{aligned}$$

Now, apply the differentiation formula (30) to arrive at

$${}_0D_t^{\alpha} e^{\lambda t} = t^{-\alpha} \sum_{k=0}^{\infty} \frac{(\lambda t)^k}{\Gamma(k+1-\alpha)}.$$

Finally, apply the definition of the Mittag–Leffler function (13) to complete the proof. □

4.3. Fractional Derivative of the Logarithm Function

Lemma 5. *The following n-th derivative formula holds true:*

$$\frac{d^n}{dt^n} \left(t^{\beta} \log t \right) = \frac{\Gamma(\beta+1)}{\Gamma(\beta-n+1)} t^{\beta-n} [\log t + \psi(\beta+1) - \psi(\beta-n+1)]. \tag{38}$$

Proof. According to Leibniz's differentiation formula [12] [Eqn. 1.4.12],

$$\frac{d^n}{dx^n}[f(x)g(x)] = \sum_{k=0}^{n} \binom{n}{k} \frac{d^{n-k}}{dx^{n-k}} f(x) \, \frac{d^k}{dx^k} g(x), \tag{39}$$

and applying the n-th derivative formula given in (30), as well as the following one (which can be easily proved by induction)

$$\frac{d^n}{dt^n} \log t = \frac{(-1)^{n-1}(n-1)!}{t^n}, \quad n = 1, 2, \ldots$$

after simplification, we arrive at

$$\begin{aligned} & \frac{d^n}{dt^n} \left(t^{\beta} \log t \right) \\ = \; & \sum_{k=0}^{n} \binom{n}{k} \frac{d^{n-k}}{dt^{n-k}} t^{\beta} \, \frac{d^k}{dt^k} \log t \\ = \; & \log t \, \frac{d^n}{dt^n} t^{\beta} + \sum_{k=1}^{n} \binom{n}{k} \frac{d^{n-k}}{dt^{n-k}} t^{\beta} \, \frac{d^k}{dt^k} \log t \\ = \; & \Gamma(\beta+1) \, t^{\beta-n} \left[\frac{\log t}{\Gamma(\beta-n+1)} + n! \sum_{k=1}^{n} \frac{(-1)^{k-1}}{k\,(n-k)!\,\Gamma(\beta-n+k+1)} \right]. \end{aligned} \tag{40}$$

In order to calculate the finite sum given in (40), consider the following function $f(z)$ which can be recast as a hypergeometric function [14] [Sect. 2.1]

$$f(z) = \sum_{k=1}^{n} \frac{z^{k-1}}{(n-k)!\,\Gamma(\beta-n+k+1)} \tag{41}$$

$$= \frac{1}{\Gamma(n)\Gamma(\beta-n+2)} \, {}_2F_1 \left(\begin{matrix} 1, 1-n \\ \beta-n+2 \end{matrix} \,\middle|\, -z \right). \tag{42}$$

On the one hand, integrating term by term in (41)

$$g(z) = \int_0^z f(t)\,dt = \sum_{k=1}^{n} \frac{z^k}{k\,(n-k)!\,\Gamma(\beta-n+k+1)}. \tag{43}$$

On the other hand, applying the integration formula given in [14] [Eqn. 2.2.3]

$$\begin{aligned} & {}_{p+1}F_{q+1}\left(\begin{matrix} a_1,\ldots,a_p,a_{p+1} \\ b_1,\ldots,b_q,b_{q+1} \end{matrix} \middle| x \right) \\ = \; & \frac{\Gamma\left(b_{q+1}\right) x^{1-b_{q+1}}}{\Gamma\left(a_{p+1}\right)\Gamma\left(b_{q+1}-a_{p+1}\right)} \\ & \int_0^x t^{a_{p+1}-1}(x-t)^{b_{q+1}-a_{p+1}-1}\,{}_pF_q\left(\begin{matrix} a_1,\ldots,a_p \\ b_1,\ldots,b_q \end{matrix} \middle| t \right) dt, \end{aligned}$$

taking $a_1 = 1$, $a_2 = 1-n$, $b_1 = \beta - n + 2$, we obtain

$$\begin{aligned} & g(z) \\ = \; & \int_0^z f(t)\,dt = \frac{1}{\Gamma(n)\Gamma(\beta-n+2)} \int_0^z {}_2F_1\left(\begin{matrix} 1, 1-n \\ \beta-n+2 \end{matrix} \middle| -t \right) dt \\ = \; & \frac{z}{\Gamma(n)\Gamma(\beta-n+2)}\,{}_3F_2\left(\begin{matrix} 1,1,1-n \\ 2,\beta-n+2 \end{matrix} \middle| -z \right) \end{aligned} \tag{44}$$

Therefore, from (43) and (44),

$$\begin{aligned} -g(-1) &= \sum_{k=1}^{n} \frac{(-1)^{k-1}}{k\,(n-k)!\,\Gamma(\beta-n+k+1)} \\ &= \frac{1}{\Gamma(n)\Gamma(\beta-n+2)}\,{}_3F_2\left(\begin{matrix} 1,1,1-n \\ 2,\beta-n+2 \end{matrix} \middle| 1 \right). \end{aligned}$$

Now, consider the reduction formula [15] [Eqn. 7.4.4(40)]

$${}_3F_2\left(\begin{matrix} 1,1,a \\ 2,b \end{matrix} \middle| 1 \right) = \frac{b-1}{a-1}[\psi(b-1) - \psi(b-a)],$$

to arrive at

$$\sum_{k=1}^{n} \frac{(-1)^{k-1}}{k\,(n-k)!\Gamma(\beta-n+k+1)} = \frac{\psi(\beta+1) - \psi(\beta-n+1)}{n!\,\Gamma(\beta-n+1)}. \tag{45}$$

Finally, substitute (45) in (40) to arrive at the desired result. □

Theorem 8. *For $\alpha > 0$, $\alpha \notin \mathbb{N}$, $\operatorname{Re}\nu > 0$, and $t > 0$, the following fractional derivative holds true:*

$${}_0D_t^{\alpha}\left[t^{\nu-1}\log t\right] = \frac{t^{\nu-\alpha-1}\,\Gamma(\nu)}{\Gamma(\nu-\alpha)}[\log t + \psi(\nu) - \psi(\nu-\alpha)]. \tag{46}$$

Proof. Apply the definition (3) and perform the change in variables $\tau = t\,u$ with $t > 0$, to obtain for $\alpha > 0$,

$$\begin{aligned} & {}_0D_t^{\alpha}\left[t^{\nu-1}\log t\right] \\ = \; & \frac{1}{\Gamma(m-\alpha)}\frac{d^m}{dt^m}\int_0^t (t-\tau)^{m-\alpha-1}\tau^{\nu-1}\log\tau\, d\tau \\ = \; & \frac{1}{\Gamma(m-\alpha)}\frac{d^m}{dt^m}\left\{t^{m-\alpha+\nu-1}\left[\log t\int_0^1 (1-u)^{m-\alpha-1}u^{\nu-1}du\right.\right. \\ & \left.\left. + \int_0^1 (1-u)^{m-\alpha-1}u^{\nu-1}\log u\, du\right]\right\}. \end{aligned} \tag{47}$$

The first integral in (47) is just a beta function (11); thus, for $\operatorname{Re}\nu > 0$, we have

$$\int_0^1 (1-u)^{m-\alpha-1}u^{\nu-1}du = \frac{\Gamma(\nu)\,\Gamma(m-\alpha)}{\Gamma(m-\alpha+\nu)},$$

and for the second one, we can apply (25); thus, for $\operatorname{Re}\nu > 0$, we have

$$\int_0^1 (1-u)^{m-\alpha-1}u^{\nu-1}\log u\, du = \frac{\Gamma(\nu)\,\Gamma(m-\alpha)}{\Gamma(m-\alpha+\nu)}[\psi(\nu)-\psi(m-\alpha+\nu)],$$

thereby

$$\begin{aligned} & {}_0D_t^{\alpha}\left[t^{\nu-1}\log t\right] \\ = \; & \frac{\Gamma(\nu)}{\Gamma(m-\alpha+\nu)} \\ & \left\{\frac{d^m}{dt^m}\left(t^{m-\alpha+\nu-1}\log t\right) + [\psi(\nu)-\psi(m-\alpha+\nu)]\frac{d^m}{dt^m}t^{m-\alpha+\nu-1}\right\}. \end{aligned} \tag{48}$$

Apply (38) to obtain

$$\begin{aligned} & \frac{d^m}{dt^m}\left(t^{m-\alpha+\nu-1}\log t\right) \\ = \; & \frac{\Gamma(m-\alpha+\nu)}{\Gamma(\nu-\alpha)}t^{-\alpha+\nu-1}[\log t + \psi(m-\alpha+\nu)-\psi(\nu-\alpha)], \end{aligned} \tag{49}$$

and apply (30) to obtain

$$\frac{d^m}{dt^m}t^{m-\alpha+\nu-1} = \frac{\Gamma(m-\alpha+\nu)}{\Gamma(\nu-\alpha)}t^{-\alpha+\nu-1}. \tag{50}$$

Insert (49) and (50) in (48), and simplify the result to complete the proof. □

5. Conclusions

On the one hand, according to (27), (46), (24) and (36), we have analytically justified that

$$\begin{aligned} {}_0D_t^{\alpha}\left[t^{\nu-1}\log t\right] &= {}_0I_t^{-\alpha}\left[t^{\nu-1}\log t\right] && (51) \\ &= \frac{t^{\nu-\alpha-1}\,\Gamma(\nu)}{\Gamma(\nu-\alpha)}[\log t + \psi(\nu)-\psi(\nu-\alpha)], \\ {}_0D_t^{\alpha}e^{\lambda t} &= {}_0I_t^{-\alpha}e^{\lambda t} = t^{-\alpha}E_{1,1-\alpha}(\lambda t)\,, && (52) \end{aligned}$$

applying the corresponding definitions of the Riemann–Liouville fractional integral (1) and the Riemann–Liouville fractional derivative (3). Note that the fractional derivatives

calculated in (51) and (52) can be obtained from the corresponding fractional integrals, substituting α by $-\alpha$. However, the corresponding derivations from the Riemann–Liouville definitions of the fractional integral and the fractional derivative in order to arrive to this conclusion are highly non-trivial.

On the other hand, from the definitions of the Weyl fractional integral (2), and the Weyl fractional derivative (4), we have calculated the novel formulas (17), and (32), i.e.,

$$ {}_{-\infty}D_t^{\alpha}|t|^{-\delta} = \frac{\Gamma(\delta+\alpha)}{\Gamma(\delta)} \frac{\cos\left(\frac{\pi\delta}{2}+\pi\alpha\right)}{\cos\left(\frac{\pi\delta}{2}\right)} t^{-\alpha-\delta} = {}_{-\infty}I_t^{-\alpha}|t|^{-\delta}. $$

Again, we can obtain the derivative formula ${}_{-\infty}D_t^{\alpha}|t|^{-\delta}$ substituting α by $-\alpha$ in the corresponding formula for ${}_{-\infty}I_t^{\alpha}|t|^{-\delta}$. Nevertheless, according to the corresponding derivations, this property is not straightforward as in the case of (51) and (52). In general, this occurs because the definition of the Riemann–Liouville fractional derivative (3) involves an m-th derivative. Meanwhile, this is not the case for the definition of the Riemann–Liouville fractional integral (1). It would be interesting to investigate the conditions under which it is satisfied that

$$ {}_aD_t^{\alpha}f(t) = {}_aI_t^{-\alpha}f(t), \tag{53} $$

from the definitions given in (1) and (3) since (53) is implicitly taken for granted in the most common literature about fractional calculus, to the knowledge of the authors.

Author Contributions: Conceptualization, F.M.; methodology, J.L.G.-S.; validation, J.L.G.-S.; formal analysis, J.L.G.-S.; investigation, J.L.G.-S.; writing—original draft preparation, J.L.G.-S.; writing—review and editing, F.M.; supervision, F.M.; project administration, F.M. All authors have read and agreed to the published version of the manuscript.

Funding: This research received no external funding.

Data Availability Statement: Data are contained within the article.

Conflicts of Interest: The authors declare no conflicts of interest.

References

1. Leibniz, G.W. Leibniz an de L'Hospital (letter from Hanover, Germany, September 30, 1695). In *Oeuvres Mathématiques de Leibniz. Correspondance de Leibniz avec Hugens, van Zulichem et le Marquis de L'Hospital*; Libr. de A. Franck: Paris, France, 1853; Volume 2, pp. 297–302.
2. Miller, K.S.; Ross, B. *An Introduction to the Fractional Calculus and Fractional Differential Equations*; John Wiley: New York, NY, USA, 1993.
3. Liouville, J. Mémoire sur quelques questions de géométrie et de mécanique, et sur un nouveau genre de calcul pour résoudre ces questions. *J. L'École Polytech.* **1832**, *13*, 1–69.
4. Podlubny, I.; Magin, R.L.; Trymorush, I. Niels Henrik Abel and the birth of fractional calculus. *Fract. Calc. Appl. Anal.* **2017**, *20*, 1068–1075. [CrossRef]
5. Samko, S.G.; Kilbas, A.A.; Marichev, O.I. *Fractional Integrals and Derivatives*; Gordon & Breach: Amsterdam, The Netherlands, 1993. [English translation from Russian, Nauka i Techika, Minsk (1987)].
6. Bateman, H.; Erdélyi, A.; Magnus, W.; Oberhettinger, F. *Tables of Integral Transforms*; McGraw-Hill: New York, NY, USA, 1954; Volume 2.
7. Mainardi, F. *Fractional Calculus and Waves in Linear Viscoelasticity: An Introduction to Mathematical Models*, 2nd ed.; World Scientific: Singapore, 2022. [1st edition 2010].
8. Podlubny, I. *Fractional Differential Equations*; Academic Press: San Diego, CA, USA, 1999.
9. Magin, R.L. *Fractional Calculus in Bioengineering*; Begell: Danbury, CT, USA, 2021. [1st edition 2006].
10. Lebedev, N.N. *Special Functions and Their Applications*; Prentice-Hall Inc.: Englewood Cliffs, NJ, USA, 1965.
11. Oldham, K.B.; Myland, J.; Spanier, J. *An Atlas of Functions: With Equator, the Atlas Function Calculator*; Springer: New York, NY, USA, 2009.
12. Olver, F.W.J.; Lozier, D.W.; Boisvert, R.F.; Clark, C.W.; Miller, B.R.; Saunders, B.V.; Cohl, H.S.; McClain, M.A. (Eds.) NIST Digital Library of Mathematical Functions. Release 1.2.0 of 2024-03-15. Available online: https://dlmf.nist.gov (accessed on 8 September 2024).
13. Spiegel, M.R. *Mathematical Handbook of Formulas and Tables*; McGraw-Hill: New York, NY, USA, 1968.

14. Andrews, G.E.; Askey, R.; Roy, R. *Special Functions*; Cambridge University Press: Cambridge, CA, USA, 1999.
15. Prudnikov, A.P.; Brychkov, Y.A.; Marichev, O.I. *Integrals and Series: More Special Functions*; CRC Press: Boca Raton, FL, USA, 1986; Volume 3.

Disclaimer/Publisher's Note: The statements, opinions and data contained in all publications are solely those of the individual author(s) and contributor(s) and not of MDPI and/or the editor(s). MDPI and/or the editor(s) disclaim responsibility for any injury to people or property resulting from any ideas, methods, instructions or products referred to in the content.

axioms

MDPI

Article

Existence of Solutions for a Coupled Hadamard Fractional System of Integral Equations in Local Generalized Morrey Spaces

Asra Hadadfard [1], Mohammad Bagher Ghaemi [1,*] and António M. Lopes [2,*]

[1] School of Mathematics and Computer Science, Iran University of Science and Technology, Tehran 16846-13114, Iran; a_hadadfard@mathdep.iust.ac.ir
[2] LAETA/INEGI, Faculty of Engineering, University of Porto, 4200-465 Porto, Portugal
* Correspondence: mghaemi@iust.ac.ir (M.B.G.); aml@fe.up.pt (A.M.L.)

Abstract: This paper introduces a new measure of non-compactness within a bounded domain of $\mathbb{R}^{\mathbb{N}}$ in the generalized Morrey space. This measure is used to establish the existence of solutions for a coupled Hadamard fractional system of integral equations in generalized Morrey spaces. To illustrate the application of the main result, an example is presented.

Keywords: non-compactness measure; hadamard fractional system of integral equations; non-compactness; boundedness

MSC: 26A33; 34A08; 45G15; 47H08

1. Introduction

Fractional calculus (FC) extends the traditional concepts of integer-order calculus by introducing fractional-order derivatives and integrals [1,2]. This generalization allows for a more flexible and comprehensive mathematical framework, which is particularly valuable for modeling complex systems that exhibit non-locality and memory effects phenomena that standard calculus struggles to address effectively. FC has emerged as a critical area of research due to its unique ability to capture and describe processes where the history of the system or its spatial interactions play a crucial role. Over the past few years, fractional calculus has gained substantial attention, with a rapidly growing body of research exploring its wide range of applications across various scientific and engineering fields [3–8]. The increasing interest in FC is largely driven by its success in modeling physical systems that require more than local and immediate effects for accurate representation. For instance, FC has proven to be highly effective in describing diffusion processes, where the rate of diffusion depends on past states, and in control theory, where systems with memory or delayed responses are better understood through fractional models. Similarly, heat conduction and electromagnetics benefit from FC's ability to model systems that involve long-range interactions and cumulative effects over time [9–11].

Results regarding compactness in the spaces $L^p(\mathbb{R}^d)$, with $1 \leq p < \infty$, and $C(K)$, meaning the space of continuous functions on a compact metric space K with values in $\mathbb{R}$, are essential for establishing the existence of solutions to functional integral, integral, and differential equations.

Kuratowski [12] proposed the first definition of the measure of non-compactness. According to his definition, letting Ω be any bounded subset of a metric space, if it is possible to cover Ω with a finite number of balls, then the smallest diameter among these balls is referred to as the Kuratowski's measure of non-compactness. Saha et al. [13] applied the measure within the Hölder space, specifically when studying nonlinear functional integral equations with changed arguments. Mehravaran et al. [14] introduced a set of measures of non-compactness in the locally Sobolev space and then used it to study the existence of solutions for a class of Volterra integro-differential nonlinear equations.

Mehravaran et al. [15] proposed a measure of non-compactness for regulated functions in a specific space, and demonstrated a Darbo-type fixed point theorem. Metwali and Vishnu [16] defined a compactness criterion in Lebesgue spaces and constructed a related measure of non-compactness. They applied it using a modified Darbo-type fixed point theorem to prove that products of n-Hammerstein integral equations have monotonic integrable solutions. Tamimi et al. [17] developed a measure of non-compactness in the generalized Morrey space and used it to address the existence of solutions to systems of nonlinear integral equations. Zhu and Han [18] used the measure of non-compactness, the convex-power condensing operator, the solution operator, and the Banach contraction principle to investigate nonlinear time fractional-order (FO) partial integro-differential equations. Zhu and Han [19] used the Schauder fixed point theorem to explore the approximate controllability of mixed-type non-autonomous FO differential equations. Zhu et al. [20] adopted the measure of non-compactness, the β-resolvent family, and fixed point theorems to study the existence and uniqueness of mild solutions for FO non-autonomous evolution equations. Banaei and Mursaleen [21] established Darbo's fixed point theorems using measures of non-compactness and weakly JS-contractive conditions in Banach spaces. They applied these results to a system of differential equations. Aghajani and Haghighi [22] employed measures of non-compactness and the Darbo fixed point theorem to establish criteria for the existence of solutions to systems of nonlinear equations in Banach spaces. Bokayev et al. [23] provided sufficient conditions for the pre-compactness of sets in the generalized Morrey spaces M^p_w. Arab et al. [24] introduced compact sets in C^k and C^k_0 spaces and developed new measures of non-compactness. They applied them to prove the existence of solutions for functional integro-differential equations.

We can generalize many important theorems from L^p to functions in generalized Morrey spaces. The benefit of working in Morrey spaces, as compared to L^p, is that we can study functions without compact support. This space controls the local integrability of functions, and it makes Morrey spaces more flexible for certain applications. Tamimi et al. [17] developed the first measure of noncompactness in the generalized Morrey spaces; this measure was defined on $\mathbb{R}^{\mathbb{N}}$, and it is a powerful tool for studying the integral equation on unbounded domains.

In this paper, we introduce the new noncompactness measure defined on a bounded domain of $\mathbb{R}^{\mathbb{N}}$. This measure can be applied to investigate the solution for integral equations on every bounded domain of the generalized Morrey spaces. By using the measure of non-compactness within generalized Morrey spaces, we investigate the existence of solutions for the Hadamard FO system of integral equations

$$\begin{cases} u(\xi) = f_1\left(\xi, u(\xi), v(\xi)), \int\limits_1^{\xi} (\ln(\frac{\xi}{\eta}))^{\alpha-1} \frac{b_1(\eta, u(\eta), v(\eta))}{\eta} d\eta\right), \\ v(\xi) = f_2\left(\xi, u(\xi), v(\xi)), \int\limits_1^{\xi} (\ln(\frac{\xi}{\eta}))^{\alpha-1} \frac{b_2(\eta, u(\eta), v(\eta))}{\eta} d\eta\right), \end{cases} \tag{1}$$

where $\xi \in [0, T]$, $\eta \in \mathbb{R}$, $\alpha \in (0, 1)$, and $f_i : [0, T] \times \mathbb{R}^3 \to \mathbb{R}$ for $i = \{1, 2\}$.

Definition 1 ([25]). *Given the function $f : [a, \infty) \to \mathbb{R}$, with $a > 0$, its left-sided Hadamard FO integral of order $\alpha > 0$ is*

$$H^{\alpha}_{a+} f(t) = \frac{1}{\Gamma(\alpha)} \int_a^t \left(\ln \frac{t}{s}\right)^{\alpha-1} \frac{f(s)}{s}\, ds,$$

assuming that the integral exists, $\Gamma(\alpha) = \int_0^{\infty} t^{\alpha-1} e^{-t} dt$, and $\ln(\cdot)$ denotes the natural logarithm function.

Definition 2 ([25]). *For $f \in C^n[a,\infty)$ and $a, \alpha > 0$, the α-order left-sided Hadamard FO derivative is*

$$H^{\alpha}_{a+}f(t) = \frac{1}{\Gamma(n-\alpha)}\left(t\frac{d}{dt}\right)^n \int_a^t \left(\ln\frac{t}{s}\right)^{n-\alpha-1} \frac{f(s)}{s}\, ds,$$

where $n-1 < \alpha \leq n$ and $n = \lceil \alpha \rceil + 1$, with $\lceil \cdot \rceil$ denoting the Gaussian function.

Hadamard first introduced the concept of Hadamard fractional-order (FO) calculus in his work [26]. This form of fractional calculus differs significantly from the more commonly known Riemann–Liouville (R-L) fractional calculus, particularly in terms of the kernel functions that define the fractional derivatives. In a recent study, Ould et al. [27] explored the uniqueness of mild solutions, as well as Ulam–Hyers and Ulam–Hyers-Rassias stability, for abstract fractional differential equations of Sobolev type with nonlocal boundary conditions. Their work employed the Hadamard derivative to achieve these results. Additionally, Maazouz et al. [28] tackled the issue of existence and uniqueness of solutions for boundary value problems related to nonlinear fractional-order pantograph equations. Their approach involved the use of a variable-order fractional derivative of Hadamard type. Furthering the exploration of Hadamard derivatives, Benkerrouche et al. [29] analyzed impulsive boundary value problems (BVP) for differential equations with variable fractional order that include the Caputo–Hadamard fractional derivative. Moreover, Ntouyas et al. [30] initiated research into fractional boundary value problems involving a combination of sequential Riemann–Liouville and Hadamard–Caputo fractional derivatives, with iterated fractional integral boundary conditions supplementing the differential equations. Indeed, the Hadamard and the R-L FO calculus use the kernel functions $k_H(t,s) = (\log \frac{t}{s})^{\alpha-1}$ and $k_{R-L}(t,s) = (t-s)^{\alpha-1}$, respectively. For any $\mu > 0$, $k_H(\mu t, \mu s) = k_H(t,s)$, while $k_{R-L}(\mu t, \mu s) = \mu^{\alpha-1}k_{R-L}(t,s) \neq k_R(t,s)$, highlighting another difference. For more information on the Hadamard FO calculus, please see references [25,30–33].

In the following, we propose a novel measure of non-compactness within a bounded domain of $\mathbb{R}^N$ in the context of generalized Morrey spaces. This newly defined measure is employed to analyze the existence of solutions for a coupled Hadamard FO system of integral equations in those spaces. Additionally, we provide an example that illustrates the applicability of the attained results and highlights potential avenues for further research and applications in a variety of fields.

The rest of this research paper is organized as follows. Section 2 introduces some basic definitions and results. Section 3 establishes a new measure of non-compactness within the framework of generalized Morrey spaces on bounded domains. Section 4 provides an example to confirm the effectiveness and applicability of this measure. Finally, Section 5 summarizes the key findings.

2. Preliminaries

This section provides some fundamental definitions and results that are necessary for the work presented in this paper.

Definition 3 ([21]). *The mapping $\mu : \Lambda_\Theta \longrightarrow [0, +\infty]$ is a measure of non-compactness in Θ if:*

*A*1. $\ker \mu := \{U \in \Lambda_\Theta : \mu(U) = 0\}$ *is Definition 3. nonempty and* $\ker \mu \subset D_\Theta$,
*A*2. $U \subseteq V \Longrightarrow \mu(U) \leq \mu(V)$,
*A*3. $\mu(\overline{U}) = \mu(U) = \mu(\operatorname{Conv} U)$,
*A*4. $\mu(cU + (1-c)V) \leq c\mu(U) + (1-c)\mu(V)$, *for each* $c \in [0,1]$,
*A*5. *If $\{U_n\}$ is a sequence of closed sets from Λ_Θ, such that $U_{n+1} \subseteq U_n$ and $\lim_{n\to\infty} \mu(U_n) = 0$, then the set $U_\infty = \bigcap_{n=1}^{\infty} U_n \neq \emptyset$, where D_Θ is the set of all precompact sets in Λ_Θ, and Λ_Θ is the set of all nonempty, bounded subsets of Θ.*

Theorem 1 ([34]). *Consider a nonempty, bounded, convex, and closed subset F within a Banach space Ω, with a continuous mapping $E : \Omega \longrightarrow \Omega$, and let μ be a measure of non-compactness on Ω. If, for any nonempty subset U of Ω, a constant $c \in [0, 1)$ exists so that*

$$\mu(EU) \leq c\mu(U),$$

then E possesses at least one fixed point in Ω.

Theorem 2 ([22]). *Consider a nonempty, bounded, convex, and closed subset E of a Banach space V, and let μ be an arbitrary measure of non-compactness on V. Suppose that, for $n \in \mathbb{N}$ and $i = 1, 2, \ldots, n$, continuous operators $\mathcal{H}_i : E^n \to E$ exist, and for any subsets $U_1, \ldots, U_n$ of E, a constant $\lambda \in [0, 1)$ exists so that*

$$\mu(\mathcal{H}_i(U_1, \ldots, U_n)) \leq \lambda \max\{\mu(U_1), \ldots, \mu(U_n)\}. \tag{2}$$

Then, for every i, there exist elements $\gamma_1^*, \ldots, \gamma_n^* \in E$, so that $\mathcal{H}_i(\gamma_1^*, \ldots, \gamma_n^*) = \gamma_i^*$.

Definition 4 ([23]). *Let $\Omega_{p\infty}^N$ be the set of all non-negative, measurable and not equivalent to zero functions $\vartheta : (0, +\infty) \longrightarrow (0, +\infty)$, which for some $\xi > 0$*

$$||\vartheta(.)r^{\frac{N}{p}}||_{L^\infty(0,\xi)} < \infty,$$

and for all $\xi > 0$

$$||\vartheta(.)||_{L^\infty(\xi,+\infty)} < \infty,$$

where $1 \leq p \leq \infty$.

Definition 5 ([23]). *The local generalized Morrey space $M_p^\vartheta \equiv M_p^\vartheta(\Omega)$ on $\Omega = [a_1, b_1] \times ... \times [a_n \times b_n] \subseteq \mathbb{R}^N$ is the finite quasi-norm*

$$||f||_p^\vartheta \equiv \sup_{\substack{u\in\Omega,\\ 0<r<diam(\Omega)}} ||\vartheta(.)||f||_{L^p(B(u,.))}||_{L^\infty(0,r)}, \tag{3}$$

where $\vartheta \in \Omega_{p\infty}^N$.

Theorem 3. *The space $M_p^\varpi(\mathbb{R}^N)$ is a non-trivial normed vector space if and only if $\varpi \in \Omega_{p\infty}^N$.*

Example 1. *Let us consider*

$$f(x) = \begin{cases} \sqrt{\pi}, & x \in [2\nu, 2\nu + 1], \\ -\sqrt{\pi}, & x \in (2\nu - 1, 2\nu), \end{cases}$$

where $\nu \in \mathbb{Z}$. If $\vartheta(r) = r^{-\frac{1}{2}}$, we have

$$\sup_{x\in\mathbb{R}} ||\varpi(.)||f||_{L^2(B(x,0))}||_{L^\infty(0,+\infty)} = \sup_{x\in\mathbb{R},r>0} |r^{-\frac{1}{2}}(\int_{x-r}^{x+r} f^2(s)ds)^{\frac{1}{2}}| = \sqrt{2\pi}.$$

Example 2. *We consider*

$$g(x) = \begin{cases} \operatorname{sech}(x), & x \in [2\nu, 2\nu + 1], \\ 0.5. \tanh(x), & x \in (2\nu + 1, 2\nu + 2), \end{cases}$$

where $\nu \in \not\in \mathbb{Z}$, *which belongs to* $M_2^{\vartheta}(\mathbb{R}$ *If* $\vartheta(r) = r^{-\frac{1}{2}}$, *and we have*

$$\sup_{x\in\mathbb{R}} ||\varpi(.)||f||_{L^2(B(x,0))}||_{L^\infty(0,+\infty)} = \sup_{x\in\mathbb{R},r>0} |r^{-\frac{1}{2}}(\int_{x-r}^{x+r} f^2(s)ds)^{\frac{1}{2}}| = \sqrt{2\pi}.$$

This shows that discontinuous functions can belong to the generalized Morrey space. Figure 1 presents a plot of this function.

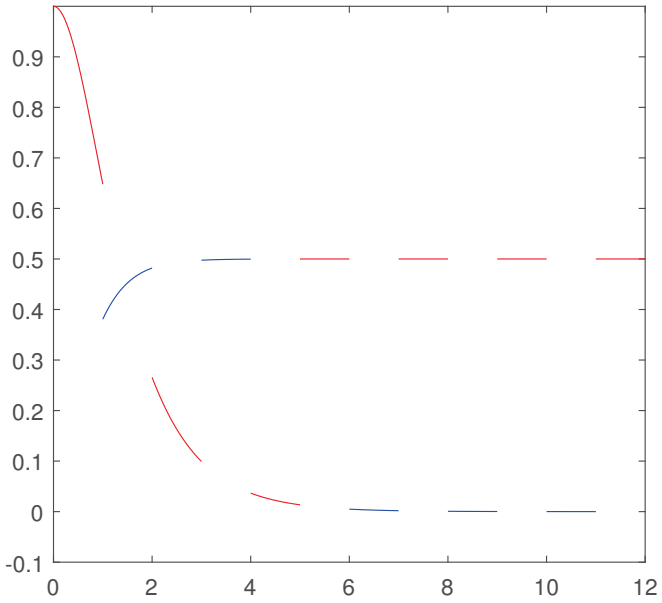

Figure 1. Morrey spaces.

Theorem 4 ([23]). *Suppose that* $\vartheta \in \Omega_{p\infty}^N$ *and* $1 \leq p \leq \infty$. *If, for a subset* Q *of* $M_p^{\vartheta}(\mathbb{R}^N)$,

D1. $\sup_{g\in Q} ||g||_p^{\vartheta} < \infty$,

D2. $\lim_{T\to\infty} \sup_{g\in Q} ||g\chi_{B^c(0,T)}||_p^{\vartheta} = 0$,

D3. $\lim_{|d|\to 0} \sup_{g\in Q} ||T_d g - g||_p^{\vartheta} = 0$,

where $T_d g(u) := g(u+d)$ *for all* $u, d \in \mathbb{R}^N$, *then the subset* Q *is precompact in* $M_p^{\vartheta}(\mathbb{R}^N)$.

Lemma 1 ([24]). *Assume that* E *is a metric space and that, for each* $\epsilon > 0$, *there exist a constant* $\gamma > 0$, *a metric space* F *and a mapping* $\psi : E \longrightarrow F$, *such that* $\psi[E]$ *is totally bounded. Moreover, for* $u, v \in E$, *if* $d(u,v) < \varepsilon$, *then* $d(\psi(u), \psi(v)) < \gamma$. *Under these conditions,* E *is totally bounded.*

3. Measure of Non-Compactness on Bounded Domains

This section establishes a novel measure of non-compactness within the framework of generalized Morrey spaces on bounded domains. This new measure builds upon existing concepts of non-compactness, offering a more refined tool for analyzing the compactness properties of sets in these spaces.

Theorem 5. *Assume that* Ω *is a compact subset of* $\mathbb{R}^N$. *If* $F \subset M_p^{\vartheta}(\Omega)$ *is bounded and equicontinuous with norm of local generalized Morrey space, then* F *is totally bounded in* $M_p^{\vartheta}(\Omega)$.

Proof. By using the equicontinuity of F and compactness of Ω for all $\varepsilon > 0$, we can obtain a finite set of $u_1, ..., u_m \in \Omega$, such that $|u - u_i| < \varepsilon$, with neighborhood $U_1, ..., U_m$ covering Ω, so that $||f(u) - f(u_i)||_p^{\vartheta} < \varepsilon$. Define $\varphi : F \longrightarrow \mathbb{R}^m$, such that $\varphi(f) := (f(u_1), ..., f(u_m))$

by boundedness of F. The image $\varphi[F]$ is totally bounded on $\mathbb{R}^m$. Additionally, if $f, g \in F$ satisfy $||\varphi(f) - \varphi(g)||_p^\vartheta < \varepsilon$, then by Lemma 1, F is totally bounded. □

Theorem 6. *Let $\mathcal{H}$ be a bounded subset of $M_p^\vartheta(\Omega)$, with $1 \leq p \leq \infty$, and*

$$\varpi(g, \varepsilon) := \sup\Big\{||T_d g - g||_p^\vartheta : |d| < \epsilon\Big\}, \tag{4}$$

$$\varpi(\mathcal{H}, \varepsilon) := \sup\{\varpi(g, \varepsilon) : g \in \mathcal{H}\}, \tag{5}$$

$$\varpi_0(\mathcal{H}) := \lim_{\epsilon \to 0} \varpi(\mathcal{H}, \varepsilon), \tag{6}$$

where $T_d g(\xi) := g(\xi + d)$ for all $\xi, d \in \Omega$. Therefore, $\varpi_0 : \Omega_{M_p^\vartheta(\Omega)} \longrightarrow \mathbb{R}^+$ is a measure of non-compactness on $M_p^\vartheta(\Omega)$.

Proof. Let $\mathcal{H} \in \Lambda_\Omega$, such that $\varpi_0(\mathcal{H}) = 0$. According to Equations (4)–(6), it holds that $\lim_{|d| \to 0} ||T_d g - g||_p^\vartheta = 0$ uniformly for all $g \in \mathcal{H}$. Therefore, by Theorem 5, we conclude that $\mathcal{H}$ is precompact. The condition $(A2)$ is straightforward, and thus $\varphi_0(\mathcal{H}) \leq \varpi_0(\bar{\mathcal{H}})$. To prove the reverse inequality, assume that $g \in \bar{\mathcal{H}}$ and that there exists a sequence $\{g_n\}_{n=1}^\infty \subset \mathcal{H}$ such that $g_n \to g$ in $M_p^\vartheta(\Omega)$. For $\epsilon > 0$, a $k \in \mathbb{N}$ exists such that, for all $m > k$, $||g - g_m||_p^\vartheta < \dfrac{\epsilon}{2}$. For each $d \in \mathbb{R}^N$ with $|d| < \varepsilon$

$$\begin{aligned} ||T_d g - g||_p^\vartheta &\leq ||T_d g - T_d g_m||_p^\vartheta + ||T_d g_m - g_m||_p^\vartheta + ||g_m - g||_p^\vartheta \\ &= ||g_m - g||_p^\vartheta + ||T_d g_m - g_m||_p^\vartheta + ||g - g_m||_p^\vartheta \\ &\leq \varepsilon + \varpi(g_m, \varepsilon). \end{aligned}$$

Therefore, $\varpi(\bar{\mathcal{H}}, \varepsilon) \leq \varepsilon + \varpi(\mathcal{H}, \varepsilon)$. Hence,

$$\varpi_0(\bar{\mathcal{H}}) \leq \varpi_0(\mathcal{H}). \tag{7}$$

This completes the proof of (A3). Because the norm has a triangular property, one can check (A4) quickly. In the following, the correctness of (A5) is verified. Suppose that $\{g_n\}$ is a sequence formed of closed sets in $\Lambda_{M_p^\vartheta}(\Omega)$, so that $g_{n+1} \subseteq g_n$ and $\lim_{n \to \infty} \varpi_0(\mathcal{H}_n) = 0$. For any $n \in \mathbb{N}$, select $g_n \in \mathcal{H}_n$. Now, it needs to be shown that g_n converges to some g_0. Suppose that one defines $H = \{g_n\}$. Then, it is necessary to prove that H is compact. Hence, it must be proven that H is equicontinuous and bounded. In the following, it is known that $\lim_{n \to \infty} \varpi_0(g_n) = 0$, so for any $\epsilon > 0$, there exists a $L > 0$ such that, for $m > L$, $\varpi_0(g_m) < \epsilon$. Then, $\|T_d g_m - g_m\|_p < \epsilon$. This implies equicontinuity of $\{g_m\}_{m=L}^\infty$. By applying Lemma 1, it can be concluded that $\{g_m\}_{m=L}^\infty$ is compact, and thus, $\{g_i\}_{i=1}^L$ is also compact. □

4. Applications within Generalized Morrey Spaces

This section illustrates the practical usefulness of the newly introduced measure of non-compactness. An example is carefully chosen to show how the new measure can be effectively applied to solve complex problems within generalized Morrey spaces.

We examine the system (1) within the framework of generalized Morrey spaces and demonstrate that if system (1) satisfies the conditions

A. Function $J_i : \mathbb{R}_+ \longrightarrow \mathbb{R}_+$ is continuous and function $f_i : \mathbb{R}^4 \longrightarrow \mathbb{R}$ is measurable. Therefore, positive constants λ_1, λ_2 and λ_3 exist, such that $0 < \lambda_1 + \lambda_2 < 1$, and

$$\begin{aligned} &|f_i(\xi_1, u_1, v_1, z_1) - f_i(\xi_2, u_2, v_2, z_2)| \leq |J_i(\xi_1) - J_i(\xi_2)| + \lambda_1 |u_1(\xi) - u_2(\xi)| + \\ &\lambda_2 |v_1(\xi) - v_2(\xi)| + \lambda_3 |z_1(\xi) - z_2(\xi)|, \end{aligned} \tag{8}$$

where $i \in \{1, 2\}$ and $\lambda_3 \in \mathbb{R}_+$.

B. The function $b_i : \mathbb{R}^3 \longrightarrow \mathbb{R}$ is bounded and continuous, with a positive constant M such that $|b_i(\xi, u, v)| \leq M$.
C. $f_{i,0}(\xi) := f_i(\xi, 0, 0, 0)$ belongs to $M_p^{\vartheta}(\Omega) \cap L^p(\Omega)$.
Then, the system (1) has at least one solution.

Theorem 7. *Under conditions A–C, the system* (1) *has at least one solution in* $M_p^{\vartheta}(\Omega)$.

Proof. We start with

$$||u||_p^{\vartheta} \equiv \sup_{\substack{u\in\Omega,\\ 0<r<\mathrm{diam}(\Omega)}} ||\omega_{(.)}||u||_{L^p(B(u,.))}||_{L^\infty(0,r)} < r_0,$$

$$||v||_p^{\vartheta} \equiv \sup_{\substack{u\in\Omega,\\ 0<r<\mathrm{diam}(\Omega)}} ||\omega_{(.)}||v||_{L^p(B(v,.))}||_{L^\infty(0,r)} < r_0,$$

and

$$F_i(u(\xi), v(\xi)) = f_i\Big(\xi, u(\xi), v(\xi), \int_1^{\xi} (\ln \frac{\xi}{\eta})^{\alpha-1} \frac{b_i(\eta, u(\eta), v(\eta))}{\eta} d\eta\Big). \tag{9}$$

According to the Cauchy–Schwartz inequality, we obtain

$$|F_i(u,v)(\xi)| \leq |f_i(\xi, u(\xi), v(\xi)), \int_1^{\xi} (\ln(\frac{\xi}{\eta}))^{\alpha-1} \frac{b_i(\eta, u(\eta), v(\eta))}{\eta} d\eta) - f_i(\xi, 0, 0, 0) + f_i(\xi, 0, 0, 0)| \tag{10}$$

$$\leq \lambda_1 |u(\xi)| + \lambda_2 |v(\xi)| + \lambda_3 M (T-1)^{\frac{1}{2}} \frac{1}{2\alpha - 1} (\ln(T))^{2\alpha-1}. \tag{11}$$

By the Lebesgue-dominated convergence theorem, we have

$$||F_i(u,v)(\xi)||_p^{\vartheta} \leq \lambda_1 ||u(\xi)||_p^{\vartheta} + \lambda_2 ||v(\xi)||_p^{\vartheta} + \lambda_3 M (T-1)^{\frac{1}{2}} \frac{1}{2\alpha - 1} (\ln(T))^{2\alpha-1}. \tag{12}$$

We choose r_0 such that

$$\frac{\lambda_3 M (T-1)^{\frac{1}{2}} (\ln(T))^{2\alpha-1}}{(2\alpha - 1)(1 - \lambda_1 - \lambda_2)} < r_0, \tag{13}$$

Therefore, we prove that F_i is a self-map. We show that $u_n \to u$ and $v_n \to v$ in B_{r_0} with norm $M_p^{\vartheta}(\Omega)$. So, we show that $F_i(u_n, v_n) \to F_i(u, v)$ for $i \in 1, 2$. By using A and C, we get

$$\begin{aligned}
&|f_i(\xi, u_n(\xi), v_n(\xi)), \int_1^{\xi} (\ln(\frac{\xi}{\eta}))^{\alpha-1} \frac{b_i(\eta, u_n(\eta), v_n(\eta))}{\eta} d\eta) \\
&\quad - f_i(\xi, u(\xi), v(\xi)), \int_1^{\xi} (\ln(\frac{\xi}{\eta}))^{\alpha-1} \frac{b_i(\eta, u(\eta), v(\eta))}{\eta} d\eta)| \\
&\leq \lambda_1 |u_n(\xi) - u(\xi)| + \lambda_2 |v_n(\xi) - v(\xi)| \\
&\quad + \lambda_3 \left| \int_1^{\xi} \left(\ln\left(\frac{\xi}{\eta}\right) \right)^{\alpha-1} \frac{b_i(\eta, u_n(\eta), v_n(\eta)) - b_i(\eta, u(\eta), v(\eta))}{\eta} d\eta \right|.
\end{aligned} \tag{14}$$

By the Lebesgue-dominated convergence theorem, we have

$$\begin{aligned}
&||f_i(\xi, u_n(\xi), v_n(\xi)), \int_1^{\xi} (\ln(\frac{\xi}{\eta}))^{\alpha-1} \frac{b_i(\eta, u_n(\eta), v_n(\eta))}{\eta} d\eta) \\
&\quad - f_i(\xi, u(\xi), v(\xi)), \int_1^{\xi} (\ln(\frac{\xi}{\eta}))^{\alpha-1} \frac{b_i(\eta, u(\eta), v(\eta))}{\eta} d\eta)||_p^{\vartheta} \\
&\leq \lambda_1 ||u_n(\xi) - u(\xi)||_p^{\vartheta} + \lambda_2 ||v_n(\xi) - v(\xi)||_p^{\vartheta} \\
&\quad + \lambda_3 \left|\left| \int_1^{\xi} \left(\ln\left(\frac{\xi}{\eta}\right) \right)^{\alpha-1} \frac{b_i(\eta, u_n(\eta), v_n(\eta)) - b_i(\eta, u(\eta), v(\eta))}{\eta} d\eta \right|\right|_p^{\vartheta}. \qquad (15)
\end{aligned}$$

Then $||F_i(u_n, v_n) - F_i(u, v)||_p^{\vartheta} \to 0$ as $n \to \infty$, confirming that F_i is continuous in the local generalized Morrey space.

Now, we show that, for the nonempty subsets $X_1, X_2 \in B_{r_0}$, we have

$$\varpi(F_i(X_1, X_2)) \leq C_1 \max \varpi(X_1, X_2), \qquad (16)$$

with $C_1 := \max\{\lambda_1, \lambda_2\}$. We choose $u \in X_1$ and $v \in X_2$. For an arbitrary $\varepsilon > 0$ and $\xi, d \in \Omega$ with $|d| < \varepsilon$, we have:

$$\begin{aligned}
&|F_i(u, v)(\xi + d) - F_i(u, v)(\xi)| = \\
&|f_i(\xi + d, u(\xi + d), v(\xi + d), \int_1^{\xi+d} (\ln(\frac{\xi + d}{\eta}))^{\alpha-1} \frac{b_i(\eta, u(\eta), v(\eta))}{\eta} d\eta) \\
&- f_i(\xi, u(\xi), v(\xi), \int_1^{\xi} (\ln(\frac{\xi}{\eta}))^{\alpha-1} \frac{b_i(\eta, u(\eta), v(\eta))}{\eta} d\eta)| \\
&< |J_i(\xi + d) - J_i(d)| + \lambda_1 |u(\xi + d) - u(\xi)| + \lambda_2 |v(\xi + d) - v(\xi)| \\
&+ \lambda_3 | \int_1^{\xi+d} (\ln(\frac{\xi + d}{\eta}))^{\alpha-1} \frac{b_i(\eta, u(\eta), v(\eta))}{\eta} d\eta - \ln(\frac{\xi}{\eta}))^{\alpha-1} \frac{b_i(\eta, u(\eta), v(\eta))}{\eta} d\eta|. \qquad (17)
\end{aligned}$$

By the Lebesgue-dominated convergence theorem, we have

$$\begin{aligned}
&||F_i(u, v)(\xi + d) - F_i(u, v)(\xi)||_p^{\vartheta} = \\
&< ||J_i(\xi + d) - J_i(d)||_p^{\vartheta} + \lambda_1 ||u(\xi + d) - u(\xi)||_p^{\vartheta} + \lambda_2 ||v(\xi + d) - v(\xi)||_p^{\vartheta} \\
&+ \lambda_3 || \int_1^{\xi+d} (\ln(\frac{\xi + d}{\eta}))^{\alpha-1} \frac{b_i(\eta, u(\eta), v(\eta))}{\eta} d\eta - \ln(\frac{\xi}{\eta}))^{\alpha-1} \frac{b_i(\eta, u(\eta), v(\eta))}{\eta} d\eta||_p^{\vartheta}. \qquad (18)
\end{aligned}$$

Applying the Riesz–Fischer and the Lebesgue-dominated convergence theorems, the proof is completed. □

Remark 1. *In a similar manner, the investigation of both finite and infinite systems of fractional integral equations within the context of generalized Morrey spaces constitutes an important area of research. For an in-depth analysis of this subject, readers are encouraged to consult the thorough examination found in reference [17].*

Example 3. *Here, we present an example that illustrates the effectiveness and applicability of Theorem 7. For every positive constant T such that $\xi \in [0, T]$, we consider a system of fractional differential equations:*

$$\begin{cases}
u(\xi) = e^{-\xi} + \dfrac{u(\xi)}{e^{\xi} + 3} + \dfrac{v(\xi)}{\xi^2 + 3} + \int_1^{\xi} (\ln(\frac{\xi}{\eta}))^{\frac{-1}{6}} \dfrac{\arctan(u(\eta) + v(\eta))}{\eta} d\eta, \\
v(\xi) = \dfrac{1}{1 + \cosh(\xi)} + \dfrac{u(\xi)}{20 + \cos(\xi)} + \dfrac{v(\xi)}{\pi + \cos^2(\xi)} + \int_1^{\xi} (\ln(\frac{\xi}{\eta}))^{\frac{-1}{6}} \dfrac{\sin(u(\eta) + v(\eta))}{\eta} d\eta.
\end{cases} \qquad (19)$$

According to system (1) *and Equation* (9), *we obtain*

$$\begin{cases} f_1(\xi,u,v,z) = e^{-\xi} + \dfrac{u}{e^{\xi}+3} + \dfrac{v}{\xi^2+3} + z, \\ f_2(\xi,u,v,z) = \dfrac{1}{1+\cosh(\xi)} + \dfrac{u}{20+\cos(\xi)} + \dfrac{v}{\pi+\cos^2(\xi)} + z. \end{cases}$$

We set $\vartheta = r^{\frac{-1}{2}}$, *and* $\alpha = \dfrac{1}{2}$. *Since* $f_1(\xi,0,0,0) = e^{-\xi}$ *and* $f_2(\xi,0,0,0) = \dfrac{1}{1+\cosh(\xi)}$, *then* $||J_1||_p^{\vartheta} \leq \sqrt{2}$, *and* $||J_2||_p^{\vartheta} \leq \dfrac{1}{\sqrt{2}}$. *Furthermore,*

$$\begin{aligned} \lambda_1 &= \max\left\{ \sup_{0\leq\xi\leq T}\left\{\frac{1}{e^{\xi}+3}\right\}, \sup_{0\leq\xi\leq T}\left\{\frac{1}{\cos(\xi)+20}\right\}\right\} = \frac{1}{3}, \\ \lambda_2 &= \max\left\{ \sup_{0\leq\xi\leq T}\left\{\frac{1}{\xi^2+3}\right\}, \sup_{0\leq\xi\leq T}\left\{\frac{1}{\cos^2(\xi)+\pi}\right\}\right\} = \frac{1}{3}, \\ \lambda_3 &= 1. \end{aligned}$$

Hence, conditions $A-C$ *are satisfied. Then, for each* $p \geq 1$, *the system* (19) *has a solution in* M_p^{ϑ}.

Example 4. *We demonstrate that the fractional integral system* (20) *possesses a solution within the space* M_p^{ϑ}:

$$\begin{cases} u(\xi) = \arctan(\xi^2+1) + \dfrac{\cos(v(\xi))}{|\sinh(\xi)|+15} + \int_1^{\xi}(\ln(\frac{\xi}{\eta}))^{-\frac{1}{6}}\dfrac{\cos(v(\eta))}{\eta}d\eta, \\ \\ v(\xi) = \tanh(\xi) + \dfrac{\arctan(u(\xi)+v(\xi))}{\xi^5+20} + \int_1^{\xi}(\ln(\frac{\xi}{\eta}))^{-\frac{1}{6}}\dfrac{\operatorname{sech}(u(\eta))}{\eta}d\eta. \end{cases} \tag{20}$$

According to system (1) *and Equation* (9), *we obtain*

$$\begin{cases} f_1(\xi,u,v,z) = \arctan(\xi^2+1) + \dfrac{\cos(v)}{|\sinh(\xi)|+15} + u, \\ f_2(\xi,u,v,z) = \tanh(\xi) + \dfrac{\arctan(u+v)}{\xi^5+20} + u. \end{cases}$$

We set $\varpi(r) = r^{\frac{-1}{3}}$, *and* $\alpha = \dfrac{1}{3}$. *Since* $f_1(\xi,0,0,0) = \arctan(\xi^2+1)$ *and* $f_2(\xi,0,0,0) = \tanh(\xi)$, *then* $||J_1||_p^{\vartheta} \leq \frac{\sqrt[3]{2}}{8}\pi^2$, *and* $||J_2||_p^{\vartheta} \leq \sqrt[3]{2}$. *Additionally,*

$$\begin{aligned} \lambda_1 &= \max\left\{0, \sup_{0\leq\xi\leq T}\left\{\frac{1}{\xi^2+20}\right\}\right\} = \frac{1}{20}, \\ \lambda_2 &= \max\left\{ \sup_{0\leq\xi\leq T}\left\{\frac{1}{|\sinh(\xi)|+15}\right\}, \sup_{0\leq\xi\leq T}\left\{\frac{1}{\xi^2+20}\right\}\right\} = \frac{1}{15}, \\ \lambda_3 &= 1. \end{aligned}$$

Hence, conditions A–C are satisfied. Then, for each $p \geq 1$, *the system* (20) *has a solution in* M_p^{ϑ}.

5. Concluding Remarks

This paper introduced a novel measure of non-compactness within a bounded domain in $\mathbb{R}^N$ for generalized Morrey spaces. This measure was utilized to demonstrate the existence of solutions for a coupled Hadamard fractional-order system of integral equations in these spaces. Examples were provided to illustrate the application of the main result.

The paper also suggested future research directions, including the study of infinite systems of integral equations in Morrey spaces and extending these results to other domains, such as Morrey spaces on $\mathbb{R}^2$.

Author Contributions: Conceptualization, A.H. and M.B.G.; formal analysis, A.H., M.B.G. and A.M.L.; investigation, A.H. and M.B.G.; methodology, A.H. and M.B.G.; software, A.H.; supervision, M.B.G.; validation, A.H., M.B.G. and A.M.L.; visualization, A.H., M.B.G. and A.M.L.; writing—original draft, A.H.; writing—review and editing, A.H., M.B.G. and A.M.L. All authors have read and agreed to the published version of the manuscript.

Funding: The authors received no financial support for this article.

Data Availability Statement: Data sharing is not applicable to this article as no new data were created or analyzed in this study.

Acknowledgments: The authors sincerely thank the editor and anonymous referee for their careful reading, constructive comments, and useful suggestions that improved the manuscript.

Conflicts of Interest: The authors declare no conflicts of interest.

References

1. Sabatier, J.; Agrawal, O.P.; Machado, J.T. *Advances in Fractional Calculus*; Springer: Berlin/Heidelberg, Germany, 2007; Volume 4.
2. Baleanu, D.; Diethelm, K.; Scalas, E.; Trujillo, J.J. *Fractional Calculus: Models and Numerical Methods*; World Scientific: Singapore, 2012; Volume 3.
3. Golbabai, A.; Nikan, O.; Nikazad, T. Numerical investigation of the time fractional mobile-immobile advection-dispersion model arising from solute transport in porous media. *Int. J. Appl. Comput. Math.* **2019**, *5*, 50. [CrossRef]
4. Al-Issa, S.M.; Kaddoura, I.H.; Rifai, N.J. Existence and Hyers-Ulam stability of solutions to the implicit second-order differential equation via fractional integral boundary conditions. *J. Math. Comput. Sci.* **2023**, *31*, 15–29. [CrossRef]
5. Can, N.H.; Nikan, O.; Rasoulizadeh, M.N.; Jafari, H.; Gasimov, Y.S. Numerical computation of the time non-linear fractional generalized equal width model arising in shallow water channel. *Thermal Sci.* **2020**, *24*, 49–58. [CrossRef]
6. El-Sayed, A.M.A.; Abdurahman, M.; Fouad, H.A. Existence and stability results for the integrable solution of a singular stochastic fractional-order integral equation with delay. *J. Math. Comput. Sci.* **2024**, *33*, 17–26. [CrossRef]
7. Al-Habahbeh, A. Exact solution for commensurate and incommensurate linear systems of fractional differential equations. *J. Math. Comput. Sci.* **2023**, *28*, 123–136. [CrossRef]
8. Oderinu, R.A.; Owolabi, J.A.; Taiwo, M. Approximate solutions of linear time-fractional differential equations. *J. Math. Comput. Sci.* **2023**, *29*, 60–72. [CrossRef]
9. Nikan, O.; Avazzadeh, Z.; Tenreiro Machado, J.A. Localized kernel-based meshless method for pricing financial options underlying fractal transmission system. *Math. Methods Appl. Sci.* **2024**, *47*, 3247–3260. [CrossRef]
10. Aghdam, Y.E.; Mesgrani, H.; Javidi, M.; Nikan, O. A computational approach for the space-time fractional advection–diffusion equation arising in contaminant transport through porous media. *Eng. Comput.* **2021**, *37*, 3615–3627. [CrossRef]
11. Nikan, O.; Golbabai, A.; Machado, J.T.; Nikazad, T. Numerical solution of the fractional Rayleigh–Stokes model arising in a heated generalized second-grade fluid. *Eng. Comput.* **2021**, *37*, 1751–1764. [CrossRef]
12. Kuratowski, K. Sur les espaces complets. *Fund. Math.* **1930**, *15*, 301–309. [CrossRef]
13. Saha, D.; Sen, M.; Sarkar, N.; Saha, S. Existence of a solution in the Holder space for a nonlinear functional integral equation. *Arm. J. Math.* **2020**, *12*, 1–8. [CrossRef]
14. Mehravaran, H.; Khanehgir, M.; Allahyari, R. A family of measures of noncompactness in the locally Sobolev spaces and its applications to some nonlinear Volterra integrodifferential equations. *J. Math.* **2018**, *2018*, 3579079. [CrossRef]
15. Mehravaran, H.; Amiri Kayvanloo, H.; Allahyari, R. Measures of noncompactness in the space of regulated functions $R(J, \mathbb{R}^{\infty})$ and its application to some nonlinear infinite systems of fractional differential equations. *Math. Sci.* **2023**, *17*, 223–232. [CrossRef]
16. Metwali, M.; Mishra, V.N. On the measure of noncompactness in $L_p(\mathbb{R}^+)$ and applications to a product of n-integral equations. *Turk. J. Math.* **2023**, *47*, 372–386. [CrossRef]
17. Tamimi, G.; Saiedinezhad, S.; Ghaemi, M. Applications of a new measure of noncompactness to the solvability of systems of nonlinear and fractional integral equations in the generalized Morrey spaces. *Fract. Calc. Appl. Anal.* **2024**, *27*, 1215–1235. [CrossRef]
18. Zhu, B.; Han, B. Existence and uniqueness of mild solutions for fractional partial integro-differential equations. *Mediterr. J. Math.* **2020**, *17*, 113. [CrossRef]
19. Zhu, B.; Han, B. Approximate controllability for mixed type non-autonomous fractional differential equations. *Qual. Theory Dyn. Syst.* **2022**, *21*, 111. [CrossRef]
20. Zhu, B.; Han, B.; Yu, W. Existence of mild solutions for a class of fractional non-autonomous evolution equations with delay. *Acta Math. Appl. Sin. Engl. Ser.* **2020**, *36*, 870–878. [CrossRef]

21. Banaei, S.; Mursaleen, M.; Parvaneh, V. Some fixed point theorems via measure of noncompactness with applications to differential equations. *Comput. Appl. Math.* **2020**, *39*, 139. [CrossRef]
22. Aghajani, A.; Haghighi, A. Existence of solutions for a system of integral equations via measure of noncompactness. *Novi Sad J. Math.* **2014**, *44*, 59–73.
23. Bokayev, N.; Burenkov, V.; Matin, D. On the pre-compactness of a set in the generalized Morrey spaces. *Aip Conf. Proc.* **2016**, *1759*, 020108. [CrossRef]
24. Arab, R.; Allahyari, R.; Shole Haghighi, A. Construction of measures of noncompactness of $C^k(\Omega)$ and $C_0^k(\Omega)$ and their application to functional integral-differential equations. *Bull. Iran. Math. Soc.* **2017**, *43*, 53–67.
25. Lv, X.; Zhao, K.; Xie, H. Stability and Numerical Simulation of a Nonlinear Hadamard Fractional Coupling Laplacian System with Symmetric Periodic Boundary Conditions. *Symmetry* **2024**, *16*, 774. [CrossRef]
26. Hadamard, J. Essai sur l'étude des fonctions données par leur développement de Taylor. *J. Math. Pures Appl.* **1892**, *8*, 101–186.
27. Ould Melha, K.; Mohammed Djaouti, A.; Latif, M.A.; Chinchane, V.L. Study of Uniqueness and Ulam-Type Stability of Abstract Hadamard Fractional Differential Equations of Sobolev Type via Resolvent Operators. *Axioms* **2024**, *13*, 131. [CrossRef]
28. Maazouz, K.; Zaak, M.D.A.; Rodríguez-López, R. Existence and uniqueness results for a pantograph boundary value problem involving a variable-order Hadamard fractional derivative. *Axioms* **2023**, *12*, 1028. [CrossRef]
29. Benkerrouche, A.; Souid, M.S.; Stamov, G.; Stamova, I. Multiterm impulsive Caputo–Hadamard type differential equations of fractional variable order. *Axioms* **2022**, *11*, 634. [CrossRef]
30. Ntouyas, S.K.; Sitho, S.; Khoployklang, T.; Tariboon, J. Sequential Riemann–Liouville and Hadamard–Caputo fractional differential equation with iterated fractional integrals conditions. *Axioms* **2021**, *10*, 277. [CrossRef]
31. Miller, K.S.; Ross, B. *An Introduction to the Fractional Calculus and Differential Equations*; Wiley: New York, NY, USA, 1993.
32. Zhou, Y. *Basic Theory of Fractional Differential Equations*; World Scientific: Singapore, 2014.
33. Chinchane, V.L.; Nale, A.B.; Panchal, S.K.; Chesneau, C.; Khandagale, A.D. On Fractional Inequalities Using Generalized Proportional Hadamard Fractional Integral Operator. *Axioms* **2022**, *11*, 266. [CrossRef]
34. Darbo, G. Punti uniti in trasformazioni a codominio non compatto. *Rend. Semin. Mat. Univ. Padova* **1955**, *24*, 84–92.

Disclaimer/Publisher's Note: The statements, opinions and data contained in all publications are solely those of the individual author(s) and contributor(s) and not of MDPI and/or the editor(s). MDPI and/or the editor(s) disclaim responsibility for any injury to people or property resulting from any ideas, methods, instructions or products referred to in the content.

fractal and fractional

MDPI

Article

Multiple Solutions for a Critical Steklov Kirchhoff Equation

Maryam Ahmad Alyami [1,*,†] and Abdeljabbar Ghanmi [2,†]

[1] Department of Mathematics and Statistics, Faculty of Sciences, University of Jeddah, Jeddah 21493, Saudi Arabia
[2] ENIT-LAMSIN, Tunis El Manar University, BP. 37, Tunis-Belvídère, Tunis 1002, Tunisia; abdeljabbar.ghanmi@lamsin.rnu.tn
* Correspondence: maalyami8@uj.edu.sa
† These authors contributed equally to this work.

Abstract: In the present work, we study some existing results related to a new class of Steklov $p(x)$-Kirchhoff problems with critical exponents. More precisely, we propose and prove some properties of the associated energy functional. In the first existence result, we use the mountain pass theorem to prove that the energy functional admits a critical point, which is a weak solution for such a problem. In the second main result, we use a symmetric version of the mountain pass theorem to prove that the investigated problem has an infinite number of solutions. Finally, in the third existence result, we use a critical point theorem proposed by Kajikiya to prove the existence of a sequence of solutions that tend to zero.

Keywords: variational methods; ψ-Hilfer fractional derivative; critical exponent; concentration-compactness principle; fractional Kirchhoff equation; Steklov problem

1. Introduction

In this study, we examine a specific class of fractional Kirchhoff-type problem with a $p(x)$-Laplacian operator, which is expressed as follows:

$$\begin{cases} M\left(\int_\Lambda \frac{1}{p(x)}\left|{}^{\mathrm{H}}\mathbb{D}_{0+}^{\omega,\nu;\psi}u\right|^{p(x)}dx\right)\mathbf{L}_{p(x)}^{\omega,\nu;\psi}u = |u|^{r(x)-2}u + \mathfrak{g}(x,u), \ in\ \Lambda=(0,T)\times(0,T), \\ \left|\mathbb{D}_{0+}^{\omega,\nu;\mu}u\right|^{p(x)-2}\frac{\partial u}{\partial v} = |u|^{s(x)-2}u \quad \text{on } \partial\Lambda, \end{cases} \tag{1}$$

where

$$\mathbf{L}_{p(x)}^{\omega,\nu;\psi}u = {}^{\mathrm{H}}\mathbb{D}_{0+}^{\omega,\nu;\psi}\left(\left|{}^{\mathrm{H}}\mathbb{D}_{0+}^{\omega,\nu;\psi}u\right|^{p(x)-2}{}^{\mathrm{H}}\mathbb{D}_{0+}^{\omega,\nu;\psi}u\right), \tag{2}$$

where ${}^{\mathrm{H}}\mathbb{D}_{0+}^{\omega,\nu;\psi}(\cdot)$ and ${}^{\mathrm{H}}\mathbb{D}_{0+}^{\omega,\nu;\psi}(\cdot)$ are ψ-Hilfer fractional partial derivatives of order $\frac{1}{p^+} < \omega < 1$ and type $0 \le \nu \le 1$. $\frac{\partial u}{\partial v}$ is the outer-unit normal derivative. p, r, and $s \in C(\overline{\Lambda})$ are such that

$$1 < p^- = \inf_\Lambda p(x) \le p^+ = \sup_\Lambda p(x) < 2,$$

$$p^+ < r(x) \le p^*(x), \text{ for all } x \in \Lambda,$$

and

$$p^+ < s(x) < p_*(x) \text{ for all } x \in \partial\Lambda,$$

where $p^*(x)$ is the critical exponent, which is defined as follows:

$$p^*(x) = \begin{cases} \frac{p(x)}{2-p(x)} \text{ if } p(x) < 2, \\ \infty \text{ if } p(x) \ge 2. \end{cases}$$

The Kirchhoff function (M) is continuous, and the nonlinearity ($\mathfrak{g}$) is of the Carathéodory type.

In recent years, considerable attention has been paid to problems involving the ψ-Hilferfractional derivative with a p-Laplacian operator [1–8]. Problems that involve the growth of the critical exponent are more complicated, since the embedding is continuous and not compact. To solve this lack of compactness, Lions [9] used the concentration-compactness principle. Recently, several problems have arisen that involve critical growth behavior. For a more thorough exploration of this subject, we recommended that interested readers consult references [10–13] and other related sources.

The investigation of problems characterized by variable exponents, critical growth, and those involving the ψ-Hilfer fractional derivative with a p-Laplacian operator has garnered considerable interest in recent years. These issues are not only intriguing but also relevant to various applications, including the modeling of electrorheological fluids [14–16], image processing [17], medicine [18], economics and finance [19,20], physics [21,22], and biology [23]. Moreover, they represent difficult mathematical problems that require a detailed examination.

The authors of [24] explored an equation with critical variable exponents.

$$\begin{cases} (-\Delta)_{p(x)}u = |u|^{r(x)-2}u + a(x)|u|^{q(x)-2}u & \text{in } \Lambda, \\ u = 0 \quad \text{on } \partial\Lambda, \end{cases}$$

where p, r, and q are such that

$$1 < p(x) < q(x) \leq r(x) \leq p^*(x), \forall\, x \in \Lambda.$$

It is assumed that the set $A = \{x \in \Lambda : r(x) = p^*(x)\}$ is not empty, which suggests the appearance of critical growth behavior. To demonstrate the existence of solutions, the authors utilized variational methods alongside the mountain pass theorem. These approaches enabled them to formulate an appropriate functional and apply critical point theory to identify non-trivial solutions to the problem.

The problems related to Kirchhoff-type problems with variable exponents are attracting significant attention and becoming increasingly important to various research groups due to a range of theoretical and practical inquiries [25–29]. Furthermore, it is important to highlight the growing interest in Kirchhoff problems involving fractional operators, which has seen a remarkable increase over the years [30–32]. The $p(x)$-Laplacian introduces more intricate nonlinearity, leading to several fundamental challenges. For approximation, the authors of [4] explored the Kirchhoff fractional $p(\xi)$-Laplacian problem without a critical exponent.

$$\begin{cases} \mathfrak{S}\left(\int_\Lambda \frac{1}{p(x)}\left|{}^{\mathrm{H}}\mathbb{D}_{0+}^{\varpi,\nu;\psi}u\right|^{p(x)}dx\right)\mathbf{L}_{p(x)}^{\varpi,\nu;\psi}u &= \mathfrak{g}(x,u),\ in\ \Lambda = [0,T]\times[0,T], \\ u &= 0,\ on\ \partial\Lambda \end{cases} \quad (P_2)$$

The authors utilized variational techniques, along with the mountain pass theorem and the fountain theorem, to demonstrate both the existence and the multiplicity of solutions for the problem (P_2).

We note that the novelty in our study compared with reference [24] is that the perturbed nonlinearity can be critical, which implies more difficulties. This is due to the embedding, which is only continuous when the exponent is critical, and to solve this we use a concentration-compactness principle. Moreover, Kirchhoff-type problems are important, since they arise in the description of nonlinear vibrations of an elastic string.

Inspired by the findings reported in reference [4], our article seeks to advance the discussion by examining the critical case of the problem mentioned above. To achieve this, we apply a recent concentration-compactness principle for ψ-Hilfer spaces with

variable exponents to analyze the weighted Kirchhoff problem (1). Our research offers a generalization, enhancement, and extension of the earlier references, incorporating additional suitable conditions. As a result, this project is of considerable significance and provides important insights.

In conclusion, our study makes a meaningful addition to the current body of literature by investigating the critical case of the Kirchhoff problem under Steklov boundary conditions. By employing robust mathematical methods and leveraging recent concentration-compactness principles, we demonstrate the existence and multiplicity of solutions for problem (1), thereby deepening the understanding of this significant area of research.

2. Preliminaries of Variational Spaces

In this section, we present the spaces related to the variational formulation of the main problem. Concerning the properties of the Lebegue spaces and the Hilfer fractional derivative ($\mathbb{D}_{0+}^{\omega,\nu;\mu}$), we refer the reader to the lemmas presented in [4,5,33,34]. Next, in order to define the working space, we begin by introducing the following set:

$$C_+(\overline{\Lambda}) = \{p \in C(\overline{\Lambda}), p(\xi) > 1, \forall \xi \in \overline{\Lambda}\}.$$

For all $p \in C_+(\overline{\Lambda})$, consider

$$p^- = \inf_{\overline{\Lambda}} p(\xi), p^+ = \sup_{\overline{\Lambda}} p(\xi).$$

Additionally, we define

$$\mathcal{L}^{p(\xi)}(\Lambda) = \left\{u : \Lambda \to \mathbb{R}, \text{ measurable} : \int_\Lambda |u(\xi)|^{p(\xi)} d\xi < \infty\right\},$$

with the norm on $\mathcal{L}^{p(\xi)}(\Lambda)$ defined as

$$|u|_{\mathcal{L}^{p(\xi)}(\Lambda)} = \inf\left\{\mu > 0 : \int_\Lambda \left|\frac{u(\xi)}{\mu}\right|^{p(\xi)} d\xi \leq 1\right\}.$$

We also define

$$\mathcal{L}^{p(\xi)}(\partial\Lambda) = \left\{u : \Lambda \to \mathbb{R}, \text{ measurable} : \int_{\partial\Lambda} |u(\xi)|^{p(\xi)} d\sigma < \infty\right\},$$

with the norm on $\mathcal{L}^{p(\xi)}(\partial\Lambda)$ defined as

$$|u|_{\mathcal{L}^{p(\xi)}(\partial\Lambda)} = \inf\left\{\mu > 0 : \int_{\partial\Lambda} \left|\frac{u(\xi)}{\mu}\right|^{p(\xi)} d\sigma \leq 1\right\}.$$

Spaces $\left(\mathcal{L}^{p(\xi)}(\Lambda), |\cdot|_{\mathcal{L}^{p(\xi)}(\Lambda)}\right)$ and $\left(\mathcal{L}^{p(\xi)}(\partial\Lambda), |\cdot|_{\mathcal{L}^{p(\xi)}(\partial\Lambda)}\right)$ are Banach spaces, which we refer to as variable-exponent Lebesgue spaces.

The μ-fractional space is expressed as [4,5]

$$\mathcal{H}_{p(\xi)}^{\omega,\nu;\mu}(\Lambda) = \left\{u \in L^{p(\xi)}(\Lambda) : \left|\mathbb{D}_{0+}^{\omega,\nu;\mu} u\right| \in L^{p(\xi)}(\Lambda)\right\}$$

with the norm

$$\| u \| = \| u \|_{\mathcal{H}_{p(\xi)}^{\omega,\nu;\mu}(\Lambda)} = \| u \|_{L^{p(\xi)}(\Lambda)} + \| \mathbb{D}_{0+}^{\omega,\nu;\mu} u \|_{L^{p(\xi)}(\Lambda)}.$$

$\mathcal{H}^{\omega,\nu;\mu}_{p(\xi),0}(\Lambda)$ denotes the closure of $C^{\infty}_{0}(\Lambda)$ in $\mathcal{H}^{\omega,\nu;\mu}_{p(\xi)}(\Lambda)$. We recall that Banach spaces $\mathcal{L}^{p(\xi)}(\Lambda)$ and $\mathcal{H}^{\omega,\nu;\mu}_{p(\xi)}(\Lambda)$ are also separable and reflexive. Moreover, if $p_1, p_2 \in C_+(\overline{\Lambda})$ such that $p_1(\xi) \leq p_2(\xi)$ for all $\xi \in \overline{\Lambda}$, then embedding $\mathcal{L}^{p_2(\xi)}(\Lambda) \hookrightarrow \mathcal{L}^{p_1(\xi)}(\Lambda)$ is continuous.

The following result is important in our proofs.

Theorem 1 (Concentration-compactness principle (see [35])). *Let $p(x)$ and $r(x)$ be two continuous functions such that*

$$p^- = \inf_{\overline{\Omega}} p(x) \leq p^+ = \sup_{\overline{\Omega}} p(x) < nand 1 < r(x) \leq p^*(x) \text{in} \Omega \subset \mathbb{R}^n.$$

Let $\{u_j\}_{j\in\mathbb{N}}$ be a weakly convergent sequence in $\mathcal{H}^{\omega,\nu;\psi}_{p(\xi)}(\Lambda)$ with a weak limit (u) such that

- $|u_n|^{r(x)} \rightharpoonup \nu$ *weakly in the sense of measures;*
- $|{}^{H}\mathbb{D}^{\omega,\nu;\psi}_{0+} u_n|^{p(x)} \rightharpoonup \psi$ *weakly in the sense of measures.*

Also assume that $A = \{x \in \Omega : r(x) = p^*(x)\}$ is nonempty. Then, for some countable index set (I), we have

$$\nu = |u|^{r(x)} + \sum_{i\in I} \nu_i \delta_{x_i}, \nu_i > 0.$$

$$\psi \geq |{}^{\mathrm{H}}\mathbb{D}^{\omega,\nu;\psi}_{0+} u|^{p(x)} + \sum_{i\in I} \mu_i \delta_{x_i}, \mu_i > 0.$$

$$S\nu_i^{\frac{1}{p^*(x_i)}} \leq \mu_i^{\frac{1}{p(x_i)}}.$$

where $\{x_i\}_{i\in I} \subset A$ and S is the best constant in the Gagliardo–Nirenberg–Sobolev inequality for variable exponents, namely

$$S = S_r(\Omega) = \inf_{\phi\in C^{\infty}_{0}(\Omega)} \frac{||{}^{\mathrm{H}}\mathbb{D}^{\omega,\nu;\psi}_{0+}\phi||_{\mathcal{L}^{p(x)}}}{||\phi||_{\mathcal{L}^{r(x)}}}.$$

Finally, we note that in our proofs, we use both the mountain pass and symmetric mountain pass theorems, which can be found in [36]; moreover, we use the following theorem:

Theorem 2 (Kajikiya theorem; see [37]). *Let E be an infinite, dimensional, real Banach space. Let $\mathfrak{J} \in C^1(E, \mathbb{R})$, satisfying the following conditions:*

(c_1) *$\mathfrak{J}$ is an even functional such that $\mathfrak{J}(0) = 0$;*
(c_2) *$\mathfrak{J}$ satisfies the (PS) condition;*
(c_3) *For any $k \in \mathbb{N}$, there exist a k-dimensional subspace of E (E_k) and a number ($r_k > 0$) such that $\sup_{E_k\cap S_{r_k}} \mathfrak{J}(u) < 0$, where $S_{r_k} = \{u \in E, ||u|| = r_k\}$.*

Then, the functional $\mathfrak{J}$ has a sequence of critical points ($\{u_k\}_{k\in\mathbb{N}}$) satisfying $||u_k|| \to 0$ as $k \to 0$.

3. Main Results

In this part, we present the principal results of this work. To do this, we make the following assumptions.

($\mathbf{H_1}$) The function $g(x, u)$ can be expressed as $a(x)h(u)$, where a and h are measurable functions satisfying the following condition: there exists $c_1 > 0$, $P, q \in C_+(\overline{\Lambda})$ such that for all $(x, u) \in \Lambda \times \mathbb{R}$, we have

$$a(x) \in \mathcal{L}^{\frac{P(x)}{P(x)-q(x)}}(\Lambda), \ h(u) \leq c_1|u|^{q(x)-1}$$

and

$$p^+ < q(x) < P(x) < p^*(x). \tag{3}$$

($\mathbf{H_2}$) There exists $t_0 > 0$ such that the Kirchhoff function (M) satisfies $M(t) \geq t_0$.
($\mathbf{H_3}$) There exists $\omega \in (0,1)$ with $1-\omega \geq \frac{1}{p^+}$ such that

$$\hat{M}(t) \geq (1-\omega)M(t)t$$

where $\hat{M}(t) = \int_0^t M(\xi)\, d\xi$.
($\mathbf{H_4}$) There exist $M_1 > 0$ and $\frac{p^+}{1-\omega} < \theta < \min(r^-, s^-)$ such that for all $x \in \Lambda$ and $|u| \geq M_1$, we have

$$0 < \theta a(x)H(u) \leq a(x)h(u)u,$$

where $H(t) = \int_0^t h(\xi)\, d\xi$.
($\mathbf{H_5}$) For all $x \in \overline{\Lambda}$, we have $h(-u) = -h(u)$.
($\mathbf{H_6}$) There exists a nonempty open ball ($B \subset \Omega$) such that

$$\lim_{t\to 0} \frac{a(x)H(t)}{|t|^{p_B^-}} = \infty uniformly for a.a. x \in B,$$

where $p_B^- = \inf_{x\in B} p(x)$.

Subsequently, we define a weak solution for the problem (1) in the following way.

Definition 1. *We assume that $u \in X$ is a weak solution for Equation (1) if, for any $v \in X$, we have*

$$\begin{aligned} M\left(\int_\Lambda \tfrac{1}{p(x)} \left|{}^{\mathrm{H}}\mathbb{D}_{0+}^{\omega,\nu;\psi} u\right|^{p(x)} dx\right) \int_\Lambda \left|{}^{\mathrm{H}}\mathbb{D}_{0+}^{\omega,\nu;\psi} u\right|^{(p(x)-2)} {}^{\mathrm{H}}\mathbb{D}_{0+}^{\omega,\nu;\psi} u\, {}^{\mathrm{H}}\mathbb{D}_{0+}^{\omega,\nu;\psi} v \\ - \int_\Lambda |u|^{r(x)-2} uv dx - \int_\Lambda a(x)h(u)v dx - \int_{\partial\Lambda} |u|^{s(x)-2} uv dx &= 0. \end{aligned}$$

We are now prepared to present and demonstrate the first key results.

Theorem 3. *Under Hypotheses ($\mathbf{H_1}$)–($\mathbf{H_4}$), problem (1) has a non-trivial weak solution.*

Theorem 4. *Under Hypotheses ($\mathbf{H_1}$)–($\mathbf{H_5}$), problem (1) has an infinite number of solutions.*

Theorem 5. *Under Hypotheses ($\mathbf{H_1}$)–($\mathbf{H_6}$), problem (1) has an infinite number of solutions ($\{v_k\}_{k\in\mathbb{N}}$) satisfying $||v_k|| \to 0$ as $k \to 0$.*

Now, we introduce the functional ($\mathfrak{J}(u)$) associated with problem (1), which characterizes the critical points and plays a key role in the existence of solutions.

$$\begin{aligned} \mathfrak{I}(u) &= \hat{M}\left(\int_\Lambda \tfrac{1}{p(x)} \left|{}^{\mathrm{H}}\mathbb{D}_{0+}^{\omega,\nu;\psi} u\right|^{p(x)} dx\right) - \int_\Lambda \tfrac{|u|^{r(x)}}{r(x)} dx - \int_\Lambda a(x)H(u)dx - \int_{\partial\Lambda} \tfrac{|u|^{s(x)}}{s(x)} dx, \\ &= L(u) - I(u) - J(u) - T(u). \end{aligned}$$

where $\hat{M}(t) = \int_0^t M(s)ds$ and

$$L(u) = \hat{M}\left(\int_\Lambda \frac{1}{p(x)} \left|{}^{\mathrm{H}}\mathbb{D}_{0+}^{\omega,\nu;\psi} u\right|^{p(x)} dx\right), I(u) = \int_\Lambda \frac{|u|^{r(x)}}{r(x)} dx, J(u) = \int_\Lambda a(x)H(u)dx and$$

$$T(u) = \int_{\partial\Lambda} \frac{|u|^{s(x)}}{s(x)} dx.$$

We recall from [25] that $L \in C^1(X, \mathbb{R})$. Moreover, for all $u, v \in X$, we have

$$< L'(u), v >= M\left(\int_\Lambda \frac{1}{p(x)}\left|{}^{\mathrm{H}}\mathbb{D}_{0+}^{\omega,\nu;\psi}u\right|^{p(x)}dx\right)\int_\Lambda \left|{}^{\mathrm{H}}\mathbb{D}_{0+}^{\omega,\nu;\psi}u\right|^{(p(x)-2)}{}^{\mathrm{H}}\mathbb{D}_{0+}^{\omega,\nu;\psi}u\,{}^{\mathrm{H}}\mathbb{D}_{0+}^{\omega,\nu;\psi}v dx.$$

We also recall the following proposition.

Proposition 1 (see [25]). *Let* $\mathfrak{L} : \mathcal{H}_{p(x)}^{\omega,\nu;\psi}(\Lambda) \to \left(\mathcal{H}_{p(x)}^{\omega,\nu;\psi}(\Lambda)\right)^*$ *be a functional defined as follows:*

$$\mathfrak{L}(u) = \int_\Lambda \frac{|{}^{\mathrm{H}}\mathbb{D}_{0+}^{\omega,\nu;\psi}u|^{p(x)}}{p(x)}dx.$$

Then the following statements hold:

1. *For all* $u, v \in \mathcal{H}_{p(x)}^{\omega,\nu;\psi}(\Lambda)$, *we have*

$$< \mathfrak{L}'(u), v >= \int_\Lambda \left|{}^{\mathrm{H}}\mathbb{D}_{0+}^{\omega,\nu;\psi}u\right|^{(p(x)-2)}{}^{\mathrm{H}}\mathbb{D}_{0+}^{\omega,\nu;\psi}u\,{}^{\mathrm{H}}\mathbb{D}_{0+}^{\omega,\nu;\psi}v dx.$$

2. *Operator* $\mathfrak{L}'$, *from X to its dual* X^*, *is continuous and bounded; moreover, it is strictly monotone.*
3. $\mathfrak{L}'$ *is a mapping of the* (S_+) *type, that is, if* $u_n \rightharpoonup u$ *in X and* $\limsup_{n\to\infty} < \mathfrak{L}'(u_n) - \mathfrak{L}'(u), u_n - u >\leq 0$, *then* $u_n \to u$ *strongly in X.*

Remark 1. *Using Hypothesis* $(\boldsymbol{H_1})$ *and the Hölder inequality,* $J \in C^1(X, \mathbb{R})$. *Therefore, for all* $u, v \in X$, *we obtain*

$$< J'(u), v >= \int_\Lambda a(x)h(u(x))v(x)dx.$$

From Proposition 1 and Remark 1, it follows that $\mathfrak{J} \in C^1(X, \mathbb{R})$. Then, for all $u, v \in X$, we have

$$\begin{aligned} < \mathfrak{J}'(u), v > &= M\left(\int_\Lambda \frac{1}{p(x)}\left|{}^{\mathrm{H}}\mathbb{D}_{0+}^{\omega,\nu;\psi}u\right|^{p(x)}dx\right)\int_\Lambda \left|{}^{\mathrm{H}}\mathbb{D}_{0+}^{\omega,\nu;\psi}u\right|^{(p(x)-2)}{}^{\mathrm{H}}\mathbb{D}_{0+}^{\omega,\nu;\psi}u\,{}^{\mathrm{H}}\mathbb{D}_{0+}^{\omega,\nu;\psi}v dx \\ &- \int_\Lambda |u|^{r(x)-2}uvdx - \int_{\partial\Lambda}|u|^{s(x)-2}uvdx - \int_\Lambda a(x)h(u(x))v(x)dx. \end{aligned}$$

Therefore, the weak solutions of the problem (1) are associated with the critical points of functional $\mathfrak{J}$.

Now, we establish a key result that offers a lower bound for functional $\mathfrak{J}(u)$ associated with the problem (1) under the assumption of $(\mathbf{H_1})$.

Lemma 1. *Assume that* $(\boldsymbol{H_1})$–$(\boldsymbol{H_3})$ *are satisfied. Then, there exist* $m, \eta > 0$ *such that, for* $u \in X$,

$$if \quad \| u \| = \rho, \ then, \ \mathfrak{J}(u) \geq d.$$

Proof. Let $u \in X$, with $\| u \| < 1$. Under Hypothesis $(\mathbf{H_1})$, for all $x \in \Lambda$, we have

$$H(u) \leq \frac{c_1}{q(x)}|u|^{q(x)}. \tag{4}$$

$1 < P(x) < p^*(x)$, $1 < r(x) \leq p^*(x), 1 < s(x) < p_*^{\omega}(x)$ proves the existence of c_3, c_4, $c_5 > 0$, such that

$$|u|_{\mathcal{L}^{P(x)}(\Lambda)} \leq c_3\| u \|, \ |u|_{\mathcal{L}^{r(x)}(\Lambda)} \leq c_4\| u \|, |u|_{\mathcal{L}^{s(x)}(\partial\Lambda)} \leq c_5\| u \|. \tag{5}$$

Now, under Hypotheses $(\mathbf{H_2})$–$(\mathbf{H_3})$, we obtain

$$\begin{aligned} L(u) &= \hat{M}\left(\int_\Lambda \frac{1}{p(x)}\left|{}^{\mathrm{H}}\mathbb{D}_{0+}^{\omega,\nu;\psi}u\right|^{p(x)}dx\right) \\ &\geq (1-\omega)M\left(\int_\Lambda \frac{1}{p(x)}\left|{}^{\mathrm{H}}\mathbb{D}_{0+}^{\omega,\nu;\psi}u\right|^{p(x)}dx\right)\int_\Lambda \frac{1}{p(x)}\left|{}^{\mathrm{H}}\mathbb{D}_{0+}^{\omega,\nu;\psi}u\right|^{p(x)}dx \qquad (6) \\ &\geq \frac{(1-\omega)t_0}{p^+}\int_\Lambda\left|{}^{\mathrm{H}}\mathbb{D}_{0+}^{\omega,\nu;\psi}u\right|^{p(x)}dx \geq \frac{(1-\omega)t_0}{p^+}||u||^{p^+}. \end{aligned}$$

Next, according to (4)–(6), we have

$$\begin{aligned} \mathfrak{J}(u) &= \hat{M}\left(\int_\Lambda \frac{1}{p(x)}\left|{}^{\mathrm{H}}\mathbb{D}_{0+}^{\omega,\nu;\psi}u\right|^{p(x)}dx\right) - \int_\Lambda a(x)H(u)dx - \int_\Lambda \frac{|u|^{r(x)}}{r(x)}dx, \\ &= L(u) - J(u) - I(u) - T(u) \\ &\geq \frac{(1-\omega)t_0}{p^+}||u||^{p^+} - \frac{c_3}{q^-}|a|_{\mathcal{L}^{\frac{P(x)}{P(x)-q(x)}}(\Lambda)}||u||^{q^-} - \frac{c_4}{r^-}||u||^{r^-} - \frac{c_5}{s^-}||u||^{s^-} \\ &\geq ||u||^{p^+}\left(\frac{(1-\omega)t_0}{p^+} - \frac{c_3}{q^-}|a|_{\mathcal{L}^{\frac{P(x)}{P(x)-q(x)}}(\Lambda)}||u||^{q^--p^+} - \frac{c_4}{r^-}||u||^{r^--p^+} - \frac{c_5}{s^-}||u||^{s^--p^+}\right) \\ &\geq ||u||^{p^+}\left(\frac{(1-\omega)t_0}{p^+} - t||u||^{\min(q^--p^+,r^--p^+,s^--p^+)}\right), \end{aligned}$$

where

$$t = \frac{c_3}{q^-}|a|_{\mathcal{L}^{\frac{P(x)}{P(x)-q(x)}}(\Lambda)} + \frac{c_4}{r^-} + \frac{c_5}{s^-}.$$

Since q^-, s^- and r^- are both greater than p^+, we can set $\| u \| = \rho$ to be sufficiently small such that

$$\frac{(1-\omega)t_0}{p^+} - t\rho^{\min(q^--p^+,r^--p^+,s^--p^+)} > 0.$$

Therefore, we obtain

$$\mathfrak{J}(u) \geq \rho^{p^+}\left(\frac{(1-\omega)t_0}{p^+} - t\,\rho^{\min(q^--p^+,r^--p^+,s^--p^+)}\right) := d > 0.$$

□

In the upcoming lemma, we demonstrate a result related to the boundedness of a Palais–Smale sequence within a space (X).

Lemma 2. *Suppose that conditions* $(\boldsymbol{H_2})$*–*$(\boldsymbol{H_4})$ *are satisfied. Let* $\{u_n\}$ *be a Palais–Smale sequence in X. Then,* $\{u_n\}$ *is bounded in* X.

Proof. Let $\{u_n\}$ be a sequence in X such that

$$\mathfrak{J}(u_n) \to c, \text{ and } \mathfrak{J}'(u_n) \to 0, \text{ in } X^*, \text{ as } n \to \infty,$$

where c is a positive constant.

Since $\mathfrak{J}(u_n) \to c$, there exists $T_1 > 0$, such that

$$|\mathfrak{J}(u_n)| \leq T_1. \qquad (7)$$

On the other hand, since we have $\mathfrak{J}'(u_n) \to 0$ in X^*, $< \mathfrak{J}'(u_n), u_n >$ converges to zero. Therefore, it is bounded. Hence, there exists $T_2 > 0$, such that

$$\left| < \mathfrak{J}'(u_n), u_n > \right| \leq T_2. \qquad (8)$$

Next, we prove, by contradiction, that $\{u_n\}$ is bounded. We consider a subsequence such that $\| u_n \| \geq 1$, and $\| u_n \| \to \infty$.

According to (7), (6) and using $p^+ < \theta < \min(r^-, s^-)$, we obtain

$$\begin{aligned} T_1 \geq \mathfrak{J}(u_n) &= L(u_n) - I(u_n) - J(u_n) - T(u_n) \\ &\geq \frac{(1-\omega)t_0}{p^+}\int_\Lambda \left|{}^{\mathrm{H}}\mathbb{D}_{0+}^{\omega,\nu;\psi}u_n\right|^{p(x)}dx - \frac{1}{r^-}\int_\Lambda |u_n|^{r(x)}dx - \frac{1}{s^-}\int_{\partial\Lambda}|u_n|^{s(x)}dx - J(u_n) \\ &\geq \frac{(1-\omega)t_0}{p^+}\int_\Lambda \left|{}^{\mathrm{H}}\mathbb{D}_{0+}^{\omega,\nu;\psi}u_n\right|^{p(x)}dx - \frac{1}{\theta}\int_\Lambda |u_n|^{r(x)}dx - \frac{1}{\theta}\int_{\partial\Lambda}|u_n|^{s(x)}dx - J(u_n). \end{aligned} \tag{9}$$

Now, according to (8) and $(\mathbf{H_2})$, we obtain

$$\begin{aligned} T_2 &\geq - < \mathfrak{J}'(u_n), u_n > \\ &= -M\left(\int_\Lambda \frac{1}{p(x)}\left|{}^{\mathrm{H}}\mathbb{D}_{0+}^{\omega,\nu;\psi}u\right|^{p(x)}dx\right)\int_\Lambda \left|{}^{\mathrm{H}}\mathbb{D}_{0+}^{\omega,\nu;\psi}u_n\right|^{p(x)}dx + \int_\Lambda |u_n|^{r(x)}dx \\ &+ \int_{\partial\Lambda}|u_n|^{s(x)}dx + < J'(u_n), (u_n) > \\ &\geq -t_0\int_\Lambda \left|{}^{\mathrm{H}}\mathbb{D}_{0+}^{\omega,\nu;\psi}u_n\right|^{p(x)}dx + \int_\Lambda |u_n|^{r(x)}dx + \int_{\partial\Lambda}|u_n|^{s(x)}dx + < J'(u_n), (u_n) > . \end{aligned}$$

By merging the inequality mentioned above with (9), we obtain

$$\begin{aligned} \theta T_1 + T_2 &\geq \left(\frac{(1-\omega)\theta}{p^+} - 1\right)t_0\int_\Lambda \left|{}^{\mathrm{H}}\mathbb{D}_{0+}^{\omega,\nu;\psi}u_n\right|^{p(x)}dx + < J'(u_n), (u_n) > -\theta J(u_n) \\ &\geq \left(\frac{(1-\omega)\theta}{p^+} - 1\right)t_0\| u_n \|^{p^-} + \int_\Lambda a(x)(h(u_n)u_n - \theta H(u_n))dx. \end{aligned}$$

Using $(\mathbf{H_4})$, we obtain

$$\theta T_1 + T_2 \geq \left(\frac{(1-\omega)\theta}{p^+} - 1\right)t_0\| u_n \|^{p^-}. \tag{10}$$

According to $(\mathbf{H_4})$ and $(\mathbf{H_2})$, $\frac{p^+}{1-\omega} < \theta$ and $t_0 > 0$; then, we have $\left(\frac{(1-\omega)\theta}{p^+} - 1\right)t_0 > 0$, so

$$\left(\frac{(1-\omega)\theta}{p^+} - 1\right)t_0\| u_n \|^{p^-} \to \infty$$

According to (10), this is absurd. Therefore, $\{u_n\}$ is bounded in X. □

Next, we introduce a set (A) defined by $A = \{x \in \Omega : r(x) = p^*(x)\}$ as nonempty set. We also define a set expressed as $A_\delta = \{x \in \Omega : dist((x, A) < \delta\}$ for $\delta > 0$. We note that $r_\delta^- = \inf_{\overline{A_\delta}} r(x)$ and $r_A^- = \inf_{\overline{A}} r(x)$.

If $\{u_n\}$ is a Palais–Smale sequence with an energy level of c, then, as stated in Theorem 1, we obtain the following convergence results:

$$|u_n|^{r(x)} \rightharpoonup \nu = |u|^{r(x)} + \sum_{i\in I}\nu_i\delta_{x_i}, \nu_i > 0. \tag{11}$$

$$|{}^{\mathrm{H}}\mathbb{D}_{0+}^{\omega,\nu;\psi}u_n|^{p(x)} \rightharpoonup \phi \geq \left|{}^{\mathrm{H}}\mathbb{D}_{0+}^{\omega,\nu;\psi}u\right|^{p(x)} + \sum_{i\in I}\mu_i\delta_{x_i}, \mu_i > 0. \tag{12}$$

$$S\nu_i^{\frac{1}{p^*(x_i)}} \leq \mu_i^{\frac{1}{p(x_i)}}. \tag{13}$$

If $I = \varnothing$, then $u_n \to u$ in $\mathcal{L}^{r(x)}(\Omega)$. It should be noted that $\{x_i\}_{i\in A} \subset A$. We aim to demonstrate that if $c < \left(\frac{1}{p^+} - \frac{1}{r_A^-}\right)S^n$, then $I = \varnothing$, where S is defined in Theorem 1.

Lemma 3. *If conditions $(\mathbf{H_1})$–$(\mathbf{H_4})$ are satisfied, let $\{u_n\}$ be a Palais–Smale sequence in X with a energy level of c. If $c < \left(\frac{1}{p^+} - \frac{1}{r_A^-}\right)S^n$, then the index set (I) is empty.*

Proof. Suppose that $I \neq \varnothing$ and let $\varphi \in C_0^\infty(\mathbb{R}^n)$ such that $\varphi(0) \neq 0$. Now, we consider the functions $\varphi_{i,\epsilon}(x) = \varphi\Big(\frac{x-x_i}{\epsilon}\Big)$. We have $< \mathfrak{J}'(u_n), \varphi_{i,\epsilon} u_n > \to 0$. Thus,

$$\begin{aligned} & < \mathfrak{J}'(u_n), \varphi_{i,\epsilon} u_n > \\ = \; & M\Big(\int_\Lambda \tfrac{1}{p(x)} \Big|{}^{\mathrm{H}}\mathbb{D}_{0+}^{\omega,\nu;\psi} u_n\Big|^{p(x)} dx\Big) \int_\Omega |{}^{\mathrm{H}}\mathbb{D}_{0+}^{\omega,\nu;\psi} u_n\Big|^{(p(x)-2)} {}^{\mathrm{H}}\mathbb{D}_{0+}^{\omega,\nu;\psi} u_n \, {}^{\mathrm{H}}\mathbb{D}_{0+}^{\omega,\nu;\psi}(\varphi_{i,\epsilon} u_n\Big) dx \\ - \; & \int_\Omega |u_n|^{r(x)} \varphi_{i,\epsilon} dx - \int_\Omega a(x) h(u_n(x)) \varphi_{i,\epsilon} u_n dx - \int_{\partial\Omega} |u_n|^{s(x)} \varphi_{i,\epsilon} dx. \end{aligned}$$

Then, we obtain

$$\begin{aligned} 0 \; = \; & \lim_{n\to\infty} \Big(M\Big(\int_\Lambda \tfrac{1}{p(x)} \Big|{}^{\mathrm{H}}\mathbb{D}_{0+}^{\omega,\nu;\psi} u_n\Big|^{p(x)} dx\Big) \int_\Omega \Big|{}^{\mathrm{H}}\mathbb{D}_{0+}^{\omega,\nu;\psi} u_n\Big|^{(p(x)-2)} {}^{\mathrm{H}}\mathbb{D}_{0+}^{\omega,\nu;\psi} u_n \, {}^{\mathrm{H}}\mathbb{D}_{0+}^{\omega,\nu;\psi}(\varphi_{i,\epsilon}) u_n dx \\ + \; & \int_\Omega \varphi_{i,\epsilon} d\mu - \int_\Omega \varphi_{i,\epsilon} d\nu - \int_\Omega a(x) h(u_n(x)) \varphi_{i,\epsilon} u_n dx - \int_{\partial\Omega} |u_n|^{s(x)} \varphi_{i,\epsilon} dx \Big). \end{aligned}$$

According to Hölder's inequality and using Hypothesis $(\mathbf{C_2})$, we have

$$\lim_{n\to\infty} \int_\Omega \Big|{}^{\mathrm{H}}\mathbb{D}_{0+}^{\omega,\nu;\psi} u_n\Big|^{(p(x)-2)} {}^{\mathrm{H}}\mathbb{D}_{0+}^{\omega,\nu;\psi} u_n \, {}^{\mathrm{H}}\mathbb{D}_{0+}^{\omega,\nu;\psi}(\varphi_{i,\epsilon}) u_n dx = 0.$$

Therefore, we obtain

$$\lim_{\epsilon\to 0} \int_\Omega a(x) h(u_n(x)) \varphi_{i,\epsilon} u_n dx = 0, \lim_{\epsilon\to 0} \int_{\partial\Omega} |u_n|^{s(x)} \varphi_{i,\epsilon} dx = 0$$

$$\lim_{\epsilon\to 0} \int_\Omega \varphi_{i,\epsilon} d\mu = \mu_i \varphi(0), \lim_{\epsilon\to 0} \int_\Omega \varphi_{i,\epsilon} d\nu = \nu_i \varphi(0).$$

Then, $(\mu_i - \nu_i)\varphi(0) = 0$, which implies $\mu_i = \nu_i$. Consequently,

$$S \nu_i^{\frac{1}{p^*(x_i)}} \leq \nu_i^{\frac{1}{p(x_i)}},$$

Thus, we conclude that $\nu_i = 0$ or $S^n \leq \nu_i$.
Now, since $r(x), s(x), \theta > p^+ > 1 - \omega$ and using Hypothesis $(\mathbf{H_4})$, we have

$$\begin{aligned} c \; = \; & \lim_{n\to\infty} \mathfrak{J}(u_n) = \lim_{n\to\infty} \Big(\mathfrak{J}(u_n) - \tfrac{1}{p^+} < \mathfrak{J}'(u_n), u_n > \Big) \\ = \; & \lim_{n\to\infty} \Big(\hat{M}\Big(\int_\Lambda \tfrac{1}{p(x)} \Big|{}^{\mathrm{H}}\mathbb{D}_{0+}^{\omega,\nu;\psi} u\Big|^{p(x)} dx\Big) - \int_\Omega \tfrac{|u_n|^{r(x)}}{r(x)} dx - \int_\Omega a(x) H(u_n) dx - \int_\Omega \tfrac{|u_n|^{s(x)}}{s(x)} dx \\ - \; & \tfrac{1}{p^+} M\Big(\int_\Lambda \tfrac{1}{p(x)} \Big|{}^{\mathrm{H}}\mathbb{D}_{0+}^{\omega,\nu;\psi} u_n\Big|^{p(x)} dx\Big) \int_\Lambda \tfrac{1}{p(x)} \Big|{}^{\mathrm{H}}\mathbb{D}_{0+}^{\omega,\nu;\psi} u_n\Big|^{p(x)} dx + \tfrac{1}{p^+} \int_\Omega a(x) h(u_n) u_n dx \\ + \; & \tfrac{1}{p^+} \int_\Omega |u_n|^{r(x)} dx + \tfrac{1}{p^+} \int_{\partial\Omega} |u_n|^{s(x)} dx \Big) \\ \geq \; & \lim_{n\to\infty} \Big((1-\omega) M\Big(\int_\Lambda \tfrac{1}{p(x)} \Big|{}^{\mathrm{H}}\mathbb{D}_{0+}^{\omega,\nu;\psi} u_n\Big|^{p(x)} dx\Big) \int_\Lambda \tfrac{1}{p(x)} \Big|{}^{\mathrm{H}}\mathbb{D}_{0+}^{\omega,\nu;\psi} u_n\Big|^{p(x)} \\ - \; & \tfrac{1}{p^+} M\Big(\int_\Lambda \tfrac{1}{p(x)} \Big|{}^{\mathrm{H}}\mathbb{D}_{0+}^{\omega,\nu;\psi} u_n\Big|^{p(x)} dx\Big) \int_\Lambda \tfrac{1}{p(x)} \Big|{}^{\mathrm{H}}\mathbb{D}_{0+}^{\omega,\nu;\psi} u_n\Big|^{p(x)} dx \\ + \; & \int_\Omega \Big(\tfrac{1}{p(x)} - \tfrac{1}{r(x)}\Big) |u_n|^{r(x)} dx + \int_{\partial\Omega} \Big(\tfrac{1}{p(x)} - \tfrac{1}{s(x)}\Big) |u_n|^{s(x)} dx \\ + \; & \tfrac{1}{p^+} \int_\Omega a(x) h_1(u_n) u_n dx - \int_\Omega a(x) H(u_n) dx \Big) \\ \geq \; & \lim_{n\to\infty} \Big(\Big(1 - \omega - \tfrac{1}{p^+}\Big) M\Big(\int_\Lambda \tfrac{1}{p(x)} \Big|{}^{\mathrm{H}}\mathbb{D}_{0+}^{\omega,\nu;\psi} u_n\Big|^{p(x)} dx\Big) \int_\Lambda \tfrac{1}{p(x)} \Big|{}^{\mathrm{H}}\mathbb{D}_{0+}^{\omega,\nu;\psi} u\Big|^{p(x)} dx \\ + \; & \int_\Omega \Big(\tfrac{1}{p^+} - \tfrac{1}{r(x)}\Big) |u_n|^{r(x)} dx + \int_{\partial\Omega} \Big(\tfrac{1}{p^+} - \tfrac{1}{s(x)}\Big) |u_n|^{s(x)} dx \\ + \; & \tfrac{1}{\theta} \int_\Omega a(x) h(u_n) u_n dx - \int_\Omega a(x) H(u_n) dx \\ \geq \; & \lim_{n\to\infty} \int_\Omega \Big(\tfrac{1}{p^+} - \tfrac{1}{r(x)}\Big) |u_n|^{r(x)} dx \\ \geq \; & \lim_{n\to\infty} \int_{A_\delta} \Big(\tfrac{1}{p^+} - \tfrac{1}{r_{A_\delta}^-}\Big) |u_n|^{r(x)} dx. \end{aligned}$$

Therefore,

$$\begin{aligned}\lim_{n\to\infty}\int_{A_\delta}\left(\frac{1}{p^+}-\frac{1}{r^-_{A_\delta}}\right)|u_n|^{r(x)}dx &= \left(\frac{1}{p^+}-\frac{1}{r^-_{A_\delta}}\right)\left(\int_{A_\delta}|u|^{r(x)}+\sum_{i\in I}\nu_i\right)\\ &\geq \left(\frac{1}{p^+}-\frac{1}{r^-_{A_\delta}}\right)\nu_i\\ &\geq \left(\frac{1}{p^+}-\frac{1}{r^-_{A_\delta}}\right)S^n.\end{aligned} \tag{14}$$

Therefore, since δ is positive and arbitrary and r is continuous, we have

$$c \geq \left(\frac{1}{p^+}-\frac{1}{r^-_A}\right)S^n.$$

Then, if $c < \left(\frac{1}{p^+}-\frac{1}{r^-_A}\right)S^n$, the index set (I) is empty. □

We now introduce the subsequent lemma that demonstrates a significant convergence result.

Lemma 4. *Assume that conditions* $(\boldsymbol{H_1})$*–*$(\boldsymbol{H_4})$ *are satisfied and let* $\{u_n\}$ *be a Palais–Smale sequence in X with an energy level of c. Then, there exists a subsequence of* $\{u_n\}$ *that converges strongly in X.*

Proof. Let $\{u_n\}$ be a $(PS)_c$ sequence in X. Then, according to Lemma 2, we know that the sequence $\{u_n\}$ is bounded in X. Therefore, there exists a subsequence still denoted by $\{u_n\}$ such that $u_n \rightharpoonup u$ weakly in X.

On the other hand, according to Lemma 3 and the compact embedding, we obtain

$$\begin{cases} u_n \to u, \ stronglyin\ \mathcal{L}^{P(x)}(\Lambda), \\ u_n \to u, \ stronglyin\ \mathcal{L}^{r(x)}(\Lambda), \\ u_n \to u, \ stronglyin\ \mathcal{L}^{s(x)}(\partial\Lambda). \end{cases}$$

Next, we prove that $u_n \to u$ strongly in X. To this end, we begin by remarking that

$$\begin{aligned}<\mathfrak{J}'(u_n),u_n-u> &= <L'(u_n),u_n-u> -\int_\Lambda|u_n|^{r(x)-2}u_n(u_n-u)dx\\ &- \int_\Lambda a(x)h(u_n)(u_n-u)dx-\int_{\partial\Lambda}|u_n|^{s(x)-2}u_n(u_n-u)dx.\end{aligned}$$

Therefore, by applying Hölder's inequality, we obtain

$$\begin{aligned}\int_\Lambda|u_n|^{r(x)-1}|u_n-u|dx &\leq |u_n-u|_{\mathcal{L}^{r(x)}}\big||u|^{r(x)-1}\big|_{\mathcal{L}^{\frac{r(x)}{r(x)-1}}}\\ &\leq |u_n-u|_{\mathcal{L}^{r(x)}}\max\left(|u_n|^{r^+-1}_{\mathcal{L}^{r(x)}},|u_n|^{r^--1}_{\mathcal{L}^{r(x)}}\right)\\ &\leq c_1|u_n-u|_{\mathcal{L}^{r(x)}}\max(||u_n||^{r^+-1},||u_n||^{r^--1}).\end{aligned}$$

This yields

$$\lim_{n\to\infty}\int_\Lambda|u_n|^{r(x)-2}u_n(u_n-u)dx=0. \tag{15}$$

Similarly, we can obtain

$$\lim_{n\to\infty}\int_{\partial\Lambda}|u_n|^{s(x)-2}u_n(u_n-u)dx=0. \tag{16}$$

Now, by using Hypothesis $(\mathbf{H_1})$ and Hölder's inequality, one has

$$\begin{aligned}\int_\Lambda a(x)h(u_n)(u_n-u)dx &\leq \int_\Lambda c_1|a(x)||u_n|^{q(x)-1}|u_n-u|dx\\ &\leq c_1|u_n-u|_{\mathcal{L}^{P(x)}}|a(x)|_{\mathcal{L}^{\frac{P(x)}{P(x)-q(x)}}}||u_n|^{q(x)-1}|_{\mathcal{L}^{\frac{P(x)}{q(x)-1}}}\\ &\leq c_1|u_n-u|_{\mathcal{L}^{P(x)}}|a(x)|_{\mathcal{L}^{\frac{P(x)}{P(x)-q(x)}}}\max(|u_n|^{q^+-1}|_{\mathcal{L}^{P(x)}},|u_n|^{q^--1}|_{\mathcal{L}^{P(x)}})\\ &\leq c_1|u_n-u|_{\mathcal{L}^{P(x)}}|a(x)|_{\mathcal{L}^{\frac{P(x)}{P(x)-q(x)}}}\max(||u_n||^{q^+-1}|,||u_n||^{q^--1}|).\end{aligned}$$

Therefore, we obtain

$$\lim_{n\to\infty}\int_\Lambda a(x)h(u_n)(u_n-u)dx=0. \tag{17}$$

On the other hand, by combining Equations (15) and (16) with Equation (17) and using the fact that $<\mathfrak{J}'(u_n),u_n-u>\to 0$, we conclude that

$$<L'(u_n),u_n-u>=M\left(\int_\Lambda\frac{1}{p(x)}\left|{}^{\mathrm{H}}\mathbb{D}_{0+}^{\omega,\nu;\psi}u\right|^{p(x)}dx\right)\int_\Lambda\left|{}^{\mathrm{H}}\mathbb{D}_{0+}^{\omega,\nu;\psi}u_n\right|^{(p(x)-2)}{}^{\mathrm{H}}\mathbb{D}_{0+}^{\omega,\nu;\psi}u_n{}^{\mathrm{H}}\mathbb{D}_{0+}^{\omega,\nu;\psi}(u_n-u)dx\to 0.$$

Since Hypothesis $(\mathbf{C_2})$ implies that $M\left(\int_\Lambda\frac{1}{p(x)}\left|{}^{\mathrm{H}}\mathbb{D}_{0+}^{\omega,\nu;\psi}u\right|^{p(x)}dx\right)\neq 0$, we obtain

$$<\mathfrak{L}'(u_n),u_n-u>=\int_\Lambda\left|{}^{\mathrm{H}}\mathbb{D}_{0+}^{\omega,\nu;\psi}u_n\right|^{(p(x)-2)}{}^{\mathrm{H}}\mathbb{D}_{0+}^{\omega,\nu;\psi}u_n{}^{\mathrm{H}}\mathbb{D}_{0+}^{\omega,\nu;\psi}(u_n-u)dx\to 0.$$

Also, the fact that $u_n\rightharpoonup u$ implies that $<\mathfrak{L}'(u),u_n-u>\to 0$.
Hence, based on the above information, we deduce that

$$\lim_{n\to\infty}<\mathfrak{L}'(u_n)-\mathfrak{L}'(u),u_n-u>=0.$$

Finally, based on the fact that the functional $\mathfrak{L}'$ is of the (S_+) type, we conclude that $u_n\to u$. □

To go deeper into the characteristics of the $\mathfrak{J}$ functional and its critical points, we present the following lemma.

Lemma 5. *If conditions $(\boldsymbol{H_2})$–$(\boldsymbol{H_4})$ hold, then there exists $u_0\in X$ such that*

$$||u_0||>\rho,\ and\ \mathfrak{J}(u_0)<0$$

where η is defined in Lemma 1.

Proof. According to $(\mathbf{H_4})$,

$$G(x,t)\geq\xi|t|^\theta,|t|\geq M_1 and x\in\Lambda. \tag{18}$$

According to Hypotheses $(\mathbf{H_2})$ and $(\mathbf{H_3})$, the function $t\longmapsto\frac{\hat{M}(t)}{t^{1/w-1}}$ is decreasing. Therefore, for all $t_0>0$, when $t>t_0$, $\frac{\hat{M}(t)}{t^{\frac{1}{w-1}}}\leq\frac{\hat{M}(t_0)}{t_0^{\frac{1}{w-1}}}$; then,

$$\hat{M}(t)\leq\hat{M}(t_0)\left(\frac{t}{t_0}\right)^{\frac{1}{1-\omega}}\leq ct^{\frac{1}{1-\omega}},\ for\ t>t_0. \tag{19}$$

Let $t>1$ be sufficiently large and let $u\in X$ be such that $\int_\Lambda|u|^\theta\neq 0$. Then, according to (18) and (19),

$$\begin{aligned}\mathfrak{J}(tu) &\leq \hat{M}\left(\int_\Lambda \frac{1}{p(x)}\left|t^{\mathrm{H}}\mathbb{D}_{0+}^{\omega,\nu;\psi}tu\right|^{p(x)}dx\right) - \int_\Lambda a(x)H(tu)dx \\ &\leq C\left(\int_\Lambda \left|{}^{\mathrm{H}}\mathbb{D}_{0+}^{\omega,\nu;\psi}u\right|^{p(x)}dx\right)^{1/1-\omega} t^{\frac{p^+}{1-\omega}} - c\xi t^\theta \int_\Lambda |u|^\theta dx.\end{aligned}$$

Since $\theta > \frac{p^+}{1-\omega}$, it follows that

$$\mathfrak{J}(tu) \to -\infty, \quad \text{as} \quad t \to \infty.$$

Therefore, we can set $t_0 > 0$ and set $u_0 = t_0 e$ such that $||u_0|| > \rho$ and $\mathfrak{J}(u_0) < 0$. This completes the proof. □

We now present a lemma that offers an important conclusion about the boundlessness of a set given specific conditions.

Lemma 6. *Under Hypotheses* $(\boldsymbol{H_1})$–$(\boldsymbol{H_4})$*, if F is a finite-dimensional subspace of X, then the set*

$$T = \{u \in F, such that \mathfrak{J}(u) \geq 0\},$$

is bounded in X.

Proof. Let $u \in T$. Then, according to (18) and (19), we have

$$\begin{aligned}\mathfrak{J}(u) &\leq \hat{M}\left(\int_\Lambda \frac{1}{p(x)}\left|t^{\mathrm{H}}\mathbb{D}_{0+}^{\omega,\nu;\psi}u\right|^{p(x)}dx\right) - \int_\Lambda a(x)H(u)dx \\ &\leq C\left(\int_\Lambda \left|{}^{\mathrm{H}}\mathbb{D}_{0+}^{\omega,\nu;\psi}u\right|^{p(x)}dx\right)^{1/1-\omega} - \xi \int_\Lambda |u|^\theta dx \\ &\leq C(||u||^{\frac{p^+}{1-\omega}} + ||u||^{\frac{p^-}{1-\omega}}) - \xi|u|^\theta_{\mathcal{L}^\theta},\end{aligned}$$

where $|.|_{\mathcal{L}^\theta}$ and $||.||$ are equivalent norms in F. Thus, there exists a positive constant (k) such that

$$||u||^\theta \leq k|u|^\theta_{\mathcal{L}^\theta}.$$

Therefore, we have

$$\mathfrak{J}(u) \leq \frac{p^+}{1-\omega}(||u||^{\frac{p^+}{1-\omega}} + ||u||^{\frac{p^-}{1-\omega}}) - \frac{\xi}{k}||u||^\theta.$$

Hence, the fact that $\frac{p^-}{1-\omega} < \frac{p^+}{1-\omega} < \theta$ implies that $\mathfrak{J}$ is bounded in X. □

Proof of Theorem 3. By combining Lemmas 1 and 4 with Lemma 5, we deduce that all conditions of the mountain pass theorem are satisfied. Therefore, this theorem ensures the existence of a critical point of the energy functional, which implies the existence of a non-trivial solution to problem (1). □

Proof of Theorem 4. First of all, we begin by remarking that $\mathfrak{J}(0) = 0$; moreover, according to condition $(\mathbf{H_5})$, $\mathfrak{J}$ is an even functional. Therefore, combining the last information with Lemmas 1, 4, and 6, we can see that all the conditions of the symmetric mountain pass theorem hold. Therefore, this theorem ensures the existence of an unbounded sequence of critical points of the functional energy, which results in the existence of infinitely many non-trivial solutions to the problem (1). □

Proof of Theorem 5. Let $k \in \mathbb{N}$ and $E_k = span\{\phi_1, \phi_2, ..., \phi_k\}$, where ϕ_i is an eigenfunction corresponding to the i-th eigenvalue of the problem expressed as $-\Delta u = \lambda u$ in B, $u = 0$ on ∂B, and it is extended on Ω by setting $\phi_i = 0$ for $x \in \Omega \setminus B$, where B is given by Hypothesis

$(\mathbf{H_6})$. Since E_k is a finitely dimensional space, there exists a positive constant (μ_k) such that for all $u \in E_k$, we have

$$\| u \| \leq \mu_k \| u \|_{p_B^-}. \tag{20}$$

On the other hand, according to Hypothesis $(\mathbf{H_6})$, we can choose

$$M_k > \frac{M_0 \mu^{p_B^-}}{p^-} \tag{21}$$

such that for a.a. $x \in B$ and for all $|t| < \varepsilon_k$, we have

$$a(x)H(t) \geq M_K |t|^{p_B^-}. \tag{22}$$

Let $r_k \in \{0, \min(1, \varepsilon_k)\}$ and $S_{r_k} = \{u \in E, ||u|| = r_k\}$. Then, according to (H_2), $\hat{M}(t) \leq M_0 t$ for all $t \geq 0$. Therefore, using Equation (22), if u is a function such that $supp(u) \subset B$, then we obtain

$$\begin{aligned}
\mathfrak{J}(u) &\leq \hat{M}\left(\int_\Lambda \frac{1}{p(x)} \left| {}^{\mathrm{H}}\mathbb{D}_{0+}^{\omega,\nu;\psi} u \right|^{p(x)} dx \right) - \int_\Lambda a(x)H(u)dx, \\
&\leq M_0 \int_\Lambda \frac{1}{p(x)} \left| {}^{\mathrm{H}}\mathbb{D}_{0+}^{\omega,\nu;\psi} u \right|^{p(x)} dx - \int_\Lambda a(x)H(u)dx, \\
&\leq \frac{M_0}{p^-} \int_B \left| {}^{\mathrm{H}}\mathbb{D}_{0+}^{\omega,\nu;\psi} u \right|^{p(x)} dx - M_K \int_B |u|^{p_B^-} dx.
\end{aligned}$$

Now, if $u \in E_k \cap S_{r_k}$, then according to Equation (20), we have

$$\begin{aligned}
\mathfrak{J}(u) &\leq \frac{M_0}{p^-} ||u||^{p_B^-} - M_K ||u||_{p_B^-}^{p_B^-} \\
&\leq \frac{M_0}{p^-} ||u||^{p_B^-} - M_K (\mu_k^{-1} ||u||)^{p_B^-} \\
&\leq \left(\frac{M_0}{p^-} - M_K \mu_k^{-p_B^-} \right) r_k^{p_B^-}.
\end{aligned}$$

Finally, according to (21), $\sup_{E_k \cap S_{r_k}} \mathfrak{J}(u) < 0$. Hence, $\mathfrak{J}$ satisfies condition (c_3) of Theorem 2. On the other hand, if $\mathfrak{J}(0) = 0$, the $\mathfrak{J}$ functional is even. Additionally, Lemmas 1 and 4 confirm that all the requirements outlined in Theorem 2 are satisfied. Therefore, we can conclude that problem (1) has a sequence of critical points ($\{u_k\}_{k \in \mathbb{N}}$) satisfying $||u_k|| \to 0$ as $k \to 0$. Thus, the proof of Theorem 5 is complete. □

4. Conclusions and Discussion

In this paper, we have proven two existing results for a Kirchhoff-type problem involving a fractional ψ-Hilfer derivative with variable exponents and critical nonlinearity. In the first main result, we studied the existence of solutions by proving that the associated energy functional satisfies the geometry of the mountain pass theorem. In the second main result, we investigated the existence an infinitely number of solutions for such a problem by using the symmetric version of the mountain pass theorem. It is noted that to manipulate the embedding for the critical exponent, we used a concentration-compactness principle.

We hope to develop other works by considering double-phase problems with singular nonlinearity.

Author Contributions: Methodology, M.A.A. and A.G.; Validation, M.A.A. and A.G.; Investigation, M.A.A. and A.G.; Writing—original draft preparation, M.A.A. and A.G.; Writing—review and editing, M.A.A. and A.G. All authors have read and agreed to the published version of the manuscript.

Funding: This work was funded by the University of Jeddah, Jeddah, Saudi Arabia, under grant No. UJ-24-DR-2511-1. Therefore, the authors thank the University of Jeddah for its technical and financial support.

Data Availability Statement: No new data were created or analyzed in this study. Data sharing is not applicable to this article.

Acknowledgments: This work was funded by the University of Jeddah, Jeddah, Saudi Arabia, under grant No. UJ-24-DR-2511-1. Therefore, the authors thank the University of Jeddah for its technical and financial support.

Conflicts of Interest: The authors declare no conflicts of interest.

References

1. Alsaedi, R.; Ghanmi, A. Variational approach for the Kirchhoff problem involving the p-Laplace operator and the p-Hilfer derivative. *Math. Methods Appl. Sci.* **2023**, *46*, 9286–9297. [CrossRef]
2. Ezati, R.; Nyamoradi, N. Existence of solutions to a Kirchhoff ψ-Hilfer fractional p-Laplacian equations. *Math. Meth. Appl. Sci.* **2021**, *44*, 12909–12920. [CrossRef]
3. Sousa, J.V.C.; Oliveira, E.C. On the ψ-Hilfer fractional derivative. *Commun. Nonlinear Sci. Numer. Simul.* **2018**, *60*, 72–91. [CrossRef]
4. Sousa, J.V.C.; Zuo, J.; O'Regan, D. The Nehari manifold for a ψ-Hilfer fractional p-Laplacian. *Appl. Anal.* **2022**, *101*, 5076–5106. [CrossRef]
5. Sousa, J.V.C. Existence and uniqueness of solutions for the fractional differential equations with p-Laplacian in $\mathbb{H}_p^{\nu,\eta;\psi}$. *J. Appl. Anal. Comput.* **2022**, *12*, 622–661.
6. Sousa, V.J.C. Nehari manifold and bifurcation for a ψ-Hilfer fractional p-Laplacian. *Math. Meth. Appl. Sci.* **2021**, *44*, 9616–9628. [CrossRef]
7. Sousa, V.J.C.; Leandro, T.S.; Ledesma, C.E.T. A variational approach for a problem involving a ψ-Hilfer fractional operator. *J. Appl. Anal. Comput.* **2021**, *11*, 1610–1630. [CrossRef]
8. Nouf, A.; Shammakh, W.M.; Ghanmi, A. Existence of solutions for a class of Boundary value problems involving Riemann Liouville derivative with respect to a function. *Filomat* **2023**, *37*, 1261–1270. [CrossRef]
9. Lions, P.L. The concentration-compactness principle in the calculus of variations. The limit case. *Rev. Mat. Iberoam.* **1985**, *1*, 145–201. [CrossRef]
10. Azorero, J.G.; Alonso, I.P. Multiplicity of solutions for elliptic problems with critical exponent or with a nonsymmetric term. *Trans. Am. Math. Soc.* **1991**, *323*, 877–895. [CrossRef]
11. Bahri, A.; Lions, P.L. On the existence of a positive solution of semilinear elliptic equations in unbounded domains. *Ann. Inst. H. Poincaré Anal. Non Linéaire* **1997**, *14*, 365–413. [CrossRef]
12. Fu, Y. The principle of concentration compactness in $L^{p(x)}$ spaces and its application. *Nonlinear Anal.* **2009**, *71*, 1876–1892. [CrossRef]
13. Ghanmi, A.; Kratou, M.; Saoudi, K.; Repovš, D. Nonlocal p-Kirchhoff equations with singular and critical nonlinearity terms. *Asympt. Anal.* **2023**, *131*, 125–143. [CrossRef]
14. Halsey, T.C. Electrorheological fluids. *Science* **1992**, *258*, 761–766. [CrossRef]
15. Mihăilescu, M.; RŘdulescu, V.D. A multiplicity result for a nonlinear degenerate problem arising in the theory of electrorheological fluids. *Proc. R. Soc. Lond. A* **2006**, *462*, 2625–2641. [CrossRef]
16. Ruzicka, M. *Electrorheological Fluids: Modelling and Mathematical Theory*; Lecture Notes in Mathematics; Springer: Berlin/Heidelberg, Germany, 2000; Volume 1784.
17. Chen, Y.; Levine, S.; Rao, M. Variable exponent, linear growth functionals in image restoration. *SIAM J. Appl. Math.* **2006**, *66*, 1383–1406. [CrossRef]
18. Ahmed, E.; Hashish, A.; Rihan, F.A. On fractional order cancer model. *J. Fract. Calc. Appl. Anal.* **2012**, *3*, 1–6.
19. Chen, W.C. Nonlinear dynamics and chaos in a fractional-order financial system. *Chaos Solit. Fract.* **2008**, *36*, 1305–1314. [CrossRef]
20. Corlay, S.; Lebovits, J.; Véhel, J.L. Multifractional stochastic volatility models. *Math. Financ.* **2014**, *24*, 364–402. [CrossRef]
21. Herrmann, R. *Fractional Calculus: An Introduction for Physicists*; World Scientific Publishing Company: Singapore, 2011.
22. Hilfer, R. *Applications of Fractional Calculus in Physics*; World Scientific Publ. Co.: Singapore, 2000; pp. 87–130.
23. Hethcote, H.W. Three basic epidemiological models. In *Applied Mathematical Ecology*; Series: Biomathematics; Springer: Berlin/Heidelberg, Germany, 1989; Volume 18.
24. Bonder, J.; Silva, A. Concentration-copactness principle for variable exponent spaces and applications. *Electr. J. Differ. Equ.* **2010**, *2010*, 141.
25. Chammem, R.; Ganmi, A.; Sahbani, A. Existence and multiplicity of solution for some Styklov problem involving $p(x)$-Laplacian operator. *Appl. Anal.* **2022**, *101*, 2401–2417. [CrossRef]
26. Chammem, R.; Sahbani, A. Existence and multiplicity of solution for some Styklov problem involving $(p_1(x), p_2(x))$-Laplacian operator. *Appl. Anal.* **2021**, *102*, 709–724. [CrossRef]
27. Dai, G.; Hao, R. Existence of solutions for a $p(x)$-Kirchhoff-type equation. *J. Math. Anal. Appl.* **2009**, *359*, 275–284. [CrossRef]
28. Dai, G.; Liu, D. Infinitely many positive solutions for a $p(x)$-Kirchhoff-type equation. *J. Math. Anal. Appl.* **2009**, *359*, 704–710. [CrossRef]
29. Dai, G.; Ma, R. Solutions for a $p(x)$-Kirchhoff type equation with Neumann boundary data. *Nonlinear Anal. Real World Appl.* **2011**, *12*, 2666–2680. [CrossRef]

30. Ambrosio, V.; Isernia, T. Concentration phenomena for a fractional Schrödinger-Kirchhoff type equation. *Math. Meth. Appl. Sci.* **2018**, *41*, 615–645. [CrossRef]
31. Fiscella, A.; Pucci, P. *p*-fractional Kirchhoff equations involving critical nonlinearities. *Nonlinear Anal. Real World Appl.* **2017**, *35*, 350–378. [CrossRef]
32. Xiang, M.; Zhang, B.; Rădulescu, V.D. Superlinear Schrödinger-Kirchhoff type problems involving the fractional p-Laplacian and critical exponent. *Adv. Nonlinear Anal.* **2020**, *9*, 690–709. [CrossRef]
33. Fan, X.; Zhang, Q.; Zhao, D. Eigenvalues of $p(x)$-Laplacian Dirichlet problem. *J. Math. Anal. Appl.* **2015**, *302*, 306–317. [CrossRef]
34. Sahbani, A. Infinitely many solutions for problems involving Laplacian and biharmonic operators. *Complex Var. Elliptic Equ.* **2023**, 1–14. [CrossRef]
35. Srivastava, H.M.; da Costa Sousa, J.V. Multiplicity of Solutions for Fractional-Order Differential Equations via the $p(x)$-Laplacian Operator and the Genus Theory. *Fract. Fract.* **2022**, *6*, 481. [CrossRef]
36. Ambrosetti, A.; Rabinowitz, P.H. Dual variational methods in critical point theory and applications. *J. Func. Anal.* **1973**, *14*, 349–381. [CrossRef]
37. Kajikiya, R. A critical point theorem related to the symmetric mountain pass lemma and its applications to elliptic equations. *J. Funct. Anal.* **2005**, *225*, 352–370. [CrossRef]

Disclaimer/Publisher's Note: The statements, opinions and data contained in all publications are solely those of the individual author(s) and contributor(s) and not of MDPI and/or the editor(s). MDPI and/or the editor(s) disclaim responsibility for any injury to people or property resulting from any ideas, methods, instructions or products referred to in the content.

mathematics

MDPI

Article

A Note on a Min–Max Method for a Singular Kirchhoff Problem of Fractional Type

Ramzi Alsaedi

Department of Mathematics, Faculty of Sciences, King Abdulaziz University, P.O. Box 80203, Jeddah 21589, Saudi Arabia; ralsaedi@kau.edu.sa or ramzialsaedi@yahoo.co.uk

Abstract: In the present work, we study a fractional elliptic Kirchhoff-type problem that has a singular term. More precisely, we start by proving some properties related to the energy functional associated with the studied problem. Then, we use the variational method combined with the min–max method to prove that the energy functional reaches its global minimum. Finally, since the energy functional has a singularity, we use the implicit function theorem to show that the point where the minimum is reached is a weak solution for the main problem. To illustrate our main result, we give an example at the end of this paper.

Keywords: variational methods; singular equations; existence of solutions; min–max method

MSC: 35A15; 35J35; 35B38

1. Introduction

In this study, we prove some existing results related to the following fractional and singular problem:

$$(Q_\mu)\begin{cases} M(A_p w)\mathrm{L}^p_{\mathbf{K}}(w)(\xi) = \frac{h(\xi)}{|w(\xi)|^{\delta(\xi)}} + \mu f(\xi, w(\xi)) \quad \text{in } \Omega, \\ \\ w = 0, \quad \text{on } \mathbb{R}^N \backslash \Omega, \end{cases}$$

where $\mu > 0$, Ω is a bounded domain of $\mathbb{R}^N$, δ is a continuous function on $\overline{\Omega}$, and $p : \mathbb{R}^N \times \mathbb{R}^N \to (1, \infty)$ is a continuous function, which satisfies

$$1 < p^- \leq p^+ < \infty, \tag{1}$$

$$p(\xi, \eta) = p(\eta, \xi), \ \forall \ (\xi, \eta) \in \overline{\Omega} \times \overline{\Omega}, \tag{2}$$

and

$$p((\xi, \eta) - (y, y)) = p(\xi, \eta), \ \ \forall \ (\xi, \eta, y) \in \mathbb{R}^N \times \mathbb{R}^N \times \mathbb{R}^N, \tag{3}$$

where

$$p^- = \inf_{\overline{\Omega}\times\overline{\Omega}} p(\xi, \eta), \text{ and } \ p^+ = \sup_{\overline{\Omega}\times\overline{\Omega}} p(\xi, \eta).$$

The operators A_p and $\mathrm{L}^p_{\mathbf{K}}$ are defined, respectively, by

$$A_p(w) = \int_{\mathbb{R}^N \times \mathbb{R}^N} \frac{|w(\xi) - w(\eta)|^{p(\xi,\eta)}}{p(\xi, \eta)} \mathbf{K}(\xi, \eta)\, d\xi d\eta, \tag{4}$$

and

$$\mathrm{L}^p_{\mathbf{K}} w(\xi) = C \int_{\mathbb{R}^N} |w(\xi) - w(\eta)|^{p(\xi,\eta)-2}(w(\xi) - w(\eta))\mathbf{K}(\xi, \eta)\, d\eta, \ \forall \ \xi \in \mathbb{R}^N, \tag{5}$$

for some normalized constant C. Finally, we assume that the function $\mathbf{K}$ is positive measurable on $\mathbb{R}^N \setminus \Omega \times \mathbb{R}^N \setminus \Omega$ and satisfies the following properties:

(B1) $\mathbf{K}(\xi,\eta) = \mathbf{K}(\eta,\xi)$ for any $(\xi,\eta) \in \mathbb{R}^N \times \mathbb{R}^N$.

(B2) There exist $k_0 > 0$ and $s \in (0,1)$, such that for all $(\xi,\eta) \in \mathbb{R}^N \times \mathbb{R}^N$ with $\xi \neq \eta$, we have

$$\mathbf{K}(\xi,\eta) \geq k_0 |\xi-\eta|^{-(N+sp(\xi,\eta))}.$$

(B3) $\varphi\,\mathbf{K} \in L^1(\mathbb{R}^N \times \mathbb{R}^N)$, where $\varphi(\xi,\eta) = \min(|\xi-\eta|^{p(\xi,\eta)}, 1)$.

We note that in the particular case when $\mathbf{K}(\xi,\eta) = \frac{1}{|\xi-\eta|^{N+sq(\xi,\eta)}}$, the operator $\mathrm{L}^p_{\mathbf{K}}$ is reduced to the fractional $p(.,.)$-Laplacian operator $(-\Delta_{p(.,.)})^s$, which is studied by many researchers (we cite, for example, the works [1–4]). A logical consequence is that every application of $(-\Delta_{q(.,.)})^s$ is also an application of $\mathrm{L}^p_{\mathbf{K}}$; so, we can find several applications of our problem in many fields like fluids, mechanics and image processing (see, for example, the reference [5]). As researchers delve deeper into understanding intricate systems and phenomena, the general non-local integro-differential operator continues to be indispensable, driving advancements in both theoretical frameworks and practical applications.

Significant attention has been directed toward investigating challenges associated with these operators. Specifically, in the literature, there are too many problems of Kirchhoff type involving variable exponents that we refer interested readers to the papers [2,6–19] and others cited therein.

For problems with singular terms arising from $\mathrm{L}^p_{\mathbf{K}}$, occurrences are quite rare and we are possibly among the first to address them through this paper. Concerning other operators like the $p(.)$-Laplacian operator, there are many published papers involving singular nonlinearities in addition; we cite, for example [9,18,20–23]. In particular, in [18], the authors considered the following problem:

$$\begin{cases} -G\left(\int_\Omega \frac{1}{q(\xi)}|\nabla u|^{q(\xi)}d\xi\right)\Delta_{q(.)}u(\xi) = h(\xi)u^{-\gamma(\xi)} - \lambda g(\xi,u(\xi)) & \text{in } \Omega, \\ u = 0, \quad \text{on } \partial\Omega, \end{cases} \tag{6}$$

where $G \in C((0,\infty),(0,\infty))$, $g \in C^1(\Omega \times \mathbb{R})$, q and γ are continuous on Ω. Under suitable assumptions and using some variational techniques combined with the min–max method, the authors proved that problem (6) has a nontrivial solution.

Recently, Ben Ali et al. [24] considered the following fractional problem:

$$\begin{cases} G\left(\int_{\Omega\times\Omega} \frac{|w(\xi)-w(\eta)|^{q(\xi,\eta)}}{q(\xi,\eta)|\xi-\eta|^{N+sq(\xi,\eta)}}d\xi d\eta\right)(-\Delta)^s_{q(.,.)}w(\xi) = \lambda h(\xi,w(\xi)) - |w(\xi)|^{p(\xi)-2}w(\xi) & \text{in } \Omega, \\ w = 0, \quad \text{on } \partial\Omega. \end{cases} \tag{7}$$

Under appropriate hypotheses and by combining Ekland's variational principle with the mountain pass theorem, the authors proved the existence of two nontrivial solutions for problem (7).

Azroul et al. [25] considered the following problem:

$$(P_K)\begin{cases} \mathrm{L}^p_{\mathbf{K}}u(\xi) = f(\xi,u(\xi)) & \text{in } \Omega, \\ u = 0, \quad \text{on } \mathbb{R}^N\setminus\Omega. \end{cases}$$

Under certain conditions, the authors showed that the problem (P_K) has a unique weak solution, and this is proven by the means of the Minty–Browder Theorem.

In this work, we continue to investigate a fractional problem of Kirchhoff type. We note that Kirchhoff-type problems often refer to problems in mathematical physics related to Kirchhoff's laws or equations. These problems typically arise in contexts like electrical

circuits, heat conduction, or wave propagation. These types of problems are introduced by Kirchhoff [14], and more precisely, the author studied the following equation:

$$\delta\frac{\partial^2\psi}{\partial u^2}-\left(\frac{t_0}{s}+\frac{\Delta}{2h}\int_0^h|\frac{\partial\psi}{\partial u}|^2\,du\right)\frac{\partial^2\psi}{\partial v^2},$$

where h represents the length of a cross and s represents the area of a cross-section; the initial axial extension is denoted by Δ and ψ denotes the lateral displacement at x and y. The novelty in our study is that the Kirchhoff function M is in a more general class of functions. The presence of the singular term also implies that the functional energy is not regular, so the direct variational method cannot be applied. We note that the presence of the non-local operator $\mathrm{L}^p_{\mathbf{K}}$ generalizes other operators in the literature. To prove the existence of solutions, we present several results and notations in Section 2, after which we present and prove the main result of this paper in Section 3. We finish our work by presenting an illustrative example.

2. Preliminaries

In this section, we introduce the functional framework within which we will examine our principal result. To accomplish this, we present the essential characteristics of variable exponent spaces. Interested readers can find further properties in [25–28] and the associated literature.

Next, we denoted by $C_+(\Omega)$ the sets of all continuous functions q such that $\inf\limits_{\xi\in\overline{\Omega}} q(\xi)>1$, and for a fixed function $w\in C_+(\Omega)$, we define

$$w^-=\inf_{\xi\in\overline{\Omega}} w(\xi)\ \text{ and }\ w^+=\sup_{\xi\in\overline{\Omega}} w(\xi).$$

Let $q\in C_+(\Omega)$. We define the space $L^{q(.)}(\Omega)$ as the set of all measurable functions w such that $\int_\Omega |w(\xi)|^{q(\xi)}d\xi<\infty$, and we equip it with the following norm:

$$|w|_{q(.)}=\inf\left\{\mu>0:\int_\Omega|\frac{w(\xi)}{\mu}|^{q(\xi)}d\xi\le 1\right\}.$$

We recall that $L^{q(.)}(\Omega)$ is a Banach space, moreover, it is separable and reflexive if and only if

$$1<q^-\le q^+<\infty.$$

Also, the Hölder inequality holds in this space.

Put

$$\rho_{q(.)}(w)=\int_\Omega|w(\xi)|^{q(\xi)}d\xi.$$

Proposition 1. *For all $w\in L^{q(.)}(\Omega)$, we have the following:*

(1) Both $|w|_{q(.)}$ and $\rho_{q(.)}(w)$ are less than one, or both greater than one, or both equal to one.

(2) $\min(|w|^{q^-}_{q(.)},|w|^{q^+}_{q(.)})\le\rho_{q(.)}(w)\le\max(|w|^{q^-}_{q(.)},|w|^{q^+}_{q(.)})$.

Also, we have the following interesting proposition.

Proposition 2. *Let m be a measurable function in $L^\infty(\mathbb{R}^N)$, and let q be a measurable function, such that for any $\xi\in\mathbb{R}^N$, we have*

$$1\le q(\xi)m(\xi)\le\infty.$$

If $0 \neq w \in L^{q(.)}(\mathbb{R}^N)$, *then, we obtain*

$$\min(|w|^{q^-}_{m(.)q(.)}, |w|^{q^+}_{m(.)q(.)}) \leq ||w|^{m(.)}|_{q(.)} \leq \max(|w|^{q^-}_{m(.)q(.)}, |w|^{q^+}_{m(.)q(.)}).$$

Now, for a function p satisfying Equations (1)–(3), we define the Sobolev space $W^{s,\overline{p}(.),p(.,.)}(\Omega)$ by

$$W^{s,\overline{p}(.),p(.,.)}(\Omega) = \left\{ w \in L^{\overline{p}(.)}(\Omega), \int_{\Omega\times\Omega} \frac{|w(\xi) - w(\eta)|^{p(\xi,\eta)}}{s^{p(\xi,\eta)}|\xi - \eta|^{N+sp(\xi,\eta)}}\, d\xi d\eta < \infty,\ \ s > 0 \right\},$$

and we endow it with the following norm:

$$||w||_{W^{s,\overline{p}(.),p(.,.)}(\Omega)} = |w|_{\overline{p}(.)} + [w]_{s,p(.,.)},$$

where $\overline{p}(\xi) = p(\xi, \xi)$, and

$$[w]_{s,p(.,.)} = \inf\left\{ s > 0 : \int_{\Omega\times\Omega} \frac{|w(\xi) - w(\eta)|^{p(\xi,\eta)}}{s^{p(\xi,\eta)}|\xi - \eta|^{N+sp(\xi,\eta)}}\, d\xi d\eta \leq 1 \right\}.$$

We denote by

$$\mathbb{B} = \left\{ w : \mathbb{R}^N \longrightarrow \mathbb{R} \text{ measurable} : w_{|\Omega} \in L^{\overline{p}(\xi)}(\Omega) \right\}.$$

Next, we define the space

$$W^{\mathbf{K},p(.,.)}(\Omega) = \left\{ w \in \mathbb{B} :\ \text{with } \int_{\Omega\times\Omega} \frac{|w(\xi) - w(\eta)|^{p(\xi,\eta)}}{s^{p(\xi,\eta)}} \mathbf{K}(\xi,\eta)\, d\xi d\eta < \infty, \text{ for some } s > 0 \right\},$$

equipped with the norm

$$||w||_{W^{\mathbf{K},p(.,.)}(\Omega)} = ||w||_{\overline{p}(.)} + [w]_{\mathbf{K},p(.,.)},$$

where

$$[w]_{\mathbf{K},p} = \inf\left\{ s > 0 : \int_{\Omega\times\Omega} \frac{|w(\xi) - w(\eta)|^{p(\xi,\eta)}}{s^{p(\xi,\eta)}} \mathbf{K}(\xi,\eta)\, d\xi d\eta \leq 1 \right\}.$$

Hereafter, we will work on the following space:

$$E := W_0^{\mathbf{K},p(.,.)}(\Omega) = \left\{ w \in W^{\mathbf{K},p(.,.)}(\Omega),\ \ w(\xi) = 0 \text{ a.e. in } \mathbb{R}^N \setminus \Omega \right\},$$

with the equivalent norm

$$||.|| = [.]_{\mathbf{K},p}.$$

We recall from [25] that this space contains $C_0^\infty(\Omega)$; moreover, the following propositions hold.

Proposition 3. *The space* $(E, ||.||)$ *is a uniformly convex Banach space. Moreover, it is reflexive and separable.*

For $w \in E$, we define the functional

$$\sigma_{\mathbf{K},p}(w) = \int_{\Omega\times\Omega} |w(\xi) - w(\eta)|^{p(\xi,y)} \mathbf{K}(\xi,\eta)\, d\xi d\eta.$$

Proposition 4 ([25])**.** *For any* $w \in E$, *we have*

$$\min\left(||w||^{p^-}, ||w||^{p^+} \right) \leq \sigma_{\mathbf{K},p}(w) \leq \max\left(||w||^{p^-}, ||w||^{p^+} \right).$$

Proposition 5 ([25]). *Let $w, w_n \in E$, $n \in \mathbb{N}$, and then, we have*

$$\lim_{n\to\infty} ||w_n - w|| = 0 \iff \lim_{n\to\infty} \sigma_{\mathbf{K},p}(w_n - w) = 0.$$

Finally, we recall again from [25] that if for any $\xi \in \overline{\Omega}$, we have

$$1 < \alpha(\xi) < p_s^*(\xi) := \frac{Np(\xi,\xi)}{N - sp(\xi,\xi)},$$

and if $\mathbf{K}$ satisfies conditions $(B1)$–$(B3)$, then we have a continuous and compact embedding from E into $L^{\alpha(.)}(\Omega)$; in particular, there is $C_\alpha > 0$, satisfying

$$|w|_{\alpha(.)} \leq C_\alpha ||w||.$$

Definition 1. *By a solution of problem (Q_μ), we mean a function $w \in E$ for which for any $\varphi \in E$, we have*

$$\begin{aligned} & M(A_P(w)) \int_{\Omega\times\Omega} |w(\xi) - w(\eta)|^{p(\xi,\eta)-2}(w(\xi) - w(\eta))(\varphi(\xi) - \varphi(\eta))\mathbf{K}(\xi,\eta)\, d\xi d\eta \\ = & \int_\Omega h(\xi)|w(\xi)|^{-\delta(\xi)}\varphi(\xi)\, d\xi + \mu \int_\Omega f(\xi, w(\xi))\varphi(\xi) d\xi. \end{aligned}$$

To prove the existence of solutions for problem (Q_μ), we associate it with the following singular functional $I_\mu : E \to \mathbb{R}$, which is defined by

$$I_\mu(w) = \widehat{M}(A_p(w)) - \int_\Omega \frac{h(\xi)}{1 - \delta(\xi)} |w(\xi)|^{1-\delta(\xi)} d\xi - \mu \int_\Omega F(\xi, w(\xi)) d\xi,$$

where

$$F(\xi,t) = \int_0^t f(\xi,s)ds, \text{ and } \widehat{M}(t) = \int_0^t M(s)ds.$$

It is worth noting that I_μ is well defined but it is non-differentiable. So, we use the min–max method to prove our existing result.

3. Main Result and Its Proof

In this section, we give and demonstrate the main result of this paper. To this aim, we assume the following hypotheses:

(N_0) The function M is continuous and positive in $\mathbb{R}$; moreover, there exist $a > 1$ and $\nu > 1$, such that

$$\frac{1}{a} t^{\nu-1} \leq M(t) \leq a t^{\nu-1}, \ \ \forall\, t \geq 0.$$

(N_1) For all $(\xi,\eta) \in \overline{\Omega} \times \overline{\Omega}$, we have

$$\nu p(\xi,\xi) < p_s^*(\xi), \quad sp(\xi,\eta) < N, \text{ and } \nu p(\xi,\xi) < \frac{N}{s}.$$

(N_2) A function h is positive almost everywhere in Ω, such that

$$h \in L^{\frac{\theta(.)}{\theta(.)+\delta(.)-1}}(\Omega),$$

for some $1 < \theta(\xi) < p_s^*(\xi)$.

(H_1) There exist $B, \alpha \in C_+(\overline{\Omega})$ and $\psi \in L^{B(\xi)}(\Omega)$, such that, for all $(\xi,\eta) \in \overline{\Omega} \times \mathbb{R}$, we have

$$f(\xi,\eta) \leq c\psi(\xi)|\eta|^{\alpha(\xi)-2}\eta, \ \text{ for some } \ c > 0,$$

and

$$\alpha(\xi) < p(\xi,\xi) < \eta p(\xi,\xi) < \frac{N}{s} < B(\xi).$$

(H_2) There exists $\Omega' \subset\subset \Omega$, $|\Omega'| > 0$, for which we have

$$f(\xi,\eta) \geq 0,\ \forall \xi \in \Omega',\ \text{and all}\ \ \eta \in \mathbb{R}.$$

Now, we state the main result of this work.

Theorem 1. *Assume that hypotheses (N_0)–(N_2) and (H_1)–(H_2) hold. If the kernel* **K** *satisfies hypotheses $(B1)$–$(B3)$, then, for each $\mu > 0$, the problem Q_μ admits a nontrivial solution.*

To prove Theorem 1, we will prove several Lemmas. The first one concerns the coercivity of the associated functional energy. In particular, we prove the following Lemma:

Lemma 1. *If the hypotheses (N_0)–(N_2) and (H_1) hold, then I_μ becomes coercive in E.*

Proof. Let $w \in E$ with $\|w\| > 1$. Then, by hypothesis (N_0), Equation (1) and Proposition 4, we obtain

$$\begin{aligned}
\widehat{M}(A_p(w)) &= \widehat{M}\bigg(\int_{\mathbb{R}^N\times\mathbb{R}^N} \frac{|w(\xi)-w(\eta)|^{p(\xi,\eta)}}{p(\xi,\eta)}\mathbf{K}(\xi,\eta)\,d\xi d\eta\bigg)\\
&= \widehat{M}\bigg(\int_{\Omega\times\Omega} \frac{|w(\xi)-w(\eta)|^{p(\xi,\eta)}}{p(\xi,\eta)}\mathbf{K}(\xi,\eta)\,d\xi d\eta\bigg)\\
&\geq \frac{1}{a\nu}\bigg(\int_{\Omega\times\Omega} |w(\xi)-w(\eta)|^{p(\xi,\eta)}\mathbf{K}(\xi,\eta)\,d\xi d\eta\bigg)^{\nu}\\
&\geq \frac{1}{p^+a\nu}\sigma^{\nu}_{\mathbf{K},p}(w)\\
&\geq \frac{1}{p^+a\nu}||w||^{\nu p^-}. \qquad (8)
\end{aligned}$$

Now, from hypothesis (N_2) and the Hölder inequality, we conclude that

$$\begin{aligned}
\int_\Omega \frac{h(\xi)}{1-\delta(\xi)}(w(\xi))^{1-\delta(\xi)}d\xi &\leq \frac{1}{1-\delta^+}\int_\Omega h(\xi)(w(\xi))^{1-\delta(\xi)}d\xi\\
&\leq \frac{1}{1-\delta^+}|h|_{\frac{\theta(.)}{\theta(.)+\delta(.)-1}}||w|^{1-\delta(.)}|_{\frac{\theta(.)}{1-\delta(.)}}. \qquad (9)
\end{aligned}$$

So, by combining Proposition 1 and the compact embedding with the fact that $1 < \theta(\xi) < q^*_s$, we conclude the existence of $c_1 > 0$ such that

$$\begin{aligned}
\int_\Omega \frac{h(\xi)}{1-\delta(\xi)}(w(\xi))^{1-\delta(\xi)}d\xi &\leq \frac{1}{1-\delta^+}|h|_{\frac{\theta(.)}{\theta(.)+\delta(.)-1}}\max(|w|^{1-\delta^+}_{\theta(.)},|w|^{1-\delta^-}_{\theta(.)})\\
&\leq \frac{c_1}{1-\delta^+}|h|_{\frac{\theta(.)}{\theta(.)+\delta(.)-1}}||w||^{1-\delta^-}. \qquad (10)
\end{aligned}$$

Next, from (H_1), the Hölder inequality and the compact embedding, we obtain

$$\begin{aligned}
\int_\Omega F(\xi,w(\xi))d\xi &\leq c\int_\Omega \psi(\xi)|w(\xi)|^{\alpha(\xi)}d\xi\\
&\leq c|\psi|_{B(.)}||w|^{\alpha(.)}|_{B'(.)}\\
&\leq c|\psi|_{B(.)}\max(|w|^{\alpha^+}_{B'(.)\alpha(.)},|w|^{\alpha^-}_{B'(.)\alpha(.)}).
\end{aligned}$$

Using (H_1), we have

$$p_s^*(\xi) - \alpha(\xi)B'(\xi) = \frac{NB(\xi)[p(\xi,\xi) - \alpha(\xi)] + p(\xi,\xi)[B(\xi)\alpha(\xi)s - N]}{(B(\xi) - 1)(N - sp(\xi,\xi))} > 0, \tag{11}$$

where

$$\frac{1}{B(\xi)} + \frac{1}{B'(\xi)} = 1.$$

In accordance with the compact embedding, we obtain the existence of $c_2 > 0$, satisfying

$$\int_\Omega F(\xi, w(\xi))d\xi \leq c_2|\psi|_{B(.)}||w||^{\alpha^+}. \tag{12}$$

Finally, by combining Equations (8) and (10) with Equation (12), we obtain

$$I_\mu(w) \geq \frac{1}{p^+a\eta}||w||^{\nu p^-} - \frac{c_1}{1-\delta^+}|h|_{\frac{\theta(.)}{\theta(.)+\delta(.)-1}}||w||^{1-\delta^-} - c_2|\psi|_{B(.)}||w||^{\alpha^+}. \tag{13}$$

Since $1 - \delta^- < \alpha^+ < \nu p^-$, we can see that $I_\mu(w) \to \infty$ as $||w|| \to \infty$. This ends the proof. □

Lemma 2. *If the hypothesis (H_2) is satisfied, then we obtain a non-negative function $0 \neq u$ in E, for which, for a sufficiently small $t > 0$, we have $I_\mu(tu) < 0$.*

Proof. We begin by fixing a function u in $C_0^\infty(\Omega)$ with $supp(u) \subset \Omega' \subset\subset \Omega$. We assume further that $u = 1$ in some subset $\Omega_1 \subset supp(u)$ and $0 \leq u \leq 1$ in Ω.

Now, let $t \in (0,1)$. Then, from hypothesis (N_0) and Proposition 4, we obtain

$$\begin{aligned}
\widehat{M}(A_p(tu)) &\leq \frac{a}{\nu}A_p^\nu(tu) \\
&\leq \frac{a}{\nu}\left(\int_{\Omega\times\Omega} t^{p(\xi,\eta)}\frac{|u(\xi) - u(\eta)|^{p(\xi,\eta)}}{p(\xi,\eta)}\mathbf{K}(\xi,\eta)\,d\xi d\eta\right)^\nu \\
&\leq \frac{a}{\nu p^-}t^{\nu p^-}\sigma_{\mathbf{K},p}^\nu(u) \\
&\leq \frac{a}{\nu p^-}t^{\nu p^-}||u||^{\nu p^-}.
\end{aligned} \tag{14}$$

So, using Equation (14) and the fact that F is a non-negative function, we obtain

$$\begin{aligned}
I_\mu(tu) &\leq \frac{a}{\nu p^-}t^{\nu p^-}||u||^{\nu p^-} - \int_\Omega \frac{h(\eta)}{1-\delta(\eta)}|tu|^{1-\delta(\eta)}d\eta \\
&\leq \frac{a}{\nu p^-}t^{\nu p^-}||u||^{\nu p^-} - t^{1-\delta^-}\frac{1}{1-\delta^-}\int_\Omega h(\eta)|u|^{1-\delta(\eta)}d\eta \\
&\leq t^{1-\delta^-}\left(t^{\nu p^- + \delta^- - 1}\frac{a}{\nu p^-}||u||^{\nu p^-} - \frac{1}{1-\delta^-}\int_\Omega h(\eta)|u|^{1-\delta(\eta)}d\eta\right).
\end{aligned}$$

Since $\frac{a}{\nu p^-}||u||^{\nu p^-} > 0$ and $\nu p^- + \delta^- - 1 > 0$, we have

$$I_\mu(tu) < 0 \text{ for } t < min(1, S),$$

where

$$S = \left(\frac{\frac{1}{1-\delta^-}\int_\Omega h(\xi)|u|^{1-\delta(\xi)}d\xi}{\frac{a}{\nu p^-}||u||^{\nu p^-}}\right)^{\frac{1}{\nu p^- + \delta^- - 1}}.$$

□

In the sequel, we put

$$m_\mu = \inf_{w \in E} I_\mu(w). \tag{15}$$

Lemma 3. *Assume that assertions* (N_1)–(N_2) *and* (H_1)–(H_2) *hold. If, in addition,* **K** *satisfies hypotheses* $(B1)$–$(B3)$*, then there exists* $w_* \in E$*, satisfying*

$$I_\mu(w_*) = m_\mu < 0.$$

Proof. Let $\{w_n\}$ be a sequence in E that satisfies

$$I_\mu(w_n) \to m_\mu. \tag{16}$$

We claim that $\{w_n\}$ is bounded in E. Indeed, if this is not true, then we have

$$||w_n|| \to \infty \ \text{ as } \ n \to \infty.$$

The coercivity of the functional I_μ implies that

$$I_\mu(w_n) \to \infty \ \text{ as } \ ||w_n|| \to \infty,$$

which contradicts with Equation (16).

Now, the reflexivity of the space E implies that we can find a sub-sequence (still denoted by $\{w_n\}$) and a function w_* in E, such that

$$\begin{cases} w_n \rightharpoonup w_* \ \textit{weakly in } E, \\ w_n \to w_* \ \textit{strongly in } L^{\alpha(.)}(\Omega), \ 1 \le \alpha(\xi) < p_s^*(\xi), \\ w_n \to w_* \ \textit{a.e in } \Omega. \end{cases} \tag{17}$$

Next, our purpose is to prove that

$$I_\mu(w) = \widehat{M}(A_p(w)) - \int_\Omega \frac{h(\xi)}{1-\delta(\xi)} |w(\xi)|^{1-\delta(\xi)} d\xi - \mu \int_\Omega F(\xi, w(\xi)) d\xi$$

is weakly lower semi-continuous on E.

By the continuity of the function $\widehat{M}$, the fact that $w_n \to u_*$ a.e in Ω, and using Fatou's lemma, we deduce that

$$\widehat{M}(A_p(w_*)) \le \lim_{n \to \infty} inf \widehat{M}(A_p(w_n)). \tag{18}$$

Now, it is shown in [29] (Theorem 2.3) that if $h \in L^{\zeta(.)}(\Omega)$ with

$$0 < \frac{\zeta(1-\delta)}{1-\zeta} < p_s^*, \tag{19}$$

then, we have

$$\lim_{n \to \infty} \int_\Omega h(\eta) |w_n(\eta)|^{1-\delta(\eta)} d\eta = \int_\Omega h(\eta) |w_*(\eta)|^{1-\delta(\eta)} d\eta. \tag{20}$$

A simple calculation shows that $\zeta = \frac{\theta(.)}{\theta(.)+\delta(.)-1}$ satisfies Equation (19). So, Equation (20) holds.

Next, we will demonstrate that

$$\lim_{n \to \infty} \int_\Omega F(\eta, w_n(\eta)) d\eta = \int_\Omega F(\eta, w_*(\eta)) d\eta. \tag{21}$$

For this purpose, let $\varepsilon > 0$; then, from hypothesis (H_1), we can find $c_\varepsilon > 0$, such that

$$|F(\eta, w_n(\eta))| \leq \frac{c_\varepsilon}{\alpha^-}|\psi(\eta)||w_n|^{\alpha(\eta).}$$

From Equation (11), we have $B^{'}(\xi)\alpha(\xi) < p_s^*$. So, from the fact that $w_n \rightharpoonup w_*$ in E, and from the compact embedding, we deduce the existence of a sub-sequence still denoted by $\{w_n\}$ that converges strongly in $L^{B^{'}(.)\alpha(.)}(\Omega)$. Thus, $w_{n\to}w_*$ a.e in Ω. Moreover, we have

$$|w_n(\xi)| \leq g(\xi), \text{ for some } g \in L^{\alpha(\xi)B^{'}(\xi)}.$$

Therefore, we obtain

$$|F(\xi, w_n(\xi))| \leq \frac{c_\varepsilon}{\alpha^-}|\psi(\xi)||g(\xi)|^{\alpha(\xi)}.$$

Hence, using the Hölder's inequality, one has

$$\int_\Omega |F(\xi, w_n(\xi))|d\xi \leq \frac{c_\varepsilon}{\alpha^-}|\psi|_{B(.)}|g|^{\alpha(.)}_{S^{'}(.)}.$$

So, if we combine Proposition 2 with the Lebesgue-dominated convergence, we obtain the result of Equation (21).

Finally, Equations (18), (20) and (21) yield to the weakly lower semi-continuity of the functional I_δ. So, we deduce

$$I_\delta(w_*) \leq \lim_{n\to\infty} inf I_\delta(w_n) = m_\delta.$$

On the other hand, from (3), we have

$$I_\delta(w_*) \geq m_\delta.$$

We conclude that

$$I_\delta(w_*) = m_\delta.$$

□

Proof of Theorem 1. From Lemma 3, we deduce that the function w_* is a global minimum for the functional I_δ. So, for all $\phi \in E$ and all $t > 0$, we have

$$I_\delta(w_* + t\phi) - I_\delta(w_*) \geq 0.$$

By dividing the last inequality by t and by letting t tend to zero, we obtain

$$\begin{aligned} & M(A_p(w_*)) \int_{\Omega\times\Omega} |w_*(\xi) - w_*(\eta)|^{p(\xi,\eta)-2}(w_*(\xi) - w_*(\eta))(\phi(\xi) - \phi(\eta))\mathbf{K}(\xi,\eta)\, d\xi d\eta \\ - & \int_\Omega h(\xi)|w_*|^{-\delta(\xi)}\phi(\xi)d\xi - \mu\int_\Omega f(\xi, w_*(\xi))\phi(\xi)d\xi \geq 0. \end{aligned}$$

As ϕ is arbitrary in E, we have the flexibility to substitute ϕ with $-\phi$ in the last inequality with the equality still preserved. Then, w_* is a weak solution to the problem (Q_δ). Furthermore, condition $I_\delta(w_*) < 0$ indicates that w_* is nontrivial. □

4. An Example

This section provides an example that improves the main result of this paper.

Example 1. *Let Ω be a bounded domain in $\mathbb{R}^N$ $(N \geq 2)$. We consider the following problem:*

$$(Q_\delta)\begin{cases} (A_p(w))^{\nu-1}(-\Delta_{p(.,.)})^s(w) = \frac{h(\xi)}{|w(\xi)|^{\delta(\xi)}} + \mu a(\xi)|w(\xi)|^{\alpha(\xi)-2}w(\xi) \quad \text{in } \Omega, \\ w = 0, \quad \text{on } \mathbb{R}^N \backslash \Omega. \end{cases}$$

It is easy to state that the problem (Q_δ) corresponds to the case when $M(t) = t^{\nu-1}$, which clearly satisfies hypothesis (N_1). On the other hand, the operator $(-\Delta_{p(.,.)})$ corresponds to the case when

$$\mathbf{K}(\xi, \eta) = \frac{1}{|\xi - \eta|^{N+sq(\xi,\eta)}}.$$

It is not difficult to prove that the last kernel satisfies conditions $(B1)$–$(B3)$. Also, problem (Q_δ) corresponds to the case

$$f(t, \xi) = a(\xi)|\xi|^{\alpha(\xi)-2}\xi,$$

with $a \in L^{B(.)}(\Omega)$. So, clearly, f satisfies condition (H_2) and the first part of condition (H_1). Assume further that α satisfies the second part of condition (N_1). Finally, if ν and p satisfy condition (N_1) and Equations (1)–(3), and, if the function h satisfies hypothesis (N_2), then Theorem 1 can be applied, ensuring that the problem (Q_δ) admits a non-trivial solution.

5. Conclusions

In this paper, we studied a singular elliptic problem of Kirchhoff type. We transformed the study from that of the existence of a weak solution to the question of the existence of extremum points of the associated functional energy. Therefore, we have proven some properties of this functional and that it reached its global minimum at a point in an appropriate function space. To prove that this point is a weak solution for the studied problem, we have used the implicit function theorem; this is due to the singular term. We note that in some special cases of the kernel $L^p_{\mathbf{K}}$ and the Kirchhoff function M, we obtained the same results as those in the literature. We hope to generalize this study to problems involving the $p(x, y)$-Laplacian operator.

Funding: This project was funded by the Deanship of Scientific Research (DSR) at King Abdulaziz University, Jeddah, under grant no. (GPIP: 1372-130-2024).

Data Availability Statement: No new data were created or analyzed in this study. Data sharing is not applicable to this article.

Acknowledgments: The authors acknowledge with thanks the DSR for technical and financial support.

Conflicts of Interest: The author declares no conflicts of interest.

References

1. Bahrouni, A. Comparison and sub-supersolution principles for the fractional $p(x)$- Laplacian. *J. Math. Anal. App.* **2018**, *458*, 1363–1372. [CrossRef]
2. Bahrouni, S.; Ounaies, H. Strauss and Lions-type theorems for the fractional Sobolev spaces with variable exponent and applications to non-local Kirchhoff-Choquard problem. *Mediterr. J. Math.* **2021**, *18*, 1–22. [CrossRef]
3. Bahrouni, A.; Radulescu, V.D. On a New Fractional Sobolev Space and Application to Non-local Variational Problems With Variable Exponent. *Discrete Contin. Dyn. Syst. S.* **2018**, *11*, 379–389.
4. Chammem, R.; Ghanmi, A.; Sahbani, A. Existence of solution for a singular fractional Laplacian problem with variable exponents and indefinite weights. *Complex Var. Ellip. Equ.* **2021**, *66*, 1320–1332. [CrossRef]
5. Ruzicka, M. Electrorheological Fluids: Modeling and Mathematical Theory. In *Lecture Notes in Mathematics*; Springer: Berlin/Heidelberg, Germany, 2000.
6. Avci, M. Existence of weak solutions for a non-local problem involving the $p(x)$-Laplace operator. *J. App. Math.* **2013**, *3*, 192–197.
7. Ayazoglu, R.; Akbulut, S.; Akkoyunlu, E. Existence and multiplicity of solutions for $p(.)$-Kirchhoff-type equations. *Turk. J. Math.* **2022**, *46*, 1342–1359. [CrossRef]
8. Azroul, E.; Benkirane, E.; Shimi, M.; Srati, M. On a class of fractional $p(x)$-Kirchhoff type. *Appl. Anal.* **2021**, *100*, 383–402. [CrossRef]

9. Ben Ali, K.; Bezzarga, M.; Ghanmi, A.; Kefi, K. Existence of Positive Solution for Kirchhoff Problems. *Complex Anal. Oper. Theory* **2019**, *13*, 115–126.
10. Binlin, Z.; Fiscella, A.; Liang, S. Infinitely many solutions for critical degenerate Kirchhoff type equations involving the fractional p-Laplacian. *Appl. Math. Optim.* **2019**, *80*, 63–80. [CrossRef]
11. Fareh, S.; Akrout, K.; Ghanmi, A.; Repovš, D.D. Multiplicity results for fractional Schrödinger-Kirchhoff systems involving critical nonlinearities. *Adv. Nonlinear Anal.* **2023**, *12*, 20220318. [CrossRef]
12. Fiscella, A.; Pucci, P. p-fractional Kirchhoff equations involving critical nonlinearities. *Nonlinear Anal. Real World Appl.* **2017**, *35*, 350–378. [CrossRef]
13. Hamdani, M.K.; Zuo, J.; Chung, N.T.; Repovs, D.D. Multiplicity of solutions for a class of fractional $p(.)$-Kirchhoff-type problems without the Ambrosetti-Rabinowitz condition. *Bound Value Probl.* **2020**, *150*, 1–16. [CrossRef]
14. Kirchhoff, G. *Vorlesungen Uber Mathematische Physik*; Teubner: Stuttgart, Germany, 1891.
15. Saoudi, K.; Ghanmi, A. A multiplicity results for a singular equation involving the $p(x)$-Laplace operator. *Complex Var. Elliptic Equ.* **2017** *62*, 695–725. [CrossRef]
16. Wang, L.; Zhang, B. Infinitely many solutions for Kirchhoff-type variable-order fractional Laplacian problems involving variable exponents. *Appl. Anal.* **2021**, *100*, 2418–2435. [CrossRef]
17. Zhang, J. Existence results for a Kirchhoff-type equations involving the fractional $p_1(x)$-$p_2(\xi)$-Laplace operator. *Collect. Math.* **2021**, *2*, 271–293.
18. Ben Ali, K.; Ghanmi, A.; Kefi, K. Min-max method involving singular $p(x)$-Kirchhoff equation. *J. Math. Physics.* **2017**, *58*, 111505. [CrossRef]
19. Chammem, R.; Ghanmi, A.; Mechergui, M. Existence of Solutions for a Singular Double Phase Kirchhoff Type Problems Involving the Fractional $q(x,.)$-Laplacian Operator. *Complex Anal. Oper. Theory* **2024**, *18*, 1–21. [CrossRef]
20. Ghanmi, A.; Saoudi, K. A multiplicity results for a singular problem involving the fractional p-Laplacian operator. *Complex Var. Elliptic Equ.* **2016**, *61*, 1199–1216. [CrossRef]
21. Ghergu, M.; Radulescu, V.D. Singular elliptic problems: Bifurcation and asymptotic analysis. *Oxford Lecture Series in Mathematics and Its Applications*; The Clarendon Press, Oxford University Press: Oxford, UK, 2008; Volume 37.
22. Coclite, M.M.; Palmieri, G. On a singular nonlinear Dirichlet problem. *Comm. Partial Differ. Equ.* **1989**, *14*, 1315–1327. [CrossRef]
23. Crandall, M.G.; Rabinowitz, P.H.; Tartar, L. On a Dirichlet problem with a singular nonlinearity. *Comm. Partial Differ. Equ.* **1977**, *2*, 193–222. [CrossRef]
24. Ben Ali, K.; Hsini, M.; Kefi, K.; Chung, T. On a Non-local Fractional $p(.,.)$-Laplacian Problem with Competing Nonlinearities. *Complex Anal. Oper. Theory* **2019**, *13*, 1377–1399.
25. Azroul, E.; Benkirane, E.; Shimi, M. General fractional Sobolev space with variable exponent and applications to non-local problems. *Adv. Oper. Theory* **2020**, *5*, 1512–1540. [CrossRef]
26. Del Pezzoc, L.M.; Rossi, J.D. Traces for fractional Sobolev spaces with variable exponents. *Adv. Oper. Throry* **2017**, *2*, 435–446.
27. Fan, X.; Zhao, D. On the spaces $L^p(\Omega)$ and $W^{m,p(\xi)}(\Omega)$. *J. Math. Anal. Appl.* **2001**, *263*, 424–446. [CrossRef]
28. Kaufmann, U.; Rossi, J.D.; Vidal, R. Fractional Sobolev spaces with variable exponents and fractional $p(x)$-Laplacian. *Electron. J. Qual. Theory Differ. Equ.* **2017**, *76*, 1–10. [CrossRef]
29. Repovš, D.D.; Saoudi, K. The Nehari manifold approach for singular equations involving the $p(x)$-Laplace operator. *Complex Var. Elliptic Equ.* **2021**, *68*, 135–149. [CrossRef]

Disclaimer/Publisher's Note: The statements, opinions and data contained in all publications are solely those of the individual author(s) and contributor(s) and not of MDPI and/or the editor(s). MDPI and/or the editor(s) disclaim responsibility for any injury to people or property resulting from any ideas, methods, instructions or products referred to in the content.

mathematics

MDPI

Article

Linearly Implicit Conservative Schemes for the Nonlocal Schrödinger Equation

Yutong Zhang [1], Bin Li [2,*] and Mingfa Fei [3]

[1] Applied Mathematics and Computational Science, School of Arts and Sciences, University of Pennsylvania, Philadelphia, PA 19104, USA
[2] School of Science, Xuchang University, Xuchang 461000, China
[3] School of Mathematics, Changsha University, Changsha 410073, China
* Correspondence: 12016072@xcu.edu.cn

Abstract: This paper introduces two high-accuracy linearly implicit conservative schemes for solving the nonlocal Schrödinger equation, employing the extrapolation technique. These schemes are based on the generalized scalar auxiliary variable approach and the symplectic Runge–Kutta method. By integrating these advanced methods, the proposed schemes aim to significantly enhance computational accuracy and efficiency, while maintaining the essential conservative properties necessary for accurate physical modeling. This offers a structured approach to handle auxiliary variables, ensuring stability and conservation, while the symplectic Runge–Kutta method provides a robust framework with high accuracy. Together, these techniques offer a powerful and reliable approach for researchers dealing with complex quantum mechanical systems described by the nonlocal Schrödinger equation, ensuring both accuracy and stability in their numerical simulations.

Keywords: nonlocal Schrödinger equation; energy-preserving schemes; extrapolation technique; symplectic Runge–Kutta method

MSC: 35R11; 65M70

1. Introduction

The nonlocal nonlinear Schrödinger (NLS) equation is a fundamental equation in quantum mechanics that extends the classical Schrödinger equation by incorporating nonlocal interactions. This modification allows for a more accurate representation of systems where the interactions cannot be adequately described by the local potentials alone. Nonlocal interactions are crucial in various physical contexts, such as in the study of quantum fluids [1], Bose–Einstein condensates [2], and in modeling long-range interactions in condensed matter physics [3]. In this paper, we consider the following nonlocal NLS equation [4]:

$$\mathrm{i}\frac{\partial u(\boldsymbol{x},t)}{\partial t} - (-\mathcal{L})^{\gamma}u(\boldsymbol{x},t) + \beta|u(\boldsymbol{x},t)|^2u(\boldsymbol{x},t) = 0, \quad \boldsymbol{x}\in\Omega\subset\mathbb{R}^2, \quad t\in(0,T], \tag{1}$$

with the initial condition

$$u(\boldsymbol{x},0) = u_0(\boldsymbol{x}), \quad \boldsymbol{x}\in\Omega,$$

where $\mathrm{i}^2 = -1$, $0 < \gamma \leq 1$, and consider the domain $\Omega := [-L,L]\times[-L,L]$. The function $u(\boldsymbol{x},t)$ represents a complex-valued wave function with period $2L$, and $u_0(\boldsymbol{x})$ is a prescribed smooth function. The constant β is a positive real number associated with focusing nonlinearity. Within a finite computational domain, the fractional Laplacian operator can be defined as [5]

$$\mathcal{L}^{\gamma}\varphi(\boldsymbol{x},t) = -\sum_{k_1\in\mathbb{Z}}\sum_{k_2\in\mathbb{Z}} |\nu_{k_1}^2+\nu_{k_2}^2|^{\frac{\gamma}{2}}\hat{\boldsymbol{\gamma}}_{\mathbf{k}}e^{\mathrm{i}\boldsymbol{\nu}_{\mathbf{k}}\cdot(\boldsymbol{x}+\boldsymbol{L})},$$

where $\nu_{k_i} = \frac{k_i\pi}{L}$ $(i=1,2)$, $\boldsymbol{\nu}_{\mathbf{k}}\cdot(\boldsymbol{x}+\boldsymbol{L}) := \sum_{i=1}^{2}\nu_{k_i}(x_i+L)$, $\hat{\boldsymbol{\gamma}}_{\mathbf{k}} = \frac{1}{(2L)^2}\int_{\Omega}\varphi(\boldsymbol{x},t)e^{-\mathrm{i}\boldsymbol{\nu}_{k}\cdot(\boldsymbol{x}+\boldsymbol{L})}d\boldsymbol{x}$.

Recently, scholars have developed many methods to obtain analytic solutions for partial differential equations, such as the Adomian decomposition method [6], the Lie symmetry approach [7], and the variational iteration method [8]. However, the analytic solution of nonlocal differential equations is generally difficult or impossible to obtain, due to the non-locality of the nonlocal operators. As a result, many numerical methods have been developed for solving nonlocal NLS equations, such as spectral methods [9], finite element methods [10], and finite difference methods [11]. These numerical approaches are essential for studying the behavior of solutions, especially in cases where traditional analytical techniques fail to provide explicit solutions, thereby enabling researchers to explore the complex dynamics of fractional differential systems.

By setting $u = p + \mathrm{i}q$, System (1) can be transformed into a pair of real-valued equations,

$$p_t = (-\mathcal{L})^{\gamma}q - \beta(p^2+q^2)q, \tag{2}$$

$$q_t = -(-\mathcal{L})^{\gamma}p + \beta(p^2+q^2)p. \tag{3}$$

We can easily demonstrate that the above system possesses a nonlocal energy conservation law under appropriate boundary conditions, which are given by

$$\mathcal{H}(p,q) = \frac{1}{2}\int_{\Omega}\Big[((-\mathcal{L})^{\gamma}p)^2 + ((-\mathcal{L})^{\gamma}q)^2\Big]d\boldsymbol{x} - \frac{\beta}{4}\int_{\Omega}(p^2+q^2)^2d\boldsymbol{x}, \tag{4}$$

where $\mathcal{H}$ represents the energy function. Utilizing the variational derivative formula with nonlocal operator [12], Systems (2) and (3) can be reformulated as an infinite-dimensional Hamiltonian system,

$$\frac{d\boldsymbol{z}}{dt} = J^{-1}\frac{\delta\mathcal{H}}{\delta\boldsymbol{z}}, \quad \text{with} \quad \boldsymbol{z} = (p,q)^T, \quad J = \begin{pmatrix} 0 & 1 \\ -1 & 0 \end{pmatrix},$$

and this representation highlights the Hamiltonian structure underlying the nonlocal system.

Structure-preserving algorithms have achieved significant success in the numerical analysis of classical differential equations, inspiring the development of similar approaches for nonlocal differential equations [13–15]. Many researchers are focused on designing numerical methods that preserve the energy of nonlocal NLS equations, especially in long-time simulations. For instance, Xiao developed an energy-preserving difference scheme for equations with nonlocal derivatives [11]. Li et al. proposed a fast finite element method that maintains the energy and mass conservation of the problem [10]. There is extensive related research in this field, and readers are encouraged to consult relevant review articles for more information [16–18]. However, many energy-preserving schemes for the nonlocal NLS equation are fully implicit, resulting in high computational costs. To address this, some researchers have recently developed linearly implicit energy-preserving schemes to reduce complexity. However, the resulting schemes have only second-accuracy in time, and exhibit poor accuracy, particularly when modeling complex physical phenomena or capturing fine details in the solution.

Over the past decade, various numerical methods have been developed to achieve high-accuracy conservative schemes for conservative systems [19,20]. However, these methods are typically fully implicit, requiring the solution of nonlinear equations at each time step, which substantially increases computational cost, particularly in large-scale

simulations. Linearly implicit schemes, on the other hand, provide a computationally efficient alternative to fully implicit methods. They offer a good balance between accuracy and computational efficiency, making them more suitable for large-scale simulations on modern computing platforms. Consequently, there is a growing interest in developing and analyzing high-accuracy linearly implicit conservative numerical schemes specifically tailored for the nonlocal NLS equation. The symplectic Runge–Kutta method is renowned for maintaining the energy and geometric properties of Hamiltonian systems, ensuring both long-term stability and accuracy in numerical simulations [21]. These strengths form a foundation for designing high-accuracy conservation schemes. This paper aims to utilize the generalized scalar auxiliary variable (GSAV) method [22] combined with the Runge–Kutta approach to develop high-accuracy, linearly implicit conservative schemes for the nonlocal NLS equation. The main goals are: (I) to develop linearly implicit high-order schemes capable of efficiently obtaining numerical solutions, and (II) to ensure the schemes conserve the system's energy, enhancing stability in simulations. Overall, the objective is to design a numerical method that achieves a balance between accuracy and computational efficiency, making it well-suited for large-scale simulations while preserving the intrinsic energy properties of the system. However, the convergence analysis of these proposed schemes has not been covered, and remains a subject for future research.

2. Semi-Discrete Conservative System

First, we derive a semi-discrete conservative system for the nonlocal NLS equation by using the Fourier pseudo-spectral method in the space direction.

2.1. Structure-Preserving Spatial Discretization

Let N_x, N_y, and N be positive even integers. Define the spatial step sizes $h_x = \frac{2L}{N_x}$ and $h_y = \frac{2L}{N_y}$, and set the time step $\tau = \frac{T}{N}$. The spatial grid points are

$$\Omega_h = \left\{ (x_i, y_j) \,\middle|\, x_i = -L + ih_x, \quad y_j = -L + jh_y, \quad 0 \le i \le N_x - 1, \quad 0 \le j \le N_y - 1 \right\}.$$

Define the vector space of grid functions on Ω_h as

$$\mathcal{V}_h = \{ \boldsymbol{v} | \boldsymbol{v} = (v_{0,0}, \cdots, v_{N_x-1,0}, v_{0,1}, \cdots, v_{N_x-1,1}, \cdots, v_{0,N_y-1}, \cdots, v_{N_x-1,N_y-1})^T \}.$$

For any $\boldsymbol{u}, \boldsymbol{v} \in \mathcal{V}_h$, the discrete inner product and norms are defined by

$$\langle \boldsymbol{u}, \boldsymbol{v} \rangle_h = h_x h_y \sum_{i=0}^{N_x-1} \sum_{j=0}^{N_y-1} u_{i,j} \overline{v}_{i,j}, \quad \|\boldsymbol{u}\| = \sqrt{\langle \boldsymbol{u}, \boldsymbol{u} \rangle_h}, \quad \|\boldsymbol{u}\|_\infty = \max_{(x_i, y_j) \in \Omega_h} |u_{i,j}|,$$

where $\overline{v}_{i,j}$ denotes the complex conjugate of $v_{i,j}$.

Let $(x_i, y_j) \in \Omega_h$ be the Fourier collocation points. Using the interpolation polynomial $I_{\mathbf{N}} p(x, y)$ to approximate $p_{\mathbf{N}}(x, y)$ of the function $p(x, y)$, which is defined by

$$I_{\mathbf{N}} p(x, y) = p_{\mathbf{N}}(x, y) = \sum_{k_1 = -N_x/2}^{N_x/2} \sum_{k_2 = -N_y/2}^{N_y/2} \tilde{p}_{k_1,k_2} \, e^{ik_1 \mu (x+L)} e^{ik_2 \mu (y+L)},$$

where $\mu = \dfrac{\pi}{L}$, the coefficients $\tilde{p}_{k_1,k_2}$ are given by

$$\tilde{p}_{k_1,k_2} = \frac{1}{N_x c_{k_1}} \frac{1}{N_y c_{k_2}} \sum_{i=0}^{N_x-1} \sum_{j=0}^{N_y-1} p(x_i, y_j) \, e^{-ik_1 \mu (x_i+L)} e^{-ik_2 \mu (y_j+L)},$$

with

$$c_{k_1} = \begin{cases} 1, & \text{if } |k_1| < N_x/2, \\ 2, & \text{if } k_1 = \pm N_x/2, \end{cases} \quad c_{k_2} = \begin{cases} 1, & \text{if } |k_2| < N_y/2, \\ 2, & \text{if } k_2 = \pm N_y/2. \end{cases}$$

Then, the nonlocal Laplacian $-(-\mathcal{L})^{\gamma} p(x,y)$ can be approximated by

$$-(-\mathcal{L})^{\gamma} p_{\mathbf{N}}(x_i, y_j) = -\sum_{\mathbf{k}=-\mathbf{N}/2}^{\mathbf{N}/2} |\mu^2 k_1^2 + \mu^2 k_2^2|^{\gamma}\, \tilde{p}_{k_1,k_2}\, e^{-i\mu \mathbf{k}\cdot(\mathbf{x}+\mathbf{L})},$$

where $\sum_{\mathbf{k}=-\mathbf{N}/2}^{\mathbf{N}/2} = \sum_{k_1=-N_x/2}^{N_x/2} \sum_{k_2=-N_y/2}^{N_y/2}$ and $\mathbf{k}\cdot(\mathbf{x}+\mathbf{L}) = k_1(x+L) + k_2(y+L)$.

We denote $\mu^2\mathbf{k}^2 = \mu^2(k_1^2 + k_2^2)$ and substitute $\tilde{p}_{k_1,k_2}$ into the equation above. The nonlocal Laplacian $-(-\mathcal{L})^{\gamma}$ can be approximated in matrix form [12],

$$-(-\mathcal{L})^{\gamma} p_{\mathbf{N}}(x_i, y_j) = (D^{\gamma}\mathbf{p})_{i+jN_x},$$

where the spectral differentiation matrix D^{γ} is symmetric with elements

$$(D^{\gamma})_{i+jN_x, l+mN_x} = -\sum_{\mathbf{k}=-\mathbf{N}/2}^{\mathbf{N}/2} \frac{1}{N_x c_{k_1}} \frac{1}{N_y c_{k_2}} |\mu^2\mathbf{k}^2|^{\gamma}\, e^{-i\mu\left[k_1(x_i - x_l) + k_2(y_j - y_m)\right]}.$$

2.2. Semi-Discrete System

By applying the Fourier pseudo-spectral method to the real-valued Equations (2) and (3), we obtain the following semi-discrete system:

$$\boldsymbol{p}_t = -D^{\gamma}\boldsymbol{q} - \beta(\boldsymbol{p}^2 + \boldsymbol{q}^2)\boldsymbol{q}, \tag{5}$$

$$\boldsymbol{q}_t = D^{\gamma}\boldsymbol{p} + \beta(\boldsymbol{p}^2 + \boldsymbol{q}^2)\boldsymbol{p}. \tag{6}$$

Theorem 1. *The proposed Schemes,* (5) *and* (6)*, can preserve the following semi-discrete energy:*

$$\frac{d}{dt}\mathcal{E}(t) = 0, \tag{7}$$

where

$$\mathcal{E}(t) = (\langle \boldsymbol{p}, D^{\gamma}\boldsymbol{p}\rangle_h + \langle \boldsymbol{q}, D^{\gamma}\boldsymbol{q}\rangle_h) + \frac{\beta}{2}\langle \boldsymbol{p}^2 + \boldsymbol{q}^2, \boldsymbol{p}^2 + \boldsymbol{q}^2\rangle_h, \tag{8}$$

where $\langle\cdot,\cdot\rangle_h$ *denotes the discrete inner product.*

Proof. Computing $\frac{d}{dt}\mathcal{E}(t)$, we can derive

$$\frac{d}{dt}\mathcal{E}(t) = 2\left\langle \frac{d}{dt}\boldsymbol{p}, D^{\gamma}\boldsymbol{p}\right\rangle_h + 2\left\langle \frac{d}{dt}\boldsymbol{q}, D^{\gamma}\boldsymbol{q}\right\rangle_h + \beta\left\langle \boldsymbol{p}^2 + \boldsymbol{q}^2, \frac{d}{dt}(\boldsymbol{p}^2 + \boldsymbol{q}^2)\right\rangle_h. \tag{9}$$

Calculating the time derivative for $\frac{d}{dt}(\boldsymbol{p}^2 + \boldsymbol{q}^2)$, we can obtain

$$\frac{d}{dt}(\boldsymbol{p}^2 + \boldsymbol{q}^2) = 2(\boldsymbol{p}\boldsymbol{p}_t + \boldsymbol{q}\boldsymbol{q}_t). \tag{10}$$

Substituting this into Equation (9), we can obtain

$$\frac{d}{dt}\mathcal{E}(t) = 2\langle \boldsymbol{p}_t, D^{\gamma}\boldsymbol{p}\rangle_h + 2\langle \boldsymbol{q}_t, D^{\gamma}\boldsymbol{q}\rangle_h + 2\beta\left\langle \boldsymbol{p}^2 + \boldsymbol{q}^2, \boldsymbol{p}\boldsymbol{p}_t + \boldsymbol{q}\boldsymbol{q}_t\right\rangle_h. \tag{11}$$

From Equations (5) and (6), we have

$$\frac{d}{dt}\mathcal{E}(t) = 2\Big\langle -D^\gamma \boldsymbol{q} - \beta(\boldsymbol{p}^2+\boldsymbol{q}^2)\boldsymbol{q}, D^\gamma \boldsymbol{p}\Big\rangle_h + 2\Big\langle D^\gamma \boldsymbol{p} + \beta(\boldsymbol{p}^2+\boldsymbol{q}^2)\boldsymbol{p}, D^\gamma \boldsymbol{q}\Big\rangle_h + 2\beta\Big\langle \boldsymbol{p}^2+\boldsymbol{q}^2, \boldsymbol{p}\Big(-D^\gamma \boldsymbol{q} - \beta(\boldsymbol{p}^2+\boldsymbol{q}^2)\boldsymbol{q}\Big) + \boldsymbol{q}\Big(D^\gamma \boldsymbol{p} + \beta(\boldsymbol{p}^2+\boldsymbol{q}^2)\boldsymbol{p}\Big)\Big\rangle_h. \tag{12}$$

Noting that

$$2\langle -D^\gamma \boldsymbol{q}, D^\gamma \boldsymbol{p}\rangle_h + 2\langle D^\gamma \boldsymbol{p}, D^\gamma \boldsymbol{q}\rangle_h = -2\langle D^\gamma \boldsymbol{q}, D^\gamma \boldsymbol{p}\rangle_h + 2\langle D^\gamma \boldsymbol{p}, D^\gamma \boldsymbol{q}\rangle_h = 0. \tag{13}$$

and

$$\begin{aligned} &2\beta^2\Big\langle \boldsymbol{p}^2+\boldsymbol{q}^2, -\boldsymbol{p}(\boldsymbol{p}^2+\boldsymbol{q}^2)\boldsymbol{q} + \boldsymbol{q}(\boldsymbol{p}^2+\boldsymbol{q}^2)\boldsymbol{p}\Big\rangle_h \\ &= 2\beta^2\Big\langle \boldsymbol{p}^2+\boldsymbol{q}^2, -\boldsymbol{p}(\boldsymbol{p}^2+\boldsymbol{q}^2)\boldsymbol{q} + \boldsymbol{q}(\boldsymbol{p}^2+\boldsymbol{q}^2)\boldsymbol{p}\Big\rangle_h = 0. \end{aligned} \tag{14}$$

After simplification, all terms sum to zero, namely

$$\frac{d}{dt}\mathcal{E}(t) = 0, \tag{15}$$

which implies that the discrete energy $\mathcal{E}(t)$ is conserved over time, i.e., $\mathcal{E}(t) = \mathcal{E}(0)$ for all $t \geq 0$. Therefore, the semi-discrete Systems (5) and (6) satisfy the energy conservation law. □

3. Equivalent System with ESAV Approach

Following the idea of the GSAV approach, we aim to apply an equivalent transformation to the real-valued Equations (5) and (6). We introduce an auxiliary variable $r(t)$ as follows:

$$r(t) = \mathcal{G}(\boldsymbol{p}, \boldsymbol{q}) := \mathcal{G}\Big(\langle \boldsymbol{p}^2+\boldsymbol{q}^2, \boldsymbol{p}^2+\boldsymbol{q}^2\rangle_h\Big), \tag{16}$$

where $\mathcal{G}$ is an invertible function. The discrete energy functional can be rewritten using the auxiliary variable $r(t)$ as

$$E(t) = \langle \boldsymbol{p}, D^\gamma \boldsymbol{p}\rangle_h + \langle \boldsymbol{q}, D^\gamma \boldsymbol{q}\rangle_h + \frac{\beta}{2}\mathcal{G}^{-1}(r). \tag{17}$$

We can express the nonlinear terms in the system using $r(t)$,

$$(\boldsymbol{p}^2+\boldsymbol{q}^2)\boldsymbol{q} = \frac{r}{\mathcal{G}(\boldsymbol{p},\boldsymbol{q})}(\boldsymbol{p}^2+\boldsymbol{q}^2)\boldsymbol{q}, \tag{18}$$

$$(\boldsymbol{p}^2+\boldsymbol{q}^2)\boldsymbol{p} = \frac{r}{\mathcal{G}(\boldsymbol{p},\boldsymbol{q})}(\boldsymbol{p}^2+\boldsymbol{q}^2)\boldsymbol{p}. \tag{19}$$

Differentiating $r(t)$ with respect to time t, we obtain

$$\frac{dr}{dt} = 4\mathcal{G}'\Big(\langle \boldsymbol{p}^2+\boldsymbol{q}^2, \boldsymbol{p}^2+\boldsymbol{q}^2\rangle_h\Big)\Big\langle \boldsymbol{p}^2+\boldsymbol{q}^2, \boldsymbol{p}\boldsymbol{p}_t + \boldsymbol{q}\boldsymbol{q}_t\Big\rangle_h, \tag{20}$$

where $\mathcal{G}'$ denotes the derivative of $\mathcal{G}$ with respect to its argument. From the property of $\mathcal{G}$, we have

$$\Big(\mathcal{G}^{-1}\Big)'(r) = \frac{1}{\mathcal{G}'(\langle \boldsymbol{p}^2+\boldsymbol{q}^2, \boldsymbol{p}^2+\boldsymbol{q}^2\rangle_h)}. \tag{21}$$

We reformulate Systems (5) and (6) as

$$\boldsymbol{p}_t = -D^\gamma \boldsymbol{q} - \beta A^{\boldsymbol{p},\boldsymbol{q}}, \tag{22}$$

$$\boldsymbol{q}_t = \quad D^\gamma \boldsymbol{p} + \beta B^{\boldsymbol{p},\boldsymbol{q}}, \tag{23}$$

$$\frac{d}{dt}\mathcal{G}^{-1}(r) = 4\langle A^{\boldsymbol{p},\boldsymbol{q}}, \boldsymbol{q}_t\rangle_h + 4\langle B^{\boldsymbol{p},\boldsymbol{q}}, \boldsymbol{p}_t\rangle_h, \tag{24}$$

where

$$A^{\boldsymbol{p},\boldsymbol{q}} = \frac{r}{\mathcal{G}(\boldsymbol{p},\boldsymbol{q})}(\boldsymbol{p}^2 + \boldsymbol{q}^2)\boldsymbol{q}, \tag{25}$$

$$B^{\boldsymbol{p},\boldsymbol{q}} = \frac{r}{\mathcal{G}(\boldsymbol{p},\boldsymbol{q})}(\boldsymbol{p}^2 + \boldsymbol{q}^2)\boldsymbol{p}. \tag{26}$$

The initial conditions for the transformed system are

$$\boldsymbol{p}(0) = \boldsymbol{p}_0, \quad \boldsymbol{q}(0) = \boldsymbol{q}_0, \quad r(0) = \mathcal{G}(\boldsymbol{p}_0, \boldsymbol{q}_0), \tag{27}$$

where $\boldsymbol{p}_0$ and $\boldsymbol{q}_0$ are the initial values of $\boldsymbol{p}$ and $\boldsymbol{q}$, respectively.

Remark 1. *By choosing different functions for $\mathcal{G}(x)$, we can derive various Scalar Auxiliary Variable (SAV) approaches, as discussed in [22]. For instance, setting $\mathcal{G}(x) = \tanh\left(\frac{x}{\mathbf{C}}\right)$ or $\mathcal{G}(x) = \exp\left(\frac{x}{\mathbf{C}}\right)$ with $\mathbf{C} > 0$ allows us to construct new numerical schemes. Notably, if we choose $\mathcal{G}(x) = \sqrt{x + \mathbf{C}}$, the GSAV approach becomes equivalent to the traditional SAV method presented in [23–25].*

Theorem 2. *Under the periodic boundary condition, Systems* (22)–(24) *possess the following modified energy conservation law:*

$$\frac{d}{dt}E(t) = 0, \tag{28}$$

where $E(t)$ is given by (17).

Proof. Computing the time derivative of $E(t)$, we can derive

$$\frac{d}{dt}E(t) = 2\langle \boldsymbol{p}_t, D^\gamma \boldsymbol{p}\rangle_h + 2\langle \boldsymbol{q}_t, D^\gamma \boldsymbol{q}\rangle_h + \frac{\beta}{2}\frac{d}{dt}\mathcal{G}^{-1}(r). \tag{29}$$

Substituting $\boldsymbol{p}_t$ and $\boldsymbol{q}_t$ from Equations (22) and (23), we obtain

$$\begin{aligned}\frac{d}{dt}E(t) &= 2\Big(\langle -D^\gamma \boldsymbol{q} - \beta A^{\boldsymbol{p},\boldsymbol{q}},\ D^\gamma \boldsymbol{p}\rangle_h + \langle D^\gamma \boldsymbol{p} + \beta B^{\boldsymbol{p},\boldsymbol{q}},\ D^\gamma \boldsymbol{q}\rangle_h\Big) - \frac{\beta}{2}\frac{d}{dt}\mathcal{G}^{-1}(r)\\ &= 2\Big(-\langle D^\gamma \boldsymbol{q},\ D^\gamma \boldsymbol{p}\rangle_h - \beta\langle A^{\boldsymbol{p},\boldsymbol{q}},\ D^\gamma \boldsymbol{p}\rangle_h\Big)\\ &\quad + 2\Big(\langle D^\gamma \boldsymbol{p},\ D^\gamma \boldsymbol{q}\rangle_h + \beta\langle B^{\boldsymbol{p},\boldsymbol{q}},\ D^\gamma \boldsymbol{q}\rangle_h\Big) + \frac{\beta}{2}\frac{d}{dt}\mathcal{G}^{-1}(r).\end{aligned} \tag{30}$$

Noting that

$$-\langle D^\gamma \boldsymbol{q},\ D^\gamma \boldsymbol{p}\rangle_h + \langle D^\gamma \boldsymbol{p},\ D^\gamma \boldsymbol{q}\rangle_h = 0.$$

Therefore,

$$\frac{d}{dt}E(t) = -2\beta\langle A^{\boldsymbol{p},\boldsymbol{q}},\ D^\gamma \boldsymbol{p}\rangle_h + 2\beta\langle B^{\boldsymbol{p},\boldsymbol{q}},\ D^\gamma \boldsymbol{q}\rangle_h + \frac{\beta}{2}\frac{d}{dt}\mathcal{G}^{-1}(r). \tag{31}$$

From Equation (24), we have

$$4(\langle A^{p,q},\ D^{\gamma}\boldsymbol{p}\rangle_h - \langle D^{\gamma}\boldsymbol{q},\ B^{p,q}\rangle_h) = \frac{d}{dt}\mathcal{G}^{-1}(r). \tag{32}$$

Substituting (32) into (31), we obtain

$$\begin{aligned}\frac{d}{dt}E(t) &= -2\beta\left(\frac{1}{4}\frac{d}{dt}\mathcal{G}^{-1}(r)\right) + \frac{\beta}{2}\frac{d}{dt}\mathcal{G}^{-1}(r)\\ &= -\frac{\beta}{2}\frac{d}{dt}\mathcal{G}^{-1}(r) + \frac{\beta}{2}\frac{d}{dt}\mathcal{G}^{-1}(r)\\ &= 0.\end{aligned} \tag{33}$$

We complete the proof. □

4. Linearly Implicit Energy-Preserving Schemes

In this section, we introduce a family of high-order fully discrete conservative schemes for approximating Systems (22)–(24) by employing symplectic Runge–Kutta methods combined with extrapolation techniques. To begin, we present essential notations related to symplectic Runge–Kutta methods (Table 1).

Table 1. Coefficients of symplectic RK methods of order 4 (top) and 6 (bottom).

$\frac{1}{2}-\frac{\sqrt{3}}{6}$	$\frac{1}{4}$	$\frac{1}{4}-\frac{\sqrt{3}}{6}$	
$\frac{1}{2}+\frac{\sqrt{3}}{6}$	$\frac{1}{4}+\frac{\sqrt{3}}{6}$	$\frac{1}{4}$	
	$\frac{1}{2}$	$\frac{1}{2}$	
$\frac{1}{2}-\frac{\sqrt{15}}{10}$	$\frac{5}{36}$	$\frac{2}{9}-\frac{\sqrt{15}}{15}$	$\frac{5}{36}-\frac{\sqrt{15}}{30}$
$\frac{1}{2}$	$\frac{5}{36}+\frac{\sqrt{15}}{24}$	$\frac{2}{9}$	$\frac{5}{36}-\frac{\sqrt{15}}{24}$
$\frac{1}{2}+\frac{\sqrt{15}}{10}$	$\frac{5}{36}+\frac{\sqrt{15}}{30}$	$\frac{2}{9}+\frac{\sqrt{15}}{15}$	$\frac{5}{36}$
	$\frac{5}{18}$	$\frac{4}{9}$	$\frac{5}{18}$

4.1. Symplectic RK Methods

We consider the ordinary differential equation

$$\frac{dw(t)}{dt} = f(t), \quad w(t_0) = w_0. \tag{34}$$

Let τ be the time step size, and define $t_n = n\tau$ for $n = 0, 1, \ldots, N$. Let a_{ij}, b_i, and $c_i = \sum_{j=1}^{s} a_{ij}$ be real numbers. Over the interval $[t_n, t_{n+1}]$, the s-stage Runge–Kutta (RK) method for solving Equation (34) is given by [21]

$$w_i = w^n + \tau\sum_{j=1}^{s} a_{ij}k_j, \quad k_i = f(t_n + c_i\tau), \quad i = 1, 2, \ldots, s, \tag{35}$$

$$w^{n+1} = w^n + \tau\sum_{i=1}^{s} b_i k_i. \tag{36}$$

If the coefficients satisfy, for $i, j = 1, 2, \ldots, s$,

$$a_{ij}b_i + a_{ji}b_j = b_i b_j, \tag{37}$$

then the RK method is symplectic, and preserves the quadratic invariants for conservative systems. We refer to Equation (37) as the condition for RK symplecticity.

Without loss of generality, we choose the $2s$-stage fourth- and sixth-order symplectic RK methods, which are provided by the Butcher tableau [21].

4.2. Construction of the Linearly Implicit Schemes

To reduce the computational complexity associated with fully implicit schemes that require nonlinear iterations during numerical simulations, this subsection uses extrapolation methods to construct linearly implicit conservative schemes, thereby improving computational efficiency. Let $t_{ni} = t_n + c_i\tau$ for $i = 1, 2, \ldots, s$ and $n = 0, 1, 2, \ldots$, where $c_1, c_2, \ldots, c_s$ are distinct real numbers, typically within $[0, 1]$. We denote the approximations of $u(x,t)$ at times t_n and t_{ni} by $\boldsymbol{u}^n$ and $\boldsymbol{u}^{ni}$, respectively. Assuming numerical solutions of u are known for $t \le t_n$, we construct the Lagrange interpolating polynomial $u^*(x,t)$ based on the points $(t_n, \boldsymbol{u}^n)$ and $(t_{ni}, \boldsymbol{u}^{ni})$. This polynomial $u^*(x,t)$ is then utilized to approximate the nonlinear terms of Systems (22)–(24) over the interval (t_n, t_{n+1}).

We proceed to apply the symplectic Runge–Kutta method to the reformulated Systems (22)–(24). By incorporating extrapolation techniques for discretizing the nonlinear terms, we derive the equations for the internal stages as follows:

$$\begin{cases} \boldsymbol{p}_i^n = \boldsymbol{p}^n + \tau \sum_{j=1}^{s} a_{ij} k_p^j, & k_p^i = -D^\gamma \boldsymbol{q} - \beta A^{\bar{\boldsymbol{p}}_i^{n,*}, \bar{\boldsymbol{q}}_i^{n,*}}, \\ \boldsymbol{q}_i^n = \boldsymbol{q}^n + \tau \sum_{j=1}^{s} a_{ij} k_q^j, & k_q^i = D^\gamma \boldsymbol{q} + \beta B^{\bar{\boldsymbol{p}}_i^{n,*}, \bar{\boldsymbol{q}}_i^{n,*}}, \\ \boldsymbol{r}_i^n = \mathcal{G}\left(\mathcal{G}^{-1}(\boldsymbol{q}^n) + \tau \sum_{j=1}^{s} a_{ij} k_r^j\right), & k_r^i = 4\left\langle A^{\bar{\boldsymbol{p}}_i^{n,*}, \bar{\boldsymbol{q}}_i^{n,*}} \right\rangle_h + 4\left\langle B^{\bar{\boldsymbol{p}}_i^{n,*}, \bar{\boldsymbol{p}}_i^{n,*}} \right\rangle_h. \end{cases} \tag{38}$$

Then, $(\boldsymbol{p}^{n+1}, \boldsymbol{q}^{n+1}, \boldsymbol{r}^{n+1})$ can be updated by

$$\begin{cases} \boldsymbol{p}^{n+1} = \boldsymbol{u}^n + \tau \sum_{i=1}^{s} b_i k_p^i, \\ \boldsymbol{q}^{n+1} = \boldsymbol{q}^n + \tau \sum_{i=1}^{s} b_i k_q^i, \\ \boldsymbol{r}^{n+1} = \boldsymbol{r}^n + \tau \sum_{i=1}^{s} b_i k_r^i, \end{cases} \tag{39}$$

For $s = 2$, the extrapolation technique for the nonlinear terms is expressed as

$$\bar{z}_1^{n,*} = (2\sqrt{3} - 4) z^{n-1} + (7\sqrt{3} - 11) z_1^{n-1} + (6 - 5\sqrt{3}) z_2^{n-1} + (10 - 4\sqrt{3}) z^n,$$

$$\bar{z}_2^{n,*} = (-2\sqrt{3} - 4) z^{n-1} + (6 + 5\sqrt{3}) z_1^{n-1} - (7\sqrt{3} + 11) z_2^{n-1} + (10 + 4\sqrt{3}) z^n.$$

These methods achieve third-order accuracy [21]. For $s = 3$, the extrapolation technique is given by

$$\bar{z}_1^{n,*} = (6\sqrt{15} - 26) z^{n-1} + \frac{33 - 5\sqrt{15}}{3} z_1^{n-1} + \frac{16\sqrt{15} - 72}{3} z_2^{n-1} + \frac{120 - 29\sqrt{15}}{3} z_3^{n-1},$$

$$\bar{z}_2^{n,*} = -17 z^{n-1} + \frac{35 + 5\sqrt{15}}{2} z_1^{n-1} - 17 z_2^{n-1} + \frac{35 - 5\sqrt{15}}{2} z_3^{n-1},$$

$$\bar{z}_3^{n,*} = (-26 - 6\sqrt{15}) z^{n-1} + \frac{120 + 29\sqrt{15}}{3} z_1^{n-1} - \frac{72 + 16\sqrt{15}}{3} z_2^{n-1} + \frac{33 + 5\sqrt{15}}{3} z_3^{n-1}.$$

where $z = p, q$. These methods attain fourth-order accuracy [21]. In the subsequent discussions, we denote Schemes (38) and (39), which satisfy the symplectic condition, as the **LI3** and **LI4** schemes for $s = 2$ and $s = 3$, respectively.

Theorem 3. *Systems* (38) *and* (39) *can inherit the following energy, i.e.,*

$$E^n = E^0,$$

where E^n *is the energy function, which has the form*

$$E^n = \langle \mathcal{D}^\gamma \boldsymbol{p}^n, \boldsymbol{p}^n \rangle_h + \langle \mathcal{D}^\gamma \boldsymbol{q}^n, \boldsymbol{q}^n \rangle_h + \frac{\beta}{2} \langle \mathcal{G}^{-1}(\boldsymbol{p}^n, \boldsymbol{q}^n), 1 \rangle_h. \tag{40}$$

Proof. First, we define

$$\Delta E = E^{n+1} - E^n = \Delta E_p + \Delta E_q + \Delta E_r, \tag{41}$$

where

$$\begin{aligned}
\Delta E_p &= \langle \mathcal{D}^\gamma \boldsymbol{p}^{n+1}, \boldsymbol{p}^{n+1} \rangle_h - \langle \mathcal{D}^\gamma \boldsymbol{p}^n, \boldsymbol{p}^n \rangle_h, \\
\Delta E_q &= \langle \mathcal{D}^\gamma \boldsymbol{q}^{n+1}, \boldsymbol{q}^{n+1} \rangle_h - \langle \mathcal{D}^\gamma \boldsymbol{q}^n, \boldsymbol{q}^n \rangle_h, \\
\Delta E_r &= \frac{\beta}{2} \Big(\langle \mathcal{G}^{-1}(\boldsymbol{r}^{n+1}), 1 \rangle_h - \langle \mathcal{G}^{-1}(\boldsymbol{r}^n), 1 \rangle_h \Big).
\end{aligned}$$

Using the updates from (39), we derive

$$\begin{aligned}
\Delta E_p &= \langle \mathcal{D}^\gamma (\boldsymbol{p}^n + \tau \sum_{i=1}^{s} b_i k_p^i), \boldsymbol{p}^n + \tau \sum_{i=1}^{s} b_i k_p^i \rangle_h - \langle \mathcal{D}^\gamma \boldsymbol{p}^n, \boldsymbol{p}^n \rangle_h, \\
\Delta E_q &= \langle \mathcal{D}^\gamma (\boldsymbol{q}^n + \tau \sum_{i=1}^{s} b_i k_q^i), \boldsymbol{q}^n + \tau \sum_{i=1}^{s} b_i k_q^i \rangle_h - \langle \mathcal{D}^\gamma \boldsymbol{q}^n, \boldsymbol{q}^n \rangle_h.
\end{aligned}$$

Expanding and simplifying using the symmetry of $\mathcal{D}^\gamma$ and the symplectic condition, (37), we obtain

$$\begin{aligned}
\Delta E_p + \Delta E_q &= \tau \sum_{i=1}^{s} b_i \Big(\langle \mathcal{D}^\gamma \boldsymbol{p}^n, k_p^i \rangle_h + \langle \mathcal{D}^\gamma \boldsymbol{q}^n, k_q^i \rangle_h \Big) + \frac{\tau^2}{2} \sum_{i,j=1}^{s} b_i b_j \Big(\langle \mathcal{D}^\gamma k_p^i, k_p^j \rangle_h + \langle \mathcal{D}^\gamma k_q^i, k_q^j \rangle_h \Big) \\
&= -\frac{\beta}{2} (\tau \sum_{i=1}^{s} b_i k_r^i).
\end{aligned} \tag{42}$$

From (39), we have

$$\Delta E_r = \frac{\beta}{2} (\langle \mathcal{G}^{-1}(\boldsymbol{r}^{n+1}), 1 \rangle_h - \langle \mathcal{G}^{-1}(\boldsymbol{r}^n), 1 \rangle_h) = \frac{\beta}{2} (\tau \sum_{i=1}^{s} b_i k_r^i). \tag{43}$$

Using the definitions of k_p^i, k_q^i, and k_r^i, along with the properties of the inner product and the symmetry of $\mathcal{D}^\gamma$, we find that the sum $\Delta E_p + \Delta E_q + \Delta E_r = 0$.

Since $\Delta E = 0$, we have $E^{n+1} = E^n$. Therefore, the numerical scheme preserves the discrete energy.

The proof is completed. □

Remark 2. *Currently, we are unable to demonstrate the convergence of the proposed scheme due to the following challenges:*

- *Obtaining convergence analysis results for high-dimensional problems is a challenging task.*
- *Incorporating a new variable and extrapolation techniques into the numerical schemes adds complexity to the system, making it harder to establish the convergence of the proposed schemes.*

In future work, we aim to address these challenges and provide a rigorous convergence proof for the schemes.

5. Numerical Examples

This section focuses on verifying the energy conservation and effectiveness of the proposed schemes. Furthermore, we present a method for comparison to evaluate their performance.

- **CN-SAV**: a second-order energy-preserving scheme for the nonlocal wave equation based on the SAV method.
- **AVF**: a second-order energy-preserving scheme for the nonlocal wave equation based on the averaged vector field (AVF) method.

Example 1. *In this subsection, we study the 1D nonlocal NLS equation*

$$iu_t - (-\Delta)^{\frac{\alpha}{2}} u + 2|u|^2 u = 0, \tag{44}$$

with the initial condition

$$u(x,0) = exp(-x^2)\exp(-ix), \tag{45}$$

and we take the space interval $\Omega = [-40, 40]$.

In practical computations, we take $\mathcal{G}(x) = \exp(x)$, and set $\mathcal{N} = 256$ to ensure that spatial discretization errors are minimal, allowing us to focus on evaluating the temporal discretization errors of the proposed energy-preserving methods. We compute the numerical errors by using the formula $\|e\|_\infty = \|z(h,\tau) - z(h,\tau/2)\|_\infty$, where $z(h,\tau)$ represent the numerical solution at (h,τ). Table 2 compares the errors and convergence rates of four numerical schemes: **CN-SAV**, **LI3**, **LI4**, and **AVF**, evaluated at $t = 1$ with different time step sizes τ and parameters γ. The **CN-SAV** and **AVF** schemes exhibit second-order convergence, as indicated by rates close to 2, confirming their expected accuracy. The LI3 scheme shows third-order convergence with rates near 3, validating its higher accuracy. Similarly, the LI4 scheme demonstrates fourth-order convergence, maintaining high precision with rates consistently close to 4. Overall, the **LI3** and **LI4** schemes provide superior performance due to their higher convergence orders, making them more suitable for applications requiring greater numerical accuracy compared to the second-order **CN-SAV** and **AVF** schemes.

Table 2. Errors and corresponding temporal observation orders of four conservative schemes with different γ at $t = 1$.

γ	τ	CN-SAV Scheme		LI3 Scheme		LI4 Scheme		AVF Scheme	
		$\|e\|_\infty$	Rate	$\|e\|_\infty$	Rate	$\|e\|_\infty$	Rate	$\|e\|_\infty$	Rate
0.6	0.01	4.15×10^{-4}	-	4.72×10^{-6}	-	6.47×10^{-7}	-	5.68×10^{-4}	-
	0.005	1.06×10^{-4}	1.97	7.33×10^{-7}	2.69	4.99×10^{-8}	3.69	1.46×10^{-4}	1.96
	0.0025	2.68×10^{-5}	1.98	1.02×10^{-7}	2.85	3.43×10^{-9}	3.86	3.68×10^{-5}	1.99
0.8	0.01	2.24×10^{-5}	-	1.53×10^{-7}	-	1.56×10^{-8}	-	1.79×10^{-3}	-
	0.005	5.95×10^{-6}	1.91	2.25×10^{-8}	2.76	1.14×10^{-9}	3.78	4.61×10^{-4}	1.95
	0.0025	1.53×10^{-6}	1.96	3.05×10^{-9}	2.89	7.68×10^{-11}	3.89	1.17×10^{-4}	1.97

Figure 1 presents a comparison of the relative errors in energy conservation for four different numerical schemes under varying values of the parameter γ. The two graphs depict the relative error of these schemes for $\gamma = 0.6$ and $\gamma = 0.8$, plotted over time. For $\gamma = 0.4$, the **CN-SAV** method exhibits oscillations in energy error, with values fluctuating between 10^{-12} and 10^{-13}, whereas the **AVF** scheme shows a steady increase in error,

starting at around 10^{-15} and rising to 10^{-13}. In contrast, the **L13** and **LI4** methods maintain significantly lower and stable errors around 10^{-14} to 10^{-15}, demonstrating excellent energy conservation properties. As γ increases to 0.6, the **CN-SAV** method experiences even larger oscillations, with errors reaching up to 10^{-11}, while the **AVF** scheme again shows a gradual increase in error, this time reaching around 10^{-11}. However, the **LI3** and **L14** methods continue to display superior performance, maintaining low relative errors similar to the case with $\gamma = 0.4$. Overall, the comparison highlights that, regardless of the value of γ, the **L13** and **L14** schemes consistently provide the best results in terms of energy conservation, while the **CN-SAV** and **AVF** schemes exhibit larger errors, with the errors growing more pronounced as γ increases.

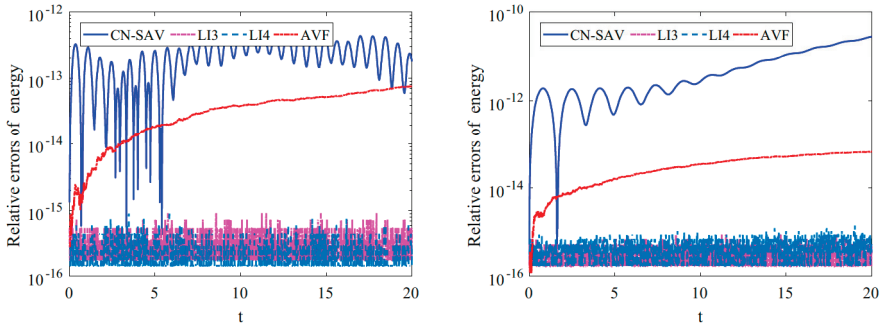

Figure 1. The relative errors of conservative laws for four schemes with $\tau = 0.01$, $h = 80/256$ for different γ.

Example 2. *We analyze the two-dimensional nonlocal NLS equation with* $\beta = 1$. *The initial condition is specified as*

$$u(x, y, 0) = \frac{2}{\sqrt{\pi}} exp(-x^2 - y^2). \tag{46}$$

For this study, we consider fractional orders $\alpha = 0.65$ *and* $\alpha = 0.95$. *The computations are carried out over the spatial domain* $\Omega = [-10, 10] \times [-10, 10]$.

Figure 2 compares the relative errors in modified energy for the **LI3** and **LI4** schemes under two different values of the parameter γ, specifically $\gamma = 0.65$ and $\gamma = 0.95$. The LI3 scheme (left plot) exhibits consistently low relative errors between 10^{-16} and 10^{-15}, with small fluctuations over time, slightly more noticeable for $\gamma = 0.65$. In the **LI4** scheme (right plot), the relative error also remains low, but with slightly larger fluctuations, especially for $\gamma = 0.65$, where the error reaches up to 10^{-14}. For $\gamma = 0.95$, both schemes perform better, with smaller fluctuations and relative errors closer to 10^{-15}. Overall, both schemes demonstrate strong energy conservation. Then, we investigate the relationship between the evolution of the soliton and the γ for nonlocal system Figure 3 displays the profile (left) and contour plot (right) of the numerical solutions for two different values of γ. The top row shows the results for $\gamma = 0.65$, where the 3D profile indicates a smooth, symmetric peak centered around $(x, y) = (0, 0)$ with values decreasing radially. The contour plot on the right confirms this radial symmetry, with evenly spaced concentric rings representing decreasing values as one moves outward from the center. The bottom row illustrates the same type of plots for $\gamma = 0.95$. Figures 3 and 4 depict the evolution of the solution, with the main difference being the height of the peak between $\gamma = 0.65$ and $\gamma = 0.95$, suggesting a slight change in the intensity of the solution based on the value of γ.

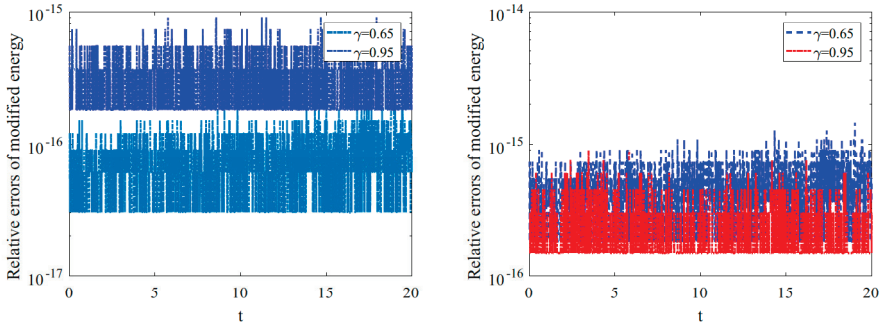

LI3 scheme **LI4** scheme

Figure 2. The relative errors of conservative laws for two schemes with $\tau = 0.01$, $h = 20/128$ for different γ.

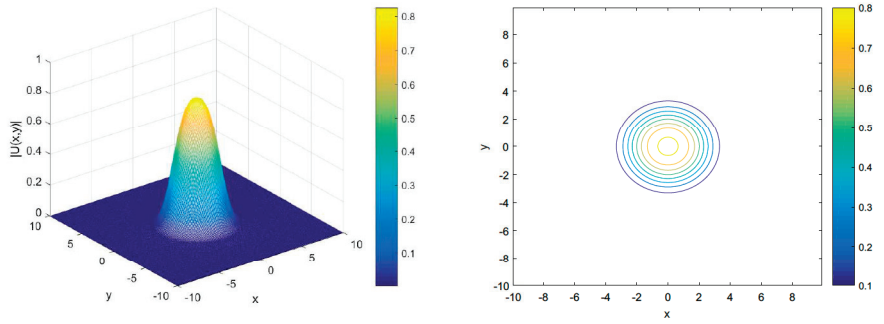

Figure 3. Profile (**left**) and contour plot (**right**) of numerical solution for $\gamma = 0.65$.

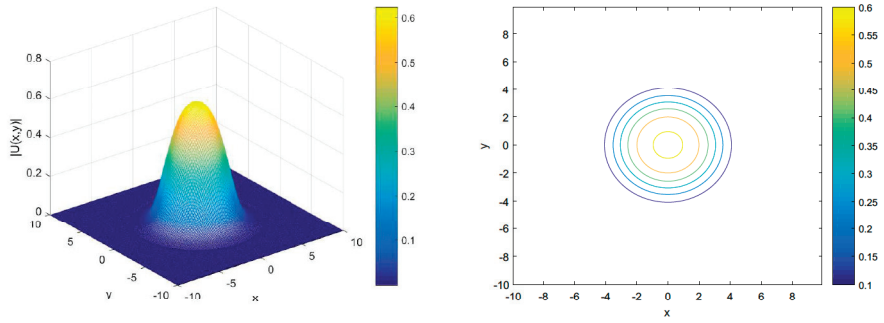

Figure 4. Profile (**left**) and contour plot (**right**) of numerical solution for $\gamma = 0.95$.

6. Conclusions

In this paper, we construct linearly implicit schemes to solve the nonlocal NLS equation. The proposed schemes offer high accuracy, and ensure preservation of the modified energy. Numerical experiments further confirm their robust stability. Moreover, these methods can be extended to other conservative differential equations. Future work will focus on overcoming the challenges of proving the convergence of these schemes and developing efficient conservative methods that can preserve the system's original energy.

Author Contributions: Methodology, Y.Z. and M.F.; software, Y.Z.; formal analysis, Y.Z.; writing—review and editing, B.L. All authors have read and agreed to the published version of the manuscript.

Funding: The research is supported by the National Natural Science Foundation of China (12201071), Natural Science Foundation of Hunan Province (2022JJ40520) and Scientific Research Fund of Hunan Province Eduation Deparment (23A0602).

Data Availability Statement: The original contributions presented in the study are included in the article, further inquiries can be directed to the corresponding author.

Conflicts of Interest: The authors declare no conflicts of interest.

References

1. Kittel, C. *Introduction to Solid State Physics*; Wiley: New York, NY, USA, 2005.
2. Boyd, R.W. *Nonlinear Optics*; Academic Press: New York, NY, USA, 2008.
3. Pethick, C.J.; Smith, H. *Bose-Einstein Condensation in Dilute Gases*; Cambridge University Press: Cambridge, UK, 2008.
4. Laskin, N. Fractional Schrödinger equation. *Phys. Rev. E* **2002**, *66*, 056108. [CrossRef] [PubMed]
5. Zeng, W.; Xiao, A.; Li, X. Error estimate of Fourier pseudo-spectral method for multidimensional nonlinear complex fractional Ginzburg-Landau equations. *Appl. Math. Lett.* **2019**, *93*, 40–45. [CrossRef]
6. Hassan, A.H. Comparison differential transformation technique with Adomian decomposition method for linear and nonlinear initial value problems. *Chaos Solitons Fract.* **2008**, *36*, 53–65. [CrossRef]
7. Shah, S.; Singh, R. Evolution of singular surface and interaction with a strong shock in reacting polytropic gases using Lie group theory. *Int. J. Non-Linear Mech.* **2019**, *116*, 173–180. [CrossRef]
8. Salkuyeh, D.K.; Ghehsareh, H.R. Convergence of the variational iteration method for the telegraph equation with integral conditions. *Numer. Methods Partial Differ. Equ.* **2011**, *27*, 1442–1455. [CrossRef]
9. Bhrawy, A.H.; Doha, E.H.; Ezz-Eldien, S.S.; Van Gorder, R.A. A new Jacobi spectral collocation method for solving 1+1 fractional Schrödinger equations and fractional coupled Schrödinger systems. *Eur. Phys. J. Plus* **2014**, *129*, 260. [CrossRef]
10. Li, M.; Gu, X.; Huang, C.; Fei, M.; Zhang, G. A fast linearized conservative finite element method for the strongly coupled nonlinear fractional Schrödinger equations. *J. Comput. Phys.* **2018**, *358*, 256–282. [CrossRef]
11. Wang, D.; Xiao, A.; Yang, W. A linearly implicit conservative difference Scheme for the space fractional coupled nonlinear Schrödinger equations. *J. Comput. Phys.* **2014**, *272*, 644–655. [CrossRef]
12. Fu, Y.; Cai, W.; Wang, Y. Structure-preserving algorithms for the two-dimensional fractional Klein-Gordon-Schrödinger equation. *Appl. Numer. Math.* **2020**, *156*, 77–93. [CrossRef]
13. Macías-Díaz, J. Numerical study of the process of nonlinear supratransmission in Riesz space-fractional sine-gordon equations. *Commun. Nonlinear Sci. Numer. Simul.* **2017**, *46*, 89–102. [CrossRef]
14. Wang, P.; Huang, C. A conservative linearized difference Scheme for the nonlinear fractional Schrödinger equation. *Numer. Algorithms* **2015**, *69*, 625–641. [CrossRef]
15. Fu, Y.; Hu, D.; Zhang, G. Arbitrary high-order exponential integrators conservative schemes for the nonlinear Gross-Pitaevskii equation. *Comput. Math. Appl.* **2022**, *121*, 102–114. [CrossRef]
16. Ran, M.; Zhang, C. A conservative difference scheme for solving the strongly coupled nonlinear fractional Schrödinger equations. *Commun. Nonlinear Sci. Numer. Simul.* **2016**, *41*, 64–83. [CrossRef]
17. Wang, P.; Huang, C. Structure-preserving numerical methods for the fractional Schrödinger equation. *Appl. Numer. Math.* **2018**, *129*, 137–158. [CrossRef]
18. Zhao, J.; Li, Y.; Xu, Y. An explicit fourth-order energy-preserving scheme for Riesz space fractional nonlinear wave equations. *Appl. Math. Comput.* **2019**, *351*, 124–138. [CrossRef]
19. Brugnano, L.; Zhang, C.; Li, D. A class of energy-conserving Hamiltonian boundary value methods for nonlinear Schrödinger equation with wave operator. *Commun. Nonlinear Sci. Numer. Simul.* **2018**, *60*, 33–49. [CrossRef]
20. Li, H.; Wang, Y.; Qin, M. A sixth order averaged vector field method. *J. Comput. Math.* **2016**, *34*, 479–498.
21. Hairer, E.; Lubich, C.; Wanner, G. *Geometric Numerical Integration: Structure-Preserving Algorithms for Ordinary Differential Equations*; Springer Science: New York, NY, USA, 2006.
22. Cheng, Q.; Liu, C.; Shen, J. Generalized SAV approaches for gradient systems. *J. Comput. Appl. Math.* **2021**, *3*, 113532. [CrossRef]
23. Shen, J.; Xu, J. Convergence and error analysis for the scalar auxiliary variable (SAV) schemes to gradient flows. *J. Comput. Phys.* **2018**, *56*, 2895–2912. [CrossRef]
24. Shen, J.; Xu, J.; Yang, J. The scalar auxiliary variable (SAV) approach for gradient flows. *J. Comput. Phys.* **2018**, *353*, 407–416. [CrossRef]
25. Shen, J.; Xu, J.; Yang, J. A new class of efficient and robust energy stable schemes for gradient flows. *SIAM Rev.* **2019**, *61*, 474–506. [CrossRef]

Disclaimer/Publisher's Note: The statements, opinions and data contained in all publications are solely those of the individual author(s) and contributor(s) and not of MDPI and/or the editor(s). MDPI and/or the editor(s) disclaim responsibility for any injury to people or property resulting from any ideas, methods, instructions or products referred to in the content.

computation

MDPI

Article

Computational Representation of Fractional Inequalities Through 2D and 3D Graphs with Applications

Muhammad Younis [1], Ahsan Mehmood [1,*], Muhammad Samraiz [2], Gauhar Rahman [3], Salma Haque [4], Ahmad Aloqaily [4] and Nabil Mlaiki [4]

[1] School of Mathematical Sciences, Shanghai Key Laboratory of PMMP, East China Normal University, 500 Dongchuan Road, Shanghai 200241, China; younismuhammad303@gmail.com
[2] Department of Mathematics, University of Sargodha, Sargodha P.O. Box 40100, Pakistan; muhammad.samraiz@uos.edu.pk
[3] Department of Mathematics & Statistics, Hazara University, Mansehra 21300, Pakistan; gauhar55uom@gmail.com or drgauhar.rahman@hu.edu.pk
[4] Department of Mathematics and Sciences, Prince Sultan University, Riyadh 11586, Saudi Arabia; shaque@psu.edu.sa (S.H.); maloqaily@psu.edu.sa (A.A.); nmlaiki@psu.edu.sa or nmlaiki20212@gmail.com (N.M.)
* Correspondence: mehmoodahsan154@gmail.com; Tel.: +86-131-6238-3863

Abstract: The aim of this research article is to use the extended fractional operators involving the multivariate Mittag–Leffler (M-M-L) function, we provide the generalization of the Hermite–Hadamard–Fejer (H-H-F) inequalities. We relate these inequalities to previously published disparities in the literature by making appropriate substitutions. In the last section, we analyze several inequalities related to the H-H-F inequalities, focusing on generalized h-convexity associated with extended fractional operators involving the M-M-L function. To achieve this, we derive two identities for locally differentiable functions, which allows us to provide specific estimates for the differences between the left, middle, and right terms in the H-H-F inequalities. Also, we have constructed specific inequalities and visualized them through graphical representations to facilitate their applications in analysis. The research bridges theoretical advancements with practical applications, providing high-accuracy bounds for complex systems involving fractional calculus.

Keywords: Hermite–Hadamard-Fejer; multivariate Mittag–Leffler function; symmetric properties; generalized h-convexity; modified (k,s)-fractional operator

1. Introduction

The study of fractional calculus and its diverse applications has received more attention in recent times. Chronologically ordering the development of this theory, we find that fractional calculus was first applied when Abel solved the Tautocrone problem [1]. Scholars have written their own books [2,3] to advance the field of fractional calculus, these books are essential to the advancement of applications of fractional calculus in mathematical modeling and applied analysis. The well-known caputo sense derivative without non-singular kernel was developed by Caputo et al. in [4], although there are still many gaps in the theory that the researchers have discovered. In order to overcome these gaps, several researchers have developed their own fractional operators with non-singular kernels [5–8]. Furthermore, the symmetric properties as well as the non-linear and non-singular extensions of fractional operators were illustrated by Wu et al. in [9]. In [10], Samraiz et al. developed the fractional derivative with non-linear and non-singular kernel, also discussed its applications in applied analysis. Consequently, fractional operators were developed

in [11,12] using different kinds of Mittag–Leffle (M-L) functions as a kernel. We direct readers to explore [13–18] for additional developments and applications on fractional calculus. Roman et al. described the fractional derivatives and their applications in time series with long-time memory and random walks in [19]. In [20], Moreles at al. introduced modeling for the mathematical study of circuit components with fractional orders, they also discussed applications of bioimpedance. In [21] the authors explore the integration of harmonic univalent functions with the generalized (p, q)-Poisson distribution, presenting a novel theoretical contribution to complex analysis and fractional calculus. It extends the classical understanding of harmonic functions by incorporating this distribution, offering new results on their univalence and injectivity properties. The study uses standard mathematical analysis techniques, providing explicit examples and graphical representations to support the theoretical claims. While the theoretical framework is solid, the article could benefit from a clearer explanation of the practical applications and real-world implications of these results. Although it makes a significant contribution to the field, a more detailed discussion on how these findings could be applied to practical problems in mathematics, physics, and engineering would strengthen the work. Using fractional calculus to simulate dielectric relaxation events in polymeric materials was demonstrated by Melo et al. in [22]. You can find a presentation of fractional integral in conjunction with wave theory in [23]. The theory of inequalities in [24,25] is closely related to convex functions (Cf) and their expansions $s-$Cf.

Definition 1. *The function $f : [\alpha, \beta] \mapsto \Re$ (Set of real numbers) is said to be Cf, if*

$$f(\ell_1 x_1 + (1 - \ell_1)x_2) \leq \ell_1 f(x_1) + (1 - \ell_1)f(x_2),$$

$\forall x_1, x_2 \in [\alpha, \beta]$ *and* $\ell_1 \in (0, 1]$.

In [25], Brechner gave the definition of s-Cf, stated by the following definition.

Definition 2. *A function $f : (0, \infty) \mapsto \Re$ is called second sense $s-$Cf for some fixed $k \epsilon (0, 1)$, is given by*

$$f(\ell_1 x_1 + \ell_2 x_2) \leq \ell_1^s f(x_1) + \ell_2^s f(x_2),$$

$\forall x_1, x_2 \in (0, \infty), 0 \leq \ell_1, \ell_2 \leq 1$, *where* $\ell_1 + \ell_2 = 1$. *This class of function is denoted as* K_s^2.

In [26,27], authors discussed novel fractional operators and class of inequalities involving novel fractional operators. Hakiki et al. described H-H-F inequalities involving second kind of $s-$Cf via Riemann–Liouville (RL) FI and novel inequalities of H-H-F kind inequalities for Cf via FI in [28,29].

Furthermore, matching nonsingular kernels and new fractional operators, like the M-L function, have also been introduced [30,31]. Diverse historical applications of fractional operators were illustrated by the researchers. The scientists have currently designed a large number of physical models [32,33]. Several of these models solve particular differential equations of fractional order using the M-L non-singular kernel [34,35]. The (k, s)-fractional calculus of the generalized M-L function was discussed by Nisar et al. [36]. For more details and applications of fractional operators, we suggest readers to [37,38]. Readers are referred to [35,39–41] for additional information and applications on fractional operators. In 1903, Gosta [42] proposed the classical M-L function. Several approaches have been taken to generalize it, such as adding two or three parameters [43].

Definition 3 ([11]). *The generalized multivariate Mittag–Leffler (M-M-L) function is defined by*

$$\xi^{(\delta_i)}_{k,\mu,(\beta_i)}(\tau_1,\tau_2,\ldots,\tau_n)=\Sigma^{\infty}_{\kappa_1,\ldots,\kappa_n=0}\frac{\Pi^n_{i=1}(\delta_i)_{\kappa_i,k}}{\Gamma_k(\mu+\Sigma^n_{i=1}(\beta_i\kappa_i))(\kappa_1)!\ldots(\kappa_n)!}(\tau_1)^{\kappa_1}(\tau_2)^{\kappa_2}\ldots(\tau_n)^{\kappa_n},$$

where $k>0$, $\beta_i,\delta_i\in C$ with $Re(\beta_i)>0$ for all $i=1,2,3,\ldots,n$. Furthermore, If we substitute $k=1$ then we obtain M-M-L function defined by Sexana et al. in [44].

Let $f:\Re\to\Re$ be Cf , $\ell_1,\ell_2\in I\subseteq\Re$ such that $\ell_1<\ell_2$, and $w:[\ell_1,\ell_2]\to\Re$ be a non-negative integrable and symmetric with respect to $\frac{\ell_1+\ell_2}{2}$, then the H-H-F inequality can be found in [45] by

$$f(\frac{\ell_1+\ell_2}{2})\int_{\ell_1}^{\ell_2}w(x)dx\leq\frac{1}{\ell_2-\ell_1}\int_{\ell_1}^{\ell_2}f(x)w(x)dx\leq\frac{f(\ell_1)+f(\ell_2)}{2}\int_{\ell_1}^{\ell_2}w(x)dx.$$

The classical H-H inequality (see also [46]) is given by the following:

$$f(\frac{\ell_1+\ell_2}{2})\leq\frac{1}{\ell_2-\ell_1}\int_{\ell_1}^{\ell_2}f(x)dx\leq\frac{f(\ell_1)+f(\ell_2)}{2}.$$

Because of the lot of applications of said inequalities, some researchers prolonged their research via functions of several classes, as an illustration [47] for Cf and [48,49] for h-Cf. In 2007, Varošanec [50] presented the concept of h-Cf, in the second sense which was a generalization of s-convexity, non-negative convexity, *P*-convexity and Godunova–Levin mappings. Chen et al. [51] presented H-H and H-H-F inequalities for generalized FI. In [52], Khan et al. generalized the conformable fractional operators and a new class of fractional operators. For details applications of fractional operators we refer readers [53,54]. Here, we have some more fundamental definitions which are indispensable for explaining the key findings in the coming results.

Definition 4 ([51]). *The incomplete beta function $B_b(\ell_1,\ell_2)$ is defined by*

$$B_b(\ell_1,\ell_2)=\int_0^b z^{\ell_1-1}(1-z)^{\ell_2-1}dz,$$

where, $0<b<1,\ell_1,\ell_2>0$.

Definition 5 ([55]). *Let $p,q\in\Re$ with $p,q>1$ and $\frac{1}{p}+\frac{1}{q}=1$, then the integral form of Hölder inequality is presented as*

$$\int_{e_1}^{e_2}|H(\imath)I(\imath)|d\imath\leq\left(\int_{e_1}^{e_2}|H(\imath)|^p d\imath\right)^{\frac{1}{p}}\left(\int_{e_1}^{e_2}|I(\imath)|^q d\imath\right)^{\frac{1}{q}},$$

with $H,I\in\mathbb{C}^1[e_1,e_2]$.

Definition 6. *The left and right-sided RLFI $I^{\varrho}_{\ell_1^+}(f)$ and $I^{\varrho}_{\ell_2^-}(f)$, of order $\varrho>0$ on $[\ell_1,\ell_2]$ are defined as*

$$I^{\varrho}_{\ell_1^+}f(p_1)=\frac{1}{\Gamma(\varrho)}\int_{\ell_1}^{p_1}(p_1-\nu)^{\varrho-1}f(\nu)d\nu,\quad p_1>\ell_1,$$

and

$$I^{\varrho}_{\ell_2^-} f(p_1) = \frac{1}{\Gamma(\varrho)} \int_{p_1}^{\ell_2} (\nu - p_1)^{\varrho-1} f(\nu) d\nu, \quad p_1 < \ell_2,$$

respectively. Here Γ *represents the Gamma function and its integral representation is given below.*

$$\Gamma(p_1) = \int_0^{\infty} \nu^{p_1-1} e^{-\nu} d\nu, \quad Re(p_1) > 0.$$

Now, we present the definition of the (k,s)-RLFI, which is defined in [56].

Definition 7. *If a function* f *is continuous on* $[a,b]$*, then the* (k,s)*-RLFI for order* $\delta > 0$ *can be defined as*

$${}^{s}_{k}\mathfrak{J}^{\delta}_{a^+} f(t_1) = \frac{(s+1)^{1-\frac{\delta}{k}}}{k\Gamma_k(\delta)} \int_{a^+}^{t_1} (t_1^{s+1} - \nu^{s+1})^{\frac{\delta}{k}-1} \nu^s f(\nu) d\nu. \tag{1}$$

The following is the definition of the fractional integral operator in its generalized form with M-M-L function as part of its kernel is defined in [11].

Definition 8. *If a function* f *is continuous on* $[a,b]$*, for* $k > 0$*,* $m \in \Re/\{-1\}$*, let the parameters* $Re(\mu) > 0$*,* τ_i*,* β_i *be complex numbers with* $Re(\beta_i) > 0, \forall i = 1,2,\ldots,n$*; and* Θ *be the strictly increasing function and differentiable then the generalized fractional integral operators for* $\delta_i > 0, \forall i = 1,2,\ldots,n$*; can be defined as*

$$\begin{aligned}
&({}^{k,m}_{\Theta}\mathfrak{J}^{\delta_i,\tau_i}_{a;\mu,\beta_i} f)(t_1) = \frac{(m+1)^{1-\frac{\mu}{k}}}{k} \int_a^{t_1} (\Theta^{m+1}(t_1) - \Theta^{m+1}(\nu))^{\frac{\mu}{k}-1} \\
&\times \xi^{\delta_i}_{k,\mu,\beta_i} \Big(\tau_1 (\Theta^{m+1}(t_1) - \Theta^{m+1}(\nu))^{\frac{\beta_1}{k}}, \tau_2 (\Theta^{m+1}(t_1) - \Theta^{m+1}(\nu))^{\frac{\beta_2}{k}}, \ldots, \\
&\tau_n (\Theta^{m+1}(t_1) - \Theta^{m+1}(\nu))^{\frac{\beta_n}{k}} \Big) \Theta^m(\nu) \Theta'(\nu) f(\nu) d\nu \\
&= \frac{(m+1)^{1-\frac{\mu}{k}}}{k} \Sigma_{\kappa_1,\ldots,\kappa_n=0}^{\infty} \frac{\Pi_{i=1}^n (\delta_i)_{\kappa_i,k} (\tau_i)^{\kappa_i}}{\Gamma_k(\mu + \Sigma_{i=1}^n (\beta_i \kappa_i))(\kappa_1)! \ldots (\kappa_n)!} \\
&\times \int_a^{t_1} (\Theta^{m+1}(t_1) - \Theta^{m+1}(\nu))^{\frac{\mu+\Sigma_{i=1}^n \beta_i \kappa_i}{k} - 1} \Theta^m(\nu) \Theta'(\nu) f(\nu) d\nu.
\end{aligned}$$

Definition 9. *If a function* f *is continuous on* $[a,b]$*, for* $k > 0$*,* $m \in \Re/\{-1\}$*, let the parameters* $Re(\mu) > 0$*,* τ_i*,* β_i *be complex numbers with* $Re(\beta_i) > 0, \forall i = 1,2,\ldots,n$*; and* Θ *be the strictly increasing function and differentiable then the left and right sided generalized fractional integral operators for* $\delta_i > 0, \forall i = 1,2,\ldots,n$*; can be defined as*

$$\begin{aligned}
&({}^{k,m}_{\Theta}\mathfrak{J}^{\delta_i,\tau_i}_{a^+;\mu,\beta_i} f)(t_1) = \frac{(m+1)^{1-\frac{\mu}{k}}}{k} \int_{a^+}^{t_1} (\Theta^{m+1}(t_1) - \Theta^{m+1}(\nu))^{\frac{\mu}{k}-1} \\
&\times \xi^{\delta_i}_{k,\mu,\beta_i} \Big(\tau_1 (\Theta^{m+1}(t_1) - \Theta^{m+1}(\nu))^{\frac{\beta_1}{k}}, \tau_2 (\Theta^{m+1}(t_1) - \Theta^{m+1}(\nu))^{\frac{\beta_2}{k}}, \ldots, \\
&\tau_n (\Theta^{m+1}(t_1) - \Theta^{m+1}(\nu))^{\frac{\beta_n}{k}} \Big) \Theta^m(\nu) \Theta'(\nu) f(\nu) d\nu \\
&= \frac{(m+1)^{1-\frac{\mu}{k}}}{k} \Sigma_{\kappa_1,\ldots,\kappa_n=0}^{\infty} \frac{\Pi_{i=1}^n (\delta_i)_{\kappa_i,k} (\tau_i)^{\kappa_i}}{\Gamma_k(\mu + \Sigma_{i=1}^n (\beta_i \kappa_i))(\kappa_1)! \ldots (\kappa_n)!} \\
&\times \int_{a^+}^{t_1} (\Theta^{m+1}(t_1) - \Theta^{m+1}(\nu))^{\frac{\mu+\Sigma_{i=1}^n \beta_i \kappa_i}{k} - 1} \Theta^m(\nu) \Theta'(\nu) f(\nu) d\nu, \ \ t_1 > a^+,
\end{aligned}$$

and

$$
\begin{aligned}
&({}^{k,m}_{\Theta}\mathfrak{J}^{\delta_i,\tau_i}_{\zeta^-;\mu,\beta_i} f)(t_1) = \frac{(m+1)^{1-\frac{\mu}{k}}}{k}\int_{\zeta^-}^{t_1}(\Theta^{m+1}(\nu)-\Theta^{m+1}(t_1))^{\frac{\mu}{k}-1}\\
&\times \xi^{\delta_i}_{k,\mu,\beta_i}\Big(\tau_1(\Theta^{m+1}(\nu)-\Theta^{m+1}(t_1))^{\frac{\beta_1}{k}}, \tau_2(\Theta^{m+1}(\nu)-\Theta^{m+1}(t_1))^{\frac{\beta_2}{k}},\ldots,\\
&\tau_n(\Theta^{m+1}(\nu)-\Theta^{m+1}(t_1))^{\frac{\beta_n}{k}}\Big)\Theta^m(\nu)\Theta'(\nu)f(\nu)d\nu\\
&= \frac{(m+1)^{1-\frac{\mu}{k}}}{k}\Sigma_{\kappa_1,\ldots,\kappa_n=0}^{\infty}\frac{\Pi_{i=1}^{n}(\delta_i)_{\kappa_i,k}(\tau_i)^{\kappa_i}}{\Gamma_k(\mu+\Sigma_{i=1}^{n}(\beta_i\kappa_i))(\kappa_1)!\ldots(\kappa_n)!}\\
&\times\int_{\zeta-}^{t_1}(\Theta^{m+1}(\nu)-\Theta^{m+1}(t_1))^{\frac{\mu+\Sigma_{i=1}^{n}\beta_i\kappa_i}{k}-1}\Theta^m(\nu)\Theta'(\nu)f(\nu)d\nu,\quad t_1<\zeta.
\end{aligned}
$$

2. A Class of Some Results

In this section we have developed H-H-F type inequalities for generalized extended fractional operator encompassing the M-M-L function.

Lemma 1. *For $k>0$, $m\in\Re/\{-1\}$, and $Re(\mu)>0$, $Re(\tau)>0$, $Re(\delta)>0$, $Re(\beta)>0$ are complex parameters, Θ be an increasing function and Υ be a differentiable on (ℓ_1,ℓ_2) with $\ell_1<\ell_2$ and $\chi:[\ell_1,\ell_2]\mapsto\Re$ be bounded. If $\Upsilon',\chi\in L[\ell_1,\ell_2]$, then the below expression holds.*

$$
\begin{aligned}
&\Upsilon\Big(\frac{\ell_1+\ell_2}{2}\Big)\Big[{}^{k,m}_{\Theta}\mathfrak{J}^{\delta_i,\tau_i}_{(\frac{\ell_1+\ell_2}{2})^+;\mu,\beta_i}\chi(\ell_2)+{}^{k,m}_{\Theta}\mathfrak{J}^{\delta_i,\tau_i}_{(\frac{\ell_1+\ell_2}{2})^-;\mu,\beta_i}\chi(\ell_1)\Big]\\
&-\Big[{}^{k,m}_{\Theta}\mathfrak{J}^{\delta_i,\tau_i}_{(\frac{\ell_1+\ell_2}{2})^+;\mu,\beta_i}\chi\Upsilon(\ell_2)+{}^{k,m}_{\Theta}\mathfrak{J}^{\delta_i,\tau_i}_{(\frac{\ell_1+\ell_2}{2})^-;\mu,\beta_i}\chi\Upsilon(\ell_1)\Big]\\
&=\frac{k}{(m+1)^{1-\frac{\mu}{k}}}\int_{\ell_1}^{\ell_2}\kappa(\nu)\Upsilon'(\nu)d\nu,
\end{aligned}
$$

where

$$
\kappa(t_1)=\begin{cases}
\dfrac{\xi^{\delta_i}_{k,\mu,\beta_i}\Big(\tau_1(\Theta^{m+1}(t_1)-\Theta^{m+1}(\nu))^{\frac{\beta_1}{k}},\ldots,\tau_n(\Theta^{m+1}(t_1)-\Theta^{m+1}(\nu))^{\frac{\beta_n}{k}}\Big)\Theta^m(\nu)\Theta'(\nu)f(\nu)d\nu}{(\Theta^{m+1}(t_1)-\Theta^{m+1}(\nu))^{\frac{\mu}{k}-1}},\\
\qquad t_1\in[\ell_1,\frac{\ell_1+\ell_2}{2}],\\
\dfrac{\xi^{\delta_i}_{k,\mu,\beta_i}\Big(\tau_1(\Theta^{m+1}(t_1)-\Theta^{m+1}(\nu))^{\frac{\beta_1}{k}},\ldots,\tau_n(\Theta^{m+1}(\nu)-\Theta^{m+1}(t_1))^{\frac{\beta_n}{k}}\Big)\Theta^m(\nu)\Theta'(\nu)f(\nu)d\nu}{(\Theta^{m+1}(\nu)-\Theta^{m+1}(t_1))^{\frac{\mu}{k}-1}}\\
\qquad t_1\in[\frac{\ell_1+\ell_2}{2},\ell_2].
\end{cases}
$$

Proof. Consider

$$
\begin{aligned}
I&=\int_{\ell_1}^{\ell_2}\kappa(\nu)\Upsilon'(\nu)d\nu\\
&=\int_{\ell_1}^{\frac{\ell_1+\ell_2}{2}}\kappa(\nu)\Upsilon'(\nu)d\nu+\int_{\frac{\ell_1+\ell_2}{2}}^{\ell_2}\kappa(\nu)\Upsilon'(\nu)d\nu\\
&=I_1+I_2.
\end{aligned}
$$

Now, taking I_1 and after employing the integration by parts

$$
\begin{aligned}
I_1 &= \int_{\ell_1}^{\frac{\ell_1+\ell_2}{2}} \kappa(\nu)\Upsilon'(\nu)d\nu \\
&= \kappa\Big(\frac{\ell_1+\ell_2}{2}\Big)\Upsilon\Big(\frac{\ell_1+\ell_2}{2}\Big) \\
&- \int_{\ell_1}^{\frac{\ell_1+\ell_2}{2}} \frac{\xi^{\delta_i}_{k,\mu,\beta_i}\Big(\tau_1(\Theta^{m+1}(\frac{\ell_1+\ell_2}{2})-\Theta^{m+1}(\nu))^{\frac{\beta_1}{k}},\ldots,\tau_n(\Theta^{m+1}(\frac{\ell_1+\ell_2}{2})-\Theta^{m+1}(\nu))^{\frac{\beta_n}{k}}\Big)}{(\Theta^{m+1}(\frac{\ell_1+\ell_2}{2})-\Theta^{m+1}(\nu))^{\frac{\mu}{k}-1}} \\
&\times \Theta^m(\nu)\Theta'(\nu)\chi(\nu)d\nu \\
&= \Upsilon\Big(\frac{\ell_1+\ell_2}{2}\Big) \\
&\times \int_{\ell_1}^{\frac{\ell_1+\ell_2}{2}} \frac{\xi^{\delta_i}_{k,\mu,\beta_i}\Big(\tau_1(\Theta^{m+1}(\frac{\ell_1+\ell_2}{2})-\Theta^{m+1}(\nu))^{\frac{\beta_1}{k}},\ldots,\tau_n(\Theta^{m+1}(\frac{\ell_1+\ell_2}{2})-\Theta^{m+1}(\nu))^{\frac{\beta_n}{k}}\Big)}{(\Theta^{m+1}(\frac{\ell_1+\ell_2}{2})-\Theta^{m+1}(\nu))^{\frac{\mu}{k}-1}} \\
&\times \Theta^m(\nu)\Theta'(\nu)\chi(\nu)d\nu \\
&- \int_{\ell_1}^{\frac{\ell_1+\ell_2}{2}} \frac{\xi^{\delta_i}_{k,\mu,\beta_i}\Big(\tau_1(\Theta^{m+1}(\frac{\ell_1+\ell_2}{2})-\Theta^{m+1}(\nu))^{\frac{\beta_1}{k}},\ldots,\tau_n(\Theta^{m+1}(\frac{\ell_1+\ell_2}{2})-\Theta^{m+1}(\nu))^{\frac{\beta_n}{k}}\Big)}{(\Theta^{m+1}(\frac{\ell_1+\ell_2}{2})-\Theta^{m+1}(\nu))^{\frac{\mu}{k}-1}} \\
&\times \Theta^m(\nu)\Theta'(\nu)\chi(\nu)\Upsilon(\nu)d\nu \\
&= \Upsilon\Big(\frac{\ell_1+\ell_2}{2}\Big)\frac{(m+1)^{1-\frac{\mu}{k}}}{k}\Sigma^{\infty}_{\kappa_1,\ldots,\kappa_n=0}\frac{\Pi^n_{i=1}(\delta_i)_{\kappa_i,k}(\tau_i)^{\kappa_i}}{\Gamma_k(\mu+\Sigma^n_{i=1}(\beta_i\kappa_i))(\kappa_1)!\ldots(\kappa_n)!} \\
&\times \int_{a^+}^{t_1}(\Theta^{m+1}(t_1)-\Theta^{m+1}(\nu))^{\frac{\mu+\Sigma^n_{i=1}\beta_i\kappa_i}{k}-1}\Theta^m(\nu)\Theta'(\nu)\chi(\nu)d\nu \\
&- \frac{(m+1)^{1-\frac{\mu}{k}}}{k}\Sigma^{\infty}_{\kappa_1,\ldots,\kappa_n=0}\frac{\Pi^n_{i=1}(\delta_i)_{\kappa_i,k}(\tau_i)^{\kappa_i}}{\Gamma_k(\mu+\Sigma^n_{i=1}(\beta_i\kappa_i))(\kappa_1)!\ldots(\kappa_n)!} \\
&\times \int_{a^+}^{t_1}(\Theta^{m+1}(t_1)-\Theta^{m+1}(\nu))^{\frac{\mu+\Sigma^n_{i=1}\beta_i\kappa_i}{k}-1}\Theta^m(\nu)\Theta'(\nu)\chi(\nu)\Upsilon(\nu)d\nu \\
&= \frac{(m+1)^{1-\frac{\mu}{k}}}{k}[\Upsilon\Big(\frac{\ell_1+\ell_2}{2}\Big)\overset{k,m}{\Theta}\mathfrak{J}^{\delta_i,\tau_i}_{(\frac{\ell_1+\ell_2}{2})^-;\mu,\beta_i}\chi(\ell_1)-\overset{k,m}{\Theta}\mathfrak{J}^{\delta_i,\tau_i}_{(\frac{\ell_1+\ell_2}{2})^-;\mu,\beta_i}\chi\Upsilon(\ell_1)]. \qquad (2)
\end{aligned}
$$

By similar arguments, it can be verified that

$$
I_2 = \frac{(m+1)^{1-\frac{\mu}{k}}}{k}[\Upsilon\Big(\frac{\ell_1+\ell_2}{2}\Big)\overset{k,m}{\Theta}\mathfrak{J}^{\delta_i,\tau_i}_{(\frac{\ell_1+\ell_2}{2})^+;\mu,\beta_i}\chi(\ell_2)-\overset{k,m}{\Theta}\mathfrak{J}^{\delta_i,\tau_i}_{(\frac{\ell_1+\ell_2}{2})^+;\mu,\beta_i}\chi\Upsilon(\ell_2)]. \qquad (3)
$$

Hence, by adding (2) and (3) we obtain,

$$
\begin{aligned}
&\frac{k}{(m+1)^{1-\frac{\mu}{k}}}\int_{\ell_1}^{\ell_2}\kappa(\nu)\Upsilon'(\nu)d\nu \\
&= \Upsilon\Big(\frac{\ell_1+\ell_2}{2}\Big)\Big[\overset{k,m}{\Theta}\mathfrak{J}^{\delta_i,\tau_i}_{(\frac{\ell_1+\ell_2}{2})^+;\mu,\beta_i}\chi(\ell_2)+\overset{k,m}{\Theta}\mathfrak{J}^{\delta_i,\tau_i}_{(\frac{\ell_1+\ell_2}{2})^-;\mu,\beta_i}\chi(\ell_1)\Big] \\
&- \Big[\overset{k,m}{\Theta}\mathfrak{J}^{\delta_i,\tau_i}_{(\frac{\ell_1+\ell_2}{2})^+;\mu,\beta_i}\chi\Upsilon(\ell_2)+\overset{k,m}{\Theta}\mathfrak{J}^{\delta_i,\tau_i}_{(\frac{\ell_1+\ell_2}{2})^-;\mu,\beta_i}\chi\Upsilon(\ell_1)\Big].
\end{aligned}
$$

Hence the required result is proved. □

Corollary 1. *If we replace* $\Theta(u)=u$, $m=0$, $\delta_i=0$, $\kappa_i=0, \forall i$ *and* $k=1$ *in Lemma 1 then we have ([28], Lemma 4),*

$$\begin{aligned}
&\Upsilon\Big(\frac{\ell_1+\ell_2}{2}\Big)\Big[\mathfrak{J}^{\mu}_{(\frac{\ell_1+\ell_2}{2})^+}\chi(\ell_2)+\mathfrak{J}^{\mu}_{(\frac{\ell_1+\ell_2}{2})^-}\chi(\ell_1)\Big]\\
&-\Big[\mathfrak{J}^{\mu}_{(\frac{\ell_1+\ell_2}{2})^+}\chi\Upsilon(\ell_2)+\mathfrak{J}^{\mu}_{(\frac{\ell_1+\ell_2}{2})^-}\chi\Upsilon(\ell_1)\Big]\\
&=\frac{1}{\Gamma(\mu)}\int_{\ell_1}^{\ell_2}\kappa(\nu)\Upsilon'(\nu)d\nu,
\end{aligned}$$

where

$$\kappa(t_1)=\begin{cases}\int_{\ell_1}^{t_1}\frac{\chi(u)du}{(u-\ell_1)^{1-\mu}}, & t_1\in[\ell_1,\frac{\ell_1+\ell_2}{2}],\\ \int_{\ell_2}^{t_1}\frac{\chi(u)du}{(\ell_2-u)^{1-\mu}}, & t_1\in[\frac{\ell_1+\ell_2}{2},\ell_2].\end{cases}$$

Theorem 1. *For $k>0$, $m\in\Re/\{-1\}$, and $Re(\mu)>0$, $Re(\tau)>0$, $Re(\delta)>0$, $Re(\beta)>0$ are complex parameters, Θ be an increasing function and Υ be a differentiable on (ℓ_1,ℓ_2) with $\ell<\ell_2$ and $\chi:[\ell_1,\ell_2]\mapsto\Re$ be bounded. If $\Upsilon',\chi\in L[\ell_1,\ell_2]$, then the below expression holds.*

$$\begin{aligned}
&F\Big(\frac{\ell_1+\ell_2}{2}\Big)\Big[{}^{k,m}_{\Theta}\mathfrak{J}^{\delta_i,\tau_i}_{(\frac{\ell_1+\ell_2}{2})^+;\mu,\beta_i}\chi(\ell_2)+{}^{k,m}_{\Theta}\mathfrak{J}^{\delta_i,\tau_i}_{(\frac{\ell_1+\ell_2}{2})^-;\mu,\beta_i}\chi(\ell_1)\Big]\\
&\le\Upsilon\Big(\frac{\ell_1+\ell_2}{2}\Big)\Big[{}^{k,m}_{\Theta}\mathfrak{J}^{\delta_i,\tau_i}_{(\frac{\ell_1+\ell_2}{2})^+;\mu,\beta_i}\chi F(\ell_2)+{}^{k,m}_{\Theta}\mathfrak{J}^{\delta_i,\tau_i}_{(\frac{\ell_1+\ell_2}{2})^-;\mu,\beta_i}\chi F(\ell_1)\Big]\\
&\le\frac{F(\ell_1)+F(\ell_2)}{2}\Big[{}^{k,m}_{\Theta}\mathfrak{J}^{\delta_i,\tau_i}_{(\frac{\ell_1+\ell_2}{2})^+;\mu,\beta_i}\chi(\ell_2)+{}^{k,m}_{\Theta}\mathfrak{J}^{\delta_i,\tau_i}_{(\frac{\ell_1+\ell_2}{2})^-;\mu,\beta_i}\chi(\ell_1)\Big],
\end{aligned}\tag{4}$$

where $F(\nu)=\Upsilon(\nu)+\tilde{\Upsilon}(\nu)$, and $\tilde{\Upsilon}(\nu)=\Upsilon(\ell_1+\ell_2-\nu)$.

Proof. As we know that Υ is Cf for all $x_1,y_1\in[\ell_1,\ell_2]$, that is

$$\Upsilon(\frac{x_1+y_1}{2})\le\frac{\Upsilon(x_1)+\Upsilon(y_1)}{2},$$

which implies, for $\nu\in[0,1]$ and substituting $x_1=\frac{\nu}{2}\ell_1+\frac{2-\nu}{2}\ell_2$, $y_1=\frac{\nu}{2}\ell_2+\frac{2-\nu}{2}\ell_1$

$$2\Upsilon(\frac{\ell_1+\ell_2}{2})\le\Upsilon(\frac{\nu}{2}\ell_1+\frac{2-\nu}{2}\ell_2)+\Upsilon(\frac{\nu}{2}\ell_2+\frac{2-\nu}{2}\ell_1).$$

By multiplying

$$\begin{aligned}
&\frac{(m+1)^{\frac{\mu}{k}-1}(\ell_2-\ell_1)}{2k}\\
&\times\frac{\xi^{\delta_i}_{k,\mu,\beta_i}\Big(\tau_1(\Theta^{m+1}(\ell_2)-\Theta^{m+1}(\frac{\nu}{2}\ell_1+\frac{2-\nu}{2}\ell_2))^{\frac{\beta_1}{k}},\ldots,\tau_n(\Theta^{m+1}(\ell_2)-\Theta^{m+1}(\frac{\nu}{2}\ell_1+\frac{2-\nu}{2}\ell_2))^{\frac{\beta_n}{k}}\Big)}{(\Theta^{m+1}(\ell_2)-\Theta^{m+1}(\frac{\nu}{2}\ell_1+\frac{2-\nu}{2}\ell_2))^{\frac{\mu}{k}-1}}\\
&\times\Theta^m(\frac{\nu}{2}\ell_1+\frac{2-\nu}{2}\ell_2)\Theta'(\frac{\nu}{2}\ell_1+\frac{2-\nu}{2}\ell_2)\chi(\frac{\nu}{2}\ell_1+\frac{2-\nu}{2}\ell_2),
\end{aligned}$$

and after simplifying and taking integration on $[0,1]$ with respect to ν, we can have

$$
\begin{aligned}
&\frac{(m+1)^{\frac{\mu}{k}-1}(\ell_2-\ell_1)}{2k}F\big(\frac{\ell_1+\ell_2}{2}\big)\\
&\times\int_0^1\frac{\xi_{k,\mu,\beta_i}^{\delta_i}\Big(\tau_1(\Theta^{m+1}(\ell_2)-\Theta^{m+1}(\frac{\nu}{2}\ell_1+\frac{2-\nu}{2}\ell_2))^{\frac{\beta_1}{k}},\ldots,\tau_n(\Theta^{m+1}(\ell_2)-\Theta^{m+1}(\frac{\nu}{2}\ell_1+\frac{2-\nu}{2}\ell_2))^{\frac{\beta_n}{k}}\Big)}{(\Theta^{m+1}(\ell_2)-\Theta^{m+1}(\frac{\nu}{2}\ell_1+\frac{2-\nu}{2}\ell_2))^{\frac{\mu}{k}-1}}\\
&\times\Theta^m\big(\frac{\nu}{2}\ell_1+\frac{2-\nu}{2}\ell_2\big)\Theta'\big(\frac{\nu}{2}\ell_1+\frac{2-\nu}{2}\ell_2\big)\chi\big(\frac{\nu}{2}\ell_1+\frac{2-\nu}{2}\ell_2\big)d\nu\\
&\leq\frac{(m+1)^{\frac{\mu}{k}-1}(\ell_2-\ell_1)}{2k}\\
&\times\int_0^1\frac{\xi_{k,\mu,\beta_i}^{\delta_i}\Big(\tau_1(\Theta^{m+1}(\ell_2)-\Theta^{m+1}(\frac{\nu}{2}\ell_1+\frac{2-\nu}{2}\ell_2))^{\frac{\beta_1}{k}},\ldots,\tau_n(\Theta^{m+1}(\ell_2)-\Theta^{m+1}(\frac{\nu}{2}\ell_1+\frac{2-\nu}{2}\ell_2))^{\frac{\beta_n}{k}}\Big)}{(\Theta^{m+1}(\ell_2)-\Theta^{m+1}(\frac{\nu}{2}\ell_1+\frac{2-\nu}{2}\ell_2))^{\frac{\mu}{k}-1}}\\
&\times\Theta^m\big(\frac{\nu}{2}\ell_1+\frac{2-\nu}{2}\ell_2\big)\Theta'\big(\frac{\nu}{2}\ell_1+\frac{2-\nu}{2}\ell_2\big)\chi\big(\frac{\nu}{2}\ell_1+\frac{2-\nu}{2}\ell_2\big)\Upsilon\big(\frac{\nu}{2}\ell_1+\frac{2-\nu}{2}\ell_2\big)d\nu\\
&+\frac{(m+1)^{\frac{\mu}{k}-1}(\ell_2-\ell_1)}{2k}\\
&\times\int_0^1\frac{\xi_{k,\mu,\beta_i}^{\delta_i}\Big(\tau_1(\Theta^{m+1}(\ell_2)-\Theta^{m+1}(\frac{\nu}{2}\ell_1+\frac{2-\nu}{2}\ell_2))^{\frac{\beta_1}{k}},\ldots,\tau_n(\Theta^{m+1}(\ell_2)-\Theta^{m+1}(\frac{\nu}{2}\ell_1+\frac{2-\nu}{2}\ell_2))^{\frac{\beta_n}{k}}\Big)}{(\Theta^{m+1}(\ell_2)-\Theta^{m+1}(\frac{\nu}{2}\ell_1+\frac{2-\nu}{2}\ell_2))^{\frac{\mu}{k}-1}}\\
&\times\Theta^m\big(\frac{\nu}{2}\ell_1+\frac{2-\nu}{2}\ell_2\big)\Theta'\big(\frac{\nu}{2}\ell_1+\frac{2-\nu}{2}\ell_2\big)\chi\big(\frac{\nu}{2}\ell_1+\frac{2-\nu}{2}\ell_2\big)\Upsilon\big(\frac{\nu}{2}\ell_1+\frac{2-\nu}{2}\ell_2\big)d\nu.
\end{aligned}
$$

By replacing $u=\frac{\nu}{2}\ell_1+\frac{2-\nu}{2}\ell_2$, we arrive at

$$
\begin{aligned}
&F\Big(\frac{\ell_1+\ell_2}{2}\Big)\big[{}_{\Theta}^{k,m}\mathfrak{J}_{(\frac{\ell_1+\ell_2}{2})^+;\mu,\beta_i}^{\delta_i,\tau_i}\chi(\ell_2)\big]\\
&\leq\Upsilon\Big(\frac{\ell_1+\ell_2}{2}\Big)\big[{}_{\Theta}^{k,m}\mathfrak{J}_{(\frac{\ell_1+\ell_2}{2})^+;\mu,\beta_i}^{\delta_i,\tau_i}\chi\Upsilon(\ell_2)+{}_{\Theta}^{k,m}\mathfrak{J}_{(\frac{\ell_1+\ell_2}{2})^+;\mu,\beta_i}^{\delta_i,\tau_i}\chi\tilde{\Upsilon}(\ell_2)\big],
\end{aligned}
$$

that is

$$
F\Big(\frac{\ell_1+\ell_2}{2}\Big)\big[{}_{\Theta}^{k,m}\mathfrak{J}_{(\frac{\ell_1+\ell_2}{2})^+;\mu,\beta_i}^{\delta_i,\tau_i}\chi(\ell_2)\big]\leq\Upsilon\Big(\frac{\ell_1+\ell_2}{2}\Big)\big[{}_{\Theta}^{k,m}\mathfrak{J}_{(\frac{\ell_1+\ell_2}{2})^+;\mu,\beta_i}^{\delta_i,\tau_i}\chi F(\ell_2)\big].\tag{5}
$$

Continuing in the same way if we multiply the below term on both sides

$$
\begin{aligned}
&\frac{(m+1)^{\frac{\mu}{k}-1}(\ell_2-\ell_1)}{2k}\\
&\times\frac{\xi_{k,\mu,\beta_i}^{\delta_i}\Big(\tau_1(\Theta^{m+1}(\frac{\nu}{2}\ell_1+\frac{2-\nu}{2}\ell_2)-\Theta^{m+1}(\ell_1))^{\frac{\beta_1}{k}},\ldots,\tau_n(\Theta^{m+1}(\frac{\nu}{2}\ell_1+\frac{2-\nu}{2}\ell_2)-\Theta^{m+1}(\ell_1))^{\frac{\beta_n}{k}}\Big)}{(\Theta^{m+1}(\frac{\nu}{2}\ell_1+\frac{2-\nu}{2}\ell_2)-\Theta^{m+1}(\ell_1))^{\frac{\mu}{k}-1}}\\
&\times\Theta^m\big(\frac{\nu}{2}\ell_1+\frac{2-\nu}{2}\ell_2\big)\Theta'\big(\frac{\nu}{2}\ell_1+\frac{2-\nu}{2}\ell_2\big)\chi\big(\frac{\nu}{2}\ell_1+\frac{2-\nu}{2}\ell_2\big),
\end{aligned}
$$

then after simplifying and taking integration on $[0,1]$ with respect to ν, we arrive at

$$
F\Big(\frac{\ell_1+\ell_2}{2}\Big)\big[{}_{\Theta}^{k,m}\mathfrak{J}_{(\frac{\ell_1+\ell_2}{2})^-;\mu,\beta_i}^{\delta_i,\tau_i}\chi(\ell_1)\big]\leq\Upsilon\Big(\frac{\ell_1+\ell_2}{2}\Big)\big[{}_{\Theta}^{k,m}\mathfrak{J}_{(\frac{\ell_1+\ell_2}{2})^-;\mu,\beta_i}^{\delta_i,\tau_i}\chi F(\ell_1)\big].\tag{6}
$$

Adding (5) and (6), we arrive at

$$F\Big(\frac{\ell_1+\ell_2}{2}\Big)\big[{}^{k,m}_{\Theta}\mathfrak{J}^{\delta_i,\tau_i}_{(\frac{\ell_1+\ell_2}{2})^+;\mu,\beta_i}\chi(\ell_2)+{}^{k,m}_{\Theta}\mathfrak{J}^{\delta_i,\tau_i}_{(\frac{\ell_1+\ell_2}{2})^-;\mu,\beta_i}\chi(\ell_1)\big]$$
$$\leq \Upsilon\Big(\frac{\ell_1+\ell_2}{2}\Big)\big[{}^{k,m}_{\Theta}\mathfrak{J}^{\delta_i,\tau_i}_{(\frac{\ell_1+\ell_2}{2})^+;\mu,\beta_i}\chi F(\ell_2)+{}^{k,m}_{\Theta}\mathfrak{J}^{\delta_i,\tau_i}_{(\frac{\ell_1+\ell_2}{2})^-;\mu,\beta_i}\chi F(\ell_1)\big]. \tag{7}$$

This shows the first half of required inequality. Now we are going to prove second half of inequality. Since, we know that Υ is Cf on $[\ell_1,\ell_2]$, after implementation, we reach

$$\Upsilon(\frac{\nu}{2}\ell_1+\frac{2-\nu}{2}\ell_2)+\Upsilon(\frac{2-\nu}{2}\tau_1+\frac{\nu}{2}\tau_2)\leq\Upsilon(\tau_1)+\Upsilon(\tau_2).$$

Continuing in the same way if we multiply the below term on both sides as in first part of inequality

$$\frac{(m+1)^{\frac{\mu}{k}-1}(\ell_2-\ell_1)}{2k}$$
$$\times\frac{\xi^{\delta_i}_{k,\mu,\beta_i}\Big(\tau_1(\Theta^{m+1}(\ell_2)-\Theta^{m+1}(\frac{\nu}{2}\ell_1+\frac{2-\nu}{2}\ell_2))^{\frac{\beta_1}{k}},\ldots,\tau_n(\Theta^{m+1}(\ell_2)-\Theta^{m+1}(\frac{\nu}{2}\ell_1+\frac{2-\nu}{2}\ell_2))^{\frac{\beta_n}{k}}\Big)}{(\Theta^{m+1}(\ell_2)-\Theta^{m+1}(\frac{\nu}{2}\ell_1+\frac{2-\nu}{2}\ell_2))^{\frac{\mu}{k}-1}}$$
$$\times\Theta^m(\frac{\nu}{2}\ell_1+\frac{2-\nu}{2}\ell_2)\Theta'(\frac{\nu}{2}\ell_1+\frac{2-\nu}{2}\ell_2)\chi(\frac{\nu}{2}\ell_1+\frac{2-\nu}{2}\ell_2),$$

then after simplifying and integrating over $[0,1]$ with respect to ν, we arrive at

$$\frac{(m+1)^{\frac{\mu}{k}-1}(\ell_2-\ell_1)}{2k}F(\frac{\ell_1+\ell_2}{2})$$
$$\times\int_0^1\frac{\xi^{\delta_i}_{k,\mu,\beta_i}\Big(\tau_1(\Theta^{m+1}(\ell_2)-\Theta^{m+1}(\frac{\nu}{2}\ell_1+\frac{2-\nu}{2}\ell_2))^{\frac{\beta_1}{k}},\ldots,\tau_n(\Theta^{m+1}(\ell_2)-\Theta^{m+1}(\frac{\nu}{2}\ell_1+\frac{2-\nu}{2}\ell_2))^{\frac{\beta_n}{k}}\Big)}{(\Theta^{m+1}(+\ell_2)-\Theta^{m+1}(\frac{\nu}{2}\ell_1+\frac{2-\nu}{2}\ell_2))^{\frac{\mu}{k}-1}}$$
$$\times\Theta^m(\frac{\nu}{2}\ell_1+\frac{2-\nu}{2}\ell_2)\Theta'(\frac{\nu}{2}\ell_1+\frac{2-\nu}{2}\ell_2)\chi(\frac{\nu}{2}\ell_1+\frac{2-\nu}{2}\ell_2)d\nu$$
$$\leq\frac{(m+1)^{\frac{\mu}{k}-1}(\ell_2-\ell_1)}{2k}$$
$$\times\int_0^1\frac{\xi^{\delta_i}_{k,\mu,\beta_i}\Big(\tau_1(\Theta^{m+1}(\ell_2)-\Theta^{m+1}(\frac{\nu}{2}\ell_1+\frac{2-\nu}{2}\ell_2))^{\frac{\beta_1}{k}},\ldots,\tau_n(\Theta^{m+1}(\ell_2)-\Theta^{m+1}(\frac{\nu}{2}\ell_1+\frac{2-\nu}{2}\ell_2))^{\frac{\beta_n}{k}}\Big)}{(\Theta^{m+1}(\ell_2)-\Theta^{m+1}(\frac{\nu}{2}\ell_1+\frac{2-\nu}{2}\ell_2))^{\frac{\mu}{k}-1}}$$
$$\times\Theta^m(\frac{\nu}{2}\ell_1+\frac{2-\nu}{2}\ell_2)\Theta'(\frac{\nu}{2}\ell_1+\frac{2-\nu}{2}\ell_2)\chi(\frac{\nu}{2}\ell_1+\frac{2-\nu}{2}\ell_2)\Upsilon(\frac{\nu}{2}\ell_1+\frac{2-\nu}{2}\ell_2)d\nu$$
$$+\frac{(m+1)^{\frac{\mu}{k}-1}(\ell_2-\ell_1)}{2k}$$
$$\times\int_0^1\frac{\xi^{\delta_i}_{k,\mu,\beta_i}\Big(\tau_1(\Theta^{m+1}(\ell_2)-\Theta^{m+1}(\frac{\nu}{2}\ell_1+\frac{2-\nu}{2}\ell_2))^{\frac{\beta_1}{k}},\ldots,\tau_n(\Theta^{m+1}(\ell_2)-\Theta^{m+1}(\frac{\nu}{2}\ell_1+\frac{2-\nu}{2}\ell_2))^{\frac{\beta_n}{k}}\Big)}{(\Theta^{m+1}(\ell_2)-\Theta^{m+1}(\frac{\nu}{2}\ell_1+\frac{2-\nu}{2}\ell_2))^{\frac{\mu}{k}-1}}$$
$$\times\Theta^m(\frac{\nu}{2}\ell_1+\frac{2-\nu}{2}\ell_2)\Theta'(\frac{\nu}{2}\ell_1+\frac{2-\nu}{2}\ell_2)\chi(\frac{\nu}{2}\ell_1+\frac{2-\nu}{2}\ell_2)\Upsilon(\frac{\nu}{2}\ell_1+\frac{2-\nu}{2}\ell_2)d\nu.$$

By replacing $u=\frac{\nu}{2}\ell_1+\frac{2-\nu}{2}\ell_2$, we obtain

$$\Upsilon\Big(\frac{\ell_1+\ell_2}{2}\Big)\big[{}^{k,m}_{\Theta}\mathfrak{J}^{\delta_i,\tau_i}_{(\frac{\ell_1+\ell_2}{2})^+;\mu,\beta_i}\chi\Upsilon(\ell_2)+{}^{k,m}_{\Theta}\mathfrak{J}^{\delta_i,\tau_i}_{(\frac{\ell_1+\ell_2}{2})^+;\mu,\beta_i}\chi\tilde{\Upsilon}(\ell_2)\big]$$
$$\leq[\Upsilon(\ell_1)+\Upsilon(\ell_2)]\Upsilon\Big(\frac{\ell_1+\ell_2}{2}\Big)\big[{}^{k,m}_{\Theta}\mathfrak{J}^{\delta_i,\tau_i}_{(\frac{\ell_1+\ell_2}{2})^+;\mu,\beta_i}\chi(\ell_2)\big].$$

This implies

$$\Upsilon\Big(\frac{\ell_1+\ell_2}{2}\Big)\,{}^{k,m}_{\Theta}\mathfrak{J}^{\delta_i,\tau_i}_{(\frac{\ell_1+\ell_2}{2})^+;\mu,\beta_i}\chi F(\ell_2)] \le \frac{F(\ell_1)+F(\ell_2)}{2}\,{}^{k,m}_{\Theta}\mathfrak{J}^{\delta_i,\tau_i}_{(\frac{\ell_1+\ell_2}{2})^+;\mu,\beta_i}\chi(\ell_2)]. \tag{8}$$

Now, by multiplying on both sides of the first half of the inequality

$$\begin{aligned}
&\frac{(m+1)^{\frac{\mu}{k}-1}(\ell_2-\ell_1)}{2k}\\
&\times\frac{\xi^{\delta_i}_{k,\mu,\beta_i}\Big(\tau_1(\Theta^{m+1}(\frac{\nu}{2}\ell_1+\frac{2-\nu}{2}\ell_2)-\Theta^{m+1}(\tau_1))^{\frac{\beta_1}{k}},\ldots,\tau_n(\Theta^{m+1}(\frac{\nu}{2}\ell_1+\frac{2-\nu}{2}\ell_2)-\Theta^{m+1}(\tau_1))^{\frac{\beta_n}{k}}\Big)}{(\Theta^{m+1}(\frac{\nu}{2}\ell_1+\frac{2-\nu}{2}\ell_2)-\Theta^{m+1}(\tau_1))^{\frac{\mu}{k}-1}}\\
&\times\Theta^m(\frac{\nu}{2}\ell_1+\frac{2-\nu}{2}\ell_2)\Theta'(\frac{\nu}{2}\ell_1+\frac{2-\nu}{2}\ell_2)\chi(\frac{\nu}{2}\ell_1+\frac{2-\nu}{2}\ell_2),
\end{aligned}$$

then, after simplifying and integrating over $[0,1]$ with respect to ν, we obtain

$$\Upsilon\Big(\frac{\ell_1+\ell_2}{2}\Big)\,{}^{k,m}_{\Theta}\mathfrak{J}^{\delta_i,\tau_i}_{(\frac{\ell_1+\ell_2}{2})^-;\mu,\beta_i}\chi F(\ell_1)] \le \frac{F(\ell_1)+F(\ell_2)}{2}\,{}^{k,m}_{\Theta}\mathfrak{J}^{\delta_i,\tau_i}_{(\frac{\ell_1+\ell_2}{2})^-;\mu,\beta_i}\chi(\ell_1)]. \tag{9}$$

Adding (8) and (9), we obtain

$$\begin{aligned}
&\Upsilon\Big(\frac{\ell_1+\ell_2}{2}\Big)\,{}^{k,m}_{\Theta}\mathfrak{J}^{\delta_i,\tau_i}_{(\frac{\ell_1+\ell_2}{2})^+;\mu,\beta_i}\chi F(\ell_2)+{}^{k,m}_{\Theta}\mathfrak{J}^{\delta_i,\tau_i}_{(\frac{\ell_1+\ell_2}{2})^-;\mu,\beta_i}\chi F(\ell_1)]\\
&\le\frac{F(\ell_1)+F(\ell_2)}{2}\,{}^{k,m}_{\Theta}\mathfrak{J}^{\delta_i,\tau_i}_{(\frac{\ell_1+\ell_2}{2})^+;\mu,\beta_i}\chi(\ell_2)+{}^{k,m}_{\Theta}\mathfrak{J}^{\delta_i,\tau_i}_{(\frac{\ell_1+\ell_2}{2})^-;\mu,\beta_i}\chi(\ell_1)].
\end{aligned}\tag{10}$$

Hence, by adding (7) and (10), we get our desired inequality. □

Example 1. *Assume that* $\chi(x) = (\Theta^{m+1}(\ell_2)-\Theta^{m+1}(x))^{\frac{\eta}{k}}$, *then the left side of above inequality* (4) *becomes*

$$\begin{aligned}
&\Big({}^{k,m}_{\Theta}\mathfrak{J}^{\delta_i,\tau_i}_{(\frac{\ell_1+\ell_2}{2})^+;\mu,\beta_i}\Big)\Big((\Theta^{m+1}(\ell_2)-\Theta^{m+1}(x))^{\frac{\eta}{k}}\Big)\\
&=\frac{(m+1)^{\frac{\mu}{k}-1}}{k}\Sigma_{n=0}^{\infty}\frac{(\delta_i)_{\kappa_i,k}(\tau_i)^{\kappa_i}}{\Gamma_k(\mu+\Sigma_{i=1}^{n}(\beta_i\kappa_i))}\\
&\times\int_{\frac{\ell_1+\ell_2}{2}}^{\ell_2}\Big(\Theta^{m+1}(\ell_2)-\Theta^{m+1}(x)\Big)^{\frac{\mu+\Sigma_{i=1}^{n}(\beta_i\kappa_i)+\eta}{k}-1}\Theta^m(x)\Theta'(x)dx\\
&=\frac{(m+1)^{-\frac{\mu}{k}}}{k}\Sigma_{n=0}^{\infty}\frac{(\delta_i)_{\kappa_i,k}(\tau_i)^{\kappa_i}}{\Gamma_k(\mu+\Sigma_{i=1}^{n}(\beta_i\kappa_i))}\\
&\times\int_{\frac{\ell_1+\ell_2}{2}}^{\ell_2}\Big(\Theta^{m+1}(\ell_2)-\Theta^{m+1}(x)\Big)^{\frac{\mu+\Sigma_{i=1}^{n}(\beta_i\kappa_i)+\eta}{k}-1}\Theta^m(x)\Theta'(x)dx\\
&=\frac{(m+1)^{-\frac{\mu}{k}}}{k}\Sigma_{n=0}^{\infty}\frac{(\delta_i)_{\kappa_i,k}(\tau_i)^{\kappa_i}}{\Gamma_k(\mu+\Sigma_{i=1}^{n}(\beta_i\kappa_i))}\frac{\Big(\Theta^{m+1}(\ell_2)-\Theta^{m+1}(\frac{\ell_1+\ell_2}{2})\Big)^{\frac{\mu+\Sigma_{i=1}^{n}(\beta_i\kappa_i)+\eta}{k}}}{\frac{\mu+\Sigma_{i=1}^{n}(\beta_i\kappa_i)+\eta}{k}}.
\end{aligned}\tag{11}$$

Similarly, we have

$$\left(\begin{smallmatrix}k,m\\ \Theta\end{smallmatrix}\mathfrak{J}^{\delta_i,\tau_i}_{(\frac{\ell_1+\ell_2}{2})^-;\mu,\beta_i}\right)\left(\Theta^{m+1}(x)-\Theta^{m+1}(\ell_1))^{\frac{\eta}{k}}\right)$$

$$=\frac{(m+1)^{-\frac{\mu}{k}}}{k}\Sigma_{n=0}^{\infty}\frac{(\delta_i)_{\kappa_i,k}(\tau_i)^{\kappa_i}}{\Gamma_k(\mu+\Sigma_{i=1}^{n}(\beta_i\kappa_i)}\frac{\left(\Theta^{m+1}(\frac{\ell_1+\ell_2}{2})-\Theta^{m+1}(\ell_1)\right)^{\frac{\mu+\Sigma_{i=1}^{n}(\beta_i\kappa_i)+\eta}{k}}}{\frac{\mu+\Sigma_{i=1}^{n}(\beta_i\kappa_i)+\eta}{k}}. \tag{12}$$

If we choose $\chi(x)=(\Theta^{m+1}(\ell_2)-\Theta^{m+1}(x))^{\frac{\eta}{k}}$ *and* $F(x)=2\Theta^{m+1}(x)$ *then the middle term of above inequality is*

$$\left(\begin{smallmatrix}k,m\\ \Theta\end{smallmatrix}\mathfrak{J}^{\delta_i,\tau_i}_{(\frac{\ell_1+\ell_2}{2})^+;\mu,\beta_i}\right)2\left((\Theta^{m+1}(x)-\Theta^{m+1}(\ell_1))^{\frac{\eta}{k}}\right)\Theta^{m+1}(x)$$
$$=\frac{2(m+1)^{\frac{\mu}{k}-1}}{k}\Sigma_{n=0}^{\infty}\frac{(\delta_i)_{\kappa_i,k}(\tau_i)^{\kappa_i}}{\Gamma_k(\mu+\Sigma_{i=1}^{n}(\beta_i\kappa_i))}$$
$$\times\int_{\frac{\ell_1+\ell_2}{2}}^{\ell_2}\left(\Theta^{m+1}(\ell_2)-\Theta^{m+1}(x)\right)^{\frac{\mu+\Sigma_{i=1}^{n}(\beta_i\kappa_i)+\eta}{k}-1}\Theta^{m+1}(x)\Theta^{m}(x)\Theta'(x)dx$$
$$=\frac{2(m+1)^{\frac{\mu}{k}-1}}{k}\Sigma_{n=0}^{\infty}\frac{(\delta_i)_{\kappa_i,k}(\tau_i)^{\kappa_i}}{\Gamma_k(\mu+\Sigma_{i=1}^{n}(\beta_i\kappa_i))}$$
$$\times\left(\frac{\left(\Theta^{m+1}(\ell_2)-\Theta^{m+1}(\frac{\ell_1+\ell_2}{2})\right)^{\frac{\mu+\Sigma_{i=1}^{n}(\beta_i\kappa_i)+\eta}{k}}}{\frac{\mu+\Sigma_{i=1}^{n}(\beta_i\kappa_i)+\eta}{k}}\right.$$
$$\left.-\frac{m+1}{\frac{\mu+\Sigma_{i=1}^{n}(\beta_i\kappa_i)+\eta}{k}}\frac{\left(\Theta^{m+1}(\ell_2)-\Theta^{m+1}(\frac{\ell_1+\ell_2}{2})\right)^{\frac{\mu+\Sigma_{i=1}^{n}(\beta_i\kappa_i)+\eta}{k}+1}}{\frac{\mu+\Sigma_{i=1}^{n}(\beta_i\kappa_i)+\eta}{k}+1}\right) \tag{13}$$

Also

$$\left(\begin{smallmatrix}k,m\\ \Theta\end{smallmatrix}\mathfrak{J}^{\delta_i,\tau_i}_{(\frac{\ell_1+\ell_2}{2})^-;\mu,\beta_i}\right)2\left((\Theta^{m+1}(x)-\Theta^{m+1}(\ell_1))^{\frac{\eta}{k}}\right)\Theta^{m+1}(x)$$
$$=\frac{2(m+1)^{\frac{\mu}{k}-1}}{k}\Sigma_{n=0}^{\infty}\frac{(\delta_i)_{\kappa_i,k}(\tau_i)^{\kappa_i}}{\Gamma_k(\mu+\Sigma_{i=1}^{n}(\beta_i\kappa_i))}$$
$$\times\left(\frac{\left(\Theta^{m+1}(\frac{\ell_1+\ell_2}{2})-\Theta^{m+1}(\ell_1)\right)^{\frac{\mu+\Sigma_{i=1}^{n}(\beta_i\kappa_i)+\eta}{k}}}{\frac{\mu+\Sigma_{i=1}^{n}(\beta_i\kappa_i)+\eta}{k}}\right.$$
$$\left.-\frac{m+1}{\frac{\mu+\Sigma_{i=1}^{n}(\beta_i\kappa_i)+\eta}{k}}\frac{\left(\Theta^{m+1}(\frac{\ell_1+\ell_2}{2})-\Theta^{m+1}(\ell_1)\right)^{\frac{\mu+\Sigma_{i=1}^{n}(\beta_i\kappa_i)+\eta}{k}+1}}{\frac{\mu+\Sigma_{i=1}^{n}(\beta_i\kappa_i)+\eta}{k}+1}\right) \tag{14}$$

So we have

$$
\begin{aligned}
&2\Theta^{m+1}\left(\frac{\ell_1+\ell_2}{2}\right)\Bigg[\frac{(m+1)^{-\frac{\mu}{k}}}{k}\Sigma_{n=0}^{\infty}\frac{(\delta_i)_{\kappa_i,k}(\tau_i)^{\kappa_i}}{\Gamma_k(\mu+\Sigma_{i=1}^{n}(\beta_i\kappa_i))}\frac{\left(\Theta^{m+1}(\ell_2)-\Theta^{m+1}\left(\frac{\ell_1+\ell_2}{2}\right)\right)^{\frac{\mu+\Sigma_{i=1}^{n}(\beta_i\kappa_i)+\eta}{k}}}{\frac{\mu+\Sigma_{i=1}^{n}(\beta_i\kappa_i)+\eta}{k}}\\
&+\frac{(m+1)^{-\frac{\mu}{k}}}{k}\Sigma_{n=0}^{\infty}\frac{(\delta_i)_{\kappa_i,k}(\tau_i)^{\kappa_i}}{\Gamma_k(\mu+\Sigma_{i=1}^{n}(\beta_i\kappa_i))}\frac{\left(\Theta^{m+1}\left(\frac{\ell_1+\ell_2}{2}\right)-\Theta^{m+1}(\ell_1)\right)^{\frac{\mu+\Sigma_{i=1}^{n}(\beta_i\kappa_i)+\eta}{k}}}{\frac{\mu+\Sigma_{i=1}^{n}(\beta_i\kappa_i)+\eta}{k}}\Bigg]\\
&\leq\Theta^{m+1}\left(\frac{\ell_1+\ell_2}{2}\right)\Bigg[\frac{2(m+1)^{\frac{\mu}{k}-1}}{k}\Sigma_{n=0}^{\infty}\frac{(\delta_i)_{\kappa_i,k}(\tau_i)^{\kappa_i}}{\Gamma_k(\mu+\Sigma_{i=1}^{n}(\beta_i\kappa_i))}\\
&\times\Bigg(\frac{\left(\Theta^{m+1}(\ell_2)-\Theta^{m+1}\left(\frac{\ell_1+\ell_2}{2}\right)\right)^{\frac{\mu+\Sigma_{i=1}^{n}(\beta_i\kappa_i)+\eta}{k}}}{\frac{\mu+\Sigma_{i=1}^{n}(\beta_i\kappa_i)+\eta}{k}}\\
&-\frac{m+1}{\frac{\mu+\Sigma_{i=1}^{n}(\beta_i\kappa_i)+\eta}{k}}\frac{\left(\Theta^{m+1}(\ell_2)-\Theta^{m+1}\left(\frac{\ell_1+\ell_2}{2}\right)\right)^{\frac{\mu+\Sigma_{i=1}^{n}(\beta_i\kappa_i)+\eta}{k}+1}}{\frac{\mu+\Sigma_{i=1}^{n}(\beta_i\kappa_i)+\eta}{k}+1}\Bigg)\\
&+\frac{2(m+1)^{\frac{\mu}{k}-1}}{k}\Sigma_{n=0}^{\infty}\frac{(\delta_i)_{\kappa_i,k}(\tau_i)^{\kappa_i}}{\Gamma_k(\mu+\Sigma_{i=1}^{n}(\beta_i\kappa_i))}\\
&\times\Theta^{m+1}\left(\frac{\ell_1+\ell_2}{2}\right)\Bigg(\frac{\left(\Theta^{m+1}\left(\frac{\ell_1+\ell_2}{2}\right)-\Theta^{m+1}(\ell_1)\right)^{\frac{\mu+\Sigma_{i=1}^{n}(\beta_i\kappa_i)+\eta}{k}}}{\frac{\mu+\Sigma_{i=1}^{n}(\beta_i\kappa_i)+\eta}{k}}\\
&-\frac{m+1}{\frac{\mu+\Sigma_{i=1}^{n}(\beta_i\kappa_i)+\eta}{k}}\frac{\left(\Theta^{m+1}\left(\frac{\ell_1+\ell_2}{2}\right)-\Theta^{m+1}(\ell_1)\right)^{\frac{\mu+\Sigma_{i=1}^{n}(\beta_i\kappa_i)+\eta}{k}+1}}{\frac{\mu+\Sigma_{i=1}^{n}(\beta_i\kappa_i)+\eta}{k}+1}\Bigg)\Bigg]\\
&\leq[\Theta^{m+1}(\ell_1)+\Theta^{m+1}(\ell_2)]\Bigg[\frac{(m+1)^{-\frac{\mu}{k}}}{k}\Sigma_{n=0}^{\infty}\frac{(\delta_i)_{\kappa_i,k}(\tau_i)^{\kappa_i}}{\Gamma_k(\mu+\Sigma_{i=1}^{n}(\beta_i\kappa_i))}\frac{\left(\Theta^{m+1}(\ell_2)-\Theta^{m+1}\left(\frac{\ell_1+\ell_2}{2}\right)\right)^{\frac{\mu+\Sigma_{i=1}^{n}(\beta_i\kappa_i)+\eta}{k}}}{\frac{\mu+\Sigma_{i=1}^{n}(\beta_i\kappa_i)+\eta}{k}}\\
&+\frac{(m+1)^{-\frac{\mu}{k}}}{k}\Sigma_{n=0}^{\infty}\frac{(\delta_i)_{\kappa_i,k}(\tau_i)^{\kappa_i}}{\Gamma_k(\mu+\Sigma_{i=1}^{n}(\beta_i\kappa_i))}\frac{\left(\Theta^{m+1}\left(\frac{\ell_1+\ell_2}{2}\right)-\Theta^{m+1}(\ell_1)\right)^{\frac{\mu+\Sigma_{i=1}^{n}(\beta_i\kappa_i)+\eta}{k}}}{\frac{\mu+\Sigma_{i=1}^{n}(\beta_i\kappa_i)+\eta}{k}}\Bigg]
\end{aligned}
\tag{15}
$$

The computational values of (15)*, are shown in Table 1, and Table 2 corresponding to the choice of parameters* $m=3$, $k=1$, $\Theta(x)=x^2$, $\eta=0.5$, $\tau_i=1$, $\kappa_i=1$, $\beta_i=1$, $\delta=0.5$ *and for some fixed values of* ℓ_1 *and* ℓ_2*. Figure 1, shows the graphical representation of* (15)*, corresponding to the choice of parameters* $0<\ell_1<2<\ell_2<4$.

For tabular values

Table 1. Tabular form presents the computational values of (15) corresponding to choice $\mu=0.5$.

ℓ_1/ℓ_2	**2.10**	**2.30**
0.10	$(4.25\times10^{00}, 1.23\times10^{01}, 2.19\times10^{01})$	$(5.56\times10^{01}, 1.39\times10^{02}, 3.72\times10^{01})$
0.50	$(6.51\times10^{00}, 2.14\times10^{01}, 2.87\times10^{01})$	$(7.83\times10^{01}, 2.26\times10^{02}, 4.91\times10^{01})$

Table 2. Tabular form presents the computational values of (15) corresponding to choice $\mu = 0.5$.

ℓ_1/ℓ_2	**2.50**	**2.70**
0.10	$(7.48 \times 10^{01}, 1.68 \times 10^{02}, 4.51 \times 10^{01})$	$(8.74 \times 10^{01}, 1.95 \times 10^{02}, 5.63 \times 10^{01})$
0.50	$(9.66 \times 10^{01}, 2.72 \times 10^{02}, 5.74 \times 10^{01})$	$(1.12 \times 10^{02}, 3.06 \times 10^{02}, 6.85 \times 10^{01})$

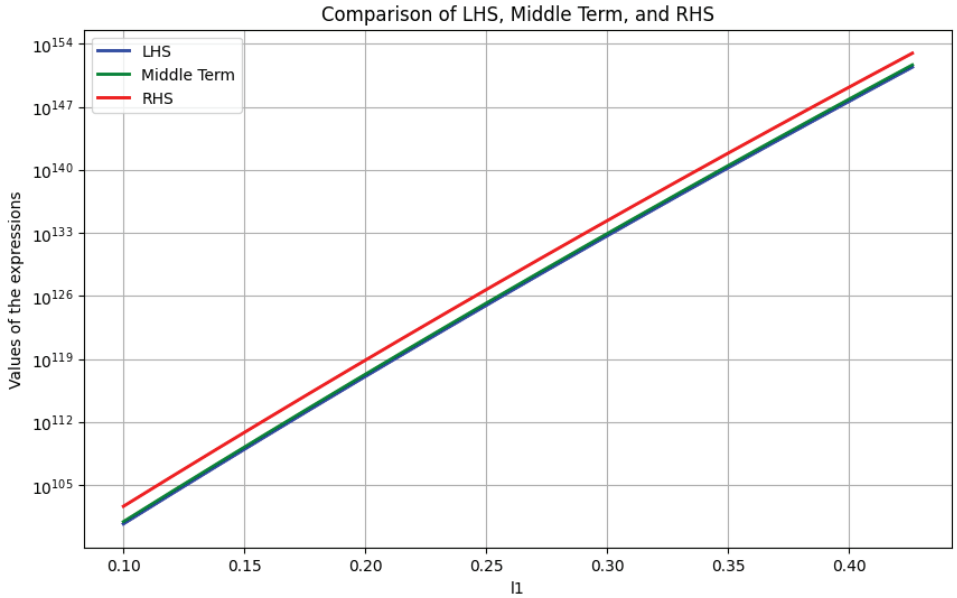

Figure 1. The graphical representation of (15) corresponding to choice $\mu = 0.5$.

Corollary 2. *If we replace* $\Theta(u) = u$, $m = 0$, $\delta_i = 0$, $\kappa_i = 0, \forall i$ *and* $k = 1$ *in Theorem 1, choose* χ *is symmetric about* $\frac{\ell_1+\ell_2}{2}$, *then we have*

$$\begin{aligned}
&F\Big(\frac{\ell_1+\ell_2}{2}\Big)\big[\mathfrak{J}^{\mu}_{(\frac{\ell_1+\ell_2}{2})^+}\chi(\ell_2)+\mathfrak{J}^{\mu}_{(\frac{\ell_1+\ell_2}{2})^-}\chi(\ell_1)\big]\\
&\leq \Upsilon\Big(\frac{\ell_1+\ell_2}{2}\Big)\big[\mathfrak{J}^{\mu}_{(\frac{\ell_1+\ell_2}{2})^+}\chi F(\ell_2)+\mathfrak{J}^{\mu}_{(\frac{\ell_1+\ell_2}{2})^-}\chi F(\ell_1)\big]\\
&\leq \frac{F(\ell_1)+F(\ell_2)}{2}\big[\mathfrak{J}^{\mu}_{(\frac{\ell_1+\ell_2}{2})^+}\chi(\ell_2)+\mathfrak{J}^{\mu}_{(\frac{\ell_1+\ell_2}{2})^-}\chi(\ell_1)\big].
\end{aligned}$$

Theorem 2. *For* $k > 0$, $m \in \Re/\{-1\}$, *and* $Re(\mu) > 0$, $Re(\tau) > 0$, $Re(\delta) > 0$, $Re(\beta) > 0$ *are complex parameters,* Θ *be an increasing function and* Υ *be a differentiable on* (ℓ_1, ℓ_2) *with* $\ell < \ell_2$ *and* $\chi : [\ell_1, \ell_2] \mapsto \Re$ *be bounded. If* $\Upsilon', \chi \in L[\ell_1, \ell_2]$ *and* $|\Upsilon'| \in K_s^2$ *on* $[\ell_1, \ell_2]$ *for any fixed* $s \in (0, 1]$, *then the H-H-F kind inequality for generalized RLFI holds.*

$$\begin{aligned}
&\Big|F\Big(\frac{\ell_1+\ell_2}{2}\Big)\Big[{}^{k,m}_{\Theta}\mathfrak{J}^{\delta_i,\tau_i}_{(\frac{\ell_1+\ell_2}{2})^+;\mu,\beta_i}\chi(\ell_2)+{}^{k,m}_{\Theta}\mathfrak{J}^{\delta_i,\tau_i}_{(\frac{\ell_1+\ell_2}{2})^-;\mu,\beta_i}\chi(\ell_1)\Big]\Big|\\
&-\Big|\Big[{}^{k,m}_{\Theta}\mathfrak{J}^{\delta_i,\tau_i}_{(\frac{\ell_1+\ell_2}{2})^+;\mu,\beta_i}\chi F(\ell_2)+{}^{k,m}_{\Theta}\mathfrak{J}^{\delta_i,\tau_i}_{(\frac{\ell_1+\ell_2}{2})^-;\mu,\beta_i}\chi F(\ell_1)\Big]\Big|\\
&\leq \frac{(m+1)^{\frac{\mu}{k}-1}||\chi||_{\infty}}{(\ell_2-\ell_1)^s(\mu+\Sigma_{i=1}^{n}(\beta_i\kappa_i))}\Sigma_{n=0}^{\infty}\frac{(\delta_i)_{\kappa_i,k}(\tau_i)^{\kappa_i}}{\Gamma_k(\mu+\Sigma_{i=1}^{n}(\beta_i\kappa_i))}\Big(|\Upsilon'(\ell_1)|+|\Upsilon'(\ell_2)|\Big)\\
&\times\Bigg[\Bigg(\int_{\ell_1}^{\frac{\ell_1+\ell_2}{2}}(\Theta^{m+1}(\nu)-\Theta^{m+1}(\ell_1))^{\frac{\mu+\Sigma_{i=1}^{n}(\beta_i\kappa_i)}{k}}+\int_{\frac{\ell_1+\ell_2}{2}}^{\ell_2}(\Theta^{m+1}(\ell_2)-\Theta^{m+1}(\nu))^{\frac{\mu+\Sigma_{i=1}^{n}(\beta_i\kappa_i)}{k}}\Bigg)\\
&\times\Big(\Big(\ell_2-\nu\Big)^s+\Big(\nu-\ell_1\Big)^s\Big)d\nu\Bigg],
\end{aligned}$$

where F *fulfilled the condition as in Theorem 1.*

Proof. By using defined s-convexity of second kind, we can write

$$\begin{aligned}
&|F'(\nu)| = |\Upsilon'(\nu) - \Upsilon'(\ell_1+\ell_2-\nu)| \leq |\Upsilon'(\nu)| + |\Upsilon'(\ell_1+\ell_2-\nu)| \\
&= \left|\Upsilon'\left(\frac{\ell_2-\nu}{\ell_2-\ell_1}\ell_1 + \frac{\nu-\ell_1}{\ell_2-\ell_1}\ell_2\right)\right| + \left|\Upsilon'\left(\frac{\nu-\ell_1}{\ell_2-\ell_1}\ell_1 + \frac{\ell_2-\nu}{\ell_2-\ell_1}\ell_2\right)\right| \\
&\leq \left(\frac{\ell_2-\nu}{\ell_2-\ell_1}\right)^s |\Upsilon'(\ell_1)| \\
&+ \left(\frac{\nu-\ell_1}{\ell_2-\ell_1}\right)^s |\Upsilon'(\ell_2)| + \left(\frac{\nu-\ell_1}{\ell_2-\ell_1}\right)^s |\Upsilon'(\ell_1)| + \left(\frac{\ell_2-\nu}{\ell_2-\ell_1}\right)^s |\Upsilon'(\ell_2)| \\
&= \left(\left(\frac{\ell_2-\nu}{\ell_2-\ell_1}\right)^s + \left(\frac{\nu-\ell_1}{\ell_2-\ell_1}\right)^s\right)\Big(|\Upsilon'(\ell_1)| + |\Upsilon'(\ell_2)|\Big).
\end{aligned}$$

Using Theorem 1, we reach

$$\begin{aligned}
&\left|F\left(\frac{\ell_1+\ell_2}{2}\right)\left[{}^{k,m}_{\Theta}\mathfrak{J}^{\delta_i,\tau_i}_{(\frac{\ell_1+\ell_2}{2})^+;\mu,\beta_i}\chi(\ell_2) + {}^{k,m}_{\Theta}\mathfrak{J}^{\delta_i,\tau_i}_{(\frac{\ell_1+\ell_2}{2})^-;\mu,\beta_i}\chi(\ell_1)\right]\right| \\
&- \left|\left[{}^{k,m}_{\Theta}\mathfrak{J}^{\delta_i,\tau_i}_{(\frac{\ell_1+\ell_2}{2})^+;\mu,\beta_i}\chi F(\ell_2) + {}^{k,m}_{\Theta}\mathfrak{J}^{\delta_i,\tau_i}_{(\frac{\ell_1+\ell_2}{2})^-;\mu,\beta_i}\chi F(\ell_1)\right]\right| \\
&\leq \frac{(m+1)^{\frac{\mu}{k}-1}}{k}\int_{\ell_1}^{\ell_2}|\kappa(\nu)||F'(\nu)|d\nu \\
&\leq \frac{(m+1)^{\frac{\mu}{k}-1}}{k} \\
&\times \left(\int_{\ell_1}^{\frac{\ell_1+\ell_2}{2}}\left|\int_{\ell_1}^{\nu}\frac{\xi^{\delta_i}_{k,\mu,\beta_i}\left(\tau_1(\Theta^{m+1}(u)-\Theta^{m+1}(\ell_1))^{\frac{\beta_1}{k}},\ldots,\tau_n(\Theta^{m+1}(u)-\Theta^{m+1}(\ell_1))^{\frac{\beta_n}{k}}\right)}{(\Theta^{m+1}(u)-\Theta^{m+1}(\ell_1))^{\frac{\mu}{k}-1}}\right.\right. \\
&\times \Theta^m(u)\Theta'(u)\chi(u)du\Bigg| \\
&\times \int_{\frac{\ell_1+\ell_2}{2}}^{\ell_2}\left|\int_{\ell_2}^{\nu}\frac{\xi^{\delta_i}_{k,\mu,\beta_i}\left(\tau_1(\Theta^{m+1}(\ell_2)-\Theta^{m+1}(u))^{\frac{\beta_1}{k}},\ldots,\tau_n(\Theta^{m+1}(\ell_2)-\Theta^{m+1}(u))^{\frac{\beta_n}{k}}\right)}{(\Theta^{m+1}(\ell_2)-\Theta^{m+1}(u))^{\frac{\mu}{k}-1}}\right. \\
&\left.\left.\times \Theta^m(u)\Theta'(u)\chi(u)du\right|\right)F'(\nu)d\nu \\
&\leq \frac{(m+1)^{\frac{\mu}{k}-1}}{k} \\
&\times \left(\int_{\ell_1}^{\frac{\ell_1+\ell_2}{2}}\left|\int_{\ell_1}^{\nu}\frac{\xi^{\delta_i}_{k,\mu,\beta_i}\left(\ell_1(\Theta^{m+1}(u)-\Theta^{m+1}(\ell_1))^{\frac{\beta_1}{k}},\ldots,\tau_n(\Theta^{m+1}(u)-\Theta^{m+1}(\ell_1))^{\frac{\beta_n}{k}}\right)}{(\Theta^{m+1}(u)-\Theta^{m+1}(\ell_1))^{\frac{\mu}{k}-1}}\right.\right. \\
&\times \Theta^m(u)\Theta'(u)\chi(u)du\Bigg| \\
&+ \int_{\frac{\ell_1+\ell_2}{2}}^{\ell_2}\left|\int_{\ell_2}^{\nu}\frac{\xi^{\delta_i}_{k,\mu,\beta_i}\left(\tau_1(\Theta^{m+1}(\ell_2)-\Theta^{m+1}(u))^{\frac{\beta_1}{k}},\ldots,\tau_n(\Theta^{m+1}(\ell_2)-\Theta^{m+1}(u))^{\frac{\beta_n}{k}}\right)}{(\Theta^{m+1}(\ell_2)-\Theta^{m+1}(u))^{\frac{\mu}{k}-1}}\right. \\
&\left.\left.\times \Theta^m(u)\Theta'(u)\chi(u)du\right|\right)F'(\nu)d\nu \\
&\leq \frac{(m+1)^{\frac{\mu}{k}-2}||\chi||_\infty\Sigma_{n=0}^{\infty}\frac{(\delta_i)_{\kappa_i,k}(\tau_i)^{\kappa_i}}{\Gamma_k(\mu+\Sigma_{i=1}^n(\beta_i\kappa_i))}}{k} \\
&\times \left[\left(\int_{\ell_1}^{\frac{\ell_1+\ell_2}{2}}\frac{[\Theta^{m+1}(\nu)-\Theta^{m+1}(\ell_1)]^{\frac{\mu+\Sigma_{i=1}^n(\beta_i\kappa_i)}{k}}}{\frac{\mu+\Sigma_{i=1}^n(\beta_i\kappa_i)}{k}} + \int_{\frac{\ell_1+\ell_2}{2}}^{\ell_2}\frac{[\Theta^{m+1}(\ell_2)-\nu^{s+}]^{\frac{\mu+\Sigma_{i=1}^n(\beta_i\kappa_i)}{k}}}{\frac{\mu+\Sigma_{i=1}^n(\beta_i\kappa_i)}{k}}\right)\right. \\
&\left.\times \left(\left(\frac{\ell_2-\nu}{\ell_2-\ell_1}\right)^s + \left(\frac{\nu-\ell_1}{\ell_2-\ell_1}\right)^s\right)\Big(|\Upsilon'(\ell_1)| + |\Upsilon'(\ell_2)|d\nu\Big)\right] \\
&\leq \frac{(m+1)^{\frac{\mu}{k}-2}||\chi||_\infty}{(\ell_2-\ell_1)^s(\mu+\Sigma_{i=1}^n(\beta_i\kappa_i))}\Sigma_{n=0}^{\infty}\frac{(\delta_i)_{\kappa_i,k}(\tau_i)^{\kappa_i}}{\Gamma_k(\mu+\Sigma_{i=1}^n(\beta_i\kappa_i))}\Big(|\Upsilon'(\ell_1)| + |\Upsilon'(\ell_2)|\Big) \\
&\times \left[\left(\int_{\ell_1}^{\frac{\ell_1+\ell_2}{2}}(\Theta^{m+1}(\nu)-\Theta^{m+1}(\ell_1))^{\frac{\mu+\Sigma_{i=1}^n(\beta_i\kappa_i)}{k}} + \int_{\frac{\ell_1+\ell_2}{2}}^{\ell_2}(\Theta^{m+1}(\ell_2)-\Theta^{m+1}(\nu))^{\frac{\mu+\Sigma_{i=1}^n(\beta_i\kappa_i)}{k}}\right)\right. \\
&\left.\times \left(\Big(\ell_2-\nu\Big)^s + \Big(\nu-\ell_1\Big)^s\right)d\nu\right].
\end{aligned}$$

We reach at desired outcome. □

Corollary 3. *If we replace* $\Theta(u) = u$, $m = 0$, $\delta_i = 0$, $\kappa_i = 0, \forall i$ *and* $p = k = 1$ *in Theorem 2 and* χ *is symmetric about* $\frac{\ell_1+\ell_2}{2}$, *then we have*

$$\begin{aligned}
&\left|F\left(\frac{\ell_1+\ell_2}{2}\right)\left[\mathfrak{J}^{\mu}_{(\frac{\ell_1+\ell_2}{2})^+}\chi(\ell_2)+\mathfrak{J}^{\mu}_{(\frac{\ell_1+\ell_2}{2})^-}\chi(\ell_1)\right]\right| - \left|\left[\mathfrak{J}^{\mu}_{(\frac{\ell_1+\ell_2}{2})^+}\chi F(\ell_2)+\mathfrak{J}^{\mu}_{(\frac{\ell_1+\ell_2}{2})^-}\chi F(\ell_1)\right]\right| \\
&\leq \frac{(m+1)^{1-\mu}(\ell_2-\ell_1)}{(\ell_2-\ell_1)\Gamma_k(\mu)}||\chi||_\infty \\
&\times\left(|\Upsilon'(\ell_1)|+|\Upsilon'(\ell_2)|\right)\left[\left(\int_{\ell_1}^{\frac{\ell_1+\ell_2}{2}}(\nu-\ell_1)^s d\nu+\int_{\frac{\ell_1+\ell_2}{2}}^{\ell_2}(\ell_2-\nu)^s\right)d\nu\right] \\
&=\frac{(m+1)^{1-\mu}(\ell_2-\ell_1)^{\mu+1}}{(\mu+1)\Gamma(\mu+1)2^{\mu+1}}||\chi||_\infty\left(|\Upsilon'(\ell_1)|+|\Upsilon'(\ell_2)|\right).
\end{aligned}$$

Proposition 1. *Furthermore, If we replace* $\Theta(u) = u$, $m = 0$, $\delta_i = 0$, $\kappa_i = 0, \forall i$ *and* $\chi = k = 1$ *in Corollary 3, so we obtain the below mid point inequality*

$$\left|(\ell_2-\ell_1)\Upsilon(\frac{\ell_1+\ell_2}{2})-\int_{\ell_1}^{\ell_2}\Upsilon(\nu)d\nu\right| \leq \frac{(\ell_2-\ell_1)^2}{8}\left(|\Upsilon'(\ell_1)|+|\Upsilon'(\ell_2)|\right).$$

Theorem 3. *For* $k > 0$, $m \in \Re/\{-1\}$, *and* $Re(\mu) > 0$, $Re(\tau) > 0$, $Re(\delta) > 0$, $Re(\beta) > 0$ *are complex parameters,* Θ *be an increasing function and* Υ *be a differentiable on* (ℓ_1, ℓ_2) *with* $\ell < \ell_2$ *and* $\chi : [\ell_1, \ell_2] \mapsto \Re$ *be bounded. If* $\Upsilon', \chi \in L[\ell_1, \ell_2]$, *then the below expression holds.*

$$\begin{aligned}
&\left|F\left(\frac{\ell_1+\ell_2}{2}\right)\left[{}^{k,m}_{\Theta}\mathfrak{J}^{\delta_i,\tau_i}_{(\frac{\ell_1+\ell_2}{2})^+;\mu,\beta_i}\chi(\ell_2)+{}^{k,m}_{\Theta}\mathfrak{J}^{\delta_i,\tau_i}_{(\frac{\ell_1+\ell_2}{2})^-;\mu,\beta_i}\chi(\ell_1)\right]\right| \\
&-\left|\left[{}^{k,m}_{\Theta}\mathfrak{J}^{\delta_i,\tau_i}_{(\frac{\ell_1+\ell_2}{2})^+;\mu,\beta_i}\chi F(\ell_2)+{}^{k,m}_{\Theta}\mathfrak{J}^{\delta_i,\tau_i}_{(\frac{\ell_1+\ell_2}{2})^-;\mu,\beta_i}\chi F(\ell_1)\right]\right| \\
&\leq \frac{(m+1)^{-\frac{\mu}{k}}||\chi||_\infty}{(\mu+\Sigma_{i=1}^n(\beta_i\kappa_i))}\Sigma_{n=0}^\infty\frac{(\delta_i)_{\kappa_i,k}(\tau_i)^{\kappa_i}}{\Gamma_k(\mu+\Sigma_{i=1}^n(\beta_i\kappa_i))} \\
&\times\left(\int_{\ell_1}^{\frac{\ell_1+\ell_2}{2}}\left(\left|(\Theta^{m+1}(\nu)-\Theta^{m+1}(\ell_1))^{\frac{\mu+\Sigma_{i=1}^n(\beta_i\kappa_i)}{k}}\right|d\nu\right)^{1-\frac{1}{q}}\left(\int_{\ell_1}^{\frac{\ell_1+\ell_2}{2}}\left|(\Theta^{m+1}(\nu)-\Theta^{m+1}(\ell_1))^{\frac{\mu+\Sigma_{i=1}^n(\beta_i\kappa_i)}{k}}\right|\right.\right. \\
&\left.\left.\times\left(\frac{\ell_2-\nu}{\ell_2-\ell_1}\right)^s(|\Upsilon'(\ell_1)|^q+\left(\frac{\nu-\ell_1}{\ell_2-\ell_1}\right)^s)|\Upsilon'(\ell_2)|^q d\nu\right)\right)^{\frac{1}{q}} \\
&+\frac{(m+1)^{-\frac{\mu}{k}}|\chi||_\infty}{(\mu+\Sigma_{i=1}^n(\beta_i\kappa_i))}\Sigma_{n=0}^\infty\frac{(\delta_i)_{\kappa_i,k}(\tau_i)^{\kappa_i}}{\Gamma_k(\mu+\Sigma_{i=1}^n(\beta_i\kappa_i))} \\
&\times\left(\int_{\frac{\ell_1+\ell_2}{2}}^{\ell_2}\left(\left|(\Theta^{m+1}(\ell_2)-\Theta^{m+1}(\nu))^{\frac{\mu+\Sigma_{i=1}^n(\beta_i\kappa_i)}{k}}\right|d\nu\right)^{1-\frac{1}{q}}\left(\int_{\frac{\ell_1+\ell_2}{2}}^{\ell_2}\left|(\Theta^{m+1}(\ell_2)-\Theta^{m+1}(\nu))^{\frac{\mu+\Sigma_{i=1}^n(\beta_i\kappa_i)}{k}}\right|\right.\right. \\
&\left.\left.\times\left(\frac{\ell_2-\nu}{\ell_2-\ell_1}\right)^s(|\Upsilon'(\ell_1)|^q+\left(\frac{\nu-\ell_1}{\ell_2-\ell_1}\right)^s)|\Upsilon'(\ell_2)|^q d\nu\right)\right)^{\frac{1}{q}}.
\end{aligned}$$

Proof. By using Theorem 1, we can write

$$
\begin{aligned}
&\left|F\left(\frac{\ell_1+\ell_2}{2}\right)\left[{}^{k,m}_{\Theta}\mathfrak{I}^{\delta_i,\tau_i}_{(\frac{\ell_1+\ell_2}{2})^+;\mu,\beta_i}\chi(\ell_2)+{}^{k,m}_{\Theta}\mathfrak{I}^{\delta_i,\tau_i}_{(\frac{\ell_1+\ell_2}{2})^-;\mu,\beta_i}\chi(\ell_1)\right]\right|\\
&-\left|\left[{}^{k,m}_{\Theta}\mathfrak{I}^{\delta_i,\tau_i}_{(\frac{\ell_1+\ell_2}{2})^+;\mu,\beta_i}\chi F(\ell_2)+{}^{k,m}_{\Theta}\mathfrak{I}^{\delta_i,\tau_i}_{(\frac{\ell_1+\ell_2}{2})^-;\mu,\beta_i}\chi F(\ell_1)\right]\right|\\
&\leq\frac{(m+1)^{\frac{\mu}{k}-1}}{k}\int_{\ell_1}^{\ell_2}|\kappa(\nu)||F'(\nu)|d\nu\\
&\leq\frac{(m+1)^{\frac{\mu}{k}-1}}{k}\Big(\int_{\ell_1}^{\ell_2}|\kappa(\nu)|d\nu\Big)^{1-\frac{1}{q}}\Big(\int_{\ell_1}^{\ell_2}|\kappa(\nu)||F'(\nu)|^q d\nu\Big)^{\frac{1}{q}}\\
&\leq\frac{(m+1)^{\frac{\mu}{k}-1}}{k}\\
&\times\left(\int_{\ell_1}^{\frac{\ell_1+\ell_2}{2}}\left|\int_{\ell_1}^{\nu}\frac{\xi^{\delta_i}_{k,\mu,\beta_i}\left(\tau_1(\Theta^{m+1}(u)-\Theta^{m+1}(\ell_1))^{\frac{\beta_1}{k}},\ldots,\tau_n(\Theta^{m+1}(u)-\Theta^{m+1}(\ell_1))^{\frac{\beta_n}{k}}\right)}{(\Theta^{m+1}(u)-\Theta^{m+1}(\ell_1))^{\frac{\mu}{k}-1}}\right.\right.\\
&\left.\times\Theta^m(u)\Theta'(u)\chi(u)du\right|d\nu\Big)^{1-\frac{1}{q}}\\
&\times\left(\int_{\ell_1}^{\frac{\ell_1+\ell_2}{2}}\left|\int_{\ell_1}^{\nu}\frac{\xi^{\delta_i}_{k,\mu,\beta_i}\left(\tau_1(\Theta^{m+1}(u)-\Theta^{m+1}(\ell_1))^{\frac{\beta_1}{k}},\ldots,\tau_n(\Theta^{m+1}(u)-\Theta^{m+1}(\ell_1))^{\frac{\beta_n}{k}}\right)}{(\Theta^{m+1}(u)-\Theta^{m+1}(\ell_1))^{\frac{\mu}{k}-1}}\right.\right.\\
&\left.\left.\times\Theta^m(u)\Theta'(u)\chi(u)du\right|\right)\left(\left(\frac{\ell_2-\nu}{\ell_2-\ell_1}\right)^s(|\Upsilon'(\ell_1)|^q+\left(\frac{\nu-\ell_1}{\ell_2-\ell_1}\right)^s)|\Upsilon'(\ell_2)|^q d\nu\right)^{\frac{1}{q}}\\
&+\frac{(m+1)^{\frac{\mu}{k}-1}}{k}\\
&\times\left(\int_{\frac{\ell_1+\ell_2}{2}}^{\ell_2}\left|\int_{\ell_2}^{\nu}\frac{\xi^{\delta_i}_{k,\mu,\beta_i}\left(\tau_1(\Theta^{m+1}(\ell_2)-\Theta^{m+1}(u))^{\frac{\beta_1}{k}},\ldots,\tau_n(\Theta^{m+1}(\ell_2)-\Theta^{m+1}(u))^{\frac{\beta_n}{k}}\right)}{(\Theta^{m+1}(\ell_2)-\Theta^{m+1}(u))^{\frac{\mu}{k}-1}}\right.\right.\\
&\left.\times\Theta^m(u)\Theta'(u)\chi(u)du\right|d\nu\Big)^{1-\frac{1}{q}}\\
&\times\left(\int_{\frac{\ell_1+\ell_2}{2}}^{\ell_2}\left|\int_{\ell_2}^{\nu}\frac{\xi^{\delta_i}_{k,\mu,\beta_i}\left(\ell_1(\Theta^{m+1}(\ell_2)-\Theta^{m+1}(u))^{\frac{\beta_1}{k}},\ldots,\tau_n(\Theta^{m+1}(\ell_2)-\Theta^{m+1}(u))^{\frac{\beta_n}{k}}\right)}{(\Theta^{m+1}(\ell_2)-\Theta^{m+1}(u))^{\frac{\mu}{k}-1}}\right.\right.\\
&\left.\left.\times\Theta^m(u)\Theta'(u)\chi(u)du\right|\right)\left(\left(\frac{\ell_2-\nu}{\ell_2-\ell_1}\right)^s(|\Upsilon'(\ell_1)|^q+\left(\frac{\nu-\ell_1}{\ell_2-\ell_1}\right)^s)|\Upsilon'(\ell_2)|^q d\nu\right)^{\frac{1}{q}}\\
&=\frac{(m+1)^{-\frac{\mu}{k}}||\chi||_\infty\Sigma_{n=0}^{\infty}\frac{(\delta_i)_{\kappa_i,k}(\tau_i)^{\kappa_i}}{\Gamma_k(\mu+\Sigma_{i=1}^n(\beta_i\kappa_i))}}{(\mu+\Sigma_{i=1}^n(\beta_i\kappa_i))}\\
&\times\left(\int_{\ell_1}^{\frac{\ell_1+\ell_2}{2}}\left(\left|(\Theta^{m+1}(\nu)-\Theta^{m+1}(\ell_1))^{\frac{\mu+\Sigma_{i=1}^n(\beta_i\kappa_i)}{k}}\right|d\nu\right)^{1-\frac{1}{q}}\left(\int_{\ell_1}^{\frac{\ell_1+\ell_2}{2}}\left|(\Theta^{m+1}(\nu)-\Theta^{m+1}(\ell_1))^{\frac{\mu+\Sigma_{i=1}^n(\beta_i\kappa_i)}{k}}\right|\right.\right.\\
&\left.\left.\times\left(\frac{\ell_2-\nu}{\ell_2-\ell_1}\right)^s(|\Upsilon'(\ell_1)|^q+\left(\frac{\nu-\ell_1}{\ell_2-\ell_1}\right)^s)|\Upsilon'(\ell_2)|^q d\nu\right)\right)^{\frac{1}{q}}\\
&+\frac{(m+1)^{-\frac{\mu}{k}}|\chi||_\infty\Sigma_{n=0}^{\infty}\frac{(\delta_i)_{\kappa_i,k}(\tau_i)^{\kappa_i}}{\Gamma_k(\mu+\Sigma_{i=1}^n(\beta_i\kappa_i))}}{(\mu+\Sigma_{i=1}^n(\beta_i\kappa_i))}\\
&\times\left(\int_{\frac{\ell_1+\ell_2}{2}}^{\ell_2}\left(\left|(\Theta^{m+1}(\ell_2)-\Theta^{m+1}(\nu))^{\frac{\mu+\Sigma_{i=1}^n(\beta_i\kappa_i)}{k}}\right|d\nu\right)^{1-\frac{1}{q}}\left(\int_{\frac{\ell_1+\ell_2}{2}}^{\ell_2}\left|(\Theta^{m+1}(\ell_2)-\Theta^{m+1}(\nu))^{\frac{\mu+\Sigma_{i=1}^n(\beta_i\kappa_i)}{k}}\right|\right.\right.\\
&\left.\left.\times\left(\frac{\ell_2-\nu}{\ell_2-\ell_1}\right)^s(|\Upsilon'(\ell_1)|^q+\left(\frac{\nu-\ell_1}{\ell_2-\ell_1}\right)^s)|\Upsilon'(\ell_2)|^q d\nu\right)\right)^{\frac{1}{q}}.
\end{aligned}
$$

This is our desired result. □

Remark 1. *For the choice of $s = 1$, $\Theta(u) = u$, $m = 0$, $\delta_i = 0$, $\kappa_i = 0, \forall i$ and $k = 1$ in the Theorem 3, then we obtain ([27], Theorem 7).*

$$\begin{aligned}
&\left|F\left(\frac{\ell_1+\ell_2}{2}\right)\left[\mathfrak{J}^{\varrho}_{(\frac{\ell_1+\ell_2}{2})^+}\chi(\ell_2)+\mathfrak{J}^{\varrho}_{(\frac{\ell_1+\ell_2}{2})^-}\chi(\tau_1)\right]\right| \\
&-\left|\left[\mathfrak{J}^{\varrho}_{(\frac{\ell_1+\ell_2}{2})^+}\chi F(\ell_2)+\mathfrak{J}^{\varrho}_{(\frac{\ell_1+\ell_2}{2})^-}\chi F(\tau_1)\right]\right| \\
&\leq \frac{||\chi||_{\infty,[\tau_1,\ell_2]}(\ell_2-\tau_1)^{\varrho+1}}{2^{\varrho+1+\frac{1}{q}}(\varrho+1)(\varrho+2)^{\frac{1}{q}}k\Gamma_k(\varrho+1)}\left[\left((\varrho+3)|\Upsilon'(\tau_1)|^q+(\varrho+1)|\Upsilon'(\ell_2)|^q\right)^{\frac{1}{q}}\right. \\
&\left.+\left((\varrho+1)|\Upsilon'(\tau_1)|^q+(\varrho+3)|\Upsilon'(\ell_2)|^q\right)^{\frac{1}{q}}\right].
\end{aligned}$$

Remark 2. *For the choice of $\Theta(u) = u$, $m = 0$, $\delta_i = 0$, $\kappa_i = 0, \forall i$ and $k = 1$ in the Theorem 3, then we obtain ([57], Theorem 5).*

$$\begin{aligned}
&\left|F\left(\frac{\ell_1+\ell_2}{2}\right)\left[\mathfrak{J}^{\varrho}_{(\frac{\ell_1+\ell_2}{2})^+}\chi(\ell_2)+\mathfrak{J}^{\varrho}_{(\frac{\ell_1+\ell_2}{2})^-,\Theta}\chi(\tau_1)\right]\right| \\
&-\left|\left[\mathfrak{J}^{\varrho}_{(\frac{\ell_1+\ell_2}{2})^+}\chi F(\ell_2)+\mathfrak{J}^{\varrho}_{(\frac{\ell_1+\ell_2}{2})^-}\chi F(\tau_1)\right]\right| \\
&\leq \frac{||\chi||_{\infty,[\tau_1,\ell_2]}(\ell_2-\tau_1)^{\varrho+1}}{2^{\varrho+1+\frac{1}{q}}(\varrho+1)(\varrho+s+1)^{\frac{1}{q}}k\Gamma_k(\varrho+1)}\left[\left(2^{\varrho+1}(\varrho+1)(\varrho+s+1)B_{\frac{1}{2}}(\varrho+1,s+1)|\Upsilon'(\tau_1)|^q\right.\right. \\
&\left.+2^{1-s}(\varrho+1)|\Upsilon'(\ell_2)|^q\right)^{\frac{1}{q}} \\
&\left.\left(2^{\varrho+1}(\varrho+1)(\varrho+s+1)B_{\frac{1}{2}}(\varrho+1,s+1)|\Upsilon'(\ell_2)|^q+2^{1-s}(\varrho+1)|\Upsilon'(\tau_1)|^q\right)^{\frac{1}{q}}\right].
\end{aligned}$$

Corollary 4. *For the choice of $s = 1$, $\Theta(u) = u$, $m = 0$, $\delta_i = 0$, $\kappa_i = 0, \forall i$ and $k = 1$ in the Theorem 3, then we arrive at the following mid-point inequality*

$$\begin{aligned}
&\left|\Upsilon(\frac{\ell_1+\ell_2}{2})\int_{\ell_1}^{\ell_2}\chi(\nu)d\nu-\int_{\ell_1}^{\ell_2}(\Upsilon\chi)(\nu)d\nu\right| \\
&\leq \frac{||\chi||(\ell_2-\ell_1)^2}{(3)^{\frac{1}{q}}8}\left[\left(2|\Upsilon'(\ell_1)|^q+|\Upsilon'(\ell_2)|^q\right)^{\frac{1}{q}}+\left(|\Upsilon'(\ell_1)|^q+2|\Upsilon'(\ell_2)|^q\right)^{\frac{1}{q}}\right].
\end{aligned}$$

Theorem 4. *For $k > 0$, $m \in \Re/\{-1\}$, and $Re(\mu) > 0$, $Re(\tau) > 0$, $Re(\delta) > 0$, $Re(\beta) > 0$ are complex parameters, Θ be an increasing function and Υ be a differentiable on (ℓ_1, ℓ_2) with $\ell < \ell_2$ and $\chi : [\ell_1, \ell_2] \mapsto \Re$ be bounded. If $\Upsilon', \chi \in L[\ell_1, \ell_2]$, then the below expression holds.*

$$\begin{aligned}
&\left|F\left(\frac{\ell_1+\ell_2}{2}\right)\left[{}^{k,m}_{\Theta}\mathfrak{J}^{\delta_i,\tau_i}_{(\frac{\ell_1+\ell_2}{2})^+;\mu,\beta_i}\chi(\ell_2)+{}^{k,m}_{\Theta}\mathfrak{J}^{\delta_i,\tau_i}_{(\frac{\ell_1+\ell_2}{2})^-;\mu,\beta_i}\chi(\ell_1)\right]\right| \\
&-\left|\left[{}^{k,m}_{\Theta}\mathfrak{J}^{\delta_i,\tau_i}_{(\frac{\ell_1+\ell_2}{2})^+;\mu,\beta_i}\chi F(\ell_2)+{}^{k,m}_{\Theta}\mathfrak{J}^{\delta_i,\tau_i}_{(\frac{\ell_1+\ell_2}{2})^-;\mu,\beta_i}\chi F(\ell_1)\right]\right| \\
&\leq \frac{(m+1)^{-\frac{\mu}{k}}||\chi||_{\infty}(\ell_2-\ell_1)^{\frac{1}{q}}}{2^{\frac{s}{q}+\frac{1}{q}}(s+1)^{\frac{1}{q}}(\mu+\Sigma_{i=1}^{n}(\beta_i\kappa_i))}\Sigma_{n=0}^{\infty}\frac{(\delta_i)_{\kappa_i,k}(\tau_i)^{\kappa_i}}{\Gamma_k(\mu+\Sigma_{i=1}^{n}(\beta_i\kappa_i))} \\
&\times\{\int_{\ell_1}^{\frac{\ell_1+\ell_2}{2}}\left(\left|(\Theta^{m+1}(\nu)-\Theta^{m+1}(\ell_1))^{\frac{p(\mu+\Sigma_{i=1}^{n}(\beta_i\kappa_i))}{k}}\right|d\nu\right)^{\frac{1}{p}}\times\left((2^{m+1}-1)(|\Upsilon'(\ell_1))|^q+|\Upsilon'(\ell_2)|^q\right)^{\frac{1}{q}} \\
&+\int_{\frac{\ell_1+\ell_2}{2}}^{\ell_2}\left(\left|(\Theta^{m+1}(\ell_2)-\Theta^{m+1}(\nu))^{\frac{p(\mu+\Sigma_{i=1}^{n}(\beta_i\kappa_i))}{k}}\right|d\nu\right)^{\frac{1}{p}}(|\Upsilon'(\ell_1)|)^q+\left((2^{m+1}-1)|\Upsilon'(\ell_2)|^q\right)^{\frac{1}{q}}\}.
\end{aligned}$$

Proof. Using Hölder's inequality, we have

$$
\begin{aligned}
&\left|F\left(\frac{\ell_1+\ell_2}{2}\right)\left[{}^{k,m}_{\Theta}\mathfrak{J}^{\delta_i,\tau_i}_{(\frac{\ell_1+\ell_2}{2})^+;\mu,\beta_i}\chi(\ell_2)+{}^{k,m}_{\Theta}\mathfrak{J}^{\delta_i,\tau_i}_{(\frac{\ell_1+\ell_2}{2})^-;\mu,\beta_i}\chi(\ell_1)\right]\right|\\
&-\left|\left[{}^{k,m}_{\Theta}\mathfrak{J}^{\delta_i,\tau_i}_{(\frac{\ell_1+\ell_2}{2})^+;\mu,\beta_i}\chi F(\ell_2)+{}^{k,m}_{\Theta}\mathfrak{J}^{\delta_i,\tau_i}_{(\frac{\ell_1+\ell_2}{2})^-;\mu,\beta_i}\chi F(\ell_1)\right]\right|\\
&\leq\frac{(m+1)^{\frac{\mu}{k}-1}}{k}\int_{\ell_1}^{\ell_2}|F'(\nu)|d\nu\\
&\leq\frac{(m+1)^{\frac{\mu}{k}-1}}{k}\Big(\int_{\ell_1}^{\ell_2}|\kappa(\nu)|^p d\nu\Big)^{\frac{1}{p}}\Big(\int_{\ell_1}^{\ell_2}|F'(\nu)|^q d\nu\Big)^{\frac{1}{q}}\\
&\leq\frac{(m+1)^{\frac{\mu}{k}-1}}{k}\\
&\times\left(\int_{\ell_1}^{\frac{\ell_1+\ell_2}{2}}\left(\left|\int_{\ell_1}^{\nu}\frac{\xi^{\delta_i}_{k,\mu,\beta_i}\left(\tau_1(\Theta^{m+1}(u)-\Theta^{m+1}(\ell_1))^{\frac{\beta_1}{k}},\ldots,\tau_n(\Theta^{m+1}(u)-\Theta^{m+1}(\ell_1))^{\frac{\beta_n}{k}}\right)}{(\Theta^{m+1}(u)-\Theta^{m+1}(\ell_1))^{\frac{\mu}{k}-1}}\right.\right.\right.\\
&\left.\left.\left.\times\Theta^m(u)\Theta'(u)\chi(u)du\right|\right)^p d\nu\right)^{\frac{1}{p}}\left(\int_{\ell_1}^{\nu}\left(\frac{\ell_2-\nu}{\ell_2-\ell_1}\right)^s(|\Upsilon'(\ell_1)|^q+\left(\frac{\nu-\ell_1}{\ell_2-\ell_1}\right)^s|\Upsilon'(\ell_2)|^q d\nu\right)^{\frac{1}{q}}\\
&+\left(\int_{\frac{\ell_1+\ell_2}{2}}^{\ell_2}\left(\left|\int_{\ell_2}^{\nu}\frac{\xi^{\delta_i}_{k,\mu,\beta_i}\left(\tau_1(\Theta^{m+1}(\ell_2)-\Theta^{m+1}(u))^{\frac{\beta_1}{k}},\ldots,\tau_n(\Theta^{m+1}(\ell_2)-\Theta^{m+1}(u))^{\frac{\beta_n}{k}}\right)}{(\Theta^{m+1}(\ell_2)-\Theta^{m+1}(u))^{\frac{\mu}{k}-1}}\right.\right.\right.\\
&\left.\left.\left.\times\Theta^m(u)\Theta'(u)\chi(u)du\right|\right)^p d\nu\right)^{\frac{1}{p}}\left(\int_{\nu}^{\ell_2}\left(\frac{\ell_2-\nu}{\ell_2-\ell_1}\right)^s(|\Upsilon'(\ell_1)|^q+\left(\frac{\nu-\ell_1}{\ell_2-\ell_1}\right)^s|\Upsilon'(\ell_2)|^q d\nu\right)^{\frac{1}{q}}\\
&=\frac{(m+1)^{\frac{\mu}{k}}||\chi||_\infty}{(\mu+\Sigma_{i=1}^n(\beta_i\kappa_i))}\Sigma_{n=0}^\infty\frac{(\delta_i)_{\kappa_i,k}(\tau_i)^{\kappa_i}}{\Gamma_k(\mu+\Sigma_{i=1}^n(\beta_i\kappa_i))}\\
&\times\left(\left(\int_{\ell_1}^{\frac{\ell_1+\ell_2}{2}}\left|(\Theta^{m+1}(\nu)-\Theta^{m+1}(\ell_1))^{\frac{\mu+\Sigma_{i=1}^n(\beta_i\kappa_i)}{k}}\right|^p d\nu\right)^{\frac{1}{p}}\right.\\
&\times\left(\int_{\ell_1}^{\nu}\left(\frac{\ell_2-\nu}{\ell_2-\ell_1}\right)^s(|\Upsilon'(\ell_1)|^q+\left(\frac{\nu-\ell_1}{\ell_2-\ell_1}\right)^s)|\Upsilon'(\ell_2)|^q d\nu\right)^{\frac{1}{q}}\\
&+\left(\int_{\frac{\ell_1+\ell_2}{2}}^{\ell_2}\left|(\Theta^{m+1}(\ell_2)-\Theta^{m+1}(\nu))^{\frac{\mu+\Sigma_{i=1}^n(\beta_i\kappa_i)}{k}}\right|^p d\nu\right)^{\frac{1}{p}}\\
&\left.\times\left(\int_{\nu}^{\ell_2}\left(\frac{\ell_2-\nu}{\ell_2-\ell_1}\right)^s(|\Upsilon'(\ell_1)|^q+\left(\frac{\nu-\ell_1}{\ell_2-\ell_1}\right)^s)|\Upsilon'(\ell_2)|^q d\nu\right)^{\frac{1}{q}}\right)\\
&=\frac{(m+1)^{-\frac{\mu}{k}}||\chi||_\infty}{(\ell_2-\ell_1)^{\frac{s}{q}}(\mu+\Sigma_{i=1}^n(\beta_i\kappa_i))}\Sigma_{n=0}^\infty\frac{(\delta_i)_{\kappa_i,k}(\tau_i)^{\kappa_i}}{\Gamma_k(\mu+\Sigma_{i=1}^n(\beta_i\kappa_i))}\\
&\times\{\int_{\ell_1}^{\frac{\ell_1+\ell_2}{2}}\left(\left|(\Theta^{m+1}(\nu)-\Theta^{m+1}(\ell_1))^{\frac{\mu+\Sigma_{i=1}^n(\beta_i\kappa_i)}{k}}\right|^p d\nu\right)^{\frac{1}{p}}\\
&\times\left(\frac{(\ell_2-\ell_1)^{m+1}(2^{m+1}-1)}{2^{m+1}(s+1)}(|\Upsilon'(\ell_1))|^q+\frac{(\ell_2-\ell_1)^{m+1}}{2^{m+1}(s+1)}|\Upsilon'(\ell_2)|^q\right)^{\frac{1}{q}}\\
&+\int_{\frac{\ell_1+\ell_2}{2}}^{\ell_2}\left(\left|(\Theta^{m+1}(\ell_2)-\Theta^{m+1}(\nu))^{\frac{\mu+\Sigma_{i=1}^n(\beta_i\kappa_i)}{k}}\right|^p d\nu\right)^{\frac{1}{p}}\\
&\times\frac{(\ell_2-\ell_1)^{m+1}}{2^{m+1}(s+1)}(|\Upsilon'(\ell_1)|)^q+\left(\frac{(\ell_2-\ell_1)^{m+1}(2^{m+1}-1)}{2^{m+1}(s+1)}|\Upsilon'(\ell_2)|^q\right)^{\frac{1}{q}}\}\\
&\leq\frac{(m+1)^{-\frac{\mu}{k}}||\chi||_\infty(\ell_2-\ell_1)^{\frac{1}{q}}}{2^{\frac{s}{q}+\frac{1}{q}}(s+1)^{\frac{1}{q}}(\mu+\Sigma_{i=1}^n(\beta_i\kappa_i))}\Sigma_{n=0}^\infty\frac{(\delta_i)_{\kappa_i,k}(\tau_i)^{\kappa_i}}{\Gamma_k(\mu+\Sigma_{i=1}^n(\beta_i\kappa_i))}\\
&\times\{\int_{\ell_1}^{\frac{\ell_1+\ell_2}{2}}\left(\left|(\Theta^{m+1}(\nu)-\Theta^{m+1}(\ell_1))^{\frac{p(\mu+\Sigma_{i=1}^n(\beta_i\kappa_i))}{k}}\right|d\nu\right)^{\frac{1}{p}}\times\left((2^{m+1}-1)(|\Upsilon'(\ell_1))|^q+|\Upsilon'(\ell_2)|^q\right)^{\frac{1}{q}}\\
&+\int_{\frac{\ell_1+\ell_2}{2}}^{\ell_2}\left(\left|(\Theta^{m+1}(\ell_2)-\Theta^{m+1}(\nu))^{\frac{p(\mu+\Sigma_{i=1}^n(\beta_i\kappa_i))}{k}}\right|d\nu\right)^{\frac{1}{p}}\times(|\Upsilon'(\ell_1)|)^q+\left((2^{m+1}-1)|\Upsilon'(\ell_2)|^q\right)^{\frac{1}{q}}\}
\end{aligned}
$$

Which is our desired result. □

Corollary 5. *If we replace* $\Theta(u) = u$, $m = 0$, $\delta_i = 0$, $\kappa_i = 0, \forall i$ *and* $s = k = 1$ *then we obtain ([28], Theorem 8).*

$$\left|\digamma\left(\frac{\ell_1+\ell_2}{2}\right)\left[\mathfrak{J}^{\mu}_{(\frac{\ell_1+\ell_2}{2})^+}\chi(\ell_2)+\mathfrak{J}^{\mu}_{(\frac{\ell_1+\ell_2}{2})^-}\chi(\ell_1)\right]\right| - \left|\left[\mathfrak{J}^{\mu}_{(\frac{\ell_1+\ell_2}{2})^+}\chi\digamma(\ell_2)+\mathfrak{J}^{\mu}_{(\frac{\ell_1+\ell_2}{2})^-}\chi\digamma(\ell_1)\right]\right|$$
$$\leq \frac{||\chi||_\infty(\ell_2-\ell_1)^{\frac{1}{q}}}{2^{\frac{3}{q}}\Gamma_(\mu+1)}\left(\int_{\ell_1}^{\frac{\ell_1+\ell_2}{2}}\left(\left|(\nu-\ell_1)^{p\mu}\right|d\nu\right)^{\frac{1}{p}}\right.$$
$$\left.\times\left(3(|\Upsilon'(\ell_1))|^q+|\Upsilon'(\ell_2)|^q\right)^{\frac{1}{q}}+\int_{\frac{\ell_1+\ell_2}{2}}^{\ell_2}\left(\left|(\ell_2-\nu)^{p\mu}\right|d\nu\right)^{\frac{1}{p}}\left(|\Upsilon'(\ell_1)|\right)^q+\left(3|\Upsilon'(\ell_2)|^q\right)^{\frac{1}{q}}\right).$$

Proposition 2. *If we replace* $\Theta(u) = u$, $m = 0$, $\delta_i = 0$, $\kappa_i = 0, \forall i$ *and* $s = k = 1$ *we obtain the following*

$$\left|\Upsilon(\frac{\ell_1+\ell_2}{2})\int_{\ell_1}^{\ell_2}\chi(\nu)d\nu-\int_{\ell_1}^{\ell_2}(\Upsilon\chi)(\nu)d\nu\right|$$
$$\leq\frac{||\chi||(\ell_2-\ell_1)^2}{(m+1)^{\frac{1}{p}}2^{\frac{4p-2}{p}}}\left[\left(3|\Upsilon'(\ell_1)|^q+|\Upsilon'(\ell_2)|^q\right)^{\frac{1}{q}}+\left(|\Upsilon'(\ell_1)|^q+3|\Upsilon'(\ell_2)|^q\right)^{\frac{1}{q}}\right].$$

3. Generalized H-H-F Type Inequalities Involving h-Convexity Associated with an Extended Fractional Operator and M-M-L Function

This section's first result reveals the M-M-L function for a generalized h-Cf and the generalized H-H-F inequality related with an extended fractional operator. In order to achieve this, the generalized supermultiplicative (s-m) mappings are necessary.

Definition 10. *Let us consider* $\aleph, \Im \in \Re$ *be invertals,* $\Im \geq (0,1)$ *and* $h \neq 0 : \Im \to \Re$ *be a positive. Also, a non-negative function* $f : \aleph \to \Re$ *is known as h-Cf if the inequality given below*

$$f(tx+(1-t)y) \leq h(t)f(x)+h(1-t)f(y)$$

holds for all $x, y \in \aleph, t \in (0,1)$.

Definition 11. *A mapping* $h : \Im \subseteq \Re \to \Re$ *is known as generalized s-m if*

$$h(xy) \geq h(x)h(y)$$

holds for all $x, y \in \Im$.

Theorem 5. *For* $k > 0$, $m \in \Re/\{-1\}$, *and* $Re(\mu) > 0$, $Re(\tau) > 0$, $Re(\delta) > 0$, $Re(\beta) > 0$ *are complex parameters, and* Θ *be an increasing function on* (ℓ_1, ℓ_2) *with* $\ell < \ell_2$, *also* $f : [\ell_1, \ell_2] \to \Re$ *be the geneeralized h-Cf and* $w : [\ell_1, \ell_2] \to \Re$, $w \geq 0$ *be symmetric pertaining to* $\frac{\ell_1+\ell_2}{2}$. *If* $f(x), w(x) \in ({}^{k,m}_{\Theta}\mathfrak{J}^{\delta_i,\tau_i}_{(\frac{\ell_1+\ell_2}{2})^+;\mu,\beta_i})[\ell_1, \ell_2]$, *then we have*

$$({}^{k,m}_{\Theta}\mathfrak{J}^{\delta_i,\tau_i}_{(\frac{\ell_1+\ell_2}{2})^+;\mu,\beta_i})f(y)w(y)$$
$$\leq\frac{f(\ell_1)+f(\ell_2)}{2}\Big({}^{k,m}_{\Theta}\mathfrak{J}^{\delta_i,\tau_i}_{(\frac{\ell_1+\ell_2}{2})^+;\mu,\beta_i}h(\frac{x-\ell_2}{\ell_1-\ell_2})w(x)(y)+({}^{k,m}_{\Theta}\mathfrak{J}^{\delta_i,\tau_i}_{(\frac{\ell_1+\ell_2}{2})^-;\mu,\beta_i}h\big(1-\frac{x-\ell_2}{\ell_1-\ell_2}\big)w(x)(y)\Big). \tag{16}$$

Proof. Let $\ell_1 < x < \frac{\ell_1+\ell_2}{2} < y < \ell_2$ exists $\nu \in (0,1)$ such that

$$x = \nu\ell_1 + (1-\nu)\ell_2$$
$$y = \nu\ell_2 + (1-\nu)\ell_1.$$

As we know that f is generalized h-Cf, we have

$$\begin{aligned} &f(\nu\ell_1 + (1-\nu)\ell_2)w\big(\nu\ell_1 + (1-\nu)\ell_2\big) \\ &\leq h(\nu)f(\ell_1) + h(1-\nu)f(\ell_2))w\big(\nu\ell_1 + (1-\nu)\ell_2\big), \end{aligned} \tag{17}$$

and

$$\begin{aligned} &f((1-\nu)\ell_1 + \nu\ell_2)w\big((1-\nu)\ell_1 + \nu\ell_2\big) \\ &\leq h(1-\nu)f(\ell_1) + h(\nu)f(\ell_2))w\big((1-\nu)\ell_1 + \nu\ell_2\big). \end{aligned} \tag{18}$$

By multiplying on both sides of (17),

$$\begin{aligned} &\frac{(m+1)^{\frac{\mu}{k}-1}(\ell_2-\ell_1)}{k} \\ &\times \frac{\xi^{\delta_i}_{k,\mu,\beta_i}\left(\tau_1(\Theta^{m+1}(\ell_2) - \Theta^{m+1}(\nu\ell_1 + (1-\nu)\ell_2))^{\frac{\beta_1}{k}}, \ldots, \tau_n(\Theta^{m+1}(\ell_2) - \Theta^{m+1}(\nu\ell_1 + (1-\nu)\ell_2))^{\frac{\beta_n}{k}}\right)}{(\Theta^{m+1}(\ell_2) - \Theta^{m+1}(\nu\ell_1 + (1-\nu)\ell_2))^{\frac{\mu}{k}-1}} \\ &\times \Theta^m(\nu\ell_1 + (1-\nu)\ell_2)\Theta'(\nu\ell_1 + (1-\nu)\ell_2), \end{aligned}$$

and after simplifying and taking integration on $[0,1]$ with respect to ν, we can have

$$\begin{aligned} &\frac{(m+1)^{\frac{\mu}{k}-1}(\ell_2-\ell_1)}{k} \\ &\times \int_0^1 \frac{\xi^{\delta_i}_{k,\mu,\beta_i}\left(\tau_1(\Theta^{m+1}(\ell_2) - \Theta^{m+1}(\nu\ell_1 + (1-\nu)\ell_2))^{\frac{\beta_1}{k}}, \ldots, \tau_n(\Theta^{m+1}(\ell_2) - \Theta^{m+1}(\nu\ell_1 + (1-\nu)\ell_2))^{\frac{\beta_n}{k}}\right)}{(\Theta^{m+1}(\ell_2) - \Theta^{m+1}(\nu\ell_1 + (1-\nu)\ell_2))^{\frac{\mu}{k}-1}} \\ &\times \Theta^m(\nu\ell_1 + (1-\nu)\ell_2)\Theta'(\nu\ell_1 + (1-\nu)\ell_2)f(\nu\ell_1 + (1-\nu)\ell_2)w(\nu\ell_1 + (1-\nu)\ell_2)d\nu \\ &\leq \frac{(m+1)^{\frac{\mu}{k}-1}(\ell_2-\ell_1)}{k} \\ &\times \int_0^1 \frac{\xi^{\delta_i}_{k,\mu,\beta_i}\left(\tau_1(\Theta^{m+1}(\ell_2) - \Theta^{m+1}(\nu\ell_1 + (1-\nu)\ell_2))^{\frac{\beta_1}{k}}, \ldots, \tau_n(\Theta^{m+1}(\ell_2) - \Theta^{m+1}(\nu\ell_1 + (1-\nu)\ell_2))^{\frac{\beta_n}{k}}\right)}{(\Theta^{m+1}(\ell_2) - \Theta^{m+1}(\nu\ell_1 + (1-\nu)\ell_2))^{\frac{\mu}{k}-1}} \\ &\times \Theta^m(\nu\ell_1 + (1-\nu)\ell_2)\Theta'(\nu\ell_1 + (1-\nu)\ell_2)\big((h(\nu)f(\ell_1) + h(1-\nu)f(\ell_2)\big)w(\nu\ell_1 + (1-\nu)\ell_2)d\nu. \end{aligned}$$

By replacing $x = (\nu\ell_1 + (1-\nu)\ell_2)$, we have

$$\begin{aligned} &({}^{k,m}_{\Theta}\mathfrak{J}^{\delta_i,\tau_i}_{(\frac{\ell_1+\ell_2}{2})^+;\mu,\beta_i})f(y)w(y) \\ &\leq f(\ell_1)({}^{k,m}_{\Theta}\mathfrak{J}^{\delta_i,\tau_i}_{(\frac{\ell_1+\ell_2}{2})^+;\mu,\beta_i}h\big(\frac{x-\ell_2}{\ell_1-\ell_2}\big)w(x))(y) + f(\ell_2)({}^{k,m}_{\Theta}\mathfrak{J}^{\delta_i,\tau_i}_{(\frac{\ell_1+\ell_2}{2})^+;\mu,\beta_i}h\big(1-\frac{x-\ell_2}{\ell_1-\ell_2}\big)w(x))(y). \end{aligned} \tag{19}$$

Continuing in the same way if we multiply the below term on both sides of (18)

$$\frac{(m+1)^{\frac{\mu}{k}-1}(\ell_2-\ell_1)}{k}$$
$$\times \frac{\xi^{\delta_i}_{k,\mu,\beta_i}\left(\tau_1(\Theta^{m+1}(\ell_2)-\Theta^{m+1}(\nu\ell_2+(1-\nu)\ell_1))^{\frac{\beta_1}{k}},\ldots,\tau_n(\Theta^{m+1}(\ell_2)-\Theta^{m+1}(\nu\ell_2+(1-\nu)\ell_1))^{\frac{\beta_n}{k}}\right)}{(\Theta^{m+1}(\ell_2)-\Theta^{m+1}(\nu\ell_2+(1-\nu)\ell_1))^{\frac{\mu}{k}-1}}$$
$$\times \Theta^m(\nu\ell_2+(1-\nu)\ell_1)\Theta'(\nu\ell_2+(1-\nu)\ell_1),$$

then after simplifying and taking integration on $[0,1]$ with respect to ν, we arrive at

$$({}^{k,m}_{\Theta}\mathfrak{J}^{\delta_i,\tau_i}_{(\frac{\ell_1+\ell_2}{2})^+;\mu,\beta_i} f(y)w(y)$$
$$\leq f(\ell_2)({}^{k,m}_{\Theta}\mathfrak{J}^{\delta_i,\tau_i}_{(\frac{\ell_1+\ell_2}{2})^+;\mu,\beta_i} h(\frac{x-\ell_2}{\ell_1-\ell_2})w(x))(y) + f(\ell_1)({}^{k,m}_{\Theta}\mathfrak{J}^{\delta_i,\tau_i}_{(\frac{\ell_1+\ell_2}{2})^+;\mu,\beta_i} h(1-\frac{x-\ell_2}{\ell_1-\ell_2})w(x))(y). \tag{20}$$

By adding (19) and (20), we obtain (16). □

Theorem 6. *For $k>0$, $m\in\Re/\{-1\}$, and $Re(\mu)>0$, $Re(\tau)>0$, $Re(\delta)>0$, $Re(\beta)>0$ are complex parameters, and Θ be an increasing function on (ℓ_1,ℓ_2) with $\ell_1<\ell_2$, also $f:[\ell_1,\ell_2]\to\Re$ be the geneeralized h-Cf with h define on $[0,max(1,\ell_2-\ell_1)]$ and $w:[\ell_1,\ell_2]\to\Re$, $w\geq 0$ be symmetric pertaining to $\frac{\ell_1+\ell_2}{2}$ and $({}^{k,m}_{\Theta}\mathfrak{J}^{\delta_i,\tau_i}_{(\frac{\ell_1+\ell_2}{2})^+;\mu,\beta_i})w>0$. [i] Then we have*

$$f(\frac{\ell_1+\ell_2}{2})\left({}^{k,m}_{\Theta}\mathfrak{J}^{\delta_i,\tau_i}_{a^+;\mu,\beta_i}\Big(w(x)+w(\ell_1+\ell_2-x)\Big)\right)(\ell_2)$$
$$\leq 2h(\frac{1}{2})\left({}^{k,m}_{\Theta}\mathfrak{J}^{\delta_i,\tau_i}_{a^+;\mu,\beta_i}\Big(w(x)f(x)+w(\ell_1+\ell_2-x)f(\ell_1+\ell_2-x)\Big)\right)(\ell_2). \tag{21}$$

[ii] Furthemore, if h, is generalized s-m and f is non-negative and

$$\frac{(m+1)^{\frac{\mu}{k}-1}}{k}$$
$$\int_{\frac{\ell_1+\ell_2}{2}}^{\ell_2}\frac{\xi^{\delta_i}_{k,\mu,\beta_i}\left(\tau_1(\Theta^{m+1}(\ell_2)-\Theta^{m+1}((1-\nu)\ell_1+(\nu)\ell_2))^{\frac{\beta_1}{k}},\ldots,\tau_n(\Theta^{m+1}(\ell_2)-\Theta^{m+1}((1-\nu)\ell_1+(\nu)\ell_2)))^{\frac{\beta_n}{k}}\right)}{(\Theta^{m+1}(\ell_2)-\Theta^{m+1}(1-\nu)\ell_1+(\nu)\ell_2))^{\frac{\mu}{k}-1}}$$
$$\times \Theta^m(1-\nu)\ell_1+(\nu)\ell_2)\Theta'(1-\nu)\ell_1+(\nu)\ell_2)$$
$$\times\left(\frac{(m+1)^{\frac{\mu}{k}-1}}{k}\right.$$
$$\left.\int_{\ell_2}^{\frac{\ell_1+\ell_2}{2}}\frac{\xi^{\delta_i}_{k,\mu,\beta_i}\left(\tau_1(\Theta^{m+1}(\ell_2)-\Theta^{m+1}(\nu\ell_1+(1-\nu)\ell_2))^{\frac{\beta_1}{k}},\ldots,\tau_n(\Theta^{m+1}(\ell_2)-\Theta^{m+1}((\nu\ell_1+(1-\nu)\ell_2))^{\frac{\beta_n}{k}}\right)}{(\Theta^{m+1}(\ell_2)-\Theta^{m+1}(\nu\ell_1+(1-\nu)\ell_2))^{\frac{\mu}{k}-1}}\right.$$
$$\left.\times\Theta^m(\nu\ell_1+(1-\nu)\ell_2)\Theta'(\nu\ell_1+(1-\nu)\ell_2)h(y-x)w(x)dx\right)w(y)dy\neq 0, h(x)>0, \tag{22}$$

then, we have

$$
\begin{aligned}
&f\big(\frac{\ell_1+\ell_2}{2}\big)\frac{(m+1)^{\frac{\mu}{k}-1}}{k}\\
&\int_{\frac{\ell_1+\ell_2}{2}}^{\ell_2}\frac{\xi_{k,\mu,\beta_i}^{\delta_i}\Big(\tau_1(\Theta^{m+1}(\ell_2)-\Theta^{m+1}((1-\nu)\ell_1+(\nu)\ell_2))^{\frac{\beta_1}{k}},\ldots,\tau_n(\Theta^{m+1}(\ell_2)-\Theta^{m+1}((1-\nu)\ell_1+(\nu)\ell_2))^{\frac{\beta_n}{k}}\Big)}{(\Theta^{m+1}(\ell_2)-\Theta^{m+1}(1-\nu)\ell_1+(\nu)\ell_2))^{\frac{\mu}{k}-1}}\\
&\times\Theta^m(1-\nu)\ell_1+(\nu)\ell_2)\Theta'(1-\nu)\ell_1+(\nu)\ell_2)\\
&\times\Bigg(\frac{(m+1)^{\frac{\mu}{k}-1}}{k}\\
&\int_{\ell_2}^{\frac{\ell_1+\ell_2}{2}}\frac{\xi_{k,\mu,\beta_i}^{\delta_i}\Big(\tau_1(\Theta^{m+1}(\ell_2)-\Theta^{m+1}(\nu\ell_1+(1-\nu)\ell_2))^{\frac{\beta_1}{k}},\ldots,\tau_n(\Theta^{m+1}(\ell_2)-\Theta^{m+1}((\nu\ell_1+(1-\nu)\ell_2))^{\frac{\beta_n}{k}}}{(\Theta^{m+1}(\ell_2)-\Theta^{m+1}(\nu\ell_1+(1-\nu)\ell_2))^{\frac{\mu}{k}-1}}\\
&\times\Theta^m(\nu\ell_1+(1-\nu)\ell_2)\Theta'(\nu\ell_1+(1-\nu)\ell_2)h(y-x)w(x)dx\Bigg)w(y)dy \qquad (23)\\
&\leq\Big({}_{\Theta}^{k,m}\mathfrak{J}_{(\frac{\ell_1+\ell_2}{2})^+;\mu,\beta_i}^{\delta_i,\tau_i}h\big(y-\frac{\ell_1+\ell_2}{2}\big)\Big)(\ell_2)\Big({}_{\Theta}^{k,m}\mathfrak{J}_{\tau_1^+;\mu,\beta_i}^{\delta_i,\tau_i}f(x)w(x)\Big)(\ell_2)\\
&+\Big({}_{\Theta}^{k,m}\mathfrak{J}_{(\frac{\ell_1+\ell_2}{2})^+;\mu,\beta_i}^{\delta_i,\tau_i}f(y)w(y)\Big)(\ell_2)\Big({}_{\Theta}^{k,m}\mathfrak{J}_{\tau_1^+;\mu,\beta_i}^{\delta_i,\tau_i}h\Big(\frac{\ell_1+\ell_2}{2}-x\Big)\Big)(\ell_2). \qquad (24)
\end{aligned}
$$

Proof. (i) Using the h-Cf if $\nu=\frac{1}{2}$, $x=\nu\ell_1+(1-\nu)\ell_2$ and $y=(1-\nu)\ell_1+(\nu)\ell_2$, then we have that

$$
\begin{aligned}
&f\Big(\frac{\ell_1+\ell_2}{2}\Big)\leq h(\frac{1}{2})\Big[f(\nu\ell_1+(1-\nu)\ell_2)+f(1-\nu)\ell_1+(\nu)\ell_2)\Big]\\
&\Leftrightarrow w(\nu\ell_1+(1-\nu)\ell_2)f\Big(\frac{\ell_1+\ell_2}{2}\Big)+w(1-\nu)\ell_1+(\nu)\ell_2)f\Big(\frac{\ell_1+\ell_2}{2}\Big)\\
&\leq 2h(\frac{1}{2})\Big[w(\nu\ell_1+(1-\nu)\ell_2)f(\nu\ell_1+(1-\nu)\ell_2)\\
&+w(1-\nu)\ell_1+(\nu)\ell_2)f(1-\nu)\ell_1+(\nu)\ell_2)\Big]. \qquad (25)
\end{aligned}
$$

By multiplying on both sides of (25),

$$
\begin{aligned}
&\frac{(m+1)^{\frac{\mu}{k}-1}(\ell_2-\ell_1)}{k}\\
&\frac{\xi_{k,\mu,\beta_i}^{\delta_i}\Big(\tau_1(\Theta^{m+1}(\ell_2)-\Theta^{m+1}(\nu\ell_1+(1-\nu)\ell_2))^{\frac{\beta_1}{k}},\ldots,\tau_n(\Theta^{m+1}(\ell_2)-\Theta^{m+1}(\nu\ell_1+(1-\nu)\ell_2))^{\frac{\beta_n}{k}}\Big)}{(\Theta^{m+1}(\ell_2)-\Theta^{m+1}(\nu\ell_1+(1-\nu)\ell_2))^{\frac{\mu}{k}-1}}\\
&\times\Theta^m(\nu\ell_1+(1-\nu)\ell_2)\Theta'(\nu\ell_1+((1-\nu)\ell_2),
\end{aligned}
$$

and after simplifying and taking integration on $[0,1]$ with respect to ν, we have

$$\frac{(m+1)^{\frac{\mu}{k}-1}(\ell_2-\ell_1)}{k}$$
$$\times\int_0^1 \frac{\xi^{\delta_i}_{k,\mu,\beta_i}\left(\tau_1(\Theta^{m+1}(\ell_2)-\Theta^{m+1}(\nu\ell_1+(1-\nu)\ell_2))^{\frac{\beta_1}{k}},\ldots,\tau_n(\Theta^{m+1}(\ell_2)-\Theta^{m+1}(\nu\ell_1+(1-\nu)\ell_2))^{\frac{\beta_n}{k}}\right)}{(\Theta^{m+1}(\ell_2)-\Theta^{m+1}(\nu\ell_1+(1-\nu)\ell_2))^{\frac{\mu}{k}-1}}$$
$$\times\Theta^m(\nu\ell_1+(1-\nu)\ell_2)\Theta'(\nu\ell_1+((1-\nu)\ell_2)$$
$$\Big(w(\nu\ell_1+(1-\nu)\ell_2)f(\frac{\ell_1+\ell_2}{2})+w(1-\nu)\ell_1+\nu\ell_2)f(\frac{\ell_1+\ell_2}{2})\Big)d\nu$$
$$\leq 2h(\frac{1}{2})\frac{(m+1)^{\frac{\mu}{k}-1}(\ell_2-\ell_1)}{k}$$
$$\times\int_0^1 \frac{\xi^{\delta_i}_{k,\mu,\beta_i}\left(\tau_1(\Theta^{m+1}(\ell_2)-\Theta^{m+1}(\nu\ell_1+(1-\nu)\ell_2))^{\frac{\beta_1}{k}},\ldots,\tau_n(\Theta^{m+1}(\ell_2)-\Theta^{m+1}(\nu\ell_1+(1-\nu)\ell_2))^{\frac{\beta_n}{k}}\right)}{(\Theta^{m+1}(\ell_2)-\Theta^{m+1}(\nu\ell_1+(1-\nu)\ell_2))^{\frac{\mu}{k}-1}}$$
$$\times\Theta^m(\nu\ell_1+(1-\nu)\ell_2)\Theta'(\nu\ell_1+((1-\nu)\ell_2)$$
$$\times\Big[w\big(\nu\ell_1+(1-\nu)\ell_2\big)f(\nu\ell_1+(1-\nu)\ell_2)+w\big((1-\nu)\ell_1+(\nu)\ell_2\big)f\big((1-\nu)\ell_1+(\nu)\ell_2\big)\Big]d\nu.$$

By replacing $x=\nu\ell_1+(1-\nu)\ell_2$, so we have

$$f(\frac{\ell_1+\ell_2}{2})\left({}^{k,m}_{\Theta}\mathfrak{I}^{\delta_i,\tau_i}_{a^+;\mu,\beta_i}\left(w(x)+w(\ell_1+\ell_2-x)\right)\right)(\ell_2)$$
$$\leq 2h(\frac{1}{2})\left({}^{k,m}_{\Theta}\mathfrak{I}^{\delta_i,\tau_i}_{a^+;\mu,\beta_i}\left(w(x)f(x)+w(\ell_1+\ell_2-x)f(\ell_1+\ell_2-x)\right)\right)(\ell_2).$$

(ii) Let h be generalized s-m and $h(\nu)>0$ for $\nu\in[0,max(1,\ell_2-\ell_1)]$. For any $x,y\in[\ell_1,\ell_2]$ such that $\ell_1<x<\frac{\ell_1+\ell_2}{2}<y\leq\ell_2$, we have

$$\frac{\ell_1+\ell_2}{2}=\Big(\frac{y-\frac{\ell_1+\ell_2}{2}}{y-x}\Big)x+\Big(\frac{\frac{\ell_1+\ell_2}{2}-x}{y-x}\Big)y\Rightarrow f(\frac{\ell_1+\ell_2}{2})$$
$$\leq h\Big(\frac{y-\frac{\ell_1+\ell_2}{2}}{y-x}\Big)f(x)+h\Big(\frac{\frac{\ell_1+\ell_2}{2}-x}{y-x}\Big)f(y). \tag{26}$$

Since h is s-m

$$h\Big(\frac{y-\frac{\ell_1+\ell_2}{2}}{y-x}\Big)\leq\frac{h(y-\frac{\ell_1+\ell_2}{2})}{h(y-x)} \tag{27}$$

and

$$h\Big(\frac{\frac{\ell_1+\ell_2}{2}-x}{y-x}\Big)\leq\frac{h(\frac{\ell_1+\ell_2}{2}-x)}{h(y-x)}. \tag{28}$$

When $f(x)\geq 0$ we have

$$h(y-x)f\Big(\frac{\ell_1+\ell_2}{2}\Big)\leq h\Big(y-\frac{\ell_1+\ell_2}{2}\Big)f(x)+h\Big(\frac{\ell_1+\ell_2}{2}-x\Big)f(y). \tag{29}$$

By multiplying weighted iterated integrals on both sides of (29),

$$\frac{(m+1)^{\frac{\mu}{k}-1}(\ell_2-\ell_1)}{k}$$
$$\frac{\xi_{k,\mu,\beta_i}^{\delta_i}\left(\tau_1(\Theta^{m+1}(\ell_2)-\Theta^{m+1}(\nu\tau_1+(1-\nu)\ell_2))^{\frac{\beta_1}{k}},\ldots,\tau_n(\Theta^{m+1}(\ell_2)-\Theta^{m+1}(\nu\ell_1+(1-\nu)\ell_2))^{\frac{\beta_n}{k}}\right)}{(\Theta^{m+1}(\ell_2)-\Theta^{m+1}(\nu\ell_1+(1-\nu)\ell_2))^{\frac{\mu}{k}-1}}$$
$$\times\Theta^m(\nu\ell_1+(1-\nu)\ell_2)\Theta'(\nu\ell_1+((1-\nu)\ell_2)w(y),$$

and after simplifying and taking integration of $w(x)$ and $w(y)$ on $[0,\frac{1}{2}]$ and $[\frac{1}{2},1]$, respectively, we have

$$\begin{aligned}
&f(\frac{\ell_1+\ell_2}{2})\frac{(m+1)^{\frac{\mu}{k}-1}(\ell_2-\ell_1)}{k}\\
&\times\int_{\frac{1}{2}}^{1}\frac{\xi_{k,\mu,\beta_i}^{\delta_i}\left(\tau_1(\Theta^{m+1}(\ell_2)-\Theta^{m+1}(1-\nu)\ell_1+\nu\ell_2)^{\frac{\beta_1}{k}},\ldots,\tau_n(\Theta^{m+1}(\ell_2)-\Theta^{m+1}(1-\nu)\ell_1+\nu\ell_2))^{\frac{\beta_n}{k}}\right)}{(\Theta^{m+1}(\ell_2)-\Theta^{m+1}(1-\nu)\ell_1+\nu\ell_2))^{\frac{\mu}{k}-1}}\\
&\times\Theta^m(1-\nu)\ell_1+\nu\ell_2)\Theta'(1-\nu)\ell_1+\nu\ell_2)\\
&\times\Bigg(\frac{(m+1)^{\frac{\mu}{k}-1}(\ell_2-\ell_1)}{k}\\
&\times\int_0^{\frac{1}{2}}\frac{\xi_{k,\mu,\beta_i}^{\delta_i}\left(\tau_1(\Theta^{m+1}(\ell_2)-\Theta^{m+1}(\nu\ell_1+(1-\nu)\ell_2))^{\frac{\beta_1}{k}},\ldots,\tau_n(\Theta^{m+1}(\ell_2)-\Theta^{m+1}(\nu\ell_1+(1-\nu)\ell_2))^{\frac{\beta_n}{k}}\right)}{(\Theta^{m+1}(\ell_2)-\Theta^{m+1}(\nu\ell_1+(1-\nu)\ell_2))^{1-\frac{\delta}{k}}}\\
&\times\Theta^m(\nu\ell_1+(1-\nu)\ell_2)\Theta'(\nu\ell_1+(1-\nu)\ell_2)h(y-x)w(x)dx\Bigg)w(y)dy\\
&\leq\frac{(m+1)^{\frac{\mu}{k}-1}(\ell_2-\ell_1)}{k}\\
&\times\int_{\frac{1}{2}}^{1}\frac{\xi_{k,\mu,\beta_i}^{\delta_i}\left(\tau_1(\Theta^{m+1}(\ell_2)-\Theta^{m+1}(1-\nu)\ell_1+\nu\ell_2)^{\frac{\beta_1}{k}},\ldots,\tau_n(\Theta^{m+1}(\ell_2)-\Theta^{m+1}(1-\nu)\ell_1+\nu\ell_2))^{\frac{\beta_n}{k}}\right)}{(\Theta^{m+1}(\ell_2)-\Theta^{m+1}(1-\nu)\ell_1+\nu\ell_2))^{\frac{\mu}{k}-1}}\\
&\times\Theta^m(1-\nu)\ell_1+\nu\ell_2)\Theta'(1-\nu)\ell_1+\nu\ell_2)h\Big(y-\frac{\ell_1+\ell_2}{2}\Big)dy\\
&\times\frac{(m+1)^{\frac{\mu}{k}-1}(\ell_2-\ell_1)}{k}\\
&\times\int_0^{\frac{1}{2}}\frac{\xi_{k,\mu,\beta_i}^{\delta_i}\left(\tau_1(\Theta^{m+1}(\ell_2)-\Theta^{m+1}(\nu\ell_1+(1-\nu)\ell_2))^{\frac{\beta_1}{k}},\ldots,\tau_n(\Theta^{m+1}(\ell_2)-\Theta^{m+1}(\nu\ell_1+(1-\nu)\ell_2))^{\frac{\beta_n}{k}}\right)}{(\Theta^{m+1}(\ell_2)-\Theta^{m+1}(\nu\ell_1+(1-\nu)\ell_2))^{1-\frac{\delta}{k}}}\\
&\times\Theta^m(\nu\ell_1+(1-\nu)\ell_2)\Theta'(\nu\ell_1+(1-\nu)\ell_2)f(x)w(x)dx\\
&+\frac{(m+1)^{\frac{\mu}{k}-1}(\ell_2-\ell_1)}{k}\\
&\times\int_{\frac{1}{2}}^{1}\frac{\xi_{k,\mu,\beta_i}^{\delta_i}\left(\tau_1(\Theta^{m+1}(\ell_2)-\Theta^{m+1}(1-\nu)\ell_1+\nu\ell_2)^{\frac{\beta_1}{k}},\ldots,\tau_n(\Theta^{m+1}(\ell_2)-\Theta^{m+1}(1-\nu)\ell_1+\nu\ell_2))^{\frac{\beta_n}{k}}\right)}{(\Theta^{m+1}(\ell_2)-\Theta^{m+1}(1-\nu)\ell_1+\nu\ell_2))^{\frac{\mu}{k}-1}}\\
&\times\Theta^m(1-\nu)\ell_1+\nu\ell_2)\Theta'(1-\nu)\ell_1+\nu\ell_2)f(y)w(y)dy\\
&\times\frac{(m+1)^{\frac{\mu}{k}-1}(\ell_2-\ell_1)}{k}\\
&\times\int_0^{\frac{1}{2}}\frac{\xi_{k,\mu,\beta_i}^{\delta_i}\left(\tau_1(\Theta^{m+1}(\ell_2)-\Theta^{m+1}(\nu\ell_1+(1-\nu)\ell_2))^{\frac{\beta_1}{k}},\ldots,\tau_n(\Theta^{m+1}(\ell_2)-\Theta^{m+1}(\nu\ell_1+(1-\nu)\ell_2))^{\frac{\beta_n}{k}}\right)}{(\Theta^{m+1}(\ell_2)-\Theta^{m+1}(\nu\ell_1+(1-\nu)\ell_2))^{1-\frac{\delta}{k}}}\\
&\times\Theta^m(\nu\ell_1+(1-\nu)\ell_2)\Theta'(\nu\ell_1+(1-\nu)\ell_2)h\Big(\frac{\ell_1+\ell_2}{2}-x\Big)dx.
\end{aligned}$$

By replacing $x=\nu\ell_1+(1-\nu)\ell_2)$ and $y=(1-\nu)\ell_1+(\nu)\ell_2)$, then we have

$$
\begin{aligned}
&f\Big(\frac{\ell_1+\ell_2}{2}\Big)\frac{(m+1)^{\frac{\mu}{k}-1}}{k}\\
&\times\int_{\frac{\ell_1+\ell_2}{2}}^{\ell_2}\frac{\xi_{k,\mu,\beta_i}^{\delta_i}\Big(\tau_1(\Theta^{m+1}(\ell_2)-\Theta^{m+1}(y)^{\frac{\beta_1}{k}},\ldots,\tau_n(\Theta^{m+1}(\ell_2)-\Theta^{m+1}(y))^{\frac{\beta_n}{k}}\Big)}{(\Theta^{m+1}(\ell_2)-\Theta^{m+1}(y)^{\frac{\mu}{k}-1}}\Theta^m(y)\Theta'(y)\\
&\times\Bigg(\frac{(m+1)^{\frac{\mu}{k}-1}}{k}\int_{\ell_1}^{\frac{\ell_1+\ell_2}{2}}\frac{\xi_{k,\mu,\beta_i}^{\delta_i}\Big(\tau_1(\Theta^{m+1}(\ell_2)-\Theta^{m+1}(x)^{\frac{\beta_1}{k}},\ldots,\tau_n(\Theta^{m+1}(\ell_2)-\Theta^{m+1}(x))^{\frac{\beta_n}{k}}\Big)}{(\Theta^{m+1}(\ell_2)-\Theta^{m+1}(x)^{\frac{\mu}{k}-1}}\\
&\times\Theta^m(x)\Theta'(x)h(y-x)w(x)dx\Bigg)w(y)dy\\
&\leq\frac{(m+1)^{\frac{\mu}{k}-1}}{k}\int_{\frac{\ell_1+\ell_2}{2}}^{\ell_2}\frac{\xi_{k,\mu,\beta_i}^{\delta_i}\Big(\tau_1(\Theta^{m+1}(\ell_2)-\Theta^{m+1}(y)^{\frac{\beta_1}{k}},\ldots,\tau_n(\Theta^{m+1}(\ell_2)-\Theta^{m+1}(y))^{\frac{\beta_n}{k}}\Big)}{(\Theta^{m+1}(\ell_2)-\Theta^{m+1}(y)^{\frac{\mu}{k}-1}}\\
&\times\Theta^m(y)\Theta'(y)h\Big(y-\frac{\ell_1+\ell_2}{2}\Big)dy\\
&\times\frac{(m+1)^{\frac{\mu}{k}-1}}{k}\int_{\ell_1}^{\frac{\ell_1+\ell_2}{2}}\frac{\xi_{k,\mu,\beta_i}^{\delta_i}\Big(\tau_1(\Theta^{m+1}(\ell_2)-\Theta^{m+1}(x)^{\frac{\beta_1}{k}},\ldots,\tau_n(\Theta^{m+1}(\ell_2)-\Theta^{m+1}(x))^{\frac{\beta_n}{k}}\Big)}{(\Theta^{m+1}(\ell_2)-\Theta^{m+1}(x)^{\frac{\mu}{k}-1}}\\
&\times\Theta^m(x)\Theta'(x)f(x)w(x)dx\\
&+\frac{(m+1)^{\frac{\mu}{k}-1}}{k}\int_{\frac{\ell_1+\ell_2}{2}}^{\ell_2}\frac{\xi_{k,\mu,\beta_i}^{\delta_i}\Big(\tau_1(\Theta^{m+1}(\ell_2)-\Theta^{m+1}(y)^{\frac{\beta_1}{k}},\ldots,\tau_n(\Theta^{m+1}(\ell_2)-\Theta^{m+1}(y))^{\frac{\beta_n}{k}}\Big)}{(\Theta^{m+1}(\ell_2)-\Theta^{m+1}(y)^{\frac{\mu}{k}-1}}\\
&\times\Theta^m(y)\Theta'(y)f(y)w(y)dy\\
&\times\frac{(m+1)^{\frac{\mu}{k}-1}}{k}\int_{\ell_1}^{\frac{\ell_1+\ell_2}{2}}\frac{\xi_{k,\mu,\beta_i}^{\delta_i}\Big(\tau_1(\Theta^{m+1}(\ell_2)-\Theta^{m+1}(x)^{\frac{\beta_1}{k}},\ldots,\tau_n(\Theta^{m+1}(\ell_2)-\Theta^{m+1}(x))^{\frac{\beta_n}{k}}\Big)}{(\Theta^{m+1}(\ell_2)-\Theta^{m+1}(x)^{\frac{\mu}{k}-1}}\\
&\times\Theta^m(x)\Theta'(x)h\Big(\frac{\ell_1+\ell_2}{2}-x\Big)dx\\
&=\Big({}^{k,m}_{\Theta}\mathfrak{J}^{\delta_i,\tau_i}_{(\frac{\ell_1+\ell_2}{2})^+;\mu,\beta_i}h\big(y-\frac{\ell_1+\ell_2}{2}\big)\Big)(\ell_2)\Big({}^{k,m}_{\Theta}\mathfrak{J}^{\delta_i,\tau_i}_{\tau_1^+;\mu,\beta_i}f(x)w(x)\Big)(\ell_2)\\
&+\Big({}^{k,m}_{\Theta}\mathfrak{J}^{\delta_i,\tau_i}_{(\frac{\ell_1+\ell_2}{2})^+;\mu,\beta_i}f(y)w(y)\Big)(\ell_2)\Big({}^{k,m}_{\Theta}\mathfrak{J}^{\delta_i,\tau_i}_{\tau_1^+;\mu,\beta_i}h\Big(\frac{\ell_1+\ell_2}{2}-x\Big)\Big)(\ell_2).
\end{aligned}
$$

□

Lemma 2. *If $f:[\ell_1,\ell_2]\to\Re$ is generalized h-Cf, then identity given below*

$$f(\ell_1+\ell_2-x)\leq\Big(h(\nu)+h(1-\nu)\Big)\Big[f(\ell_1)+f(\ell_2)\Big]-f(x),\tag{30}$$

hold for all $x\in[\ell_1,\ell_2]$ and $\nu\in[0,1]$.

Proof. We skip the proof of Lemma 2 here, because essentially it is very identical with that of (Lemma 1, [58]). □

Theorem 7. *For $k>0$, $m\in\Re/\{-1\}$, and $Re(\mu)>0$, $Re(\tau)>0$, $Re(\delta)>0$, $Re(\beta)>0$ are complex parameters, and Θ be an increasing function on (ℓ_1,ℓ_2) with $\ell<\ell_2$, also the geneeralized h-Cf $f:[\ell_1,\ell_2]\to\Re$ and $w:[\ell_1,\ell_2]\to\Re$, $w\geq0$ both are symmetric pertaining to $\frac{\ell_1+\ell_2}{2}$, then we have*

$$f(\frac{\ell_1+\ell_2}{2})\left({}^{k,m}_{\Theta}\mathfrak{J}^{\delta_i,\tau_i}_{((\frac{\ell_1+\ell_2}{2})^+;\mu,\beta_i}w(x)\right)(\ell_2)$$
$$\leq 2h(\frac{1}{2})\left({}^{k,m}_{\Theta}\mathfrak{J}^{\delta_i,\tau_i}_{((\frac{\ell_1+\ell_2}{2})^+;\mu,\beta_i}\left(w(x)f(x)+\left(\big(h(\nu)+h(1-\nu)\big)\big(f(\ell_1)+f(\ell_2)\big)-f(x)\right)w(x)\right)\right)(\ell_2).$$

Proof. We have

$$f(\frac{\ell_1+\ell_2}{2})\left({}^{k,m}_{\Theta}\mathfrak{J}^{\delta_i,\tau_i}_{((\frac{\ell_1+\ell_2}{2})^+;\mu,\beta_i}\Big(w(x)+w(\ell_1+\ell_2-x)\Big)\right)(\ell_2)$$
$$\leq h(\frac{1}{2})\left({}^{k,m}_{\Theta}\mathfrak{J}^{\delta_i,\tau_i}_{((\frac{\ell_1+\ell_2}{2})^+;\mu,\beta_i}\Big(w(x)f(x)+w(\ell_1+\ell_2-x)f(\ell_1+\ell_2-x)\Big)\right).$$

Since w is symmetric

$$f(\frac{\ell_1+\ell_2}{2})\left({}^{k,m}_{\Theta}\mathfrak{J}^{\delta_i,\tau_i}_{((\frac{\ell_1+\ell_2}{2})^+;\mu,\beta_i}w(x)\right)(\ell_2)$$
$$\leq 2h(\frac{1}{2})\left({}^{k,m}_{\Theta}\mathfrak{J}^{\delta_i,\tau_i}_{(\frac{\ell_1+\ell_2}{2})^+;\mu,\beta_i}\left(w(x)f(x)+\left(\big(h(\nu)+h(1-\nu)\big)\big(f(\ell_1)+f(\ell_2)\big)-f(x)\right)w(x)\right)\right)(\ell_2).$$
□

Example 2. *If we choose* $w(x)=1, f(x)=\Theta^{m+1}(x)$ *and* $h(x)=1$, *we have*

$$f(\frac{\ell_1+\ell_2}{2})\left({}^{k,m}_{\Theta}\mathfrak{J}^{\delta_i,\tau_i}_{(\frac{\ell_1+\ell_2}{2})^+;\mu,\beta_i}w(x)\right)(\ell_2)$$
$$=\left(\frac{(m+1)^{-\frac{\mu}{k}}}{k}\sum_{n=0}^{\infty}\frac{(\delta_i)_{\kappa_i,k}(\tau_i)^{\kappa_i}}{\Gamma_k(\mu+\Sigma_{i=1}^n(\beta_i\kappa_i))(\frac{\mu+\Sigma_{i=1}^n(\beta_i\kappa_i)}{k})}\left((\Theta^{m+1}(\ell_2)-\Theta^{m+1}(\frac{\ell_1+\ell_2}{2})\right)^{\frac{\mu+\Sigma_{i=1}^n(\beta_i\kappa_i)}{k}},\right.$$

and

$$2h(\frac{1}{2})\left({}^{k,m}_{\Theta}\mathfrak{J}^{\delta_i,\tau_i}_{(\frac{\ell_1+\ell_2}{2})^+;\mu,\beta_i}\left(w(x)f(x)+\left(\big(h(\nu)+h(1-\nu)\big)\big(f(\tau_1)+f(\ell_2)\big)-f(x)\right)w(x)\right)\right)(\ell_2)$$
$$=4\left(\frac{(m+1)^{-\frac{\mu}{k}}}{k}\sum_{n=0}^{\infty}\frac{(\delta_i)_{\kappa_i,k}(\tau_i)^{\kappa_i}}{\Gamma_k(\mu+\Sigma_{i=1}^n(\beta_i\kappa_i)(\frac{\mu+\Sigma_{i=1}^n(\beta_i\kappa_i)}{k})}\left(\Theta^{m+1}(\ell_2)-\Theta^{m+1}(\frac{\ell_1+\ell_2}{2})\right)^{\frac{\mu+\Sigma_{i=1}^n(\beta_i\kappa_i)}{k}}.\right.$$

By comparing above results we have

$$\frac{(m+1)^{-\frac{\mu}{k}}}{k}\sum_{n=0}^{\infty}\frac{(\delta_i)_{\kappa_i,k}(\tau_i)^{\kappa_i}}{\Gamma_k(\mu+\Sigma_{i=1}^n(\beta_i\kappa_i)(\frac{\mu+\Sigma_{i=1}^n(\beta_i\kappa_i)}{k})}\left(\Theta^{m+1}(\ell_2)-\Theta^{m+1}(\frac{\ell_1+\ell_2}{2})\right)^{\frac{\mu+\Sigma_{i=1}^n(\beta_i\kappa_i)}{k}}$$
$$\leq 4\left(\frac{(m+1)^{-\frac{\mu}{k}}}{k}\sum_{n=0}^{\infty}\frac{(\delta_i)_{\kappa_i,k}(\tau_i)^{\kappa_i}}{\Gamma_k(\mu+\Sigma_{i=1}^n(\beta_i\kappa_i)(\frac{\mu+\Sigma_{i=1}^n(\beta_i\kappa_i)}{k})}\left(\Theta^{m+1}(\ell_2)-\Theta^{m+1}(\frac{\ell_1+\ell_2}{2})\right)^{\frac{\mu+\Sigma_{i=1}^n(\beta_i\kappa_i)}{k}}.\right. \tag{31}$$

The computational values of (31), *are shown in Tables 3 and 4 corresponding to the choice of parameters* $m=2, k=1, \Theta(x)=x^2, \mu=2, \tau_i=1, \beta_i=0.5, \kappa_i=0.5, \mu=0.5$ *for some fixed values of* ℓ_1 *and* ℓ_2. *Figure 2, shows the graphical representation of* (31), *corresponding to the choice of parameters* $0<\ell_1=1<\ell_2=4$.

Table 3. The computational values of (31) corresponding to choice $\mu = 0.5$ are as follows:

$\ell_1/\ell 2$	**2.00**	**2.40**	**2.80**
1.00	$(6.93 \times 10^{00}, 2.77 \times 10^{01})$	$(2.37 \times 10^{01}, 9.49 \times 10^{01})$	$(9.60 \times 10^{01}, 3.84 \times 10^{02})$
1.20	$(4.76 \times 10^{00}, 1.91 \times 10^{01})$	$(1.64 \times 10^{01}, 6.55 \times 10^{01})$	$(6.46 \times 10^{01}, 2.58 \times 10^{02})$
1.40	$(3.08 \times 10^{00}, 1.23 \times 10^{01})$	$(1.09 \times 10^{01}, 4.37 \times 10^{01})$	$(4.25 \times 10^{01}, 1.70 \times 10^{02})$
1.60	$(1.81 \times 10^{00}, 7.23 \times 10^{00})$	$(7.02 \times 10^{00}, 2.81 \times 10^{01})$	$(2.72 \times 10^{01}, 1.09 \times 10^{02})$
1.80	$(8.48 \times 10^{-01}, 3.39 \times 10^{00})$	$(4.25 \times 10^{00}, 1.70 \times 10^{01})$	$(1.69 \times 10^{01}, 6.76 \times 10^{01})$
2.00	$(0.00 \times 10^{00}, 0.00 \times 10^{00})$	$(2.34 \times 10^{00}, 9.35 \times 10^{00})$	$(1.01 \times 10^{01}, 4.05 \times 10^{01})$

Table 4. The computational values of (31) corresponding to choice $\mu = 0.5$.

$\ell_1/\ell 2$	**3.20**	**3.60**	**4.00**
1.00	$(4.80 \times 10^{02}, 1.92 \times 10^{03})$	$(3.03 \times 10^{03}, 1.21 \times 10^{04})$	$(2.43 \times 10^{04}, 9.70 \times 10^{04})$
1.20	$(3.12 \times 10^{02}, 1.25 \times 10^{03})$	$(1.89 \times 10^{03}, 7.57 \times 10^{03})$	$(1.46 \times 10^{04}, 5.83 \times 10^{04})$
1.40	$(1.98 \times 10^{02}, 7.94 \times 10^{02})$	$(1.16 \times 10^{03}, 4.64 \times 10^{03})$	$(8.57 \times 10^{03}, 3.43 \times 10^{04})$
1.60	$(1.24 \times 10^{02}, 4.94 \times 10^{02})$	$(6.96 \times 10^{02}, 2.78 \times 10^{03})$	$(4.95 \times 10^{03}, 1.98 \times 10^{04})$
1.80	$(7.52 \times 10^{01}, 3.01 \times 10^{02})$	$(4.09 \times 10^{02}, 1.64 \times 10^{03})$	$(2.80 \times 10^{03}, 1.12 \times 10^{04})$
2.00	$(4.47 \times 10^{01}, 1.79 \times 10^{02})$	$(2.35 \times 10^{02}, 9.42 \times 10^{02})$	$(1.55 \times 10^{03}, 6.20 \times 10^{03})$

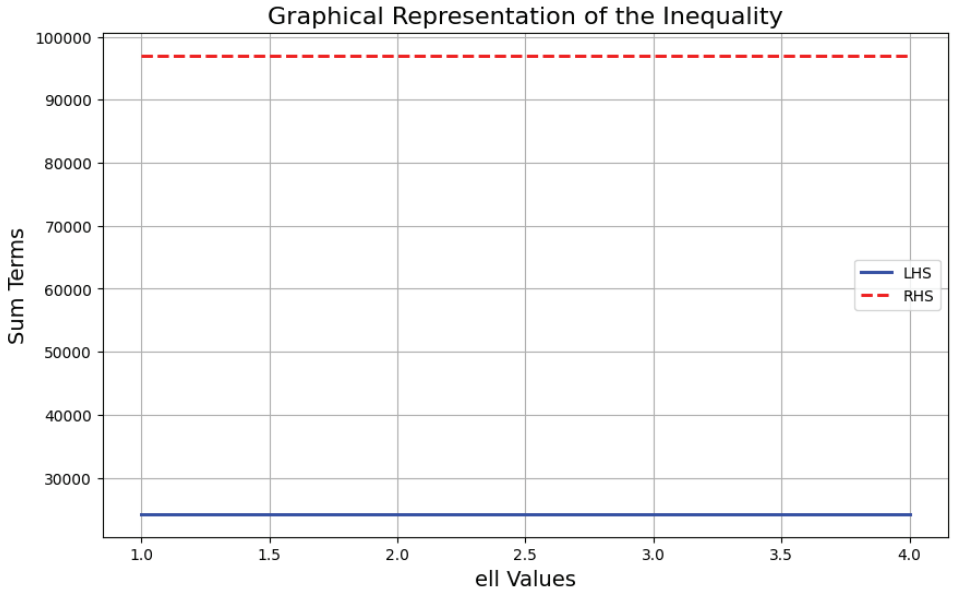

Figure 2. The graphical representation of (31) corresponding to choice $\mu = 0.5$.

Theorem 8. *For $k > 0$, $m \in \Re/\{-1\}$, and $Re(\eta) > 0$, $Re(\varrho) > 0$, $Re(\lambda) > 0$, $Re(\gamma) > 0$ are complex parameters, and Θ be an increasing function on (ℓ_1, ℓ_2) with $\ell_1 < \ell_2$, also $f : [\ell_1, \ell_2] \to \Re$ be the geneeralized h-Cf, $h : \Re \to \Re$ be non-negative function and $w : [\ell_1, \ell_2] \to \Re$, $w \geq 0$ be symmetric pertaining to $\frac{\ell_1+\ell_2}{2}$ and $f(x), w(x) \in ({}^{k,m}_{\Theta}\mathfrak{J}^{\delta_i,\tau_i}_{(\frac{\ell_1+\ell_2}{2})^+;\mu,\beta_i})[\ell_1, \ell_2]$. Then the subsequent the inequality*

$$\begin{aligned}
&\left({}^{k,m}_{\Theta}\mathfrak{J}^{\delta_i,\tau_i}_{(\frac{\ell_1+\ell_2}{2})^+;\mu,\beta_i}\right) f(x)w(x) \\
&\leq \frac{f(\ell_1)+f(\ell_2)}{2}\left({}^{k,m}_{\Theta}\mathfrak{J}^{\delta_i,\tau_i}_{(\frac{\ell_1+\ell_2}{2})^+;\mu,\beta_i}\left(h\left(\frac{\ell_2-x}{\ell_2-\ell_1}\right)+h\left(\frac{x-\ell_1}{\ell_2-\ell_1}\right)\right)w(x)\right)(\ell_2), \qquad (32)
\end{aligned}$$

holds for all $\nu \in (0, 1)$.

Proof. Using Lemma 2 and the symmetricalness of the weight w, we have

$$\frac{f\left(\frac{\ell_1+\ell_2}{2}\right)\left({}^{k,m}_{\Theta}\mathfrak{J}^{\delta_i,\tau_i}_{(\frac{\ell_1+\ell_2}{2})^+;\mu,\beta_i}\right)w(x)}{2h(\frac{1}{2})}=\frac{\left({}^{k,m}_{\Theta}\mathfrak{J}^{\delta_i,\tau_i}_{(\frac{\ell_1+\ell_2}{2})^+;\mu,\beta_i}\right)f\left(\frac{\ell_1+\ell_2-x+x}{2}\right)w(x)}{2h(\frac{1}{2})}$$
$$\leq\frac{\left({}^{k,m}_{\Theta}\mathfrak{J}^{\delta_i,\tau_i}_{(\frac{\ell_1+\ell_2}{2})^+;\mu,\beta_i}\right)h(\frac{1}{2})\Big[f(\ell_1+\ell_2-x)+f(x)\Big]w(x)}{2h(\frac{1}{2})}$$
$$=(\frac{1}{2})\left({}^{k,m}_{\Theta}\mathfrak{J}^{\delta_i,\tau_i}_{(\frac{\ell_1+\ell_2}{2})^+;\mu,\beta_i}\right)\Big[f(\ell_1+\ell_2-x)w(\ell_1+\ell_2-x)+f(x)w(x)\Big]$$
$$=\left({}^{k,m}_{\Theta}\mathfrak{J}^{\delta_i,\tau_i}_{(\frac{\ell_1+\ell_2}{2})^+;\mu,\beta_i}\right)f(x)w(x).$$

Which is the left part of the inequality. Alternatively, we have

$$\left({}^{k,m}_{\Theta}\mathfrak{J}^{\delta_i,\tau_i}_{(\frac{\ell_1+\ell_2}{2})^+;\mu,\beta_i}f(x)w(x)\right)(\ell_2)$$
$$=\frac{1}{2}({}^{k,m}_{\Theta}\mathfrak{J}^{\delta_i,\tau_i}_{(\frac{\ell_1+\ell_2}{2})^+;\mu,\beta_i})\Big[f(x)w(x)+f(\ell_1+\ell_2-x)w(\ell_1+\ell_2-x)\Big]$$
$$=\frac{1}{2}\left({}^{k,m}_{\Theta}\mathfrak{J}^{\delta_i,\tau_i}_{(\frac{\ell_1+\ell_2}{2})^+;\mu,\beta_i}\big(f(x)+f(\ell_1+\ell_2-x)\big)w(x)\right)(\ell_2)$$
$$=\frac{1}{2}\left({}^{k,m}_{\Theta}\mathfrak{J}^{\delta_i,\tau_i}_{(\frac{\ell_1+\ell_2}{2})^+;\mu,\beta_i}\left(f(\frac{\ell_2-x}{\ell_2-\ell_1}\ell_1+\frac{x-\ell_1}{\ell_2-\ell_1}\ell_2)\right.\right.$$
$$\left.\left.+f\left(\frac{x-\ell_1}{\ell_2-\ell_1}\ell_1+\frac{\ell_2-x}{\ell_2-\ell_1}\ell_2\right)\right)w(x)\right)(\ell_2)$$
$$\leq\frac{1}{2}\left({}^{k,m}_{\Theta}\mathfrak{J}^{\delta_i,\tau_i}_{(\frac{\ell_1+\ell_2}{2})^+;\mu,\beta_i}\big(h\left(\frac{\ell_2-x}{\ell_2-\ell_1}\right)f(\ell_1)+h\left(\frac{x-\ell_1}{\ell_2-\ell_1}\right)f(\ell_2)\right.$$
$$\left.+h(\frac{x-\ell_1}{\ell_2-\ell_1})f(\ell_1)+h(\frac{\ell_2-x}{\ell_2-\ell_1})f(\ell_2)\big)w(x)\right)(\ell_2)$$
$$=\frac{f(\ell_1)+f(\ell_2)}{2}\left({}^{k,m}_{\Theta}\mathfrak{J}^{\delta_i,\tau_i}_{(\frac{\ell_1+\ell_2}{2})^+;\mu,\beta_i}\big(h(\frac{\ell_2-x}{\ell_2-\ell_1})+h(\frac{x-\ell_1}{\ell_2-\ell_1})\big)w(x)\right)(\ell_2).$$

□

Example 3. *For graphical representation we choose $f(x)=\Theta^{m+1}(x)$, $w(x)=x$ and $h(x)=x$ in (32), we have*

$$\frac{(m+1)^{\frac{\mu}{k}-1}}{k}\Sigma_{n=0}^{\infty}\frac{(\delta_i)_{\kappa_i,k}(\tau_i)^{\kappa_i}}{\Gamma_k(\mu+\Sigma_{i=1}^{n}(\beta_i\kappa_i))}$$
$$\times\left(\frac{\left(\Theta^{m+1}(\ell_2)-\Theta^{m+1}(\frac{\ell_1+\ell_2}{2})\right)^{\frac{\mu+\Sigma_{i=1}^{n}(\beta_i\kappa_i)+\eta}{k}}}{\frac{\mu+\Sigma_{i=1}^{n}(\beta_i\kappa_i)+\eta}{k}}\right.$$
$$\left.-\frac{m+1}{\frac{\mu+\Sigma_{i=1}^{n}(\beta_i\kappa_i)}{k}}\frac{\left(\Theta^{m+1}(\ell_2)-\Theta^{m+1}(\frac{\ell_1+\ell_2}{2})\right)^{\frac{\mu+\Sigma_{i=1}^{n}(\beta_i\kappa_i)}{k}+1}}{\frac{\mu+\Sigma_{i=1}^{n}(\beta_i\kappa_i)}{k}+1}\right)$$
$$\leq[\Theta^{m+1}(\ell_2)+\Theta^{m+1}(\ell_1)]\left(\frac{(m+1)^{-\frac{\mu}{k}}}{k}\sum_{n=0}^{\infty}\frac{(\delta_i)_{\kappa_i,k}(\tau_i)^{\kappa_i}}{\Gamma_k(\mu+\Sigma_{i=1}^{n}(\beta_i\kappa_i)(\frac{\mu+\Sigma_{i=1}^{n}(\beta_i\kappa_i)}{k})}\right.$$
$$\left.\times\left(\Theta^{m+1}(\ell_2)-\Theta^{m+1}(\frac{\ell_1+\ell_2}{2})\right)^{\frac{\mu+\Sigma_{i=1}^{n}(\beta_i\kappa_i)}{k}}\right).\tag{33}$$

The computational values of (33)*, are shown in Tables 5 and 6 corresponding to the choice of parameters* $m = 2$, $k = 1$, $\Theta(x) = x^2$, $\mu = 2$, $\tau_i = 1$, $\beta_i = 0.5$, $\kappa_i = 0.5$, *and for some fixed values of* ℓ_1 *and* ℓ_2. *The Figure 3, shows the two-dimensional graphical representation of* (33)*, corresponding to the choice of parameters* $0 < \ell_1 = 1 < \ell_2 = 4$. *The Figure 4 shows the three-dimensional graphical representation of* (33) *corresponding to the choice of parameters* $0 < \mu < 1$.

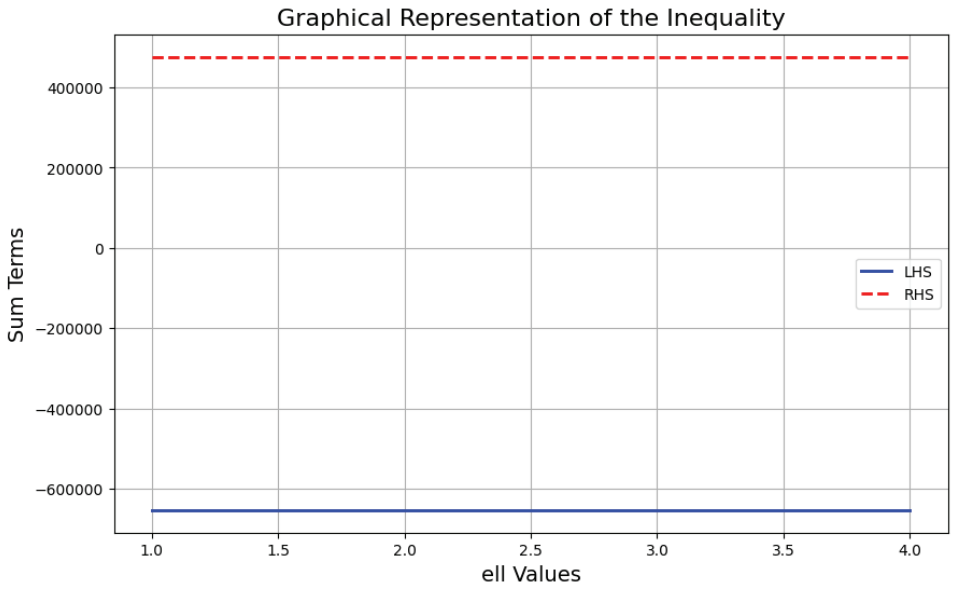

Figure 3. The two-dimensional graphical representation of (33) corresponding to choice $\mu = 0.5$.

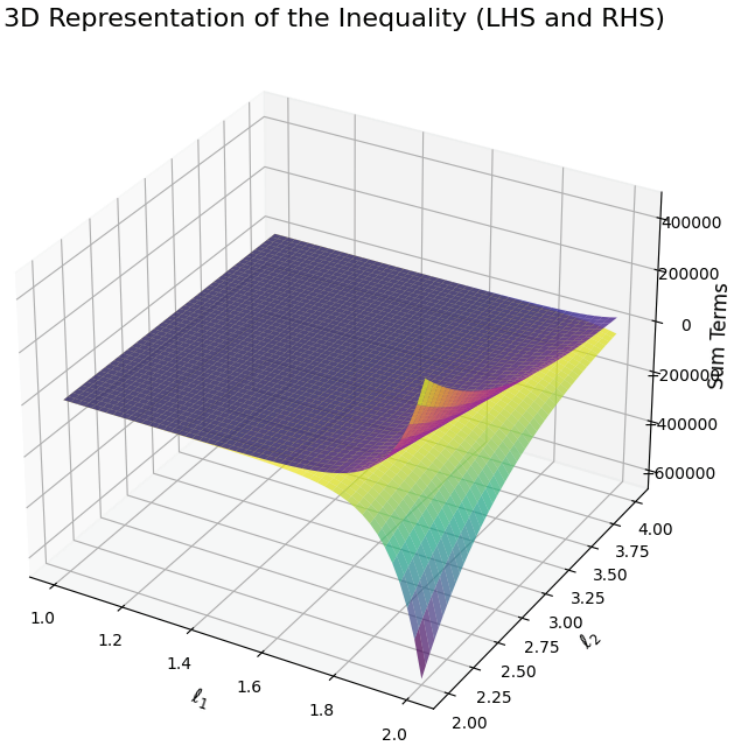

Figure 4. The three-dimensional graphical representation of (33) corresponding to choice $0 \leq \mu \leq 1$.

For tabular values

Table 5. The computational values of (33) corresponding to choice $\mu = 0.5$.

ℓ_1/ℓ_2	**2.10**	**2.30**	**2.50**
0.10	$(4.12 \times 10^{01}, 3.14 \times 10^{01})$	$(5.23 \times 10^{01}, 4.16 \times 10^{01})$	$(6.98 \times 10^{01}, 5.69 \times 10^{01})$
0.30	$(5.29 \times 10^{01}, 4.21 \times 10^{01})$	$(6.43 \times 10^{01}, 5.25 \times 10^{01})$	$(8.44 \times 10^{01}, 7.07 \times 10^{01})$
0.50	$(6.47 \times 10^{01}, 5.29 \times 10^{01})$	$(7.62 \times 10^{01}, 6.34 \times 10^{01})$	$(9.89 \times 10^{01}, 8.08 \times 10^{01})$
0.70	$(7.65 \times 10^{01}, 6.36 \times 10^{01})$	$(8.82 \times 10^{01}, 7.42 \times 10^{01})$	$(1.10 \times 10^{02}, 9.09 \times 10^{01})$
0.90	$(8.83 \times 10^{01}, 7.43 \times 10^{01})$	$(1.00 \times 10^{02}, 8.51 \times 10^{01})$	$(1.24 \times 10^{02}, 1.04 \times 10^{02})$
1.00	$(1.00 \times 10^{02}, 8.57 \times 10^{01})$	$(1.13 \times 10^{02}, 9.45 \times 10^{01})$	$(1.39 \times 10^{02}, 1.17 \times 10^{02})$

Table 6. The computational values of (33) corresponding to choice $\mu = 0.5$.

ℓ_1/ℓ_2	**2.70**	**2.90**	**3.00**
0.10	$(8.72 \times 10^{01}, 7.22 \times 10^{01})$	$(1.04 \times 10^{02}, 8.75 \times 10^{01})$	$(1.16 \times 10^{02}, 9.87 \times 10^{01})$
0.30	$(1.03 \times 10^{02}, 8.78 \times 10^{01})$	$(1.21 \times 10^{02}, 1.05 \times 10^{02})$	$(1.34 \times 10^{02}, 1.17 \times 10^{02})$
0.50	$(1.20 \times 10^{02}, 9.89 \times 10^{01})$	$(1.40 \times 10^{02}, 1.16 \times 10^{02})$	$(1.55 \times 10^{02}, 1.30 \times 10^{02})$
0.70	$(1.32 \times 10^{02}, 1.10 \times 10^{02})$	$(1.53 \times 10^{02}, 1.29 \times 10^{02})$	$(1.69 \times 10^{02}, 1.43 \times 10^{02})$
0.90	$(1.48 \times 10^{02}, 1.27 \times 10^{02})$	$(1.72 \times 10^{02}, 1.49 \times 10^{02})$	$(1.88 \times 10^{02}, 1.64 \times 10^{02})$
1.00	$(1.64 \times 10^{02}, 1.38 \times 10^{02})$	$(1.90 \times 10^{02}, 1.58 \times 10^{02})$	$(2.06 \times 10^{02}, 1.72 \times 10^{02})$

4. Discussion

In the first table, the comparison of the LHS, Middle Term, and RHS in the graphs and tables reveals that the RHS is generally larger than both the LHS and Middle Term, with the values increasing as ℓ_1 and ℓ_2 increase. The Middle Term tends to be closer to the LHS in magnitude, suggesting its role as a balancing factor between the two sides. As ℓ_2 increases, the RHS grows more rapidly compared to the LHS and Middle Term, indicating that the RHS is more sensitive to changes in ℓ_2. The inequality appears to hold in the form $LHS \leq MiddleTerm \leq RHS$ across the tested values, with the LHS being consistently smaller than or equal to the Middle Term, and the Middle Term smaller than or equal to the RHS. This confirms the validity of the inequality and suggests that while the terms grow with ℓ_1 and ℓ_2, the RHS exhibits the fastest growth. These observations highlight that the inequality holds true in the given range, with the terms influenced differently by ℓ_1 and ℓ_2, and the RHS proving to be the dominant term in terms of magnitude. In the remaining graphs and tables demonstrate that for all combinations of ℓ_1 and ℓ_2, the RHS values are consistently greater than the corresponding LHS values, indicating that the inequality is satisfied in all cases. This suggests that the inequality becomes more pronounced for larger ℓ_1 and ℓ_2, with the RHS serving as a more accurate upper bound, confirming the robustness of the inequality in these conditions.

5. Conclusions

In recent times, mathematical fractional inequalities have found their way into various domains such as the material sciences, heat conduction, viscoelasticity, time series analysis, circuits, human body modeling, and shear waves. While inequalities, itself may not directly take note of issues of educational access, high-quality research, and mathematical advancement—topics such as inequality contribute to the larger objective of improving educational through the dissemination of knowledge, the development of critical thinking abilities, and the encouragement of mathematical literacy among researchers. In this work, we extended the well-known H-H-F inequalities by introducing generalized fractional operators involving the M-M-L function. Through the derivation of two key identities for locally differentiable functions, we were able to provide more accurate estimates of the differences between the left, middle, and right terms in the H-H-F inequalities. These

generalized inequalities offer valuable insights into generalized convexity and the behavior of fractional operators in various mathematical contexts. The practical applications of these inequalities are significant, particularly in fields such as optimization, fractional calculus, and applied analysis. For instance, the improved inequalities can aid in more precise bounding of functions and contribute to solving complex problems in areas such as signal processing, system modeling, and the study of fractional differential equations. The graphical representations included in this study serve to visualize these inequalities, providing a useful tool for researchers and practitioners. Overall, the results presented in this paper lay a foundation for further exploration of fractional inequalities and their applications in real-world problems. Future research could extend these methods to higher-dimensional settings and explore their potential in new areas such as financial modeling and the modeling of physical systems in plasma physics. Researchers can apply our defined operator to generalized Opial-type, Chebyshev-type, and composite Cf inequality problems, among other types of inequalities. These inequalities play a vital role in computing the special means. Specifically, we have looked into some of the well-known H-H-F inequality's relations to generalized h-convexity and extended fractional operators. In order to achieve this goal, two identities for local differentiable mappings are created. From these identities, we may derive estimates for the difference between the center and right parts of the H-H-F inequality as well as the difference between the left and central inequality.

Author Contributions: All authors contributed equally and significantly in writing this article. All authors have read and agreed to the published version of the manuscript.

Funding: This work does not receive any external funding.

Data Availability Statement: The data used to support the findings of this study are available from the corresponding author upon request.

Acknowledgments: The authors S. Haque, A. Aloqaily and Nabil Mlaiki would like to thank Prince Sultan University for the funding support and for the support through the TAS research lab.

Conflicts of Interest: The authors declare that they have no conflicts of interest.

References

1. Abel, N. Solution de quelques problemes l'aide d'integrales definies. *Mag. Naturv.* **1823**, 55–63.
2. Kilbas, A.A.; Srivastava, H.H.; Trujillo, J.J. *Theory and Applications of Fractional Differential Equations*; Elsevier B.V.: Amsterdam, The Netherlands, 2006.
3. Oldham, K.B.; Spanier, J. *The Fractional Calculus*; Academic Press: New York, NY, USA, 1974.
4. Caputo, M.; Fabrizio, M. A new definition of fractional derivative without singular kernel. *Prog. Frac. Differ. Appl.* **2015**, *2*, 73–85.
5. Losada, J.; Nieto, J.J. Properties of a new fractional derivative without singular kernel. *Prog. Fract. Differ. Appl.* **2015**, *1*, 87–92.
6. Yang, X.J.; Srivastava, H.M.; Machado, J.A.T. A new fractional derivative without a singular kernel: Application to the moddeling of the steady heat flow. *Therm. Sci.* **2016**, *20*, 753–756. [CrossRef]
7. Fernandez, A.; Ozarslan, M.A.; Baleanu, D. On fractional calculus with general analytic kernels. *Appl. Math. Comput.* **2019**, *354*, 248–265. [CrossRef]
8. Teodoro, G.S.; Machado, J.A.T.; de Oliveira, E.C. A review of definitions of fractional derivatives and other operators. *J. Comput. Phys.* **2019**, *388*, 195–208. [CrossRef]
9. Wu, S.; Samraiz, M.; Mehmood, A.; Jarad, J.; Naheed, S. Some symmetric propertise and applications of weighted fractional integral operator. *Fractals* **2023**, *31*, 2340011. [CrossRef]
10. Samraiz, M.; Mehmood, A.; Iqbal, S.; Naheed, S.; Rehman, G.; Chu, Y.M. Generalized fractional operator with applications in mathematical physics. *Chaos Solition Fractals* **2022**, *16*, 112830. [CrossRef]
11. Samraiz, M.; Mehmood, A.; Naheed, S.; Rehman, G.; Kashuri, A.; Nonlaopon, K. On novel fractional Operators involving the multivariate M-L function. *Mathematics* **2022**, *10*, 3991. [CrossRef]
12. Huang, W.H.; Samraiz, M.; Mehmood, A.; Baleanu, D.; Rehman, G.; Naheed, S. Modified Atangana- Baleanu Fractional operators Involving generalized Mittag-Leffler function. *Alexanderia Eng. J.* **2023**, *75*, 639–648. [CrossRef]

13. Cho, Y.; Kim, I.; Sheen, D. A fractional-order model for MINMOD Millennium. *Math. Biosci.* **2015**, *262*, 36–45. [CrossRef] [PubMed]
14. Magin, R.L.; Ovadia, M. Modeling the cardiac tissue electrode interface using fractional calculus. *J. Vib. Control* **2008**, *1*, 1431–1442. [CrossRef]
15. Chen, W.; Pang,G. A new definition of fractional Laplacian with application to modeling three-dimensional nonlocal heat conduction. *J. Comput. Phys.* **2016**, *309*, 350–367. [CrossRef]
16. Grahovac, N.M.; Zigic, M.M. Modelling of the hamstring muscle group by use of fractional derivatives. *Comput. Math. Appl.* **2010**, *59*, 1695–1700. [CrossRef]
17. Rossikhin, Y.A.; Shitikova, M.Y. Analysis of two colliding fractionally damped spherical shells in modelling blunt human head impacts. *Cent. Eur. J. Phys.* **2013**, *11*, 760–778. [CrossRef]
18. Balci, M.A. Fractional virus epidemic model on financial networks. *Open Math.* **2016**, *14*, 1074– 1086. [CrossRef]
19. Roman, H.E.; Porto, M. Fractional derivatives of random walks: Time series with long-time memory. *Phys. Rev. E* **2008**, *78*, 031127. [CrossRef]
20. Moreles, M.A.; Lainez, R. Mathematical modelling of fractional order circuit elements and bioimpedance applications. *Commun. Nonlinear Sci. Numer. Simul.* **2017**, *46*, 81–88. [CrossRef]
21. Yalçın, S.; Bayram, H. On harmonic univalent functions involving q-Poisson distribution series. *MJPS* **2021**, *8*, 105–111.
22. Reyes-Melo, E.; Martinez-Vega, J.; Guerrero-Salazar, C.; Ortiz-Mendez, U. Application of fractional calculus to the modeling of dielectric relaxation phenomena in polymeric materials. *J. Appl. Polym. Sci.* **2005**, *98*, 923–935. [CrossRef]
23. Carcione, J.M. Theory and modeling of constant-QP- and S -waves using fractional time derivatives. *Geophysics* **2009**, *74*, 1–11. [CrossRef]
24. Jensen, J.L.W.V. Sur les fonctions convexes et les inegalites entre les valeurs moyennes. *Acta Math.* **1905**, *30*, 175–193. [CrossRef]
25. Breckner, W.W. Stetigkeitsaussagen fur eine Klasse verallgemein konvexer Funktionen in topologischen linearen Raumen. *Publ. Inst. Math.* **1978**, *23*, 13–20.
26. Jarad, F.; Ugurlu, E.; Abdeljawad, T.; Baleanu, D. On a new class of fractional operators. *Adv. Differ. Equ.* **2017**, *2017*, 247. [CrossRef]
27. Set, E.; Iscan, I.; Sarikaya, M.Z.; Ozdemir, M.E. On new inequalities of Hermite-Hadamard-Fejer' type for convex functions via fractional integrals. *Appl. Math. Comput.* **2015**, *259*, 875–881. [CrossRef]
28. Gradshteyn, I.S.; Ryzhik, I.M. *Table of Integrals Series and Products*, 7 Eds.; Academic Press: San Diego, CA, USA, 1980.
29. Sarikaya, M.Z.; Dahmani, Z.; Kiris, M.E.; Ahmad, F. (k, s)-Riemann-Liouville fractional integral and applications. *Hacet. J. Math. Stat.* **2016**, *45*, 77–89. [CrossRef]
30. Gorenflo, R.; Kilbas, A.A.; Mainardi, F.; Rogosin, S.V. *Mittag-Leffler Functions, Related Topics and Applications*; Springer Monographs in Mathematics; Springer: New York, NY, USA, 2014.
31. Akgül, E.K.; Akgül, A.; Yavuz, M. New illustrative application of integral transform to financial models with different fractional derivatives. *Chaos Solitions Fractals* **2021**, *146*, 110877. [CrossRef]
32. Yavuz, M.; Sene, N. Approximation solution of the model describing fluid flow using generalized laplace transform method and heat balance integral method. *Axioms* **2020**, *9*, 123. [CrossRef]
33. Yavuz, M.; Abdeljawad, T. Nonlinear regularized long-wave with a new integral transformation applied to the fractional derivative with power and Mittag-Leffler kernel. *Adv. Differ. Equ.* **2020**, *2020*, 367. [CrossRef]
34. Yavuz, M.; Ozdemir, N. Comparison the new fractional derivative operators involving exponential and Mittag-Leffler kernal. *Discrete Contin. Dyn. Syst. Ser. S.* **2020**, *13*, 995–1006.
35. Podlubny, I. *Fractional Differential Equations*; Academic Press: San Diego, CA, USA, 1999.
36. Nisar, K.S.; Rahman, G.; Baleanu, D.; Mubeen, S.; Arshad, M. The (k, s)-fractional calculus of k Mittag-Leffler function. *Adv. Differ. Equ.* **2017**, *2017*, 118. [CrossRef]
37. Baleanu, D.; Diethelm, K.; Scalas, E.; Trujillo, J.J. *Fractional Calculus: Models and Numerical Methods, Series on Complexity, Nonlinearity and Chaos*; World Scientific: Singapore, 2012.
38. Mainardi, F. *Fractional Calculus and Waves in Linear Viscoelasticity: An Introduction to Mathematical Models*; World Scientific Publishing Company: Singapore; Hackensack, NJ, USA; London, UK, 2010.
39. Zhao, D.; Luo, M. Representations of acting processes and memory effects: General fractional derivative and its application to theory of heat conduction with finite wave speeds. *Appl. Math. Comput.* **2019**, *49*, 531–544. [CrossRef]
40. Chen, S.B.; Rashid, S.; Noor, M.A.; Ashraf, R.; Chu, Y.M. A new approach on fractional calculus and probability density function. *AIMS Math.* **2020**, *5*, 7041–7054. [CrossRef]
41. Samraiz, M.; Umer, M.; Abduljawad, T.; Naheed, S.; Rahman, G.; Shah, K. On Riemann-type weighted fractional operator and solution to cauchy problems. *Comput. Model. Eng. Sci.* **2022**, *136*, 901–917. [CrossRef]
42. Mittag-Leffler, M.G. Sur la nouvelle fonction E(x). *C. R. Acad. Sci.* **1903**, *137*, 5548.

43. Garg, M.; Manohar, P.; Kalla, S.L. A Mittag-Leffler-type function of two variables. *Int. Transf. Spec. Funct.* **2013**, *24*, 9344. [CrossRef]
44. Saxena, R.K.; Kalla, S.L.; Saxena, R. Multivariate analogue of generalised Mittag-Leffler function. *Int. Transf. Spec. Funct.* **2011**, *22*, 533–548.
[CrossRef]
45. Fej, L. Über die Fourierreihen. II. *Math. Naturwiss Anz. Ungar. Akad. Wiss.* **1906**, *24*, 369–390.
46. Hadamard, J. Étude sur les propriétés des fonctions entières et en particulier d'une fonction considérée par Riemann. *J. Mathématiques Pures Appliquées* **1893**, *9*, 171–215.
47. Tseng, K.L.; Yang, G.S.; Hsu, K.C. Some inequalities for differentiable mappings and applications to Fejér inequality and weighted trapezoidal formula. *Taiwan J. Math.* **2011**, *15*, 1737–1747. [CrossRef]
48. Delavar, M.R.; Dargomir, S.S. Trapezoidal type inequalities related to h-convex functions with applications. *Rev. R. Acad. Cienc Exactas Fís Nat. Ser.-A Math.* **2019**, *113*, 1487–1498. [CrossRef]
49. Matloka, M. Weighted Simpson type inequalities for h-convex functions. *J. Non-Linear Sci. Appl.* **2017**, *10*, 5770–5780. [CrossRef]
50. Varošanec, S. On h-convexity. *J. Math. Anal. Appl.* **2007**, *326*, 303–311. [CrossRef]
51. Chen, H.; Katugampola, U.N. Hermite-Hadamard and Hermite-Hadamard-Fejer type inequalities for generalized fractional integrals. *J. Math. Anal. Appl.* **2017**, *446*, 1274–1291. [CrossRef]
52. Khan, T.U.; Khan, M.A. Generalized conformable fractional operators. *J. Comput. Appl. Math.* **2019**, *346*, 378–389. [CrossRef]
53. Samko, S.G.; Kilbas, A.A.; Marichev, O.I. *Fractional Integrals and Derivatives, Theory and Applications*; Gordon and Breach: Montreux, Switzerland, 1993.
54. Agarwal, P.; Nieto, J.J. Some fractional integral formulas for the Mittag-Leffler type function with four parameters. *Open Math.* **2015**, *13*, 537–546. [CrossRef]
55. Hölder, O.L. *Nachrichten von der Königl Gesel Schaft der Wissenschaften und der Georg-August-Universität zu Göttingen*; Dieterichsche Verlags-Buchhandlung: Gottingen, Germany, 1889; pp. 38–47.
56. Alqudah, M.A.; Mohammed, P.O.; Abdeljawad, T. Solution of Singular integral equation via Riemann-Liouville fractional integral. *Math. Prob. Eng.* **2020**, *1*, 1250970. [CrossRef]
57. Hakiki, M.T.; Wibowo, A. Hermite-Hadamard-Fejer type inequalities for s-convex functions in the second sense via Riemann-Liouville fractional integral. *J. Phys. Conf. Ser.* **2020**, *1442*, 012039. [CrossRef]
58. Sarikaya, M.Z.; Set, E.; Özdemir, M.E. On some new inequalities of Hadamard type involving h-convex functions. *Acta Math. Univ. Comeniane* **2010**, *79*, 265–272.

Disclaimer/Publisher's Note: The statements, opinions and data contained in all publications are solely those of the individual author(s) and contributor(s) and not of MDPI and/or the editor(s). MDPI and/or the editor(s) disclaim responsibility for any injury to people or property resulting from any ideas, methods, instructions or products referred to in the content.

fractal and fractional

MDPI

Article

Comparison Principle Based Synchronization Analysis of Fractional-Order Chaotic Neural Networks with Multi-Order and Its Circuit Implementation

Rongbo Zhang, Kun Qiu *, Chuang Liu, Hongli Ma and Zhaobi Chu

School of Electrical Engineering and Automation, Hefei University of Technology, Hefei 230009, China; 2022210486@mail.hfut.edu.cn (R.Z.); 2022170433@mail.hfut.edu.cn (C.L.); 2023010050@mail.hfut.edu.cn (H.M.); zbchu@hfut.edu.cn (Z.C.)

* Correspondence: qiukun@hfut.edu.cn

Abstract: This article investigates non-fragile synchronization control and circuit implementation for incommensurate fractional-order (IFO) chaotic neural networks with parameter uncertainties. In this paper, we explore three aspects of the research challenges, i.e., theoretical limitations of uncertain IFO systems, the fragility of the synchronization controller, and the lack of circuit implementation. First, we establish an IFO chaotic neural network model incorporating parametric uncertainties, extending beyond conventional commensurate-order architectures. Second, a novel, non-fragile state-error feedback controller is designed. Through the formulation of FO Lyapunov functions and the application of inequality scaling techniques, sufficient conditions for asymptotic synchronization of master–slave systems are rigorously derived via the multi-order fractional comparison principle. Third, an analog circuit implementation scheme utilizing FO impedance units is developed to experimentally validate synchronization efficacy and accurately replicate the system's dynamic behavior. Numerical simulations and circuit experiments substantiate the theoretical findings, demonstrating both robustness against parameter perturbations and the feasibility of circuit realization.

Keywords: chaotic neural networks; uncertainty; synchronization control; state feedback control; circuits design

1. Introduction

Neural networks, as brain-inspired computational architectures, find ubiquitous applications spanning medical diagnostics, financial forecasting, information processing systems, and pattern-recognition algorithms [1–4]. Recent technological innovation has driven considerable research interest in chaotic neural networks, owing to their distinctive nonlinear dynamic characteristic [5–7]. The synchronization of such systems has emerged as a central research challenge, spurring rigorous investigations into control strategies, including impulsive control [8], adaptive control [9], fuzzy control [10], and feedback control [11]. Nevertheless, these methodologies consistently encounter fundamental limitations in maintaining robustness and operational precision when addressing complex nonlinear systems.

Fractional-order (FO) calculus has established itself as a compelling framework for characterizing dynamical properties in complex nonlinear systems. Compared to integer-order models, FO frameworks demonstrate enhanced characterization accuracy for electrochemical phenomena, particularly in voltage output regulation and state-of-charge

estimation [12]. Particularly in scenarios involving memory effects, FO calculus intrinsically encodes temporal correlations through its hereditary operators, facilitating accurate forecasting in operational scenarios spanning neural networks, bioengineering, quantum systems, and signal-processing architecture [13–18]. Particularly in neural network architectures, the incorporation of FO calculus empowers neural models to more accurately characterize neuronal dynamical properties, yielding broad applicability spanning signal-processing architectures, image encryption schemes, and secure communication protocols [19–22]. Consequently, investigating synchronization control in FO chaotic neural networks holds substantial theoretical importance and applied potential across interdisciplinary domains.

While notable advances exist in FO chaotic neural network research, current studies predominantly address commensurate FO system dynamics [23–25]. However, practical systems frequently possess multiple different orders and demonstrate heightened dynamical complexity, formally categorized as IFO chaotic systems. Their intricate dynamical characteristics render conventional analytical approaches developed for uniform FO systems inadequate for such configurations. Research on IFO chaotic systems is still in its early stages, with some seminal contributions appearing in the recent literature. Notable advances include the generalized projective synchronization framework under external perturbations [26]. In addition, their seminal study of the glucose-insulin regulatory mechanism introduced a pioneering approach to stabilize chaotic attractors, providing important insights into the application of IFO dynamics to biophysically relevant systems [27]. Recent investigations [28,29] establish rigorous synchronization criteria for IFO systems. Capitalizing on neural networks' inherent approximation capabilities, ref. [30] introduced adaptive control to resolve undetermined control directionality while developing neural-driven synchronization strategies for generalized projective IFO chaotic systems with uncertain nonlinearities. While pioneering investigations exist, a persistent theoretical–practical disconnect persists in synchronization control methodologies for IFO chaotic neural networks.

Practical implementations inevitably confront parametric uncertainties stemming from measurement inaccuracies and exogenous disturbances, which critically degrade Lyapunov stability margins and compromise synchronization control precision in neural networks. Consequently, robust synchronization control of chaotic neural networks with parametric uncertainties has become a critical research focus, demanding novel adaptive strategies. Deepika pioneered a FO sliding mode control strategy to achieve finite-time robust synchronization for uncertain chaotic/hyperchaotic systems, effectively addressing nonlinear coupling dynamics and parametric perturbations [31]. While Hajipour developed an adaptive synchronization scheme for IFO Arneodo systems with quadrivariable parametric uncertainties, their Lyapunov-based control law enables asymptotic state synchronization between coupled IFO chaotic oscillators through rigorous stability guarantees [32]. However, contemporary research remains predominantly confined to deterministic system formulations, whereas robust controller synthesis incorporating uncertainty quantification—particularly non-fragile control architectures resilient to parametric perturbations—still faces fundamental challenges in both theoretical analysis and engineering implementation.

While numerical simulation remains indispensable in theoretical exploration, circuit implementation constitutes a critical validation phase for confirming result fidelity in nonlinear dynamical systems. The aforementioned studies [33,34] have achieved FO implementations, yet the circuit-level realization of synchronization control for IFO chaotic neural networks remains unexplored, with current findings limited to numerical simulations lacking hardware validation. This study investigates synchronization control and circuit implementation of IFO chaotic neural networks, addressing parametric uncertainties induced by measurement inaccuracies and external perturbations. Concurrently, a

non-fragile state-error feedback controller is developed to achieve robust synchronization in IFO chaotic neural networks through dual compensation mechanisms for parametric perturbations and quantization errors. The main innovations of this paper are:

- This work investigates IFO chaotic neural networks with inherent parametric uncertainties, establishing enhanced generality through multi-order dynamics compared to existing chaotic system formulations.
- Ensures the state synchronization of the master–slave system can still be accomplished with a certain degree of robustness when the control protocol parameters have relatively small perturbations.
- Using the principle of multiple FO comparison, sufficient conditions are given to achieve synchronization of master–slave systems, and the obtained sufficient conditions are also applicable to FO chaotic systems of the same metric as well as integer orders.
- The design of the IFO uncertain chaotic neural network synchronization control circuit is completed, and the circuit simulation is carried out by Mutisim and the results coincide with the numerical simulation results of Matlab, which verifies the validity of the FO operator as well as the correctness of the circuit design.

The paper is organized as follows. Section 2 focuses on system description and generalization of the underlying theory. Section 3 is the main content. In Section 4, Simulation results are given for an IFO chaotic neural network analog circuit and the physical circuit is completed. Finally, Section 5 outlines the main conclusions.

The notations and their descriptions are displayed in Table 1.

Table 1. Notations and their descriptions.

Notations	Descriptions
R^n	set of n-dimensional real vectors
$R^{p\times q}$	set of $p \times q$ real matrices
I	the identity matrix with appropriate dimension
$\otimes$	the Kronecker product
$\mathrm{diag}(\cdots)$	a block diagonal matrix
$H_+^{p\times q}$	the real symmetric positive definite $p \times q$ matrix set
X^T	the transpose of the matrix X
X^{-1}	the inverse of the matrix X
$X > 0\ (< 0)$	a real symmetric and positive (negative) definite matrix
$\oplus_{i=1}^{k} x_i$	equivalent to $\mathrm{diag}(x_1, x_2, \cdots, x_n)$

2. System Description and Basics

This section will introduce the theory of FO calculus and some necessary lemmas.

2.1. Fractional Calculus

The commonly used definitions of FO derivatives can be categorized into the following three: the Riemann–Liouville, Caputo, and Grunwald–Letnikov definitions. The Caputo derivative is widely adopted in control engineering due to its seamless compatibility with the integer-order system when the FO ω attains integer values. It degenerates to classical integer-order differentiation, particularly advantageous for hybrid control architectures integrating fractional and integer-order dynamics.

Definition 1 ([35]). *The Riemann–Liouville fractional derivative can be defined as:*

$$ {}_{t_0}^{RL}D_{0,t}^{\omega} f(t) = \frac{1}{\Gamma(n-\omega)} \frac{d^n}{dt^n} \int_0^t \frac{f(\tau)}{(t-\tau)^{\omega-n+1}} d\tau, \tag{1} $$

where $\omega > 0$ being positive real non-integer numbers, n is the smallest positive integer greater than ω, i.e., $n-1 \leqslant \omega < n$.

Definition 2 ([35]). *The Caputo FO derivative can be written for a differentiable function $f(t)$:*

$$ {}_{t_0}^{C}D_{0,t}^{\omega} f(t) = \frac{1}{\Gamma(n-\omega)} \int_0^t \frac{f^{(n)}(\tau)}{(t-\tau)^{1-n+\omega}} d\tau, \tag{2} $$

where $\Gamma(n-\omega) = \int_0^{\infty} e^{-t} t^{n-\omega-1} dt$ denotes the Euler gamma function.

Definition 3 ([35]). *The Grunwald–Letnikov derivative of order ω is*

$$ {}_{t_0}^{GL}D_{0,t}^{\omega} f(t) = \lim_{h \to 0} \frac{1}{h^{\omega}} \sum_{j=0}^{[(t-t_0)/h]} (-1)^j \binom{\omega}{j} f(t-jh). \tag{3} $$

Please note that the Caputo derivative is widely applicable in practice and will be used in this paper. From now on, to simplify the notation, we will use D_t^{ω}, which means we omit the left superscript and the operator limit.

2.2. Relevant Lemmas

Lemma 1 ([36]). *For a continuous function $x(t) \in R^n$ and any given symmetric positive definite matrix $P \in R^{n \times n}$ we verify that*

$$ D_t^{\omega} \left(x^T(t) P x(t) \right) \leq \left(x^T(t) P \right) D_t^{\omega} x(t) + \left(D_t^{\omega} x(t) \right)^T P x(t), \tag{4} $$

where $\omega \in (0, 1]$.

Lemma 2 ([37]). *(Principle of Comparing Multi-order FO Systems) Consider the following FO differential inequalities with initial conditions $V_i(0, x_i(0)) = V_{i0} \geqslant 0$ and $V_i(0, x_i(0)) \leqslant W_i(0, y_i(0)), i = 1, 2, \cdots, n$ and conditions:*

$$ \begin{aligned} & D_t^{\omega_1} V_1(t, x_1(t)) \leq D_t^{\omega_1} W_1(t, y_1(t)), \\ & D_t^{\omega_2} V_2(t, x_2(t)) \leq D_t^{\omega_2} W_2(t, y_2(t)), \\ & \vdots \\ & D_t^{\omega_n} V_n(t, x_n(t)) \leq D_t^{\omega_n} W_n(t, y_n(t)). \end{aligned} \tag{5} $$

If previous inequalities hold, then the following inequalities hold:

$$ \begin{aligned} & V_1(x_i(t)) \leq W_i(y_i(t)), \forall t > 0, i = 1, 2, \cdots, n, \\ & V(x(t)) \leq W(y(t)), \forall t > 0, \end{aligned} \tag{6} $$

where V and W: $[0, \infty) \times R^n \to [0, \infty)$ are continuously differentiable functions.

Lemma 3 ([38]). *The FO multi-order system $D_t^{\overline{\omega}} x(t) = A_0 x(t) + B_0 u(t), \overline{\omega} = (\omega_1, \omega_2, \cdots, \omega_n)^T$, is stabilizable under the state feedback controller $u(t) = Kx(t)$, if there exist symmetric positive*

definite matrices $P_i \in H_+^{t_i \times t_i}, i = 1, 2, \cdots k$, *the matrices* $H \in R^{n\times n}$,$Q \in R^{p\times n}$, *the following equation holds:*

$$\begin{aligned} &M + sym\left\{ \left(\begin{bmatrix} I_n \\ -A_0 \end{bmatrix} \otimes I_2 \right)(H \otimes I_2)([I_n \ I_n] \otimes I_2) \right\} \\ &+sym\left\{ \left(\begin{bmatrix} 0_{n\times p} \\ -B_0 \end{bmatrix} \otimes I_2 \right)(Q \otimes I_2)([I_n \ I_n] \otimes I_2) \right\} < 0. \end{aligned} \tag{7}$$

Moreover, the controller feedback gain is given by $K = QH^{-1}$.

2.3. System Description

We consider the uncertain IFO neural network master chaotic system:

$$\frac{d^{\omega_i} x_i(t)}{dt^{\omega_i}} = -(c_i + \Delta c_i)x_i(t) + \sum_{j=1}^{n} \left(a_{ij} + \Delta a_{ij}\right) f_j\left(x_j(t)\right) + I_i. \tag{8}$$

The matrix representation of the system is formulated as:

$$\frac{d^{\overline{\omega}} x(t)}{dt^{\overline{\omega}}} = -(C + \Delta C)x(t) + (A + \Delta A)f(x(t)) + I, \tag{9}$$

where $i = \{1, 2, \cdots, n\}$, n is the number of neurons in the network, $\overline{\omega} = (\omega_1, \omega_2, \cdots, \omega_n)^T$ belongs to $(0, 1]$. $x(t) = (x_1(t), x_2(t), \cdots, x_n(t))^T \in R^n$ is the state of the neuron at the moment t,$f(x(t)) = (f_1(x(t)), f_2(x(t)), \cdots, f_n(x(t)))^T$ is the excitation nonlinear function of the neuron. $C = \mathrm{diag}(c_1, \cdots, c_n)$, $A = \left(a_{ij}\right)_{n\times n}$ are the weight matrices from the j-th neuron to the i-th neuron. $I = (I_1, I_2, \cdots, I_n)^T$ is an external input. $\Delta A = \left(\Delta a_{ij}\right)_{n\times n} \in R^{n\times n}$ and $\Delta C = \left(\Delta c_{ij}\right)_{n\times n} \in R^{n\times n}$ are uncertain parameter perturbation matrices.

System (9) can be described in vector form:

$$\begin{aligned} \begin{bmatrix} \frac{d^{\omega_1} x_1(t)}{dt^{\omega_1}} \\ \frac{d^{\omega_2} x_2(t)}{dt^{\omega_2}} \\ \vdots \\ \frac{d^{\omega_n} x_n(t)}{dt^{\omega_n}} \end{bmatrix} &= -\begin{bmatrix} c_{11} + \Delta c_{11} & c_{12} + \Delta c_{12} \cdots & c_{1n} + \Delta c_{1n} \\ c_{21} + \Delta c_{21} & c_{22} + \Delta c_{22} \cdots & c_{2n} + \Delta c_{2n} \\ \vdots & \vdots & \ddots \quad \vdots \\ c_{n1} + \Delta c_{n1} & c_{n2} + \Delta c_{n2} & \cdots c_{nn} + \Delta c_{nn} \end{bmatrix} \begin{bmatrix} x_1(t) \\ x_2(t) \\ \vdots \\ x_n(t) \end{bmatrix} \\ &+ \begin{bmatrix} a_{11} + \Delta a_{11} & a_{12} + \Delta a_{12} \cdots & a_{1n} + \Delta a_{1n} \\ a_{21} + \Delta a_{21} & a_{22} + \Delta a_{22} \cdots & a_{2n} + \Delta a_{2n} \\ \vdots & \vdots & \ddots \quad \vdots \\ a_{n1} + \Delta a_{n1} & a_{n2} + \Delta a_{n2} & \cdots a_{nn} + \Delta a_{nn} \end{bmatrix} \begin{bmatrix} f_1(x(t)) \\ f_2(x(t)) \\ \vdots \\ f_n(x(t)) \end{bmatrix} + \begin{bmatrix} I_1 \\ I_2 \\ \vdots \\ I_n \end{bmatrix}. \end{aligned} \tag{10}$$

where the uncertainty matrix elements satisfy $\left|\Delta a_{ij}\right| \leqslant \overline{a}_{ij}$, $\left|\Delta c_{ij}\right| \leqslant \overline{c}_{ij}$. $\overline{a}_{ij}, \overline{c}_{ij}$ are positive constants. The excitation function f_j of a neuron is Lipschitz continuous, i.e., there exists $L_j (j = 1, 2, \cdots, n)$ such that $\left|f_j(u_j) - f_j(v_j)\right| \leqslant L_j|u_j - v_j|, \forall u_j, v_j \in R$.

Remark 1. *It should be pointed out that widely used excitation functions in neural networks are Lipschitz continuous. It accommodates standard excitation functions, ensures theoretical analysis, and aligns with practical requirements.*

We assume the IFO neural network slave chaotic system:

$$\frac{d^{\omega_i} y_i(t)}{dt^{\omega_i}} = -(c_i + \Delta c_i)y_i(t) + \sum_{j=1}^{n} \left(a_{ij} + \Delta a_{ij}\right) f_j\left(y_j(t)\right) + I_i + u_i(t). \tag{11}$$

Its matrix form is

$$\frac{d^{\overline{\omega}}y(t)}{dt^{\overline{\omega}}} = -(C+\Delta C)y(t) + (A+\Delta A)f(y(t)) + I + u(t). \tag{12}$$

It can also be written as:

$$\begin{aligned}\begin{bmatrix} \frac{d^{\omega_1}y_1(t)}{dt^{\omega_1}} \\ \frac{d^{\omega_2}y_2(t)}{dt^{\omega_2}} \\ \vdots \\ \frac{d^{\omega_n}y_n(t)}{dt^{\omega_n}} \end{bmatrix} &= -\begin{bmatrix} c_{11}+\Delta c_{11} & c_{12}+\Delta c_{12} & \cdots & c_{1n}+\Delta c_{1n} \\ c_{21}+\Delta c_{21} & c_{22}+\Delta c_{22} & \cdots & c_{2n}+\Delta c_{2n} \\ \vdots & \vdots & \ddots & \vdots \\ c_{n1}+\Delta c_{n1} & c_{n2}+\Delta c_{n2} & \cdots & c_{nn}+\Delta c_{nn} \end{bmatrix} \begin{bmatrix} y_1(t) \\ y_2(t) \\ \vdots \\ y_n(t) \end{bmatrix} \\ &+ \begin{bmatrix} a_{11}+\Delta a_{11} & a_{12}+\Delta a_{12} & \cdots & a_{1n}+\Delta a_{1n} \\ a_{21}+\Delta a_{21} & a_{22}+\Delta a_{22} & \cdots & a_{2n}+\Delta a_{2n} \\ \vdots & \vdots & \ddots & \vdots \\ a_{n1}+\Delta a_{n1} & a_{n2}+\Delta a_{n2} & \cdots & a_{nn}+\Delta a_{nn} \end{bmatrix} \begin{bmatrix} f_1(y(t)) \\ f_2(y(t)) \\ \vdots \\ f_n(y(t)) \end{bmatrix} + \begin{bmatrix} I_1 \\ I_2 \\ \vdots \\ I_n \end{bmatrix} + \begin{bmatrix} u_1(t) \\ u_2(t) \\ \vdots \\ u_n(t) \end{bmatrix}.\end{aligned} \tag{13}$$

where $y(t) = (y_1(t), \cdots, y_n(t))^T \in R^n$ stands for slave system state. C, A and $f(\cdot)$ are consistent with those in Equation (8). $u(t) = (u_1(t), \cdots, u_n(t))^T$ is the external control input.

The synchronization error is defined as the difference between the states of the master and slave systems and is expressed as follows:

$$e(t) = y(t) - x(t). \tag{14}$$

From (8), (11), and (14), it follows that the error system can be written in the following form:

$$\frac{d^{\overline{\omega}}e(t)}{dt^{\overline{\omega}}} = -(C+\Delta C)e(t) + (A+\Delta A)(f(y(t)) - f(x(t))) + u(t), \tag{15}$$

where $e(t) = (e_1(t), \cdots, e_n(t))^T$.

Our goal is to design a non-fragile feedback controller:

$$u(t) = (K+\Delta K)e(t), \tag{16}$$

where $K = \mathrm{diag}(k_1, k_2, \cdots, k_n)$ is the feedback gain, $\Delta K = \mathrm{diag}(\Delta k_1, \Delta k_2, \cdots, \Delta k_n)$, $|\Delta k_i| \leqslant \overline{k}_i$.

The error system is

$$\frac{d^{\overline{\omega}}e(t)}{dt^{\overline{\omega}}} = [(K+\Delta K) - (C+\Delta C)]e(t) + (A+\Delta A)(f(y(t)) - f(x(t))), \tag{17}$$

or

$$\frac{d^{\omega_i}e_i(t)}{dt^{\omega_i}} = -\sum_{j=1}^{n}\left(c_{ij}+\Delta c_{ij}\right)e_j(t) + (k_i+\Delta k_i)e_i(t) + \sum_{j=1}^{n}\left(a_{ij}+\Delta a_{ij}\right)(f_i(y(t)) - f_i(x(t))). \tag{18}$$

Herein, the control objective is that the trajectory of the slave asymptotically approaches the one of the master, for given master and slave initial conditions, $x(0)$ and $y(0)$, respectively. This translates into:

$$\lim_{t\to\infty}\|e(t)\| = \lim_{t\to\infty}\|y(t) - x(t)\| = 0. \tag{19}$$

System (17) can also be written as:

$$\begin{bmatrix} \frac{d^{\omega_1}e_1(t)}{dt^{\omega_1}} \\ \frac{d^{\omega_2}e_2(t)}{dt^{\omega_2}} \\ \vdots \\ \frac{d^{\omega_n}e_n(t)}{dt^{\omega_n}} \end{bmatrix} = -\begin{bmatrix} (c_{11}+\Delta c_{11}-k_1-\Delta k_1) & (c_{12}+\Delta c_{12}) & \cdots & (c_{1n}+\Delta c_{1n}) \\ (c_{21}+\Delta c_{21}) & (c_{22}+\Delta c_{22}-k_2-\Delta k_2) & \cdots & (c_{1n}+\Delta c_{1n}) \\ \vdots & \vdots & \ddots & \vdots \\ (c_{n1}+\Delta c_{n1}) & (c_{n2}+\Delta c_{n2}) & \cdots & (c_{nn}+\Delta c_{nn}-k_n-\Delta k_n) \end{bmatrix} \begin{bmatrix} e_1(t) \\ e_2(t) \\ \vdots \\ e_n(t) \end{bmatrix} + \begin{bmatrix} a_{11}+\Delta a_{11} & a_{12}+\Delta a_{12} & \cdots & a_{1n}+\Delta a_{1n} \\ a_{21}+\Delta a_{21} & a_{22}+\Delta a_{22} & \cdots & a_{2n}+\Delta a_{2n} \\ \vdots & \vdots & \ddots & \vdots \\ a_{n1}+\Delta a_{n1} & a_{n2}+\Delta a_{n2} & \cdots & a_{nn}+\Delta a_{nn} \end{bmatrix} \begin{bmatrix} f_1(y(t))-f_1(x(t)) \\ f_2(y(t))-f_2(x(t)) \\ \vdots \\ f_n(y(t))-f_n(x(t)) \end{bmatrix}. \tag{20}$$

Then, the design problem involving (8) and (11) can be transformed into a stability problem for the error system (17).

Remark 2. *In the existing literature [23–25], the synchronization control design addresses the commensurate-order case $\omega_i = \omega$. It is not difficult to find that commensurate order is a special case of incommensurate-order systems. It is more general to investigate IFO chaotic neural networks, which provide a more accurate description of the dynamics of complex systems and offer additional possibilities. Although the synchronous control of IFO chaotic systems has been studied in the literature [29] based on linear feedback, the results therein cannot be directly generalized to the IFO chaotic neural networks studied in this paper.*

3. Main Elements

In this section, we establish the following theorem as a fundamental theoretical result of this work, and the following theorem provides a sufficient stabilization condition.

Theorem 1. *If there exist matrices $P_i \in H_+^{t_i \times t_i}, i = 1, 2, \cdots k$, $H \in H_+^{n\times n}$ and $Q \in H^{p\times n}$ such that $BQ > 0$ holds and satisfies*

$$\begin{aligned} &M + \mathrm{sym}\left\{ \left(\begin{bmatrix} I_n \\ -\widetilde{A} \end{bmatrix} \otimes I_2 \right)(H \otimes I_2)([I_n I_n] \otimes I_2) \right\} \\ &+\mathrm{sym}\left\{ \left(\begin{bmatrix} 0_{n\times p} \\ -B \end{bmatrix} \otimes I_2 \right)(Q \otimes I_2)([I_n I_n] \otimes I_2) \right\} < 0, \end{aligned} \tag{21}$$

where

$$\widetilde{A} = \begin{bmatrix} \widetilde{\varphi}_{11} & \widetilde{\varphi}_{12} & \cdots & \widetilde{\varphi}_{1n} \\ \widetilde{\varphi}_{21} & \widetilde{\varphi}_{22} & \cdots & \widetilde{\varphi}_{2n} \\ \vdots & \vdots & \ddots & \vdots \\ \widetilde{\varphi}_{n1} & \widetilde{\varphi}_{n2} & \cdots & \widetilde{\varphi}_{nn} \end{bmatrix},$$

$$\widetilde{\varphi}_{ii} = -2c_{ii} - 2\overline{c}_{ii} + 2(|a_{ii}| + \overline{a}_{ii})L_{ii} + 2k_i + 2\overline{k}_i + \sum_{j=1, i\neq j}^{n} \left(-|c_{ij}| - \overline{c}_{ij} + (|a_{ij}| + \overline{a}_{ij})L_{ij}\right),$$

$$\widetilde{\varphi}_{ij} = \sum_{j=1, i\neq j}^{n} \left(-|c_{ij}| - \overline{c}_{ij} + (|a_{ij}| + \overline{a}_{ij})L_{ij}\right) \ (i = 1, 2, \cdots, n, i \neq j),$$

then system (17) is stable. Additionally, the feedback gain is $K = QH^{-1}$.

Proof. For the error system (17), we choose the following Lyapunov candidate function

$$V(t) = \sum_{i=1}^{n} V_i(t) = \sum_{i=1}^{n} {e_i}^2(t), \tag{22}$$

With Lemma 1 in mind, and calculating the ω_i-order derivatives of $V_i(t)$ along the solution of (17), yields:

$$
\begin{aligned}
D_t^{\omega_1} V_1(t) &\leqslant 2e_1(t) D_t^{\omega_1} e_1(t) \\
&= 2e_1(t)\Bigg(-\sum_{j=1}^{n} (c_{1j} + \Delta c_{1j}) e_j(t) + (k_1 + \Delta k_1) e_1(t) \\
&+ \sum_{j=1}^{n} (a_{1j} + \Delta a_{1j})(f_1(y(t)) - f_1(x(t)))\Bigg) \\
&\leqslant \sum_{j=2}^{n} \left(-|c_{1j}| - \bar{c}_{1j} + \left(|a_{1j}| + \bar{a}_{1j}\right) L_{1j}\right) e_1^2(t) \\
&+ \left(-2c_{11} - 2\bar{c}_{11} + 2(|a_{11}| + \bar{a}_{11}) L_{11} + 2k_1 + 2\bar{k}_1\right) e_1^2(t) \\
&+ (-|c_{12}| - \bar{c}_{12} + (|a_{12}| + \bar{a}_{12}) L_{12}) e_2^2(t) \\
&+ \cdots + (-|c_{1n}| + \bar{c}_{1n} + (|a_{1n}| + \bar{a}_{1n}) L_{1n}) e_n^2(t) \\
&= \sum_{j=2}^{n} \left(-|c_{1j}| - \bar{c}_{1j} + \left(|a_{1j}| + \bar{a}_{1j}\right) L_{1j}\right) V_1(t) \\
&+ \left(-2c_{11} - 2\bar{c}_{11} + 2(|a_{11}| + \bar{a}_{11}) L_{11} + 2k_1 + 2\bar{k}_1\right) V_1(t) \\
&+ (-|c_{12}| - \bar{c}_{12} + (|a_{12}| + \bar{a}_{12}) L_{12}) V_2(t) \\
&+ \cdots + (-|c_{1n}| - \bar{c}_{1n} + (|a_{1n}| + \bar{a}_{1n}) L_{1n}) V_n(t) \\
D_t^{\omega_2} V_2(t) &\leqslant 2e_2(t) D_t^{\omega_2} e_2(t) \\
&= 2e_2(t)\Bigg(-\sum_{j=1}^{n} (c_{2j} + \Delta c_{2j}) e_j(t) + (k_2 + \Delta k_2) e_2(t) \\
&+ \sum_{j=1}^{n} (a_{2j} + \Delta a_{2j})(f_2(y(t)) - f_2(x(t)))\Bigg) \\
&\leqslant \sum_{j=1, j\neq 2}^{n} \left(-|c_{2j}| - \bar{c}_{2j} + \left(|a_{2j}| + \bar{a}_{2j}\right) L_{2j}\right) e_2^2(t) \\
&+ \left(-2c_{22} - 2\bar{c}_{22} + 2(|a_{22}| + \bar{a}_{22}) L_{22} + 2k_2 + 2\bar{k}_2\right) e_2^2(t) \\
&+ (-|c_{21}| - \bar{c}_{21} + (|a_{21}| + \bar{a}_{21}) L_{21}) e_1^2(t) \\
&+ \cdots + (-|c_{2n}| - \bar{c}_{2n} + (|a_{2n}| + \bar{a}_{2n}) L_{2n}) e_n^2(t) \\
&= \sum_{j=1, j\neq 2}^{n} \left(-|c_{2j}| - \bar{c}_{2j} + \left(|a_{2j}| + \bar{a}_{2j}\right) L_{2j}\right) V_2(t) \\
&+ \left(-2c_{22} - 2\bar{c}_{22} + 2(|a_{22}| + \bar{a}_{22}) L_{22} + 2k_2 + 2\bar{k}_2\right) V_2(t) \\
&+ (-|c_{21}| - \bar{c}_{21} + (|a_{21}| + \bar{a}_{21}) L_{21}) V_1(t) \\
&+ \cdots + (-|c_{2n}| - \bar{c}_{2n} + (|a_{2n}| + \bar{a}_{2n}) L_{2n}) V_n(t) \\
&\vdots
\end{aligned}
$$

$$
\begin{aligned}
D_t^{\omega_n} V_n(t) &\leqslant 2e_n(t) D_t^{\omega_n} e_n(t) \\
&= 2e_n(t)\Bigg(-\sum_{j=1}^{n} (c_{nj} + \Delta c_{nj}) e_j(t) + (k_n + \Delta k_n) e_n(t) \\
&+ \sum_{j=1}^{n} (a_{nj} + \Delta a_{nj})(f_i(y(t)) - f_i(x(t)))\Bigg) \\
&\leqslant \sum_{j=1}^{n-1} \left(-|c_{nj}| - \bar{c}_{nj} + \left(|a_{nj}| + \bar{a}_{nj}\right) L_{nj}\right) e_n^2(t) \\
&+ \left(-2c_{nn} - 2\bar{c}_{nn} + 2(|a_{nn}| + \bar{a}_{nn}) L_{nn} + 2k_n + 2\bar{k}_n\right) e_n^2(t) \qquad (23) \\
&+ (-|c_{n1}| - \bar{c}_{n1} + (|a_{n1}| + \bar{a}_{n1}) L_{n1}) e_1^2(t) \\
&+ \cdots + (-|c_{nn-1}| - \bar{c}_{nn-1} + (|a_{nn-1}| + \bar{a}_{nn-1}) L_{nn-1}) e_{n-1}^2(t) \\
&= \sum_{j=1}^{n-1} \left(-|c_{nj}| - \bar{c}_{nj} + \left(|a_{nj}| + \bar{a}_{nj}\right) L_{nj}\right) V_n(t) \\
&+ \left(-2c_{nn} - 2\bar{c}_{nn} + 2(|a_{nn}| + \bar{a}_{nn}) L_{nn} + 2k_n + 2\bar{k}_n\right) V_n(t) \\
&+ (-|c_{n1}| - \bar{c}_{n1} + (|a_{n1}| + \bar{a}_{n1}) L_{n1}) V_1(t) \\
&+ \cdots + (-|c_{nn-1}| - \bar{c}_{nn-1} + (|a_{nn-1}| + \bar{a}_{nn-1}) L_{nn-1}) V_{n-1}(t).
\end{aligned}
$$

From (23), the corresponding comparison system is as follows:

$$\begin{bmatrix} D_t^{\omega_1} W_1(t) \\ D_t^{\omega_2} W_2(t) \\ \vdots \\ D_t^{\omega_n} W_n(t) \end{bmatrix} = \begin{bmatrix} \overline{\varphi}_{11} & \overline{\varphi}_{12} & \cdots & \overline{\varphi}_{1n} \\ \overline{\varphi}_{21} & \overline{\varphi}_{22} & \cdots & \overline{\varphi}_{2n} \\ \vdots & \vdots & \ddots & \vdots \\ \overline{\varphi}_{n1} & \overline{\varphi}_{n2} & \cdots & \overline{\varphi}_{nn} \end{bmatrix} \begin{bmatrix} W_1(t) \\ W_2(t) \\ \vdots \\ W_n(t) \end{bmatrix}, \tag{24}$$

where

$$\widetilde{\varphi}_{ii} = -2c_{ii} - 2\overline{c}_{ii} + 2(|a_{ii}| + \overline{a}_{ii})L_{ii} + 2k_i + 2\overline{k}_i + \sum_{j=1, i\neq j}^{n} \left(-|c_{ij}| - \overline{c}_{ij} + \left(|a_{ij}| + \overline{a}_{ij}\right)L_{ij}\right), \tag{25}$$

$$\widetilde{\varphi}_{ij} = \sum_{j=1, i\neq j}^{n} \left(-|c_{ij}| - \overline{c}_{ij} + \left(|a_{ij}| + \overline{a}_{ij}\right)L_{ij}\right) \ (i = 1, 2, \cdots, n, i \neq j). \tag{26}$$

The system can be rewritten to:

$$D_t^{\overline{\omega}} W(t) = \widetilde{A}W(t) + B\overline{K}W(t) = \widetilde{A}W(t) + Bu(t), \tag{27}$$

$$\widetilde{\varphi}_{ii} = \widetilde{\varphi}_{ii} - 2k_i, \widetilde{\varphi}_{ij} = \widetilde{\varphi}_{ij}, \tag{28}$$

where $W(t) = (W_1(t), W_2(t), \cdots, W_n(t))^T$, it follows from Lemma 3 that the controlled system (27) is stable if the appropriate condition is satisfied, i.e., $W(t) \to 0$. Based on the comparison principle of FO systems with multi-order, we have $V(t) \leqslant W(t)$. Therefore, the error system (17) is also stable. This ends the proof. □

Remark 3. *Recent works have studied the stability and stabilization of IFO uncertain nonlinear systems based on the comparison principle but have not considered the synchronization control problem [36]. In literature [27], the authors studied the synchronization problem of IFO chaotic systems with linear feedback control based on the comparative principle. It is a great pity that the presence of uncertainty is not considered, and only numerical simulation results are available.*

4. Numerical Examples

4.1. Numerical Simulation

The state equation of an uncertain IFO neural network master system can be represented by the following equation:

$$\begin{cases} D_t^{\omega_1} x_1(t) = -(1 + \Delta c_{11})x_1 + 2\tanh x_1 - \tanh x_2, \\ D_t^{\omega_2} x_2(t) = -(1 + \Delta c_{22})x_2 + 1.7\tanh x_1 + 1.71\tanh x_2 + 1.1\tanh x_3, \\ D_t^{\omega_3} x_3(t) = -(2 + \Delta c_{33})x_3 - 2.6\tanh x_1 - 2.8\tanh x_2 + 1.25\tanh x_3, \end{cases} \tag{29}$$

where $\omega_1 = 0.99$, $\omega_2 = 0.993$, $\omega_3 = 1$. Parameter uncertainties are chosen as $\Delta c_{11} = 0.2\sin(t)$, $\Delta c_{22} = 0.3\sin(t)$, $\Delta c_{33} = 0.1\sin(t)$. The 3-D chaotic attractors of the system (29) when its initial state is selected as $x(0) = (0.5, 0.2, -0.5)^T$ is shown in Figure 1. In addition, Figure 2 shows the projection of the chaotic attractor of the system (29) on $x_1(t) - x_2(t)$, $x_2(t) - x_3(t)$, $x_1(t) - x_3(t)$. Based on the boundedness and phase space diagram of the system (29), we can observe the Lipschitz constant $L_{11} = 2$, $L_{12} = 1$, $L_{13} = 0$, $L_{21} = 1.7$, $L_{22} = 1.71$, $L_{23} = 1.1$, $L_{31} = 2.6$, $L_{32} = 2.8$, $L_{33} = 1.25$.

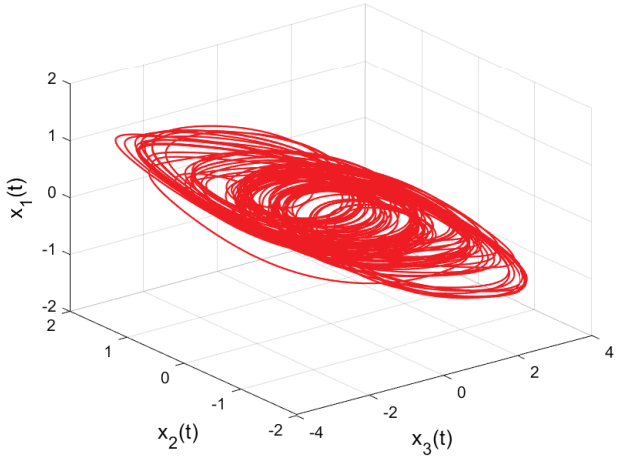

Figure 1. 3-D chaotic attractors for the IFO neural network system (29).

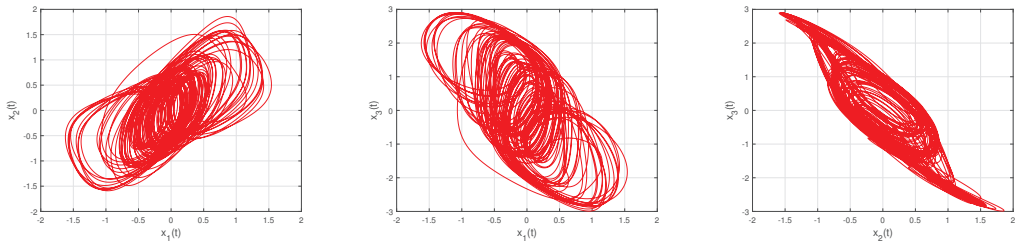

(**a**) (**b**) (**c**)

Figure 2. Examples of phase diagrams for chaotic systems with FO neural networks: (**a**) chaotic attractor on the $x_1(t) - x_2(t)$ space; (**b**) chaotic attractor projected on the $x_1(t) - x_3(t)$ plane; (**c**) chaotic attractor on the $x_2(t) - x_3(t)$ space.

The slave system can be selected as follows:

$$\begin{cases} D_t^{\omega_1} y_1(t) = -(1+\Delta c_{11})y_1 + 2\tanh y_1 - \tanh y_2 + u_1, \\ D_t^{\omega_2} y_2(t) = -(1+\Delta c_{22})y_2 + 1.7\tanh y_1 + 1.71\tanh y_2 + 1.1\tanh y_3 + u_2, \\ D_t^{\omega_3} y_3(t) = -(2+\Delta c_{33})y_3 - 2.6\tanh y_1 - 2.8\tanh y_2 + 1.25\tanh y_3 + u_3. \end{cases} \tag{30}$$

The initial state of the slave system (30) is chosen as $y(0) = (0.3, 0.5, -0.7)^T$. Define the state error as $e_1(t) = y_1(t) - x_1(t)$; $e_2(t) = y_2(t) - x_2(t)$; $e_3(t) = y_3(t) - x_3(t)$ and define that $u_i(t) = (k_i + \Delta k_i)e_i(t)$, $i = 1, 2, 3$. Therefore, the state equation of the error system is:

$$\begin{cases} D_t^{\omega_1} e_1(t) = & -(1+\Delta c_{11})e_1 + 2(\tanh y_1 - \tanh x_1) - (\tanh y_2 - \tanh x_2) + (k_1 + \Delta k_1)e_1, \\ D_t^{\omega_2} e_2(t) = & -(1+\Delta c_{22})e_2 + 1.7(\tanh y_1 - \tanh x_1) + 1.71(\tanh y_2 - \tanh x_2) \\ & +1.1(\tanh y_3 - \tanh x_3) + (k_2 + \Delta k_2)e_2, \\ D_t^{\omega_3} e_3(t) = & -(2+\Delta c_{33})e_3 - 2.6(\tanh y_1 - \tanh x_1) - 2.8(\tanh y_2 - \tanh x_2) \\ & +1.25(\tanh y_3 - \tanh x_3) + (k_3 + \Delta k_3)e_3, \end{cases} \tag{31}$$

where $\Delta k_i = 0.1\sin(t), i = 1, 2, 3$.

By calculation, we can obtain $\widetilde{A} = \begin{bmatrix} 6.8 & 1 & 0 \\ 1.7 & 7.82 & 1.1 \\ 2.6 & 2.8 & 11.9 \end{bmatrix}$, $B = I_3$.

Based on the constraints of the LMI in Theorem 1, the following feasible solution is obtained using the LMI control toolbox in Matlab (i.e., YALMIP):

$$Q = \begin{bmatrix} 33.8773 & 0 & 0 \\ 0 & 48.3640 & 0 \\ 0 & 0 & 77.1769 \end{bmatrix}, H = \begin{bmatrix} -2.5839 & 0 & 0 \\ 0 & -3.5697 & 0 \\ 0 & 0 & -11.5700 \end{bmatrix},$$

$$K = QH^{-1} = \begin{bmatrix} -13.1110 & 0 & 0 \\ 0 & -13.5485 & 0 \\ 0 & 0 & -6.6704 \end{bmatrix},$$

$$P_1 = 25.3066, P_2 = 27.4804, P_3 = 34.2507.$$

The master and slave state trajectories of the IFO neural network systems (29) and (30) are shown in Figure 3, which effectively verify that synchronization has been achieved. Meanwhile, Figure 4 shows the synchronization errors of the error system (31), and the results shown in Figure 4 demonstrate the effectiveness of the designed controller.

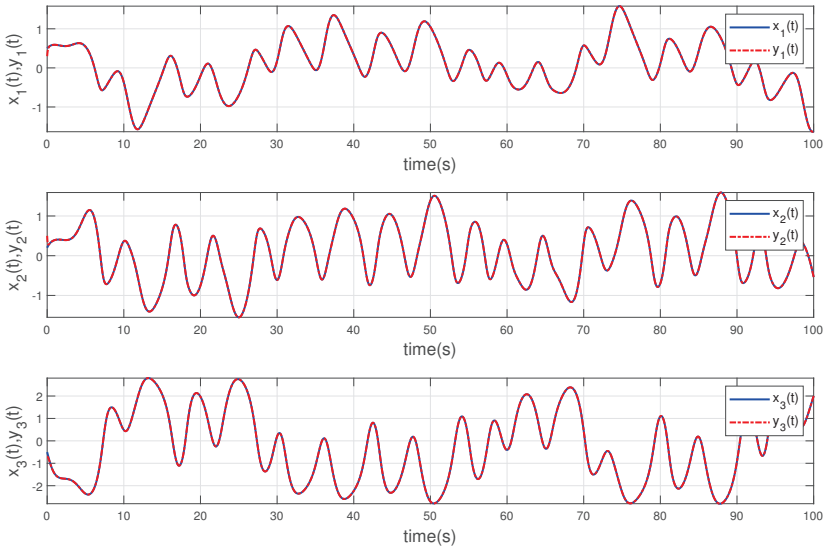

Figure 3. Master and slave state trajectories of the IFO neural network systems (29) and (30).

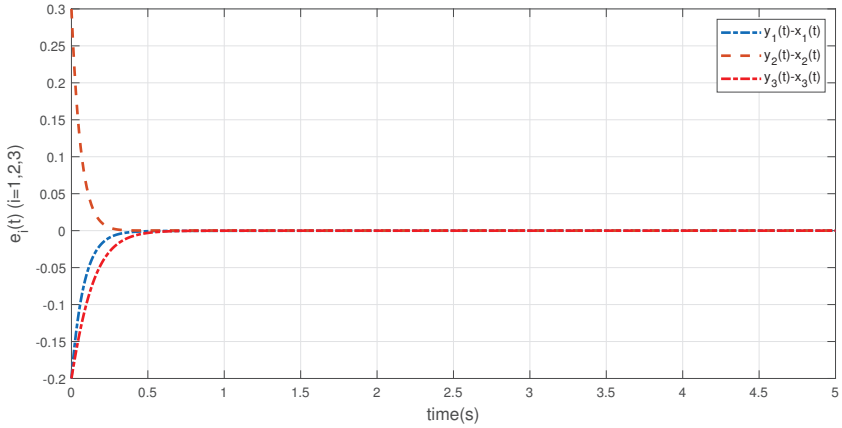

Figure 4. Synchronization errors of IFO neural network systems (29) and (30).

4.2. Circuit Implementation

To enable hardware-level verification of dynamic performance and support subsequent engineering development, the corresponding analog circuit is implemented in this study.

4.2.1. Realization of the FO Circuit

To characterize the FO system's frequency-domain behavior, we develop a frequency-domain approximation circuit for dynamic analysis. In the scope of $[10^{-2}\ 10^{2}]$ rad/s for ω, there exists an approximation expression with maximum distortion 0.2 dB [39]:

$$\frac{9.77237\left(1+1.890215\times10^{-6}s\right)\left(1+9.32603\times10^{-4}s\right)(1+0.097701s)}{(1+8.49753\times10^{-6}s)\left(1+8.90215\times10^{-4}s\right)(1+0.0932603s)(1+9.77s)} = 1/s^{0.99}, \tag{32}$$

where s denotes the complex frequency.

The corresponding transfer function $F(s)$ to realize the unit circuit is given in the analog circuit:

$$\frac{\left(\frac{C_o}{C_1}+\frac{C_o}{C_2}\right)\left[s^2+\frac{\left(\frac{C_2}{R_1}+\frac{C_1}{R_2}\right)s+\frac{R_1+R_2}{R_1R_2}}{C_1C_2}\right]}{C_o(s+1/R_1C_1)(s+1/R_2C_2)} = F(s), \tag{33}$$

where C_o denotes the specific capacitance, C_1 and C_2 are the selected capacitors, and R_1 and R_2 represent the selected resistors.

Based on the aforementioned approximation method, the approximate transfer function of $1/s^{0.993}$ is defined in the frequency domain with a maximum deviation of 0.2 dB within the range of 0.01∼100 rad/s, as follows [40]:

$$\frac{9.84011\left(1+1.80095\times10^{-5}s\right)\left(1+1.35765\times10^{-2}s\right)}{(1+1.71934\times10^{-5}s)(1+1.29612\times10^{-2}s)(1+9.77079s)} = 1/s^{0.993}. \tag{34}$$

The corresponding transfer function $F(s)$ to realize the unit circuit is given in the analog circuit:

$$\frac{\left(\frac{C_o}{C_1}+\frac{C_o}{C_2}+\frac{C_o}{C_3}\right)\left[s^2+\frac{\left(\frac{C_2+C_3}{R_1}+\frac{C_1+C_3}{R_2}+\frac{C_1+C_2}{R_3}\right)s+\frac{R_1+R_2+R_3}{R_1R_2R_3}}{C_1C_2+C_1C_3+C_2C_3}\right]}{C_o(s+1/R_1C_1)(s+1/R_2C_2)(s+1/R_3C_3)} = F(s), \tag{35}$$

where C_o is the specific capacitance, C_1, C_2 and C_3 denote the selected capacitors, and R_1, R_2 and R_3 are the selected resistors.

In order to build a unit circuit of $F(s)$, the circuit diagram corresponding to fractional order and their parameters are displayed in Table 2.

Table 2. The circuit diagram corresponding to fractional order and their parameters.

Fractional Order	Circuit Diagram	Circuit Parameters	
ω = 0.99		C_1 = 10.002 nF C_2 = 208.054 nF	R_1 = 976.784 MΩ R_2 = 448.251 kΩ
ω = 0.993	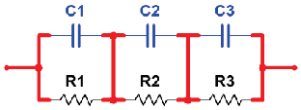	C_1 = 9.93018 nF C_2 = 208.9 nF C_3 = 199.7 nF	R_1 = 983.949 MΩ R_2 = 62.0449 kΩ R_3 = 80.0960 Ω

4.2.2. Design of the Multisim Circuits

According to the system Equation (31), the circuit model of the ternary cellular neural network is constructed by applying the principles of the inverting adder circuit, the inverting integrator circuit, and the inverting circuit in analog circuitry. This model is then integrated with the output function module and the FO module and simulated in Multisim, as illustrated in Figure 5.

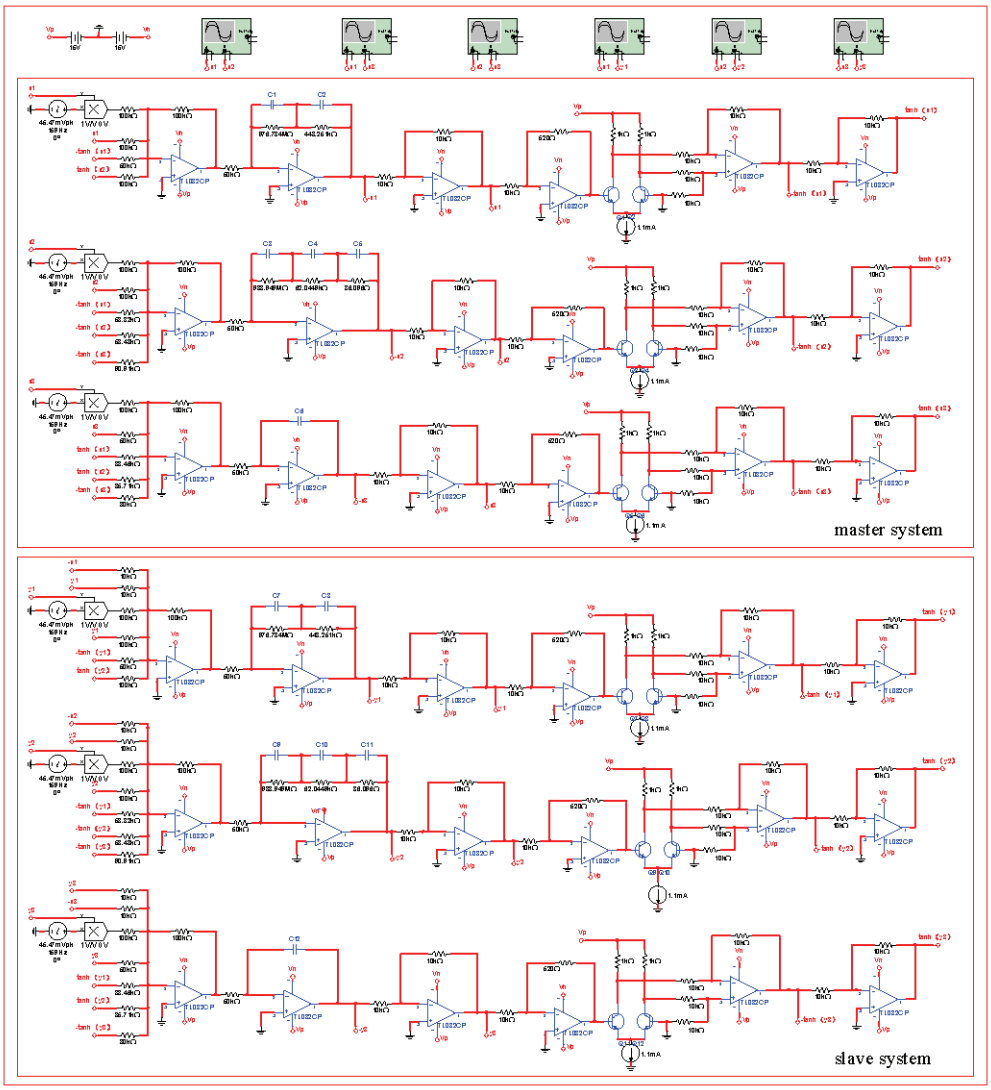

Figure 5. Overall circuit synchronization diagram.

The phase portrait of the chaotic attractor generated by the IFO neural network system is depicted in Figure 6, while Figure 7 illustrates the relationship between the corresponding synchronization state vectors. These figures demonstrate that the master–slave system achieves synchronization through the regulation of the linear feedback controller. Furthermore, the results align with both the Matlab simulation and the circuit simulation outcomes, thereby validating the correctness of the circuit design presented in this section.

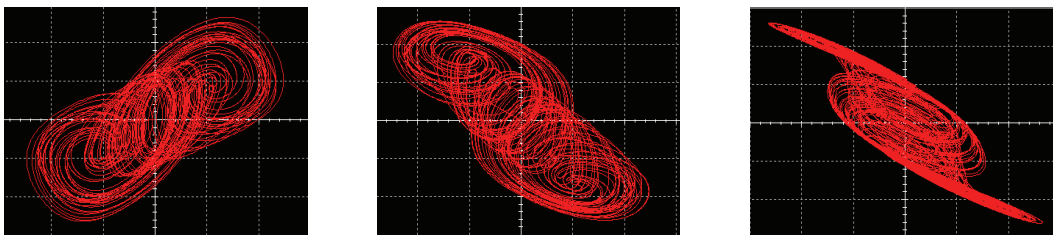

(**a**) (**b**) (**c**)

Figure 6. IFO Phase trajectory diagram of a chaotic neural network system: (**a**) $x_1(t) - x_2(t)$ phase diagram (**b**) $x_1(t) - x_3(t)$ phase diagram (**c**) $x_2(t) - x_3(t)$ phase diagram.

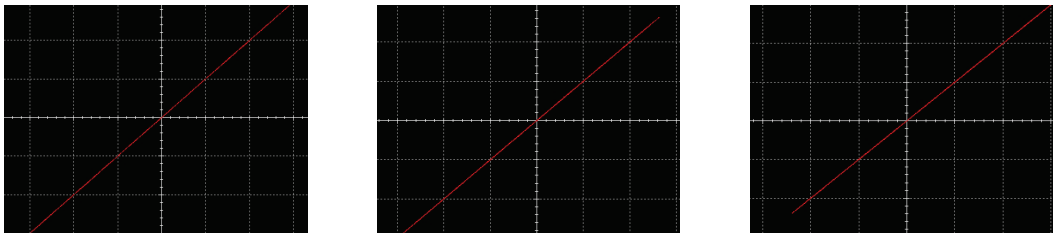

(**a**) (**b**) (**c**)

Figure 7. Synchronization curves for master–slave IFO chaotic neural network systems: (**a**) $x_1(t) - x_2(t)$ phase diagram (**b**) $x_1(t) - x_3(t)$ phase diagram (**c**) $x_2(t) - x_3(t)$ phase diagram.

5. Conclusions

This paper addressed the synchronization control and circuit implementation of IFO chaotic neural networks with parameter uncertainties. By establishing a dynamic model for IFO systems, the study breaks through the limitations of traditional commensurate-order frameworks, offering a more generalized approach for analyzing complex neural networks. A novel non-fragile state-error feedback controller was designed to ensure robust synchronization under parameter perturbations, supported by FO Lyapunov functions and the multi-order fractional comparison principle. Sufficient conditions for asymptotic synchronization were derived, applicable to both commensurate and integer-order systems. Furthermore, the proposed synchronization strategy was validated through numerical simulations and circuit experiments, demonstrating consistency between theoretical predictions and circuit implementation. Future work may focus on extending the framework to higher-dimensional systems and exploring real-world applications under more complex environmental conditions.

Author Contributions: Methodology, writing—original draft preparation, R.Z.; software, C.L.; validation, Z.C.; data curation, H.M.; writing—review and editing, supervision and project administration, K.Q. All authors have read and agreed to the published version of the manuscript.

Funding: This work was supported by the National Natural Science Funds of China (No. 62202138), Anhui Provincial Key Research and Development Project (202304a05020060) and Anhui Provincial Natural Science Outstanding Youth Foundation (2408085J038) and 2024 University Student Innovative Experiment Program at Hefei University of Technology (X2024103591).

Data Availability Statement: No new data were created or analyzed in this study. Data sharing is not applicable to this article.

Conflicts of Interest: The authors declare no conflicts of interest.

References

1. Che, H.; Wang, J. A Two-Timescale Duplex Neurodynamic Approach to Biconvex Optimization. *IEEE Trans. Neural Netw. Learn. Syst.* **2019**, *30*, 2503–2514. [CrossRef] [PubMed]
2. Chen, W.; Ding, D.; Dong, H.; Wei, G. Distributed Resilient Filtering for Power Systems Subject to Denial-of-Service Attacks. *IEEE Trans. Syst. Man Cybern. Syst.* **2019**, *49*, 1688–1697. [CrossRef]
3. Ding, D.; Wang, Z.; Han, Q.L. A Set-Membership Approach to Event-Triggered Filtering for General Nonlinear Systems Over Sensor Networks. *IEEE Trans. Autom. Control* **2020**, *65*, 1792–1799. [CrossRef]
4. Zong, G.; Ren, H.; Karimi, H.R. Event-Triggered Communication and Annular Finite-Time Filtering for Networked Switched Systems. *IEEE Trans. Cybern.* **2021**, *51*, 309–317. [CrossRef] [PubMed]
5. Chen, M.; Shao, S.Y.; Shi, P.; Shi, Y. Disturbance-Observer-Based Robust Synchronization Control for a Class of Fractional-Order Chaotic Systems. *IEEE Trans. Circuits Syst. II Express Briefs* **2017**, *64*, 417–421. [CrossRef]
6. Heng, L.; Sheng-Gang, L.; Ye-Guo, S.; Hong-Xing, W. Prescribed performance synchronization for fractional-order chaotic systems. *Chin. Phys. B* **2015**, *24*, 157–164.

7. Liu, X.; Li, C.; Ge, S.S.; Li, D. Time-Synchronized Control of Chaotic Systems in Secure Communication. *IEEE Trans. Circuits Syst. I: Regul. Pap.* **2022**, *69*, 3748–3761. [CrossRef]
8. Xu, Y.; Wang, H.; Liu, X.; Li, W. Quasi-synchronization of heterogenous fractional-order dynamical networks with time-varying delay via distributed impulsive control. *Chaos Solitons Fractals* **2021**, *142*, 110465.
9. Aadhithiyan, S.; Raja, R.; Zhu, Q.; Alzabut, J.O.; Niezabitowski, M.; Lim, C.P. Modified projective synchronization of distributive fractional order complex dynamic networks with model uncertainty via adaptive control. *Chaos Solitons Fractals* **2021**, *147*, 110853. [CrossRef]
10. Zambrano-Serrano, E.; Bekiros, S.; Platas-Garza, M.A.; Posadas-Castillo, C.; Agarwal, P.; Jahanshahi, H.; Aly, A.A. On chaos and projective synchronization of a fractional difference map with no equilibria using a fuzzy-based state feedback control. *Phys. A Stat. Mech. Its Appl.* **2021**, *578*, 126100. [CrossRef]
11. Zhang, K.; Wang, H.O.; Fang, H. Feedback control and hybrid projective synchronization of a fractional-order Newton–Leipnik system. *Commun. Nonlinear Sci. Numer. Simul.* **2012**, *17*, 317–328. [CrossRef]
12. Xiong, R.; Tian, J.; Shen, W.; Sun, F. A Novel Fractional Order Model for State of Charge Estimation in Lithium Ion Batteries. *IEEE Trans. Veh. Technol.* **2019**, *68*, 4130–4139. [CrossRef]
13. Liu, X.; Mou, J.; Zhang, Y.; Cao, Y. A New Hyperchaotic Map Based on Discrete Memristor and Meminductor: Dynamics Analysis, Encryption Application, and DSP Implementation. *IEEE Trans. Ind. Electron.* **2024**, *71*, 5094–5104. [CrossRef]
14. Sha, Y.; Mou, J.; Banerjee, S.; Zhang, Y. Exploiting Flexible and Secure Cryptographic Technique for Multidimensional Image Based on Graph Data Structure and Three-Input Majority Gate. *IEEE Trans. Ind. Informatics* **2024**, *20*, 3835–3846. [CrossRef]
15. Lundstrom, B.N.; Higgs, M.H.; Spain, W.J.; Fairhall, A.L. Fractional differentiation by neocortical pyramidal neurons. *Nat. Neurosci.* **2008**, *11*, 1335–1342. [CrossRef] [PubMed]
16. Kamal, F.M.; Elsonbaty, A.; Elsaid, A. A novel fractional nonautonomous chaotic circuit model and its application to image encryption. *Chaos Solitons Fractals* **2021**, *144*, 110686. [CrossRef]
17. Gökdoğan, A.; Merdan, M.; Yildirim, A. A multistage differential transformation method for approximate solution of Hantavirus infection model. *Commun. Nonlinear Sci. Numer. Simul.* **2012**, *17*, 1–8. [CrossRef]
18. Xingce, L.; Jun, M.; Jue, W.; Santo, B.; Peng, L. Dynamical Analysis of a Novel Fractional-Order Chaotic System Based on Memcapacitor and Meminductor. *Fractal Fract.* **2022**, *6*, 671. [CrossRef]
19. Liu, X.; Tong, X.; Wang, Z.; Zhang, M. Efficient high nonlinearity S-box generating algorithm based on third-order nonlinear digital filter. *Chaos Solitons Fractals* **2021**, *150*, 111109. [CrossRef]
20. Shi, Q.; An, X.; Xiong, L.; Yang, F.; Zhang, L. Dynamic analysis of a fractional-order hyperchaotic system and its application in image encryption. *Phys. Scr.* **2022**, *97*, 045201. [CrossRef]
21. Bao, H.; Park, J.H.; Cao, J. Synchronization of fractional-order complex-valued neural networks with time delay. *Neural Networks* **2016**, *81*, 16–28. [CrossRef] [PubMed]
22. Xiong, J.-J.; Zhang, G.-B.; Wang, J.-X.; Yan, T.-H. Improved Sliding Mode Control for Finite-Time Synchronization of Nonidentical Delayed Recurrent Neural Networks. *IEEE Trans. Neural Netw. Learn. Syst.* **2020**, *31*, 2209–2216. [CrossRef]
23. Rakkiyappan, R.; Cao, J.; Velmurugan, G. Existence and Uniform Stability Analysis of Fractional-Order Complex-Valued Neural Networks With Time Delays. *IEEE Trans. Neural Netw. Learn. Syst.* **2015**, *26*, 84–97. [CrossRef] [PubMed]
24. Yang, S.; Yu, J.; Hu, C.; Jiang, H. Quasi-projective synchronization of fractional-order complex-valued recurrent neural networks. *Neural Networks* **2018**, *104*, 104–113. [CrossRef]
25. Hong-Li, L.; Cheng, H.; Jinde, C.; Haijun, J.; Ahmed, A. Quasi-projective and complete synchronization of fractional-order complex-valued neural networks with time delays. *Neural Netw.* **2019**, *118*, 102–109.
26. Boulkroune, A.; Bouzeriba, A.; Bouden, T. Fuzzy generalized projective synchronization of incommensurate fractional-order chaotic systems. *Neurocomputing* **2016**, *173*, 606–614. [CrossRef]
27. Qi, F.; Qu, J.; Chai, Y.; Chen, L.; Lopes, A.M. Synchronization of Incommensurate Fractional-Order Chaotic Systems Based on Linear Feedback Control. *Fractal Fract.* **2022**, *6*, 221. [CrossRef]
28. Debbouche, N.; Almatroud, A.O.; Ouannas, A.; Batiha, I.M. Chaos and coexisting attractors in glucose-insulin regulatory system with incommensurate fractional-order derivatives. *Chaos Solitons Fractals* **2021**, *143*, 110575. [CrossRef]
29. Chen, L.; Xue, M.; Lopes, A.M.; Wu, R.; Zhang, X.; Chen, Y. New Synchronization Criterion of Incommensurate Fractional-Order Chaotic Systems. *IEEE Trans. Circuits Syst. II: Express Briefs* **2024**, *71*, 455–459. [CrossRef]
30. Zouari, F.; Boulkroune, A.; Ibeas, A. Neural adaptive quantized output-feedback control-based synchronization of uncertain time-delay incommensurate fractional-order chaotic systems with input nonlinearities. *Neurocomputing* **2017**, *237*, 200–225. [CrossRef]
31. Deepika, D.; Kaur, S.; Narayan, S. Uncertainty and disturbance estimator based robust synchronization for a class of uncertain fractional chaotic system via fractional order sliding mode control. *Chaos Solitons Fractals* **2018**, *115*, 196–203. [CrossRef]
32. Hajipour, A.; Aminabadi, S.S. Synchronization of chaotic Arneodo system of incommensurate fractional order with unknown parameters using adaptive method. *Optik* **2016**, *127*, 7704–7709. [CrossRef]

33. Xu, S.; Wang, X.; Ye, X. A new fractional-order chaos system of Hopfield neural network and its application in image encryption. *Chaos Solitons Fractals* **2022**, *157*, 111889. [CrossRef]
34. Ma, T.; Mou, J.; Li, B.; Banerjee, S.; Yan, H. Study on the Complex Dynamical Behavior of the Fractional-Order Hopfield Neural Network System and Its Implementation. *Fractal Fract.* **2022**, *6*, 637. [CrossRef]
35. Podlubny, I. *Fractional Differential Equations*; Mathematics in Science and Engineering; Academic Press: Cambridge, MA, USA, 1999.
36. Chen, L.; Guo, W.; Gu, P.; Lopes, A.M.; Chu, Z.; Chen, Y. Stability and Stabilization of Fractional-Order Uncertain Nonlinear Systems With Multiorder. *IEEE Trans. Circuits Syst. II Express Briefs* **2023**, *70*, 576–580. [CrossRef]
37. Lenka, B.K. Fractional comparison method and asymptotic stability results for multivariable fractional order systems. *Commun. Nonlinear Sci. Numer. Simul.* **2018**, *69*, 398–415. [CrossRef]
38. Lu, J.G.; Zhu, Z.; Ma, Y.D. Robust stability and stabilization of multi-order fractional-order systems with interval uncertainties: An LMI approach. *Int. J. Robust Nonlinear Control* **2021**, *31*, 4081–4099. [CrossRef]
39. Luo, S.; Song, Y.; Lewis, F.L.; Garrappa, R. Neuroadaptive Optimal Fixed-Time Synchronization and its Circuit Realization for Unidirectionally Coupled FO Self-Sustained Electromechanical Seismograph Systems. *IEEE Trans. Cybern.* **2023**, *53*, 2454–2466. [CrossRef]
40. Luo, S.; Song, Y.; Lewis, F.L.; Deng, G. Dynamical Analysis, Circuit Design, and Fuzzy Prescribed Performance Backstepping Control of the FO Weakly Coupled MEMS Resonators. *IEEE Trans. Fuzzy Syst.* **2024**, *32*, 1768–1781. [CrossRef]

Disclaimer/Publisher's Note: The statements, opinions and data contained in all publications are solely those of the individual author(s) and contributor(s) and not of MDPI and/or the editor(s). MDPI and/or the editor(s) disclaim responsibility for any injury to people or property resulting from any ideas, methods, instructions or products referred to in the content.

symmetry

MDPI

Article

Fractional and Higher Integer-Order Moments for Fractional Stochastic Differential Equations

Arsalane Chouaib Guidoum [1,2,†], Fatimah A. Almulhim [3,*,†], Mohammed Bassoudi [4,†], Kamal Boukhetala [2,†] and Mohammed B. Alamari [5,†]

[1] Department of Mathematics and Computer Science, Faculty of Sciences and Technology, University of Tamanghasset, Tamanghasset 11000, Algeria; acguidoum@univ-tam.dz
[2] Laboratory MSTD, Faculty of Mathematics, University of Science and Technology Houari Boumediene, P.O. Box 32, El Alia 16111, Algeria; kamel.boukhetala@usthb.edu.dz
[3] Department of Mathematical Sciences, College of Science, Princess Nourah bint Abdulrahman University, P.O. Box 84428, Riyadh 11671, Saudi Arabia
[4] Department of Science and Technology, Faculty of Technology, Amar Teledji University, Laghouat 03000, Algeria; m.bassoudi@lagh-univ.dz
[5] Department of Mathematics, College of Science, King Khalid University, Abha 62529, Saudi Arabia; malamari@kku.edu.sa
* Correspondence: faalmulhim@pnu.edu.sa
† These authors contributed equally to this work.

Abstract: This study investigates the computation of fractional and higher integer-order moments for a stochastic process governed by a one-dimensional, non-homogeneous linear stochastic differential equation (SDE) driven by fractional Brownian motion (fBm). Unlike conventional approaches relying on moment-generating functions or Fokker–Planck equations, which often yield intractable expressions, we derive explicit closed-form formulas for these moments. Our methodology leverages the Wick–Itô calculus (fractional Itô formula) and the properties of Hermite polynomials to express moments efficiently. Additionally, we establish a recurrence relation for moment computation and propose an alternative approach based on generalized binomial expansions. To validate our findings, Monte Carlo simulations are performed, demonstrating a high degree of accuracy between theoretical and empirical results. The proposed framework provides novel insights into stochastic processes with long-memory properties, with potential applications in statistical inference, mathematical finance, and physical modeling of anomalous diffusion.

Keywords: fractional moments; higher-order moments; fractional Brownian motion; Wick–Itô formula; long-memory process; Hermite polynomials; stochastic differential equations

MSC: 39A50; 60G22; 33C45; 65C05

1. Introduction

Long-memory processes, defined by extended-range dependencies, have attracted considerable attention due to their diverse applications across multiple scientific fields. These include physics [1–5], biology and life sciences [6–9], economics and financial mathematics [10–14], as well as other areas of science and engineering [15,16]. Among the prominent models for capturing long memory, fractional Brownian motion (fBm) has emerged as a robust and well-established framework for describing the long-range dependence exhibited by certain time series. When analyzing data characterized by long-range dependence, fBm serves as a natural alternative to standard Brownian motion, which is

limited by the independence of its increments. Fractional Brownian motion was initially introduced by Kolmogorov [17] and later popularized within the statistical community by Mandelbrot and Ness [18]. For a deeper exploration of equations driven by fBm, readers are encouraged to consult the works of Maslowski and Nualart [19], Mishura [20], Ascione et al. [21]. Ullah et al. [22] have recently investigated fractional SDEs under relaxed regularity assumptions, such as non-Lipschitz conditions, and established general results on the existence and mean-square stability of their solutions. Overall, fBm provides a rich mathematical framework for modeling various stochastic processes influenced by memory effects and external factors, making it a versatile tool in the study of dynamic systems.

Computing the fractional and higher integer-order moments of a stochastic process is a fundamental challenge in stochastic analysis, particularly when the process is driven by fBm. This difficulty arises primarily due to the non-Markovian nature of fBm, which introduces memory effects into the system and significantly complicates its analysis compared to standard Brownian motion. In the context of linear SDEs driven by fBm, the presence of random excitation whether additive or multiplicative significantly amplifies the analytical challenges. Consequently, approximate solutions frequently become essential in practical applications.

Typically, one computes a process's moments either by integrating a power function against its density function or by differentiating its moment-generating function. These moments are essential, as they offer valuable insights into the distribution's form and variability. For example, higher-order moments are instrumental in characterizing skewness and kurtosis, as well as addressing parametric statistical inference challenges for various classes of stochastic processes governed by SDEs [23,24]. A detailed exploration of statistical inference for fractional diffusion processes can be found in [25]. For linear SDEs driven by fBm, the determination of transition density functions frequently requires solving the associated Fokker–Planck equations (or Kolmogorov backward equations) [26]. While density functions or moment-generating functions can sometimes be derived under specific conditions [27,28], the computation of fractional and higher-order moments remains highly non-trivial. This complexity is particularly pronounced due to the lack of explicit analytical solutions for the Fokker–Planck equations in the presence of fBm. In these situations, numerical techniques such as Monte Carlo simulations [29,30] offer a viable alternative for approximating the process's moments. Analytical techniques to characterize fractional stochastic systems have also been explored through spectral density analysis, providing useful insights into their dynamic response under stochastic excitation (see [31]). However, these techniques primarily focus on frequency-domain properties. Our study complements these methods by providing analytical results in terms of fractional and higher-order moments, offering a robust statistical characterization in the time domain.

Our main objective in this study is to determine the fractional and higher integer-order moments of a linear stochastic process driven by fBm. By examining these moments, one gains a deeper understanding of the process's statistical behavior, encompassing its mean, variance, skewness, and kurtosis. Fractional moments, in particular, are indispensable when the distribution of the process exhibits inverse power-law tails, which often render integer-order moments undefined or non-existent. Rather than relying on traditional approaches, such as deriving the density or moment-generating functions—which are often infeasible in this context—we leverage the unique properties of fBm to obtain explicit formulas for the pth moments. Beyond reducing computational complexity, these formulas serve as an effective tool for validating the accuracy of numerical simulations within stochastic modeling. By calculating these moments, researchers can deepen their understanding of the process's statistical properties and enhance their capability to accurately forecast its

temporal evolution. This methodology establishes a solid framework for analyzing the dynamics of stochastic systems characterized by long-memory behavior.

The structure of the paper is as follows. Section 2 revisits essential results that form the foundation of our study. Section 3 details our main contributions, where we derive explicit formulas for both the fractional and higher integer-order moments of the process. In Section 4, a numerical Monte Carlo simulation is presented to compute the moments of the propagation process, which are then compared with the analytical expressions derived earlier. Finally, Section 5 wraps up the paper by summarizing the primary findings and outlining possible directions for future research.

2. Preliminaries

In this section, we present the foundational definitions of fractional Brownian motion (fBm) and fractional calculus that will underpin our analysis throughout the paper.

Let $(\Omega, \mathcal{F}, \mathbb{P})$ denote a probability space, and consider the stochastic process $\mathbb{X} = \{X_t, t \geq 0\}$ defined on this space, where each X_t takes values in $\mathbb{R}$ for all $t \geq 0$. We now consider $\mathbb{X}$ as the solution to a linear stochastic differential equation driven by fBm:

$$\begin{cases} \mathrm{d}X_t = \underbrace{\left(\alpha \dfrac{g^{(k+1)}(t)}{g^{(k)}(t)} X_t + \beta\, g^{(k)}(t)^{\alpha}\right)}_{\mu(x,t)} dt + \underbrace{\gamma\, g^{(k)}(t)^{\alpha}}_{\sigma(t)} \mathrm{d}W_t^H \\ X_0 = x_0 \in \mathbb{R} \,\text{at}\, t_0 \end{cases} \tag{1}$$

We assume that X_t is well-defined for all $t \geq 0$. In Equation (1), the process $\{W_t^H, t \geq 0\}$ denotes a fractional Brownian motion (fBm) with Hurst index $H \in (0,1)$. Although fBm does not possess the martingale property, it exhibits behavior similar to Brownian motion, enhanced by long-memory effects governed by H. The drift $\mu(x,t)$ and diffusion $\sigma(t)$ coefficients are given time-dependent functions that satisfy the necessary regularity conditions—such as Lipschitz continuity and bounded growth—to ensure the existence and uniqueness of the solution (see e.g., [32–34]). Furthermore, for parameters $\alpha, \beta \in \mathbb{R}$ and $\gamma > 0$, we assume that $g(t)$ is piecewise continuous on $(-\infty, +\infty)$ and that its kth derivative $g^{(k)}(t)$ is non-zero for all $t \geq 0$ with $k \in \mathbb{N}$.

The model (1) encapsulates a complex system and subsumes several well-known stochastic processes as special cases. For example, when $\alpha = 0$, the stochastic process reduces to a fractional Merton model [35]. Moreover, if $\alpha \in \mathbb{Z}^-$, $k \in \mathbb{N}^+$, and $g(t) = \ln(t - T)$, it corresponds to a fractional Brownian bridge process with time-dependent diffusion (see Section 4.3). Additionally, when $\alpha < 0$, $k = 0$, and $g(t) = t + 1$, the model becomes the fractional Ornstein–Uhlenbeck process [36] with mean $(\beta t + x_0)g(t)^{\alpha}$ and variance $\gamma^2 g(t)^{2\alpha} t^{2H}$ (see Section 4.4). In the specific case where $H = 1/2$, exact higher integer-order moments for similar models have already been established in [37]. These results provide a comprehensive analytical foundation for understanding the behavior of such processes under standard Brownian motion. Below, we describe a few essential definitions of fBm.

Definition 1. *A fractional Brownian motion (fBm)* $\{W_t^H, t \geq 0\}$ *of Hurst index* $H \in (0,1)$ *on* $(\Omega, \mathcal{F}, \mathbb{P})$ *is a centered Gaussian process which satisfies:*

1. $\mathbb{E}(W_t^H) = 0$ *for all* $t \geq 0$.
2. $\mathbb{E}\left((W_t^H - W_s^H)^2\right) = |t-s|^{2H}$ *for all* $s, t \geq 0$.
3. $\mathbb{E}(W_s^H W_t^H) = \dfrac{1}{2}\left(t^{2H} + s^{2H} - |t-s|^{2H}\right)$ *for all* $s, t \geq 0$.
4. $\{W_t^H, t \geq 0\}$ *has continuous sample paths* $\mathbb{P}$*-a.s.*

From condition 3, it is evident that the components of this process are independent. Moreover, conditions 1 and 3 immediately imply that $W_0^H = 0$ $\mathbb{P}$-a.s. When $H = 1/2$, fBm reduces to the standard Brownian motion. The Hurst parameter H not only determines the sign of the correlation between increments but also governs the regularity of the sample paths. In particular, for $H > 1/2$ (a long-memory process), the increments are positively correlated, while for $H < 1/2$ (a short-memory process), they are negatively correlated. It is important to note that fBm is neither a semimartingale nor a Markov process unless $H = 1/2$, which means that many of the powerful techniques available in stochastic analysis cannot be applied when dealing with fBm. Nonetheless, one can construct a stochastic calculus of variations with respect to the Gaussian process $\{W_t^H,\, t \geq 0\}$, which is closely related to Malliavin calculus [38,39]. Comprehensive surveys on this subject can be found in [33,34].

Lemma 1 (Wick–Itô formula for fBm [40])**.** *If X_t satisfies that*

$$\mathrm{d}X_t = \mu(x,t)\,dt + \sigma(t)\,\mathrm{d}W_t^H$$

where μ, σ are given functions. Furthermore, let $f \in C^2(\mathbb{R})$, and assume that $f'(X)$ and $f''(X)$ exist and are continuous for $X \in \mathbb{R}$. Then, it has

$$\mathrm{d}f(t,X_t) = \left[\frac{\partial f(t,X_t)}{\partial t} + \mu(t,X_t)\frac{\partial f(t,X_t)}{\partial x} + H\,t^{2H-1}\,\sigma^2(t)\,\frac{\partial^2 f(t,X_t)}{\partial x^2}\right]dt + \sigma(t)\,\frac{\partial f(t,X_t)}{\partial x}\,\mathrm{d}W_t^H \tag{2}$$

It is worth noting that when $H = \frac{1}{2}$ is substituted into (2)*, the classical Itô formula for standard Brownian motion is recovered.*

In this work, it is assumed that the process X_t has finite moments of all orders. More formally, for every $p > 0$, it holds that $\mathbb{E}\left(X_t^p\right) < \infty$, with the $\mathbb{E}\left(X_t^0\right) \equiv 1$. Applying Formula (2) to the process Y_t:

$$Y_t = f(t,X_t) = g^{(k)}(t)^{-\alpha}\,X_t$$

by assuming $t_0 = 0$, which results in

$$\mathrm{d}Y_t = \beta\,dt + \gamma\,\mathrm{d}W_t^H \Leftrightarrow Y_t = Y_0 + \beta\,t + \gamma\,W_t^H \tag{3}$$

consequently, the explicit solution to (1) can be readily obtained:

$$X_t = g^{(k)}(t)^{\alpha}\left(\frac{x_0}{g^{(k)}(0)^{\alpha}} + \beta\,t + \gamma\,W_t^H\right) \tag{4}$$

To compute the moments of the process X_t, we apply the expectation to both sides of (4). In this work, we assume that the Hurst index satisfies $H \in \left(\frac{1}{2}, 1\right)$.

3. Main Results

In this section, we outline the key results of our work. The first theorem establishes a method for calculating the fractional and higher integer-order moments of model (1) using Hermite polynomials. The second theorem provides a system of differential equations with a recurrence relation for calculating its moments. Additionally, we present a third theorem offering an alternative calculus using a generalized binomial expansion.

Theorem 1 (*p*th moments using Hermite polynomials without the recurrence relations)**.** *Suppose that $g(t)$ is a piecewise continuous function defined on $(-\infty, +\infty)$ and that for every $k \in \mathbb{N}$, its kth derivative satisfies $g^{(k)}(t) \neq 0$ for all $t \geq 0$. Let the parameters $\alpha, \beta \in \mathbb{R}$, $\gamma > 0$, and the Hurst index $H \in \left(\frac{1}{2}, 1\right)$. Then, for $p > 0$, the pth moment of* (1) *is given by:*

$$\mathbb{E}\left(X_t^p\right) = \begin{cases} x_0^p & \text{if } t = 0 \\ \Psi_p(H,t) \times \mathcal{H}_p\Big(\Theta(H,t)\Big) & \text{if } t > 0 \end{cases} \tag{5}$$

where the functions $\Psi_p(H,t)$ and $\Theta(H,t)$ satisfy the following expressions:

$$\Psi_p(H,t) = 2^{-\frac{p}{2}} \left(\frac{g^{(k)}(t)^{\alpha}\,\gamma}{\mathrm{i}}\right)^p t^{pH} \quad \text{and} \quad \Theta(H,t) = \frac{\mathrm{i}\sqrt{2}}{2}\left(\frac{g^{(k)}(0)^{-\alpha}\,x_0 + \beta\, t}{\gamma}\right) t^{-H}$$

where $\mathrm{i} = \sqrt{-1}$*, and $\mathcal{H}_p(x)$ represents the pth Hermite polynomial evaluated at x, defined by*

$$\mathcal{H}_p(x) = \begin{cases} (-1)^p\, \mathrm{e}^{x^2} \dfrac{\mathrm{d}^p}{\mathrm{d}x^p}\, \mathrm{e}^{-x^2} & \text{if } p \in \mathbb{N}^+ \quad (\text{Integer} - \text{order}) \\ 2^p \sqrt{\pi} \left[\dfrac{1}{\Gamma\left(\frac{1}{2} - \frac{p}{2}\right)} \mathcal{M}\left(-\frac{p}{2}, \frac{1}{2}, x^2\right) - \dfrac{2x}{\Gamma\left(-\frac{p}{2}\right)} \mathcal{M}\left(\frac{1}{2} - \frac{p}{2}, \frac{3}{2}, x^2\right) \right] & \text{if } p \in \mathbb{Q}^+ \quad (\text{Fractional} - \text{order}) \end{cases}$$

where $\mathcal{M}(a,b,z)$ is called the Kummer's function (the Kummer's function is also known as the confluent hypergeometric function of the first kind with notation ${}_1F_1(a;b;z)$.) (see [41] p. 322) and $\Gamma(x)$ is a gamma function.

Proof. From (4), the stochastic process Y_t is recognized as a fBm with a constant drift β and diffusion coefficient γ, characterized by the mean $\mu_t = y_0 + \beta\, t$ and variance $\sigma_t^2 = \gamma^2\, t^{2H}$. Hence, the conditional on $Y_0 = y_0$, Y_t is Gaussian distributed:

$$Y_t \mid Y_0 = y_0 \sim \mathcal{N}\left(y_0 + \beta\, t\ ,\ \gamma^2\, t^{2H}\right)$$

For $m > 0$, the moments of Y_t are given by Willink [42]:

$$\mathbb{E}(Y_t^m) = \begin{cases} y_0^m & \text{if } t = 0 \\ 2^{-\frac{m}{2}}\, (-\mathrm{i}\,\sigma_t)^m \mathcal{H}_m\left(\dfrac{\mu_t}{\sqrt{2}\sigma_t}\mathrm{i}\right) & \text{if } t > 0 \end{cases}$$

Then, we introduce the following change of variable:

$$\begin{aligned} y = g^{(k)}(t)^{-\alpha}\, x \Leftrightarrow x &= g^{(k)}(t)^{\alpha}\, y \\ \Leftrightarrow x^p &= \left(g^{(k)}(t)\right)^{\alpha p} y^p \quad \text{holds for all } p > 0 \end{aligned}$$

Therefore, we obtain

$$\mathbb{E}\left(X_t^p\right) = \left(g^{(k)}(t)\right)^{\alpha p} \mathbb{E}\left(Y_t^p\right)$$

Hence, by substituting the last expression into the moments of Y_t, we obtain

$$\mathbb{E}\Big(X_t^p\Big) = \begin{cases} x_0^p & \text{if } t = 0 \\ 2^{-\frac{p}{2}} \left(\dfrac{g^{(k)}(t)^{\alpha}\, \sigma_t}{\mathrm{i}} \right)^p \mathcal{H}_p\Big(\dfrac{\mu_t}{\sqrt{2}\sigma_t} \mathrm{i} \Big) & \text{if } t > 0 \end{cases}$$

by inserting the expression of μ_t and σ_t into last equation with $y_0 = g^{(k)}(0)^{-\alpha}\, x_0$, and using properties of Hermite polynomial $\mathcal{H}_p(x)$ in both cases for $p \in \mathbb{N}^+$ and $p \in \mathbb{Q}^+$. Thus, the proof is complete. □

Theorem 2 (pth moments using recursive differential equations)**.** *For all $t \geq 0$ and $p > 0$, the pth moments of* (1) *satisfy the recursive differential equations:*

$$\begin{cases} \dfrac{d}{dt}\mathbb{E}\Big(X_t^p\Big) = a_p(t)\, \mathbb{E}\Big(X_t^p\Big) + b_p(t)\, \mathbb{E}\Big(X_t^{p-1}\Big) + c_p(H,t)\, \mathbb{E}\Big(X_t^{p-2}\Big) \\ \quad \mathbb{E}\Big(X_0^p\Big) = x_0^p \end{cases} \tag{6}$$

where $a_p(t)$, $b_p(t)$ and $c_p(H,t)$ satisfy the following expressions:

$$a_p(t) = \alpha\, p\, \frac{g^{(k+1)}(t)}{g^{(k)}(t)}, b_p(t) = \beta\, p \left(g^{(k)}(t)\right)^{\alpha} \text{and } c_p(H,t) = \gamma^2\, p\, (p-1) \left(g^{(k)}(t)\right)^{2\alpha} H\, t^{2H-1},$$

where the general solution of (6) *is expressed by the following recurrence relation:*

$$\begin{aligned} \mathbb{E}\Big(X_t^p\Big) = \Bigg[p \int_0^t \Bigg[\beta \left(g^{(k)}(s)\right)^{-\alpha\,(p-1)} \mathbb{E}\Big(X_s^{p-1}\Big) + \gamma^2\, (p-1) \left(g^{(k)}(s)\right)^{-\alpha\,(p-2)} H\, s^{2H-1}\, \mathbb{E}\Big(X_s^{p-2}\Big) \Bigg] ds \\ + x_0^p \Big(g^{(k)}(0)\Big)^{-\alpha\, p} \Bigg] \times \Big(g^{(k)}(t)\Big)^{\alpha\, p} \end{aligned} \tag{7}$$

with $\mathbb{E}(X_t^0) \equiv 1$ and $\mathbb{E}\Big(X_t^{-p}\Big) \equiv 0$.

Proof. We consider the change of variable $f(t,x) = x^p$, and by applying the Formula (2), the corresponding SDE are obtained

$$\begin{aligned} dX_t^p = p \left(\alpha\, \frac{g^{(k+1)}(t)}{g^{(k)}(t)}\, X_t^p + \beta\, g^{(k)}(t)^{\alpha}\, X_t^{p-1} + (p-1)\, \gamma^2\, H\, t^{2H-1}\, g^{(k)}(t)^{2\alpha}\, X_t^{p-2} \right) dt \\ + p\gamma\, g^{(k)}(t)^{\alpha}\, X_t^{p-1}\, dW_t^H \end{aligned}$$

The preceding equation may be rewritten in its integral form as

$$\begin{aligned} X_t^p = X_0^p + p \int_0^t \left[\alpha\, \frac{g^{(k+1)}(s)}{g^{(k)}(s)}\, X_s^p + \beta\, g^{(k)}(s)^{\alpha}\, X_s^{p-1} + (p-1)\, \gamma^2\, H\, s^{2H-1}\, g^{(k)}(s)^{2\alpha}\, X_s^{p-2} \right] ds \\ + p\,\gamma \int_0^t g^{(k)}(s)^{\alpha}\, X_s^{p-1}\, dW_s^H \end{aligned}$$

By applying the expectation to both sides of the previous equation and leveraging the properties of stochastic integrals, we derive

$$\mathbb{E}\Big(X_t^p\Big) = \mathbb{E}\Big(X_0^p\Big) + p\,\mathbb{E}\left(\int_0^t \left[\alpha\,\frac{g^{(k+1)}(s)}{g^{(k)}(s)}\,X_s^p + \beta\,g^{(k)}(s)^{\alpha}\,X_s^{p-1} + (p-1)\,\gamma^2\,H\,s^{2H-1}\,g^{(k)}(s)^{2\alpha}\,X_s^{p-2}\right] ds\right)$$
$$+ p\,\gamma\,\underbrace{\mathbb{E}\left(\int_0^t g^{(k)}(s)^{\alpha}\,X_s^{p-1}\,dW_s^H\right)}_{0}$$
$$= X_0^p + p\int_0^t \left[\alpha\,\frac{g^{(k+1)}(s)}{g^{(k)}(s)}\,\mathbb{E}\Big(X_s^p\Big) + \beta\,g^{(k)}(s)^{\alpha}\,\mathbb{E}\Big(X_s^{p-1}\Big) + (p-1)\,\gamma^2\,H\,s^{2H-1}\,g^{(k)}(s)^{2\alpha}\,\mathbb{E}\Big(X_s^{p-2}\Big)\right] ds$$

Subsequently, by differentiating with respect to t on both sides, one obtains the recurrence relation corresponding to the differential equation

$$\frac{d}{dt}\mathbb{E}\Big(X_t^p\Big) = \underbrace{\alpha\,p\,\frac{g^{(k+1)}(t)}{g^{(k)}(t)}}_{a_p(t)}\,\mathbb{E}\Big(X_t^p\Big) + \underbrace{\beta\,p\,g^{(k)}(t)^{\alpha}}_{b_p(t)}\,\mathbb{E}\Big(X_t^{p-1}\Big) + \underbrace{\gamma^2\,p\,(p-1)\,g^{(k)}(t)^{2\alpha}\,H\,t^{2H-1}}_{c_p(H,t)}\,\mathbb{E}\Big(X_t^{p-2}\Big)$$

where we set $a_0(t) \equiv 0$, $b_0(t) \equiv 0$ and $c_0(H,t) \equiv 0$.

If $p = 1$, the terms $\mathbb{E}\Big(X_t^{p-1}\Big)$ and $\mathbb{E}\Big(X_t^{p-2}\Big)$ vanish because $p-1 < 0$ and $p-2 < 0$. Hence, the recurrence simplifies to

$$\frac{d}{dt}\mathbb{E}(X_t) = a_1(t)\mathbb{E}(X_t)$$

this is a first-order linear differential equation, and its solution can be obtained by integrating:

$$\mathbb{E}(X_t) = x_0 \exp\left(\int_0^t a_1(s)ds\right)$$

substituting the expression for $a_1(t)$, we get:

$$\mathbb{E}(X_t) = x_0 \exp\left(\alpha\int_0^t \frac{g^{(k+1)}(s)}{g^{(k)}(s)}ds\right) = x_0\left(\frac{g^{(k)}(t)}{g^{(k)}(0)}\right)^{\alpha}.$$

□

Lemma 2. *The moments* $\mathbb{E}\Big(X_t^p\Big)$ *defined by* (5) *satisfy the recursive differential Equation* (6)*, i.e., expression* (5) *is a solution of* (6)*.*

Proof. We differentiate expression (5) with respect to t by the product rule,

$$\frac{d}{dt}\mathbb{E}\Big(X_t^p\Big) = \frac{d}{dt}\Big[x_0^p + \Psi_p(H,t)\,\mathcal{H}_p\big(\Theta(H,t)\big)\Big] = \mathcal{H}_p\big(\Theta(H,t)\big)\,\frac{d}{dt}\Psi_p(H,t) + \Psi_p(H,t)\,\frac{d}{dt}\mathcal{H}_p\big(\Theta(H,t)\big). \tag{8}$$

Since $\mathcal{H}_p(\cdot)$ is a function of $\Theta(H,t)$, the chain rule yields

$$\frac{d}{dt}\mathcal{H}_p\big(\Theta(H,t)\big) = \mathcal{H}_p'\big(\Theta(H,t)\big)\,\frac{d}{dt}\Theta(H,t),$$

by the classical derivative property of Hermite polynomials,

$$\mathcal{H}_p'(x) = 2p\,\mathcal{H}_{p-1}(x),$$

so that

$$\frac{d}{dt}\mathcal{H}_p\big(\Theta(H,t)\big) = 2p\,\mathcal{H}_{p-1}\big(\Theta(H,t)\big)\,\frac{d}{dt}\Theta(H,t),$$

thus,

$$(8) \Leftrightarrow \frac{d}{dt}\mathbb{E}\Big(X_t^p\Big) = \underbrace{\mathcal{H}_p\big(\Theta(H,t)\big)\,\frac{d}{dt}\Psi_p(H,t)}_{\text{Term 1}} + \underbrace{2p\,\Psi_p(H,t)\,\mathcal{H}_{p-1}\big(\Theta(H,t)\big)\,\frac{d}{dt}\Theta(H,t)}_{\text{Term 2}}, \quad (9)$$

we now compute the derivatives of $\Psi_p(H,t)$ and $\Theta(H,t)$. First, from the definition of the functions $\Psi_p(H,t)$ and $\Theta(H,t)$ given by Theorem 1, we obtain

$$\frac{d}{dt}\Psi_p(H,t) = \Psi_p(H,t)\left[\alpha p\,\frac{g^{(k+1)}(t)}{g^{(k)}(t)} + p\,\frac{H}{t}\right],$$

and,

$$\frac{d}{dt}\Theta(H,t) = \frac{\mathrm{i}\sqrt{2}}{2}\frac{\beta}{\gamma}t^{-H} - \frac{H}{t}\,\Theta(H,t),$$

by substituting the last expressions into Equation (9), we obtain

$$\text{Term 1} = \Psi_p(H,t)\left[\alpha p\,\frac{g^{(k+1)}(t)}{g^{(k)}(t)} + p\,\frac{H}{t}\right]\mathcal{H}_p\big(\Theta(H,t)\big),$$

since, by definition, we have $\mathbb{E}\Big(X_t^p\Big) = \Psi_p(H,t)\,\mathcal{H}_p\Big(\Theta(H,t)\Big)$, the first term can be written as

$$\text{Term 1} = \alpha p\,\frac{g^{(k+1)}(t)}{g^{(k)}(t)}\mathbb{E}\Big(X_t^p\Big) + p\,\frac{H}{t}\Psi_p(H,t)\,\mathcal{H}_p\Big(\Theta(H,t)\Big)$$

however, we now use the classical recurrence relation for Hermite polynomials

$$\mathcal{H}_p(x) = 2x\,\mathcal{H}_{p-1}(x) - 2(p-1)\,\mathcal{H}_{p-2}(x)$$

Taking $x = \Theta(H,t)$, we can express

$$\mathcal{H}_p\Big(\Theta(H,t)\Big) = 2\,\Theta(H,t)\,\mathcal{H}_{p-1}\Big(\Theta(H,t)\Big) - 2(p-1)\,\mathcal{H}_{p-2}\Big(\Theta(H,t)\Big)$$

Thus, the Term 1 becomes

$$\text{Term 1} = \alpha p\,\frac{g^{(k+1)}(t)}{g^{(k)}(t)}\mathbb{E}\Big(X_t^p\Big) + p\,\frac{H}{t}\Psi_p(H,t)\Big[2\,\Theta(H,t)\,\mathcal{H}_{p-1}\Big(\Theta(H,t)\Big) - 2(p-1)\,\mathcal{H}_{p-2}\Big(\Theta(H,t)\Big)\Big] \quad (10)$$

and Term 2 can be written as

$$\text{Term 2} = 2p\,\Psi_p(H,t)\,\mathcal{H}_{p-1}\Big(\Theta(H,t)\Big)\left[\frac{\mathrm{i}\sqrt{2}}{2}\frac{\beta}{\gamma}t^{-H} - \frac{H}{t}\,\Theta(H,t)\right] \quad (11)$$

by adding the two simplified terms (10) and (11), we obtain

$$\begin{aligned}\frac{d}{dt}\mathbb{E}\Big(X_t^p\Big) &= \text{Term 1} + \text{Term 2}\\ &= \alpha p\,\frac{g^{(k+1)}(t)}{g^{(k)}(t)}\mathbb{E}\Big(X_t^p\Big) + \mathrm{i}\sqrt{2}\,p\,\frac{\beta}{\gamma}t^{-H}\,\Psi_p(H,t)\,\mathcal{H}_{p-1}\Big(\Theta(H,t)\Big) - 2p(p-1)\frac{H}{t}\,\Psi_p(H,t)\,\mathcal{H}_{p-2}\Big(\Theta(H,t)\Big) \quad (12)\end{aligned}$$

Furthermore, by considering the ratio

$$\mathrm{R}(H,t) = \frac{\Psi_p(H,t)}{\Psi_{p-1}(H,t)} = \frac{1}{\sqrt{2}}\Big(\frac{\gamma}{\mathrm{i}}\Big)\,g^{(k)}(t)^{\alpha}\,t^{H},$$

then,

$$\Psi_p(H,t)\,\mathcal{H}_{p-1}\Big(\Theta(H,t)\Big) = \mathrm{R}(H,t)\,\mathbb{E}\Big(X_t^{p-1}\Big) \tag{13}$$

and, analogously,

$$\Psi_p(H,t)\,\mathcal{H}_{p-2}\Big(\Theta(H,t)\Big) = \mathrm{R}(H,t)^2\,\mathbb{E}\Big(X_t^{p-2}\Big) \tag{14}$$

by substituting the expressions (13) and (14) into Equation (12), we obtain the final recursive form

$$\begin{aligned}(8) \Leftrightarrow \frac{d}{dt}\mathbb{E}\Big(X_t^p\Big) &= \alpha p\,\frac{g^{(k+1)}(t)}{g^{(k)}(t)}\mathbb{E}\Big(X_t^p\Big) + \mathrm{i}\sqrt{2}\,p\,\frac{\beta}{\gamma}t^{-H}\,\mathrm{R}(H,t)\,\mathbb{E}\Big(X_t^{p-1}\Big) - 2p(p-1)\frac{H}{t}\,\mathrm{R}(H,t)^2\,\mathbb{E}\Big(X_t^{p-2}\Big)\\ &= \underbrace{\alpha\,p\,\frac{g^{(k+1)}(t)}{g^{(k)}(t)}}_{a_p(t)}\,\mathbb{E}\Big(X_t^p\Big) + \underbrace{\beta\,p\,g^{(k)}(t)^{\alpha}}_{b_p(t)}\,\mathbb{E}\Big(X_t^{p-1}\Big) + \underbrace{\gamma^2\,p\,(p-1)\,g^{(k)}(t)^{2\alpha}\,H\,t^{2H-1}}_{c_p(H,t)}\,\mathbb{E}\Big(X_t^{p-2}\Big)\end{aligned}$$

thus, the proof is complete. □

Remark 1. *Theorem 1 establishes an explicit formula for both the fractional and higher integer-order moments of* (1) *using Hermite polynomials, thereby eliminating the need for recurrence relations. Alternatively, Theorem 2 expresses these moments explicitly through recurrence relations, allowing them to be computed with ease. However, in situations where additional constraints are imposed or the previous theorems become difficult to apply, we present in the following theorem an alternative formula for a simpler computation of the pth moment of* (1).

Theorem 3 (*p*th moments using a generalized binomial expansion)**.** *Let the conditions of Theorem 1 be valid; the pth moments of* (1) *are given by*

$$\mathbb{E}\Big(X_t^p\Big) = \frac{\Big[g^{(k)}(t)^{\alpha}\,\mu_t\Big]^p}{2\sqrt{\pi}}\sum_{j=0}^{\lfloor p\rfloor}\binom{p}{j}\Big(1+(-1)^j\Big)\Gamma\Big(\frac{1+j}{2}\Big)\left(\frac{\sqrt{2}\sigma_t}{\mu_t}\right)^j \tag{15}$$

where $\lfloor x\rfloor$ *denotes the greatest integer not greater than* x*, and* μ_t*,* σ_t *are given by*

$$\mu_t = \Big(g^{(k)}(0)^{-\alpha}\,x_0 + \beta\,t\Big) \quad \textit{and} \quad \sigma_t = \gamma\,t^H$$

Proof. From (4), and for all $p > 0$, we have

$$X_t^p = g^{(k)}(t)^{\alpha p}\Big(g^{(k)}(0)^{-\alpha}\,x_0 + \beta\,t + \gamma\,W_t^H\Big)^p$$

we rewrite X_t^p by the generalized binomial expansion for any real exponent $p > 0$

$$X_t^p = g^{(k)}(t)^{\alpha p}\sum_{j=0}^{\infty}\binom{p}{j}\Big(g^{(k)}(0)^{-\alpha}\,x_0 + \beta\,t\Big)^{p-j}\Big(\gamma\,W_t^H\Big)^j$$

where the generalized binomial coefficient is defined as

$$\binom{p}{j} = \frac{p(p-1)\cdots(p-j+1)}{j!} \quad \text{for } j \geq 1,\ \binom{p}{0} = 1.$$

By applying the expectation to both sides of the last equation, we obtain

$$\mathbb{E}\left(X_t^p\right) = \mathbb{E}\left(g^{(k)}(t)^{\alpha p}\sum_{j=0}^{\infty}\binom{p}{j}\left(g^{(k)}(0)^{-\alpha}x_0+\beta\,t\right)^{p-j}\left(\gamma\,W_t^H\right)^j\right)$$
$$= \left[g^{(k)}(t)^{\alpha}\left(g^{(k)}(0)^{-\alpha}x_0+\beta\,t\right)\right]^p\sum_{j=0}^{\infty}\binom{p}{j}\left(\frac{\gamma}{g^{(k)}(0)^{-\alpha}x_0+\beta\,t}\right)^j\mathbb{E}\left[\left(W_t^H\right)^j\right]$$

However, since fBm W_t^H is a centered Gaussian process, its odd moments vanish. Therefore, when taking the expectation, only even powers contribute. In our final expression, we effectively sum over the indices up to $j=\lfloor p\rfloor$, which provides the proper truncation by analytic continuation. Then, the known moments of fBm W_t^H are given by

$$\mathbb{E}\left[\left(W_t^H\right)^j\right] = \frac{2^{-1+\frac{j}{2}}}{\sqrt{\pi}}\left(1+(-1)^j\right)\Gamma\left(\frac{1+j}{2}\right)t^{jH}$$

Hence, we define $\mu_t = \left(g^{(k)}(0)^{-\alpha}x_0+\beta\,t\right)$ and $\sigma_t = \gamma\,t^H$, and by substituting these expressions into $\mathbb{E}\left(X_t^p\right)$, we obtain

$$\mathbb{E}\left(X_t^p\right) = \frac{\left[g^{(k)}(t)^{\alpha}\left(g^{(k)}(0)^{-\alpha}x_0+\beta\,t\right)\right]^p}{2\sqrt{\pi}}\sum_{j=0}^{\lfloor p\rfloor}\binom{p}{j}\left(1+(-1)^j\right)\Gamma\left(\frac{1+j}{2}\right)\left(\frac{\sqrt{2}\,\gamma\,t^H}{g^{(k)}(0)^{-\alpha}x_0+\beta\,t}\right)^j$$
$$= \frac{\left[g^{(k)}(t)^{\alpha}\,\mu_t\right]^p}{2\sqrt{\pi}}\sum_{j=0}^{\lfloor p\rfloor}\binom{p}{j}\left(1+(-1)^j\right)\Gamma\left(\frac{1+j}{2}\right)\left(\frac{\sqrt{2}\sigma_t}{\mu_t}\right)^j$$

Therefore, the last equation holds for all $p>0$. □

Corollary 1. *Under the assumptions of Theorem 1. Let*

$$Y_t \mid Y_0 = y_0 \sim \mathcal{N}\left(\underbrace{y_0+\beta\,t}_{\mu_t},\ \underbrace{\gamma^2\,t^{2H}}_{\sigma_t^2}\right)$$

and assume that X_t and Y_t are related by $x = g^{(k)}(t)^{\alpha}\,y$. Then, by employing the moment-generating function (MGF) of Y_t together with the generalized binomial expansion, one obtains that the pth moment of X_t as given in (15) *of Theorem 3.*

Proof. Recall that the moment-generating function (MGF) for a normally distributed variable $Y\sim\mathcal{N}(\mu,\sigma^2)$ is given by:

$$\mathrm{M}_Y(u) = \mathbb{E}\left(e^{uY}\right) = \exp\left(\mu\,u+\frac{\sigma^2}{2}\,u^2\right)$$

In principle, the pth moment can be computed by differentiating

$$\mathbb{E}(Y^p) = \left.\frac{d^p}{du^p}\mathrm{M}_Y(u)\right|_{u=0}$$

However, for non-integer p, this method is not directly applicable. Instead, we use an expansion based on the generalized binomial theorem. Write $Y_t = \mu_t + (Y_t - \mu_t)$. Then, by the generalized binomial expansion (which holds for any real exponent $p > 0$), we have

$$Y_t^p = \Big(\mu_t + (Y_t - \mu_t)\Big)^p = \sum_{j=0}^{\infty} \binom{p}{j} \mu_t^{p-j} (Y_t - \mu_t)^j, \tag{16}$$

Since $Y_t - \mu_t$ is a centered Gaussian process (i.e., $Y_t - \mu_t \sim \mathcal{N}(0, \sigma_t^2)$), all its odd moments vanish

$$\mathbb{E}\Big[(Y_t - \mu_t)^j\Big] = 0 \quad \text{for } j \text{ odd}$$

for even j, say $j = 2k$, we have (see [43])

$$\mathbb{E}\Big[(Y_t - \mu_t)^{2k}\Big] = \sigma_t^{2k}\,(2k-1)!! \qquad \text{where} \quad z!! = \sqrt{\frac{2^{z+1}}{\pi}}\,\Gamma\Big(\frac{z}{2}+1\Big) \tag{17}$$

note that by introducing the factor

$$1 + (-1)^j = \begin{cases} 2, & \text{if } j \text{ is even,} \\ 0, & \text{if } j \text{ is odd,} \end{cases}$$

we can write the moment as a sum over j (from 0 to $\lfloor p \rfloor$, where $\lfloor p \rfloor$ denotes the greatest integer less than or equal to p), and taking the expectation in (16), we have

$$\mathbb{E}\Big(Y_t^p\Big) = \frac{1}{2}\sum_{j=0}^{\lfloor p \rfloor} \binom{p}{j} \Big(1 + (-1)^j\Big)\, \mu_t^{p-j}\, \mathbb{E}\Big[(Y_t - \mu_t)^j\Big] \tag{18}$$

For even j, writing $j = 2k$, we replace the moment (17) by its expression

$$\mathbb{E}\Big[(Y_t - \mu_t)^j\Big] = \frac{\Big(\sqrt{2}\,\sigma_t\Big)^j}{\sqrt{\pi}}\,\Gamma\Big(\frac{1+j}{2}\Big) \tag{19}$$

by substituting expression (19) into Equation (18), we obtain

$$\mathbb{E}\Big(Y_t^p\Big) = \frac{1}{2\sqrt{\pi}}\sum_{j=0}^{\lfloor p \rfloor} \binom{p}{j} \Big(1 + (-1)^j\Big)\, \mu_t^{p-j}\, \Big(\sqrt{2}\,\sigma_t\Big)^j\, \Gamma\Big(\frac{1+j}{2}\Big). \tag{20}$$

Recalling that

$$\mathbb{E}\Big(X_t^p\Big) = \Big(g^{(k)}(t)\Big)^{\alpha p}\, \mathbb{E}\Big(Y_t^p\Big)$$

we substitute expression (20) in the last equation. Thus, we arrive at the final expression:

$$\mathbb{E}\Big(X_t^p\Big) = \frac{\Big[\big(g^{(k)}(t)\big)^{\alpha}\, \mu_t\Big]^p}{2\sqrt{\pi}} \sum_{j=0}^{\lfloor p \rfloor} \binom{p}{j} \Big(1 + (-1)^j\Big)\, \Gamma\Big(\frac{1+j}{2}\Big) \left(\frac{\sqrt{2}\,\sigma_t}{\mu_t}\right)^j$$

This is precisely the closed-form expression given in Theorem 3. □

4. Numerical Simulation

In this section, we carry out a numerical experiment to evaluate the fractional and higher integer-order moments of the model (1). The exact moments, as derived earlier,

are computed and then compared against the simulation outcomes obtained via a Monte Carlo approach. For this purpose, we use the R [44] packages Sim.DiffProc [45] and yumia [46,47] to simulate the solution of (1) numerically. Recent numerical studies have addressed the challenges associated with solving fractional differential equations driven by stochastic processes, highlighting significant computational considerations (see [48]). The R code used to perform these simulations is available as Supplementary Materials at https://github.com/acguidoum-git/supplementary_material. In all examples in this section, we simulate 100,000 sample paths over the interval $t \in [0, T]$ and compute the approximate pth moment, denoted by $m_p(t)$, which covers both fractional and higher integer orders. Subsequently, the formulas from Theorems 1 and 3 are used to determine the exact moments, $\mathbb{E}\left(X_t^p\right)$. In the last example, explicit expressions for the fractional moments of the fractional Ornstein–Uhlenbeck process are presented. To facilitate a direct numerical comparison, the moments are scaled to a common basis. The scaled pth moment, $M_p(t)$, is defined as

$$M_p(t) \triangleq \sqrt[p]{m_p(t)} = \sqrt[p]{\mathbb{E}\left(X_t^p\right)}$$

4.1. Linear Time-Dependent Function

As a numerical example for evaluating both fractional and higher integer-order moments, we examine the following process. For this example, the parameters are set as

$$\alpha = -\frac{1}{2}, \quad \beta = 14, \quad \gamma = 6, \quad g(t) = 2t + 1, \quad \text{and} \quad k = 0,$$

where

$$g^{(0)}(t) = 2t + 1 \neq 0 \quad \text{for all } t \geq 0.$$

We then consider the following fractional SDE

$$\begin{cases} \mathrm{d}X_t = \left(-\dfrac{1}{2t+1}\, X_t + \dfrac{14}{\sqrt{2t+1}}\right) dt + \dfrac{6}{\sqrt{2t+1}}\, \mathrm{d}W_t^H \\ X_0 = 30,\ t \in [0, 5] \end{cases} \tag{21}$$

from (5), it is known that for all $p \geq 0$, the p^{th} moments of the solution to (21) are given by

$$\mathbb{E}\left(X_t^p\right) = \begin{cases} 30^p & \text{if } t = 0 \\ 2^{-\frac{p}{2}} \left(-6\mathrm{i}\sqrt{\dfrac{t^{2H}}{2t+1}}\right)^p \mathcal{H}_p\left(\dfrac{\mathrm{i}\sqrt{2}(7t+15)}{6\, t^H}\right) & \text{if } t > 0 \end{cases}$$

In Figure 1, we display a visual comparison between the moments obtained via the Monte Carlo simulation $m_p(t)$ (represented by continuous lines) and the exact values $\mathbb{E}\left(X_t^p\right)$ (represented by dashed lines). This comparison covers both fractional and higher integer-order moments, with orders p chosen from the set $\left\{\frac{l}{2} : l = 1, \ldots, 10\right\}$, over the time interval $t \in [0, 5]$.

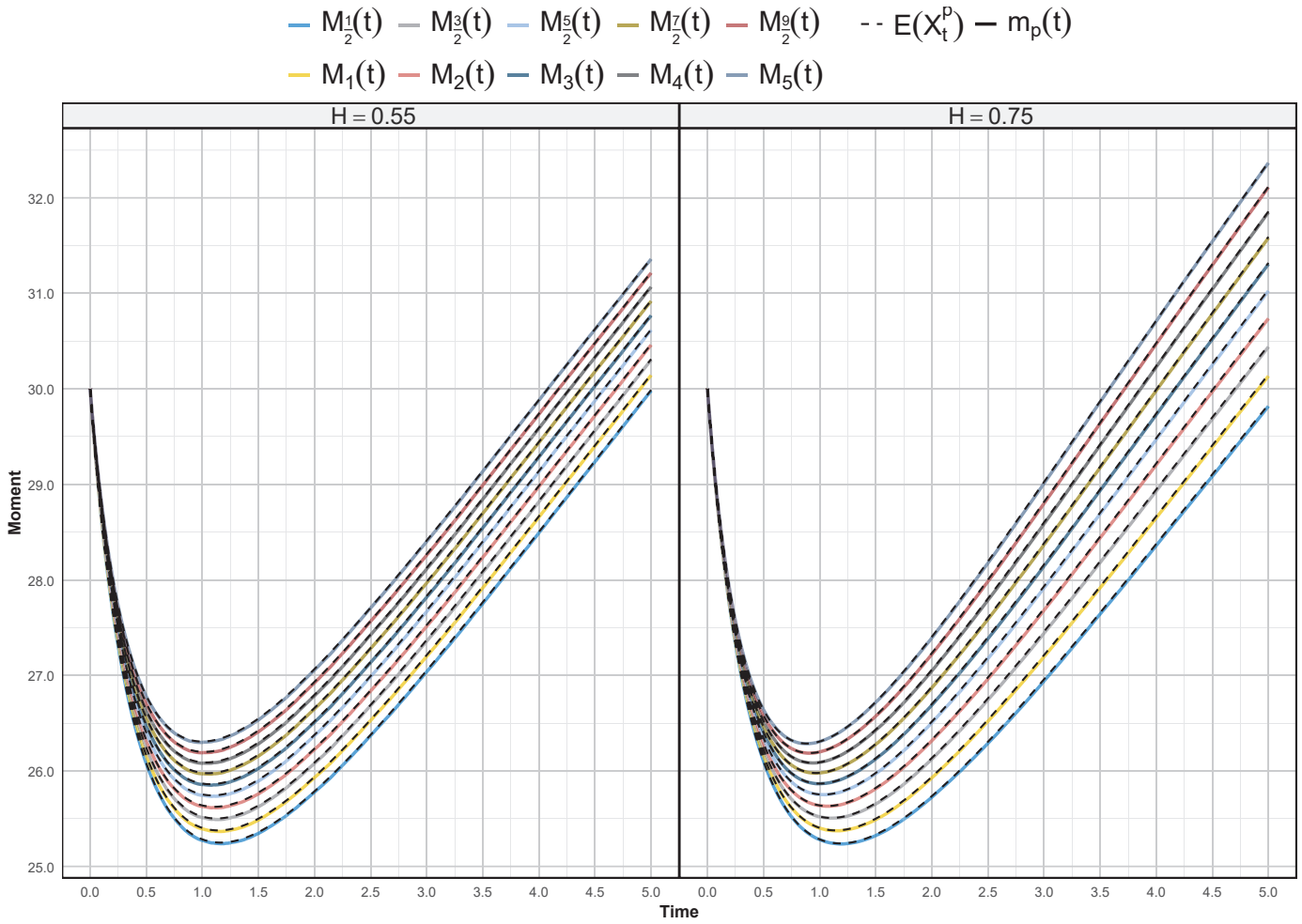

Figure 1. The pth approximate $m_p(t)$ and exact moments $\mathbb{E}\left(X_t^p\right)$ of (21), where $p = \left\{\frac{l}{2} : l = 1, \ldots, 10\right\}$. (**Left**): Hurst index $H = 0.55$. (**Right**): $H = 0.75$.

4.2. Non-Linear Time-Dependent Function

In this example, we are interested only in fractional moments. Consider a more complex fractional SDE

$$g(t) = \cos(t + \pi) \quad \text{and} \quad k = 4, \text{ where } g^{(4)}(t) = \cos(t + \pi)$$

and with the parameters $\alpha = \beta = \gamma = 2$. Hence, the model under consideration is

$$\begin{cases} \mathrm{d}X_t = -2\big(\tan(t+\pi)X_t - \cos^2(t+\pi)\big)\,dt + 2\cos^2(t+\pi)\,\mathrm{d}W_t^H \\ X_0 = 20,\ t \in [0, 10] \end{cases} \tag{22}$$

Following Equation (15), for all $p \geq 0$, the moments of the solution to (22) are given by

$$\mathbb{E}\left(X_t^p\right) = \frac{\left(\cos^2(t+\pi)(20+2t)\right)^p}{2\sqrt{\pi}} \sum_{j=0}^{\lfloor p \rfloor} \binom{p}{j} \left(1 + (-1)^j\right) \Gamma\left(\frac{1+j}{2}\right) \left(\frac{\sqrt{2}}{10+t}\right)^j t^{jH}$$

Figure 2 presents the Monte Carlo simulation results, computed using (15), for the fractional moments corresponding to $p = \left\{\frac{1}{6}, \frac{22}{5}, \frac{67}{7}, \frac{78}{5}, \frac{93}{4}\right\}$; over the time interval $t \in [0, 10]$. Notice that the same results are obtained when using Formula (5).

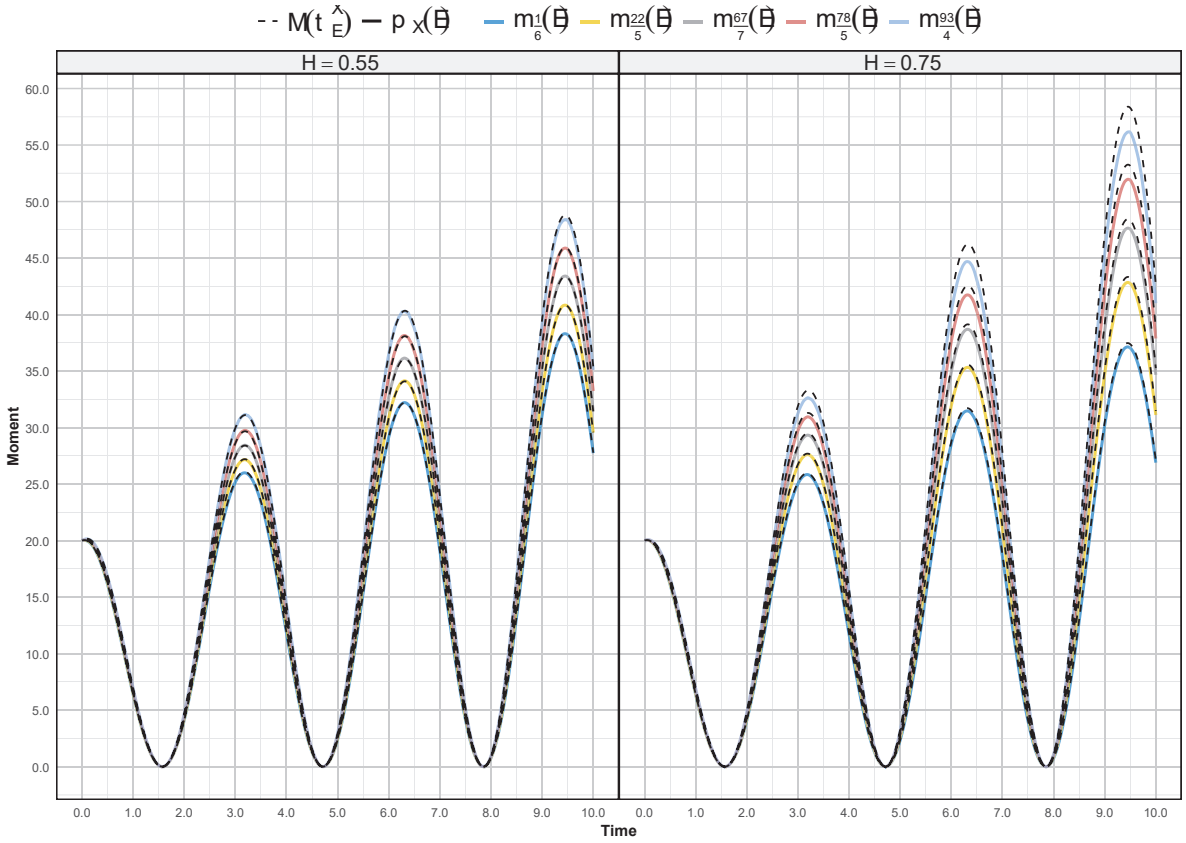

Figure 2. The pth approximate $m_p(t)$ and exact moments $\mathbb{E}\left(X_t^p\right)$ of (22), where $p = \left\{\frac{1}{6}, \frac{22}{5}, \frac{67}{7}, \frac{78}{5}, \frac{93}{4}\right\}$. (**Left**): Hurst index $H = 0.55$. (**Right**): $H = 0.75$.

4.3. Fractional Brownian Bridge Process

In this example, we consider the parameters $\alpha = -1$, $\beta = 0$, $\gamma = 1$ and the function $g(t)$ is defined by

$$g^{(k)}(t) = \begin{cases} \ln(t-20) & \text{if } k = 0 \\ (-1)^{k-1} \dfrac{\Gamma(k)}{(t-20)^k} & \text{if } k = 1, 2, 3, \ldots \end{cases}$$

for any $k \in \mathbb{N}^+$, we obtain fractional Brownian bridge process

$$\begin{cases} \mathrm{d}X_t = \dfrac{k}{t-20} X_t \, dt + \dfrac{(t-20)^k}{(-1)^{k-1}\,\Gamma(k)} \, \mathrm{d}W_t^H \\ X_0 = 10, \; t \in [0, 20] \end{cases} \tag{23}$$

From (5), for every $p > 0$, the exact moments of (23) are given by

$$\mathbb{E}\left(X_t^p\right) = \begin{cases} 10^p & \text{if } t = 0 \\ 2^{-\frac{p}{2}} \left(\dfrac{-\mathrm{i}(t-20)^k \, t^H}{(-1)^{k-1}\,\Gamma(k)} \right)^p \mathcal{H}_p\left(\dfrac{10\,\mathrm{i}(-1)^{k-1}\,\Gamma(k)}{\sqrt{2}\,(-20)^k \, t^H} \right) & \text{if } t > 0 \end{cases}$$

As illustrated in Figure 3, the continuous lines exhibit rough and irregular behavior due to approximation errors in the simulated sample paths, whereas the dashed lines form smooth curves since they represent the exact high integer-order moment values. By computing the moments up to a sufficiently high order, we can gain insights into the statistical properties of (23), such as its mean, variance, skewness, and kurtosis. To illustrate, using the last

expression for $p = \{1, 2, 3, 4\}$ and $k \in \mathbb{N}^+$, we explicitly obtain the first, second, third, and fourth moments.

$$\begin{aligned}
\mathbb{E}(X_t) &= 10(-1)^{-k}\left(-1+\frac{t}{20}\right)^k \\
\mathbb{E}\left(X_t^2\right) &= (-1)^{-2k}\left(-1+\frac{t}{20}\right)^{2k}\left(100+\frac{20^{2k}}{\Gamma(k)^2}\times t^{2H}\right) \\
\mathbb{E}\left(X_t^3\right) &= 10(-1)^{-3k}\left(-1+\frac{t}{20}\right)^{3k}\left(100+3\times\frac{20^{2k}}{\Gamma(k)^2}\times t^{2H}\right) \\
\mathbb{E}\left(X_t^4\right) &= (-1)^{-4k}\left(-1+\frac{t}{20}\right)^{4k}\left(10000+600\times\frac{20^{2k}}{\Gamma(k)^2}\times t^{2H}+3\times\frac{20^{4k}}{\Gamma(k)^4}\times t^{4H}\right)
\end{aligned}$$

These explicit expressions not only enable us to calculate the higher-order moments directly but also allow us to derive the variance in an analytical manner. In particular, the variance, defined as $\mathbb{V}\mathrm{ar}(X_t) = \mathbb{E}(X_t^2) - [\mathbb{E}(X_t)]^2$, can be determined directly from the first and second moments.

$$\mathbb{V}\mathrm{ar}(X_t) = \frac{(-1)^{-2k}}{\Gamma(k)^2}\,(-20+t)^{2k}\,t^{2H}$$

This analytic form provides precise insights into the central tendency and dispersion of the process, thereby facilitating a rigorous assessment of its distributional characteristics. Moreover, with the availability of closed-form expressions for the moments, one can readily analyze the impact of long-range dependence and other parameters on the overall behavior of the stochastic process, further enhancing both theoretical understanding and practical applications.

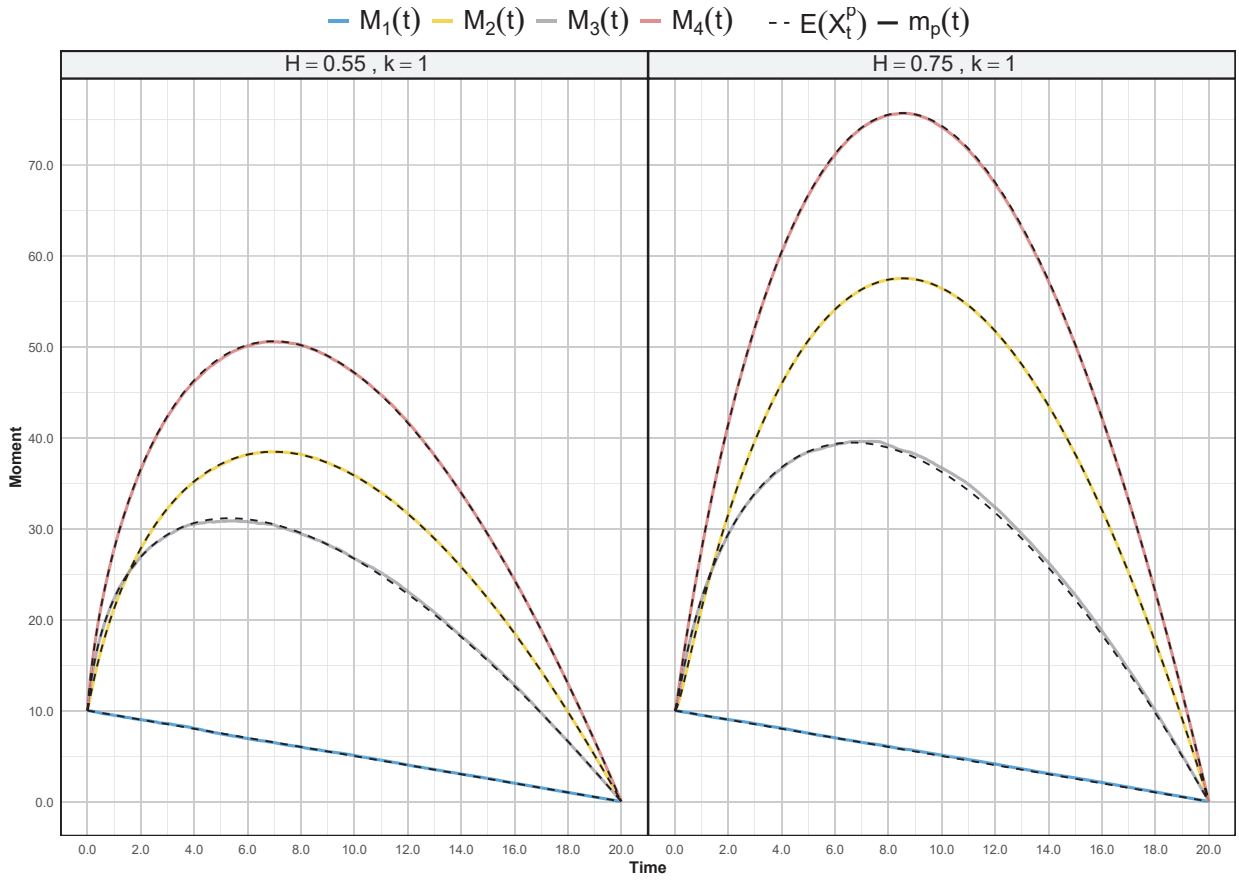

Figure 3. *Cont.*

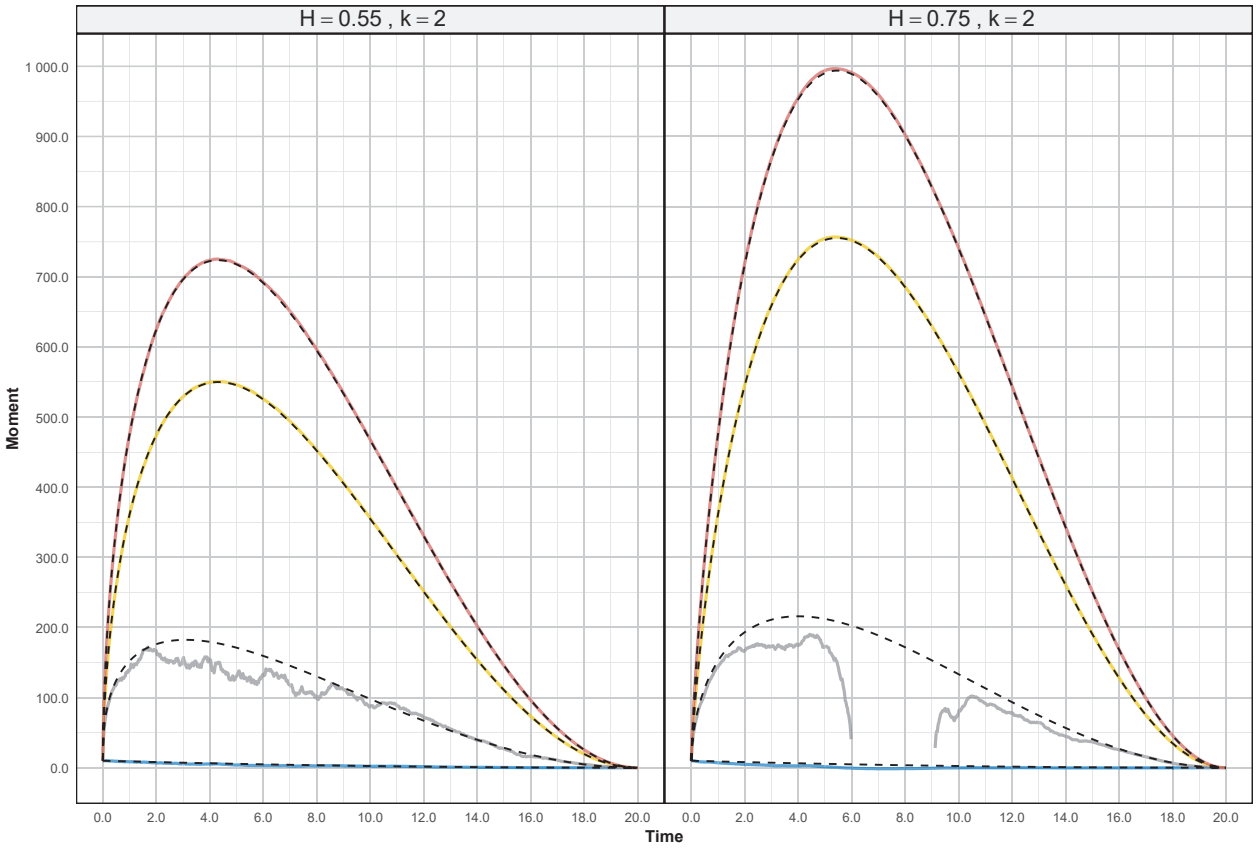

Figure 3. The 1st–4th approximate $m_p(t)$ and exact moments $\mathbb{E}\left(X_t^p\right)$ of (23) where top $k = 1$ and bottom $k = 2$. (**Left**): Hurst index $H = 0.55$. (**Right**): $H = 0.75$.

4.4. Fractional Ornstein–Uhlenbeck Process

Let us consider a particle moving in a viscoelastic medium (e.g., a polymer gel or cellular cytoplasm). The medium's mechanical memory leads to anomalous diffusion, which can be modeled by a SDE with fractional Brownian motion (fBm). The model captures both the time-dependent friction and the long-term memory ($H > 1/2$). We use Equation (1) with the following parameters:

- Function: $g(t) = t + 1$, with $k = 0 \;\Rightarrow\; g^{(0)}(t) = t + 1$.
- Parameters: $\alpha = -2$ (mean reversion), $\beta = 0$ (no external drift), $\gamma = 1$ (volatility), $H = 0.55$ (long memory).

$$\begin{cases} \mathrm{d}X_t = -\dfrac{2}{t+1} X_t \, dt + \dfrac{1}{(t+1)^2} \, \mathrm{d}W_t^H \\ X_0 = 10, \; t \in [0,5] \end{cases} \tag{24}$$

from (5), for all $p \geq 0$, the pth moments of (24) are given by

$$\mathbb{E}\left(X_t^p\right) = \begin{cases} 10^p & \text{if } t = 0 \\ 2^{-\frac{p}{2}} \left(-\mathrm{i} \sqrt{\dfrac{t^{2H}}{(t+1)^4}} \right)^p \mathcal{H}_p \left(5\mathrm{i} \sqrt{\dfrac{2}{t^{2H}}} \right) & \text{if } t > 0 \end{cases}$$

The results obtained in this example underscore the unique insights offered by fractional moments when analyzing complex stochastic processes driven by fractional Brownian motion. In our case, the model describes a particle moving in a viscoelastic medium—a scenario where the medium's memory effects result in anomalous diffusion. Unlike tradi-

tional moments that provide measures for dispersion, skewness, and kurtosis, fractional moments capture the behavior of the process at non-integer orders, offering a more delicate probe into its dynamics.

By explicitly deriving the fractional moments for orders such as $p = \{1/4, 1/2, \dots\}$, we demonstrate that even though these moments do not directly yield classical measures of dispersion or asymmetry, they still provide valuable information about the underlying distribution. They help reveal the influence of the long memory (as characterized by the Hurst index $H = 0.55$) on the process, particularly how the interplay between the time-dependent drift and diffusion components shapes the evolution of the system. Moreover, the close agreement between the Monte Carlo simulation results and the analytically derived fractional moments—as illustrated in Figure 4 on a logarithmic scale—reinforces the robustness of the proposed method. In summary, while fractional moments may not directly allow the computation of dispersion, skewness, and kurtosis, they serve as an indispensable tool for characterizing the complex statistical properties of anomalously diffusing systems, thereby enhancing our overall understanding of such processes.

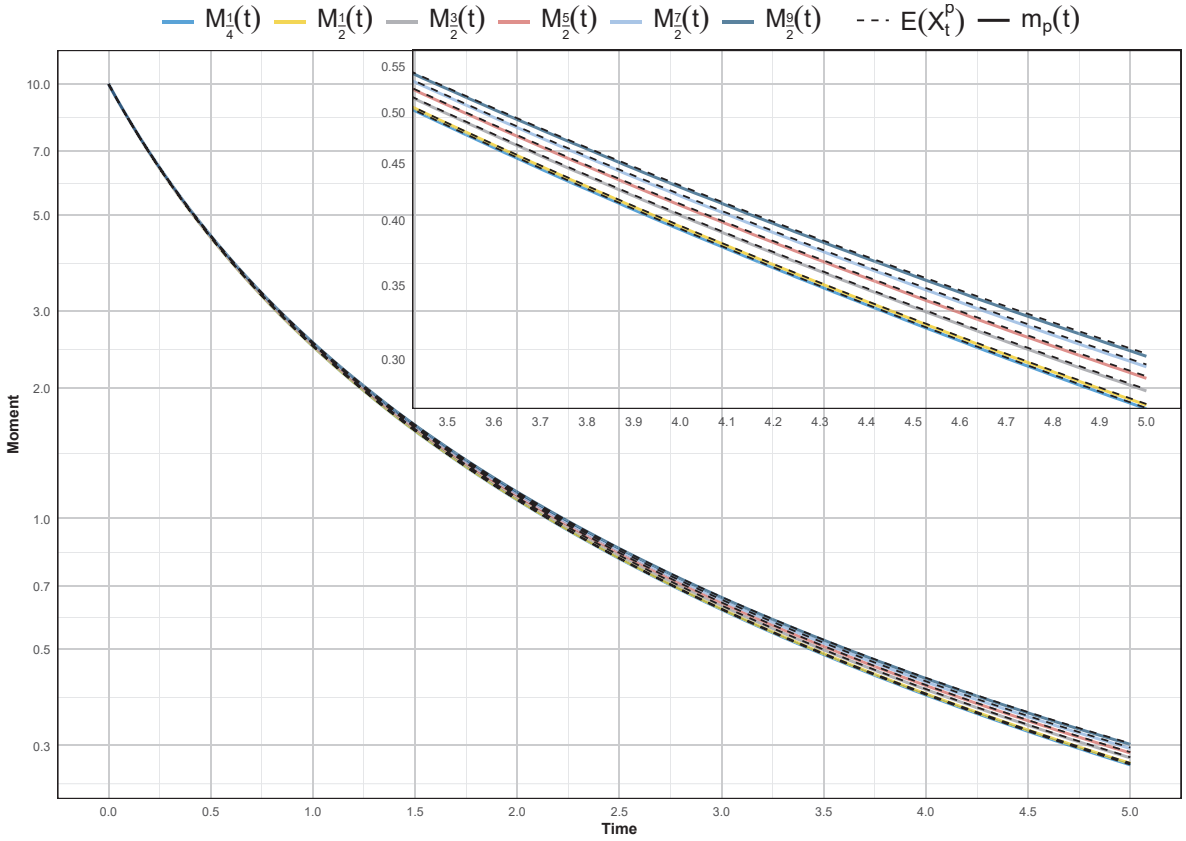

Figure 4. The pth approximate $m_p(t)$ and exact moments $\mathbb{E}\left(X_t^p\right)$ of (24), where $p = \{l/2 : l = 1, 3, 5, 7, 9\}$ and Hurst index $H = 0.55$.

In the Figure 5, we illustrated the evolution of fractional-order moments associated with the fractional Ornstein–Uhlenbeck (fOU) process for various values of the Hurst exponent $H = \{0.5, 0.6, 0.7, 0.8, 0.9, 1.0\}$ and different orders $p = \{1/4, 1/2, 3/2, 5/2, 7/2, 9/2\}$. This visualization highlights the influence of long-range dependence on the statistical properties of the process over time. The results indicate that the moments exhibit a strong dependency on both H and p, revealing distinct scaling behaviors. Specifically, for smaller values of H, the process exhibits a faster decay in moment magnitudes, indicating weaker persistence and stronger mean reversion. Conversely, higher values of H correspond to a slower decay, reflecting stronger long-memory effects characteristic of the fOU process.

Additionally, increasing the order p amplifies these differences, particularly in the tail behavior of the process. This is evident in the non-linearity observed in moment growth, which is more pronounced for larger H. The curvature of the moment trajectories suggests that higher-order moments capture subtle deviations from Gaussianity, influenced by the underlying memory structure.

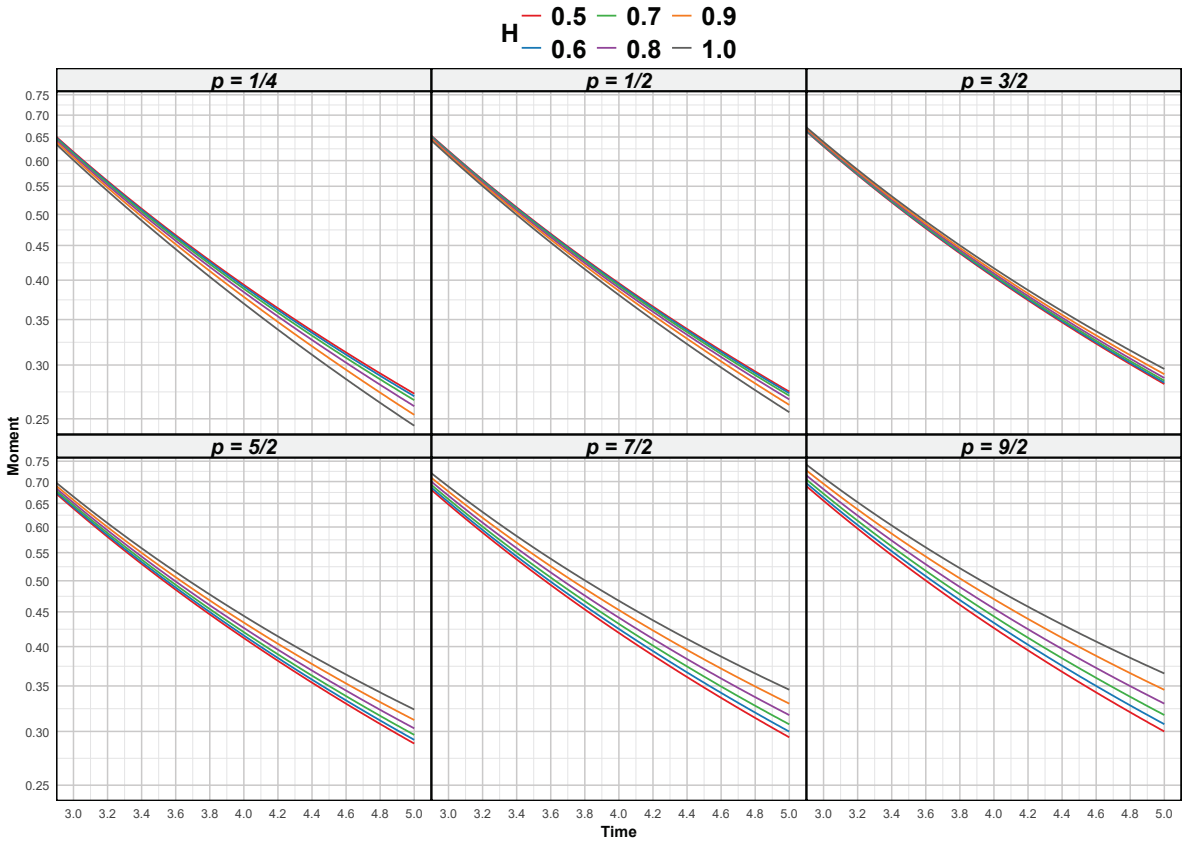

Figure 5. Evolution of exact fractional moments $\mathbb{E}\left(X_t^p\right)$ of (24) with various values of the order p and Hurst parameter H.

Overall, these results provide a deeper insight into the impact of the Hurst exponent on the statistical moments of the fOU process. The Figure 5 serves as empirical evidence of how long-range dependence modulates the higher-order dynamics of the process, emphasizing the need for accurate moment estimation when characterizing such systems.

Table 1 presents the exact fractional moments of (24), computed for various values of the fractional order p and Hurst parameter H, evaluated at different time points t. The results highlight the influence of the long-range dependence parameter H on the evolution of fractional moments.

The analysis of fractional moments of (24) as a function of the Hurst parameter H reveals distinct trends depending on the order p as shown in Figure 6. When $p < 1$, the moments exhibit a decreasing behavior as H increases, indicating that higher long-range dependencies in the process lead to a reduction in expected values of fractional powers. This suggests that for small moment orders, stronger memory effects (higher H) contribute to a more stable and less dispersed process. Conversely, when $p > 1$, the moments show a monotonic increase with H, highlighting the fact that long memory amplifies large fluctuations in the process. Interestingly, for $p = 1$, the moments remain approximately stable across different values of H, suggesting an equilibrium point where the effects of long-range dependence do not significantly alter the mean behavior of the process. These contrasting behaviors underline the non-trivial interaction between fractional moment

orders and memory effects, which has important implications for understanding the statistical properties of stochastic processes driven by fractional Brownian motion.

Table 1. Exact fractional moments $\mathbb{E}\left(X_t^p\right)$ of model (24), computed for various fractional orders p and Hurst parameters $H \in (0.5, 1.0)$, evaluated at time points $t = \{0, 1, 2, 3, 4, 5\}$.

	p	H	Time					
			0.0	**1.0**	**2.0**	**3.0**	**4.0**	**5.0**
$\mathbb{E}(X_t^p)$	$\frac{1}{4}$	0.5	10.0000	2.4905	1.1026	0.6177	0.3937	0.2722
		0.6	10.0000	2.4905	1.1013	0.6158	0.3915	0.2699
		0.7	10.0000	2.4905	1.0998	0.6134	0.3885	0.2663
		0.8	10.0000	2.4905	1.0980	0.6103	0.3841	0.2609
		0.9	10.0000	2.4905	1.0960	0.6063	0.3779	0.2534
		1.0	10.0000	2.4905	1.0936	0.6008	0.3694	0.2442
	$\frac{1}{2}$	0.5	10.0000	2.4937	1.1055	0.6202	0.3958	0.2741
		0.6	10.0000	2.4937	1.1046	0.6189	0.3944	0.2726
		0.7	10.0000	2.4937	1.1036	0.6174	0.3925	0.2704
		0.8	10.0000	2.4937	1.1024	0.6154	0.3897	0.2670
		0.9	10.0000	2.4937	1.1011	0.6128	0.3858	0.2621
		1.0	10.0000	2.4937	1.0996	0.6093	0.3804	0.2556
	$\frac{3}{2}$	0.5	10.0000	2.5063	1.1167	0.6297	0.4040	0.2813
		0.6	10.0000	2.5063	1.1175	0.6309	0.4053	0.2826
		0.7	10.0000	2.5063	1.1185	0.6323	0.4070	0.2845
		0.8	10.0000	2.5063	1.1196	0.6341	0.4093	0.2871
		0.9	10.0000	2.5063	1.1208	0.6364	0.4124	0.2908
		1.0	10.0000	2.5063	1.1223	0.6393	0.4165	0.2960
	$\frac{5}{2}$	0.5	10.0000	2.5186	1.1276	0.6388	0.4117	0.2879
		0.6	10.0000	2.5186	1.1300	0.6421	0.4153	0.2916
		0.7	10.0000	2.5186	1.1327	0.6462	0.4200	0.2965
		0.8	10.0000	2.5186	1.1359	0.6513	0.4261	0.3031
		0.9	10.0000	2.5186	1.1395	0.6574	0.4339	0.3118
		1.0	10.0000	2.5186	1.1436	0.6650	0.4438	0.3232
	$\frac{7}{2}$	0.5	10.0000	2.5542	1.1758	0.6672	0.4295	0.3036
		0.6	10.0000	2.5542	1.1784	0.6710	0.4336	0.3080
		0.7	10.0000	2.5542	1.1814	0.6753	0.4385	0.3134
		0.8	10.0000	2.5542	1.1850	0.6804	0.4443	0.3199
		0.9	10.0000	2.5542	1.1891	0.6864	0.4511	0.3276
		1.0	10.0000	2.5542	1.1937	0.6933	0.4590	0.3366
	$\frac{9}{2}$	0.5	10.0000	2.5664	1.1862	0.6755	0.4363	0.3094
		0.6	10.0000	2.5664	1.1890	0.6795	0.4407	0.3141
		0.7	10.0000	2.5664	1.1922	0.6839	0.4459	0.3197
		0.8	10.0000	2.5664	1.1960	0.6892	0.4519	0.3265
		0.9	10.0000	2.5664	1.2003	0.6955	0.4589	0.3345
		1.0	10.0000	2.5664	1.2051	0.7027	0.4669	0.3438

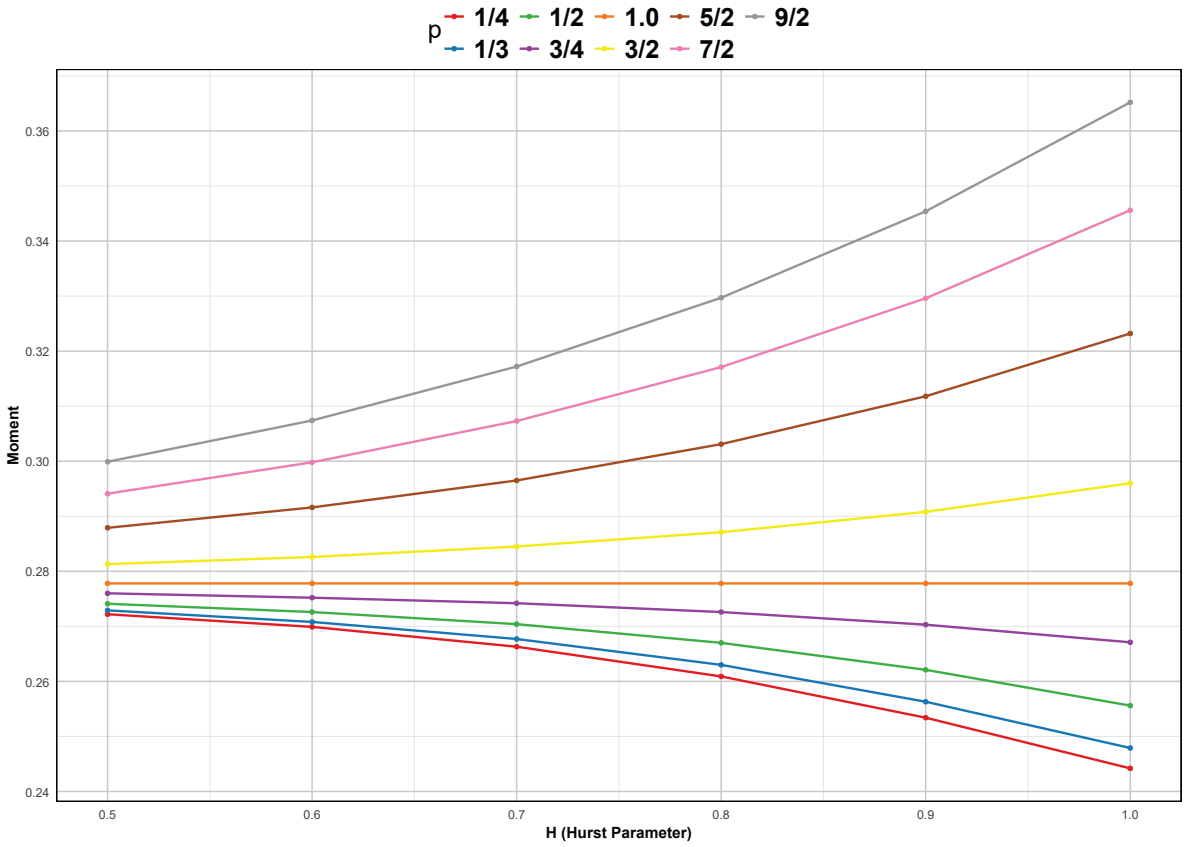

Figure 6. Impact of the Hurst parameter H on exact fractional moments $\mathbb{E}\left(X_t^p\right)$ of (24) with different order p at time $t = 5$.

5. Conclusions and Perspectives

This study has provided a comprehensive analysis of fractional and higher integer-order moments in stochastic processes governed by stochastic differential equations (SDEs) driven by fractional Brownian motion (fBm). By leveraging Wick–Itô calculus and Hermite polynomials, explicit closed-form expressions for these moments were derived, offering a more tractable and efficient alternative to classical approaches. The results reveal a fundamental interaction between the moment order p and the Hurst parameter H, illustrating three distinct regimes: a decreasing trend of moments for $p < 1$ as H increases, a stable behavior for $p = 1$, and an increasing trend for $p > 1$. These findings underscore the profound influence of long-memory effects on the statistical properties of fractional processes, particularly in their higher-order moments, which are crucial for understanding the dynamics of complex systems.

The numerical validation, conducted through Monte Carlo simulations, confirms the robustness of the theoretical results, demonstrating their accuracy in capturing the underlying stochastic dynamics. The ability to explicitly characterize the moments of fractional processes opens new perspectives in both theoretical and applied domains. In mathematical finance, these results provide a valuable tool for modeling asset price dynamics in markets exhibiting long-range dependence, improving volatility estimation and risk management strategies. In statistical inference, the derived moment expressions establish a solid foundation for efficient parameter estimation in fractional models, enhancing the accuracy of empirical studies. Similarly, in physics and engineering, the proposed framework can be applied to describe anomalous diffusion processes, turbulence models, and a variety of physical systems where memory effects play a crucial role. These insights contribute to a

deeper understanding of the mechanisms governing non-Markovian dynamics and their impact on real-world phenomena.

Despite the significant theoretical advancements, several challenges remain. One limitation of the current approach is its reliance on linear fractional SDEs, which may not fully capture the complexity of real-world systems exhibiting non-linearity and strong non-Gaussian behavior. A natural extension of the present work is to move beyond the linear class of fractional SDEs and investigate genuinely non-linear dynamics. In such cases, the Gaussian change of variable and the Hermite-based moment closure adopted here no longer yield a finite hierarchy of moment equations. Complementary tools are therefore required: perturbative expansions around the linear reference case, moment-closure approximations, chaos expansions grounded in Malliavin calculus, or high-order numerical schemes that combine spectral methods with Monte Carlo sampling. Developing a systematic framework along these lines will be a central focus of our future research.

Additionally, while this study focuses on one-dimensional processes, extending these results to multidimensional fractional SDEs would allow for a deeper investigation of interacting systems with long-memory characteristics, such as coupled financial assets, multi-component diffusion models, or climate variables. Furthermore, integrating these findings into machine learning frameworks could enhance predictive modeling for time series exhibiting non-Markovian behavior. The exploration of fractional moment-based techniques in real-world applications remains an exciting avenue for further investigation, with potential implications in finance, climatology, biophysics, and beyond.

In summary, this work provides a solid mathematical foundation for the study of fractional moments in stochastic processes, bridging theoretical developments with practical applications. The interplay between long-memory effects and higher-order moments offers valuable insights into a wide range of complex systems, setting the stage for further advancements in both theoretical and applied research.

Supplementary Materials: The R (software version 4.5.0) code is available on GitHub at https://github.com/acguidoum-git/supplementary_material (accessed on 15 March 2025), enabling readers to replicate the results.

Author Contributions: Conceptualization, A.C.G. and K.B.; methodology, A.C.G., K.B. and F.A.A.; software, A.C.G.; validation, A.C.G., F.A.A. and M.B.; formal analysis, A.C.G., M.B. and M.B.A.; investigation, K.B. and M.B.A.; writing—original draft preparation, A.C.G., K.B., F.A.A. and M.B.; writing—review and editing, A.C.G., K.B. and M.B.A.; visualization, A.C.G. and M.B.; supervision, A.C.G., K.B. and M.B.A.; project administration, A.C.G. and K.B.; funding acquisition, F.A.A. All authors have read and agreed to the published version of the manuscript.

Funding: This research was funded by Princess Nourah bint Abdulrahman University Researchers Supporting Project number (PNURSP2025R515), Princess Nourah bint Abdulrahman University, Riyadh, Saudi Arabia, and the Deanship of Scientific Research and Graduate Studies at King Khalid University through the Research Groups Program under grant number R.G.P. 1/41/46.

Institutional Review Board Statement: Not applicable.

Informed Consent Statement: Not applicable.

Data Availability Statement: The original contributions presented in this study are included in the article. Further inquiries can be directed to the corresponding author.

Acknowledgments: The authors gratefully acknowledge the editor and the anonymous reviewers for their careful and thorough evaluation of the manuscript. Their constructive feedback and insightful suggestions have greatly contributed to enhancing the clarity, rigor, and overall quality of this work. We also thank and extend their appreciation to the funders of this work: (1) Princess Nourah bint Abdulrahman University Researchers Supporting Project Number (PNURSP2025R515), Princess

Nourah bint Abdulrahman University, Riyadh, Saudi Arabia; (2) The Deanship of Scientific Research at King Khalid University through the Research Groups Program under Grant Number R.G.P. 1/41/46.

Conflicts of Interest: The authors declare no conflicts of interest.

References

1. Klebaner, F.C. *Introduction to Stochastic Calculus with Applications*, 2nd ed.; Imperial College Press: London, UK, 2005. [CrossRef]
2. Allen, E. Mathematical Modelling: Theory and Applications. In *Modeling with Itô Stochastic Differential Equations*, 1st ed.; Springer: Berlin/Heidelberg, Germany, 2007; Volume 22. [CrossRef]
3. Jedrzejewski, F. *Modèles Aléatoires et Physique Probabiliste*; Springer: Berlin/Heidelberg, Germany, 2009. [CrossRef]
4. Freidlin, M.I.; Wentzell, A.D. Grundlehren der mathematischen Wissenschaften. In *Random Perturbations of Dynamical Systems*; Springer: Berlin/Heidelberg, Germany, 2012; Volume 260. [CrossRef]
5. Živorad, T.; Sandev, T.; Metzler, R.; Dubbeldam, J. Generalized space–time fractional diffusion equation with composite fractional time derivative. *Phys. A Stat. Mech. Its Appl.* **2012**, *391*, 2527–2542. [CrossRef]
6. Lange, K. Statistics for Biology and Health. In *Mathematical and Statistical Methods for Genetic Analysis*, 2nd ed.; Springer: Berlin/Heidelberg, Germany, 2002. [CrossRef]
7. Han, X.; Kloeden, P.E. Probability Theory and Stochastic Modelling. In *Random Ordinary Differential Equations and Their Numerical Solution*, 1st ed.; Springer: Berlin/Heidelberg, Germany, 2017; Volume 85. [CrossRef]
8. Panik, M.J. *Stochastic Differential Equations: An Introduction with Applications in Population Dynamics Modeling*; John Wiley & Sons: Hoboken, NJ, USA, 2017. [CrossRef]
9. Atangana, A.; İgret Araz, S. Industrial and Applied Mathematics. In *Fractional Stochastic Differential Equations: Applications to Covid-19 Modeling*, 1st ed.; Springer Nature: Singapore, 2022. [CrossRef]
10. Rolski, T.; Schmidli, H.; Schmidt, V.; Teugels, J. *Stochastic Processes for Insurance and Finance*; John Wiley & Sons: Hoboken, NJ, USA, 2008. [CrossRef]
11. Iacus, S.M. *Option Pricing and Estimation of Financial Models with R*; John Wiley & Sons: Hoboken, NJ, USA, 2011. [CrossRef]
12. Nguyen Tien, D. Fractional stochastic differential equations with applications to finance. *J. Math. Anal. Appl.* **2013**, *397*, 334–348. [CrossRef]
13. Rostek, S.; Schöbel, R. A note on the use of fractional Brownian motion for financial modeling. *Econ. Model.* **2013**, *30*, 30–35. [CrossRef]
14. Mackevicius, V. *Stochastic Models of Financial Mathematics*, 1st ed.; Elsevier: Amsterdam, The Netherlands, 2016. [CrossRef]
15. Primak, S.; Kontorovich, V.; Lyandres, V. *Stochastic Methods and Their Applications to Communications, Stochastic Differential Equations Approach*; John Wiley & Sons: Hoboken, NJ, USA, 2004. [CrossRef]
16. Henderson, D.; Plaschko, P. *Stochastic Differential Equations in Science and Engineering*; World Scientific: Singapore, 2006. [CrossRef]
17. Kolmogorov, A.N. Wienersche spiralen und einige andere interessante kurven in hilbertscen raum, cr (doklady). *Acad. Sci. URSS* **1940**, *26*, 115–118.
18. Mandelbrot, B.B.; Ness, J.W.V. Fractional Brownian Motions, Fractional Noises and Applications. *SIAM Rev.* **1968**, *10*, 422–437. [CrossRef]
19. Maslowski, B.; Nualart, D. Evolution equations driven by a fractional Brownian motion. *J. Funct. Anal.* **2003**, *202*, 277–305. [CrossRef]
20. Mishura, Y.S. *Stochastic Calculus for Fractional Brownian Motion and Related Processes*, 1st ed.; Lecture Notes in Mathematics; Springer: Berlin/Heidelberg, Germany, 2008. [CrossRef]
21. Ascione, G.; Mishura, Y.; Pirozzi, E. *Fractional Deterministic and Stochastic Calculus*; De Gruyter: Berlin, Germany; Boston, MA, USA, 2024. [CrossRef]
22. Ullah, R.; Farooq, M.; Faizullah, F.; Alghafli, M.A.; Mlaiki, N. Fractional stochastic functional differential equations with non-Lipschitz condition. *AIMS Math.* **2025**, *10*, 7127–7143. [CrossRef]
23. Bishwal, J.P.N. *Parameter Estimation in Stochastic Differential Equations*, 1st ed.; Lecture Notes in Mathematics; Springer: Berlin/Heidelberg, Germany, 2008. [CrossRef]
24. Bishwal, J.P.N. *Parameter Estimation in Stochastic Volatility Models*, 1st ed.; Springer: Cham, Switzerland, 2012. [CrossRef]
25. Rao, B.P. *Statistical Inference for Fractional Diffusion Processes*, 1st ed.; John Wiley & Sons, Ltd.: Hoboken, NJ, USA, 2010. [CrossRef]
26. Risken, H. *The Fokker-Planck Equation: Methods of Solution and Applications*, 2nd ed.; Springer Series in Synergetics; Springer: Berlin/Heidelberg, Germany, 1996; Volume 18. [CrossRef]
27. Živorad, T.; Ralf, M.; Stefan, G. Fractional characteristic functions, and a fractional calculus approach for moments of random variables. *Fract. Calc. Appl. Anal.* **2022**, *25*, 1307–1323. [CrossRef]

28. Cottone, G.; Di Paola, M.; Metzler, R. Fractional calculus approach to the statistical characterization of random variables and vectors. *Phys. A Stat. Mech. Its Appl.* **2010**, *389*, 909–920. [CrossRef]
29. Graham, C.; Talay, D. Stochastic Modelling and Applied Probability. In *Stochastic Simulation and Monte Carlo Methods: Mathematical Foundations of Stochastic Simulation*, 1st ed.; Springer: Berlin/Heidelberg, Germany, 2013; Volume 68. [CrossRef]
30. Thomopoulos, N.T. *Essentials of Monte Carlo Simulation: Statistical Methods for Building Simulation Models*, 1st ed.; Springer: Berlin/Heidelberg, Germany, 2013. [CrossRef]
31. Li, M. PSD and Cross-PSD of Responses of Seven Classes of Fractional Vibrations Driven by fGn, fBm, Fractional OU Process, and von Kármán Process. *Symmetry* **2024**, *16*, 635. [CrossRef]
32. Russo, F.; Vallois, P. Stochastic calculus with respect to continuous finite quadratic variation processes. *Stochastics Stoch. Rep.* **2000**, *70*, 1–40. [CrossRef]
33. Nualart, D.; Răşcanu, A. Differential equations driven by fractional Brownian motion. *Collect. Math.* **2002**, *53*, 55–81.
34. Guerra, J.; Nualart, D. Stochastic Differential Equations Driven by Fractional Brownian Motion and Standard Brownian Motion. *Stoch. Anal. Appl.* **2008**, *26*, 1053–1075. [CrossRef]
35. Merton, R.C. Theory of Rational Option Pricing. *Bell J. Econ. Manag. Sci.* **1973**, *4*, 141–183. [CrossRef]
36. Cheridito, P.; Kawaguchi, H.; Maejima, M. Fractional Ornstein-Uhlenbeck processes. *Electron. J. Probab.* **2003**, *8*, 1–14. [CrossRef]
37. Guidoum, A.C.; Boukhetala, K. Exact higher-order moments for linear non-homogeneous stochastic differential equation. *Model Assist. Stat. Appl.* **2023**, *18*, 321–329. [CrossRef]
38. Decreusefond, L.; Üstünel, A.S. Stochastic Analysis of the Fractional Brownian Motion. *Potential Anal.* **2001**, *10*, 177–214. [CrossRef]
39. Alòs, E.; Mazet, O.; Nualart, D. Stochastic Calculus with Respect to Gaussian Processes. *Ann. Probab.* **2001**, *29*, 766–801. [CrossRef]
40. Bender, C. An Itô formula for generalized functionals of a fractional Brownian motion with arbitrary Hurst parameter. *Stoch. Process. Their Appl.* **2003**, *104*, 81–106. [CrossRef]
41. Olver, F.W.; Lozier, D.W.; Boisvert, R.F.; Clark, C.W. *NIST Handbook of Mathematical Functions*, 1st ed.; Cambridge University Press: New York, NY, USA, 2010.
42. Willink, R. Normal moments and Hermite polynomials. *Stat. Probab. Lett.* **2005**, *73*, 271–275. [CrossRef]
43. Winkelbauer, A. Moments and Absolute Moments of the Normal Distribution. *arXiv* **2014**. [CrossRef]
44. R Core Team. *R: A Language and Environment for Statistical Computing*; R Foundation for Statistical Computing: Vienna, Austria, 2025. Available online: https://www.r-project.org/ (accessed on 15 March 2025).
45. Guidoum, A.C.; Boukhetala, K. Performing Parallel Monte Carlo and Moment Equations Methods for Itô and Stratonovich Stochastic Differential Systems: R Package Sim.DiffProc. *J. Stat. Softw.* **2020**, *96*, 1–82. [CrossRef]
46. Brouste, A.; Fukasawa, M.; Hino, H.; Iacus, S.M.; Kamatani, K.; Koike, Y.; Masuda, H.; Nomura, R.; Ogihara, T.; Shimuzu, Y.; et al. The yuima Project: A Computational Framework for Simulation and Inference of Stochastic Differential Equations. *J. Stat. Softw.* **2014**, *57*, 1–51. [CrossRef]
47. Iacus, S.M.; Yoshida, N. *Simulation and Inference for Stochastic Processes with* yuima*: A Comprehensive R Framework for SDEs and Other Stochastic Processes*; Springer: Berlin/Heidelberg, Germany, 2018. [CrossRef]
48. Burlon, A. On the numerical solution of fractional differential equations under white noise processes. *Probabilistic Eng. Mech.* **2023**, *73*, 103465. [CrossRef]

Disclaimer/Publisher's Note: The statements, opinions and data contained in all publications are solely those of the individual author(s) and contributor(s) and not of MDPI and/or the editor(s). MDPI and/or the editor(s) disclaim responsibility for any injury to people or property resulting from any ideas, methods, instructions or products referred to in the content.

computation

MDPI

Article

Fractional Order Mathematical Model for Predicting and Controlling Dengue Fever Spread Based on Awareness Dynamics

Ahmed S. Rashed [1,2,3,*], Mahy M. Mahdy [2], Samah M. Mabrouk [2] and Rasha Saleh [2]

[1] Department of Mathematical Sciences, Saveetha School of Engineering, Saveetha Institute of Medical and Technical Sciences, Chennai 602105, Tamil Nadu, India
[2] Department of Physics and Engineering Mathematics, Faculty of Engineering, Zagazig University, Zagazig 44519, Egypt; mmahdy@eng.zu.edu.eg (M.M.M.); samahmm@gmail.com (S.M.M.); rasha.dar20@gmail.com (R.S.)
[3] Basic Science Department, Faculty of Engineering, Delta University for Science and Technology, Gamasa 11152, Egypt
* Correspondence: ahmed.s.rashed@gmail.com

Abstract: Dengue fever (DF) is considered one of the most rapidly spreading infectious diseases, which is primarily transmitted to humans by bites from infected Aedes mosquitoes. The current investigation considers the spread patterns of dengue disease with and without host population awareness. It is assumed that some individuals decrease their contact with infected mosquitoes by adopting precautionary behaviors due to their awareness of the disease. Certain susceptible groups actively prevent mosquito bites, and a few infected are isolated to reduce further infections. The basic reproduction number and population dynamics are modeled by a system of fractional-order differential equations. The system of equations is solved using the Adomian Decomposition Method (ADM) since it converges rapidly to the exact solution and can give explicit analytical solutions. Solutions derived are analyzed and plotted for different fractional orders, providing useful insights into population dynamics and contributing to a better understanding of the initiation and control of disease.

Keywords: dengue fever; Adomian decomposition method; fractional order derivatives; basic reproduction number

1. Introduction

During these days, the COVID-19 pandemic has intimately linked the world and brought along many negative changes. It used to be presumed that the coronavirus was an endemic illness, but it quickly ballooned out of control and turned into a worldwide pandemic. There have been suspicions lately that some individuals who are diagnosed display the symptoms of dengue fever, which are very much like the ones of dengue fever [1]. Dengue fever [2,3] refers to the flu caused by the virus a person gets through the bites of mosquitoes, which are carriers. The production of more already infected mosquitoes allows viruses to survive and spread in case of warm weather and rainfall. The first known cases of the onset of dengue fever occurred in 1779 in Cairo, Egypt, and Batavia, Indonesia [4]. By the year 1818, the number of dengue fever cases that were reported had reached 50,000. The disease has symptoms like high temperature and body pain, in addition to such symptoms as a skin rash; in more serious cases, vision loss and muscle pains are also noted. Normally, it can cause internal bleeding and shock if the patient is in a critical condition. However, symptomatic treatment can relieve the side effects since, as of now, there is no specific cure for the disease in question.

Mathematical models are the backbone of natural sciences, as they can be utilized to study human interactions and the surrounding environment [5]. Monitoring the spread dynamics of infectious diseases is important to estimate outbreaks and formulate policies to stop them [5,6]. To analyze the biological model behavior, several advanced methods have been applied, such as the meshless method [7], the Jacobi elliptic equation method [8], the variational iterative method [9], the Sine–Gordon expansion method [10], the finite difference method [9], the generalized Kudryashov method [11], the Sine–Cosine method [12], and others [13–16].

Several researchers have investigated the dynamics of dengue fever (DF) using mathematical and statistical models. The differential transform method [17] was applied to obtain the series solution of the DF model. Numerical simulations conducted in these studies analyzed the long-term behavior of the DF model and demonstrated that treatment plays a crucial role in reducing the disease burden within a population. Additionally, the Adams–Bashforth–Moulton predictor–corrector scheme was utilized to approximate the solution of the DF model [18]. Furthermore, a mathematical DF model was proposed and analyzed [19] to study the transmission dynamics of the virus in a human population while accounting for the effects of treatment. Previous studies [20–22] significantly enhanced the mathematical modeling of dengue control via mosquito population management and Wolbachia-mediated treatment. Wan and Xu [20] constructed a deterministic model that incorporated Wolbachia infection dynamics and dengue transmission, applying optimal control theory to determine cost-minimizing release strategies in cases of high mortality among infected immature mosquitoes. Their findings indicated that increased larval mortality hindered Wolbachia establishment and hence diminished its efficacy for the treatment of dengue. Wang et al. [21] introduced a stochastic vector–host model with environmental stochasticity in the form of white noise and demonstrated the dynamics of mosquito and human infection levels as a function of changes in death rates and life stage switching. Their analysis verified that controlling mosquito mortality rates significantly lowered the prevalence of dengue, as a key finding also obtained by numerical simulations with Fuzhou, China, data. Zhang et al. [22] set up an impulsive differential system to investigate Wolbachia-based population suppression and replacement strategies, including sex ratios, release time, and cytoplasmic incompatibility. Their bifurcation and sensitivity analyses demonstrated that the performance of these techniques was significantly influenced by initial mosquito densities, release parameters, and selection of Wolbachia strain. These studies collectively provide a comprehensive comprehension of the operational and ecological processes required to control dengue effectively. Jan et al. [23] reported a study in which they exemplified the very important role played by memory and non-Markovian dynamics in the propagation of dengue. They developed a fractional-order model accounting for asymptomatic carriers with the use of Caputo–Fabrizio (CF) and Atangana–Baleanu (AB) derivatives. They quantified the basic reproduction number as well as the sensitivity analysis using the PRCC method. Simulations revealed that reducing the fractional-order parameter had a significant effect on the infected population number, and the AB model played a more important role in this sense than the CF model. Moreover, they discovered that decreasing the mosquito bite rate could significantly lower the disease rate. Jajarmi et al. [24] formulated a new model of dengue epidemics based on the fractional differential equation. The new model was established and confirmed from Cape Verde's 2009 genuine epidemic data. Equilibrium states and system stability were discussed. Simulation outcomes determined that the use of the exponential kernel adequately delineated the start of the epidemic but not the Mittag–Leffler kernel for the remaining stages. The application of the combined kernel was accurate in simulating the entire disease dynamics. The authors suggested two control strategies that efficiently

stabilized the disease-free equilibrium in simulations. Fatmawati et al. [25] established a fractional-order model of dengue transmission involving carrier and partially immune classes. They applied fractional calculus to study the system and estimated the basic reproduction number based on the next-generation method. Memory effects and vector biting rate were crucial to studying and controlling dengue transmission, as demonstrated by the work. Srivastava et al. [26] presented a new fractional-order model of dengue with asymptomatic carriers and reinfection, studied through the Liouville–Caputo and Atangana–Baleanu methods. Existence, uniqueness, and boundedness of the solutions were confirmed, and the basic reproduction number was approximated using the next-generation approach. Sensitivity analysis identified the most critical determinants of the dynamics of illness. Their finding indicated that input parameters and the fractional order had significant roles in infection patterns. Boulaaras et al. [27] introduced a fractional-order complex dengue model with vaccination, reinfection, and carrier dynamics based on the Caputo–Fabrizio framework. They estimated the basic reproduction number using the next-generation matrix and examined the local stability at the disease-free equilibrium. Numerical experiments demonstrated the influence of altering the fractional order and input parameters on disease behavior.

It identified the most important parameters that would be applied to eliminate dengue and gave some suggestions on how disease modeling can be enhanced through the use of fractional calculus.

The novelty of this study is in its application of a fractional-order mathematical model to analyze the transmission dynamics of dengue fever, considering awareness-based prevention strategies. This is a departure from previous models that mainly rely on integer-order differential equations; in this work, fractional calculus is employed to describe the memory effects and long-range effects of disease progression in a better manner. In addition, the Adomian Decomposition Method (ADM) is utilized to analytically solve the system and provides a highly convergent analytical approximation that is more computationally efficient as opposed to numerical methods. Furthermore, by explicitly incorporating public awareness and behavioral responses into the model, this study provides a more realistic representation of disease control dynamics, thereby making it different from other studies performed previously, which focused only on interactions between the vector and the host. The organization of the manuscript is as follows: Section 2 describes the mathematical equation of the dengue fever model. Section 3 explains the mathematical approach and then applies it. Section 4 gives a case study along with the analysis of the model. Finally, Section 5 reports the conclusion of the research.

2. Mathematical Model Formulation of Dengue Fever

The mathematical model of DF transmission divides the populations into two main parts, namely, human hosts and mosquito vectors. The host population (N_h) consists of five distinct compartments: those who are fully susceptible (S_h), susceptible with partial immunity (S_{hk}), individuals with symptomatic infections (I_h), those with asymptomatic infections (I_{hA}), and recovered individuals (R_h). The mosquito population (N_v) is divided into two categories, the susceptible (S_v) and infectious (I_v) groups. The model considers the dynamics of natural population through birth and death rates, denoted by μ_h for humans and μ_v for mosquitoes. While the dengue-related death rate in humans is considered negligible, mosquitoes are modeled with equal birth and death rates (μ_v). For simplicity, different dengue strains are considered the same in the mathematical model. The transmission of DF occurs when infected mosquitoes bite susceptible humans. The rate of disease spread depends on multiple factors, including the mosquito biting rate (b), transmission probabilities, and the numbers of susceptible and infected individuals in both populations.

The transmission probability from humans to mosquitoes is denoted as β_h for fully susceptible individuals and β_{hk} for partially immune individuals. The model assumes that fully susceptible individuals have a higher transmission probability than those with partial immunity ($\beta_h > \beta_{hk}$). The relation $\frac{b}{N_h}$ is known as the number of mosquito bites a human receives from each one, and then $\frac{b\beta_h}{N_h} I_v$, $\frac{b\beta_{hk}}{N_h} I_v$, $\frac{b\beta_v}{N_h} I_v$ represent the infection rates per susceptible human and each susceptible vector. Therefore, the initial infection from susceptible S_h and the second infection from susceptible S_{hk} are both included in the infected class (I_h). A percentage v of the recovered persons (R_h) lose immunity and join the susceptible class with just partial immunity (S_{hk}). These dynamics are mathematically formalized through a system of fractional order differential equations based on these assumptions and relationships [28–30].

$$\begin{cases} \frac{dS_h}{dt} = \mu_h N_h - \frac{\beta_h b}{N_h} S_h I_v - \mu_h S_h, \\ \frac{dS_{hk}}{dt} = -\frac{\beta_{hk} b}{N_h} S_{hk} I_v - \mu_h S_{hk} + v R_h, \\ \frac{dI_h}{dt} = (1-\psi)\frac{\beta_h b}{N_h} S_h I_v - (\mu_h + \tau + \gamma) I_h + \frac{\beta_{hk} b}{N_h} S_{hk} I_v, \\ \frac{dI_{hA}}{dt} = \psi \frac{\beta_h b}{N_h} S_h I_v - (\mu_h + \gamma) I_{hA} \\ \frac{dR_h}{dt} = \gamma(I_h + I_{hA}) + \tau I_h - (v + \mu_h) R_h, \\ \frac{dS_v}{dt} = \mu_v N_v - \frac{\beta_h b}{N_h} (I_h + I_{hA}) S_v - \mu_v S_v, \\ \frac{dI_v}{dt} = \frac{\beta_v b}{N_h} I_h + I_{hA} S_v - \mu_v I_v \end{cases}. \quad (1)$$

For better and generalized modeling, the fractional derivatives are employed, which are inherently nonlocal, meaning they depend not just on the value at a single time point but on the entire history of the function. In epidemics, the future state of the system does not depend only on the current number of infections but also on past exposures, recoveries, or immunity loss. Accordingly, and from a mathematical point of view, a study on the effect of different fractional orders, α, is introduced to secure different models, which could describe different situations.

$$\begin{cases} D_t^\alpha S_h = \mu_h N_h - \frac{\beta_h b}{N_h} S_h I_v - \mu_h S_h, \\ D_t^\alpha S_{hk} = -\frac{\beta_{hk} b}{N_h} S_{hk} I_v - \mu_h S_{hk} + v R_h, \\ D_t^\alpha I_h = (1-\psi)\frac{\beta_h b}{N_h} S_h I_v - (\mu_h + \tau + \gamma) I_h + \frac{\beta_{hk} b}{N_h} S_{hk} I_v, \\ D_t^\alpha I_{hA} = \psi \frac{\beta_h b}{N_h} S_h I_v - (\mu_h + \gamma) I_{hA} \\ D_t^\alpha R_h = \gamma(I_h + I_{hA}) + \tau I_h - (v + \mu_h) R_h, \\ D_t^\alpha S_v = \mu_v N_v - \frac{\beta_h b}{N_h} (I_h + I_{hA}) S_v - \mu_v S_v, \\ D_t^\alpha I_v = \frac{\beta_v b}{N_h} I_h + I_{hA} S_v - \mu_v I_v \end{cases}, \quad (2)$$

with an initial condition,

$$S_h(0) = n_1, S_{hk}(0) = n_2, I_h(0) = n_3, I_{hA}(0) = n_4, R_h(0) = n_5, S_v(0) = n_6, I_v(0) = n_7, \quad (3)$$

where D_t^α satisfies the definition of the Caputo derivative, with order α defined as follows:

$$D^\alpha f(s) = \frac{1}{\Gamma(\mathrm{n} - \alpha)} \int_0^s (s-t)^{\mathrm{n}-\alpha-1} \left(f^{(n)}(t) \right) dt, \quad n - 1 < \alpha \leq n, n \in \mathrm{N}, s > 0. \quad (4)$$

3. The Adomian Decomposition Method

To find the solution of the system (2), the Adomian Decomposition Method (ADM) [31,32] starts with deeming this system in an operator form and then evaluating the inverse operator for the system.

$$\begin{cases} S_h = D_t^{-\alpha}\mu_h N_h - D_t^{-\alpha}\frac{\beta_h b}{N_h} S_h I_v - D_t^{-\alpha}\mu_h S_h, \\ S_{hk} = -D_t^{-\alpha}\frac{\beta_{hk} b}{N_h} S_{hk} I_v - D_t^{-\alpha}\mu_h S_{hk} + D_t^{-\alpha} v R_h, \\ I_h = D_t^{-\alpha}(1-\psi)\frac{\beta_h b}{N_h} S_h I_v - D_t^{-\alpha}(\mu_h + \tau + \gamma) I_h + D_t^{-\alpha}\frac{\beta_{hk} b}{N_h} S_{hk} I_v, \\ I_{hA} = D_t^{-\alpha}\psi\frac{\beta_h b}{N_h} S_h I_v - D_t^{-\alpha}(\mu_h + \gamma) I_{hA} \\ R_h = D_t^{-\alpha}\gamma(I_h + I_{hA}) + D_t^{-\alpha}\tau I_h - D_t^{-\alpha}(v + \mu_h) R_h, \\ S_v = D_t^{-\alpha}\mu_v N_v - D_t^{-\alpha}\frac{\beta_h b}{N_h}(I_h + I_{hA}) S_v - D_t^{-\alpha}\mu_v S_v, \\ I_v = D_t^{-\alpha}\frac{\beta_v b}{N_h} I_h + D_t^{-\alpha} I_{hA} S_v - D_t^{-\alpha}\mu_v I_v \end{cases}. \quad (5)$$

According to ADM assumptions, the following series are introduced:

$$S_h = \sum_{n=0}^{\infty} S_{hn}, S_{hk} = \sum_{n=0}^{\infty} S_{hkn}, I_h = \sum_{n=0}^{\infty} I_{hn}, I_{hA} = \sum_{n=0}^{\infty} I_{hAn}, R_h = \sum_{n=0}^{\infty} R_{hn}, S_v = \sum_{n=0}^{\infty} S_{vn}, I_v = \sum_{n=0}^{\infty} I_{vn}. \quad (6)$$

The sum of nonlinear components can be described as follows:

$$\begin{cases} S_h I_v = \sum_{n=0}^{\infty} A_n = \sum_{m=0}^{\infty} S_{hm} I_{v(n-m)}, \\ S_{hk} I_v = \sum_{n=0}^{\infty} B_n = \sum_{m=0}^{\infty} S_{hkm} I_{v(m-k)}, \\ I_{hA} S_v = \sum_{n=0}^{\infty} C_n = \sum_{k=0}^{\infty} I_{hAm} S_{v(m-k)}, \\ I_h S_v = \sum_{n=0}^{\infty} D_n = \sum_{k=0}^{\infty} I_{hm} S_{v(m-k)}. \end{cases}, \quad (7)$$

where n = 0, 1, 2, . . ., n.

The Adomian polynomials A_n, B_n, C_n, and D_n are obtained as follows:

$$\begin{cases} A_0 = S_{h0} I_{v0} \\ A_1 = S_{h0} I_{v1} + S_{h1} I_{v0} \\ A_2 = S_{h0} I_{v2} + S_{h1} I_{v1} + S_{h2} I_{v0} \\ A_3 = S_{h0} I_{v3} + S_{h1} I_{v2} + S_{h2} I_{v1} + S_{h3} I_{v0} \\ \cdots\cdots \end{cases}, \quad (8)$$

$$\begin{cases} B_0 = S_{hk0} I_{v0} \\ B_1 = S_{hk0} I_{v1} + S_{hk1} I_{v0} \\ B_2 = S_{hk0} I_{v2} + S_{hk1} I_{v1} + S_{hk2} I_{v0} \\ B_3 = S_{hk0} I_{v3} + S_{hk1} I_{v2} + S_{hk2} I_{v1} + S_{hk3} I_{v0} \\ \cdots\cdots \end{cases}, \quad (9)$$

$$\begin{cases} C_0 = I_{hA0} S_{v0} \\ C_1 = I_{hA0} S_{v1} + I_{hA1} S_{v0} \\ C_2 = I_{hA0} S_{v2} + I_{hA1} S_{v1} + I_{hA2} S_{v0} \\ C_3 = I_{hA0} S_{v3} + I_{hA1} S_{v2} + I_{hA2} S_{v1} + I_{hA3} S_{v0} \\ \cdots\cdots \end{cases}, \quad (10)$$

$$\begin{cases} D_0 = I_{h0} S_{v0} \\ D_1 = I_{h0} S_{v1} + I_{h1} S_{v0} \\ D_2 = I_{h0} S_{v2} + I_{h1} S_{v1} + I_{h2} S_{v0} \\ D_3 = I_{h0} S_{v3} + I_{h1} S_{v2} + I_{h2} S_{v1} + I_{h3} S_{v0} \\ \cdots\cdots \end{cases}. \quad (11)$$

Then, substituting Equalities (6)–(11) into System (5), yields the following results:

$$\sum_{n=0}^{\infty} S_{hn} = n_1 + D_t^{-\alpha}\mu_h N_h - D_t^{-\alpha}\frac{\beta_h b}{N_h}\sum_{n=0}^{\infty} A_n - D_t^{-\alpha}\mu_h \sum_{n=0}^{\infty} S_{hn}, \tag{12}$$

$$\sum_{n=0}^{\infty} S_{hkn} = n_2 - D_t^{-\alpha}\frac{\beta_{hk} b}{N_h}\sum_{n=0}^{\infty} B_n - D_t^{-\alpha}\mu_h \sum_{n=0}^{\infty} S_{hkn} + D_t^{-\alpha} v \sum_{n=0}^{\infty} R_{hn}, \tag{13}$$

$$\sum_{n=0}^{\infty} I_{hn} = n_3 + D_t^{-\alpha}(1-\psi)\frac{\beta_h b}{N_h}\sum_{n=0}^{\infty} A_n - D_t^{-\alpha}(\mu_h + \tau + \gamma)\sum_{n=0}^{\infty} I_{hn} + D_t^{-\alpha}\frac{\beta_{hk} b}{N_h}\sum_{n=0}^{\infty} B_n, \tag{14}$$

$$\sum_{n=0}^{\infty} I_{hAn} = n_4 + D_t^{-\alpha}\psi\frac{\beta_h b}{N_h}\sum_{n=0}^{\infty} A_n - D_t^{-\alpha}(\mu_h + \gamma)\sum_{n=0}^{\infty} I_{hAn}, \tag{15}$$

$$\sum_{n=0}^{\infty} R_{hn} = n_5 + D_t^{-\alpha}\gamma\sum_{n=0}^{\infty} I_{hn} + D_t^{-\alpha}\gamma\sum_{n=0}^{\infty} I_{hAn} + D_t^{-\alpha}\tau\sum_{n=0}^{\infty} I_{hn} - D_t^{-\alpha}(v + \mu_h)\sum_{n=0}^{\infty} R_{hn}, \tag{16}$$

$$\sum_{n=0}^{\infty} S_{vn} = n_6 + D_t^{-\alpha}\mu_v N_v - D_t^{-\alpha}\frac{\beta_h b}{N_h}\sum_{n=0}^{\infty} D_n - D_t^{-\alpha}\frac{\beta_h b}{N_h}\sum_{n=0}^{\infty} C_n - D_t^{-\alpha}\mu_v \sum_{n=0}^{\infty} S_{vn}, \tag{17}$$

$$\sum_{n=0}^{\infty} I_{vn} = n_7 + D_t^{-\alpha}\frac{\beta_v b}{N_h}\sum_{n=0}^{\infty} I_{hn} + D_t^{-\alpha}\sum_{n=0}^{\infty} C_n - D_t^{-\alpha}\mu_v \sum_{n=0}^{\infty} I_{vn}. \tag{18}$$

Considering the Caputo integral properties, yields the following:

$$S_{h0} = n_1,\ S_{hk0} = n_2, I_{h0} = n_3, I_{hA0} = n_4, R_{h0} = n_5, S_{v0} = n_6, I_{v0} = n_7, \tag{19}$$

$$S_{h(m+1)} = \frac{\mu_h N_h}{\Gamma(\alpha+1)}t^{\alpha} - \frac{\beta_h b}{N_h\Gamma(\alpha+1)}t^{\alpha}A_m - \frac{\mu_h}{\Gamma(\alpha+1)}t^{\alpha}S_{hm}, \quad m = 0, 1, 2, \ldots, \tag{20}$$

$$S_{hk(m+1)} = -\frac{\beta_{hk} b}{N_h\Gamma(\alpha+1)}t^{\alpha}B_m - \frac{\mu_h}{\Gamma(\alpha+1)}t^{\alpha}S_{hkm} + \frac{v}{\Gamma(\alpha+1)}t^{\alpha}R_{hm}, \tag{21}$$

$$I_{h(m+1)} = \frac{(1-\psi)\beta_h b}{N_h\Gamma(\alpha+1)}t^{\alpha}A_m - \frac{(\mu_h + \tau + \gamma)}{\Gamma(\alpha+1)}t^{\alpha}I_{hm} + \frac{\beta_{hk} b}{N_h\Gamma(\alpha+1)}t^{\alpha}B_m, \tag{22}$$

$$I_{hA(m+1)} = \psi\frac{\beta_h b}{N_h\Gamma(\alpha+1)}t^{\alpha}A_m - \frac{(\mu_h + \gamma)}{\Gamma(\alpha+1)}t^{\alpha}I_{hAm}, \tag{23}$$

$$R_{h(m+1)} = \frac{\gamma}{\Gamma(\alpha+1)}t^{\alpha}I_{hm} + \frac{\gamma}{\Gamma(\alpha+1)}t^{\alpha}I_{hAm} + \frac{\tau}{\Gamma(\alpha+1)}t^{\alpha}I_{hm} - \frac{(v+\mu_h)}{\Gamma(\alpha+1)}t^{\alpha}R_{hm}, \tag{24}$$

$$S_{v(m+1)} = \frac{\mu_v N_v}{\Gamma(\alpha+1)}t^{\alpha} - \frac{\beta_h b}{N_h\Gamma(\alpha+1)}t^{\alpha}D_m - \frac{\beta_h b}{N_h\Gamma(\alpha+1)}t^{\alpha}C_m - \frac{\mu_v N_v}{\Gamma(\alpha+1)}t^{\alpha}S_{vm}, \tag{25}$$

$$I_{v(m+1)} = \frac{\beta_v b}{N_h\Gamma(\alpha+1)}t^{\alpha}I_{hm} + \frac{t^{\alpha}}{\Gamma(\alpha+1)}C_m - \frac{\mu_v}{\Gamma(\alpha+1)}t^{\alpha}I_{vm}. \tag{26}$$

4. Results and Discussion

The numerical simulations are carried out using the parameter values in Table 1.

Table 1. Parameter information.

Symbol	Physical Meaning	Value	References
N_h	Constant host population size	8,266,000	[33]
s_h	Susceptible people	8,065,518	[33]
s_{hk}	Susceptible people with partial immunity	200,000	[33]
I_h	Symptomatic infected people	200	[33]
I_{hA}	Asymptomatic infected people	282	[33]

Table 1. *Cont.*

Symbol	Physical Meaning	Value	References
R_h	Recovered people	0	[33]
N_v	Vector (mosquito) population size	50,000	Assumed
s_v	Susceptible mosquitoes	49,000	Assumed
I_v	Infected mosquitoes	1000	Assumed
μ_h	Death rates of humans per capita	0.0000457/day	[3,28–30]
μ_v	Death rates of mosquitoes per capita	0.03/day	[3,28–30]
β_h	The transmission probability from vector to human (effective contact rate)	0.75	[3,28–30]
β_{hk}	The transmission probability from vector to human with partial immunity (effective contact rate)	1	Assumed
β_v	The transmission probability from human to vector (effective contact rate)	0.75	[3,28–30]
b	Average bite per mosquito per day	0.3/day	[3,28–30]
$b\beta_v$	Effective contact rate, human to vector	0.3750000	[28]
$b\beta_h$	Effective contact rate, vector to human	0.75	[28]
γ	Recovery rate in the host population, time -1	0.14286/day	[3,28–30]
ψ	Proportion of asymptomatic infection rate of people	0.009	[34]
n_1	$S_h(0)$	0.9757	$\frac{s_h}{N_h}$
n_2	$S_{hk}(0)$	0.0242	$\frac{s_{hk}}{N_h}$
n_3	$I_h(0)$	0.0000242	$\frac{I_h}{N_h}$
n_4	I_{hA0}	0.000034	$\frac{I_{hA}}{N_h}$
n_5	R_{h0}	0	$\frac{R_h}{N_h}$
n_6	$S_v(0)$	0.98	$\frac{s_V}{N_V}$
n_7	$I_v(0)$	0.02	$\frac{I_V}{N_V}$

At $\alpha = 1$, the results can be obtained in the following form:

$$S_h = 0.9757 + 1511.0248t - 0.0519t^2 + 1.5902 * 10^{-6}t^3 + 1.5074 * 10^{-6}t^4 + \cdots, \quad (27)$$

$$S_{hk} = 0.0242 - 1.106 * 10^{-6}t + 5.10427 * 10^{-11}t^2 - 89.5916 * 10^{-12}t^3 + 6.7197 * 10^{-8}t^4 + \cdots, \quad (28)$$

$$I_h = 0.0000242 - 3.4578 * 10^{-6}t + 1.091929 * 10^{-6}t^2 - 135.44 * 10^{-9}t^3 - 1.546 * 10^{-6}t^4 + \cdots, \quad (29)$$

$$I_{hA} = 0.000034 - 4.85726 * 10^{-6}t + 699.68182 * 10^{-9}t^2 - 99.27595 * 10^{-9}t^3 - 2.778 * 10^{-8}t^4 + \cdots, \quad (30)$$

$$R_h = 1.07344 * 10^{-5}t + 229.668 * 10^{-9}t^2 - 136.752 * 10^{-9}t^3 - 3.9443 * 10^{-8}t^4 + \cdots, \quad (31)$$

$$S_v = 0.98 + 6000t - 6.75 * 10^6t^2 + 6.75 * 10^9t^3 - 5.0625 * 10^{12}t^4, + \cdots, \quad (32)$$

$$I_v = 0.02 - 5.6668 * 10^{-4}t + 0.153t^2 - 153.017t^3 + 114.76 * 10^3t^4 + \cdots. \quad (33)$$

For $\alpha = \frac{1}{2}$, the results are given hereafter.

$$S_h = 0.9757 + 1.705009 * 10^3t^{0.5} - 21.980781 * 10^{-3}t + 15.14401281 * 10^{-6}t^{\frac{3}{2}} + 1.70092t^2 + \cdots, \quad (34)$$

$$S_{hk} = 0.0242 - 1.247939 * 10^{-6} t^{0.5} + 64.934982 * 10^{-12} t - 128.74597 * 10^{-12} t^{\frac{3}{2}} + 7.5823695 * 10^{-8} t^2 + \cdots . \quad (35)$$

$$I_h = 0.0000242 - 3.9017948 * 10^{-6} t^{0.5} + 1.378081386 * 10^{-6} t - 6.559415133 * 10^{-6} t^{\frac{3}{2}} - 1.744474 * 10^{-6} t^2 + \cdots . \quad (36)$$

$$I_{hA} = 0.000034 - 5.480831 * 10^{-6} t^{0.5} + 892.59524487 * 10^{-9} t - 200.917186 * 10^{-9} t^{\frac{3}{2}} - 3.1346373 * 10^{-8} t^2 + \cdots . \quad (37)$$

$$R_h = 12.112473 * 10^{-6} t^{0.5} - 1.952752 * 10^{-6} t + 43.9112769 * 10^{-8} t^{\frac{3}{2}} - 4.45066595 * 10^{-8} t^2 + \cdots . \quad (38)$$

$$S_v = 0.98 + 6.770276 * 10^{3} t^{0.5} - 8.594367 * 10^{6} t + 9.6977046 * 10^{9} t^{\frac{3}{2}} - 5.712419 * 10^{12} t^2 + \cdots . \quad (39)$$

$$I_v = 0.02 - 639.429906 * 10^{-6} t^{0.5} + 194.8056 * 10^{-3} t - 219.839968 t^{\frac{3}{2}} + 129.49279 * 10^{3} t^2 + \cdots . \quad (40)$$

In the same way, other results can be obtained for different values of α. The fractional order in the mathematical model is used to describe memory effects, hereditary properties, and anomalous dynamics in systems in physics, epidemiology, and engineering. The fractional order α $(0 < \alpha \leq 1)$ includes a concept of history dependence and non-locality, which cannot be achieved with the standard integer-order models.

To verify the existing model, the obtained results are compared against results published by Z. Ullah [35] for significant epidemiological compartments, such as susceptible and infected populations. From this comparison, the accuracy of the ADM model versus the Laplace adomian method in simulating the transmission of dengue can be established, as well as deviations or improvements from previous results. Figures 1 and 2 show high agreement between the presented model and literature.

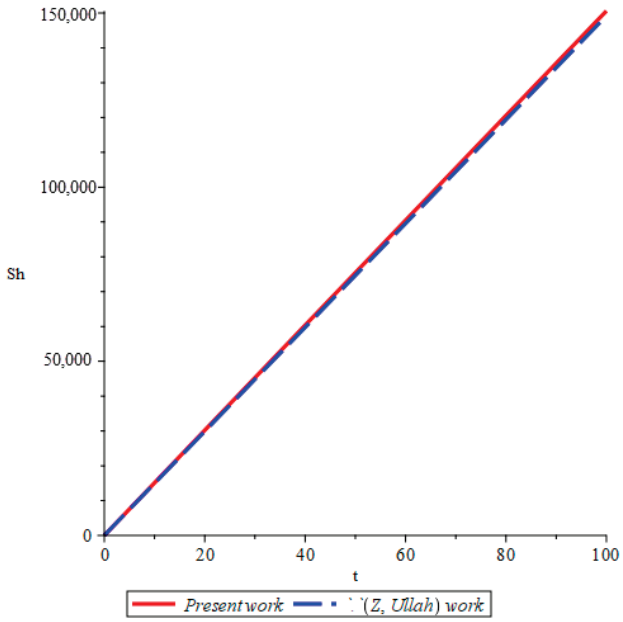

Figure 1. Comparison between the present S_h and Z. Ullah's work [35] at $\alpha = 1$.

Figure 3 illustrates the time evolution of the susceptible population S_h as a function of time (days) with various values of the fractional order parameter α. The fractional order derivative causes memory effects within the model, one of the most significant characteristics of fractional calculus. This figure indicates how the memory parameter α controls the susceptibility dynamics in a fractional-order epidemic model. For small α values (e.g., $\alpha = 0.1$), the buildup of susceptibility is far slower. This behavior illustrates the extremely strong memory effect of the fractional model: the system "remembers" more of its past states, which can be interpreted in epidemiological terms as long-term immunity, delayed exposure, or environmental survival that slows the progression of individuals into the susceptible class. These delays could simulate some scenarios where elder infections

impart long-term partial immunity or where environmental conditions reduce immediate re-exposure. As α increases, the curve steepens, with a faster accumulation of susceptibles. This corresponds to weaker memory effects, where individuals lose immunity or become re-exposed to the disease vector more quickly. Biologically, this can be attributed to waning immunity, rapid mosquito–human transmission cycles, or environmental feedbacks that reinforce the rate at which susceptibility accumulates, such as mosquito breeding increases due to climatic changes or human migration into endemic areas. At the largest considered value of $\alpha = 0.5$, the susceptibility increases nearly exponentially with time and reaches significantly larger values than the other curves. This is the behavior of a system in which past states have little effect, and the disease dynamics are more like a typical first-order system. The steep increase in susceptibility may be due to hastened disease transmission cycles, perhaps fueled by urbanization, waning immunity at the population level, or disruption of vector control policies. The monotonicity and increasing convexity of the curves with increasing α support the reasoning that memory decay leads to faster replenishment of the susceptible pool. Thus, higher values of α weaken the dampening effect of the past disease dynamics, pointing to the importance of temporal memory in disease control and recurrence.

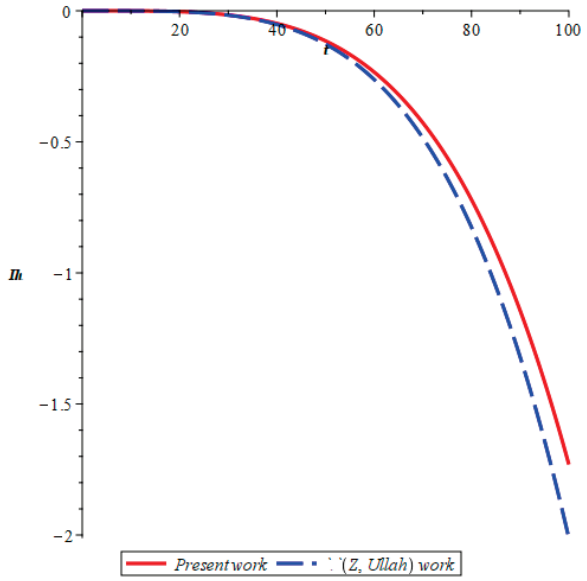

Figure 2. Comparison between the present I_h and Z. Ullah's work [35] at $\alpha = 1$.

Figure 4 illustrates the temporal evolution of the partially immune susceptible population S_{hk} for different values of the fractional-order parameter α. The graph shows a steady decrease in S_{hk} across all values of α, suggesting a progressive loss of partial immunity and movement towards alternative disease states, including full susceptibility or infection. This trend illustrates the immunological dynamics in diseases such as dengue, where partial immunity, typically acquired through previous exposure to various serotypes, diminishes over time. The fractional-order derivative α significantly influences this behavior by incorporating memory effects into the system. At reduced values of α, the system demonstrates enhanced memory, indicating that previous states exert a more extended impact on current dynamics. The slower decrease in S_{hk} indicates that individuals maintain partial immunity for an extended period, which consequently delays susceptibility and slows the epidemic's progression. As α increases, the memory effect diminishes, resulting in a more rapid decline in S_{hk}. This suggests that immunity diminishes more rapidly, enabling quicker shifts between disease states and promoting faster epidemic spread. This may indicate a situation in which protective immunity is transient or where environmental and immunological

factors facilitate a more rapid decline in protection. The fractional-order model's capacity to represent nuanced behavior underscores its significance in modeling real-world infectious disease dynamics, particularly in scenarios where immune memory, reinfection risk, and cross-protection are essential for comprehending long-term disease propagation patterns.

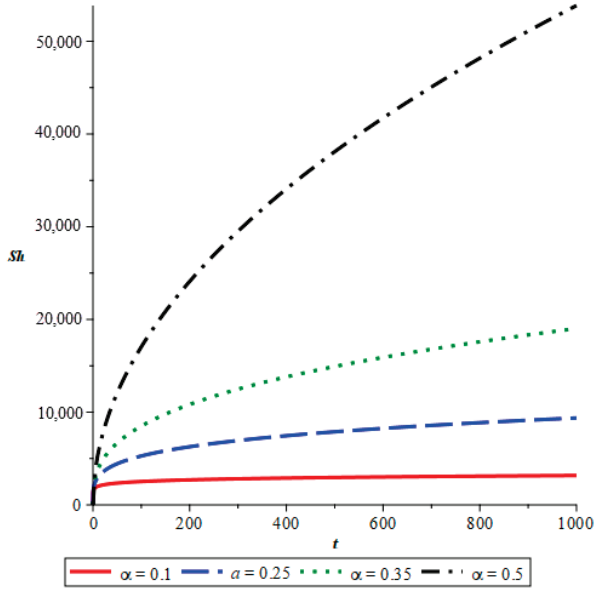

Figure 3. Susceptible people, S_h at different fractional orders.

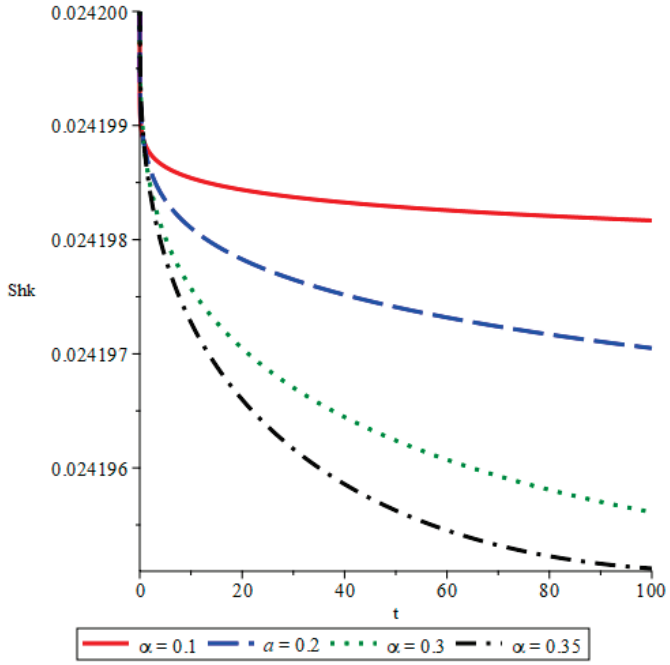

Figure 4. Susceptible people with partial immunity, s_{hk} at different fractional orders.

Figure 5 depicts the symptomatic infected human population. The rate and amount of this reduction depend significantly on the selection of α, the memory or inherited characteristics of the system. In fractional calculus models, the parameter $\alpha \in (0, 1]$ determines the amount to which previous states affect current behavior, with smaller values giving more weight to historical influence and larger values approximating conventional models that assume nearly instantaneous dynamics. At lower values of α (say, $\alpha = 0.05$ and 0.1), the memory effect is stronger in the sense that the spread of infection is more

inertial due to the persistent effect of earlier infection rates. This causes the decline of I_h to be slower, as the system retains past symptomatic loads, potentially indicating responses delayed to intervention strategies or prolonged durations of illness and recovery. In contrast, large values for α (e.g., $\alpha = 0.2$ and 0.3) are indicative of low memory systems that facilitate rapid state change. This results in a more rapid reduction in symptomatic disease, probably indicating more effective public health measures, such as a rapid diagnosis, treatment, effective vaccination programs, or mosquito control causing rapid reduction in transmission. Continuous decrease in I_h with increased α might reflect enhanced host immunity or behavioral reduction in contact with vectors. This result highlights the role of dynamical memory in predicting the efficiency of control measures from an epidemiological perspective. The capability of the fractional model to account for various levels of system memory enables a more general and realistic modeling of disease progression, especially for vector-borne infections such as dengue, where immune response, onset of treatment, and delay of vector exposure are quantities that decide the outcome. Consequently, the determination of α provides a robust modeling method to simulate varied public health scenarios and guide best intervention practices.

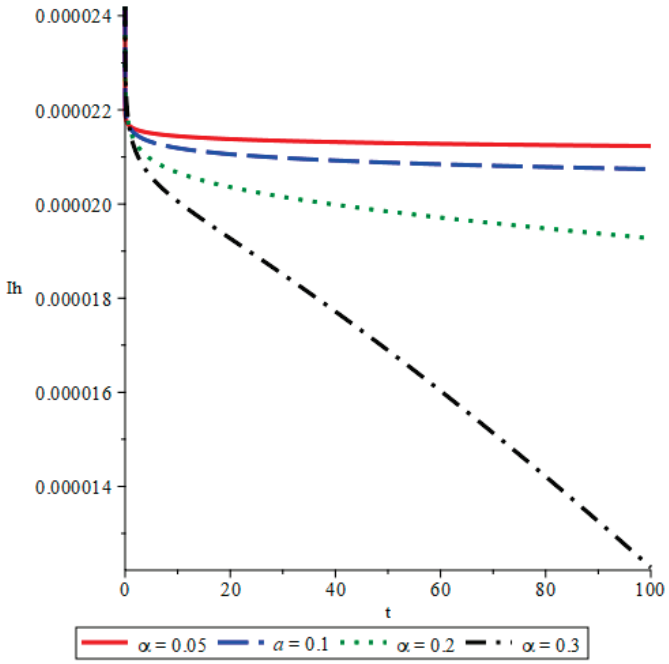

Figure 5. Symptomatic infection, I_h at different fractional orders.

Figure 6 displays the temporal behavior of the population of asymptomatic infected individuals I_{hA} in a fractional-order model of dengue fever, showing how this population evolves over time with different values of the fractional-order parameter α. The fractional-order parameter α, determining the effect of memory in fractional calculus, plays an important role in how fast asymptomatic patients decline. At lower α values, the decline is slower, suggesting a longer duration of asymptomatic carriers within the community. Conversely, large values of α result in a steeper decline, suggesting rapid elimination of the silent infections. This trend illustrates that more powerful memory effects in systems (more negative α) keep past infection processes going for extended time intervals, possibly because of late immune response or persistence of the virus in the environment. Epidemiologically, the faster disappearance of I_{hA} with larger α might indicate better public health interventions, e.g., increased diagnosis and quarantine of asymptomatic carriers, greater access to healthcare, or greater community immunity. The asymptomatic course in I_{hA} is nearly indistinguishable from that of symptomatic disease I_{hA}, but the fraction

of asymptomatic disease begins at slightly elevated levels, consistent with known dengue epidemiology, in which most patients are subclinical but still facilitate transmission. The figure highlights the advantages of fractional-order models in describing the complexity of infectious disease dynamics and the parameter α as a quantitative metric of biological processes and the effectiveness of interventions.

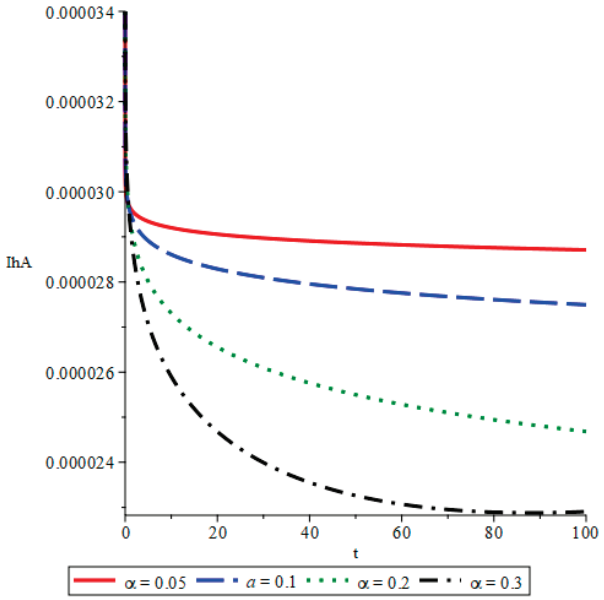

Figure 6. Asymptomatic infected people, I_{hA} at different fractional orders.

Figure 7 illustrates the recovery time course of recovered population $R_h(t)$ in a fractional-order dengue disease model as illustrates the continued increase in recoveries by time over the range of the fractional-order parameter α. This rise is consistent with earlier-found reductions in both symptomatic (I_h) and asymptomatic (I_{hA}) infective individuals and would indicate ongoing clearing of infection from within the population. The growth rate of recovery is significantly affected by the value of α, with large fractional orders (e.g., $\alpha = 0.3$) producing a more rapid and higher rate of recovery accumulation. It indicates that as the influence of memory in the system diminishes, reaching the classical case, sick individuals recover more quickly. This may indicate stronger immune responses and effective healthcare infrastructures.

Smaller values of α indicate a slow recovery, in agreement with long-term memory effects that may be due to biological or logistical delays, e.g., delayed diagnosis, limited access to treatment, or inherently longer durations of recovery. From the modeling perspective, fractional calculus provides a more in-depth explanation of epidemic disease processes in real life by considering memory and genetic characteristics of infectious disease development. As such, parameter α is a valuable instrument to study the role of systemic and biological delays in recovery outcomes and provides a congenial framework to evaluate the contribution of public health interventions and individual recovery paths in dengue transmission.

Figure 8 displays the time dynamics of the infected mosquito population $I_v(t)$ of the fractional-order dengue model, which indicates an explicit correlation with the fractional-order parameter α. As time goes on, the infected mosquitoes grow in number, with the amount of this growth depending to a large extent on the value of α. For higher values, e.g., $\alpha = 0.3$, I_v growth is rapid and roughly linear, echoing increased transmission dynamics between humans and mosquito vectors. This could simulate situations with minimal memory effects, perhaps because of high vector biting rates, favorable weather conditions,

or inefficient vector control measures. In contrast, lower values of α (e.g., 0.05 and 0.1) result in a much more gradual rise in mosquito infections, suggesting better suppression of transmission cycles. These scenarios may represent significant environmental limits on mosquito populations, effective public health measures, or behavioral changes that limit human–vector contact. The synchrony between infected mosquito trends and the foregoing reductions in human infections is indicative of the coupled dynamics of host–vector transmission in the model. The fractional-order derivative effectively captures memory effects in mosquito infection dynamics, including incubation lag and infection accumulation slowness. As a result, α is a critical parameter in the modeling and control of vector-borne diseases such as dengue. These results emphasize the importance of early and sustained vector control interventions, particularly in scenarios with high α values, where transmission may rapidly increase and saturate public health systems.

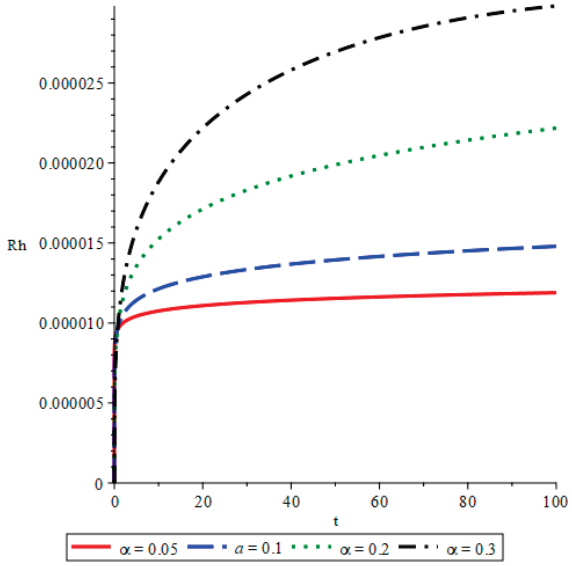

Figure 7. Recovered people, R_h, at different fractional orders.

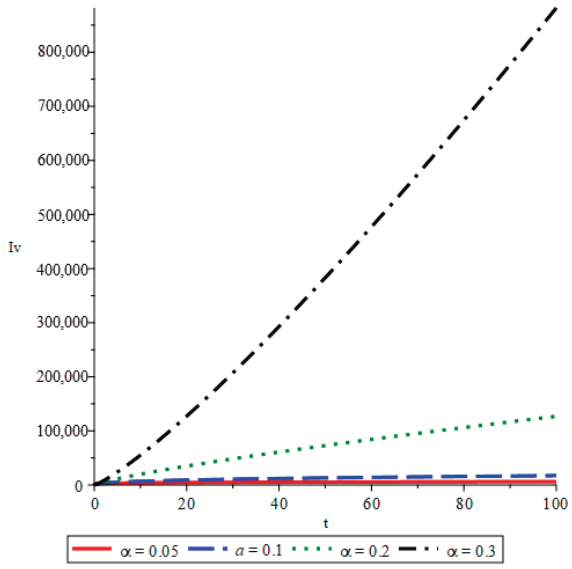

Figure 8. Infected mosquitos, I_V at different fractional orders.

5. Conclusions

This paper has investigated the analytical solutions of the mathematical model of dengue fever by applying an approximate method called the Adomian Decomposition

Method. The solutions obtained using this method are approximate series solutions. The following remarks have been drawn:

1. The study verifies that the use of a fractional-order differential model offers a more realistic representation of dengue fever transmission dynamics than integer-order models. The inclusion of memory effects and hereditary properties enhances prediction accuracy and supports improved control strategies.
2. The simulations reveal that smaller fractional orders (α) lead to longer disease persistence due to stronger memory effects, while larger α values result in faster infection reduction. This demonstrates that interventions altering the transmission rate significantly influence disease development.
3. The study confirms that infected mosquito populations closely follow the patterns of human infections. High values of α lead to explosive vector transmission, validating the need for mosquito control measures, such as the use of insecticides and the elimination of breeding sites.
4. The outcomes show that an increase in recovery corresponds to a decline in both symptomatic and asymptomatic infections.

The Government of India published National Guidelines for Clinical Management of Dengue Fever [36] to highlight key public health suggestions for the control and management of dengue fever. These suggestions included early case detection and categorization for early treatment, public education about warning signs and mosquito control, and enhancement of primary healthcare systems for early diagnosis and referral. The guidelines endorse careful fluid management, especially during the critical period, and discourage the use of nonsteroidal anti-inflammatory drugs (NSAIDs) due to the threat of bleeding. Special caution is exercised in vulnerable groups such as children, pregnant women, and those with the presence of comorbidities. Intensive surveillance, vector control, and public awareness campaigns are also essential components of India's dengue control program.

Author Contributions: Conceptualization, A.S.R., S.M.M. and R.S.; methodology, M.M.M., S.M.M. and R.S.; validation, A.S.R. and M.M.M.; formal analysis, A.S.R., M.M.M., S.M.M. and R.S.; investigation, M.M.M. and S.M.M.; writing—original draft preparation, A.S.R., M.M.M., S.M.M. and R.S.; writing—review and editing, A.S.R. and S.M.M.; visualization, A.S.R. and M.M.M. All authors have read and agreed to the published version of the manuscript.

Funding: This research received no external funding.

Data Availability Statement: The authors confirm that the data supporting the findings of this study are available within the article.

Conflicts of Interest: The authors declare no conflict of interest.

Nomenclature

N_h	constant host (human) population size
S_h	number of susceptible in host population
S_{hk}	number of susceptible with partial immunity in host population
I_h	number of symptomatic infected in host population
I_{hA}	number of asymptomatic infected in host population
R_h	number of recovered in host population
N_v	vector (mosquito) population size
S_v	number of susceptible in the vector population
I_v	number of infectives in the vector population

References

1. Eegunjobi, A.S.; Anyanwu, M.C.; Neossi-Nguetchue, S.N. Modelling the super-infection of two strains of dengue virus. *J. Egypt. Math. Soc.* **2023**, *31*, 1. [CrossRef]
2. Ogunlade, S.T.; Meehan, M.T.; Adekunle, A.I.; McBryde, E.S. A systematic review of mathematical models of dengue transmission and vector control: 2010–2020. *Viruses* **2023**, *15*, 254. [CrossRef] [PubMed]
3. Aguiar, M.; Anam, V.; Blyuss, K.B.; Estadilla, C.D.S.; Guerrero, B.V.; Knopoff, D.; Kooi, B.W.; Srivastav, A.K.; Steindorf, V.; Stollenwerk, N. Mathematical models for dengue fever epidemiology: A 10-year systematic review. *Phys. Life Rev.* **2022**, *40*, 65–92. [CrossRef] [PubMed]
4. Naaly, B.Z.; Marijani, T.; Isdory, A.; Ndendya, J.Z. Mathematical modeling of the effects of vector control, treatment and mass awareness on the transmission dynamics of dengue fever. *Comput. Methods Programs Biomed. Update* **2024**, *6*, 100159. [CrossRef]
5. El-Sayed, A.M.; Arafa, A.A.; Hanafy, I.M.; Gouda, M.I. A Fractional-Order Model of Dengue Fever with Awareness Effect: Numerical Solutions and Asymptotic Stability Analysis. *Progr. Fract. Differ. Appl.* **2022**, *8*, 267–274.
6. Dwivedi, A.; Keval, R. Analysis for transmission of dengue disease with different class of human population. *Epidemiol. Methods* **2021**, *10*, 20200046. [CrossRef]
7. Lin, S.; Cao, X.; Zheng, H.; Li, Y.; Li, W. An improved meshless numerical manifold method for simulating complex boundary seepage problems. *Comput. Geotech.* **2023**, *155*, 105211. [CrossRef]
8. Fendzi-Donfack, E.; Kumar, D.; Tala-Tebue, E.; Nana, L.; Nguenang, J.P.; Kenfack-Jiotsa, A. Construction of exotical soliton-like for a fractional nonlinear electrical circuit equation using differential-difference Jacobi elliptic functions sub-equation method. *Results Phys.* **2022**, *32*, 105086. [CrossRef]
9. Abdulazeez, S.T.; Modanli, M. Solutions of fractional order pseudo-hyperbolic telegraph partial differential equations using finite difference method. *Alex. Eng. J.* **2022**, *61*, 12443–12451. [CrossRef]
10. Ali, K.K.; Wazwaz, A.-M.; Osman, M. Optical soliton solutions to the generalized nonautonomous nonlinear Schrödinger equations in optical fibers via the sine-Gordon expansion method. *Optik* **2020**, *208*, 164132. [CrossRef]
11. Ouahid, L.; Owyed, S.; Abdou, M.; Alshehri, N.A.; Elagan, S. New optical soliton solutions via generalized Kudryashov's scheme for Ginzburg–Landau equation in fractal order. *Alex. Eng. J.* **2021**, *60*, 5495–5510. [CrossRef]
12. Fendzi-Donfack, E.; Temgoua, G.W.K.; Djoufack, Z.I.; Kenfack-Jiotsa, A.; Nguenang, J.P.; Nana, L. Exotical solitons for an intrinsic fractional circuit using the sine-cosine method. *Chaos Solitons Fractals* **2022**, *160*, 112253. [CrossRef]
13. Mohamed, N.A.; Rashed, A.S.; Melaibari, A.; Sedighi, H.M.; Eltaher, M.A. Effective numerical technique applied for Burgers' equation of (1+1)-, (2+1)-dimensional, and coupled forms. *Math. Methods Appl. Sci.* **2021**, *44*, 10135–10153. [CrossRef]
14. Rashed, A.S.; Inc, M.; Saleh, R. Extensive novel waves evolution of three-dimensional Yu–Toda–Sasa–Fukuyama equation compatible with plasma and electromagnetic applications. *Mod. Phys. Lett. B* **2023**, *37*, 2250195. [CrossRef]
15. Mohamed, M.; Mabrouk, S.M.; Rashed, A.S. Mathematical Investigation of the Infection Dynamics of COVID-19 Using the Fractional Differential Quadrature Method. *Computation* **2023**, *11*, 198. [CrossRef]
16. Rashed, A.S.; Mostafa, A.N.M.; Mabrouk, S.M. Abundant families of solutions for (4+1)-dimensional Fokas fractional differential equation using New sub-equation method. *Sci. Afr.* **2024**, *23*, e02107. [CrossRef]
17. Eguda, F.; Andrawus, J.; Babuba, S. The Solution of a Mathematical Model for Dengue Fever Transmission Using Differential Transformation Method. *J. Niger. Soc. Phys. Sci.* **2019**, *1*, 82–87. [CrossRef]
18. Agarwal, P.; Singh, R.; Ul Rehman, A. Numerical solution of hybrid mathematical model of dengue transmission with relapse and memory via Adam–Bashforth–Moulton predictor-corrector scheme. *Chaos Solitons Fractals* **2021**, *143*, 110564. [CrossRef]
19. Eguda, A.J.; Yakubu, F. Analysis of a mathematical model to investigate the dynamics of dengue fever. *J. Appl. Sci. Environ. Manag.* **2017**, *21*, 626–638. [CrossRef]
20. Wan, H.; Xu, J. How Does the Enhanced Mortality of *Wolbachia*-Infected Immature Mosquitoes Affect Dengue Transmission? *Int. J. Biomath.* **2024**, 2450045. [CrossRef]
21. Wang, Z.; Cai, S.; Chen, G.; Zheng, K.; Wei, F.; Jin, Z.; Mao, X.; Xie, J. Dynamics of a Dengue Transmission Model with Multiple Stages and Fluctuations. *Mathematics* **2024**, *12*, 2491. [CrossRef]
22. Zhang, X.; Tang, S.; Cheke, R.A.; Zhu, H. Modeling the Effects of Augmentation Strategies on the Control of Dengue Fever with an Impulsive Differential Equation. *Bull. Math. Biol.* **2016**, *78*, 1968–2010. [CrossRef] [PubMed]
23. Jan, R.; Khan, M.A.; Kumam, P.; Thounthong, P. Modeling the transmission of dengue infection through fractional derivatives. *Chaos Solitons Fractals* **2019**, *127*, 189–216. [CrossRef]
24. Jajarmi, A.; Arshad, S.; Baleanu, D. A new fractional modelling and control strategy for the outbreak of dengue fever. *Phys. A Stat. Mech. Its Appl.* **2019**, *535*, 122524. [CrossRef]
25. Jan, R.; Khan, M.A.; Khan, Y.; Ullah, S. A new model of dengue fever in terms of fractional derivative. *Math. Biosci. Eng.* **2020**, *17*, 5267–5287. [CrossRef]
26. Srivastava, H.M.; Jan, R.; Jan, A.; Deebani, W.; Shutaywi, M. Fractional-calculus analysis of the transmission dynamics of the dengue infection. *Chaos Interdiscip. J. Nonlinear Sci.* **2021**, *31*, 053130. [CrossRef]

27. Boulaaras, S.; Jan, R.; Khan, A.; Ahsan, M. Dynamical analysis of the transmission of dengue fever via Caputo-Fabrizio fractional derivative. *Chaos Solitons Fractals X* **2022**, *8*, 100072. [CrossRef]
28. Gurung, D. Mathematical Model of Dengue Fever with and without awareness in Host Population. *Int. J. Adv. Eng. Res. Appl. (IJAERA)* **2015**, *1*, 239.
29. Andraud, M.; Hens, N.; Marais, C.; Beutels, P. Dynamic epidemiological models for dengue transmission: A systematic review of structural approaches. *PLoS ONE* **2012**, *7*, e49085. [CrossRef]
30. Garba, S.M.; Gumel, A.B.; Abu Bakar, M.R. Backward bifurcations in dengue transmission dynamics. *Math. Biosci.* **2008**, *215*, 11–25. [CrossRef]
31. Tatari, M.; Dehghan, M.; Razzaghi, M. Application of the Adomian decomposition method for the Fokker–Planck equation. *Math. Comput. Model.* **2007**, *45*, 639–650. [CrossRef]
32. Wazwaz, A.-M. A reliable modification of Adomian decomposition method. *Appl. Math. Comput.* **1999**, *102*, 77–86. [CrossRef]
33. Khan, M.A.; Atangana, A. Modeling the dynamics of novel coronavirus (2019-nCov) with fractional derivative. *Alex. Eng. J.* **2020**, *59*, 2379–2389. [CrossRef]
34. Nazir, G.; Zeb, A.; Shah, K.; Saeed, T.; Khan, R.A.; Ullah Khan, S.I. Study of COVID-19 mathematical model of fractional order via modified Euler method. *Alex. Eng. J.* **2021**, *60*, 5287–5296. [CrossRef]
35. Ullah, Z. Analytical Solution of the Mathematical Model of Dengue Fever by the Laplace Adomian Decomposition Method. *Commun. Nonlinear Anal.* **2023**, *2*, 1–17.
36. National Center for Vector Borne Diseases Control-India. National Guidelines for Clinical Management of Dengue Fever. 2023. Available online: https://ncvbdc.mohfw.gov.in (accessed on 15 May 2025).

Disclaimer/Publisher's Note: The statements, opinions and data contained in all publications are solely those of the individual author(s) and contributor(s) and not of MDPI and/or the editor(s). MDPI and/or the editor(s) disclaim responsibility for any injury to people or property resulting from any ideas, methods, instructions or products referred to in the content.

axioms

MDPI

Article

Existence and Uniqueness of Solutions for Singular Fractional Integro-Differential Equations with p-Laplacian and Two Kinds of Fractional Derivatives

Fang Wang [1], Lishan Liu [1,2,*], Haibo Gu [2], Lina Ma [2] and Yonghong Wu [3]

[1] School of Mathematical Sciences, Qufu Normal University, Qufu 273165, China; wangfangmath@qfnu.edu.cn
[2] School of Mathematical Sciences, Xinjiang Normal University, Urumqi 830017, China; hbgu_math@163.com (H.G.); mln@xjnu.edu.cn (L.M.)
[3] Department of Mathematics and Statistics, Curtin University, Perth, WA 6845, Australia; y.wu@curtin.edu.au
* Correspondence: mathlls@163.com or lls@qfnu.edu.cn

Abstract

The paper is devoted to the study of a class of singular high-order fractional integro-differential equations with p-Laplacian operator, involving both the Riemann–Liouville fractional derivative and the Caputo fractional derivative. First, we investigate the problem by the method of reducing the order of fractional derivative. Then, by using the Schauder fixed point theorem, the existence of solutions is proved. The upper and lower bounds for the unique solution of the problem are established under various conditions by employing the Banach contraction mapping principle. Furthermore, four numerical examples are presented to illustrate the applications of our main results.

Keywords: p-Laplacian operator; fractional integro-differential equations; Riemann–Liouville and Caputo fractional derivative; Riemann–Stieltjes integral boundary conditions; infinite point boundary conditions

MSC: 26A33; 34A08; 34B16

1. Introduction

In recent years, fractional boundary value problems have appeared widely in many fields of science, such as the characterization of the behavior for viscoelastic materials [1], the development of algorithms for signal and image processing [2], and so on. To cite a specific instance, by introducing fractional derivatives to describe the relationship between strain and strain force, in [3], the author introduced fractional models to describe the creep, stress relaxation, and hysteresis of viscoelastic materials by incorporating fractional derivatives into the relationship between strain and stress. The theoretical results obtained are closer to the actual situation, which provides an important theoretical basis for the study of the properties of actual viscoelastic materials. Many scholars have conducted in-depth and extensive research in this field [4–8], and they have obtained significant results for the heat equation [9], the impulsive problem [10], and the system [11].

In addition, as a crucial tool for modeling fluid mechanics, the p-Laplacian equations have been studied by many researchers [12–16]. For example, Turbulence is a state of fluid flow in physics, and the study of turbulent characteristics in porous media has always been a hot topic in the field. Since this process is influenced by many parameters, research on turbulent flow fields in porous media is extremely complex. Therefore, modeling this

process has remained a key issue both domestically and internationally. In [12], the author introduced the following differential equation with a p-Laplacian operator to describe the mechanical phenomenon of turbulence in porous media:

$$(\phi_p(u'(t)))' = f(t, u(t), u'(t)).$$

This work represented a significant step forward in the study of p-Laplacian differential equations. Specifically, the introduction of the p-Laplacian operator into fractional differential equations has been a key development, which has increasingly become a hot topic in research.

In the case of problems containing a type of fractional derivative, the existence and uniqueness of solutions have been extensively studied. In particular, the Riemann–Liouville fractional differential equations have been received considerable attention. For example, in [17] the author considered the following problem:

$$\begin{cases} D_{0+}^{\beta}\phi_p(D_{0+}^{\alpha}u(t)) = f(t, u(t)), \quad 0 < t < 1, \\ u(0) = 0,\ D_{0+}^{\gamma}u(1) = \sum_{i=1}^{m-2} \xi_i D_{0+}^{\gamma}u(\eta_i), \\ D_{0+}^{\alpha}u(0) = 0,\ \phi_p(D_{0+}^{\alpha}u)(1) = \sum_{i=1}^{m-2} \rho_i \phi_p(D_{0+}^{\alpha}u)(\eta_i), \end{cases}$$

where $1 < \alpha,\ \beta \leq 2,\ 3 < \alpha + \beta \leq 4,\ 0 < \gamma \leq 1,\ \alpha - \gamma > 1,\ 0 < \xi_i, \rho_i, \eta_i \leq 1$, $\sum_{i=1}^{m-2} \xi_i \eta_i^{\alpha-\gamma-1} < 1, \sum_{i=1}^{m-2} \rho_i \eta_i^{\alpha-\gamma-1} < 1, f : [0,1] \times \mathbb{R}_+ \to \mathbb{R}_+$ is continuous.

By using the Banach contraction mapping principle, the author established the uniqueness result for this problem. Further, by using the fixed point theorem of mixed monotone operators, in [18], the authors obtained the existence of positive solutions to the same problem. Building on this foundation, the study in [19] extended the analysis to a class of fractional differential equations with a generalized Laplacian operator. Following a methodology similar to [19], the work in [20] further incorporated a fractional integral operator into the nonlinear term. In contrast, in [21], the authors introduced a fractional derivative in the nonlinear term, which necessitated an analysis within a function space framework distinct from that employed in the preceding works.

On the other hand, fractional differential equations involving the Caputo derivative have also been investigated. For instance, in [22], the authors investigated a class of integro-differential equations by applying the generalized contraction principle. Subsequently, the studies presented in [23,24] extended the research to the existence of positive solutions. Furthermore, the works in [25,26] made significant strides by establishing both the existence and uniqueness of solutions. While the authors of [27] investigated the generalized system of fractional differential equations, the study in [28] focused on a class of generalized Caputo fractional boundary value problems. It is worth noting that the analyses in [23–25] were particularly complex due to the inclusion of derivatives of functions in their nonlinear terms. Moreover, the impulsive problem addressed in [25] contributed to the analytical complexity of the study.

In contrast to the aforementioned studies, in [29], the author studied the following initial value problem:

$$\begin{cases} {}^{c}D_{0+}^{\beta}(\phi_p({}^{c}D_{0+}^{\alpha}x(t))) = t^{-\gamma}f(t, x(t)) \quad 0 < t < 1, \\ x(0) = x_0,\ ({}^{c}D_{0+}^{\alpha}x)(0) = x_{\alpha},\ x_0, x_{\alpha} \in \mathbb{R}, \end{cases}$$

where $0 \leq \gamma < \alpha, \beta \leq 1$, $f : [0,1] \times \mathbb{R} \to \mathbb{R}$ is continuous. By means of the Schaefer's fixed point theorem, the authors established existence results for this problem.

Specifically, the various types of multi-point boundary value problems are an active area of research [25,26,30–32]. For instance, in [26], the authors studied the existence and uniqueness of solutions to the following problems:

$$\begin{cases} (r\,{}^cD_{0+}^{\sigma_1} + (1-r)I_{0+}^{\sigma_2})z(t) = f(t,z(t)) + {}^cD_{0+}^{\sigma_3}g(t,z(t)), \quad 0 \leq t \leq T, \\ z(0) = 0, \\ r({}^cD_{0+}^{\nu_1}z)(T) + (1-r)({}^cD_{0+}^{\nu_2}z)(T) = a_0, \end{cases}$$

where $\sigma_1, \sigma_3 \in (1,2]$ $(\sigma_1 > \sigma_3)$, $\sigma_2 \in (0,1]$, $0 < \nu_1, \nu_2 < \sigma_1 - \sigma_3$, $r \in [0,1]$, $f, g : [0,T] \times \mathbb{R} \to \mathbb{R}$ are continuous. The authors provided examples and presented numerical data in tables and figures to demonstrate the theoretical results.

It is worth mentioning that in [33], the authors investigated fixed point theorems in a class of generalized metric spaces and applied them to a type of nonlinear fractional differential equation problem, which represented a highly novel field of research. Recently, in [34], the authors investigated the following problem with generalized Caputo fractional derivative:

$$\begin{cases} {}_c^{\varrho}D_{0+}^{\sigma}x(t) = -f(t,x(t)), \quad \theta \leq t \leq \vartheta, \\ x(\theta) = \lambda_1,\ x(\vartheta) = \lambda_2. \end{cases}$$

where $1 < \sigma \leq 2$, $f : [\theta, \vartheta] \times \mathbb{R} \to \mathbb{R}$ is continuous. The authors proved the uniqueness of the solution by applying the Banach contraction mapping principle under the condition that the nonlinear term satisfies the Lipschitz condition. It is worth noting that the authors verified the theoretical results through an approximate approach to the parameter.

Furthermore, the problems, which contain two types of fractional derivatives, have been studied recently. For instance, building upon the work of [35], in [36], the authors investigated the following problem:

$$\begin{cases} D_{0+}^{\alpha}\phi_p({}^cD_{0+}^{\beta}u(t)) = f(t,u(t),{}^cD_{0+}^{\beta}u(t)), \quad 0 < t < 1, \\ ({}^cD_{0+}^{\beta}u)(0) = u'(0) = 0, \\ u(1) = r_1u(\eta),\ ({}^cD_{0+}^{\beta}u)(1) = r_2({}^cD_{0+}^{\beta}u)(\xi), \end{cases}$$

where $\alpha, \beta \in (1,2]$, $r_1, r_2 > 2$, $f : [0,1] \times [0,+\infty) \times (-\infty,0] \to [0,+\infty)$ is continuous. By the method of lower and upper solutions, the authors obtained the existence of positive solutions. In [37], the authors applied the same method to a class of integral boundary value problems. Building upon [36], the work in [38] modified the boundary conditions and successfully established the existence of at least three positive solutions using the Leggett–Williams fixed point theorem. Subsequently, in [39], the authors extended the research scope significantly by generalizing the mixed derivative problem to a system of fractional differential equations. Further, in [40], the authors combined the quantum fractional derivative with the Riemann–Liouville derivative, applying the same method as in [38] to investigate multiple positive solutions.

Inspired by the above-mentioned work, we study the following fractional boundary value problem involving the p-Laplacian operator:

$$\begin{cases} -{}^{c}D_{0+}^{\delta}\phi_p(D_{0+}^{\alpha}u(t)) + f(t,u(t),(Hu)(t),D_{0+}^{\beta}u(t)) = 0, \quad 0 < t < 1, \\ u(0) = D_{0+}^{\gamma_1}u(0) = \cdots = D_{0+}^{\gamma_{n-2}}u(0) = 0, \\ D_{0+}^{\alpha}u(0) = 0, \quad (\phi_p(D_{0+}^{\alpha}u))''(0) = 0, \\ \phi_p(D_{0+}^{\alpha}u(1)) = k_0\int_0^1 b_0(s)\phi_p(D_{0+}^{\alpha}u(s))ds, \\ D_{0+}^{z_0}u(1) = k_1\int_0^1 b_1(s)D_{0+}^{z_1}u(s)dA_1(s) + k_2\int_0^{\zeta} b_2(s)D_{0+}^{z_2}u(s)dA_2(s) \\ \qquad\qquad + k_3\sum_{i=1}^{\infty} a_i D_{0+}^{z_3}u(\xi_i), \end{cases} \tag{1}$$

where $2 < \delta \le 3$, $n-1 < \alpha \le n$ $(n \ge 3)$, $n-3 < \beta \le n-2$, $1 < \alpha - \beta \le 2$, $j-1 < \gamma_j \le j$ $(j = 1,2,\ldots,n-2)$, $\beta - \gamma_j \le n-2-j$ $(j = 1,2,\ldots,n-2)$, $\beta \le z_l \le z_0 \le \alpha - 1$ $(l = 1,2,3)$; $k_l \ge 0$ $(l = 0,1,2,3)$, $0 < \zeta \le 1$, $a_i \ge 0$, $0 < \xi_i < 1$ $(i = 1,2,\ldots)$; $b_l \in L^1(0,1)$, $b_l : (0,1) \to \mathbb{R}_+$ $(l = 0,1,2)$ is continuous, $(Hu)(t) = \int_0^t h(t,s)u(s)ds$ with the bounded function $h \in L^1(0,1)$, $h : (0,1) \to \mathbb{R}_+$ is continuous, and $\int_0^1 \cdot dA_i(s)$ represent the standard Riemann–Stieltjes integral, in which $A_i : [0,1] \to \mathbb{R}$ $(i = 1,2)$ is function of bounded variation and $f : (0,1) \times \mathbb{R}^3 \to \mathbb{R}$ is continuous.

Remark 1. *In this paper, we always use the following notation:* ${}^{c}D_{0+}^{\alpha}$ *denotes the Caputo fractional derivative of order* α, D_{0+}^{β} *denotes the Riemann–Liouville fractional derivative of order* β, ϕ_p *denotes the p-Laplacian operator as* $\phi_p(s) = |s|^{p-2}s$ *with* $p > 1$, *and the inverse function of* ϕ_p *is* $\phi_q(x) = |x|^{q-2}x$ *with* $1/p + 1/q = 1$.

Let $x(t) = D_{0+}^{\beta}u(t)$, $t \in [0,1]$. Then, the problem (1) changes to the following problem:

$$\begin{cases} -{}^{c}D_{0+}^{\delta}\phi_p(D_{0+}^{\alpha-\beta}x(t)) + f(t,I_{0+}^{\beta}x(t),(\mathcal{H}x)(t),x(t)) = 0, \quad 0 < t < 1, \\ D_{0+}^{\gamma_{n-2}-\beta}x(0) = 0, \\ D_{0+}^{\alpha-\beta}x(0) = 0, \quad (\phi_p(D_{0+}^{\alpha-\beta}x))''(0) = 0, \\ \phi_p(D_{0+}^{\alpha-\beta}x(1)) = k_0\int_0^1 b_0(s)\phi_p(D_{0+}^{\alpha-\beta}x(s))ds, \\ D_{0+}^{z_0-\beta}x(1) = k_1\int_0^1 b_1(s)D_{0+}^{z_1-\beta}x(s)dA_1(s) \\ \qquad\qquad + k_2\int_0^{\zeta} b_2(s)D_{0+}^{z_2-\beta}x(s)dA_2(s) \\ \qquad\qquad + k_3\sum_{i=1}^{\infty} a_i D_{0+}^{z_3-\beta}x(\xi_i), \end{cases} \tag{2}$$

where $1 < \alpha - \beta \le 2$, $(\mathcal{H}x)(t) = \int_0^t h(t,s)I_{0+}^{\beta}x(s)ds$.

The innovation of our paper includes the following four points. First of all, as far as we know, there has been no research focusing on the problem (1) with more complex boundary conditions. The key characteristic of the problem (1) is that it involves two kinds of fractional derivatives, and the nonlinear term contains both integral operator and fractional derivatives. In the process of reducing the order of problem (1) in Lemma 5, since two types of fractional derivatives need to be considered, and the boundary conditions simultaneously involve integral and infinite-point conditions, the difficulty of the order reduction analysis is increased. On the other hand, the complexity of the boundary conditions leads to a rather cumbersome form of the Green's function, which also complicates the proof process of Lemma 9 and Lemma 10. It is necessary to carefully

consider the relationship of the relevant parameters to ensure the acquisition of good properties of the solution.

Secondly, by the method of reduction of order, we transform the problem (1) into a new equivalent lower-order problem (2), in which the nonlinear term has no fractional derivative. Accordingly, we denote the Banach space $C[0,1]$ with the norm

$$\|x\| = \sup_{0\le t\le 1} |x(t)|.$$

As a result, we discuss the problem (2) in the space $C[0,1]$, whereas the problem (1) requires consideration in a complex functional space endowed with fractional derivatives. For details of the method of reduction of order, we refer the readers to [41–45] and so on. If the reduced-order method is not employed, all arguments must be developed within the more complex space $Y = \{x | x \in C[0,1], D^{\beta}_{0^+} x \in C[0,1]\}$ with the norm

$$\|x\| = \sup_{0\le t\le 1} |x(t)| + \sup_{0\le t\le 1} |D^{\beta}_{0^+} x(t)|.$$

This necessitates the prior establishment of several key properties of the operator $(D^{\beta}_{0^+} T)$, whether by applying the Schauder fixed point theorem in Theorem 1 or the Banach contraction mapping principle in Theorems 2–5. Consequently, the process entails considerably heavier computations and greater theoretical difficulty.

Thirdly, as far as we know, many studies have established uniqueness results for p-Laplacian boundary value problems by using the Banach contraction mapping principle. In this case, the nonlinear term is required to satisfy the Lipschitz condition, cf. [17,35,46]. In fact, a function $g : [0,1] \times I \to \mathbb{R}$ is said to satisfy the Lipschitz condition on the interval I if there exists a constant $L > 0$ such that

$$|g(t,x_1) - g(t,x_2)| \le L|x_1 - x_2|, \quad \forall\, x_1, x_2 \in I,\ t \in [0,1].$$

This condition implies that g is uniformly continuous on I. This is a very strong condition, so its applications are limited in many studies. However, we obtain the uniqueness results for the problem (1) under more general conditions, which allow the nonlinear term to be singular at time variables $t = 0$ and $t = 1$. In the proofs of Theorems 2–5, we relax the classical Lipschitz condition by allowing the constant to be a function, thereby accommodating certain singularities in the nonlinear term. Using the integrability of the Lipschitz function, we have proved the conclusion.

Finally, it is worth pointing out that the estimation of solutions for the problem (1) has not been considered before. Especially, the validity of the results is proved by numerical examples.

Due to the complexity of the problem (1), the examples constructed in Section 5 must incorporate numerous parameters, resulting in a sophisticated case study. We hope that these examples can offer practical guidance for real-world problems.

The rest of the paper is organized as follows. In Section 2, we present some relevant definitions and lemmas, transform the problem (1) into an equivalent low-order problem (2), and obtain some significant properties of the relevant Green's function. In Section 3, we give the main proof for the existence results of the problem (1). In Section 4, we establish the uniqueness result of the problem (1). In Section 5, we give four numerical examples to illustrate our theoretical results.

2. Preliminaries and Lemmas

Definition 1. *The Riemann–Liouville fractional integral of order $v > 0$ of a function $u : (0, \infty) \to \mathbb{R}$ is given by*

$$I_{0^+}^{v} u(t) = \frac{1}{\Gamma(v)} \int_0^t (t - \eta)^{v-1} u(\eta) d\eta,$$

where the right-hand side exists a.e. on $(0, \infty)$.

Definition 2. *The Riemann–Liouville fractional derivative of order $v > 0$ of a continuous function $u : (0, \infty) \to \mathbb{R}$ is given by*

$$D_{0^+}^{v} u(t) = \left(\frac{d}{dt}\right)^n I_{0^+}^{n-v} u(t),$$

where the right-hand side exists a.e. on $(0, \infty)$, where $n - 1 < v < n$ (n is a positive integer). In particular, if $v = n$, then $D_{0^+}^{v} u(t) = u^{(n)}(t)$.

Definition 3. *The Caputo fractional derivative of order $v > 0$ of a continuous function $u : (0, \infty) \to \mathbb{R}$ is given by*

$${}^{c}D_{0^+}^{v} u(t) = I_{0^+}^{n-v} u^{(n)}(t),$$

with the right-hand side pointwise defined on $(0, \infty)$, $n - 1 < v < n$ (n is a positive integer). In particular, if $v = n$, then ${}^{c}D_{0^+}^{v} u(t) = u^{(n)}(t)$.

Lemma 1 ([47]). *Let $u \in C(0, 1) \cap L^1(0, 1)$. Then, the equation*

$$D_{0^+}^{v} u(t) = 0$$

has

$$u(t) = \sum_{i=1}^{n} b_i t^{v-i},$$

as the unique solution, where $n - 1 < v \leq n$ (n is a positive integer), $b_1, \cdots, b_n \in \mathbb{R}$.

Lemma 2 ([47]). *Let $u, D_{0^+}^{v} u \in C(0, 1) \cap L^1(0, 1)$. Then,*

$$I_{0^+}^{v} D_{0^+}^{v} u(t) = u(t) + \sum_{i=1}^{n} b_i t^{v-i},$$

where $n - 1 < v \leq n$ (n is a positive integer), $b_1, \cdots, b_n \in \mathbb{R}$.

Lemma 3 ([4]). *Let $u \in AC^n[0, 1]$. Then,*

$$I_{0^+}^{v} {}^{c}D_{0^+}^{v} u(t) = u(t) + \sum_{i=0}^{n-1} b_i t^i,$$

where $n - 1 < v \leq n$ (n is a positive integer), $b_0, \cdots, b_{n-1} \in \mathbb{R}$.

Lemma 4 ([4]). *If $u \in L^1(0, 1)$, $v_1 \geq v_2 > 0$, then*

$$D_{0^+}^{v_1} I_{0^+}^{v_1} u(t) = u(t), \quad D_{0^+}^{v_2} I_{0^+}^{v_1} u(t) = I_{0^+}^{v_1 - v_2} u(t).$$

Lemma 5. *Suppose that $u \in C[0, 1]$ is a solution of the problem* (1)*, then $x = D_{0^+}^{\beta} u$ is a solution of the problem* (2)*. Conversely, if $x \in C[0, 1]$ is a solution of the problem* (2)*, then $u = I_{0^+}^{\beta} x$ is a solution of the problem* (1)*.*

Proof. Let $x = D^{\beta}_{0^+}u$, where $u \in C[0,1]$ is a solution of the problem (1). By Lemma 2, we have

$$u(i) = I^{\beta}_{0^+}x(t) - c_1t^{\beta-1} - \ldots - c_{n-2}t^{\beta-(n-2)}, \quad c_i \in \mathbb{R},\ i = 1,2,\cdots,n-2.$$

Since $u(0) = D^{\gamma_1}_{0+}u(0) = \cdots = D^{\gamma_{n-3}}_{0+}u(0) = 0$, we obtain $c_{n-2} = \cdots = c_1 = 0$. It follows that

$$u(t) = I^{\beta}_{0^+}x(t), \quad t \in [0,1]. \tag{3}$$

Consequently, it follows that

$$(Hu)(t) = \int_0^t h(t,s)u(s)ds = \int_0^t h(t,s)I^{\beta}_{0^+}x(s)ds = (\mathcal{H}x)(t), \tag{4}$$

$$\begin{aligned} D^{\alpha}_{0^+}u(t) &= \frac{d^n}{dt^n}I^{n-\alpha}_{0^+}u(t) = \frac{d^n}{dt^n}I^{n-\alpha}_{0^+}(I^{\beta}_{0^+}x(t)) = \frac{d^n}{dt^n}I^{n-(\alpha-\beta)}_{0^+}x(t) \\ &= \frac{d^2}{dt^2}\left(\frac{d^{n-2}}{dt^{n-2}}I^{n-2}_{0^+}\right)I^{2-(\alpha-\beta)}_{0^+}x(t) \\ &= \frac{d^2}{dt^2}I^{2-(\alpha-\beta)}_{0^+}x(t) \\ &= D^{\alpha-\beta}_{0^+}x(t) \end{aligned} \tag{5}$$

and

$$D^{\gamma_{n-2}}_{0+}u(t) = D^{\gamma_{n-2}-\beta}_{0+}x(t),\ D^{z_i}_{0^+}u(t) = D^{z_i-\beta}_{0^+}x(t),\ i = 0,1,2,3. \tag{6}$$

From (3), (4) and (5), we have

$$\begin{aligned} &{}^cD^{\delta}_{0+}\phi_p(D^{\alpha-\beta}_{0+}x(t)) - f(t, I^{\beta}_{0+}x(t), (\mathcal{H}x)(t), x(t)) \\ &= {}^cD^{\delta}_{0+}\phi_p(D^{\alpha}_{0+}u(t)) - f(t, u(t), (Hx)(t), D^{\beta}_{0+}u(t)) = 0, \end{aligned} \tag{7}$$

$$D^{\alpha-\beta}_{0+}x(0) = D^{\alpha}_{0+}u(0) = 0, \quad (\phi_p(D^{\alpha-\beta}_{0+}x))''(0) = (\phi_p(D^{\alpha}_{0+}u))''(0) = 0 \tag{8}$$

and

$$\begin{aligned} \phi_p(D^{\alpha-\beta}_{0+}x(1)) &= \phi_p(D^{\alpha}_{0+}u(1)) \\ &= k_0\int_0^1 b_0(s)\phi_p(D^{\alpha}_{0+}u(s))ds, \\ &= k_0\int_0^1 b_0(s)\phi_p(D^{\alpha-\beta}_{0+}x(s))ds. \end{aligned} \tag{9}$$

By using (6), we obtain

$$D^{\gamma_{n-2}-\beta}_{0+}x(0) = D^{\gamma_{n-2}}_{0+}u(0) = 0 \tag{10}$$

and

$$\begin{aligned} D^{z_0-\beta}_{0+}x(1) =& k_1\int_0^1 b_1(s)D^{z_1-\beta}_{0+}x(s)dA_1(s) + k_2\int_0^{\eta} b_2(s)D^{z_2-\beta}_{0+}x(s)dA_2(s) \\ &+ k_3\sum_{i=1}^{\infty} a_iD^{z_3-\beta}_{0+}x(\xi_i). \end{aligned} \tag{11}$$

Combining (7)–(11), we conclude that $x = D^{\beta}_{0^+}u$ is a solution of the problem (2).

Conversely, let $x \in C[0,1]$ be a solution of the problem (2). Then, $u = I_{0+}^{\beta} x$ is a solution of the problem (1). Since the proof is similar to that of Lemma 3 in [44], we omit it here. □

Remark 2. *According to Lemma 5, we deduce that, under the assumption that* $1 < \alpha - \beta \leq 2$, *the problem* (1) *is equivalent to the problem* (2). *Consequently, we focus on establishing the results for the problem* (2) *in the following.*

Lemma 6. *Let* $W \in C(0,1) \cap L^1(0,1)$. *Then, the problem*

$$\begin{cases} D_{0+}^{\alpha-\beta} x(t) + W(t) = 0, \quad 0 < t < 1, \quad 1 < \alpha - \beta \leq 2, \\ D_{0+}^{\gamma_n - 2 - \beta} x(0) = 0, \\ D_{0+}^{z_0 - \beta} x(1) = k_1 \displaystyle\int_0^1 b_1(s) D_{0+}^{z_1 - \beta} x(s) dA_1(s) \\ \qquad\qquad + k_2 \displaystyle\int_0^{\zeta} b_2(s) D_{0+}^{z_2 - \beta} x(s) d\Lambda_2(s) \\ \qquad\qquad + k_3 \displaystyle\sum_{i=1}^{\infty} a_i D_{0+}^{z_3 - \beta} x(\xi_i), \end{cases} \tag{12}$$

has a unique solution

$$x(t) = \int_0^1 G(t,s) W(s) ds,$$

where

$$\begin{aligned} G(t,s) =& P_0(t,s) + t^{\alpha-\beta-1} \left(\int_0^1 P_1(\tau,s) b_1(\tau) dA_1(\tau) \right) \\ &+ t^{\alpha-\beta-1} \left(\int_0^{\zeta} P_2(\tau,s) b_2(\tau) dA_2(\tau) \right) \\ &+ t^{\alpha-\beta-1} \sum_{i=1}^{\infty} a_i P_3(\xi_i, s), \end{aligned} \tag{13}$$

in which

$$P_0(t,s) = \frac{1}{\Gamma(\alpha-\beta)} \begin{cases} t^{\alpha-\beta-1}(1-s)^{\alpha-z_0-1} - (t-s)^{\alpha-\beta-1}, & s \leq t, \\ t^{\alpha-\beta-1}(1-s)^{\alpha-z_0-1}, & t \leq s, \end{cases} \tag{14}$$

$$P_i(t,s) = \frac{k_i}{\sigma_1 \Gamma(\alpha-\beta)\Gamma(\alpha-z_i)} \begin{cases} t^{\alpha-z_i-1}(1-s)^{\alpha-z_0-1} - (t-s)^{\alpha-z_i-1}, & s \leq t, \\ t^{\alpha-z_i-1}(1-s)^{\alpha-z_0-1}, & t \leq s, \end{cases} \tag{15}$$

$(i = 1,2,3)$

$$\varrho_1 - \frac{k_1}{\Gamma(\alpha-z_1)} \int_0^1 s^{\alpha-z_1-1} b_1(s) dA_1(s), \tag{16}$$

$$\varrho_2 = \frac{k_2}{\Gamma(\alpha-z_2)} \int_0^{\zeta} s^{\alpha-z_2-1} b_2(s) dA_2(s), \tag{17}$$

$$\varrho_3 = \frac{k_3}{\Gamma(\alpha-z_3)} \sum_{i=1}^{\infty} a_i \xi_i^{\alpha-z_3-1}, \tag{18}$$

$$\sigma_1 = \frac{1}{\Gamma(\alpha-z_0)} - \varrho_1 - \varrho_2 - \varrho_3 \neq 0. \tag{19}$$

Obviously, $G : [0,1] \times [0,1] \to \mathbb{R}$ *is continuous.*

Proof. By Lemma 2, Equation (12) can be written as

$$x(t) = c_1 t^{\alpha-\beta-1} + c_2 t^{\alpha-\beta-2} - I_{0+}^{\alpha-\beta} W(t), \quad c_1, c_2 \in \mathbb{R}.$$

Since $D_{0+}^{\gamma_{n-2}-\beta} x(0) = 0$, we obtain $c_2 = 0$. Thus,

$$x(t) = c_1 t^{\alpha-\beta-1} - I_{0+}^{\alpha-\beta} W(t). \tag{20}$$

Applying $D_{0+}^{z_i-\beta}$ $(i = 0, 1, 2, 3)$ on both sides of (20), we have

$$D_{0+}^{z_i-\beta} x(t) = c_1 \frac{\Gamma(\alpha-\beta)}{\Gamma(\alpha-z_i)} t^{\alpha-z_i-1} - I_{0+}^{\alpha-z_i} W(t), \quad i = 0, 1, 2, 3. \tag{21}$$

Substituting (21) into the second boundary condition of (12), we derive

$$\begin{aligned} c_1 = & \Bigg\{ \frac{1}{\Gamma(\alpha-z_0)} \int_0^1 (1-s)^{\alpha-z_0-1} W(s) ds \\ & - \frac{k_1}{\Gamma(\alpha-z_1)} \int_0^1 \left(\int_0^s (s-\tau)^{\alpha-z_1-1} W(\tau) d\tau \right) b_1(s) dA_1(s) \\ & - \frac{k_2}{\Gamma(\alpha-z_2)} \int_0^\zeta \left(\int_0^s (s-\tau)^{\alpha-z_2-1} W(\tau) d\tau \right) b_2(s) dA_2(s) \\ & - \frac{k_3}{\Gamma(\alpha-z_3)} \sum_{i=1}^{\infty} a_i \int_0^{\xi_i} (\xi_i - s)^{\alpha-z_3-1} W(s) ds \Bigg\} \frac{1}{\sigma_1 \Gamma(\alpha-\beta)}, \end{aligned} \tag{22}$$

Substituting c_1 into (20) and simplifying, we deduce that

$$\begin{aligned} x(t) = & - \frac{1}{\Gamma(\alpha-\beta)} \int_0^t (t-s)^{\alpha-\beta-1} W(s) ds \\ & + \Bigg\{ \frac{1}{\Gamma(\alpha-z_0)} \int_0^1 (1-s)^{\alpha-z_0-1} W(s) ds \\ & - \frac{k_1}{\Gamma(\alpha-z_1)} \int_0^1 \left(\int_0^s (s-\tau)^{\alpha-z_1-1} W(\tau) d\tau \right) b_1(s) dA_1(s) \\ & - \frac{k_2}{\Gamma(\alpha-z_2)} \int_0^\zeta \left(\int_0^s (s-\tau)^{\alpha-z_2-1} W(\tau) d\tau \right) b_2(s) dA_2(s) \\ & - \frac{k_3}{\Gamma(\alpha-z_3)} \sum_{i=1}^{\infty} a_i \int_0^{\xi_i} (\xi_i - s)^{\alpha-z_3-1} W(s) ds \Bigg\} \frac{t^{\alpha-\beta-1}}{\sigma_1 \Gamma(\alpha-\beta)} \\ = & \int_0^1 P_0(t,s) W(s) ds \\ & + \int_0^1 t^{\alpha-\beta-1} \left(\int_0^1 P_1(\tau,s) b_1(\tau) dA_1(\tau) \right) W(s) ds \\ & + \int_0^1 t^{\alpha-\beta-1} \left(\int_0^\zeta P_2(\tau,s) b_2(\tau) dA_2(\tau) \right) W(s) ds \\ & + \int_0^1 t^{\alpha-\beta-1} \sum_{j=1}^{\infty} a_i P_3(\xi_i, s) W(s) ds \\ = & \int_0^1 G(t,s) W(s) ds. \end{aligned} \tag{23}$$

The proof is complete. □

Lemma 7. *Let $W \in C(0,1) \cap L^1(0,1)$. Then, the following problem*

$$\begin{cases} {}^cD^{\delta}_{0+}x(\theta) + W(\theta) = 0, \quad 0 < \theta < 1, \\ \phi_q(x(0)) = x''(0) = 0, \\ x(1) = k_0 \int_0^1 b_0(s)x(s)ds, \end{cases} \tag{24}$$

has a unique solution

$$x(\theta) = \int_0^1 V(\theta, s)W(s)ds,$$

where $\phi_q = \phi_p^{-1}$,

$$V(\theta, s) = V_1(\theta, s) + V_2(\theta, s), \tag{25}$$

in which

$$V_1(\theta, s) = \frac{1}{\Gamma(\delta)} \begin{cases} \theta(1-s)^{\delta-1} - (\theta - s)^{\delta-1}, \ s \le \theta, \\ \theta(1-s)^{\delta-1}, \ \theta \le s, \end{cases} \tag{26}$$

$$V_2(\theta, s) = \frac{k_0\theta}{\sigma_2} \int_0^1 V_1(\tau, s)b_0(\tau)d\tau, \tag{27}$$

$$\sigma_2 = 1 - k_0 \int_0^1 \theta b_0(\theta)d\theta \neq 0. \tag{28}$$

Proof. Obviously, the problem (24) can be written as

$$x(\theta) = b_0 + b_1\theta + b_2\theta^2 - I^{\delta}_{0+}W(\theta).$$

The boundary condition $\phi_q(x(0)) = 0$ implies that $x(0) = 0$. Substituting this result and the condition $x''(0) = 0$ into the above equation yields that $b_0 = b_2 = 0$. Thus,

$$x(\theta) = b_1\theta - I^{\delta}_{0+}W(\theta). \tag{29}$$

Note that the boundary condition $x(1) = k_0 \int_0^1 b_0(s)x(s)ds$. We infer that

$$b_1 = \frac{1}{\Gamma(\delta)} \int_0^1 (1-s)^{\delta-1}W(s)ds + k_0 \int_0^1 b_0(s)x(s)ds. \tag{30}$$

It follows that

$$\begin{aligned} x(\theta) =& \frac{1}{\Gamma(\delta)} \int_0^1 \theta(1-s)^{\delta-1}W(s)ds + k_0 \int_0^1 \theta b_0(s)x(s)ds \\ & - \frac{1}{\Gamma(\delta)} \int_0^{\theta} (\theta - s)^{\delta-1}W(s)ds \\ =& \int_0^1 V_1(\theta, s)W(s)ds + k_0\theta \int_0^1 b_0(s)x(s)ds. \end{aligned} \tag{31}$$

Multiplying Equation (31) on both sides by $b_0(\theta)$ and integrating on $(0,1)$, we have

$$\begin{aligned}\int_0^1 b_0(\theta)x(\theta)d\theta &= \int_0^1 b_0(\theta)\left(\int_0^1 V_1(\theta,s)W(s)ds\right)d\theta \\ &\quad + k_0\int_0^1 \theta b_0(\theta)\left(\int_0^1 b_0(s)x(s)ds\right)d\theta \\ &= \int_0^1\left(\int_0^1 V_1(\tau,s)b_0(\tau)d\tau\right)W(s)ds \\ &\quad + \left(k_0\int_0^1 \theta b_0(\theta)d\theta\right)\left(\int_0^1 b_0(s)x(s)ds\right). \end{aligned} \tag{32}$$

Then, we obtain

$$\int_0^1 b_0(\theta)x(\theta)d\theta = \frac{1}{\sigma_2}\int_0^1\left(\int_0^1 V_1(\tau,s)b_0(\tau)d\tau\right)W(s)ds. \tag{33}$$

Substituting (33) into (31), we have

$$\begin{aligned} x(\theta) &= \int_0^1 V_1(\theta,s)W(s)ds + \frac{k_0\theta}{\sigma_2}\int_0^1\left(\int_0^1 V_1(\tau,s)b_0(\tau)d\tau\right)W(s)ds \\ &= \int_0^1 V_1(\theta,s)W(s)ds + \int_0^1 V_2(\theta,s)W(s)ds \\ &= \int_0^1 V(\theta,s)W(s)ds. \end{aligned} \tag{34}$$

□

Lemma 8. *Let $W \in C(0,1)\cap L^1(0,1)$. Then, the following problem*

$$\begin{cases} -{}^cD_{0+}^{\delta}\phi_p(D_{0+}^{\alpha-\beta}x(t)) + W(t) = 0, \quad 0 < t < 1, \\ D_{0+}^{\gamma_{n-2}-\beta}x(0) = D_{0+}^{\alpha-\beta}x(0) = (\phi_p(D_{0+}^{\alpha-\beta}x))''(0) = 0, \\ \phi_p(D_{0+}^{\alpha-\beta}x(1)) = k_0\displaystyle\int_0^1 b_0(s)\phi_p(D_{0+}^{\alpha-\beta}x(s))ds, \\ D_{0+}^{z_0-\beta}x(1) = k_1\displaystyle\int_0^1 b_1(s)D_{0+}^{z_1-\beta}x(s)dA_1(s) \\ + k_2\displaystyle\int_0^{\zeta} b_2(s)D_{0+}^{z_2-\beta}x(s)dA_2(s) + k_3\sum_{i=1}^{\infty} a_i D_{0+}^{z_3-\beta}x(\xi_i), \end{cases} \tag{35}$$

has a unique solution

$$x(t) = \int_0^1 G(t,s)\phi_q\left(\int_0^1 V(s,\tau)W(\tau)d\tau\right)ds,$$

where $G(t,s)$ and $V(t,s)$ are defined in Lemmas 6 and 7, respectively.

Proof. Let $h(t) = -\phi_p(D_{0+}^{\alpha-\beta}x(t))$. Then, we can resolve the problem (35) into the following two problems:

$$\begin{cases} {}^cD_{0+}^{\delta}h(t) + W(t) = 0, \ 0 < t < 1, \\ \phi_q(h(0)) = h''(0) = 0, \\ h(1) = k_0\displaystyle\int_0^1 b_0(s)h(s)ds \end{cases} \tag{36}$$

and

$$\begin{cases} D_{0+}^{\alpha-\beta}x(t)+\phi_q(h(t))=0, \quad 0<t<1, \\ D_{0+}^{\gamma_{n-2}-\beta}x(0)=0, \\ D_{0+}^{z_0-\beta}x(1)=k_1\int_0^1 b_1(s)D_{0+}^{z_1-\beta}x(s)dA_1(s) \\ +k_2\int_0^\zeta b_2(s)D_{0+}^{z_2-\beta}x(s)dA_2(s)+k_3\sum_{i=1}^{\infty}a_iD_{0+}^{z_3-\beta}x(\xi_i). \end{cases} \tag{37}$$

From Lemma 7, the problem (36) has a unique solution:

$$h(t)=\int_0^1 V(t,s)W(s)ds. \tag{38}$$

From Lemma 6, the problem (37) has a unique solution:

$$x(t)=\int_0^1 G(t,s)\phi_q(h(s))ds. \tag{39}$$

Therefore, the problem (35) has a unique solution:

$$x(t)=\int_0^1 G(t,s)\phi_q\left(\int_0^1 V(s,\tau)W(\tau)d\tau\right)ds.$$

□

Lemma 9. *Let* $\int_0^1 s^{\alpha-z_1-1}b_1(s)dA_1(s)\geq 0$, $\int_0^\zeta s^{\alpha-z_2-1}b_2(s)dA_2(s)\geq 0$, $\sum_{i=1}^{\infty}a_i\xi_i^{\alpha-z_3-1}<+\infty$, $k_i\geq 0\,(i=1,2,3)$, $\sigma_1>0$ *(defined in Lemma 6). Then,* $G(t,s)$ *has the following properties:*

(1) $t^{\alpha-\beta-1}J(s)\leq G(t,s)\leq \Upsilon t^{\alpha-\beta-1}(1-s)^{\alpha-z_0-1}$, *where*

$$J(s)=\Upsilon_0J_0(s)+\Upsilon_1J_1(s)+\Upsilon_2J_2(s)+\Upsilon_3J_3(s),\ \Upsilon=\Upsilon_0+\Upsilon_1+\Upsilon_2+\Upsilon_3,$$

in which

$$\Upsilon_0=\frac{1}{\Gamma(\alpha-\beta)},\ \Upsilon_1=\frac{k_1}{\sigma_1\Gamma(\alpha-\beta)\Gamma(\alpha-z_1)}\int_0^1\tau^{\alpha-z_1-1}b_1(\tau)dA_1(\tau),$$

$$\Upsilon_2=\frac{k_2}{\sigma_1\Gamma(\alpha-\beta)\Gamma(\alpha-z_2)}\int_0^\zeta\tau^{\alpha-z_2-1}b_2(\tau)dA_2(\tau),$$

$$\Upsilon_3=\frac{k_3}{\sigma_1\Gamma(\alpha-\beta)\Gamma(\alpha-z_3)}\sum_{i=1}^{\infty}a_i\xi_i^{\alpha-z_3-1},$$

$$J_0(s)=(1-s)^{\alpha-z_0-1}\Big(1-(1-s)^{z_0-\beta}\Big),$$

$$J_i(s)=(1-s)^{\alpha-z_0-1}\big(1-(1-s)^{z_0-z_i}\big),\ i=1,2,3.$$

(2) $G(t,s)\geq 0$, $t,s\in[0,1]\times[0,1]$.

Proof. (1) For $s\leq t$,

$$\begin{aligned} P_0(t,s)=&\frac{1}{\Gamma(\alpha-\beta)}\Big(t^{\alpha-\beta-1}(1-s)^{\alpha-z_0-1}-(t-s)^{\alpha-\beta-1}\Big)\\ \geq&\frac{t^{\alpha-\beta-1}}{\Gamma(\alpha-\beta)}(1-s)^{\alpha-z_0-1}\Big(1-(1-s)^{z_0-\beta}\Big)\\ =&\Upsilon_0t^{\alpha-\beta-1}J_0(s), \end{aligned}$$

$$\begin{aligned} P_0(t,s) \leq & \frac{1}{\Gamma(\alpha-\beta)} t^{\alpha-\beta-1}(1-s)^{\alpha-z_0-1} \\ = & \Upsilon_0 t^{\alpha-\beta-1}(1-s)^{\alpha-z_0-1}. \end{aligned}$$

For $t \leq s$,

$$\begin{aligned} P_0(t,s) = & \frac{1}{\Gamma(\alpha-\beta)} t^{\alpha-\beta-1}(1-s)^{\alpha-z_0-1} \\ \geq & \frac{1}{\Gamma(\alpha-\beta)} t^{\alpha-\beta-1}(1-s)^{\alpha-z_0-1}\left(1-(1-s)^{z_0-\beta}\right) \\ = & \Upsilon_0 t^{\alpha-\beta-1} J_0(s), \\ & P_0(t,s) = \Upsilon_0 t^{\alpha-\beta-1}(1-s)^{\alpha-z_0-1}. \end{aligned}$$

Similarly, we obtain

$$P_i(t,s) \geq \frac{k_i t^{\alpha-z_i-1} J_i(s)}{\sigma_1 \Gamma(\alpha-\beta)\Gamma(\alpha-z_i)},\ i=1,2,3,$$

$$P_i(t,s) \leq \frac{k_i t^{\alpha-z_i-1}(1-s)^{\alpha-z_0-1}}{\sigma_1 \Gamma(\alpha-\beta)\Gamma(\alpha-z_i)},\ i=1,2,3.$$

Thus, we have

$$\begin{aligned} G(t,s) = & P_0(t,s) + t^{\alpha-\beta-1}\left(\int_0^1 P_1(\tau,s) b_1(\tau) dA_1(\tau)\right) \\ & + t^{\alpha-\beta-1}\left(\int_0^\zeta P_2(\tau,s) b_2(\tau) dA_2(\tau)\right) + t^{\alpha-\beta-1}\sum_{i=1}^{\infty} a_i P_3(\xi_i,s) \\ \geq & t^{\alpha-\beta-1}\Upsilon_0 J_0(s) + t^{\alpha-\beta-1}\Upsilon_1 J_1(s) + t^{\alpha-\beta-1}\Upsilon_2 J_2(s) + t^{\alpha-\beta-1}\Upsilon_3 J_3(s) \\ = & t^{\alpha-\beta-1} J(s), \end{aligned}$$

$$\begin{aligned} G(t,s) \leq & \Upsilon_0 t^{\alpha-\beta-1}(1-s)^{\alpha-z_0-1} + \Upsilon_1 t^{\alpha-\beta-1}(1-s)^{\alpha-z_0-1} \\ & + \Upsilon_2 t^{\alpha-\beta-1}(1-s)^{\alpha-z_0-1} + \Upsilon_3 t^{\alpha-\beta-1}(1-s)^{\alpha-z_0-1} \\ = & \Upsilon t^{\alpha-\beta-1}(1-s)^{\alpha-z_0-1}. \end{aligned}$$

Moreover, from the above proof, (2) is true, clearly. □

Lemma 10. *Let $\sigma_2 > 0$ (defined in Lemma 7). Then, the following properties hold:*

(1) $\frac{1}{\Gamma(\delta)} t(1-t^{\delta-2})(1-s)^{\delta-1} \leq V_1(t,s) \leq \frac{1}{\Gamma(\delta)} t(1-s)^{\delta-1}$.

(2) $\frac{\Xi_1}{\Gamma(\delta)} t(1-s)^{\delta-1} \leq V_2(t,s) \leq \frac{\Xi_2}{\Gamma(\delta)} t(1-s)^{\delta-1}$, *where*

$$\Xi_1 = \frac{k_0}{\sigma_2}\int_0^1 \tau(1-\tau^{\delta-2}) b_0(\tau) d\tau,\ \Xi_2 = \frac{k_0}{\sigma_2}\int_0^1 \tau b_0(\tau) d\tau.$$

(3) $\Lambda_1 t(1-t^{\delta-2})(1-s)^{\delta-1} \leq V(t,s) \leq \Lambda_2 t(1-s)^{\delta-1}$, *where*

$$\Lambda_1 = \frac{1}{\Gamma(\delta)}(1+\Xi_1),\ \Lambda_2 = \frac{1}{\Gamma(\delta)}(1+\Xi_2).$$

(4) *for $\iota > 0$,*

$$\int_0^1 V(t,s) s^\iota ds = \frac{\mathcal{B}(\iota+1,\delta)}{\Gamma(\delta)}(t - t^{\delta+\iota} + \varpi t),$$

where $\varpi = \frac{k_0}{\sigma_2}\int_0^1 (\tau - \tau^{\delta+\iota}) b_0(\tau) d\tau$.

(5) $V(t,s) \geq 0, t, s \in [0,1] \times [0,1]$.

Proof. (1) For $s \leq t$,

$$\begin{aligned} V_1(t,s) \geq & \frac{1}{\Gamma(\delta)}\left(t(1-s)^{\delta-1} - t^{\delta-1}(1-s)^{\delta-1}\right) \\ = & \frac{1}{\Gamma(\delta)} t(1-t^{\delta-2})(1-s)^{\delta-1}, \end{aligned}$$

$$V_1(t,s) \leq \frac{1}{\Gamma(\delta)} t(1-s)^{\delta-1}.$$

For $t \leq s$,

$$V_1(t,s) \geq \frac{1}{\Gamma(\delta)} t(1-t^{\delta-2})(1-s)^{\delta-1},$$

$$V_1(t,s) = \frac{1}{\Gamma(\delta)} t(1-s)^{\delta-1}.$$

(2) It follows from (1) that

$$\begin{aligned} V_2(t,s) &= \frac{k_0 t}{\sigma_2} \int_0^1 V_1(\tau,s) b_0(\tau) d\tau \\ &\geq \frac{k_0}{\sigma_2 \Gamma(\delta)} \left(\int_0^1 \tau(1-\tau^{\delta-2}) b_0(\tau) d\tau \right) t(1-s)^{\delta-1} \\ &= \frac{\Xi_1}{\Gamma(\delta)} t(1-s)^{\delta-1}, \end{aligned}$$

$$\begin{aligned} V_2(t,s) &= \frac{k_0 t}{\sigma_2} \int_0^1 V_1(\tau,s) b_0(\tau) d\tau \\ &\leq \frac{k_0}{\sigma_2 \Gamma(\delta)} \left(\int_0^1 \tau b_0(\tau) d\tau \right) t(1-s)^{\delta-1} \\ &= \frac{\Xi_2}{\Gamma(\delta)} t(1-s)^{\delta-1}. \end{aligned}$$

(3) On the basis of (1) and (2), we obtain

$$\begin{aligned} V(t,s) \geq & \frac{1}{\Gamma(\delta)} t(1-t^{\delta-2})(1-s)^{\delta-1} + \frac{\Xi_1}{\Gamma(\delta)} t(1-s)^{\delta-1} \\ \geq & \left(\frac{1}{\Gamma(\delta)} + \frac{\Xi_1}{\Gamma(\delta)} \right) t(1-t^{\delta-2})(1-s)^{\delta-1} \\ = & \Lambda_1 t(1-t^{\delta-2})(1-s)^{\delta-1}. \end{aligned}$$

$$\begin{aligned} V(t,s) \leq & \frac{1}{\Gamma(\delta)} t(1-s)^{\delta-1} + \frac{\Xi_2}{\Gamma(\delta)} t(1-s)^{\delta-1} \\ = & \Lambda_2 t(1-s)^{\delta-1}. \end{aligned}$$

(4) For $\iota > 0$,

$$\begin{aligned} \int_0^1 V_1(t,s) s^\iota ds &= \frac{1}{\Gamma(\delta)} \left(\int_0^1 t(1-s)^{\delta-1} s^\iota ds - \int_0^t (t-s)^{\delta-1} s^\iota ds \right) \\ &= \frac{\mathcal{B}(\iota+1,\delta)}{\Gamma(\delta)} (t - t^{\delta+\iota}), \end{aligned}$$

$$\begin{aligned}\int_0^1 V_2(t,s)s^\iota ds &= \int_0^1 \left(\frac{k_0 t}{\sigma_2}\int_0^1 V_1(\tau,s)b_0(\tau)d\tau\right)s^\iota ds\\ &= \frac{k_0 t}{\sigma_2}\int_0^1\left(\int_0^1 V_1(\tau,s)s^\iota ds\right)b_0(\tau)d\tau\\ &= \frac{k_0\mathcal{B}(\iota+1,\delta)t}{\sigma_2\Gamma(\delta)}\int_0^1(\tau-\tau^{\delta+\iota})b_0(\tau)d\tau,\\ &= \frac{\mathcal{B}(\iota+1,\delta)}{\Gamma(\delta)}\varpi t,\end{aligned}$$

where $\varpi = \frac{k_0}{\sigma_2}\int_0^1(\tau-\tau^{\delta+\iota})b_0(\tau)d\tau$. It follows that

$$\int_0^1 V(t,s)s^\iota ds = \frac{\mathcal{B}(\iota+1,\delta)}{\Gamma(\delta)}(t-t^{\delta+\iota}+\varpi t).$$

From the above proof, (5) is true. The proof is complete. □

Lemma 11 ([35]). (1) *If* $1<p\le 2$, $|x_1|, |x_2| \ge x_0 > 0$, *and* $x_1x_2>0$, *then*

$$|\phi_p(x_1)-\phi_p(x_2)| \le (p-1)x_0^{p-2}|x_1-x_2|.$$

(2) *If* $p>2$, $|x_1|, |x_2| \le X_0$, *then*

$$|\phi_p(x_1)-\phi_p(x_2)| \le (p-1)X_0^{p-2}|x_1-x_2|.$$

(3) *If* $1<p\le 2$, *then for* $x_1, x_2 \ge 0$,

$$2^{p-2}(\phi_p(x_1)+\phi_p(x_2)) \le \phi_p(x_1+x_2) \le \phi_p(x_1)+\phi_p(x_2).$$

(4) *If* $p>2$, *then for* $x_1, x_2 \ge 0$,

$$\phi_p(x_1)+\phi_p(x_2) \le \phi_p(x_1+x_2) \le 2^{p-2}(\phi_p(x_1)+\phi_p(x_2)).$$

Remark 3. *In this paper,* $\Gamma(t)$ *represents the Gamma function*

$$\Gamma(t) = \int_0^{+\infty} s^{t-1}e^{-s}ds, \quad t>0,$$

and $\mathcal{B}(t,s)$ *represents the Beta function*

$$\mathcal{B}(t,s) = \int_0^1 l^{t-1}(1-l)^{s-1}dl,\ t>0,\ s>0.$$

In the following, we define two operators $T_1, T : C[0,1] \to C[0,1]$ *by*

$$(T_1x)(t) = \int_0^1 V(t,s)f(s, I_{0^+}^{\beta}x(s), \mathcal{H}x(s), x(s))ds,\ t\in[0,1],$$

$$(Tx)(t) = \int_0^1 G(t,s)\phi_q((T_1x)(s))ds,\ t\in[0,1].$$

It is easy to verify that if T *has a fixed point* x *in* $C[0,1]$, *then* x *is a solution of the problem* (2) *on* $[0,1]$.

3. Existence of Solutions

In this section, we give the following hypothesis:

For $(\mathbf{A_0})$, there exist non-negative functions $a_i \in L^2(0,1)$ $(i = 0,1,2,3)$ such that for a.e. $t \in (0,1)$, and for any $(x_1, x_2, x_3) \in \mathbb{R}^3$,

$$|f(t, x_1, x_2, x_3)| \leq a_0(t) + \sum_{i=1}^{3} a_i(t)|x_i|^{\theta_i},$$

where $\theta_i \in (0, p-1)$ $(i = 1,2,3)$.

In the following, for any $r > 0$, we denote

$$\begin{aligned} K_r =& \Lambda_2 \Big(\mathcal{B}^{\frac{1}{2}}(1, 2\delta - 1)\|a_0\|_{L_2} + \mathcal{B}^{\frac{1}{2}}(2\beta\theta_1 + 1, 2\delta - 1)(\Gamma(\beta+1))^{-\theta_1}\|a_1\|_{L_2} r^{\theta_1} \\ &+ \mathcal{B}^{\frac{1}{2}}(1, 2\delta - 1)(\Gamma(\beta+1))^{-\theta_2} M_h^{\theta_2}\|a_2\|_{L_2} r^{\theta_2} + \mathcal{B}^{\frac{1}{2}}(1, 2\delta - 1)\|a_3\|_{L_2} r^{\theta_3} \Big), \end{aligned} \tag{40}$$

where $\|a_i\|_{L_2} = \left(\int_0^1 a_i^2(t)dt \right)^{\frac{1}{2}}$ $(i = 0,1,2,3)$, $M_h = \sup_{t\in[0,1]} \int_0^t h(t,s)s^\beta ds$, and Λ_2 is defined in Lemma 10.

Lemma 12. *Let $C_i \geq 0$ $(i = 1,2,3,4)$ and considering the function*

$$\mathcal{C}(t) = t^{p-1} - C_1 t^{\theta_1} - C_2 t^{\theta_2} - C_3 t^{\theta_3} - C_4, \quad t \in [0, +\infty).$$

Since $\theta_i \in (0, p-1)$ $(i = 1,2,3)$, we derive that $\mathcal{C}(t) \to +\infty$ $(t \to +\infty)$. Thus, there exists $t_0 > 0$ such that

$$\mathcal{C}(t) \geq 0, \quad \forall\, t \geq t_0.$$

Lemma 13. *Suppose that $(\mathbf{A_0})$ holds. Then, for any $r > 0$, $T : S_r \to C[0,1]$ is well defined, where $S_r = \{x \in C[0,1] : \|x\| \leq r\}$.*

Proof. For any $x \in S_r$, we have

$$\left| I_{0^+}^{\beta} x(t) \right| \leq I_{0^+}^{\beta} |x(t)| \leq \frac{\|x\|}{\Gamma(\beta)} \int_0^t (t-s)^{\beta-1} ds \leq \frac{r t^\beta}{\Gamma(\beta+1)}, \ t \in [0,1], \tag{41}$$

$$\begin{aligned} |(\mathcal{H}x)(t)| &\leq \int_0^t h(t,s) I_{0^+}^{\beta} |x(s)| ds \leq \frac{r}{\Gamma(\beta+1)} \int_0^t h(t,s) s^\beta ds \\ &\leq \frac{M_h r}{\Gamma(\beta+1)}, \ t \in [0,1]. \end{aligned} \tag{42}$$

Based on $(\mathbf{A_0})$, Lemma 10(3) and the above analysis, we derive that for any $x \in S_r$,

$$
\begin{aligned}
&|T_1x(t)|\\
=&\left|\int_0^1 V(t,s)f(s,I_{0^+}^{\beta}x(s),\mathcal{H}x(s),x(s))ds\right|\\
\le&\int_0^1 V(t,s)\Big(a_0(s)+a_1(s)|I_{0^+}^{\beta}x(s)|^{\theta_1}+a_2(s)|\mathcal{H}x(s)|^{\theta_2}+a_3(s)|x(s)|^{\theta_3}\Big)ds\\
\le&\int_0^1 V(t,s)\left(a_0(s)+\frac{a_1(s)s^{\beta\theta_1}r^{\theta_1}}{(\Gamma(\beta+1))^{\theta_1}}+\frac{a_2(s)M_h^{\theta_2}r^{\theta_2}}{(\Gamma(\beta+1))^{\theta_2}}+a_3(s)r^{\theta_3}\right)ds\\
\le&\Lambda_2 t\left(\int_0^1(1-s)^{\delta-1}a_0(s)ds+\frac{r^{\theta_1}}{(\Gamma(\beta+1))^{\theta_1}}\int_0^1(1-s)^{\delta-1}a_1(s)s^{\beta\theta_1}ds\right.\\
&\left.+\frac{M_h^{\theta_2}r^{\theta_2}}{(\Gamma(\beta+1))^{\theta_2}}\int_0^1(1-s)^{\delta-1}a_2(s)ds+r^{\theta_3}\int_0^1(1-s)^{\delta-1}a_3(s)ds\right)\\
\le&\Lambda_2 t\left\{\left(\int_0^1(1-s)^{2\delta-2}ds\right)^{\frac{1}{2}}\left(\int_0^1 a_0^2(s)ds\right)^{\frac{1}{2}}\right.\\
&+\frac{r^{\theta_1}}{(\Gamma(\beta+1))^{\theta_1}}\left(\int_0^1 s^{2\beta\theta_1}(1-s)^{2\delta-2}ds\right)^{\frac{1}{2}}\left(\int_0^1 a_1^2(s)ds\right)^{\frac{1}{2}}\\
&+\frac{M_h^{\theta_2}r^{\theta_2}}{(\Gamma(\beta+1))^{\theta_2}}\left(\int_0^1(1-s)^{2\delta-2}ds\right)^{\frac{1}{2}}\left(\int_0^1 a_2^2(s)ds\right)^{\frac{1}{2}}\\
&\left.+r^{\theta_3}\left(\int_0^1(1-s)^{2\delta-2}ds\right)^{\frac{1}{2}}\left(\int_0^1 a_3^2(s)ds\right)^{\frac{1}{2}}\right\}\\
=&\Lambda_2 t\Big(\mathcal{B}^{\frac{1}{2}}(1,2\delta-1)\|a_0\|_{L_2}+\mathcal{B}^{\frac{1}{2}}(2\beta\theta_1+1,2\delta-1)(\Gamma(\beta+1))^{-\theta_1}\|a_1\|_{L_2}r^{\theta_1}\\
&+\mathcal{B}^{\frac{1}{2}}(1,2\delta-1)(\Gamma(\beta+1))^{-\theta_2}M_h^{\theta_2}\|a_2\|_{L_2}r^{\theta_2}+\mathcal{B}^{\frac{1}{2}}(1,2\delta-1)\|a_3\|_{L_2}r^{\theta_3}\Big)\\
=&K_r t,\ t\in[0,1],
\end{aligned}
\tag{43}
$$

which, together with Lemma 9(1), implies

$$
\begin{aligned}
|Tx(t)|=&\left|\int_0^1 G(t,s)\phi_q(T_1x(s))ds\right|\\
\le&\int_0^1 G(t,s)\phi_q(K_r s)ds\\
=&K_r^{q-1}\int_0^1 G(t,s)s^{q-1}ds\\
\le&K_r^{q-1}\int_0^1\Upsilon t^{\alpha-\beta-1}(1-s)^{\alpha-z_0-1}s^{q-1}ds\\
=&\Upsilon\mathcal{B}(q,\alpha-z_0)K_r^{q-1}t^{\alpha-\beta-1}<+\infty,\quad t\in[0,1].
\end{aligned}
\tag{44}
$$

Therefore, we deduce that $T:S_r\to C[0,1]$ is well defined. □

Theorem 1. *Suppose that* $(\mathbf{A_0})$ *holds. Then, the problem* (1) *has a solution* u_1*, and there exists* $r_1>0$ *such that*

$$|u_1(t)|\le\frac{r_1}{\Gamma(\beta+1)}t^{\beta},\quad t\in[0,1].$$

Proof. Considering the function $\mathcal{C}(t)$ (in Lemma 12) with

$$\mathcal{C}_1=(\Upsilon\mathcal{B}(q,\alpha-z_0))^{p-1}\Lambda_2\mathcal{B}^{\frac{1}{2}}(2\beta\theta_1+1,2\delta-1)(\Gamma(\beta+1))^{-\theta_1}\|a_1\|_{L_2},$$

$$\mathcal{C}_2 = (\Upsilon\mathcal{B}(q,\alpha-z_0))^{p-1}\Lambda_2\mathcal{B}^{\frac{1}{2}}(1,2\delta-1)(\Gamma(\beta+1))^{-\theta_2}M_h^{\theta_2}\|a_2\|_{L_2},$$

$$\mathcal{C}_3 = (\Upsilon\mathcal{B}(q,\alpha-z_0))^{p-1}\Lambda_2\mathcal{B}^{\frac{1}{2}}(1,2\delta-1)\|a_3\|_{L_2},$$

$$\mathcal{C}_4 = (\Upsilon B(q,\alpha-z_0))^{p-1}\Lambda_2 B^{\frac{1}{2}}(1,2\delta-1)\|a_0\|_{L_2},$$

we can infer that there exists an r_1 that is sufficiently large such that $\mathcal{C}(r_1) > 0$, i.e.,

$$\Upsilon\mathcal{B}(q,\alpha-z_0)K_{r_1}^{q-1} \le r_1. \tag{45}$$

Let $S_{r_1} = \{x \in C[0,1] : \|x\| \le r_1\}$, and we prove $T : S_{r_1} \to S_{r_1}$, firstly. Taking account of (44) and (45), we infer that for any $x \in S_{r_1}$,

$$|Tx(t)| \le \Upsilon\mathcal{B}(q,\alpha-z_0)K_{r_1}^{q-1} \le r_1,\ t \in [0,1], \tag{46}$$

which means $T : S_{r_1} \to S_{r_1}$. In the following, we give the proof that $T : S_{r_1} \to S_{r_1}$ is completely continuous.

Let $\{x_n\} \subset C[0,1]$ be a sequence satisfying $x_n \to x_0$, as $n \to +\infty$. Since $f \in C((0,1)\times\mathbb{R}^3,\mathbb{R})$, for fixed $\tau \in (0,1)$, $f(\tau,x,y,z)$ is uniformly continuous in regard to x, y and z on $[-r_1,r_1]^3$. Thus, for any $\varepsilon > 0$, there exists $\delta = \delta(\tau,\varepsilon) > 0$ such that, for any x_i, $y_i, z_i \in [-r_1,r_1]$ $(i = 1,2)$, which satisfy $|x_1 - x_2| < \delta$,$|y_1 - y_2| < \delta$ and $|z_1 - z_2| < \delta$,

$$|f(\tau,x_1,y_1,z_1) - f(\tau,x_2,y_2,z_2)| < \varepsilon. \tag{47}$$

As $x_n \to x_0$ $(n \to +\infty)$, for $\tilde{\delta} = \min\{\delta,\Gamma(\beta+1)\delta,\Gamma(\beta+1)M_h^{-1}\delta\}$, there exists $N_0 > 0$, such that for any $n \ge N_0$,

$$\|x_n - x_0\| < \tilde{\delta} \le \delta.$$

Evidently, we have

$$|x_n(\tau) - x_0(\tau)| < \tilde{\delta} \le \delta, \tag{48}$$

$$|I_{0^+}^{\beta}x_n(\tau) - I_{0^+}^{\beta}x_0(\tau)| < \frac{\tilde{\delta}}{\Gamma(\beta+1)} \le \delta, \tag{49}$$

$$|\mathcal{H}x_n(\tau) - \mathcal{H}x_0(\tau)| < \frac{M_h\tilde{\delta}}{\Gamma(\beta+1)} \le \delta. \tag{50}$$

Hence, by (47)–(50), we infer that for any $n \ge N_0$,

$$|f(\tau,I_{0^+}^{\beta}x_n(\tau),\mathcal{H}x_n(\tau),x_n(\tau)) - f(\tau,I_{0^+}^{\beta}x_0(\tau),\mathcal{H}x_0(\tau),x_0(\tau))| < \varepsilon. \tag{51}$$

That is, for any $\tau \in (0,1)$,

$$|f(\tau,I_{0^+}^{\beta}x_n(\tau),\mathcal{H}x_n(\tau),x_n(\tau)) - f(\tau,I_{0^+}^{\beta}x_0(\tau),\mathcal{H}x_0(\tau),x_0(\tau))| \to 0,\ n \to +\infty. \tag{52}$$

Further, by $(\mathbf{A_0})$, we know

$$\begin{aligned}&|f(\tau,I_{0^+}^{\beta}x_n(\tau),\mathcal{H}x_n(\tau),x_n(\tau)) - f(\tau,I_{0^+}^{\beta}x_0(\tau),\mathcal{H}x_0(\tau),x_0(\tau))|\\ \le& 2a_0(\tau) + 2a_1(\tau)r_1^{\theta_1} + 2a_2(\tau)r_1^{\theta_2} + 2a_3(\tau)r_1^{\theta_3},\quad \tau \in (0,1).\end{aligned}$$

It is clear that $2a_0 + 2r_1^{\theta_1}a_1 + 2r_1^{\theta_2}a_2 + 2r_1^{\theta_3}a_3 \in L^1(0,1)$, by using $(\mathbf{A_0})$. Accordingly, by means of the Lebesgue dominated convergence theorem, we obtain

$$\begin{aligned}
&|T_1x_n(s) - T_1x_0(s)| \\
=&\int_0^1 V(s,\tau)\Big|f(\tau, I_{0+}^{\beta}x_n(\tau), \mathcal{H}x_n(\tau), x_n(\tau)) - f(\tau, I_{0+}^{\beta}x_0(\tau), \mathcal{H}x_0(\tau), x_0(\tau))\Big|d\tau \\
\leq&\Lambda_2\int_0^1 \Big|f(\tau, I_{0+}^{\beta}x_n(\tau), \mathcal{H}x_n(\tau), x_n(\tau)) - f(\tau, I_{0+}^{\beta}x_0(\tau), \mathcal{H}x_0(\tau), x_0(\tau))\Big|d\tau \\
\to&0, \quad s \in [0,1].
\end{aligned} \tag{53}$$

Based on the continuity of ϕ_q, we have

$$|\phi_q(T_1x_n(s)) - \phi_q(T_1x_0(s))| \to 0, \quad s \in [0,1]. \tag{54}$$

By (43), we know

$$|\phi_q(T_1x_n(s)) - \phi_q(T_1x_0(s))| \leq 2K_{r_1}^{q-1}, \quad s \in [0,1].$$

Thus, based on Lemma 9(1) and the Lebesgue control convergence theorem, we obtain

$$\begin{aligned}
&|(Tx_n)(t) - (Tx_0)(t)| \\
=&\left|\int_0^1 G(t,s)(\phi_q(T_1x_n(s)) - \phi_q(T_1x_0(s)))ds\right| \\
\leq&\Upsilon\int_0^1 \big|\phi_q(T_1x_n(s)) - \phi_q(T_1x_0(s))\big|ds \to 0, \quad t \in [0,1].
\end{aligned} \tag{55}$$

Therefore, we conclude that $T : S_{r_1} \to S_{r_1}$ is continuous. □

Next, we prove TS_{r_1} is equicontinuous. With the help of the uniformly continuity of $G(t,s)$ on $[0,1] \times [0,1]$, we infer that, for any $\tilde{\varepsilon} > 0$, there exists $\delta = \delta(\tilde{\varepsilon}) > 0$ such that, for any $t_1, t_2 \in [0,1]$ that satisfy $|t_1 - t_2| < \delta$,

$$|G(t_1,s) - G(t_2,s)| < K_{r_1}^{1-q}\tilde{\varepsilon}, \quad s \in [0,1].$$

Hence, for any $x \in S_{r_1}$,

$$\begin{aligned}
&|Tx(t_1) - Tx(t_2)| \\
=&\left|\int_0^1 G(t_1,s)\phi_q(T_1x(s))ds - \int_0^1 G(t_2,s)\phi_q(T_1x(s))ds\right| \\
\leq&\int_0^1 |G(t_1,s) - G(t_2,s)|\phi_q(T_1x(s))ds \\
\leq&K_{r_1}^{q-1}\int_0^1 |G(t_1,s) - G(t_2,s)|ds < \tilde{\varepsilon},
\end{aligned} \tag{56}$$

which implies that TS_{r_1} is equicontinuous. In addition, based on (46), we observe that TS_{r_1} is uniformly bounded. Hence, we deduce that $T : S_{r_1} \to S_{r_1}$ is completely continuous. It follows from the Schauder fixed point theorem that T has a fixed point $x_1 \in S_{r_1}$. That is, the problem (2) has a solution x_1, which satisfies $\|x_1\| \leq r_1$. Moreover, from Lemma 5, we derive that theproblem (1) has a solution $u_1 = I_{0+}^{\beta}x_1$, which satisfies

$$|u_1(t)| \leq \frac{r_1}{\Gamma(\beta+1)}t^{\beta}, \quad t \in [0,1].$$

□

4. Uniqueness of Solutions

In this section, we prove the uniqueness of solutions for the cases $1 < q \leq 2$ and $q > 2$ separately. We give the following hypotheses:

$(\mathbf{A_1})$ There exist $\kappa > 0$ and $\iota > 0$ such that

$$f(t,x,y,z) \geq \kappa t^{\iota}, \quad \forall\, (t,x,y,z) \in (0,1) \times \mathbb{R}^3.$$

$(\mathbf{A_2})$ There exist $\kappa > 0$ and $\iota > 0$ such that

$$f(t,x,y,z) \leq -\kappa t^{\iota}, \quad \forall\, (t,x,y,z) \in (0,1) \times \mathbb{R}^3.$$

$(\mathbf{A_3})$ There exists non-negative function $\mathcal{F} \in C(0,1)$, which satisfies $(1-t)^{\delta-1}\mathcal{F} \in L^1(0,1)$, such that

$$|f(t,x,y,z)| \leq \mathcal{F}(t), \quad \forall\, (t,x,y,z) \in (0,1) \times \mathbb{R}^3.$$

$(\mathbf{A_4})$ There exist non-negative functions $l_i \in L^2(0,1)$ $(i = 1,2,3)$ such that for a.e. $t \in (0,1)$, and for any $(x_j, y_j, z_j) \in \mathbb{R}^3$ $(j = 1,2)$,

$$|f(t,x_1,y_1,z_1) - f(t,x_2,y_2,z_2)| \leq l_1(t)|x_1 - x_2| + l_2(t)|y_1 - y_2| + l_3(t)|z_1 - z_2|.$$

$(\mathbf{A_5})$ For any $r > 0$, there exist non-negative functions $l_{i,r} \in L^2(0,1)$ $(i = 1,2,3)$ such that for a.e. $t \in (0,1)$, and for any $(x_j, y_j, z_j) \in [-r,r]^3$ $(j = 1,2)$,

$$|f(t,x_1,y_1,z_1) - f(t,x_2,y_2,z_2)| \leq l_{1,r}(t)|x_1 - x_2| + l_{2,r}(t)|y_1 - y_2| + l_{3,r}(t)|z_1 - z_2|.$$

For convenience, we denote

$$M_h = \sup_{t\in[0,1]} \int_0^t h(t,s)s^{\beta} ds, \tag{57}$$

$$M_f = \int_0^1 (1-\tau)^{\delta-1} f(\tau,0,0,0) d\tau, \tag{58}$$

$$M_{\mathcal{F}} = \int_0^1 (1-\tau)^{\delta-1} \mathcal{F}(\tau) d\tau, \tag{59}$$

$$\begin{aligned}\mathcal{L} =& \Lambda_2 \Big(\mathcal{B}^{\frac{1}{2}}(2\beta+1, 2\delta-1)(\Gamma(\beta+1))^{-1} \|l_1\|_{L^2} \\ &+ M_h \mathcal{B}^{\frac{1}{2}}(1, 2\delta-1)(\Gamma(\beta+1))^{-1} \|l_2\|_{L^2} + \mathcal{B}^{\frac{1}{2}}(1, 2\delta-1)\|l_3\|_{L^2} \Big),\end{aligned} \tag{60}$$

$$\begin{aligned}\mathcal{L}_r =& \Lambda_2 \Big(\mathcal{B}^{\frac{1}{2}}(2\beta+1, 2\delta-1)(\Gamma(\beta+1))^{-1} \|l_{1,r}\|_{L^2} \\ &+ M_h \mathcal{B}^{\frac{1}{2}}(1, 2\delta-1)(\Gamma(\beta+1))^{-1} \|l_{2,r}\|_{L^2} + \mathcal{B}^{\frac{1}{2}}(1, 2\delta-1)\|l_{3,r}\|_{L^2} \Big) \ (\forall r > 0),\end{aligned} \tag{61}$$

$$\mathcal{M}_1 = (q-1)\left(\frac{\kappa \mathcal{B}(\iota+1, \delta)}{\Gamma(\delta)} \varpi \right)^{q-2} \mathcal{L} \Upsilon \mathcal{B}(q, \alpha - z_0), \tag{62}$$

$$\mathcal{M}_2 = (q-1)(\Lambda_2 M_{\mathcal{F}})^{q-2} \mathcal{L} \Upsilon \mathcal{B}(q, \alpha - z_0), \tag{63}$$

where $\|x\|_{L^2} = \left(\int_0^1 x^2(t) dt \right)^{\frac{1}{2}}$.

Lemma 14. *Suppose that* $(\mathbf{A_4})$ *holds. Then, for any* $x, y \in C[0,1]$,

$$|(T_1 x)(t) - (T_1 y)(t)| \leq \mathcal{L} t \|x - y\|, \ t \in [0,1].$$

Proof. For any $x, y \in C[0,1]$, we have

$$\left|I_{0^+}^{\beta}x(t) - I_{0^+}^{\beta}y(t)\right| \leq \frac{t^{\beta}}{\Gamma(\beta+1)}\|x-y\|,\ t \in [0,1], \tag{64}$$

$$|(\mathcal{H}x)(t) - (\mathcal{H}y)(t)| \leq \frac{M_h}{\Gamma(\beta+1)}\|x-y\|,\ t \in [0,1], \tag{65}$$

which, together with $(\mathbf{A_4})$ and Lemma 10(3), yields

$$\begin{aligned}
&|(T_1x)(t) - (T_1y)(t)| \\
\leq &\int_0^1 V(t,s)\left|f(s, I_{0^+}^{\beta}x(s), (\mathcal{H}x)(s), x(s))ds - f(s, I_{0^+}^{\beta}y(s), (\mathcal{H}y)(s), y(s))\right|ds \\
\leq &\int_0^1 V(t,s)\Big(l_1(s)|I_{0^+}^{\beta}x(s) - I_{0^+}^{\beta}y(s)| + l_2(s)|(\mathcal{H}x)(s) - (\mathcal{H}y)(s)| \\
&+ l_3(s)|x(s) - y(s)|\Big)ds \\
\leq &\left(\Lambda_2\int_0^1 t(1-s)^{\delta-1}\left(\frac{s^{\beta}l_1(s)}{\Gamma(\beta+1)} + \frac{M_h l_2(s)}{\Gamma(\beta+1)} + l_3(s)\right)ds\right)\|x-y\| \\
\leq &\left(\frac{1}{\Gamma(\beta+1)}\left(\int_0^1 (1-s)^{2\delta-2}s^{2\beta}ds\right)^{\frac{1}{2}}\left(\int_0^1 l_1^2(s)ds\right)^{\frac{1}{2}}\right. \\
&+ \frac{M_h}{\Gamma(\beta+1)}\left(\int_0^1 (1-s)^{2\delta-2}ds\right)^{\frac{1}{2}}\left(\int_0^1 l_2^2(s)ds\right)^{\frac{1}{2}} \\
&\left.+\left(\int_0^1 (1-s)^{2\delta-2}ds\right)^{\frac{1}{2}}\left(\int_0^1 l_3^2(s)ds\right)^{\frac{1}{2}}\right)\Lambda_2 t\|x-y\| \\
= &\left(\frac{\mathcal{B}^{\frac{1}{2}}(2\beta+1, 2\delta-1)\|l_1\|_{L^2}}{\Gamma(\beta+1)} + \frac{M_h\mathcal{B}^{\frac{1}{2}}(1, 2\delta-1)\|l_2\|_{L^2}}{\Gamma(\beta+1)}\right. \\
&\left.+ \mathcal{B}^{\frac{1}{2}}(1, 2\delta-1)\|l_3\|_{L^2}\right)\Lambda_2 t\|x-y\| \\
= &\mathcal{L}t\|x-y\|,\ t \in [0,1].
\end{aligned} \tag{66}$$

□

4.1. Uniqueness of Solutions for $1 < q \leq 2$

Lemma 15. *Suppose that $(\mathbf{A_1})$ and $(\mathbf{A_4})$ hold. Then, $T : C[0,1] \to C[0,1]$ is well defined.*

Proof. By means of $(\mathbf{A_1})$ and Lemma 10(4), we know, for any $x \in C[0,1]$,

$$\begin{aligned}
(T_1x)(t) &= \int_0^1 V(t,s)f(s, I_{0^+}^{\beta}x(s), (\mathcal{H}x)(s), x(s))ds \geq \kappa\int_0^1 V(t,s)s^{\iota}ds \\
&= \frac{\kappa\mathcal{B}(\iota+1,\delta)}{\Gamma(\delta)}(t - t^{\delta+\iota} + \varpi t),\ t \in [0,1],
\end{aligned} \tag{67}$$

which, together with (66) and Lemma 11(1), implies that for any $x, y \in C[0,1]$,

$$\begin{aligned}
&\left|\phi_q((T_1x)(t)) - \phi_q((T_1y)(t))\right| \\
\leq &(q-1)\left(\frac{\kappa\mathcal{B}(\iota+1,\delta)}{\Gamma(\delta)}(t - t^{\delta+\iota} + \varpi t)\right)^{q-2}|(T_1x)(t) - (T_1y)(t)| \\
\leq &(q-1)\left(\frac{\kappa\mathcal{B}(\iota+1,\delta)}{\Gamma(\delta)}\varpi t\right)^{q-2}\mathcal{L}t\|x-y\| \\
= &(q-1)\left(\frac{\kappa\mathcal{B}(\iota+1,\delta)}{\Gamma(\delta)}\varpi\right)^{q-2}\mathcal{L}t^{q-1}\|x-y\|, \quad t \in (0,1].
\end{aligned} \tag{68}$$

Meanwhile,

$$\begin{aligned}
&\left|\phi_q((T_1x)(0)) - \phi_q((T_1y)(0))\right| \\
=&\left|\phi_q\left(\int_0^1 V(0,s)f(s, I_{0^+}^{\beta}x(s), (\mathcal{H}x)(s), x(s))ds\right)\right. \\
&\left.-\phi_q\left(\int_0^1 V(0,s)f(s, I_{0^+}^{\beta}y(s), (\mathcal{H}y)(s), y(s))ds\right)\right| = 0
\end{aligned} \tag{69}$$

follows from $V(0,s) = 0$, for $s \in [0,1]$. Thus, combining with (66), we obtain

$$\begin{aligned}
|Tx(t)| =&\left|\int_0^1 G(t,s)\phi_q((T_1x)(s))ds\right| \\
\leq& \int_0^1 G(t,s)\left|\phi_q\left(\int_0^1 V(s,\tau)f(\tau, I_{0^+}^{\beta}x(\tau), (\mathcal{H}x)(\tau), x(\tau))d\tau\right)\right. \\
&\left.- \phi_q\left(\int_0^1 V(s,\tau)f(\tau,0,0,0)d\tau\right)\right|ds \\
&+ \int_0^1 G(t,s)\left|\phi_q\left(\int_0^1 V(s,\tau)f(\tau,0,0,0)d\tau\right)\right|ds \\
\leq&(q-1)\left(\frac{\kappa\mathcal{B}(\iota+1,\delta)}{\Gamma(\delta)}\varpi\right)^{q-2}\mathcal{L}\|x\|\int_0^1 G(t,s)s^{q-1}ds \\
&+ \int_0^1 G(t,s)\phi_q\left(\int_0^1 \Lambda_2 s(1-\tau)^{\delta-1}f(\tau,0,0,0)d\tau\right)ds \\
\leq&(q-1)\left(\frac{\kappa\mathcal{B}(\iota+1,\delta)}{\Gamma(\delta)}\varpi\right)^{q-2}\mathcal{L}\|x\|\int_0^1 \Upsilon t^{\alpha-\beta-1}(1-s)^{\alpha-z_0-1}s^{q-1}ds \\
&+ \int_0^1 \Upsilon t^{\alpha-\beta-1}(1-s)^{\alpha-z_0-1}(\Lambda_2 M_f)^{q-1}s^{q-1}ds \\
\leq&(q-1)\left(\frac{\kappa\mathcal{B}(\iota+1,\delta)}{\Gamma(\delta)}\varpi\right)^{q-2}\mathcal{L}\Upsilon\mathcal{B}(q,\alpha-z_0)\|x\| \\
&+ \Upsilon(\Lambda_2 M_f)^{q-1}\mathcal{B}(q,\alpha-z_0) < +\infty,\ t \in [0,1].
\end{aligned} \tag{70}$$

Thus, we deduce that $T : C[0,1] \to C[0,1]$ is well defined. □

Theorem 2. *Suppose that* $(\mathbf{A_1})$ *and* $(\mathbf{A_4})$ *hold. Then, the problem* (1) *has a unique solution* u_2 *provided that* $\mathcal{M}_1 < 1$. *Moreover, the solution* u_2 *satisfies*

$$u_2(t) \geq \Theta(t), \quad t \in [0,1],$$

where $\Theta(t)$ *defined in* (75).

Proof. Based on Lemma 15, we know, for any $x, y \in C[0,1]$,

$$\begin{aligned}
&|Tx(t) - Ty(t)| \\
=&\left| \int_0^1 G(t,s)\phi_q((T_1x)(s))ds - \int_0^1 G(t,s)\phi_q((T_1y)(s))ds \right| \\
\leq& \int_0^1 G(t,s)\left|\phi_q((T_1x)(s)) - \phi_q((T_1y)(s))\right|ds \\
\leq&(q-1)\left(\frac{\kappa\mathcal{B}(\iota+1,\delta)}{\Gamma(\delta)}\varpi\right)^{q-2}\mathcal{L}\|x-y\|\int_0^1 G(t,s)s^{q-1}ds \\
\leq&(q-1)\left(\frac{\kappa\mathcal{B}(\iota+1,\delta)}{\Gamma(\delta)}\varpi\right)^{q-2}\mathcal{L}\|x-y\| \\
&\times\int_0^1 \Upsilon t^{\alpha-\beta-1}(1-s)^{\alpha-z_0-1}s^{q-1}ds \\
\leq&(q-1)\left(\frac{\kappa\mathcal{B}(\iota+1,\delta)}{\Gamma(\delta)}\varpi\right)^{q-2}\mathcal{L}\Upsilon\mathcal{B}(q,\alpha-z_0)\|x-y\| \\
=&\mathcal{M}_1\|x-y\|,\ t\in[0,1].
\end{aligned} \tag{71}$$

That is,

$$\|Tx - Ty\| \leq \mathcal{M}_1\|x-y\|.$$

Since $\mathcal{M}_1 < 1$, we can infer that $T : C[0,1] \to C[0,1]$ is a contraction mapping. It follows from the Banach contraction mapping principle that T has a unique fixed point x_2 in $C[0,1]$, i.e., the problem (2) has a unique solution x_2. Furthermore, by means of Lemma 5, we deduce that the problem (1) has a unique solution $u_2 = I_{0^+}^{\beta}x_2$.

In the following, we prove that the solution u_2 has a lower bound given by (74). Based on (67) and Lemma 11(3), we have

$$\begin{aligned}
x_2(t) = (Tx_2)(t) &= \int_0^1 G(t,s)\phi_q((T_1x_2)(s))ds \\
&\geq \left(\frac{\kappa\mathcal{B}(\iota+1,\delta)}{\Gamma(\delta)}\right)^{q-1}\int_0^1 G(t,s)\phi_q\Big(s - s^{\delta+\iota} + \varpi s\Big)ds \\
&\geq 2^{q-2}\left(\frac{\kappa\mathcal{B}(\iota+1,\delta)}{\Gamma(\delta)}\right)^{q-1}\int_0^1 G(t,s)\Big(\phi_q(s - s^{\delta+\iota}) + \phi_q(\varpi s)\Big)ds \\
&\geq 2^{q-2}\left(\frac{\kappa\mathcal{B}(\iota+1,\delta)}{\Gamma(\delta)}\right)^{q-1}\int_0^1 G(t,s)\Big(s^{q-1} - s^{(\delta+\iota)(q-1)} + (\varpi s)^{q-1}\Big)ds \\
&= \mu(t),\ t\in[0,1],
\end{aligned} \tag{72}$$

where

$$\begin{aligned}
\mu(t) =&2^{q-2}\left(\frac{\kappa\mathcal{B}(\iota+1,\delta)}{\Gamma(\delta)}\right)^{q-1}\Big\{M_\Upsilon t^{\alpha-\beta-1} - \Upsilon_0\Big(\mathcal{B}(q,\alpha-\beta)t^{q+\alpha-\beta-1} \\
&-\mathcal{B}((\delta+\iota)(q-1)+1,\alpha-\beta)t^{(\delta+\iota)(q-1)+\alpha-\beta} \\
&+\varpi^{q-1}\mathcal{B}(q,\alpha-\beta)t^{q+\alpha-\beta-1}\Big)\Big\},
\end{aligned} \tag{73}$$

with

$$\begin{aligned}M_{\Upsilon} =&\Big(\mathcal{B}(q,\alpha-z_0)-\mathcal{B}((\delta+\iota)(q-1)+1,\alpha-z_0)+\varpi^{q-1}\mathcal{B}(q,\alpha-z_0)\Big)\Upsilon\\&-(1+\varpi^{q-1})\mathcal{B}(q,\alpha-z_1)\Upsilon_{1,1}+\mathcal{B}((\delta+\iota)(q-1)+1,\alpha-z_1)\Upsilon_{1,2}\\&-(1+\varpi^{q-1})\mathcal{B}(q,\alpha-z_2)\Upsilon_{2,1}+\mathcal{B}((\delta+\iota)(q-1)+1,\alpha-z_2)\Upsilon_{2,2}\\&-(1+\varpi^{q-1})\mathcal{B}(q,\alpha-z_3)\Upsilon_{3,1}+\mathcal{B}((\delta+\iota)(q-1)+1,\alpha-z_3)\Upsilon_{3,2},\end{aligned}$$

$$\Upsilon_{1,1}=\frac{k_1}{\sigma_1\Gamma(\alpha-\beta)\Gamma(\alpha-z_1)}\int_0^1\tau^{q+\alpha-z_1-1}b_1(\tau)dA_1(\tau),$$

$$\Upsilon_{1,2}=\frac{k_1}{\sigma_1\Gamma(\alpha-\beta)\Gamma(\alpha-z_1)}\int_0^1\tau^{(\delta+\iota)(q-1)+\alpha-z_1}b_1(\tau)dA_1(\tau),$$

$$\Upsilon_{2,1}=\frac{k_2}{\sigma_1\Gamma(\alpha-\beta)\Gamma(\alpha-z_2)}\int_0^\zeta\tau^{q+\alpha-z_2-1}b_2(\tau)dA_2(\tau),$$

$$\Upsilon_{2,2}=\frac{k_2}{\sigma_1\Gamma(\alpha-\beta)\Gamma(\alpha-z_2)}\int_0^\zeta\tau^{(\delta+\iota)(q-1)+\alpha-z_2}b_2(\tau)dA_2(\tau),$$

$$\Upsilon_{3,1}=\frac{k_3}{\sigma_1\Gamma(\alpha-\beta)\Gamma(\alpha-z_3)}\sum_{i=1}^{\infty}a_i\xi_i^{q+\alpha-z_3-1},$$

$$\Upsilon_{3,2}=\frac{k_3}{\sigma_1\Gamma(\alpha-\beta)\Gamma(\alpha-z_3)}\sum_{i=1}^{\infty}a_i\xi_i^{(\delta+\iota)(q-1)+\alpha-z_3}.$$

Consequently, we obtain

$$\begin{aligned}u_2(t)=&I_{0^+}^{\beta}x_2(t)\geq\frac{1}{\Gamma(\beta)}\int_0^t(t-s)^{\beta-1}\mu(s)ds\\=&\frac{2^{q-2}}{\Gamma(\beta)}\left(\frac{\kappa\mathcal{B}(\iota+1,\delta)}{\Gamma(\delta)}\right)^{q-1}\Bigg(M_{\Upsilon}\int_0^t(t-s)^{\beta-1}s^{\alpha-\beta-1}ds\\&-\Upsilon_0\mathcal{B}(q,\alpha-\beta)\int_0^t(t-s)^{\beta-1}s^{q+\alpha-\beta-1}ds\\&+\Upsilon_0\mathcal{B}((\delta+\iota)(q-1)+1,\alpha-\beta)\int_0^t(t-s)^{\beta-1}s^{(\delta+\iota)(q-1)+\alpha-\beta}ds\\&-\Upsilon_0\varpi^{q-1}\mathcal{B}(q,\alpha-\beta)\int_0^t(t-s)^{\beta-1}s^{q+\alpha-\beta-1}ds\Bigg)\\=&\Theta(t),\ t\in[0,1],\end{aligned}\tag{74}$$

where

$$\begin{aligned}\Theta(t)=&2^{q-2}\left(\frac{\kappa\mathcal{B}(\iota+1,\delta)}{\Gamma(\delta)}\right)^{q-1}\Bigg(M_{\Upsilon}\frac{\Gamma(\alpha-\beta)}{\Gamma(\alpha)}t^{\alpha-1}-\Upsilon_0\frac{\Gamma(q+\alpha-\beta)\mathcal{B}(q,\alpha-\beta)}{\Gamma(q+\alpha)}t^{q+\alpha-1}\\&+\Upsilon_0\frac{\Gamma((\delta+\iota)(q-1)+\alpha-\beta+1)\mathcal{B}((\delta+\iota)(q-1)+1,\alpha-\beta)}{\Gamma((\delta+\iota)(q-1)+\alpha+1)}t^{(\delta+\iota)(q-1)+\alpha}\\&-\Upsilon_0\varpi^{q-1}\frac{\Gamma(q+\alpha-\beta)\mathcal{B}(q,\alpha-\beta)}{\Gamma(q+\alpha)}\mathcal{B}(q,\alpha-\beta)t^{q+\alpha-1}\Bigg).\end{aligned}\tag{75}$$

Remark 4. *Given that the lengthy expression of $G(t,s)$ and the resulting elaborate computation for*

$$\int_0^1 G(t,s)\Big(s^{q-1}-s^{(\delta-\iota)(q-1)}+(\varpi s)^{q-1}\Big)ds,$$

we provide the detailed calculation below for completeness. By calculation, we obtain

$$\begin{aligned}
&\int_0^1 P_0(t,s)\Big(s^{q-1}-s^{(\delta+\iota)(q-1)}+(\varpi s)^{q-1}\Big)ds\\
=&\frac{1}{\Gamma(\alpha-\beta)}\int_0^1 t^{\alpha-\beta-1}(1-s)^{\alpha-z_0-1}\Big(s^{q-1}-s^{(\delta+\iota)(q-1)}+(\varpi s)^{q-1}\Big)ds\\
&-\frac{1}{\Gamma(\alpha-\beta)}\int_0^t (t-s)^{\alpha-\beta-1}\Big(s^{q-1}-s^{(\delta+\iota)(q-1)}+(\varpi s)^{q-1}\Big)ds\\
=&\frac{t^{\alpha-\beta-1}}{\Gamma(\alpha-\beta)}\Big(\mathcal{B}(q,\alpha-z_0)-\mathcal{B}((\delta+\iota)(q-1)+1,\alpha-z_0)+\varpi^{q-1}\mathcal{B}(q,\alpha-z_0)\Big)\\
&-\frac{1}{\Gamma(\alpha-\beta)}\Big(t^{q+\alpha-\beta-1}\mathcal{B}(q,\alpha-\beta)-t^{(\delta+\iota)(q-1)+\alpha-\beta}\mathcal{B}((\delta+\iota)(q-1)+1,\\
&\alpha-\beta)+\varpi^{q-1}t^{q+\alpha-\beta-1}\mathcal{B}(q,\alpha-\beta)\Big),
\end{aligned}\tag{76}$$

$$\begin{aligned}
&\int_0^1\left(\int_0^1 P_1(\tau,s)b_1(\tau)dA_1(\tau)\right)\Big(s^{q-1}-s^{(\delta+\iota)(q-1)}+(\varpi s)^{q-1}\Big)ds\\
=&\int_0^1\left(\int_0^1 P_1(\tau,s)\Big(s^{q-1}-s^{(\delta+\iota)(q-1)}+(\varpi s)^{q-1}\Big)ds\right)b_1(\tau)dA_1(\tau)\\
=&\frac{k_1}{\sigma_1\Gamma(\alpha-\beta)\Gamma(\alpha-z_1)}\int_0^1\tau^{\alpha-z_1-1}b_1(\tau)dA_1(\tau)\\
&\times\Big(\mathcal{B}(q,\alpha-z_0)-\mathcal{B}((\delta+\iota)(q-1)+1,\alpha-z_0)+\varpi^{q-1}\mathcal{B}(q,\alpha-z_0)\Big)\\
&-\frac{k_1}{\sigma_1\Gamma(\alpha-\beta)\Gamma(\alpha-z_1)}\Big(\mathcal{B}(q,\alpha-z_1)\int_0^1\tau^{q+\alpha-z_1-1}b_1(\tau)dA_1(\tau)\\
&-\mathcal{B}((\delta+\iota)(q-1)+1,\alpha-z_1)\int_0^1\tau^{(\delta+\iota)(q-1)+\alpha-z_1}b_1(\tau)dA_1(\tau)\\
&+\varpi^{q-1}\mathcal{B}(q,\alpha-z_1)\int_0^1\tau^{q+\alpha-z_1-1}b_1(\tau)dA_1(\tau)\Big),
\end{aligned}\tag{77}$$

$$\begin{aligned}
&\int_0^1\left(\int_0^\zeta P_2(\tau,s)b_2(\tau)dA_2(\tau)\right)\Big(s^{q-1}-s^{(\delta+\iota)(q-1)}+(\varpi s)^{q-1}\Big)ds\\
=&\int_0^\zeta\left(\int_0^1 P_2(\tau,s)\Big(s^{q-1}-s^{(\delta+\iota)(q-1)}+(\varpi s)^{q-1}\Big)ds\right)b_2(\tau)dA_2(\tau)\\
=&\frac{k_2}{\sigma_1\Gamma(\alpha-\beta)\Gamma(\alpha-z_2)}\int_0^\zeta\tau^{\alpha-z_2-1}b_2(\tau)dA_2(\tau)\\
&\times\Big(\mathcal{B}(q,\alpha-z_0)-\mathcal{B}((\delta+\iota)(q-1)+1,\alpha-z_0)+\varpi^{q-1}\mathcal{B}(q,\alpha-z_0)\Big)\\
&-\frac{k_2}{\sigma_1\Gamma(\alpha-\beta)\Gamma(\alpha-z_2)}\Big(\mathcal{B}(q,\alpha-z_2)\int_0^\zeta\tau^{q+\alpha-z_2-1}b_2(\tau)dA_2(\tau)\\
&-\mathcal{B}((\delta+\iota)(q-1)+1,\alpha-z_2)\int_0^\zeta\tau^{(\delta+\iota)(q-1)+\alpha-z_2}b_2(\tau)dA_2(\tau)\\
&+\varpi^{q-1}\mathcal{B}(q,\alpha-z_2)\int_0^\zeta\tau^{q+\alpha-z_2-1}b_2(\tau)dA_2(\tau)\Big),
\end{aligned}\tag{78}$$

and

$$\begin{aligned}
&\int_0^1 \sum_{i=1}^{\infty} a_i P_3(\xi_i, s)\Big(s^{q-1} - s^{(\delta+\iota)(q-1)} + (\varpi s)^{q-1}\Big)ds \\
=&\frac{k_3}{\sigma_1\Gamma(\alpha-\beta)\Gamma(\alpha-z_3)}\Big(\mathcal{B}(q,\alpha-z_0) - \mathcal{B}((\delta+\iota)(q-1)+1,\alpha-z_0) \\
&+ \varpi^{q-1}\mathcal{B}(q,\alpha-z_0)\Big)\sum_{i=1}^{\infty} a_i\xi_i^{\alpha-z_3-1} \\
&- \frac{k_3}{\sigma_1\Gamma(\alpha-\beta)\Gamma(\alpha-z_3)}\Big(\mathcal{B}(q,\alpha-z_3)\sum_{i=1}^{\infty} a_i\xi_i^{q+\alpha-z_3-1} \\
&- \mathcal{B}((\delta+\iota)(q-1)+1,\alpha-z_3)\sum_{i=1}^{\infty} a_i\xi_i^{(\delta+\iota)(q-1)+\alpha-z_3} \\
&+ \varpi^{q-1}\mathcal{B}(q,\alpha-z_3)\sum_{i=1}^{\infty} a_i\xi_i^{q+\alpha-z_3-1}\Big). \qquad (79)
\end{aligned}$$

From (76)–(79)*, we deduce that*

$$\begin{aligned}
&\int_0^1 G(t,s)\Big(\phi_q(s) - \phi_q(s^{\delta+\iota}) + \phi_q(\varpi s)\Big)ds \\
=&M_\Upsilon t^{\alpha-\beta-1} - \Upsilon_0\Big(\mathcal{B}(q,\alpha-\beta)t^{q+\alpha-\beta-1} \\
&- \mathcal{B}((\delta+\iota)(q-1)+1,\alpha-\beta)t^{(\delta+\iota)(q-1)+\alpha-\beta} + \varpi^{q-1}\mathcal{B}(q,\alpha-\beta)t^{q+\alpha-\beta-1}\Big). \qquad (80)
\end{aligned}$$

□

Theorem 3. *Suppose that* $(\mathbf{A_2})$ *and* $(\mathbf{A_4})$ *hold. Then, the problem* (1) *has a unique solution* u_3 *provided that* $\mathcal{M}_1 < 1$*. Moreover, the solution* u_3 *satisfies*

$$u_3(t) \leq -\Theta(t), \quad t \in [0,1].$$

Proof. Let $g(t,x,y,z) = -f(t,x,y,z)$. Then the proof is similar to Theorem 2. So, we omit the details here. □

4.2. Uniqueness of Solutions for $q > 2$

Theorem 4. *Suppose that* $(\mathbf{A_3})$ *and* $(\mathbf{A_4})$ *hold. Then the problem* (1) *has a unique solution* u_4 *provided that* $\mathcal{M}_2 < 1$*. Moreover, the solution* u_4 *satisfies*

$$|u_4(t)| \leq \frac{(\Lambda_2 M_{\mathcal{F}})^{q-1}\Upsilon\mathcal{B}(q,\alpha-z_0)\Gamma(\alpha-\beta)}{\Gamma(\alpha)}t^{\alpha-1}, \quad t \in [0,1].$$

Proof. By using $(\mathbf{A_3})$ and Lemma 10(3), we infer that for any $x \in C[0,1]$,

$$\begin{aligned}
|(T_1x)(t)| \leq& \int_0^1 V(t,s)|f(s, I_{0^+}^{\beta}x(s), (\mathcal{H}x)(s), x(s))|ds \\
\leq& \int_0^1 V(\iota,s)\mathcal{F}(s)ds \\
\leq& \Lambda_2 t\int_0^1 (1-s)^{\delta-1}\mathcal{F}(s)ds \\
=& \Lambda_2 M_{\mathcal{F}} t, \ t \in [0,1], \qquad (81)
\end{aligned}$$

which, together with Lemma 11(2) and Lemma 14, implies that for any $x, y \in C[0,1]$,

$$\begin{aligned}
&\left|\phi_q((T_1x)(t)) - \phi_q((T_1y)(t))\right| \\
\leq &(q-1)(\Lambda_2 M_{\mathcal{F}} t)^{q-2}|(T_1x)(t) - (T_1y)(t)| \\
\leq &(q-1)(\Lambda_2 M_{\mathcal{F}})^{q-2}\mathcal{L}t^{q-1}\|x-y\|, \quad t \in [0,1].
\end{aligned} \tag{82}$$

Hence, for any $x, y \in C[0,1]$,

$$\begin{aligned}
&|Tx(t) - Ty(t)| \\
\leq &\int_0^1 G(t,s)\left|\phi_q((T_1x)(s)) - \phi_q((T_1y)(s))\right|ds \\
\leq &(q-1)(\Lambda_2 M_{\mathcal{F}})^{q-2}\mathcal{L}\|x-y\| \int_0^1 G(t,s)s^{q-1}ds \\
\leq &(q-1)(\Lambda_2 M_{\mathcal{F}})^{q-2}\mathcal{L}\|x-y\| \int_0^1 \Upsilon t^{\alpha-\beta-1}(1-s)^{\alpha-z_0-1}s^{q-1}ds \\
\leq &(q-1)(\Lambda_2 M_{\mathcal{F}})^{q-2}\mathcal{L}\Upsilon\mathcal{B}(q,\alpha-z_0)\|x-y\| \\
= &\mathcal{M}_2\|x-y\|, \ t \in [0,1].
\end{aligned} \tag{83}$$

That is,

$$\|Tx - Ty\| \leq \mathcal{M}_2\|x-y\|. \tag{84}$$

Since $\mathcal{M}_2 < 1$, we deduce that $T : C[0,1] \to C[0,1]$ is a contraction mapping. Thus, by the Banach contraction mapping principle, we know that T has a unique fixed point x_4 in $C[0,1]$, i.e., the problem (2) has a unique solution x_4. Moreover, by using (81) and Lemma 9, we find an upper bound of x_4 on $[0,1]$:

$$\begin{aligned}
|x_4(t)| = &|Tx_4(t)| \\
\leq &\int_0^1 G(t,s)\phi_q(|(T_1x_4)(s)|)ds \\
\leq &(\Lambda_2 M_{\mathcal{F}})^{q-1}\int_0^1 G(t,s)\phi_q(s)ds \\
\leq &(\Lambda_2 M_{\mathcal{F}})^{q-1}\int_0^1 \Upsilon t^{\alpha-\beta-1}(1-s)^{\alpha-z_0-1}s^{q-1}ds \\
= &(\Lambda_2 M_{\mathcal{F}})^{q-1}\Upsilon\mathcal{B}(q,\alpha-z_0)t^{\alpha-\beta-1}, \quad t \in [0,1].
\end{aligned} \tag{85}$$

Finally, by using Lemma 5, we deduce that the problem (1) has a unique solution $u_4 = I_{0^+}^{\beta}x_4$, which satisfies

$$|u_4(t)| \leq \frac{(\Lambda_2 M_{\mathcal{F}})^{q-1}\Upsilon\mathcal{B}(q,\alpha-z_0)\Gamma(\alpha-\beta)}{\Gamma(\alpha)}t^{\alpha-1}, \quad t \in [0,1]. \tag{86}$$

□

Lemma 16. *Suppose that* $1 \leq M_h \leq \Gamma(\beta+1)$ *and* $(\mathbf{A_5})$ *hold. Then, for any* $x, y \in S_r$,

$$|T_1x(t) - T_1y(t)| \leq \mathcal{L}_r t\|x-y\|, \quad t \in [0,1].$$

Proof. Obviously, for any $x \in S_r$,

$$\left|I_{0^+}^{\beta}x(t)\right| \leq \frac{rt^{\beta}}{\Gamma(\beta+1)} \leq r, \ t \in [0,1], \tag{87}$$

$$|(\mathcal{H}x)(t)| \leq \frac{r}{\Gamma(\beta+1)} \int_0^t h(t,s)s^{\beta} ds \leq \frac{M_h r}{\Gamma(\beta+1)} \leq r,\ t \in [0,1]. \tag{88}$$

Then, similar to the proof of Lemma 14, we can prove that

$$|(T_1 x)(t) - (T_1 y)(t)| \leq \mathcal{L}_r t \|x - y\|,\ t \in [0,1]. \tag{89}$$

□

Lemma 17. *Suppose that* $(\mathbf{A_5})$ *and the following conditions hold:*

(i) $1 \leq M_h \leq \Gamma(\beta+1)$;

(ii) *There exists* $r > 0$ *such that the function*

$$U(r) = r - Z(r)(q-1)^{-1}\mathcal{L}_r^{-1}(\mathcal{L}_r r + \Lambda_2 M_f) \geq 0, \tag{90}$$

where

$$Z(r) = (q-1)(\mathcal{L}_r r + \Lambda_2 M_f)^{q-2}\mathcal{L}_r \Upsilon \mathcal{B}(q, \alpha - z_0).$$

Then, $T : S_r \to S_r$ *is well defined.*

Proof. From (87) and (88), we know, for any $x \in S_r$,

$$\left| I_{0^+}^{\beta} x(t) \right| \leq r,\ |(\mathcal{H}x)(t)| \leq r,\ t \in [0,1]. \tag{91}$$

Thus, based on Lemma 16 and Lemma 10(3), we deduce that for any $x \in S_r$,

$$\begin{aligned} |T_1 x(t)| =& \left| \int_0^1 V(t,s) f(s, I_{0^+}^{\beta} x(s), (\mathcal{H}x)(s), x(s)) ds \right| \\ \leq& \left| \int_0^1 V(t,s) \Big(f(s, I_{0^+}^{\beta} x(s), (\mathcal{H}x)(s), x(s)) - f(s,0,0,0) \Big) ds \right| \\ &+ \left| \int_0^1 V(t,s) f(s,0,0,0) ds \right| \\ \leq& \mathcal{L}_r r t + \Lambda_2 M_f t,\ t \in [0,1]. \end{aligned} \tag{92}$$

Hence, we have

$$\begin{aligned} |Tx(t)| =& \left| \int_0^1 G(t,s)\phi_q(T_1 x(s)) ds \right| \\ \leq& \int_0^1 G(t,s)\phi_q\Big(\mathcal{L}_r r s + \Lambda_2 M_f s\Big) ds \\ \leq& (\mathcal{L}_r r + \Lambda_2 M_f)^{q-1} \int_0^1 \Upsilon t^{\alpha-\beta-1}(1-s)^{\alpha-z_0-1} s^{q-1} ds \\ \leq& (\mathcal{L}_r r + \Lambda_2 M_f)^{q-1} \Upsilon \mathcal{B}(q, \alpha - z_0) \leq r, \end{aligned} \tag{93}$$

which means $T : S_r \to S_r$ is well defined. □

Theorem 5. *Suppose that* $(\mathbf{A_5})$ *and the following conditions hold:*

(i) $1 \leq M_h \leq \Gamma(\beta+1)$;

(ii) *There exists* $r_* > 0$ *such that* $Z(r_*) < 1$ *and* $U(r_*) \geq 0$.

Then, the problem (1) *has a unique solution* u_5*, which satisfies*

$$|u_5(t)| \leq \frac{r_*}{\Gamma(\beta+1)} t^{\beta}, \quad t \in [0,1].$$

Proof. By Lemma 17, we know $T : S_{r_*} \to S_{r_*}$ is well defined. In the following, we prove that T is a contraction mapping. Indeed, based on (92), Lemma 16 and Lemma 11(2), we know, for any $x, y \in S_{r_*}$,

$$\begin{aligned}
&\left|\phi_q(T_1x(t)) - \phi_q(T_1y(t))\right| \\
\leq&(q-1)(\mathcal{L}_{r_*}r_*t + \Lambda_2 M_f t)^{q-2}|T_1x(t) - T_1y(t)| \\
\leq&(q-1)(\mathcal{L}_{r_*}r_*t + \Lambda_2 M_f t)^{q-2}\mathcal{L}_{r_*}t\|x-y\| \\
=&(q-1)(\mathcal{L}_{r_*}r_* + \Lambda_2 M_f)^{q-2}\mathcal{L}_{r_*}t^{q-1}\|x-y\|, \quad t \in [0,1].
\end{aligned} \tag{94}$$

Thus, for any $x, y \in S_{r_*}$,

$$\begin{aligned}
&|Tx(t) - Ty(t)| \\
\leq&\int_0^1 G(t,s)\left|\phi_q(T_1x(s))ds - \phi_q(T_1y(s))\right|ds \\
\leq&(q-1)(\mathcal{L}_{r_*}r_* + \Lambda_2 M_f)^{q-2}\mathcal{L}_{r_*}\|x-y\|\int_0^1 G(t,s)s^{q-1}ds \\
\leq&(q-1)(\mathcal{L}_{r_*}r_* + \Lambda_2 M_f)^{q-2}\mathcal{L}_{r_*}\Upsilon\mathcal{B}(q,\alpha - z_0)\|x-y\| \\
=&Z(r_*)\|x-y\|,\ t \in [0,1].
\end{aligned} \tag{95}$$

Since $Z(r_*) < 1$, $T : S_{r_*} \to S_{r_*}$ is a contraction mapping. In view of the Banach contraction mapping principle, we deduce that T has a unique fixed point x_5 in S_{r_*}, i.e., the problem (2) has a unique solution x_5 satisfying $\|x_5\| \leq r_*$. Moreover, by using Lemma 5, we deduce that the problem (1) has a unique solution $u_5 = I_{0^+}^{\beta}x_5$, which satisfies

$$|u_5(t)| \leq \frac{r_*}{\Gamma(\beta+1)}t^{\beta}, \quad t \in [0,1]. \tag{96}$$

□

5. Examples

Example 1. *We consider the following problem:*

$$\begin{cases}
-{}^cD_{0+}^{\frac{5}{2}}\phi_5(u'''(t)) + \dfrac{4.1472\times10^8}{\sqrt{\pi}}\left(t^{\frac{3}{2}} - 8t^{\frac{5}{2}} + \dfrac{144}{7}t^{\frac{7}{2}}\right. \\
\left.-\dfrac{64}{3}t^{\frac{9}{2}} + \dfrac{256}{33}t^{\frac{11}{2}}\right) = 0, \quad 0 < t < 1, \\
u(0) = u'(0) = u'''(0) = \left(\phi_5(u'''(0))\right)'' = \phi_5(u'''(1)) = 0, \\
u'(1) = \dfrac{3(2^{\frac{7}{4}}-1)}{3\times2^{\frac{17}{5}} - 2^{\frac{99}{20}} + 2^{\frac{16}{5}}}\displaystyle\sum_{i=1}^{\infty}2^{-i}u'(2^{\frac{16-5i}{20}}).
\end{cases} \tag{97}$$

Proof. Let $p = 5$, $\delta = \frac{5}{2}$, $\alpha = 3$ $(n = 3)$, $\beta = 1$, $\gamma_1 = 1$, $z_i = 1$ $(i = 0,1,2,3)$, $\zeta = \frac{1}{7}$, $k_0 = 0$, $k_1 = 0$, $k_2 = \frac{1}{3}$, $k_3 = 3(2^{\frac{7}{4}}-1)(3\times2^{\frac{17}{5}} - 2^{\frac{99}{20}} + 2^{\frac{16}{5}})^{-1}$, $b_0(s) = s^{-\frac{1}{2}}$, $b_1(s) = s^{-\frac{1}{2}}$, $b_2(s) \equiv 0$, $a_i = 2^{-i}$, $\xi_i = 2^{\frac{16-5i}{20}}$ $(i = 1,2,\ldots)$, $(Hu)(t) = \int_0^t u(s)ds$,

$$A_1(t) = \begin{cases}\Gamma(\dfrac{6}{5}), & t \in \left[0, \dfrac{10}{11}\right), \\ \Gamma(\dfrac{11}{5}), & t \in \left[\dfrac{10}{11}, 1\right],\end{cases} \quad A_2(t) = \begin{cases}\Gamma(\dfrac{8}{7}), & t \in \left[0, \dfrac{2}{7}\right), \\ 3, & t \in \left[\dfrac{2}{7}, 1\right].\end{cases}$$

$$f(t,u,v,w) = \frac{4.1472\times10^8}{\sqrt{\pi}}\left(t^{\frac{3}{2}} - 8t^{\frac{5}{2}} + \frac{3856}{3465}t^{\frac{13}{2}} - \frac{464}{105}t^{\frac{1}{2}}u + \frac{7712}{1155}t^{\frac{1}{2}}v + \frac{72}{35}t^{\frac{1}{2}}w\right).$$

Then, we can regard the problem (97) as a specific case of the problem (1). Let $\theta_1 = \theta_2 = \theta_3 = 1$, and

$$a_0(t) = \frac{4.1472 \times 10^8}{\sqrt{\pi}}\left(t^{\frac{3}{2}} - 8t^{\frac{5}{2}} + \frac{3856}{3465}t^{\frac{13}{2}}\right), \quad a_1(t) = \frac{1282.8672 \times 10^7}{7\sqrt{\pi}}t^{\frac{1}{2}},$$

$$a_2(t) = \frac{21322.1376 \times 10^7}{77\sqrt{\pi}}t^{\frac{1}{2}}, \quad a_3(t) = \frac{597.1968 \times 10^7}{7\sqrt{\pi}}t^{\frac{1}{2}}.$$

Obviously, $a_i \in L^2(0,1)$ $(i = 0,1,2,3)$ and f satisfies the condition $(\mathbf{A_0})$. Let $r_1 = \frac{3}{2}$. Then, all the assumptions of Theorem 1 are fulfilled. With these data, we obtain a solution u_1 to the problem (97) and establish an upper bound for u_1. Figure 1 and Table 1 show that the solution u_1 has an upper bound. This thereby verifies the validity and effectiveness of Theorem 1. □

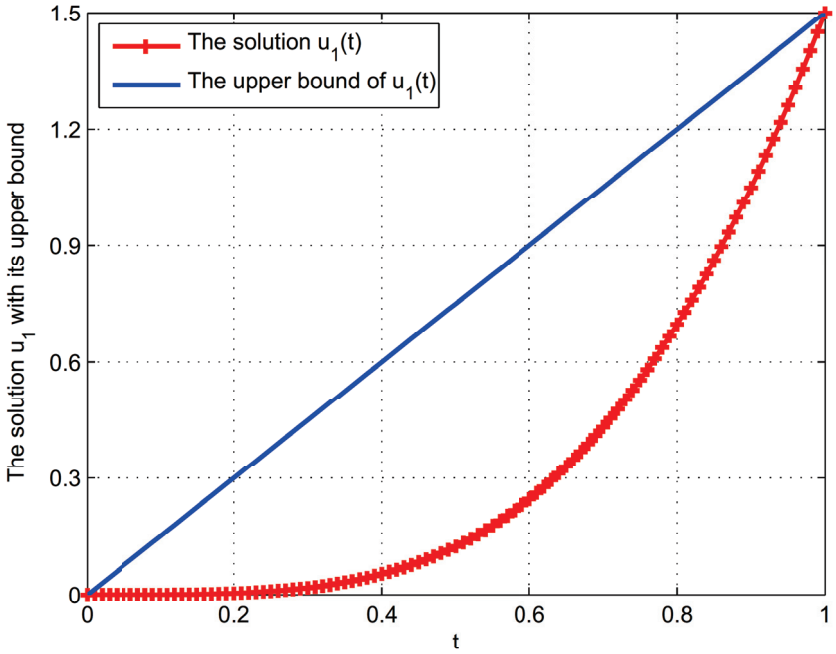

Figure 1. Trajectory of the model (97) solution.

Table 1. The solution u_1 with its upper bound.

t	0	0.2	0.4	0.6	0.8	1
$u_1(t)$	0	0.0037	0.0538	0.2462	0.6963	1.5000
The upper bound of $u_1(t)$	0	0.3000	0.6000	0.9000	1.2000	1.5000

Example 2. *We consider the following problem:*

$$\begin{cases} -{}^cD^3_{0+}\phi_2\left(D^{\frac{5}{2}}_{0+}u(t)\right) + \dfrac{315\sqrt{\pi}}{8} = 0, \quad 0 < t < 1, \\ u(0) = u'(0) = D^{\frac{5}{2}}_{0+}u(0) = \left(\phi_2\left(D^{\frac{5}{2}}_{0+}u(0)\right)\right)'' = 0, \\ \phi_2\left(D^{\frac{5}{2}}_{0+}u(1)\right) = 0, \quad u'(1) = 0. \end{cases} \tag{98}$$

Proof. Let $p = 2$, $\delta = 3$, $\alpha = \frac{5}{2}$ $(n = 3)$, $\beta = \frac{3}{4}$, $\gamma_1 = 1$, $z_0 = 1$, $z_1 = \frac{4}{5}$, $z_2 = \frac{5}{6}$, $z_3 = \frac{6}{7}$, $\zeta = \frac{13}{14}$, $k_0 = k_1 = 0$, $k_2 = 2$, $k_3 = 1$, $a_i \equiv 0$, $\xi_i = 2^{-i}$ $(i = 1, 2, \ldots)$, $b_0(s) = s^{\frac{1}{3}}$, $b_1(s) = s^{-\frac{1}{2}}$, $b_2(s) \equiv 0$, $(Hu)(t) = \int_0^t u(s)ds$,

$$A_1(t) = \begin{cases} \frac{5}{7}, & t \in \left[0, \frac{1}{7}\right), \\ \frac{6}{7}, & t \in \left[\frac{1}{7}, 1\right], \end{cases} \quad A_2(t) = \begin{cases} \frac{5}{8}, & t \in \left[0, \frac{1}{3}\right), \\ \frac{8}{9}, & t \in \left[\frac{1}{3}, 1\right]. \end{cases}$$

$$f(t,u,v,w) = |u| + |v| + |w| + \frac{315\sqrt{\pi}}{8} - \frac{13}{9}t^{\frac{3}{2}} + t^{\frac{7}{2}} - \frac{8}{33}t^{\frac{11}{2}} - \frac{26}{45}t^{\frac{5}{2}} + \frac{2}{9}t^{\frac{9}{2}} - \frac{16}{429}t^{\frac{13}{2}} - \frac{\sqrt{\pi}}{\Gamma(3/4)}\left(\frac{13}{9}t^{\frac{3}{4}} - \frac{20}{11}t^{\frac{11}{4}} + \frac{128}{209}t^{\frac{19}{4}}\right).$$

Then, we can regard the problem (98) as the problem (1). It is easy to check that f satisfies $(\mathbf{A_1})$ and $(\mathbf{A_4})$ with $\kappa = 10$, $\iota = 2$, $l_1(t) = l_2(t) = l_3(t) = 1$. And, $\mathcal{M}_1 = 0.1258 < 1$. Thus, all the assumptions of Theorem 2 are fulfilled. With these data, the numerical results in Figures 2 and 3 and Table 2 show that the solution u_2 has a lower bound. Among them, Figure 2 illustrates the relationship between the solution u_2 and its lower bound. For a clearer visualization of the lower bound's trajectory, we provide Figure 3. Thus, this numerical example confirms Theorem 2. □

Table 2. The solution u_2 with its lower bound.

t	0	0.2	0.4	0.6	0.8	1
$u_2(t)$	0	0.1257	0.3265	0.5186	0.6467	0.6869
The lower bound of $u_2(t)$	0	0.0023	0.0061	0.0098	0.0123	0.0120

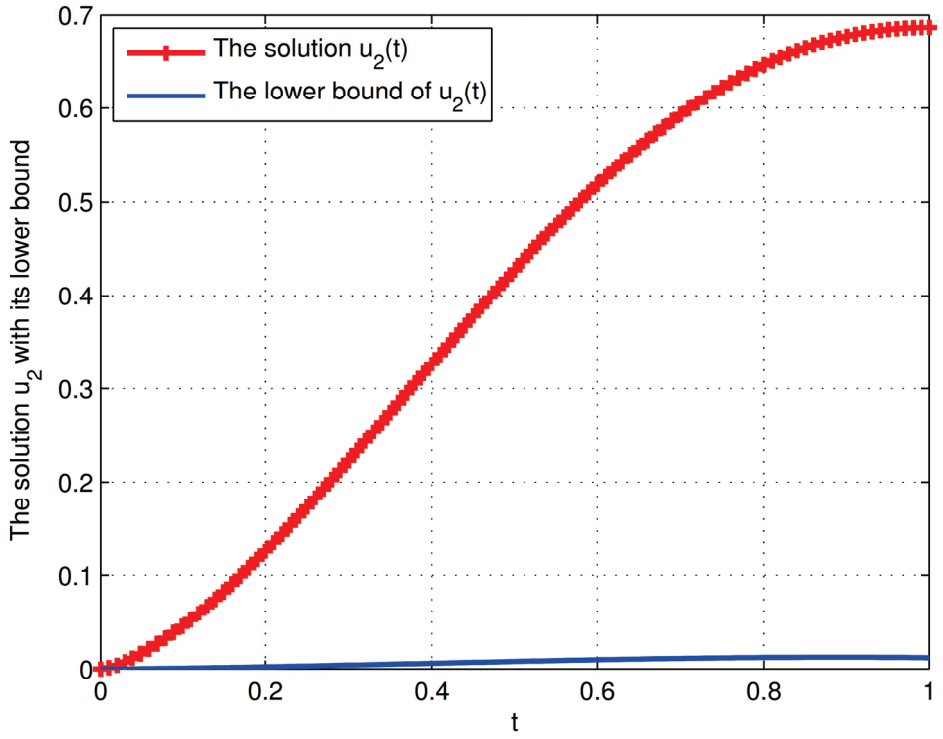

Figure 2. Trajectory 1 of the model (98).

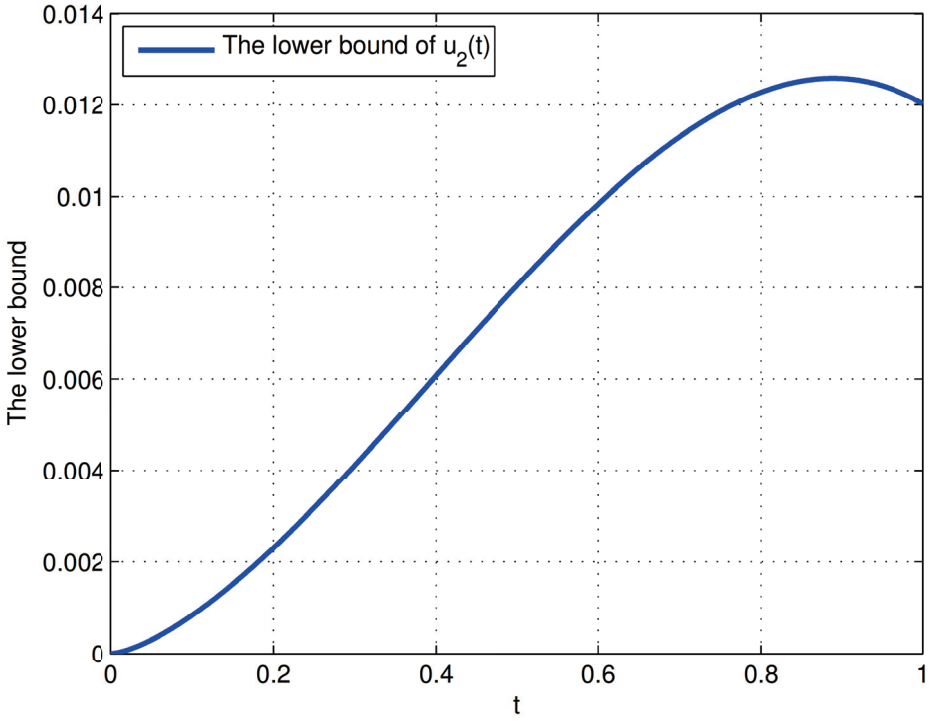

Figure 3. Trajectory 2 of the model (98).

Example 3. *We consider the following equation:*

$$\begin{cases} -{}^{c}D_{0+}^{\frac{21}{10}}\phi_{\frac{3}{2}}\left(D_{0+}^{\frac{11}{5}}u(t)\right)+\dfrac{792\Gamma(\frac{1}{5})}{125000\Gamma(\frac{1}{10})}\left(\dfrac{897\Gamma(\frac{3}{5})}{17\Gamma(\frac{2}{5})}\right)^{\frac{1}{2}}t^{\frac{1}{10}}=0, \quad 0<t<1,\\ u(0)=u'(0)=D_{0+}^{\frac{11}{5}}u(0)=\left(\phi_{\frac{3}{2}}\left(D_{0+}^{\frac{11}{5}}u(0)\right)\right)''=0,\\ \phi_{\frac{3}{2}}\left(D_{0+}^{\frac{11}{5}}u(1)\right)=3\displaystyle\int_0^1 s^{-\frac{1}{5}}\phi_{\frac{3}{2}}(D_{0+}^{\frac{11}{5}}u(s))ds,\\ D_{0+}^{\frac{6}{5}}u(1)=\dfrac{8}{\Gamma(\frac{32}{5})}\displaystyle\int_0^1 s^{-\frac{1}{2}}D_{0+}^{\frac{11}{10}}u(s)dA_1(s)\\ +\dfrac{8}{\Gamma(\frac{32}{5})}\displaystyle\int_0^{\frac{10}{11}} s^{-\frac{4}{5}}D_{0+}^{\frac{4}{5}}u(s)dA_2(s)+\dfrac{1}{2\Gamma(\frac{32}{5})}\sum_{i=1}^{\infty}\Gamma(\frac{67}{10})2^{-\frac{1}{2}i}D_{0+}^{\frac{9}{10}}u(2^{-\frac{5}{57}i}), \end{cases} \tag{99}$$

where

$$A_1(t)=\begin{cases}1, & \iota\in\left[0,\dfrac{1}{2}\right),\\ 1+\Gamma\left(\dfrac{13}{2}\right), & t\in\left[\dfrac{1}{2},1\right],\end{cases} \qquad A_2(t)=\begin{cases}1, & \iota\in\left[0,\dfrac{1}{2}\right),\\ 1+\Gamma\left(\dfrac{34}{5}\right), & t\in\left[\dfrac{1}{2},1\right].\end{cases}$$

Proof. Let $p=\frac{3}{2}$, $\delta=\frac{21}{10}$, $\alpha=\frac{11}{5}$ $(n=3)$, $\beta=1$, $\gamma_1=1$, $z_0=\frac{6}{5}$, $z_1=\frac{11}{10}$, $z_2=\frac{4}{5}$, $z_3=\frac{9}{10}$, $k_0=3$, $k_1=\frac{8}{\Gamma(\frac{32}{5})}$, $k_2=\frac{8}{\Gamma(\frac{32}{5})}$, $k_3=\frac{1}{2\Gamma(\frac{32}{5})}$, $\zeta=\frac{10}{11}$, $b_0(s)=s^{-\frac{1}{5}}$, $b_1(s)=s^{-\frac{1}{2}}$, $b_2(s)=s^{-\frac{4}{5}}$, $(Hu)(t)=\int_0^t u(s)ds$,

$$f(t,u,v,w)=\frac{792\Gamma(\frac{1}{5})}{125000\Gamma(\frac{1}{10})}\left(\frac{897\Gamma(\frac{3}{5})}{17\Gamma(\frac{2}{5})}\right)^{\frac{1}{2}}\frac{t^{\frac{1}{10}}(\frac{t^{\frac{33}{5}}}{10^6}+1)(\frac{5t^{\frac{38}{5}}}{38\times10^6}+1)(\frac{33t^{\frac{28}{5}}}{5\times10^6}+1)}{(|u|+1)(|v|+1)(|w|+1)}.$$

Then, we can regard the problem (99) as the problem (1). Let

$$\mathcal{F}(t) = \frac{792\Gamma(\frac{1}{5})}{125000\Gamma(\frac{1}{10})}\left(\frac{897\Gamma(\frac{3}{5})}{17\Gamma(\frac{2}{5})}\right)^{\frac{1}{2}} t^{\frac{1}{10}}\left(\frac{t^{\frac{33}{5}}}{10^6}+1\right)\left(\frac{5t^{\frac{38}{5}}}{38\times 10^6}+1\right)\left(\frac{33t^{\frac{28}{5}}}{5\times 10^6}+1\right)$$

and

$$l_i(t) = \frac{792\Gamma(\frac{1}{5})}{125000\Gamma(\frac{1}{10})}\left(\frac{897\Gamma(\frac{3}{5})}{17\Gamma(\frac{2}{5})}\right)^{\frac{1}{2}} t^{\frac{1}{10}}\left(\frac{t^{\frac{33}{5}}}{10^6}+1\right)\left(\frac{5t^{\frac{38}{5}}}{38\times 10^6}+1\right)\left(\frac{33t^{\frac{28}{5}}}{5\times 10^6}+1\right)(i=1,2,3).$$

It is easy to check that f satisfies conditions $(\mathbf{A_3})$ and $(\mathbf{A_4})$. Moreover, by using the above data, we obtain $\mathcal{M}_2 \leq 0.0029 < 1$. Therefore, all the assumptions of Theorem 4 are fulfilled. With these data, the numerical results in Figures 4 and 5 as well as Table 3 show that the solution u_4 has an upper bound. Among them, Figure 4 illustrates the relationship between the solution u_4 and its upper bound. For a clearer visualization of the trajectory of solution u_4, we provide Figure 5. Therefore, this numerical example demonstrates the validity of Theorem 4. □

Table 3. The solution u_4 with its upper bound.

t	0	0.2	0.4	0.6	0.8	1
$u_4(t)$ $(\times 10^{-6})$	0	0.0000	0.0024	0.0343	0.2293	1.0000
The upper bound of $u_4(t)$ $(\times 10^{-4})$	0	0.7665	1.7610	2.8646	4.0457	5.2879

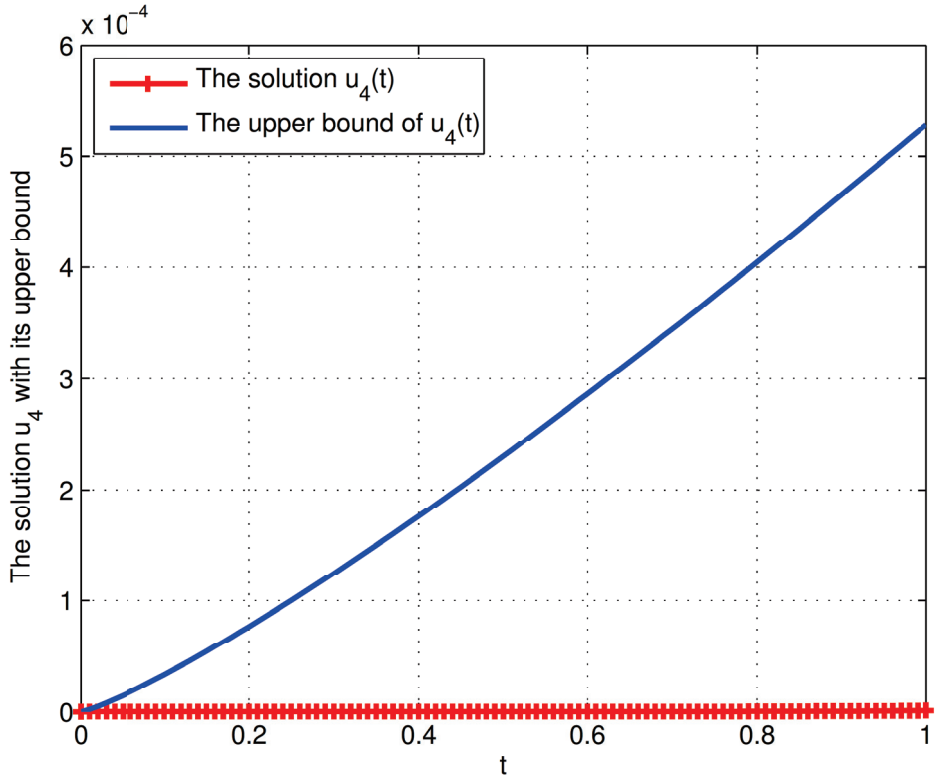

Figure 4. Trajectory 1 of the model (99) solution.

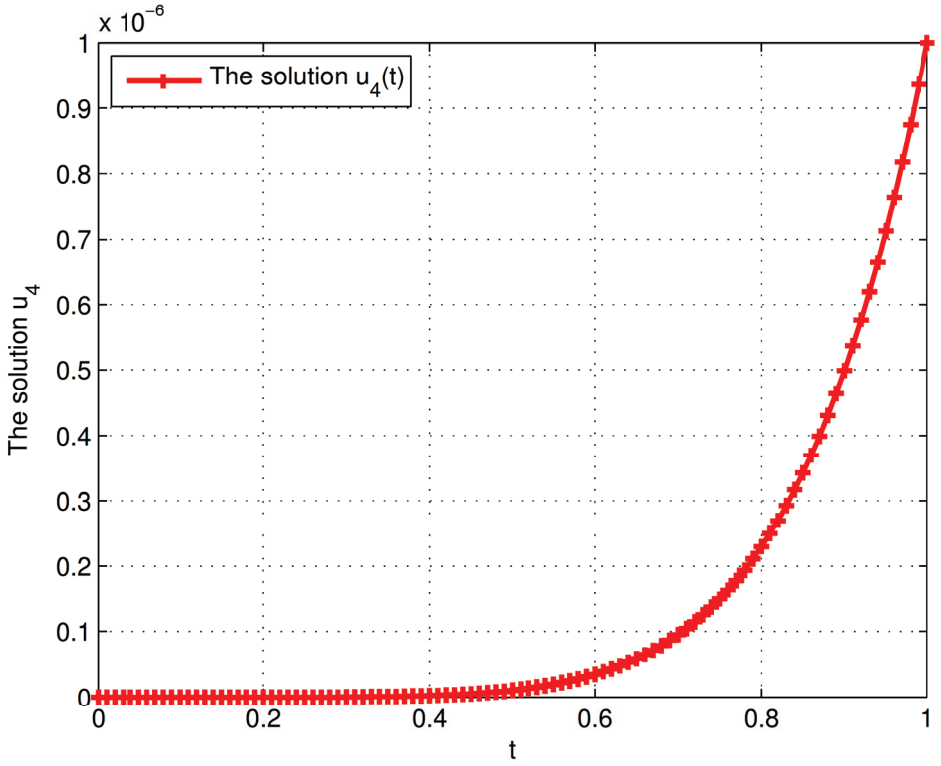

Figure 5. Trajectory 2 of the model (99) solution.

Example 4. *We consider the following problem:*

$$\begin{cases} -{}^{c}D^{3}_{0+}\phi_{\frac{3}{2}}\left(D^{\frac{7}{2}}_{0+}u(t)\right)+\dfrac{3}{5}=0, \quad 0<t<1, \\ u(0)=D^{\frac{6}{7}}_{0+}u(0)=D^{\frac{13}{7}}_{0+}u(0)=0, \\ D^{\frac{7}{2}}_{0+}u(0)=0, \quad (\phi_{\frac{3}{2}}(D^{\frac{7}{2}}_{0+}u(0)))''=0, \\ \phi_{\frac{3}{2}}(D^{\frac{7}{2}}_{0+}u(1))=\dfrac{7}{2}\displaystyle\int_0^1 s^{-\frac{1}{2}}\phi_{\frac{3}{2}}(D^{\frac{7}{2}}_{0+}u(s))ds, \\ D^{\frac{5}{2}}_{0+}u(1)=1152\displaystyle\int_0^1 D^{\frac{1}{2}}_{0+}u(s)dA_1(s) \\ +64\displaystyle\int_0^{\frac{10}{11}} D^{\frac{3}{2}}_{0+}u(s)dA_2(s)+4\sum_{i=1}^{\infty}2^{-\frac{1}{2}i}D^{\frac{3}{2}}_{0+}u(2^{-\frac{1}{16}i}), \end{cases} \tag{100}$$

where

$$A_1(t)=\begin{cases} 1, & t\in\left[0,\dfrac{1}{2}\right), \\ 9, & t\in\left[\dfrac{1}{2},1\right], \end{cases} \quad A_2(t)=\begin{cases} 3, & t\in\left[0,\dfrac{1}{2}\right), \\ 11, & t\in\left[\dfrac{1}{2},1\right]. \end{cases}$$

Proof. Let $p=\frac{3}{2}$, $\delta=3$, $\alpha=\frac{7}{2}$ $(n=4)$, $\beta=\frac{3}{2}$, $\gamma_1=\frac{6}{7}$, $\gamma_2=\frac{13}{7}$, $z_0=\frac{5}{2}$, $z_1=\frac{1}{2}$, $z_2=z_3=\frac{3}{2}$, $k_0=\frac{72}{9}$, $k_1=1152$, $k_2=64$, $k_3=4$, $\zeta=\frac{10}{11}$, $a_i=2^{-\frac{1}{2}i}$, $\xi_i=2^{-\frac{1}{16}i}$ $(i=1,2,\ldots)$, $b_0(s)=s^{-\frac{1}{2}}$, $b_1(s)\equiv 1$, $b_2(s)\equiv 1$, $(Hu)(t)=\Gamma(\frac{7}{2})\int_0^t u(s)ds$,

$$f(t,u,v,w)=\frac{3\left(\frac{2^{12}}{363738375\sqrt{\pi}}t^{\frac{19}{2}}+1\right)\left(\frac{2^{10}}{509233725}t^{\frac{21}{2}}+1\right)\left(\frac{1}{5600}t^{8}+1\right)}{5(|u|+1)(|v|+1)(|w|+1)}.$$

Then, we can regard the problem (100) as the problem (1). By using the above data, it is easy to check that f satisfies the condition $(\mathbf{A_5})$ with

$$l_{i,r}(t) = \frac{3}{5}\left(\frac{2^{12}t^{\frac{19}{2}}}{363738375\sqrt{\pi}} + 1\right)\left(\frac{2^{10}t^{\frac{21}{2}}}{509233725} + 1\right)\left(\frac{t^8}{5600} + 1\right) \ (i = 1, 2, 3).$$

Let $r_* = 1$. Then, by calculation, we have $U(r_*) > 0$, $Z(r_*) \leq 0.0245 < 1$, and $1 < M_h = \Gamma(\beta + 1) = \Gamma(2.5)$. Thus, all the assumptions of Theorem 5 are fulfilled. With these data, the numerical results in Figures 6 and 7 and Table 4 show that the solution u_5 has an upper bound. Among them, Figure 6 illustrates the relationship between the solution u_5 and its upper bound. For a clearer visualization of the trajectory of solution u_5, we provide Figure 7. Therefore, these numerical results validate the validity of Theorem 5. □

Table 4. The solution u_5 with its upper bound.

t	0	0.2	0.4	0.6	0.8	1
$u_5(t)$ $(\times 10^{-5})$	0	0.0000	0.0001	0.0050	0.0763	0.6353
The upper bound of $u_5(t)$	0	0.0673	0.1903	0.3496	0.5383	0.7523

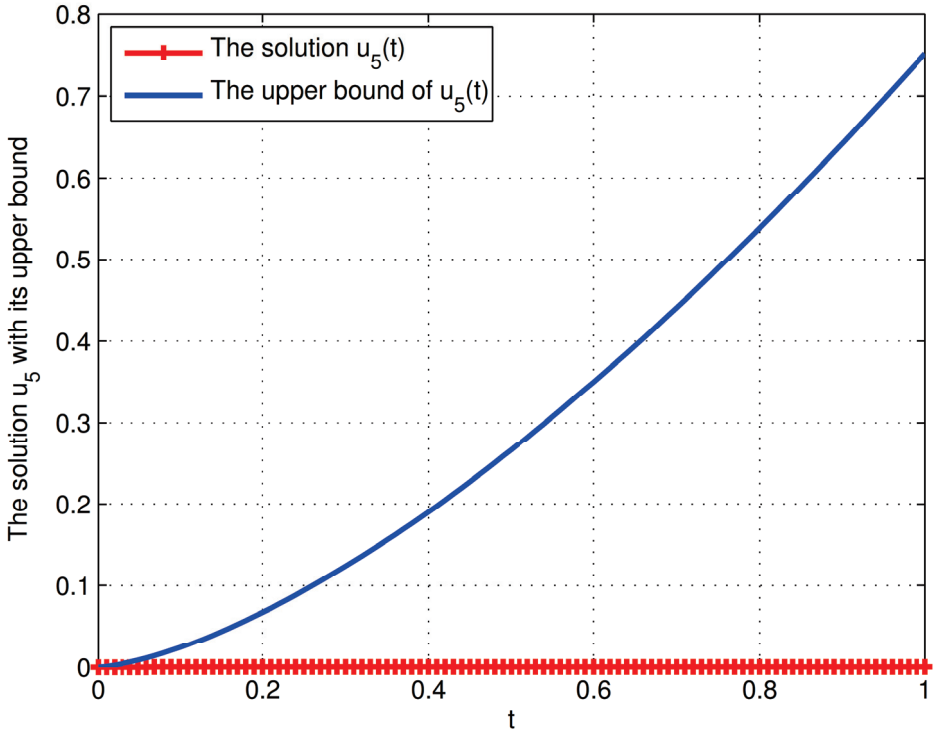

Figure 6. Trajectory 1 of the model (100) solution.

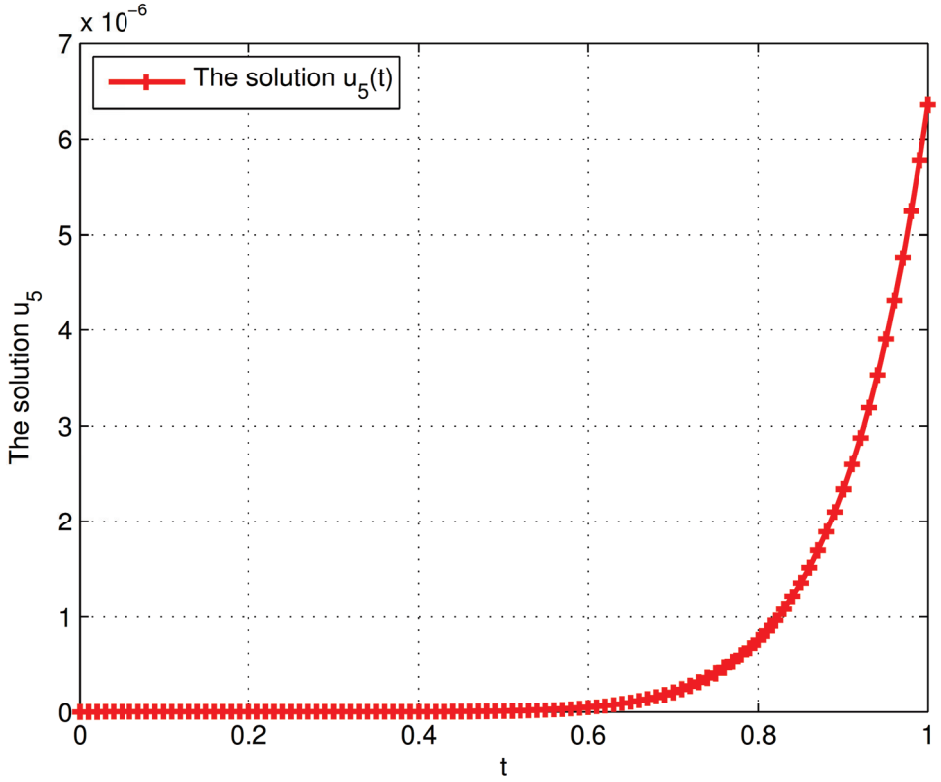

Figure 7. Trajectory 2 of the model (100) solution.

6. Conclusions

In this paper, we have addressed the problem of fractional differential equations with the p-Laplacian operator. By the method of reducing the order of fractional derivative, even when the nonlinear term involves fractional derivatives, we can still study the problem in the function space $C[0,1]$, which significantly simplifies our analysis. By employing the Schauder fixed point theorem and the Banach contraction principle, we established the existence and uniqueness of solutions. We have systematically validated our theoretical results through numerical examples, tabulated data, and graphical analyses. Furthermore, through analysis of the properties of Green's function, we developed and applied a novel approach to approximate solutions. This approach demonstrated effectiveness and practicality in estimating solutions. Notably, the generalized boundary conditions adopted in this work provided a powerful modeling tool for physics phenomena.

Author Contributions: Conceptualization, F.W. and L.L.; methodology, F.W. and L.L.; resources, F.W. and L.L.; funding acquisition, L.L.; writing—original draft preparation, F.W.; writing—review and editing, L.L., H.G., L.M. and Y.W.; supervision, L.L.; project administration, F.W., L.L., H.G. and Y.W. All authors have read and agreed to the published version of the manuscript.

Funding: This research was supported by the National Natural Science Foundation of China (11871302), the ARC Discovery Project Grant (DP230102079) and the Natural Science Foundation of Shandong Province (ZR2022MA009).

Data Availability Statement: No new data were created or analyzed in this study.

Conflicts of Interest: The authors declare no conflicts of interest.

References

1. Mainardi, F. *Fractional Calculus and Waves in Linear Viscoelasticity: An Introduction to Mathematical Models*; Imperial College Press: London, UK, 2010.
2. Valvano, S.; Alaimo, A.; Orlando, C. Analytical analysis of sound transmission in passive damped multilayered shells. *Compos. Struct.* **2020**, *253*, 112742. [CrossRef]
3. Bagley, R.L.; Torvik, P.J. A theoretical basis for the application of fractional calculus to viscoelasticity. *J. Rheol.* **1983**, *27*, 201–210. [CrossRef]
4. Kilbas, A.A.; Srivastava, H.M.; Trujillo, J.J. Theory and Applications of Fractional Differential Equations. In *North-Holland Mathematics Studies*; Elsevier Science B.V.: Amsterdam, The Netherlands, 2006; Volume 204.
5. Henderson, J.; Luca, R. *Boundary Value Problems for Systems of Differential, Difference and Fractional Equations: Positive Solutions*; Elsevier: Amsterdam, The Netherlands, 2016.
6. Podlubny, I. *Fractional Differential Equations*; Academic Press: San Diego, CA, USA, 1999.
7. Samko, S.G.; Kilbas, A.A.; Marichev, O.I. *Fractional Integrals and Derivatives: Theory and Applications*; Gordon and Breach Science Publishers: Philadelphia, PA, USA, 1993.
8. Kukushkin, M. On solvability of the Sonin–Abel equation in the Weighted Lebesgue space. *Fractal Fract.* **2021**, *5*, 77. [CrossRef]
9. Derbissaly, B.; Kirane, M.; Sadybekov, M. Inverse source problem for two-term time-fractional diffusion equation with nonlocal boundary conditions. *Fractal Fract.* **2024**, *183*, 114897. [CrossRef]
10. Zhang, L.; Liu, X.; Jia, M.; Yu, Z. Piecewise conformable fractional impulsive differential system with delay: Existence, uniqueness and Ulam stability. *J. Appl. Math. Comput.* **2024**, *70*, 1543–1570. [CrossRef]
11. Rahul, R.; Halder, S.; Kazemi, M.; Samei, M.E. A study on solvability and an iterative method for infinite systems of fractional integro-differential equations. *Bol. Soc. Mat. Mex.* **2025**, *31*, 73. [CrossRef]
12. Leibenson, L.S. General problem of the movement of a compressible fluid in a porous medium. *Izv. Akad. Nauk Kirgiz. SSSR* **1983**, *9*, 7–10.
13. Li, K.; Liu, B. Grow-up of weak solutions in a p-Laplacian pseudo-parabolic problem. *Nonlinear Anal. Real World Appl.* **2022**, *68*, 103657. [CrossRef]
14. Amoroso, E.; Bonanno, G.; Perera, K. Nonlinear elliptic p-Laplacian equations in the whole space. *Nonlinear Anal.* **2023**, *236*, 113364. [CrossRef]
15. Gallo, M.; Squassina, M. Concavity and perturbed concavity for p-Laplace equations. *J. Differ. Equ.* **2025**, *440*, 113452. [CrossRef]
16. Zhang, L.; Hou, W.; Nieto, J.J.; Wang, G. An anisotropic tempered fractional p-Laplacian model involving logarithmic nonlinearity. *Evol. Equ. Control Theory* **2024**, *13*, 1–11. [CrossRef]
17. Jong, K. Existence and uniqueness of positive solutions of a kind of multi-point boundary value problems for nonlinear fractional differential equations with p-Laplacian operator. *Mediterr. J. Math.* **2018**, *15*, 129. [CrossRef]
18. Jong, K.; Choi, H.; Ri, Y. Existence of positive solutions of a class of multi-point boundary value problems for p-Laplacian fractional differential equations with singular source terms. *Commun. Nonlinear Sci. Numer. Simulat.* **2019**, *72*, 272–281. [CrossRef]
19. Cheng, T.; Xu, X. Existence results for multi-point boundary value problem to singular fractional differential equations with a positive parameter. *J. Appl. Math. Comput.* **2022**, *68*, 3721–3746. [CrossRef]
20. Henderson, J.; Luca, R.; Tudorache, A. On a fractional differential equation with r-Laplacian operator and nonlocal boundary conditions. *Mathematics* **2022**, *10*, 3139. [CrossRef]
21. Feng, X.; Li, Y. Solvability of a fractional boundary value problem with problem with p-Laplacian operator on an infinite interval. *J. Appl. Anal. Comput.* **2023**, *13*, 3087–3106. [CrossRef]
22. Samei, M.E.; Karimi, L.; Kaabar, M.K.A. To investigate a class of multi-singular pointwise defined fractional q–integro-differential equation with applications. *AIMS Math.* **2022**, *7*, 7781–7816. [CrossRef]
23. Zhang, L.; Zhang, W.; Liu, X.; Jia, M. Positive solutions of fractional p-Laplacian equations with integral boundary value and two parameters. *J. Inequal. Appl.* **2020**, *2020*, 2. [CrossRef]
24. Guo, L.; Zhao, J.; Dong, S.; Hou, X. Existence of multiple positive solutions for Caputo fractional differential equation with infinite-point boundary value conditions. *J. Appl. Anal. Comput.* **2022**, *12*, 1786–1800. [CrossRef]
25. Chu, L.; Hu, W.; Su, Y.; Yun, Y. Existence and uniqueness of solutions to four-point impulsive fractional differential equations with p-Laplacian operator. *Mathematics* **2022**, *10*, 1852. [CrossRef]
26. Rezapour, S.; Boulfoul, A.; Tellab, B.; Samei, M.E.; Etemad, S.; George, R. Fixed point theory and the Liouville-Caputo integro-differential FBVP with multiple nonlinear terms. *J. Funct. Spaces* **2022**, *2022*, 6713533. [CrossRef]
27. Nazari, S.; Samei, M.E. An existence of the solution for generalized system of fractional q-differential inclusions involving p-Laplacian operator and sequential derivatives. *Bound. Value Probl.* **2024**, *2024*, 117. [CrossRef]
28. Baitiche, Z.; Derbazi, C.; Wang, G. Monotone iterative method for nonlinear fractional p-Laplacian differential equation in terms of Ψ-Caputo fractional derivative equipped with a new class of nonlinear boundary conditions. *Math. Methods Appl. Sci.* **2022**, *45*, 967–976. [CrossRef]

29. Hasanov, M. Initial value problems for fractional p-Laplacian equations with singularity. *AIMS Math.* **2024**, *9*, 12800–12813. [CrossRef]
30. Wang, G.; Yuan, H.; Baleanu, D. Stability analysis, existence and uniqueness of solutions for a fractional conformable p-Laplacian coupled boundary value problem on the disilane graph. *Qual. Theory Dyn. Syst.* **2024**, *23*, 218. [CrossRef]
31. Etemad, S.; Iqbal, I.; Samei, M.E.; Rezapour, S.; Alzabut, J.; Sudsutad, W.; Goksel, I. Some inequalities on multi-functions for applying in the fractional Caputo–Hadamard jerk inclusion system. *J. Inequal. Appl.* **2022**, *2022*, 84. [CrossRef]
32. Mursaleen, M.; Savaş, E. Solvability of an infinite system of fractional differential equations with p-Laplacian operator in a new tempered sequence space. *J. Pseudo-Differ. Oper. Appl.* **2023**, *14*, 57. [CrossRef]
33. Guran, L.; Mitrović, Z.; Reddy, G.; Belhenniche, A.; Radenović, S. Applications of a fixed point result for solving nonlinear fractional and integral differential equations. *Fractal Frac.* **2021**, *5*, 211. [CrossRef]
34. Bekri, Z.; Aljohani, S.; Samei, M.; Akgül, A.; Belhenniche, A.; Aloqaily, A.; Mlaiki, N. Unique solution analysis for generalized Caputo-type fractional BVP via Banach contraction. *Eur. J. Pure Appl. Math.* **2025**, *18*, 5979. [CrossRef]
35. Liu, X.; Jia, M.; Xiang, X. On the solvability of a fractional differential equation model involving the p-Laplacian operator. *Comput. Math. Appl.* **2012**, *64*, 3267–3275. [CrossRef]
36. Liu, X.; Jia, M.; Ge, W. The method of lower and upper solutions for mixed fractional four-point boundary value problem with p-Laplacian operator. *Appl. Math. Lett.* **2017**, *65*, 56–62. [CrossRef]
37. Wei, C.; Liu, X.; Jia, M.; Zhang, L. The monotone iterative method for the integral boundary value problems of fractional p-Laplacian equations with delay. *Int. J. Nonlinear Sci. Numer. Simul.* **2021**, *22*, 23–32. [CrossRef]
38. Liu, X.; Jia, M. The positive solutions for integral boundary value problem of fractional p-Laplacian equation with mixed derivatives. *Mediterr. J. Math.* **2017**, *14*, 94. [CrossRef]
39. Ahmad, B.; Agarwal, R.P.; Broom, A.; Alsaedi, A. On a coupled integro-differential system involving mixed fractional derivatives and integrals of different orders. *Acta Math. Sci.* **2021**, *41*, 1366–1384. [CrossRef]
40. Nyamoradi, N.; Ntouyas, S.K.; Tariboon, J. Existence of positive solutions to boundary value problems with mixed Riemann–Liouville and Quantum fractional derivatives. *Fractal Fract.* **2023**, *7*, 685. [CrossRef]
41. Wang, Y.; Liu, L.; Zhang, X.; Wu, Y. Positive solutions of an abstract fractional semipositone differential system model for bioprocesses HIV infection. *Appl. Math. Comput.* **2015**, *258*, 312–324. [CrossRef]
42. Zhang, X.; Liu, L.; Wu, Y.; Wiwatanapataphee, B. The spectral analysis for a singular fractional differential equation with a signed measure. *Appl. Math. Comput.* **2015**, *257*, 252–263. [CrossRef]
43. Wang, F.; Liu, L.; Wu, Y. Existence and uniqueness of solutions for a class of higher-order fractional boundary value problems with the nonlinear term satisfying some inequalities. *J. Inequal. Appl.* **2020**, *2020*, 196. [CrossRef]
44. Wang, F.; Liu, L.; Kong, D.; Wu, Y. Existence and uniqueness of positive solutions for a class of nonlinear fractional differential equations with mixed-type boundary value conditions. *Nonlinear Anal. Model. Control* **2019**, *24*, 73–94. [CrossRef]
45. Guo, L.; Liu, L.; Wu, Y. Iterative unique positive solutions for singular p-Laplacian fractional differential equation system with several parameters. *Nonlinear Anal. Model. Control* **2018**, *23*, 182–203. [CrossRef]
46. Ahmad, B.; Ntouyas, S.K.; Alsaedi, A.; Alalwi, K.A. Sequential fractional differential equations with parametric type anti-periodic boundary conditions. *J. Appl. Anal. Comput.* **2025**, *15*, 2921–2934. [CrossRef] [PubMed]
47. Bai, Z.; Lv, H. Positive solutions for boundary value problem of nonlinear fractional differential equation. *J. Math. Anal. Appl.* **2005**, *311*, 495–505. [CrossRef]

Disclaimer/Publisher's Note: The statements, opinions and data contained in all publications are solely those of the individual author(s) and contributor(s) and not of MDPI and/or the editor(s). MDPI and/or the editor(s) disclaim responsibility for any injury to people or property resulting from any ideas, methods, instructions or products referred to in the content.

computation

MDPI

Article

A Study of the Efficiency of Parallel Computing for Constructing Bifurcation Diagrams of the Fractional Selkov Oscillator with Variable Coefficients and Memory

Dmitriy Tverdyi * and Roman Parovik

Institute of Cosmophysical Research and Radio Wave Propagation FEB RAS, Mirnaya Street 7, 684034 Paratunka, Kamchatka, Russia; parovik@ikir.ru

* Correspondence: tverdyi@ikir.ru

Abstract

This paper presents a comprehensive performance analysis and practical implementation of a parallel algorithm for constructing bifurcation diagrams of the fractional Selkov oscillator with variable coefficients and memory (SFO). The primary contribution lies in the systematic benchmarking and validation of a coarse-grained parallelization strategy (MapReduce) applied to a computationally intensive class of problems—fractional-order systems with hereditary effects. We investigate the efficiency of a parallel algorithm that leverages central processing unit (CPU) capabilities to compute bifurcation diagrams of the Selkov fractional oscillator as a function of the characteristic time scale. The parallel algorithm is implemented in the ABMSelkovFracSim 2.0 software package using Python 3.13. This package also incorporates the Adams–Bashforth–Moulton numerical algorithm for obtaining numerical solutions to the Selkov fractional oscillator, thereby accounting for heredity (memory) effects. The Selkov fractional oscillator is a system of nonlinear ordinary differential equations with Gerasimov–Caputo derivatives of fractional order variables and non-constant coefficients, which include a characteristic time scale parameter to ensure dimensional consistency in the model equations. This paper evaluates the efficiency, speedup, and cost of the parallel algorithm, and determines its optimal configuration based on the number of worker processes. The optimal number of processes required to achieve maximum efficiency for the algorithm is determined. We apply the TAECO approach to evaluate the efficiency of the parallel algorithm: T (execution time), A (acceleration), E (efficiency), C (cost), O (cost optimality index). Graphs illustrating the efficiency characteristics of the parallel algorithm as functions of the number of CPU processes are provided.

Keywords: parallel algorithm; efficiency; speedup; cost; cost optimality index; Selkov fractional oscillator; Adams-Bashforth-Moulton numerical algorithm; bifurcation diagrams; Python

1. Introduction

Constructing bifurcation diagrams for various dynamic systems is of great practical importance, as it allows one to identify various regimes depending on changes in key parameters [1–3]. One such dynamic system, in our opinion, is the Selkov oscillator due to its important application in applied problems, for example, in biology for describing glycolytic reactions [4,5] or in seismology for describing microseisms [6]. From a mathematical perspective, the Selkov oscillator is a dynamic system consisting of two nonlinear first-

order ordinary differential equations that describes various oscillatory regimes, including self-oscillations.

A generalization of the Selkov oscillator to the case of memory effects is the fractional Selkov oscillator [7]. Memory effects here indicate that the current state of the system depends on previous states, i.e., on its prehistory [8–10]. These effects can be described using the theory of fractional calculus using fractional derivatives [11–13]. In this case, the Selkov fractional oscillator is a nonlinear system of two ordinary differential equations of fractional orders. The introduction of fractional derivatives also entails the introduction of an additional parameter—a characteristic time scale—to match the dimensions of the right- and left-hand sides of the model equations, which is important in the study of dynamic regimes [14].

In previous work [7,15], a quantitative and qualitative analysis of the Selkov fractional oscillator was conducted for cases where the orders of the fractional derivatives were constant and where the characteristic time scale was chosen to be unity. There, the system's equilibrium points were studied, the Adams–Bashforth–Moulton numerical algorithm was implemented to construct oscillograms and phase trajectories, and regular and chaotic regimes were also investigated using the maximum Lyapunov exponents [16].

Further development of the Selkov fractional oscillator involved introducing derivatives of fractional variable order [17–19], which also resulted in non-constant coefficients in the model equations [20–22]. Quantitative and qualitative analyses were conducted using an adapted Adams–Bashforth–Moulton algorithm, various oscillatory modes were investigated, and 2D and 3D bifurcation diagrams were constructed. These algorithms were implemented in the ABMSelkovFracSim 2.0 software package using the Python programming language and the PyCharm 2025.2 environment [23,24].

Constructing bifurcation diagrams is a rather computationally intensive task, as it requires repeatedly solving a system of fractional differential equations numerically. This leads to significant computational time expenditures [21,22]. Therefore, a parallel version of the bifurcation diagram calculation, depending on the characteristic time scale, was developed using Python tools. However, the parallel computation algorithm has not been studied for its efficiency depending on CPU processes. Therefore, in this paper, we examine its efficiency by addressing this gap and taking into account the available number of CPU processes, similar to the approach in [25].

The novelty and contribution of this work are as follows:

- We present a reproducible performance analysis (benchmarking) of a parallel MapReduce algorithm applied to the computationally demanding task of constructing bifurcation diagrams for a fractional-order system with memory (SFO). The analysis uses the TAECO metric set (Time, Acceleration, Efficiency, Cost, Cost Optimality Index).
- We provide practical guidelines for configuring parallel computations for similar parametric studies in fractional dynamics, including determining the optimal number of worker processes (found to be equal to the number of physical CPU cores in our test system).
- The parallel algorithm is integrated into the user-friendly ABMSelkovFracSim 2.0 software package, making high-performance bifurcation analysis accessible to researchers without expertise in parallel programming.
- This study highlights the limitations and trade-offs of the applied parallelization strategy, offering insights for future developments, such as hybrid CPU-GPU implementations.

Thus, this work contributes to the computational practice and software engineering for scientific computing, providing a validated tool and methodology for accelerating the analysis of complex fractional dynamical systems [26–28].

The remainder of this article is structured as follows: Section 2 introduces the necessary background and key concepts. Section 3 presents the problem statement. Section 4

https://doi.org/10.3390/computation14020032

details the Adams–Bashforth–Moulton numerical algorithm for solving the SFO system. Section 5 provides an overview of the ABMSelkovFracSim 2.0 software package. Section 6 describes the parallel algorithm for constructing bifurcation diagrams, including its detailed configuration and practical recommendations. Section 7 presents a performance analysis of the parallel algorithm with respect to the number of CPU worker processes. Finally, Section 8 concludes this paper.

2. Preliminaries

Definition 1. *The Gerasimov–Caputo fractional derivative of variable order* $0 < \alpha(t) < 1$ *of a function* $x(t) \in C^1[0,T]$ *has the following form [19]:*

$$\partial_{0t}^{\alpha(t)} x(t) = \frac{1}{\Gamma(1-\alpha(t))} \int_0^t \frac{\dot{x}(\tau)d\tau}{(t-\tau)^{\alpha(t)}}, \tag{1}$$

where $\alpha(t)$ *is a function from the class* $C[0,T]$*, and* $\Gamma(\cdot)$ *is the gamma function.*

Remark 1. *In the case where the variable order* $\alpha(t)$ *is constant, we arrive at the Gerasimov–Caputo fractional derivative, which has been studied quite well [29,30].*

Remark 2. *Here, we will not dwell on the properties of the fractional derivative (1), but we will point out that they can be studied in review articles [17,19], and refer to the relevant literature sources.*

Definition 2. *A bifurcation diagram is a graphical representation of changes in the structure of solutions of a dynamic system when the parameters change. It shows how the stable and unstable states of the system change depending on the values of the parameters.*

3. Statement of the Problem

Consider the following dynamic system:

$$\begin{cases} \partial_{0t}^{\alpha_1(t)} x(t) = -v_1(t)x(t) + w_1(t)y(t) + h_1(t)x^2(t)y(t), x(0) = x_0, \\ \partial_{0t}^{\alpha_2(t)} y(t) = v_2(t) - w_2(t)y(t) - h_2(t)x^2(t)y(t), y(0) = y_0. \end{cases} \tag{2}$$

where $x(t), y(t) \in C^1[0,T]$ are the unknown solution functions; $v_1(t) = \theta^{1-\alpha_1(t)}$, $v_2(t) = v_0\theta^{1-\alpha_2(t)}$, $w_1(t) = w_0\theta^{1-\alpha_1(t)}, w_2(t) = w_0\theta^{1-\alpha_2(t)}, h_1(t) = h_0\theta^{1-\alpha_1(t)}$, $h_2(t) = h_0\theta^{1-\alpha_2(t)}$ are functions from the class $C[0,T]$; θ is a parameter with time dimension; v_0, w_0, h_0 are given constants; $t \in [0,T]$ is the current process time; $T > 0$ is the simulation time; and x_0, y_0 are positive constants responsible for the initial conditions.

The fractional derivative operators of variable orders $0 < \alpha_1(t), \alpha_2(t) < 1$ in the dynamic system (2) are understood in the sense of Gerasimov–Caputo (1). Following the work in [21], we choose the following four types of functions $\alpha_1(t)$ and $\alpha_2(t)$:

1. Constant fractional orders:

$$\alpha_1(t) = a_1 = \text{const}, \qquad \alpha_2(t) = a_2 = \text{const},$$

   where $a_1, a_2 \in (0,1]$ are constant values of the fractional orders. Note that when $a_1 = a_2 = 1$, we arrive at the classical Selkov oscillator proposed by [4].
2. Cosine dependence:

$$\alpha_1(t) = a_1 - k_1\cos(\phi_1 t + f_1), \qquad \alpha_2(t) = a_2 - k_2\cos(\phi_2 t + f_2),$$

https://doi.org/10.3390/computation14020032

where $a_1, a_2 \in (0, 1]$ are the initial order values; $k_1, k_2 \in \mathbb{R}^+$ are the oscillation amplitudes; $\phi_1, \phi_2 \in \mathbb{R}^+$ are the oscillation frequencies; and $f_1, f_2 \in \mathbb{R}$ are the initial phases.

3. Exponential dependence:

$$\alpha_1(t) = a_1 - k_1 \exp(-\phi_1 t), \qquad \alpha_2(t) = a_2 - k_2 \exp(-\phi_2 t),$$

where $a_1, a_2 \in (0, 1]$ are the limiting values as $t \to \infty$, $k_1, k_2 \in \mathbb{R}^+$ are the initial deviations, and $\phi_1, \phi_2 \in \mathbb{R}^+$ are the rates of exponential decay.

4. Linear dependence:

$$\alpha_1(t) = \max(a_1 - k_1 t, \varepsilon), \qquad \alpha_2(t) = \max(a_2 - k_2 t, \varepsilon),$$

where $a_1, a_2 \in (0, 1]$ are the initial values at $t = 0$, $k_1, k_2 \in \mathbb{R}^+$ are the coefficients of linear decrease, and $\varepsilon = 0.01$ is the lower boundary for computational stability.

Definition 3. *The dynamic system (2) will be called a Selkov fractional oscillator with variable coefficients and memory, or simply a Selkov fractional oscillator (SFO).*

Remark 3. *It should be noted that in [31,32], a special case of the SFO (2) was investigated for* $\theta = 1$.

However, the characteristic time scale θ, as further studies of bifurcation diagrams [20–22] showed, plays an important role in the dynamics of the SFO. Therefore, as test examples, we will use the calculation of bifurcation diagrams depending on the values of the parameter θ.

4. Adams–Bashforth–Moulton Method

To study the SFO (2), we use the Adams–Bashforth–Moulton numerical method (ABM) from the family of predictor–corrector methods. The ABM has been studied and discussed in detail in [33–36]. We adapt this method to solve the SFO (2). To carry this out on a uniform grid of N points with step $\tau = T/N$, we introduce the functions $x^p_{k+1}, y^p_{k+1}, k = 0, \ldots, N-1$, which will be determined by the Adams–Bashforth formula (predictor):

$$\begin{cases} x^p_{k+1} = x_0 + \dfrac{\tau^{\alpha_{1,k}}}{\Gamma(\alpha_{1,k}+1)} \sum\limits_{j=0}^{k} \theta^1_{j,k+1}\Big(-v_{1,j}x_j + w_{1,j}y_j + h_{1,j}x_j^2 y_j\Big), \\ y^p_{k+1} = y_0 + \dfrac{\tau^{\alpha_{2,k}}}{\Gamma(\alpha_{2,k}+1)} \sum\limits_{j=0}^{k} \theta^2_{j,k+1}\Big(v_{2,j} - w_{2,j}y_j - h_{2,j}x_j^2 y_j\Big), \\ \theta^i_{j,k+1} = (k-j+1)^{\alpha_{i,k}} - (k-j)^{\alpha_{i,k}}, i = 1, 2. \end{cases} \tag{3}$$

For the corrector (Adams–Moulton formula), we obtain the following:

$$\begin{cases} x_{k+1} = x_0 + A_k\Big(-v_{1,k+1}x^p_{k+1} + w_{1,k+1}y^p_{k+1} + h_{1,k+1}x^{p\,2}_{k+1}y^p_{k+1}\Big) + \\ + A_k\left(\sum\limits_{j=0}^{k} \rho^1_{j,k+1}\Big(-v_{1,j}x_j + w_{1,j}y_j + h_{1,j}x_j^2 y_j\Big)\right), \\ y_{k+1} = y_0 + B_k\Big(v_{2,k+1} - w_{2,k+1}y^p_{k+1} - h_{2,k+1}x^{p\,2}_{k+1}y^p_{k+1}\Big) + \\ + B_k \sum\limits_{j=0}^{k} \rho^2_{j,k+1}\Big(v_{2,j} - w_{2,j}y_j - h_{2,j}x_j^2 y_j\Big). \end{cases} \tag{4}$$

where $A_k = \dfrac{\tau^{\alpha_{1,k}}}{\Gamma(\alpha_{1,k}+2)}$, $B_k = \dfrac{\tau^{\alpha_{2,k}}}{\Gamma(\alpha_{2,k}+2)}$, and weight coefficients in (3) are determined by the following formula:

https://doi.org/10.3390/computation14020032

$$\rho_{j,k+1}^{i} = \begin{cases} k^{\alpha_{i,k}+1} - (k-\alpha_{i,k})(k+1)^{\alpha_{i,k}}, j = 0, \\ (k-j+2)^{\alpha_{i,k}+1} + (k-j)^{\alpha_{i,k}+1} \text{-} 2(k-j+1)^{\alpha_{i,k}+1}, 1 \le j \le k, \\ 1, j = k+1, \\ i = 1, 2. \end{cases}$$

Formulas (3) and (4) constitute a modified ABM method adapted for the fractional-order SFO system with variable exponents ($\alpha_{1,k}, \alpha_{2,k}$) and coefficients. A key advantage of the ABM method is that it avoids solving nonlinear systems of equations at each step, thereby reducing the computational cost. However, the primary computational burden arises from the need to store the entire history (memory) of the solution vectors x_j and y_j, a characteristic feature of fractional integro-differential methods.

Remark 4. *The presented ABM method is explicit in its implementation, despite the use of the implicit Adams–Moulton Formula (4). Therefore, the ABM method is conditionally stable, like most explicit methods. It should also be noted that the order of accuracy of the ABM method is higher than that of the nonlocal explicit finite-difference scheme. The properties of the numerical ABM method (3) and (4), as well as convergence and stability issues, can be studied in [20–22].*

Based on Remark 4, the functions $\alpha_1(t)$ in the test examples for this article were chosen to be monotonically decreasing or not rapidly changing on the interval (0, 1), and the sampling step τ was chosen as it is small enough to prevent the solution from exhibiting unphysical oscillations or error growth.

The numerical algorithm ABM (3) and (4) was implemented in the ABMSelkovFracSim 2.0 software package for four types of $\alpha_1(t), \alpha_2(t)$ functions. We will refer to them as follows: ABMSelkovFracConst, ABMSelkovFracCos, ABMSelkovFracExp, and ABMSelkovFracLine.

5. ABMSelkovFracSim 2.0 Software Package

The authors of [22] provide a detailed description of the ABM software package. We will focus on the module for calculating bifurcation diagrams (the Bifurcation Analysis mode, Figure 1).

Figure 1 shows a screenshot of the main window in Bifurcation Analysis mode. The interface allows the user to input values for key SFO parameters, select one of four calculation methods based on the types of functions $\alpha_1(t)$ and $\alpha_2(t)$, and define the range and step size for the key parameter θ. Additionally, the user can specify the number of CPU worker processes to be used for the efficient parallel computation of the bifurcation diagram.

The left side of the ABMSelkovFracSim 2.0 software interface in the Bifurcation Analysis mode shows visualizations of the calculation results in the form of bifurcation diagrams and graphs of the functions $x(\theta), y(\theta)$. In Figure 1, the bifurcation diagram shows two ranges of parameter θ values, within which different dynamic SFO modes exist [21].

Remark 5. *It should be noted that the following useful information is displayed in the interface for the user of the ABMSelkovFracSim 2.0 software package: the time taken to calculate the bifurcation diagram, the number of processed points during the simulation and the progress bar of the algorithm's operation, and the possible presence of errors in the calculation.*

Next, we will discuss in more detail the implementation of the parallel part of the bifurcation diagram calculation algorithm in the ABMSelkovFracSim 2.0 software.

https://doi.org/10.3390/computation14020032

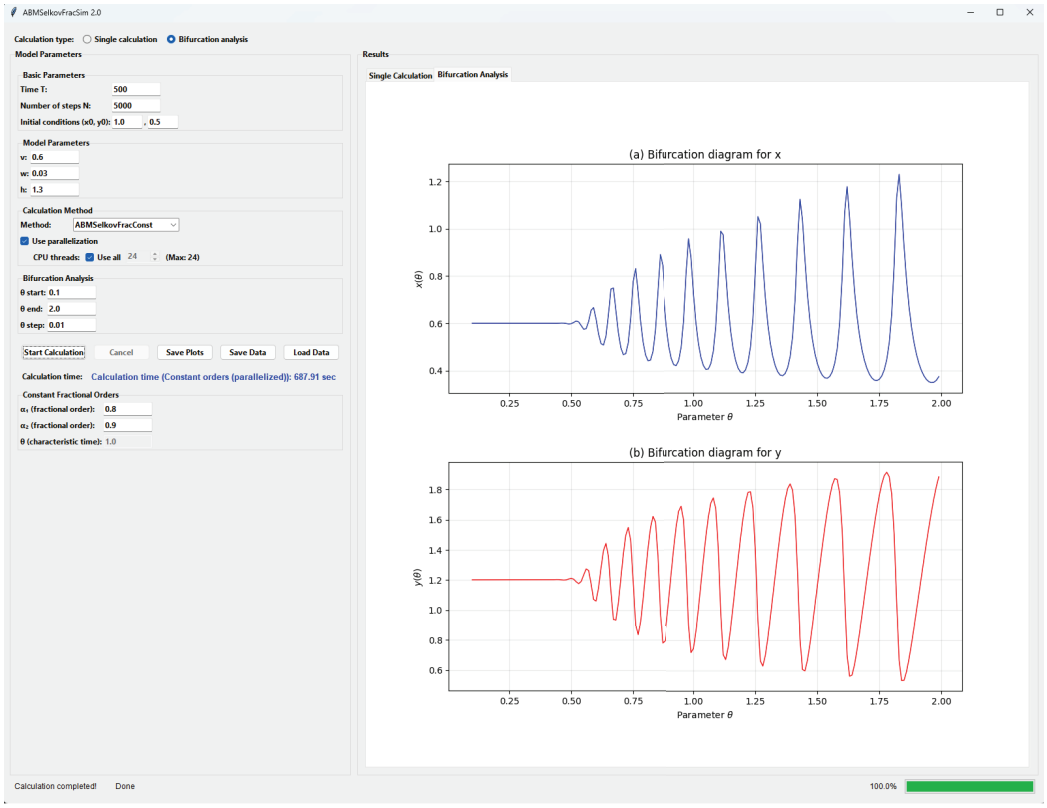

Figure 1. A screenshot of the main window of the ABMSelkovFracSim 2.0 software package in the Bifurcation Analysis mode.

6. Parallel Implementation of the Bifurcation Diagram Calculation Algorithm

Parallel implementation of algorithms is an important and relevant task in reducing their execution time. There are many approaches and technologies for parallelizing algorithms; these can be studied, for example, in [37,38]. In this section, we will describe a parallelization method based on the built-in libraries of the Python 3.13 programming language [23].

Because the numerical ABM algorithm (3) and (4) cannot be parallelized at the level of individual time steps due to data dependencies between the solution grid functions x_k and y_k, we adopt a parametric parallelization approach. Specifically, we parallelize the multiple independent computations required for each discrete value of the parameter θ within a specified interval. That is, the operating principle of our parallel algorithm consists of the following steps: a separate independent process is created for each value of the parameter θ; processes are executed in parallel on multiple processor cores; the results are collected after all calculations are completed. This is the classic "MapReduce" approach, where Map is the distribution of calculations across processes, and Reduce is the collection and merging of the results. This approach is optimal for parametric studies, where each calculation is independent of the others.

To implement this approach, we will use Native Python Multiprocessing (Python Multiprocessing, ProcessPoolExecutor) technology from the Python Standard Library (Algorithm 1).

https://doi.org/10.3390/computation14020032

Algorithm 1 Bifurcation analysis with parallel computing

Step 1: The user runs the bifurcation analysis
Step 2: Create a list of values $\theta = [\theta_1, \theta_2, \ldots, \theta_n]$
for $i = 1$ to n **do**
    Create a task T_i to evaluate for $\theta = \theta_i$
end for
Step 4: Initialize **ProcessPoolExecutor** with N processes
Step 5: Assign tasks $T_1, T_2, \ldots, T_n$ to processes
Step 6: ▷ Parallel execution
for $k = 1$ to N **in parallel do**
    Independently compute results for assigned tasks
end for
Step 7: Collect all results from processes
Step 8: Combine results into a single data structure
Step 9: Build a common bifurcation graph

Remark 6. *Let's highlight the key features of Algorithm 1:*

1. *Data parallelism: each value of θ_i is processed independently.*
2. *Process-based parallelism: the implementation uses separate operating system processes, not threads, to circumvent Python's Global Interpreter Lock (GIL) and achieve true concurrent execution.*
3. *Master–worker pattern: the master process distributes tasks, and workers perform computations.*
4. *Fault tolerance: an error in one process does not affect others.*
5. *Dynamic load balancing: ProcessPoolExecutor automatically distributes tasks.*

Remark 7. *It is important to note that Pythonuses multiprocessing, not threading, for computationally intensive tasks. This is due to the GIL, which makes threading ineffective for numerical calculations. Each Python process has its own interpreter and memory, allowing for full utilization of multi-core processors. Therefore, in this paper, the term "worker processes" refers to operating system processes created via ProcessPoolExecutor.*

We do not use other CPU parallelization technologies here for the following reasons: OpenMP is used for parallelization within a single process [39], which is not possible in our case. MPI is used for distributed computing on clusters, which is also not necessary in our case [40]. Threading: threads in Python have a GIL and are not suitable for numerical calculations [41].

6.1. Parallel Configuration

The parallel configuration of the ABM software suite consists of the following steps:

- Partitioning strategy: The data parallelism strategy is used. The initial set of values for the parameter θ (e.g., $[\theta_1, \theta_2, \ldots, \theta_n]$) is partitioned into n independent tasks.
- Task granularity: Each task has a coarse-grained granularity. This includes a full calculation of the system dynamics (solving a system of differential equations) for a single value of θ using the Adams–Bashforth–Moulton method. This granularity is optimal because the computation time for a single θ significantly exceeds the overhead of process creation and interprocess communication.
- Process binding/pinning: Not used in the current implementation. Processes are scheduled by the operating system. We acknowledge that pinning processes to specific physical cores (e.g., using taskset on Linux or libraries like numexpr and affinity) could reduce the overhead of process migration between cores and improve cache utilization, especially on NUMA systems. This optimization is planned for future releases.
- Result aggregation method: the MapReduce model is used.

https://doi.org/10.3390/computation14020032

- Map: The main process creates a pool of worker processes and distributes tasks (theta values) among them using ProcessPoolExecutor.map() or submit(). This function provides dynamic load balancing.
- Reduce: Upon completion of the computation, the main process collects the results (the x(theta) and y(theta) values at the final point in time). The results are returned in the order in which the tasks were completed (as_completed), but to plot the correct bifurcation diagram, they are then sorted in ascending θ (see the update_bifurcation_plots function in the code). This ensures that the graph will be plotted correctly, regardless of the order in which the calculations were completed.

6.2. Practical Recommendations and Limitations

Based on our performance analysis, we provide the following practical recommendations for users of the ABMSelkovFracSim 2.0 package and for researchers implementing similar parallel parametric studies:

- The optimal number of worker processes is typically equal to the number of physical CPU cores. In our tests, eight processes (matching eight physical cores) yielded the best efficiency–cost trade-off. Using more processes than physical cores leads to diminishing returns due to increased overhead.
- For memory-intensive fractional-order problems, the coarse-grained parallelism (one process per parameter value) is effective because the computation time for each task is large compared to inter-process communication costs.
- The TAECO metrics provide a comprehensive view of parallel performance. Users should monitor not only speedup (A_p) but also efficiency (E_p) and cost optimality (O_p) to assess the true benefit of parallelization.
- Limitations: The current implementation is designed for shared-memory systems (multi-core CPUs). It does not support distributed memory (cluster) environments. Also, parallel efficiency is limited by the inherently serial parts of the algorithm (Amdahl's law). For future work, hybrid CPU-GPU parallelism could be explored to accelerate the internal ABM solver itself.

We now turn to the main goal of our article: studying the efficiency of a parallel algorithm for calculating bifurcation diagrams.

7. Analysis of Algorithm Efficiency Based on Average Execution Time

7.1. Methodology of Performance Evaluation and Fairness of Comparison

In this study, we follow the following methodology:

1. **Identical computational code:** The sequential version of the algorithm ($p = 1$) uses exactly the same code for numerical solution of the SFO (ABM method, Formulas (3) and (4)) as each task in the parallel pool. This guarantees that identical numerical work is compared for each parameter value θ. The difference lies only in the way the loop over θ is organized: a sequential `for` loop versus task distribution across processes using `ProcessPoolExecutor`.
2. **Accounting for all stages:** The measured execution time $T_p(N)$ includes all stages common to both versions: data initialization, the loop (or task scheduling) over θ, numerical integration of system (2) for each θ, and collection of result arrays. Visualization time (plotting) is excluded from measurements as it is performed single-threaded after calculations are completed and is identical in both cases.
3. **Overhead of parallelization:** The parallel version inevitably incurs additional costs: creating and managing a process pool, serializing/deserializing data for inter-process communication, and synchronization. The presence of these costs is not a drawback

https://doi.org/10.3390/computation14020032

of the method but represents its inherent property. Precisely to account for these and analyze total costs, we use the extended TAECO metric set, not just speedup. The decrease in efficiency E_p and increase in cost optimality index O_p for $p > 8$ (Figures 2–4) are direct evidence of the growing role of these overheads.

4. **Discussion of possible optimizations:** We acknowledge that the sequential Python implementation is not highly optimized for single-core performance. It could potentially be accelerated through vectorization of operations (NumPy libraries), just-in-time (JIT) compilation (Numba), or a C/C++ implementation of the computational kernel. However, such optimizations are beyond the scope of this paper, which focuses on evaluating the effectiveness of the MapReduce parallelization strategy for parametric studies of fractional calculus problems. The chosen baseline sequential code is typical and easily reproducible, allowing us to clearly isolate and evaluate the gains from parallelization itself. Optimizing performance on a single-core system is an important but separate task that can be considered for future development of the ABMSelkovFracSim package.
5. **Time measurement methodology**: All execution time measurements were conducted using wall-clock time by calling the high-precision time.perf_counter() timer from the Python standard library. This allows for accounting for all factors affecting the actual speedup of a parallel algorithm, including the overhead of organizing parallel computations. To ensure measurement stability, a single warm-up run was performed before each series of experiments (for a fixed number of processes p and problem size N), the results of which were not taken into account. All experiments were conducted on a dedicated workstation with unnecessary background processes disabled to minimize the impact of external workloads on the results.

Thus, the presented comparison is valid for the stated goal: demonstrating that the parallel strategy based on `ProcessPoolExecutor` provides significant and measurable acceleration for the computationally intensive task of constructing bifurcation diagrams of the SFO, with optimal use of computational resources ($p \approx N_{\text{physical_cores}}$).

7.2. Experimental Setup and Reproducibility

To ensure transparency and facilitate reproducibility of our results, we provide a detailed description of the experimental setup. All performance measurements were conducted on a workstation with the following hardware and software configuration:

- **CPU:** AMD Ryzen 7 7800X3D (8 physical cores, 16 logical threads due to Simultaneous Multithreading), base clock 4.2 GHz, boost frequency up to 5.0 GHz, L2 cache: 8 MB (1 MB per core), L3 cache: 96 MB (64 MB 3D V-Cache + 32 MB standard).
- **RAM:** 32 GB DDR5.
- **Operating system:** Microsoft Windows 10 Pro 64-bit (build 22H2).
- **Python environment:** Python 3.13.0. The main libraries used were the standard Python multiprocessing module and NumPy for numerical operations. A full list of dependencies for the ABMSelkovFracSim 2.0 package is available from the authors upon reasonable request.
- **System settings:** The Windows power plan was set to "High Performance." No specific CPU affinity (core pinning) was enforced for the Python processes; they were managed by the default OS scheduler. Background applications were minimized during testing.

Reproducibility statement: The ABMSelkovFracSim 2.0 software package, which contains the complete implementation of the sequential and parallel algorithms described in this paper, is proprietary software developed within the framework of the state assignment of IKIR FEB RAS. Due to institutional policies and licensing restrictions, the

https://doi.org/10.3390/computation14020032

source code cannot be publicly distributed at this time. However, to enable verification and reproduction of the key performance results, the authors provide the following:

1. A detailed description of the algorithm (Section 6) and its configuration (Sections 6.1 and 6.2).
2. The exact mathematical formulation of the problem (Section 3) and the numerical method (Section 4).
3. The complete set of parameters used for all test examples (Sections 7.2–7.4).
4. The raw measurement data (average execution time and standard deviation) for all experiments, presented in Tables 1–3.

The computational experiments can be reproduced by implementing the Adams–Bashforth–Moulton method (Equations (3) and (4)) for the SFO system (Equation (2)) and applying the parallel MapReduce pattern (Algorithm 1) using Python's `ProcessPoolExecutor` with the parameters specified in the test examples. For access to the compiled software package for verification purposes or for any additional information required to replicate this study, interested researchers are encouraged to contact the corresponding author directly.

Remark 8. *It should be noted that the obtained values for the optimal number of processes* $(p = 8)$ *directly correspond to the number of physical cores of the test processor. This is an expected result for problems with coarse-grained parallelism and intensive memory usage, typical for parametric studies of dynamic systems. However, the performance and optimal efficiency point of a parallel algorithm may demonstrate sensitivity to a specific hardware architecture: processor topology (e.g., the number of cores per die, the presence of simultaneous multithreading technology-SMT/HT), cache hierarchy and size, as well as the memory subsystem configuration (NUMA vs. UMA). On systems with a different configuration (e.g., with a higher number of cores but a smaller shared L3 cache, or in server multiprocessor NUMA configurations), the balance between speedup and overhead may shift, which can potentially change the empirically determined value of* p_{opt}*. Therefore, the tuning recommendations provided (starting with a number of processes equal to the number of physical cores) should be considered as a starting point for fine-tuning in a particular computing environment.*

All timing measurements presented in this section were performed for the complete parallel computation cycle of the bifurcation diagram within a single call of the `Bifurcation analysis` function. The measured execution time $T_p^i(N)$ includes (1) initialization of the process pool (`ProcessPoolExecutor`); (2) task distribution (Map): serialization of parameters and their transfer to worker processes; (3) parallel execution: solving system (2) for each value of the parameter θ using the Adams–Bashforth–Moulton numerical method (3) and (4)—the most computationally intensive part; (4) collection of results (Reduce): deserialization and aggregation of the results from all processes. The measurement does not include stages unrelated to parallel computations: initialization of the graphical user interface (GUI), loading parameters from input fields, and, most importantly, final visualization (plotting). Plotting is performed single-threaded after all computations and synchronization are completed. This separation allows us to evaluate the performance of the parallel computational component of the algorithm in isolation.

Let us analyze the efficiency of the parallel computation algorithm of the ABM-SelkovFracSim 2.0 software package in the mode of calculating and constructing a bifurcation diagram (Bifurcation analysis).

7.3. Performance Metrics and Methodology

Since each run of the bifurcation analysis yields slightly different execution times T (in seconds), and the number of experiments is finite, we treat T as a discrete random variable characterized by a distribution function and an expected value:

https://doi.org/10.3390/computation14020032

$$T_p(N) = \frac{1}{L}\sum_{i=1}^{L} T_p^i(N), \tag{5}$$

where i is the index of the Bifurcation analysis numerical experiment; L is the sample size; p is the number of worker processes; and N is the number of nodes in the uniform grid of the numerical method, i.e., the size of the input data.

The standard deviation of the execution time for a given number of worker processes p and problem size N is calculated as follows:

$$\sigma_p(N) = \sqrt{\frac{1}{L-1}\sum_{i=1}^{L}\Big(T_p^i(N) - T_p(N)\Big)^2}. \tag{6}$$

The values of $T_p(N)$ and $\sigma_p(N)$ for the test examples are presented in Tables 1–3.

The efficiency of a parallel algorithm measures how effectively it utilizes the available computational resources (worker processes) compared to the sequential version. It is defined as the ratio of the speedup achieved to the number of processes used. However, as the number of worker processes increases, hardware and software limitations on parallel speedup become more pronounced. These limitations include the high time costs of parallelizing the task and reassembling all computational results [42], known as Amdahl's law [43,44]. To represent various data on average execution time, we will use the following parameters in [sec]:

- $T_1(N)$—the execution time of a test example of size N required by the sequential Bifurcation analysis algorithm;
- $T_p(N)$—the execution time of a test example of size N required by the parallel Bifurcation analysis algorithm on a machine with $p \geq 2$ worker processes.

Let us calculate $T_p(N)$ for different numbers of used worker processes p in [units] with a step of 1.

To obtain efficiency estimates, data on average execution time are considered in terms of (TAECO) [25], applicable to algorithms: T (execution time), A (acceleration, speedup), E (efficiency), C (cost), O (cost-optimal indicator).

- $A_p(N)$—is the speedup of the algorithm, in [units], provided by the parallel version of the algorithm compared to the sequential one, and is calculated as follows:

$$A_p(N) = \frac{T_1(N)}{T_p(N)}. \tag{7}$$

- $E_p(N)$—is the efficiency of the algorithm, in [units/process], of using a given number p of worker processes and is defined by the following ratio:

$$E_p(N) = \frac{T_1(N)}{p \cdot T_p(N)} = \frac{A_p(N)}{p}, \tag{8}$$

  moreover, by definition, the sequential algorithm has the greatest efficiency, $E_1(N) = 1$. Therefore, for a parallel algorithm, it is better if $E_p(N) \to 1$.
- $C_p(N)$—the cost of the algorithm, in [sec. $\times$ process], which is determined by the product of a given number p of worker processes and the T execution time of the parallel algorithm. The cost is determined by the following ratio:

$$C_p(N) = p \cdot T_p(N). \tag{9}$$

https://doi.org/10.3390/computation14020032

- $O_p(N)$—is the cost-optimal indicator (COI) of the algorithm, in [units × process], characterized by a cost proportional to the complexity of the most efficient sequential algorithm:

$$O_p(N) = \frac{C_p(N)}{T_1(N)}, \tag{10}$$

and the closer the value is to 1, the better, i.e., the cheaper the use of the parallel algorithm in terms of engaging worker processes.

7.4. Test Examples

The calculations of efficiency indicators (5)–(10) and their visualization were performed in the MatlabR2025b computer mathematics system.

Example 1. *For the first example, we will choose the ABMSelkovFracCos method and the following parameter values for FOS (2): $T = 200, N = 3000, x_0 = 1, y_0 = 0.5, v_0 = 0.6, w_0 = 0.03$, $h_0 = 1.3$, $a_1 = 0.8, a_2 = 0.9, k_1 = 0.04, k_2 = 0.02, \phi_1 = 3.5, \phi_2 = 1.5$, $f_1 = f_2 = 0$.*

$$\alpha_1(t) = 0.8 - 0.04\cos(3.5t), \quad \alpha_2(t) = 0.9 - 0.02\cos(1.5t).$$

In the Bifurcation Analysis mode with all the same parameters, the calculation method ABMSelkovFracCos is used, but with $\theta \in [0.1, 2.0]$ and step $h = 0.01$. To obtain the average execution time according to (5), we define $L = 10$, which will allow for smoother graphs for both average time and efficiency analysis.

The results are shown in Table 1 and Figure 2 below.

Table 1. Average execution time $T_p(N)$ and standard deviation $\sigma_p(N)$ of the Test Example 1 with a varying number of worker processes.

p, [Processes]	$T_p(3000)$, [s]	$\sigma_p(3000)$, [s]
1	4765	70.0003
2	2612	53.1686
3	1645	56.8393
4	1251	33.7665
5	1023	19.4882
6	868	8.9697
7	775	4.9542
8	759	11.2071
9	716	8.8097
10	629	7.6884
11	601	4.5814
12	589	13.8840
13	568	2.0790
14	558	3.5340
15	544	1.8409
16	536	1.8974

Figure 2 presents the results of the efficiency analysis of the parallel Bifurcation Analysis algorithm for the ABMSelkovFracCos method compared to its sequential counterpart. The results are presented as histograms for greater clarity. Parallelization, specific to this computer, allows for a maximum speedup of up to 8.9 times.

Figure 2 shows a dependence close to exponential: average execution time vs. number of worker processes. Increasing the number of worker processes at $p \leq 8$ gives a greater performance gain compared to the sequential algorithm, but increasing the number of worker processes at $p > 8$ yields less and less performance gain. In the COI estimate, we see the opposite trend: the cost of using parallel algorithms does not change until around

https://doi.org/10.3390/computation14020032

$p = \pm 7$, and then increases linearly and proportionally to the growth in the number of worker processes. Consequently, at $p = 8$ we have the best efficiency coefficient of the parallel algorithm $E_8(3000) = 0.785$ in relation to the cost of using the parallel algorithm $O_8(3000) = 1.27 \to 1$ while obtaining a speedup of 6.28 times. As a result, we can say that the Bifurcation Analysis mode is optimally parallelized on 7–8 processes, which, depending on the maximum number of CPUs of a particular computer, will allow for running several copies of the ABMSelkovFracSim 2.0 software package itself for simultaneous work in several windows.

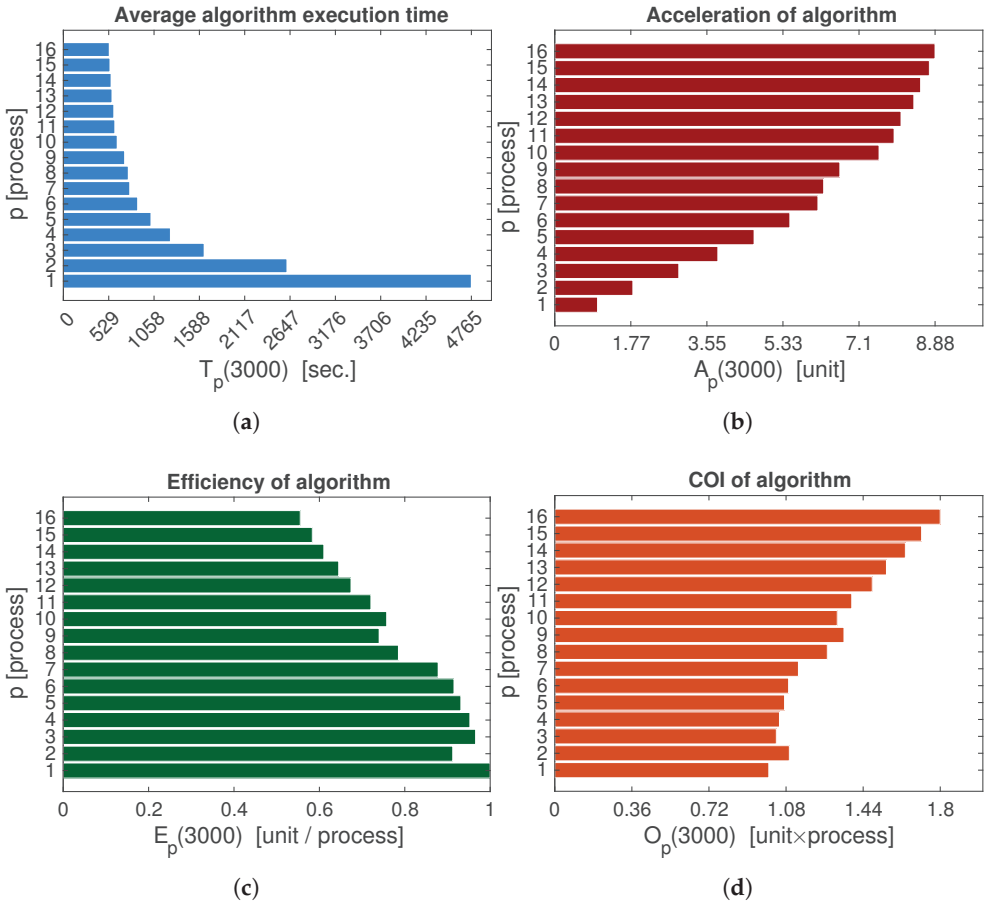

Figure 2. Average execution time and efficiency estimation of a parallel algorithm implementing Bifurcation analysis (Example 1): **(a)** $T_p(3000)$, **(b)** $A_p(3000)$, **(c)** $E_p(3000)$, **(d)** $O_p(3000)$.

An analysis of the standard deviation values $\sigma_p(3000)$ for the parallel algorithm for calculating bifurcation diagrams (Example 1, ABMSelkovFracCos method) allows us to draw the following conclusions:

1. In all cases, the standard deviation is of less than 1.4% of the corresponding average execution time $T_p(3000)$. For example, for $p = 8$: $\sigma_8(3000) = 11.2071$ s at $T_8(3000) = 759$ s, which is approximately 1.4%. Such a relatively small spread indicates high stability and reproducibility of the measurements, confirming the reliability of the presented average values for efficiency analysis.
2. A tendency toward a decrease in the absolute value of the standard deviation is observed as the number of processes p increases:
   - For sequential execution ($p = 1$), $\sigma_1 = 70.0$ s is the highest value.
   - At maximum utilization ($p = 16$), $\sigma_{16} = 1.8974$ s—the value has decreased by more than three times.

   This may be due to two factors:

https://doi.org/10.3390/computation14020032

- Smoothing out random system impacts: During parallel execution, multiple independent computing processes distributed over time statistically "average out" the impact of random fluctuations in system load (background processes, interrupts, caching), which can lead to more noticeable deviations in a sequential run.
- Reducing task execution time: With a larger p, the overall execution time T_p is significantly reduced. During this shorter period of time, the system is less likely to be subject to significant background impacts, which reduces variability.

3. The most important range from a practical perspective is p from 6 to 8 (where the best trade-off between speedup and efficiency is observed, see Figure 2). In this range, the standard deviation is 8–11 s, which is relatively small. This means that the recommendation for choosing the optimal number of processes $(p = 8)$ is statistically robust—with repeated runs, the execution time will fluctuate only slightly, and the expected speedup will be achieved with a high probability.
4. User interpretation: The small standard deviation, especially in the region of the optimal p, gives the user of the ABMSelkovFracSim 2.0 package high confidence in the predictability of computation times. This is important for planning computational experiments. The presented standard deviation data confirm that the execution time measurements are statistically reliable. The observed pattern of decreasing σ_p with increasing p is consistent with the expected behavior of the parallel version of the algorithm and further substantiates the possibility of choosing the optimal configuration $(p = 8)$ not only based on the average speedup criterion but also on the criterion of low result variability.

Example 2. *To evaluate the efficiency of the parallel version of the calculation algorithm, we will choose the ABMSelkovFracExp method.*

$$\alpha_1(t) = 0.8 - 0.04\exp(-3.5t), \alpha_2(t) = 0.9 - 0.02\exp(-1.5t).$$

We will select the parameter values from Example 1. To obtain the average time (5), the sample size is $L = 10$.

The results are shown in Table 2 and Figure 3 below.

In the case of Test Example 2 for the ABMSelkovFracExp method, parallelization, for this particular computer, allows for a maximum speedup of ≈9 times. The estimates for (Figure 3) have the same trends as for Test Example 1 (Figure 2). However, for $p \leq 5$, the cost of using parallel algorithms $O_{p\to5}(3000) \approx 1$, and therefore $E_{p\to5}(3000) \to 1$, i.e., almost as effective as the sequential algorithm, with a 5-fold performance increase.

Table 2 shows that the absolute values of σ_p decrease with increasing p: for $p = 1$: $\sigma_1 = 82.5486$ s; for $p = 16$: $\sigma_{16} = 1.0750$ s; a decrease of more than 70 times is observed, which is even more pronounced than in Example 1. The relative standard deviation is small: in the region of the optimal $p = 8$:

$$\frac{\sigma_8}{T_8} \approx \frac{4.3512}{748} \approx 0.58\%.$$

This indicates very high measurement stability.

Example 3. *Let us consider a parallel version of the algorithm for the ABMSelkovFracLinear method. For simplicity, we set* $k_1 = k_2 = 0.001$.

$$\alpha_1(t) = \max(0.8 - 0.001t, 0.01), \alpha_2(t) = \max(0.9 - 0.001t, 0.01),$$

https://doi.org/10.3390/computation14020032

The remaining parameter values are left unchanged.

Table 2. Average execution time $T_p(N)$ and standard deviation $\sigma_p(N)$ of the Test Example 2 with a varying number of worker processes.

p, [Processes]	$T_p(3000)$, [s]	$\sigma_p(3000)$, [s]
1	4766	82.5486
2	2439	43.2883
3	1660	23.0169
4	1260	20.8180
5	1024	6.1364
6	862	7.9589
7	780	6.5693
8	748	4.3512
9	658	1.9889
10	628	6.1427
11	604	5.5538
12	577	6.4326
13	560	1.8886
14	550	5.5538
15	538	1.5811
16	531	1.0750

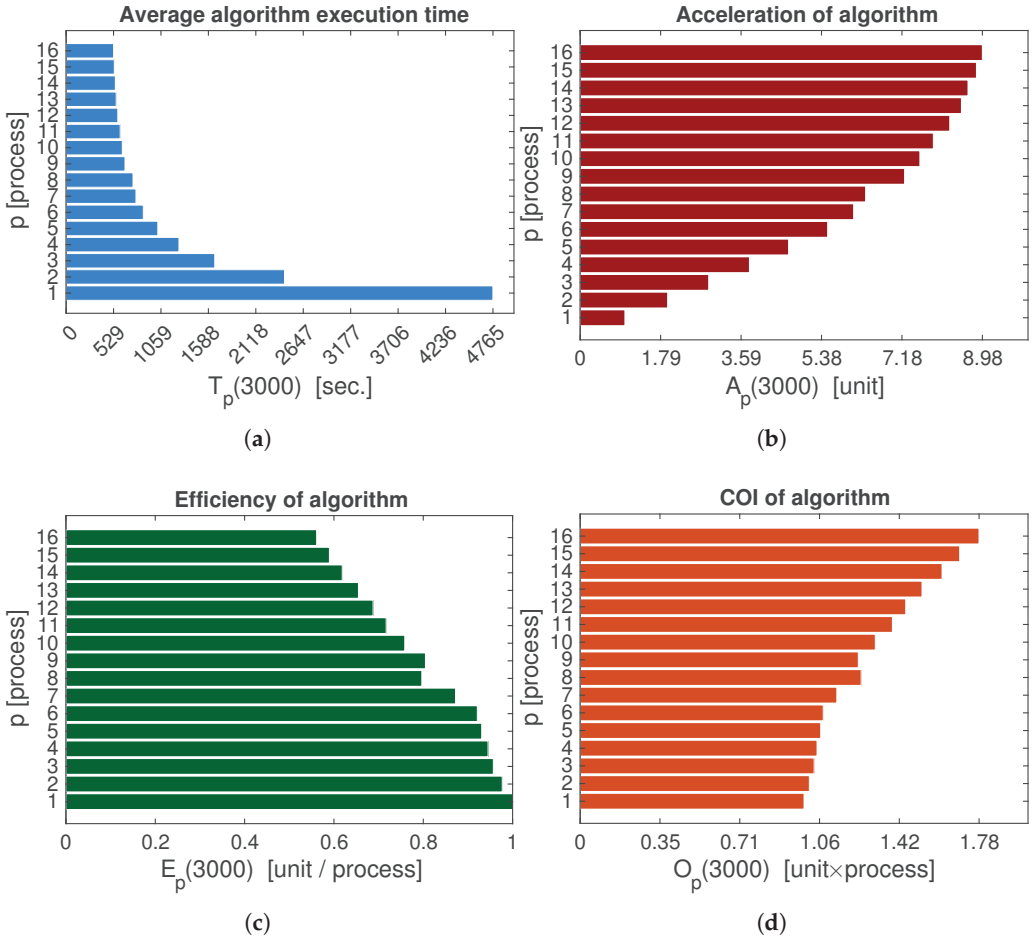

Figure 3. Average execution time and efficiency estimation of a parallel algorithm implementing Bifurcation Analysis (Example 2): **(a)** $T_p(3000)$, **(b)** $A_p(3000)$, **(c)** $E_p(3000)$, **(d)** $O_p(3000)$.

The results are shown in Table 3 and Figure 4 below.

https://doi.org/10.3390/computation14020032

Table 3. Average execution time $T_p(N)$ and standard deviation $\sigma_p(N)$ of the Test Example 3 with a varying number of worker processes.

p, [Processes]	$T_p(3000)$, [s]	$\sigma_p(3000)$, [s]
1	4660	71.4165
2	2462	34.7890
3	1681	29.0366
4	1262	15.8328
5	1032	11.1679
6	876	6.3034
7	785	8.0994
8	717	13.2665
9	657	1.5776
10	631	6.0882
11	603	4.1846
12	573	3.2728
13	563	2.1108
14	553	1.2649
15	545	1.2649
16	540	1.1972

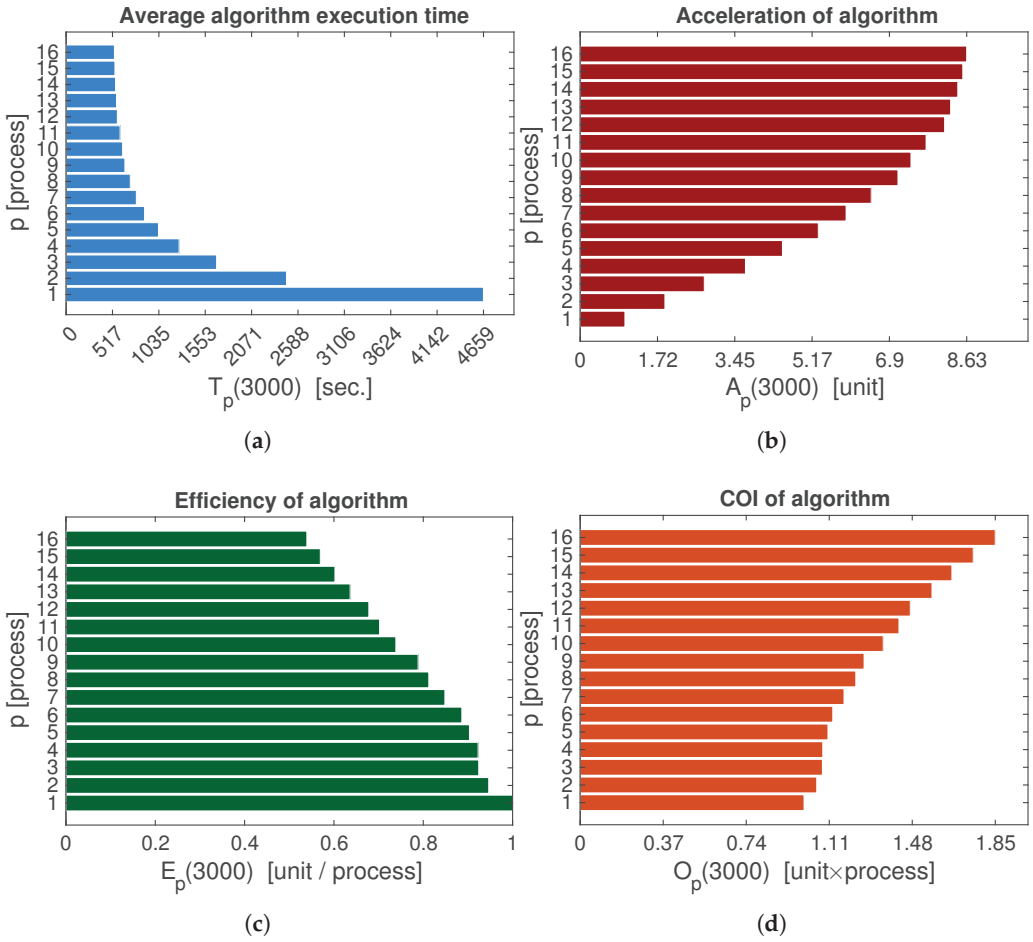

Figure 4. Average execution time and efficiency estimation of a parallel algorithm implementing Bifurcation Analysis (Example 3): (**a**) $T_p(3000)$, (**b**) $A_p(3000)$, (**c**) $E_p(3000)$, (**d**) $O_p(3000)$.

From Table 3, we can draw the following conclusions:

1. The standard deviation also decreases with increasing p:
   - for $p = 1 : \sigma_1 = 71.4165$ s;
   - for $p = 16 : \sigma_{16} = 1.1972$ s;

https://doi.org/10.3390/computation14020032

- A decrease of approximately 60 times.

2. In the optimal region of $p = 8$:

$$\frac{\sigma_8}{T_8} \approx \frac{13.2665}{717} \approx 1.85\%.$$

This is slightly higher than in Examples 1 and 2, but still less than 2%, indicating acceptable stability.

For Test Example 3 for ABMSelkovFracLinear, parallelization allows for a maximum speedup of ≈8.6 times. The efficiency estimates (Figure 4) show trends similar to those for Test Example 2 (Figure 2).

8. Conclusions

This article presents a performance analysis and practical implementation of a parallel algorithm for constructing bifurcation diagrams of the fractional Selkov oscillator with variable coefficients and memory. The main contribution is a reproducible benchmarking study that validates the effectiveness of a coarse-grained parallelization strategy (MapReduce) for this computationally intensive class of problems. This article investigated the performance of a parallel algorithm, implemented with Python's multiprocessing library, for computing bifurcation diagrams of the Selkov fractional oscillator. Using the TAECO metric set (Time, Acceleration, Efficiency, Cost, Cost Optimality), we evaluated the algorithm for three ABM variants: ABMSelkovFracCos, ABMSelkovFracExp, and ABMSelkovFracLinear. On a test system supporting up to sixteen worker processes, all three methods exhibited similar performance trends. The parallel algorithm achieved a speedup of 8–9 times compared to the sequential version, with an optimal resource allocation of 8 worker processes. Therefore, the implementation of a parallel algorithm for calculating bifurcation diagrams of the fractional oscillator in the ABM software package is justified. This study provides practical guidelines for configuring parallel computations and highlights the limitations of the current approach.

The presented performance analysis and conclusions are valid for the specific hardware and software configuration used in this study (see Section 7.1). The observed optimal number of processes ($p = 8$) corresponds to the number of physical cores in the test CPU. While the coarse-grained MapReduce parallelism strategy is generally effective for parametric studies, its efficiency metrics (speedup, optimal process count) are inherently dependent on the system architecture, workload characteristics (grid size N, parameter range), and software environment. To generalize these findings, cross-platform benchmarking on different CPU architectures (Intel, ARM), operating systems, and with varying problem sizes is necessary. Such future work would help develop adaptive configuration guidelines for a broader range of computational environments.

The obtained results and performance conclusions are valid for the hardware configuration studied. Cross-platform benchmarking is necessary to formulate more general recommendations and test the algorithm's robustness to different architectures. As a further development of this research, we plan to conduct a comprehensive analysis of the algorithm's scalability and efficiency on heterogeneous hardware, including the following:

- Intel Core i7/i9 processors of various generations with a cache hierarchy different from AMD.
- Server platforms based on AMD EPYC or Intel Xeon processors with NUMA architecture and a large number of computing cores.
- Systems with various RAM and I/O subsystem configurations.

https://doi.org/10.3390/computation14020032

This study will help identify common patterns and dependencies, minimize the risk of algorithm overfitting to a single hardware topology, and develop adaptive strategies for configuring parallel computing for a wide range of fractal dynamics problems.

Further development of research on this topic may be associated with the use of heterogeneous parallel programming structures, for example, CPU-GPU architecture, similar to [45–47].

We note that another promising direction for further research is a detailed comparative analysis of the accuracy and stability of various numerical schemes for the class of fractional-order systems with variable exponents and coefficients, which includes SFO. Such research will allow us to optimize the choice of a computing kernel for parametric calculations and will be the subject of our separate future work.

Author Contributions: Conceptualization, R.P. and D.T.; methodology, R.P. and D.T.; software, R.P. and D.T.; validation, R.P. and D.T.; formal analysis, R.P. and D.T.; investigation, D.T.; data curation, D.T.; writing—original draft preparation, R.P. and D.T.; writing—review and editing, R.P.; visualization, D.T.; supervision, R.P. All authors have read and agreed to the published version of the manuscript.

Funding: This work was carried out within the framework of the state assignment of IKIR FEB RAS (reg. No. 124012300245-2).

Data Availability Statement: The original contributions presented in this study are included in this article. Further inquiries can be directed to the corresponding author.

Conflicts of Interest: The authors declare no conflicts of interest.

Abbreviations

The following abbreviations are used in this manuscript:

ABM	Adams–Bashforth–Moulton Numerical Method
CPU	Central Processing Unit
GIL	Global Interpreter Lock
GPU	Graphics Processing Unit
HT	Hyper-Threading
MPI	Message Passing Interface
NUMA	Non-Uniform Memory Access
OpenMP	Open Multi-Processing
RAM	Random Access Memory
SFO	Selkov Fractional Oscillator
SMT	Simultaneous Multithreading
UMA	Uniform Memory Access

References

1. Sinet, S.; Bastiaansen, R.; Kuehn, C.; von der Heydt, A.S.; Dijkstra, H.A. Approximating the bifurcation diagram of weakly and strongly coupled leading-following systems. *Chaos Interdiscip. J. Nonlinear Sci.* **2025**, *35*, 063135. [CrossRef]
2. Li, X.; Liu, G.; Liu, J.; Chen, Y. Unveiling Pseudo-Period-Tripling Bifurcations in Nonlinear Dynamical Systems. *Int. J. Bifurc. Chaos* **2025**, *35*, 2550156. [CrossRef]
3. Gong, R.; Xu, J.; Liu, T.; Qin, Y.; Wei, Z. Bifurcation and Chaos in DCM Voltage-Fed Isolated Boost Full-Bridge Converter. *Electronics* **2025**, *14*, 260. [CrossRef]
4. Sel'kov, E.E. Self-Oscillations in Glycolysis 1. A Simple Kinetic Model. *Eur. J. Biochem.* **1968**, *4*, 79–86. [CrossRef] [PubMed]
5. Dhatt, S.; Chaudhury, P. Study of oscillatory dynamics in a Selkov glycolytic model using sensitivity analysis. *Indian J. Phys.* **2025**, *96*, 1649–1654. [CrossRef]
6. Makovetsky, V.I.; Dudchenko, I.P.; Zakupin, A.S. Auto oscillation model of microseism's sources. *Geosist. Pereh. Zon* **2017**, *4*, 37–46.

7. Parovik, R.I. Studies of the fractional Selkov dynamical system for describing the self-oscillatory regime of microseisms. *Mathematics* **2022**, *10*, 4208. [CrossRef]
8. Volterra, V. *Functional Theory, Integral and Integro-Differential Equations*; Dover Publications: Mineola, NY, USA, 2005.
9. Nyerere, N.; Edward, S. Modeling Chlamydia transmission with caputo fractional derivatives: Exploring memory effects and control strategies. *Model. Earth Syst. Environ.* **2025**, *11*, 307. [CrossRef]
10. Awadalla, M.; Sharif, A.A. A Fractional Calculus Approach to Energy Balance Modeling: Incorporating Memory for Responsible Forecasting. *Mathematics* **2026**, *14*, 223. [CrossRef]
11. Nakhushev, A.M. *Fractional Calculus and Its Applications*: Fizmatlit: Moscow, Russia, 2003.
12. Kilbas, A.A.; Srivastava, H.M.; Trujillo, J.J. *Theory and Applications of Fractional Differential Equations*; Elsevier: Amsterdam, The Netherlands, 2006.
13. García, J.J.R.; Escalante-Martínez, J.E.; Rojano, F.A.G.; Fuentes, J.C.M.; Torres, L. *Advances in Fractional Calculus*; Springer: Cham, Switzerland, 2025.
14. Gómez Aguilar, J.F.; Córdova-Fraga, T.; Tórres-Jiménez, J.; Escobar-Jiménez, R.F.; Olivares-Peregrino, V.H.; Guerrero-Ramírez, G.V. Nonlocal Transport Processes and the Fractional Cattaneo-Vernotte Equation. *Math. Probl. Eng.* **2026**, *2016*, 7845874.
15. Parovik, R.I.; Rakhmonov, Z.; Rakhim Zunnunov, R. Study of Chaotic and Regular Modes of the Fractional Dynamic System of Selkov. *EPJ Web Conf.* **2021**, *254*, 02014. [CrossRef]
16. Zhou, S.; Zhang, Q.; He, S.; Zhang, Y. What is the lowest cost to calculate the Lyapunov exponents from fractional differential equations? *Nonlinear Dyn.* **2025**, *113*, 14825–14871. [CrossRef]
17. Sun, H.; Chang, A.; Zhang, Y.; Chen, W. A Review on Variable-Order Fractional Differential Equations: Mathematical Foundations, Physical Models, Numerical Methods and Applications. *Fract. Calc. Appl. Anal.* **2019**, *22*, 27–59. [CrossRef]
18. Ortigueira, M.D.; Valério, D.; Machado, J.T. Variable order fractional systems. *Commun. Nonlinear Sci. Numer. Simul.* **2019**, *71*, 231–243. [CrossRef]
19. Patnaik, S.; Hollkamp, J.P.; Semperlotti, F. Applications of variable-order fractional operators: A review. *Proc. R. Soc. A Math. Phys. Eng. Sci.* **2020**, *476*, 20190498. [CrossRef]
20. Parovik, R.I. Selkov's Dynamic System of Fractional Variable Order with Non-Constant Coefficients. *Mathematics* **2025**, *13*, 372. [CrossRef]
21. Parovik, R.I. Study of dynamic modes of fractional Selkov oscillator with variable coefficients using bifurcation diagrams. *Comput. Math. Model.* **2025**. [CrossRef]
22. Parovik, R.I. ABMSelkovFracSim 2.0 software package for quantitative and qualitative analysis of the Selkov fractional oscillator. *Vestn. KRAUNC. Fiz.-Mat. Nauk.* **2025**, *53*, 75–92.
23. Shaw, Z.A. *Learn Python the Hard Way*; Addison-Wesley Professional: Boston, MA, USA, 2024.
24. Van Horn, B.M.; Nguyen, Q. *Hands-On Application Development with PyCharm: Build Applications Like a Pro with the Ultimate Python Development Tool*; Packt Publishing Ltd.: Birmingham, UK, 2023.
25. Tverdyi, D. A. An Analysis of the Computational Complexity and Efficiency of Various Algorithms for Solving a Nonlinear Model of Radon Volumetric Activity with a Fractional Derivative of a Variable Order. *Computation* **2025**, *13*, 252. [CrossRef]
26. Kulczycki, P.; Józef, K.; Janusz K. *Fractional Dynamical Systems: Methods, Algorithms and Applications*; Springer Nature: Cham, Switzerland, 2022.
27. Munoz-Pacheco, J.M.; Wei, Z.; Volos, C.; Sambas, A. Future challenges in the fractional-order dynamical systems: From mathematics to applications. *Front. Appl. Math. Stat.* **2023**, *9*, 1324660. [CrossRef]
28. Gao, B.; Shukur, A.; Marwan, M.; Wang, N. On the complex dynamics of simple integer to fractional-order sine chaotic oscillators. *Fractals* **2026**, *34*, 2550115. [CrossRef]
29. Novozhenova, O.G. Life And Science of Alexey Gerasimov, One of the Pioneers of Fractional Calculus in Soviet Union. *Fract. Calc. Appl. Anal.* **2017**, *20*, 790–809. [CrossRef]
30. Caputo, M.; Fabrizio, M. On the notion of fractional derivative and applications to the hysteresis phenomena. *Meccanica* **2017**, *52*, 3043–3052. [CrossRef]
31. Parovik, R.I. Qualitative analysis of Selkov's fractional dynamical system with variable memory using a modified Test 0–1 algorithm. *Vestn. KRAUNC. Fiz.-Mat. Nauk.* **2023**, *45*, 9–23.
32. Parovik, R.I. Selkov dynamic system with variable heredity for describing Microseismic regimes. In *Solar-Terrestrial Relations and Physics of Earthquake Precursors: Proceedings of the XIII International Conference*; Dmitriev, A., Lichtenberger, J., Mandrikova, O., Nahayo, E., Eds.; Springer Nature: Cham, Switzerland, 2023; pp. 166–178.
33. Diethelm, K.; Ford, N.J.; Freed, A.D. A Predictor-Corrector Approach for the Numerical Solution of Fractional Differential Equations. *Nonlinear Dyn.* **2002**, *29*, 3–22. [CrossRef]
34. Yang, C.; Liu, F. A computationally effective predictor-corrector method for simulating fractional order dynamical control system. *ANZIAM J.* **2005**, *47*, 168. [CrossRef]

35. Garrappa, R. Numerical solution of fractional differential equations: A survey and a software tutorial. *Mathematics* **2018**, *6*, 16. [CrossRef]
36. Naveen, S.; Parthiban, V. Qualitative analysis of variable-order fractional differential equations with constant delay. *Math. Methods Appl. Sci.* **2024**, *47*, 2981–2992. [CrossRef]
37. Sino, M.; Domazet, E. Scalable Parallel Processing: Architectural Models, Real-Time Programming, and Performance Evaluation. *Eng. Proc.* **2025**, *104*, 60.
38. Meng, X.; He, X.; Hu, C.; Lu, X.; Li, H. A Review of Parallel Computing for Large-scale Reservoir Numerical Simulation. *Arch. Comput. Methods Eng.* **2025**, *32*, 4125–4162. [CrossRef]
39. Zhou, X.; Wang, C. Research on optimization of data mining algorithm based on OpenMP. *SPIE* **2025**, *13560*, 850–857.
40. Himstedt, K. Multiple execution of the same MPI application: Exploiting parallelism at hotspots with minimal code changes. *GEM-Int. J. Geomath.* **2025**, *16*, 1–28. [CrossRef]
41. Wicaksono, D.; Soewito, B. Application of the multi-threading method and Python script for the network automation. *J. Syntax Lit.* **2024**, *9*, 3614.
42. Rauber, T.; Runger, G. *Parallel Programming for Multicore and Cluster Systems*; Springer: New York, NY, USA, 2013.
43. Al-hayanni, M.A.N.; Xia, F.; Rafiev, A.; Romanovsky, A., Shafik, R.; Yakovlev, A. Amdahl's Law in the Context of Heterogeneous Many-core Systems-ASurvey. *IET Comput. Digit.* **2020**, *14*, 133–148. [CrossRef]
44. Poolla, C.; Saxena, R. On extending Amdahl's law to learn computer performance. *Microprocess. Microsystems* **2023**, *96*, 104745. [CrossRef]
45. Skorych, V.; Dosta, M. Parallel CPU–GPU computing technique for discrete element method. *Concurr. Comput. Pract. Exp.* **2022**, *34*, e6839. [CrossRef]
46. Alaei, M.; Yazdanpanah, F. A survey on heterogeneous CPU–GPU architectures and simulators. *Concurr. Comput. Pract. Exp.* **2025**, *37*, e8318. [CrossRef]
47. Vaithianathan, M. The Future of Heterogeneous Computing: Integrating CPUs GPUs and FPGAs for High-Performance Applications. *Int. J. Emerg. Trends Comput. Sci. Inf. Technol.* **2025**, *1*, 12–23. [CrossRef]

Disclaimer/Publisher's Note: The statements, opinions and data contained in all publications are solely those of the individual author(s) and contributor(s) and not of MDPI and/or the editor(s). MDPI and/or the editor(s) disclaim responsibility for any injury to people or property resulting from any ideas, methods, instructions or products referred to in the content.

https://doi.org/10.3390/computation14020032

fractal and fractional

MDPI

Article

Global Dynamics of a Fractional-Order Anthrax Transmission Model with Distributed Delays and Beddington–DeAngelis Incidence

Sheng-Hu Xu * and Liang-Jia Dong

School of Mathematics and Information Science, North Minzu University, Yinchuan 750021, China; dlj@stu.nmu.edu.cn
* Correspondence: xushh@nmu.edu.cn

Abstract

This paper presents a novel mathematical framework for anthrax transmission by integrating Caputo fractional derivatives, distributed delays, and a Beddington–DeAngelis incidence function. The proposed model captures memory effects in disease progression, temporal heterogeneities in pathogen release, and saturation phenomena in host–pathogen interactions. We establish the well-posedness of the system and derive the basic reproduction number $\mathcal{R}_0$, which serves as a sharp threshold for disease dynamics: when $\mathcal{R}_0 \leq 1$, the disease-free equilibrium is globally asymptotically stable; when $\mathcal{R}_0 > 1$, a unique endemic equilibrium emerges and is globally stable. Theoretical analysis demonstrates that the fractional order modulates convergence rates through memory effects, while distributed delays influence oscillatory behaviors and time to equilibrium. Numerical simulations validate these findings and illustrate the impacts of key parameters on disease transmission. The results provide a scientific foundation for designing targeted public health interventions in anthrax control.

Keywords: Caputo fractional derivative; distributed delay; Beddington–DeAngelis incidence rate; Lyapunov functional

1. Introduction

Anthrax, caused by the spore-forming bacterium *Bacillus anthracis*, is a severe zoonotic disease affecting both animals and humans [1,2]. The pathogen exhibits remarkable environmental persistence, allowing contaminated soil and water to serve as long-term reservoirs of infection [3,4]. Ungulate herbivores such as cattle, sheep, goats, and horses are particularly susceptible, often succumbing within 24–48 h post-infection [5,6]. Human infections primarily occur through contact with infected animals or contaminated animal products, manifesting as cutaneous, gastrointestinal, or pulmonary forms, the latter two being associated with high mortality rates [7,8]. Outbreaks continue to be reported worldwide, underscoring the need for effective control strategies, especially in resource-limited settings where anthrax poses significant threats to livestock economies and public health [9,10].

Mathematical models have become indispensable tools for understanding transmission dynamics and evaluating intervention policies [11]. Early deterministic frameworks, such as the model by Hahn and Furniss [12], examined the role of environmental contamination and animal carcasses in driving anthrax epizootics. Subsequent extensions incorporated animal movement, carcass ingestion, and time delays [13,14]. However, these

models often assumed immediate death upon infection, neglecting the biologically relevant lag between infection and death, a factor that may crucially influence outbreak trajectories and control efficacy.

The incidence function, which describes the rate at which susceptible individuals become infected, is a core component in the construction of epidemic models. With the development of nonlinear dynamics, researchers have refined model formulations to more realistically characterize disease transmission processes. For example, the nonlinear infection rate function proposed by Capasso and Serio [15] captures the saturation effect of infection rates and associated socio-psychological impacts; Dimarco et al. [16] used nonlinear incidence models to reveal the regulatory role of heterogeneity in epidemic spread; Bondesan et al. [17] derived population-level dynamic behaviors via multi-scale modeling, providing theoretical support for the analysis of complex systems.

Among the improved model formulations, the Beddington–DeAngelis incidence Beddington–DeAngelis incidence rate

$$\frac{\beta SP}{1 + aS + bP}$$

has been widely applied. The parameter $a \geq 0$ quantifies the mutual interference effect among susceptible hosts, reflecting the decline in per capita contact rates due to crowding or competition; the parameter $b \geq 0$ characterizes the saturation effect related to pathogen density. When $a = 0$ and $b = 0$, the Beddington–DeAngelis incidence reduces to the classical bilinear form βSP; when $a = 0$ or $b = 0$, it degenerates to the Holling type II incidence $\frac{\beta SP}{1+bP}$ or pure interference effect form $\frac{\beta SP}{1+aS}$, respectively. Within the anthrax model framework, the interference term aS characterizes intraspecific competition among grazing herbivores, which reduces the per capita contact probability of individuals with contaminated areas, while the saturation term bP reflects the physiological upper limit of infection probability at high spore concentrations. As shown in Section 4 (Remark 4), the factor $(1 + aS_0)$ is incorporated into the denominator of the basic reproduction number $\mathcal{R}_0$, directly raising the threshold for disease persistence; meanwhile, the endemic pathogen level P^* derived in Theorem 3 is inversely related to parameter b, confirming that both saturation mechanisms jointly constrain the magnitude of epidemic outbreaks.

Recent advances in fractional calculus have enriched epidemiological modeling by capturing memory effects and non-local interactions [18,19]. Unlike integer-order derivatives, fractional derivatives reflect the dependence of system dynamics on historical states, offering more realistic descriptions of immune responses and pathogen mutation processes [20,21]. The Caputo fractional derivative, in particular, is widely adopted in biological models and models in other fields due to its compatibility with standard initial conditions [22,23]. Meanwhile, the Beddington–DeAngelis incidence function has been successfully applied in various epidemic models to describe saturation effects and behavioral changes [24,25].

The integration of Caputo fractional derivatives into our model is motivated by three biological mechanisms unique to anthrax ecology, which are characterized by:

- **Long memory of environmental persistence**: Bacillus anthracis spores can survive in soil for decades to over a century, and historically contaminated sites ("cursed fields") can trigger new outbreaks after decades of quiescence [26,27]. Current infection risk thus depends on the cumulative historical abundance of pathogens rather than just present concentrations, exhibiting non-Markovian characteristics that integer-order instantaneous rate frameworks fail to capture [28].
- **Power-law decay of immunity**: Herd immunity levels are jointly governed by cumulative exposure and vaccination histories, with decay processes following a power-law

https://doi.org/10.3390/fractalfract10030175

instead of exponential pattern [29], structurally consistent with the Mittag–Leffler memory kernel of Caputo derivatives [29].

- **Subdiffusive behavior of outbreak data**: Empirical evidence shows that anthrax outbreak time series exhibit heavy-tailed distributions and subdiffusive features [30,31], which cannot be fitted by integer-order exponential kernels but are well characterized by fractional-order power-law kernels [32].

In this study, we propose a novel fractional-order anthrax transmission model that simultaneously incorporates distributed delays and a Beddington–DeAngelis incidence rate. The model is formulated as the following system of Caputo fractional differential equations:

$$\begin{cases} {}_0^C D_t^\gamma S(t) = \Lambda - \mu S(t) - \frac{\beta P(t) S(t)}{1 + aS(t) + bP(t)}, \\ {}_0^C D_t^\gamma C(t) = \beta \int_0^\infty g_1(\tau) \frac{P(t-\tau) S(t-\tau)}{1 + aS(t-\tau) + bP(t-\tau)} \mathrm{d}\tau - (\phi + d) C(t), \\ {}_0^C D_t^\gamma P(t) = \alpha \int_0^\infty g_2(\tau) C(t-\tau) \mathrm{d}\tau - (\phi + \varepsilon) P(t), \end{cases} \tag{1}$$

with initial conditions

$$S(\theta) = \varphi_1(\theta), \quad C(\theta) = \varphi_2(\theta), \quad P(\theta) = \varphi_3(\theta), \quad \theta \in (-\tau, 0],$$

where φ_i are bounded and nonnegative continuous functions. Here, $S(t)$, $C(t)$, and $P(t)$ denote the populations of susceptible animals, carcasses of animals killed by anthrax, and free anthrax spores in the environment, respectively. The parameter $\gamma \in (0, 1]$ is the order of the Caputo fractional derivative, which introduces memory into the system dynamics [33,34]. The meanings of the remaining parameters are shown in Table 1. The functions $g_1(\tau)$ and $g_2(\tau)$ are normalized kernel functions representing distributed delays in the infection process and the spore release process, satisfying $\int_0^\infty g_i(\tau) d\tau = 1$, $i = 1, 2$. The incidence rate follows the Beddington–DeAngelis form $\frac{\beta PS}{1 + aS + bP}$, which captures both saturation effects and interactive influences between susceptible hosts and pathogens [24,25].

Table 1. Model parameters and their meanings.

Parameter	Meaning	Unit
Λ	Birth rate	individuals $\cdot \mathrm{day}^{-1}$
β	Transmission rate	day^{-1}
μ	Natural mortality rate	day^{-1}
ϕ	Environmental purification rate	day^{-1}
d	Natural decomposition rate of carcasses	day^{-1}
α	Spore release rate	$\mathrm{pathogen} \cdot \mathrm{carcass}^{-1} \cdot \mathrm{day}^{-1}$
ε	Decay rate of free spores in the environment	day^{-1}
τ	Time delay variable	day

The fractional-order anthrax model developed herein incorporates three key mechanistic features that have not been concurrently investigated in prior theoretical frameworks for anthrax transmission dynamics. These include: (i) fractional-order dynamics, which capture memory effects and non-local interactions inherent to pathogen transmission and environmental persistence processes [35,36]; (ii) distributed time delays, which provide a more biologically realistic representation of the lag periods between host infection and mortality, as well as between carcass persistence and spore release into the environment [37,38]; and (iii) a Beddington–DeAngelis incidence function, which generalizes the pathogen-host contact process to account for saturation effects in both host population and pathogen density [24,25].

https://doi.org/10.3390/fractalfract10030175

The remainder of this paper is organized as follows. Section 2 provides essential preliminaries on fractional calculus. Section 3 addresses the existence, uniqueness, and boundedness of solutions. Section 4 derives $\mathcal{R}_0$ and establishes the existence of equilibria. Section 5 presents stability analyses. Section 6 performs sensitivity analysis and illustrates theoretical results via numerical simulations. Finally, Section 7 concludes the paper and suggests future research directions.

2. Preliminaries

This section collects fundamental definitions and auxiliary lemmas from fractional calculus that underpin the stability analysis developed in subsequent sections.

Definition 1 (Riemann-Liouville fractional integral [39]). *For a function $f : \mathbb{R}_+ \to \mathbb{R}$ and $0 < \gamma < 1$, the Riemann-Liouville fractional integral of order γ is defined as*

$$I^{\gamma}_{[0,t]} f(t) = \frac{1}{\Gamma(\gamma)} \int_0^t (t-s)^{\gamma-1} f(s)\, ds.$$

Definition 2 (Caputo fractional derivative [39]). *For a function $f \in C^1([0,+\infty), \mathbb{R})$ and $0 < \gamma < 1$, the Caputo fractional derivative of order γ is defined as*

$${}^{C}_{0}D^{\gamma}_{t} f(t) = \frac{1}{\Gamma(1-\gamma)} \int_0^t \frac{f'(s)}{(t-s)^{\gamma}}\, ds.$$

Definition 3 (Riemann-Liouville fractional derivative [33]). *For a function $f \in C^1([0,+\infty), \mathbb{R})$ and $0 < \gamma < 1$, the Riemann-Liouville fractional derivative of order γ is defined as*

$${}^{RL}_{0}D^{\gamma}_{t} f(t) = \frac{1}{\Gamma(1-\gamma)} \frac{d}{dt} \int_0^t \frac{f(s)}{(t-s)^{\gamma}}\, ds.$$

Definition 4 (Mittag–Leffler function [34]). *The two-parameter Mittag–Leffler function is defined by*

$$E_{\eta_1,\eta_2}(z) = \sum_{k=0}^{\infty} \frac{z^k}{\Gamma(k\eta_1 + \eta_2)}, \quad \eta_1 > 0,\ \eta_2 > 0,\ z \in \mathbb{C}.$$

When $\eta_2 = 1$, we denote $E_{\eta_1}(z) := E_{\eta_1,1}(z)$.

Lemma 1 (Fractional differential inequality [40]). *Let $\psi(t) \in C[0,\infty)$ satisfy the Caputo fractional differential inequality*

$${}^{C}_{0}D^{\gamma}_{t} \psi(t) + n_1 \psi(t) \le n_2$$

with initial condition $\psi(0) = \psi_0$, where $0 < \gamma \le 1$, and $n_1, n_2 \in \mathbb{R}$ with $n_1 \neq 0$. Then

$$\psi(t) \le \left(\psi_0 - \frac{n_2}{n_1}\right) E_{\gamma,1}(-n_1 t^{\gamma}) + \frac{n_2}{n_1}.$$

Lemma 2 (Existence and uniqueness for fractional delay systems [41]). *Consider the fractional differential system with time delay*

$$\begin{cases} {}^{C}_{0}D^{\gamma}_{t} x(t) = f(t, x(t), x(t-\tau)), & t \ge t_0, \\ x^{(k)}(t) = \phi_k(t), & t_0 - h \le t \le t_0, \end{cases}$$

https://doi.org/10.3390/fractalfract10030175

where f is continuous in a neighborhood of $(t_0, x(t_0), x(t_0-\tau))$. If f satisfies a Lipschitz condition with respect to all variables except t, and the initial function $\phi_k(t)$ is defined on $[t_0-h, t_0]$, then there exists a unique continuous solution on $[t_0, t_0+h]$ for some $h > 0$.

Lemma 3 (Routh–Hurwitz stability condition for fractional systems [41])**.** *Consider the fractional-order dynamical system*

$$ {}_0^C D_t^\gamma \mathbf{x}(t) = f(\mathbf{x}), \quad \gamma \in (0,1], $$

with equilibrium $\mathbf{x}^*$ and linearized characteristic equation

$$ P(\lambda) = \lambda^n + b_1\lambda^{n-1} + \cdots + b_{n-1}\lambda + b_n = 0, \quad b_i \in \mathbb{R}. $$

Define the Hurwitz determinants as

$$ H_1 = b_1, \quad H_2 = \begin{vmatrix} b_1 & 1 \\ b_3 & b_2 \end{vmatrix}, \quad H_3 = \begin{vmatrix} b_1 & 1 & 0 \\ b_3 & b_2 & b_1 \\ b_5 & b_4 & b_3 \end{vmatrix}, \quad \ldots $$

If $H_k > 0$ for $k = 1, 2, \ldots, n$, then the system is locally asymptotically stable at $\mathbf{x}^*$ for any $\gamma \in (0,1]$.

Remark 1 (Stability condition [42])**.** *The necessary and sufficient condition for stability of a fractional-order system is that all characteristic roots λ satisfy*

$$ |\arg(\lambda)| > \frac{\gamma\pi}{2}. $$

The Routh–Hurwitz condition in Lemma 3 ensures that all roots lie in the open left-half complex plane $\{\lambda \in \mathbb{C} : \Re(\lambda) < 0\}$, which is a subset of the sectorial stability region $\{\lambda \in \mathbb{C} : |\arg(\lambda)| > \gamma\pi/2\}$.

Lemma 4 (Fractional derivative of convex functions [43])**.** *Let $V : \Omega \to \mathbb{R}$ and $x : [t_0, \infty) \to \Omega$ be continuous and differentiable, where $\Omega \subseteq \mathbb{R}^n$. If $V(x(t))$ is convex on Ω, then for any $t \geq t_0$ and $\gamma \in (0,1)$,*

$$ {}_{t_0}^C D_t^\gamma V(x(t)) \leq \left(\frac{\partial V(x(t))}{\partial x(t)} \right)^T {}_{t_0}^C D_t^\gamma x(t). $$

Lemma 5 (Composition rule [44])**.** *For $\gamma \in \mathbb{R}^+$, $k = [\gamma]$, $t \in [0,T]$, and $f \in C[0,T]$, the following holds*

$$ {}_0^C D_t^\gamma I_{[0,t]}^\gamma f(t) = f(t). $$

These definitions and lemmas provide the essential mathematical foundation for analyzing the fractional-order anthrax transmission model with distributed delays. The Mittag–Leffler function plays a crucial role in solving fractional differential equations, while the stability lemmas enable rigorous analysis of the system's equilibrium points.

Remark 2. *The Caputo fractional derivative is preferred over the Riemann–Liouville definition because it admits integer-order initial conditions with direct epidemiological meaning, preserves constant equilibria, and yields $\mathcal{R}_0$ without reformulation. Its nonlocal kernel captures memory effects arising from prolonged spore persistence and delayed immune responses, while the fractional order γ serves as a tunable parameter whose influence on $\mathcal{R}_0$ reveals memory-dependent threshold behavior inaccessible to integer-order models.*

https://doi.org/10.3390/fractalfract10030175

3. Existence, Uniqueness and Boundedness of Solutions

This section establishes the fundamental properties of solutions to the fractional-order anthrax transmission model (1), including non-negativity, boundedness, and uniqueness. These properties ensure the biological plausibility of the model and provide the foundation for subsequent dynamical analysis.

Theorem 1 (Well-posedness of solutions)**.** *For any positive initial condition*

$$X(0) = (S(0), C(0), P(0)) \in \Gamma,$$

there exists a unique, non-negative, and bounded solution

$$X(t) = (S(t), C(t), P(t)) \in \Gamma$$

to system (1) *that remains in* $\mathbb{R}^3_+$ *for all* $t \geq 0$*, where the positively invariant set* Γ *is defined as*

$$\Gamma = \left\{ (S, C, P) \in \mathbb{R}^3_+ : S \leq M_1,\ C \leq M_2,\ P \leq M_3 \right\}$$

with the bounds M_1*,* M_2*, and* M_3 *specified in the proof.*

Proof. The proof is divided into three parts: (i) non-negativity, (ii) boundedness, and (iii) uniqueness of solutions.

(i) Non-negativity of solutions. From system (1), we examine the behavior of each variable when it approaches zero

$$\begin{aligned}
{}^{C}_{0}D^{\gamma}_{t} S(t)\Big|_{S=0} &= \Lambda \geq 0, \\
{}^{C}_{0}D^{\gamma}_{t} C(t)\Big|_{C=0} &= \beta \int_0^{\infty} g_1(\tau) \frac{P(t-\tau)S(t-\tau)}{1 + aS(t-\tau) + bP(t-\tau)}\, d\tau \geq 0, \\
{}^{C}_{0}D^{\gamma}_{t} P(t)\Big|_{P=0} &= \alpha \int_0^{\infty} g_2(\tau) C(t-\tau)\, d\tau \geq 0.
\end{aligned}$$

According to the generalized mean value theorem for fractional differential equations [45], these inequalities imply that $S(t) \geq 0$, $C(t) \geq 0$, and $P(t) \geq 0$ for all $t \geq 0$.

(ii) Boundedness of solutions. We establish uniform bounds for each state variable.

Bound for $S(t)$*:* From the first equation of (1),

$${}^{C}_{0}D^{\gamma}_{t} S(t) = \Lambda - \mu S(t) - \frac{\beta P(t) S(t)}{1 + aS(t) + bP(t)} \leq \Lambda - \mu S(t).$$

Applying Lemma 1 [40] yields

$$S(t) \leq \left(S(0) - \frac{\Lambda}{\mu} \right) E_{\gamma,1}(-\mu t^{\gamma}) + \frac{\Lambda}{\mu}.$$

Thus,

$$\limsup_{t \to \infty} S(t) \leq M_1, \quad \text{where } M_1 = \max\left\{ S(0), \frac{\Lambda}{\mu} \right\}.$$

Bound for $C(t)$*:* Since $S(t) \leq M_1$ and $P(t) \geq 0$,

$$\frac{\beta P(t) S(t)}{1 + aS(t) + bP(t)} \leq \frac{\beta M_1 P(t)}{1 + bP(t)} \leq \frac{\beta M_1}{b}.$$

https://doi.org/10.3390/fractalfract10030175

From the second equation of (1),

$$ {}_0^C D_t^\gamma C(t) \le \frac{\beta M_1}{b} - (\phi + d)C(t). $$

Applying Lemma 1 again gives

$$ C(t) \le \left(C(0) - \frac{\beta M_1}{b(\phi + d)} \right) E_{\gamma,1}(-(\phi + d)t^\gamma) + \frac{\beta M_1}{b(\phi + d)}. $$

Hence,

$$ \limsup_{t \to \infty} C(t) \le M_2, \quad \text{where } M_2 = \max\left\{ C(0), \frac{\beta M_1}{b(\phi + d)} \right\}. $$

Bound for $P(t)$: From the third equation of (1) and $C(t) \le M_2$,

$$ {}_0^C D_t^\gamma P(t) \le \alpha M_2 - (\phi + \varepsilon)P(t). $$

Thus,

$$ \limsup_{t \to \infty} P(t) \le M_3, \quad \text{where } M_3 = \max\left\{ P(0), \frac{\alpha M_2}{\phi + \varepsilon} \right\}. $$

The above bounds confirm that all solutions remain within the compact set Γ.

(iii) Uniqueness of solutions. We demonstrate that the right-hand side of system (1) satisfies a Lipschitz condition on Γ, which guarantees local existence and uniqueness by the Banach fixed-point principle [44].

Define the vector function $G : \Gamma \to \mathbb{R}^3$ as

$$ G(X) = \begin{pmatrix} G_1(S, C, P) \\ G_2(S, C, P) \\ G_3(S, C, P) \end{pmatrix}, $$

where

$$ \begin{aligned} G_1(S, C, P) &= \Lambda - \mu S - \frac{\beta PS}{1 + aS + bP}, \\ G_2(S, C, P) &= \beta \int_0^\infty g_1(\tau) \frac{P(t - \tau)S(t - \tau)}{1 + aS(t - \tau) + bP(t - \tau)} \, d\tau - (\phi + d)C, \\ G_3(S, C, P) &= \alpha \int_0^\infty g_2(\tau) C(t - \tau) \, d\tau - (\phi + \varepsilon)P. \end{aligned} $$

Let $M = \max\{M_1, M_2, M_3\} > 0$. Define $f(S, P) = \frac{\beta PS}{1 + aS + bP}$. For $S, P \in [0, M]$, the partial derivatives are bounded

$$ \begin{aligned} \left| \frac{\partial f}{\partial S} \right| &= \left| \frac{\beta P(1 + bP)}{(1 + aS + bP)^2} \right| \le \beta M(1 + bM) = L_{11}, \\ \left| \frac{\partial f}{\partial P} \right| &= \left| \frac{\beta S(1 + aS)}{(1 + aS + bP)^2} \right| \le \beta M(1 + aM) = L_{12}. \end{aligned} $$

For G_1, we have

$$ \begin{aligned} |G_1(X_1) - G_1(X_2)| &\le \mu |S_1 - S_2| + |f(S_1, P_1) - f(S_2, P_2)| \\ &\le \mu |S_1 - S_2| + L_{11}|S_1 - S_2| + L_{12}|P_1 - P_2| \\ &\le L_1(|S_1 - S_2| + |P_1 - P_2|), \end{aligned} $$

https://doi.org/10.3390/fractalfract10030175

where $L_1 = \max\{\mu + L_{11}, L_{12}\}$.

For G_2, define

$$H(t) = \int_0^\infty g_1(\tau) \frac{P(t-\tau)S(t-\tau)}{1 + aS(t-\tau) + bP(t-\tau)}\, d\tau.$$

Since $\int_0^\infty g_1(\tau)d\tau = 1$ and f is Lipschitz continuous,

$$\begin{aligned} |H(t, X_1) - H(t, X_2)| &\leq \int_0^\infty g_1(\tau)|f(S_1(t-\tau), P_1(t-\tau)) - f(S_2(t-\tau), P_2(t-\tau))|\, d\tau \\ &\leq L_{11}\|S_1 - S_2\|_\infty + L_{12}\|P_1 - P_2\|_\infty. \end{aligned}$$

Thus

$$\begin{aligned} |G_2(X_1) - G_2(X_2)| &\leq \beta(L_{11}\|S_1 - S_2\|_\infty + L_{12}\|P_1 - P_2\|_\infty) + (\phi + d)|C_1 - C_2| \\ &\leq L_2(\|S_1 - S_2\|_\infty + |C_1 - C_2| + \|P_1 - P_2\|_\infty), \end{aligned}$$

where $L_2 = \max\{\beta L_{11}, \beta L_{12}, \phi + d\}$.

For G_3, define

$$K(t) = \int_0^\infty g_2(\tau)C(t-\tau)\, d\tau.$$

Similarly,

$$|K(t, X_1) - K(t, X_2)| \leq \|C_1 - C_2\|_\infty,$$

and

$$\begin{aligned} |G_3(X_1) - G_3(X_2)| &\leq \alpha\|C_1 - C_2\|_\infty + (\phi + \varepsilon)|P_1 - P_2| \\ &\leq L_3(\|C_1 - C_2\|_\infty + |P_1 - P_2|), \end{aligned}$$

where $L_3 = \max\{\alpha, \phi + \varepsilon\}$.

Combining these estimates, for any $X_1, X_2 \in \Gamma$,

$$\|G(X_1) - G(X_2)\| \leq L\|X_1 - X_2\|,$$

where $L = \max\{L_1 + L_2, L_2 + L_3, L_1 + L_2 + L_3\}$. By Lemma 2 [41], this Lipschitz condition guarantees the existence of unique solution to system (1) for any non-negative initial condition in Γ. □

Remark 3. *The positively invariant set Γ represents the biologically feasible region where the numbers of susceptible animals, carcasses, and spores remain non-negative and bounded. The bounds M_1, M_2, and M_3 depend explicitly on model parameters, providing quantitative constraints on population sizes.*

The well-posedness established in Theorem 1 guarantees that system (1) is mathematically sound and suitable for analyzing long-term dynamical behavior, which will be addressed in subsequent sections.

4. Basic Reproduction Number and Existence of Endemic Equilibrium

The basic reproduction number $\mathcal{R}_0$ serves as a crucial epidemiological threshold that quantifies the transmission potential of an infectious disease. It represents the expected number of secondary infections produced by a single infected individual in a completely susceptible population. Typically, if $\mathcal{R}_0 < 1$, the disease will eventually die out; if $\mathcal{R}_0 > 1$, the disease is likely to persist, indicating the need for intervention measures.

https://doi.org/10.3390/fractalfract10030175

In this section, we derive the basic reproduction number for the fractional-order anthrax transmission model (1) using the next-generation matrix method [46]. This approach remains applicable to fractional-order epidemic models [23] and involves constructing two matrices F and V that transform the disease transmission process into mathematically tractable forms. Here, F represents the transmission rates from infected compartments to new infections, while V characterizes the transition rates among infected compartments.

Theorem 2 (Basic reproduction number)**.** *For system* (1)*, the disease-free equilibrium is* $E_0 = (\Lambda/\mu, 0, 0)$*. The basic reproduction number is*

$$\mathcal{R}_0 = \frac{\beta\alpha\Lambda}{\mu(\phi+d)(\phi+\varepsilon)(1+a\Lambda/\mu)}.$$

Proof. We consider the infected compartments $C(t)$ and $P(t)$. At the disease-free equilibrium $E_0 = (S_0, 0, 0)$, the matrices F and V are constructed as follows

The transmission matrix F contains the rates at which new infections appear

$$F = \begin{pmatrix} 0 & \dfrac{\beta S_0}{1+aS_0} \\ 0 & 0 \end{pmatrix}.$$

The transition matrix V contains the rates of transfer between compartments

$$V = \begin{pmatrix} \phi+d & 0 \\ -\alpha & \phi+\varepsilon \end{pmatrix}.$$

The inverse of V is computed as

$$V^{-1} = \begin{pmatrix} \dfrac{1}{\phi+d} & 0 \\ \dfrac{\alpha}{(\phi+d)(\phi+\varepsilon)} & \dfrac{1}{\phi+\varepsilon} \end{pmatrix}.$$

The next-generation matrix is then

$$FV^{-1} = \begin{pmatrix} \dfrac{\beta\alpha S_0}{(\phi+d)(\phi+\varepsilon)(1+aS_0)} & \dfrac{\beta S_0}{(\phi+\varepsilon)(1+aS_0)} \\ 0 & 0 \end{pmatrix}.$$

The spectral radius (dominant eigenvalue) of FV^{-1} is

$$\mathcal{R}_0 = \rho(FV^{-1}) = \frac{\beta\alpha S_0}{(\phi+d)(\phi+\varepsilon)(1+aS_0)}.$$

This completes the derivation. □

Remark 4. *The expression for* $\mathcal{R}_0$ *reveals the combined influence of transmission parameters* (β, α)*, environmental persistence* (ϕ, ε)*, carcass decomposition* (d)*, and saturation effects* (a)*. The factor* $(1 + aS_0)$ *in the denominator reflects the inhibitory effect of host density on transmission, characteristic of the Beddington–DeAngelis incidence.*

Having established the basic reproduction number, we now examine the existence and uniqueness of the endemic equilibrium when $\mathcal{R}_0 > 1$.

https://doi.org/10.3390/fractalfract10030175

Theorem 3 (Existence and uniqueness of endemic equilibrium). *If $\mathcal{R}_0 > 1$, then system* (1) *admits a unique endemic equilibrium $E^* = (S^*, C^*, P^*)$, where*

$$S^* = \frac{\Lambda b\alpha + (\phi+\varepsilon)(\phi+d)}{b\alpha\mu + \beta\alpha - a(\phi+\varepsilon)(\phi+d)},$$
$$C^* = \frac{\alpha(a\Lambda+\mu)(\mathcal{R}_0-1)}{b\alpha\mu + \beta\alpha - a(\phi+\varepsilon)(\phi+d)},$$
$$P^* = \frac{(\phi+\varepsilon)(a\Lambda+\mu)(\mathcal{R}_0-1)}{b\alpha\mu + \beta\alpha - a(\phi+\varepsilon)(\phi+d)}.$$

Proof. At an endemic equilibrium, the time derivatives in system (1) vanish, yielding the algebraic system

$$\begin{cases} \Lambda - \mu S^* - \dfrac{\beta P^* S^*}{1 + aS^* + bP^*} = 0, \\ \beta \displaystyle\int_0^\infty g_1(\tau) \frac{P^* S^*}{1 + aS^* + bP^*}\, d\tau - (\phi+d)C^* = 0, \\ \alpha \displaystyle\int_0^\infty g_2(\tau) C^*\, d\tau - (\phi+\varepsilon)P^* = 0. \end{cases} \tag{2}$$

Using the normalization conditions $\int_0^\infty g_1(\tau)d\tau = 1$ and $\int_0^\infty g_2(\tau)d\tau = 1$, system (2) simplifies to

$$\begin{cases} \Lambda = \mu S^* + \dfrac{\beta P^* S^*}{1 + aS^* + bP^*}, \\ \dfrac{\beta P^* S^*}{1 + aS^* + bP^*} = (\phi+d)C^*, \\ \alpha C^* = (\phi+\varepsilon)P^*. \end{cases} \tag{3}$$

From the third equation, we obtain

$$C^* = \frac{\phi+\varepsilon}{\alpha} P^*.$$

Substituting into the second equation gives

$$\frac{\beta P^* S^*}{1 + aS^* + bP^*} = (\phi+d) \cdot \frac{\phi+\varepsilon}{\alpha} P^*.$$

Assuming $P^* \neq 0$ (which holds for an endemic equilibrium), we have

$$\frac{\beta S^*}{1 + aS^* + bP^*} = \frac{(\phi+\varepsilon)(\phi+d)}{\alpha}.$$

Solving for P^* yields

$$P^* = \frac{1}{b}\left(\frac{\beta\alpha S^*}{(\phi+\varepsilon)(\phi+d)} - 1 - aS^* \right).$$

Substituting this expression into the first equation of (3)

$$\begin{aligned} \Lambda &= \mu S^* + \frac{(\phi+\varepsilon)(\phi+d)}{\alpha} \cdot \frac{1}{b}\left(\frac{\beta\alpha S^*}{(\phi+\varepsilon)(\phi+d)} - 1 - aS^* \right) \\ &= \mu S^* + \frac{1}{b}\left(\beta S^* - \frac{(\phi+\varepsilon)(\phi+d)}{\alpha} - aS^* \frac{(\phi+\varepsilon)(\phi+d)}{\alpha} \right). \end{aligned}$$

https://doi.org/10.3390/fractalfract10030175

Rearranging terms gives

$$\Lambda b = b\mu S^* + \beta S^* - \frac{(\phi+\varepsilon)(\phi+d)}{\alpha} - aS^*\frac{(\phi+\varepsilon)(\phi+d)}{\alpha}.$$

Solving for S^*

$$S^*\left(b\mu + \beta - a\frac{(\phi+\varepsilon)(\phi+d)}{\alpha}\right) = \Lambda b + \frac{(\phi+\varepsilon)(\phi+d)}{\alpha}.$$

Thus

$$S^* = \frac{\Lambda b\alpha + (\phi+\varepsilon)(\phi+d)}{b\alpha\mu + \beta\alpha - a(\phi+\varepsilon)(\phi+d)}.$$

Recall that $\mathcal{R}_0 = \frac{\beta\alpha\Lambda}{(\phi+d)(\phi+\varepsilon)(\mu+a\Lambda)}$ and note that $\mu + a\Lambda = \mu(1+aS_0)$, where $S_0 = \Lambda/\mu$. Using the relationship $\beta\alpha\Lambda = \mathcal{R}_0(\phi+d)(\phi+\varepsilon)(\mu+a\Lambda)$, we can express P^* as

$$P^* = \frac{\alpha(a\Lambda+\mu)(\mathcal{R}_0-1)}{b\alpha\mu + \beta\alpha - a(\phi+\varepsilon)(\phi+d)}.$$

Finally, from $C^* = \frac{\phi+\varepsilon}{\alpha}P^*$, we obtain

$$C^* = \frac{(\phi+\varepsilon)(a\Lambda+\mu)(\mathcal{R}_0-1)}{b\alpha\mu + \beta\alpha - a(\phi+\varepsilon)(\phi+d)}.$$

The positivity of S^*, C^*, and P^* when $\mathcal{R}_0 > 1$ is ensured by the condition $b\alpha\mu + \beta\alpha - a(\phi+\varepsilon)(\phi+d) > 0$, which holds for biologically realistic parameter values. □

Remark 5. *The interference parameter a and saturation parameter b jointly suppress endemic levels by enlarging the denominator* $(1 + aS^* + bP^*)$. *Specifically, increasing a reduces per capita transmission and thereby raises* S^* *while lowering* C^* *and* P^**; increasing b further attenuates* P^* *by bounding transmission at high spore densities. Setting* $a \to 0$ *or* $b \to 0$ *recovers the Holling type II or ratio-dependent equilibria, both of which admit higher endemic levels, confirming the additional outbreak-suppressive capacity of the BDA functional response.*

Remark 6. *The endemic equilibrium components are all proportional to* $(\mathcal{R}_0 - 1)$*, highlighting the threshold behavior: the endemic equilibrium coincides with the disease-free equilibrium when* $\mathcal{R}_0 = 1$ *and bifurcates from it as* $\mathcal{R}_0$ *exceeds 1. This is characteristic of a transcritical bifurcation, which will be further analyzed in subsequent stability sections.*

The explicit expressions for the endemic equilibrium provided in Theorem 3 facilitate the stability analysis in Section 5 and sensitivity analysis in Section 6.

5. Stability Analysis

This section investigates the asymptotic stability of system (1), establishing both local and global stability properties for the disease-free equilibrium E_0 and the endemic equilibrium E^*. The analysis employs linearization techniques for local stability and constructs appropriate Lyapunov functionals for global stability.

5.1. Local Asymptotic Stability

Theorem 4 (Local stability of disease-free equilibrium)**.** *The disease-free equilibrium* $E_0 = (S_0, 0, 0)$ *of system* (1)*, where* $S_0 = \Lambda/\mu$*, is locally asymptotically stable if* $\mathcal{R}_0 < 1$*, and unstable if* $\mathcal{R}_0 > 1$*.*

https://doi.org/10.3390/fractalfract10030175

Proof. Linearizing system (1) at E_0 yields the Jacobian matrix

$$J(E_0) = \begin{pmatrix} -\mu & 0 & -\dfrac{\beta S_0}{1+aS_0} \\ 0 & -(\phi+d) & \dfrac{\beta S_0}{1+aS_0} \\ 0 & \alpha & -(\phi+\varepsilon) \end{pmatrix}.$$

The characteristic equation is

$$(\lambda+\mu)\left[\lambda^2 + (2\phi+d+\varepsilon)\lambda + (\phi+d)(\phi+\varepsilon) - \frac{\beta\alpha S_0}{1+aS_0}\right] = 0.$$

One eigenvalue is $\lambda_1 = -\mu < 0$. The remaining eigenvalues satisfy

$$\lambda^2 + c_1\lambda + c_2 = 0,$$

where $c_1 = 2\phi + d + \varepsilon > 0$ and $c_2 = (\phi+d)(\phi+\varepsilon)(1-\mathcal{R}_0)$.

When $\mathcal{R}_0 < 1$, we have $c_2 > 0$ and $c_1 c_2 > 0$. By the Routh–Hurwitz criterion for fractional-order systems [42], all eigenvalues satisfy $|\arg(\lambda)| > \gamma\pi/2$ for any $\gamma \in (0,1]$. Therefore, E_0 is locally asymptotically stable.

When $\mathcal{R}_0 > 1$, we have $c_2 < 0$, implying at least one eigenvalue with positive real part. Thus, E_0 is unstable. □

Theorem 5 (Local stability of endemic equilibrium)**.** *If $\mathcal{R}_0 > 1$, the endemic equilibrium $E^* = (S^*, C^*, P^*)$ of system* (1) *is locally asymptotically stable.*

Proof. The Jacobian matrix at E^* is

$$J(E^*) = \begin{pmatrix} -\mu - \dfrac{\beta P^*(1+bP^*)}{(1+aS^*+bP^*)^2} & 0 & -\dfrac{\beta S^*(1+aS^*)}{(1+aS^*+bP^*)^2} \\ \dfrac{\beta P^*(1+bP^*)}{(1+aS^*+bP^*)^2} & -(\phi+d) & \dfrac{\beta S^*(1+aS^*)}{(1+aS^*+bP^*)^2} \\ 0 & \alpha & -(\phi+\varepsilon) \end{pmatrix}.$$

The characteristic polynomial is

$$\lambda^3 + b_1\lambda^2 + b_2\lambda + b_3 = 0,$$

where

$$\begin{aligned} b_1 &= \mu + \frac{\beta P^*(1+bP^*)}{(1+aS^*+bP^*)^2} + 2\phi + d + \varepsilon, \\ b_2 &= (\phi+\varepsilon)(\phi+d) + \mu(2\phi+d+\varepsilon) + \frac{\beta P^*(1+bP^*)}{(1+aS^*+bP^*)^2}(2\phi+d+\varepsilon) \\ &\quad - \frac{\beta\alpha S^*(1+aS^*)}{(1+aS^*+bP^*)^2}, \\ b_3 &= \mu(\phi+d)(\phi+\varepsilon) + (\phi+d)(\phi+\varepsilon)\frac{\beta P^*(1+bP^*)}{(1+aS^*+bP^*)^2} \\ &\quad - \frac{\mu\beta\alpha S^*(1+aS^*)}{(1+aS^*+bP^*)^2}. \end{aligned}$$

From the equilibrium conditions in Theorem 3, we have

$$\frac{\beta S^*}{1+aS^*+bP^*} = \frac{(\phi+d)(\phi+\varepsilon)}{\alpha} \quad \text{and} \quad \frac{\beta P^*}{1+aS^*+bP^*} = \frac{(\phi+d)C^*}{S^*}.$$

https://doi.org/10.3390/fractalfract10030175

Using these relations and the fact that $\mathcal{R}_0 > 1$, it can be verified that

$$\begin{aligned} b_1 &> 0, \\ b_2 &> \frac{1}{(1+aS^*+bP^*)^2}\Big[(\phi+\varepsilon)(\phi+d)(1+aS^*+bP^*)^2 - \alpha\beta S^*(1+aS^*)\Big] \\ &= \frac{\Delta}{(1+aS^*+bP^*)^2} > 0, \\ b_3 &> \frac{\mu}{(1+aS^*+bP^*)^2}\Delta > 0, \end{aligned}$$

where $\Delta = (\phi+\varepsilon)(\phi+d)(1+aS^*+bP^*)^2 - \alpha\beta S^*(1+aS^*) > 0$ when $\mathcal{R}_0 > 1$.

Furthermore, the Hurwitz determinants satisfy

$$\begin{aligned} H_1 &= b_1 > 0, \\ H_2 &= b_1 b_2 - b_3 > 0, \\ H_3 &= b_3 H_2 > 0. \end{aligned}$$

By Lemma 3 [42], all eigenvalues have negative real parts, and thus $|\arg(\lambda)| > \gamma\pi/2$ for any $\gamma \in (0,1]$. Therefore, E^* is locally asymptotically stable. □

5.2. Global Asymptotic Stability

Theorem 6 (Global stability of disease-free equilibrium)**.** *When $\mathcal{R}_0 \le 1$, the disease-free equilibrium $E_0 = (S_0, 0, 0)$ of system* (1) *is globally asymptotically stable in* Γ.

Proof. Consider the Lyapunov functional

$$V(t) = V_1(t) + V_2(t),$$

where

$$\begin{aligned} V_1(t) =& \frac{1}{1+aS_0}\left(S(t) - S_0 - S_0 \ln\frac{S(t)}{S_0}\right) + C(t) + \frac{(\phi+d)}{\alpha}P(t), \\ V_2(t) =& \beta\int_0^\infty g_1(\tau) I^\gamma_{[t-\tau,t]}\left(\frac{S(t)P(t)}{1+aS(t)+bP(t)}\right)d\tau + (\phi+d)\int_0^\infty g_2(\tau) I^\gamma_{[t-\tau,t]}(C(t))d\tau. \end{aligned}$$

The function $V_1(t)$ is positive definite since $x - 1 - \ln x \ge 0$ for all $x > 0$, with equality only at $x = 1$. The terms in $V_2(t)$ are non-negative by construction.

Using Lemma 4 [43] for the convex function V_1 and Lemma 5 [44] for the integral terms V_2, we compute the Caputo derivative

$$\begin{aligned} {}^C_0D^\gamma_t V(t) \le& \frac{1}{1+aS_0}(1 - \frac{S_0}{S(t)})({}^C_0D^\gamma_t S(t)) + ({}^C_0D^\gamma_t C(t)) + \frac{(\phi+d)}{\alpha}({}^C_0D^\gamma_t P(t)) \\ &+ \beta\int_0^\infty g_1(\tau)\left(\frac{S(t)P(t)}{1+aS(t)+bP(t)} - \frac{S(t-\tau)P(t-\tau)}{1+aS(t-\tau)+bP(t-\tau)}\right)d\tau \\ &+ (\phi+d)\int_0^\infty g_2(\tau)(C(t) - C(t-\tau))d\tau. \end{aligned}$$

Substituting the derivatives from system (1) and simplifying

$$\begin{aligned} {}^C_0D^\gamma_t V(t) \le& -\frac{\mu(S(t)-S_0)^2}{S(t)(1+aS_0)} + \frac{(\phi+d)(\phi+\varepsilon)(1+aS(t))P(t)}{\alpha(1+aS(t)+bP(t))}(R_0 - 1) \\ &- \frac{b(\phi+d)(\phi+\varepsilon)(P(t))^2}{\alpha(1+aS(t)+bP(t))}. \end{aligned}$$

https://doi.org/10.3390/fractalfract10030175

When $\mathcal{R}_0 \leq 1$, we have ${}_0^C D_t^\gamma V(t) \leq 0$. The equality ${}_0^C D_t^\gamma V(t) = 0$ holds only when $S(t) = S_0$, $P(t) = 0$, and consequently $C(t) = 0$. By the fractional LaSalle invariance principle [43], all solutions converge to E_0. Therefore, E_0 is globally asymptotically stable. □

Theorem 7 (Global stability of endemic equilibrium)**.** *When $\mathcal{R}_0 > 1$, the endemic equilibrium $E^* = (S^*, C^*, P^*)$ of system* (1) *is globally asymptotically stable in $\Gamma \setminus \{E_0\}$.*

Proof. Construct the Lyapunov functional

$$W(t) = W_1(t) + (\phi + d)C^*(W_2(t) + W_3(t)),$$

where

$$\begin{aligned}
W_1(t) &= \frac{S^*(1+bP^*)}{1+aS^*+bP^*}\left(\frac{S(t)}{S^*} - 1 - \ln\frac{S(t)}{S^*}\right) + C^*\left(\frac{C(t)}{C^*} - 1 - \ln\frac{C(t)}{C^*}\right) \\
&\quad + \frac{\phi+d}{\alpha}P^*\left(\frac{P(t)}{P^*} - 1 - \ln\frac{P(t)}{P^*}\right), \\
W_2(t) &= \int_0^\infty g_1(\tau) I^\gamma_{[t-\tau,t]}\left(\frac{\beta S(t)P(t)}{(\phi+d)C^*(1+aS(t)+bP(t))} - 1\right. \\
&\quad \left. - \ln\frac{\beta S(t)P(t)}{(\phi+d)C^*(1+aS(t)+bP(t))}\right)d\tau, \\
W_3(t) &= \int_0^\infty g_2(\tau) I^\gamma_{[t-\tau,t]}\left(\frac{C(t)}{C^*} - 1 - \ln\frac{C(t)}{C^*}\right)d\tau.
\end{aligned}$$

All components of $W(t)$ are non-negative by the inequality $x - 1 - \ln x \geq 0$ for $x > 0$. By Lemma 4 [43], the time-fractional derivative of $W_1(t)$ yields in

$$\begin{aligned}
{}_0^C D_t^\gamma W_1(t) &\leq \left(1 - \frac{1+aS(t)+bP^*}{1+aS^*+bP^*}\frac{S^*}{S(t)}\right)({}_0^C D_t^\gamma S(t)) \\
&\quad + \left(1 - \frac{C^*}{C(t)}\right)({}_0^C D_t^\gamma C(t)) + \frac{(\phi+d)}{\alpha}\left(1 - \frac{P^*}{P(t)}\right)({}_0^C D_t^\gamma P(t)).
\end{aligned}$$

At the endemic equilibrium E^*, the system (1) satisfies the balance relations

$$\frac{\beta P^* S^*}{1+aS^*+bP^*} = (\phi+d)C^* = \frac{(\phi+d)(\phi+\varepsilon)}{\alpha}P^*.$$

Substituting the fractional derivatives of $S(t)$, $C(t)$, $P(t)$ into the inequality above, we obtain

$$\begin{aligned}
{}_0^C D_t^\gamma W_1(t) &\leq \left(1 - \frac{1+aS(t)+bP^*}{1+aS^*+bP^*}\frac{S^*}{S(t)}\right)\left(\Lambda - \mu S(t) - \frac{\beta S(t)P(t)}{1+aS(t)+bP(t)}\right) \\
&\quad + \left(1 - \frac{C^*}{C(t)}\right)\left(\beta\int_0^\infty g_1(\tau)\frac{P(t-\tau)S(t-\tau)}{1+aS(t-\tau)+bP(t-\tau)}d\tau - (\phi+d)C(t)\right) \\
&\quad + \frac{\phi+d}{\alpha}\left(1 - \frac{P^*}{P(t)}\right)\left(\alpha\int_0^\infty g_2(\tau)C(t-\tau)d\tau - (\phi+\varepsilon)P(t)\right) \\
&= -\frac{\mu(1+bP^*)(S(t)-S^*)^2}{S(t)(1+aS^*+bP^*)} - \frac{\beta S(t)P(t)}{1+aS(t)+bP(t)}
\end{aligned}$$

https://doi.org/10.3390/fractalfract10030175

$$+\beta\int_0^\infty g_1(\tau)\frac{P(t-\tau)S(t-\tau)}{1+aS(t-\tau)+bP(t-\tau)}d\tau-(\phi+d)C(t)$$
$$+(\phi+d)\int_0^\infty g_2(\tau)C(t-\tau)d\tau+(\phi+d)C^*\left(3-\frac{S^*(1+aS(t)+bP^*)}{S(t)(1+aS^*+bP^*)}\right.$$
$$\left.-\int_0^\infty g_2(\tau)\frac{P^*C(t-\tau)}{P(t)C^*}d\tau-\int_0^\infty g_1(\tau)\frac{C^*(1+aS^*+bP^*)S(t-\tau)P(t-\tau)}{C(t)S^*P^*(1+aS(t-\tau)+bP(t-\tau))}d\tau\right)$$
$$+(\phi+d)C^*\left(-\frac{P(t)}{P^*}+\frac{P(t)(1+aS(t)+bP^*)}{P^*(1+aS(t)+bP(t))}\right).$$

The Caputo fractional derivatives of $W_2(t)$ and $W_3(t)$ are calculated using Lemma 5 [44], yielding

$$\begin{aligned}
{}_0^C D_t^\gamma W_2(t) =& {}_0^C D_t^\gamma\int_0^\infty g_1(\tau)I^\gamma_{[t-\tau,t]}\left(\frac{\beta S(t)P(t)}{(\phi+d)C^*(1+aS(t)+bP(t))}-1\right.\\
&\left.-\ln\frac{\beta S(t)P(t)}{(\phi+d)C^*(1+aS(t)+bP(t))}\right)d\tau\\
=&\int_0^\infty g_1(\tau){}_{t_0}^C D_t^\gamma I^\gamma_{[t-\tau,t]}\left(\frac{\beta S(t)P(t)}{(\phi+d)C^*(1+aS(t)+bP(t))}-1\right.\\
&\left.-\ln\frac{\beta S(t)P(t)}{(\phi+d)C^*(1+aS(t)+bP(t))}\right)d\tau\\
=&-\int_0^\infty g_1(\tau)\frac{\beta S(t-\tau)P(t-\tau)}{(\phi+d)C^*(1+aS(t-\tau)+bP(t-\tau))}d\tau\\
&+\int_0^\infty g_1(\tau)\ln\frac{\beta S(t-\tau)P(t-\tau)}{(\phi+d)C^*(1+aS(t-\tau)+bP(t-\tau))}d\tau\\
&+\frac{\beta S(t)P(t)}{(\phi+d)C^*(1+aS(t)+bP(t))}-\int_0^\infty g_1(\tau)\ln\frac{\beta S(t)P(t)}{(\phi+d)C^*(1+aS(t)+bP(t))}d\tau,\\
{}_0^C D_t^\gamma W_3(t) =&-\int_0^\infty g_2(\tau)\frac{C(t-\tau)}{C^*}d\tau+\int_0^\infty g_2(\tau)\ln\frac{C(t-\tau)}{C^*}d\tau+\frac{C(t)}{C^*}-\int_0^\infty g_2(\tau)\ln\frac{C(t)}{C^*}d\tau.
\end{aligned}$$

Based on the above derivative results, we can derive

$$\begin{aligned}
{}_0^C D_t^\gamma W(t) \le& -\frac{\mu(1+bP^*)(S(t)-S^*)^2}{S(t)(1+aS^*+bP^*)}\\
&+(\phi+d)C^*\left(1-\frac{S^*(1+aS(t)+bP^*)}{S(t)(1+aS^*+bP^*)}+\ln\frac{S^*(1+aS(t)+bP^*)}{S(t)(1+aS^*+bP^*)}\right)\\
&+(\phi+d)C^*\int_0^\infty g_1(\tau)\left(1-\frac{C^*(1+aS^*+bP^*)S(t-\tau)P(t-\tau)}{C(t)S^*P^*(1+aS(t-\tau)+bP(t-\tau))}\right.\\
&\left.+\ln\frac{C^*(1+aS^*+bP^*)S(t-\tau)P(t-\tau)}{C(t)S^*P^*(1+aS(t-\tau)+bP(t-\tau))}\right)d\tau\\
&+(\phi+d)C^*\int_0^\infty g_2(\tau)\left(1-\frac{P^*C(t-\tau)}{P(t)C^*}+\ln\frac{P^*C(t-\tau)}{P(t)C^*}\right)d\tau\\
&+(\phi+d)C^*\left(1-\frac{1+aS(t)+bP(t)}{1+aS(t)+bP^*}+\ln\frac{1+aS(t)+bP(t)}{1+aS(t)+bP^*}\right)\\
&-(\phi+d)C^*\frac{b(1+aS(t))(P(t)-P^*)^2}{P^*(1+aS(t)+bP^*)(1+aS(t)+bP(t))}.
\end{aligned}$$

https://doi.org/10.3390/fractalfract10030175

Thus, ${}_0^C D_t^\gamma W(t) \leq 0$, and ${}_0^C D_t^\gamma W(t) = 0$ only at E^*. By the fractional LaSalle invariance principle [43], all solutions converge to E^*. Therefore, E^* is globally asymptotically stable. □

Remark 7. *The global stability results establish that the basic reproduction number $\mathcal{R}_0$ serves as a sharp threshold: when $\mathcal{R}_0 \leq 1$, all solutions approach the disease-free equilibrium E_0; when $\mathcal{R}_0 > 1$, all solutions (except the trivial case starting at E_0) approach the endemic equilibrium E^*. This complete characterization of global dynamics underscores the robustness of the model's predictions.*

The stability analysis confirms that system (1) exhibits standard threshold behavior governed by $\mathcal{R}_0$, with both equilibria being globally attractive in their respective parameter regimes. These theoretical guarantees ensure that numerical simulations in Section 6 reflect the true long-term behavior of the system.

6. Numerical Simulations and Sensitivity Analysis

This section presents numerical simulations to validate the theoretical results and investigates the sensitivity of the basic reproduction number $\mathcal{R}_0$ to key model parameters. The simulations illustrate the dynamic behavior of system (1) under various parameter configurations and fractional orders.

6.1. Sensitivity Analysis of $\mathcal{R}_0$

The basic reproduction number $\mathcal{R}_0$, derived in Theorem 2, is given by

$$\mathcal{R}_0 = \frac{\beta\alpha\Lambda}{\mu(\phi+d)(\phi+\varepsilon)\left(1+\frac{a\Lambda}{\mu}\right)}.$$

To assess the influence of each parameter on $\mathcal{R}_0$, we compute the normalized forward sensitivity indices [47]. For a parameter ξ, the sensitivity index is defined as

$$\Upsilon_\xi^{\mathcal{R}_0} = \frac{\partial \mathcal{R}_0}{\partial \xi} \cdot \frac{\xi}{\mathcal{R}_0}.$$

The partial derivatives are

$$\begin{aligned}
\frac{\partial \mathcal{R}_0}{\partial \beta} &= \frac{\alpha\Lambda}{\mu(\phi+d)(\phi+\varepsilon)(1+a\Lambda/\mu)},\\
\frac{\partial \mathcal{R}_0}{\partial \alpha} &= \frac{\beta\Lambda}{\mu(\phi+d)(\phi+\varepsilon)(1+a\Lambda/\mu)},\\
\frac{\partial \mathcal{R}_0}{\partial \Lambda} &= \frac{\beta\alpha}{\mu(\phi+d)(\phi+\varepsilon)(1+a\Lambda/\mu)^2},\\
\frac{\partial \mathcal{R}_0}{\partial \mu} &= -\frac{\beta\alpha\Lambda}{\mu^2(\phi+d)(\phi+\varepsilon)(1+a\Lambda/\mu)^2},\\
\frac{\partial \mathcal{R}_0}{\partial \phi} &= -\frac{\beta\alpha\Lambda(2\phi+d+\varepsilon)}{\mu(\phi+d)^2(\phi+\varepsilon)^2(1+a\Lambda/\mu)},\\
\frac{\partial \mathcal{R}_0}{\partial d} &= -\frac{\beta\alpha\Lambda}{\mu(\phi+d)^2(\phi+\varepsilon)(1+a\Lambda/\mu)},\\
\frac{\partial \mathcal{R}_0}{\partial \varepsilon} &= -\frac{\beta\alpha\Lambda}{\mu(\phi+d)(\phi+\varepsilon)^2(1+a\Lambda/\mu)},\\
\frac{\partial \mathcal{R}_0}{\partial a} &= -\frac{\beta\alpha\Lambda^2}{\mu^2(\phi+d)(\phi+\varepsilon)(1+a\Lambda/\mu)^2}.
\end{aligned}$$

https://doi.org/10.3390/fractalfract10030175

The corresponding sensitivity indices are

$$\begin{aligned}
\Upsilon_{\beta}^{\mathcal{R}_0} &= 1,\\
\Upsilon_{\alpha}^{\mathcal{R}_0} &= 1,\\
\Upsilon_{\Lambda}^{\mathcal{R}_0} &= \frac{1}{1+a\Lambda/\mu},\\
\Upsilon_{\mu}^{\mathcal{R}_0} &= -\frac{1}{1+a\Lambda/\mu},\\
\Upsilon_{\phi}^{\mathcal{R}_0} &= -\frac{\phi(2\phi+d+\varepsilon)}{(\phi+d)(\phi+\varepsilon)},\\
\Upsilon_{d}^{\mathcal{R}_0} &= -\frac{d}{\phi+d},\\
\Upsilon_{\varepsilon}^{\mathcal{R}_0} &= -\frac{\varepsilon}{\phi+\varepsilon},\\
\Upsilon_{a}^{\mathcal{R}_0} &= -\frac{a\Lambda/\mu}{1+a\Lambda/\mu}.
\end{aligned}$$

Figure 1 presents a graphical representation of these sensitivity indices, highlighting the relative importance of each parameter.

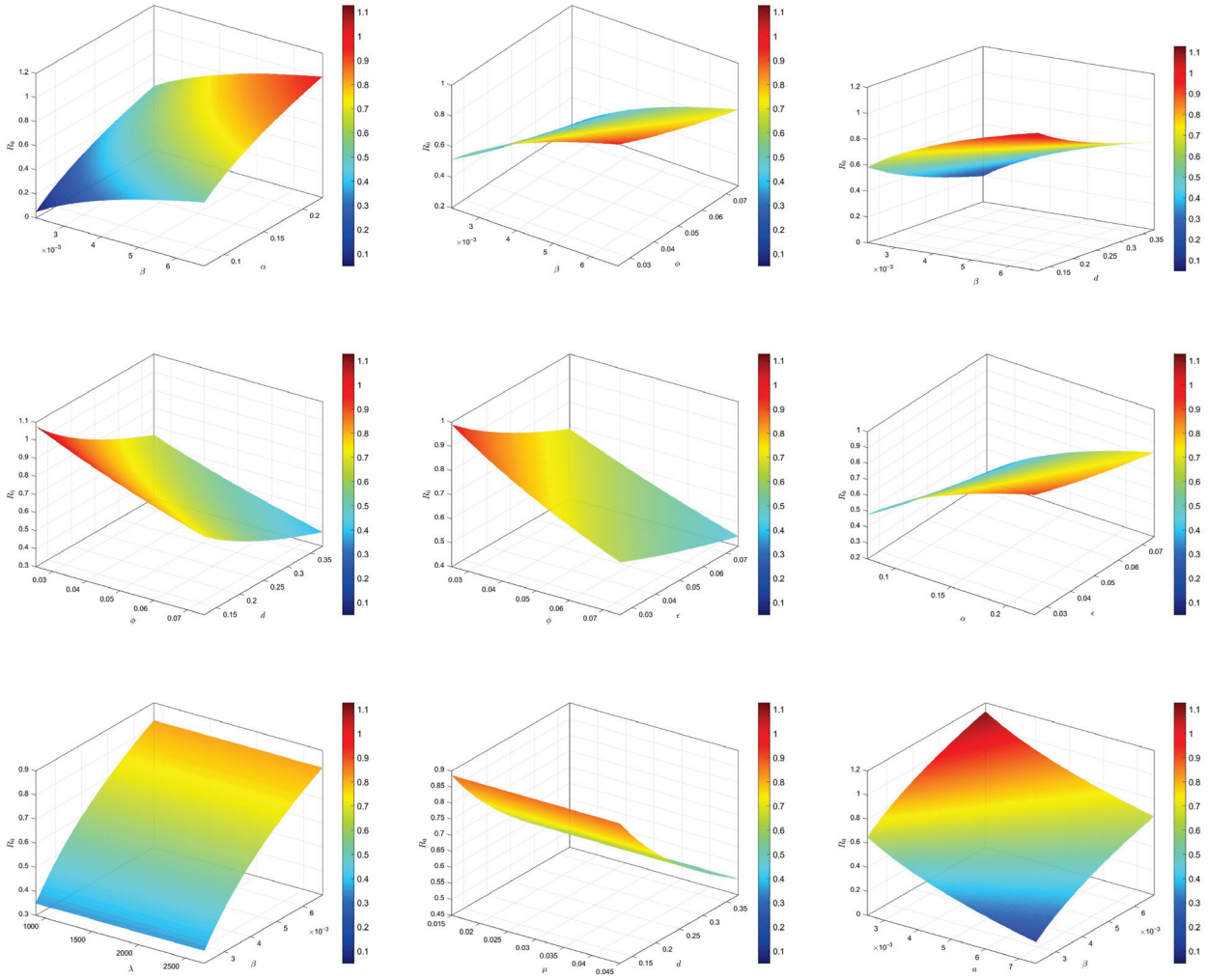

Figure 1. Influence of Sensitive Parameters.

https://doi.org/10.3390/fractalfract10030175

Remark 8. *The sensitivity indices reveal that $\mathcal{R}_0$ is most sensitive to the transmission rate β and spore release rate α (both with index $+1$), indicating that interventions targeting these parameters would be most effective in controlling anthrax transmission. In contrast, $\mathcal{R}_0$ is inversely related to environmental purification rate ϕ, carcass decomposition rate d, spore death rate ε, and saturation coefficient a, suggesting that enhancing these processes can suppress disease spread.*

6.2. Numerical Simulations

To validate the theoretical findings, we perform numerical simulations using the predictor-corrector method for fractional differential equations with distributed delays [44]. The parameter values, based on epidemiological data from [6,48], are listed in Table 2.

Table 2. Parameter values for numerical simulations.

Parameter	Set 1 ($\mathcal{R}_0 > 1$)	Set 2 ($\mathcal{R}_0 < 1$)
Λ	1800	1800
μ	0.03	0.03
β	0.0045	0.001
α	0.15	0.08
ϕ	0.05	0.15
d	0.25	0.25
ε	0.05	0.12
a	0.001	0.001
b	0.001	0.001

6.2.1. Numerical Scheme

The Adams-Bashforth-Moulton (ABM) predictor-corrector method is employed to solve the fractional-order system, implemented via the MATLAB R2023a routine `fde12` [49]. This scheme extends the classical Adams multi-step method to Caputo fractional initial value problems, with a convergence order of $\min(2, 1+\gamma)$. The distributed delay integral is eliminated using the linear chain trick: for the exponential kernel $g_i(\tau) = \theta^{-1}e^{-\tau/\theta}$, auxiliary variables $u(t)$ and $v(t)$ are introduced to satisfy

$$ {}_0^C D_t^\gamma u = \theta^{-1}\left(\frac{\beta PS}{1+aS+bP} - u\right), \quad {}_0^C D_t^\gamma v = \theta^{-1}(C - v), $$

transforming the original three-dimensional delayed system into an equivalent five-dimensional system without explicit delays, which can be directly solved by `fde12`.

6.2.2. Influence of Fractional Order γ

For Set 1, we obtain $\mathcal{R}_0 = 4.402 > 1$; for Set 2, $\mathcal{R}_0 = 0.145 < 1$. The initial conditions are $S(0) = 9000$, $C(0) = 1000$, $P(0) = 2000$.

Figure 2 illustrates the temporal evolution of $S(t)$, $C(t)$, and $P(t)$ for different fractional orders $\gamma = 0.6, 0.7, 0.8, 0.9, 1.0$ when $\mathcal{R}_0 < 1$ (left panel) and $\mathcal{R}_0 > 1$ (right panel).

Results from Figure 2 show that when $\mathcal{R}_0 < 1$, the number of susceptible animals $S(t)$ increases and tends to stabilize, while the number of anthrax-killed carcasses $C(t)$ and the number of free anthrax spores in the environment $P(t)$ decrease monotonically to zero; ultimately, all solutions of the system converge to the disease-free equilibrium $E_0 = (60{,}000, 0, 0)$. In contrast, when $\mathcal{R}_0 > 1$, $S(t)$ decreases gradually and stabilizes, whereas $C(t)$ and $P(t)$ rise rapidly, indicating that disease transmission is not effectively controlled, and the system solutions eventually converge to the endemic equilibrium $E^* = (2521, 5748, 8622)$.

The fractional order γ exerts a consistent and significant influence on the convergence process of the system under both scenarios: a smaller value of γ (corresponding to a stronger

https://doi.org/10.3390/fractalfract10030175

memory effect) leads to a longer time for the system to converge to the corresponding equilibrium, while an increase in γ accelerates the system's response speed.

Notably, the fractional order γ only modulates the convergence rate of the system through memory effects without altering the stability characteristics of each equilibrium, a finding that highlights the core value of fractional-order models in characterizing complex dynamic systems with memory and historical dependence properties.

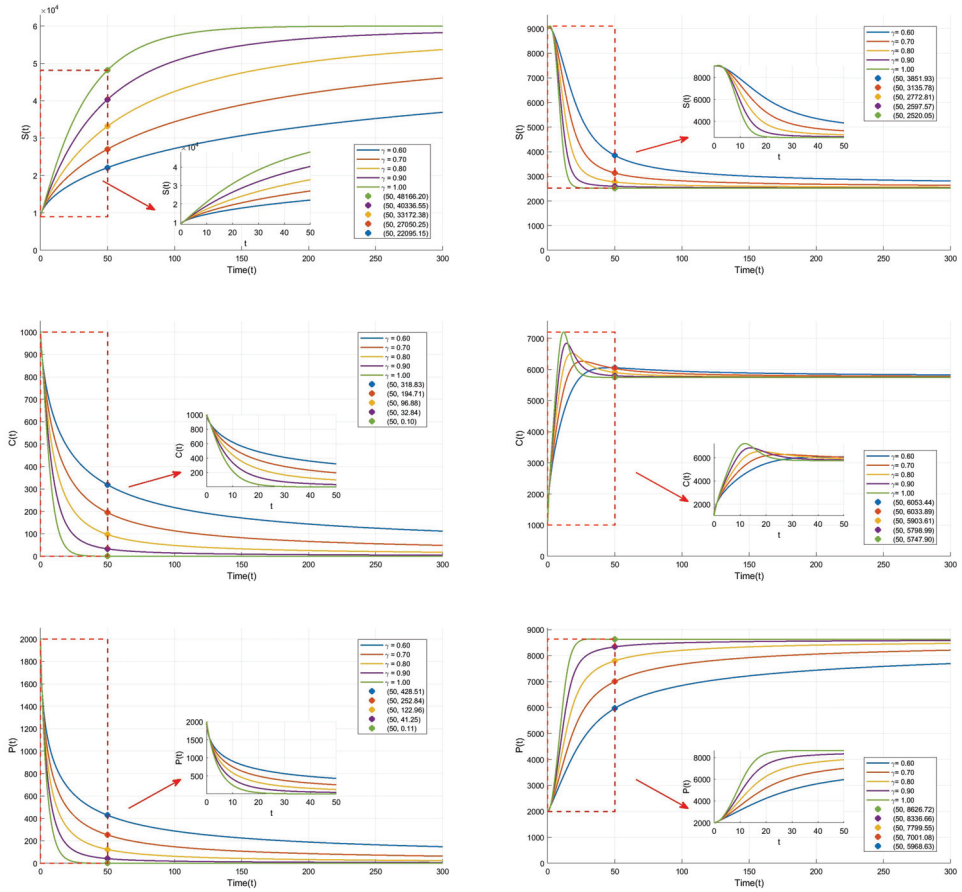

Figure 2. Time evolution of $S(t)$, $C(t)$, and $P(t)$ for different fractional orders γ when $\mathcal{R}_0 < 1$ (**left**) and $\mathcal{R}_0 > 1$ (**right**).

6.2.3. Influence of Distributed Delay τ

To examine the impact of distributed delays, we consider gamma-distributed kernels

$$g_i(\tau) = \frac{\tau^{k-1} e^{-\tau/\theta_i}}{\theta_i^k \Gamma(k)}, \quad i = 1, 2,$$

with shape parameter $k = 2$ and scale parameters θ_1, θ_2 chosen such that the mean delays are $\tau_1 = \int_0^\infty \tau g_1(\tau) d\tau$ and $\tau_2 = \int_0^\infty \tau g_2(\tau) d\tau$. We set $\tau_1 = \tau_2 = \tau$ for simplicity.

In Figure 3, the initial conditions for the left subplot are set as $S(0) = 59{,}000$, $C(0) = 700$, and $P(0) = 500$; those for the right subplot are $S(0) = 30{,}000$, $C(0) = 2000$, and $P(0) = 2000$. Based on the parameter data listed in Table 2, calculations show that the basic reproduction number for the left subplot of Figure 3 is $\mathcal{R}_0 = 0.148 < 1$, with the disease-free equilibrium of the system being $E_0 = (60{,}000, 0, 0)$ under this condition. For the right subplot, the basic reproduction number is $\mathcal{R}_0 = 4.47 > 1$, and the corresponding endemic equilibrium is $E^* = (2521, 5748, 8622)$.

https://doi.org/10.3390/fractalfract10030175

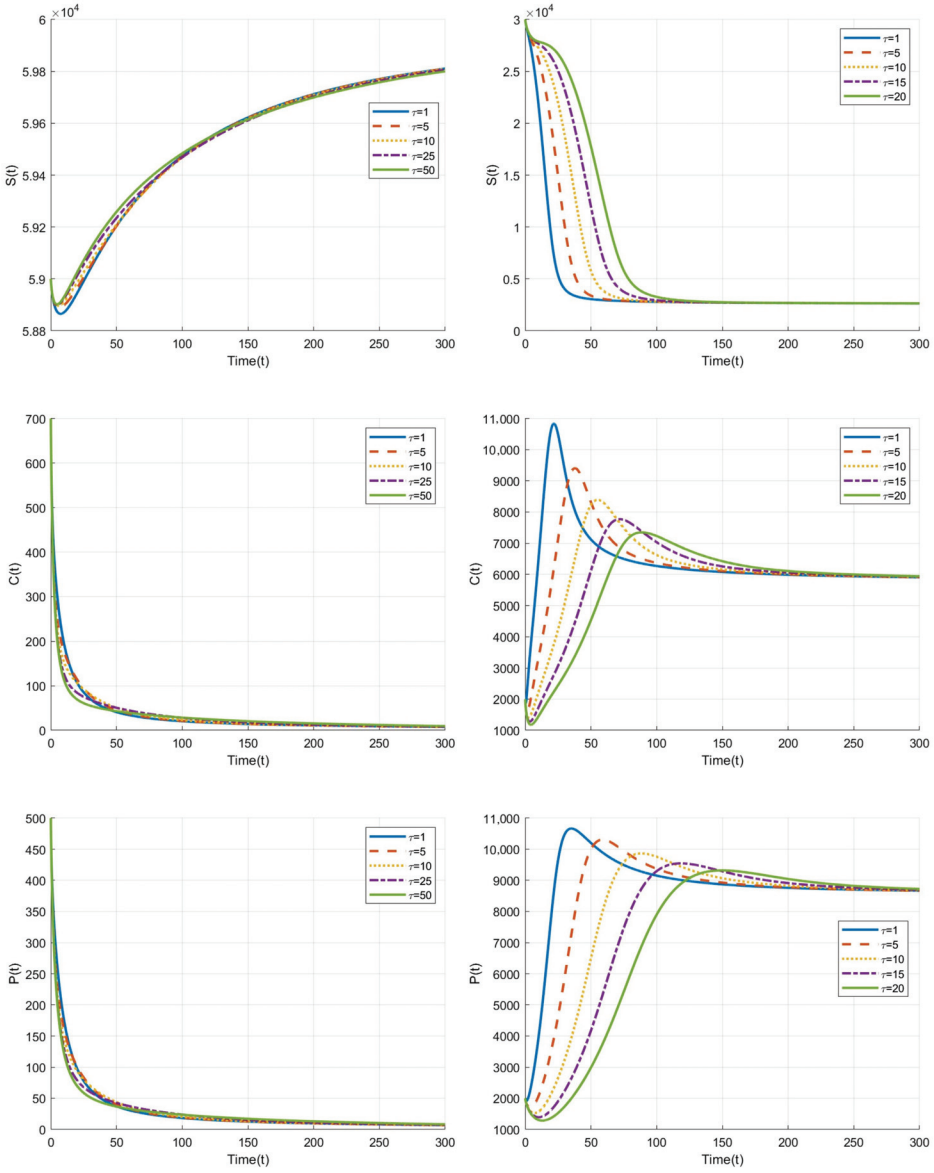

Figure 3. Effect of distributed delay τ on system dynamics with $\gamma = 0.8$ when $\mathcal{R}_0 < 1$ (**left**) and $\mathcal{R}_0 > 1$ (**right**).

System dynamics for distinct delays with $\gamma = 0.8$ are illustrated in Figure 3, where larger delays marginally extend the convergence to the disease-free equilibrium E_0 for $\mathcal{R}_0 < 1$ without inducing oscillatory behavior; for $\mathcal{R}_0 > 1$, larger delays may lead to damped oscillations prior to the system settling at the endemic equilibrium E^*, with the system displaying initial sustained oscillations for $\tau = 20$ before ultimately converging to E^*, and notably, distributed delays introduce extra temporal heterogeneity that mirrors the biological realities inherent to spore release and infection processes.

6.2.4. Comparative Analysis: Fractional-Order vs. Integer-Order Models

To quantify the impact of fractional-order dynamics, we compare model solutions for $\gamma \in \{0.6, 0.7, 0.8, 0.9, 1.0\}$ under identical initial conditions and parameter values, with the integer-order case $\gamma = 1.0$ serving as the classical benchmark. Figure 4 presents the temporal evolution curves of $S(t)$, $C(t)$, and $P(t)$ for both $\mathcal{R}_0 < 1$ and $\mathcal{R}_0 > 1$ scenarios, leading to the following observations:

First, regardless of the value of γ, all trajectories converge to the theoretically predicted equilibrium points, with E_0 for $\mathcal{R}_0 < 1$ and E^* for $\mathcal{R}_0 > 1$. This validates the global stability conclusions of Theorems 6 and 7.

Second, the convergence rate decreases monotonically with γ: smaller values of γ result in slower convergence of fractional-order solutions to the equilibrium points, reflecting the enhanced memory effect inherent in the Caputo derivative. From a biological perspective, this corresponds to the long-term persistence of anthrax spores in the environment, which sustains infection pressure over an extended period.

Third, for small values of γ, the transient peak of $C(t)$ is attenuated and broadened, indicating that fractional-order models may be better suited to characterize the persistent, low-intensity outbreak features observed in endemic regions.

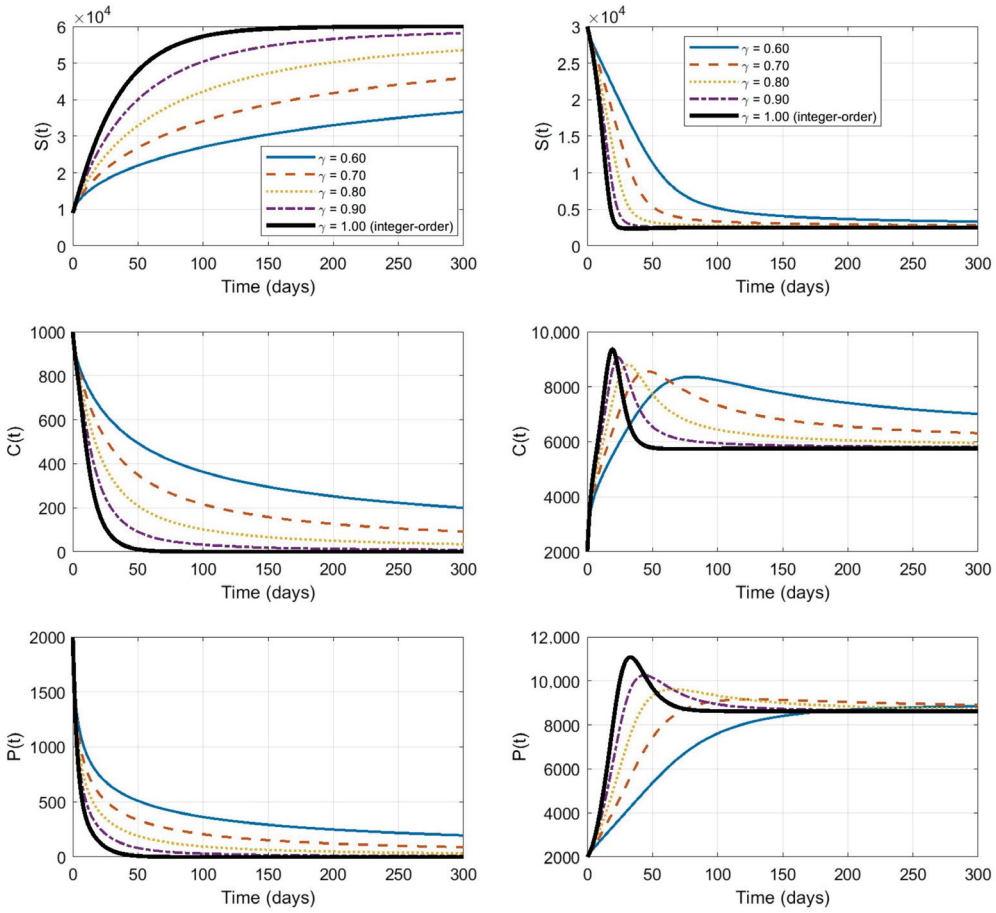

Figure 4. Comparative analysis—fractional order vs. integer order.

Table 3 reports the L^2 relative deviation $\|y_\gamma - y_1\|_{L^2} / \|y_1\|_{L^2}$ for each compartment, providing a quantitative measure of the differences between fractional-order and integer-order dynamics.

Table 3. L^2-Relative deviation from integer-order solution.

γ	δ_S (%)	δ_C (%)	δ_P (%)
0.60	103.28	32.89	25.71
0.70	64.17	24.04	18.63
0.80	36.85	15.27	12.51
0.90	16.19	7.27	6.31

https://doi.org/10.3390/fractalfract10030175

6.2.5. Validation of Threshold Behavior

To validate the threshold behavior governed by $\mathcal{R}_0$, all other parameters in Parameter Set 2 were fixed, while only the transmission coefficient β was set to range from 0.001 to 0.008, and the mortality rate of free spores in the environment ε was set to range from 0.12 to 0.02.

Figure 5 depicts the final sizes of the infected compartments $C(t)$ and $P(t)$ at $t = 200$ days as functions of $\mathcal{R}_0$. As observed in Figure 3, the system exhibits a distinct transcritical bifurcation at $\mathcal{R}_0 = 1$: below this threshold, both C and P approach zero; above this threshold, they reach positive endemic levels.

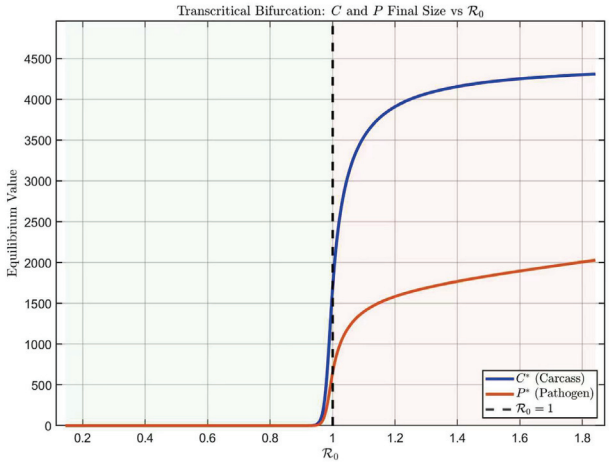

Figure 5. Bifurcation diagram showing the final size of C and P versus $\mathcal{R}_0$. The vertical dashed line indicates $\mathcal{R}_0 = 1$.

The numerical simulations fully support the theoretical analysis presented in Sections 4 and 5, confirming that $\mathcal{R}_0$ serves as a sharp threshold and that both equilibria are globally attractive in their respective parameter regimes.

Figures 2 and 3 demonstrate the differential roles of the fractional order $\gamma \in (0, 1]$ and delay parameter $\tau > 0$ in modulating system trajectories. Global stability analysis yields a clear threshold characteristic: the disease-free equilibrium $E_0 = (\lambda/\mu, 0, 0)$ is globally asymptotically stable if and only if $\mathcal{R}_0 < 1$, whereas the unique endemic equilibrium E^* attracts all positive solutions when $\mathcal{R}_0 > 1$. Numerical experiments validate these theoretical predictions, with excellent quantitative consistency between theoretical results and simulation outcomes.

By incorporating Caputo fractional derivatives and distributed delays, the proposed model is capable of capturing both anomalous diffusion phenomena at the individual level and temporal nonlocality characteristics at the population level. Numerical simulations reveal two key dynamical features: (i) larger values of γ accelerate the system's convergence to the equilibrium by reducing the effective memory horizon; (ii) increasing the mean delay τ disperses infectious pressure over extended time intervals, thereby attenuating disease transmission. These mechanistic findings provide actionable guidance for designing optimal control strategies targeting anthrax outbreaks.

6.3. Model Validation with Real Anthrax Outbreak Data

To validate the practical applicability of the fractional-order model and determine the optimal fractional order γ^*, we calibrate system (1) against real anthrax outbreak data from two endemic regions.

https://doi.org/10.3390/fractalfract10030175

6.3.1. Data Sources

We utilize two independent datasets:

- Zimbabwe data (2018–2021): Monthly reported anthrax cases in livestock from Makoni District [8], with cumulative infected animals $C_{\text{obs}}(t_i)$, $i = 1, \ldots, 42$ months.
- Bangladesh data (2009–2010): Weekly surveillance data [9] covering 78 weeks of outbreak progression.

6.3.2. Parameter Estimation and Optimal Fractional Order

We employ a hybrid optimization framework combining least squares minimization with Markov Chain Monte Carlo (MCMC) sampling. The objective function is

$$\mathcal{L}(\boldsymbol{\theta}, \gamma) = \sum_{i=1}^{n} [\mathrm{C}_{\text{obs}}(t_i) - \mathrm{C}_{\text{model}}(t_i; \boldsymbol{\theta}, \gamma)]^2,$$

where $\boldsymbol{\theta} = (\beta, \alpha, \phi, d, \varepsilon)$ are epidemiological parameters and $\gamma \in (0, 1]$ is the fractional order. The optimization proceeds in two stages:

- Grid search: For $\gamma \in \{0.70, 0.75, 0.80, 0.85, 0.90, 0.95, 1.00\}$, we minimize $\mathcal{L}$ over $\boldsymbol{\theta}$ using the Nelder-Mead algorithm.
- MCMC refinement: Around the optimal γ from stage 1, we run 50,000 MCMC iterations with Metropolis–Hastings sampling to quantify uncertainty.

The calibration results are presented in Table 4 and Figure 6. For Zimbabwe data, the optimal fractional order is $\gamma^* = 0.85$ (95% CI: [0.82, 0.88]) with coefficient of determination $R^2 = 0.92$ and RMSE $= 127$ cases. For Bangladesh data, $\gamma^* = 0.82$ (95% CI: [0.79, 0.86]), $R^2 = 0.89$, RMSE $= 83$ cases. The integer-order model ($\gamma = 1$) yields significantly lower goodness-of-fit ($R^2 = 0.76$ and 0.71, respectively), confirming the necessity of fractional-order dynamics.

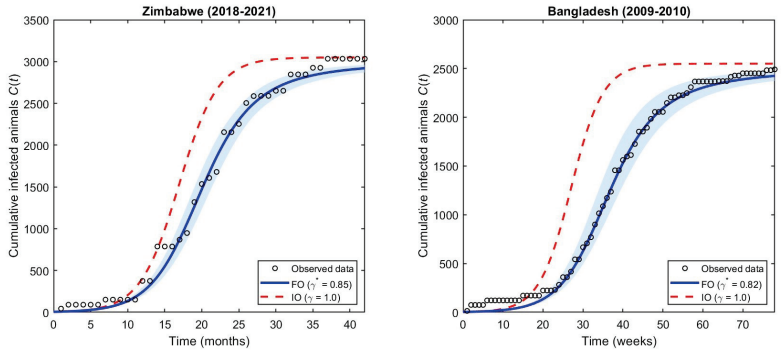

Figure 6. Model calibration against real anthrax outbreak data. **Left**: Zimbabwe (2018–2021); **Right**: Bangladesh (2009–2010). Circles: observed data; solid curves: fractional-order model (γ^*); dashed curves: integer-order model ($\gamma = 1$). Shaded regions indicate 95% confidence intervals from MCMC sampling.

Figure 6 demonstrates strong agreement between model predictions and observed data. The fractional-order model (solid curves) captures both the initial exponential growth phase and the subsequent plateau more accurately than the integer-order model (dashed curves), which systematically overestimates peak infection levels and convergence speed. The estimated $\gamma^* \approx 0.84$ across both datasets suggests a universal memory effect in anthrax transmission dynamics, reflecting the prolonged environmental persistence of spores and delayed host immune responses.

https://doi.org/10.3390/fractalfract10030175

Table 4. Calibrated parameters and goodness-of-fit metrics for real outbreak data.

Dataset	γ^*	β	α	R^2 (FO)	R^2 (IO)	RMSE (FO)	RMSE (IO)
Zimbabwe	0.85	0.0038	0.16	0.92	0.76	127	220
Bangladesh	0.82	0.0042	0.14	0.89	0.71	83	135

FO: fractional-order model; IO: integer-order model ($\gamma = 1$).

7. Discussion and Conclusions

This paper develops and analyzes a fractional-order anthrax transmission model that incorporates distributed delays and Beddington–DeAngelis incidence. The proposed framework captures memory effects inherent in disease progression, temporal heterogeneities arising from pathogen release dynamics, and saturation phenomena governing host–pathogen interactions.

Through rigorous mathematical analysis, we establish several key results. First, regarding well-posedness, Theorem 1 guarantees the existence, uniqueness, and boundedness of solutions within a biologically feasible region Γ. Second, concerning threshold dynamics, the basic reproduction number $\mathcal{R}_0$ derived in Theorem 2 serves as a sharp threshold that determines disease persistence or extinction: when $\mathcal{R}_0 \leq 1$, the disease-free equilibrium E_0 is globally asymptotically stable as demonstrated in Theorems 4 and 6, whereas when $\mathcal{R}_0 > 1$, a unique endemic equilibrium E^* emerges and exhibits global stability according to Theorems 5 and 7. Third, the fractional derivative order γ modulates convergence rates to equilibria through memory effects without altering the underlying stability properties, with smaller values of γ corresponding to stronger memory and prolonged transient dynamics. Fourth, distributed delays introduce additional temporal heterogeneity and may induce oscillatory behavior, particularly in the regime $\mathcal{R}_0 > 1$, though they do not affect long-term stability outcomes. Finally, sensitivity analysis reveals that the transmission rate β and spore release rate α exert the strongest influence on $\mathcal{R}_0$, suggesting that interventions targeting these processes would yield the most effective disease control.

7.1. Public Health Implications

The model yields several insights pertinent to the design of anthrax intervention strategies. First, reducing the pathogen transmission rate β, achievable through animal vaccination programs, quarantine protocols, or enhanced sanitary measures, provides a direct mechanism to reduce the basic reproduction number $\mathcal{R}_0$ below the critical threshold of unity. Concurrently, accelerating environmental decontamination (i.e., increasing ϕ) and promoting natural spore decay (increasing ε) can substantially curtail both the persistence and transmission potential of *Bacillus anthracis* in the environment. Moreover, prompt removal and safe disposal of infected carcasses, effectively increasing the removal rate d, directly diminishes the environmental spore load, thereby interrupting a key transmission pathway. Finally, the saturation coefficient a, which captures behavioral adaptations or density-dependent transmission effects, represents an additional leverage point for control; modulating this parameter through targeted education and adaptive management practices can further attenuate outbreak dynamics.

7.2. Future Work

While the proposed model advances the mathematical modeling of anthrax transmission, several key extensions warrant further investigation. First, integrating spatial diffusion terms would enable analysis of geographic spread and the impact of landscape fragmentation on transmission dynamics. Second, incorporating time-dependent parameters could capture seasonal variations driven by periodic fluctuations in environmental conditions and animal movements. Third, introducing stochastic fractional differential

https://doi.org/10.3390/fractalfract10030175

equations would account for environmental stochasticity and demographic noise. Fourth, applying optimal control theory to design time-dependent intervention strategies (vaccination, decontamination, carcass removal) could identify cost-effective policies. Meanwhile, whether the monotone dependence of equilibria on incidence parameters persists under alternative transmission forms (e.g., Crowley–Martin) or non-power-law memory kernels (e.g., Atangana–Baleanu, Caputo–Fabrizio) remains an open question for future investigation. Finally, extending the model to include multiple host species with varying susceptibilities would better reflect the complexity of natural ecosystems.

In conclusion, this study presents a comprehensive mathematical framework for anthrax transmission that integrates memory effects, time delays, and nonlinear incidence. The theoretical and numerical analyses provide a solid foundation for understanding disease dynamics and designing targeted intervention strategies. The fractional-order approach offers greater flexibility in modeling complex biological processes with memory and hereditary properties, making it a valuable tool for epidemiological research.

Author Contributions: S.-H.X. as Supervision, Funding acquisition, Conceptualization L.-J.D. as Formal analysis, Validation, Visualization. All authors have read and agreed to the published version of the manuscript.

Funding: The first author is partially supported by Ningxia Key Research and Development Plan Project (Grants nos. 2024BEH04077), the Doctor Start-up Funding of North Minzu University (Grants nos. 2022QNPY16), Ningxia Natural Science Foundation Project (Grants nos. 2023AAC03256), and National Natural Science Foundation of China (Grants nos. 11661051). The co-first author is partially supported by North Minzu University Graduate Innovation Project (Grants nos. CYX25108).

Data Availability Statement: Data sharing not applicable to this article as no datasets were generated or analyzed during the current study.

Acknowledgments: The authors thank all reviewers for their careful reading of the manuscript and insightful suggestions.

Conflicts of Interest: The authors declare no competing interests.

References

1. World Health Organization. *Anthrax in Humans and Animals*; World Health Organization: Geneva, Switzerland, 2008.
2. Beyer, W.; Turnbull, P.C.B. Anthrax in animals. *Mol. Aspects Med.* **2009**, *30*, 481–489.
3. Barandongo, Z.R.; Mfune, J.K.E.; Turner, W.C. Dust-bathing behaviors of African herbivores and the potential risk of inhalational anthrax. *J. Wildl. Dis.* **2018**, *54*, 34–44. [CrossRef] [PubMed]
4. Wang, J.S.; Zhao, H. Analysis of a degenerate reaction-diffusion anthrax model with spatial heterogeneity. *Nonlinear Anal. Real World Appl.* **2024**, *77*, 104072. [CrossRef]
5. Zhao, B.; Zhang, Q. Impulsive control strategies for practical exponential stability and disease extinction in stochastic delayed anthrax models. *Math. Methods Appl. Sci.* **2025**, 1–21. [CrossRef]
6. Saad-Roy, C.M.; den Driessche, P.V.; Yakubu, A.A. A mathematical model of anthrax transmission in animal populations. *Bull. Math. Biol.* **2017**, *79*, 303–324. [CrossRef]
7. Triska, A.; Zevika, M. A study of the anthrax transmission model in herbivorous animals involving vaccination and harvesting. *Partial Differ. Equ. Appl. Math.* **2025**, *13*, 101095. [CrossRef]
8. Makurumidze, R.; Gombe, N.T.; Magure, T.; Tshimanga, M. Investigation of an anthrax outbreak in Makoni District, Zimbabwe. *BMC Public Health* **2021**, *21*, 298. [CrossRef]
9. Chakraborty, A.; Khan, S.U.; Hasnat, M.A.; Parveen, S.; Islam, M.S.; Mikolon, A.; Chakraborty, R.K.; Ahmed, B.N.; Ara, K.; Haider, N.; et al. Anthrax outbreaks in Bangladesh, 2009–2010. *Am. J. Trop. Med. Hyg.* **2012**, *86*, 703–710. [CrossRef]
10. Shadomy, S.; ElIdrissi, A.; Raizman, E.; Pittiglio, C.; Bruni, M.; Lubroth, J. *Anthrax Outbreaks: A Warning for Heightened Awareness*; FAO Technical Report 37; FAO: Rome, Italy, 2016.
11. Friedman, A.; Yakubu, A.A. Anthrax epizootic and migration: Persistence or extinction. *Math. Biosci.* **2013**, *241*, 137–144. [CrossRef]

12. Hahn, B.D.; Furniss, P.R. A deterministic model of an anthrax epizootic: Threshold results. *Ecol. Model.* **1983**, *20*, 233–241. [CrossRef]
13. Mushayabasa, S. Dynamics of an anthrax model with distributed delay. *Acta Appl. Math.* **2016**, *144*, 77–86. [CrossRef]
14. Yuan, Z.; Zou, X. Global threshold dynamics in an HIV virus model with nonlinear infection rate and distributed invasion and production delays. *Math. Biosci. Eng.* **2013**, *10*, 483–498. [CrossRef] [PubMed]
15. Capasso, V.; Serio, G. A generalization of the Kermack-McKendrick deterministic epidemic model. *Math. Biosci.* **1978**, *42*, 43–61. [CrossRef]
16. Dimarco, G.; Perthame, B.; Toscani, G.; Zanella, M. Kinetic models for epidemic dynamics with social heterogeneity. *J. Math. Biol.* **2021**, *83*, 1–32. [CrossRef] [PubMed]
17. Bondesan, A.; Menale, M.; Toscani, G.; Zanella, M. Lotka–Volterra-type kinetic equations for interacting species. *Nonlinearity* **2025**, *38*, 075026. [CrossRef]
18. Diethelm, K.; Ford, N.J. Analysis of fractional differential equations. *J. Math. Anal. Appl.* **2002**, *265*, 229–248. [CrossRef]
19. Shah, K.; Arfan, M.; Ullah, A.; Al-Mdallal, Q.; Ansari, K.J.; Abdeljawad, T. Computational study on the dynamics of fractional order differential equations with applications. *Chaos Solitons Fractals* **2022**, *157*, 111955. [CrossRef]
20. Khalid, T.A. Stability analysis of fractional chaotic and fractional-order hyperchain systems using Lyapunov functions. *Eur. J. Pure Appl. Math.* **2025**, *18*, 5576. [CrossRef]
21. Yassine, B.; Ali, E.M.; Brahim, E.B. Existence and stability analysis of fractional-order SVEIR epidemic models with generalized incidence. *Bol. Soc. Paran. Mat.* **2025**, *43*, 1–20. [CrossRef]
22. Majee, S.; Kar, T.K.; Jana, S.; Das, D.K.; Nieto, J. Complex dynamics and fractional-order optimal control of an epidemic model with saturated treatment and incidence. *Int. J. Bifurc. Chaos* **2023**, *33*, 2350192. [CrossRef]
23. Li, J.; Tan, X.; Wu, W.; Zou, X. A Caputo fractional derivative dynamic model of hepatitis E with optimal control based on particle swarm optimization. *AIP Adv.* **2024**, *14*, 045125. [CrossRef]
24. Zhu, H.; Zou, X. Impact of delays in cell infection and virus production on HIV-1 dynamics. *Math. Med. Biol.* **2008**, *25*, 99–112. [CrossRef] [PubMed]
25. Xu, S.; Hu, Y. Dynamic analysis of a Caputo fractional-order SEIR model with a general incidence rate. *Sci. Rep.* **2025**, *15*, 17561. [CrossRef]
26. Turnbull, P.C.B. Introduction: Anthrax history, disease and ecology. In *Current Topics in Microbiology and Immunology*; Koehler, T.M., Ed.; Springer: Berlin/Heidelberg, Germany, 2002; Volume 271, pp. 1–19.
27. Van Ness, M. Ecology of anthrax. *Science* **1971**, *172*, 1303–1307. [CrossRef] [PubMed]
28. Metzler, R.; Klafter, J. The random walk's guide to anomalous diffusion: A fractional dynamics approach. *Phys. Rep.* **2000**, *339*, 1–77. [CrossRef]
29. Mainardi, F. *Fractional Calculus and Waves in Linear Viscoelasticity*; Imperial College Press: London, UK, 2010.
30. Barandongo, Z.R.; Dolfi, A.C.; Bruce, S.A.; Rysava, K.; Huang, Y.-H.; Joel, H.; Hassim, A.; Kamath, P.L.; van Heerden, H.; Turner, W.C. The persistence of time: The lifespan of Bacillus anthracis spores in environmental reservoirs. *Res. Microbiol.* **2023**, *174*, 104029. [CrossRef]
31. Diethelm, K. A fractional calculus based model for the simulation of an outbreak of dengue fever. *Nonlinear Dynam.* **2013**, *71*, 613–619. [CrossRef]
32. Boukhouima, A.; Hattaf, K.; Lotfi, E.M.; Mahrouf, M.; Torres, D.F.M.; Yousfi, N. Lyapunov functions for fractional-order systems in biology: Methods and applications. *Chaos Solitons Fractals* **2020**, *140*, 110224. [CrossRef]
33. Lakshmikantham, V.; Leela, S.; Devi, J.V. *Theory of Fractional Dynamic Systems*; Cambridge Scientific Publishers: Cambridge, UK, 2009.
34. Liu, F.; Meerschaert, M.M.; Momani, S.; Leonenko, N.N.; Chen, W.; Agrawal, O.P. Fractional differential equations. *Int. J. Differ. Equ.* **2010**, *2010*, 553–563. [CrossRef]
35. Wu, Z.; Cai, Y.; Wang, Z.; Wang, W. Global stability of a fractional order SIS epidemic model. *J. Differ. Equ.* **2023**, *352*, 221–248. [CrossRef]
36. Janagaraj, R.; Jones, G.M.; Selvam, A.G.M. Discretization fractional-order SEIR worm propagation model in computer networks. *TWMS J. Appl. Eng. Math.* **2025**, *15*, 342–352.
37. Nelson, P.W.; Perelson, A.S. A model of HIV-1 pathogenesis that includes an intracellular delay. *Math. Biosci.* **2000**, *163*, 201–215. [CrossRef] [PubMed]
38. Nelson, P.W.; Perelson, A.S. Mathematical analysis of delay differential equation models of HIV-1 infection. *Math. Biosci.* **2002**, *179*, 73–94. [CrossRef]
39. Badri, V.; Tavazoei, M.S. Stability analysis of fractional order time-delay systems: Constructing new Lyapunov functions from those of integer order counterparts. *IET Control Theory Appl.* **2019**, *13*, 2476–2481. [CrossRef]
40. Aguila-Camacho, N.; Duarte-Mermoud, M.A.; Gallegos, J.A. Lyapunov functions for fractional order systems. *Commun. Nonlinear Sci. Numer. Simul.* **2014**, *19*, 2951–2957. [CrossRef]

41. Hu, R.; Aziz, M.H.N.; Aruchunan, E.; Mohamed, N.A. Modeling and analysis of a delayed fractional order COVID-19 SEIHRM model with media coverage in Malaysia. *Sci. Rep.* **2025**, *15*, 25305. [CrossRef]
42. Ahmed, E.; El-Sayed, A.M.A.; El-Saka, H.A. On some Routh-Hurwitz conditions for fractional order differential equations and their applications in Lorenz, Rössler, Chua and Chen systems. *Phys. Lett. A* **2006**, *358*, 1–4. [CrossRef]
43. Gallegos, J.A.; Duarte-Mermoud, M.A. On the Lyapunov theory for fractional order systems. *Appl. Math. Comput.* **2016**, *287*, 161–170. [CrossRef]
44. Diethelm, K. *The Analysis of Fractional Differential Equations*; Lecture Notes in Mathematics, 2004; Springer: Berlin, Germany, 2010.
45. Odibat, Z.M.; Shawagfeh, N.T. Generalized Taylor's formula. *Appl. Math. Comput.* **2007**, *186*, 286–293. [CrossRef]
46. Van den Driessche, P. Reproduction numbers of infectious disease models. *Infect. Dis. Model.* **2017**, *2*, 288–303. [CrossRef]
47. Xu, S.H.; Hu, Y.H. Brucellosis threshold dynamics: A time-fractional-order diffusion model with generalized incidence rate functions. *Adv. Contin. Discret. Model.* **2025**, *175*, 1–36. [CrossRef]
48. Mushayabasa, S.; Marijani, T.; Masocha, M. Dynamical analysis and control strategies in modeling anthrax. *Comput. Appl. Math.* **2017**, *36*, 1333–1348. [CrossRef]
49. Garrappa, R. Numerical solution of fractional differential equations: A survey and a software tutorial. *Mathematics* **2018**, *6*, 16. [CrossRef]

Disclaimer/Publisher's Note: The statements, opinions and data contained in all publications are solely those of the individual author(s) and contributor(s) and not of MDPI and/or the editor(s). MDPI and/or the editor(s) disclaim responsibility for any injury to people or property resulting from any ideas, methods, instructions or products referred to in the content.

symmetry

MDPI

Article

Partial Approximate Controllability of a Three-Parameter Damped Fractional Diffusion Control System with Nonlinear Perturbations

Zhichao Lu, Shiyou Lin * and Tingting Hu

School of Mathematics and Statistics, Hainan Normal University, Haikou 571158, China;
202412070100011@hainnu.edu.cn (Z.L.); 202412070100003@hainnu.edu.cn (T.H.)
* Correspondence: 050105@hainnu.edu.cn

Abstract

In this paper, we investigate the partial approximate controllability of a class of fractional diffusion control systems with three-parameter damping and nonlinear perturbations. First, based on the theory of (μ, ν, ξ, e, k)-resolvent families developed in our previous work, we define the mild solution of the system. Then, by constructing a proper objective functional and using the strict convexity, we prove the existence and uniqueness of the minimal norm control. Furthermore, employing the Arzelà–Ascoli theorem and variational inequalities, we establish the precompactness of the solution family and derive the key controllability estimate. Finally, we provide an example to illustrate the effectiveness of our theoretical results.

Keywords: three-parameter damping; fractional diffusion system; partial approximate controllability; resolvent family; nonlinear perturbation

MSC: 35R11; 34K37; 35B65

1. Introduction

Fractional calculus has evolved into a robust mathematical framework for modeling complex dynamic behaviors characterized by memory effects and nonlocal properties—hallmark features of many physical, engineering, and biological systems, including viscoelastic vibrations, anomalous diffusion, and damping control of aerospace composite materials [1–3]. Among the diverse class of fractional evolution systems, the Riemann–Liouville abstract fractional Cauchy problem (RLAFCP) stands as a cornerstone framework, has garnered extensive attention from the research community owing to its rigorous theoretical underpinnings and broad practical applicability [4,5]. The systematic theoretical foundation of Riemann–Liouville fractional calculus was first established by Kilbas et al. [6] and Podlubny [7], which has since become the fundamental bedrock for subsequent investigations into various fractional evolution equations.

Damped RLAFCP research has advanced substantially over recent decades. Mei and Peng [8] pioneered two-parameter damped models in their seminal work, systematically establishing the (α, β, c)-resolvent family theory for solution well-posedness analysis. Recent extensions of the resolvent family method include generalized frameworks for multi-parameter damped systems [9], exponential stability analysis of RL-type fractional damped systems [10], and variable-order damping term integration [11], thus enriching the theoretical system. However, this line of research is limited by its failure to capture

multi-scale damping effects-an inherent feature of practical systems. Building on this, the authors' prior work [12] generalized the two-parameter model to a three-parameter framework by incorporating an additional lower-order fractional damping term, rigorously defining the (μ, ν, ξ, e, k)-resolvent family and proving strong solution existence and uniqueness. This addressed the theoretical gap of the three-parameter damped RLAFCP, but only focused on solution well-posedness, neglecting controllability, which is critical for practical system regulation.

Notably, fractional damped system research encompasses two primary derivative frameworks: Riemann–Liouville (RL) and Caputo. While Caputo-type fractional resolvent families [13] are well-suited for systems with well-defined initial states, existing controllability studies for both frameworks remain confined to two-parameter damping, leaving a gap for three-parameter RL-type systems with nonlocal conditions. In the field of fractional system controllability analysis, Abdul Haq [14] made a notable contribution by investigating the partial approximate controllability of nonlocal semi-linear systems with two Riemann–Liouville fractional derivatives. Via an approximate system and fixed point method, Haq relaxed the Lipschitz continuity constraint on the nonlinear term, offering a valuable approach for non-Lipschitz semi-linear system analysis. Recent fractional system controllability studies have extended the framework to coupled and impulsive systems with nonlocal initial conditions [15], but remain limited to two-parameter damping models, unable to capture the high, medium, and low-frequency energy dissipation prevalent in complex engineering scenarios.

Other relevant studies further underscore key research gaps. Liu [16] proposed a multi-term numerical model for fractional diffusion-wave equations but lacked rigorous abstract operator theory. Almeida and Malinowska [17] explored damping-related applications of fractional differential equations without addressing controllability. Zhu et al. [18] studied resolvent operators for fractional evolution equations, focusing solely on linear systems and excluding nonlinear perturbations and nonlocal initial conditions, which lays a theoretical foundation for the analysis of three-parameter damped fractional systems. Zhou [19] and Suhaib [20] advanced the theoretical foundation of three-parameter fractional systems by investigating solution well-posedness and regularity of fractional damped wave equations, respectively. Yang [21] and Li et al. [22] examined the approximate controllability of Riemann–Liouville fractional systems, but restricted to single or two-parameter damping. For engineering applications like elastic beams, Bahreini et al. [23] developed numerical frameworks for nonlocal Euler–Bernoulli beam analysis, while controllability under three-parameter damping remains unaddressed. Qiu et al. [24] and George et al. [25] provided critical references for high-order fractional damped systems via stability and well-posedness studies of damped viscoelastic fractional damped Euler–Bernoulli beam equations, respectively.

Despite these advances, several critical research gaps remain:

(1) Existing three-parameter damped fractional system studies only focus on the well-posedness of solutions [18–20], while the key controllability problem in practical engineering applications is rarely addressed;
(2) The representative controllability results represented by Haq [14] are strictly limited to two-parameter damping models, which cannot characterize the high, medium, and low-frequency multi-scale damping effects in complex engineering systems;
(3) The controllability analysis with non-Lipschitz nonlinear terms has not been developed in the three-parameter damping framework [26], lacking the support of corresponding resolvent family theory and variational methods.

To address these gaps, this paper investigates the existence of mild solutions and partial-approximate controllability of a semi-linear system involving three Riemann–

https://doi.org/10.3390/sym18050721

Liouville fractional derivatives, nonlocal initial conditions, and nonlinear perturbations. The targeted system is formulated as follows:

$$\begin{cases} D_{\hat{t}}^{\mu} u(\hat{t}) + eD_{\hat{t}}^{\nu} u(\hat{t}) + kD_{\hat{t}}^{\xi} u(\hat{t}) = Au(\hat{t}) + Bv(\hat{t}) + \Phi(\hat{t}, u(\hat{t})), \quad \mu > \frac{1}{2}, \hat{t} \in (0, \vartheta]; \\ \lim\limits_{\hat{t} \to 0^+} I_{\hat{t}}^{1-\mu} u(\hat{t}) = \xi_0 - \eta(u); \end{cases} \tag{1}$$

In this paper, we investigate the partial approximate controllability of System (1) involving three-parameter damping and nonlinear perturbations, where $0 < \xi < \nu < \mu \leq 1$, and the condition $\mu > \frac{1}{2}$ is imposed to ensure the space $C_{1-\mu}$ is dense in L_2. Herein, $D_{\hat{t}}^{\delta}$ ($\delta = \mu, \nu, \xi$) denotes the Riemann–Liouville fractional derivative of order δ with respect to time $\hat{t}$, and $I_{\hat{t}}^{1-\mu}$ is the corresponding $1-\mu$ order Riemann–Liouville fractional integral. The state variable $u(\cdot) \in L_2([0, \vartheta]; \mathbb{X})$, and the weighted space $C_{1-\mu}([0, \vartheta]; \mathbb{X}) = \{\omega : \hat{t}^{1-\mu}\omega(\hat{t}) \in C([0, \vartheta]; \mathbb{X})\}$ is introduced to accommodate the singularity of $D_{\hat{t}}^{\mu}$ at $\hat{t} = 0$. Control variable $v(\cdot) \in L_2([0, \vartheta]; \mathbb{X}')$. The linear operator $A : D(A) \subseteq \mathbb{X} \to \mathbb{X}$ is densely defined and closed on $\mathbb{X}$, and generates a Riemann–Liouville fractional (μ, ν, ξ, e, k)-resolvent family $\{S(\hat{t})\}_{\hat{t}>0}$, which is a core tool for analyzing the dynamic behavior of the system. Bounded linear operator $B : \mathbb{X}' \to \mathbb{X}$ maps control inputs to the state space. Nonlinear term $\Phi : [0, \vartheta] \times \mathbb{X} \to \mathbb{X}$ describes nonlinear perturbations in practical complex systems, with $\xi_0 \in \mathbb{X}$ the initial state. Nonlocal function $\eta : C_{1-\mu}([0, \vartheta]; \mathbb{X}) \to \mathbb{X}$ replaces the classical local initial condition, allowing the model to accurately capture the memory and hereditary nonlocal properties of systems like viscoelasticity and anomalous diffusion.

Contribution of the paper:

1. We extend the classical two-parameter damped fractional systems in [14] to a three-parameter damped system with nonlocal initial conditions and nonlinear perturbations, and define the three-parameter Mittag-Leffler function and (μ, ν, ξ, e, k)-resolvent family, and fill the theoretical gap of controllability for three-parameter damped fractional systems.
2. Without requiring the Lipschitz continuity of the nonlinear term, we prove the existence of mild solutions by combining the properties of the three-parameter resolvent family and the Schauder fixed-point theorem, which breaks through the constraint of nonlinear terms in the two-parameter framework [14].
3. We prove that the partial-approximate controllability of linear systems can imply the controllability of semi-linear systems with three-parameter damping, and generalize the conclusion from second-order spatial operators to fourth-order spatial operators, and adapt to engineering scenarios such as damped vibration of elastic beams [23].

2. Preliminaries

To define the mild solution of the proposed system, we first introduce the Banach space $C_{1-\mu}([0, \vartheta]; \mathbb{X}) = \{\omega : \hat{t}^{1-\mu}\omega(\hat{t}) \in C([0, \vartheta]; \mathbb{X})\}$ with the norm $\|\omega\|_{C_{1-\mu}} = \sup_{\hat{t} \in (0,\vartheta]} \{\hat{t}^{1-\mu} \|\omega(\hat{t})\|_{\mathbb{X}}\}$. This space is specifically constructed to accommodate the singularity of the Riemann–Liouville fractional derivative at $\hat{t} = 0$, ensuring the well-definedness of the solution. Let $\|B\| = \lambda_B$ denote the operator norm of B, $L(\mathbb{X})$ be the set of all bounded linear operators from $\mathbb{X}$ to itself, $\mathbb{R}^+$ represent the set of positive real numbers, and $T : \mathbb{X} \to \mathbb{X}_0$ be a projection map where $\mathbb{X}_0$ is a closed subspace of $\mathbb{X}$. Before proceeding to the definition of the mild solution, we first recall the fundamental concepts of Riemann–Liouville fractional integral and derivative, which are the core of classical fractional calculus theory [6,7] and serve as the mathematical foundation for subsequent analysis.

https://doi.org/10.3390/sym18050721

Definition 1. *The μ-order Riemann–Liouville fractional derivative with respect to the time variable $\hat{t}$ is given by*

$$D_{\hat{t}}^{\mu}\varphi(\hat{t}) = \frac{1}{\Gamma(n-\mu)}\left(\frac{d}{d\hat{t}}\right)^{n}\int_{0}^{\hat{t}}(\hat{t}-s)^{n-\mu-1}\varphi(s)\,ds,$$

where $n = [\mu]+1$ and $\Gamma(\cdot)$ stands for the gamma function, with $0 < \xi < \nu < \mu \leq 1$, the same holds for ν, ξ. This is a classical and widely adopted definition in the field of fractional calculus [4,14].

Definition 2. *The μ-order Riemann–Liouville fractional integral with respect to the time variable $\hat{t}$ is given by*

$$I_{\hat{t}}^{\mu}\varphi(\hat{t}) = \frac{1}{\Gamma(\mu)}\int_{0}^{\hat{t}}(\hat{t}-s)^{\mu-1}\varphi(s)ds,$$

where $\Gamma(\cdot)$ stands for the gamma function, with $0 < \xi < \nu < \mu \leq 1$, the same holds for ν, ξ. As a fundamental and well-established notion in fractional calculus, this definition is commonly referenced in relevant studies [4,14].

Definition 3. *Three-Parameter Mittag-Leffler function is defined by*

$$E_{\mu-\nu,\mu-\xi,\mu}(z,w) = \sum_{k=0}^{\infty}\sum_{m=0}^{\infty}\frac{z^{k}w^{m}}{\Gamma((\mu-\nu)k+(\mu-\xi)m+\mu)k!m!}.$$

where $z, \omega \in \mathbb{C}$ with $\mathbb{C}$ being the set of complex numbers and $\Gamma(\cdot)$ stands for the gamma function. This novel three-parameter Mittag-Leffler function is motivated by our previous work [12]. If $\xi = \mu$, then it reduces to the classical two-parameter Mittag-Leffler function denoted by $E_{\mu-\nu,\mu}(\cdot) = \sum_{k=0}^{\infty}\frac{z^{k}}{\Gamma((\mu-\nu)k+\mu)}$; if $\nu = \mu$ and $\xi = \mu$ simultaneously, it is denoted by the single-parameter Mittag-Leffler function $E_{\mu}(\cdot) = \sum_{n=0}^{\infty}\frac{(z)^{n}}{\Gamma(\mu n+\mu)}$. This definition is formally proposed as a new contribution in this manuscript. It serves as a natural generalization of the classical two-parameter Mittag-Leffler function, with its foundational framework rooted in the existing studies [8,14].

Definition 4. *The three-parameter Mittag-Leffler integral operator is defined by*

$$\mathbb{E}_{\hat{t}}^{\mu-\nu,\mu-\xi,\mu,-e,-k}\varphi(\hat{t}) = \int_{0}^{\hat{t}}(\hat{t}-s)^{\mu-1}E_{\mu-\nu,\mu-\xi,\mu}\left(-e(\hat{t}-s)^{\mu-\nu},-k(\hat{t}-s)^{\mu-\xi}\right)\varphi(s)ds.$$

where $\hat{t} > 0$, $0 < \xi < \nu < \mu \leq 1$, $e, k \in \mathbb{R}$. It is specifically constructed by integrating the newly proposed three-parameter Mittag-Leffler function and the theoretical framework derived from our previous research [12].

Definition 5. *A family $\{S(\hat{t})\}_{\hat{t}\in\mathbb{R}^{+}} \subset L(\mathbb{X})$ is called a Riemann–Liouville Fractional (μ,ν,ξ,e,k)-resolvent family on the Banach space $\mathbb{X}$ if it satisfies the following conditions:*

(a) For any $\xi \in \mathbb{X}$, the mapping $\hat{t} \mapsto S(\hat{t})\xi$ is strongly continuous on $(0,\infty)$, and satisfies the initial limit condition

$$\lim_{\hat{t}\to 0^{+}}\Gamma(\mu)\hat{t}^{1-\mu}S(\hat{t})\xi = \xi;$$

(b) For all $\hat{t}, s > 0$, the operators commute, i.e., $S(\hat{t})S(s) = S(s)S(\hat{t})$;

(c) For all $\hat{t}, s > 0$, the resolvent identity holds

$$S(s)\mathbb{E}_{\hat{t}}^{\mu-\nu,\mu-\xi,\mu,-e,-k}S(\hat{t}) - \mathbb{E}_{s}^{\mu-\nu,\mu-\xi,\mu,-e,-k}S(s)S(\hat{t})$$

$$= s^{\mu-1}E_{\mu-\nu,\mu-\xi,\mu}\left(-es^{\mu-\nu},-ks^{\mu-\xi}\right)\mathbb{E}_{\hat{t}}^{\mu-\nu,\mu-\xi,\mu,-e,-k}S(\hat{t})$$

https://doi.org/10.3390/sym18050721

$$-\hat{t}^{\mu-1}E_{\mu-\nu,\mu-\xi,\mu}\left(-e\hat{t}^{\mu-\nu},-k\hat{t}^{\mu-\xi}\right)\mathbb{E}_{s}^{\mu-\nu,\mu-\xi,\mu,-e,-k}S(s).$$

This definition is established as a new concept in this manuscript. It extends the two-parameter (α,β,c)-resolvent family proposed in [8] and further generalizes our prior research on three-parameter damped fractional systems [12].

Definition 6. *The operator A defined by*

$$A\xi=\Gamma(2\mu)\lim_{\hat{t}\to 0^{+}}\frac{\hat{t}^{1-\mu}S(\hat{t})\xi-E_{\mu-\nu,\mu-\xi,\mu}\left(-e\hat{t}^{\mu-\nu},-k\hat{t}^{\mu-\xi}\right)\xi}{\hat{t}^{\mu}},\quad \textit{for } \xi\in D(A),$$

where

$$D(A)=\left\{\xi\in\mathbb{X}:\lim_{\hat{t}\to 0^{+}}\frac{\hat{t}^{1-\mu}S(\hat{t})\xi-E_{\mu-\nu,\mu-\xi,\mu}\left(-e\hat{t}^{\mu-\nu},-k\hat{t}^{\mu-\xi}\right)\xi}{\hat{t}^{\mu}}\ \textit{exists}\right\};$$

is known as the generator of the Riemann–Liouville fractional (μ,ν,ξ,e,k)-resolvent family $\{S(\hat{t})\}_{\hat{t}>0}$.

This novel generator definition is developed on the basis of the two-parameter fractional resolvent family generator framework in [8] and combined with our previous research work [12].

Lemma 1. *Let $\mathbb{X}$ be a Banach space, and let $\{S(\hat{t})\}_{\hat{t}>0}$ be the Riemann–Liouville fractional (μ,ν,ξ,e,k)-resolvent family generated by the operator A in Definition 6. Then the resolvent family $\{S(\hat{t})\}_{\hat{t}>0}$ and its generator A satisfy the following properties:*

(a) For any $\xi\in D(A)$, $S(\hat{t})\xi\in D(A)$ and $AS(\hat{t})\xi=S(\hat{t})A\xi$ for all $\hat{t}>0$;

(b) For any $\xi\in\mathbb{X}$ and all $\hat{t}>0$, the resolvent family admits the decomposition

$$S(\hat{t})\xi=\hat{t}^{\mu-1}E_{\mu-\nu,\mu-\xi,\mu}\left(-e\hat{t}^{\mu-\nu},-k\hat{t}^{\mu-\xi}\right)\xi+A\mathbb{E}_{\hat{t}}^{\mu-\nu,\mu-\xi,\mu,-e,-k}S(\hat{t})\xi;$$

(c) For any $\xi\in D(A)$ and all $\hat{t}>0$, the generator A commutes with the multi-parameter Mittag-Leffler integral operator

$$S(\hat{t})\xi=\hat{t}^{\mu-1}E_{\mu-\nu,\mu-\xi,\mu}\left(-e\hat{t}^{\mu-\nu},-k\hat{t}^{\mu-\xi}\right)\xi+\mathbb{E}_{\hat{t}}^{\mu-\nu,\mu-\xi,\mu,-e,-k}S(\hat{t})A\xi.$$

Remark 1. *The properties of the (μ,ν,ξ,e,k)-resolvent family in this lemma are consistent with the general properties of multi-parameter damped resolvent families proposed in [9,11], and further extend the property conclusions of two-parameter resolvent families in [8], which verifies the rationality of the definition of the three-parameter resolvent family in this paper.*

Definition 7. *A function $u\in C_{1-\mu}([0,\vartheta];\mathbb{X})$ is said to be a mild solution if it satisfies the following integral equation for all $\hat{t}\in(0,\vartheta]$:*

$$u(\hat{t})=S(\hat{t})(\xi_0-\eta(u))+\int_0^{\hat{t}}S(\hat{t}-s)(Bv(s)+\Phi(s,u(s)))ds. \tag{2}$$

where $C_{1-\mu}([0,\vartheta];\mathbb{X})=\left\{\omega:\hat{t}^{1-\mu}\omega(\hat{t})\in C([0,\vartheta];\mathbb{X})\right\}$ with the norm $\|\omega\|_{C_{1-\mu}}=\sup_{\hat{t}\in(0,\vartheta]}\hat{t}^{1-\mu}\|\omega(\hat{t})\|_{\mathbb{X}}$, and $\{S(\hat{t})\}_{\hat{t}>0}$ is the Riemann–Liouville fractional (μ,ν,ξ,e,k)-resolvent family generated by the operator A.

This definition is introduced as a new mild solution concept in this manuscript. It is tailored to the three-parameter damped fractional system framework, with reference to the classical mild solution definition for two-parameter fractional dynamical systems [8,14].

https://doi.org/10.3390/sym18050721

Definition 8. *The system (1) is said to be partial-approximately controllable if for each $\varepsilon > 0$ and every target state $u_\vartheta \in \mathbb{X}_0$, there exists a control $v \in U = L^2([0,\vartheta];\mathbb{X}')$ such that the corresponding mild solution $u \in C_{1-\mu}([0,\vartheta];\mathbb{X})$ of the system satisfies*

$$\|Tu(\vartheta) - u_\vartheta\|_{\mathbb{X}} \leq \varepsilon.$$

where $T : \mathbb{X} \to \mathbb{X}_0$ is a projection operator, and $\mathbb{X}'$ is a Hilbert space corresponding to the control space.

This definition constitutes a generalization of the standard partial approximate controllability concept. It is extended from the two-parameter fractional system framework [14] to the newly proposed three-parameter damped fractional system setting.

Remark 2. *The proposed (μ,ν,ξ,e,k)-resolvent family is a three-parameter generalization of the (ς,μ,κ)-resolvent family introduced by Haq [14]. It degenerates into the classical two-parameter resolvent family when $\xi = \mu$, which verifies the compatibility of the definition.*

Remark 3. *The weighted continuous space $C_{1-\mu}([0,\vartheta];\mathbb{X})$ is a dense subset of the state space $Z = L^2([0,\vartheta];\mathbb{X})$ when the highest fractional order μ of the (1) satisfies $0 < \xi < \nu < \mu \leq 1$. The condition $\mu > \frac{1}{2}$ is imposed to handle the singularity of the Riemann–Liouville fractional derivative at $\hat{t} = 0$ and guarantee the density of the weighted space.*

Remark 4. *Since the Riemann–Liouville fractional (μ,ν,ξ,e,k)-resolvent family $\{S(\hat{t})\}_{\hat{t}>0}$ admits a singularity at $\hat{t} = 0$, we cannot assume the uniform boundedness of $\{S(\hat{t})\}_{\hat{t}>0}$ on any interval of the form $(0,\alpha]$ with $\alpha > 0$. However, the weighted resolvent family $\hat{t}^{1-\mu}S(\hat{t})$ is uniformly bounded on every bounded interval contained in $\mathbb{R}^+$.*

Hypothesis 1. *The Riemann–Liouville fractional (μ,ν,ξ,e,k)-resolvent family $\{S(\hat{t})\}_{\hat{t}>0} \subset L(\mathbb{X})$ satisfies that $\hat{t}^{1-\mu}S(\hat{t})$ is uniformly continuous and compact on $(0,\vartheta]$, and there exists a constant $\lambda_S > 0$ such that*

$$\left\|\hat{t}^{1-\mu}S(\hat{t})\right\| \leq \lambda_S, \text{ for all } 0 < \hat{t} \leq \vartheta;$$

Hypothesis 2. *The nonlinear term $\Phi : [0,\vartheta] \times \mathbb{X} \to \mathbb{X}$ is continuous on $[0,\vartheta] \times \mathbb{X}$, and there exists a non-negative continuous function $g \in C([0,\vartheta];\mathbb{R}^+)$ such that*

$$\left\|\Phi(\hat{t},\xi)\right\| \leq g(\hat{t}), \text{ for all } (\hat{t},\xi) \in [0,\vartheta] \times \mathbb{X};$$

Hypothesis 3. *The nonlocal function $\eta : C_{1-\mu}([0,\vartheta];\mathbb{X}) \to \mathbb{X}$ is continuous, and there exists a positive constant $\lambda_\eta > 0$ such that*

$$\|\eta(u)\| \leq \lambda_\eta, \text{ for all } u \in C_{1-\mu}([0,\vartheta];\mathbb{X});$$

Hypothesis 4. *There exists a constant $b \in (0,\vartheta)$ and a prescribed kernel $h(\eta;s) \in L^2([0,\vartheta] \times [0,\vartheta];\mathbb{R}^+)$ such that for any $u_1, u_2 \in C_{1-\mu}([0,\vartheta];\mathbb{X})$ with $u_1(\hat{t}) = u_2(\hat{t})$ for all $\hat{t} \in [b,\vartheta]$, we have $\eta(u_1) = \eta(u_2)$. The kernel $h(\eta;s)$ is bounded, measurable and independent of u.*

Hypothesis 5. *The corresponding linear system of (1) with the nonlinear perturbation term Φ and the nonlocal function η eliminated is partially approximately controllable in the sense of Definition 7, and the mild solution of the linear system is given by*

$$u(\hat{t}) = S(\hat{t})\xi_0 + \int_0^{\hat{t}} S(\hat{t}-s)Bv(s)ds, \text{ for all } \hat{t} \in (0,\vartheta]. \tag{3}$$

https://doi.org/10.3390/sym18050721

Remark 5. *The condition (H4) implies that η is allowed to depend on $u \in C_{1-\mu}([0,\vartheta];\mathbb{X})$ for $\hat{t} \in [b,\vartheta]$ only.*

Remark 6. *For $0 < \hat{t} < \vartheta$ and $\xi \in \mathbb{X}_0$, $B^*S^*(\vartheta-\hat{t})T^*\xi = 0$ implies $\xi = 0$ if and only if system (1) is partially approximately controllable.*

Proof. Suppose $B^*S^*(\vartheta-\hat{t})T^*\xi = 0$ for all $\hat{t} \in (0,\vartheta)$. By the definition of the controllability operator and the duality pairing, we have

$$\langle \xi,\, TS(\vartheta-\hat{t})Bv\rangle = \langle B^*S^*(\vartheta-\hat{t})T^*\xi,\, v\rangle = 0$$

for all controls v. Since the linear system is partially approximately controllable by Assumption (H_5), the set $\{TS(\vartheta-\hat{t})Bv \mid v \in L^2(0,\vartheta;\mathbb{X}')\}$ is dense in $\mathbb{X}_0$. Hence $\xi = 0$. The converse follows directly from the definition of partial approximate controllability.

Let us define

$$\chi_{\varepsilon,n}(y;u) = \frac{1}{2}\int_0^{\vartheta}(\vartheta-s)^{1-\mu}\|B^*S^*(\vartheta-s)T^*y\|^2\,ds + \varepsilon\|y\| + \langle y, \Theta_n(u)\rangle, \tag{4}$$

where

$$\Theta_n(u) = TS(\vartheta)\left(\xi_0 - \Gamma(\mu)n^{\mu-1}S\left(\frac{1}{n}\right)\eta(u)\right) + \int_0^{\vartheta} TS(\vartheta-s)\Phi\big(s,u(s)\big)ds - u_{\vartheta};$$

and the mapping $G : C_{1-\mu}([0,\vartheta];\mathbb{X}) \to \mathbb{X}_0$ is given by

$$G(u) = TS(\vartheta)\left(\xi_0 - \Gamma(\mu)n^{\mu-1}S\left(\frac{1}{n}\right)\eta(u)\right) + \int_0^{\vartheta} TS(\vartheta-s)\Phi\big(s,u(s)\big)ds.$$

Consider the closed ball

$$\widetilde{S}(0,\alpha) = \big\{u \in C_{1-\mu}([0,\vartheta];\mathbb{X}) : \|u\|_{C_{1-\mu}} \le \alpha\big\}.$$

□

Lemma 2. *The operator $G : \widetilde{S}(0,\alpha) \to \mathbb{X}_0$ is compact.*

Proof. We verify the compactness of operator G by the Arzelà-Ascoli theorem, which requires the set $\{G(u) : u \in \widetilde{S}(0,\alpha)\}$ to be uniformly bounded and equicontinuous in $\mathbb{X}_0$.

1. **Boundedness of the domain**. By definition, the closed ball $\widetilde{S}(0,\alpha)$ is bounded in the weighted space $C_{1-\mu}([0,\vartheta];\mathbb{X})$.
2. **Uniform boundedness**. For any $u \in \widetilde{S}(0,\alpha)$, by the definition of G, Assumption (H_1) ($\|\hat{t}^{1-\mu}S(\hat{t})\| \le \lambda_S$) and Assumption (H_3) ($\|\eta(u)\| \le \lambda_\eta$), we have

$$\begin{aligned}\|G(u)\|_{\mathbb{X}_0} &= \left\|TS(\vartheta)\left(\xi_0 - \Gamma(\mu)n^{\mu-1}S\left(\frac{1}{n}\right)\eta(u)\right) + \int_0^{\vartheta} TS(\vartheta-s)\Phi(s,u(s))ds\right\|_{\mathbb{X}_0}\\ &\le \|T\|\lambda_S\|\xi_0\| + \|T\|\lambda_S^2\Gamma(\mu)\vartheta^{\mu-1}\lambda_\eta + \|T\|\lambda_S\int_0^{\vartheta}(\vartheta-s)^{1-\mu}g(s)ds.\end{aligned}$$

   The right-hand side is a constant independent of u, so $\{G(u)\}$ is uniformly bounded.
3. **Equicontinuity**. For any $u \in \widetilde{S}(0,\alpha)$ and $\hat{t}_1, \hat{t}_2 \in (0,\vartheta]$, by the uniform continuity of $\hat{t}^{1-\mu}S(\hat{t})$ (Assumption (H_1)) and the boundedness of g (Assumption (H_2)), the difference

$$\|G(u)(\hat{t}_2) - G(u)(\hat{t}_1)\|_{\mathbb{X}_0}$$

https://doi.org/10.3390/sym18050721

can be uniformly controlled by $|\hat{t}_2 - \hat{t}_1|$, independent of u. Thus $\{G(u)\}$ is equicontinuous.

By the Arzelà–Ascoli theorem, $\{G(u)\}$ is precompact in $\mathbb{X}_0$, which implies that the operator $G : \widetilde{S}(0,\alpha) \to \mathbb{X}_0$ is compact. □

Remark 7. *The precompactness of the set*

$$\left\{TS(\vartheta)\left(\xi_0 - \Gamma(\mu)n^{\mu-1}S\left(\frac{1}{n}\right)\eta(u)\right) : u \in \widetilde{S}(0,\alpha)\right\}$$

in $\mathbb{X}$ *follows directly from the compactness of G by Lemma 2.*

3. Well-Posedness of Mild Solutions

The following lemma reveals the asymptotic property of the objective functional constructed in this paper, which is a key step in proving the existence of mild solutions and is consistent with the variational method used in the controllability analysis of fractional systems [27,28].

Lemma 3. *For any* $\widetilde{S}(0,\alpha)$,

$$\lim_{\|y\|\to\infty} \inf_{u\in\widetilde{S}(0,\alpha)} \frac{\chi_{\varepsilon,n}(y;u)}{\|y\|} \geq \varepsilon. \tag{5}$$

Proof. First, we show that $\Theta_n : \widetilde{S}(0,\alpha) \to \mathbb{X}_0$ is continuous for every n. Take $u_\varrho, u \in \widetilde{S}(0,\alpha)$ with $\lim_{\varrho\to\infty} \|u_\varrho - u\|_{C_{1-\mu}} = 0$. From (H2), we have $\lim_{\varrho\to\infty} \|\widetilde{\Phi}(u_\varrho) - \widetilde{\Phi}(u)\|_{C_{1-\mu}} = 0$, where $\widetilde{\Phi} : C_{1-\mu}([0,\vartheta];\mathbb{X}) \to C_{1-\mu}([0,\vartheta];\mathbb{X})$ is given as $(\widetilde{\Phi}(u))(\hat{t}) = \Phi(\hat{t}, u(\hat{t}))$. Now

$$\begin{aligned}
&\|\Theta_n(u_\varrho) - \Theta_n(u)\|_{\mathbb{X}_0} \\
&\leq \left\|\Gamma(\mu)TS(\vartheta)n^{\mu-1}S\left(\frac{1}{n}\right)(\eta(u_\varrho) - \eta(u))\right\| + \left\|\int_0^\vartheta TS(\vartheta - s)\big(\Phi(s,u_\varrho(s)) - \Phi(s,u(s))\big)ds\right\| \\
&\leq \Gamma(\mu)\vartheta^{\mu-1}\lambda_S^2\|T\|\|\eta(u_\varrho) - \eta(u)\| + \lambda_S\|T\|\int_0^\vartheta (\vartheta - s)^{1-\mu}s^{\mu-1}\|(\widetilde{\Phi}(u_\varrho))(s) - (\widetilde{\Phi}(u))(s)\|ds \\
&\leq \Gamma(\mu)\vartheta^{\mu-1}\lambda_S^2\|T\|\|\eta(u_\varrho) - \eta(u)\| + \frac{\lambda_S\vartheta^{2\mu-1}(\Gamma(\mu))^2}{\Gamma(2\mu)}\|T\|\|\widetilde{\Phi}(u_\varrho) - \widetilde{\Phi}(u)\|_{C_{1-\mu}} \\
&\to 0 \quad \text{as } \varrho \to \infty.
\end{aligned}$$

If (5) is not true, we are able to get sequences $y_\varrho \in \mathbb{X}$ and $u_\varrho \in \widetilde{S}(0,\alpha)$, with $\|y_\varrho\| \to \infty$ verifying

$$\lim_{\varrho\to\infty} \frac{\chi_{\varepsilon,n}(y_\varrho;u_\varrho)}{\|y_\varrho\|} < \varepsilon. \tag{6}$$

As $\{\Theta_n(u_\varrho) : \varrho \geq 1\} \subset \text{Range}(G)$ is precompact. Therefore, by picking a subsequence, we suppose that

$$\Theta_n(u_\varrho) \to \Theta_n \in \mathbb{X}. \tag{7}$$

Denote $\widehat{y}_\varrho = \frac{y_\varrho}{\|y_\varrho\|}$. Due to boundedness of $\widehat{y}_\varrho$ we are able to pick a subsequence (denoted as $\widehat{y}_\varrho$) such that $\widehat{y}_\varrho \to \widehat{y}$. Since $S(\cdot)$ is compact, one can see that

$$B^*S^*(\vartheta - \cdot)T^*\widehat{y}_\varrho \to B^*S^*(\vartheta - \cdot)T^*\widehat{y} \quad \text{in } C_{1-\mu}([0,\vartheta];\mathbb{X}). \tag{8}$$

From (5), one can obtain

$$\frac{\chi_{\varepsilon,n}(y_\varrho;u_\varrho)}{\|y_\varrho\|} = \frac{\|y_\varrho\|}{2}\int_0^\vartheta (\vartheta - s)^{1-\mu}\|B^*S^*(\vartheta - s)T^*\widehat{y}_\varrho\|^2 ds + \varepsilon\|\widehat{y}_\varrho\| + \langle\widehat{y}_\varrho, \Theta_n(u_\varrho)\rangle.$$

https://doi.org/10.3390/sym18050721

Since $\|y_\varrho\| \to \infty$, from (6)–(8) and Fatou's lemma, we get

$$\int_0^\vartheta (\vartheta - s)^{1-\mu} \|B^* S^*(\vartheta - s) T^* \widehat{y}_\varrho\|^2 ds \le \underline{\lim}_{\varrho\to\infty} \int_0^\vartheta (\vartheta - s)^{1-\mu} \|B^* S^*(\vartheta - s) T^* \widehat{y}_\varrho\|^2 ds = 0.$$

By (H5), $\widehat{y} = 0$ and hence, $\widehat{y}_\varrho \to 0 \in \mathbb{X}$. Thus

$$\underline{\lim}_{\varrho\to\infty} \frac{\chi_{\varepsilon,n}(y_\varrho; u_\varrho)}{\|y_\varrho\|} \ge \underline{\lim}_{\varrho\to\infty} \big(\varepsilon \|\widehat{y}_\varrho\| + \langle \widehat{y}_\varrho, \Theta_n(u_\varrho)\rangle\big) = \varepsilon,$$

which is a contradiction. □

Remark 8. *To each $\varphi \in \widetilde{S}(0,\alpha)$, the function $y \mapsto \chi_{\varepsilon,n}(y;\varphi)$ is continuous and strictly convex.*

Remark 9. *To each $\varphi \in C_{1-\mu}([0,\vartheta];\mathbb{X})$, $\chi_{\varepsilon,n}(\cdot;\varphi)$ admits exactly one minimum $\widetilde{y}_{\varepsilon,n}$ defining a bounded map $\Psi_{\varepsilon,n} : C_{1-\mu}([0,\vartheta];\mathbb{X}) \to \mathbb{X}$ on $\widetilde{S}(0,\alpha)$ for each fixed $\varepsilon > 0$, that is there exists a $\delta_\varepsilon > 0$ verifying $\|\Psi_{\varepsilon,n}(\varphi)\| < \delta_\varepsilon$ for $\varphi \in \widetilde{S}(0,\alpha)$, $n = 1, 2, \ldots$.*

Note: The proof of this lemma is adapted from [14], with modifications to fit the setting of the Riemann–Liouville-type abstract fractional Cauchy problem with multi-parameter damping terms studied in this paper. We have replaced the original operators $S(\cdot)$ and spaces $C_{1-\mu}$ from our problem setup, and aligned all notations and assumptions to ensure rigor and self-consistency in our framework.

Lemma 4. *If $u_\varrho, u \in \widetilde{S}(0,\alpha)$ satisfy*

$$\lim_{\varrho\to\infty} \|u_\varrho - u\|_{C_{1-\mu}} = 0,$$

then

$$\lim_{\varrho\to\infty} \|\Psi_{\varepsilon,n}(u_\varrho) - \Psi_{\varepsilon,n}(u)\|_{\mathbb{X}} = 0.$$

Proof. Boundedness of $\widetilde{y}_{\varepsilon,n,\varrho} = \Psi_{\varepsilon,n}(u_\varrho)$ enables us to assume that $\widetilde{y}_{\varepsilon,n,\varrho} \rightharpoonup \widehat{y}_{\varepsilon,n}$. By optimality of $\widetilde{y}_{\varepsilon,n,\varrho} = \Psi_{\varepsilon,n}(u_\varrho)$ and $\widetilde{y}_{\varepsilon,n} = \Psi_{\varepsilon,n}(u)$, one obtains

$$\begin{aligned}
\chi_{\varepsilon,n}(\widetilde{y}_{\varepsilon,n}; u) &\le \chi_{\varepsilon,n}(\widehat{y}_{\varepsilon,n}; u) \le \underline{\lim}_{\varrho\to\infty} \chi_{\varepsilon,n}(\widetilde{y}_{\varepsilon,n,\varrho}; u_\varrho) \\
&\le \overline{\lim}_{\varrho\to\infty} \chi_{\varepsilon,n}(\widetilde{y}_{\varepsilon,n,\varrho}; z_\varrho) \le \lim_{\varrho\to\infty} \chi_{\varepsilon,n}(\widetilde{y}_{\varepsilon,n}; u_\varrho) \\
&= \chi_{\varepsilon,n}(\widetilde{y}_{\varepsilon,n}; u).
\end{aligned}$$

Above shows that $\widehat{y}_{\varepsilon,n}$ also minimize $\chi_{\varepsilon,n}(\cdot; u)$. It means $\widehat{y}_{\varepsilon,n} = \widetilde{y}_{\varepsilon,n}$. Therefore

$$\lim_{\varrho\to\infty} \chi_{\varepsilon,n}(\widetilde{y}_{\varepsilon,n,\varrho}; u_\varrho) = \chi_{\varepsilon,n}(\widetilde{y}_{\varepsilon,n}; u),$$

$$\lim_{\varrho\to\infty} \int_0^\vartheta (\vartheta - s)^{1-\mu} \|B^* S^*(\vartheta - s) T^* \widetilde{y}_{\varepsilon,n,\varrho}\|^2 ds = \int_0^\vartheta (\vartheta - s)^{1-\mu} \|B^* S^*(\vartheta - s) T^* \widetilde{y}_{\varepsilon,n}\|^2 ds,$$

$$\lim_{\varrho\to\infty} \langle \widetilde{y}_{\varepsilon,n,\varrho}, \Theta_n(u_\varrho)\rangle = \langle \widetilde{y}_{\varepsilon,n}, \Theta_n(u)\rangle,$$

and

$$\|\widetilde{y}_{\varepsilon,n,\varrho}\| \le \lim_{\varrho\to\infty} \|\widetilde{y}_{\varepsilon,n,\varrho}\|.$$

From above relations, one has

$$\|\widetilde{y}_{\varepsilon,n}\| = \lim_{\varrho\to\infty} \|\widetilde{y}_{\varepsilon,n,\varrho}\|. \tag{9}$$

https://doi.org/10.3390/sym18050721

Since $\mathbb{X}$ is a Hilbert space therefore, the result holds.

Now we prove that the operator $\mathcal{Q}_{\varepsilon,n} : C_{1-\mu}([0,\vartheta];\mathbb{X}) \to C_{1-\mu}([0,\vartheta];\mathbb{X})$ given by

$$(\mathcal{Q}_{\varepsilon,n}u)(\hat{t}) = S(\hat{t})\left(\xi_0 - \Gamma(\mu)n^{\mu-1}S\left(\frac{1}{n}\right)\eta(u)\right) + \int_0^{\hat{t}} S(\hat{t}-s)\big(Bv_{\varepsilon,n}(s,u) + \Phi(s,u(s))\big)ds, \tag{10}$$

with

$$\begin{aligned} u_{\varepsilon,n}(s,u) &= (\vartheta - s)^{1-\mu}B^*S^*(\vartheta - s)T^*\Psi_{\varepsilon,n}(u) \\ &= (\vartheta - s)^{1-\mu}B^*S^*(\vartheta - s)T^*\widetilde{y}_{\varepsilon,n}; \end{aligned} \tag{11}$$

has a fixed point.

In this paper, we use the Schauder to prove the existence of fixed points, which is a classic method for solving the existence of solutions for fractional nonlinear systems [28] and is especially suitable for the analysis of non-lipschitz nonlinear fractional systems with non-compact semigroups. □

Remark 10. *The continuity of the mapping $\Psi_{\varepsilon,n}$ is a necessary condition for the continuity of the operator $\mathcal{Q}_{\varepsilon,n}$, and its proof method refers to the variational analysis method for fractional system controllability in [14,29], which is adapted to the three-parameter damping framework in this paper.*

Theorem 1. *The map $\mathcal{Q}_{\varepsilon,n}$ has a fixed point for $n = 1, 2, \ldots$.*

Proof. Step 1: $\mathcal{Q}_{\varepsilon,n}$ is continuous.

Let $u_i \to u$ in $C_{1-\mu}([0,\vartheta];\mathbb{X})$ as $i \to \infty$. Then,

$$\begin{aligned} &\hat{t}^{1-\mu}\|(\mathcal{Q}_{\varepsilon,n}u_i)(\hat{t}) - (\mathcal{Q}_{\varepsilon,n}u)(\hat{t})\| \\ &\leq \Gamma(\mu)\lambda_S^2\|\eta(u_i) - \eta(u)\| + \frac{\lambda_S\vartheta^\mu(\Gamma(\mu))^2}{\Gamma(2\mu)}\big(\|\widetilde{\Phi}(u_i) - \widetilde{\Phi}(u)\|_{C_{1-\mu}} + \lambda_B\|u_{\varepsilon,n}(\cdot,u_i) - u_{\varepsilon,n}(\cdot,u)\|_{C_{1-\mu}}\big). \end{aligned}$$

From the continuity of $\widetilde{\Phi}$ and $u_{\varepsilon,n}$, we obtain $\|\mathcal{Q}_{\varepsilon,n}u_i - \mathcal{Q}_{\varepsilon,n}u\|_{C_{1-\mu}} \to 0$ as $i \to \infty$.

Step 2:

$$\begin{aligned} &\hat{t}^{1-\mu}\|(\mathcal{Q}_{\varepsilon,n}u)(\hat{t})\| \\ &\leq \lambda_S\|\xi_0\| + \Gamma(\mu)\lambda_S^2\lambda_\eta + \frac{\vartheta\lambda_S}{\mu}\big(\lambda_S\lambda_B^2\|T\|\delta_\varepsilon + \|g\|\big) = \alpha(\varepsilon), \end{aligned}$$

which implies $\mathcal{Q}_{\varepsilon,n}\big(\widetilde{S}(0,\alpha(\varepsilon))\big) \subset \widetilde{S}(0,\alpha(\varepsilon))$.

Step 3: $\mathcal{Q}_{\varepsilon,n}$ is compact for $n = 1, 2, \ldots$

We first verify the two core conditions of the Arzelà-Ascoli theorem for the function family $\{\mathcal{Q}_{\varepsilon,n}u : u \in \widetilde{S}(0,\alpha(\varepsilon))\} \subset C_{1-\mu}([0,\vartheta];\mathbb{X})$:

(1) Uniform Boundedness. For any $u \in \widetilde{S}(0,\alpha(\varepsilon))$ and $\hat{t} \in (0,\vartheta]$, by Step 2 we have

$$\hat{t}^{1-\mu}\|(\mathcal{Q}_{\varepsilon,n}u)(\hat{t})\|_{\mathbb{X}} \leq \alpha(\varepsilon),$$

where $\alpha(\varepsilon)$ is a constant independent of u and $\hat{t}$. By the definition of the norm $\|\cdot\|_{C_{1-\mu}}$, we get

$$\|\mathcal{Q}_{\varepsilon,n}u\|_{C_{1-\mu}} = \sup_{\hat{t}\in(0,\vartheta]} \hat{t}^{1-\mu}\|(\mathcal{Q}_{\varepsilon,n}u)(\hat{t})\|_{\mathbb{X}} \leq \alpha(\varepsilon),$$

which means the family $\{\mathcal{Q}_{\varepsilon,n}u : u \in \widetilde{S}(0,\alpha(\varepsilon))\}$ is uniformly bounded in $C_{1-\mu}([0,\vartheta];\mathbb{X})$.

(2) Equicontinuity. Let $\hat{t}_1, \hat{t}_2 \in (0,\vartheta]$ with $\hat{t}_1 < \hat{t}_2$. For any $u \in \widetilde{S}(0,\alpha(\varepsilon))$, since $0 < \hat{t}_1 < \hat{t}_2$ and $1 - \mu > 0$, we have

$$\hat{t}_1^{1-\mu}\|(\mathcal{Q}_{\varepsilon,n}u)(\hat{t}_1) - (\mathcal{Q}_{\varepsilon,n}u)(\hat{t}_2)\|_{\mathbb{X}} \leq \hat{t}_2^{1-\mu}\|(\mathcal{Q}_{\varepsilon,n}u)(\hat{t}_1) - (\mathcal{Q}_{\varepsilon,n}u)(\hat{t}_2)\|_{\mathbb{X}}.$$

https://doi.org/10.3390/sym18050721

By Assumption (H_1), $\hat{t}^{1-\mu}S(\hat{t})$ is uniformly continuous on $(0,\vartheta]$. Thus for any $\epsilon>0$, there exists $\delta>0$ such that

$$|\hat{t}_2-\hat{t}_1|<\delta \implies \left\|\hat{t}_1^{1-\mu}S(\hat{t}_1)-\hat{t}_2^{1-\mu}S(\hat{t}_2)\right\|_{L(\mathbb{X})}<\frac{\epsilon}{C},$$

where

$$C=\|\xi_0\|+\Gamma(\mu)\lambda_\eta+\vartheta^\mu(\lambda_B\delta_\varepsilon+\|g\|_C)$$

is a constant independent of u.

By the boundedness of B, the uniform bound of Φ (H_2), and the boundedness of $\Psi_{\varepsilon,n}$, the integral term in $\mathcal{Q}_{\varepsilon,n}u$ can be uniformly estimated. Combining the above inequalities, we obtain

$$\hat{t}^{1-\mu}\|(\mathcal{Q}_{\varepsilon,n}u)(\hat{t}_1)-(\mathcal{Q}_{\varepsilon,n}u)(\hat{t}_2)\|_{\mathbb{X}}<\epsilon,\quad \forall u\in\widetilde{S}(0,\alpha(\varepsilon)).$$

Thus $\{\mathcal{Q}_{\varepsilon,n}u\}$ is equicontinuous on $(0,\vartheta]$.

For $\hat{t}\to 0^+$, by the singularity-mitigating property of $C_{1-\mu}([0,\vartheta];\mathbb{X})$ and the uniform boundedness of $\hat{t}^{1-\mu}S(\hat{t})$ (H_1), the family is equicontinuous at $\hat{t}=0$.

Since $\{\mathcal{Q}_{\varepsilon,n}u\}$ is uniformly bounded and equicontinuous on the compact interval $[0,\vartheta]$, by the Arzelà–Ascoli theorem, the family is precompact in $C_{1-\mu}([0,\vartheta];\mathbb{X})$. The compactness of $\hat{t}^{1-\mu}S(\hat{t})$ is preserved under integration, so the operator $\mathcal{Q}_{\varepsilon,n}$ is compact on $\widetilde{S}(0,\alpha(\varepsilon))$. □

Lemma 5. *If*

$$\lim_{n\to\infty}\|u_{\varepsilon,n}-u_\varepsilon\|_{C_{1-\mu}}=0,$$

then

$$\lim_{n\to\infty}\|\Psi_{\varepsilon,n}(u_{\varepsilon,n})-\Psi_\varepsilon(u_\varepsilon)\|=0$$

and

$$\lim_{n\to\infty}\|u_{\varepsilon,n}(s,u_{\varepsilon,n})-u_\varepsilon(s,u_\varepsilon)\|_C=0.$$

Proof. From definition, $\Psi_{\varepsilon,n}(u_{\varepsilon,n})$ and $\Psi_\varepsilon(u_\varepsilon)$ are minimizers of

$$\chi_{\varepsilon,n}(y;u_{\varepsilon,n})=\int_0^\vartheta(\vartheta-s)^{1-\mu}\|B^*S^*(\vartheta-s)\mathrm{T}^*y\|^2ds+\varepsilon\|y\|+\langle y,\Theta_n(u_{\varepsilon,n})\rangle,$$

and

$$\chi_\varepsilon(y;u_\varepsilon)=\int_0^\vartheta(\vartheta-s)^{1-\mu}\|B^*S^*(\vartheta-s)\mathrm{T}^*y\|^2ds+\varepsilon\|y\|+\langle y,\Theta(u_\varepsilon)\rangle.$$

respectively. In view of the boundedness of $\Psi_{\varepsilon,n}(u_{\varepsilon,n})$, we are able to take $\Psi_{\varepsilon,n}(u_{\varepsilon,n})\rightharpoonup\hat{\Psi}_\varepsilon\in\mathbb{X}$. Due to the optimality of $\Psi_{\varepsilon,n}(u_{\varepsilon,n})$ and $\Psi_\varepsilon(u_\varepsilon)$,

$$\chi_\varepsilon(\Psi_\varepsilon(u_\varepsilon);u_\varepsilon)\le\chi_\varepsilon(\hat{\Psi}_\varepsilon;u_\varepsilon)\le\underline{\lim}_{n\to\infty}\chi_{\varepsilon,n}(\Psi_{\varepsilon,n}(u_{\varepsilon,n});u_{\varepsilon,n}),\tag{12}$$

and

$$\begin{aligned}\underline{\lim}_{n\to\infty}\chi_{\varepsilon,n}(\Psi_{\varepsilon,n}(u_{\varepsilon,n});u_{\varepsilon,n})&\le\overline{\lim}_{n\to\infty}\chi_{\varepsilon,n}(\Psi_{\varepsilon,n}(u_{\varepsilon,n});u_{\varepsilon,n})\\&\le\lim_{n\to\infty}\chi_{\varepsilon,n}(\Psi_\varepsilon(u_\varepsilon);u_{\varepsilon,n})=\chi_\varepsilon(\Psi_\varepsilon(u_\varepsilon);u_\varepsilon).\end{aligned}\tag{13}$$

From (12) and (13), one has

$$\chi_\varepsilon(\Psi_\varepsilon(u_\varepsilon);u_\varepsilon)=\chi_\varepsilon(\hat{\Psi}_\varepsilon;u_\varepsilon),$$

$$\underline{\lim}_{n\to\infty}\chi_{\varepsilon,n}(\Psi_{\varepsilon,n}(u_{\varepsilon,n});u_{\varepsilon,n})=\overline{\lim}_{n\to\infty}\chi_{\varepsilon,n}(\Psi_{\varepsilon,n}(u_{\varepsilon,n});u_{\varepsilon,n})=\chi_\varepsilon(\Psi_\varepsilon(u_\varepsilon);u_\varepsilon).$$

https://doi.org/10.3390/sym18050721

which implies that $\hat{\Psi}_\varepsilon$ is a minimizer of $\chi_\varepsilon(\cdot; u_\varepsilon)$. Consequently, $\hat{\Psi}_\varepsilon = \Psi_\varepsilon(u_\varepsilon)$. Hence,

$$\lim_{n\to\infty} \chi_{\varepsilon,n}(\Psi_{\varepsilon,n}(u_{\varepsilon,n}); u_{\varepsilon,n}) = \chi_\varepsilon(\Psi_\varepsilon(u_\varepsilon); u_\varepsilon).$$

which further implies

$$\lim_{n\to\infty} \int_0^\vartheta (\vartheta - s)^{1-\mu} \|B^* S^*(\vartheta - s) \mathrm{T}^* \Psi_{\varepsilon,n}(u_{\varepsilon,n})\|^2 ds = \int_0^\vartheta (\vartheta - s)^{1-\mu} \|B^* S^*(\vartheta - s) \mathrm{T}^* \Psi_\varepsilon(u_\varepsilon)\|^2 ds,$$

$$\lim_{n\to\infty} \langle \Psi_{\varepsilon,n}(u_{\varepsilon,n}), \Theta_n(u_{\varepsilon,n}) \rangle = \langle \Psi_\varepsilon(u_\varepsilon), \Theta(u_\varepsilon) \rangle,$$

and

$$\|\Psi_\varepsilon(u_\varepsilon)\| \leq \lim_{n\to\infty} \|\Psi_{\varepsilon,n}(u_{\varepsilon,n})\|.$$

From the above relations, we obtain

$$\|\Psi_\varepsilon(u_\varepsilon)\| = \lim_{n\to\infty} \|\Psi_{\varepsilon,n}(u_{\varepsilon,n})\|. \tag{14}$$

Since $\Psi_{\varepsilon,n}(u_{\varepsilon,n}) \rightharpoonup \Psi_\varepsilon(u_\varepsilon)$ and $\mathbb{X}$ is a Hilbert space, strong convergence follows.

Now we prove that $\mathcal{Q}_\varepsilon : C_{1-\mu}([0,\vartheta];\mathbb{X}) \to C_{1-\mu}([0,\vartheta];\mathbb{X})$ given by

$$(\mathcal{Q}_\varepsilon u)(\hat{t}) = S(\hat{t})(\xi_0 - \eta(u)) + \int_0^{\hat{t}} S(\hat{t} - s)\big(Bu_\varepsilon(s,u) + \Phi(s,u(s))\big) ds,$$

with

$$\begin{aligned} u_\varepsilon(s,u) &= (\vartheta - s)^{1-\mu} B^* S^*(\vartheta - s) T^* \Psi_\varepsilon(u) \\ &= (\vartheta - s)^{1-\mu} B^* S^*(\vartheta - s) T^* \tilde{y}_\varepsilon. \end{aligned}$$

has a fixed point. □

Theorem 2. *The map $\mathcal{Q}_\varepsilon$ has a fixed point.*

Proof. Let

$$E = \{u_{\varepsilon,n} \in C_{1-\mu}([0,\vartheta];\mathbb{X}) : \mathcal{Q}_{\varepsilon,n} u_{\varepsilon,n} = u_{\varepsilon,n},\ n \geq 1\},$$

$$E_{1-\mu} = \{w_{\varepsilon,n}(\hat{t}) : w_{\varepsilon,n}(\hat{t}) = \hat{t}^{1-\mu} u_{\varepsilon,n}(\hat{t}),\ u_{\varepsilon,n} \in E\},$$

and

$$E_{1-\mu}(0) = \{w_{\varepsilon,n}(0) : w_{\varepsilon,n} \in E_{1-\mu}\}.$$

where

$$\begin{aligned} w_{\varepsilon,n}(0) &= \lim_{\hat{t}\to 0^+} \hat{t}^{1-\mu} u_{\varepsilon,n}(\hat{t}) \\ &= \lim_{\hat{t}\to 0^+} \hat{t}^{1-\mu} S(\hat{t}) \left(\xi_0 - \Gamma(\mu) n^{\mu-1} S\left(\frac{1}{n}\right)\eta(u)\right) \\ &= \frac{1}{\Gamma(\mu)} \left(\xi_0 - \Gamma(\mu) n^{\mu-1} S\left(\frac{1}{n}\right)\eta(u)\right). \end{aligned}$$

Step 1: $E_{1-\mu}(0)$ is precompact in $\mathbb{X}$.

For $w_{\varepsilon,n} \in E_{1-\mu}$, $n \geq 1$, define

$$\widehat{w}_{\varepsilon,n}(\hat{t}) = t^{1-\mu} \widehat{u}_{\varepsilon,n}(\hat{t}) = \begin{cases} w_{\varepsilon,n}(\hat{t}), & b \leq \hat{t} \leq \vartheta; \\ w_{\varepsilon,n}(b), & 0 \leq \hat{t} < b. \end{cases}$$

Then $\{\widehat{w}_{\varepsilon,n} : n = 1, 2, \dots\}$ is equicontinuous and uniformly bounded. Hence from Arzela theorem it contains a convergent subsequence in $C([0,\vartheta];\mathbb{X})$. Thus we are able to take $\widehat{w}_{\varepsilon,n} \to \widehat{w}_\varepsilon \in C([0,\vartheta];\mathbb{X})$. It means, $\widehat{u}_{\varepsilon,n} \to \widehat{u}_\varepsilon \in C_{1-\mu}[0,\vartheta];\mathbb{X})$, here $\widehat{u}_\varepsilon(\hat{t}) = \hat{t}^{\mu-1} \widehat{w}_\varepsilon(\hat{t})$. From (H_4), we get $\eta(u_{\varepsilon,n}) = \eta(\widehat{u}_{\varepsilon,n}) \to \eta(\widehat{u}_\varepsilon)$. Now,

https://doi.org/10.3390/sym18050721

$$\begin{aligned}\|w_{\varepsilon,n}(0)-\frac{1}{\Gamma(\mu)}(\xi_0-\eta(\widehat{u}_\varepsilon))\| &= \left\|\frac{1}{\Gamma(\mu)}\left(\xi_0-\Gamma(\mu)n^{\mu-1}S\left(\frac{1}{n}\right)\eta(u_{\varepsilon,n})\right)-\frac{1}{\Gamma(\mu)}(\xi_0-\eta(\widehat{u}_\varepsilon))\right\|\\ &\le \frac{1}{\Gamma(\mu)}\left\|\Gamma(\mu)n^{\mu-1}S\left(\frac{1}{n}\right)\eta(u_{\varepsilon,n})-\eta(\widehat{u}_\varepsilon)\right\|\\ &\le \frac{1}{\Gamma(\mu)}\left(\left\|\Gamma(\mu)n^{\mu-1}S\left(\frac{1}{n}\right)\eta(u_{\varepsilon,n})-\Gamma(\mu)n^{\mu-1}S\left(\frac{1}{n}\right)\eta(\widehat{u}_\varepsilon)\right\|\right.\\ &\quad\left.+\left\|\Gamma(\mu)n^{\mu-1}S\left(\frac{1}{n}\right)\eta(\widehat{u}_\varepsilon)-\eta(\widehat{u}_\varepsilon)\right\|\right)\\ &\le \lambda_S\|\eta(u_{\varepsilon,n})-\eta(\widehat{u}_\varepsilon)\|+\frac{1}{\Gamma(\mu)}\left\|\Gamma(\mu)n^{\mu-1}S\left(\frac{1}{n}\right)\eta(\widehat{u}_\varepsilon)-\eta(\widehat{u}_\varepsilon)\right\|\\ &\to 0 \quad \text{as } n\to\infty.\end{aligned}$$

Therefore $E_{1-\mu}(0)$ is precompact in $\mathbb{X}$.

Step 2: The set $E_{1-\mu}(\hat{t})=\{w_{\varepsilon,n}(\hat{t})=\hat{t}^{1-\mu}u_{\varepsilon,n}(\hat{t}),\ u_{\varepsilon,n}\in E\}$ is precompact in $\mathbb{X}$ for every fixed $\hat{t}>0$.

Step 3: $E_{1-\mu}$ is equicontinuous at $\hat{t}=0$.

We have

$$\begin{aligned}\|w_{\varepsilon,n}(\hat{t})-w_{\varepsilon,n}(0)\| &\le \left\|\hat{t}^{1-\mu}S(\hat{t})\left(\xi_0-\Gamma(\mu)n^{\mu-1}S\left(\frac{1}{n}\right)\eta(u_{\varepsilon,n})\right)-\frac{1}{\Gamma(\mu)}\left(\xi_0-\Gamma(\mu)n^{\mu-1}S\left(\frac{1}{n}\right)\eta(u_{\varepsilon,n})\right)\right\|\\ &\quad+\lambda_S\hat{t}^{\mu}\sup_{s\in[0,\hat{t}]}\|Bv_{\varepsilon,n}(s,u_{\varepsilon,n}(s))+\Phi(s,u_{\varepsilon,n}(s))\|\int_0^{\hat{t}}(\hat{t}-s)^{\mu-1}ds\\ &\le \left\|\left(\hat{t}^{1-\mu}S(\hat{t})-\frac{1}{\Gamma(\mu)}I\right)\xi_0\right\|+\left\|\left(\hat{t}^{1-\mu}S(\hat{t})-\frac{1}{\Gamma(\mu)}I\right)\Gamma(\mu)n^{\mu-1}S\left(\frac{1}{n}\right)\eta(u_{\varepsilon,n})\right\|\\ &\quad+\frac{\lambda_S\hat{t}}{\mu}\left(\lambda_S\lambda_B^2\|T\|\delta_\varepsilon+\|g\|_C\right)\\ &\to 0 \quad \text{as } \hat{t}\to 0^+.\end{aligned}$$

Hence, $E_{1-\mu}$ is equicontinuous at $\hat{t}=0$.

Step 4: $E_{1-\mu}$ is equicontinuous on $(0,\vartheta]$.

Let $\vartheta_1,\vartheta_2\in(0,\vartheta)$ with $\vartheta_1<\vartheta_2$ and $h\in(0,\vartheta_1)$, and $\xi_s(v_\varepsilon,u_{\varepsilon,n})=Bv_\varepsilon(s,u_{\varepsilon,n}(s))+\Phi(s,u_{\varepsilon,n}(s))$. Then for $w_{\varepsilon,n}\in E_{1-\mu}$, one has

$$\begin{aligned}&\|w_{\varepsilon,n}(\vartheta_2)-w_{\varepsilon,n}(\vartheta_1)\|\\ &\le \left\|\left(\vartheta_2^{1-\mu}S(\vartheta_2)-\vartheta_1^{1-\mu}S(\vartheta_1)\right)\left(\xi_0-\Gamma(\mu)n^{\mu-1}S\left(\frac{1}{n}\right)\eta(u_{\varepsilon,n})\right)\right\|\\ &\quad+\left\|\vartheta_2^{1-\mu}\int_0^{\vartheta_2}S(\vartheta_2-s)\xi_s(v_\varepsilon,u_{\varepsilon,n})ds-\vartheta_1^{1-\mu}\int_0^{\vartheta_1}S(\vartheta_1-s)\xi_s(v_\varepsilon,u_{\varepsilon,n})ds\right\|\\ &\le \left\|\left(\vartheta_2^{1-\mu}S(\vartheta_2)-\vartheta_1^{1-\mu}S(\vartheta_1)\right)\left(\xi_0-\Gamma(\mu)n^{\mu-1}S\left(\frac{1}{n}\right)\eta(u_{\varepsilon,n})\right)\right\|\\ &\quad+\left\|\left(\vartheta_2^{1-\mu}-\vartheta_1^{1-\mu}\right)\int_0^{\vartheta_2}S(\vartheta_2-s)\xi_s(v_\varepsilon,u_{\varepsilon,n})ds\right\|\\ &\quad+\vartheta_1^{1-\mu}\left\|\int_0^{\vartheta_2}S(\vartheta_2-s)\xi_s(v_\varepsilon,u_{\varepsilon,n})ds-\int_0^{\vartheta_1}S(\vartheta_1-s)\xi_s(v_\varepsilon,u_{\varepsilon,n})ds\right\|\\ &= I_1+I_2+I_3.\end{aligned}$$

From uniform continuity of $\hat{t}^{1-\mu}S(\hat{t})$ and (H_3), we get

$$I_1=\left\|\left(\vartheta_2^{1-\mu}S(\vartheta_2)-\vartheta_1^{1-\mu}S(\vartheta_1)\right)\left(\xi_0-\Gamma(\mu)n^{\mu-1}S\left(\frac{1}{n}\right)\eta(u_{\varepsilon,n})\right)\right\|\to 0 \text{ as } \vartheta_2-\vartheta_1\to 0 \tag{15}$$

https://doi.org/10.3390/sym18050721

for all $w_{\varepsilon,n} \in E_{1-\mu}$.

Now,

$$I_2 \leq \frac{\lambda_S}{\mu}\left(\vartheta_2^{1-\mu} - \vartheta_1^{1-\mu}\right)\vartheta_2^{\mu}\left(\lambda_S\lambda_B^2\|T\|\delta_\varepsilon + \|g\|_C\right) \to 0 \quad \text{as } \vartheta_2 - \vartheta_1 \to 0. \tag{16}$$

For $\vartheta_1 - h > 0$, one has

$$\begin{aligned}
I_3 &= \left\| \int_0^{\vartheta_1 - h} \Big((\vartheta_2 - s)^{1-\mu} S(\vartheta_2 - s) - (\vartheta_1 - s)^{1-\mu} S(\vartheta_1 - s) \Big) (\vartheta_2 - s)^{\mu-1} \xi_s(v_\varepsilon, u_{\varepsilon,n})\, ds \right\| \\
&\quad + \left\| \int_{\vartheta_1 - h}^{\vartheta_1} \Big((\vartheta_2 - s)^{1-\mu} S(\vartheta_2 - s) - (\vartheta_1 - s)^{1-\mu} S(\vartheta_1 - s) \Big) (\vartheta_2 - s)^{\mu-1} \xi_s(v_\varepsilon, u_{\varepsilon,n})\, ds \right\| \\
&\quad + \left\| \int_0^{\vartheta_1} (\vartheta_1 - s)^{1-\mu} S(\vartheta_1 - s) \Big((\vartheta_2 - s)^{\mu-1} - (\vartheta_1 - s)^{\mu-1} \Big) \xi_s(v_\varepsilon, u_{\varepsilon,n})\, ds \right\| \\
&\quad + \left\| \int_{\vartheta_1}^{\vartheta_2} (\vartheta_2 - s)^{\mu-1} (\vartheta_2 - s)^{1-\mu} S(\vartheta_2 - s) \xi_s(v_\varepsilon, u_{\varepsilon,n})\, ds \right\| \\
&\leq \frac{1}{\mu}\left(\lambda_S\lambda_B^2\|T\|\delta_\varepsilon + \|g\|_C\right)\left(\vartheta_2^{\mu} - (\vartheta_2 - \vartheta_1 + h)^{\mu}\right) \\
&\quad \cdot \sup_{s\in[0,\vartheta_1 - h]} \left\| (\vartheta_2 - s)^{1-\mu} S(\vartheta_2 - s) - (\vartheta_1 - s)^{1-\mu} S(\vartheta_1 - s) \right\| \\
&\quad + 2\lambda_S\left((\vartheta_2 - \vartheta_1 + h)^{\mu} - (\vartheta_2 - \vartheta_1)^{\mu}\right) + \lambda_S\left(\vartheta_2^{\mu} - \vartheta_1^{\mu} - (\vartheta_2 - \vartheta_1)^{\mu}\right) + \lambda_S(\vartheta_2 - \vartheta_1)^{\mu} \\
&\to 0 \quad \text{as } \vartheta_2 - \vartheta_1 \to 0.
\end{aligned} \tag{17}$$

From (15)–(17), $E_{1-\mu}$ is equicontinuous on $(0, \vartheta]$. Therefore, $E_{1-\mu}$ is precompact in $C([0,\vartheta];\mathbb{X})$ and we are able to take $w_{\varepsilon,n} \to w_\varepsilon \in C([0,\vartheta];\mathbb{X})$ as $n \to \infty$, that is, $u_{\varepsilon,n} \to u_\varepsilon \in C_{1-\mu}([0,\vartheta];\mathbb{X})$ as $n \to \infty$, here $u_\varepsilon(\hat{t}) = \hat{t}^{\mu-1} w_\varepsilon(\hat{t})$. Taking $n \to \infty$ in $\mathcal{Q}_{\varepsilon,n} u_{\varepsilon,n} = u_{\varepsilon,n}$, we obtain

$$u_\varepsilon(\hat{t}) = S(\hat{t})(\xi_0 - \eta(u_\varepsilon)) + \int_0^{\hat{t}} S(\hat{t} - s)(Bv_\varepsilon(s, u_\varepsilon(s)) + \Phi(s, u_\varepsilon(s)))ds.$$

□

4. PartialControllability Result

From above discussion, for each $\varepsilon > 0$ we can get a $z_\varepsilon \in C_{1-\mu}([0,\vartheta];\mathbb{X})$ verifying

$$u_\varepsilon(\hat{t}) = S(\hat{t})(\xi_0 - \eta(u_\varepsilon)) + \int_0^{\hat{t}} S(\hat{t} - s)(Bv_\varepsilon(s, u_\varepsilon(s)) + \Phi(s, u_\varepsilon(s)))ds,$$

with $v_\varepsilon(s, u_\varepsilon) = (\vartheta - s)^{1-\mu} B^* S^*(\vartheta - s) T^* \Psi_\varepsilon(u_\varepsilon)$. Next we show the partial controllability of system (1).

Theorem 3. *The system (1) is partially approximately controllable.*

Due to strict convexity of χ_ε, $\chi_\varepsilon(y, u_\varepsilon)$ has a unique minimizer $\widetilde{y}_\varepsilon \in \mathbb{X}$ satisfying

$$\chi_\varepsilon(\widetilde{y}_\varepsilon; u_\varepsilon) = \min_{y\in\mathbb{X}} \chi_\varepsilon(y; u_\varepsilon).$$

Now, for any $\xi \in \mathbb{X}$ and $\alpha \in \mathbb{R}$ one can write

$$\chi_\varepsilon(\widetilde{y}_\varepsilon; u_\varepsilon) \leq \chi_\varepsilon(\widetilde{y}_\varepsilon + \alpha\xi, u_\varepsilon),$$

https://doi.org/10.3390/sym18050721

which means

$$\begin{aligned}\varepsilon\|\widetilde{y}_\varepsilon\| \le \frac{\alpha^2}{2}\int_0^\vartheta (\vartheta-s)^{1-\mu}\|\langle B^*S^*(\vartheta-s)T^*\xi\|^2\,ds \\ + \alpha\int_0^\vartheta (\vartheta-s)^{1-\mu}\langle B^*S^*(\vartheta-s)T^*\widetilde{y}_\varepsilon, B^*S^*(\vartheta-s)T^*\xi\rangle\,ds \\ + \varepsilon\|\widetilde{y}_\varepsilon+\alpha\xi\| + \alpha\langle\xi,\Theta(u_\varepsilon)\rangle.\end{aligned}$$

Dividing by $\alpha > 0$ and taking $\alpha \to 0^+$, one can get

$$\begin{aligned}-\langle\xi,\Theta(u_\varepsilon)\rangle &\le \int_0^\vartheta (\vartheta-s)^{1-\mu}\langle B^*S^*(\vartheta-s)T^*\widetilde{y}_\varepsilon, B^*S^*(\vartheta-s)T^*\xi\rangle ds + \varepsilon\underline{\lim}_{\alpha\to0^+}\frac{\|\widetilde{y}_\varepsilon+\alpha\xi\|-\|\widetilde{y}_\varepsilon\|}{\alpha} \\ &\le \int_0^\vartheta (\vartheta-s)^{1-\mu}\langle B^*S^*(\vartheta-s)T^*\widetilde{y}_\varepsilon, B^*S^*(\vartheta-s)T^*\xi\rangle ds + \varepsilon\|\xi\|.\end{aligned}$$

In similar fashion with $\alpha < 0$, one can get

$$-\langle\xi,\Theta(u_\varepsilon)\rangle \ge \int_0^\vartheta (\vartheta-s)^{1-\mu}\langle B^*S^*(\vartheta-s)T^*\widetilde{y}_\varepsilon, B^*S^*(\vartheta-s)T^*\xi\rangle ds - \varepsilon\|\xi\|.$$

Thus,

$$\left|\int_0^\vartheta (\vartheta-s)^{1-\mu}\langle B^*S^*(\vartheta-s)T^*\widetilde{y}_\varepsilon, B^*S^*(\vartheta-s)T^*\xi\rangle ds + \langle\xi,\Theta(u_\varepsilon)\rangle\right| \le \varepsilon\|\xi\|. \tag{18}$$

But, for $v_\varepsilon = (\vartheta-s)^{1-\mu}B^*S^*(\vartheta-s)T^*\widetilde{y}_\varepsilon$, one can get

$$\begin{aligned}&\int_0^\vartheta (\vartheta-s)^{1-\mu}\langle B^*S^*(\vartheta-s)T^*\widetilde{y}_\varepsilon, B^*S^*(\vartheta-s)T^*\xi\rangle ds + \langle\xi,\Theta(u_\varepsilon)\rangle \\ &= \left\langle\int_0^\vartheta (\vartheta-s)^{1-\mu}TSBB^*S^*(\vartheta-s)T^*\widetilde{y}_\varepsilon ds + \Theta(u_\varepsilon),\xi\right\rangle \\ &= \left\langle\int_0^\vartheta T^*S^*(\vartheta-s)B^*u_s(s,u_{\varepsilon,n})ds + \Theta(u_\varepsilon),\xi\right\rangle \\ &= \langle Tu_\varepsilon(\vartheta)-u_\vartheta,\xi\rangle,\end{aligned} \tag{19}$$

since

$$\Theta(u_\varepsilon) = TS(\vartheta)(\xi_0-\eta(u_\varepsilon)) + \int_0^\vartheta TS(\vartheta-s)\Phi(s,u_\varepsilon(s))ds - u_\vartheta.$$

From (18) and (19), one has

$$\begin{aligned}&|\langle Tu_\varepsilon(\vartheta)-u_\vartheta,\xi\rangle| \le \varepsilon\|\xi\| \text{ for all } \xi\in\mathbb{X}, \\ &\implies |\langle Tu_\varepsilon(\vartheta)-u_\vartheta, Tu_\varepsilon(\vartheta)-u_\vartheta\rangle| \le \varepsilon\|Tu_\varepsilon(\vartheta)-u_\vartheta\|, \\ &\implies \|Tu_\varepsilon(\vartheta)-u_\vartheta\| \le \varepsilon.\end{aligned}$$

Since $\varepsilon > 0$ is arbitrary and the existence of the corresponding mild solution u_ε is guaranteed by Theorem 1, System (1) satisfies the condition of partial approximate controllability in Definition 7, for any target state $u_\vartheta \in \mathbb{X}_0$. This completes the proof.

5. Example

To verify the effectiveness of the theoretical results in this paper, we consider a one-dimensional fourth-order fractional damped Euler–Bernoulli beam system, which is a typical high-order fractional diffusion system in engineering [23–25]. For $0 < \xi < \nu < \mu \le 1$, where the condition $\mu > \frac{1}{2}$ is imposed to ensure the density of the weighted space $C_{1-\mu}$ in

https://doi.org/10.3390/sym18050721

L^2, consider the following semi-linear fractional system involving three Riemann–Liouville fractional derivatives and nonlocal initial conditions:

$$\begin{cases} D_{\hat{t}}^{\mu}\omega(\hat{t},\sigma) + eD_{\hat{t}}^{\nu}\omega(\hat{t},\sigma) + kD_{\hat{t}}^{\xi}\omega(\hat{t},\sigma) = r^4\frac{\partial^4}{\partial\sigma^4}\omega(\hat{t},\sigma) + Bv(\hat{t},\sigma) + \Phi(\hat{t},\omega(\hat{t},\sigma)), & \hat{t}\in(0,1]; \\ \omega(\hat{t},0) = \omega(\hat{t},1) = 0, \quad \frac{\partial^2}{\partial\sigma^2}\omega(\hat{t},0) = \frac{\partial^2}{\partial\sigma^2}\omega(\hat{t},1) = 0, & \hat{t}\in(0,1]; \\ \lim\limits_{\hat{t}\to 0^+} I_{\hat{t}}^{1-\mu}\omega(\hat{t},\sigma)_{\hat{t}=0} = \xi_0(\sigma) - \dfrac{1}{1+\left|\sum_{i=0}^{n}\int_0^1 h(\sigma,s)\omega(\vartheta_i,s)ds\right|}, & \vartheta_i\in(0,1]; \end{cases} \tag{20}$$

We refer to the above one-dimensional fourth-order fractional damped Euler–Bernoulli beam system as System (20) for short in the following analysis, where $e, k \in \mathbb{R}$ are damping coefficients, $r > 0$ is a constant, $\xi_0 \in L_2[0,1]$ is the initial state, with $n \in \mathbb{N}$, $0 = \vartheta_0 < \vartheta_1 < \cdots < \vartheta_n < 1$ and $h(\cdot,\cdot) \in L_2([0,1]\times[0,1];\mathbb{R}^+)$ being a non-negative integrable kernel.

Step 1 : Define the state space and fourth-order operator A

Take the Hilbert space $\mathbb{X} = L_2[0,1]$ and the linear fourth-order operator $A : D(A) \subset \mathbb{X} \to \mathbb{X}$ given by

$$Af = r^4\frac{d^4 f}{d\sigma^4},$$

with the domain

$$D(A) = \left\{ f \in W^{4,2}(0,1) : f(0) = f(1) = 0,\ f''(0) = f''(1) = 0 \right\},$$

where $W^{4,2}(0,1)$ denotes the Sobolev space of functions with square-integrable derivatives up to order 4 on $[0,1]$.

The operator A has a complete orthonormal system of eigenfunctions $\{q_n(\sigma)\}_{n=1}^{\infty}$ in $\mathbb{X}$

$$q_n(\sigma) = \sin(n\pi\sigma), \quad n = 1,2,\ldots,$$

corresponding to the eigenvalues

$$\lambda_n = -r^4 n^4\pi^4, \quad n = 1,2,\ldots.$$

Then, A generates a strongly continuous (μ,ν,ξ,e,k)-resolvent family $\{S(\hat{t})\}_{\hat{t}>0} \subset L(\mathbb{X})$ with the explicit spectral form

$$(S(\hat{t})z)(\sigma) = \sum_{n=1}^{\infty}\hat{t}^{\mu-1}E_{\mu-\nu,\mu-\xi,\mu}\left(-e\lambda_n\hat{t}^{\mu-\nu}, -k\lambda_n\hat{t}^{\mu-\xi}\right)\langle z, q_n\rangle_{\mathbb{X}}\sin(n\pi\sigma),$$

where $E_{\alpha,\beta,\gamma}(a,b)$ is the three-parameter Mittag-Leffler function defined in your paper, and $\langle\cdot,\cdot\rangle_{\mathbb{X}}$ is the $L_2[0,1]$ inner product.

Step 2: Verify Assumption (H_1)

For the resolvent family $\{S(\hat{t})\}_{\hat{t}>0}$, the weighted operator $\hat{t}^{1-\mu}S(\hat{t})$ satisfies

$$\left\|\hat{t}^{1-\mu}S(\hat{t})\right\|_{L(\mathbb{X})} \le \sup_{n\in\mathbb{N}}\left|E_{\mu-\nu,\mu-\xi,\mu}\left(-e\lambda_n\hat{t}^{\mu-\nu}, -k\lambda_n\hat{t}^{\mu-\xi}\right)\right| =: \lambda_S,$$

where $\lambda_S > 0$ is a constant. Moreover, $\hat{t}^{1-\mu}S(\hat{t})$ is uniformly continuous and compact on $(0,1]$ due to the compactness of A and the spectral decay of λ_n. Thus, Assumption (H_1) is satisfied. The compactness and uniform boundedness of the weighted resolvent family are the core properties for the controllability analysis of high-order fractional damped systems [9,25], which are also the key assumptions in this paper. The compactness and uniform boundedness of the weighted resolvent family are the core properties for the

https://doi.org/10.3390/sym18050721

controllability analysis of high-order fractional damped systems [9,25], which are also the key assumptions in this paper.

Step 3: Define the control space and control operator B

We define the closed subspace $\mathbb{X}' \subset \mathbb{X}$ as follows:

$$\mathbb{X}' = \left\{ v = \sum_{n=2}^{\infty} \alpha_n q_n(\sigma) : \sum_{n=2}^{\infty} \alpha_n^2 < \infty \right\},$$

where the first-order mode q_1 is excluded for the following rationality.

Mathematical rationality: This setting ensures the validity of the key partial approximate controllability condition in Assumption (H_5) and the boundedness of the control operator B.

Physical rationality: $q_1(\sigma) = \sin(\pi\sigma)$ is the first-order natural vibration mode of the Euler–Bernoulli beam, which is inherently stable and does not need active control in engineering practice. endowed with the norm

$$\|v\|_{\mathbb{X}'} = \left(\sum_{n=2}^{\infty} \alpha_n^2 \right)^{\frac{1}{2}}.$$

The linear bounded control operator $B : \mathbb{X}' \to \mathbb{X}$ is defined by

$$Bv = 2\alpha_2 q_1(\sigma) + \sum_{n=2}^{\infty} \alpha_n q_n(\sigma),$$

where $v = \sum_{n=2}^{\infty} \alpha_n q_n(\sigma) \in \mathbb{X}'$. The term $2\alpha_2 q_1$ is specially designed to realize the effective coupling between the control input and the first-order mode q_1. It is straightforward to check that $\|B\| = \lambda_B < \infty$, satisfying the boundedness condition of B in your paper.

Step 4: Rewrite the system in abstract form

Let $\widetilde{\omega}(\hat{t}) = \omega(\hat{t}, \cdot)$, $\widetilde{v}(\hat{t}) = v(\hat{t}, \cdot)$, $\widetilde{\xi}_0 = \xi_0(\cdot)$, and $C_{1-\mu}([0, \vartheta]\mathbb{X})$. Then, the concrete system (20) can be rewritten as the abstract three-parameter damped fractional system in this paper.

$$\begin{cases} D_{\hat{t}}^{\mu} \widetilde{\omega}(\hat{t}) + eD_{\hat{t}}^{\nu} \widetilde{\omega}(\hat{t}) + kD_{\hat{t}}^{\xi} \widetilde{\omega}(\hat{t}) = A\widetilde{\omega}(\hat{t}) + B\widetilde{v}(\hat{t}) + \Phi(\hat{t}, \widetilde{\omega}(\hat{t})), \quad \hat{t} \in (0, 1]; \\ \lim\limits_{\hat{t} \to 0^+} I_{\hat{t}}^{1-\mu} \widetilde{\omega}(\hat{t}) = \widetilde{\xi}_0 - \eta(\widetilde{\omega}); \end{cases} \tag{21}$$

Here, Equation (21) represents the abstract form of the illustrative system, referred to as System (21). where the nonlocal function $\eta : C_{1-\mu}([0, 1]; \mathbb{X}) \to \mathbb{X}$ is defined as

$$\eta(\omega) = \frac{1}{1 + \left| \sum_{i=0}^{n} \int_0^1 h(\sigma, s)\omega(\vartheta_i, s)ds \right|},$$

with the norm $\|\omega\|_{C_{1-\mu}} = \sup_{\hat{t} \in (0,1]} \hat{t}^{1-\mu} \|\omega(\hat{t})\|_{\mathbb{X}}$.

Step 5: Verify assumptions (H_2)–(H_4)

1. Assumption (H_2).

Choose the nonlinear perturbation term $\Phi : [0, 1] \times \mathbb{X} \to \mathbb{X}$ as

$$\Phi(\hat{t}, \omega(\hat{t}, \sigma)) = \frac{(1 + \hat{t}^2 + \cos^2 \hat{t}) \sin(\omega(\hat{t}, \sigma))}{2 + \hat{t}^3 + \cos(\omega(\hat{t}, \sigma)) + e^{\omega(\hat{t}, \sigma)}}.$$

It is continuous on $[0, 1] \times \mathbb{X}$ and satisfies

$$\|\Phi(\hat{t}, \omega)\|_{\mathbb{X}} \leq 1 + \hat{t}^2 + \cos^2 \hat{t} =: g(\hat{t}), \text{ for all } (\hat{t}, \omega) \in [0, 1] \times \mathbb{X},$$

https://doi.org/10.3390/sym18050721

where $g \in C([0,1];\mathbb{R}^+)$. Thus, (H_2) is satisfied.

2. Assumption (H_3)

For the nonlocal function η, we have

$$\|\eta(\omega)\|_{\mathbb{X}} \leq 1 =: \lambda_\eta, \text{ for all } \omega \in C_{1-\mu}([0,1];\mathbb{X}),$$

and η is continuous on $C_{1-\mu}([0,1];\mathbb{X})$. Thus, (H_3) is satisfied.

3. Assumption (H_4)

Take $b = \vartheta_n \in (0,1)$. For any $\omega_1, \omega_2 \in C_{1-\mu}([0,1];\mathbb{X})$ with $\omega_1(\hat{t}) = \omega_2(\hat{t})$ for all $\hat{t} \in [b,1]$, we have $\eta(\omega_1) = \eta(\omega_2)$. Thus, (H_4) is satisfied.

Step 6: Verify Assumption (H_5)

The linearized system of (21) is

$$\begin{cases} D_{\hat{t}}^{\mu}\widetilde{\omega}(\hat{t}) + eD_{\hat{t}}^{\nu}\widetilde{\omega}(\hat{t}) + kD_{\hat{t}}^{\xi}\widetilde{\omega}(\hat{t}) = A\widetilde{\omega}(\hat{t}) + B\widetilde{v}(\hat{t}), \quad \hat{t} \in (0,1]; \\ \lim\limits_{\hat{t}\to 0^+} I_{\hat{t}}^{1-\mu}\widetilde{\omega}(\hat{t}) = \widetilde{\xi}_0. \end{cases}$$

By the definition of B and the projection $T : \mathbb{X} \to \mathbb{X}_0$, where $\mathbb{X}_0 = \overline{\text{Range}(\mathcal{U})}$, $\mathcal{U}$ is the controllability operator, we obtain

$$B^*S^*(\vartheta - \hat{t})T^*\xi = 0 \implies \xi = 0, \text{ for all } \xi \in \mathbb{X}_0, \hat{t} \in (0,1).$$

This equivalence implies the linear system is partially approximately controllable on $\mathbb{X}_0 \subset \mathbb{X}$, satisfying Assumption (H_5).

Conclusion All assumptions (H_1)–(H_5) in the paper are satisfied for the fourth-order system (20). By the main controllability theorem in Section 4, the three-parameter damped semi-linear fractional fourth-order system (20) is partially approximately controllable on the closed subspace $\mathbb{X}_0 \subset L_2[0,1]$.

6. Conclusions

This paper investigates the existence of mild solutions and partial approximate controllability for semilinear Riemann–Liouville fractional fourth-order systems with three-parameter damping, nonlocal initial conditions and nonlinear perturbations. Using the (μ,ν,ξ,e,k)-resolvent family and three-parameter Mittag-Leffler function, we relax the Lipschitz condition via approximate systems, the Schauder fixed-point theorem and functional minimization, and prove the well-posedness of mild solutions and partial approximate controllability in $\mathbb{X}_0 \subset L_2[0,1]$. A one-dimensional elastic beam example verifies the theoretical results under (H_1)–(H_5). The results can be extended to general high-order fractional damped systems [24,25].

The core contributions are threefold: extending two-parameter damping to a three-parameter framework and defining the related Mittag-Leffler function and resolvent family to fill the theoretical gap; focusing on fourth-order spatial operators to supplement the controllability research of high-order fractional damped systems; and relaxing the Lipschitz constraint without extra strong assumptions to ensure the universality of results.

This study enriches the controllability theory of fractional systems, extends the application of the resolvent family method, and provides theoretical support for the control design of one-dimensional high-order engineering systems with multi-scale damping.

Limitations: this work is limited to one-dimensional systems [20]; exact and optimal control are not involved [29], and only linear bounded control operators and constant-order

https://doi.org/10.3390/sym18050721

damping are considered, while unbounded operators and variable-order damping are still open [11].

Future work will extend the model to high-dimensional cases, study exact and optimal control, and introduce complex perturbations. We will also generalize the three-parameter damping framework to singular kernel fractional calculus [19], explore the controllability of systems with impulses and delays [15,29], and carry out numerical simulations [24] to improve the theory and application value.

In summary, this work proposes a new framework for the controllability analysis of multi-parameter high-order fractional damped systems, and the conclusions are applicable to more general fractional systems with both theoretical and engineering significance.

Author Contributions: Conceptualization, S.L.; methodology, S.L. and Z.L.; validation, Z.L., S.L. and T.H.; formal analysis and investigation, S.L. and Z.L.; resources, S.L.; writing—original draft preparation, Z.L.; writing—review and editing, Z.L., S.L. and T.H.; supervision, S.L.; project administration, S.L.; funding acquisition, S.L. All authors have read and agreed to the published version of the manuscript.

Funding: This research was supported by the following funding bodies: Hainan Provincial Natural Science Foundation (Grant number 125RC745) and National Natural Science Foundation of China (Grant number 11761027).

Data Availability Statement: All the data contained in this paper can be obtained by contacting the corresponding author upon request.

Acknowledgments: The authors would like to convey their deepest thanks and utmost honor to the editors and referees involved.

Conflicts of Interest: The authors affirm that there is no conflicts of interest.

References

1. Mishra, V.N.; Gupta, A.; Sarangi, S.K. Viscoelastic materials and composites: A comprehensive review on mechanics, modeling, and design configurations for vibration control in structural application. *Multiscale Multidiscip. Model. Exp. Des.* **2025**, *8*, 470. [CrossRef]
2. Baleanu, D.; Sajjadi, S.S.; Jajarmi, A.; Defterli, Ö. On a nonlinear dynamical system with both chaotic and nonchaotic behaviors: A new fractional analysis and control. *Adv. Differ. Equ.* **2021**, *2021*, 234. [CrossRef]
3. Suzuki, J.L.; Gulian, M.; Zayernouri, M.; D'Elia, M. Fractional Modeling in Action: A Survey of Nonlocal Models for Subsurface Transport, Turbulent Flows, and Anomalous Materials. *J. Peridynamics Nonlocal Model.* **2023**, *5*, 392–459. [CrossRef]
4. Li, K.X.; Peng, J.G.; Jia, J.X. Cauchy problems for fractional differential equations with Riemann–Liouville fractional derivatives. *J. Funct. Anal.* **2012**, *263*, 476–510. [CrossRef]
5. Saha, K.K.; Sukavanam, N.; Pan, S. Existence and uniqueness of solutions to fractional differential equations with fractional boundary conditions. *Alex. Eng. J.* **2023**, *72*, 147–155. [CrossRef]
6. Kilbas, A.A.; Srivastava, H.M.; Trujillo, J.J. *Theory and Applications of Fractional Differential Equations*; North-Holland Mathematics Studies; Elsevier Science: Amsterdam, The Netherlands, 2006; Volume 204, pp. 1–340. Available online: https://www.elsevier.com/books/theory-and-applications-of-fractional-differentialequations/kilbas/978-0-444-51832-3 (accessed on 19 April 2026).
7. Podlubny, I. *Fractional Differential Equations: An Introduction to Fractional Derivatives, Fractional Differential Equations, to Methods of Their Solution and Some of Their Applications*; Elsevier: Amsterdam, The Netherlands, 1999; Volume 198, pp. 1–309. Available online: https://www.sciencedirect.com/book/978-0-12-558840-9/fractional-differential-equations (accessed on 19 April 2026).
8. Mei, Z.; Peng, J.G. Riemann–Liouville abstract fractional Cauchy problem with damping. *Indag. Math.* **2014**, *25*, 145–161. [CrossRef]
9. Pomaro, B.; Majorana, C.E. Parametric resonance of fractional multiple-degree-of-freedom damped beam systems. *Acta Mech.* **2021**, *232*, 4897–4918. [CrossRef]
10. Aslam, M.F.; Hao, J.H.; Boulaaras, S.; Bashir, L. Global existence and exponential stability of a fractionally damped plate equation with past history. *Electron. Res. Arch.* **2025**, *33*, 4363–4381. [CrossRef]
11. Almeida, R.; Tavares, D.; Torres, D.F.M. *The Variable-Order Fractional Calculus of Variations*; Springer: Cham, Switzerland, 2019. [CrossRef]

12. Lu, Z.C.; Lin, S.Y.; Hu, T.T. Research on the existence and uniqueness of solutions to fractional diffusion equations with three-parameter damping terms. *Axioms* **2026**, *15*, 136. [CrossRef]
13. Hu, T.T.; Lin, S.Y.; Lu, Z.C. Solution Operators for Caputo-type Fractional Evolution Equations with Damping. *Axioms* **2026**, *15*, 179. [CrossRef]
14. Haq, A. Partial-approximate controllability of semi-linear systems involving two Riemann-Liouville fractional derivatives. *Chaos Solitons Fractals* **2022**, *157*, 111923. [CrossRef]
15. Gassem, F.; Almalahi, M.; Aldwoah, K. Stability and Controllability of Coupled Neutral Impulsive ϱ-Fractional System with Mixed Delays. *Fractal Fract.* **2026**, *10*, 3. [CrossRef]
16. Liu, F.W.; Meerschaert, M.M.; McGough, R.J.; Zhuang, P.H.; Liu, Q.X. Numerical methods for solving the multi-term time-fractional wave-diffusion equation. *Fract. Calc. Appl. Anal.* **2013**, *16*, 9–25. [CrossRef] [PubMed]
17. Almeida, R.; Malinowska, A.B.; Monteiro, M.T.T. Fractional differential equations with a Caputo derivative with respect to a kernel function and their applications. *Math. Methods Appl. Sci.* **2018**, *41*, 336–352. [CrossRef]
18. Zhu, S.; Dai, P.; Qu, Y.; Li, G. Subordination principle and approximation of fractional resolvents and applications to fractional evolution equations. *Fract. Calc. Appl. Anal.* **2023**, *26*, 781–799. [CrossRef]
19. Zhou, Y. Well-Posedness and Regularity of Fractional Wave Equations. In *Fractional Diffusion and Wave Equations*; Springer: Cham, Switzerland, 2024; pp. 151–234. [CrossRef]
20. Suhaib, K.; Malik, S.A.; Ilyas, A. Existence and uniqueness results for a multi-parameters nonlocal diffusion equation. *Rep. Math. Phys.* **2022**, *90*, 203–219. [CrossRef]
21. Yang, H.; Li, Y.X. Approximate controllability of Riemann-Liouville fractional stochastic evolution systems. *J. Appl. Anal. Comput.* **2023**, *13*, 2809–2826. [CrossRef]
22. Li, X.M.; Liu, X.G.; Tang, M.L. Approximate controllability of fractional evolution inclusions with damping. *Chaos Solitons Fractals* **2021**, *148*, 111073. [CrossRef]
23. Bahreini, A.; Asgari, A.; Akbarzadeh Bengar, H. Numerical Fractional Calculus Framework for Nonlocal Euler-Bernoulli Beam Deflection Analysis. *Fractal Fract.* **2026**, *10*, 2. [CrossRef]
24. Qiu, W.; Zheng, X.; Guo, T.; Xiao, X. Finite Difference Method for Nonlinear Damped Viscoelastic Euler-Bernoulli Beam Model. *Numer. Methods Partial Differ. Equ.* **2025**, *41*, e70051. [CrossRef]
25. George, R.E.; Oyelami, B.O. Analytical solution of the fractional-order Euler–Bernoulli beam equation. *Electron. J. Math.* **2025**, *9*, 102–112. [CrossRef]
26. Mahmudov, N.I. Partial-approximate controllability of nonlocal fractional evolution equations via approximating method. *Appl. Math. Comput.* **2018**, *334*, 227–238. [CrossRef]
27. Mishra, K.K.; Dubey, S. Approximate Controllability of Nonlocal Fractional Control System. *Qual. Theory Dyn. Syst.* **2024**, *23*, 232. [CrossRef]
28. Sharma, A.; Mishra, S.N.; Shukla, A. Schauder's fixed point theorem approach for stability analysis of nonlinear fractional difference equations. *Chaos Solitons Fractals* **2024**, *188*, 115586. [CrossRef]
29. Aberqi, A.; Ech-chaffani, Z.; Karite, T. Approximate controllability of fractional differential systems with nonlocal conditions of order $q \in [1, 2]$. *arXiv* **2024**, arXiv:2411.10766. [CrossRef]

Disclaimer/Publisher's Note: The statements, opinions and data contained in all publications are solely those of the individual author(s) and contributor(s) and not of MDPI and/or the editor(s). MDPI and/or the editor(s) disclaim responsibility for any injury to people or property resulting from any ideas, methods, instructions or products referred to in the content.

computation

MDPI

Article

Complex-Order Gold Rush Optimizer Algorithm

Sixuan Chen [1], Xiaobo Wu [1], Tao Wang [1,2,*], Hongli Ma [1], Xiang Li [1] and Lisheng Yin [1]

[1] School of Electrical Engineering and Automation, Hefei University of Technology, Hefei 230009, China; 2023210804@mail.hfut.edu.cn (S.C.); 2018170339@mail.hfut.edu.cn (X.W.); 2023010050@mail.hfut.edu.cn (H.M.); lixiang@hfut.edu.cn (X.L.)

[2] National Key Laboratory of Autonomous Intelligent Unmanned Systems, Beijing Institute of Technology, Beijing 100081, China

* Correspondence: twang@hfut.edu.cn

Abstract

This study proposes an enhanced variant of the gold rush optimizer (GRO) algorithm, termed the complex-order gold rush optimizer (CoGRO) algorithm, to address two inherent theoretical limitations of the original GRO. First, GRO employs a random initialization strategy that lacks ergodicity and uniform coverage, leading to insufficient population diversity and a higher risk of premature convergence. Second, its position update mechanism relies solely on current-time information without incorporating historical search experience, which restricts the algorithm's ability to model long-term dependencies and escape local optima in complex multimodal landscapes. To overcome these deficiencies, we introduce a chaotic LCS1 initialization to enhance population diversity through improved ergodic coverage, and we embed a complex-order derivative mechanism into the migration and collaboration updates to provide infinite memory capability. A comprehensive sensitivity analysis is conducted to examine the influence of control parameters on CoGRO's performance, leading to the identification of an optimal parameter configuration. The effectiveness of the proposed algorithm is evaluated using the CEC2022 benchmark suite through ablation studies and comparative analyses with state-of-the-art algorithms. Experimental results on the CEC2022 benchmark suite comprising 12 test functions demonstrate that CoGRO significantly outperforms the original GRO, achieving an average solution accuracy improvement of 0.84% and an average standard deviation reduction of 67.6 across all 12 functions, with particularly notable improvements on hybrid and composition functions. Wilcoxon signed-rank tests confirm the statistical significance of these improvements ($p < 0.05$). These results confirm the feasibility and effectiveness of CoGRO as an improved optimization method for complex engineering problems.

Keywords: gold rush optimizer; complex-order; chaotic initialization

1. Introduction

Intelligent optimization algorithms can generally be divided into four major categories: evolutionary algorithms, including Genetic Algorithm (GA) [1] and Differential Evolution (DE) [2]; swarm intelligence algorithms, such as Particle Swarm Optimization (PSO) [3] and Ant Colony Optimization (ACO) [4]; physics-based algorithms, for instance Simulated Annealing (SA) [5] and Gravitational Search Algorithm (GSA) [6]; and human-inspired algorithms, among which are Teaching–Learning-Based Optimization (TLBO) [7], Imperialist Competitive Algorithm (ICA) [8], and the recently proposed Gold Rush Optimizer. Among these classes, human-inspired algorithms simulate human social behaviors or

historical events to drive the optimization search process. The Gold Rush Optimizer (GRO), formally introduced by Kamran Zolfi in 2023 [9], falls into this category. Motivated by the 19th-century North American Gold Rush, GRO establishes a multi-stage search framework by mimicking three core behaviors: migration, collaboration, and mining. Compared with other classical algorithms, GRO is characterized by its simple structure and ease of implementation while possessing strong global search ability that dynamically balances exploration and exploitation [10].

Nevertheless, despite its structural simplicity, GRO still exhibits noticeable shortcomings relative to other human-inspired algorithms including Teaching–Learning-Based Optimization (TLBO) and the Imperialist Competitive Algorithm (ICA). TLBO adopts a two-phase teacher-learner update mechanism that effectively balances exploration and exploitation [11], whereas ICA maintains population diversity through competition among imperialist colonies [12]. In comparison, GRO employs random initialization without ergodic coverage, which frequently leads to insufficient initial population diversity. Furthermore, its position updates rely solely on real-time information and ignore historical search experiences, making the algorithm susceptible to premature convergence into local optima. To alleviate such limitations in metaheuristic algorithms, various improvement strategies have been reported in the literature. For example, the random average marine predators algorithm [13] introduces stochastic averaging operations to balance exploration and exploitation during the search process. Weng et al. [14] proposed a hybrid sine cosine algorithm that incorporates vertical and horizontal crossover mechanisms with pattern search to enhance population diversity and accelerate convergence, effectively addressing the issues of local optima stagnation and slow convergence in the standard SCA. Nonlinear sine cosine and safe experimentation dynamics algorithms [15] adopt adaptive parameter adjustment and safety constraint mechanisms to avoid premature convergence. Polar bear optimization [16] has also been successfully applied to industrial computed tomography with incomplete data, demonstrating its effectiveness in handling real-world engineering problems. These methods provide meaningful references for algorithmic enhancement. In this study, we adopt a distinct yet complementary improvement scheme: chaotic LCS1 initialization to enrich population diversity, and complex-order derivatives to embed historical memory into position updates. These strategies can also be flexibly combined with the aforementioned methods in future research.

Despite its drawbacks, GRO is selected as the baseline algorithm in this work for two main reasons. First, unlike TLBO with its two-phase update rule and ICA with multiple empire-related parameters, GRO adopts a concise three-strategy framework with fewer control parameters, making it more convenient for theoretical analysis and structural modification. Second, recent studies have verified that GRO achieves competitive performance on both unimodal and multimodal optimization problems despite its simplicity, implying that its core search logic is inherently effective and that targeted improvements can further enhance its performance. Therefore, by addressing its two critical deficiencies—insufficient initialization diversity and lack of historical memory—we aim to elevate GRO to a performance level comparable to more advanced algorithms. This is the primary motivation of the present work.

Based on the above discussions, this paper proposes an improved complex-order Gold Rush Optimizer (CoGRO). The main contributions are summarized as follows:

1. An initialization scheme based on LCS1 chaotic mapping is introduced to improve population diversity, enabling initial individuals to be distributed more uniformly within the search space and thus enhancing the starting quality of the global search.
2. Complex-order derivatives are integrated into the migration and collaboration update stages of GRO, granting the algorithm long-term memory of historical search information and improving its adaptability and guidance precision in complex multimodal scenarios.

https://doi.org/10.3390/computation14060124

3. In contrast to the original GRO, which uses random initialization and memoryless updates, the proposed CoGRO innovatively combines chaotic LCS1 initialization with complex-order derivative-based position updating. This hybrid mechanism helps maintain population diversity during the entire search process and supports effective escape from local optima. Extensive experiments on the CEC2022 benchmark functions show that CoGRO outperforms the original GRO and several state-of-the-art algorithms in both solution accuracy and convergence stability, verifying the effectiveness and universality of the proposed improvements.

The remainder of this paper is organized as follows. Section 2 introduces the basic theoretical definitions used in this study. Section 3 briefly reviews the standard GRO algorithm. Section 4 details the proposed improved strategies. Section 5 presents comprehensive experimental results and analyses of CoGRO. Finally, Section 6 concludes the main findings of this work.

2. Preliminary Mathematical Concepts

To ensure the rigor and reproducibility of the proposed algorithm, this section establishes the theoretical foundation for incorporating historical memory into the optimization process by introducing fundamental concepts from fractional calculus and complex-order derivatives. Fractional calculus extends traditional integer-order calculus and provides a powerful framework for modeling memory and hereditary effects. Among various definitions of fractional derivatives, the Grunwald–Letnikov (G-L) formulation is particularly well-suited for numerical implementation.

Definition 1 ([17] (Grunwald-Letnikov Fractional Derivative)). *For a function $f(t) \in C^{m+1}([t_0, +\infty), \mathbb{R})$, its α-th order G-L derivative is defined as:*

$$ {}_{t_0}D_t^{\alpha} f(t) = \lim_{h \to 0} \frac{1}{h^{\alpha}} \sum_{k=0}^{\lfloor (t-t_0)/h \rfloor} (-1)^k \binom{\alpha}{k} f(t - kh), \tag{1} $$

where $\alpha \in (m-1, m)$ is the order of the derivative, $m \in \mathbb{N}^+$; h is the step size; the binomial coefficient $\binom{\alpha}{k} = \frac{\Gamma(\alpha+1)}{\Gamma(k+1)\Gamma(\alpha-k+1)}$, and $\Gamma(\cdot)$ denotes the Gamma function.

In practical discrete-time systems, when the sampling period T is sufficiently small and the truncation order r is appropriately chosen, Equation (1) *can be approximated as:*

$$ D^{\alpha} f(t) = \frac{1}{T^{\alpha}} \sum_{k=0}^{r} (-1)^k \frac{\Gamma(\alpha+1) f(t-kT)}{\Gamma(k+1)\Gamma(\alpha-k+1)}, \tag{2} $$

This discrete-time approximation is used for numerical implementation in the proposed algorithm.

Extending fractional derivatives to the complex domain yields complex-order derivative operators. The extension of the Grunwald–Letnikov formulation to complex orders is valid when the function $f(t)$ is analytic and the parameters satisfy $|\alpha|, |\beta| < 1$, which guarantees the decay of the series coefficients. Under these conditions, the Gamma function $\Gamma(\alpha \pm i\beta + 1)$ is well-defined for complex arguments, and the binomial coefficients $\binom{\alpha \pm i\beta}{k}$ exhibit the same rapid decay properties as in the real case, ensuring absolute convergence of the series [18,19]. With the sampling period $T = 1$ adopted in this work, the truncation error introduced by limiting the summation to $r = 3$ is bounded by $O(z^{-4})$, which is negligible for numerical implementation. The resulting complex-order derivative operators not only capture the attenuation of historical information but also introduce oscillatory behavior through the imaginary part, enabling a more nuanced balance between exploration and exploitation [17]. From the perspective of complex-order calculus, the derivative order can

https://doi.org/10.3390/computation14060124

be further generalized to the conjugate complex pair $\alpha \pm i\beta$, leading to the G-L formulation of the complex-order derivative:

$$D^{\alpha \pm i\beta} f(t) = \frac{1}{T^{\alpha \pm i\beta}} \sum_{k=0}^{r} (-1)^k \frac{\Gamma(\alpha \pm i\beta + 1) f(t - kh)}{\Gamma(k+1)\Gamma(\alpha \pm i\beta - k + 1)}, \tag{3}$$

This formulation preserves the memory characteristics of fractional-order derivatives while introducing frequency-domain selection and phase modulation mechanisms through the imaginary component.

Definition 2 ([18] (Complex-Order Derivative Operators)). *Based on the unified complex-order derivative operator $D^{\alpha \pm i\beta}$ defined above, we construct two real-valued conjugate operators for practical implementation. Let $\alpha \in \mathbb{R}$ and $\beta \in \mathbb{R}$. The two operators corresponding to the complex order $\alpha + j\beta$ are defined as:*

$$\varphi_1(\alpha, \beta)(f) = \frac{D^{\alpha + j\beta} + D^{\alpha - j\beta}}{2}(f), \tag{4}$$

$$\varphi_2(\alpha, \beta)(f) = \frac{D^{\alpha + j\beta} - D^{\alpha - j\beta}}{2j}(f). \tag{5}$$

where f is a real-valued function. Thus, φ_1 and φ_2 represent the real and imaginary parts of the complex-order derivative, respectively, ensuring that the position update remains in the real domain. Expanding f as a Taylor series around $z = 0$ yields explicit expressions for φ_1 and φ_2:

$$\begin{aligned} \varphi_1(\alpha, \beta) &= 1 - \alpha z^{-1} + \frac{1}{2}(\alpha^2 - \alpha - \beta^2) z^{-2} \\ &\quad - \frac{1}{6}\left[\alpha^3 - 3\alpha^2 + \alpha(2 - 3\beta^2) + 3\beta^2\right] z^{-3} + \cdots \end{aligned} \tag{6}$$

$$\begin{aligned} \varphi_2(\alpha, \beta) &= -\beta z^{-1} - \frac{1}{2}\beta(1 - 2\alpha) z^{-2} \\ &\quad - \frac{1}{6}\beta\left(3\alpha^2 - 6\alpha - \beta^2 + 2\right) z^{-3} - \cdots \end{aligned} \tag{7}$$

From Equations (6) *and* (7)*, it is evident that φ_1 primarily governs the attenuation amplitude of historical information, while φ_2 introduces phase modulation. Their combination enables refined control over the search trajectory.*

3. Classic GRO Algorithm

The classical GRO algorithm [9] is inspired by the historical event of the 19th-century Gold Rush. By simulating the behavior of gold prospectors searching for gold deposits, it constructs a search mechanism comprising three strategies: migration, mining, and collaboration. During the iterative process of the algorithm, each prospector (i.e., search individual) updates its position by executing one of these three operations, thereby progressively approaching the global optimal solution within the solution space.

3.1. Migration

When a miner moves toward the current optimal gold deposit, the position update formula is:

$$X_{i,d}(t+1) = X_{i,d}(t) + A_1 \times (C_1 \times X_{best} - X_{i,d}(t)). \tag{8}$$

Here, X_{best} denotes the current optimal prospector position, i.e., the optimal gold deposit location; $X_{i,d}(t)$ represents the current position of the i-th prospector in the d-th dimension; C_1 is a random vector within the range $[0, 2]$; and $A_1 = 1 + l_1(r_1 - \frac{1}{2})$, where r_1 is a random

https://doi.org/10.3390/computation14060124

vector in $[0, 1]$ and l_1 is the convergence factor. Figure 1 illustrates the 2D schematic diagram of this migration process.

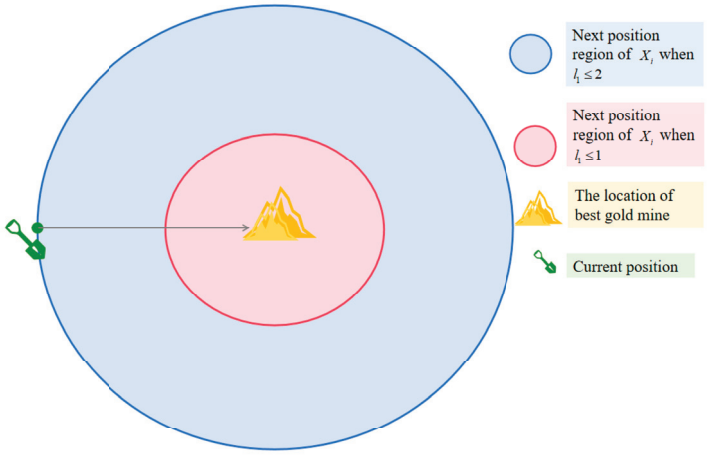

Figure 1. Migration schematic diagram (2D).

3.2. Mining

When a prospector performs local exploration near a randomly selected mining point, its position update formula is as follows:

$$X_{i,d}(t+1) = X_{g_1,d}(t) + A_2 \times (X_{i,d}(t) - X_{g_1,d}(t)). \tag{9}$$

Here, A_2 is a coefficient vector. When $|A_2| < 1$, the local exploitation strategy is executed; when $|A_2| > 1$, the random exploration strategy is executed. Figure 2 shows the 2D schematic diagram of this mining process.

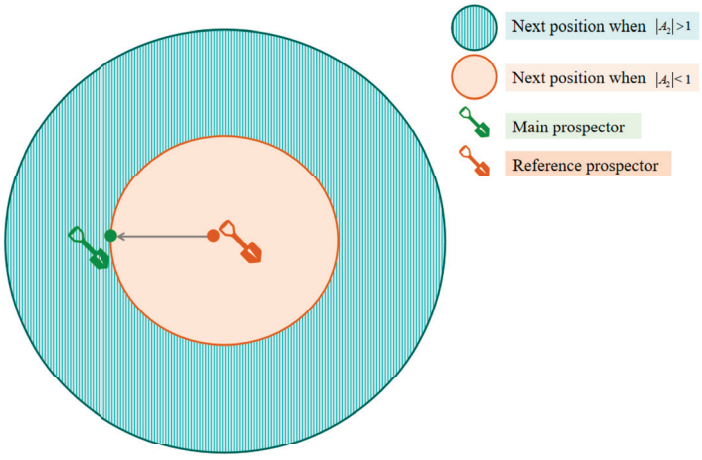

Figure 2. Mining schematic diagram (2D).

3.3. Collaboration

Two prospectors jointly determine the search area, while a third prospector searches randomly within this area:

$$X_{i,d}(t+1) = X_{i,d}(t) + r_1 \times (X_{g_1,d}(t) - X_{g_2,d}(t)). \tag{10}$$

where $X_{g_1,d}(t)$ and $X_{g_2,d}(t)$ denote the positions of the two randomly selected prospectors; r_1 is the random coefficient used for random search within the area. Figure 3 illustrates the 2D schematic diagram of this collaboration mechanism.

https://doi.org/10.3390/computation14060124

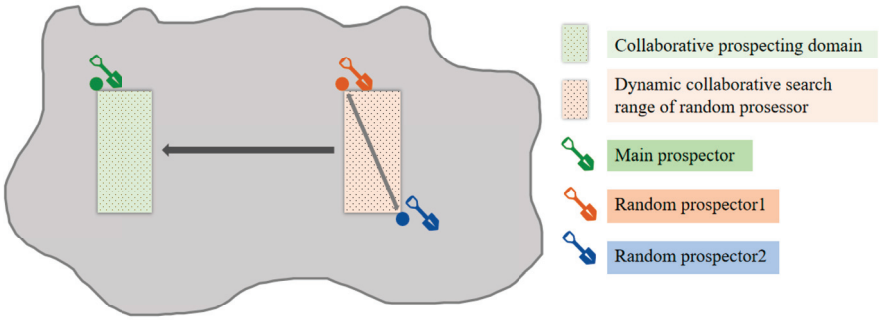

Figure 3. Collaboration schematic diagram (2D).

The pseudocode of the classical GRO algorithm is shown in Algorithm 1:

Algorithm 1: Classical GRO algorithm.

begin;
Initialize t, l_1, l_2;
while *the termination criteria is not met* **do**
  for $i = 1$ **to** N **do**
    Randomly select $g_1, g_2 \in \{1, \ldots, N\} \setminus \{i\}$, $g_1 \neq g_2$;
    Update parameters l_1, l_2;
    Update X_{best};
    $m = \text{rand}(0, 1)$;
    if $m < 1/3$ **then**
      for $d = 1$ **to** D **do**
        $r_1 = \text{rand}(0, 1)$;
        $X_{i,d}(t+1) = X_{i,d}(t) + r_1 \times (X_{g_1,d}(t) - X_{g_2,d}(t))$;
      end
    else if $m < 2/3$ **then**
      for $d = 1$ **to** D **do**
        $r_1 = \text{rand}(0, 1)$;
        $A_2 = 2 \times l_2 \times r_1 - l_2$;
        $X_{i,d}(t+1) = X_{g_1,d}(t) + A_2 \times (X_{i,d}(t) - X_{g_1,d}(t))$;
      end
    else
      for $d = 1$ **to** D **do**
        $r_1 = \text{rand}(0, 1)$, $r_2 = \text{rand}(0, 1)$;
        $C_1 = 2 \times r_2$;
        $A_1 = 1 + l_1 \times (r_1 - 0.5)$;
        $X_{i,d}(t+1) = X_{i,d}(t) + A_1 \times (C_1 \times X_{best} - X_{i,d}(t))$;
      end
    end
  end
  $t = t + 1$;
end
end;

4. The Proposed CoGRO Algorithm

4.1. Initialization Based on Chaotic LCS1

GRO suffers from uneven initial population distribution, which may cause the algorithm to easily get stuck in local optima [20] and exhibit low search efficiency. To generate a more uniformly distributed and diverse initial population [21], we incorporate chaos into the initialization process [22]. Leveraging the ergodicity [23], randomness [24], and sensitivity [25] to initial conditions of chaotic mappings, this approach effectively avoids issues such as population clustering and premature convergence that may arise from random initialization, thereby establishing a solid foundation for subsequent iterative searches. Among various chaotic mappings, LCS1 is a composite chaotic mapping, integrating the dynamic characteristics of both the Logistic and Sine mappings. Compared to traditional Logistic or Tent mappings, LCS1 exhibits more complex chaotic behavior and a more uniform ergodic distribution. This enables it to cover the solution space more comprehensively, thereby further enhancing population diversity and global exploration capabilities [26].

Therefore, we employ the LCS1 mapping to generate chaotic sequences for each explorer across dimensions, obtaining initial values with good exploratory properties through iterative computation:

$$x_{n+1} = \Phi_{\mathrm{LCS1}}(x_n; r) = \frac{1}{2}\left\{1 + \cos\left[\pi\left(4rx_n(1 - x_n) + (1 - r)\sin(\pi x_n) - 0.5\right)\right]\right\}. \quad (11)$$

where $x_n \in [0, 1]$ is the chaotic variable value at the n-th iteration, and $r \in (0, 1)$ is a hybrid control parameter that adjusts the complexity of the chaotic behavior. By combining the dynamics of both maps, the LCS1 generator produces chaotic sequences with more uniform distribution characteristics compared to traditional pseudo-random number generators.The uniform distribution property of LCS1 is supported by the Frobenius–Perron framework: Lawnik [27] proved that chaotic maps with constant Frobenius–Perron density generate uniformly distributed sequences, while Anikin et al. [28] established the general conditions for such behavior. As a composite map, LCS1 inherits favorable ergodic properties from its Logistic and Sine components [29]. During the population initialization phase, N chaotic sequences of different dimensions are first generated using Equation (11). These sequences are then mapped onto the decision variable's search space $[L, UI]$ via a linear transformation:

$$X_{i,d} = L_d + (U_d - L_d) \cdot x_{i,d}, \quad i = 1, \ldots, N,\ d = 1, \ldots, D. \quad (12)$$

where N is the population size, D is the problem dimension, L_d and U_d are the lower and upper bounds of the d-th dimension, respectively, and $x_{i,d}$ is the chaotic value generated by the LCS1 map. This initialization strategy ensures that initial individuals are uniformly distributed across the solution space, thereby providing a solid foundation for subsequent global search by preventing premature clustering and enhancing the algorithm's exploratory capacity from the very first generation.

The final initialization matrix is obtained as follows:

$$M_{GPchaos} = \begin{bmatrix} x_{11} & x_{12} & \cdots & x_{1D} \\ x_{21} & x_{22} & \cdots & x_{2D} \\ \vdots & \vdots & \ddots & \vdots \\ x_{N1} & x_{N2} & \cdots & x_{ND} \end{bmatrix}. \quad (13)$$

This process ensures that the initial population possesses sufficient randomness and spatial coverage while satisfying the constraints, thereby enhancing the classical GRO into a GRO incorporating chaotic initialization.

https://doi.org/10.3390/computation14060124

4.2. The Complex-Order Position Adaptation Laws

Although GRO features a simple structure and is easy to implement, it relies solely on current-time information during iterative updates, lacking the ability to remember and utilize historical search experience. This limitation restricts the algorithm's capacity to model long-term dependencies in complex optimization environments. When confronted with multi-modal or high-dimensional problems, it tends to get stuck in local optima and exhibits reduced convergence efficiency.

As a generalization of fractional derivatives, complex-order derivatives possess infinite memory capacity and continuous state ranges. Recent studies have demonstrated that fractional-order operators inherently maintain population diversity and prevent premature convergence. Specifically, Yousri et al. [30] proved that the fractional-order memory mechanism enables effective sharing of best knowledge and historical experiences among search agents, with the explicit goal of escaping local solutions and avoiding immature convergence. Similarly, Fernandez et al. [31] established that fractional-order operators enhance convergence robustness and achieve a superior trade-off between exploration and exploitation through their intrinsic memory and non-local characteristics. The mathematical treatment of fractional systems with inherent delays or memory effects is crucial for stability, and the use of complex-order derivatives allows for a more nuanced modulation of this historical information during the optimization trajectory, analogous to the fractional differential transformation method applied to fractional delay differential equations [32].

As a natural extension of fractional-order calculus, complex-order derivatives inherit and further enhance these beneficial properties. They effectively capture historical information within particle trajectories, enabling the algorithm to balance current states with past paths during search. This enhances the ability to escape local optima, improving both solution accuracy and convergence efficiency.

The practical validity of combining fractional/complex-order operators with heuristic search has been demonstrated beyond optimization algorithm design. Recent studies have successfully applied such hybrid approaches to solve ill-posed inverse problems for fractional diffusion equations, where parameters such as derivative orders and boundary conditions are identified using metaheuristic algorithms [33]. This cross-domain success further supports the rationale for embedding complex-order mechanisms into the GRO framework.

Therefore, based on the integer-order version of the gold rush optimizer incorporating chaotic initialization, we introduce new parameters α and β. By applying Equation (2) to refine the core formula of GRO, we derive the current complex-order gold rush optimizer—CoGRO. The specific improvements are as follows:

First, for the migration strategy: when the iteration count $t \leq 4$, the original integer-order gold rush optimizer formula is retained. When $t > 4$, Equation (8) is rewritten as:

$$X_{i,d}(t+1) - X_{i,d}(t) = A_1 \cdot D_1. \tag{14}$$

On the left is the discrete version of the derivative with order $\alpha = 1$. Setting $T = 1$ yields the following expression:

$$D^{\alpha}[X_{i,d}(t+1)] = A_1 \cdot D_1. \tag{15}$$

The G-L definition based on fractional differentiation concepts [17] is:

$$D^{\alpha}x(t) = \frac{1}{T^{\alpha}} \sum_{k=0}^{r} (-1)^k \frac{\Gamma(\alpha+1)x(t-kh)}{\Gamma(k+1)\Gamma(\alpha-k+1)}. \tag{16}$$

https://doi.org/10.3390/computation14060124

From the perspective of complex order, the order of the position derivative can be further generalized to the conjugate complex pair $\alpha \pm i\beta$, namely:

$$D^{\alpha \pm i\beta} x(t) = \frac{1}{T^{\alpha \pm i\beta}} \sum_{k=0}^{r} (-1)^k \frac{\Gamma(\alpha \pm i\beta + 1) x(t - kh)}{\Gamma(k+1)\Gamma(\alpha \pm i\beta - k + 1)}. \tag{17}$$

This approach not only preserves smoothness and memory effects but also introduces frequency-domain selection and phase modulation mechanisms, thereby enabling dynamic offset control over the evolution direction. Based on the first three terms of the differential in Equation (8), we derive the migration formula for complex-order GRO:

$$\begin{aligned} X_{i,d}(t+1) = {} & \alpha \times X_{i,d}(t) - \frac{1}{2}(\alpha^2 - \alpha - \beta^2) \times X_{i,d}(t-1) \\ & + \frac{1}{6}(\alpha^3 - 3\alpha^2 + \alpha(2 - 3\beta^2) + 3\beta^2) \times X_{i,d}(t-2) \\ & - \frac{1}{24}(\alpha^4 + \beta^4 - 6\alpha^3 - 6\alpha^2\beta^2 + 11(\alpha^2 - \beta^2) + 18\alpha\beta^2 - 6\alpha) \times X_{i,d}(t-3) \\ & + A_1 \times (C_1 \times X_{best} - X_{i,d}(t)). \end{aligned} \tag{18}$$

Similarly, we have applied the same improvements to the collaboration formula. When $t \leq 4$, we continue to use Equation (10); when $t > 4$, the collaboration formula is modified as follows:

$$\begin{aligned} X_{i,d}(t+1) = {} & \alpha \times X_{i,d}(t) - \frac{1}{2}(\alpha^2 - \alpha - \beta^2) \times X_{i,d}(t-1) \\ & + \frac{1}{6}(\alpha^3 - 3\alpha^2 + \alpha(2 - 3\beta^2) + 3\beta^2) \times X_{i,d}(t-2) \\ & - \frac{1}{24}(\alpha^4 + \beta^4 - 6\alpha^3 - 6\alpha^2\beta^2 + 11(\alpha^2 - \beta^2) + 18\alpha\beta^2 - 6\alpha) \times X_{i,d}(t-3) \\ & + r_1 \times (X_{g_1,d}(t) - X_{g_2,d}(t)). \end{aligned} \tag{19}$$

Since the mining formula Equation (9) does not incorporate the previous position information $X_{i,d}(t)$ into $X_{i,d}(t+1)$, it is not subject to multi-order optimization and retains the original formula. At this point, we have completed the complex-order improvement of the algorithm. It can be seen from Equations (18) and (19) that the position update of a particle depends not only on its own position at the previous moment but also incorporates historical state information up to $t-3$, exhibiting short-memory characteristics. The choice of truncation depth $r-3$ is justified by the Taylor series expansion of the complex-order operators: the coefficients of the series decay rapidly as the order increases. For $|\alpha|, |\beta| < 1$, the magnitude of the coefficient for the z^{-4} term is an order of magnitude smaller than that of the z^{-3} term, and the contribution of historical terms beyond $t-3$ becomes negligible. Therefore, retaining terms up to $t-3$ captures the dominant memory effects while maintaining computational efficiency. This feature helps maintain the diversity and uniform distribution of the population to a certain extent, laying the foundation for global search. It is worth noting that the position update at each moment is associated with the position data from the previous three moments, allowing the algorithm to dynamically adjust the optimization direction based on the particle's historical motion trajectory, thereby enhancing the accuracy of local search and facilitating faster convergence to the global optimum.The pseudocode of the proposed CoGRO algorithm is shown in Algorithm 2.

https://doi.org/10.3390/computation14060124

Algorithm 2: The proposed CoGRO algorithm.

begin;
Chaotic initialization using LCS1 mapping, and setting t = 1;
while *the termination criteria is not met* **do**
  Initialize l_1, l_2;
  for $i = 1$ **to** N **do**
    Randomly select $g_1, g_2 \in \{1, \ldots, N\} \setminus \{i\}$, $g_1 \neq g_2$;
    Update parameters l_1, l_2;
    Update X_{best};
    $m = \text{rand}(0, 1)$;
    if $m < 1/3$ **then**
      for $d = 1$ **to** D **do**
        $r_1 = \text{rand}(0, 1)$;
        if $t < 4$ **then**
          $X_{i,d}(t+1) = X_{i,d}(t) + r_1 \times (X_{g_1,d}(t) - X_{g_2,d}(t))$;
        else
          $X_{i,d}(t+1) = \alpha \times X_{i,d}(t) - \frac{1}{2}(\alpha^2 - \alpha - \beta^2) \times X_{i,d}(t-1) + \frac{1}{6}(\alpha^3 - 3\alpha^2 + \alpha(2 - 3\beta^2) + 3\beta^2) \times X_{i,d}(t-2) - \frac{1}{24}(\alpha^4 + \beta^4 - 6\alpha^3 - 6\alpha^2\beta^2 + 11(\alpha^2 - \beta^2) + 18\alpha\beta^2 - 6\alpha) \times X_{i,d}(t-3) + r_1 \times (X_{g_1,d}(t) - X_{g_2,d}(t))$;
        end
      end
    else if $m < 2/3$ **then**
      for $d = 1$ **to** D **do**
        $r_1 = \text{rand}(0, 1)$;
        $A_2 = 2 \times l_2 \times r_1 - l_2$;
        $X_{i,d}(t+1) = X_{g_1,d}(t) + A_2 \times (X_{i,d}(t) - X_{g_1,d}(t))$;
      end
    else
      for $d = 1$ **to** D **do**
        $r_1 = \text{rand}(0, 1)$, $r_2 = \text{rand}(0, 1)$;
        $C_1 = 2 \times r_2$;
        $A_1 = 1 + l_1 \times (r_1 - 0.5)$;
        if $t < 4$ **then**
          $X_{i,d}(t+1) = X_{i,d}(t) + A_1 \times (C_1 \times X_{best} - X_{i,d}(t))$;
        else
          $X_{i,d}(t+1) = \alpha \times X_{i,d}(t) - \frac{1}{2}(\alpha^2 - \alpha - \beta^2) \times X_{i,d}(t-1) + \frac{1}{6}(\alpha^3 - 3\alpha^2 + \alpha(2 - 3\beta^2) + 3\beta^2) \times X_{i,d}(t-2) - \frac{1}{24}(\alpha^4 + \beta^4 - 6\alpha^3 - 6\alpha^2\beta^2 + 11(\alpha^2 - \beta^2) + 18\alpha\beta^2 - 6\alpha) \times X_{i,d}(t-3) + A_1 \times (C_1 \times X_{best} - X_{i,d}(t))$;
        end
      end
    end
  end
  $t = t + 1$;
end
end;

https://doi.org/10.3390/computation14060124

5. Performance Test of the CoGRO

To comprehensively evaluate the optimization performance of the CoGRO algorithm and the effectiveness of its improvement mechanisms, four interrelated sets of numerical experiments are designed in this study: parameter sensitivity analysis, truncation depth analysis, ablation study, and comparative experiments.

5.1. Parameters' Sensitivity Analysis of the CoGRO

To ensure the performance stability and the rationality of parameter selection for the proposed CoGRO algorithm, a systematic sensitivity analysis is conducted on its key control parameters, α and β. The experiments are carried out using the CEC2022 benchmark suite as the evaluation platform. This suite comprises 12 complex optimization problems with distinct mathematical characteristics (denoted as Function 1 to 12), which comprehensively reflect the algorithm's performance on unimodal, multimodal, hybrid, and composition functions. The specific definitions and mathematical properties of the test functions are presented in Table 1.

Table 1. Benchmark functions adopted from CEC2022.

	No.	Functions	F_i^*
Unimodal Function	1	Shifted and full Rotated Zakharov Function	300
Basic Functions	2	Shifted and full Rotated Rosenbrock's Function	400
	3	Shifted and full Rotated Expanded Schaffer's F6 Function	600
	4	Shifted and full Rotated Non-Continuous Rastrigin's Function	800
	5	Shifted and full Rotated Levy Function	900
Hybrid Functions	6	Hybrid Function 1 (N = 3)	1800
	7	Hybrid Function 2 (N = 6)	2000
	8	Hybrid Function 3 (N = 5)	2200
Composition Functions	9	Composition Function 1 (N = 5)	2300
	10	Composition Function 2 (N = 4)	2400
	11	Composition Function 3 (N = 5)	2600
	12	Composition Function 4 (N = 6)	2700
Search range: $[-100, 100]^D$			

We conducted 121 test runs on each test function, varying α and β from 0 to 1 in increments of 0.1. Each experiment employed a population size of 30 particles, a maximum iteration count of $D \times 1000$ (where D is the dimension, $D = 10$), and was repeated 30 times. Evaluation is based on three metrics: Mean, Standard Deviation (std), and Minimum (min). The total computational cost is approximately $121 \times 30 \times 12 \times 10{,}000 = 4.356 \times 10^8$ function evaluations, which is acceptable given the offline nature of parameter tuning and is consistent with similar studies in the literature. The final results display the optimal parameter pairs adapted for each test function. Based on the comprehensive sensitivity analysis across all 12 test functions, CoGRO maintains competitive performance when α ranges from 0.5 to 0.9 and β ranges from 0 to 0.3. Below, we present the top five parameter combinations for Function 5 in Table 2 and the parameter sensitivity analysis heatmap in Figure 4. Detailed simulation results for all functions are available in Appendix A.

As shown in the table, the optimal parameter combination is $(\alpha = 0.7, \beta = 0.4)$, which achieves a mean fitness of 9.0000×10^2 with a remarkably low standard deviation of 1.3257×10^{-4}. This indicates that the configuration not only delivers high solution accuracy but also demonstrates exceptional stability across repeated runs. Moreover, its minimum value exactly reaches the theoretical optimum of 9.0000×10^2, further confirming its convergence reliability. The second-ranked combination $(\alpha = 1.0, \beta = 0.0)$ attains the

https://doi.org/10.3390/computation14060124

same mean fitness yet exhibits a standard deviation of 2.0019×10^{-2}—approximately two orders of magnitude higher than that of the top configuration. This contrast highlights that while several parameter pairs can yield comparable solution accuracy, they differ considerably in terms of algorithmic stability, underscoring the importance of considering both precision and robustness during parameter selection. The remaining top-ranked combinations suggest that configurations with low α and high β can also produce competitive results, albeit with slightly higher variability (standard deviations around 2.00×10^{-2}). This reflects a certain degree of complementarity between the two parameters—the phase modulation governed by β can partially compensate for the memory attenuation controlled by α.

Table 2. Top 5 Parameter Combinations for Function 5.

Rank	Alpha	Beta	Mean	Std	Min
1	0.7	0.4	9.0000×10^2	1.3257×10^{-4}	9.0000×10^2
2	1.0	0.0	9.0000×10^2	2.0019×10^{-2}	9.0000×10^2
3	0.2	0.8	9.0000×10^2	2.0031×10^{-2}	9.0000×10^2
4	0.1	0.9	9.0000×10^2	2.0009×10^{-2}	9.0000×10^2
5	0.0	0.9	9.0000×10^2	2.0001×10^{-2}	9.0000×10^2

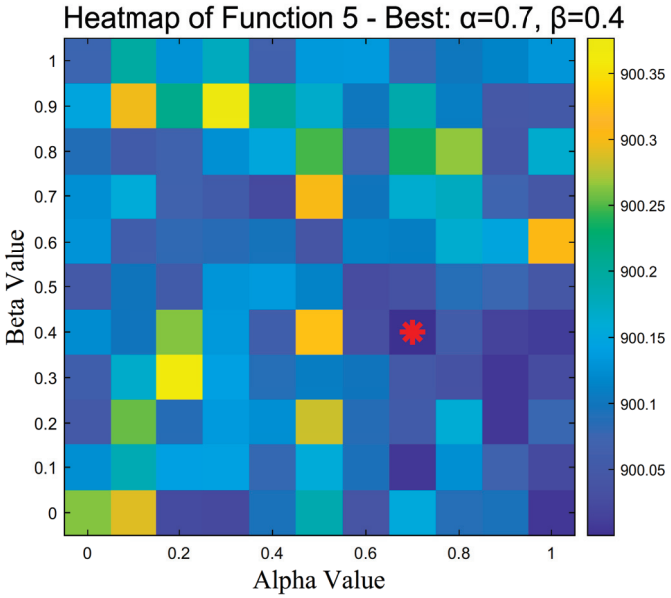

Figure 4. Heatmap of Function 5.

As illustrated in the figure, the region around ($\alpha = 0.7, \beta = 0.4$) exhibits the deepest blue coloration, indicating that this parameter combination achieves the best performance on Function 5, while also confirming that parameter selection significantly influences algorithmic performance. Examining the α axis reveals that when β is held constant, increasing α from 0 to 0.7 leads to progressive performance improvement, whereas values exceeding 0.8 result in slight degradation while maintaining relative stability. Along the β axis, optimal performance concentrates in the moderate range of $\beta = 0.3$ to 0.5, with either excessively high or low β values causing marginal performance deterioration. The heatmap displays a distinct diagonal distribution pattern, suggesting an interaction between α and β: larger α values require moderate β values to achieve optimal performance, while smaller α values can still yield acceptable results when paired with higher β values. Finally, the predominantly light and uniform coloration across most regions indicates that the CoGRO

https://doi.org/10.3390/computation14060124

algorithm maintains good robustness over a wide parameter range, with performance degradation occurring only in localized peripheral areas.

From the above parameter sensitivity analysis experiments, it can be seen that the real part α controls the decay rate of historical information: a larger α preserves more past information to enhance local exploitation, while a smaller α emphasizes recent states to promote exploration. The imaginary part β introduces an oscillatory component $e^{-i\beta \ln(t)}$ that periodically modulates memory contributions, thereby reducing directional correlation among particles and preventing synchronous convergence. As demonstrated in the complex-order PSO literature [18,19], the optimal parameter region is $\alpha \in [0.5, 0.9]$ and $\beta \in [0, 0.3]$, within which the algorithm achieves a balance between exploration and exploitation. The convergence curves in Appendix C confirm that the algorithm converges stably within this parameter range.

5.2. Truncation Depth Analysis

To quantitatively justify the choice of truncation depth $r = 3$ in Equations (18) and (19), we conducted comparative experiments with different truncation depths $r = 1, 2, 3$ on the CEC2022 benchmark suite. The algorithm with truncation depth 1 is denoted as CoGRO1, with depth 2 as CoGRO2, and with depth 3 as CoGRO3. Except for the truncation depth, all other parameter settings are identical among the three algorithms. All experiments were conducted at a fixed dimension of $D = 10$. To ensure fair comparison, universal algorithmic parameters were held constant across all methods. Specifically, the population size was set to $D \times 10$, and the maximum number of iterations was set to $D \times 1000$. Each optimization result was obtained from 30 independent runs to ensure statistical reliability. The experimental results for Function 4 are presented in the Figure 5 and Table 3 below, and all detailed results are provided in Appendix B.

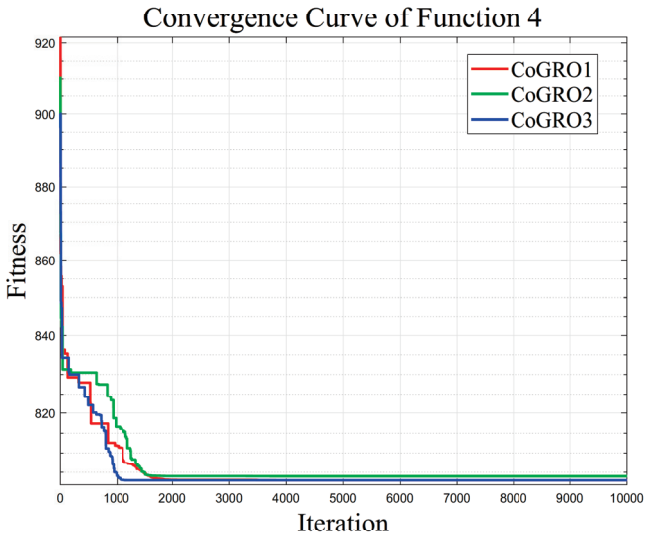

Figure 5. Convergence Curve of Function 4.

Table 3. Results of the truncation depth analysis for Function 4.

Method	Mean	Std	Best	Rank
CoGRO1	8.0689×10^2	1.8188×10^0	8.0299×10^2	3
CoGRO2	8.0638×10^2	3.5632×10^0	8.0398×10^2	2
CoGRO3	$\mathbf{8.0571 \times 10^2}$	$\mathbf{2.2746 \times 10^0}$	$\mathbf{8.0298 \times 10^2}$	**1**

https://doi.org/10.3390/computation14060124

As shown in the results of Function 4, CoGRO3 achieves the optimal performance in terms of mean fitness, best fitness, and overall rank. Meanwhile, its convergence curve exhibits a faster descent rate, enabling the algorithm to converge to the vicinity of the optimal solution earlier and maintain stable performance thereafter. These results demonstrate that the complex-order improvement strategy significantly enhances the solution accuracy and convergence efficiency of the algorithm and enables a superior exploration–exploitation balance on this test function.

5.3. Ablation Study of CoGRO

An ablation study systematically removes or modifies specific components of a model to observe their impact on overall performance, thereby validating the contribution of each component to the model's effectiveness. This approach functions as a controlled variable method. In this work, the complex-order gold rush optimizer (CoGRO) incorporates two key enhancements: the application of complex-order derivatives (Module A) and chaotic initialization (Module B). To evaluate the individual contribution of these modules, three ablated variants of CoGRO were developed: CoGRO-A (with Module A removed), CoGRO-B (with Module B removed), and CoGRO-AB (with both modules removed).

The performance of CoGRO, CoGRO-A, CoGRO-B, and CoGRO-AB was evaluated on the 12 benchmark functions from the CEC2022 test suite. All experiments were conducted at a fixed dimension of $D = 10$. To ensure fair comparison, universal algorithmic parameters were held constant across all methods. Specifically, the population size was set to $D \times 10$, and the maximum number of iterations was set to $D \times 1000$. Each optimization result was obtained from 30 independent runs to ensure statistical reliability. Following the parameter sensitivity analysis in Section 5.3, the CoGRO and CoGRO-B algorithms adopted the optimal α and β parameter combinations for each respective function. For CoGRO-A and CoGRO, the LCS1 coupling coefficient was maintained at 0.7, with all other parameters consistent with the standard GRO algorithm. Algorithmic performance was assessed using three key metrics: mean, standard deviation, and minimum value. The comprehensive results are presented in Table 4. The experimental outcomes demonstrate that CoGRO-AB—the variant with both modules removed—exhibited the poorest performance. This finding substantiates the critical contribution of both Module A and Module B to the overall efficacy of the CoGRO algorithm. For a detailed exposition of the results, please refer to Appendix C.

Table 4. Comparison Results.

Method	CoGRO-AB	CoGRO-A	CoGRO-B	CoGRO
Total Rank	4	3	2	1

5.4. Comparative Experiments

To validate the advantage of complex-order over fractional-order ($\beta = 0$), we first compare CoGRO with its fractional-order counterpart FGRO (i.e., CoGRO with $\beta = 0$) under identical parameter configurations ($\alpha = 0.7$, population size $N = D \times 10$, maximum iterations $T_{\max} = D \times 1000$) without per-function parameter tuning. Table 5 presents the comparison results on CEC2022 Functions 1 to 12.

The results demonstrate that CoGRO outperforms FGRO on the majority of test functions, achieving higher solution accuracy and better stability. This confirms that introducing the imaginary part β—i.e., extending fractional-order to complex-order—effectively enhances the algorithm's global search capability and convergence reliability.

https://doi.org/10.3390/computation14060124

Table 5. Comparison results of FGRO vs. CoGRO on CEC2022 Functions 1–12.

	Function 1				Function 2			
Method	Mean	Std	Best	w-Test	Mean	Std	Best	w-Test
FGRO	3.0000×10^{2}	8.6926×10^{-8}	3.0000×10^{2}	+	4.0003×10^{2}	3.8646×10^{-2}	4.0000×10^{2}	=
CoGRO	$\mathbf{3.0000} \times 10^{2}$	$\mathbf{8.3918} \times 10^{-9}$	$\mathbf{3.0000} \times 10^{2}$		$\mathbf{4.0004} \times 10^{2}$	$\mathbf{4.1153} \times 10^{-2}$	$\mathbf{4.0000} \times 10^{2}$	
	Function 3				Function 4			
Method	Mean	Std	Best	w-Test	Mean	Std	Best	w-Test
FGRO	6.0000×10^{2}	3.6055×10^{-7}	6.0000×10^{2}	+	8.0593×10^{2}	2.3814×10^{0}	8.0199×10^{2}	+
CoGRO	$\mathbf{6.0000} \times 10^{2}$	$\mathbf{2.5946} \times 10^{-7}$	$\mathbf{6.0000} \times 10^{2}$		$\mathbf{8.0353} \times 10^{2}$	$\mathbf{1.1311} \times 10^{0}$	$\mathbf{8.0099} \times 10^{2}$	
	Function 5				Function 6			
Method	Mean	Std	Best	w-Test	Mean	Std	Best	w-Test
FGRO	9.0000×10^{2}	6.2804×10^{-9}	9.0000×10^{2}	+	2.1098×10^{3}	6.0157×10^{2}	1.8368×10^{3}	+
CoGRO	$\mathbf{9.0000} \times 10^{2}$	$\mathbf{6.0456} \times 10^{-9}$	$\mathbf{9.0000} \times 10^{2}$		$\mathbf{1.8475} \times 10^{3}$	$\mathbf{3.0192} \times 10^{1}$	$\mathbf{1.8011} \times 10^{3}$	
	Function 7				Function 8			
Method	Mean	Std	Best	w-Test	Mean	Std	Best	w-Test
FGRO	2.0009×10^{3}	5.6468×10^{-1}	2.0000×10^{3}	+	2.2057×10^{3}	6.7043×10^{0}	2.2001×10^{3}	+
CoGRO	$\mathbf{2.0004} \times 10^{3}$	$\mathbf{5.4691} \times 10^{-1}$	$\mathbf{2.0000} \times 10^{3}$		$\mathbf{2.2044} \times 10^{3}$	$\mathbf{3.8543} \times 10^{0}$	$\mathbf{2.2003} \times 10^{3}$	
	Function 9				Function 10			
Method	Mean	Std	Best	w-Test	Mean	Std	Best	w-Test
FGRO	2.5293×10^{3}	3.7535×10^{-11}	2.5293×10^{3}	+	2.5071×10^{3}	2.6542×10^{1}	2.5001×10^{3}	+
CoGRO	$\mathbf{2.5293} \times 10^{3}$	$\mathbf{2.7141} \times 10^{-12}$	$\mathbf{2.5293} \times 10^{3}$		$\mathbf{2.5001} \times 10^{3}$	$\mathbf{2.7711} \times 10^{-2}$	$\mathbf{2.5000} \times 10^{3}$	
	Function 11				Function 12			
Method	Mean	Std	Best	w-Test	Mean	Std	Best	w-Test
FGRO	2.6100×10^{3}	5.4772×10^{1}	2.6000×10^{3}	=	2.8642×10^{3}	1.1465×10^{0}	2.8614×10^{3}	=
CoGRO	$\mathbf{2.6150} \times 10^{3}$	$\mathbf{6.0420} \times 10^{1}$	$\mathbf{2.6000} \times 10^{3}$		$\mathbf{2.8641} \times 10^{3}$	$\mathbf{1.3635} \times 10^{0}$	$\mathbf{2.8612} \times 10^{3}$	

Having established the advantage of complex-order over fractional-order, we further evaluate CoGRO against several classical and state-of-the-art algorithms on the CEC2022 benchmark suite, including Particle Swarm Optimization (PSO), Grey Wolf Optimizer (GWO), Genetic Algorithm (GA), as well as two modern highly competitive algorithms: EA4eig and MadDE. To maintain fairness and scientific validity, all algorithms are configured with identical population sizes and termination criteria: the population size is set to $N = D \times 10$, where $D = 10$ denotes the problem dimension, and the maximum number of iterations is set to $T_{\max} = D \times 1000$. The specific control parameters for each comparative algorithm are configured strictly following the recommendations in their respective original literature.

To mitigate the impact of stochastic variability on the experimental outcomes, each algorithm is independently executed 30 times on every test function. The best value (Best), mean (Mean), standard deviation (Std), Wilcoxon rank-sum test results (w-test), and average CPU time (Avg Time) obtained from the 30 runs are recorded as performance evaluation metrics. The mean value reflects the convergence accuracy of the algorithm, the standard deviation assesses its stability and robustness, the w-test evaluates the statistical significance of performance differences between algorithms, and the average CPU time measures the computational efficiency. Taking the unimodal Function 10 as an illustrative example, Table 6 summarizes the statistical results of the compared algorithms on this function, and Figure 6 depicts their average convergence curves. Complete experimental results and convergence curves for the remaining functions are presented in Appendix D.

https://doi.org/10.3390/computation14060124

Table 6. Comparison Results of Function 10.

Method	Best	Mean	Std	Avg Time	w-Test
CoGRO	$\mathbf{2.50 \times 10^3}$	$\mathbf{2.50 \times 10^3}$	$\mathbf{2.77 \times 10^{-2}}$	**8.42**	
EA4eig	2.50×10^3	2.50×10^3	2.89×10^{-2}	5.90	+
GA	2.50×10^3	2.54×10^3	5.82×10^1	2.95	+
GWO	2.50×10^3	2.53×10^3	4.96×10^1	3.73	+
MadDE	2.50×10^3	2.50×10^3	1.91×10^1	6.85	+
PSO	2.50×10^3	2.50×10^3	1.67×10^{-1}	3.64	+

Note: "+" denotes that CoGRO is significantly better than the corresponding algorithm ($p < 0.05$).

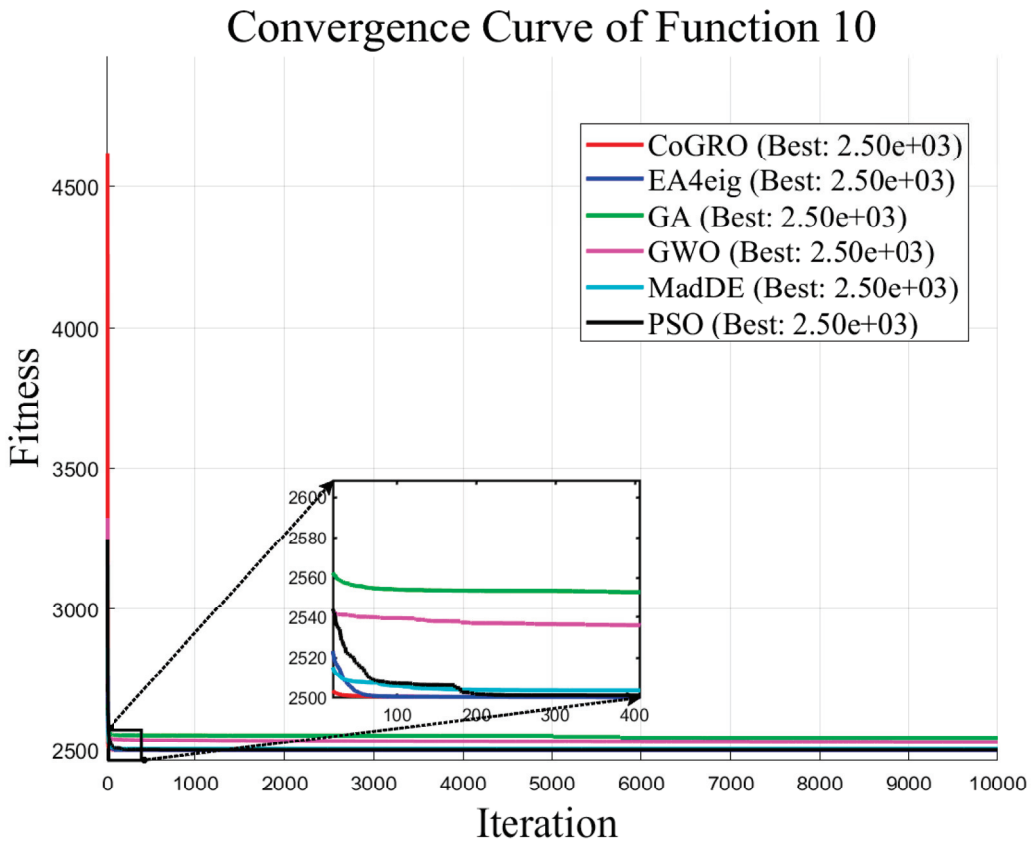

Figure 6. Convergence curve of Function 10.

On Function 10, CoGRO matches the best value (2.50×10^3) and mean of EA4eig, MadDE, and PSO. CoGRO achieves the lowest standard deviation (2.77×10^{-2}) among all algorithms, demonstrating the best convergence consistency and robustness. CoGRO (8.42 s) is slower than GA, PSO, GWO, and EA4eig but comparable to MadDE. Wilcoxon tests confirm CoGRO's statistically significant performance. Overall, CoGRO reaches the global optimum with superior stability, offering clear advantages in accuracy and robustness despite slightly higher computational cost.

From Table 7, it can be seen that CoGRO achieves the highest number of best results (9 out of 12 functions), demonstrating superior overall performance. Compared to EA4eig, CoGRO shows comparable performance with a slight advantage (3 better, 3 worse, 6 equal) while significantly outperforming GA, GWO, and PSO (12 better, 0 worse). Although MadDE occasionally surpasses CoGRO (1 worse), it fails to achieve the best on any function, highlighting CoGRO's robustness and effectiveness.

https://doi.org/10.3390/computation14060124

Table 7. Summary of Wilcoxon test results.

w-Test	Better	Equal	Worse	Best
CoGRO				9
EA4eig	3	6	3	3
GA	12	0	0	0
GWO	12	0	0	0
MadDE	6	5	1	0
PSO	12	0	0	0

6. Conclusions

This paper extends the classical GRO algorithm based on complex calculus theory, proposing the CoGRO algorithm, which integrates chaotic initialization and a complex-order update mechanism. The effectiveness of the key improvement strategies is systematically evaluated on the CEC2022 benchmark suite through parameter sensitivity analysis and ablation experiments. The results indicate that chaotic initialization significantly enhances population diversity, while the complex-order derivative operator endows the algorithm with long-term memory capabilities for historical information. Their combined effect effectively strengthens CoGRO's global search accuracy and convergence stability. Furthermore, comparative experiments with classical algorithms, including PSO, GA, and GWO, confirm that CoGRO exhibits significant advantages in both solution accuracy and convergence efficiency. Although there is still room for improvement in local performance aspects such as convergence speed, CoGRO's overall optimization capability is superior to that of several existing comparison algorithms. Future work will focus on introducing adaptive parameter adjustment mechanisms and validating the algorithm's application in practical engineering optimization problems.

Author Contributions: Methodology, H.M.; software, X.W.; validation and data curation, L.Y. and X.L.; writing—original draft preparation, S.C.; writing—review and editing, T.W. and X.L.; supervision and project administration, T.W. All authors have read and agreed to the published version of the manuscript.

Funding: This research was funded by the opening project of the State Key Laboratory of Autonomous Intelligent Unmanned Systems (ZZKF2025-1-10).

Data Availability Statement: The original contributions presented in this study are included in the article. Further inquiries can be directed to the corresponding author.

Conflicts of Interest: The authors declare no conflicts of interest.

Appendix A

Table A1. Top 5 parameter combinations for Functions 1–6.

Function 1					Function 2				
(α, β)	Mean	Std	Best	Rank	(α, β)	Mean	Std	Best	Rank
(1.0, 0.0)	3.0000×10^{2}	1.0911×10^{-13}	3.0000×10^{2}	1	(0.7, 0.3)	4.0003×10^{2}	5.2822×10^{-2}	4.0000×10^{2}	1
(0.6, 0.5)	3.0002×10^{2}	3.1769×10^{-2}	3.0000×10^{2}	2	(0.5, 0.5)	4.0022×10^{2}	8.9106×10^{-1}	4.0000×10^{2}	2
(0.9, 0.2)	3.0002×10^{2}	3.8159×10^{-2}	3.0000×10^{2}	3	(0.8, 0.3)	4.0027×10^{2}	9.5797×10^{-1}	4.0000×10^{2}	3
(1.0, 0.1)	3.0003×10^{2}	6.8814×10^{-2}	3.0000×10^{2}	4	(0.6, 0.0)	4.0029×10^{2}	8.8762×10^{-1}	4.0000×10^{2}	4
(0.7, 0.4)	3.0008×10^{2}	1.1898×10^{-1}	3.0000×10^{2}	5	(0.1, 0.1)	4.0032×10^{2}	1.0786×10^{0}	4.0000×10^{2}	5

https://doi.org/10.3390/computation14060124

Table A1. *Cont.*

Function 3					Function 4				
(α, β)	Mean	Std	Best	Rank	(α, β)	Mean	Std	Best	Rank
(0.5, 0.2)	6.0000×10^{2}	6.1596×10^{-5}	6.0000×10^{2}	1	(0.1, 0.8)	8.0558×10^{2}	2.3203×10^{0}	8.0166×10^{2}	1
(1.0, 0.9)	6.0000×10^{2}	7.8005×10^{-5}	6.0000×10^{2}	2	(0.3, 0.7)	8.0559×10^{2}	2.1647×10^{0}	8.0199×10^{2}	2
(0.9, 0.3)	6.0000×10^{2}	6.9478×10^{-5}	6.0000×10^{2}	3	(0.2, 1.0)	8.0566×10^{2}	1.9845×10^{0}	8.0201×10^{2}	3
(0.3, 0.2)	6.0000×10^{2}	7.1212×10^{-5}	6.0000×10^{2}	4	(0.0, 0.9)	8.0588×10^{2}	2.1641×10^{0}	8.0199×10^{2}	4
(1.0, 0.6)	6.0000×10^{2}	6.6798×10^{-5}	6.0000×10^{2}	5	(0.0, 0.8)	8.0599×10^{2}	2.6388×10^{0}	8.0254×10^{2}	5
Function 5					Function 6				
(α, β)	Mean	Std	Best	Rank	(α, β)	Mean	Std	Best	Rank
(0.7, 0.4)	9.0000×10^{2}	1.3257×10^{-4}	9.0000×10^{2}	1	(0.1, 0.8)	2.1571×10^{3}	6.5789×10^{2}	1.8506×10^{3}	1
(1.0, 0.0)	9.0000×10^{2}	2.0019×10^{-2}	9.0000×10^{2}	2	(1.0, 0.0)	2.1583×10^{3}	5.0330×10^{2}	1.8530×10^{3}	2
(0.2, 0.8)	9.0000×10^{2}	2.0031×10^{-2}	9.0000×10^{2}	3	(0.9, 0.9)	2.2250×10^{3}	4.7052×10^{2}	1.8745×10^{3}	3
(0.1, 0.9)	9.0000×10^{2}	2.0009×10^{-2}	9.0000×10^{2}	4	(0.9, 0.3)	2.2513×10^{3}	4.9895×10^{2}	1.8265×10^{3}	4
(0.0, 0.9)	9.0000×10^{2}	2.0001×10^{-2}	9.0000×10^{2}	5	(0.8, 0.9)	2.2908×10^{3}	5.1411×10^{2}	1.8563×10^{3}	5

Table A2. Top 5 parameter combinations for Functions 7–12.

Function 7					Function 8				
(α, β)	Mean	Std	Best	Rank	(α, β)	Mean	Std	Best	Rank
(0.6, 0.1)	2.0044×10^{3}	5.8970×10^{0}	2.0001×10^{3}	1	(0.9, 0.1)	2.2075×10^{3}	5.7492×10^{0}	2.2016×10^{3}	1
(0.1, 0.9)	2.0044×10^{3}	6.0472×10^{0}	2.0000×10^{3}	2	(1.0, 0.0)	2.2085×10^{3}	7.9965×10^{0}	2.2003×10^{3}	2
(0.8, 0.3)	2.0046×10^{3}	5.4599×10^{0}	2.0000×10^{3}	3	(1.0, 0.2)	2.2088×10^{3}	7.1631×10^{0}	2.2028×10^{3}	3
(0.5, 0.0)	2.0047×10^{3}	6.3519×10^{0}	2.0001×10^{3}	4	(1.0, 0.1)	2.2101×10^{3}	6.8932×10^{0}	2.2030×10^{3}	4
(1.0, 0.0)	2.0048×10^{3}	7.3188×10^{0}	2.0000×10^{3}	5	(0.9, 0.3)	2.2103×10^{3}	8.1814×10^{0}	2.2016×10^{3}	5
Function 9					Function 10				
(α, β)	Mean	Std	Best	Rank	(α, β)	Mean	Std	Best	Rank
(1.0, 0.0)	2.5293×10^{3}	1.8070×10^{-13}	2.5293×10^{3}	1	(0.9, 0.2)	2.5002×10^{3}	5.7998×10^{-2}	2.5000×10^{3}	1
(0.9, 0.3)	2.5293×10^{3}	2.3678×10^{-6}	2.5293×10^{3}	2	(0.4, 0.6)	2.5002×10^{3}	7.4642×10^{-2}	2.5001×10^{3}	2
(1.0, 0.1)	2.5293×10^{3}	6.6201×10^{-6}	2.5293×10^{3}	3	(0.8, 0.2)	2.5002×10^{3}	4.6619×10^{-2}	2.5001×10^{3}	3
(0.9, 0.2)	2.5293×10^{3}	8.8897×10^{-6}	2.5293×10^{3}	4	(0.7, 0.2)	2.5002×10^{3}	6.0885×10^{-2}	2.5001×10^{3}	4
(1.0, 0.2)	2.5293×10^{3}	1.0989×10^{-5}	2.5293×10^{3}	5	(0.2, 0.7)	2.5002×10^{3}	5.5681×10^{-2}	2.5001×10^{3}	5
Function 11					Function 12				
(α, β)	Mean	Std	Best	Rank	(α, β)	Mean	Std	Best	Rank
(0.3, 0.6)	2.6000×10^{3}	4.7505×10^{-6}	2.6000×10^{3}	1	(0.9, 0.3)	2.8630×10^{3}	1.6189×10^{0}	2.8589×10^{3}	1
(0.0, 0.7)	2.6000×10^{3}	3.0998×10^{-5}	2.6000×10^{3}	2	(1.0, 0.2)	2.8632×10^{3}	1.4686×10^{0}	2.8594×10^{3}	2
(0.2, 0.0)	2.6000×10^{3}	5.3157×10^{-5}	2.6000×10^{3}	3	(1.0, 0.1)	2.8634×10^{3}	1.6734×10^{0}	2.8599×10^{3}	3
(0.5, 0.0)	2.6000×10^{3}	6.6388×10^{-5}	2.6000×10^{3}	4	(1.0, 0.3)	2.8635×10^{3}	1.5317×10^{0}	2.8591×10^{3}	4
(1.0, 0.0)	2.6000×10^{3}	5.3832×10^{-5}	2.6000×10^{3}	5	(1.0, 0.0)	2.8635×10^{3}	1.4425×10^{0}	2.8587×10^{3}	5

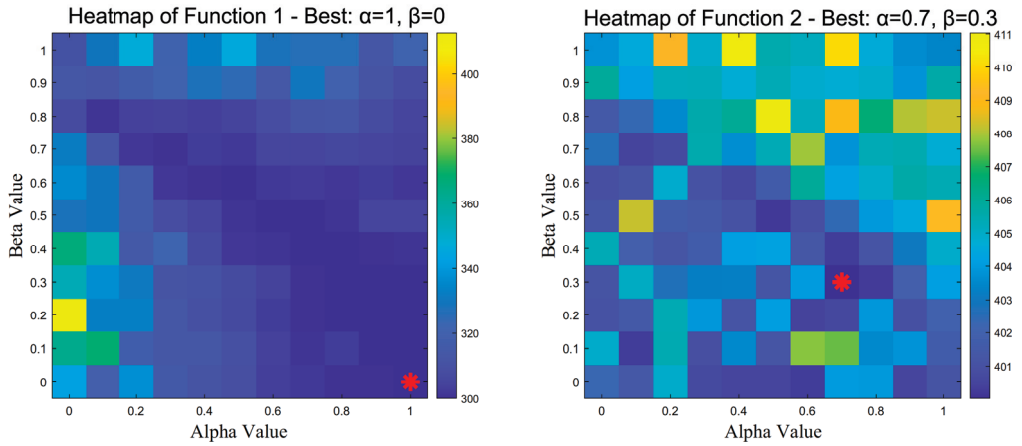

Figure A1. *Cont.*

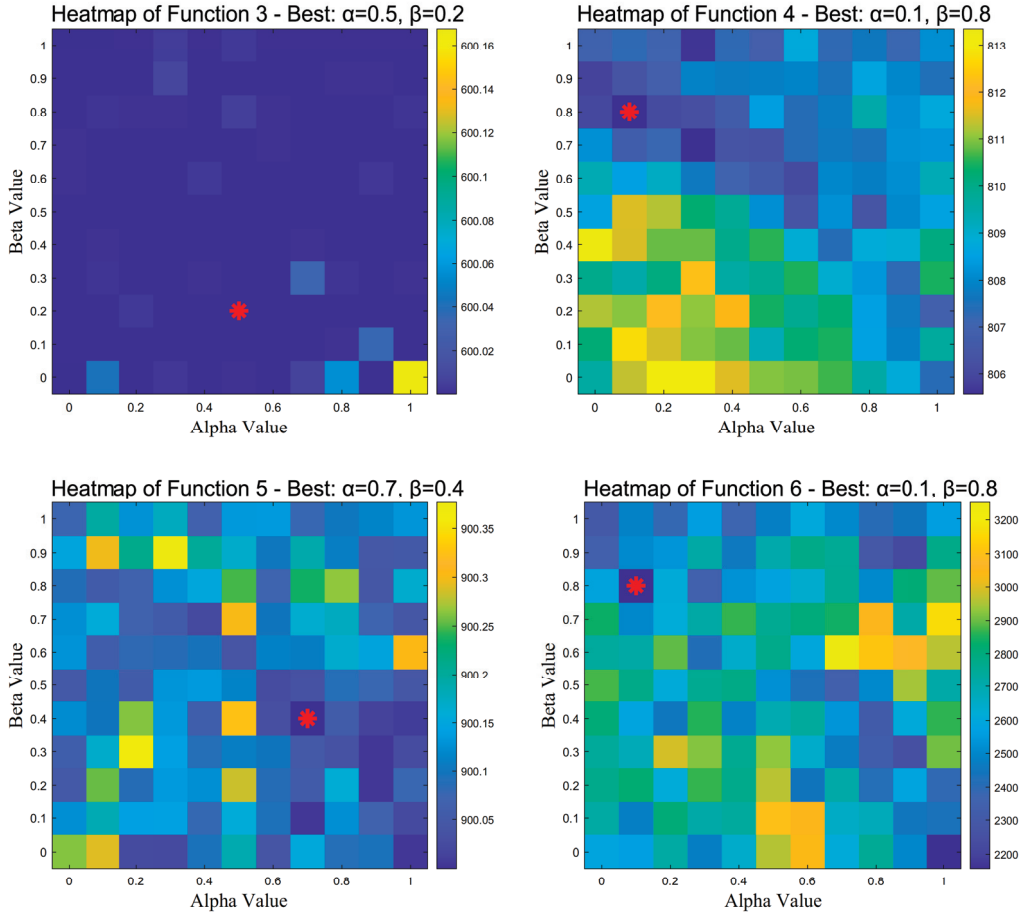

Figure A1. Heatmap of Functions 1–6.

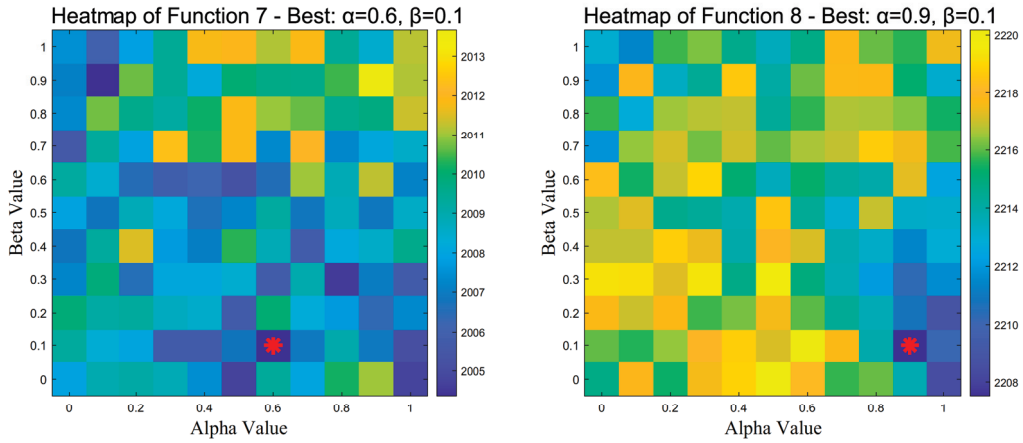

Figure A2. *Cont.*

https://doi.org/10.3390/computation14060124

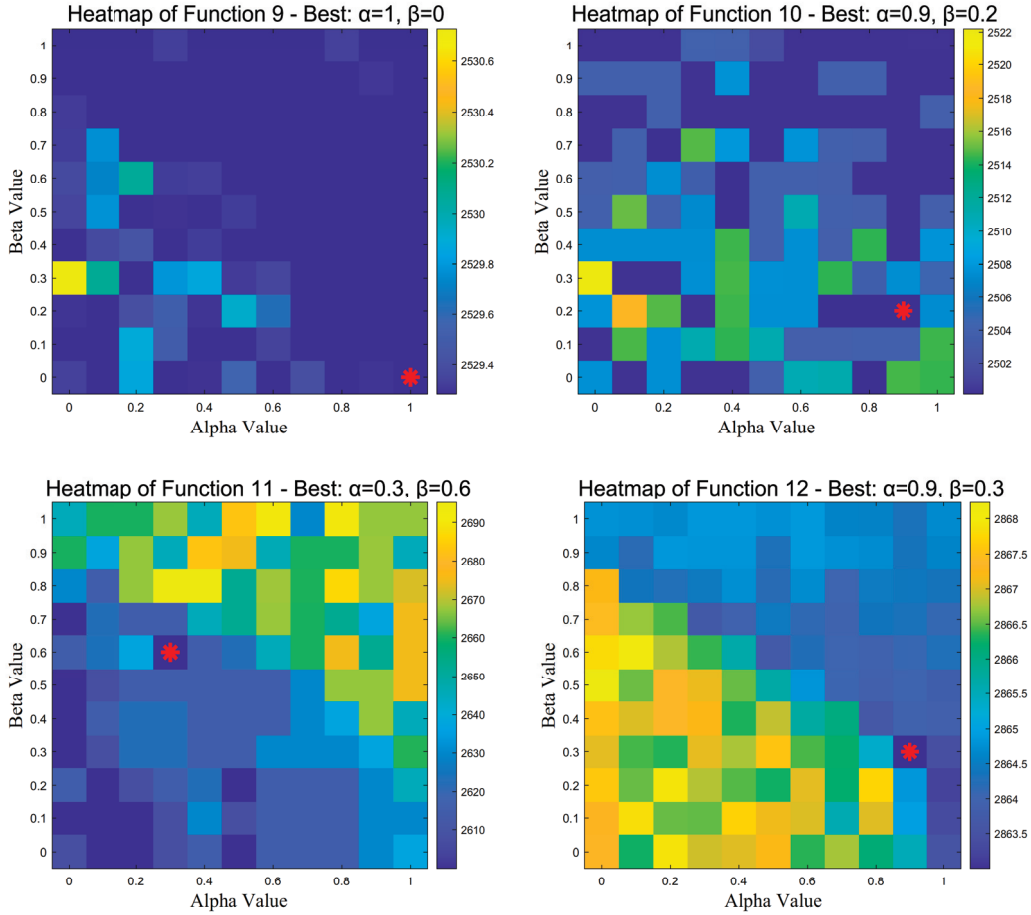

Figure A2. Heatmap of Functions 7–12.

Appendix B

Table A3. Results of the truncation depth analysis for Functions 1–6.

	Function 1				Function 2			
Method	Mean	Std	Best	Rank	Mean	Std	Best	Rank
CoGRO1	3.0000×10^{2}	3.5704×10^{-8}	3.0000×10^{2}	3	4.0003×10^{2}	3.6981×10^{-2}	4.0000×10^{2}	3
CoGRO2	3.0000×10^{2}	2.7174×10^{-8}	3.0000×10^{2}	2	4.0003×10^{2}	3.5971×10^{-2}	4.0000×10^{2}	2
CoGRO3	$\mathbf{3.0000} \times 10^{2}$	$\mathbf{1.1109} \times 10^{-9}$	$\mathbf{3.0000} \times 10^{2}$	**1**	$\mathbf{4.0002} \times 10^{2}$	$\mathbf{3.8210} \times 10^{-2}$	$\mathbf{4.0000} \times 10^{2}$	**1**
	Function 3				Function 4			
Method	Mean	Std	Best	Rank	Mean	Std	Best	Rank
CoGRO1	6.0000×10^{2}	8.2477×10^{-14}	6.0000×10^{2}	3	8.0689×10^{2}	1.8188×10^{0}	8.0299×10^{2}	3
CoGRO2	6.0000×10^{2}	7.9443×10^{-8}	6.0000×10^{2}	2	8.0638×10^{2}	3.5632×10^{0}	8.0398×10^{2}	2
CoGRO3	$\mathbf{6.0000} \times 10^{2}$	$\mathbf{6.3886} \times 10^{-14}$	$\mathbf{6.0000} \times 10^{2}$	**1**	$\mathbf{8.0571} \times 10^{2}$	$\mathbf{2.2746} \times 10^{0}$	$\mathbf{8.0298} \times 10^{2}$	**1**
	Function 5				Function 6			
Method	Mean	Std	Best	Rank	Mean	Std	Best	Rank
CoGRO1	9.0000×10^{2}	8.7479×10^{-9}	9.0000×10^{2}	3	2.1106×10^{3}	5.0751×10^{2}	1.8421×10^{3}	3
CoGRO2	9.0000×10^{2}	3.8418×10^{-9}	9.0000×10^{2}	2	2.0879×10^{3}	3.1164×10^{2}	1.8608×10^{3}	2
CoGRO3	$\mathbf{9.0000} \times 10^{2}$	$\mathbf{2.6498} \times 10^{-9}$	$\mathbf{9.0000} \times 10^{2}$	**1**	$\mathbf{2.0608} \times 10^{3}$	$\mathbf{2.5483} \times 10^{2}$	$\mathbf{1.8396} \times 10^{3}$	**1**

https://doi.org/10.3390/computation14060124

Table A4. Results of the truncation depth analysis for Functions 7–12.

	Function 7				Function 8			
Method	Mean	Std	Best	Rank	Mean	Std	Best	Rank
CoGRO1	2.0010×10^{3}	6.0635×10^{-1}	2.0000×10^{3}	3	2.2120×10^{3}	1.0004×10^{1}	2.2009×10^{3}	3
CoGRO2	2.0012×10^{3}	8.3360×10^{-1}	2.0000×10^{3}	2	2.2066×10^{3}	8.2072×10^{0}	2.2003×10^{3}	2
CoGRO3	$\mathbf{2.0009} \times 10^{3}$	$\mathbf{4.6483} \times 10^{-1}$	$\mathbf{2.0000} \times 10^{3}$	**1**	$\mathbf{2.2053} \times 10^{3}$	$\mathbf{2.7249} \times 10^{0}$	$\mathbf{2.2005} \times 10^{3}$	**1**
	Function 9				Function 10			
Method	Mean	Std	Best	Rank	Mean	Std	Best	Rank
CoGRO1	2.5293×10^{3}	3.7956×10^{-12}	2.5293×10^{3}	2	2.5002×10^{3}	1.2309×10^{-2}	2.5002×10^{3}	3
CoGRO2	2.5293×10^{3}	4.2820×10^{-12}	2.5293×10^{3}	3	2.5001×10^{3}	5.1174×10^{-2}	2.5001×10^{3}	2
CoGRO3	$\mathbf{2.5293} \times 10^{3}$	$\mathbf{1.5753} \times 10^{-12}$	$\mathbf{2.5293} \times 10^{3}$	**1**	$\mathbf{2.5001} \times 10^{3}$	$\mathbf{2.5890} \times 10^{-2}$	$\mathbf{2.5001} \times 10^{3}$	**1**
	Function 11				Function 12			
Method	Mean	Std	Best	Rank	Mean	Std	Best	Rank
CoGRO1	2.8700×10^{3}	1.2312×10^{2}	2.6000×10^{3}	3	2.8647×10^{3}	1.0047×10^{0}	2.8614×10^{3}	2
CoGRO2	2.8400×10^{3}	1.3328×10^{2}	2.6000×10^{3}	2	2.8640×10^{3}	1.3980×10^{0}	2.8612×10^{3}	1
CoGRO3	$\mathbf{2.8250} \times 10^{3}$	$\mathbf{9.2338} \times 10^{1}$	$\mathbf{2.6000} \times 10^{3}$	**1**	$\mathbf{2.8637} \times 10^{3}$	$\mathbf{1.4092} \times 10^{0}$	$\mathbf{2.8614} \times 10^{3}$	**3**

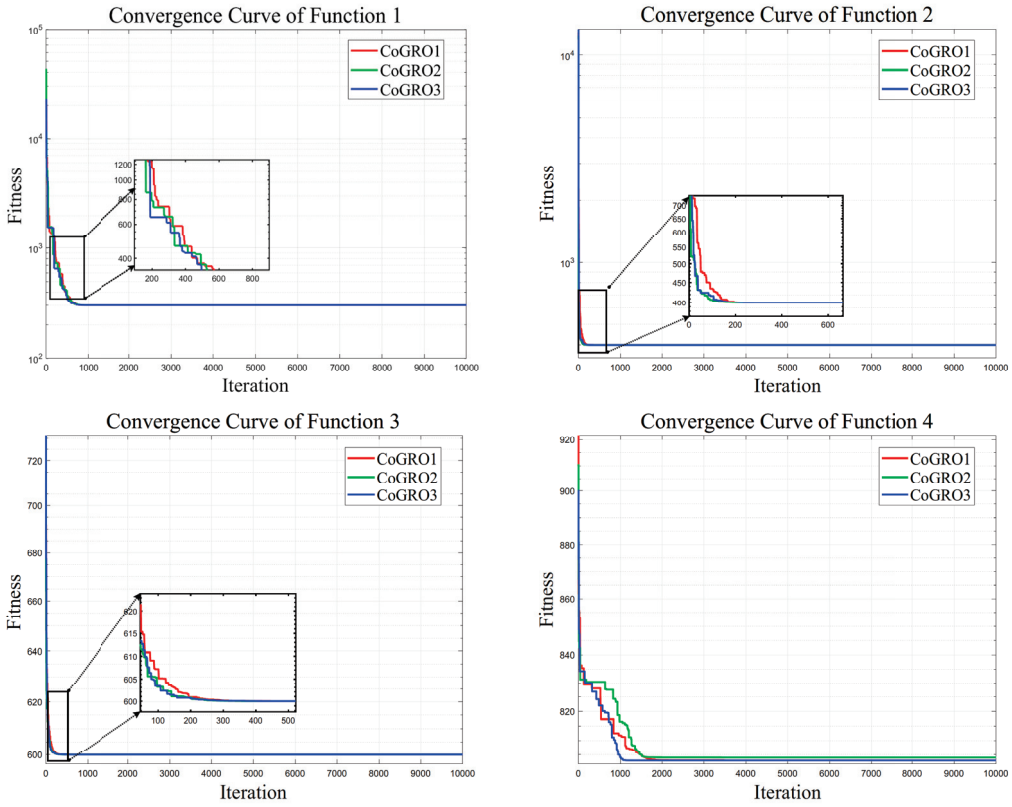

Figure A3. *Cont.*

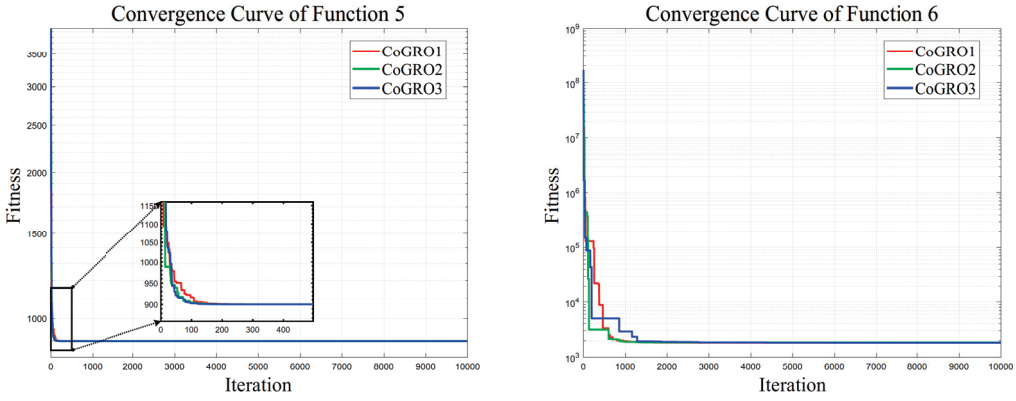

Figure A3. Convergencecurve of Functions 1–6.

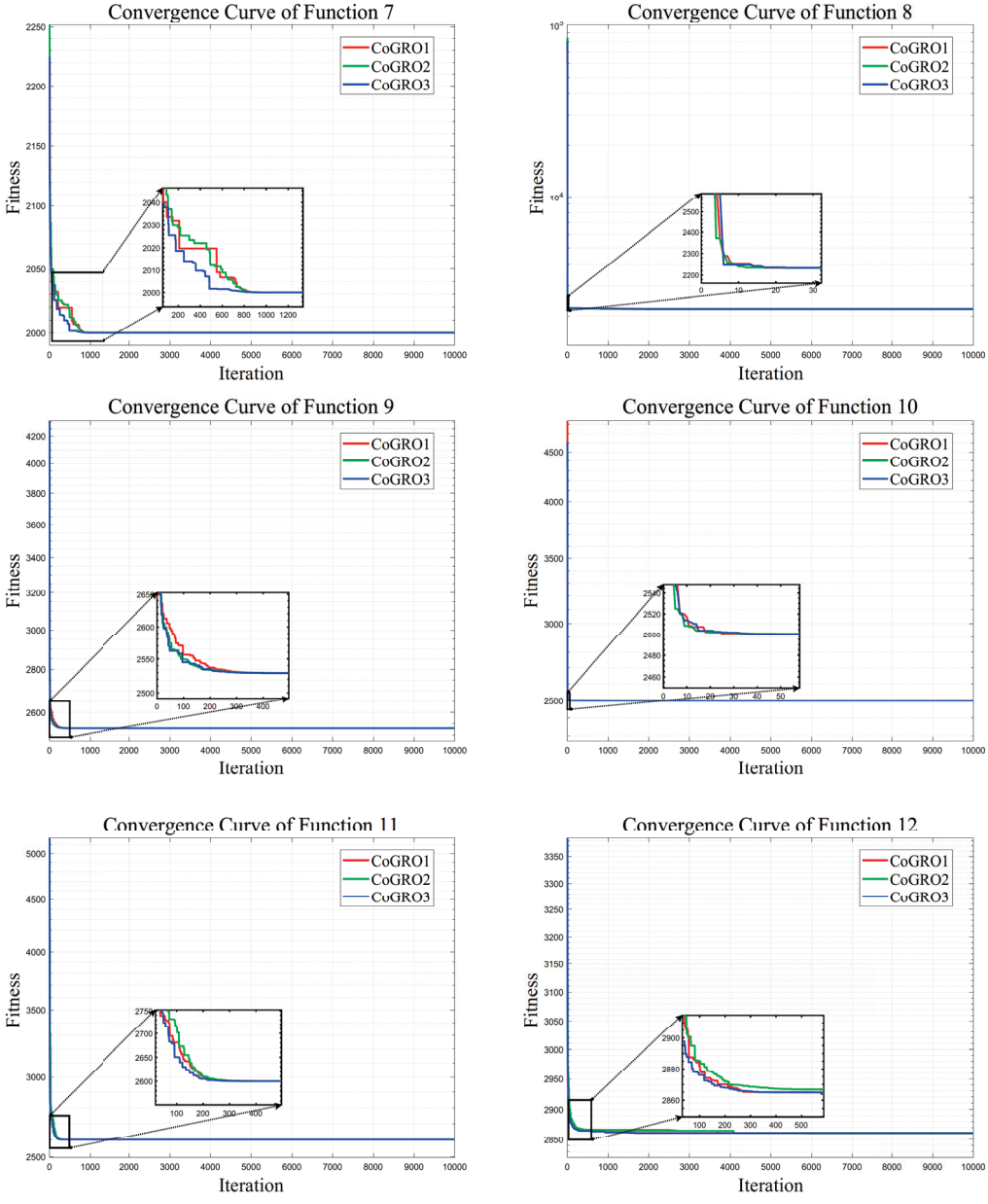

Figure A4. Convergencecurve of Functions 7–12.

https://doi.org/10.3390/computation14060124

Appendix C

Table A5. Results of the ablation study for Functions 1–6.

	Function 1				Function 2			
Method	Mean	Std	Best	Rank	Mean	Std	Best	Rank
CoGRO-AB	3.0000×10^{2}	1.1881×10^{-13}	3.0000×10^{2}	2	4.0014×10^{2}	7.2682×10^{-1}	4.0000×10^{2}	4
CoGRO-A	3.0000×10^{2}	5.0507×10^{-14}	3.0000×10^{2}	1	4.0003×10^{2}	6.2726×10^{-2}	4.0000×10^{2}	3
CoGRO-B	3.0002×10^{2}	3.1769×10^{-2}	3.0000×10^{2}	4	4.0003×10^{2}	5.2822×10^{-2}	4.0000×10^{2}	2
CoGRO	$\mathbf{3.0000} \times 10^{2}$	$\mathbf{9.0742} \times 10^{-9}$	$\mathbf{3.0000} \times 10^{2}$	**3**	$\mathbf{4.0003} \times 10^{2}$	$\mathbf{4.5528} \times 10^{-2}$	$\mathbf{4.0000} \times 10^{2}$	**1**
	Function 3				Function 4			
Method	Mean	Std	Best	Rank	Mean	Std	Best	Rank
CoGRO-AB	6.0017×10^{2}	7.4966×10^{-1}	6.0000×10^{2}	4	8.0836×10^{2}	3.2345×10^{0}	8.0298×10^{2}	4
CoGRO-A	6.0005×10^{2}	2.1467×10^{-1}	6.0000×10^{2}	3	8.0776×10^{2}	2.6145×10^{0}	8.0298×10^{2}	3
CoGRO-B	6.0000×10^{2}	1.5496×10^{-4}	6.0000×10^{2}	2	8.0551×10^{2}	2.6135×10^{0}	8.0100×10^{2}	2
CoGRO	$\mathbf{6.0000} \times 10^{2}$	$\mathbf{2.5946} \times 10^{-7}$	$\mathbf{6.0000} \times 10^{2}$	**1**	$\mathbf{8.0274} \times 10^{2}$	$\mathbf{1.8511} \times 10^{0}$	$\mathbf{8.0000} \times 10^{2}$	**1**
	Function 5				Function 6			
Method	Mean	Std	Best	Rank	Mean	Std	Best	Rank
CoGRO-AB	9.0000×10^{2}	1.0159×10^{-1}	9.0000×10^{2}	4	2.1583×10^{3}	5.0330×10^{2}	1.8530×10^{3}	4
CoGRO-A	9.0000×10^{2}	2.0019×10^{-2}	9.0000×10^{2}	3	2.1153×10^{3}	1.0075×10^{2}	1.8354×10^{3}	3
CoGRO-B	9.0000×10^{2}	1.3257×10^{-4}	9.0000×10^{2}	2	2.1148×10^{3}	3.0767×10^{2}	1.8441×10^{3}	2
CoGRO	$\mathbf{9.0000} \times 10^{2}$	$\mathbf{3.4181} \times 10^{-9}$	$\mathbf{9.0000} \times 10^{2}$	**1**	$\mathbf{2.0192} \times 10^{3}$	$\mathbf{2.6768} \times 10^{2}$	$\mathbf{1.8373} \times 10^{3}$	**1**

Table A6. Results of the ablation study for Functions 7–12.

	Function 7				Function 8			
Method	Mean	Std	Best	Rank	Mean	Std	Best	Rank
CoGRO-AB	2.0048×10^{3}	7.3188×10^{0}	2.0000×10^{3}	4	2.2089×10^{3}	8.0431×10^{0}	2.2006×10^{3}	4
CoGRO-A	2.0030×10^{3}	4.3911×10^{0}	2.0000×10^{3}	3	2.2085×10^{3}	7.9965×10^{0}	2.2003×10^{3}	3
CoGRO-B	2.0022×10^{3}	2.1860×10^{0}	2.0000×10^{3}	2	2.2075×10^{3}	5.7492×10^{0}	2.2016×10^{3}	2
CoGRO	$\mathbf{2.0010} \times 10^{3}$	$\mathbf{1.1916} \times 10^{0}$	$\mathbf{2.0000} \times 10^{3}$	**1**	$\mathbf{2.2037} \times 10^{3}$	$\mathbf{2.7183} \times 10^{0}$	$\mathbf{2.2009} \times 10^{3}$	**1**
	Function 9				Function 10			
Method	Mean	Std	Best	Rank	Mean	Std	Best	Rank
CoGRO-AB	2.5293×10^{3}	3.2991×10^{-13}	2.5293×10^{3}	2	2.5541×10^{3}	5.5301×10^{1}	2.5001×10^{3}	4
CoGRO-A	2.5293×10^{3}	1.8070×10^{-13}	2.5293×10^{3}	1	2.5112×10^{3}	3.3733×10^{1}	2.5001×10^{3}	3
CoGRO-B	2.5293×10^{3}	4.4348×10^{-6}	2.5293×10^{3}	4	2.5002×10^{3}	5.7998×10^{-2}	2.5000×10^{3}	2
CoGRO	$\mathbf{2.5293} \times 10^{3}$	$\mathbf{4.1832} \times 10^{-12}$	$\mathbf{2.5293} \times 10^{3}$	**3**	$\mathbf{2.5001} \times 10^{3}$	$\mathbf{2.7008} \times 10^{-2}$	$\mathbf{2.5000} \times 10^{3}$	**1**
	Function 11				Function 12			
Method	Mean	Std	Best	Rank	Mean	Std	Best	Rank
CoGRO-AB	2.6225×10^{3}	7.3443×10^{1}	2.6000×10^{3}	4	2.8635×10^{3}	1.4425×10^{0}	2.8587×10^{3}	4
CoGRO-A	2.6150×10^{3}	6.7082×10^{1}	2.6000×10^{3}	3	2.8633×10^{3}	2.2540×10^{0}	2.8594×10^{3}	3
CoGRO-B	2.6000×10^{3}	4.7505×10^{-6}	2.6000×10^{3}	2	2.8630×10^{3}	1.6189×10^{0}	2.8589×10^{3}	2
CoGRO	$\mathbf{2.6000} \times 10^{3}$	$\mathbf{4.1730} \times 10^{-13}$	$\mathbf{2.6000} \times 10^{3}$	**1**	$\mathbf{2.8624} \times 10^{3}$	$\mathbf{1.3059} \times 10^{0}$	$\mathbf{2.8594} \times 10^{3}$	**1**

https://doi.org/10.3390/computation14060124

Appendix D

Table A7. Comparison results of Functions 1–12.

	Function 1					Function 2				
Method	Mean	Std	Best	Avg Time	w-Test	Mean	Std	Best	Avg Time	w-Test
CoGRO	$\mathbf{3.0000 \times 10^{2}}$	$\mathbf{0.0000 \times 10^{0}}$	$\mathbf{3.0000 \times 10^{2}}$	**6.58**		$\mathbf{4.0003 \times 10^{2}}$	$\mathbf{4.0831 \times 10^{-2}}$	$\mathbf{4.0000 \times 10^{2}}$	**6.52**	
EA4eig	3.0000×10^{2}	0.0000×10^{0}	3.0000×10^{2}	5.25	=	4.0200×10^{2}	2.0200×10^{0}	4.0000×10^{2}	5.24	=
GA	3.0600×10^{2}	4.0800×10^{0}	3.0000×10^{2}	1.69	+	4.0700×10^{2}	1.1200×10^{1}	4.0000×10^{2}	1.67	+
GWO	6.2700×10^{2}	6.7800×10^{2}	3.0700×10^{2}	2.33	+	4.1000×10^{2}	8.2300×10^{0}	4.0100×10^{2}	2.32	+
MadDE	3.0000×10^{2}	9.4900×10^{-7}	3.0000×10^{2}	4.62	=	4.0000×10^{2}	1.7900×10^{-2}	4.0000×10^{2}	4.95	=
PSO	5.1700×10^{2}	8.1800×10^{1}	4.0300×10^{2}	1.33	+	4.2400×10^{2}	1.6900×10^{1}	4.0400×10^{2}	1.34	+
	Function 3					Function 4				
Method	Mean	Std	Best	Avg Time	w-Test	Mean	Std	Best	Avg Time	w-Test
CoGRO	$\mathbf{6.0000 \times 10^{2}}$	$\mathbf{0.0000 \times 10^{0}}$	$\mathbf{6.0000 \times 10^{2}}$	**7.77**		$\mathbf{8.0400 \times 10^{2}}$	$\mathbf{1.1300 \times 10^{0}}$	$\mathbf{8.0100 \times 10^{2}}$	**7.23**	
EA4eig	6.0000×10^{2}	0.0000×10^{0}	6.0000×10^{2}	6.07	=	8.0600×10^{2}	1.9700×10^{0}	8.0200×10^{2}	5.36	+
GA	6.0000×10^{2}	1.0900×10^{-2}	6.0000×10^{2}	5.13	+	8.2600×10^{2}	1.0200×10^{1}	8.1000×10^{2}	2.06	+
GWO	6.0000×10^{2}	3.8200×10^{-1}	6.0000×10^{2}	3.84	+	8.1000×10^{2}	4.1900×10^{0}	8.0400×10^{2}	2.71	+
MadDE	6.0000×10^{2}	6.4800×10^{-8}	6.0000×10^{2}	7.06	+	8.0200×10^{2}	7.9000×10^{-1}	8.0000×10^{2}	5.17	-
PSO	6.0700×10^{2}	1.6000×10^{0}	6.0300×10^{2}	2.81	+	8.2300×10^{2}	4.4800×10^{0}	8.1200×10^{2}	1.72	+
	Function 5					Function 6				
Method	Mean	Std	Best	Avg Time	w-Test	Mean	Std	Best	Avg Time	w-Test
CoGRO	$\mathbf{9.0000 \times 10^{2}}$	$\mathbf{0.0000 \times 10^{0}}$	$\mathbf{9.0000 \times 10^{2}}$	**6.66**		$\mathbf{1.8524 \times 10^{3}}$	$\mathbf{2.6783 \times 10^{1}}$	$\mathbf{1.8132 \times 10^{3}}$	**6.70**	
EA4eig	9.0000×10^{2}	0.0000×10^{0}	9.0000×10^{2}	5.44	=	1.8000×10^{3}	8.7200×10^{-3}	1.8000×10^{3}	4.94	-
GA	9.3700×10^{2}	3.3200×10^{1}	9.0000×10^{2}	2.16	+	3.6400×10^{3}	1.5200×10^{3}	1.8600×10^{3}	1.81	+
GWO	9.0200×10^{2}	3.3700×10^{0}	9.0000×10^{2}	2.98	+	5.4200×10^{3}	2.3800×10^{3}	1.9400×10^{3}	2.49	+
MadDE	9.0000×10^{2}	0.0000×10^{0}	9.0000×10^{2}	5.43	=	1.8500×10^{3}	5.9300×10^{1}	1.8000×10^{3}	4.45	=
PSO	9.1400×10^{2}	7.7800×10^{0}	9.0300×10^{2}	1.78	+	9.8600×10^{4}	1.0400×10^{5}	1.2300×10^{4}	1.48	+
	Function 7					Function 8				
Method	Mean	Std	Best	Avg Time	w-Test	Mean	Std	Best	Avg Time	w-Test
CoGRO	$\mathbf{2.0000 \times 10^{3}}$	$\mathbf{5.8900 \times 10^{-1}}$	$\mathbf{2.0000 \times 10^{3}}$	**8.08**		$\mathbf{2.2000 \times 10^{3}}$	$\mathbf{3.8500 \times 10^{0}}$	$\mathbf{2.2000 \times 10^{3}}$	**9.39**	
EA4eig	2.0000×10^{3}	0.0000×10^{0}	2.0000×10^{3}	11.34	-	2.2000×10^{3}	5.5400×10^{-3}	2.2000×10^{3}	6.28	=
GA	2.0100×10^{3}	9.9000×10^{0}	2.0000×10^{3}	3.41	+	2.2100×10^{3}	8.5900×10^{0}	2.2000×10^{3}	3.86	+
GWO	2.0200×10^{3}	9.4300×10^{0}	2.0000×10^{3}	6.59	+	2.2200×10^{3}	9.9000×10^{0}	2.2000×10^{3}	4.62	+
MadDE	2.0000×10^{3}	7.4400×10^{-1}	2.0000×10^{3}	7.29	=	2.2100×10^{3}	8.2200×10^{0}	2.2000×10^{3}	8.50	+
PSO	2.0400×10^{3}	5.5400×10^{0}	2.0200×10^{3}	3.28	+	2.2200×10^{3}	3.5100×10^{0}	2.2200×10^{3}	3.71	+
	Function 9					Function 10				
Method	Mean	Std	Best	Avg Time	w-Test	Mean	Std	Best	Avg Time	w-Test
CoGRO	$\mathbf{2.5300 \times 10^{3}}$	$\mathbf{2.7100 \times 10^{-12}}$	$\mathbf{2.5300 \times 10^{3}}$	**8.97**		$\mathbf{2.5000 \times 10^{3}}$	$\mathbf{2.7700 \times 10^{-2}}$	$\mathbf{2.5000 \times 10^{3}}$	**8.42**	
EA4eig	2.5300×10^{3}	0.0000×10^{0}	2.5300×10^{3}	6.08	-	2.5000×10^{3}	2.8900×10^{-2}	2.5000×10^{3}	5.90	+
GA	2.5300×10^{3}	2.6800×10^{1}	2.5300×10^{3}	3.32	+	2.5400×10^{3}	5.8200×10^{1}	2.5000×10^{3}	2.95	+
GWO	2.5300×10^{3}	1.4100×10^{1}	2.5300×10^{3}	3.94	+	2.5300×10^{3}	4.9600×10^{1}	2.5000×10^{3}	3.73	+
MadDE	2.5300×10^{3}	6.6600×10^{-7}	2.5300×10^{3}	7.68	+	2.5000×10^{3}	1.9100×10^{1}	2.5000×10^{3}	6.85	+
PSO	2.5600×10^{3}	5.4700×10^{0}	2.5400×10^{3}	3.03	+	2.5000×10^{3}	1.6700×10^{-1}	2.5000×10^{3}	3.64	+

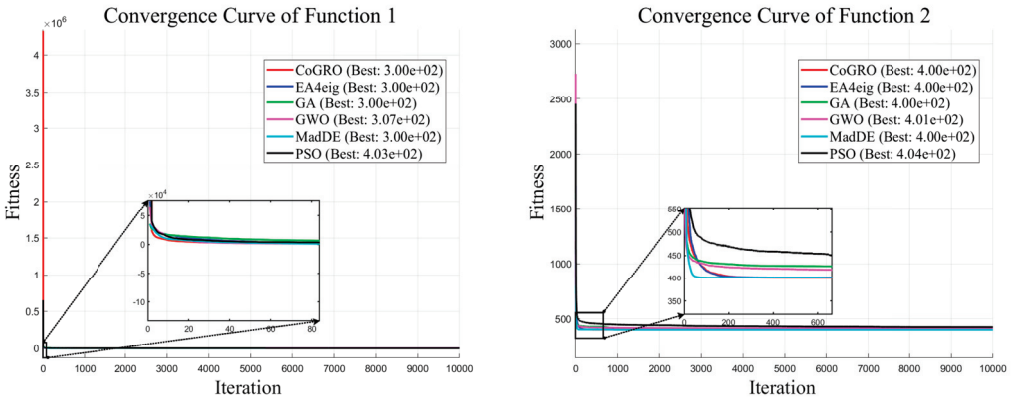

Figure A5. *Cont.*

https://doi.org/10.3390/computation14060124

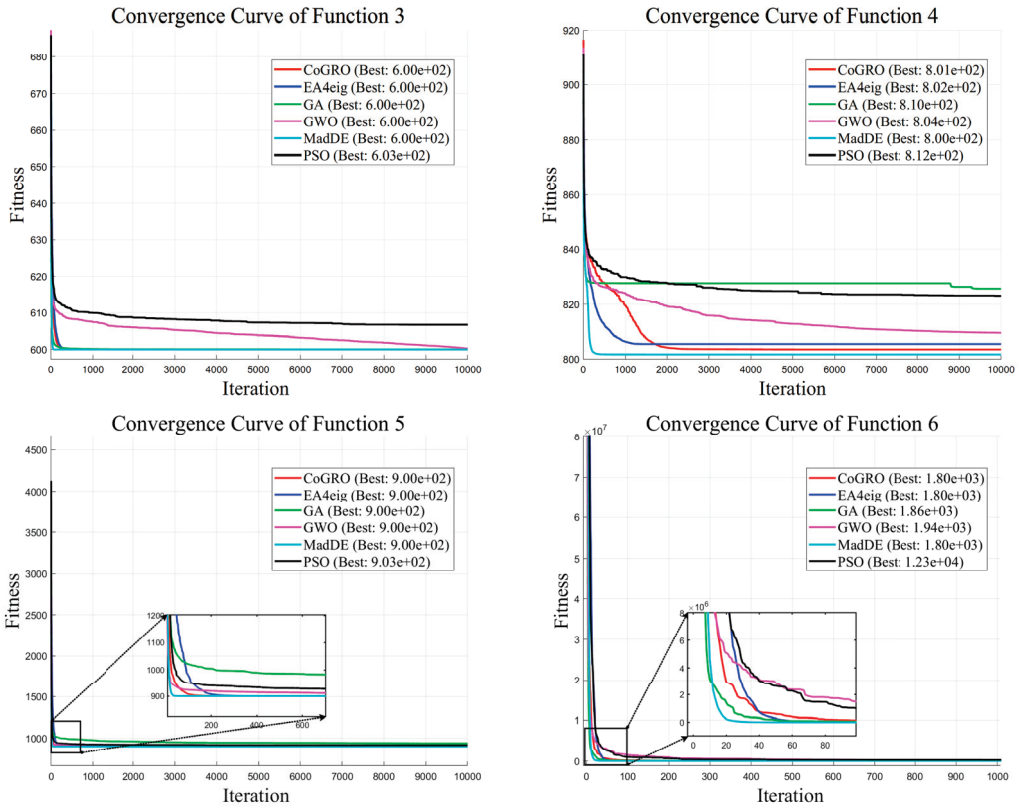

Figure A5. Convergence curve of Functions 1–6.

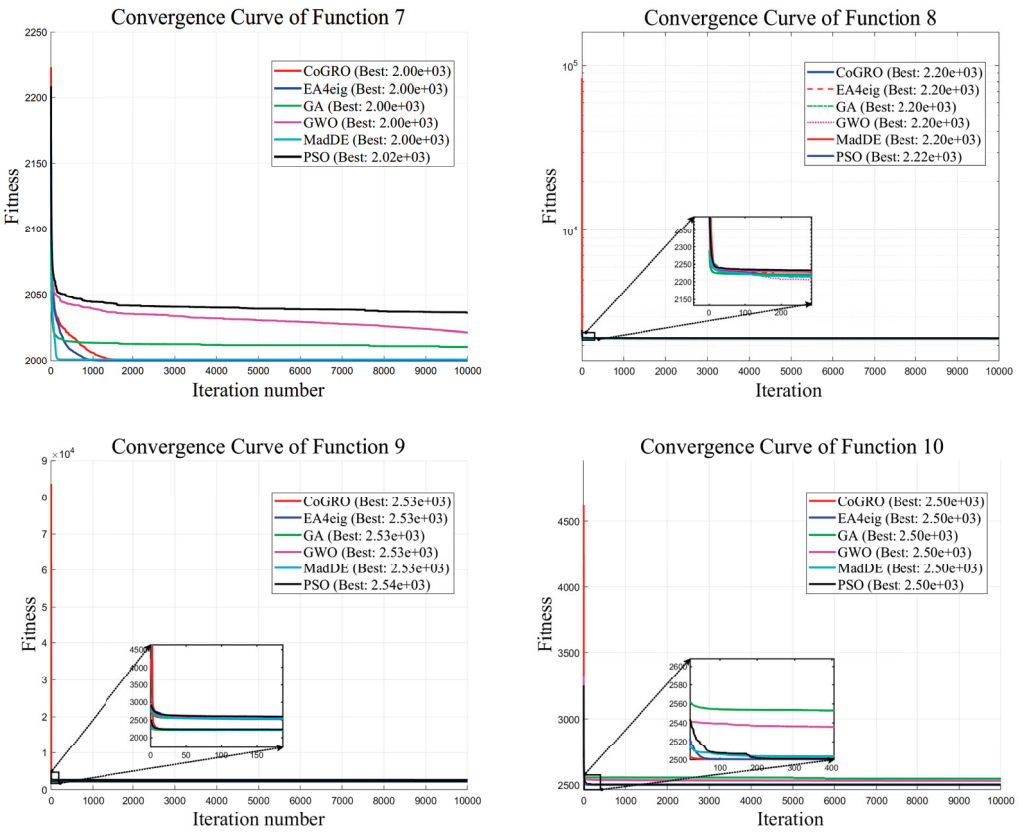

Figure A6. *Cont.*

https://doi.org/10.3390/computation14060124

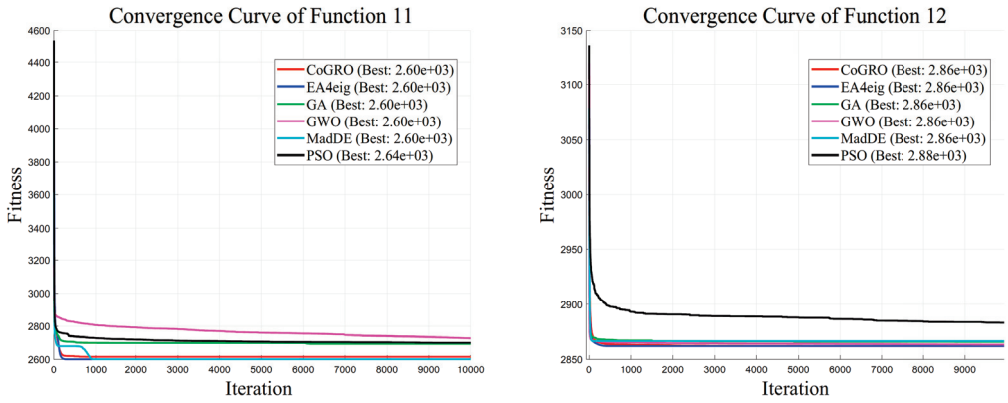

Figure A6. Convergence curve of Functions 7–12.

References

1. Al-Terkawi, L. Survey on distributed parallel genetic algorithms for large-scale data analysis. *Computing* **2026**, *108*, 6. [CrossRef]
2. Brest, J.; Sepesy Maučec, M. Comparative study of modern differential evolution algorithms: Perspectives on mechanisms and performance. *Mathematics* **2025**, *13*, 1556. [CrossRef]
3. Lyu, C.; Ma, Z.; Luo, X.; Shi, Y. Dynamic stochastic reorientation particle swarm optimization for adaptive latent factor analysis in high-dimensional sparse matrices. *IEEE Trans. Knowl. Data Eng.* **2025**, *38*, 222–234. [CrossRef]
4. Abir, A.R.; Nayeem, M.A.; Rahman, M.S.; Arefeen, M.A. GTG-ACO: Graph Transformer Guided Ant Colony Optimization for learning heuristics and pheromone dynamics for combinatorial optimization. *Swarm Evol. Comput.* **2025**, *99*, 102147. [CrossRef]
5. Tsoulos, I.G.; Charilogis, V.; Tsalikakis, D. Optimizing the Bounds of Neural Networks Using a Novel Simulated Annealing Method. *AppliedMath* **2026**, *6*, 23. [CrossRef]
6. Hashemi, A.; Dowlatshahi, M.B.; Nezamabadi-Pour, H. Gravitational search algorithm: Theory, literature review, and applications. In *Handbook of AI-based Metaheuristics*; CRC Press: Boca Raton, FL, USA, 2021; pp. 119–150.
7. Dastan, M.; Shojaee, S.; Hamzehei-Javaran, S.; Goodarzimehr, V. Hybrid teaching–learning-based optimization for solving engineering and mathematical problems. *J. Braz. Soc. Mech. Sci. Eng.* **2022**, *44*, 431. [CrossRef]
8. Sadeghi Moghadam, M.; Parvin, H.; Bagheri Fard, K.; Yagoubian, S.H. Solving dynamic optimization problems with an Improved Imperialis Competition Algorithm. *Signal Data Process.* **2025**, *22*, 3–30. [CrossRef]
9. Zolfi, K. Gold rush optimizer: A new population-based metaheuristic algorithm. *Oper. Res. Decis.* **2023**, *33*, 113–150. [CrossRef]
10. Zhang, Y.; Adegboye, O.R.; Feda, A.K.; Agyekum, E.B.; Kumar, P. Dynamic gold rush optimizer: Fusing worker adaptation and salp navigation mechanism for enhanced search. *Sci. Rep.* **2025**, *15*, 15779. [CrossRef]
11. Abaeifar, A.; Barati, H.; Tavakoli, A.R. Inertia-weight local-search-based TLBO algorithm for energy management in isolated micro-grids with renewable resources. *Int. J. Electr. Power Energy Syst.* **2022**, *137*, 107877. [CrossRef]
12. Tang, Y.; Zhou, F. An improved imperialist competition algorithm with adaptive differential mutation assimilation strategy for function optimization. *Expert Syst. Appl.* **2023**, *211*, 118686. [CrossRef]
13. Mohd Tumari, M.Z.; Ahmad, M.A.; Suid, M.H.; Ghazali, M.R.; Tokhi, M.O. An improved marine predators algorithm tuned data-driven multiple-node hormone regulation neuroendocrine-PID controller for multi-input–multi-output gantry crane system. *J. Low. Freq. Noise Vib. Act. Control* **2023**, *42*, 1666–1698. [CrossRef]
14. Weng, X.; Xuan, P.; Heidari, A.A.; Cai, Z.; Chen, H.; Mansour, R.F.; Ragab, M. A vertical and horizontal crossover sine cosine algorithm with pattern search for optimal power flow in power systems. *Energy* **2023**, *271*, 127000. [CrossRef]
15. Suid, M.; Ahmad, M. A novel hybrid of nonlinear sine cosine algorithm and safe experimentation dynamics for model order reduction. *Autom. Časopis Za Autom. Mjer. Elektron. Računarstvo I Komun.* **2023**, *64*, 34–50. [CrossRef]
16. Połap, D.; Woźniak, M. Polar bear optimization algorithm: Meta-heuristic with fast population movement and dynamic birth and death mechanism. *Symmetry* **2017**, *9*, 203. [CrossRef]
17. Chen, L.; Wu, X.; Lopes, A.M.; Wang, D.; Gu, P.; Zhu, M.; Chen, Y. Complex-Order Quantum-Behaved Particle Swarm Optimization with Double Jump-Out Strategy. *IEEE Trans. Emerg. Top. Comput. Intell.* **2025**, *9*, 3469–3487. [CrossRef]
18. Machado, J.T.; Pahnehkolaei, S.M.A.; Alfi, A. Complex-order particle swarm optimization. *Commun. Nonlinear Sci. Numer. Simul.* **2021**, *92*, 105448. [CrossRef]
19. Pahnehkolaei, S.M.A.; Alfi, A.; Machado, J.T. Particle swarm optimization algorithm using complex-order derivative concept: A comprehensive study. *Appl. Soft Comput.* **2021**, *111*, 107641. [CrossRef]
20. Liu, W.; Dou, Z.; Yan, Y.; Zhou, T.; Chen, J. Research on Optimal Scheduling of the Combined Cooling, Heating, and Power Microgrid Based on Improved Gold Rush Optimization Algorithm. *Electronics* **2025**, *14*, 3135. [CrossRef]

21. Peng, W.; Wu, R.; Wang, Y.; Wang, J. Improved Egret Swarm Optimization Algorithm with mixed multi-strategy for system evaluation. *Math. Comput. Simul.* **2026**, *243*, 362–381. [CrossRef]
22. Lan, L.; Qi, Z. An enhanced parrot optimizer with multiple strategies for wireless sensor network node deployment. *Sci. Rep.* **2026**, *16*, 1285. [CrossRef]
23. Tao, P.; Aihara, K.; Chen, L. Brain-Inspired Chaotic Graph Backpropagation for Combinatorial Optimization. In *IEEE Transactions on Neural Networks and Learning Systems*; IEEE: New York, NY, USA, 2026; pp. 1–13.
24. Choi, H.; Kim, G.; Song, H.Y.; Shin, S.; Lee, C.; Noh, H. Some New Maximally Chaotic Discrete Maps. *Entropy* **2026**, *28*, 131. [CrossRef]
25. Htiti, M.; Akharraz, I.; Ahaitouf, A. A novel one-dimensional chaotic map with improved sine map dynamics. *Int. J. Electr. Comput. Eng.* **2025**, *15*, 2128. [CrossRef]
26. Serbet, F.; Kaya, T. New comparative approach to multi-level thresholding: Chaotically initialized adaptive meta-heuristic optimization methods. *Neural Comput. Appl.* **2025**, *37*, 8371–8396.
27. Lawnik, M. Generation of Numbers with the Distribution Close to Uniform with the Use of Chaotic Maps. In *International Conference on Simulation and Modeling Methodologies, Technologies and Applications*; SCITEPRESS: Setúbal, Portugal, 2014; Volume 2, pp. 451–455.
28. Anikin, V.; Arkadaksky, S.S.; Kuptsov, S.; Remizov, A.; Vasilenko, L. Lyapunov exponent for chaotic 1D maps with uniform invariant distribution. *Bull. Russ. Acad. Sci. Phys.* **2008**, *72*, 1684–1688. [CrossRef]
29. Drmota, M.; Tichy, R.F. *Sequences, Discrepancies and Applications*; Springer: Berlin/Heidelberg, Germany, 2006.
30. Yousri, D.; Abd Elaziz, M.; Oliva, D.; Abraham, A.; Alotaibi, M.A.; Hossain, M.A. Fractional-order comprehensive learning marine predators algorithm for global optimization and feature selection. *Knowl.-Based Syst.* **2022**, *235*, 107603. [CrossRef]
31. Fernandez, E.; Victor, H.; Isabela, B.; Ricardo, C. The Role of Fractional Calculus in Modern Optimization: A Survey of Algorithms, Applications, and Open Challenges. *Mathematics* **2025**, *13*, 3172. [CrossRef]
32. Yadav, S.K.; Methi, G. Application of fractional differential transform method and Bell polynomial for solving system of fractional delay differential equations. *Partial Differ. Equ. Appl. Math.* **2024**, *12*, 100971. [CrossRef]
33. Brociek, R.; Goik, M.; Miarka, J.; Pleszczynski, M.; Napoli, C. Solution of inverse problem for diffusion equation with fractional derivatives using metaheuristic optimization algorithm. *Informatica* **2024**, *35*, 453–481. [CrossRef]

Disclaimer/Publisher's Note: The statements, opinions and data contained in all publications are solely those of the individual author(s) and contributor(s) and not of MDPI and/or the editor(s). MDPI and/or the editor(s) disclaim responsibility for any injury to people or property resulting from any ideas, methods, instructions or products referred to in the content.

mathematics

MDPI

Article

Hydrometeorological Disaster Insurance Modeling Based on Fractional Differential Equations for Climate Change Mitigation Within the Framework of SDG 13

Hanifah Al Affiani [1], Muhamad Deni Johansyah [2,*], Endang Rusyaman [2], Sukono [2], Nurfadhlina Binti Abdul Halim [3], Alim Jaizul Wahid [1], Moch Panji Agung Saputra [2], Astrid Sulistya Azahra [4] and Aceng Sambas [5,6,7]

[1] Master Program in Mathematics, Faculty of Mathematics and Natural Sciences, Universitas Padjadjaran, Jatinangor, Sumedang 45363, Indonesia; hanifah21004@mail.unpad.ac.id (H.A.A.); alim24002@mail.unpad.ac.id (A.J.W.)
[2] Department of Mathematics, Faculty of Mathematics and Natural Sciences, Universitas Padjadjaran, Jatinangor, Sumedang 45363, Indonesia; sukono@unpad.ac.id (S.); moch16006@mail.unpad.ac.id (M.P.A.S.)
[3] Faculty of Science and Technology, University Sains Islam Malaysia, Bandar Baru Nilai, Nilai 71800, Negeri Sembilan, Malaysia; nurfadhlina@usim.edu.my
[4] Doctoral Program in Mathematics, Faculty of Mathematics and Natural Sciences, Universitas Padjadjaran, Jatinangor, Sumedang 45363, Indonesia; astrid23002@mail.unpad.ac.id
[5] Faculty of Informatics and Computing, Universiti Sultan Zainal Abidin, Campus Besut, Kuala 22200, Terengganu, Malaysia; acengsambas@unisza.edu.my
[6] Department of Mathematical Sciences, Saveetha School of Engineering, Saveetha Institute of Medical and Technical Sciences (SIMATS), Chennai 602105, Tamilnadu, India
[7] Department of Mechanical Engineering, Universitas Muhamadiyah Tasikmalaya, Tamansari Gobras, Tasikmalaya 46196, Indonesia
* Correspondence: muhamad.deni@unpad.ac.id

Abstract

Rainfall-index-based disaster insurance is an efficient approach to mitigating hydrometeorological losses. However, conventional premium pricing models generally assume memoryless stochastic dynamics that do not fully capture the long-range dependence inherent in rainfall data. This study develops a hydrometeorological disaster insurance model within a fractional Black–Scholes framework to incorporate long-memory effects. The model is formulated using fractional differential equations and solved semi-analytically by integrating the Daftardar–Jafari Method (DJM) with the Kashuri–Fundo (KF) transform, yielding a closed-form solution expressed in terms of the Mittag–Leffler function. The proposed contract is structured as parametric rainfall insurance with a multi-layer payout mechanism based on percentiles corresponding to minor, moderate, and severe housing damage. The results show that variations in the fractional-order parameter significantly affect premium estimation. In particular, $\delta = 0.5$ recovers the classical model and tends to generate higher premiums than the fractional model with $\delta_1 = 0.23153$, whereas the model with $\delta_2 = 0.73153$ yields lower premiums. These findings indicate that fractional-order parameterization can accommodate diverse risk characteristics and policyholders' economic capacities, enabling more adaptive, risk-sensitive premium structures. In line with SDG 13 (Climate Action), the proposed framework offers a climate-responsive disaster-mitigation strategy through accessible, actuarially relevant insurance design.

Keywords: hydrometeorological disaster insurance; rainfall index-based; fractional Black–Scholes model; climate change; SDG 13 (Climate Action)

MSC: 34A08; 60G22; 91B30; 91G80; 62P05; 86A08

1. Introduction

Hydrometeorological risks, such as floods and droughts, are strongly influenced by high rainfall variability, both spatially and temporally. High-intensity rainfall can trigger floods that directly damage infrastructure and settlements, while prolonged low rainfall can lead to droughts that disrupt community livelihoods [1,2]. Within the global framework, efforts to mitigate these risks align with achieving SDG target 13, which emphasizes strengthening resilience and adaptive capacity to climate-related disasters. In recent decades, the increase in extreme rainfall events has amplified risk exposure to physical assets, including residential buildings, particularly in areas with high vulnerability [3,4]. Climate projections further indicate that extreme wet events will continue to intensify throughout the 21st century, while certain regions simultaneously experience longer dry periods, increasing dual exposure to both flood and drought risks [5–7].

From a modeling perspective, rainfall is a stochastic process because it is influenced by complex, uncertain atmospheric dynamics. Therefore, stochastic approaches are important in representing rainfall variability and in evaluating hydrometeorological risks more realistically. In this context, the integration of weather statistics and financial models has evolved through the concept of weather derivatives, as proposed by Jewson and Brix (2005) and Alaton et al. (2002) [8,9]. One of the models widely used within this framework is the Black–Scholes model, introduced by Black and Scholes (1973) and further developed in modern derivatives literature by Hull (2018) [10,11]. In the context of rainfall-index-based insurance, the contract structure can be represented analogously to a financial option, so that the premium can be expressed as the discounted expected value of the payoff.

However, the classical Black–Scholes approach has limitations in representing the complex dynamics of rainfall. This model is based on a geometric Brownian motion process that is memoryless and therefore cannot capture long-range dependence, which frequently appears in hydrometeorological data. To address this limitation, a fractional approach based on the concept of fractional Brownian motion by Mandelbrot & Van Ness (1968) is utilized [12]. This concept was later formalized within the framework of stochastic calculus by Biagini et al. (2008) and further developed by Bender & Viitasaari (2016) [13,14].

The development of the fractional Black–Scholes model has been further extended in various studies. Necula (2002) showed that models based on fractional Brownian motion with a Hurst parameter can capture long-range dependence that classical models cannot [15]. This is reinforced by Comte and Renault (1998), who identified memory structures in financial market volatility [16], and by the development of fractional stochastic calculus by Hu and Øksendal (2003), which serves as the mathematical foundation for memory-based financial models [17]. Furthermore, Chen et al. (2015) developed the formulation of fractional Black–Scholes partial differential equations and demonstrated their flexibility in representing complex stochastic systems [18], while He and Lin (2021) showed that fractional approaches are able to improve accuracy in modeling derivative pricing in systems with memory-dependent volatility [19].

In the hydrometeorological context, Lovejoy and Mandelbrot (1985) highlighted that rainfall processes exhibit fractional characteristics through the Noah effect and Hurst law, indicating the presence of persistence and long-range dependence that cannot be adequately captured by classical stochastic models [20]. This observation provides a strong theoretical basis for adopting fractional approaches in rainfall-based risk modeling, particularly in applications where memory effects play an important role in determining future dynamics.

To obtain analytical insights from such models, a variety of semi-analytical techniques have been developed for solving fractional differential equations. Among these, the DJM, introduced by Daftardar-Gejji and Jafari (2006), offers an iterative framework capable of generating convergent series solutions without the need for linearization or discretization [21]. Integral transform techniques have also been extensively employed to simplify the treatment of fractional operators and improve analytical tractability [22]. More recently, the KF transform has emerged as a promising alternative for systematically handling fractional differential systems [23]. Furthermore, advances in fractional differential equation theory have extended the analysis of existence, uniqueness, and controllability to increasingly sophisticated settings involving Ψ-Hilfer operators and stochastic integro-differential systems, reflecting the growing mathematical maturity and applicability of fractional frameworks in risk-sensitive modeling [24]. These developments motivate integrating the DJM and the Kashuri–Fundo transform in the present study to derive a semi-analytical solution to the fractional Black–Scholes model while preserving its underlying memory characteristics.

In line with these developments, research on determining premiums for rainfall-index-based insurance using the Black–Scholes model has made significant progress, as demonstrated by Kalfin et al. (2022) and Purwandari et al. (2024) [25,26]. Efforts to integrate fractional approaches remain relatively limited, as seen in the study by Azahra et al. (2025), which developed a fractional Black–Scholes model for rainfall index-based premium determination but was still limited to the agricultural context [27,28]. These findings indicate that developing fractional models in the broader context of disaster insurance remains an open research opportunity.

The determination of insurance premiums and compensation thresholds in this study employs the Historical Burn Analysis (HBA) method, which transforms historical climate observations into risk indices by directly utilizing past disaster records to estimate trigger and exit values. This approach has been widely adopted in weather index-based insurance due to its objectivity and transparency in linking measurable climatic variables to compensation mechanisms [25,29]. However, HBA alone is insufficient for capturing rainfall's stochastic dynamics; it requires integration with a probabilistic pricing framework to produce actuarially sound premium estimates [25,27,30]. This gap motivates combining HBA with the fractional Black–Scholes model as the core methodological contribution of this study.

In addition, approaches that simultaneously model the risks of excess rainfall (floods) and rainfall deficit (droughts) within a unified framework remain relatively limited, even though the characteristics of extreme rainfall exhibit complex long-range dependence and temporal persistence patterns associated with climate variability and hydrometeorological processes [31–34]. Therefore, there remains a need to develop approaches that are not only capable of representing rainfall dynamics more realistically through fractional Black–Scholes models, but also of integrating multi-risk modeling and solution strategies based on a more comprehensive combination of methods [27,35–38]. From a risk financing perspective, parametric insurance schemes based on objectively measurable indices have been recognized as a promising complement to conventional indemnity-based insurance, particularly in contexts where post-disaster recovery funds are limited and transparent, pre-arranged claim mechanisms are needed [39]. This further motivates the development of mathematically rigorous index-based insurance frameworks that provide actuarially sound, verifiable premium structures.

To address these limitations, this study develops a parametric disaster insurance model based on rainfall indices, using a fractional Black–Scholes framework to capture long-memory effects. The research is structured as follows. First, the current state of hydrometeorological disaster insurance research is examined, identifying the gap in mod-

https://doi.org/10.3390/10.3390/math14132277

els that simultaneously address long-range dependence, multi-risk scenarios (flood and drought), and semi-analytical solvability. Second, the required mathematical theories are presented, encompassing fractional calculus (Caputo derivative), the KF integral transform, the Mittag–Leffler function, the fractional Black–Scholes framework, and the DJM. Third, the proposed method is formulated as a parametric rainfall-index insurance model with a multi-layer payout structure, solved semi-analytically using the combined DJM–KF approach. Finally, the feasibility and advantages of the proposed method are demonstrated through a case study in Bandung, West Java, comparing fractional and standard Black–Scholes premiums and evaluating compensation mechanisms via the HBA method.

The main contributions of this study are as follows. First, the fractional Black–Scholes equation is solved semi-analytically using a novel combination of the DJM and the KF transform, yielding a general closed-form solution expressed in terms of the Mittag–Leffler function. Second, a unified parametric insurance model is developed that simultaneously addresses flood and drought risk within a single framework, with a multi-layer compensation structure differentiated by housing damage severity. Third, the study provides empirical evidence that the fractional-order parameter can be calibrated to match the long-memory characteristics of observed rainfall data, enabling adaptive and inclusive premium structures consistent with SDG 13 objectives. Thus, this study not only contributes to the development of mathematical models in index-based insurance but also has practical implications for supporting hydrometeorological disaster risk mitigation strategies and strengthening climate change adaptation efforts in line with the achievement of SDG 13.

2. Mathematical Preliminaries and Notation

This section introduces the fundamental mathematical concepts used throughout this study. Fractional calculus extends classical calculus by allowing derivatives and integrals of non-integer order, enabling the modeling of systems with memory and hereditary properties. In the context of hydrometeorological modeling, the utility of fractional calculus lies in its ability to represent persistent memory effects inherent in rainfall processes, which classical stochastic models based on standard Brownian motion fail to capture. The following subsections present the key definitions and properties of the Caputo fractional derivative, the KF integral transform, and the Mittag–Leffler function, which collectively form the mathematical foundation of the fractional Black–Scholes framework developed in this study.

This capability has been demonstrated in hydrological modeling, where fractional-order operators based on the Caputo derivative have been applied to represent memory effects and long-term dependencies across key components of the water cycle, including rainfall, surface water, and groundwater dynamics, yielding improved accuracy compared to classical integer-order approaches [40].

Definition 1 ([22]). *The Caputo fractional derivative, for a function f to x of real order δ, where $n-1 < \delta \leq n$, satisfies the following condition:*

$$D^{\delta} f(t) = \begin{cases} f^{(n)}(t), & \delta = n \in N \\ \frac{1}{\Gamma(n-\delta)} \int_0^t (x-\tau)^{n-\delta-1} f^{(n)}(t) dt, & n-1 < \delta < n. \end{cases} \quad (1)$$

The Caputo fractional derivative is selected in this study for three principal reasons. First, unlike the Riemann–Liouville derivative, the Caputo derivative allows initial conditions to be expressed in terms of classical integer-order derivatives, which carry direct physical interpretations and are consistent with standard observational data [22,41]. Second, the Caputo operator is well-suited for modeling memory effects in systems where

https://doi.org/10.3390/10.3390/math14132277

the initial state is known, as in rainfall-based insurance, where historical data serve as the starting point for premium computation. Third, the Caputo derivative commutes with the KF transform in a manner that yields a tractable algebraic structure (Theorem 1), enabling the systematic derivation of the DJM–KF solution scheme. While other operators, such as the Hilfer, Ψ-Caputo, and Ψ-Hilfer derivatives, offer greater generality through interpolation parameters or kernel flexibility, they introduce additional complexity that is not required given the data-driven estimation of δ in this study. Nevertheless, the DJM iterative decomposition framework in Section 3 is operator-agnostic in structure: provided the chosen fractional derivative admits a compatible integral transform with a known convolution property analogous to Theorem 1, the solution procedure can be adapted accordingly. This extensibility is noted as a direction for future research.

Consider the following fractional differential equation with the Caputo derivative:

$$D_t^{\delta} u(x,t) = f(x,t) + Lu(x,t) + Nu(x,t),\ t > 0, x \in \mathbb{R}, 0 < \delta \leq 1, \tag{2}$$

with the initial condition $u(x,0) = g(x)$, where D_t^{δ} denotes the fractional derivative operator (in the Caputo sense), L is a linear operator, N is a nonlinear operator, $f(x,t)$ represents the nonhomogeneous term, and $u(x,t)$ is the unknown function to be determined [22,35,41].

Furthermore, the integral transform used in this study is the KF Transform, which is defined as follows [23]:

$$\mathcal{K}[u(x,t)](v) = A(v) = \frac{1}{v}\int_0^{\infty} e^{-\frac{t}{v^2}}\, u(x,t)dt, \quad t \geq 0,\ -k_1 < v < k_2, \tag{3}$$

The inverse of the KF transform is denoted by

$$\mathcal{K}^{-1}[A(v)] = u(x,t),\ \ t \geq 0. \tag{4}$$

For δ as a fractional number, the KF transform satisfies [23]:

$$\mathcal{K}\left[t^{\delta}\right] = \Gamma(\delta+1)v^{2\delta+1}, \tag{5}$$

thus, its inverse is given by

$$\mathcal{K}^{-1}\left[v^{2\delta+1}\right] = \frac{t^{\delta}}{\Gamma(\delta+1)}. \tag{6}$$

Theorem 1 ([23])**.** *The following property of the KF transform with respect to the Caputo fractional derivative holds:*

$$\mathcal{K}\left[D^{\delta}u(x,t)\right] = \frac{A(v)}{v^{2\delta}} - \sum_{k=0}^{n-1}\frac{u^k(0)}{v^{2(\delta-k)-1}},\ \ n-1 < \delta \leq n. \tag{7}$$

This transform possesses properties with respect to the Caputo fractional derivative that enable the systematic solution of fractional differential equations.

Definition 2 ([22])**.** *The Mittag–Leffler function $E_{\delta}(z)$ plays an important role in representing solutions of fractional differential equations and is defined as follows:*

$$E_{\delta}(z) = \sum_{k=0}^{\infty}\frac{z^k}{\Gamma(1+\delta k)},\ Re(\delta) > 0. \tag{8}$$

This function is a generalization of the exponential function, since for $\delta = 1$, it holds that [22,42]:

https://doi.org/10.3390/10.3390/math14132277

$$E_1(z)\sum_{k=0}^{\infty}\frac{z^k}{\Gamma(1+k)}=\sum_{k=0}^{\infty}\frac{z^k}{k!}=e^z. \tag{9}$$

Since the exponential function constitutes an essential component of the classical Black–Scholes formulation, the standard Black–Scholes model is briefly reviewed before introducing its fractional counterpart. The classical Black–Scholes model is one of the fundamental frameworks in financial mathematics used to determine derivative prices based on the stochastic dynamics of the underlying variable [10,11]. This model assumes that the underlying variable follows a geometric Brownian motion process, expressed as:

$$dS_t = \mu S_t dt + \sigma S_t dW_t, \tag{10}$$

where S_t is the value of the underlying variable at time t, μ is the growth rate, σ is the volatility, and W_t is a standard Brownian motion [10,11]. Based on this assumption, the Black–Scholes partial differential equation for the contract value $V(S,t)$ is obtained as follows [10]:

$$\frac{\partial V}{\partial t}+\frac{1}{2}\sigma^2S^2\frac{\partial^2V}{\partial S^2}+rS\frac{\partial V}{\partial S}-rV=0, \tag{11}$$

where r denotes the risk-free interest rate. This equation yields an analytical solution for European option pricing, enabling consistent and arbitrage-free valuation of the contract [11]. In particular, the prices of call options and put options, respectively, are given by [10,11]:

$$C_B = S_0N(d_1)-Ke^{-rt}N(d_2), \tag{12}$$

$$P_B = Ke^{-rt}N(-d_2)-S_0N(-d_1), \tag{13}$$

with the cumulative distribution terms d_1 and d_2 represented as follows:

$$d_1=\frac{\ln\left(\frac{S_0}{K}\right)+\left(r+\frac{\sigma^2}{2}\right)t}{\sigma\sqrt{t}}, \tag{14}$$

$$d_2=\frac{ln\left(\frac{S_0}{K}\right)+\left(r-\frac{\sigma^2}{2}\right)t}{\sigma\sqrt{t}}. \tag{15}$$

Although the classical Black–Scholes model has provided a strong mathematical framework for determining risk-based contract pricing and has been widely adapted in the insurance context, it has a fundamental limitation arising from the assumption that the geometric Brownian motion process in Equation (10) is memoryless [10,11]. Within this framework, the dynamics of the underlying variable depend only on the current state and do not account for historical effects, making it less capable of representing natural phenomena such as rainfall, which often exhibit long-range dependence and temporal persistence [13, 16,20,31].

Several studies have shown that hydrometeorological data, including rainfall, possess fractal characteristics and significant memory effects, which cannot be adequately explained using classical stochastic models based on standard Brownian motion [12,20,31,43]. This is demonstrated through the concept of fractional Brownian motion $B_{H(t)}$, which has the following covariance property:

$$E[B_H(t)B_H(s)]=\frac{1}{2}\left(t^{2H}+s^{2H}-|t-s|^{2H}\right) \tag{16}$$

with parameter $H\in(0,1)$ as the Hurst exponent that measures the degree of long-range dependence, where $H>0.5$ indicates the presence of persistence in the data [12,14]. This

https://doi.org/10.3390/10.3390/math14132277

characteristic is recognized through the Joseph effect and the Noah effect, which indicate that climate systems possess memory structures that cannot be captured by classical Brownian models [12,31].

To address this limitation, the development of fractional models is carried out by replacing the standard Brownian process in the Black–Scholes model with fractional Brownian motion, enabling the model to better capture memory effects and temporal dependence [15,18,19,27,44]. In general, the dynamics of the underlying variable in the fractional model can be expressed as [13–15]:

$$dS_t = \mu S_t dt + \sigma S_t dB_H(t). \tag{17}$$

To incorporate both long-range dependence and memory effects, the classical framework is extended by introducing fractional Brownian motion in the stochastic process and a fractional-order derivative in the governing equation [13,15,19,44]:

$$\frac{\partial^\delta V}{\partial t^\delta} + \frac{1}{2}\sigma^2 S^2 \frac{\partial^2 V}{\partial S^2} + rS\frac{\partial V}{\partial S} - rV = 0, \tag{18}$$

with $0 < \delta \leq 1$ as the fractional order representing memory effects in the system. This approach allows the model to capture long-term dynamics more realistically, making it more suitable for modeling rainfall-based hydrometeorological risks that are complex and non-stationary [31,43,45,46].

In this study, the cumulative distribution in the Black–Scholes model represents the probability that the rainfall index exceeds a certain threshold, thereby triggering claim payments. In the fractional model, this probability is influenced by long-memory effects modeled through the fractional-order parameter, as follows [27,47]:

$$d_2 = \frac{\ln\left(\frac{S_0}{K}\right) + rt - \frac{1}{2}\sigma^2 t^{2\delta}}{\sigma\sqrt{t^{2\delta}}}, \tag{19}$$

when $\delta = \frac{1}{2}$, Equation (19) reduces to the classical Black–Scholes formulation. Substituting $\delta = \frac{1}{2}$ yields $t^{2\delta} = t^{2(\frac{1}{2})} = t$, so that Equation (19) becomes the classical d_2 expression in Equation (15). Consequently, $\delta = \frac{1}{2}$ acts as the boundary between the fractional and classical regimes, and the fractional order parameter δ governs the degree of memory intensity in the model. Values of δ closer to zero indicate weaker memory intensity and greater deviation from the classical model, while values of δ closer to one correspond to stronger temporal persistence and more pronounced long-range dependence in the dynamics of the underlying process [12,18,19]. The well-posedness of the fractional Black–Scholes equation under the Caputo derivative has been established by reformulating it as an integral equation and applying Banach's fixed-point theorem under Lipschitz continuity conditions, guaranteeing the existence and uniqueness of its solution [41,44].

3. Daftardar Gejji–Jafari Method (DJM)

As the basis for the development of the combined DJM and KF method, the following nonlinear differential equation is introduced [21]:

$$u = f + L(u) + N(u), \tag{20}$$

where f is a given function, L is a linear operator, and N is a nonlinear operator. The DJM assumes that the solution can be represented as an infinite series expansion, allowing the nonlinear problem to be decomposed into a sequence of recursive terms [21,44]:

https://doi.org/10.3390/10.3390/math14132277

$$u = \sum_{i=0}^{\infty} u_i. \tag{21}$$

The DJM decomposes the nonlinear operator into iterative components to construct successive approximations without requiring linearization, perturbation assumptions, or discretization procedures [21,44]:

$$\sum_{i=0}^{\infty} u_i = f + L\left(\sum_{i=0}^{\infty} u_i\right) + N\left(\sum_{i=0}^{\infty} u_i\right). \tag{22}$$

Consequently, the approximate solution at the k-th iteration can be expressed as a truncated series expansion, where convergence toward the exact solution is achieved through recursive correction terms [21,27,44]:

$$u = \sum_{i=0}^{k-1} u_i. \tag{23}$$

4. Identification of Long-Term Effects and Fractional Order Estimation

The identification of long-term effects and fractional order estimation are carried out by evaluating memory characteristics through the Hurst exponent obtained from the Hurst statistical test. This approach is used to assess whether the data pattern exhibits random behavior, short-term dependence, or long-term persistence through the rescaled range (R/S) analysis framework [31]. Once the presence of long-term effects is identified, the magnitude of memory in the system is further estimated through the determination of the fractional order using the Geweke–Porter–Hudak (GPH) method [32]. This method is based on spectral analysis and Ordinary Least Squares (OLS) regression, enabling flexible and representative estimation of the fractional order in capturing long-term dynamics in time-series data [32]. According to Azahra [27] in her study on the application of the fractional Black–Scholes model in rainfall-based agricultural insurance using daily rainfall data, the steps of the Hurst statistical test using the rescaled range method are presented as follows:

$$R_i = \max_{0 \le i \le n} \sum_{i=1}^{n} \left(h_i - \overline{h}\right) - \min_{0 \le i \le n} \sum_{i=1}^{n} \left(h_i - \overline{h}\right), \tag{24}$$

where h_i represents rainfall data on the i-th day, $\overline{h}$ denotes the average rainfall, and R_i represents the cumulative deviation range of rainfall data [27]. Meanwhile, the standard deviation of rainfall data on the i-th day is expressed as follows:

$$s_i = \sqrt{\frac{1}{n}\sum_{i=1}^{n}\left(h_i - \overline{h}\right)^2}. \tag{25}$$

The estimation of the Hurst value requires a logarithmic transformation of the R/S statistic, yielding the following relation [31]:

$$(R/S)_i = ci^H, \tag{26}$$

where c is a constant, and the Hurst exponent for rainfall data is estimated using the following equation [31]:

$$H = \frac{\log(R/S)_i}{\log(i)}. \tag{27}$$

https://doi.org/10.3390/10.3390/math14132277

Furthermore, the Hurst exponent has several interpretations, namely $H = \frac{1}{2}$ indicates that the rainfall data are random, $0 < H < \frac{1}{2}$ represents short-term dependence, and $\frac{1}{2} < H < 1$ indicates long-term dependence [12,31].

5. Materials and Methods

5.1. Materials

This study was conducted in the city of Bandung, West Java, which exhibits complex spatial characteristics. It is located in a basin surrounded by mountains and active fault lines and is traversed by various river networks. This topographical condition makes Bandung highly vulnerable to hydrometeorological disasters, such as floods and droughts, as well as potential geological hazards including landslides and volcanic activity from nearby mountainous regions. In addition, the presence of dense watershed systems and land-use changes further increases the risk of surface runoff accumulation, particularly during periods of extreme rainfall events. Previous studies have shown that changes in precipitation patterns and climate variability significantly contribute to the increased frequency and intensity of hydrometeorological hazards, especially in urban areas with complex environmental conditions [43,45,46,48]. Moreover, multi-hazard assessments in Bandung indicate substantial vulnerability arising from the interaction between climatic, topographic, and anthropogenic factors [36,48,49]. Therefore, these spatial characteristics make the Bandung region a highly relevant area for the development of rainfall index-based disaster insurance models to support risk mitigation efforts and strengthen climate change adaptation strategies [25,28,29]. The spatial map of the study area, sourced from the Dashboard Pencegahan Bencana, Badan Nasional Penanggulangan Bencana (BNPB) (https://dashboardpencegahan.bnpb.go.id/peta/das, accessed on 3 January 2026), is presented in Figure 1.

Figure 1. Spatial Map of Bandung. Source: Dashboard Pencegahan Bencana, BNPB, https://dashboardpencegahan.bnpb.go.id/peta/das (accessed on 3 January 2025).

These characteristics make Bandung a representative region for studying rainfall index-based disaster insurance models. The high complexity of risks, including the possibility of multiple hydrometeorological events occurring within the same period, such as floods and droughts, requires a modeling framework capable of capturing rainfall dynamics more realistically. Previous studies have shown that rainfall variability and extreme climate

events exhibit complex temporal behavior, including persistence and long-range dependence patterns, which cannot always be adequately represented by conventional stochastic approaches [12,20,33,43]. Therefore, this study employs a fractional Black–Scholes model to incorporate long-memory effects in rainfall data, with the expectation of producing premium estimates that more accurately reflect actual risk conditions in the Bandung region.

The model used in this study is constructed based on secondary data, including daily rainfall data obtained from NASA POWER (https://power.larc.nasa.gov/data-access-viewer, accessed on 3 January 2026) and disaster loss data sourced from the National Disaster Management Agency ("Badan Nasional Penanggulangan Bencana" (BNPB)) through its website (https://gis.bnpb.go.id, accessed on 3 January 2026) for the Bandung area, West Java Province, Indonesia. The observation period covers six years, from 1 November 2019 to 31 October 2025. The collected rainfall and disaster datasets are subsequently processed and categorized according to Indonesia's seasonal characteristics, including the rainy season, dry season, and two transitional periods [43]. Furthermore, rainfall observations are analyzed to determine the trigger index and exit index values, which serve as the basis for premium calculations in rainfall index-based disaster insurance models.

5.2. Methods

The methodology in this study is structured sequentially to ensure a systematic premium determination process. First, the HBA method is applied to historical rainfall and disaster loss data to identify trigger and exit threshold values for each seasonal period. Second, the long-range dependence of the rainfall index data is assessed through the Hurst exponent using R/S analysis, confirming the presence of memory effects that justify the use of a fractional modeling approach. Third, the fractional order parameter is estimated from the rainfall data using the GPH method, yielding the values used in the fractional Black-Scholes framework. Fourth, insurance premiums are computed using both the standard and fractional Black-Scholes models based on the estimated parameters, and compensation values are determined according to the multi-layer payout structure established from the HBA thresholds.

5.2.1. Historical Burn Analysis Method

The HBA method is employed to transform historical climate datasets into risk indices, determine trigger and exit thresholds, and establish the basis for premium calculations. This approach has been widely used in weather index-based insurance because it directly utilizes historical observations to estimate risk levels and potential compensation mechanisms [25–27]. Although HBA has demonstrated effectiveness in hydrometeorological risk analysis, particularly for flood and drought events, its implementation requires long-term historical datasets, appropriate index construction, and policy support to ensure both social and economic feasibility [29,30].

Compensation in rainfall index-based disaster insurance is determined through trigger and exit values. Compensation is initiated when the rainfall index exceeds or falls below a predetermined threshold, depending on the type of disaster event considered. No compensation is provided when the rainfall index remains within the normal range. Meanwhile, when the rainfall index falls between the trigger and exit values, partial compensation is paid by the insurer to the insured according to the predefined payout structure [25–27]. The steps used to determine rainfall trigger and exit indices based on the HBA approach are described as follows [27]:

(1) Data Collection and Preprocessing

The initial stage of the study begins with collecting historical datasets representing disaster conditions within the study area. The primary variables consist of hydrometeoro-

https://doi.org/10.3390/10.3390/math14132277

logical indicators, particularly rainfall observations obtained at an appropriate temporal resolution according to disaster-event characteristics. In addition, disaster loss records and supporting datasets are incorporated to strengthen the relationship analysis between rainfall indices and actual disaster impacts. Subsequently, the collected datasets undergo preprocessing procedures, including completeness checking, treatment of missing values, and temporal standardization to ensure data consistency and suitability for further analysis.

(2) Determination of the Period

The determination of the index-window period is conducted to identify the temporal interval most relevant to disaster occurrence. Historical observations are analyzed to examine seasonal patterns and the frequency of extreme events. Furthermore, the relationship between rainfall index variables and disaster impact data is assessed using the Pearson product–moment correlation coefficient to identify the period that exhibits the strongest association with disaster occurrences:

$$r_{xy} = \frac{n\sum x_i y_i - \sum x_i \sum y_i}{\sqrt{\left(n\sum x_i^2 - (\sum x_i)^2\right)\left(n\sum y_i^2 - (\sum y_i)^2\right)}} \tag{28}$$

where x_i represents rainfall index observations and y_i denotes disaster impact observations. The Pearson product–moment correlation coefficient is used to identify the strength of the relationship between rainfall variables and disaster occurrences within a given observation period.

(3) Adjustment and Aggregation of Index Data

After determining the index window period, rainfall data within the selected period are further processed through an aggregation procedure. Daily rainfall observations are accumulated into ten-day rainfall indices (dasarian), denoted by D_j, $j = 1,\ 2,\ 3$, within the index window period calculated for each season (divided into four time intervals) that has been previously determined. The formulas used are as follows:

$$D_1 = \sum_{i=1}^{10} h_i,\ D_2 = \sum_{i=11}^{20} h_i,\ D_3 = \sum_{i=21}^{30} h_i, \tag{29}$$

where h_i represents daily rainfall observations.

The adjusted ten-day rainfall index D'_j, with $j = 1,\ 2,\ 3$, is subsequently determined under the following assumptions:

- Rainfall observations are bounded using lower and upper thresholds of 2 mm/day and 100 mm/day, respectively.
- Rainfall values below the lower threshold are replaced by 2 mm/day, whereas rainfall values exceeding the upper threshold are replaced by 100 mm/day.

These adjustments are introduced to reduce the influence of extreme observations and ensure that the resulting rainfall index provides a stable and proportional representation of disaster conditions for insurance calculations. The average adjusted cumulative rainfall $\overline{A'_m}$ is then calculated as:

$$\overline{A'_m} = \frac{\sum_{j=1}^{n} D'_j}{n},\ m = 1,\ 2,\ 3,\ 4. \tag{30}$$

(4) Calculation of the Mean ($\overline{u}$) and Sample Standard Deviation (σ)

https://doi.org/10.3390/10.3390/math14132277

To validate the distributional assumptions of the rainfall data, distribution parameters are estimated from the transformed rainfall index values. These parameters are represented by the mean and standard deviation values and are calculated as follows:

$$\overline{u} = \frac{1}{n-1}\sum_{m=2}^{n} \ln\left(\frac{\overline{A_m}}{\overline{A_m}-1}\right) \tag{31}$$

$$\sigma = \sqrt{\frac{1}{n-2}\left(\sum_{m=2}^{n}\left(\ln\left(\frac{\overline{A_m}}{\overline{A_m}-1}\right)-\overline{u}\right)^2\right)} \tag{32}$$

The estimated mean value $\overline{u}$ and standard deviation σ are subsequently employed in the Anderson–Darling goodness-of-fit test to assess whether the selected probability distribution adequately represents rainfall behavior as part of the model validation process.

(5) Determination of Trigger and Exit Values

The trigger and exit index values are determined based on the historical distribution of adjusted rainfall index data. This process is conducted by analyzing all historical index realizations to identify the threshold at which losses begin to occur and the maximum compensation level. The exit value represents the worst-case condition corresponding to the maximum payout level and is calculated as follows:

$$Exit = \min\overline{A'_m},\ \ m = 1,\ 2,\ 3, \ldots, \tag{33}$$

The trigger value indicates the condition under which losses begin to occur. The rainfall trigger index G is determined based on the percentile value of the adjusted average total rainfall data as follows:

$$P_k = \text{data at potition } \frac{k(n+1)}{100},\ k \in \mathbb{C}, k < 100, \tag{34}$$

The determination of trigger and exit values ensures that the insurance scheme remains objective and consistent with actual disaster conditions while maintaining transparency in the compensation mechanism.

5.2.2. Determination of the Fractional-Order Parameter

Following the determination of trigger and exit values through the HBA method, the next stage involves identifying whether the rainfall index data exhibit long-range dependence characteristics. This identification is essential because the presence of memory effects in the data serves as the primary justification for employing a fractional rather than a classical Black-Scholes framework in premium determination. The long-term memory structure is first assessed through the Hurst exponent obtained via the R/S analysis method, as described in Section 4. Once long-range dependence is confirmed, the degree of memory in the system is quantified by estimating the fractional order parameter using the Geweke-Porter-Hudak (GPH) method, which is based on spectral analysis and OLS regression on the periodogram of the time series data [32]. Subsequently, Azahra [27] applies the GPH method to determine the fractional-order parameter δ, with the following steps:

(1) Determining the harmonic frequencies ω_j for each observation and the optimal bandwidth m:

$$\omega_j = (2\ \pi.j/n), j = 1,2,3,\ldots,mm = g(n) = \left[n^{0.5}\right], \tag{35}$$

(2) Determining the periodogram value:

https://doi.org/10.3390/10.3390/math14132277

$$I_z(\omega_j) = \frac{1}{2\pi}\left\{\gamma_0 + 2\sum_{i=1}^{n-1}\gamma_i \cos(i.\omega_j)\right\},\ \omega_j \in (-\pi, \pi), \tag{36}$$

where γ_i represents the autocovariance value at the i-th step [29].

(3) Determining the response variable Y_j and the predictor variable X_j:

$$Y_j = \ln(I_z(\omega_j)), \tag{37}$$

$$X_j = \ln\left(\frac{1}{4\sin^2(\omega_j/2)}\right), \tag{38}$$

(4) Determining the fractional-order parameter δ using the Ordinary Least Squares (OLS) method:

$$\hat{\delta} = \frac{\sum_{j=1}^{m}(X_j - \overline{X})(Y_j - \overline{Y})}{\sum_{j=1}^{m}(X_j - \overline{X})^2},\ j = 1,\ 2,\ 3, \ldots, m. \tag{39}$$

The fractional order δ_1 is directly estimated from historical rainfall data in Bandung using the GPH method via Equation (39), which applies OLS regression on the periodogram in the frequency domain. This value reflects the degree of long-range dependence present in the observed rainfall time series, where $\delta_1 < 0.5$ corresponds to a process with intermediate memory. To analyze the sensitivity of the model across a broader range of fractional orders, a second fractional order δ_2 is introduced analytically. Consider the sequence:

$$\phi_n = \frac{1}{2} + \frac{\delta_1}{n}, \quad n \in \mathbb{N}. \tag{40}$$

This sequence satisfies two properties. First, $\phi_n > 0.5$ for all n, since $\delta_1 > 0$. Second, the sequence converges to the classical limit:

$$\lim_{n\to\infty}\phi_n = \frac{1}{2}, \tag{41}$$

which is consistent with the recovery of the standard Black-Scholes model at $\delta = 0.5$, as established in Equation (19). Taking $n = 1$ yields:

$$\delta_2 = \phi_1 = \frac{1}{2} + \delta_1. \tag{42}$$

This value represents the upper bound of the fractional order range examined in this study. Therefore, variations in δ_1 and δ_2 are introduced to evaluate the sensitivity of the model to changes in fractional order and to investigate the influence of memory effects on the resulting premium values.

5.2.3. Conceptual Framework of Hydrometeorological Index Insurance

Rainfall index-based hydrometeorological insurance is a parametric insurance scheme in which claim payments are determined based on the realization of a predefined rainfall index without requiring direct assessment of actual losses in the field. This mechanism employs a trigger index as the threshold for claim activation, thereby increasing objectivity, accelerating the claim settlement process, and reducing administrative costs compared with conventional loss-based insurance schemes [25,26,29,30].

Premium determination in this study is conducted using an option-pricing analogy. This approach is adopted because the structure of hydrometeorological risk, including both excess rainfall and rainfall deficiency, exhibits mathematical similarities to the payoff structure of financial option contracts. The Black–Scholes model provides a probabilistic

https://doi.org/10.3390/10.3390/math14132277

framework for premium estimation based on the stochastic behavior and volatility of rainfall indices while enabling systematic determination of compensation values according to realized index conditions without requiring individual loss assessments [8–11].

Within this framework, the Black–Scholes equation is adapted by mapping financial variables into a hydrometeorological context. The average cumulative rainfall is considered as the underlying variable, the rainfall trigger index serves as the strike value, and the option payoff corresponds to the insurance claim payment. Through this analogy, the insurance premium can be estimated using an option-pricing mechanism with adjustments to the interpretation of model parameters according to hydrometeorological characteristics [10,11,25].

Although the parameters d_1 and d_2 are jointly used in the Black–Scholes formulation, the subsequent analysis in this study focuses primarily on d_2 since it directly reflects the cumulative probability associated with rainfall index deviations relative to the trigger threshold and therefore has a more direct interpretation in the insurance claim mechanism. Meanwhile, d_1 mainly contributes to the intermediate pricing formulation and sensitivity interpretation within the option framework [10,11,19,27].

The insured risk is determined based on deviations of the rainfall index from the trigger index specified in the insurance contract. This study considers two principal categories of hydrometeorological risk, namely excess rainfall and rainfall deficiency, which are represented through call option and put option analogies, respectively.

For excess rainfall conditions that may potentially lead to flood events, the insurance contract is modeled using a call-option framework. Claims are activated when the average cumulative rainfall during the insurance period exceeds the predetermined trigger value. The payoff and premium functions are expressed as follows [10,25–27]:

$$\text{Payoff} = \begin{cases} K, \ if \ \text{A}_0 > G \\ 0, \ if \ \text{A}_0 \leq G \end{cases}, \tag{43}$$

$$\text{Premium} = \text{K}e^{-rT}N(d_2). \tag{44}$$

Conversely, rainfall deficiency risk that may potentially cause drought conditions is represented through a put-option framework. Claims are paid when the average cumulative rainfall falls below the trigger value. The payoff and premium functions are formulated as follows [10,25–27]:

$$\text{Payoff} = \begin{cases} K, \ if \ \text{A}_0 < G \\ 0, \ if \ \text{A}_0 \geq G \end{cases}, \tag{45}$$

$$\text{Premium} = Ke^{-rT}N(-d_2). \tag{46}$$

In this formulation, K denotes the insured amount, $\overline{A_0}$ represents the average cumulative rainfall during the insurance period, G is the rainfall trigger index, r is the risk-free interest rate, and T is the insurance period. Furthermore, $N(.)$ represents the cumulative standard normal distribution function, where $N(d_2)$ and $N(-d_2)$ indicate the probabilities that the rainfall index exceeds or falls below the trigger threshold, corresponding to the call and put option structures, respectively [10,11]. In this context, the cumulative distribution value d_2 acts as a probabilistic link between the stochastic dynamics of rainfall behavior and the likelihood of claim occurrence. By incorporating memory effects through a fractional order parameter, the modified d_2 formulation can be written as follows [10,25–27]:

$$d_2 = \frac{\ln\left(\frac{\overline{A_0}}{G}\right) + rT - \frac{\sigma^2}{2}T^{2\delta}}{\sigma\sqrt{T^{2\delta}}}, \tag{47}$$

https://doi.org/10.3390/10.3390/math14132277

where δ denotes the fractional order parameter representing memory effects within the rainfall dynamics. This formulation enables hydrometeorological risks to be represented mathematically within an option-pricing framework, allowing insurance premiums to reflect both the probability of extreme events and the variability characteristics of rainfall indices in a more realistic manner [25,27,33].

5.2.4. Rainfall Index Scheme and Claim Function Within the Fractional Model Framework

The rainfall data used in this study are divided into several seasonal periods based on the climatic characteristics of Indonesia and further adjusted according to the actual rainfall patterns observed in the study data [43]. This adjustment is necessary because rainfall conditions may vary across regions and time periods, resulting in seasonal characteristics that differ from the general climate patterns reported in previous studies.

The classification of seasonal periods is important because variations in rainfall intensity may significantly affect the magnitude of hydrometeorological disaster risk, including flood and drought events, as well as influence the probability of loss occurrence and the determination of premium and compensation values in rainfall-based parametric insurance schemes. Although Indonesia generally experiences rainy seasons, dry seasons, and transitional periods influenced by monsoon systems and large-scale climate variability [43], the classification adopted in this study is determined according to the observed rainfall behavior within the dataset to ensure that the rainfall index more accurately reflects the actual conditions of the Bandung region.

Therefore, periods with relatively higher rainfall intensity are identified as high-risk periods for excess-rainfall events, while periods with lower rainfall intensity are associated with increased drought risk. The resulting seasonal classification used in this study is presented in Table 1 [27].

Table 1. Classification of High-Intensity Rainfall.

No	Rainfall Index (mm/day)	Criteria
1	<20	Light rain
2	20–50	Moderate rain
3	50–100	Heavy rain
4	100–150	Very heavy rain
5	>150	Extreme rain

Based on Table 1, periods categorized as having high rainfall intensity exhibit relatively large average rainfall values compared to other observation periods. These conditions indicate an increased potential for hydrometeorological disasters, including floods, inundation, landslides, and infrastructure damage associated with extreme rainfall events. High rainfall intensity may increase surface runoff, reduce soil infiltration capacity, and intensify water pressure on slopes and drainage systems, thereby increasing the probability of flood and landslide occurrence [33,45].

Furthermore, regions experiencing substantial rainfall accumulation within relatively short periods tend to face more severe impacts, including damage to roads, bridges, drainage systems, and residential infrastructure, compared with regions experiencing lower rainfall intensity [7,30,33,43,50]. Such conditions may directly affect socioeconomic activities and increase the magnitude of financial losses associated with hydrometeorological disasters [3].

Meanwhile, periods classified as having relatively low rainfall intensity generally represent conditions with lower rainfall accumulation and may correspond to dry periods or transition phases toward drier conditions, as identified from the observed rainfall data

https://doi.org/10.3390/10.3390/math14132277

and presented in Table 2 [27]. These periods are also important within the rainfall index insurance framework because prolonged rainfall deficits may increase the risk of drought and associated economic losses.

Table 2. Classification of Low-Intensity Rainfall.

No	Rainfall Index (mm/day)	Criteria
1	≤1.000	Very Dry
2	1.001–2.000	Dry
3	2.001–3.000	Moderate
4	3.001–4.000	Wet
5	>4.000	Very Wet

Based on Table 2, periods with low rainfall intensity indicate relatively low and more stable rainfall conditions. These periods generally correspond to dry conditions or transitional periods characterized by a lower probability of extreme rainfall events. However, persistent rainfall deficits over extended periods may increase the potential for drought conditions and associated socioeconomic impacts. Prolonged drought may also contribute indirectly to structural damage in residential areas through soil shrinkage and land subsidence processes, which can result in wall cracks, floor deformation, foundation instability, and an increased susceptibility to environmental hazards such as fires under extremely dry conditions.

The development of rainfall index-based insurance schemes requires a compensation mechanism that is transparent, objective, and directly linked to measurable climatic variables. In this scheme, G_S is defined as the lower trigger rainfall index representing the minimum rainfall threshold at which compensation payments begin, while G_L denotes the upper trigger rainfall index corresponding to the maximum compensation threshold. These trigger values establish the range within which insurance claims are activated and determine the progression of compensation payments according to rainfall conditions.

This approach aims to reduce moral hazard and improve the efficiency of the claim process, since payments are determined based on objective rainfall index values rather than direct field verification of damages [25–27,33]. Consequently, the compensation mechanism is represented through a piecewise function describing the relationship between the rainfall index and the proportion of claim payments, as illustrated in Figure 2a.

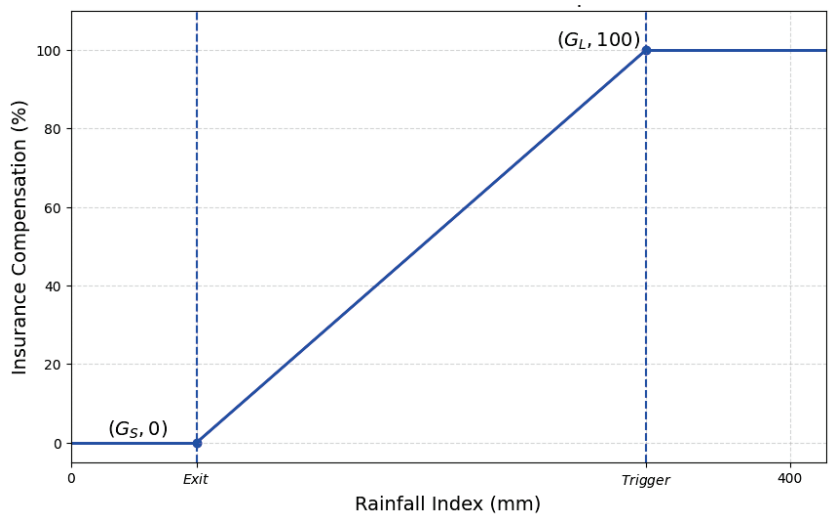

(a)

Figure 2. *Cont.*

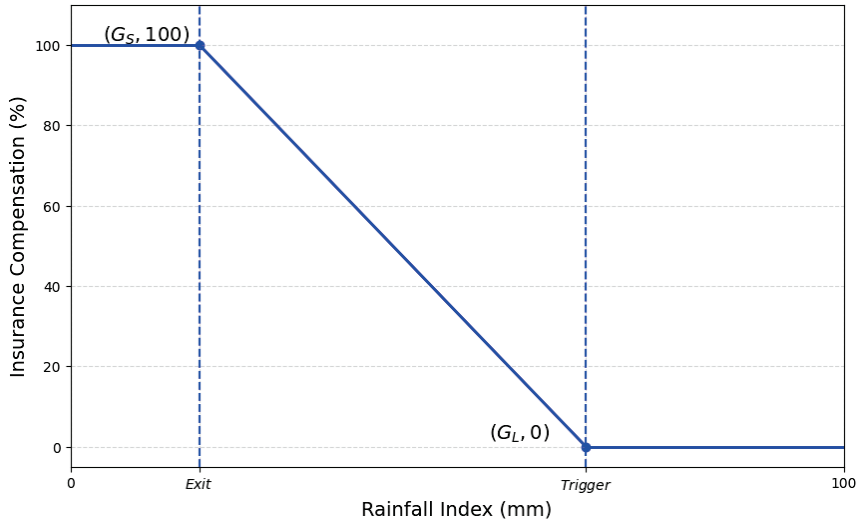

(**b**)

Figure 2. (**a**) Rainfall Index-Based Flood Insurance Compensation Scheme. (**b**) Rainfall Index-Based Drought Insurance Compensation Scheme.

Based on Figure 2a, compensation begins to be provided when the rainfall index reaches the initial trigger point G. After exceeding this value, the compensation increases linearly with increasing rainfall until it reaches the maximum compensation level of 100% at point G_L. If rainfall continues to increase beyond G_L, the compensation value remains constant at the maximum level, reflecting an extreme loss condition that has reached saturation. In addition to the trigger value as the initial point for claim payments, exit and trigger values are also established to represent extreme conditions in which losses have reached the maximum level. The claim function for flood disasters can be expressed as follows [25–27]:

$$Compensation = \frac{Rainfall\ Index - Exit}{Trigger - Exit} \times K \tag{48}$$

Meanwhile, for periods characterized by low rainfall intensity, the compensation scheme is developed according to drought-related conditions, as illustrated in Figure 2b.

Based on Figure 2b, maximum compensation of 100% is provided when the rainfall index is at or below the initial trigger point G_S. Subsequently, the compensation decreases linearly as rainfall increases until it reaches zero at point G_L. If rainfall exceeds G_L, no compensation is provided because such conditions no longer represent drought risk. The claim amount is then determined through an index-based claim function modeled as follows [25–27]:

$$Compensation = \frac{Trigger - Rainfall\ Index}{Trigger - Exit} \times K. \tag{49}$$

6. Results

6.1. Solution of the Fractional Black–Scholes Model Using the DJM–KF Method

This subsection discusses the solution of the fractional Black–Scholes partial differential equation by utilizing the combined theorem of the KF Transform and the DJM decomposition method. This approach enables the systematic solution of partial differential equations through a combination of integral transforms and series decomposition schemes. Suppose the following fractional differential equation is given:

$$D_t^{\delta} u(x,t) = f(x,t) + L[u(x,t)], \quad 0 < \delta \leq 1, \tag{50}$$

https://doi.org/10.3390/10.3390/math14132277

where D_t^{δ} denotes the fractional derivative (in the Caputo sense), L is a linear differential operator, and $f(x,t)$ is a given function. By applying the KF transform to both sides of the fractional differential Equation (50), we obtain

$$\mathcal{K}[D_t^{\delta}u(x,t)\Big] = \mathcal{K}[f(x,t)] + \mathcal{K}[Lu(x,t)], \tag{51}$$

and by using the transform property with respect to the Caputo fractional derivative, the following relation is obtained:

$$\frac{A(v)}{v^{2\delta}} - \frac{u(x,0)}{v^{2\delta-1}} = \mathcal{K}[f(x,t)] + \mathcal{K}[Lu(x,t)] + \mathcal{K}[Nu(x,t)], \tag{52}$$

where $A(v) = \mathcal{K}[u(x,t)]$ by multiplying both sides by $v^{2\delta}$, the equation can be rewritten as follows:

$$A(v) = vu(x,0) + v^{2\delta}\mathcal{K}[f(x,t)] + v^{2\delta}\mathcal{K}[Lu(x,t)] + v^{2\delta}\mathcal{K}[Nu(x,t)]. \tag{53}$$

Furthermore, by applying the inverse KF transform, the following expression is obtained:

$$\begin{aligned} \mathcal{K}^{-1}[A(v)] &= \mathcal{K}^{-1}\Big[vu(x,0) + v^{2\delta}\mathcal{K}[f(x,t)] - v^{2\delta}\mathcal{K}[Lu(x,t)] - v^{2\delta}\mathcal{K}[Nu(x,t)]\Big] \\ u(x,t) &= u(x,0) + \mathcal{K}^{-1}\Big[v^{2\delta}\mathcal{K}[f(x,t)] - v^{2\delta}\mathcal{K}[Lu(x,t)] - v^{2\delta}\mathcal{K}[Nu(x,t)]\Big]. \end{aligned} \tag{54}$$

Following the DJM method, the solution $u(x,t)$ and the nonlinear operator $Nu(x,t)$, introduced previously in Equations (21) and (22), respectively, are obtained as follows:

$$\sum_{n=0}^{\infty} u_n(x,t) = u(x,0) + \mathcal{K}^{-1}\Big[v^{2\delta}\mathcal{K}[f(x,t)] - v^{2\delta}\mathcal{K}[Lu(x,t)] - v^{2\delta}\mathcal{K}[Nu(x,t)]\Big] \tag{55}$$

To construct the iterative solution procedure, Equation (50) is decomposed according to the Daftardar–Gejji and Jafari Method (DJM), where the solution is represented as a sum of recursive components. The initial approximation is obtained from the source term and initial condition, while the subsequent terms are generated iteratively from the linear and nonlinear operators. Therefore, Equation (55) can be rewritten as follows:

$$\begin{aligned} u_0 + u_1 + u_2 + \cdots &= u(0) + \mathcal{K}^{-1}\left[v^{2\delta}\mathcal{K}[f(x,t)]\right] - \mathcal{K}^{-1}\left[v^{2\delta}\mathcal{K}[Lu(x,t)]\right] - \mathcal{K}^{-1}\left[v^{2\delta}\mathcal{K}\left[\sum_{n=0}^{\infty} G_n\right]\right] \\ &= u(0) + \mathcal{K}^{-1}\left[v^{2\delta}\mathcal{K}[f(x,t)]\right] - \mathcal{K}^{-1}\left[v^{2\delta}\mathcal{K}[L(u_0 + u_1 + u_2 + \cdots)]\right] \\ &\quad -\mathcal{K}^{-1}\left[v^{2\delta}\mathcal{K}[(G_0 + G_1 + G_2 + \cdots)]\right]. \end{aligned} \tag{56}$$

Thus, the combined theorem is obtained from the recursive relation of the fractional differential equation solution using the DJM and the KF Transform as follows:

$$\begin{aligned} u_0 &= u(x,0) + \mathcal{K}^{-1}\Big[v^{2\delta}\mathcal{K}[u(x,t)]\Big] \\ u_1 &= -\mathcal{K}^{-1}\Big[v^{2\delta}\mathcal{K}[Lu_0]\Big] - \mathcal{K}^{-1}\Big[v^{2\delta}\mathcal{K}[(G_0)]\Big] \\ u_2 &= -\mathcal{K}^{-1}\Big[v^{2\delta}\mathcal{K}[Lu_1]\Big] - \mathcal{K}^{-1}\Big[v^{2\delta}\mathcal{K}[(G_1)]\Big] \\ u_3 &= -\mathcal{K}^{-1}\Big[v^{2\delta}\mathcal{K}[Lu_2]\Big] - \mathcal{K}^{-1}\Big[v^{2\delta}\mathcal{K}[(G_2)]\Big] \\ u_{n+1} &= -\mathcal{K}^{-1}\Big[v^{2\delta}\mathcal{K}[L(u_n)]\Big] - \mathcal{K}^{-1}\Big[v^{2\delta}\mathcal{K}[(G_n)]\Big],\ n \geq 0. \end{aligned} \tag{57}$$

https://doi.org/10.3390/10.3390/math14132277

Furthermore, this formulation is applied to the fractional Black–Scholes model. By performing a standard variable transformation, the fractional Black–Scholes equation can be reduced into the form

$$D_\tau^\delta u(x,\tau) = Lu(x,\tau), \tag{58}$$

with the linear operator

$$Lu = \frac{\partial^2 V}{\partial x^2} + (k-1)\frac{\partial V}{\partial x} - ku, \tag{59}$$

with the initial condition $u(x,0) = \max\{e^x - 1, 0\}$. Based on the combined DJM and KF theorem, the recursive solution of the fractional Black–Scholes equation is given by

$$u(x,0) = \max\{e^x - 1, 0\}, \tag{60}$$

$$u_{n+1}(x,\tau) = \mathcal{K}^{-1}\left(v^{2\delta}\mathcal{K}[L(u_n(x,\tau))]\right),\ n \geq 0, \tag{61}$$

By further expansion using the properties of the KF transform, the initial terms of the solution are obtained as

$$\begin{array}{ll} u_0(x,\tau) & = u(x,0) = \max\{e^x - 1, 0\}, \\ u_1(x,\tau) & = \mathcal{K}^{-1}\left(v^{2\delta}\mathcal{K}[L(u_0(x,\tau))]\right) \\ & = \frac{\tau^\delta}{\Gamma(\delta+1)}\left[k.\max\{e^x, 0\} - k.\max\{e^x - 1, 0\}\right], \\ u_2(x,\tau) & = \mathcal{K}^{-1}\left(v^{2\delta}\mathcal{K}[L(u_1(x,\tau))]\right) \\ & = \frac{\tau^{2\delta}}{\Gamma(2\delta+1)}\left[-k^2.\max\{e^x, 0\} + k^2.\max\{e^x - 1, 0\}\right], \end{array} \tag{62}$$

and in general,

$$u_n(x,\tau) = \mathcal{K}^{-1}\left(v^{2\delta}\mathcal{K}[L(u_{n-1}(x,\tau))]\right) = \frac{\tau^{n\delta}}{\Gamma(n\delta+1)}\left[(-k)^n.\max\{e^x - 1, 0\} - (-k)^n.\max\{e^x, 0\}\right], \tag{63}$$

Thus, by summing all terms, the solution of the fractional Black–Scholes model is obtained as

$$u(x,\tau) = \sum_{n=0}^{\infty} u_n(x,\tau) = \max\{e^x - 1, 0\}E_\delta(-k\tau)^n + \max\{e^x, 0\}\left(1 - E_\delta\left(-k\tau^\delta\right)\right), \tag{64}$$

where $E_\delta(z)$ denotes the Mittag–Leffler function.

6.2. Statistical Characteristics of Hydrometeorological Data

This section presents the statistical characteristics of the hydrometeorological data used in this study, with a particular focus on rainfall dynamics and their implications for disaster risk modeling. Based on the rainfall intensity classifications presented in Tables 1 and 2, the observation period in this study is divided into four periods. Period 1 (P1), namely November–March, represents the rainy season with the highest rainfall intensity and variability. Period 2 (P2), namely April–June, represents the transition phase from the rainy season to the dry season. Period 3 (P3), namely July–August, reflects the dry season characterized by low and relatively stable rainfall. Period 4 (P4), namely September–October, represents the transition phase from the dry season to the rainy season. This classification is conducted based on the meteorological characteristics of rainfall during each observation period.

6.2.1. Rainfall Data and Disaster Events

This section discusses the relationship between rainfall data and disaster events during each observation period. Rainfall data are used to describe the meteorological patterns

https://doi.org/10.3390/10.3390/math14132277

occurring throughout the year, while disaster event data are used to identify the impacts arising from changes in rainfall intensity. To facilitate the analysis, rainfall data are grouped according to the previously defined seasonal periods. Thus, Table 3 presents the differences in rainfall characteristics across each period and their relationship to potential disasters.

Table 3. Rainfall Accumulation and Disaster Events in Each Observation Period.

No	Year	Period	Accumulated Rainfall (mm)	Number of Disaster Event	Type of Damaging House			Disaster Losses (IDR)
					Low	Med	High	
1	2019–2020	P1	2337.36	444	3368	1301	1141	158,010,000,000
2	2020	P2	1016.93	161	526	242	168	25,230,000,000
3	2020	P3	160.11	68	120	38	20	4,140,000,000
4	2020	P4	645.38	175	1881	748	447	77,475,000,000
5	2020–2021	P1	2077.48	657	3315	905	606	113,235,000,000
6	2021	P2	676.41	255	821	258	141	28,515,000,000
7	2021	P3	189.54	77	171	107	83	10,755,000,000
8	2021	P4	463.16	173	398	182	80	16,230,000,000
9	2021–2022	P1	1596.97	660	3446	1044	598	118,890,000,000
10	2022	P2	825.23	215	780	202	130	25,560,000,000
11	2022	P3	338.59	90	1076	101	34	21,210,000,000
12	2022	P4	726.57	158	693	279	122	26,085,000,000
13	2022–2023	P1	1617.57	323	29678	17026	13965	1,793,850,000,000
14	2023	P2	640.44	168	706	348	105	27,330,000,000
15	2023	P3	95.87	130	114	85	35	6,360,000,000
16	2023	P4	59.03	192	1359	221	71	31,275,000,000
17	2023–2024	P1	2078.24	265	14392	1619	918	319,530,000,000
18	2024	P2	667.28	76	1812	497	138	50,370,000,000
19	2024	P3	386.45	41	115	56	11	4,065,000,000
20	2024	P4	412.67	61	4877	2031	977	192,705,000,000
21	2024–2025	P1	1867.2	135	4017	1581	1160	177,285,000,000
22	2025	P2	798.21	101	677	390	206	34,215,000,000
23	2025	P3	436.52	60	484	179	51	15,690,000,000
24	2025	P4	596.14	51	1844	157	97	38,190,000,000

Based on Table 3, periods with high rainfall accumulation tend to be followed by a greater number of disaster events, housing damage, and total losses. This is particularly evident in Period 1 (P1), which represents the rainy season. In contrast, Period (P3), which represents the dry season, generally exhibits lower rainfall accumulation, fewer disaster events, and less housing damage.

These findings are consistent with the results of the Pearson correlation analysis using Equation (28), which shows a coefficient value of 0.7181 between rainfall accumulation and the number of disaster events. This value indicates a strong positive linear relationship, implying that an increase in rainfall tends to be followed by an increase in the number of disaster events. Therefore, rainfall can be used as an important indicator in determining risk levels within rainfall-based parametric insurance schemes.

The dynamics of rainfall over time need to be analyzed by visualizing the trends of accumulated rainfall during each observation period. This aims to identify patterns of rainfall variation across years, including fluctuations, increasing or decreasing trends, as well as the possible presence of anomalies, as presented in Figure 3.

As shown in Figure 3, Period P1 is the most critical period, where high rainfall is strongly associated with a high number of disaster events. Meanwhile, P3 represents the safest period. Periods P2 and P4 exhibit more varied patterns, indicating that not only rainfall accumulation, but also other factors (such as disaster type or regional vulnerability) may influence the number of disaster events. Furthermore, the relationship between rainfall accumulation and the number of disaster events is presented in Figure 4. This relationship is important for determining whether increases in rainfall are followed by increases in the frequency of disaster events during each period.

https://doi.org/10.3390/10.3390/math14132277

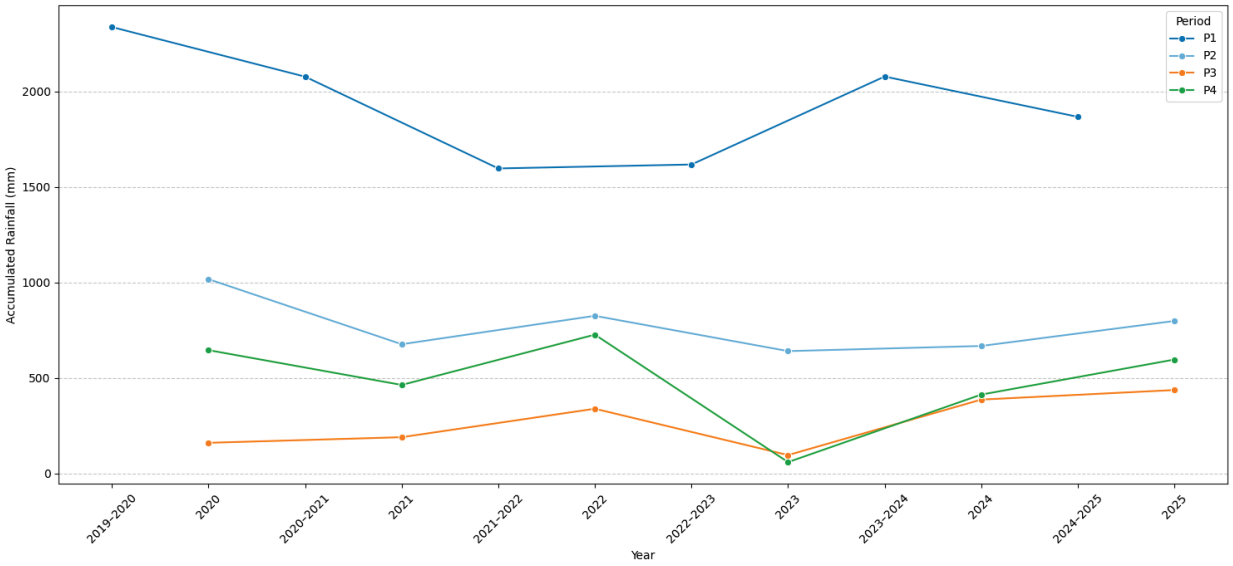

Figure 3. Rainfall Trend Graph for Each Observation Period.

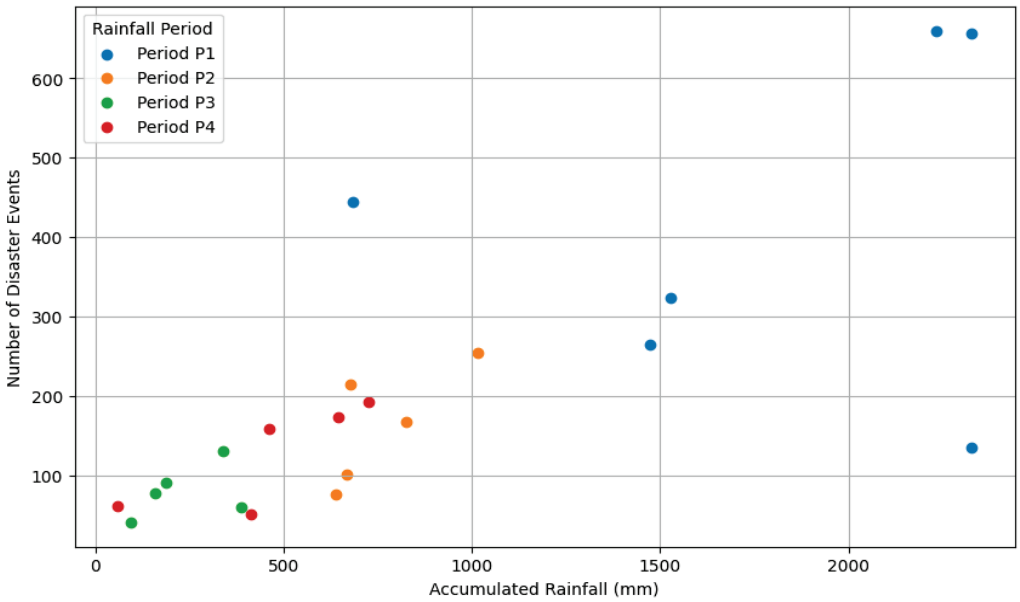

Figure 4. Relationship Between Accumulated Rainfall and Number of Disaster Events by Observation Period.

Based on Figure 4, it can be observed that higher rainfall accumulation tends to be associated with a greater number of disaster events. Data points in Period P1 tend to appear at higher rainfall and disaster-event values compared to other periods, whereas Period P3 is concentrated at lower values. This pattern supports the previous Pearson correlation results, which indicated a strong positive linear relationship between rainfall and the number of disaster events. In addition to analyzing rainfall patterns and disaster-event frequency, this study also considers the economic losses caused by disasters. Loss estimation is calculated based on disaster-event data for each period (P1–P4) to examine how financial impacts evolve over time. Figure 5 aims to identify disaster-loss trends, detect significant spikes (extreme losses), and compare loss levels across periods. This analysis is important in the context of developing index insurance models, since loss values constitute a primary component in premium determination and risk management.

The visualization presented in Figure 5 successfully illustrates the trend of rainfall accumulation across the four seasonal periods, namely P1 (November–March), P2 (April–June),

https://doi.org/10.3390/10.3390/math14132277

P3 (July–August), and P4 (September–October), throughout the observation years. In general, Period P1 exhibits the highest rainfall accumulation and coincides with a large number of disaster events and high loss values. However, an exception is observed in P1 of 2022, where rainfall was at a moderate level but was followed by extremely high losses. P3 consistently shows the lowest rainfall accumulation and can therefore be categorized as the driest period, with relatively low numbers of disaster events and disaster losses. This indicates that rainfall is not the sole factor influencing disaster losses. High loss values are likely affected by other factors such as regional vulnerability, population density, infrastructure conditions, or the severity of impacts on houses experiencing moderate to severe damage. Therefore, although rainfall has a strong relationship with the number of disaster events, the magnitude of the resulting losses is also influenced by regional characteristics and the severity of the damage incurred.

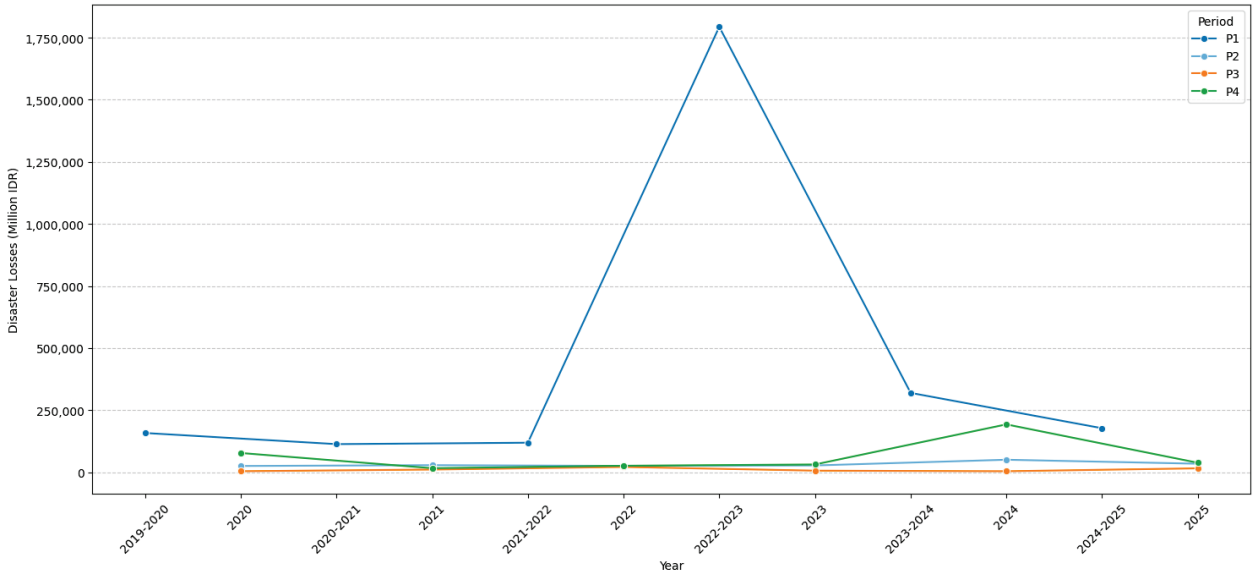

Figure 5. Graph of Disaster Loss Accumulation by Observation Period.

6.2.2. Normal Distribution Testing for Data in Each Period

Normal distribution testing is conducted on rainfall data for each observation period to determine whether the data follow a normal distribution. This information is important because several statistical methods and parametric models require the assumption of normality in order to produce more valid estimation results. In this study, normality testing is carried out separately for each period to identify differences in rainfall distribution characteristics between the rainy season, dry season, and transitional periods.

The calculation of the normal distribution begins by grouping daily rainfall data into ten-day periods $(D_j,\ j = 1,\ 2,\ 3)$, namely accumulated rainfall over 10 days. Thus, each observation month consists of three ten-day periods. Dasarian 1 represents rainfall accumulation from days 1–10, Dasarian 2 from days 11–20, and Dasarian 3 from day 21 until the end of the month according to the number of days in that month. The grouped data for each period are presented in Appendix A. As an example, the following presents the calculation of rainfall accumulation data for 1–10 November 2019, corresponding to Dasarian 1 of November:

- $D_1 = 26.53 + 14.46 + 14.58 + 7.69 + 8.23 + 4.26 + 2.85 + 0.13 + 0.92 + 1.72 = 81.37$
- $D_2 = 5.72 + 0.29 + 3.41 + 10.56 + 7.21 + 0.8 + 0.07 + 0.11 + 4.2 + 12.47 = 44.84$
- $D_3 = 8.91 + 6.25 + 16.95 + 8.96 + 7.73 + 7.64 + 4.71 + 1.9 + 3.39 + 16.87 = 83.31$

https://doi.org/10.3390/10.3390/math14132277

Furthermore, the ten-day rainfall data are adjusted using a lower threshold and an upper threshold, denoted by $D_j{}'$. The lower threshold is assumed to represent the minimum rainfall level that does not cause drought disasters, namely 2 mm/day, while the upper threshold is assumed to represent the maximum rainfall level that still does not trigger flood disasters, namely 100 mm/day. These lower and upper threshold values are determined based on the rainfall intensity classifications presented in Tables 1 and 2.

This adjustment is carried out to restrict rainfall values within a range that is still considered normal with respect to disaster risk. Accordingly, daily rainfall data below 2 mm/day are replaced with 2 mm/day, while daily rainfall data exceeding 100 mm/day are replaced with 100 mm/day. As an example, the following presents the calculation of adjusted daily rainfall accumulation data for 1–31 November 2019. Subsequently, the adjusted ten-day rainfall data for each observation period are presented in Table 4:

- $D'_1 = 26.53 + 14.46 + 14.58 + 7.69 + 8.23 + 4.26 + 2.85 + 2 + 2 + 2 = 84.6$ mm
- $D'_2 = 5.72 + 2 + 3.41 + 10.56 + 7.21 + 2 + 2 + 2 + 4.2 + 12.47 = 51.57$ mm
- $D'_3 = 8.91 + 6.25 + 16.95 + 8.96 + 7.73 + 7.64 + 4.71 + 2 + 3.39 + 16.87 = 83.41$ mm

Table 4. Adjusted Ten-Day Rainfall Throughout the Observation Period.

Month / Period 1	j	$D_j{}'$ (mm) 2019–2020	2020–2021	2021–2022	2022–2023	2023–2024	2024–2025
November	1	84.6	163.82	198.05	165.86	66.59	141.22
	2	51.57	62.77	139.6	124.59	103.53	183.89
	3	83.41	128.91	116.96	125.04	191.66	207.5
December	1	75.24	120.9	136.63	133.38	98.85	165.49
	2	154.64	86.29	121.7	89.85	38.31	105.13
	3	245.37	112.49	114.84	121.63	131.14	63.81
January	1	135.96	125.54	64.18	51.75	306.15	98.28
	2	59.69	97.28	120.92	33.32	125.74	127.08
	3	224.32	123.19	43.52	88.31	164.7	233.33
February	1	206.26	228.92	117.36	42.22	138.99	49.08
	2	203.78	134.05	81.03	137.98	200.26	98.49
	3	222.52	91.94	51.76	183.98	116.93	148.18
March	1	85.02	123.43	92.38	116.07	165.32	171.14
	2	285.79	263.75	132.8	106.62	136.8	60.06
	3	231.92	95.99	83.44	110.5	115.86	35.86
Month / Period 2	j	$D_j{}'$ (mm) **2020**	**2021**	**2022**	**2023**	**2024**	**2025**
April	1	120.41	55.31	79.77	42.53	108.51	95.97
	2	128.29	119.95	185.9	107.91	106.19	60.53
	3	112.31	44.86	97	124.59	107.23	69.94
May	1	105.26	51.86	90.67	160.55	39.23	48.47
	2	144.91	58.88	78.37	42	31.65	80.59
	3	249.49	109	84.38	35.99	77.12	165.61
June	1	62.4	34.82	93.73	41.89	77.87	73.67
	2	59.65	128.97	54.9	76.98	53.52	128.88
	3	51.41	100.76	69.96	41.49	104.13	93.52
Month / Period 3	j	$D_j{}'$ (mm) **2020**	**2021**	**2022**	**2023**	**2024**	**2025**
July	1	70.75	35.63	34.92	71.69	250.87	134.86
	2	34.44	22.73	145.96	20	20	20
	3	24.02	49.9	43.59	22.82	22	39.13
August	1	21.5	77.4	32.85	26.93	83.85	55.16
	2	51.76	36.03	72.69	20	20	89.95
	3	22	24.71	50.92	23.4	22	141.41
Month / Period 4	j	$D_j{}'$ (mm) **2020**	**2021**	**2022**	**2023**	**2024**	**2025**
September	1	47.27	35.5	157.41	20	72.14	41.27
	2	60.25	81.44	78.33	21.61	51.83	127.85
	3	108.17	66.63	68.41	20	165.52	93.09
October	1	61.63	31.26	178.37	22.52	35.19	82.89
	2	176.58	120.65	103.98	27.42	27.8	78.53
	3	211.83	150.36	144.08	41.49	41.65	186.11

https://doi.org/10.3390/10.3390/math14132277

After calculating the ten-day rainfall values throughout the observation period as presented in Table 4, the next step is to compute the average daily rainfall for each observation year within each period, denoted by $\overline{A_m}$, $m = 1, 2, 3, \ldots 6$ where m represents the average rainfall in the first observation year. This calculation is performed to obtain a general overview of rainfall characteristics in each period and to facilitate comparisons across observation years. The resulting average daily rainfall values are presented in Table 5. As an illustration, the following example shows the calculation of the average daily rainfall for Period 1 during the 2019–2020 observation year.

$$\overline{A_m} = \frac{84.6 + 51.57 + 83.41 + 75.24 + \ldots + 231.92}{15} = \frac{2350.09}{15} = 156.6727$$

Table 5. Average Rainfall for Each Period.

m	$\overline{A_m}$ (mm)			
	Period 1	**Period 2**	**Period 3**	**Period 4**
1	156.6727	114.9033	37.41167	110.955
2	130.618	78.26778	41.06667	80.97333
3	107.678	92.74222	63.48833	121.7633
4	108.74	74.88111	30.80667	25.50667
5	140.0553	78.38333	69.78667	65.68833
6	125.9027	90.79778	80.085	101.6233

Based on the average rainfall data for each period presented in Table 5, the mean value ($\overline{u}$) and sample standard deviation (σ) are subsequently calculated using Equations (36) and (37). These two parameters are then used in normal distribution testing using the Anderson–Darling method with a significance level of ($\alpha = 0.05$). The hypotheses used in the Anderson–Darling test are as follows:

- H_0: The data follow a normal distribution.
- H_1: The data do not follow a normal distribution.

The testing criteria are defined as follows:

- If p-value $> \alpha$, then H_0 is accepted, indicating that the data are considered normally distributed.
- If p-value $\leq \alpha$, then H_0 is rejected, indicating that the data are considered not normally distributed.

The results of the calculations of the mean value ($\overline{u}$), sample standard deviation (σ), and p-value for each period are presented in Table 6.

Table 6. Mean Values, Standard Deviations, and Rainfall p-values for Each Period.

Period	$\overline{u}$	σ	p**-Value**
1	−0.04373	0.184602497	0.168672119
2	−0.04709	0.242175346	0.198409825
3	0.152221	0.568581645	0.449942658
4	−0.01757	0.973756134	0.235922811

Based on Table 6, all p-values are greater than 0.05; therefore, H_0 is accepted. These results indicate that the data in Period 1, Period 2, Period 3, and Period 4 follow a normal distribution and can therefore be used in the subsequent data processing stages. The Anderson–Darling test serves as an initial evaluation of the suitability of the rainfall data distribution, which forms the basis for index construction in the hydrometeorological disaster insurance scheme using the Black–Scholes approach.

https://doi.org/10.3390/10.3390/math14132277

6.2.3. Calculation of the Average Total Ten-Day Rainfall in Each Period

The average rainfall data for each period are ordered from the smallest to the largest values, denoted by $\overline{A'_m}$. This ordering is performed to determine the rainfall exit and trigger values for each period. The exit value is defined as the lowest rainfall value from the ordered data, while the trigger value is determined based on a specified percentile of the ordered average total rainfall. Thus, rainfall thresholds for each period can be established more systematically according to the characteristics of the data distribution. The results of the determination of exit and trigger values are presented in Table 7.

Table 7. Average Rainfall Values in Ascending Order for Each Period.

$\overline{A'_m}$ (mm)			
Period 1	**Period 2**	**Period 3**	**Period 4**
107.678	74.881	30.807	25.507
108.740	78.268	37.412	65.688
125.903	78.383	41.067	80.973
130.618	90.798	63.488	101.623
140.055	92.742	69.787	110.955
156.673	114.903	80.085	121.763

Based on Table 7, the exit values for each period can be determined, namely 107.678 mm for Period 1, 74.881 mm for Period 2, 30.807 mm for Period 3, and 25.507 mm for Period 4. In addition, the highest average rainfall value in each period is used as a reference for determining the largest trigger, denoted by G_L. The G_L value for Period 1 is 156.673 mm, for Period 2 is 114.903 mm, for Period 3 is 80.085 mm, and for Period 4 is 121.763 mm.

6.2.4. Determination of Rainfall Trigger Values for Each Period

Next, the rainfall trigger values for each period are determined. These trigger values are used as thresholds in the compensation payment scheme of parametric insurance, both for high-rainfall and low-rainfall conditions. The trigger values are determined based on specific percentiles of the ordered average rainfall data, thereby representing the rainfall characteristics of each period more objectively. The results of the rainfall trigger determination for each period are presented in Table 8.

Table 8. Trigger Values for Each Period.

Percentile	**Trigger (*G*)**			
	Period 1	**Period 2**	**Period 3**	**Period 4**
1%	107.7311	75.05044444	31.13692	27.51575
5%	107.9435	75.72777778	32.45792	35.55208
10%	108.209	76.57444444	34.10917	45.5975
15%	108.4745	77.42111111	35.76042	55.64292
20%	108.74	78.26777778	37.41167	65.68833
25%	113.0306667	78.29666667	38.32542	69.50958
30%	117.3213333	78.32555556	39.23917	73.33083
35%	121.612	78.35444444	40.15292	77.15208
40%	125.9026667	78.38333333	41.06667	80.97333
45%	127.0815	81.48694444	46.67208	86.13583
50%	128.2603333	84.59055556	52.2775	91.29833
55%	129.4391667	87.69416667	57.88292	96.46083
60%	130.618	90.79777778	63.48833	101.6233
65%	132.9773333	91.28388889	65.06292	103.9563
70%	135.3366667	91.77	66.6375	106.2892
75%	137.696	92.25611111	68.21208	108.6221
80%	140.0553333	92.74222222	69.78667	110.955
85%	144.2096667	98.2825	72.36125	113.6571
90%	148.364	103.8227778	74.93583	116.3592
95%	152.5183333	109.3630556	77.51042	119.0613
100%	156.6726667	114.9033333	80.085	121.7633

https://doi.org/10.3390/10.3390/math14132277

After obtaining the trigger values in Table 8, and referring to Tables 1 and 2, disaster events occur when rainfall intensity falls within the categories of very heavy rain and extreme rain for flood risk, and within the categories of very dry and dry for drought risk. Therefore, the percentile value for both flood and drought risks is determined as $\frac{2}{5} \times 100\% = 40\%$. This trend indicates that, for flood risk, the percentile values begin at the 40th percentile and continue through the 45th, 50th, 55th, up to the 100th percentile. Meanwhile, for drought risk, the trend shows that percentile values begin at the 1st percentile and continue through the 5th, 10th, 15th, and up to the 40th percentile [27].

6.3. Premium Calculation Based on the Standard Black–Scholes Model

This section presents the calculation of insurance premiums using the standard Black–Scholes model. The standard Black–Scholes model is employed as a classical approach under the assumption of a memoryless process. Premium calculation begins by determining the value of d_2 based on Equation (19) with $\delta = 1/2$ (memoryless model), where the standard deviation value σ refers to Table 5. Meanwhile, the risk-free interest rate is calculated using the formula $r = \ln(i + 1)$, where i denotes the Indonesian interest rate of 4.65%. Thus, the value obtained is $r = \ln(4.65\% + 1) = 0.045451263$. Another required component is T, namely the length of the observation period in years, obtained by dividing the number of months in each period by 12. For Period 1, the observation period consists of 5 months, yielding $T = \frac{5}{12} = 0.41667$. For Period 1, $\overline{A_0} = 156.672$ mm, while the value of G is adjusted according to the percentile data in Table 7. As an example, for the 40th percentile with $G = 125.903$ mm, the value of d_2 is calculated as follows:

$$d_2 = \frac{\ln\left(\frac{156.672}{125.903}\right) + \left(0.045451263 - \frac{(0.184602497)^2}{2}\right)(0.41667)}{0.184602497\sqrt{0.41667}} = 0.80594.$$

Subsequently, the premium value is calculated using Equation (44). The premiums are then grouped according to the categories of lightly damaged, moderately damaged, and heavily damaged houses by adjusting the initial damage data obtained from BNPB. In addition, the value of K used refers to the compensation amounts provided by BNPB according to each category of housing damage.

As an example, premium calculations for the 40th to the 100th percentiles in Period 1 are carried out using the previously obtained d_2 values and compensation amounts corresponding to each housing damage category. The overall premium calculation results for all percentiles and damage categories are presented in Table 9.

$$\text{Premium} = IDR\ 15{,}000{,}000\ e^{-(0.0454513)(0.41667)} N(0.80594) = 11{,}625{,}673.$$

Based on Table 9, it can be observed that the premium values tend to decrease as the percentile values increase. This occurs because, at higher percentiles, the rainfall threshold value G becomes closer to the average rainfall $\overline{A_0}$, thereby reducing the probability of claim occurrence. In addition, premiums for heavily damaged houses are consistently higher than those for moderately and lightly damaged houses, since the compensation amounts provided are also greater.

In Period 2, which represents the rainy-to-dry season transition, premium values can be determined using trigger values that exceed the exit values of both the rainy and dry season periods, according to the established insurance compensation scheme. Period 2 consists of 3 observation months, thus $T = \frac{3}{12} = 0.25$ with $\overline{A_0} = 114.903$ mm, while the

https://doi.org/10.3390/10.3390/math14132277

value of G is adjusted according to the percentile data in Table 8. As an example, for the 90th percentile with $G = 103.823$ mm, the value of d_2 can be calculated as follows:

$$d_2 = \frac{\ln\left(\frac{114.903}{103.823}\right) + \left(0.04545 - \frac{(0.242175)^2}{2}\right)(0.25)}{0.242176\sqrt{0.25}} = 0.21769.$$

Subsequently, the premium calculation for the 90th percentile in Period 2, as an example, is performed using the previously obtained d_2 value and the compensation amount corresponding to each housing damage category. The premium calculation follows Equation (44), and the overall results for all percentiles and damage categories are presented in Table 10.

$$\text{Premium} = \text{IDR } 15{,}000{,}000\, e^{-(0.0454513)(0.25)} N(0.21769) = \text{IDR } 8{,}693{,}119$$

Table 9. Premium Values of the Standard Black–Scholes Model for Period 1.

Percentile	G	d_2	Premium (IDR)		
			Low	Medium	High
40%	125.903	0.80594	11,625,673	23,251,347	46,502,693
45%	127.082	0.77336	11,485,580	22,971,161	45,942,321
50%	128.260	0.74107	11,343,255	22,686,510	45,373,019
55%	129.439	0.70908	11,198,832	22,397,665	44,795,329
60%	130.618	0.67738	11,052,451	22,104,901	44,209,803
65%	132.977	0.61478	10,754,157	21,508,314	43,016,629
70%	135.337	0.55329	10,449,713	20,899,426	41,798,853
75%	137.696	0.49285	10,140,264	20,280,529	40,561,057
80%	140.055	0.43345	9,826,952	19,653,905	39,307,809
85%	144.210	0.33124	9,269,295	18,538,591	37,077,182
90%	148.364	0.23193	8,709,052	17,418,103	34,836,207
95%	152.518	0.13536	8,151,726	16,303,452	32,606,904
100%	156.673	0.04140	7,602,300	15,204,599	30,409,199

Table 10. Premium Values of the Standard Black–Scholes Model for Period 2.

Percentile	G	d_2	Premium (IDR)		
			Low	Medium	High
95%	109.363	0.11035	8,066,847	16,133,694	32,267,388
100%	114.903	0.00832	7,464,509	14,929,019	29,858,038

Based on Table 10, the premium values also tend to decrease, following the same trend observed in the premiums for Period 1. This occurs because the transition period from the wet season to the dry season may still trigger flood disasters if rainfall during the period remains high. Intense short-duration rainfall during the transition season can increase surface runoff and cause flooding, particularly in vulnerable areas. For Period 3, the observation duration is $T = \frac{2}{12} = 0.166667$, with $\overline{A_0} = 30.807$ mm, while the value of G is adjusted according to the percentile data in Table 8. As an example, for the 5th percentile with $G = 32.458$ mm, the value of d_2 can be calculated as follows:

$$d_2 = \frac{\ln\left(\frac{30.807}{32.458}\right) + \left(0.045451 - \frac{(0.568581645)^2}{2}\right)(0.166667)}{0.568581\sqrt{0.166667}} = -0.04374.$$

Subsequently, the premium calculation for the 1st to the 40th percentiles in Period 3 follows Equation (43). As an example, the calculation is performed using the previ-

https://doi.org/10.3390/10.3390/math14132277

ously obtained d_2 value and the compensation amount corresponding to each housing damage category.

$$\text{Premium} = IDR\ 15{,}000{,}000\ e^{-(0.0454513)(0.166667)} N(0.04374) = 7{,}703{,}077$$

Based on Table 11, it can be observed that premium values during Period 3, which represents the dry season, tend to increase as the percentile values increase. This indicates that the higher the rainfall threshold used, the greater the probability that actual rainfall falls below that threshold, thereby increasing drought risk and the probability of claim occurrence. This result is consistent with the insurance scheme established previously. In Period 4, which represents the dry-to-wet season transition, premium values can be determined using trigger values that exceed the exit values of both the rainy and dry season periods. In this case, $T = \frac{2}{12} = 0.166667$, with $\overline{A_0} = 27.51575$, while the value of G is adjusted according to the percentile data in Table 8. As an example, for the 5th percentile with $G = 27.51575$ mm, the value of d_2 can be calculated as follows:

$$d_2 = \frac{\ln\left(\frac{27.515}{27.515}\right) + \left(0.045451 - \frac{(0.973756134)^2}{2}\right)(0.166667)}{0.9737561\sqrt{0.166667}} = -0.02995.$$

Table 11. Premium Values of the Standard Black–Scholes Model for Period 3.

Percentile	G	d_2	Premium (IDR)		
			Low	Medium	High
5%	32.458	−0.26243	8,984,248	17,968,496	35,936,992
10%	34.109	−0.47620	10,168,204	20,336,407	40,672,814
15%	35.760	−0.67987	11,190,498	22,380,996	44,761,991
20%	37.412	−0.87434	12,043,915	24,087,829	48,175,658
25%	38.325	−0.97830	12,445,900	24,891,800	49,783,600
30%	39.239	−1.07980	12,800,936	25,601,873	51,203,745
35%	40.153	−1.17897	13,112,228	26,224,456	52,448,912
40%	41.067	−1.27591	13,383,333	26,766,667	53,533,333

Subsequently, the premium calculation for the 5th percentile in Period 4, as an example, is carried out using the previously obtained d_2 value and the compensation amount corresponding to each housing damage category. The premium calculations follow Equations (44) and (46), adjusted according to rainfall conditions. The overall premium calculation results for all percentiles and damage categories are presented in Table 12.

$$\text{Premium} = IDR\ 15{,}000{,}000\ e^{-(0.0454513)(0.166667)} N(0.02995) = 7{,}621{,}258$$

Table 12. Premium Values of the Standard Black–Scholes Model for Period 4.

Percentile	G	d_2	Premium (IDR)		
			Low	Medium	High
1%	27.516	−0.17971	8,504,986	17,009,972	34,019,945
75%	108.622	0.09295	7,764,638	15,529,276	31,058,552
80%	110.955	0.06889	7,405,333	14,810,666	29,621,331
85%	113.657	0.04540	7,054,595	14,109,189	28,218,378
90%	116.359	0.02244	6,713,208	13,426,416	26,852,833
95%	119.061	0.00000	6,381,815	12,763,630	25,527,260
100%	121.763	0.11420	8,081,030	16,162,059	32,324,118

https://doi.org/10.3390/10.3390/math14132277

Based on Table 12, during Period 4, which represents the transition from the dry season to the rainy season, drought risk may still occur if the increase in rainfall is slow or if the onset of the rainy season is delayed, as indicated by the 1st percentile. Furthermore, flood risk may also occur when rainfall increases beyond the exit value of Period 1, as indicated by the 75th to 100th percentiles. These conditions are consistent with the established insurance scheme, which considers the potential risks corresponding to rainfall values exceeding the exit threshold.

6.4. Premium Calculation Using the Fractional Black–Scholes Model

In this study, premiums are calculated using the fractional Black–Scholes model to accommodate the stochastic characteristics of rainfall data that exhibit temporal dependence. Parameter estimation shows that the value of H, calculated using Equation (27), is $H = 0.6385886$, indicating the presence of long-range dependence in the rainfall data. The fractional-order parameter δ, calculated using Equation (32), is obtained as $\delta_1 = 0.2315363$. Furthermore, to analyze the sensitivity of the model, δ_2 is determined using the convergence of the sequence $(\delta_1)_n = \left(\frac{1}{2} + 0.231536\, e^n\right)$, which converges to $\frac{1}{2}$ or $\lim_{n\to\infty}(\delta_1)_n = \frac{1}{2}$. This refers to Equation (19), where substituting $\delta = \frac{1}{2}$ yields the standard Black-Scholes model. Accordingly, the value obtained is $\delta_2 = 0.73153$. The obtained values are then substituted into Equation (19) to determine d_2, and the calculation results are presented in Table 13. For each period, the values of T, $\overline{A_0}$, and G are the same as those used in the standard Black–Scholes model. The main difference lies in the formulation of d_2 which incorporates the fractional orders δ_1 and δ_2.

Table 13. Premium Values of the Fractional Black–Scholes Model for Period 1.

Percentile	G	d_2 (δ_1 = 0.231536)	Low-Premium	d_2 (δ_2 = 0.731536)	Low-Premium
40%	125.903	1.50086	13,736,935	0.99165	14,595,693
45%	127.082	1.43903	13,613,669	0.98920	14,559,686
50%	128.260	1.37778	13,480,235	0.98619	14,515,284
55%	129.439	1.31708	13,336,436	0.98251	14,461,121
60%	130.618	1.25693	13,182,141	0.97806	14,395,747
65%	132.977	1.13817	12,841,608	0.96647	14,225,161
70%	135.337	1.02149	12,459,137	0.95059	13,991,333
75%	137.696	0.90683	12,036,167	0.92962	13,682,687
80%	140.055	0.79412	11,575,256	0.90292	13,289,657
85%	144.210	0.60019	10,682,935	0.84084	12,376,002
90%	148.364	0.41178	9,710,580	0.75991	11,184,875
95%	152.518	0.22856	8,689,806	0.66356	9,766,656
100%	156.673	0.05027	7,654,383	0.55804	8,213,510

As an example, for the 40th percentile with $G = 125.9026667$ mm, the value of d_2 can be calculated as follows:

$$d_2 = \frac{\ln\left(\frac{156.67267}{125.90267}\right) + \left(0.04545(0.41667)\right) - \left(\frac{(0.184603)^2}{2}(0.41667)^{2(0.23)}\right)}{0.184602497\sqrt{(0.41667)^{2(0.23)}}} = 1.00063.$$

Based on Table 13, it can be observed that the premium values in the fractional Black–Scholes model tend to decrease as the percentile values increase for both fractional-order values used, namely $\delta_1 = 0.231536$ and $\delta_2 = 0.731536$. In addition, the premiums generated with $\delta_2 > 0.5$ are consistently lower than those obtained with $\delta_1 < 0.5$. This indicates that an increase in the fractional order, which represents a stronger long-memory effect, influences the reduction of premium estimates. Therefore, the selection of the fractional-order value

https://doi.org/10.3390/10.3390/math14132277

becomes an important factor in determining premium values within the fractional model. Furthermore, the premium calculations for the 95th and 100th percentiles in Period 2, as examples, are performed using the previously obtained d_2 values and compensation amounts corresponding to each housing damage category. The overall premium calculation results for all percentiles and damage categories are presented in Table 14.

Table 14. Premium Values of the Fractional Black–Scholes Model for Period 2.

Percentile	G	d_2 (δ_1 = 0.231536)	Low-Premium	d_2 (δ_2 = 0.731536)	Low-Premium
95%	109.363	0.25813	8,216,509	0.64801	10,996,985
100%	114.903	−0.02316	7,343,138	0.08543	7,920,114

Based on Table 14, it can be observed that the premium values in the fractional Black–Scholes model for Period 2 tend to decrease at higher percentiles. In addition, the premiums generated with $\delta_2 = 0.731536 > 0.5$ are consistently lower than those obtained with $\delta_1 = 0.231536 < 0.5$. This indicates that an increase in the fractional order influences the reduction of premium estimates. From an interpretative perspective, this condition reflects that, during the transitional period, although rainfall remains relatively high, the probability of extreme events triggering maximum claims becomes smaller at higher percentile thresholds, resulting in lower calculated premium values. For Period 3, which represents the dry season, the trigger window begins similarly to the standard model. The difference lies in the calculation of d_2 and the premium values for the 5th to the 100th percentiles, which are presented in Table 15.

Table 15. Premium Values of the Fractional Black–Scholes Model for Period 3.

Percentile	G	d_2 (δ_1 = 0.231536)	Low-Premium	d_2 (δ_2 = 0.731536)	Low-Premium
5%	32.458	−0.27823	9,074,740	−0.29827	9,188,916
10%	34.109	−0.41038	9,813,905	−0.62196	10,912,262
15%	35.760	−0.53627	10,482,022	−0.93034	12,265,278
20%	37.412	−0.65649	11,079,414	−1.22480	13,244,411
25%	38.325	−0.72075	11,380,472	−1.38221	13,644,436
30%	39.239	−0.78349	11,661,296	−1.53590	13,959,638
35%	40.153	−0.84480	11,922,653	−1.68606	14,203,620
40%	41.067	−0.90472	12,165,385	−1.83284	14,389,390

Based on Table 15, it can be observed that the premium values in the fractional Black–Scholes model for Period 3, representing the dry season, tend to increase as the percentile values increase. In addition, the premiums generated with $\delta_2 = 0.731536 > 0.5$ are consistently lower than those obtained with $\delta_1 = 0.231536 < 0.5$. This indicates that an increase in the fractional order influences the reduction of premium estimates.

From an interpretative perspective, during the dry season, the higher the rainfall threshold used, the greater the probability that actual rainfall falls below that threshold, thereby increasing drought risk and the likelihood of claims, which is reflected in the increasing premium values.

In Period 4, which represents the transitional season, drought risk is indicated at the 1st percentile, while flood risk appears from the 75th to the 100th percentiles. The overall premium calculation results for all percentiles and damage categories are presented in Table 16.

https://doi.org/10.3390/10.3390/math14132277

Table 16. Premium Values of the Fractional Black–Scholes Model for Period 4.

Percentile	G	d_2 (δ_1 = 0.231536)	Low-Premium	d_2 (δ_2 = 0.731536)	Low-Premium
1%	27.516	−0.30977	9,254,124	−0.10242	8,050,618
75%	108.622	−0.13219	6,660,619	0.33256	9,382,675
80%	110.955	−0.16523	6,466,545	0.25163	8,922,179
85%	113.657	−0.20265	6,248,082	0.15998	8,389,488
90%	116.359	−0.23918	6,036,343	0.07049	7,861,692
95%	119.061	−0.27488	5,831,242	−0.01695	7,342,758
100%	121.763	−0.30977	5,632,677	−0.10242	6,836,184

Based on Table 16, it can be observed that the premium values in the fractional Black–Scholes model for Period 4 exhibit a different pattern compared to the previous periods, namely tending to decrease at higher percentiles for drought risk, while increasing at certain percentiles representing flood risk. In addition, the premiums generated with $\delta_2 = 0.731536 > 0.5$ remain lower than those obtained with $\delta_1 = 0.231536 < 0.5$ under most conditions. This indicates that the influence of the fractional order on premium estimation remains consistent; however, the characteristics of premium changes are strongly affected by transitional seasonal conditions, in which rainfall dynamics become more complex.

Overall, the premium mechanism in the rainfall index-based insurance model exhibits a consistent pattern that aligns with the hydrometeorological risk characteristics of each period. Premium values in the fractional Black–Scholes model are influenced by changes in percentile values and fractional orders, where increasing percentile values may either increase or decrease premiums depending on the dominant type of risk, such as drought or flood risk.

6.5. Compensation Calculation Using the HBA Method

As part of the development of the index-based insurance scheme, the determination of compensation values constitutes an important stage to ensure that the claim payment mechanism reflects the actual level of risk occurrence. Therefore, this study employs the HBA method to calculate compensation amounts based on the historical distribution of rainfall indices adjusted according to the previously established threshold and exit levels. The compensation calculation is performed using Equation (45) for flood risk and Equation (46) for drought risk.

This indicates that the 60th, 65th, 70th, 75th, 80th, 85th, 90th, 95th, and 100th percentiles are used for flood risk determination. Meanwhile, the 5th, 10th, 15th, 20th, 25th, 30th, 35th, and 40th percentiles are used to determine compensation for drought risk. For Period 2, representing the rainy-to-dry season transition, the highest percentiles whose rainfall indices fall within the disaster-prone category according to Table 1 are selected. Similarly, for Period 4, representing the dry-to-rainy season transition, the smallest percentiles whose rainfall indices fall within the disaster-prone category according to Table 2 are selected.

The compensation calculation results for various rainfall index values are presented in Table 17. As an example, the following presents the compensation calculation for Period 1 with $exit = 107.678$ mm, $trigger = 125.903$ mm, and $rainfall\ index = 107.860$ mm, $K = 15,000,000$:

$$Compensation = \frac{107.860 - 107.678}{125.903 - 107.678}.\text{IDR } 15{,}000{,}000 = \text{IDR } 150{,}000.$$

https://doi.org/10.3390/10.3390/math14132277

Table 17. Compensation Values for Period 1 (Rainy Season).

Percentile	Exit (mm)	Trigger (mm)	Rainfall Index (mm)	Compensation (IDR)
40%	107.678	125.903	≤107.678	0
			107.860	150,000
			109.500	1,500,000
			111.323	3,000,000
			113.145	4,500,000
			114.968	6,000,000
			116.790	7,500,000
			118.613	9,000,000
			120.435	10,500,000
			122.258	12,000,000
			124.080	13,500,000
			≥125.903	15,000,000

Based on Table 17, it can be observed that the compensation amount in the rainfall index-based insurance scheme increases gradually as the rainfall index value increases. This compensation structure follows a parametric mechanism determined by the trigger and exit thresholds, in which no payment is provided when the index value is below a specified threshold, while compensation increases proportionally until reaching the maximum value of IDR 15,000,000. This pattern indicates that the higher the rainfall intensity exceeding the threshold, the greater the assumed level of damage, resulting in higher compensation values provided to the insured, up to the predetermined maximum limit.

Based on Table 18, it can be observed that the compensation amount in the rainfall index-based insurance scheme during the rainy-to-dry season transition increases gradually as the rainfall index value increases. This mechanism continues to follow the predetermined trigger and exit thresholds, where no payment is provided when the index value is below the threshold, and compensation increases until reaching the maximum value of IDR 15,000,000. This indicates that during the transitional period, although rainfall conditions begin to decline, increases in rainfall index values exceeding certain thresholds may still reflect increasing levels of risk, resulting in proportionally higher compensation provided to the insured according to the severity of the risk.

Table 18. Compensation Values for Period 2 (Rainy-to-Dry Season Transition).

Percentile	Exit (mm)	Trigger (mm)	Rainfall Index (mm)	Compensation (IDR)
95%	109.363	114.903	≤109.363	0
			109.418	150,000
			109.917	1,500,000
			110.471	3,000,000
			111.025	4,500,000
			111.579	6,000,000
			112.133	7,500,000
			112.687	9,000,000
			113.241	10,500,000
			113.795	12,000,000
			114.349	13,500,000
			≥114.903	15,000,000

For Period 3, representing the dry season, the compensation structure is determined based on rainfall index values lying between the exit and trigger thresholds. This calculation

aims to represent the severity level of the drought occurring during the period. The complete compensation calculation for the 5th percentile is presented in Table 19.

Table 19. Compensation Values for Period 3 (Dry Season).

Percentile	Exit (mm)	Trigger (mm)	Rainfall Index (mm)	Compensation (IDR)
5%	30.807	32.458	≤30.807	15,000,000
			30.823	14,850,000
			30.972	13,500,000
			31.137	12,000,000
			31.302	10,500,000
			31.467	9,000,000
			31.632	7,500,000
			31.797	6,000,000
			31.963	4,500,000
			32.128	3,000,000
			32.293	1,500,000
			≥32.458	0

Table 19 shows that the compensation amount decreases as the rainfall index increases. This reflects that higher rainfall during the dry season corresponds to lower drought severity, resulting in smaller compensation amounts until eventually reaching zero. Meanwhile, in Period 4, which represents the transition phase from the dry season to the rainy season, the compensation structure is again determined based on rainfall index values while considering the established exit and trigger thresholds. During this period, rainfall begins to increase; therefore, the compensation mechanism is designed to capture changes in risk levels from dry conditions toward wetter conditions.

Table 20 shows that the compensation amount decreases gradually as the rainfall index increases. This suggests that higher rainfall during the transitional period corresponds to lower drought risk, resulting in smaller compensation amounts that eventually reach zero. This pattern confirms that the index-based insurance scheme can adjust claim payments in proportion to changes in rainfall.

Table 20. Compensation Values for Period 4 (Dry-to-Rainy Season Transition).

Percentile	Exit (mm)	Trigger (mm)	Rainfall Index (mm)	Compensation (IDR)
1%	25.50666667	27.516	25.507	15,000,000
			25.527	14,850,000
			25.708	13,500,000
			25.908	12,000,000
			26.109	10,500,000
			26.310	9,000,000
			26.511	7,500,000
			26.712	6,000,000
			26.913	4,500,000
			27.114	3,000,000
			27.315	1,500,000
			27.516	0

Overall, the compensation structure demonstrates a clear relationship with the rainfall index. Under flood-risk conditions, compensation increases with rainfall intensity, whereas under drought-risk conditions, compensation decreases with rainfall intensity. This in-

https://doi.org/10.3390/10.3390/math14132277

dicates that the implemented scheme is capable of proportionally representing the risk severity through the trigger and exit thresholds.

7. Discussion

The developed model integrates both the standard and fractional Black–Scholes approaches to estimate rainfall-index-based insurance premiums. The standard model assumes a memoryless stochastic process, whereas the fractional model accommodates long-memory effects through the fractional order. With a Hurst exponent value of $H > 0.5$, the data indicate the presence of long-range dependence. Therefore, the fractional approach is theoretically more representative of rainfall dynamics. Analytically, the fractional Black–Scholes model is solved using a combination of the DJM method and the KF transform, yielding an efficient semi-analytical solution without requiring complex numerical discretization.

The DJM–KF approach offers several advantages over existing methods for solving fractional Black–Scholes equations. Sugandha et al. [44] previously applied the DJM to the fractional Black–Scholes equation and demonstrated its convergence without linearization or discretization; the present study extends this foundation by combining DJM with the KF transform, yielding a structurally distinct solution pathway that produces a closed-form result expressed through the Mittag–Leffler function. Compared to purely numerical methods such as finite difference schemes and the Adams–Bashforth–Moulton predictor-corrector approach, the DJM–KF yields a closed-form semi-analytical solution expressible through the Mittag–Leffler function, which provides direct insight into solution behavior as a function of the fractional order δ. Compared to transform-only approaches such as the Laplace-based method used in Azahra et al. [27], the KF transform offers a structurally different convolution property (Theorem 1) that integrates naturally with the DJM iterative decomposition, producing a general recursive formula applicable to both linear and nonlinear operators. Furthermore, unlike perturbation-based or Adomian decomposition methods that require explicit computation of Adomian polynomials, the DJM directly decomposes the nonlinear operator without such preprocessing, reducing computational overhead while maintaining convergence [21,44,51].

To provide a clearer comparison between the standard Black–Scholes model and the fractional model with two different fractional-order values, namely δ_1 and δ_2, the premium calculation results for Period 1 are visualized in Figure 6. This visualization aims to illustrate the differences in premium patterns and magnitudes among the models with respect to changes in rainfall values.

Based on the graph, it can be observed that the fractional model with $\delta_2 > 0.5$ produces lower premium values compared to the fractional model with $\delta_1 < 0.5$ and the standard model at most observation points. Meanwhile, the standard model tends to produce higher premium values. This difference indicates that the selection of the fractional order has a significant influence on premium estimation, where larger fractional-order values reflect stronger long-memory effects and result in more conservative premium estimates. To provide a clearer comparison between the standard Black–Scholes model and the fractional model with two different fractional-order values, namely δ_1 and δ_2, the premium calculation results for Period 2 are visualized in Figure 7.

Based on Figure 7, it can be observed that during the rainy-to-dry season transition, the fractional model with δ_1 tends to produce lower premiums compared to the standard model, whereas δ_2 produces relatively higher premiums. This difference indicates that the selection of the fractional order provides flexibility in premium determination, allowing insurance schemes to be designed in a more adaptive, responsive, and flexible manner according to the observed rainfall index conditions without neglecting risk balance.

https://doi.org/10.3390/10.3390/math14132277

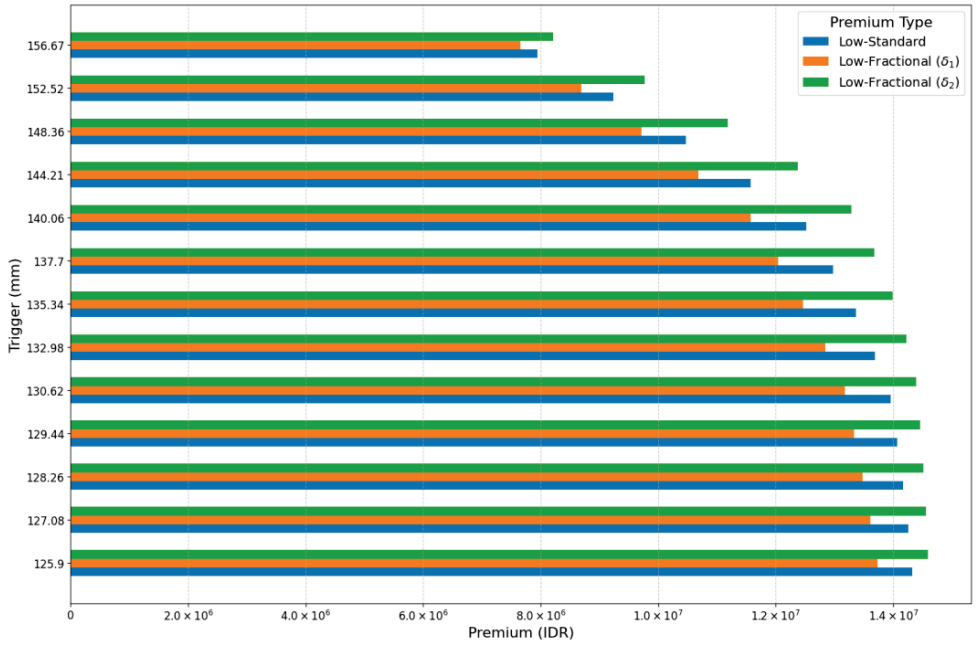

Figure 6. Premium Graph for Period 1 under the Standard and Fractional Models.

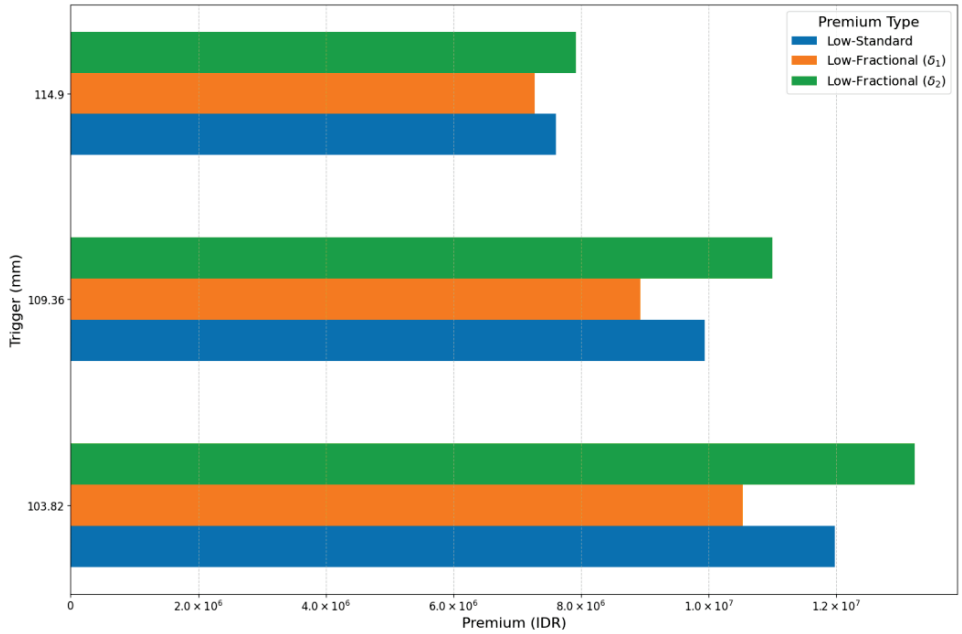

Figure 7. Premium Graph for Period 2 under the Standard and Fractional Models.

To provide a clearer comparison between the standard Black–Scholes model and the fractional model with two different fractional-order values, namely δ_1 and δ_2, the premium calculation results for Period 3 are visualized in Figure 8.

Based on Figure 8, it can be observed that during the dry season, the fractional model with δ_1 tends to produce lower premiums compared to the standard model, whereas δ_2 produces relatively higher premiums. This difference confirms that the fractional-order value influences premium estimation, particularly under dry-season conditions associated with increased drought risk. To provide a clearer comparison between the standard Black–Scholes model and the fractional model with two different fractional-order values, namely δ_1 and δ_2, the premium calculation results for Period 4 are visualized in Figure 9.

https://doi.org/10.3390/10.3390/math14132277

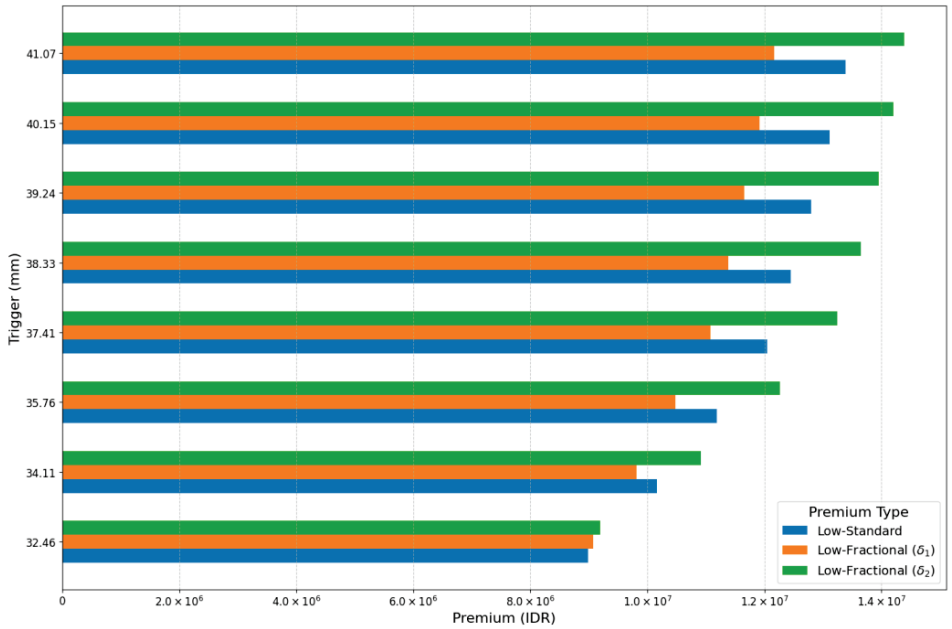

Figure 8. Premium Graph for Period 3 under the Standard and Fractional Models.

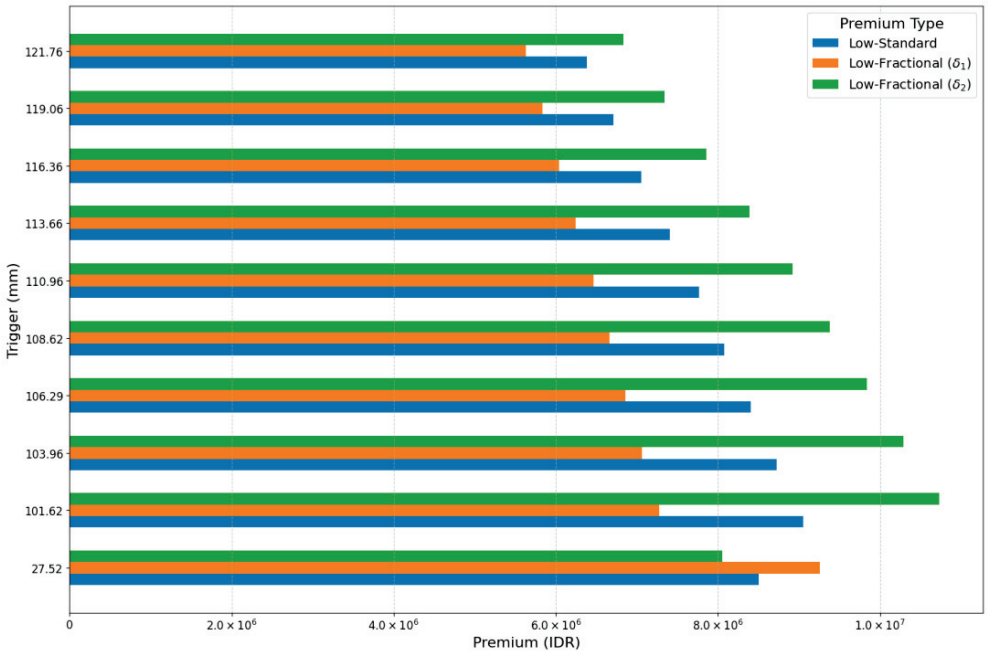

Figure 9. Premium Graph for Period 4 under the Standard and Fractional Models.

Based on Figure 9, it can be observed that during the dry-to-rainy season transition, the fractional model with δ_1 tends to produce lower premiums compared to the standard model, whereas δ_2 produces relatively higher premiums. This difference indicates that the selection of the fractional order provides flexibility in premium determination. In Period 4, two possible risks are simultaneously detected, namely drought risk at the trigger value of 27.52 mm and flood risk at the trigger value of 108.62 mm. Therefore, the insurance scheme can be designed in a more adaptive, responsive, and flexible manner according to the observed rainfall index conditions without neglecting risk balance.

A sensitivity analysis further reveals two structural patterns across all periods. With respect to the fractional order, a shift from $\delta_1 = 0.231536$ to $\delta_2 = 0.731536$ consistently produces lower premium values, with the magnitude of reduction ranging from approximately 5% to 25% depending on the period and percentile threshold, confirming that δ should

https://doi.org/10.3390/10.3390/math14132277

be estimated rigorously from observed data rather than assigned arbitrarily. With respect to percentile thresholds, premiums decrease monotonically as the threshold increases in flood-risk periods (P1, P2), while the opposite pattern holds in drought-risk periods (P3, P4), consistent with the underlying exceedance probability structure of each risk type. These directional sensitivities are robust across both the standard and fractional models.

Overall, the standard model tends to produce higher premium values compared to the fractional model with (δ_1) whereas the fractional model with (δ_2) tends to produce lower premiums. These differences indicate that the selection of the fractional order can be adjusted according to the level of risk and the economic capacity of society. In the context of SDG 13 (Climate Action), this approach may be utilized as a disaster mitigation strategy through the determination of adaptive premium schemes, for example, by setting lower premiums to improve accessibility for vulnerable groups, while applying higher premiums for segments with stronger financial capacity. Consequently, the insurance scheme can remain inclusive without neglecting the principle of risk balance, thereby avoiding losses for insurers while simultaneously strengthening community resilience against disaster risks.

Regarding model validation, this study employs two complementary approaches. First, the standard Black–Scholes model $(\delta = 0.5)$ serves as an internal benchmark: the fractional model is designed to reduce to the classical model at this value, which has been verified analytically and confirmed numerically through the convergence of premium values as $\delta \to 0.5$. Second, the HBA method provides an external reference by transforming historical disaster loss records into empirically grounded trigger and exit thresholds, ensuring that the compensation structure reflects actual historical risk conditions rather than purely theoretical distributions. A full comparison with independently computed premiums from alternative actuarial models (such as the collective risk model of Kalfin et al. [25] or the modified Black–Scholes model of Purwandari et al. [26]) is limited by differences in data period, geographic scope, and model assumptions, as detailed in Table 21. Future validation using out-of-sample rainfall and loss data is recommended to further assess predictive accuracy.

The comparison reveals three key advantages of the proposed model. First, it is the only framework that simultaneously addresses both flood and drought risks within a unified parametric structure, enabling multi-hazard premium estimation in a single period (as demonstrated in Period 4). Second, while Azahra et al. [27] applied the fractional Black–Scholes model to agricultural insurance covering both flood and drought risks in the context of crop failure and production loss, this study extends the framework to hydrometeorological disaster insurance specifically targeting residential infrastructure damage across multiple severity levels (minor, moderate, and severe).

This constitutes a substantively different application domain, with distinct compensation structures, trigger mechanisms, and socioeconomic implications. Third, the multi-layer payout structure tied to housing damage categories (minor, moderate, severe) provides a more granular, actuarially sound compensation mechanism than single-layer schemes in prior studies.

A critical distinction across these studies lies in their treatment of temporal memory in rainfall dynamics. Kalfin et al. [25] employed a collective risk model based on the pure premium principle, which assumes that disaster occurrences follow a standard Poisson process, a memoryless framework that does not account for long-range dependence or persistence patterns in historical rainfall data. Purwandari et al. [26] advanced the premium determination framework by incorporating cross-subsidies and regional economic growth into the Black-Scholes model. However, the underlying stochastic process remains geometric Brownian motion, which assumes independent increments and therefore cannot

capture memory effects in rainfall volatility. Azahra et al. [27] made an important step forward by introducing the fractional Black-Scholes model with a Caputo derivative, explicitly incorporating memory effects through a fractional order parameter estimated from historical data. Nevertheless, their application remained within the agricultural insurance domain. The present study builds on this foundation by extending the fractional framework to the hydrometeorological disaster insurance context, where memory effects play an equally critical role: the Hurst exponent $H = 0.6386$ confirms long-range dependence in the Bandung rainfall series, and the fractional order directly influences premium sensitivity across all four seasonal risk periods, as demonstrated in Tables 13–16.

Table 21. Methodological Comparison with Related Studies.

Aspect	Kalfin et al. (2022) [25]	Purwandari et al. (2024) [26]	Azahra et al. (2025) [27]	This Study
Base Model	Collective Risk Model	Modified Black–Scholes	Fractional Black–Scholes	Fractional Black–Scholes
Application Model	Natural disaster	Natural disaster	Agricultural insurance	Hydrometeorological disaster insurance
Memory Effect	Not considered	Not considered	Considered	Considered
Solution Method	Pure premium principle	Analytical closed-form	DJM–Laplace Transform	DJM–KF Transform
Risk Coverage	Flood & drought (aggregate)	Flood only	Flood & drought (crop context)	Flood & drought (disaster/housing context, unified multi-layer)
Index Structure	Disaster loss index	Rainfall index	Rainfall index	Rainfall index (multi-period)
Premium Flexibility	Fixed by region	Fixed by economic growth factor	Varies by fractional order	Varies by fractional order & seasonal period
Payout Structure	Aggregate	Single-layer	Single-layer	Multi-layer (minor/moderate/severe damage)

8. Conclusions

This study develops a hydrometeorological disaster insurance model based on the fractional Black–Scholes equation that accommodates long-memory effects in rainfall dynamics. With a Hurst exponent value of $H > 0.5$, the fractional approach becomes more representative in capturing long-range dependence characteristics compared to the standard memoryless model. Analytically, the model is solved using a combination of the DJM method and the KF transform, resulting in an efficient semi-analytical solution.

The results demonstrate systematic findings across all four seasonal periods. In Period 1 (rainy season, November–March), flood risk dominates with premium values ranging from IDR 7.6–11.6 million (standard model) and IDR 7.7–13.7 million (fractional model, δ_1), decreasing as the percentile threshold increases. In Period 2 (wet-to-dry transition, April–June), both flood risk at higher percentiles and early drought signals are captured, with premiums sensitive to the onset of seasonal change. In Period 3 (dry season, July–August), drought risk is the primary concern, and premium values increase with rising percentile thresholds, reflecting a greater probability of rainfall deficit. In Period 4 (dry-to-wet transition, September–October), the model simultaneously detects dual risks: drought at trigger 27.52 mm and flood at trigger 108.62 mm, demonstrating the framework's capacity for multi-hazard premium estimation within a single period. Across all periods, the standard model ($\delta = 0.5$) consistently produces higher premiums than the fractional model with $\delta_1 = 0.231536$, while the fractional model with $\delta_2 = 0.731536$ yields the lowest premiums. These systematic variations confirm that the fractional order parameter can be calibrated to the risk appetite and economic capacity of policyholders, providing a flexible and risk-sensitive premium structure.

https://doi.org/10.3390/10.3390/math14132277

In the context of disaster insurance as a risk-transfer mechanism, these differences relate to SDG 13, particularly in developing resilience against climate-related risks. Premium adjustments based on fractional-order strengthening provide broader protection for various social groups without neglecting risk balance, thereby maintaining financial sustainability.

Nevertheless, this study has several limitations that open avenues for future research. First, the assumption of a lognormal distribution for the rainfall index may not fully capture the heavy-tailed behavior observed in extreme rainfall events; future work could explore alternative distributional assumptions, such as the generalized Pareto or stable distributions, within the fractional framework. Second, spatial factors and land-use changes are not incorporated in the current model; integration of spatially distributed rainfall data across multiple stations would improve the representativeness of the trigger mechanism. Third, the Caputo derivative used in this study could be extended to more general fractional operators, including the Hilfer derivatives, which offer additional flexibility in capturing mixed initial-value and boundary-value memory structures, as demonstrated in recent theoretical developments. Fourth, long-term climate projections incorporating scenario data could be integrated to assess how evolving rainfall patterns under climate change affect premium sustainability over multi-decadal horizons. Overall, the fractional Black–Scholes model provides both theoretical and practical contributions to the development of index-based disaster insurance that is more responsive to climate change dynamics.

Author Contributions: Conceptualization, H.A.A., M.D.J., E.R. and S.; methodology, H.A.A., M.D.J., E.R., S. and N.B.A.H.; validation, M.P.A.S., H.A.A., A.S.A. and A.J.W.; formal analysis, M.D.J., E.R., H.A.A. and S.; investigation, M.P.A.S., H.A.A., A.S.A., S., A.J.W. and A.S.; resources, E.R., H.A.A. and S.; data curation, M.P.A.S., H.A.A. and A.S.A.; writing—original draft preparation, M.D.J., E.R., H.A.A. and S.; writing—review and editing, M.P.A.S., H.A.A., A.S.A., S. and N.B.A.H.; visualization, H.A.A., A.S.A., S. and A.S.; supervision, M.D.J., E.R., H.A.A. and S.; project administration, H.A.A., A.S.A., N.B.A.H. and A.J.W.; funding acquisition, M.D.J. All authors have read and agreed to the published version of the manuscript.

Funding: This scientific work was supported by the Equity-WCU Research Grant, Universitas Padjadjaran, number: 5578/UN6.3.1/PT.00/2025.

Data Availability Statement: The original contributions presented in this study are included in the article. Further inquiries can be directed to the corresponding author.

Acknowledgments: The authors are grateful to Universitas Padjadjaran (Unpad) for providing Article Processing Charge (APC) support. The APC for this article was funded by Unpad through the Indonesian Endowment Fund for Education (LPDP) on behalf of the Indonesian Ministry of Higher Education, Science and Technology, and managed under the EQUITY Program (Contract No. 4303/B3/DT.03.08/2025 and 3927/UN6.RKT/HK.07.00/2025).

Conflicts of Interest: The authors declare no conflicts of interest.

Abbreviations

The following abbreviations are used in this manuscript:

DJM	Daftardar Gejji–Jafari Method
SDG	Sustainable Development Goals
KF	Kashuri–Fundo
GPH	Geweke–Porter–Hudak
HBA	Historical Burn Analysis
IDR	Indonesian Rupiah

Appendix A

Table A1. Dasarian rainfall data for each observation period.

Month / Period 1	j	D_j (mm)					
		2019–2020	**2020–2021**	**2021–2022**	**2022–2023**	**2023–2024**	**2024–2025**
November	1	84.6	163.82	198.05	165.86	66.59	141.22
	2	51.57	62.77	139.6	124.59	103.53	183.89
	3	83.41	128.91	116.96	125.04	191.66	207.5
December	1	75.24	120.9	136.63	133.38	98.85	165.49
	2	154.64	86.29	121.7	89.85	38.31	105.13
	3	245.37	112.49	114.84	121.63	131.14	63.81
January	1	135.96	125.54	64.18	51.75	306.15	98.28
	2	59.69	97.28	120.92	33.32	125.74	127.08
	3	224.32	123.19	43.52	88.31	164.7	233.33
February	1	206.26	228.92	117.36	42.22	138.99	49.08
	2	203.78	134.05	81.03	137.98	200.26	98.49
	3	222.52	91.94	51.76	183.98	116.93	148.18
March	1	85.02	123.43	92.38	116.07	165.32	171.14
	2	285.79	263.75	132.8	106.62	136.8	60.06
	3	231.92	95.99	83.44	110.5	115.86	35.86
Month / Period 2	j	D_j (mm)					
		2020	**2021**	**2022**	**2023**	**2024**	**2025**
April	1	120.41	55.31	79.77	42.53	108.51	95.97
	2	128.29	119.95	185.9	107.91	106.19	60.53
	3	112.31	44.86	97	124.59	107.23	69.94
May	1	105.26	51.86	90.67	160.55	39.23	48.47
	2	144.91	58.88	78.37	42	31.65	80.59
	3	249.49	109	84.38	35.99	77.12	165.61
June	1	62.4	34.82	93.73	41.89	77.87	73.67
	2	59.65	128.97	54.9	76.98	53.52	128.88
	3	51.41	100.76	69.96	41.49	104.13	93.52
Month / Period 3	j	D_j (mm)					
		2020	**2021**	**2022**	**2023**	**2024**	**2025**
July	1	70.75	35.63	34.92	71.69	250.87	134.86
	2	34.44	22.73	145.96	20	20	20
	3	24.02	49.9	43.59	22.82	22	39.13
August	1	21.5	77.4	32.85	26.93	83.85	55.16
	2	51.76	36.03	72.69	20	20	89.95
	3	22	24.71	50.92	23.4	22	141.41
Month / Period 4	j	D_j (mm)					
		2020	**2021**	**2022**	**2023**	**2024**	**2025**
September	1	47.27	35.5	157.41	20	72.14	41.27
	2	60.25	81.44	78.33	21.61	51.83	127.85
	3	108.17	66.63	68.41	20	165.52	93.09
October	1	61.63	31.26	178.37	22.52	35.19	82.89
	2	176.58	120.65	103.98	27.42	27.8	78.53
	3	211.83	150.36	144.08	41.49	41.65	186.11

https://doi.org/10.3390/10.3390/math14132277

References

1. Dai, A. Increasing Drought under Global Warming in Observations and Models. *Nat. Clim. Change* **2013**, *3*, 52–58. [CrossRef]
2. Ward, P.; Jongman, B.; Aerts, J. A Global Framework for Future Costs and Benefits of River-Flood Protection in Urban Areas. *Nat. Clim. Change* **2017**, *7*, 642–646. [CrossRef]
3. Jongman, B. Effective Adaptation to Rising Flood Risk. *Nat. Commun.* **2018**, *9*, 1986. [CrossRef] [PubMed]
4. Winsemius, H.C.; Aerts, J.C.J.H.; van Beek, L.P.H.; Bierkens, M.F.P.; Bouwman, A.; Jongman, B.; Kwadijk, J.C.J.; Ligtvoet, W.; Lucas, P.L.; van Vuuren, D.P.; et al. Global Drivers of Future River Flood Risk. *Nat. Clim. Change* **2016**, *6*, 381–385. [CrossRef]
5. Kurniadi, A.; Weller, E.; Min, S.-K.; Seong, M.-G. Future Projections of Extreme Rainfall Events in Indonesia. *Int. J. Climatol.* **2024**, *44*, 1435–1451. [CrossRef]
6. Hariadi, M.H.; van der Schrier, G.; Steeneveld, G.-J.; Sutanto, S.J.; Sutanudjaja, E.; Ratri, D.N.; Sopaheluwakan, A.; Klein Tank, A. A High-Resolution Perspective of Extreme Rainfall and River Flow under Extreme Climate Change in Southeast Asia. *Hydrol. Earth Syst. Sci.* **2024**, *28*, 1935–1956. [CrossRef]
7. Giuzio, M.; Rousova, L.; Kapadia, S.; Kumar, H.; Mazzotta, L.; Parker, M.; Zafeiris, D. Climate Change, Catastrophes, Insurance and the Macroeconomy. *Eur. Econ. Rev.* **2026**, *182*, 105210. [CrossRef]
8. Jewson, S.; Brix, A.; Ziehmann, C. *Weather Derivative Valuation: The Meteorological, Statistical, Financial and Mathematical Foundations*; Cambridge University Press: Cambridge, UK, 2005.
9. Alaton, P.; Djehiche, B.; Stillberger, D. On Modelling and Pricing Weather Derivatives. *Appl. Math. Financ.* **2002**, *9*, 1–20. [CrossRef]
10. Black, F.; Scholes, M. The Pricing of Options and Corporate Liabilities. *J. Political Econ.* **1973**, *81*, 637–654. [CrossRef] [PubMed]
11. Hull, J.C. *Options, Futures, and Other Derivatives*, 10th ed.; Pearson: London, UK, 2018.
12. Mandelbrot, B.B.; Van Ness, J.W. Fractional Brownian Motions, Fractional Noises and Applications. *SIAM Rev.* **1968**, *10*, 422–437. [CrossRef]
13. Bender, C.; Viitasaari, L. Fractional Brownian Motion in Financial Modeling. In *Wiley StatsRef: Statistics Reference Online*; Wiley: Hoboken, NJ, USA, 2016.
14. Biagini, F.; Hu, Y.; Øksendal, B.; Zhang, T. *Stochastic Calculus for Fractional Brownian Motion and Applications*; Springer: London, UK, 2008.
15. Necula, C. Option Pricing in a Fractional Brownian Motion Environment. *DOFIN Acad. Econ. Stud. Buchar. Rom.* **2002**, 1–19. [CrossRef]
16. Comte, F.; Renault, E. Long Memory in Continuous-Time Stochastic Volatility Models. *Math. Financ.* **1998**, *8*, 291–323. [CrossRef]
17. Hu, Y.; Øksendal, B. Fractional White Noise Calculus and Applications to Finance. *Infin. Dimens. Anal. Quantum Probab. Relat. Top.* **2003**, *6*, 1–32. [CrossRef]
18. Chen, W.; Xu, X.; Zhu, S.-P. Analytically Pricing Double Barrier Options Based on a Time-Fractional Black-Scholes Equation. *Comput. Math. Appl.* **2015**, *69*, 1407–1419. [CrossRef]
19. He, X.-J.; Lin, S. A Fractional Black-Scholes Model with Stochastic Volatility and European Option Pricing. *Expert Syst. Appl.* **2021**, *178*, 114983. [CrossRef]
20. Lovejoy, S.; Mandelbrot, B.B. Fractal Properties of Rain, and a Fractal Model. *Tellus A* **1985**, *37*, 209–232. [CrossRef]
21. Daftardar-Gejji, V.; Jafari, H. An Iterative Method for Solving Nonlinear Functional Equations. *J. Math. Anal. Appl.* **2006**, *316*, 753–763. [CrossRef]
22. Podlubny, I. *Fractional Differential Equations*; Academic Press: San Diego, CA, USA, 1999.
23. Kashuri, A.; Fundo, A. A New Integral Transform. *Adv. Theor. Appl. Math.* **2013**, *8*, 27–43.
24. Sharma, O.P.K.; Vats, R.K. Qualitative Analysis of the Nonlinear Psi-Hilfer Fractional Neutral-Type Delayed Integro-Differential Stochastic System: Existence, Uniqueness and Controllability. *Int. J. Syst. Sci.* **2025**, 1–25. [CrossRef]
25. Kalfin; Sukono; Supian, S.; Mamat, M. Insurance Premium Determination Model and Innovation for Economic Recovery Due to Natural Disasters in Indonesia. *Computation* **2022**, *10*, 174. [CrossRef]
26. Purwandari, T.; Hidayat, Y.; Sukono; Kalfin; Ibrahim, R.A.; Subiyanto. Development of the Black-Scholes Model for Determining Insurance Premiums to Mitigate the Risk of Disaster Losses Using the Principles of Mutual Cooperation and Regional Economic Growth. *Risks* **2024**, *12*, 110. [CrossRef]
27. Azahra, A.S.; Johansyah, M.D.; Sukono. The Development of Fractional Black-Scholes Model Solution Using the Daftardar-Gejji Laplace Method for Determining Rainfall Index-Based Agricultural Insurance Premiums. *Mathematics* **2025**, *13*, 1725. [CrossRef]
28. Azahra, A.S.; Johansyah, M.D.; Sukono. Agricultural Insurance Premium Determination Model for Risk Mitigation Based on Rainfall Index: Systematic Literature Review. *Risks* **2024**, *12*, 205. [CrossRef]
29. Tellman, B.; Lall, U.; Islam, A.K.M.S.; Bhuyan, M.A. Satellite-Based Flood Index Insurance. *Earths Future* **2022**, *10*, e2021EF002418. [CrossRef]
30. Collier, B.; Skees, J.; Barnett, B. Weather Index Insurance and Climate Change: Opportunities and Challenges in Lower Income Countries. *Geneva Pap. Risk Insur. Issues Pract.* **2009**, *34*, 401–424. [CrossRef]
31. Hurst, H.E. Long-Term Storage Capacity of Reservoirs. *Trans. Am. Soc. Civ. Eng.* **1951**, *116*, 770–799. [CrossRef]

32. Geweke, J.; Porter-Hudak, S. The Estimation and Application of Long Memory Time Series Models. *J. Time Ser. Anal.* **1983**, *4*, 221–238. [CrossRef]
33. Marengo, J.A.; Alves, L.M.; Ambrizzi, T.; Young, A.; Barreto, N.J.C.; Ramos, A.M. Trends in Extreme Rainfall and Hydrogeometeorological Disasters in the Metropolitan Area of Sao Paulo: A Review. *Ann. N. Y. Acad. Sci.* **2020**, *1469*, 5–20. [CrossRef] [PubMed]
34. Abrego-Perez, A.L.; Boonman, T.M.; Valencia Arboleda, C.F. Index Insurance for Simultaneous Flooding and Drought Risks with Insufficient Data: A Two-Step Approach. *Stoch. Environ. Res. Risk Assess.* **2025**, *39*, 2769–2788. [CrossRef]
35. Atangana, A.; Baleanu, D. New Fractional Derivatives with Non-Local and Non-Singular Kernel: Theory and Application to Heat Transfer Model. *Therm. Sci.* **2016**, *20*, 763–769. [CrossRef]
36. Crummy, J.; Gunawan, E.; Hussain, E.; Hanifa, R.; Sagala, S.; Nurfiani, D. Understanding Multi-Hazard Risk and Resilience in Bandung, Indonesia. In Proceedings of the EGU General Assembly 2026, Vienna, Austria, 3–8 May 2026.
37. Turvey, C.G.; Shee, A.; Marr, A. Addressing Fractional Dimensionality in the Application of Weather Index Insurance and Climate Risk Financing in Agricultural Development: A Dynamic Triggering Approach. *Weather Clim. Soc.* **2019**, *11*, 901–915. [CrossRef]
38. Curioso, B.A.; Esquivel, M.L.; Guerreiro, G.R.; Krasii, N.P.; Sousa, P.A.C. A First Step Toward a CAT Model Framework: An ODE-Based Risk Analysis of Urban Floods Triggered by Meteorological Events. *Risks* **2026**, *14*, 83. [CrossRef]
39. Pleterski, N. Parametric Insurance for Sustainable Disaster Risk Finance: Legal, Data, and Governance Pathways in Slovenia and Croatia. *Sustainability* **2025**, *17*, 9643. [CrossRef]
40. Sherly, K.; Veeresha, P. Fractional Operator-Based Mathematical Model for Hydrological Cycle Analysis with Machine Learning Integration. *Model. Earth Syst. Environ.* **2025**, *11*, 168. [CrossRef]
41. Diethelm, K. *The Analysis of Fractional Differential Equations*; Springer: Berlin, Germany, 2010.
42. Gorenflo, R.; Kilbas, A.A.; Mainardi, F.; Rogosin, S. *V Mittag-Leffler Functions, Related Topics and Applications*; Springer: Berlin, Germany, 2014.
43. Alsepan, G.; Minobe, S. Relations between Interannual Variability of Regional-Scale Indonesian Precipitation and Large-Scale Climate Modes during 1960–2007. *J. Clim.* **2020**, *33*, 5271–5291. [CrossRef]
44. Sugandha, A.; Rusyaman, E.; Sukono; Carnia, E. A New Solution to the Fractional Black-Scholes Equation Using the Daftardar-Gejji Method. *Mathematics* **2023**, *11*, 4887. [CrossRef]
45. Kirschbaum, D.; Stanley, T.; Zhou, Y. Changes in Extreme Precipitation and Landslides Over High Mountain Asia. *Geophys. Res. Lett.* **2020**, *47*, e2019GL085347. [CrossRef]
46. Guild, R.; Wang, X.; Russon, A.E. Tracking Deforestation, Drought, and Fire Occurrence in Kutai National Park, Indonesia. *Remote Sens.* **2022**, *14*, 5630. [CrossRef]
47. Zhang, H.; Liu, F.; Turner, I.; Yang, Q. Numerical Solution of the Time Fractional Black-Scholes Model Governing European Options. *Comput. Math. Appl.* **2016**, *71*, 1772–1783. [CrossRef]
48. Sen, S.; Nayak, N.C.; Mohanty, W.K.; Keshri, C.K. Vulnerability and Risk Perceptions of Hydrometeorological Disasters: A Study of a Coastal District of Odisha, India. *GeoJournal* **2023**, *88*, 711–731. [CrossRef]
49. Akhtar, Z.; Sajjad, M.; Imran, M.; Ofli, F. Risk Mapping in Managing Flood Vulnerability in Disaster Management. In *International Handbook of Disaster Research*; Springer Nature: Singapore, 2023; pp. 743–776.
50. Huang, J.; Li, Y.; Wang, Z. Climate Risk Adaptation through Disaster Insurance: Understanding Purchase Behavior of Farmers Threatened by Flash Floods in Rural China. *Clim. Risk Manag.* **2026**, *47*, 100787. [CrossRef]
51. Edeki, S.O.; Jena, R.M.; Chakraverty, S.; Baleanu, D. Coupled Transform Method for Time-Space Fractional Black-Scholes Option Pricing Model. *Alex. Eng. J.* **2020**, *59*, 3239–3246. [CrossRef]

Disclaimer/Publisher's Note: The statements, opinions and data contained in all publications are solely those of the individual author(s) and contributor(s) and not of MDPI and/or the editor(s). MDPI and/or the editor(s) disclaim responsibility for any injury to people or property resulting from any ideas, methods, instructions or products referred to in the content.

fractal and fractional

MDPI

Article

Optimal Control of Riemann–Liouville Fractional Stochastic Systems with Three-Parameter Damping

Zhi-Chao Lu [1], Ting-Ting Hu [1] and Shi-You Lin [1,2,*]

[1] School of Mathematics and Statistics, Hainan Normal University, Haikou 571158, China; 202412070100011@hainnu.edu.cn (Z.-C.L.); 202412070100003@hainnu.edu.cn (T.-T.H.)
[2] Key Laboratory of Data Science and Intelligence Education, Ministry of Education, Hainan Normal University, Haikou 571158, China
* Correspondence: 050105@hainnu.edu.cn

Abstract

This paper studies mild solutions and Bolza optimal control for Riemann–Liouville fractional stochastic integro-differential systems incorporating fourth-order diffusion, time-varying control, non-instantaneous impulses, and infinite delay. Based on our self-developed (μ, ν, ξ, e, k)-resolvent family, we derive the mild solution formulation and prove its existence via the Krasnoselskii–Schaefer fixed-point theorem. Using the Arzelá-Ascoli theorem, Mazur's lemma, and Balder's lower semicontinuity principle, we further establish the existence of optimal control pairs. A numerical example from Euler–Bernoulli beam dynamics illustrates the theoretical results.

Keywords: Riemann–Liouville fractional derivative; three-parameter damping; non-instantaneous impulses; infinite delay; optimal control; resolvent family

1. Introduction

Fractional calculus has broken through the limitations of classical integer-order calculus and emerged as a powerful mathematical framework for characterizing memory, heredity, and nonlocality in complex dynamical systems. It has been extensively applied in viscoelastic mechanics, anomalous diffusion, vibration control, biomedical engineering, and other fields [1–3]. Compared with the Caputo fractional derivative, the Riemann–Liouville fractional derivative allows the state function to have discontinuities at the initial moment, covers a wider solution space, and is more suitable for constructing dynamic models with singular initial states and impulse perturbations [4–6]. In recent years, the theory of multi-term Riemann–Liouville fractional differential equations has been further developed, and fruitful results have been achieved on the existence of solutions and approximate controllability for damped fractional evolution equations and inclusions [7,8].

Most of the existing studies focus on two-parameter damping models composed of two fractional derivative terms [9,10], which cannot fully reflect the coupled high, medium, and low-frequency damping characteristics in actual engineering scenarios. To fill this gap, this paper introduces a three-parameter fractional damping term $D_t^{\mu}x(t) + eD_t^{\nu}x(t) + kD_t^{\xi}x(t)$, which extends the classical two-parameter damping structure and enhances the modeling capability for complex damping phenomena. Meanwhile, a fourth-order diffusion operator A is adopted to meet the dynamic modeling requirements of high-order structural systems such as Euler–Bernoulli beams and thin plates. This setting compensates for the limited applicability of second-order operators in large-deflection and high-dimensional diffusion problems [11–13].

Impulse effects widely exist in practical systems including structural vibration, drug delivery, and power system disturbance, which can be divided into instantaneous impulses and non-instantaneous impulses [14–16]. Different from instantaneous impulses that only act at t_i discrete time points, non-instantaneous impulses are triggered suddenly at t_i and act continuously on the interval (t_i, ς_i). This feature is more consistent with continuous evolution processes in real systems, such as drug absorption and pollutant diffusion [17,18]. Random disturbances represented by Brownian motion $dW(t)$ and the infinite delay effect determined by the historical state x_t play an essential role in accurate modeling. The stochastic integro-differential term with infinite delay $\mathcal{M}(t, x_t, \int_0^t g(t, \varsigma, x_\varsigma)d\varsigma)dW(t)$ simultaneously describes random noise, memory integration, and historical state dependence. This formulation thus better captures the real dynamic behavior of the system [19–21].

In the field of optimal control, fractional stochastic systems with impulses and delays have attracted extensive attention. With the help of resolvent family theory, fixed-point theorems and stochastic analysis methods, scholars have successively established the existence results of mild solutions and optimal controls for various systems [22]. Nevertheless, the current research literature still has the following limitations:

1. Most models only adopt two-parameter damping, and optimal control research on coupled three-parameter damping and fourth-order diffusion systems is still insufficient;
2. Control operators are mostly time-invariant, while the time-varying control operator $\mathcal{B}(t)$, which is more consistent with practical control requirements, has been rarely studied;
3. A unified analytical framework combining Riemann–Liouville fractional calculus, non-instantaneous impulses, infinite delay, stochastic integro-differential dynamics, and time-varying control has not been established. Moreover, the supporting resolvent family theory and corresponding existence criteria for such comprehensive systems require further development and refinement.

Driven by the above analysis and recent research progress, this paper constructs a class of multi-term Riemann–Liouville fractional stochastic impulsive integro-differential systems with three-parameter damping, fourth-order diffusion, infinite delay, and time-varying control in a Hilbert space. The specific form of the system is as follows:

$$\begin{cases} D_t^{\mu}x(t) + eD_t^{\nu}x(t) + kD_t^{\xi}x(t) = Ax(t) + B(t)u(t) + \mathcal{M}\left(t, x_t, \int_0^t g(t, \varsigma, x_\varsigma)d\varsigma\right)dW(t), \\ t \in (\varsigma_i, t_{i+1}], i = 0, 1, \ldots, q, \\ x(t) = h_i(t, x_t),\ t \in (t_i, \varsigma_i], \quad i = 1, 2, \ldots, q, \\ \lim\limits_{t\to 0^+} I_t^{1-\mu}x(t) = \varphi(0) \in \mathcal{B}_\hbar, \quad I_t^{1-\mu}x(t)\Big|_{t=\varsigma_i} = h_i(\varsigma_i, x_{\varsigma_i}), \end{cases} \tag{1}$$

Here, D_t^{μ}, D_t^{ν}, and D_t^{ξ} denote Riemann–Liouville fractional derivatives, and $I_t^{1-\mu}$ is the Riemann–Liouville fractional integral. A is a fourth-order diffusion operator, $B(t)$ is a time-varying control operator, x_t denotes the infinite delay state, $dW(t)$ denotes a Brownian motion, h_i represents the non-instantaneous impulsive condition, and $\mathcal{B}_\hbar$ is the standard phase space for infinite delay systems. Throughout this paper, we assume $0 < \xi < \nu < \mu \leq 1$, which ensures the three-parameter damping structure is well-defined. System (1) unifies three-parameter fractional damping, fourth-order linear operators, time-varying control, non-instantaneous impulses, infinite delay, and stochastic disturbances, and thus possesses strong universality and practical value. The overall framework of this system is illustrated in Figure 1.

https://doi.org/10.3390/fractalfract10070490

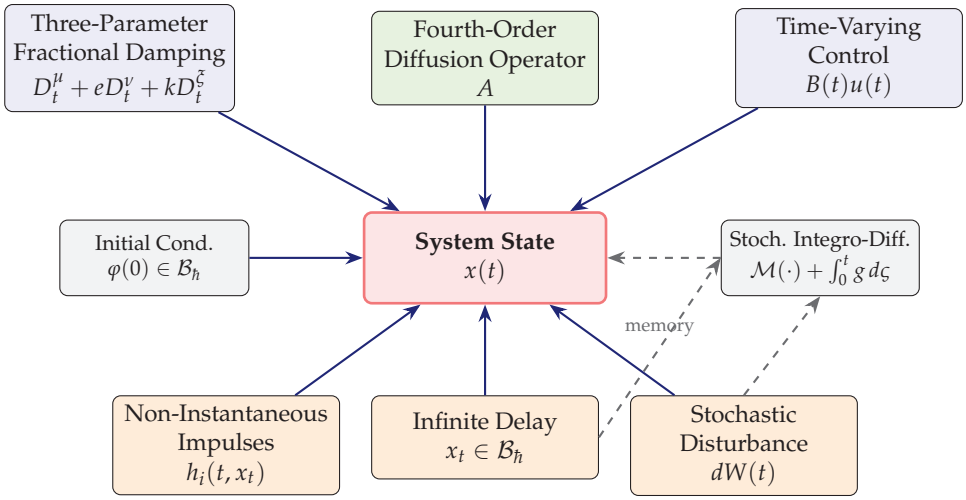

Figure 1. Schematic diagram of the system framework for the Riemann–Liouville fractional stochastic integro-differential system (1) with three-parameter damping. The three driving mechanisms (fractional damping $D_t^\mu + eD_t^\nu + kD_t^\xi$, fourth-order diffusion operator A, and time-varying control $B(t)u(t)$) govern the system state $x(t)$. The non-instantaneous impulses h_i, infinite delay state x_t, and stochastic disturbance $dW(t)$—coupled through the integro-differential operator $\mathcal{M}(\cdot)$—act as perturbation and memory mechanisms. The initial condition $\varphi(0) \in \mathcal{B}_h$ is defined in the phase space for infinite delay systems.

Remark 1. *Equation (1) is expressed in formal differential form for presentation clarity. Throughout this paper, the term $dW(t)$ is interpreted in the Itô sense, and the rigorous mathematical meaning of the stochastic system is given by the mild solution formulation defined in Section 2. In the mild solution framework, all stochastic terms are rigorously defined as Itô stochastic convolutions with the (μ, ν, ξ, e, k)-resolvent family, which avoids the mathematical ambiguity of directly applying fractional derivatives to irregular stochastic processes.*

Main Contributions :

1. A unified model containing three-parameter fractional damping, fourth-order diffusion, time-varying control, non-instantaneous impulses, and infinite delay is proposed, which extends the existing two-parameter damping and time-invariant control frameworks;
2. The mild solution of the system is defined based on the (μ, ν, ξ, e, k)-resolvent family tailored for three-parameter damping, and the existence of mild solutions is proved by combining the Krasnoselskii–Schaefer fixed-point theorem and stochastic analysis;
3. Under the assumptions of convexity and lower semicontinuity of the cost functional, the existence of optimal control pairs for the Bolza problem is derived by using the Mazur lemma and lower semicontinuity theory;
4. The abstract results are applied to a fourth-order fractional stochastic diffusion system, which illustrates the effectiveness and applicability of the theoretical conclusions.

The remainder of this paper is structured as follows:

1. Section 2 provides the necessary mathematical preliminaries, including key definitions, lemmas, and standing assumptions related to fractional calculus, resolvent families, the phase space $\mathcal{B}_h$, and stochastic analysis. These preliminaries lay the foundation for our subsequent theoretical developments.
2. Section 3 is dedicated to establishing the existence of mild solutions for the proposed system via fixed-point arguments. This result serves as the cornerstone for the subsequent optimal control analysis.

https://doi.org/10.3390/fractalfract10070490

3. Section 4 addresses the existence of optimal controls, building directly upon the mild solution framework derived in Section 3.
4. Section 5 presents a numerical example based on a fourth-order fractional diffusion system to illustrate the applicability of our theoretical findings.
5. Section 6 concludes the paper with a summary of the main contributions, along with a discussion of potential extensions and future research directions.

2. Preliminaries

This section presents the fundamental concepts, standard definitions, and key lemmas that lay the foundation for analyzing the fractional-order system with three-parameter damping in the subsequent sections. The main notations used in this paper are summarized in Table 1.

Let $\{e_k\}_{k\geq 1}$ be a complete orthonormal basis for U with corresponding non-negative eigenvalues $\lambda_k \geq 0$ for all $k \geq 1$. A U-valued Wiener process $W(t)$ is referred to as a Q-Wiener process if it possesses the following spectral expansion

$$W(t) = \sum_{k=1}^{\infty} \sqrt{\lambda_k} e_k \beta_k(t),$$

where $\beta_k(t) = \frac{1}{\sqrt{\lambda_k}} \langle W(t), e_k \rangle_U$ forms a sequence of mutually independent real-valued Brownian motions. The corresponding covariance operator $Q : U \to U$ is a linear, non-negative, and symmetric operator with a finite trace. To simplify the construction of stochastic integrals driven by $W(t)$, we introduce the subspace $U_0 = Q^{\frac{1}{2}}(U) \subset U$ endowed with the inner product $\langle x, z \rangle_{U_0} = \langle Q^{-\frac{1}{2}} x, Q^{-\frac{1}{2}} z \rangle_U$.

The space of Hilbert–Schmidt operators mapping from U_0 to $\mathcal{H}$ is denoted by $L_2^0 = L_2(U_0; \mathcal{H})$, which constitutes a separable Hilbert space equipped with the norm:

$$\|\psi\|_{L_2^0}^2 = \mathrm{Tr}\Big((\psi Q^{\frac{1}{2}})(\psi Q^{\frac{1}{2}})^*\Big),$$

where $\mathrm{Tr}(\cdot)$ represents the trace operator and $(\cdot)^*$ denotes the adjoint operator.

For a fixed delay parameter $d > 0$, we define the space of bounded measurable functions as

$$\mathcal{B} = \{\varphi : [-d, 0] \to \mathcal{H} \mid \varphi \text{ is measurable and uniformly bounded}\},$$

which is equipped with the supremum norm $\|\varphi\|_{[-d,0]} = \sup_{t\in[-d,0]} \|\varphi(t)\|$.

Inspired by the phase space framework introduced by Yan [23], we present the abstract phase space $\mathcal{B}_\hbar$ for systems with infinite delay. Let $\hbar : (-\infty, 0] \to (0, \infty)$ be a continuous weight function such that $l = \int_{-\infty}^{0} \hbar(t)dt < \infty$. The space $\mathcal{B}_\hbar$ is defined by

$$\mathcal{B}_\hbar = \Bigg\{ \varphi : (-\infty, 0] \to \mathcal{H} : \ (E\|\varphi(\theta)\|^p)^{\frac{1}{p}} \text{ is a measurable and bounded}$$

$$\text{function on } [-d, 0] \text{ and } \int_{-\infty}^{0} \hbar(\varsigma) \sup_{\varsigma\leq\theta\leq 0} (E\|\varphi(\theta)\|^p)^{\frac{1}{p}} d\varsigma < \infty \Bigg\},$$

with the norm

$$\|\varphi\|_{\mathcal{B}_\hbar} = \int_{-\infty}^{0} \hbar(t) \sup_{t\leq\theta\leq 0} (E\|\varphi(\theta)\|^p)^{\frac{1}{p}} dt.$$

It can be readily verified that $(\mathcal{B}_\hbar, \|\cdot\|_{\mathcal{B}_\hbar})$ is a Banach space that satisfies the fundamental axioms put forward by Ansari et al. [17], as listed below:

https://doi.org/10.3390/fractalfract10070490

(a) For any function $x : (-\infty, T] \to \mathcal{H}$ with $x_0 = \varphi \in \mathcal{B}_\hbar$ and $x|_{[0,T]} \in PC([0,T];\mathcal{H})$ (the space of piecewise continuous $\mathcal{H}$-valued processes), the following hold for all $t \in [0,T]$:

1. $x_t \in \mathcal{B}_\hbar$, where $x_t(\theta) = x(t+\theta)$ for $\theta \le 0$;
2. There exists a constant $\tilde{M} > 0$ such that $\|x(t)\|_{\mathcal{H}} \le \tilde{M}\|x_t\|_{\mathcal{B}_\hbar}$;
3. There exist functions $\mathcal{L}, \mathcal{N} : [0,\infty) \to [1,\infty)$ (with $\mathcal{L}$ continuous and $\mathcal{N}$ locally bounded) such that

$$\|x_t\|_{\mathcal{B}_\hbar} \le \mathcal{L}(t-\sigma) \sup_{\sigma \le \varsigma \le t} \|x(\varsigma)\|_{\mathcal{H}} + \mathcal{N}(t-\sigma)\|x_\sigma\|_{\mathcal{B}_\hbar}$$

for all $0 \le \sigma \le t \le T$.

(b) The phase space $\mathcal{B}_\hbar$ is complete.

Remark 2. *For non-impulsive functional differential equations, the continuity of the mapping $t \mapsto x_t$ constitutes a standard axiom for the phase space $\mathcal{B}_\hbar$; see Corduneanu [24]. However, this property is no longer valid in impulsive delay systems due to the non-instantaneous state jumps in state trajectories, and is therefore omitted from the foregoing axiomatic framework.*

Definition 1. *The μ-order Riemann–Liouville fractional integral is defined as*

$$I_t^\mu f(t) = \frac{1}{\Gamma(\mu)} \int_0^t (t-\varsigma)^{\mu-1} f(\varsigma) d\varsigma, \quad t > 0,$$

where $\Gamma(\cdot)$ denotes the Gamma function and $\mu > 0$.

Definition 2. *For any $0 < \mu \le 1$, the μ-order Riemann–Liouville fractional derivative with respect to the time variable t is given by*

$$D_t^\mu f(t) = \frac{d}{dt} I_t^{1-\mu} f(t).$$

As a fundamental notion in fractional calculus, the above definitions are commonly employed in the relevant literature [10,25].

Definition 3. *The three-parameter bivariate Mittag–Leffler-type function is defined by*

$$E_{\mu,\nu,\xi}(z,w) = \sum_{k=0}^{\infty} \sum_{m=0}^{\infty} \frac{z^k w^m}{\Gamma(\mu k + \nu m + \xi)\, k!\, m!},$$

where $\Gamma(\cdot)$ denotes the gamma function. This generalized function is introduced in our previous work [25] and tailored for the multi-term fractional damping structure.

When $w = 0$, only the term with index $m = 0$ remains (noting $0! = 1$), so the double series reduces to a single series:

$$E_{\mu,\nu,\xi}(z,0) = \sum_{k=0}^{\infty} \frac{z^k}{\Gamma(\mu k + \xi)\, k!}.$$

In particular, setting $\xi = \mu$ further yields

$$E_{\mu,\nu,\mu}(z,0) = \sum_{k=0}^{\infty} \frac{z^k}{\Gamma(\mu k + \mu)\, k!}.$$

https://doi.org/10.3390/fractalfract10070490

If we additionally set $\nu = \mu$ with $w = 0$, the function reduces to a single-parameter Mittag-Leffler type function with factorial weight:

$$E_{\mu,\mu,\mu}(z,0) = \sum_{k=0}^{\infty} \frac{z^k}{\Gamma(\mu k + \mu)\, k!}.$$

We remark that the classical two-parameter Mittag-Leffler function takes the form $E_{\alpha,\beta}(z) = \sum_{k=0}^{\infty} \frac{z^k}{\Gamma(\alpha k+\beta)}$ without factorial weights [10,26]. Our definition extends the classical framework by introducing factorial weights and a second variable to match the three-parameter fractional damping operator.

Definition 4. *The three-parameter Mittag-Leffler integral operator is defined by*

$$\mathbb{E}_t^{\mu-\nu,\mu-\xi,\mu,-e,-k} f(t) = \int_0^t (t-\varsigma)^{\mu-1} E_{\mu-\nu,\mu-\xi,\mu}\big(-e(t-\varsigma)^{\mu-\nu}, -k(t-\varsigma)^{\mu-\xi}\big) f(\varsigma)\, d\varsigma, \quad t > 0.$$

where $t > 0$, $0 < \xi < \nu < \mu \leq 1$, $e, k \in \mathbb{R}$. This formulation is explicitly constructed by integrating the newly proposed three-parameter Mittag-Leffler function into the theoretical framework developed in Refs. [10,25,26].

Definition 5. *A family $\{R_{\mu,\nu,\xi,e,k}(t)\}_{t>0}$ is called a Riemann–Liouville fractional (μ,ν,ξ,e,k)-resolvent family on the Banach space $\mathbb{X}$ if it satisfies the following conditions:*

(a) For any $x \in \mathbb{X}$, the mapping $t \mapsto \{R_{\mu,\nu,\xi,e,k}(t)\}x$ is strongly continuous on $(0,\infty)$, and satisfies the initial limit condition

$$\lim_{t\to 0^+} \Gamma(\mu) t^{1-\mu} R_{\mu,\nu,\xi,e,k}(t)x = x;$$

(b) For all $t, \varsigma > 0$, the operators commute, i.e., $R_{\mu,\nu,\xi,e,k}(t)R_{\mu,\nu,\xi,e,k}(\varsigma) = R_{\mu,\nu,\xi,e,k}(\varsigma)R_{\mu,\nu,\xi,e,k}(t)$;

(c) For all $t, \varsigma > 0$, the resolvent identity holds

$$\begin{aligned} &R_{\mu,\nu,\xi,e,k}(\varsigma)\mathbb{E}_t^{\mu-\nu,\mu-\xi,\mu,-e,-k} R_{\mu,\nu,\xi,e,k}(t) - \mathbb{E}_\varsigma^{\mu-\nu,\mu-\xi,\mu,-e,-k} R_{\mu,\nu,\xi,e,k}(\varsigma) R_{\mu,\nu,\xi,e,k}(t) \\ &= \varsigma^{\mu-1} E_{\mu-\nu,\mu-\xi,\mu}\Big(-e\varsigma^{\mu-\nu}, -k\varsigma^{\mu-\xi}\Big)\mathbb{E}_t^{\mu-\nu,\mu-\xi,\mu,-e,-k} R_{\mu,\nu,\xi,e,k}(t) \\ &-t^{\mu-1} E_{\mu-\nu,\mu-\xi,\mu}\Big(-e\varsigma^{\mu-\nu}, -k\varsigma^{\mu-\xi}\Big)\mathbb{E}_\varsigma^{\mu-\nu,\mu-\xi,\mu,-e,-k} R_{\mu,\nu,\xi,e,k}(\varsigma). \end{aligned}$$

This generalizes the two-parameter (α,β,c)-resolvent family from [10], and further expands our earlier investigations on three-parameter damped fractional systems in [25] together with the related theories presented in [17].

Remark 3. *The existence and generation theorem for the (μ,ν,ξ,e,k)-resolvent family was rigorously established in our previous published work [25]. We take this resolvent family as a fundamental analytical tool throughout the present paper without repeating redundant derivations for brevity.*

Lemma 1. *Let $\mathbb{X}$ be a Banach space, and let $\{R_{\mu,\nu,\xi,e,k}(t)\}_{t>0}$ be the Riemann–Liouville fractional (μ,ν,ξ,e,k)-resolvent family generated by the operator A. Then,*

(a) For any $x \in D(A)$, $R_{\mu,\nu,\xi,e,k}(t)x$ is well-defined and $AR_{\mu,\nu,\xi,e,k}(t)x = R_{\mu,\nu,\xi,e,k}(t)Ax$ for all $t > 0$;

(b) For any $x \in \mathbb{X}$ and all $t > 0$, the resolvent family admits the decomposition

$$R_{\mu,\nu,\xi,e,k}(t)x = t^{\mu-1} E_{\mu-\nu,\mu-\xi,\mu}\Big(-et^{\mu-\nu}, -kt^{\mu-\xi}\Big)x + A\mathbb{E}_t^{\mu-\nu,\mu-\xi,\mu,-e,-k} R_{\mu,\nu,\xi,e,k}(t)x;$$

https://doi.org/10.3390/fractalfract10070490

(c) For any $x \in D(A)$ and all $t > 0$, the generator A commutes with the multi-parameter Mittag-Leffler integral operator

$$R_{\mu,\nu,\xi,e,k}(t)x = t^{\mu-1}E_{\mu-\nu,\mu-\xi,\mu}\left(-et^{\mu-\nu}, -kt^{\mu-\xi}\right)x + \mathbb{E}_t^{\mu-\nu,\mu-\xi,\mu,-e,-k}R_{\mu,\nu,\xi,e,k}(t)Ax.$$

The proof of this lemma can be found in [25].

Lemma 2 ([17]). *For any predictable process $f(\cdot)$ taking values in the Banach space $\mathbb{X}$, the following estimate holds:*

$$\sup_{\varsigma\in[0,t]} E\left\|\int_0^{\varsigma} f(s)dW(s)\right\|_{\mathbb{X}}^{2p} \le C_{p,\mu,\nu,\xi,e,k}\left(\int_0^t \left(E\|f(s)\|_{\mathbb{X}}^{2p}\right)^{\frac{1}{p}}ds\right)^p, \quad t \in [0,\infty),$$

where $p \ge 1$ and $C_{p,\mu,\nu,\xi,e,k}$ is a positive constant depending only on p, μ, ν, ξ, e, k.

Remark 4. *The constant $C_{p,\mu,\nu,\xi,e,k}$ in Lemma 2 arises from combining the classical Burkholder–Davis–Gundy inequality (which yields a constant depending only on p) with the resolvent kernel bound $\|R_{\mu,\nu,\xi,e,k}(t-\varsigma)\| \le K(t-\varsigma)^{\mu-1}$. After substituting this bound into the BDG estimate and evaluating the resulting singular integral, all parameter-dependent coefficients are absorbed into the final constant, which therefore depends on p, μ, ν, ξ, e, k.*

Lemma 3 ([27]). *Let $\{t^{1-\mu}R_{\mu,\nu,\xi,e,k}(t), t > 0\}$ be compact and equicontinuous. Then,*

1. $\lim_{h\to 0^+}\left\|(t+h)^{1-\mu}R_{\mu,\nu,\xi,e,k}(t+h) - \Gamma(\mu)h^{1-\mu}R_{\mu,\nu,\xi,e,k}(h)t^{1-\mu}R_{\mu,\nu,\xi,e,k}(t)\right\| = 0;$
2. $\lim_{h\to 0^+}\left\|t^{1-\mu}R_{\mu,\nu,\xi,e,k}(t) - \Gamma(\mu)h^{1-\mu}R_{\mu,\nu,\xi,e,k}(h)(t-h)^{1-\mu}R_{\mu,\nu,\xi,e,k}(t-h)\right\| = 0.$

Theorem 1 (Krasnoselskii-Schaefer Fixed Point Theorem). *Let Q_1 and Q_2 be a contraction operator and a completely continuous operator, respectively, on a Banach space $\mathbb{X}$. If the set*

$$G = \left\{x \in \mathbb{X} : \omega Q_1\left(\frac{x}{\omega}\right) + \omega Q_2 x = x,\ \omega \in (0,1)\right\}$$

is bounded in $\mathbb{X}$, then the equation $Q_1x + Q_2x = x$ has at least one solution in $\mathbb{X}$.

Let the operator $B \in L^\infty([0,a]; L(Y;\mathcal{H}))$, where $L^\infty([0,a]; L(Y;\mathcal{H}))$ represents the space of all measurable and uniformly bounded operator-valued functions with the norm $\|B\|_\infty$. The control function u belongs to $L^p_{\mathcal{F}}([0,a];Y)$, which is the separable Banach space consisting of all measurable, $\mathcal{F}_t$-adapted, Y-valued stochastic processes satisfying $E\int_0^a \|u(t)\|^p dt < \infty$. The norm of this space is given by $\|u\|_{L^p_{\mathcal{F}}} = \left(E\int_0^a \|u(t)\|^p dt\right)^{\frac{1}{p}}$. We assume $p > 1$, which ensures that the control space $L^p_{\mathcal{F}}([0,a];Y)$ is a reflexive Banach space. Let U be a non-empty, closed, bounded, and convex subset of Y. The set of admissible controls is defined as

$$U_{ad} = \left\{u(\cdot) \in L^p_{\mathcal{F}}([0,a];Y); u(t) \in U \text{ a.e. } t \in [0,a]\right\}.$$

By the Eberlein–Šmulian theorem, every bounded subset of a reflexive space is weakly sequentially compact. Since U_{ad} is closed and convex, it follows from Mazur's lemma that U_{ad} is weakly closed.

Consider the space $PC \equiv PC([0,a]; L^p(\Omega;\mathcal{H}))$ composed of $\mathcal{F}_t$-adapted $L^p(\Omega;\mathcal{H})$-valued stochastic processes $\{x(t) : t \in [0,a]\}$ such that $x(t)$ is continuous at $t \ne t_i$,

https://doi.org/10.3390/fractalfract10070490

left-continuous on $[0,a]$, and $\lim_{t\to t_i^+} x(t)$ exists for all $i=1,2,\ldots,q$. This space is a Banach space equipped with the norm

$$\|x\|_{PC} = \max_{i=0,1,\ldots,q} \sup_{t\in(\varsigma_i,\varsigma_{i+1}]} \left(E\|(t-\varsigma_i)^{1-\mu}x(t)\|^p\right)^{\frac{1}{p}}.$$

We further introduce the space

$$\mathcal{B}_b = \left\{x:(-\infty,a]\to\mathcal{H} \mid x|_{[0,a]}\in PC \text{ and } x_0=\varphi\in\mathcal{B}_\hbar\right\},$$

endowed with the seminorm

$$\|x\|_{\mathcal{B}_b} = \|\varphi\|_{\mathcal{B}_\hbar} + \max_{i=0,1,\ldots,q} \sup_{t\in(\varsigma_i,\varsigma_{i+1}]} \left(E\|(t-\varsigma_i)^{1-\mu}x(t)\|^p\right)^{\frac{1}{p}}.$$

Lemma 4. *We recall the following result from [16]. Let $x\in\mathcal{B}_b$, then for any $t\in(\varsigma_i,\varsigma_{i+1}]$, $x_t\in\mathcal{B}_\hbar$ and*

$$l(E\|x(t)\|^p)^{\frac{1}{p}} \le \|x_t\|_{\mathcal{B}_\hbar} \le \|x_0\|_{\mathcal{B}_\hbar} + l\sup_{t\in[\varsigma_i,\varsigma_{i+1}]}\left(E\left\|(t-\varsigma_i)^{1-\mu}x(t)\right\|^p\right)^{\frac{1}{p}},$$

where $l=\int_{-\infty}^0 \hbar(s)ds<\infty$.

Basic Assumptions.

The following assumptions are introduced to derive the main results.

Assumption 1. *$t^{1-\mu}R_{\mu,\nu,\xi,e,k}(t)$ is uniformly continuous and compact, and there exists a constant $K>0$ such that*

$$\|t^{1-\mu}R_{\mu,\nu,\xi,e,k}(t)\|\le K,\quad 0<t\le a.$$

Assumption 2. *For each pair $(t,\varsigma)\in D=\{(t,\varsigma)\in[0,a]\times[0,a]:\varsigma\le t\}$, the function $g(t,\varsigma,\cdot):\mathcal{B}_\hbar\to\mathcal{H}$ is continuous and*

$$E\|g(t,\varsigma,\varphi)\|^p \le m_g\theta_g\left(\|\varphi\|^p_{\mathcal{B}_\hbar}\right),$$

where m_g is a constant and $\theta_g:[0,\infty)\to[0,\infty)$ is non-decreasing and continuous.

Assumption 3. *The function $\mathcal{M}:[0,a]\times\mathcal{B}_\hbar\times\mathcal{H}\to L_2^0$ fulfills the Carathodory condition:*

1. *For almost all $t\in[0,a]$, $\mathcal{M}(t,\cdot,\cdot):\mathcal{B}_\hbar\times\mathcal{H}\to L_2^0$ is continuous; for each $(\psi,x)\in\mathcal{B}_\hbar\times\mathcal{H}$, $\mathcal{M}(\cdot,\psi,x):[0,a]\to L_2^0$ is measurable.*
2. *There exist a non-decreasing continuous function $\Theta_{\mathcal{M}}:\mathbb{R}^+\cup\{0\}\to\mathbb{R}^+$ and a continuous function $m_{\mathcal{M}}\in L^1([0,a];\mathbb{R})$ such that*

$$E\|\mathcal{M}(t,\varphi,x)\|^p_{L_2^0} \le m_{\mathcal{M}}(t)\Theta_{\mathcal{M}}\left(\|\varphi\|^p_{\mathcal{B}_\hbar}+E\|x\|^p\right)$$

with

$$\int_1^\infty \frac{1}{\Theta_{\mathcal{M}}(\varsigma)+\theta_g(\varsigma)}d\varsigma=\infty.$$

Assumption 4. *The function $h_i:(t_i,\varsigma_i]\times\mathcal{B}_\hbar\to\mathcal{H}$ is continuous, and there exist positive constants $L_{h_i},M_{h_i}>0$ for $i=1,2,\ldots,q$ such that*

$$E\|h_i(t,\varphi_1)-h_i(t,\varphi_2)\|^p\le L_{h_i}\|\varphi_1-\varphi_2\|^p_{\mathcal{B}_\hbar},$$

https://doi.org/10.3390/fractalfract10070490

$$E\|h_i(t,\varphi)\|^p \le L_{h_i}\Big(1+\|\varphi\|^p_{\mathcal{B}_\hbar}\Big).$$

The following constants are introduced:

$$p(2\mu-1)>2,$$

which ensures the integrability of the singular resolvent kernel (derived in Lemma 6).

$$\begin{aligned}
&d^*=\frac{1}{1-L}2^{p-1}a^{\frac{p-2}{2}}C_pK^p\times\left(\frac{p-2}{-p-2+2p\mu}\right);\\
&r''=r'+a^p m_g\theta_g(r');\\
&L=\max_{i=1,2,\dots,q}\Big\{2^{p-1}l^pL_{h_i}a^{p(1-\mu)}+2^{p-1}l^pL_{h_i}K^p\Big\}<1;\\
&\bar\gamma(t)=\max\Big\{d^*m_{\mathcal{M}}(t),a^{p-1}m_g\Big\}.
\end{aligned}$$

Remark 5. *Based on the (μ,ν,ξ,e,k)-resolvent family introduced in Definitions 4 and 5 and its decomposition property in Lemma 1, we briefly justify the variation-of-constants form of mild solutions before giving its formal definition.*

We first consider the system on a single continuous evolution interval $t\in(0,t_1]$, and rewrite the equation as

$$D^\mu_t x(t)+eD^\nu_t x(t)+kD^\xi_t x(t)-Ax(t)=B(t)u(t)+\mathcal{M}\left(t,x_t,\int_0^t g(t,\varsigma,x_\varsigma)d\varsigma\right)\frac{dW(t)}{dt},$$

where the right-hand side is regarded as a generalized nonhomogeneous forcing term. Applying the three-parameter Mittag–Leffler integral operator $\mathbb{E}_t^{\mu-\nu,\mu-\xi,\mu,-e,-k}$ (Definition 4) to both sides and using the resolvent identity in Lemma 1 (b) to eliminate the multi-term fractional derivatives, we obtain the integral form of the solution:

$$x(t)=R_{\mu,\nu,\xi,e,k}(t)\varphi(0)+\int_0^t R_{\mu,\nu,\xi,e,k}(t-\varsigma)\left[B(\varsigma)u(\varsigma)d\varsigma+\mathcal{M}\left(\varsigma,x_\varsigma,\int_0^\varsigma g(\varsigma,\tau,x_\tau)d\tau\right)dW(\varsigma)\right]$$

Definition 6. *An $\mathcal{F}_t$-adapted stochastic process $\{x(t):t\in(-\infty,a]\}$ is termed a mild solution of problem (1) (cf. Definition 2.7 in [17]) if $x_0=\varphi\in\mathcal{B}_\hbar$, $x|_{[0,a]}\in PC$; for each $u\in U_{ad}$, there exists $a=a(u)>0$ such that for any $t\in[0,a]$, $x(t)$ satisfies*

$$x(t)=\begin{cases}
R_{\mu,\nu,\xi,e,k}(t)\varphi(0)+\displaystyle\int_0^t R_{\mu,\nu,\xi,e,k}(t-\varsigma)B(\varsigma)u(\varsigma)d\varsigma\\
\quad+\displaystyle\int_0^t R_{\mu,\nu,\xi,e,k}(t-\varsigma)\mathcal{M}\left(\varsigma,x_\varsigma,\int_0^\varsigma g(\varsigma,\tau,x_\tau)d\tau\right)dW(\varsigma),t\in(0,t_1]\\
h_i(t,x_t),t\in(t_i,\varsigma_i],\ i=1,2,\dots,q.\\
\\
R_{\mu,\nu,\xi,e,k}(t-\varsigma_i)h_i(\varsigma_i,x_{\varsigma_i})+\displaystyle\int_{\varsigma_i}^t R_{\mu,\nu,\xi,e,k}(t-\varsigma)B(\varsigma)u(\varsigma)d\varsigma\\
\quad+\displaystyle\int_{\varsigma_i}^t R_{\mu,\nu,\xi,e,k}(t-\varsigma)\mathcal{M}\left(\varsigma,x_\varsigma,\int_0^\varsigma g(\varsigma,\tau,x_\tau)d\tau\right)dW(\varsigma),t\in(\varsigma_i,t_{i+1}],\ i=1,2,\dots,q.
\end{cases}\tag{2}$$

https://doi.org/10.3390/fractalfract10070490

Table 1. Summary of principal notation used throughout the paper.

Symbol	Description
$\mathcal{H}, U, Y$	Separable Hilbert spaces: state, noise, and control spaces
$(\Omega, \mathcal{F}, \{\mathcal{F}_t\}_{t\geq 0}, \mathbb{P})$	Filtered complete probability space
$W(t)$	Q-Wiener process on U with covariance operator Q
$L(U;\mathcal{H})$	Banach space of bounded linear operators from U to $\mathcal{H}$
$L_2^0 = L_2(U_0;\mathcal{H})$	Space of Hilbert–Schmidt operators from $U_0 = Q^{1/2}(U)$ to $\mathcal{H}$
$\mathcal{B}_\hbar$	Phase space for infinite delay with weight function $\hbar$
$\mathcal{B}_b$	Extended phase space incorporating non-instantaneous impulses
$PC([0,a];L^p(\Omega;\mathcal{H}))$	Space of piecewise continuous $\mathcal{F}_t$-adapted processes
U_{ad}	Admissible control set
$L^p_{\mathcal{F}}([0,a];Y)$	Space of p-integrable $\mathcal{F}_t$-adapted Y-valued processes ($p>1$)
D_t^α, I_t^α	Riemann–Liouville fractional derivative and integral of order α
$E_{\mu,\nu,\xi}(z,w)$	Three-parameter bivariate Mittag-Leffler type function
$\mathbb{E}_t^{\mu-\nu,\mu-\xi,\mu,-e,-k}$	Three-parameter Mittag-Leffler integral operator
$R_{\mu,\nu,\xi,e,k}(t)$	(μ,ν,ξ,e,k)-resolvent family generated by operator A
A	Linear sectorial operator (e.g., fourth-order diffusion operator)
$B(t)$	Time-varying control operator
$\mathcal{M}$	Nonlinear stochastic coefficient operator
g	Nonlinear delay interaction kernel
h_i	Non-instantaneous impulsive operator at the i-th impulse
μ, ν, ξ	Fractional orders satisfying $0<\xi<\nu<\mu\leq 1$
e, k	Damping parameters
p	Moment order ($p>1$)
t_i, ς_i	Impulse onset and termination times, $i=1,\ldots,q$

3. Solvability Results

This section is devoted to establishing the existence of mild solutions for system (1) by means of fixed-point techniques. We introduce the operator $Q:\mathcal{B}_b\to\mathcal{B}_b$ as follows:

$$(Qx)(t)=\begin{cases}\varphi(t), t\in(-\infty,0],\\ \\ R_{\mu,\nu,\xi,e,k}(t)\varphi(0)+\displaystyle\int_0^t R_{\mu,\nu,\xi,e,k}(t-\varsigma)B(\varsigma)u(\varsigma)d\varsigma\\ \quad+\displaystyle\int_0^t R_{\mu,\nu,\xi,e,k}(t-\varsigma)\mathcal{M}\left(\varsigma,x_\varsigma,\int_0^\varsigma g(\varsigma,\tau,x_\tau)d\tau\right)dW(\varsigma),\quad t\in(0,t_1],\\ h_i(t,x_t), t\in(t_i,\varsigma_i],\ i=1,2,\ldots,q,\\ \\ R_{\mu,\nu,\xi,e,k}(t-\varsigma_i)h_i(\varsigma_i,x_{\varsigma_i})+\displaystyle\int_{\varsigma_i}^t R_{\mu,\nu,\xi,e,k}(t-\varsigma)B(\varsigma)u(\varsigma)d\varsigma\\ \quad+\displaystyle\int_{\varsigma_i}^t R_{\mu,\nu,\xi,e,k}(t-\varsigma)\mathcal{M}\left(\varsigma,x_\varsigma,\int_0^\varsigma g(\varsigma,\tau,x_\tau)d\tau\right)dW(\varsigma),\quad t\in(\varsigma_i,t_{i+1}],\\ i=1,2,\ldots,q.\end{cases}$$

Our goal is to verify that the operator Q admits at least one fixed point.

For any $\varphi\in\mathcal{B}_\hbar$, define

$$\tilde{\varphi}(t)=\begin{cases}\varphi(t), t\in(-\infty,0],\\ \\ R_{\mu,\nu,\xi,e,k}(t)\varphi(0), t\in[0,a].\end{cases}$$

https://doi.org/10.3390/fractalfract10070490

Then, one has $\tilde{\varphi} \in \mathcal{B}_b$. To convert the fixed-point problem for x into a homogeneous one, we introduce the change of variable $x(t) = \nu(t) + \tilde{\varphi}(t)$ for $t \in (-\infty, a]$, where $\nu_0 = 0$. It is readily seen that x satisfies system (1) if and only if $\nu_0 = 0$ and

$$\nu(t) = \begin{cases} \displaystyle\int_0^t R_{\mu,\nu,\xi,e,k}(t-\varsigma)B(\varsigma)u(\varsigma)d\varsigma \\ \quad + \displaystyle\int_0^t R_{\mu,\nu,\xi,e,k}(t-\varsigma)\mathcal{M}\left(\varsigma, \nu_\varsigma + \tilde{\varphi}_\varsigma, \int_0^\varsigma g(\varsigma,\tau,\nu_\tau+\tilde{\varphi}_\tau)d\tau\right)dW(\varsigma), \quad t \in (0, t_1] \\ h_i(t, \nu_t + \tilde{\varphi}_t), t \in (t_i, \varsigma_i],\ i = 1, 2, \ldots, q, \\ R_{\mu,\nu,\xi,e,k}(t-\varsigma_i)h_i(\varsigma_i, \nu_{\varsigma_i} + \tilde{\varphi}_{\varsigma_i}) + \displaystyle\int_{\varsigma_i}^t R_{\mu,\nu,\xi,e,k}(t-\varsigma)B(\varsigma)u(\varsigma)d\varsigma \\ \quad + \displaystyle\int_{\varsigma_i}^t R_{\mu,\nu,\xi,e,k}(t-\varsigma)\mathcal{M}\left(\varsigma, \nu_\varsigma + \tilde{\varphi}_\varsigma, \int_0^\varsigma g(\varsigma,\tau,\nu_\tau+\tilde{\varphi}_\tau)d\tau\right)dW(\varsigma), t \in (\varsigma_i, t_{i+1}], \\ i = 1, 2, \ldots, q. \end{cases}$$

Introduce the space $\mathcal{B}_b^0 = \{\nu \in \mathcal{B}_b : \nu_0 = 0 \in \mathcal{B}_\hbar\}$, which is a Banach space equipped with the norm

$$\begin{aligned} \|\nu\|_b &= \|\nu_0\| + \max_{i=0,1,2,\ldots,q} \sup_{t\in(\varsigma_i,\varsigma_{i+1}]} \left(E\left\|(t-\varsigma_i)^{1-\mu}\nu(t)\right\|^p\right)^{\frac{1}{p}} \\ &= \max_{i=0,1,2,\ldots,q} \sup_{t\in(\varsigma_i,\varsigma_{i+1}]} \left(E\left\|(t-\varsigma_i)^{1-\mu}\nu(t)\right\|^p\right)^{\frac{1}{p}}. \end{aligned}$$

For some constant $r \geq 0$, set $B_r = \{\nu \in \mathcal{B}_b^0 : \|\nu\|_b^p \leq r\}$. Clearly, B_r is a nonempty, closed, bounded, and convex subset of $\mathcal{B}_b^0$. Moreover, for any $\nu \in B_r$, the estimate holds:

$$\begin{aligned} \|\nu_t + \tilde{\varphi}_t\|_{\mathcal{B}_\hbar}^p &\leq 2^{p-1}\left(\|\nu_t\|_{\mathcal{B}_\hbar}^p + \|\tilde{\varphi}_t\|_{\mathcal{B}_\hbar}^p\right) \\ &\leq 4^{p-1}\left[l^p \sup_{\varsigma\in[0,t]} E\left\|\varsigma^{1-\mu}\nu(\varsigma)\right\|^p + \|\tilde{\varphi}_0\|_{\mathcal{B}_\hbar}^p + l^p \sup_{\varsigma\in[0,t]} E\left\|\varsigma^{1-\mu}\varphi(\varsigma)\right\|^p\right] \qquad (3) \\ &\leq 4^{p-1}\left[l^p r + l^p K^p \|\varphi(0)\|^p + \|\varphi\|_{\mathcal{B}_\hbar}^p\right] = r'. \end{aligned}$$

Define an operator $\bar{Q} : \mathcal{B}_b^0 \to \mathcal{B}_b^0$ by

$$(\bar{Q}\nu)(t) = \begin{cases} 0, & t \in (-\infty, 0], \\ \displaystyle\int_0^t R_{\mu,\nu,\xi,e,k}(t-\varsigma)B(\varsigma)u(\varsigma)d\varsigma \\ \quad + \displaystyle\int_0^t R_{\mu,\nu,\xi,e,k}(t-\varsigma)\mathcal{M}\left(\varsigma, \nu_\varsigma + \tilde{\varphi}_\varsigma, \int_0^\varsigma g(\varsigma,\tau,\nu_\tau+\tilde{\varphi}_\tau)d\tau\right)dW(\varsigma), & t \in (0, t_1], \\ h_i(t, \nu_t + \tilde{\varphi}_t), & t \in (t_i, \varsigma_i],\ i = 1, 2, \ldots, q, \\ R_{\mu,\nu,\xi,e,k}(t-\varsigma_i)h_i(\varsigma_i, \nu_{\varsigma_i} + \tilde{\varphi}_{\varsigma_i}) + \displaystyle\int_{\varsigma_i}^t R_{\mu,\nu,\xi,e,k}(t-\varsigma)B(\varsigma)u(\varsigma)d\varsigma \\ \quad + \displaystyle\int_{\varsigma_i}^t R_{\mu,\nu,\xi,e,k}(t-\varsigma)\mathcal{M}\left(\varsigma, \nu_\varsigma + \tilde{\varphi}_\varsigma, \int_0^\varsigma g(\varsigma,\tau,\nu_\tau+\tilde{\varphi}_\tau)d\tau\right)dW(\varsigma), & t \in (\varsigma_i, t_{i+1}]. \end{cases}$$

It is straightforward to verify that for $x(t) = \nu(t) + \tilde{\varphi}(t)$, the operators Q and $\bar{Q}$ satisfy the relation $(Qx)(t) = (\bar{Q}\nu)(t) + \tilde{\varphi}(t)$. Therefore, x is a fixed point of Q if and only if ν is a fixed point of $\bar{Q}$.

Decompose $\bar{Q} = \bar{Q}_1 + \bar{Q}_2$, where $\bar{Q}_1$ and $\bar{Q}_2$ are given by

https://doi.org/10.3390/fractalfract10070490

$$(\bar{Q}_1\nu)(t)=\begin{cases}\displaystyle\int_0^t R_{\mu,\nu,\xi,e,k}(t-\varsigma)B(\varsigma)u(\varsigma)d\varsigma, & t\in(0,t_1],\\ h_i(t,\nu_t+\tilde{\varphi}_t), & t\in(t_i,\varsigma_i],\ i=1,2,\ldots,q,\\ R_{\mu,\nu,\xi,e,k}(t-\varsigma_i)h_i(\varsigma_i,\nu_{\varsigma_i}+\tilde{\varphi}_{\varsigma_i})+\displaystyle\int_{\varsigma_i}^t R_{\mu,\nu,\xi,e,k}(t-\varsigma)B(\varsigma)u(\varsigma)d\varsigma, & t\in(\varsigma_i,t_{i+1}],\end{cases}$$

$$(\bar{Q}_2\nu)(t)=\begin{cases}\displaystyle\int_0^t R_{\mu,\nu,\xi,e,k}(t-\varsigma)\mathcal{M}\Big(\varsigma,\nu_\varsigma+\tilde{\varphi}_\varsigma,\int_0^\varsigma g(\varsigma,\tau,\nu_\tau+\tilde{\varphi}_\tau)d\tau\Big)dW(\varsigma), & t\in(0,t_1],\\ 0, & t\in(t_i,\varsigma_i],\ i=1,2,\ldots,q,\\ \displaystyle\int_{\varsigma_i}^t R_{\mu,\nu,\xi,e,k}(t-\varsigma)\mathcal{M}\Big(\varsigma,\nu_\varsigma+\tilde{\varphi}_\varsigma,\int_0^\varsigma g(\varsigma,\tau,\nu_\tau+\tilde{\varphi}_\tau)d\tau\Big)dW(\varsigma), & t\in(\varsigma_i,t_{i+1}].\end{cases}$$

We proceed to verify that $\bar{Q}_1$ and $\bar{Q}_2$ satisfy all assumptions of Theorem 1.

Lemma 5. *Assume that (1)–(4) hold and*

$$L=\max_{1\le i\le q}\left\{2^{p-1}l^pL_{h_i}a^{p(1-\mu)}+2^{p-1}l^pL_{h_i}K^p\right\}<1.$$

Thus, $\bar{Q}_1:\mathcal{B}_b^0\to\mathcal{B}_b^0$ is a contraction operator.

Proof. Take any $y,\nu\in\mathcal{B}_b^0$. For $t\in(0,t_1]$, one obtains

$$t^{1-\mu}\|(\bar{Q}_1\nu)(t)-(\bar{Q}_1y)(t)\|=0.$$

Note that the integral term of $\overline{Q}_1$ on non-impulsive intervals depends only on the control input and is independent of the state variable. It thus vanishes identically in the difference of two states, and the overall contraction constant is solely determined by the Lipschitz constants of the impulsive mappings h_i.

For $t\in(t_i,\varsigma_i]$, $i=1,2,\ldots,q$, by Lemma 4, it follows that

$$\begin{aligned}E\big\|(t-\varsigma_{i-1})^{1-\mu}\big((\bar{Q}_1\nu)(t)-(\bar{Q}_1y)(t)\big)\big\|^p&\le a^{p(1-\mu)}E\big\|h_i(t,\nu_t+\tilde{\varphi}_t)-h_i(t,y_t+\tilde{\varphi}_t)\big\|^p\\&\le 2^{p-1}a^{p(1-\mu)}l^pL_{h_i}\|\nu-y\|_b^p.\end{aligned}$$

(Note: For the impulsive interval $t\in(t_i,\varsigma_i]$, the weight function subscript is ς_{i-1}, whereas for the post-impulsive interval $t\in(\varsigma_i,t_{i+1}]$, the subscript is ς_i; see the definition of $\|\cdot\|_b$.) For any $t\in(\varsigma_i,t_{i+1}]$, $i=1,2,\ldots,q$, we derive

$$\begin{aligned}&E\big\|(t-\varsigma_i)^{1-\mu}\big((\bar{Q}_1\nu)(t)-(\bar{Q}_1y)(t)\big)\big\|^p\\=&E\Big\|(t-\varsigma_i)^{1-\mu}R_{\mu,\nu,\xi,e,k}(t-\varsigma_i)[h_i(\varsigma_i,\nu_{\varsigma_i}+\tilde{\varphi}_{\varsigma_i})-h_i(\varsigma_i,y_{\varsigma_i}+\tilde{\varphi}_{\varsigma_i})]\Big\|^p\\\le&K^pE\big\|h_i(\varsigma_i,\nu_{\varsigma_i}+\tilde{\varphi}_{\varsigma_i})-h_i(\varsigma_i,y_{\varsigma_i}+\tilde{\varphi}_{\varsigma_i})\big\|^p\\\le&2^{p-1}K^pl^pL_{h_i}\|\nu-y\|_b^p.\end{aligned}$$

Taking the supremum with respect to $t\in[0,a]$ yields

$$\|\bar{Q}_1\nu-\bar{Q}_1y\|_b^p\le L\|\nu-y\|_b^p,$$

which implies that $\bar{Q}_1$ is a contraction operator. □

Lemma 6. *Under Assumptions (1)–(4), the operator $\bar{Q}_2$ is completely continuous.*

https://doi.org/10.3390/fractalfract10070490

Proof. The proof proceeds in three steps. We first show that $\bar{Q}_2$ maps bounded sets to bounded sets in $\mathcal{B}_b^0$. For this purpose, it suffices to prove that there exists a positive constant $\mathcal{Z}$ such that

$$\|\bar{Q}_2\nu\|_b^p \leq \mathcal{Z} \quad \text{for all } \nu \in B_r.$$

Under the integrability condition $p(2\mu-1) > 2$, applying Hölder's inequality with conjugate exponents $\frac{p}{2}$ and $\frac{p}{p-2}$, we obtain

$$\begin{aligned}
&E\left\|(t-\varsigma_i)^{1-\mu}(\bar{Q}_2\nu)(t)\right\|^p \\
&\leq a^{p(1-\mu)}E\left\|\int_{\varsigma_i}^t R_{\mu,\nu,\xi,e,k}(t-\varsigma)\mathcal{M}\left(\varsigma,\nu_\varsigma+\tilde{\varphi}_\varsigma,\int_0^\varsigma g(\varsigma,\tau,\nu_\tau+\tilde{\varphi}_\tau)\mathrm{d}\tau\right)\mathrm{d}W(\varsigma)\right\|^p \\
&\leq a^{p(1-\mu)}C_p\left[\int_{\varsigma_i}^t\left(E\left\|R_{\mu,\nu,\xi,e,k}(t-\varsigma)\mathcal{M}\left(\varsigma,\nu_\varsigma+\tilde{\varphi}_\varsigma,\int_0^\varsigma g(\varsigma,\tau,\nu_\tau+\tilde{\varphi}_\tau)\mathrm{d}\tau\right)\right\|^p\right)^{\frac{2}{p}}\mathrm{d}\varsigma\right]^{\frac{p}{2}} \\
&\leq a^{p(1-\mu)}C_pK^p\left[\int_{\varsigma_i}^t(t-\varsigma)^{p(\mu-1)}\left(E\left\|\mathcal{M}\left(\varsigma,\nu_\varsigma+\tilde{\varphi}_\varsigma,\int_0^\varsigma g(\varsigma,\tau,\nu_\tau+\tilde{\varphi}_\tau)\mathrm{d}\tau\right)\right\|^p\right)^{\frac{2}{p}}\mathrm{d}\varsigma\right]^{\frac{p}{2}} \\
&\leq a^{p(1-\mu)}C_pK^p\left[\int_{\varsigma_i}^t(t-\varsigma)^{2(\mu-1)}m_{\mathcal{M}}^{\frac{2}{p}}(\varsigma)\Theta_{\mathcal{M}}^{\frac{2}{p}}\big(r'+(t_{i+1}-\varsigma_i)^p m_g\Theta_g(r')\big)\mathrm{d}\varsigma\right]^{\frac{p}{2}} \\
&\leq a^{p(1-\mu)}C_pK^p\Theta_{\mathcal{M}}(r'')\left[\left(\int_{\varsigma_i}^t(t-\varsigma)^{\frac{2p(\mu-1)}{p-2}}\mathrm{d}\varsigma\right)^{\frac{p-2}{p}}\left(\int_{\varsigma_i}^t m_{\mathcal{M}}(\varsigma)\mathrm{d}\varsigma\right)^{\frac{2}{p}}\right]^{\frac{p}{2}} \\
&\leq a^{p(1-\mu)}C_pK^p\Theta_{\mathcal{M}}(r'')\left(\frac{p-2}{-p-2+2p\mu}\right)^{\frac{p-2}{2}}(t_{i+1}-\varsigma_i)^{\frac{-p-2+2p\mu}{2}}\int_{\varsigma_i}^t m_{\mathcal{M}}(\varsigma)\mathrm{d}\varsigma \\
&= K_i.
\end{aligned}$$

Taking $\mathcal{Z} = \max_{i=0,1,\ldots,q} K_i$, we conclude that $\|\bar{Q}_2\nu\|_b^p \leq \mathcal{Z}$ for all $\nu \in B_r$, i.e., $\bar{Q}_2$ maps bounded sets to bounded sets in $\mathcal{B}_b^0$.

Next, we prove that the family $\bar{Q}_2(B_r)$ is equicontinuous in $\mathcal{B}_b^0$. For any $s_1, s_2 \in (\varsigma_i, s_{i+1}]$ with $s_1 < s_2$ and $x \in B_r$, consider

$$\begin{aligned}
&E\left\|(t-\varsigma_i)^{1-\mu}[(\bar{Q}_2\nu)(t_1)-(\bar{Q}_2\nu)(t_2)]\right\|^p \\
&\leq C_p^1(t_1)E\left\|t_2^{1-\mu}[(\bar{Q}_2\nu)(t_1)-(\bar{Q}_2\nu)(t_2)]\right\|^p \\
&\leq C_p^1(t_1)E\left\|t_1^{1-\mu}\bar{Q}_2\nu(t_1)-t_2^{1-\mu}\bar{Q}_2\nu(t_2)\right\|^p + C_p^1(t_1)E\left\|t_1^{1-\mu}\bar{Q}_2\nu(t_1)-t_2^{1-\mu}\bar{Q}_2\nu(t_1)\right\|^p \\
&\leq C_p^1(t_1)E\left\|t_1^{1-\mu}\bar{Q}_2\nu(t_1)-t_2^{1-\mu}\bar{Q}_2\nu(t_2)\right\|^p + C_p^1(t_1)E\|\bar{Q}_2\nu(t_1)\|^p\left|t_2^{1-\mu}-t_1^{1-\mu}\right|^p \\
&\to 0.
\end{aligned}$$

Since $t^{1-\mu}R_{\mu,\nu,\xi,e,k}(t-\varsigma)$ is uniformly continuous and $|t_1^{1-\mu}-t_2^{1-\mu}| \to 0$ as $t_1 \to t_2$, both terms tend to 0 as $t_1 \to t_2$, which implies that $\bar{Q}_2(B_r)$ is equicontinuous in $\mathcal{B}_b^0$.

Finally, we show that $\bar{Q}_2$ is continuous on $\mathcal{B}_b^0$. Let $\{\nu^n\}_{n=0}^\infty \subseteq \mathcal{B}_b^0$ be a sequence such that $\nu^n \to \nu$ in $\mathcal{B}_b^0$ as $n \to \infty$. Then, $E\|(t-\varsigma_i)^{1-\alpha}\nu^n(t)\|^p \leq r$ for all n and almost all $t \in [0,a]$, so $\nu^n, \nu \in B_r$. For any $t \in (\varsigma_i, t_{i+1}]$ $(i = 0,1,\ldots,q)$, we have

$$\mathcal{M}\left(\varsigma,\nu_\varsigma^n+\tilde{\varphi}_\varsigma,\int_0^\varsigma g(\varsigma,\tau,\nu_\tau^n+\tilde{\varphi}_\tau)\mathrm{d}\tau\right) \to \mathcal{M}\left(\varsigma,\nu_\varsigma+\tilde{\varphi}_\varsigma,\int_0^\varsigma g(\varsigma,\tau,\nu_\tau+\tilde{\varphi}_\tau)\mathrm{d}\tau\right)$$

https://doi.org/10.3390/fractalfract10070490

as $n \to \infty$, Since $\{\nu^n\} \subset B_r$, by the a priori estimate of the phase space norm, we have $\|\nu_\varsigma^n + \tilde{\varphi}_\varsigma\|_{\mathcal{B}_h}^p \le r'$ for all n and almost all $\varsigma \in [0, a]$, and the integral term $E\|\int_0^\varsigma g(\varsigma, \tau, \nu_\tau^n + \tilde{\varphi}_\tau)d\tau\|^p$ also admits a uniform upper bound independent of n. Substituting into the growth condition in Assumption (3) yields

$$E\left\|\mathcal{M}\left(\varsigma, \nu_\varsigma^n + \tilde{\varphi}_\varsigma, \int_0^\varsigma g(\varsigma, \tau, \nu_\tau^n + \tilde{\varphi}_\tau)d\tau\right)\right\|_{L_2^0}^p \le m_{\mathcal{M}}(\varsigma) \cdot C_r,$$

where the constant C_r depends only on the radius r of the bounded set and is independent of n. Combined with the integrability of the singular kernel $(t-\varsigma)^{p(\mu-1)}$ under the condition $p(2\mu-1) > 2$, it follows that the sequence of integrands admits an integrable dominating function independent of the approximating sequence, by Assumptions (2) and (3) and the dominated convergence theorem. This implies that $\bar{Q}_2 x^n \to \bar{Q}_2 x$ in $\mathcal{B}_b^0$ as $n \to \infty$, so $\bar{Q}_2$ is continuous.

Combining Steps 1–3, $\bar{Q}_2$ maps bounded sets to bounded and equicontinuous sets in $\mathcal{B}_b^0$, and is continuous. By the Arzelá-Ascoli theorem,

$$\begin{aligned}
&E\left\|(t-\varsigma_i)^{1-\mu}[\bar{Q}_2\nu^n(t) - \bar{Q}_2\nu(t)]\right\|^p \\
&\le a^{p(1-\mu)}C_p\left[\int_{\varsigma_i}^t\left(E\left\|R_{\mu,\nu,\xi,e,k}(t-\varsigma)\left[\mathcal{M}\left(\varsigma, \nu_\varsigma^n + \tilde{\varphi}_\varsigma, \int_0^\varsigma g(\varsigma, \tau, \nu^n + \tilde{\varphi}_\tau)\,\mathrm{d}\tau\right)\right.\right.\right.\right. \\
&\left.\left.\left.\left.-\mathcal{M}\left(\varsigma, \nu_\varsigma + \tilde{\varphi}_\varsigma, \int_0^\varsigma g(\varsigma, \tau, \nu_\tau + \tilde{\varphi}_\tau)\,\mathrm{d}\tau\right)\right]\right\|_{L_2^0}^p\right)^{\frac{2}{p}}\mathrm{d}\varsigma\right]^{\frac{p}{2}} \\
&\le a^{p(1-\mu)}C_pK^p\left[\int_{\varsigma_i}^t(t-\varsigma)^{2(\mu-1)}\left(E\left\|\mathcal{M}\left(\varsigma, \nu_\varsigma^n + \tilde{\varphi}_\varsigma, \int_0^\varsigma g(\varsigma, \tau, \nu^n + \tilde{\varphi}_\tau)\,\mathrm{d}\tau\right)\right.\right.\right. \\
&\left.\left.\left.-\mathcal{M}\left(\varsigma, \nu_\varsigma + \tilde{\varphi}_\varsigma, \int_0^\varsigma g(\varsigma, \tau, \nu_\tau + \tilde{\varphi}_\tau)\,\mathrm{d}\tau\right)\right\|_{L_2^0}^p\right)^{\frac{2}{p}}\mathrm{d}\varsigma\right]^{\frac{p}{2}} \\
&\le a^{p(1-\mu)}C_pK^p\left(\frac{p-2}{-p-2+2p\mu}\right)^{\frac{p}{2}-1}(t_{i+1}-\varsigma_i)^{\frac{p}{2}-1} \\
&\int_{\varsigma_i}^t E\left\|\mathcal{M}\left(\varsigma, \nu_\varsigma^n + \tilde{\varphi}_\varsigma, \int_0^\varsigma g(\varsigma, \tau, \nu^n + \tilde{\varphi}_\tau)\,\mathrm{d}\tau\right) - \mathcal{M}\left(\varsigma, \nu_\varsigma + \tilde{\varphi}_\varsigma, \int_0^\varsigma g(\varsigma, \tau, \nu_\tau + \tilde{\varphi}_\tau)\,\mathrm{d}\tau\right)\right\|_{L_2^0}^p\mathrm{d}\varsigma \\
&\to 0 \quad \text{as } n \to \infty.
\end{aligned}$$

Hence, $\bar{Q}_2$ is continuous. □

Remark 6. *The condition $p(2\mu-1) > 2$ is used throughout the proof of Lemma 6 to guarantee the integrability of the singular resolvent kernel $(t-s)^{2(\mu-1)}$ in the p-th moment estimates of stochastic convolutions. We derive this condition as follows.*

After applying the Burkholder–Davis–Gundy inequality and substituting the resolvent bound $\|R(t-\varsigma)\| \le K(t-\varsigma)^{\mu-1}$, we obtain an integral of the form

$$\int_{\varsigma_i}^t (t-\varsigma)^{2(\mu-1)}\mathbb{E}\|\mathcal{M}(\cdot)\|^2 d\varsigma.$$

Applying Hölder's inequality with exponents $\frac{p}{2}$ and $\frac{p}{p-2}$, the kernel exponent becomes

$$\alpha = \frac{2p(\mu-1)}{p-2}.$$

https://doi.org/10.3390/fractalfract10070490

The singular integral $\int_{\varsigma_i}^{t}(t-\varsigma)^{\alpha}d\varsigma$ *converges if and only if* $\alpha > -1$. *Substituting* α *and rearranging:*

$$\frac{2p(\mu-1)}{p-2} > -1 \quad \Longleftrightarrow \quad 2p(\mu-1) > -(p-2) \quad \Longleftrightarrow \quad p(2\mu-1) > 2.$$

This justifies the integrability condition stated in Section 2.

Lastly, we prove that $\bar{Q}_2$ maps B_r into a precompact set in $\mathcal{H}$. Let

$$V = \Big\{ z \in \mathcal{B}_b^0 : z(t) = t^{1-\mu}(\bar{Q}_2 \nu)(t),\ \nu \in B_r,\ t \in [0,a] \Big\}.$$

We prove that the set $V(t) = \{z(t) \mid z \in V\}$ is precompact in the Hilbert space $\mathcal{H}$ for all $t \in [0,a]$. The case $t = 0$ is trivial, as $V(0) = \{0\}$ is a singleton and thus trivially precompact in $\mathcal{H}$. For $t > 0$, we introduce an auxiliary set $V^{\varepsilon}(t) = \{z^{\varepsilon}(t) \mid \nu \in B_r\} \subseteq \mathcal{H}$, where

$$\begin{aligned} z^{\varepsilon}(t) &= \Gamma(\mu)\varepsilon^{1-\mu} R_{\mu,\nu,\xi,e,k}(\varepsilon) t^{1-\mu} \\ &\quad \times \int_{\varsigma_i}^{t-\varepsilon} R_{\mu,\nu,\xi,e,k}(t-\varsigma-\varepsilon)\mathcal{M}\Big(\varsigma, \nu_\varsigma + \tilde{\varphi}_\varsigma, \int_0^{\varsigma} g(\varsigma,\tau,\nu_\tau+\tilde{\varphi}_\tau)\mathrm{d}\tau\Big)\mathrm{d}W(\varsigma). \end{aligned}$$

Under Assumption (1), the operator $\varepsilon^{1-\mu} R_{\mu,\nu,\xi,e,k}(\varepsilon)$ is compact for any $\varepsilon > 0$, which guarantees that $V^{\varepsilon}(t)$ is precompact in $\mathcal{H}$ for each $t \in (0,a]$. This follows from the fact that a compact linear operator maps every bounded set into a relatively compact set, and the stochastic integral term maps B_r into a bounded subset of H. We now show that the approximation error tends to zero uniformly with respect to all $\nu \in B_r$. Fix $t \in (\varsigma_i, t_{i+1}]$ with $i = 0,1,2,\ldots,q$, and take $\delta \in (\varepsilon, t)$, we have

$$\begin{aligned} &E\Big\|(t-\varsigma_i)^{1-\mu}[z(t)-z^{\varepsilon}(t)]\Big\|^p \\ &\le a^{p(1-\mu)} E\|z(t)-z^{\varepsilon}(t)\|^p \\ &\le a^{2p(1-\mu)} E\Big\| \int_{\varsigma_i}^{t} R_{\mu,\nu,\xi,e,k}(t-\varsigma)\mathcal{M}\Big(\varsigma,\nu_\varsigma+\tilde{\varphi}_\varsigma,\int_0^{\varsigma} g(\varsigma,\tau,\nu_\tau+\tilde{\varphi}_\tau)\mathrm{d}\tau\Big)\mathrm{d}W(\varsigma) \\ &\quad -\Gamma(\mu)\varepsilon^{1-\mu} R_{\mu,\nu,\xi,e,k}(\varepsilon) t^{1-\mu} \int_{\varsigma_i}^{t-\varepsilon} R_{\mu,\nu,\xi,e,k}(t-\varsigma-\varepsilon)\mathcal{M}\Big(\varsigma,\nu_\varsigma+\tilde{\varphi}_\varsigma,\int_0^{\varsigma} g(\varsigma,\tau,\nu_\tau+\tilde{\varphi}_\tau)\mathrm{d}\tau\Big)\mathrm{d}W(\varsigma)\Big\|^p \\ &\le 3^{p-1}a^{2p(1-\mu)} E\Big\| \int_{\varsigma_i}^{t-\varepsilon} R_{\mu,\nu,\xi,e,k}(t-\varsigma)\mathcal{M}\Big(\varsigma,\nu_\varsigma+\tilde{\varphi}_\varsigma,\int_0^{\varsigma} g(\varsigma,\tau,\nu_\tau+\tilde{\varphi}_\tau)\mathrm{d}\tau\Big)\mathrm{d}W(\varsigma) \\ &\quad -\Gamma(\mu)\varepsilon^{1-\mu} R_{\mu,\nu,\xi,e,k}(\varepsilon) \int_{\varsigma_i}^{t-\varepsilon} (t-\varsigma-\varepsilon)^{1-\mu} R_{\mu,\nu,\xi,e,k}(t-\varsigma-\varepsilon)(t-\varsigma)^{\mu-1} \\ &\quad \times\mathcal{M}\Big(\varsigma,\nu_\varsigma+\tilde{\varphi}_\varsigma,\int_0^{\varsigma} g(\varsigma,\tau,\nu_\tau+\tilde{\varphi}_\tau)\mathrm{d}\tau\Big)\mathrm{d}W(\varsigma)\Big\|^p \\ &\quad +3^{p-1}a^{2p(1-\mu)} E\Big\|\varepsilon^{1-\mu} R_{\mu,\nu,\xi,e,k}(\varepsilon)\Gamma(\mu)\int_{\varsigma_i}^{t-\varepsilon}(t-\varsigma-\varepsilon)^{1-\mu} R_{\mu,\nu,\xi,e,k}(t-\varsigma-\varepsilon)\Big[(t-\varsigma)^{\mu-1} \\ &\quad -(t-\varsigma-\varepsilon)^{\mu-1}\Big]\mathcal{M}\Big(\varsigma,\nu_\varsigma+\tilde{\varphi}_\varsigma,\int_0^{\varsigma} g(\varsigma,\tau,\nu_\tau+\tilde{\varphi}_\tau)d\tau\Big)dW(\varsigma)\Big\|^p \\ &\quad +3^{p-1}a^{2p(1-\mu)}K^p E\Big\| \int_{t-\varepsilon}^{t}(t-\varsigma)^{\mu-1}\mathcal{M}\Big(\varsigma,\nu_\varsigma+\tilde{\varphi}_\varsigma,\int_0^{\varsigma} g(\varsigma,\tau,\nu_\tau+\tilde{\varphi}_\tau)d\tau\Big)dW(\varsigma)\Big\|^p \\ &\le 6^{p-1}a^{2p(1-\mu)} E\Big\| \int_{\varsigma_i}^{t-\delta}\Big[(t-\varsigma)^{1-\mu} R_{\mu,\nu,\xi,e,k}(t-\varsigma) - \Gamma(\mu)\varepsilon^{1-\mu} R_{\mu,\nu,\xi,e,k}(\varepsilon) \end{aligned}$$

https://doi.org/10.3390/fractalfract10070490

$$
\begin{aligned}
&\times(t-\varsigma-\varepsilon)^{1-\mu}R_{\mu,\nu,\xi,e,k}(t-\varsigma-\varepsilon)\Big](t-\varsigma)^{\mu-1}\mathcal{M}\bigg(\varsigma,\nu_\varsigma+\tilde{\varphi}_\varsigma,\int_0^\varsigma g(\varsigma,\tau,\nu_\tau+\tilde{\varphi}_\tau)d\tau\bigg)dW(\varsigma)\bigg\|^p\\
&+6^{p-1}a^{2p(1-\mu)}E\bigg\|\int_{t-\delta}^{t-\varepsilon}\Big[(t-\varsigma)^{1-\mu}R_{\mu,\nu,\xi,e,k}(t-\varsigma)-\Gamma(\mu)\varepsilon^{1-\mu}R_{\mu,\nu,\xi,e,k}(\varepsilon)\\
&\times(t-\varsigma-\varepsilon)^{1-\mu}R_{\mu,\nu,\xi,e,k}(t-\varsigma-\varepsilon)\Big](t-\varsigma)^{\mu-1}\mathcal{M}\bigg(\varsigma,\nu_\varsigma+\tilde{\varphi}_\varsigma,\int_0^\varsigma g(\varsigma,\tau,\nu_\tau+\tilde{\varphi}_\tau)d\tau\bigg)dW(\varsigma)\bigg\|^p\\
&+3^{p-1}a^{2p(1-\mu)}K^{2p}(\Gamma(\mu))^pE\bigg\|\int_{\varsigma_i}^{t-\varepsilon}\Big[(t-\varsigma)^{\mu-1}-(t-\varsigma-\varepsilon)^{\mu-1}\Big]\\
&\times\mathcal{M}\bigg(\varsigma,\nu_\varsigma+\tilde{\varphi}_\varsigma,\int_0^\varsigma g(\varsigma,\tau,\nu_\tau+\tilde{\varphi}_\tau)d\tau\bigg)dW(\varsigma)\bigg\|^p\\
&+3^{p-1}a^{2p(1-\mu)}K^pE\bigg\|\int_{t-\varepsilon}^{t}(t-\varsigma)^{\mu-1}\mathcal{M}\bigg(\varsigma,\nu_\varsigma+\tilde{\varphi}_\varsigma,\int_0^\varsigma g(\varsigma,\tau,\nu_\tau+\tilde{\varphi}_\tau)d\tau\bigg)dW(\varsigma)\bigg\|^p\\
\le\ &6^{p-1}a^{2p(1-\mu)}C_p\Theta_{\mathcal{M}}(r'')\bigg[\int_{\varsigma_i}^{t-\delta}\Big\|(t-\varsigma)^{1-\mu}R_{\mu,\nu,\xi,e,k}(t-\varsigma)-\Gamma(\mu)\varepsilon^{1-\mu}R_{\mu,\nu,\xi,e,k}(\varepsilon)\\
&\times(t-\varsigma-\varepsilon)^{1-\mu}R_{\mu,\nu,\xi,e,k}(t-\varsigma-\varepsilon)\Big\|^2(t-\varsigma)^{2(\mu-1)}m_{\mathcal{M}}^{\frac{2}{p}}(\varsigma)d\varsigma\bigg]^{\frac{p}{2}}\\
&+6^{p-1}a^{2p(1-\mu)}C_p\Theta_{\mathcal{M}}(r'')\bigg[\int_{t-\delta}^{t-\varepsilon}\Big\|(t-\varsigma)^{1-\mu}R_{\mu,\nu,\xi,e,k}(t-\varsigma)-\Gamma(\mu)\varepsilon^{1-\mu}R_{\mu,\nu,\xi,e,k}(\varepsilon)\\
&\times(t-\varsigma-\varepsilon)^{1-\mu}R_{\mu,\nu,\xi,e,k}(t-\varsigma-\varepsilon)\Big\|^2(t-\varsigma)^{2(\mu-1)}m_{\mathcal{M}}^{\frac{2}{p}}(\varsigma)d\varsigma\bigg]^{\frac{p}{2}}\\
&+3^{p-1}a^{2p(1-\mu)}K^{2p}C_p\\
&\times\Theta_{\mathcal{M}}(r'')(\Gamma(\mu))^p\int_{\varsigma_i}^{t-\varepsilon}\Big((t-\varsigma)^{\mu-1}-(t-\varsigma-\varepsilon)^{\mu-1}\Big)^pd\varsigma\bigg(\int_{\varsigma_i}^{t-\varepsilon}m_{\mathcal{M}}^{\frac{2}{p-2}}(\varsigma)d\varsigma\bigg)^{\frac{p-2}{2}}\\
&+3^{p-1}a^{2p(1-\mu)}K^p\\
&\times E\bigg\|\int_{t-\varepsilon}^{t}(t-\varsigma)^{1-\mu}R_{\mu,\nu,\xi,e,k}(t-\varsigma)^{\mu-1}\mathcal{M}\bigg(\varsigma,\nu_\varsigma+\tilde{\varphi}_\varsigma,\int_0^\varsigma g(\varsigma,\tau,\nu_\tau+\tilde{\varphi}_\tau)d\tau\bigg)dW(\varsigma)\bigg\|^p.
\end{aligned}
$$

From Lemma 3, combined with the absolute continuity of integrals and the arbitrariness of ε and δ, the right-hand side of the foregoing expression tends to zero as $\varepsilon,\delta\to0^+$. For any fixed $t\in(\varsigma_i,t_{i+1}]$, we accordingly derive that

$$\lim_{\varepsilon\to0^+}\|z(t)-z^\varepsilon(t)\|_{\mathcal{H}}=0.$$

This yields the precompactness of $V(t)$ in $\mathcal{H}$, since $V(t)$ can be approximated arbitrarily closely by a family of precompact subsets of $\mathcal{H}$. Notably, all error bounds in the above derivation depend only on the radius r of the bounded set, not on the specific element $\nu\in B_r$. Hence, the above convergence is uniform for all $\nu\in B_r$. Since $V(t)$ can be uniformly approximated by precompact sets $V^\varepsilon(t)$ with arbitrarily small Hausdorff distance, it follows from a standard characterization of relative compactness in Banach spaces that $V(t)$ itself is relatively compact in $\mathcal{H}$.

By virtue of the Arzelá–Ascoli theorem, we further conclude that the operator $\bar{Q}_2$ is completely continuous. To investigate the solvability of system (1), we now consider the auxiliary equation $x(t)=\omega\bar{Q}x(t)$ with $\omega\in(0,1)$.

Lemma 7. *Suppose that Assumptions (1)–(4) are satisfied. Then, there exists an a priori bound $\tilde{K}>0$, which depends on a, the functions Θ_g, $\Theta_{\mathcal{M}}$, and the constant $\bar{\gamma}$, such that*

$$\|x_t\|_{\mathcal{B}_h}^p\le\tilde{K},t\in[0,a].$$

https://doi.org/10.3390/fractalfract10070490

Proof. By virtue of Assumptions (1)–(4) and Hölder's inequality, for all $t \in (0, t_1]$, we derive that

$$\begin{aligned}
E\|t^{1-\mu}x(t)\|^p &\le 2^{p-1}a^{p(1-\mu)}E\left\|\int_0^t R_{\mu,\nu,\xi,e,k}(t-\varsigma)B(\varsigma)u(\varsigma)\,\mathrm{d}\varsigma\right\|^p + 2^{p-1}a^{p(1-\mu)} \\
&\quad \times E\left\|\int_0^t R_{\mu,\nu,\xi,e,k}(t-\varsigma)\mathcal{M}\left(\varsigma, x_\varsigma, \int_0^\varsigma g(\varsigma,\tau,x_\tau)\,\mathrm{d}\tau\right)\mathrm{d}W(\varsigma)\right\|^p \\
&\le 2^{p-1}a^{p(1-\mu)}K^pE\left[\int_0^t (t-\varsigma)^{\mu-1}\|B(\varsigma)u(\varsigma)\|\,\mathrm{d}\varsigma\right]^p + 2^{p-1}a^{p(1-\mu)}C_p \\
&\quad \times \left[\int_0^t (t-\varsigma)^{2(\mu-1)}m_{\mathcal{M}}^{\frac{2}{p}}(\varsigma)\Theta_{\mathcal{M}}^{\frac{2}{p}}\left(\|x_\varsigma\|_{\mathcal{B}_h}^p + E\left\|\int_0^\varsigma g(\varsigma,\tau,x_\tau)\,\mathrm{d}\tau\right\|^p\right)\mathrm{d}\varsigma\right]^{\frac{p}{2}} \\
&\le 2^{p-1}a^{p(1-\mu)}K^p\|B\|_\infty^p\left(\frac{p-1}{p\mu-1}\right)^{p-1}t_1^{p\mu-1}\|u\|_{L_{\mathcal{F}}^p}^p \\
&\quad + 2^{p-1}a^{p(1-\mu)}C_pK^p\left(\frac{p-2}{-p-2+2p\mu}\right)^{\frac{p-2}{2}}t_1^{\frac{-p-2+2p\mu}{2}} \\
&\quad \times \int_0^t m_{\mathcal{M}}(\varsigma)\Theta_{\mathcal{M}}\left(\|x_\varsigma\|_{\mathcal{B}_h}^p + t_1^{p-1}m_g\int_0^\varsigma \Theta_g\left(\|x_\tau\|_{\mathcal{B}_h}^p\right)\mathrm{d}\tau\right)\mathrm{d}\varsigma. \qquad (4)
\end{aligned}$$

Next, for each $t \in (t_i, \varsigma_i]$ with $i = 1, 2, \ldots, q$, it holds that

$$\begin{aligned}
\mathbb{E}\|(t-\varsigma_{i-1})^{1-\mu}x(t)\|^p &\le a^{p(1-\mu)}\mathbb{E}\|h_i(t,x_t)\|^p \\
&\le a^{p(1-\mu)}L_{h_i}\left(1+\|x_t\|_{\mathcal{B}_h}^p\right). \qquad (5)
\end{aligned}$$

(Note: For the impulsive interval $t \in (t_i, \varsigma_i]$, the weight function subscript is ς_{i-1}, whereas for the post-impulsive interval $t \in (\varsigma_i, t_{i+1}]$, the subscript is ς_i; see the definition of $\|\cdot\|_b$.)

In a similar fashion, for any $t \in (\varsigma_i, t_{i+1}]$ $(i = 1, 2, \ldots, q)$, we derive that

$$\begin{aligned}
&\mathbb{E}\left\|(t-\varsigma_i)^{1-\mu}\nu(t)\right\|^p \\
&\le 3^{p-1}\mathbb{E}\left\|(t-\varsigma_i)^{1-\mu}R_{\mu,\nu,\xi,e,k}(t-\varsigma_i)h_i(\varsigma_i,x_{\varsigma_i})\right\|^p + 3^{p-1}a^{p(1-\mu)}\mathbb{E}\left\|\int_{\varsigma_i}^t R_{\mu,\nu,\xi,e,k}(t-\varsigma)B(\varsigma)u(\varsigma)\,d\varsigma\right\|^p \\
&\quad + 3^{p-1}a^{p(1-\mu)}\mathbb{E}\left\|\int_{\varsigma_i}^t R_{\mu,\nu,\xi,e,k}(t-\varsigma)\mathcal{M}\left(\varsigma, x_\varsigma, \int_0^\varsigma g(\varsigma,\tau,x_\tau)\,d\tau\right)dW(\varsigma)\right\|^p \\
&\le 3^{p-1}K^pL_{h_i}\left(1+\|x_{\varsigma_i}\|_{\mathcal{B}_h}^p\right) + 3^{p-1}a^{p(1-\mu)}K^p\mathbb{E}\left[\int_{\varsigma_i}^t (t-\varsigma)^{\mu-1}\|B(\varsigma)u(\varsigma)\|\,d\varsigma\right]^p \\
&\quad + 3^{p-1}a^{p(1-\mu)}C_pK^p\left[\int_{\varsigma_i}^t (t-\varsigma)^{2(\mu-1)}m_{\mathcal{M}}^{\frac{2}{p}}(\varsigma)\Theta_{\mathcal{M}}^{\frac{2}{p}}\left(\|x_\varsigma\|_{\mathcal{B}_h}^p + \mathbb{E}\left\|\int_0^\varsigma g(\varsigma,\tau,x_\tau)\,d\tau\right\|^p\right)d\varsigma\right]^{\frac{p}{2}} \\
&\le 3^{p-1}K^pL_{h_i}\left(1+\|x_{\varsigma_i}\|_{\mathcal{B}_h}^p\right) + 3^{p-1}a^{p(1-\mu)}K^p\|B\|_\infty^p\left(\frac{p-1}{p\mu-1}\right)^{p-1}(t_{i+1}-\varsigma_i)^{p\mu-1}\|u\|_{L_{\mathcal{F}}^p}^p \\
&\quad + 3^{p-1}a^{p(1-\mu)}C_pK^p\left(\frac{p-2}{-p-2+2p\mu}\right)^{\frac{p-2}{2}}(t_{i+1}-\varsigma_i)^{\frac{-p-2+2p\mu}{2}} \\
&\quad \times \int_{\varsigma_i}^t m_{\mathcal{M}}(\varsigma)\Theta_{\mathcal{M}}\left(\|x_\varsigma\|_{\mathcal{B}_h}^p + t_{i+1}^{p-1}m_g\int_0^\varsigma \Theta_g(\|x_\tau\|_{\mathcal{B}_h}^p)\,d\tau\right)d\varsigma. \qquad (6)
\end{aligned}$$

Combining inequalities (4)–(6), for all $t \in [0, a]$, it holds that

$$\begin{aligned}
E\|(t-\varsigma_i)^{1-\mu}x(t)\|^p &\le M^* + a^{p(1-\mu)}\max_{i=1,\ldots,q}L_{h_i}\|x_t\|_{\mathcal{B}_h}^p + 3^{p-1}\max_{i=1,\ldots,q}L_{h_i}\|x_{\varsigma_i}\|_{\mathcal{B}_h}^pK^p \\
&\quad + 3^{p-1}C_pK^pa^{\frac{p-2}{2}}\left(\frac{p-2}{-p-2+2p\mu}\right)^{\frac{p-2}{2}}\int_0^t m_{\mathcal{M}}(\varsigma)\Theta_{\mathcal{M}}\left(\|x_\varsigma\|_{\mathcal{B}_h}^p + a^{p-1}m_g\int_0^\varsigma \Theta_g(\|x_\tau\|_{\mathcal{B}_h}^p)\,d\tau\right)d\varsigma,
\end{aligned}$$

https://doi.org/10.3390/fractalfract10070490

where

$$M^* = \max_{i=1,2,\ldots,q}\left\{3^{p-1}K^p L_{h_i} + a^{p(1-\mu)}L_{h_i} + 3^{p-1}a^{p(1-\mu)}K^p\|B\|_\infty^p\left(\frac{p-1}{p\mu-1}\right)^{p-1}(t_{i+1}-\varsigma_i)^{p\mu-1}\|u\|_{L_{\mathcal{F}}^p}^p\right\}.$$

Consequently, in view of Lemma 4, for each $t \in [0,a]$, it follows that

$$\begin{aligned}\|x_t\|_{\mathcal{B}_h}^p &\le 2^{p-1}\|\varphi\|_{\mathcal{B}_h}^p + 2^{p-1}l^p \sup_{t\in[0,a]}\left\{E\|(t-\varsigma_i)^{1-\mu}x(t)\|^p\right\}\\ &\le 2^{p-1}\|\varphi\|_{\mathcal{B}_h}^p + 2^{p-1}l^p\Bigg\{M^* + a^{p(1-\mu)}\max_{i=1,\ldots,q}L_{h_i}\|x_t\|_{\mathcal{B}_h}^p + 3^{p-1}\max_{i=1,\ldots,q}L_{h_i}\|x_{t_i}\|_{\mathcal{B}_h}^p K^p + 3^{p-1}C_pK^p\\ &\quad\times\left(\frac{p-2}{-p-2+2p\mu}\right)^{\frac{p-2}{2}}a^{\frac{p-2}{2}}\int_0^t m_{\mathcal{M}}(\varsigma)\Theta_{\mathcal{M}}\left(\|x_\varsigma\|_{\mathcal{B}_h}^p + a^{p-1}m_g\int_0^\varsigma\Theta_g(\|x_\tau\|_{\mathcal{B}_h}^p)\,d\tau\right)d\varsigma\Bigg\}.\end{aligned}$$

Define the non-decreasing function $\sigma(t) := \sup_{0\le\tau\le t}\|x_\tau\|_{\mathcal{B}_h}^p$ for $t \in [0,a]$. Then we obtain

$$\begin{aligned}\sigma(t) &\le 2^{p-1}\left(\|\varphi\|_{\mathcal{B}_h}^p + l^pM^*\right) + 2^{p-1}l^p\Bigg\{a^{p(1-\mu)}\max_{i=1,\ldots,q}L_{h_i} + 3^{p-1}\max_{i=1,\ldots,q}L_{h_i}K^p\}\sigma(t) + 6^{p-1}C_pK^p\\ &\quad\times\left(\frac{p-2}{-p-2+2p\mu}\right)^{\frac{p-2}{2}}a^{\frac{p-2}{2}}\int_0^t m_{\mathcal{M}}(s)\Theta_{\mathcal{M}}\left(\sigma(s) + a^{p-1}m_g\int_0^s\Theta_g(\sigma(\tau))\,d\tau\right)ds.\end{aligned}$$

Since $L < 1$, we have

$$\sigma(t) \le \frac{1}{1-L}2^{p-1}\left(\|\varphi\|_{\mathcal{B}_h}^p + l^pM^*\right) + d^*\int_0^t m_{\mathcal{M}}(s)\Theta_{\mathcal{M}}\left(\sigma(s) + a^{p-1}m_g\int_0^s\Theta_g(\sigma(\tau))\,d\tau\right)ds.$$

Let $\kappa(t)$ denote the right-hand side of the aforementioned inequality. Then $\kappa(0) = \frac{2^{p-1}}{1-L}\left(\|\varphi\|_{\mathcal{B}_h}^p + l^pM^*\right)$ and $\sigma(t) \le \kappa(t)$ for all $t \in [0,a]$. Furthermore,

$$\begin{aligned}\kappa'(t) &\le d^*m_{\mathcal{M}}(t)\Theta_{\mathcal{M}}\left(\sigma(t) + a^{p-1}m_g\int_0^t\Theta_g(\sigma(s))\,ds\right)\\ &\le d^*m_{\mathcal{M}}(t)\Theta_{\mathcal{M}}\left(\kappa(t) + a^{p-1}m_g\int_0^t\Theta_g(\kappa(\varsigma))\,d\varsigma\right).\end{aligned}$$

Define the auxiliary function $\gamma(t) = \kappa(t) + a^{p-1}m_g\int_0^t\Theta_g(\kappa(\varsigma))\,d\varsigma$. Then $\gamma(0) = \kappa(0)$ and $\kappa(t) \le \gamma(t)$ for all $t \in [0,a]$. Moreover,

$$\begin{aligned}\gamma'(t) &= \kappa'(t) + a^{p-1}m_g\Theta_g(\kappa(t))\\ &\le d^*m_{\mathcal{M}}(t)\Theta_{\mathcal{M}}(\gamma(t)) + a^{p-1}m_g\Theta_g(\gamma(t))\\ &\le \bar{\gamma}(t)\left[\Theta_{\mathcal{M}}(\gamma(t)) + \Theta_g(\gamma(t))\right].\end{aligned}$$

It then follows that

$$\int_{\gamma(0)}^{\gamma(t)}\frac{d\varsigma}{\Theta_{\mathcal{M}}(\varsigma)+\Theta_g(\varsigma)} \le \int_0^a\bar{\gamma}(t)\,dt < \infty.$$

Combined with the divergence condition $\int_1^\infty\frac{d\varsigma}{\Theta_{\mathcal{M}}(\varsigma)+\Theta_g(\varsigma)} = \infty$ in Assumption (3), $\gamma(t)$ cannot blow up on the finite interval $[0,a]$; otherwise, the left-hand integral would diverge to infinity, contradicting the boundedness of the right-hand side. Hence there exists a constant $\tilde{K} > 0$ such that $\gamma(t) \le \tilde{K}$ uniformly for all $t \in [0,a]$. Consequently, we conclude that $\|x_t\|_{\mathcal{B}_h}^p \le \sigma(t) \le \kappa(t) \le \gamma(t) \le \tilde{K}$. □

https://doi.org/10.3390/fractalfract10070490

Theorem 2. *Suppose that Assumptions (1)–(4) hold true. Then, system (1) possesses at least one mild solution over* $[0, a]$ *for any admissible control* $u \in U_{\text{ad}}$.

Proof. We first define the set

$$G = \Big\{ \nu \in \mathcal{B}_b^0 : \nu = \omega \bar{Q}_1\Big(\frac{\nu}{\omega}\Big) + \omega \bar{Q}_2(\nu), \text{ for some } \omega \in (0,1) \Big\}.$$

We now verify the boundedness of the set G in the norm of $\mathcal{B}_b^0$. For any $\nu \in G$, by definition there exists $\omega \in (0,1)$ such that $\nu = \omega \bar{Q}_1(\nu/\omega) + \omega \bar{Q}_2(\nu)$.

By the triangle inequality and the properties of $\bar{Q}_1$ (contraction, Lemma 5) and $\bar{Q}_2$ (uniformly bounded on bounded sets, Lemma 6), we obtain

$$\|\nu\|_b^p \le 2^{p-1}\omega^p \Big(L \Big\| \frac{\nu}{\omega} \Big\|_b^p + \big\| \bar{Q}_1(0) \big\|_b^p \Big) + 2^{p-1}\omega^p \mathcal{Z}.$$

Combining this with the a priori bound $\|x_t\|_{\mathcal{B}_h}^p \le \tilde{K}$ from Lemma 7, we further derive that

$$\begin{aligned} \|\nu\|_b^p &= \max_{i=0,1,\ldots,q} \sup_{t \in (\varsigma_i, \varsigma_{i+1}]} \Big(E \Big\| (t-\varsigma_i)^{1-\mu} \nu(t) \Big\|^p \Big) \\ &\le 2^{p-1} l^{-p} a^{p(1-\mu)} \tilde{K} + 2^{p-1} K^p \|\varphi(0)\|^p. \end{aligned}$$

Since the right-hand side is a constant independent of ν and ω, the set G is uniformly bounded in $\mathcal{B}_b^0$. Note that the a priori estimate established in Lemma 7 precisely guarantees the boundedness of the set G, thereby verifying the hypothesis of Theorem 1. According to Theorem 1, the operator $\bar{Q}$ admits at least one fixed point $\nu^* \in \mathcal{B}_b^0$. Set $x(t) = \nu^*(t) + \tilde{\varphi}(t)$ for all $t \in (-\infty, a]$. It is easy to verify that x is a fixed point of operator Q, which demonstrates that x is a mild solution to system (1). □

Remark 7. *It should be noted that Assumptions (1)–(4) are only sufficient to guarantee the existence of mild solutions for system 1. Under the current continuity and growth conditions on the nonlinear mappings* $\mathcal{M}$ *and* g*, the uniqueness of mild solutions is not ensured in general. To derive a uniqueness result, additional Lipschitz-type restrictions on the nonlinear terms would be required, which lies outside the scope of the present paper.*

4. Existence of Stochastic Optimal Controls

This section investigates the optimal control problem for the proposed three-parameter damped fractional stochastic system. By virtue of the compactness of resolvent operators, Mazur lemma and lower semicontinuity theory, we establish the existence result of optimal control pairs, and extend the optimal control theory to the Riemann–Liouville fractional stochastic impulsive integro-differential system with infinite delay, time-varying control operator and three-parameter damping.

Consider the Bolza problem (P): find an optimal control pair $(x^0, u^0) \in \mathcal{B}_b \times U_{ad}$, for all $u \in U_{ad}$ such that

$$J(x^0, u^0) \le J(x^u, u),$$

where x^u denotes the mild solution of system (1) corresponding to the admissible control u, and the cost functional $J : \mathcal{B}_b \times U_{ad} \to \mathbb{R}$ is defined by

$$J(x^u, u) = E \int_0^a P(t, x_t^u, x^u(t), u(t))dt + E\psi(x^u(a)).$$

To derive the existence of optimal controls, the following assumptions compatible with the framework of three-parameter damped systems are imposed on the running cost functional P and the terminal cost functional ψ:

https://doi.org/10.3390/fractalfract10070490

Assumption 5. *The functional $P : [0,a] \times \mathcal{B}_\hbar \times \mathcal{H} \times Y \to \mathbb{R} \cup \{\infty\}$ satisfies:*

1. *P is Borel measurable;*
2. *$P(t, z_1, x, \cdot)$ is convex on Y for any $z_1 \in \mathcal{B}_\hbar$, $x \in \mathcal{H}$ and almost all $t \in [0,a]$;*
3. *$P(t, \cdot, \cdot, \cdot)$ is sequentially lower semicontinuous on $\mathcal{B}_\hbar \times \mathcal{H} \times Y$ for almost all $t \in [0,a]$;*
4. *There exist constants $r_1, r_2 \geq 0$, $r_3 > 0$ and a non-negative function $\mathscr{C} \in L^1([0,a];\mathbb{R})$ such that*

$$P(t, z_1, x, u) \geq \mathscr{C}(t) + r_1\|z_1\|_{\mathcal{B}_\hbar} + r_2\|x\|_{\mathcal{H}} + r_3\|u\|_Y^p.$$

Assumption 6. *The functional $\psi : \mathcal{H} \to \mathbb{R}$ is non-negative and continuous.*

Next, we prove the complete continuity of the linear control operator, which is the key to establishing the existence of optimal controls. This operator is constructed based on the three-parameter (μ, ν, ξ, e, k)-resolvent family $R_{\mu,\nu,\xi,e,k}(\cdot)$ tailored for the damped system.

Remark 8. *Assumptions (5) and (6) cover the standard conditions guaranteeing the existence of optimal controls via the direct method in the calculus of variations:*

1. Condition (5)-2 ensures the running cost $P(t, \cdot, \cdot, \cdot)$ is convex with respect to the control variable u.

2. Condition (5)-3 states the sequential lower semicontinuity of P on $B_\hbar \times H \times Y$, which forms the basis for the weak lower semicontinuity of the integral cost functional.

3. The growth condition in (5)-4 provides a coercive lower bound of the cost with respect to the control norm, which guarantees that every minimizing sequence of controls is bounded in $L^p_{\mathcal{F}}([0,a];Y)$.

Lemma 8. *Define the operator $\mathcal{L} : L^p_{\mathcal{F}}([0,a];Y) \to \mathcal{B}_b$ by*

$$(\mathcal{L}u)(t) = \begin{cases} \displaystyle\int_0^t R_{\mu,\nu,\xi,e,k}(t-\varsigma)B(\varsigma)u(\varsigma)d\varsigma, & t \in (0, t_1], \\ 0, & t \in (t_i, \varsigma_i], i = 1, 2, \ldots, q, \\ \displaystyle\int_{\varsigma_i}^t R_{\mu,\nu,\xi,e,k}(t-\varsigma)B(\varsigma)u(\varsigma)d\varsigma, & t \in (\varsigma_i, t_{i+1}], i = 1, 2, \ldots, q, \end{cases}$$

Thus, the operator $\mathcal{L}$ is completely continuous.

Proof. Let $\{u^n\}$ be a bounded sequence in $L^p_{\mathcal{F}}([0,a];Y)$, and denote $\Theta_n(t) = (\mathcal{L}u^n)(t)$ for $t \in [0,a]$. By Assumption (1), the weighted resolvent operator $t^{1-\mu}R_{\mu,\nu,\xi,e,k}(t)$ is uniformly bounded and compact, so $E\|\Theta_n(t)\|^p$ is uniformly bounded for any fixed $t \in [0,a]$.

The operator $\mathcal{L}$ is linear and continuous. Referring to the proof steps of the complete continuity of $\bar{Q}_2$ in Lemma 6, it can be verified that $\mathcal{L}$ maps bounded sets into equicontinuous and precompact sets in $\mathcal{B}_b$. By the Arzelá-Ascoli theorem, $\mathcal{L}$ is a completely continuous operator. □

Theorem 3. *If Assumptions (1)–(6) hold, then the Bolza problem (P) admits at least one optimal control pair $(x^0, u^0) \in \mathcal{B}_b \times U_{ad}$.*

Proof. Without loss of generality, we set $\inf\{J(x^u, u) \mid u \in U_{\text{ad}}\} = \epsilon < \infty$. In view of Assumptions (5) and (6), we derive

$$\begin{aligned} J(x^u, u) \geq E\int_0^a \mathscr{C}(t)dt + r_1\int_0^a E\|x_t^u\|_{\mathcal{B}_\hbar}dt + r_2E\int_0^a \|x^u(t)\|_{\mathcal{H}}dt \\ + r_3E\int_0^a \|u(t)\|_Y^p dt + E\psi(x^u(a)) \geq -\rho > -\infty, \end{aligned}$$

https://doi.org/10.3390/fractalfract10070490

where $\rho > 0$ is a positive constant, which implies $\epsilon > -\infty$. According to the definition of infimum, there exists a minimizing sequence $\{(x^n, u^n)\} \subset A_{\text{ad}}$ such that $J(x^n, u^n) \to \epsilon$ as $n \to \infty$, where

$$A_{ad} = \{(x, u) \mid x \text{ is the mild solution of system (1) corresponding to } u \in U_{ad}\}.$$

Since $p > 1$ and $L^p_{\mathcal{F}}([0, a]; Y)$ is reflexive, the bounded sequence $\{u^n\} \subseteq U_{\text{ad}}$ is weakly sequentially compact by the Eberlein–Šmulian theorem. Hence, we can choose a subsequence, still denoted by $\{u^n\}$, such that u^n converges weakly to some $u^0 \in L^p_{\mathcal{F}}([0, a]; Y)$ as $n \to \infty$. Furthermore, since U_{ad} is a closed and convex subset, by Mazur's lemma it is weakly closed, which guarantees that the weak limit u^0 belongs to U_{ad}.

Let x^n denote the mild solution of system (1) corresponding to u^n, which satisfies

$$x^n(t) = \begin{cases} \varphi(t), & t \in (-\infty, 0], \\ R_{\mu,\nu,\xi,e,k}(t)\varphi(0) + \int_0^t R_{\mu,\nu,\xi,e,k}(t-\varsigma)B(\varsigma)u^n(\varsigma)d\varsigma \\ \quad + \int_0^t R_{\mu,\nu,\xi,e,k}(t-\varsigma)\mathcal{M}\Big(\varsigma, x^n_\varsigma, \int_0^\varsigma g(\varsigma,\tau,x^n_\tau)d\tau\Big)dW(\varsigma), & t \in (0, t_1], \\ h_i(t, x^n_t), & t \in (t_i, \varsigma_i], i = 1, \ldots, q, \\ R_{\mu,\nu,\xi,e,k}(t-\varsigma_i)h_i(\varsigma_i, x^n_{\varsigma_i}) + \int_{\varsigma_i}^t R_{\mu,\nu,\xi,e,k}(t-\varsigma)B(\varsigma)u^n(\varsigma)d\varsigma \\ \quad + \int_{\varsigma_i}^t R_{\mu,\nu,\xi,e,k}(t-\varsigma)\mathcal{M}\Big(\varsigma, x^n_\varsigma, \int_0^\varsigma g(\varsigma,\tau,x^n_\tau)d\tau\Big)dW(\varsigma), & t \in (\varsigma_i, t_{i+1}], i = 1, \ldots, q. \end{cases}$$

Denote $\mathcal{M}_n(\varsigma) = \mathcal{M}\Big(\varsigma, x^n_\varsigma, \int_0^\varsigma g(\varsigma,\tau,x^n_\tau)d\tau\Big)$. By (3), $\{\mathcal{M}_n(\cdot)\}$ is bounded in $L^p([0, a]; \mathcal{L}^0_2)$, so there exist a subsequence and $\widehat{\mathcal{M}}(\cdot) \in L^p([0, a]; \mathcal{L}^0_2)$ such that $\mathcal{M}_n(\cdot)$ converges weakly to $\widehat{\mathcal{M}}(\cdot)$ in $L^p([0, a]; \mathcal{L}^0_2)$. By Lemma 8, $\mathcal{L}\mathcal{M}_n$ converges to $\mathcal{L}\widehat{\mathcal{M}}$ in $\mathcal{B}_b$ as $n \to \infty$.

Consider the controlled system with the weak limit control u^0 and the perturbation term $\widehat{M}$:

$$\begin{cases} D^\mu_t x(t) + eD^\nu_t x(t) + kD^\xi_t x(t) = Ax(t) + B(t)u^0(t) + \widehat{\mathcal{M}}(t)dW(t), & t \in (\varsigma_i, t_{i+1}], \\ x(t) = h_i(t, x_t), & t \in (t_i, \varsigma_i], \\ \lim\limits_{t\to 0^+} I^{1-\mu}_t x(t) = \varphi(0) \in \mathcal{B}_\hbar, \quad I^{1-\mu}_t x(t)\Big|_{t=\varsigma_i} = h_i(\varsigma_i, x_{\varsigma_i}). \end{cases} \tag{7}$$

Note that for system (7), the stochastic coefficient $\widehat{\mathcal{M}}(t)$ is independent of ψ and y, so $\Theta_{\mathcal{M}}$ reduces to a constant function and the growth condition in (3) is automatically satisfied. Therefore, all Assumptions (1)–(4) hold for system (7).

By virtue of Theorem 2, we readily deduce that the system (7) admits a mild solution, which satisfies the following piecewise integral equation:

$$\hat{x}(t) = \begin{cases} \varphi(t), t \in (-\infty, 0], \\ R_{\mu,\nu,\xi,e,k}(t)\varphi(0) + \int_0^t R_{\mu,\nu,\xi,e,k}(t-\varsigma)B(\varsigma)u^0(\varsigma)\,d\varsigma + \int_0^t R_{\mu,\nu,\xi,e,k}(t-\varsigma)\widehat{\mathcal{M}}(\varsigma)\,dW(\varsigma), t \in (0, t_1], \\ h_i(t, \hat{x}_t), t \in (t_i, \varsigma_i],\ i = 1, 2, \ldots, q, \\ R_{\mu,\nu,\xi,e,k}(t-\varsigma_i)h_i(\varsigma_i, \hat{x}_{\varsigma_i}) + \int_{\varsigma_i}^t R_{\mu,\nu,\xi,e,k}(t-\varsigma)B(\varsigma)u^0(\varsigma)\,d\varsigma \\ + \int_{\varsigma_i}^t R_{\mu,\nu,\xi,e,k}(t-\varsigma)\widehat{\mathcal{M}}(\varsigma)\,dW(\varsigma), t \in (\varsigma_i, t_{i+1}],\ i = 1, 2, \ldots, q. \end{cases}$$

Let $x^n(t) = \nu^n(t) + \tilde{\varphi}(t)$ and $\hat{x}(t) = \hat{v}(t) + \tilde{\varphi}(t)$, where $\nu^n, \hat{v} \in \mathcal{B}^0_b$ and $\tilde{\varphi} : (-\infty, a] \to \mathcal{H}$ is a given function. For $t \in (0, t_1]$, we have

https://doi.org/10.3390/fractalfract10070490

$$
\begin{aligned}
E\left\|t^{1-\mu}(\nu^n(t)-\hat{v}(t))\right\|^p &\le 2^{p-1}a^{p(1-\mu)}E\left\|\int_0^t R_{\mu,\nu,\xi,e,k}(t-\varsigma)B(\varsigma)\left[u^n(\varsigma)-u^0(\varsigma)\right]d\varsigma\right\|^p \\
&\quad + 2^{p-1}a^{p(1-\mu)}E\left\|\int_0^t R_{\mu,\nu,\xi,e,k}(t-\varsigma)\left[\mathcal{M}_n(\varsigma)-\widehat{\mathcal{M}}(\varsigma)\right]dW(\varsigma)\right\|^p \\
&\le 2^{p-1}a^{p(1-\mu)}K^p\left[\int_0^t(t-\varsigma)^{\mu-1}\|B(\varsigma)\|\left\|u^n(\varsigma)-u^0(\varsigma)\right\|d\varsigma\right]^p \\
&\quad + 2^{p-1}a^{p(1-\mu)}C_pK^p\left[\int_0^t(t-\varsigma)^{\mu-1}E\left\|\mathcal{M}_n(\varsigma)-\widehat{\mathcal{M}}(\varsigma)\right\|_{L_2^0}^p d\varsigma\right]^{\frac{2}{p}} \\
&\le 2^{p-1}a^{p(1-\mu)}K^p\|B\|_\infty^p\left(\frac{p-1}{p\mu-1}\right)^{p-1}t_1^{p\mu-1}\int_0^t E\left\|u^n(\varsigma)-u^0(\varsigma)\right\|^p d\varsigma \\
&\quad + 2^{p-1}a^{p(1-\mu)}K^pC_p\left(\frac{p-2}{2p\mu-p-2}\right)^{\frac{p-2}{2}}t_1^{\frac{2p\mu-p-2}{2}}\int_0^t E\left\|\mathcal{M}_n(\varsigma)-\widehat{\mathcal{M}}(\varsigma)\right\|_{L_2^0}^p d\varsigma.
\end{aligned}
$$

For any $t\in(t_i,\varsigma_i]$, $i=1,2,\ldots,q$, we derive

$$
\begin{aligned}
E\left\|(t-\varsigma_{i-1})^{1-\mu}[\nu^n(t)-\hat{v}(t)]\right\|^p &\le a^{p(1-\mu)}E\|h_i(t,\nu_t^n+\tilde{\varphi}_t)-h_i(t,\hat{v}_t+\tilde{\varphi}_t)\|^p \\
&\le a^{p(1-\mu)}L_{h_i}^p\|\nu_t^n-\hat{v}_t\|_{\mathcal{B}_h}^p \\
&\le 2^{p-1}a^{p(1-\mu)}L_{h_i}^p l^p\|\nu^n-\hat{v}\|_b^p.
\end{aligned}
$$

Similarly, for any $t\in(\varsigma_i,t_{i+1}]$, $i=1,2,\ldots,q$, we decompose the error into three parts:

$$
E\left\|(t-\varsigma_i)^{1-\mu}[\nu^n(t)-\hat{v}(t)]\right\|^p \le 3^{p-1}\left[\mathscr{C}_n^{(1)}(t)+\mathscr{C}_n^{(2)}(t)+\mathscr{C}_n^{(3)}(t)\right],
$$

where

$$
\begin{aligned}
\mathscr{C}_n^{(1)}(t) &= E\left\|(t-\varsigma_i)^{1-\mu}R_{\mu,\nu,\xi,e,k}(t-\varsigma_i)\left[h_i\left(\varsigma_i,\nu_{\varsigma_i}^n+\tilde{\varphi}_{\varsigma_i}\right)-h_i(\varsigma_i,\hat{v}_{\varsigma_i}+\tilde{\varphi}_{\varsigma_i})\right]\right\|^p \\
&\le 2^{p-1}K^pL_{h_i}^p l^p\|\nu^n-\hat{v}\|_b^p, \\
\mathscr{C}_n^{(2)}(t) &= E\left\|(t-\varsigma_i)^{1-\mu}\int_{\varsigma_i}^t R_{\mu,\nu,\xi,e,k}(t-\varsigma)B(\varsigma)\left[u^n(\varsigma)-u^0(\varsigma)\right]d\varsigma\right\|^p \\
&\le a^{p(1-\mu)}K^p\|B\|_\infty^p E\left[\int_{\varsigma_i}^t(t-\varsigma)^{\mu-1}\left\|u^n(\varsigma)-u^0(\varsigma)\right\|d\varsigma\right]^p \\
&\le a^{p(1-\mu)}K^p\|B\|_\infty^p\left(\frac{p-1}{p\mu-1}\right)^{p-1}(t_{i+1}-\varsigma_i)^{p\mu-1}\int_{\varsigma_i}^t E\left\|u^n(\varsigma)-u^0(\varsigma)\right\|^p d\varsigma,
\end{aligned}
$$

$$
\begin{aligned}
\mathscr{C}_n^{(3)}(t) &= E\left\|(t-\varsigma_i)^{1-\mu}\int_{\varsigma_i}^t R_{\mu,\nu,\xi,e,k}(t-\varsigma)\left[\mathcal{M}_n(\varsigma)-\widehat{\mathcal{M}}(\varsigma)\right]dW(\varsigma)\right\|^p \\
&\le a^{p(1-\mu)}K^pC_p\left[\int_{\varsigma_i}^t(t-\varsigma)^{p(\mu-1)}E\left\|\mathcal{M}_n(\varsigma)-\widehat{\mathcal{M}}(\varsigma)\right\|_{L_2^0}^p \mathrm{d}\varsigma\right]^{\frac{p}{2}} \\
&\le a^{p(1-\mu)}K^pC_p\left(\frac{p-2}{-p-2+2p\mu}\right)^{\frac{p-2}{2}}(t_{i+1}-\varsigma_i)^{\frac{-p-2+2p\mu}{2}}\int_{\varsigma_i}^t E\left\|\mathcal{M}_n(\varsigma)-\widehat{\mathcal{M}}(\varsigma)\right\|_{L_2^0}^p \mathrm{d}\varsigma.
\end{aligned}
$$

Accordingly, for all $t\in[0,a]$, it holds that

$$
\|\nu^n-\hat{v}\|_b^p \le L\|\nu^n-\hat{v}\|_b^p+\xi_n^1(t)+\xi_n^2(t),
$$

https://doi.org/10.3390/fractalfract10070490

where

$$\xi_n^1(t) = 3^{p-1}a^{p-1}K^p\|B\|_\infty^p\left(\frac{p-1}{p\mu-1}\right)^{p-1}\int_0^t E\left\|u^n(\varsigma)-u^0(\varsigma)\right\|^p \mathrm{d}\varsigma,$$

$$\xi_n^2(t) = 3^{p-1}a^{\frac{p-2}{2}}K^pC_p\left(\frac{p-2}{-p-2+2p\mu}\right)^{\frac{p-2}{2}}\int_{\varsigma_i}^t E\left\|\mathcal{M}_n(\varsigma)-\widehat{\mathcal{M}}(\varsigma)\right\|^p \mathrm{d}\varsigma.$$

This immediately yields

$$\|v^n-\hat{v}\|_b^p \le \frac{\xi_n^1(t)+\xi_n^2(t)}{1-L}.$$

Combining Lebesgue's dominated convergence theorem with Lemma 8, we deduce that

$$\int_0^t E\left\|u^n(\varsigma)-u^0(\varsigma)\right\|^p \mathrm{d}\varsigma \to 0 \quad \text{as } n\to\infty,$$

$$\int_0^t E\left\|\mathcal{M}_n(\varsigma)-\widehat{\mathcal{M}}(\varsigma)\right\|_{L_2^0}^p \mathrm{d}\varsigma \to 0 \quad \text{as } n\to\infty.$$

Hence, $\xi_n^1(t), \xi_n^2(t) \to 0$ as $n\to\infty$, which implies that $v^n \to \hat{v}$ in $\mathcal{B}_b^0$ and equivalently $x^n \to \hat{x}$ in $\mathcal{B}_b$ as $n\to\infty$.

In light of Assumption (3), it follows that

$$\mathcal{M}_n(\cdot) \to \mathcal{M}\left(\cdot, x_\cdot, \int_0^\cdot g(\cdot,\tau,x_\tau)\mathrm{d}\tau\right) \quad \text{in } \mathcal{B}_b^0 \text{ as } n\to\infty.$$

Utilizing the uniqueness of limits in $\mathcal{B}_b^0$, we obtain $\widehat{\mathcal{M}}(t) = \mathcal{M}\left(t, \hat{x}_t, \int_0^t g(t,\varsigma,\hat{x}_\varsigma)\mathrm{d}\tau\right)$. Consequently, the limit function $\hat{x}$ fulfills the mild solution formulation of fractional-order system (1), that is

$$\hat{x}(t) = \begin{cases} \varphi(t), & t\in(-\infty,0], \\ R_{\mu,\nu,\xi,e,k}(t)\varphi(0) + \displaystyle\int_0^t R_{\mu,\nu,\xi,e,k}(t-\varsigma)B(\varsigma)u^0(\varsigma)\mathrm{d}\varsigma & \\ \quad + \displaystyle\int_0^t R_{\mu,\nu,\xi,e,k}(t-\varsigma)\mathcal{M}\left(t,\hat{x}_t,\int_0^\varsigma g(\varsigma,\tau,\hat{x}_\tau)\mathrm{d}\tau\right)\mathrm{d}W(\varsigma), & t\in(0,t_1], \\ h_i(t,\hat{x}_t), & t\in(t_i,\varsigma_i], i=1,2,\ldots,q, \\ R_{\mu,\nu,\xi,e,k}(t-\varsigma_i)h_i(\varsigma_i,\hat{x}_{\varsigma_i}) + \displaystyle\int_{\varsigma_i}^t R_{\mu,\nu,\xi,e,k}(t-\varsigma)B(\varsigma)u^0(\varsigma)\mathrm{d}\varsigma & \\ \quad + \displaystyle\int_{\varsigma_i}^t R_{\mu,\nu,\xi,e,k}(t-\varsigma)\mathcal{M}\left(t,\hat{x}_t,\int_0^\varsigma g(\varsigma,\tau,\hat{x}_\tau)\mathrm{d}\tau\right)\mathrm{d}W(\varsigma), & t\in(\varsigma_i,t_{i+1}], i=1,2,\ldots,q, \end{cases}$$

which constitutes a mild solution to the Riemann–Liouville fractional-order system (1) associated with the optimal control u^0.

In light of Assumption (5), we verify all hypotheses of Balder's theorem [28] step by step:

(1) The admissible control set U_{ad} is nonempty, convex, closed and bounded in $L_{\mathcal{F}}^p([0,a];Y)$;
(2) The solution operator corresponding to system (1) is weakly continuous and sequentially relatively compact in B_b;
(3) The cost functional $J(x,u)$ is sequentially weakly lower semicontinuous on $B_b\times U_{ad}$ and bounded from below.

According to Balder's theorem [28], the integral functional

$$(x_t, x(t), u(t)) \mapsto \int_0^a P(t,x_t,x(t),u(t))dt$$

https://doi.org/10.3390/fractalfract10070490

is sequentially weakly lower semicontinuous on B_b. Since the cost functional J is weakly lower semicontinuous and bounded from below, it attains its infimum at $(\hat{x}, u^0) \in B_b \times U_{ad}$. That is,

$$\begin{aligned}\epsilon &= \lim_{n\to\infty} E\int_0^a P(t, x_t^n, x^n(t), u^n(t))\mathrm{d}t + \lim_{n\to\infty} E\psi(x^n(t))\\ &\geq E\int_0^a P\Big(t, \hat{x}_t, \hat{x}(t), u^0(t)\Big)\mathrm{d}t + E\psi(\hat{x}(a))\\ &= J\Big(\hat{x}, u^0\Big) \geq \epsilon.\end{aligned}$$

This leads to the conclusion that the cost functional J admits a minimum at $(\hat{x}, u^0) \in \mathcal{B}_b \times U_{ad}$. □

5. Example

As elaborated in the introduction, multi-term Riemann–Liouville fractional differential equations serve as a dominant mathematical tool for characterizing anomalous diffusion with memory and nonlocal features. To illustrate the applicability and effectiveness of the theoretical findings established in this work, we present a fourth-order fractional stochastic diffusion system equipped with three-parameter damping and non-instantaneous impulses. By means of an abstract operator-theoretic formulation, the parabolic distributed-parameter system is recast into the infinite-dimensional abstract system 1.

To be specific, consider the following partial impulsive stochastic integro-differential equation:

$$\begin{cases} D_t^{\mu}X(t,\xi) + eD_t^{\nu}X(t,\xi) + kD_t^{\xi}X(t,\xi) = -r^4\dfrac{\partial^4 X(t,\xi)}{\partial\xi^4} + Cu(t,\xi)\\ \quad + \Big(\int_{-\infty}^t a_1(t)a_2(\varsigma - t)X(\varsigma,\xi)\,d\varsigma + \int_0^t\int_{-\infty}^{\varsigma} b_1(t)b_2(\tau)b_3(\varsigma-\tau)X(\varsigma,\xi)\,d\tau d\varsigma\Big)dW(t),\\ \quad (t,\xi) \in (\varsigma_i, t_{i+1}]\times[0,1],\ i = 0,1,\ldots,q,\ u \in U_{\mathrm{ad}},\\ X(t,\xi) = \int_{-\infty}^t g_i(\varsigma - t)X(\varsigma,\xi)\,d\varsigma, \quad (t,\xi) \in (t_i,\varsigma_i]\times[0,1],\ i = 1,2,\ldots,q,\\ X(t,0) = X(t,1) = 0,\ X''(t,0) = X''(t,1) = 0, \quad t \in [0,a],\\ \lim\limits_{t\to 0^+} I_t^{1-\mu}X(t,\xi) = \varphi(0,\xi), \quad \xi \in [0,1],\\ I_t^{1-\mu}X(t,\xi)\Big|_{t=\varsigma_i} = \int_{-\infty}^{\varsigma_i} g_i(\varsigma - \varsigma_i)X(\varsigma,\xi)\,d\varsigma, \end{cases} \tag{8}$$

with the associated cost functional

$$\begin{aligned}J(X^u, u)(\xi) = E\int_0^a \Big(\int_{[0,1]}\int_{-\infty}^0 \|X^u(t+\tau,\xi)\|^2 d\tau d\xi + \int_{[0,1]}\|X^u(t,\xi)\|^2 d\xi\\ + \int_{[0,1]}\|u(t,\xi)\|^2 d\xi\Big)dt + E\int_{[0,1]}\|X^u(a,\xi)\|^2 d\xi.\end{aligned}$$

Set the state space and control space as $\mathcal{H} = Y = L^2[0,1]$, and let $W(t)$ be a one-dimensional Wiener process defined on a filtered complete probability space. Define the fourth-order differential operator $A : D(A) \subset \mathcal{H} \to \mathcal{H}$ by

$$Ax = -r^4\frac{\partial^4 x}{\partial\xi^4},$$

with domain

$$D(A) = \Big\{x \in H^{4,2}(0,1) : x(0) = x(1) = 0,\ x''(0) = x''(1) = 0\Big\}.$$

https://doi.org/10.3390/fractalfract10070490

It can be verified that A generates a Riemann–Liouville fractional (μ,ν,ξ,e,k)-resolvent family $\left\{R_{\mu,\nu,\xi,e,k}(t)\right\}_{t>0}$ of the form

$$\Big(R_{\mu,\nu,\xi,e,k}(t)x\Big)(\xi)=\sum_{n=1}^{\infty}t^{\mu-1}E_{\mu-\nu,\mu-\xi,\mu}\Big(-e\lambda_n t^{\mu-\nu},-k\lambda_n t^{\mu-\xi}\Big)x_n\sin(n\pi\xi),$$

where $\lambda_n=-r^4n^4\pi^4$ are the eigenvalues of A, $\{\sin(n\pi\xi):n\in\mathbb{N}\}$ denotes the corresponding eigenfunctions, and any $x\in\mathcal{H}$ admits the Fourier sine expansion

$$x(\xi)=\sum_{n=1}^{\infty}x_n\sin(n\pi\xi).$$

Next, we endow the phase space $\mathcal{B}_\hbar$ for infinite delay systems with the norm

$$\|\varphi\|_{\mathcal{B}_\hbar}=\int_{-\infty}^{0}\hbar(s)\sup_{s\le\theta\le0}(E\|\varphi(\theta)\|^p)^{\frac{1}{p}}ds,$$

where the weight function is chosen as $\hbar(t)=e^{3t}$ for $t<0$, yielding the integral constant

$$l=\int_{-\infty}^{0}\hbar(t)dt=\frac{1}{3}.$$

The admissible control set is defined by

$$U_{\mathrm{ad}}=\left\{u(\cdot,\xi):[0,1]\to Y\,\middle|\,u\text{ is }\mathcal{F}_t\text{-adapted, measurable, and }\|u\|_{L^p_{\mathcal{F}}}\le\mu_1\right\},$$

with a fixed constant $\mu_1>0$. The control operator is taken as

$$B(t)u(t,\xi)=Cu(t,\xi),$$

where $C>0$ is a constant control coefficient.

Under the above settings, by letting

$$X(t,\cdot)=x(t),\quad x(t)(\xi)=X(t,\xi),\quad (t,\xi)\in[0,a]\times[0,1],$$

and

$$\varphi(t)(\xi)=\varphi(t,\xi),\quad (t,\xi)\in(-\infty,0]\times\mathcal{B}_\hbar,$$

the distributed-parameter system (8) is exactly transformed into the abstract system (1).

Define the cost functionals $P:[0,a]\times\mathcal{B}_\hbar\times\mathcal{H}\times Y\to\mathbb{R}\cup\{\infty\}$ and $\psi:\mathcal{H}\to\mathbb{R}$ as follows:

$$P(t,x_t^u,x^u(t),u(t))(\xi)=\int_{[0,1]}\int_{-\infty}^{0}|x^u(t+\tau)(\xi)|^2d\tau d\xi+\int_{[0,1]}|x^u(t)(\xi)|^2d\xi+\int_{[0,1]}|u(t)(\xi)|^2d\xi,$$
$$\psi(x^u(a))(\xi)=\int_{[0,1]}|x^u(a,\xi)|^2d\xi.$$

The nonlinear mappings are introduced as below :

1. The integral operator $g:[0,a]\times[0,a]\times\mathcal{B}_\hbar\to\mathcal{H}$:

$$g(t,\tau,\psi)(\xi)=\int_{-\infty}^{0}b_1(t)b_2(\tau)b_3(\theta)\psi(\theta)(\xi)d\theta;$$

2. The stochastic operator $\mathcal{M}:[0,a]\times\mathcal{B}_\hbar\times\mathcal{H}\to L_2^0$:

https://doi.org/10.3390/fractalfract10070490

$$\mathcal{M}\left(t,\psi,\int_0^t g(t,\varsigma,\psi)d\varsigma\right)(\xi)=\int_{-\infty}^0 a_1(t)a_2(\theta)\psi(\theta)(\xi)d\theta+\int_0^t\int_{-\infty}^0 b_1(t)b_2(\tau)b_3(\theta)\psi(\theta)(\xi)d\theta d\tau;$$

3. The non-instantaneous impulsive operators $h_i:(t_i,\varsigma_i]\times\mathcal{B}_\hbar\to\mathcal{H}$ $(i=1,2,\ldots,q)$:

$$h_i(t,\psi)(\xi)=\int_{-\infty}^0 g_i(\theta)\psi(\theta)(\xi)d\theta.$$

Assume that the coefficient functions a_1,a_2,b_j,g_i $(j=1,2,3)$ are continuous and satisfy

$$\begin{aligned}
k_1&=\left(\int_{-\infty}^0 e^{-6\theta}|b_3(\theta)|^2d\theta\right)^{\frac{1}{2}}<\infty,\\
k_2&=\left(\int_{-\infty}^0 e^{-6\theta}|a_2(\theta)|^2d\theta\right)^{\frac{1}{2}}<\infty,\\
d_i&=\left(\int_{-\infty}^0 e^{-6\theta}|g_i(\theta)|^2d\theta\right)^{\frac{1}{2}}<\infty,\quad i=1,2,\ldots,q.
\end{aligned}$$

Based on the above boundedness assumptions, we derive the p-th moment estimates for operators g, $\mathcal{M}$ and h_i successively.

For the nonlinear mapping $g(t,\tau,\psi)$, by virtue of Hölder's inequality and monotonicity of expectation, we obtain

$$\begin{aligned}
E\|g(t,\tau,\psi)\|^p&\le E\left[|b_1(t)b_2(\tau)|\left(\int_{-\infty}^0 e^{-6\theta}|b_3(\theta)|^2d\theta\right)^{\frac{1}{2}}\left(\int_{-\infty}^0 e^{6\theta}\|\psi(\theta)\|^2d\theta\right)^{\frac{1}{2}}\right]^p\\
&\le|b_1(t)b_2(\tau)k_1|^p\left(\int_{-\infty}^0 e^{3\theta}\sup_{\theta\le s\le 0}(E\|\psi(s)\|^p)^{\frac{1}{p}}d\theta\right)^p\\
&\le m_g\|\psi\|_{\mathcal{B}_\hbar}^p,
\end{aligned}$$

where $m_g=\sup\limits_{t,\tau\in[0,a]}|b_1(t)b_2(\tau)k_1|^p$. This validates Assumption (2).

For the stochastic operator $\mathcal{M}$, applying Hölder's inequality and Jensen's inequality yields

$$\begin{aligned}
E\|\mathcal{M}(t,\psi,y)\|_{L_2^0}^p&\le 2^{p-1}\left(|a_1(t)k_2|^p+1\right)\left(\|\psi\|_{\mathcal{B}_\hbar}^p+E\|y\|^p\right)\\
&=m_{\mathcal{M}}(t)\left(\|\psi\|_{\mathcal{B}_\hbar}^p+E\|y\|^p\right),
\end{aligned}$$

where $m_{\mathcal{M}}(t)=2^{p-1}\left(|a_1(t)k_2|^p+1\right)\in L^1([0,a];\mathbb{R})$, which confirms Assumption (3).

For the impulsive operators h_i, a similar calculation gives

$$E\|h_i(t,\psi)\|^p\le d_i^p\left(1+\|\psi\|_{\mathcal{B}_\hbar}^p\right),$$

and the Lipschitz continuity estimate

$$E\|h_i(t,\psi_1)-h_i(t,\psi_2)\|^p\le L_{h_i}\|\psi_1-\psi_2\|_{\mathcal{B}_\hbar}^p$$

holds with $L_{h_i}=d_i^p$, verifying Assumption (4).

In conclusion, all hypotheses of Theorem 3 and Balder's theorem are fulfilled. Therefore, the corresponding Bolza optimal control problem admits at least one optimal pair $(\hat{x},u^0)\in\mathcal{B}_b\times U_{\mathrm{ad}}$.

To visualize the dynamic behavior of the system, we numerically compute the mild solution $X(t,\xi)$ via the (μ,ν,ξ,e,k)-resolvent family representation, where the resolvent

https://doi.org/10.3390/fractalfract10070490

kernel is evaluated using the Talbot numerical inverse Laplace transform. Figure 2 presents the simulation results: panel (a) displays the three-dimensional solution surface $X(t,\xi)$ evolving over the spatio-temporal domain, while panel (b) shows the two-dimensional cross-sectional profiles at representative time instants $t = 0.2$, $t = 0.5$, and $t = 1.0$.

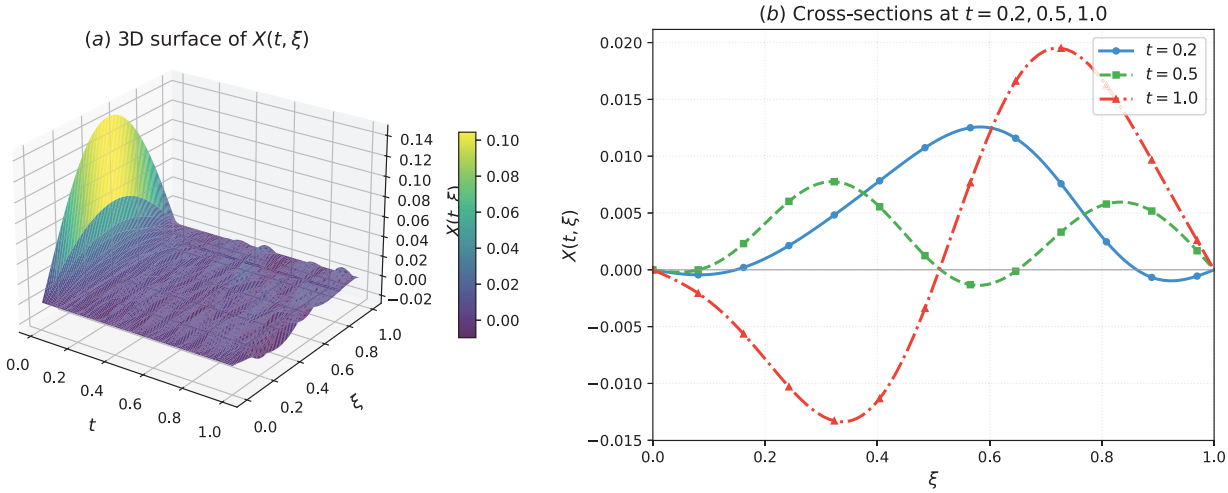

Figure 2. Numerical simulation of the fourth-order fractional stochastic diffusion system in Section 5 with parameters $\mu = 0.8$, $\nu = 0.5$, $\xi = 0.3$, $e = 0.1$, $k = 0.2$, $r = 1$, and initial condition $\varphi(0,\xi) = \sin(\pi\xi)$, computed on the spatio-temporal domain $t \in [0,1]$, $\xi \in [0,1]$: (**a**) three-dimensional surface plot of the solution $X(t,\xi)$ evolving over time $t \in [0,1]$ and space $\xi \in [0,1]$, illustrating the decay of the solution profile driven by the fourth-order diffusion and three-parameter fractional damping; (**b**) cross-sectional profiles of $X(t,\cdot)$ at representative time instants $t = 0.2$, $t = 0.5$, and $t = 1.0$, demonstrating the temporal evolution of the spatial distribution over $\xi \in [0,1]$.

6. Conclusions

This paper investigates the existence of mild solutions and the corresponding optimal control problems for a class of Riemann–Liouville fractional stochastic integro-differential systems with three-parameter damping, fourth-order diffusion, infinite delays, and non-instantaneous impulses in Hilbert spaces. Based on the (μ,ν,ξ,e,k)-resolvent family theory applicable to multi-term fractional systems, this paper first rigorously defines the mild solutions for the considered non-autonomous stochastic system. Under the verifiable boundedness and continuity assumptions imposed on system coefficients, the existence of mild solutions is strictly proved by combining the Krasnoselskii–Schaefer fixed-point theorem and stochastic analysis approaches. On this basis, with the help of the Mazur lemma, the Arzelá–Ascoli theorem and Balder's lower semicontinuity criterion, we prove the existence of optimal control pairs for the corresponding Bolza optimal control problem by overcoming the non-convexity and infinite-dimensional features of the problem. The validity of theoretical results is illustrated by a concrete example constructed on a fourth-order fractional stochastic diffusion system, which demonstrates that the results of this paper can be employed for modeling and analyzing complex damped diffusion processes.

The main contributions of this paper are embodied in three aspects. A unified analytical framework integrating three-parameter fractional damping, fourth-order diffusion operators, non-instantaneous impulses, infinite delays, and stochastic disturbances is established in this paper, which notably extends the research scope of existing two-parameter damping models and provides a universal tool for analyzing high-dimensional fractional systems with complex memory and hysteresis effects. Meanwhile, the introduction of (μ,ν,ξ,e,k)-resolvent family theory into fractional stochastic impulsive systems with infinite delays enriches the mathematical methodologies for solving multi-term fractional

https://doi.org/10.3390/fractalfract10070490

evolution equations and opens up new research routes for damped fractional systems. Furthermore, the derived theoretical results can be directly applied to the dynamic modeling of high-dimensional structures including Euler–Bernoulli beams and thin plates, laying a solid theoretical foundation for the design and optimization of control strategies for complex damped diffusion systems in engineering and applied sciences.

This paper presents a range of promising future research directions. The current research framework can be generalized to the scenarios involving Markovian switching, state-dependent impulses, or fractional Brownian motion, so as to more precisely characterize practical systems with abrupt variations or long-range dependence. Further explorations can be made on the partial approximate controllability, optimal output tracking and robust control problems of three-parameter damped systems, so as to address practical control issues not covered in this work. In addition, building upon the numerical simulation presented in Section 5, future work may focus on developing more efficient numerical algorithms and further exploring the dynamic characteristics and control performance of the model in practical engineering applications.

Overall, this paper offers new perspectives and rigorous mathematical tools for the analysis and control of complex fractional stochastic systems, and the obtained results possess potential application values in diverse fields including structural engineering, materials science, and mathematical physics.

Author Contributions: Conceptualization, S.-Y.L.; methodology, Z.-C.L. and S.-Y.L.; validation, Z.-C.L., T.-T.H. and S.-Y.L.; formal analysis and investigation, Z.-C.L., T.-T.H. and S.-Y.L.; resources, S.-Y.L.; writing—original draft preparation, Z.-C.L.; writing—review and editing, Z.-C.L., T.-T.H. and S.-Y.L.; supervision, S.-Y.L.; project administration, S.-Y.L.; funding acquisition, S.-Y.L. All authors have read and agreed to the published version of the manuscript.

Funding: This work was supported by the Hainan Provincial Natural Science Foundation (Grant No. 125RC745), the National Natural Science Foundation of China (Grant No. 11761027), and the National Social Sciences Foundation of China (Grant No. 23BJY026).

Data Availability Statement: The original contributions presented in this study are included in the article. Further inquiries can be directed to the corresponding author(s).

Acknowledgments: The authors thank the editors and referees for their valuable comments and suggestions.

Conflicts of Interest: The authors declare no conflict of interest. The funders had no role in the design of the study; in the collection, analyses, or interpretation of data; in the writing of the manuscript; or in the decision to publish the results.

References

1. Mishra, V.N.; Gupta, A.; Sarangi, S.K. Viscoelastic materials and composites: A comprehensive review on mechanics, modeling, and design configurations for vibration control in structural application. *Multiscale Multidiscip. Model. Exp. Des.* **2025**, *8*, 470. [CrossRef]
2. Baleanu, D.; Sajjadi, S.S.; Jajarmi, A.; Defterli, Ö. On a nonlinear dynamical system with both chaotic and nonchaotic behaviors: A new fractional analysis and control. *Adv. Differ. Equ.* **2021**, *2021*, 234. [CrossRef]
3. Suzuki, J.L.; Gulian, M.; Zayernouri, M.; D'Elia, M. Fractional Modeling in Action: A Survey of Nonlocal Models for Subsurface Transport, Turbulent Flows, and Anomalous Materials. *J. Peridynamics Nonlocal Model.* **2023**, *5*, 392–459. [CrossRef]
4. Podlubny, I. An Introduction to Fractional Derivatives, Fractional Differential Equations, to Methods of Their Solution and Some of Their Applications. In *Mathematics in Science and Engineering*; Academic Press: New York, NY, USA, 1998; Volume 198.
5. Kilbas, A.A.; Srivastava, H.M.; Trujillo, J.J. *Theory and Applications of Fractional Differential Equations*; North-Holland Mathematics Studies; Elsevier: Amsterdam, The Netherlands, 2006; Volume 204, pp. 1–340. Available online: https://www.elsevier.com/books/theory-and-applications-of-fractional-differential-equations/kilbas/978-0-444-51832-3 (accessed on 1 July 2026).
6. Li, K.X.; Peng, J.G.; Jia, J.X. Cauchy problems for fractional differential equations with Riemann–Liouville fractional derivatives. *J. Funct. Anal.* **2012**, *263*, 476–510. [CrossRef]

7. Chen, P.; Zhang, X.; Li, Y. Existence and Approximate Controllability of Fractional Evolution Equations with Nonlocal Conditions Via Resolvent Operators. *Fract. Calc. Appl. Anal.* **2020**, *23*, 268–291. [CrossRef]
8. Li, X.; Liu, X.; Tang, M. Approximate controllability of fractional evolution inclusions with damping. *Chaos Solitons Fractals* **2021**, *148*, 111073. [CrossRef]
9. Haq, A. Partial-approximate controllability of semi-linear systems involving two Riemann–Liouville fractional derivatives. *Chaos Solitons Fractals* **2022**, *157*, 111923. [CrossRef]
10. Mei, Z.; Peng, J.G. Riemann–Liouville abstract fractional Cauchy problem with damping. *Indag. Math.* **2014**, *25*, 145–161. [CrossRef]
11. Bahreini, A.; Asgari, A.; Akbarzadeh Bengar, H. Numerical Fractional Calculus Framework for Nonlocal Euler-Bernoulli Beam Deflection Analysis. *Fractal Fract.* **2026**, *10*, 109. [CrossRef]
12. Xing, Z.; Wen, L. Numerical analysis and fast implementation of a fourth-order difference scheme for two-dimensional space-fractional diffusion equations. *Appl. Math. Comput.* **2019**, *346*, 155–166. [CrossRef]
13. Jafari, A.; Aftabi Sani, A. Free vibration analysis of Euler-Bernoulli beams modeled by spatial-fractional differential equation. *Results Eng.* **2024**, *24*, 102972. [CrossRef]
14. Hernandez, E.; O'Regan, D. On a new class of abstract impulsive differential equations. *Proc. Am. Math. Soc.* **2013**, *141*, 1641–1649. [CrossRef]
15. Dhayal, R.; Malik, M.; Abbas, S. Existence, stability and controllability results of stochastic differential equations with non-instantaneous impulses. *Int. J. Control* **2022**, *95*, 1719–1730. [CrossRef]
16. Guo, Y.; Shu, X.-B.; Li, Y.; Xu, F. The existence and Hyers-Ulam stability of solution for an impulsive Riemann–Liouville fractional neutral functional stochastic differential equation with infinite delay of. *Bound. Value Probl.* **2019**, *2019*, 59. [CrossRef]
17. Ansari, S.; Malik, M.; Dhayal, R. Optimal controls for multi-term fractional stochastic integro-differential equations with impulses and infinite delay. *Int. J. Syst. Sci.* **2025**, *56*, 1862–1883. [CrossRef]
18. Yan, Z.; Jia, X. Optimal controls of fractional impulsive partial neutral stochastic integro-differential systems with infinite delay in Hilbert spaces. *Int. J. Control Autom. Syst.* **2017**, *15*, 1051–1068. [CrossRef]
19. Da Prato, G.; Zabczyk, J. Stochastic Equations in Infinite Dimensions. In *Encyclopedia of Mathematics and Its Applications*; Cambridge University Press: Cambridge, UK, 2010; Volume 45. [CrossRef]
20. Lin, A.; Ren, Y.; Xia, N. On neutral impulsive stochastic integro-differential equations with infinite delays via fractional operators. *Math. Comput. Model.* **2010**, *51*, 413–424. [CrossRef]
21. Chalishajar, D.; Kasinathan, R. Optimal control for neutral stochastic systems with infinite time delay and deviated argument. *Results Control Optim.* **2022**, *9*, 100181. [CrossRef]
22. Balasubramaniam, P.; Tamilalagan, P. The Solvability and Optimal Controls for Impulsive Fractional Stochastic Integro-Differential Equations via Resolvent Operators. *J. Optim. Theory Appl.* **2017**, *174*, 139–155. [CrossRef]
23. Yan, B. Boundary value problems on the half-line with impulses and infinite delay. *J. Math. Anal. Appl.* **2001**, *259*, 94–114. [CrossRef]
24. Corduneanu, C. Functional Differential Equations with Infinite Delay. *SIAM Rev.* **1992**, *34*, 504–505. [CrossRef]
25. Lu, Z.C.; Lin, S.Y.; Hu, T.T. Research on the existence and uniqueness of solutions to fractional diffusion equations with three-parameter damping terms. *Axioms* **2026**, *15*, 136. [CrossRef]
26. Gorenflo, R.; Kilbas, A.A.; Mainardi, F.; Rogosin, S.V. *Mittag-Leffler Functions, Related Topics and Applications*; Springer: Berlin/Heidelberg, Germany, 2014.
27. Ji, S.; Yang, D.D. Solutions to Riemann–Liouville fractional integrodifferential equations via fractional resolvents. *Adv. Differ. Equ.* **2019**, *2019*, 524. [CrossRef]
28. Balder, E.J. Necessary and sufficient conditions for. *Nonlinear Anal. Theory Methods Appl.* **1987**, *11*, 1399–1404. [CrossRef]

Disclaimer/Publisher's Note: The statements, opinions and data contained in all publications are solely those of the individual author(s) and contributor(s) and not of MDPI and/or the editor(s). MDPI and/or the editor(s) disclaim responsibility for any injury to people or property resulting from any ideas, methods, instructions or products referred to in the content.

fractal and fractional

MDPI

Article

On the Solution Variability of Random-Order Fractional Differential Equations with Orders on Bounded Supports

Zafer Bekiryazici

Department of Mathematics, Recep Tayyip Erdogan University, Rize 53100, Türkiye;
zafer.bekiryazici@erdogan.edu.tr

Abstract

In this study, random-order FDEs are studied with a focus on the variability of their solutions and random orders when the order of differentiation is governed by a probability distribution. Fractional differential equations (FDEs) offer a generalized modeling approach that enables the analysis of nonlocality and memory effects. However, the deterministic framework for studying FDEs neglects the random nature of real-life events. In this regard, four continuous probability distributions with bounded support (uniform, Beta, triangle and Bates) are used to analyze the variability of the solutions depending on the random order, which is defined to vary between [0.65, 0.95] according to these probability distributions with identical expected values. Monte-Carlo simulations with $N = 2^{15}$ repetitions are performed to investigate the random-order FDEs using a predictor-corrector approach. Results show that the decrease in the deviation from the uniform distribution to the Bates distribution is reflected in the random characteristics of the solutions and the order of differentiation to almost the same extent. The findings indicate that the average solutions obtained with random orders from each distribution show almost identical results, whereas the variability changes significantly based on the distribution of the order of differentiation. This information provides useful guidance in working with probabilistic models instead of deterministic systems for uncertainty quantification or sensitivity analysis.

Keywords: random-order fractional differential equation; Caputo derivative; bounded support; simulation; Beta distribution

MSC: 34A08; 34F05

1. Introduction

Differential equations are the primary tools for modeling real-life events in a wide range of areas from mathematical biology [1,2] to social sciences [3]. Although ordinary differential equations (ODEs) constitute the foundation for a significant part of these modeling studies, the increased usability and capability of mathematical software and the developments in stochastic and fractional calculus have caused an increased diversity in these studies. Numerical investigation of models, theoretical investigations about the stability and existence and uniqueness of solutions and various other aspects of the models have been extensively studied for systems consisting of ODEs. Yet, especially since the late twentieth century, the use of ODEs as primary tools for modeling has gradually shifted toward the use of other forms of equations. Stochastic, delay and fuzzy differential equations are some of the other forms that are used in mathematical modeling. However,

among these classes of equations, one specific class that has become a prominent tool for mathematical modeling is differential equations with fractional order derivatives.

Most studies on fractional calculus date its history back to the 17th century to Leibniz's inquiry about the meaning of a derivative of order ½. The introduction of the Caputo fractional derivative by Michel Caputo in the mid-twentieth century can be considered a milestone that has paved the way for the widespread use of fractional differential equations (FDEs) today [4]. FDEs provide the means to analyze memory effects and nonlocality in models and have received the attention of many researchers. Additionally, the introduction of new fractional derivatives alongside Riemann-Liouville and Caputo derivatives, such as the Atangana-Baleanu and Caputo-Fabrizio derivatives, has provided a broad range of investigation opportunities.

Studies using FDEs are generally performed on a deterministic level in mathematical modeling. However, certain events in nature possess a significant level of uncertainty that cannot be neglected. The implementation of probabilistic components in FDEs is generally done using random coefficients or stochastic noise terms. Some of the studies on random fractional differential equations include the study by Burgos et al., where mean-square analysis of random FDEs is studied [5] and the study by Villafuerte, which analyzes second-order linear fractional differential equations with random inhomogeneous parts [6]. The application of polynomial chaos [7], Galerkin method [8], Laplace transform [9] and random variable transformation technique [10] has been given for the investigation of random FDEs. These equations have been used to investigate modeling problems in mechanical engineering [11], random microbial growth [12], malware spread [13] and tea cultivation [14]. Investigation of uncertainty along with fractional differential equations is also done in other forms containing stochastic processes and partial differential equations (PDEs). The study by Su uses random fractional PDEs for modeling water movement in soils [15], and Heris et al. have studied the Darboux problem of random fractional PDEs with infinite delay [16]. Studies that are performed within the stochastic framework can be exemplified by [17], which focuses on a malnutrition model and [18], where a financial chaotic model is studied with the Atangana-Baleanu (AB) fractional derivative. Many studies involving other fractional derivatives such as the Atangana-Baleanu-Caputo derivative or the conformable derivative can also be found [19,20]. Overall, it can be said that the literature focuses mostly on the use of the Caputo fractional derivative [10,21,22], and although there are various studies on the probabilistic dynamics of solution processes in random and stochastic FDEs [5,23,24], applications of these equations are also used within modeling studies in various areas such as finance, acoustics and epidemiology [25–27].

It is seen that most studies focusing on FDEs treat the fractional order as a deterministic constant where the value is either hypothetically determined or identified using existing data. The use of estimates depending on a limited number of observations or uncertainty from measurement errors may lead to unclear memory effects that cannot be represented by a single deterministic order. Hence, using random orders may provide a more suitable modeling framework for studies in a variety of disciplines, such as those focusing on microscale physics where the uncertainty in transport media could be investigated with a random fractional order of differentiation. In this study, the random dynamics of FDEs will be studied for the case where the order of differentiation is a random variable. The order of the Caputo-type fractional derivative α will be assumed as a random variable governed by a probability density with bounded support. Here, changing the original constant fractional order into a measurable mapping $\alpha^* : \Omega \to (0, 1)$ defined on a probability space $(\Omega, \mathcal{F}, P)$ yields a random-order fractional equation. These FDEs will be studied numerically for a comparative analysis of the possible variations caused by the changes in the probability density driving the random orders. Results for the variability of the solutions and the

https://doi.org/10.3390/fractalfract10080561

random orders will be analyzed for several probability distributions defined on bounded supports. Although the amount of research on random-order FDEs is not at the same level as the research on general FDEs, there are some important studies on the topic. The studies by Sun et al. and Patnaik et al. present reviews on random and variable-order FDEs [28,29]. There are also several studies on the application of variable- or random-order FDEs focused on mean square displacement behaviors of anomalous diffusions [30], fractional advection-diffusion equation [31], chaotic financial systems [32], contaminant transport through porous media [33], mass transport equation [34], fractional Schrödinger equation [35] and fractional Telegraph equation [36]. Other studies that use finite difference schemes [37], a wavelet approach [38], Bessel wavelet functions [39] and a collocation method with Lagrange polynomials [40] have also been given in the literature for the analysis of random or variable-order FDEs.

An overall summary of the literature on FDEs of random order shows that most of the studies, some of which are listed above, focus on the use of various numerical approximation methods such as wavelet approaches or finite difference schemes. Another focal point in the literature is to study specific equations such as fractional Schrödinger or Telegraph equations, or to study equation systems modeling financial systems or contaminant transport with random components. Hence, it can be said that studies concentrate on the numerical analysis of FDEs or handle the equations from a modeling perspective. Despite the considerable amount of research conducted in this area, the issue of the statistical characteristics of the solutions in relation to the probability density of the random order remains largely unexplored. In this regard, this study focuses on the variability of the solutions of FDEs with random orders that are governed by four continuous probability distributions. A Monte-Carlo approach based on pathwise simulation of the random-order FDEs will be used for analysis. Fractional orders with identical expectations that are uniform, Beta, triangular and Bates distributed are analyzed numerically, and simulation results are used to comment on the random characteristics of the orders and the solutions, as well as to compare the findings for each distribution with each other and their theoretical estimates. The numerical characteristics of random variables and how the variability of the outcomes changes with respect to the distribution of the random variable are clearly known. It is hypothesized that changing the orders of the random variables should reflect this change in variability in relation to the probability distribution. In this regard, the study focuses on the effects of the distributions of the orders on the solutions, in terms of the deviation and width of the three-sigma interval for the expected solution caused by the changes in the probability density. The study also aims to underline that different probability distributions provide similar results for average solutions—the counterpart of the deterministic solution obtained in the general case of FDEs—and hence all distributions are equally suitable for obtaining an approximation to the expected solution.

This paper is organized as follows: Section 2 contains the fundamental information related to fractional calculus and the randomization of the orders, Section 3 presents the numerical applications for different types of equations, and Section 4 contains the conclusion and discussion.

2. Preliminaries and Randomization

Fundamental definitions related to Caputo-type fractional derivatives and the probability distributions used for the random orders of the FDEs are given in this section.

Definition 1 ([41]). *Let $\nu \in \mathbb{R}_+$. The operator J_a^ν, defined on $L_1[a,b]$ by*

$$J_a^\nu f(t) = \frac{1}{\Gamma(\nu)} \int_a^t (t-\tau)^{\nu-1} f(\tau) d\tau, \tag{1}$$

https://doi.org/10.3390/fractalfract10080561

for $a \leq t \leq b$, is called the Riemann–Liouville fractional integral operator of the order ν. For $\nu = 0$, the identity operator $J_a^0 = I$ is obtained.

Definition 2 ([41]). *Let $\nu \in \mathbb{R}_+$ and $m = \lceil \nu \rceil$, where $\lceil \nu \rceil$ is the ceiling function and denotes the smallest integer that is larger than ν. The operator D_a^ν, defined by*

$$D_a^\nu f(t) = D^m J_a^{m-\nu} f(t), \tag{2}$$

is called the Riemann–Liouville fractional derivative operator of the order ν. For $\nu = 0$, $D_a^0 = I$ is obtained.

Definition 3 ([4]). *Let $n = \lceil \alpha \rceil$. Then, the Caputo fractional derivative operator ${}^C D_t^\alpha$ is given as follows:*

$${}^C D_t^\alpha f(t) = \frac{1}{\Gamma(n-\alpha)} \int_0^t \frac{f^{(n)}(\tau)}{(t-\tau)^{\alpha+1-n}} d\tau. \tag{3}$$

Caputo fractional derivative is one of the most frequently used fractional differentiation operators in FDEs [42,43] because of its compatibility with integer-ordered differential equations in terms of the initial and boundary conditions used with these equations.

Randomization of Fractional Orders

The integer-ordered derivatives in generic Bernoulli, Euler, Clairaut and Riccati-type ordinary differential equations will be transformed into Caputo-type fractional derivatives to obtain four random-order FDEs. Then, the fractional orders in the equations will be transformed into (continuous) uniform, Beta, triangular, and Bates distributed random variables. All the listed probability distributions are continuous with bounded supports, which can be generalized to any interval $[a, b]$. Using a random variable, which is a measurable function, $X : \Omega \to \mathbb{R}$ defined on the probability space $(\Omega, \mathcal{F}, P)$ with the mentioned probability densities, the random order α^* will be defined as follows:

$$\alpha^* = c + \varepsilon X_i, \; i \in \{1, 2, 3, 4\}. \tag{4}$$

The (continuous) uniform distribution is defined on any bounded support $[a, b]$ and its probability density function (pdf) is given by $f(x) = 1/(b-a)$ for $x \in [a, b]$ where $a, b \in \mathbb{R}$. This random variable is denoted as $X \sim U(a, b)$ and has the expected value $\mu_X = (a+b)/2$. The standard version of the (continuous) uniform distribution has the bounded support $[0, 1]$, the pdf $f(x) = 1$, the expected value $E(X) = 1/2$ and is denoted as $X \sim U(0, 1)$.

The Beta distribution is another probability distribution defined on the bounded support $[0, 1]$ and this interval can be extended in the modified version of the distribution called the generalized Beta distribution. A Beta-distributed random variable X is denoted as $X \sim Beta(u, v)$, where u and v are the shape parameters, and has the pdf

$$f(x) = \frac{1}{B(u, v)} x^{u-1} (1-x)^{v-1}, u > 0, v > 0, x \in [0, 1]. \tag{5}$$

Here, $B(u, v)$ is the Beta function, and the distribution is symmetrical for the case $u = v$. The expected value is $u/(u+v)$, which means that the symmetrically distributed Beta random variable X also has an expected value of $E(X) = 1/2$.

The next two distributions can be obtained by using independent standard continuous uniform random variables. The first one, the standard triangle (or triangular) distribution, has the bounded support $[0, 1]$ and the pdf

https://doi.org/10.3390/fractalfract10080561

$$f(x) = \begin{cases} \frac{2x}{p}, & 0 \le x \le p, \\ \frac{2(1-x)}{1-p}, & p < x \le 1, \\ 0, & \text{otherwise}, \end{cases} \tag{6}$$

where the shape parameter $p \in [0,1]$ corresponds to the mode (or the vertex) and the random variable X with this pdf is denoted as $X \sim Tri(p)$ or $X \sim Tri(0,p,1)$. The generalized triangle distribution is the modified version of this distribution with an arbitrary bounded support $[a,b]$, where a and b are the lower and upper limits for the random variable. The generalized triangular random variable is denoted as $X \sim Tri(a,b,p)$ and the mean, or expected value, is given by $\mu_X = (a+b+p)/3$. Hence, the expected value for $X \sim Tri(p)$ becomes $E(X) = 1/2$ for $p = 1/2$, which corresponds to the symmetrical form of the distribution, with an isosceles triangle-shaped PDF. The standard triangle random variable X with $p = 1/2$ can be obtained as the mean of two independent standard continuous uniform random variables $X_1 \sim U(0,1)$ and $X_2 \sim U(0,1)$, i.e., $X = (X_1 + X_2)/2$.

The last probability distribution, the Bates distribution, is a generalization of the relationship between independent standard continuous uniform random variables and the standard triangle random variable mentioned above. Bates distribution is obtained as the average of n independent standard continuous uniform random variables. Bates distribution coincides with the standard (continuous) uniform distribution for $n = 1$ and the standard triangle distribution with $p = 1/2$ for $n = 2$. The pdf of a Bates-distributed random variable is given by

$$f(x) = \frac{n}{2(n-1)!} \sum_{k=0}^{n} (-1)^k C(n,k)(nx-k)^{n-1} sgn(nx-k), \tag{7}$$

for $x \in [0,1]$ [44]. Here, $sgn(x)$ is the signum function and $C(n,k)$ denotes the number of combinations of k elements from a set of n elements. A Bates-distributed random variable X can be denoted as $X \sim Bates(n)$ with n showing the number of uniform random variables being averaged. It is also clear that this definition yields the expected value of $X \sim Bates(n)$ as $\mu_X = 1/2$, since all of the independent uniform random variables have the same expectation.

Although any probability distribution could be used to randomize the order of differentiation, certain limitations on the selection would provide a clearer presentation of the main idea. Using uniform, Beta, triangular and Bates distributions results in a selection of probability densities that will provide symmetrical variability within their supports with different deviation rates. Additionally, these distributions have bounded supports, which provide a more convenient numerical investigation. Defining the random order as $\alpha^* = c + \varepsilon X_i$ for suitable ε, c enables the limitation of the random order to remain fractional, i.e., $0 < \alpha^* < 1$, preventing complications for the selection of a suitable numerical method. Any expected value for α^* can be obtained for suitable values of ε, c, which enables a comparison of the results obtained for the expected values and the results from a deterministic study where $E(\alpha^*) = \alpha$.

If $X_1 \sim U(0,1), X_2 \sim Beta(u,v), X_3 \sim Tri(0,p,1), X_4 \sim Bates(3)$, then

$$P(0 \le X_i \le 1) = 1 \text{ and } c = 0.65, \varepsilon = 0.3 \Rightarrow P(0.65 \le \alpha^* \le 0.95) = 1 \tag{8}$$

with

$$E(\alpha^*) = 0.80 \text{ for } X_i,\ i \in \{1,2,3,4\}. \tag{9}$$

This support for the random order was selected to ensure that the order of differentiation stays fractional, i.e., $\alpha < 1$, getting sufficiently close to the classical case for $\alpha = 1$. However, as the order of differentiation goes below a certain level, the solutions of the models may

https://doi.org/10.3390/fractalfract10080561

diverge significantly from the remaining solutions, especially around $\alpha = 0.50$. Fractional derivatives are often related to memory effects, and this would correspond to a case where the memory effect is too strong. Hence, the support $[0.65, 0.95]$ enables the analysis of fractional models incorporating weak and moderate memory effects, which are frequently used for modeling studies. Although the pattern of change in variability caused by the change in the order of differentiation may be preserved outside this range, it may be difficult to observe this pattern outside this interval, especially when $\alpha < 0.50$.

Although all of the random variables $X_1 \sim U(0,1)$, $X_2 \sim Beta(u,v)$ with $u = v = 2$, $X_3 \sim Tri(0,p,1)$ with $p = 1/2$ and $X_4 \sim Bates(n)$ for $n = 3$ have identical expectations $E(X_i) = 1/2$ for $i \in \{1,2,3,4\}$, their standard deviations vary:

$$Var(X_1) = \frac{1}{12}, Var(X_2) = \frac{1}{20}, Var(X_3) = \frac{1}{24}, Var(X_4) = \frac{1}{36}. \tag{10}$$

This also affects the variance of the random order

$$Var(\alpha^*) = Var(c + \varepsilon X_i) = \varepsilon^2 Var(X_i). \tag{11}$$

Hence, a Bates-distributed random order has one-third the variance of a standard uniformly distributed random order. In fact, the coefficients of variation (CV) for these distributions are obtained as follows. For the percentage notation of CV, i.e., $CV(X_i) = 100 \times std(X_i)/E(X_i)$, one can find that

$$CV(X_1) = 57.74\%,\ CV(X_2) = 44.72\%,\ CV(X_3) = 40.82\%,\ CV(X_4) = 33.33\%. \tag{12}$$

Meaning that the random fractional orders $\alpha_i^* = c + \varepsilon X_i$ for $i \in \{1,2,3,4\}$ have the following CV for $c = 0.65, \varepsilon = 0.3$:

$$CV(\alpha_1) = 10.83\%,\ CV(\alpha_2) = 8.39\%,\ CV(\alpha_3) = 7.65\%,\ CV(\alpha_4) = 6.25\%. \tag{13}$$

All of these random variables can be generated using the Statistics and Machine Learning Toolbox in MATLAB R2025b (The MathWorks, Inc., Natick, MA, USA). The function "betarnd" generates Beta-distributed random numbers, whereas the function "unifrnd" can be used to create uniform random numbers as well as triangular and Bates-distributed random numbers using the aforementioned relationships.

The variability of the random orders $\alpha_i^* = c + \varepsilon X_i, i \in \{1,2,3,4\}$, for $X_1 \sim U(0,1)$, $X_2 \sim Beta(u,v)$ with $u = v = 2$, $X_3 \sim Tri(0,p,1)$ with $p = 1/2$ and $X_4 \sim Bates(n)$ for $n = 3$ have been shown below in Figure 1. Note that the uniformly distributed random orders (shown with black squares) are much more scattered around their mean $E(\alpha_1) = 0.80$ compared to the Bates-distributed random orders (red upside-down triangles), which are more concentrated around the same mean $E(\alpha_4) = 0.80$. This is a visualization of the difference in the coefficients of variation for both probability distributions.

The identical expectations for these distributions enable a similar randomization of deterministic problems, whereas the difference in variation means some distributions may be more suitable in specific applications. The suitability of the distribution should be assessed according to the physical properties of the system being investigated. A uniform distribution would be a more suitable selection when an assessment of uncertainty is needed, but the variability of the order of differentiation is not relevant. Since all values of a uniform random variable are equally likely, this distribution may be suitable in applications related to the investigation of memory effects in preliminary modeling studies or the study of newly identified materials. In applications where a specific value within the interval is more likely, the peak value of the triangular distribution may be more suitable for

https://doi.org/10.3390/fractalfract10080561

randomization. The peak value of the probability density may be used to model expert judgment values or certain elements in engineering design studies, while the variability within the support may still opt for other possible values of the fractional order. Beta distribution provides a more versatile modeling ability since the shape parameters of the distribution may be used to obtain a symmetric/skewed or concave/convex probability density. This diversity may be suitable in representing the transition from modeling the current state of the system ($D^{\alpha}y(t) = f(t, y)$ with $\alpha = 0$) to modeling the change in time ($D^{\alpha}y(t) = f(t, y)$ with $\alpha = 1$) in a system related to diffusion or biology. Bates distribution is based on the average of multiple independent uniform random variables and may be a suitable selection for modeling systems under the effect of multiple factors, such as meteorological models related to temperature or humidity.

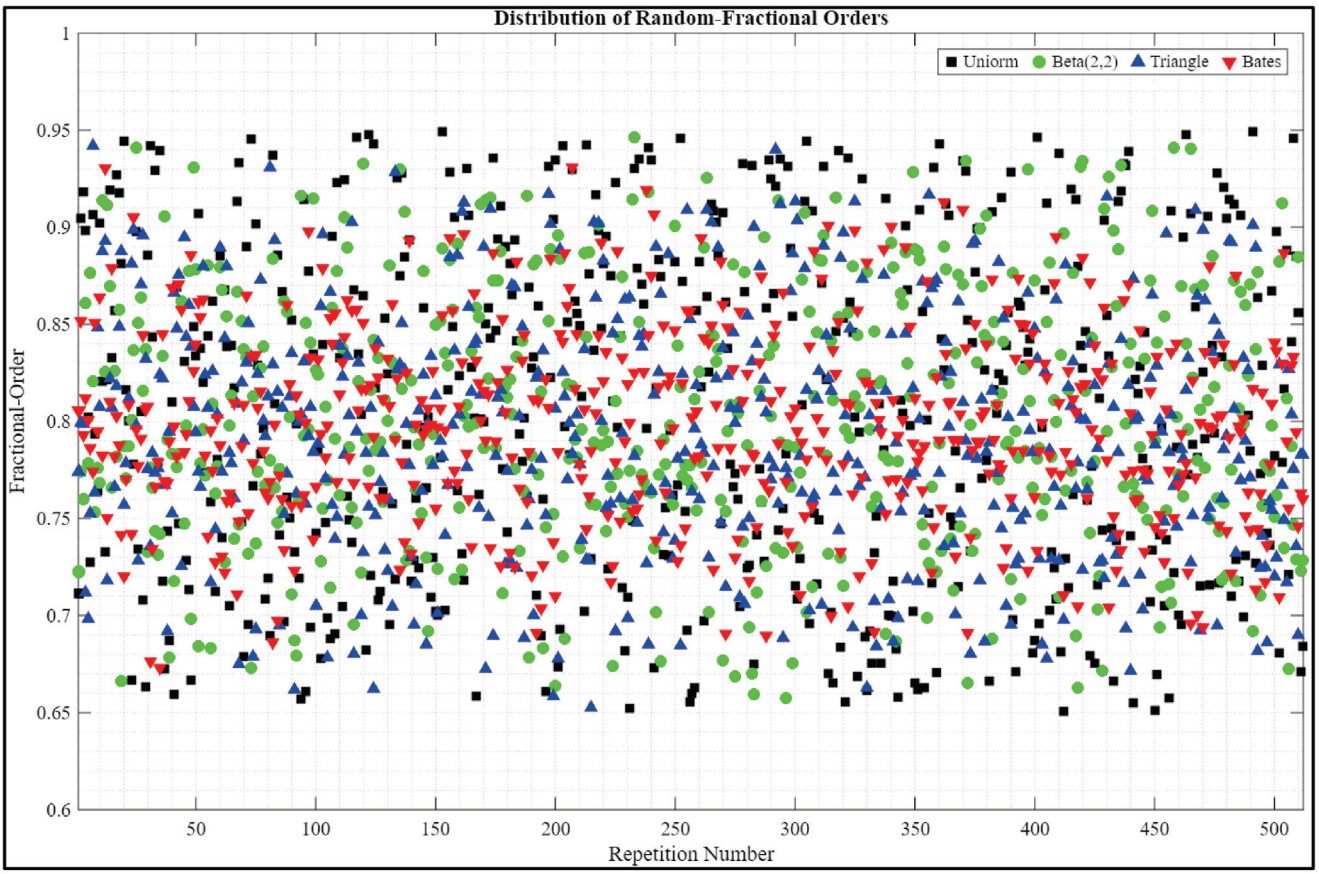

Figure 1. Distribution of selected random orders for (i) uniform distribution, (ii) Beta distribution, (iii) triangular distribution and (iv) Bates distribution.

A random variable $X : \Omega \to \mathbb{R}$ is a measurable function that maps events in the sample space to real numbers, meaning that $\alpha^* \in \mathbb{R}$ for each trial. Although the orders vary for each repetition, they are still constants such that $0 < \alpha^* < 1$, a result guaranteed by the selection of probability densities with bounded supports. Hence, fractional approximation methods can be used to analyze the random-order FDEs for each separate repetition. There are numerous methods in the literature, some of which have been mentioned earlier. Here, the fde12 method will be used to obtain the numerical solution of the equations. fde12 algorithm [45] is a predictor-corrector approach and has been used in many studies to analyze Caputo-type FDEs [14]. The fractional initial value problem ${}^{C}D^{\alpha}_{0,t}u(t) = f(t, u(t))$, $u^{j}(0) = u^{j}_{0}$ for $j = 0, 1, \ldots, m-1$ and $\alpha \in (m-1, m), m \in \mathbb{Z}^{+}$ is analyzed with the predictor-corrector scheme in the fde12 algorithm, and the solutions of

https://doi.org/10.3390/fractalfract10080561

the Caputo-type fractional IVP will be used to obtain the characteristics for the random orders and the solutions of the FDEs [45,46].

Using the numerical approximations for the expected value and standard deviation of the solutions, three-sigma coverage intervals for the solutions of the random-order FDEs will be analyzed. A coverage interval of K sigma is of the form $[\mu - K\sigma, \mu + K\sigma]$ and covers a certain amount of the values of the random variable. According to the distribution of the random variable and the value of K, the portion of the support that is covered by the interval changes. As $\alpha_1^* = c + \varepsilon X_1$ with $X_1 \sim U(0,1)$, the probability that a certain solution of the random-order FDE with the random order α_1 is covered by intervals of K standard deviations are given below:

$$P(\mu_{\alpha_1} - K \times std(\alpha_1) < \alpha_1^* < \mu_{\alpha_1} + K \times std(\alpha_1)) = \int_{\mu_{\alpha_1} - K \times std(\alpha_1)}^{\mu_{\alpha_1} + K \times std(\alpha_1)} \frac{1}{0.30} dx = \frac{K}{\sqrt{3}}.$$

This means that for $K = 1, 2, 3$ the covered intervals and their probabilities are as follows: For $K = 1$ the interval $[0.7134, 0.8866]$ covers 57.74% of the solutions—or there is a 0.5774 probability that this interval contains a solution of the FDE with the random order α_1^*. For $K = 2$ and $K = 3$, the intervals become larger than the support of α_1^*, meaning that there is *a* probability of 1 that the solutions fall within the coverage interval. As the distribution changes, these probabilities vary. However, since $K = 3$ for all four distributions cover the support in each case, coverage intervals for three standard deviations will be analyzed.

3. Numerical Examples

The numerical characteristics of the solutions for fractional differential equations with random orders are exemplified with four generic ordinary differential equations that have been transformed into random-order FDEs with distinct probability distributions that govern the orders of differentiation. The deterministic ODEs used to exemplify Bernoulli, Euler, Clairaut and Riccati differential equations were generated as numerical representatives of each class. It should be noted here that the fractional-order FDEs are solved using fde12 in MATLAB, designed to analyze a deterministic fractional IVP. The Monte Carlo simulation was suitably implemented to ensure independence between realizations of the random-order FDE, generating a fractional-order separately for each repetition of the simulation, providing one independent deterministic realization each time to be solved numerically.

Example 1. *Fractional Bernoulli equation: Consider the following Bernoulli differential equation with the Caputo-type fractional derivative:*

$$^{C}C_t^{\alpha_i^*} y = -4y + \frac{t}{y}, y(1) = 1. \tag{14}$$

The original ordinary-deterministic version of this initial value problem (IVP) admits the exact solution $y(t) = \left(\sqrt{8t - 1 + 25\exp(8 - 8t)}\right)/4\sqrt{2}$. The fractional-order α is replaced by random-fractional orders $\alpha_i^* = c + \varepsilon X_i, i \in \{1, 2, 3, 4\}, X_i : \Omega \to \mathbb{R}$ for $X_1 \sim U(0,1)$, $X_2 \sim Beta(2,2)$, $X_3 \sim Tri(0, 1/2, 1)$ and $X_4 \sim Bates(3)$. The numerical solution $y(t)$ from fde12 ($h = 0.01$) is repeatedly obtained for $N = 2^{15}$ trials for each probability distribution to investigate its characteristics. The coefficients of variation (CV) for each $\alpha_i^*, i \in \{1, 2, 3, 4\}$ and three-sigma interval of the expected values for the solution $E(y(t))$ calculated with $k = 3$ standard deviations for the uniform distribution are shown below (Figure 2). Note that maximum and minimum values for the coverage intervals and the solutions for each distribution have been marked on the figure.

https://doi.org/10.3390/fractalfract10080561

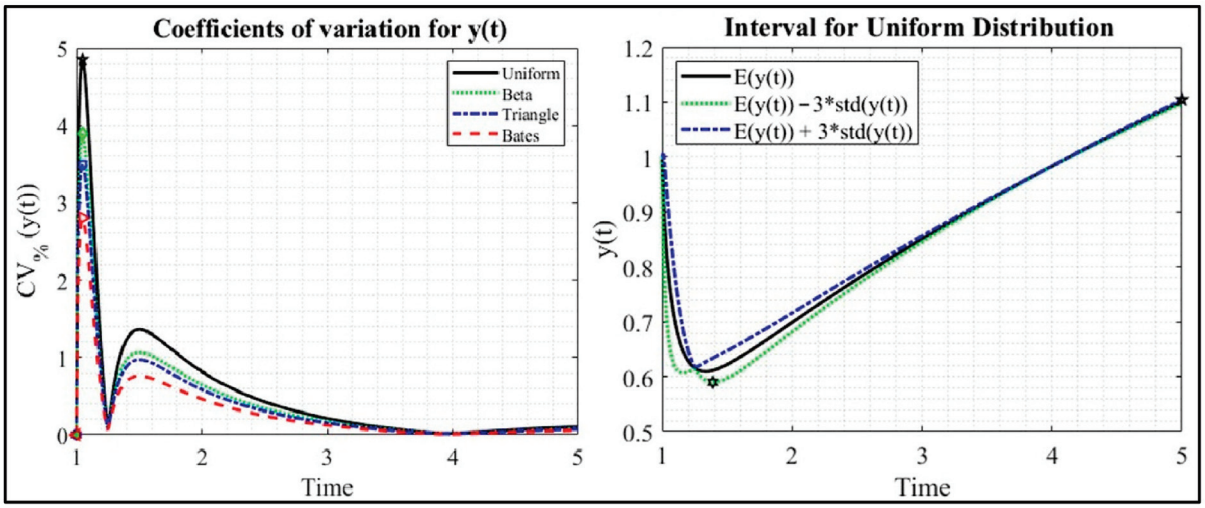

Figure 2. Coefficients of variation for all distributions (**left**) and the three-sigma interval for the uniform distribution (**right**) for the Bernoulli FDE.

Here, the three-sigma intervals of the form $[E(y) - 3std(y), (y) + 3std(y)]$ are used. The solid black line shows the expected value, whereas the green dotted line and blue dash-dotted line are the lower and upper ends of the interval, respectively. The graph for the uniform distribution is used for the three-sigma intervals since the graphs for the other distributions are almost identical. The results for the coefficients of variation in (13) are also reflected in this graph, where the variability decreases along with the CV for each probability distribution.

The maximum and minimum values for the solution, along with their timing, are given below for each distribution (Table 1).

Table 1. Extreme values for the expected solution of the Bernoulli FDE.

	Uniform	**Beta**	**Triangle**	**Bates**
$E(y(t))_{Min}$	$0.6100, t = 1.33$	$0.6101, t = 1.33$	$0.6101, t = 1.33$	$0.6102, t = 1.33$
$E(y(t))_{Max}$	$1.1008, t = 5.00$	$1.1007, t = 5.00$	$1.1007, t = 5.00$	$1.1007, t = 5.00$

The maxima for the CV of the solution $y(t)$ changes with respect to the distribution of the random fractional order as follows: $Max(CV(y(t))) = 4.9379\%$ for uniform distribution, 3.8470% for Beta distribution, 3.5262% for the triangle distribution and 2.8858% for Bates distribution, all obtained at the same moment $t = 1.05$. The minima for the CV are identical: $Min(CV(y(t))) = 0.00\%$ at the starting point, but other common minima are also found at $t = 1.25$ and around $t = 4.00$ changing between 0.06–0.12% and 0.01–0.02% respectively.

It should be noted that while the expected values for the random orders are $E(\alpha_i^*) = 0.80$ for $\alpha_i^* = c + \varepsilon X_i, i \in \{1, 2, 3, 4\}$, this value can only be achieved as $N \to \infty$ in the simulation. Since the simulation has been performed with $N = 2^{15}$ repetitions, the random orders α_i^* have shown different characteristics for each probability distribution. For uniform distribution, since $\alpha_1 = c + \varepsilon X_1$ where $c = 0.65, \varepsilon = 0.3$ and $X_1 \sim U(0, 1)$, it is seen that the generated 2^{15} orders vary within $[0.65, 0.95]$ with an expected value $E(\alpha_1) = 0.8002$ and standard deviation $std(\alpha_1) = 0.0867$ that results in the maximum relative standard deviation $CV(\alpha_1) = 10.8364\%$. The results for all characteristics of $\alpha_i^*, i \in \{1, 2, 3, 4\}$ are given in the table below (Table 2). Results show that the probability characteristics for each distribution are in accordance with their theoretical expectations. According to the law of large numbers, the calculated $CV(\alpha_i), i \in \{1, 2, 3, 4\} \to CV(\alpha)$ for each distribution as $N \to \infty$.

https://doi.org/10.3390/fractalfract10080561

Table 2. Calculated deviation in the results compared to the theoretical values for the Bernoulli FDE.

	Range	Expectation $E(\alpha^*)$	Deviation $std(\alpha^*)$	Coefficient of Variation	
				Calculated	Expected
Uniform	$\alpha_1 \in [0.6500, 0.9500]$	0.8002	0.0867	$CV(\alpha_1) = 10.8364\%$	10.83%
Beta	$\alpha_2 \in [0.6514, 0.9496]$	0.8001	0.0670	$CV(\alpha_2) = 8.3769\%$	8.39%
Triangle	$\alpha_3 \in [0.6506, 0.9494]$	0.8000	0.0614	$CV(\alpha_3) = 7.6700\%$	7.65%
Bates	$\alpha_4 \in [0.6577, 0.9459]$	0.8000	0.0498	$CV(\alpha_4) = 6.2230\%$	6.25%

The coefficient of variation changes the width of the interval for the expected solution obtained for three standard deviations, which is expected to contain around 99.73% of the values for a normal distribution, i.e., $P(\mu - 3\sigma \leq X \leq \mu + 3\sigma) = 0.9973$ for $X \sim N(\mu, \sigma^2)$. This probability differs from the probability distributions used in the study. For instance, at $t = 1.4$, the expected solutions of $y(t)$ and the intervals for three standard deviations for each distribution are obtained as follows. For the uniform distribution $E(y(t)) = 0.6125$ whereas the solution could be between $[0.5897, 0.6354]$. For the Beta distribution $E(y(t)) = 0.6128$ and the interval is obtained as $[0.5952, 0.6304]$. For the triangular distribution $E(y(t)) = 0.6129$ and the interval $[0.5967, 0.6290]$ contains the solution. For the Bates distribution $E(y(t)) = 0.6130$ and the three-sigma interval is obtained as $[0.5999, 0.6261]$. It is seen that the increase in the theoretical variance from the Bates distribution to the uniform distribution is also seen in the width of the three-sigma intervals containing the expected solutions, which is in accordance with the results obtained for the coefficients of variation.

Example 2. *Fractional Euler differential equation:*

$$^{C}C_t^{\alpha_i^*} y = -3\frac{y}{t} + 4, y(1) = 4. \tag{15}$$

The original ODE has the exact solution $y(t) = t + 3/t^3$ and the random-order FDE (15) is obtained for each $\alpha_i^*, i \in \{1, 2, 3, 4\}$ by introducing Caputo-type derivatives in the original equation. Note that the time domain $[1, T]$ does not contain $t = 0$ which causes a singularity. The three-sigma intervals for the expected solution of the random-order FDE with Beta distribution and coefficients of variation of the solutions are shown below along with marked extreme values (Figure 3). The graph for the Beta distribution has been used for the figure for a concise presentation since the figures for the three-sigma intervals do not have noticeable differences. Once again, the simulation has been done by using $N = 2^{15}$ repetitions and a step size of $h = 0.01$.

The extreme values for the solution of the fractional Euler differential equation are given for each probability distribution along with their timing (Table 3). The values are once again similar for each distribution in terms of their magnitudes and timings.

Table 3. Extreme values for the expected solution of the Euler FDE.

	Uniform	Beta	Triangle	Bates
$E(y(t))_{Min}$	$2.4287, t = 1.55$	$2.4282, t = 1.54$	$2.4277, t = 1.54$	$2.4276, t = 1.54$
$E(y(t))_{Max}$	$4.9781, t = 5.00$	$4.9767, t = 5.00$	$4.9765, t = 5.00$	$4.9759, t = 5.00$

The maximum CV for each distribution is obtained as $Max(CV(y(t))) = 4.4524\%$ for the uniform distribution, 3.4773% for the Beta distribution, 3.1756% for the triangle distribution and 2.5947% for the Bates distribution, all obtained at $t = 1.08$ and zero

https://doi.org/10.3390/fractalfract10080561

minimum CV for all cases at the beginning of the process. Here, other common minima are also found between 0.09–0.20% at $t = 1.4$ and between 0.02–0.05% at $t = 4.79$. The similarity between the results for the calculated CV of the random orders and the theoretical results for their probability distributions is shown in the table below (Table 4).

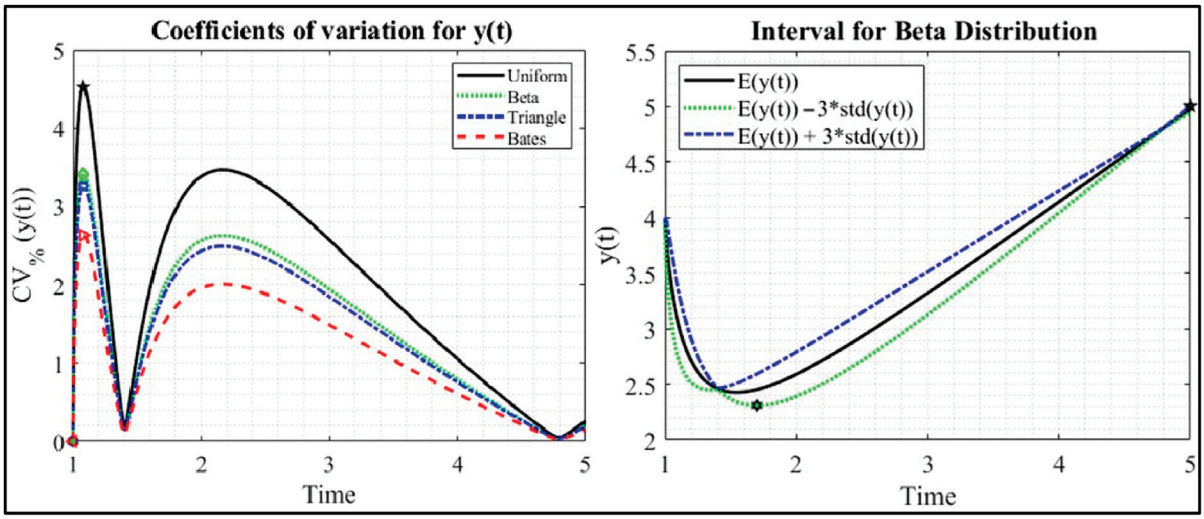

Figure 3. Coefficients of variation for all distributions (**left**) and the three-sigma interval for the Beta distribution (**right**) for the Euler FDE.

Table 4. Calculated deviation and theoretical values for each probability distribution.

	Range	Expectation $E(\alpha^*)$	Deviation $std(\alpha^*)$	Coefficient of Variation	
				Calculated	Expected
Uniform	$\alpha_1 \in [0.6500, 0.9500]$	0.8003	0.0864	$CV(\alpha_1) = 10.7901\%$	10.83%
Beta	$\alpha_2 \in [0.6514, 0.9494]$	0.7995	0.0671	$CV(\alpha_2) = 8.3956\%$	8.39%
Triangle	$\alpha_3 \in [0.6509, 0.9493]$	0.8003	0.0613	$CV(\alpha_3) = 7.6610\%$	7.65%
Bates	$\alpha_4 \in [0.6547, 0.9438]$	0.7998	0.0500	$CV(\alpha_4) = 6.2458\%$	6.25%

The decrease in the deviation from uniform distribution to Bates distribution can also be seen in three-sigma intervals. The expected solution at $t = 1.4$ is obtained as $E(y(t)) = 0.6125$ for the uniform distribution, whereas its interval for three standard deviations is $[0.5897, 0.6354]$. For the Beta distribution, the expected solution $E(y(t)) = 0.6128$ could vary between $[0.5952, 0.6304]$. For the triangular distribution, the expected solution $E(y(t)) = 0.6129$ has the three-sigma interval $[0.5967, 0.6290]$. For the Bates distribution $E(y(t)) = 0.6130$ could be obtained within $[0.5999, 0.6261]$.

Example 3. *Fractional Clairaut differential equation:*

$$y = t\,{}^{C}C_{t}^{\alpha_i^*} y + 2\,{}^{C}C^{\alpha_i^*} y, y(0) = 4. \tag{16}$$

The original Clairaut ODE has the exact solution $y(t) = 2t + 4$ (and a singular solution $t = -2$). The coefficients of variation for the solution of the fractional Clairaut differential equation and the three-sigma interval of the expected solution for a triangular distribution are shown below along with marked extreme values (Figure 4).

The change in the coefficient of variation is similar to the case observed in the fractional Bernoulli and Euler differential equations. The maximum values for the CV and the expected values of the solution are given below (Table 5).

https://doi.org/10.3390/fractalfract10080561

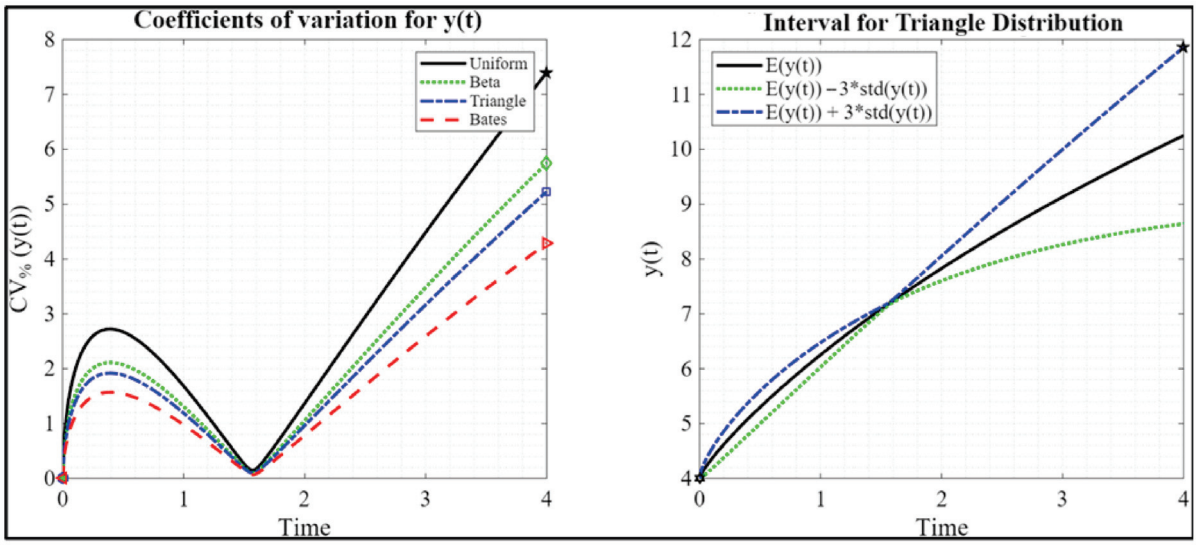

Figure 4. Coefficients of variation for all distributions (**left**) and the three-sigma interval for the triangular distribution (**right**) for the Clairaut FDE.

Table 5. Extreme values for the expected solution of the Clairaut FDE.

	Uniform	**Beta**	**Triangle**	**Bates**
$E(y(t))_{Max}$	$10.2560, t = 4.00$	$10.2539, t = 4.00$	$10.2488, t = 4.00$	$10.2495, t = 4.00$
$CV(y(t))_{Max}$	$7.3976, t = 4.00$	$5.7478, t = 4.00$	$5.2269, t = 4.00$	$4.2844, t = 4.00$

The minimum values for the expected solution are identical for each case, as $Min(E(y(t))) = 4.0000$ at $t = 4.00$ and similarly for the coefficient of variation as $CV(y(t))_{Min} = 0.00\%$ initially. A second common local minimum CV is obtained at $t = 1.57$ between 0.06–1.15%. A comparison of calculated CV and the theoretical values is given below (Table 6).

Table 6. Calculated deviation and theoretical CV values for the Clairaut FDE.

	Range	**Expectation** $E(\alpha^*)$	**Deviation** $std(\alpha^*)$	**Coefficient of Variation**	
				Calculated	**Expected**
Uniform	$\alpha_1 \in [0.6500, 0.9500]$	0.8007	0.0866	$CV(\alpha_1) = 10.8160\%$	10.83%
Beta	$\alpha_2 \in [0.6504, 0.9495]$	0.8005	0.0672	$CV(\alpha_2) = 8.3945\%$	8.39%
Triangle	$\alpha_3 \in [0.6505, 0.9488]$	0.8000	0.0611	$CV(\alpha_3) = 7.6343\%$	7.65%
Bates	$\alpha_4 \in [0.6592, 0.9417]$	0.8001	0.0500	$CV(\alpha_4) = 6.2524\%$	6.25%

The change in the level of deviation with respect to the probability distribution of the fractional order can be further analyzed through the expected solution at the end of the process. At $t = 4.00$, the expected solution and the intervals for three standard deviations are obtained as follows for each case: $E(y(t)) = 10.2560$ and the solution is expected to be between $[7.9799, 12.5321]$ for uniform distribution, $E(y(t)) = 10.2539$ and the solution is expected to be between $[8.4858, 12.0220]$ for Beta distribution, $E(y(t)) = 10.2488$ and the solution is expected to be between $[8.6417, 11.8559]$ for the triangle distribution and $E(y(t)) = 10.2495$ and the solution is expected to be between $[8.9321, 11.5668]$ for the Bates distribution.

https://doi.org/10.3390/fractalfract10080561

Example 4. *Fractional Riccati differential equation:*

$$^{C}C_{t}^{\alpha_i^*} y = 4 + 4yt^2 - ty^2, y(0) = 0. \quad (17)$$

The ODE version of this IVP has the exact solution $y(t) = 4t$. The maximum values for the CV and the expected values of the solution are given below (Table 7).

Table 7. Extreme values for the expected solution of the Riccati FDE.

	Uniform	Beta	Triangle	Bates
$E(y(t))_{Max}$	$16.0219, t = 4.00$	$16.0177, t = 4.00$	$16.0153, t = 4.00$	$16.0128, t = 4.00$
$CV(y(t))_{Max}$	$41.4320, t = 0.01$	$32.7501, t = 0.01$	$29.8597, t = 0.01$	$24.6715, t = 0.01$

The minimum values for the expected solution are identical for each probability distribution, as $Min(E(y(t))) = 0.0000$ at $t = 0.00$. The calculated CV values are compared to the theoretical values below (Table 8). The excessive CV values seen initially may be caused by the initial value of the problem, since the solution starts from $y(0) = 0$.

Table 8. Calculated deviation and the theoretical CV values for the Riccati FDE.

	Range	Expectation $E(\alpha^*)$	Deviation $std(\alpha^*)$	Coefficient of Variation	
				Calculated	Expected
Uniform	$\alpha_1 \in [0.6500, 0.9500]$	0.8002	0.0865	$CV(\alpha_1) = 10.8159\%$	10.83%
Beta	$\alpha_2 \in [0.6514, 0.9492]$	0.8008	0.0672	$CV(\alpha_2) = 8.3882\%$	8.39%
Triangle	$\alpha_3 \in [0.6515, 0.9488]$	0.8000	0.0608	$CV(\alpha_3) = 7.6027\%$	7.65%
Bates	$\alpha_4 \in [0.6562, 0.9450]$	0.8000	0.0501	$CV(\alpha_4) = 6.2680\%$	6.25%

It is seen that the average value for the random fractional order is obtained within $[0.7995, 0.8008]$ for these four fractional differential equations using uniform, Beta, triangle and Bates distributions. The average calculated from $N = 2^{15}$ repetitions is expected to approach the theoretical expectation $E(\alpha^*) = 0.8000$ as $N \to \infty$ according to the law of large numbers. Similarly, the results for the variances—and consequently, the coefficients of variation—are expected to approach their theoretical values given in (10) and (13) as $N \to \infty$.

Since a finite number of repetitions are used to estimate the expected value and variance of the solutions for the random-order FDEs, Monte-Carlo error and confidence intervals with the standard error of the estimated mean could be analyzed. However, a simulation using $N = 2^{15}$ repetitions would mean that such a large sample would lead to minimal standard error due to the $\mathcal{O}\left(N^{-1/2}\right)$ convergence rate for Monte-Carlo estimates. For random-order Riccati FDE with uniform distribution, the distribution with the highest standard deviation, a CV of 10.8159%, was obtained for the random order. If the standard error $std(\alpha^*)/\sqrt{N}$ was analyzed with $N = 2^{15}$, a maximum value of 4.78×10^{-4} would be obtained also corresponding to a 95% confidence interval of full maximal width 1.873×10^{-3} for the expected value of the random order. While changing sample size may affect the standard error, the convergence rate $\mathcal{O}\left(N^{-1/2}\right)$ means using $N = 2^{20}$ simulations would likely decrease the error margin to around 8.45×10^{-5}.

4. Discussion and Conclusions

This study focuses on the characteristics related to the variability of solutions and random orders in fractional differential equations with orders governed by various probability

https://doi.org/10.3390/fractalfract10080561

distributions on bounded supports. There are numerous studies in the literature that focus on analyzing fractional differential equations with random or variable orders. However, most of these studies focus on numerical methods to solve FDEs of variable or random orders such as finite difference schemes or wavelet approaches [37,38]; or their applications in various modeling problems such as the fractional advection-diffusion equation or chaotic financial systems [31,32]. Collocation methods and Taylor approximation-based approaches have also been utilized in studies concentrating on approximate solutions of FDEs containing fractional derivatives in the Riemann-Liouville or Caputo senses [47,48]. Rather than focusing on numerical approximation, this study investigates a different aspect of random-order FDEs and underlines variability caused by the probability distribution of the random order. Caputo fractional derivative has been used to exemplify FDEs due to its physical interpretability, compatibility with classical calculus and its widespread use in modeling studies. Results on the coefficients of variation and three-sigma intervals are given along with expected solutions of the FDEs and average orders to show how the simulated cases follow the theoretical values for the distributions. The theoretical CV values for uniform, Beta, triangular and Bates distributions, calculated as 10.83%, 8.39%, 7.65% and 6.25%, respectively, are obtained in four numerical examples. The solutions of the simulated Bernoulli, Euler, Clairaut and Riccati FDEs calculated from $N = 2^{15}$ repetitions all follow these theoretical values for the random orders. Note that as the number of repetitions approaches infinity, the calculated values are also expected to approach their theoretical values, according to the law of large numbers. Additionally, the variability of solutions for each FDE also follows the ratios of the CVs of the probability distributions given in (12). For instance, ratios of the coefficients of variation for Beta and Bates distributions compared to the maximum CV of the solution obtained for Clairaut FDE are obtained as follows.

$$\frac{CV(Beta)}{CV(Bates)} = \frac{44.72}{33.33} = 1.3417, \quad \frac{CV(y(t))_{Max}}{CV(y(t))_{Max}} = \frac{5.7478}{4.2844} = 1.3416. \tag{18}$$

Other examples can also be given for different probability distributions and FDEs. For instance, the ratios of the CVs for Uniform and Bates distributions are $\frac{CV(Uniform)}{CV(Triangle)} = \frac{57.74}{40.82} = 1.4145$, whereas the maximum CV of the solutions for the Euler FDE gives $\frac{CV(y(t))_{Max}}{CV(y(t))_{Max}} = \frac{4.4525}{3.1756} = 1.4021$. The change in the variability in the results of random-order FDEs is also shown with a comparison of the three-sigma intervals for expected solutions. A summary of the variability comparison results can be found below (Table 9). The agreement rates of CVs have been obtained by percentage of absolute difference between calculated and theoretical CVs for the random orders. The table summarizes the results for almost identical average solutions (expected solution range) and the results for the CV and the order or relative deviation rates for each FDE and distribution (the width of the range of minimum and maximum expected solutions).

Table 9. A summary of variability characteristics.

Equation	Agreement Rates of CV (α^*)	Order of CV for $y(t)$	Expected Solution Range Width	
			Min	Max
Bernoulli	0.0591–0.4320%	Uniform > Beta > Tri > Bates	0.0002	0.0001
Euler	0.0667–0.3684%	Uniform > Beta > Tri > Bates	0.0011	0.0022
Clairaut	0.0348–0.2052%	Uniform > Beta > Tri > Bates	0.0000	0.0072
Riccati	0.0215–0.6183%	Uniform > Beta > Tri > Bates	0.0000	0.0091

https://doi.org/10.3390/fractalfract10080561

The support of the random order has been altered to investigate if the correspondence between theoretical and observed CVs is preserved for cases closer to the boundaries (when $\alpha \to 1$) or when the width of the support is smaller. If $c = 0.85$ and $\varepsilon = 0.1$ for the random order $\alpha^* = c + \varepsilon X_i$ with $X_1 \sim U(0,1), X_2 \sim Beta(u,v), X_3 \sim Tri(0,0.5,1), X_4 \sim Bates(3)$, it is seen that $\alpha^* \in [0.85, 0.95]$ with $E(\alpha^*) = 0.9$. In this scenario, the maximum values for theoretical and calculated CVs for the random order and the solutions are obtained as follows (Table 10).

Table 10. Variability results for $\alpha^* \in [0.85, 0.95]$.

CV	Uniform	Beta	Triangle	Bates
α^*—Theoretical	3.2075%	2.4845%	2.2553%	1.8558%
α^*—Calculated	3.2087%	2.4928%	2.2568%	1.8544%
$y(t)$—Calculated	1.5973%	1.2420%	1.1245%	0.9243%

The variability pattern is preserved on the boundary region for the random order as well. When $\alpha^* \in [0.94, 0.99]$, the alignment of the theoretically calculated CVs for the random order continues: 1.4957–1.4990% for uniform, 1.1586–1.1566% for Beta, 1.0576–1.0543% for triangular and 0.8636–0.8640% for Bates along with the CV for the solutions 0.7808%, 0.6025%, 0.5493% and 0.4502% respectively. Note that all simulations have been performed using $N = 2^{15}$ repetitions. These results show that the variability characteristics of the distributions can also be observed in the simulated sample of random orders and the solutions when the bounded support of the random order becomes narrower or shifts to the integer-order boundary as well.

Overall, it can be said that this study contributes to the current literature with its distribution-specific investigation for the variability in the solutions of random-order FDEs. It should be stated here that these findings are related to the results of the simulations, carried out within a limited timeframe and for fractional orders with a bounded support $[0.65, 0.95]$. Further analysis could focus on general properties of the Caputo derivative and the conditions which guarantee this relationship.

A certain amount of modeling studies that use FDEs also consider the random nature of the events being investigated. Recent studies that use a fractional modeling approach along with probabilistic elements have discussed the findings from both the random and the deterministic perspectives. A fractional malnutrition model with random perturbations [17], a fractional Lassa-fever model with varying kernels [49], a fractional model for tea cultivation [14] and a study on random vibration of linear systems [50] are some of the studies that provide deterministic and random elements at the same time. A comparison of random and deterministic results shows that the results for the expected values obtained from the random perspective match the solutions obtained from the deterministic perspective. This study contributes to this phenomenon with the results obtained for the expected values, especially for the random orders. Although results change as $\alpha_i^* = c + \varepsilon X_i, i \in \{1,2,3,4\}$ varies within the interval $[0.65, 0.95]$, the average solutions obtained from the random order FDEs for $N = 2^{15}$ repetitions approach the deterministic results through the expected values. Both the average random orders $E(\alpha^*)$ approach their expected value of 0.80 in all four numerical examples, and the expected solutions $E(y(t))$ approach the deterministic solution $y(t)$. Hence, this study adds to the literature focused on deterministic-random modeling studies using FDEs.

A figure showing the convergence of the Monte-Carlo estimate for the random order of fractional differentiation (for Beta distribution $\alpha^* = c + \varepsilon X$ for $X \sim Beta(u,v)$ with $u = v = 2$) has been given below, showing how the absolute error $|E(\alpha^*) - 0.80|$ decreases

https://doi.org/10.3390/fractalfract10080561

with an increase in the number of simulations (Figure 5). Note that the change in mean fractional order error (blue line) has been compared to the theoretical Monte-Carlo convergence rate $\mathcal{O}\left(N^{-1/2}\right)$ shown with the red dashed line using a log-log convergence plot.

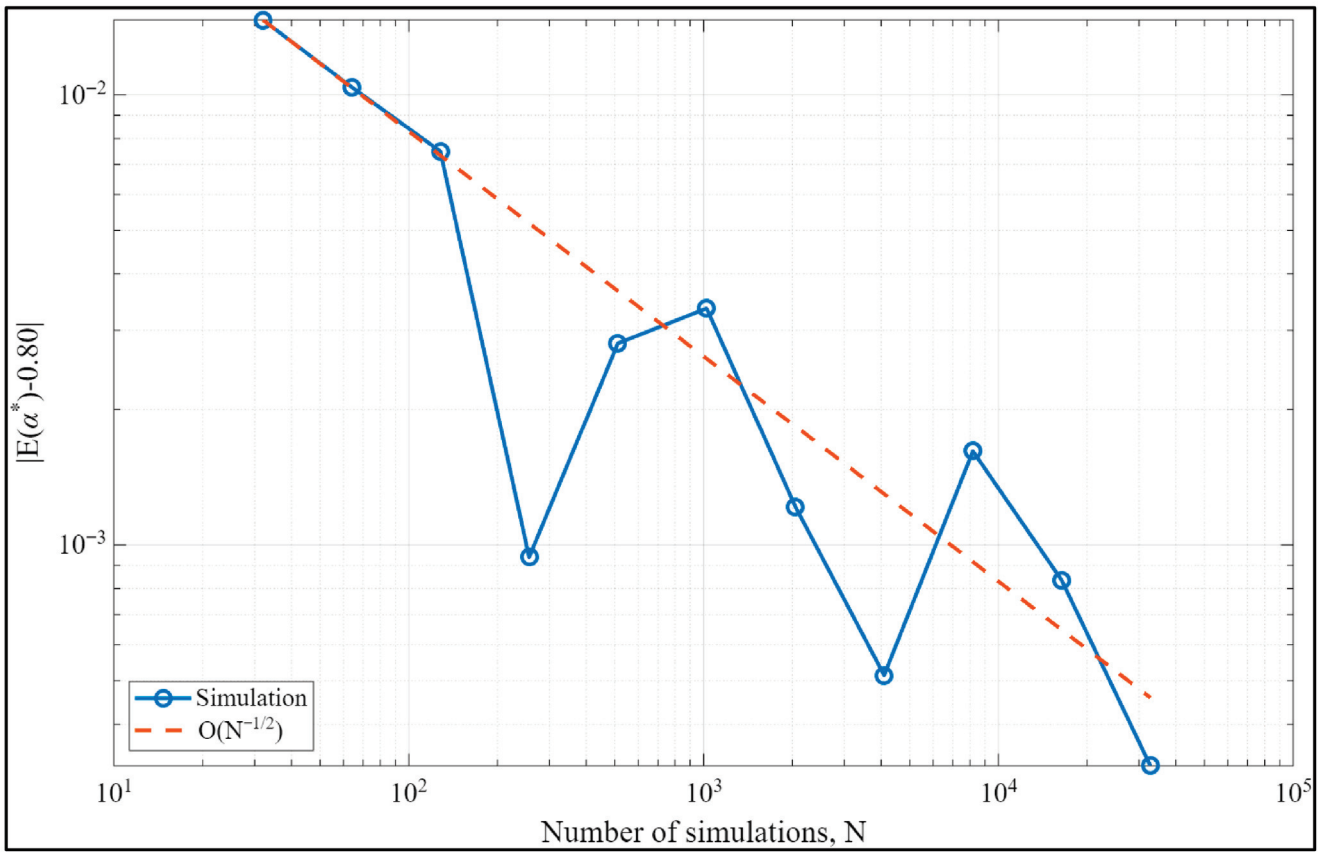

Figure 5. Log-log convergence plot of the Monte Carlo error.

The study aims to highlight the changing variability in the solutions and the random orders of fractional differential equations, and certain limitations in study design ensure a focus on these aspects. The probability distributions investigated in this study are all defined on a bounded support. This ensures that the random order α^* always remains a fractional order such that $0 < \alpha^* < 1$. Further analysis can focus on the case where the order is still not an integer but is also allowed to exceed $\alpha = 1$. L2 method and other numerical methods could be used to analyze the case where $\alpha > 1$. Note that this would also cause other issues such as the need for extra initial conditions. The probability distributions are all assumed to be symmetrical in this study, whereas further investigation could focus on skewed distributions. Probability distributions defined on the whole $\mathbb{R}$ could also be used with certain conditions that guarantee $\alpha^* > 0$. However, the limitations in this study were implemented to guarantee a concise investigation focusing on the changes in variability characteristics related to the distribution of the random orders. Further limitations on the numerical method, fixed parameters for all distributions and the use of univariate distributions may be the foundation for future studies. Although these restrictions were used to ensure a focus on the relationship between the variability of the solutions and the probability density of the random order, more detailed analysis could provide useful results on the numerical characteristics of the solutions and the convergence of numerical solutions. Results show that although the selection of the probability distribution affects the variability of the results of the FDEs, the expected solutions still meet the deterministic case, meaning that the random orders could be used as an alternative to the fixed order

https://doi.org/10.3390/fractalfract10080561

values used in deterministic studies. It should be noted that in cases where the randomized order has excessive variance, this may affect the correspondence of the model output to the real system being modeled. Nevertheless, in most cases where the randomized fractional order provides a useful tool for modeling uncertainty, the average solutions provide a valuable alternative to the solutions of deterministic models.

Funding: This study has been supported by the Recep Tayyip Erdoğan University Development Foundation (Grant number: 02026007001453).

Data Availability Statement: The original contributions presented in this study are included in the article. Further inquiries can be directed to the corresponding author.

Conflicts of Interest: The author declares no conflict of interest.

References

1. Le, M.; Kurt, H.I.; Yaprak, R. Analytical and numerical analysis of boundedness in a two-species Keller–Segel model with weak nonlinear sensitivity. *Commun. Nonlinear Sci. Numer. Simul.* **2026**, *154*, 109563. [CrossRef]
2. Li, X.; Guo, Y. Dynamics analysis and numerical simulations of a stochastic delayed epidemic model with double disease driven by Lévy noise. *AIMS Math.* **2026**, *11*, 3038–3095. [CrossRef]
3. Cobb, L. Stochastic differential equations for the social sciences. In *Mathematical Frontiers of the Social and Policy Sciences*; Routledge: New York, NY, USA, 2019; pp. 37–68.
4. Caputo, M. Linear models of dissipation whose Q is almost frequency independent—II. *Geophys. J. Int.* **1967**, *13*, 529–539. [CrossRef]
5. Burgos, C.; Cortés, J.C.; Villafuerte, L.; Villanueva, R.J. Mean square calculus and random linear fractional differential equations: Theory and applications. *Appl. Math. Nonlinear Sci.* **2017**, *2*, 317–328. [CrossRef]
6. Villafuerte, L. Solution processes for second-order linear fractional differential equations with random inhomogeneous parts. *Math. Comput. Simul.* **2023**, *210*, 17–48. [CrossRef]
7. González-Parra, G.; Chen-Charpentier, B.; Arenas, A.J. Polynomial chaos for random fractional order differential equations. *Appl. Math. Comput.* **2014**, *226*, 123–130. [CrossRef]
8. Jornet, M. On the convergence of the Galerkin method for random fractional differential equations. *Fract. Calc. Appl. Anal.* **2024**, *27*, 1852–1865. [CrossRef]
9. Burgos, C.; Cortés, J.C.; Villafuerte, L.; Villanueva, R.J. Solving random fractional second-order linear equations via the mean square Laplace transform: Theory and statistical computing. *Appl. Math. Comput.* **2022**, *418*, 126846. [CrossRef]
10. Burgos, C.; Calatayud, J.; Cortés, J.C.; Navarro-Quiles, A. A full probabilistic solution of the random linear fractional differential equation via the random variable transformation technique. *Math. Methods Appl. Sci.* **2018**, *41*, 9037–9047. [CrossRef]
11. Navarro, E.L. Advances on Differential Equations with Uncertainties and Their Applications to Probabilistic Mechanics Engineering. Ph.D. Thesis, Universitat Politècnica de València, Valencia, Spain, 2024.
12. Bevia, V.J.; Simón, C.B.; Cortés, J.C.; Micó, R.J.V. Uncertainty quantification of random microbial growth in a competitive environment via probability density functions. *Fractal Fract.* **2021**, *5*, 26. [CrossRef]
13. Bekiryazici, Z. Utilizing fractional derivatives and sensitivity analysis in a random framework: A model-based approach to the investigation of random dynamics of malware spread. *Bound. Value Probl.* **2024**, *2024*, 109. [CrossRef]
14. Bekiryazici, Z. A randomized fractional modeling of pest management dynamics for tea plant (*Camellia sinensis*) with parameter adaptation to Turkish data. *Bound. Value Probl.* **2026**, *2026*, 39. [CrossRef]
15. Su, N. Random fractional partial differential equations and solutions for water movement in soils: Theory and applications. *Hydrol. Process.* **2023**, *37*, e14844. [CrossRef]
16. Heris, A.; Salim, A.; Benchohra, M.; Karapınar, E. Fractional partial random differential equations with infinite delay. *Results Phys.* **2022**, *37*, 105557. [CrossRef]
17. Chu, Y.M.; Rashid, S.; Karim, S.; Khalid, A.; Elagan, S.K. Deterministic-stochastic analysis of fractional differential equations malnutrition model with random perturbations and crossover effects. *Sci. Rep.* **2023**, *13*, 14824. [CrossRef] [PubMed]
18. Liping, C.; Khan, M.A.; Atangana, A.; Kumar, S. A new financial chaotic model in Atangana–Baleanu stochastic fractional differential equations. *Alex. Eng. J.* **2021**, *60*, 5193–5204. [CrossRef]
19. Kurt, A.; Taşbozan, O. Exact solution for nonlinear acoustics model with conformable derivative. *J. Math. Sci. Model.* **2025**, *8*, 22–27. [CrossRef]
20. Zerbib, S.; Hilal, K.; Kajounı, A. On the study of semilinear fractional differential equations involving Atangana–Baleanu–Caputo derivative. *Univ. J. Math. Appl.* **2023**, *6*, 122–129. [CrossRef]

21. Sun, H.; Chen, Y.; Chen, W. Random-order fractional differential equation models. *Signal Process.* **2011**, *91*, 525–530. [CrossRef]
22. Pedjeu, J.C.; Ladde, G.S. Stochastic fractional differential equations: Modeling, method and analysis. *Chaos Solitons Fractals* **2012**, *45*, 279–293. [CrossRef]
23. Lupulescu, V.; Ntouyas, S.K. Random fractional differential equations. *Int. Electron. J. Pure Appl. Math.* **2012**, *4*, 119–136.
24. Cortés, J.C.; Jódar, L.; Romero, J.V.; Roselló, M.D. A comparative study of the numerical approximation of the random Airy differential equation. *Comput. Math. Appl.* **2011**, *62*, 3411–3417. [CrossRef]
25. Ali, I.; Khan, S.U. A dynamic competition analysis of stochastic fractional differential equation arising in finance via pseudospectral method. *Mathematics* **2023**, *11*, 1328. [CrossRef]
26. Chu, Y.M.; Sultana, S.; Rashid, S.; Alharthi, M.S. Dynamical analysis of the stochastic COVID-19 model using piecewise differential equation technique. *CMES-Comput. Model. Eng. Sci.* **2023**, *137*, 2427–2464. [CrossRef]
27. Bekiryazici, Z. Sensitivity analysis and random dynamics for a mathematical model of tuberculosis transmission. *Commun. Stat. Simul. Comput.* **2024**, *53*, 6009–6021. [CrossRef]
28. Sun, H.; Chang, A.; Zhang, Y.; Chen, W. A review on variable-order fractional differential equations: Mathematical foundations, physical models, numerical methods and applications. *Fract. Calc. Appl. Anal.* **2019**, *22*, 27–59. [CrossRef]
29. Patnaik, S.; Hollkamp, J.P.; Semperlotti, F. Applications of variable-order fractional operators: A review. *Proc. Math. Phys. Eng. Sci.* **2020**, *476*, 20190498. [CrossRef] [PubMed]
30. Sun, H.; Chen, W.; Sheng, H.; Chen, Y. On mean square displacement behaviors of anomalous diffusions with variable and random orders. *Phys. Lett. A* **2010**, *374*, 906–910. [CrossRef]
31. Tayebi, A.; Shekari, Y.; Heydari, M.H. A meshless method for solving two-dimensional variable-order time fractional advection–diffusion equation. *J. Comput. Phys.* **2017**, *340*, 655–669. [CrossRef]
32. Soradi-Zeid, S.; Jahanshahi, H.; Yousefpour, A.; Bekiros, S. King algorithm: A novel optimization approach based on variable-order fractional calculus with application in chaotic financial systems. *Chaos Solitons Fractals* **2020**, *132*, 109569. [CrossRef]
33. Jahan, S.; Yadav, P.; Shah, K.; Abdeljawad, T. An efficient wavelet technique for solving variable-order fractional equations arising in contaminant transport through porous media. *Fractals* **2025**, *33*, 2540238. [CrossRef]
34. Atangana, A.; Kilicman, A. On the generalized mass transport equation to the concept of variable fractional derivative. *Math. Probl. Eng.* **2014**, *2014*, 542809. [CrossRef]
35. Ray, S.S. Two competent novel techniques based on two-dimensional wavelets for nonlinear variable-order Riesz space-fractional Schrödinger equations. *J. Comput. Appl. Math.* **2023**, *424*, 114971. [CrossRef]
36. Heydari, M.H.; Shakiba, A.; Avazzadeh, Z.; Cattani, C. Second kind Chebyshev wavelets for solving the variable-order space-time fractional telegraph equation. In *Special Functions and Analysis of Differential Equations*; Chapman & Hall/CRC: Boca Raton, FL, USA, 2020; pp. 63–85.
37. Sun, H.; Chen, W.; Li, C.; Chen, Y. Finite difference schemes for variable-order time fractional diffusion equation. *Int. J. Bifurc. Chaos* **2012**, *22*, 1250085. [CrossRef]
38. Heydari, M.H.; Avazzadeh, Z.; Haromi, M.F. A wavelet approach for solving multi-term variable-order time fractional diffusion-wave equation. *Appl. Math. Comput.* **2019**, *341*, 215–228. [CrossRef]
39. Dehestani, H.; Ordokhani, Y.; Razzaghi, M. Fractional-order Bessel wavelet functions for solving variable-order fractional optimal control problems with estimation error. *Int. J. Syst. Sci.* **2020**, *51*, 1032–1052. [CrossRef]
40. Kumar, S.; Gupta, V. Collocation method with Lagrange polynomials for variable-order time-fractional advection–diffusion problems. *Math. Methods Appl. Sci.* **2024**, *47*, 1113–1131. [CrossRef]
41. Diethelm, K. *The Analysis of Fractional Differential Equations: An Application-Oriented Exposition Using Differential Operators of Caputo Type*; Springer: Berlin/Heidelberg, Germany, 2010.
42. Şengül, S.; Bekiryazici, Z.; Merdan, M. Approximate solutions of fractional differential equations using optimal q-homotopy analysis method: A case study of Abel differential equations. *Fractal Fract.* **2024**, *8*, 533. [CrossRef]
43. Duman, O. Controllability analysis of fractional-order delay differential equations via contraction principle. *J. Math. Sci. Model.* **2024**, *7*, 121–127. [CrossRef]
44. Arnholt, A.T.; Bauldry, W.C.; Rupasinghe, H.S.; Don, A.; Watagoda, L.C.P. Examining the "n≥30 Is Sufficiently Large for the Sampling Distribution of X to Follow a Normal Distribution" Caveat. *BEIO* **2018**, *34*, 182–198.
45. Predictor-Corrector PECE. Method for Fractional Differential Equations, MathWorks File Exchange, 2000. Available online: https://www.mathworks.com/matlabcentral/fileexchange/32918-predictor-corrector-pecemethod-for-fractional-differential-equations (accessed on 14 May 2024).
46. Diethelm, K.; Freed, A.D. The FracPECE subroutine for the numerical solution of differential equations of fractional order. *Forsch. Wiss. Rechn.* **1999**, *1998*, 57–71.
47. Didgar, M.; Ekhlasi, F. An approximate approach for fractional relaxation-oscillation equation based on Taylor expansion. *Int. J. Math. Comput. Eng.* **2025**, *3*, 435–454. [CrossRef]

48. Önal, M.; Karaagac, B.; Esen, A. An efficient higher-order trigonometric cubic B-spline collocation method for time-fractional Burgers equations. *Int. J. Math. Comput. Eng.* **2026**, *4*, 211–234. [CrossRef]
49. Rashid, S.; Karim, S.; Akgül, A.; Bariq, A.; Elagan, S.K. Novel insights for a nonlinear deterministic-stochastic class of fractional-order Lassa fever model with varying kernels. *Sci. Rep.* **2023**, *13*, 15320. [CrossRef] [PubMed]
50. Pirrotta, A.; Kougioumtzoglou, I.A.; Di Matteo, A.; Fragkoulis, V.C.; Pantelous, A.A.; Adam, C. Deterministic and random vibration of linear systems with singular parameter matrices and fractional derivative terms. *J. Eng. Mech.* **2021**, *147*, 04021031. [CrossRef]

Disclaimer/Publisher's Note: The statements, opinions and data contained in all publications are solely those of the individual author(s) and contributor(s) and not of MDPI and/or the editor(s). MDPI and/or the editor(s) disclaim responsibility for any injury to people or property resulting from any ideas, methods, instructions or products referred to in the content.

MDPI AG
Grosspeteranlage 5
4052 Basel
Switzerland
Tel.: +41 61 683 77 34

MDPI Books Editorial Office
E-mail: books@mdpi.com
www.mdpi.com/books

Disclaimer/Publisher's Note: The title and front matter of this reprint are at the discretion of the Topic Editors. The publisher is not responsible for their content or any associated concerns. The statements, opinions and data contained in all individual articles are solely those of the individual Editors and contributors and not of MDPI. MDPI disclaims responsibility for any injury to people or property resulting from any ideas, methods, instructions or products referred to in the content.

Academic Open
Access Publishing

mdpi.com

ISBN 978-3-7258-9216-7